CHAPTER 1
INTRODUCTION

by Ted Belytschko
Northwestern University

1.1 NONLINEAR FINITE ELEMENTS IN DESIGN

Nonlinear finite element analysis is an essential component of computer-aided design. Testing of prototypes is increasingly being replaced by simulation with nonlinear finite element methods because this provides a more rapid and less expensive way to evaluate design concepts and design details. For example, in the field of automotive design, simulation of crashes is replacing full scale tests, both for the evaluation of early design concepts and details of the final design, such as accelerometer placement for airbag deployment, padding of the interior, and selection of materials and component cross-sections for meeting crashworthiness criteria. In many fields of manufacturing, simulation is speeding the design process by allowing simulation of processes such as sheet-metal forming, extrusion of parts, and casting. In the electronics industries, simulation is replacing drop-tests for the evaluation of product durability.

For both users and developers of nonlinear finite element programs, an understanding of the fundamental concepts of nonlinear finite element analysis is essential. Without an understanding of the fundamentals, a user must treat the finite element program as a black box that provides simulations. However, even more so than linear finite element analysis, nonlinear finite element analysis confronts the user with many choices and pitfalls. Without an understanding of the implication and meaning of these choices and difficulties, a user is at a severe disadvantage.

The purpose of this book is to describe the methods of nonlinear finite element analysis for solid mechanics. Our intent is to provide an integrated treatment so that the reader can gain an understanding of the fundamental methods, a feeling for the comparative usefulness of different approaches and an appreciation of the difficulties which lurk in the nonlinear world. At the same time, enough detail about the implementation of various techniques is given so that they can be programmed.

Nonlinear analysis consists of the following steps:

1. development of a model;

2. formulation of the governing equations;

3. discretization of the equations;

4. solution of the equations;

5. interpretation of the results.

Modeling is a term that tends to be used for two distinct tasks in engineering. The older definition emphasizes the extraction of the essential elements of mechanical behavior. The objective in this approach is to identify the simplest model which can replicate the behavior of interest. In this approach, model development is the process of identifying the ingredients of the model which can provide the qualitative and quantitative predictions.

A second approach to modeling, which is becoming more common in industry, is to develop a detailed, single model of a design and to use it to examine all of the engineering criteria which are of interest. The impetus for this approach to modeling is that it costs far more to make a model or mesh for an engineering product than can be saved through reduction of the model by specializing it for each application. For example, the same finite element model of a laptop computer can be used for a drop-test simulation, a linear static analysis and a thermal analysis. By using the same model for all of these analyses, a significant amount of engineering time can be saved. While this approach is not recommended in all situations, it is becoming commonplace in industry. In the near future the finite element model may serve as a prototype that can be used for checking many aspects of a design's performance. The decreasing cost of computer time and the increasing speed of computers make this approach highly cost-effective. However the user of finite element software must still able to evaluate the suitability of a model for a particular analysis and understand its limitations.

The formulation of the governing equations and their discretization is largely in the hands of the software developers today. However, a user who does not understand the fundamentals of the software faces many perils, for some approaches and software may be unsuitable. Furthermore, to convert experimental data to input, the user must be aware of the stress and strain measures used in the program and by the experimentalist who provided material data. The user must understand the sensitivity of response to the data and how to asses it. An effective user must be aware of the likely sources of error, how to check for these errors and estimate their magnitudes, and the limitations and strengths of various algorithms.

The solution of the discrete equations also presents a user with many choices. An inappropriate choice will result in very long run-times which can prevent him from obtaining the results within the time schedule. An understanding of the advantages and disadvantages and the approximate computer time required for various solution procedures are invaluable in the selection of a good strategy for developing a reasonable model and selecting the solution procedure.

The user's role is most crucial in the interpretation of results. In addition to the approximations inherent even in linear finite element models, nonlinear analyses are often sensitive to many factors that can make a single simulation quite misleading. Nonlinear solids can undergo instabilities, their response can be sensitive to imperfections, and the results can depend dramatically on material parameters. Unless the user is aware of these phenomena, the possibility of a misinterpretation of simulation results is quite possible.

In spite of these many pitfalls, our views on the usefulness and potential of nonlinear finite element analyses are very sanguine. In many industries, nonlinear finite element analysis have shortened design cycles and dramatically reduced the need for prototype tests. Simulations, because of the wide variety of output they produce and the ease of doing what-ifs, can lead to tremendous improvements of the engineer's understanding of the basic physics of a product's behavior under various environments. While tests give the gross but important result of whether the product withstands a certain environment, they usually provide little of the detail of the behavior of the product on which a redesign can be based if the product does not meet a test. Computer simulations, on the other hand, give detailed histories of stress and strain and other state variables, which in the hands of a good engineer give valuable insight into how to redesign the product .

Like many finite element books, this book presents a large variety of methods and recipes for the solution of engineering and scientific problems by the finite element method. However, in order to preserve a pedagogic character, we have interwoven several themes into the book which we feel are of central importance in nonlinear analysis. These include the following:

1. the selection of appropriate methods for the problem at hand;

2. the selection of a suitable mesh description and kinematic and kinetic descriptions for a given problem;

3. the examination of stability of the solution and the solution procedure;

4. an awareness of the smoothness of the response of the model and its implication on the quality and cost of the solution;

5. the role of major assumptions and the likely sources of error.

The selection of an appropriate mesh description, i.e. whether a Lagrangian, Eulerian or arbitrary Lagrangian Eulerian mesh is used, is very important for many of the large deformation problems encountered in process simulation and failure analysis. The effects of mesh distortion need to be understood, and the advantages of different types of mesh descriptions should be borne in mind in the selection. There are many situations where a continuous remeshing or arbitrary Lagrangian Eulerian description is most suitable.

The issue of the stability of solution is central in the simulation of nonlinear processes. In numerical simulation, it is possible to obtain solutions which are not physically stable and therefore quite meaningless. Many solutions are sensitive to imperfections or material and load parameters; in some cases, there is even sensitivity to the mesh employed in the solution. A knowledgeable user of nonlinear finite element software must be aware of these characteristics and the associated pitfalls. Otherwise the results obtained by elaborate computer simulations can be quite misleading and lead to incorrect design decisions.

The issue of smoothness is also ubiquitous in nonlinear finite element analysis. Lack of smoothness degrades the robustness of most algorithms and can introduce undesirable noise into the solution. Techniques have been developed which improve the smoothness of the response; these are generally called regularization procedures. However, regularization procedures are often not

based on physical phenomena and in many cases the constants associated with the regularization are difficult to determine. Therefore, an analyst is often confronted with the dilemma of whether to choose a method which leads to smoother solutions or to deal with a discontinuous response. An understanding of the effects of regularization parameters, the presence of hidden regularizations, such as penalty methods in contact-impact, and an appreciation of the benefits of these methods is highly desirable.

The accuracy and stability of solutions is a difficult consideration in nonlinear analysis. These issues manifest themselves in many ways. For example, in the selection of an element, the analyst must be aware of stability and locking characteristics of various elements. A judicious selection of an element for a problem involves factors such as the stability of the element for the problem at hand, the expected smoothness of the solution and the magnitude of deformations expected. In addition, the analyst must be aware of the complexity of nonlinear solutions: the appearance of bifurcation points and limit points, the stability and instability of equilibrium branches. The possibility of both physical and numerical instabilities must be kept in mind and checked in a solution.

Thus the informed use of nonlinear software in both industry and research requires considerable understanding of nonlinear finite element methods. It is the objective of this book to provide this understanding and to make the reader aware of the many interesting challenges and opportunities in nonlinear finite element analysis.

1.2. RELATED BOOKS AND HISTORY OF NONLINEAR FINITE ELEMENTS

Several excellent texts and monographs devoted either entirely or partially to nonlinear finite element analysis have already been published. Books dealing only with nonlinear finite element analysis include Oden(1972), Crisfield(1991), Kleiber(1989), and Zhong(1993). Oden's work is particularly noteworthy since it pioneered the field of nonlinear finite element analysis of solids and structures. Some of the books which are partially devoted to nonlinear analysis are Belytschko and Hughes(1983), Zienkiewicz and Taylor(1991), Bathe(1995) and Cook, Plesha and Malkus(1989). These books provide useful introductions to nonlinear finite element analysis. As a companion book, a treatment of linear finite element analysis is also useful. The most comprehensive are Hughes (1987) and Zienkiewicz and Taylor(1991).

Nonlinear finite element methods have many roots. Not long after the linear finite element method appeared through the work of the Boeing group and the famous paper of Cough, Topp, and Martin (??), engineers in several venues began extensions of the method to nonlinear, small displacement static problems, Incidentally, it is hard to convey the excitement of the finite element community and the disdain of classical researchers for the method. For example, for many years the *Journal of Applied Mechanics* banned papers, either tacitly, because it was considered of no scientific substance [sentence does not finish]. The excitement in the method was fueled by Ed Wilson's liberal distribution of his first programs. In many laboratories throughout the world, engineers developed new applications by modifying and extending these early codes.

This account form those in many other books in that the focus is not on the published works, buut on the software. In nonlinear finite element analysis, as in many endeavors in this information-computer age, te software represents a more meaningful indication of the state-of-the-art than the literature since it represents what can be applied in practice.

Among the first papers on nonlinear finite element methods were Marcal and King (??) and Gallagher (??). Pedro Marcal taught at Brown in those early years of nonlinear FEM, but he soon set up a firm to market the first nonlinear finite element program in 196?; the program was called MARC and is still a major player in the commercial software scene.

At about the same time, John Swanson (??) was developing a nonlinear finite element program at Westinghouse for nuclear applications. He left Westinghouse in 19?? to market the program ANSYS, which for the period 1980-90 dominated the commercial nonlinear finite element scene.

Two other major players in the early commercial nonlinear finite element scene were David Hibbitt and Klaus-Jürgen Bathe. David worked with Pedro Marcal until 1972, and then co-founded HKS, which markets ABAQUS. Jürgen launched his program, ADINA, shortly after obtaining his Ph.D. at Berkeley under the tutelage of Ed Wilson while teaching at MIT.

All of these programs through the early 1990's focused on static solutions and dynamic solutions by implicit methods. There were terrific advances in these methods in the 1970's, generated mainly by the Berkeley researchers and those with Berkeley roots: Thomas J.R. Hughes, Michael Ortiz, Juan Simo, and Robert Taylor (in order of age), were the most fertile contributors, but there are many other who are referenced throughout this book.

Explicit finite element methods probably have many different origins, depending on your viewpoint. Most of us were strongly influenced by the work in the DOE laboratories, such as the work of Wilkins (??) at Lawrence Livermore and Harlow (??) at Los Alamos.

In ???, Costantino (??) developed what was probably the first explicit finite element program. It was limit to linear materials and small deformations, and computed the internal nodal forces by multiplying a banded form of **K** by the nodal displacements. It was used primarily on IBM 7040 series computers, which cost millions of dollars and had a speed of far less than 1 megaflop and 32,000 words of RAM. The stiffness matrix was stored on a tape and the progress of a calculation could be gauged by watching the tape drive; after every step, the tape drive would reverse to permit a read of the stiffness matrix.

In 1969, in order to sell a proposal to the Air Force, we conceived what has come to be known as the element-by-element technique: the computation of the nodal forces without use of a stiffness matrix. The resulting program, SAMSON, was a two-dimensional finite element program which was used for a decade by weapons laboratories in the U.S. In 1972, the program was extended to fully nonlinear three-dimensional transient analysis of structures and was called WRECKER. This funding program was provided by the U.S. Department of Transportation by a visionary program manager, Lee Ovenshire, who dreamt in the early 1970's that crash testing of automobiles could be replaced by simulation. However, it was not to be, for at that time a simulation of a 300-element nodal

over ?? msec of simulation time took 30 hours of computer time, which cost the equivalent of three years of salary of an Assistant Professor ($35,000). The program funded several other pioneering efforts, Hughes' work on contact-impact (??) and Ted Shugar and Carly Ward's work on the modeling of the head at Port Hueneme. But the DOT decided around 1975 that simulation was too expensive (such is the vision of some bureaucrats) and shifted all funds to testing, bringing this far flung research effort to a screeching halt. WRECKER remained barely alive for the next decade at Ford.

Parallel work proceeded at the DOE national laboratories. In 1975, Sam Key completed PRONTO, which also featured the element-by-element explicit method. However, his program suffered from the restrictive dissemination policies of Sandia.

The key work in the promulgation of explicit finite element codes was John Hallquist's work at Lawrence Livermore Laboratories. John drew on the work which preceded his with discernment, he interacted closely with many Berkeley researchers such as Bob Taylor, Tom Hughes, and Juan Simo. Some of the key elements of his success were the development of contact-impact interfaces with Dave Benson, his awesome programming productivity and the wide dissemination of the resulting codes, DYNA-2D and DYNA-3D. In contrast to Sandia, LLN seemed to place no impediments on the distribution of the program and it was soon to be found in many government and academic laboratories and in industry throughout the world.

Key factors in the success of the DYNA codes was the use of one-point quadrature elements and the degree of vectorization which was achieved by john Hallquist. The latter issue has become somewhat irrelevant with the new generation of computers, but this combination enabled the simulation with models of suffiecient sizeto make full-scale simulation of problems such as car crash meaningful. The one-point quadrature elements with consistent hourglass control discussed in Chapter 8 increased the speed of three-dimensional analysis by almost an order of magnitude over fully integrated three-dimensional elements.

1.3 NOTATION

Nonlinear finite element analysis represents a nexus of three fields: (1) linear finite element methods, which evolved out of matrix methods of structural analysis; (2) nonlinear continuum mechanics; and (3) mathematics, including numerical analysis, linear algebra and functional analysis, Hughes(1996). In each of these fields a standard notation has evolved. Unfortunately, the notations are quite different, and at times contradictory or overlapping. We have tried to keep the variety of notation to a minimum and both consistent within the book and with the relevant literature. To make a reasonable presentation possible, both the notation of the finite element literature and continuum mechanics are used.

Three types of notation are used: 1. indicial notation, 2. tensor notation and 3. matrix notation. Equations in continuum mechanics are written in tensor and indicial notation. The equations pertaining to the finite element implementation are given in indicial or matrix notation.

Indicial Notation. In indicial notation, the components of tensors or matrices are explicitly specified. Thus a vector, which is a first order tensor, is denoted in

indicial notation by x_i, where the range of the index is the number of dimensions n_S. *Indices repeated twice in a term are summed*, in conformance with the rules of Einstein notation. For example in three dimensions, if x_i is the position vector with magnitude r

$$r^2 = x_i x_i = x_1 x_1 + x_2 x_2 + x_3 x_3 = x^2 + y^2 + z^2 \tag{1.3.1}$$

where the second equation indicates that $x_1 = x, x_2 = y, x_3 = z$; we will always write out the coordinates as x, y and z rather than using subscripts to avoid confusion with nodal values. For a vector such as the velocity v_i in three dimensions, $v_1 = v_x, v_2 = v_y, v_3 = v_z$; numerical subscripts are avoided in writing out expressions to avoid confusing components with node numbers. *Indices which refer to components of tensors are always lower case*.

Nodal indices are always indicated by upper case Latin letters, e.g. v_{iI} is the velocity at node *I. Upper case indices repeated twice are summed over their range*, which depends on the context. When dealing with an element, the range is over the nodes of the element, whereas when dealing with a mesh, the range is over the nodes of the mesh. Thus the velocity at a node *I* is written as v_{iI}, where v_{iI} is the *i*-component at node *I.*

A second order tensor is indicated by two subscripts. For example, for the second order tensor E_{ij}, the components are $E_{11} = E_{xx}, E_{21} = E_{yx}$, etc.. We will usually use indicial notation for Cartesian components but in a few of the more advanced sections we also use curvilinear components.

Indicial notation at times leads to spaghetti-like equations, and the resulting equations are often only applicable to Cartesian coordinates. For those who dislike indicial notation, it should be pointed out that it is almost unavoidable in the implementation of finite element methods, for in programming the finite element equations the indices must be specified.

Tensor Notation. Tensor notation is frequently used in continuum mechanics because tensor expression are independent of the coordinate systems. Thus while Cartesian indicial equations only apply to Cartesian coordinates, expressions in tensor notation can be converted to other coordinates such as cylindrical coordinates, curvilinear coordinates, etc. Furthermore, equations in tensor notation are much easier to memorize. A large part of the continuum mechanics and finite element literature employs tensor notation, so a serious student should become familiar with it.

In tensor notation, we indicate tensors of order one or greater in boldface. Lower case bold-face letters are almost always used for first order tensors, while upper case, bold-face letters are used for higher order tensors. For example, a velocity vector is indicated by $\mathbf{v}$ in tensor notation, while the second order tensor, such as $\mathbf{E}$, is written in upper case. The major exception to this are the physical stress tensor $\boldsymbol{\sigma}$, which is a second order tensor, but is denoted by a lower case symbol. Equation(1.3.1) is written in tensor notation as

$$r^2 = \mathbf{x} \cdot \mathbf{x} \tag{1.3.2}$$

where a dot denotes a contraction of the inner indices; in this case, the tensors on the RHS have only one index so the contraction applies to those indices.

Tensor expressions are distinguished from matrix expressions by using dots and colons between terms, as in $\mathbf{a} \cdot \mathbf{b}$, and $\mathbf{A} \cdot \mathbf{B}$. The symbol ":" denotes the contraction of a pair of repeated indices which appear in the same order, so

$$\mathbf{A} : \mathbf{B} \equiv A_{ij} B_{ij} \tag{1.3.3}$$

The symbol " $\cdot\cdot$" denotes the contraction of the outer repeated indices and the inner repeated indices, as in

$$\mathbf{A} \cdot\cdot \mathbf{B} = A_{ij} B_{ji} = \mathbf{A}^T : \mathbf{B} \tag{1.3.4}$$

If one of the tensors is symmetric, the expressions in Eqs. (1.3.3) and (1.3.4) are equivalent. This notation can also be used for contraction of higher order matrices. For example, the usual expression for a constitutive equation given below on the left is written in tensor notation as shown on the right

$$\sigma_{ij} = C_{ijkl} \varepsilon_{kl} \qquad \boldsymbol{\sigma} = \mathbf{C} : \boldsymbol{\varepsilon} \tag{1.3.5}$$

The functional dependence of a variable will be indicated at the beginning of a development in the standard manner by listing the independent variables. For example, $\mathbf{v}(\mathbf{x}, t)$ indicates that the velocity $\mathbf{v}$ is a function of the space coordinates $\mathbf{x}$ and the time t. In subsequent appearances of $\mathbf{v}$, the identity of the independent variables in implied. We will not hang symbols all around the variable. This notation, which has evolved in a some of the finite element literature, violates esthetics, and is reminiscent of laundry hanging from the balconies of tenements. We will attach short words to some of the symbols. This is intended to help a reader who delves into the middle of the book. It is not intended that such complex symbols be used working through equations. Mathematical symbols and equations should be kept as simple as possible.

Matrix Notation. In implementation of finite element methods, we will often use matrix notation. We will use the same notations for matrices as for tensors and but will not use connective symbols. Thus Eq. (2) in matrix notation is written as

$$r^2 = \mathbf{x}^T \mathbf{x} \tag{1.3.6}$$

All first order matrices will be denoted by lower case boldface letters, such as $\mathbf{v}$, *and will be considered column matrices.* Examples of column matrices are

$$\mathbf{x} = \begin{Bmatrix} x \\ y \\ z \end{Bmatrix} \qquad \mathbf{v} = \begin{Bmatrix} v_1 \\ v_2 \\ v_3 \end{Bmatrix} \tag{1.3.7}$$

Usually rectangular matrices, of which second tensors are a special case, will be denoted by upper case boldface, such as **A.** The transpose of a matrix is denoted by a superscript "T" , and the first index always refers to a row number, the second to a column number. Thus a 2x2 matrix **A** and a 2x3 matrix **B** are written out as (the order of a matrix is also written with number of rows by number of columns, with rows always first):

$$\mathbf{A} = \begin{bmatrix} A_{11} & A_{12} \\ A_{21} & A_{22} \end{bmatrix} \qquad \mathbf{B} = \begin{bmatrix} B_{11} & B_{12} & B_{13} \\ B_{21} & B_{22} & B_{23} \end{bmatrix} \tag{1.3.8}$$

In summary, we show the quadratic form associated with **A** in three notations

$$\mathbf{x}^{\mathbf{T}}\mathbf{A}\mathbf{x} = \mathbf{x}\cdot\mathbf{A}\cdot\mathbf{x} = x_i A_{ij} x_j \tag{1.3.9}$$

The above are all equivalent: the first is matrix notation, the second in tensor notation, the third in indicial notation.

Second-order tensors are often converted to Voigt. Voigt notation is described in the Glossary.

1.4. MESH DESCRIPTIONS

One of the themes of this book is partially the different descriptions that are used in the formulation of the governing equations and the discretization of the continuum mechanics. We will classify the finite element model in three parts, Belytschko (1977):

1. the mesh description;

2. the kinetic description, which is determined by the choice of the stress tensor and the form of the momentum equation;

3. the kinematic description, which is determined by the choice of the strain measure.

In this Section, we will introduce the types of mesh descriptions. For this purpose, it is useful to introduce some definitions and concepts which will be used throughout this book. The first are the definitions of material coordinates and spatial coordinates. Spatial coordinates are denoted by **x**; spatial coordinates are also called Eulerian coordinates. A spatial (or Eulerian coordinate) specifies the location of a point in space. The material coordinates, also called Lagrangian coordinates, are denoted by **X**. The material coordinate labels a material point: each material point has a unique material coordinate, which is usually taken to be its spatial coordinate in the initial configuration of the body, so at t=0, **X**=**x**. Since in a deforming body, the positions of the material points change with time, the spatial coordinates of material points will be functions of time.

The *motion* or deformation of a body can be described by a function $\boldsymbol{\phi}(\mathbf{X}, t)$, with the material coordinates X and the time t as the independent

variables. This function gives the spatial positions of the material points as a function of time through:

$$\mathbf{x} = \boldsymbol{\phi}(\mathbf{X}, t) \tag{1.4.1}$$

This is also called a map between the initial and current configurations. The displacement of a material point is the difference between its current position and its original position, so it is given by

$$\mathbf{u}(X, t) = \boldsymbol{\phi}(X, t) - \mathbf{X} \tag{1.4.2}$$

To illustrate these definitions, consider the following motion in one dimension:

$$x = \phi(X, t) = (1 - X)t + \tfrac{1}{2} Xt^2 + X \tag{1.4.3}$$

This motion is shown in Fig. 1.1; the motion of several points are plotted in space time to exhibit their trajectories; we obviously cannot plot the motion of all material points since there are an infinite number. The velocity of a material point is the time derivative of the motion with the material coordinate fixed, i.e. the velocity is given by

$$v(X, t) = \frac{\partial \phi(X, t)}{\partial t} = 1 + X(t - 1) \tag{1.4.4}$$

The mesh description is based on the choice of independent variables. For purposes of illustration, let us consider the velocity field. We can describe the velocity field as a function of the Lagrangian (material) coordinates, as in Eq. (1.4.4) or we can describe the velocity as a function of the Eulerian (spatial) coordinates

$$\bar{\mathbf{v}}(\mathbf{x}, t) = \mathbf{v}\left(\boldsymbol{\phi}^{-1}(\mathbf{x}, t), t\right) \tag{1.4.5}$$

In the above we have placed a bar over the velocity symbol to indicate that the velocity field when expressed in terms of the spatial coordinate x and the time t will not be the same function as that given in Eq. (1.4.4), although in the remainder of the book we will usually not distinguish different functions which are used to represent the same field. We have also used the concept of an inverse map which to express the material coordinates in terms of the spatial coordinates

$$X = \varphi^{-1}(x, t) \tag{1.4.6}$$

Such inverse mappings can generally not be expressed in closed form for arbitrary motions, but for the simple motion given in Eq. (1.4.3) it is given by

$$X = \frac{x - t}{\frac{1}{2}t^2 - t + 1} \tag{1.4.7}$$

Substituting the above into (3) gives

$$\bar{v}(x,t) = 1 + \frac{(x-t)(t-1)}{\frac{1}{2}t^2 - t + 1} = \frac{1 - x + xt - \frac{1}{2}t^2}{\frac{1}{2}t^2 - t + 1} \tag{1.4.8}$$

Equations (1.4.4) and (1.4.8) give the same physical velocity fields, but express them in terms of different independent variables, so that they are different functions. Equation (1.4.4) is called a Lagrangian (material) description for it expresses the dependent variable in terms of the Lagrangian (material) coordinate. Equation (1.4.8) is called an Eulerian (spatial) description, for it expresses the dependent variable as a function of the Eulerian (spatial) coordinates. Henceforth in this book, we will not use different symbols for these different functions, but keep in mind that if the same field variable is expressed in terms of different independent variables, then the functions must be different. In other words, a symbol for a dependent field variable is associated with the field, not the function.

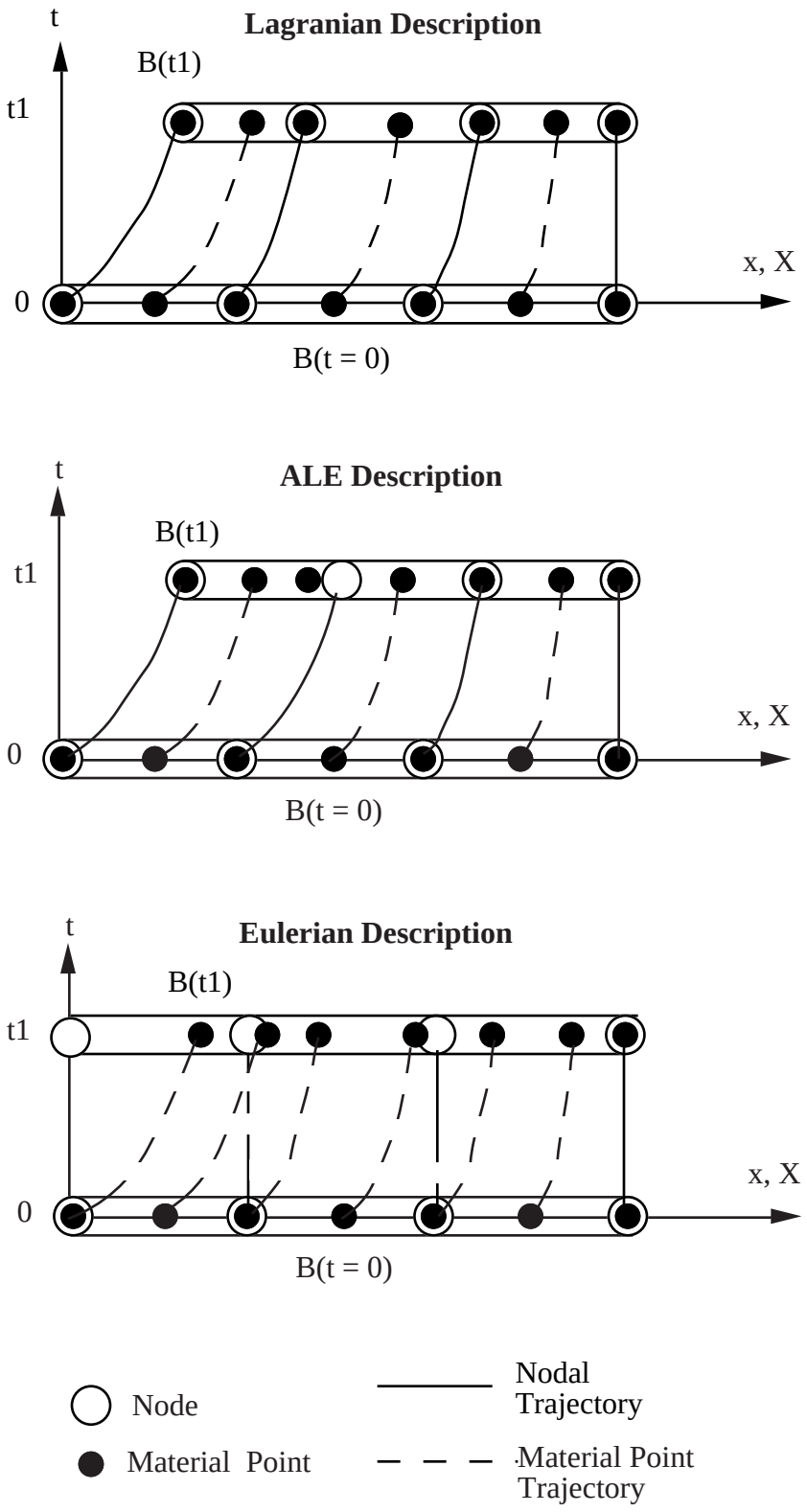

Fig. 1.1 Space time depiction of a one dimensional Lagrangian, Eulerian, and ALE (arbitrary Lagrangian Eulerian) elements.

The differences between Lagrangian and Eulerian meshes are most clearly seen in terms of the behavior of the nodes. If the mesh is Eulerian, the Eulerian coordinates of nodes are fixed, i.e. the nodes are coincident with spatial points. If the mesh is Lagrangian, the Lagrangian (material) coordinates of nodes are time invariant, i.e. the nodes are coincident with material points. This is illustrated in Fig. 1.1 for the mapping given by Eq. (1.4.3). In the Eulerian mesh, the nodal trajectories are vertical lines and material points pass across element interfaces. In the Lagrangian mesh, nodal trajectories are coincident with material point trajectories, and no material passes between elements. Furthermore, element quadrature points remain coincident with material points in Lagrangian meshes, whereas in Eulerian meshes the material point at a given quadrature point changes with time. We will see later that this complicates the treatment of materials in which the stress is history-dependent.

The comparative advantages of Eulerian and Lagrangian meshes can be seen even in this simple one-dimensional example. Since the nodes are coincident with material points in the Lagrangian mesh, boundary nodes remain on the boundary throughout the evolution of the problem. This simplifies the imposition of boundary conditions in Lagrangian meshes. In Eulerian meshes, on the other hand, boundary nodes do not remain coincident with the boundary. Therefore, boundary conditions must be imposed at points which are not nodes, and as we shall see later, this engenders significant complications in multi-dimensional problems. Similarly, if a node is placed on an interface between two materials, it remains on the interface in a Lagrangian mesh, but not in an Eulerian mesh.

In Lagrangian meshes, since the material points remain coincident with mesh points, the elements deform with the material. Therefore, elements in a Lagrangian mesh can become severely distorted. This effect is apparent in a one-dimensional problem only in the element lengths: in Eulerian meshes, the element length are constant in time, whereas in Lagrangian meshes, element lengths change with time. In multi-dimensional problems, these effects are far more severe, and elements can get very distorted. Since element accuracy degrades with distortion, the magnitude of deformation that can be simulated with a Lagrangian mesh is limited. Eulerian elements, on the other hand, are unchanged by the deformation of the material, so no degradation in accuracy occurs because of material deformation.

To illustrate the differences between Eulerian and Lagrangian mesh descriptions in two dimensions, a two dimensional example will be considered. In two dimensions, the spatial coordinates are denoted by $\mathbf{x} = [x, y]^T$ and the material coordinates by $\mathbf{X} = \mathbf{[}X, Y\mathbf{]}^T$. The deformation mapping is given by

$$\mathbf{x} = \boldsymbol{\phi}(\mathbf{X}, t) \tag{1.4.9}$$

where $\boldsymbol{\phi}(\mathbf{X}, t)$ is a vector function, i.e. it gives a vector for every pair of the independent variables. For every pair of material coordinates and time, this function gives the pair of spatial coordinates corresponding to the current position of the material particles. Writing out the above expression gives

$$\begin{aligned} x &= \phi_1(X, Y, t) \\ y &= \phi_2(X, Y, t) \end{aligned} \tag{1.4.10}$$

As an example of a motion, consider pure shear in which the map is given by

$$x = X + tY$$
$$y = Y \tag{1.4.11}$$

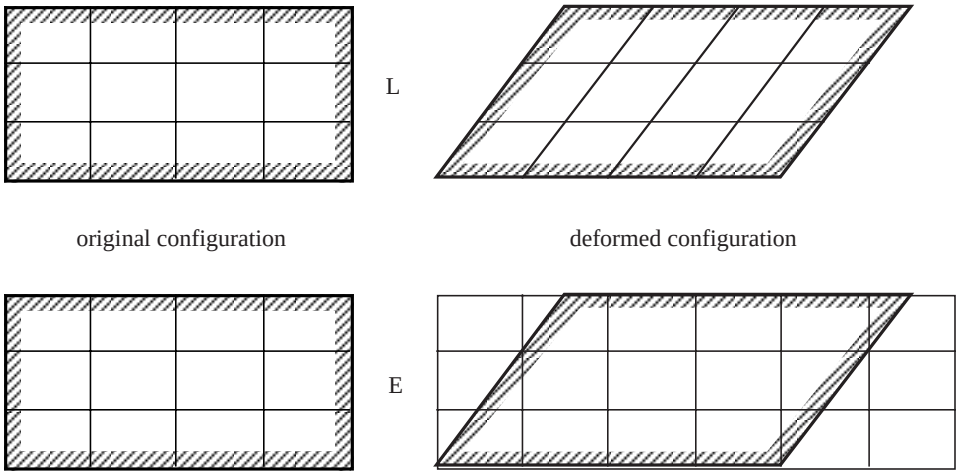

Fig. 1.2 Two dimensional shearing of a block showing Lagrangian (L) and Eulerian (E) elements.

In a Lagrangian mesh, the nodes are coincident with material (Lagrangian) points, so the nodes remain coincident with material points, so

for Lagrangian nodes, $\mathbf{X}_I = \text{constant in time}$

For an Eulerian mesh, the nodes are coincident with spatial (Eulerian) points, so we can write

for Eulerian nodes, $\mathbf{x}_I = \text{constant in time}$

Points on the edges of elements behave similarly to the nodes: in Lagrangian meshes, element edges remain coincident with material lines, whereas in Eulerian meshes, the element edges remain fixed in space.

To illustrate this statement we show Lagrangian and Eulerian meshes for the shear deformation given by Eq. (11) in Fig. 1.2. As can be seen from the figure, a Lagrangian mesh is like an etching on the material: as the material is deformed, the etching deforms with it. An Eulerian mesh is like an etching on a sheet of glass held in front of the material: as the material deforms, the etching is unchanged and the material passes across it.

The advantages and disadvantages of the two types of meshes are similar to those in one dimension. In a Lagrangian mesh, element edges and nodes which are initially on the boundary remain on the boundary, whereas in Eulerian meshes edges and nodes which are initially on the boundary do not remain on the boundary. Thus, in Lagrangian meshes, element edges (lines in two dimensions, surfaces in three dimensions) remain coincident with boundaries and material interfaces. In Eulerian meshes, element sides do not remain coincident with boundaries or material interfaces. Hence tracking methods or approximate

methods, such as volume of fluid approaches, have to be used for treating moving boundaries treated by Eulerian meshes; such as volume of fluid methods described in Section 5.?. Furthermore, an Eulerian mesh must be large enough to enclose the material in its deformed state. On the other hand, since Lagrangian meshes deform with the material, and they become distorted in the simulations of severe deformations. In Eulerian meshes, elements remain fixed in space, so their shapes never change.

A third type of mesh is an arbitrary Lagrangian Eulerian mesh, in which the nodes are programmed to move so that the advantages of both Lagrangian and Eulerian meshes can be exploited. In this type of mesh, the nodes can be programmed to move arbitrarily, as shown in Fig. 1.1. Usually the nodes on the boundaries are moved to remain on the boundaries, while the interior nodes are moved to minimize mesh distortion. This type of mesh is described and discussed further in Chapter 7.

REFERENCES

T. Belytschko (1976), Methods and Programs for Analysis of Fluid-Structure Systems," *Nuclear Engineering and Design*, **42** , 41-52.

T. Belytschko and T.J.R. Hughes (1983), *Computational Methods for Transient Analysis*, North-Holland, Amsterdam.

K.-J. Bathe (1996), *Finite Element Procedures,* Prentice Hall, Englewood Cliffs, New Jersey.

R.D. Cook, D.S. Malkus, and M.E. Plesha (1989), *Concepts and Applications of Finite Element Analysis,* 3rd ed., John Wiley.

M.A. Crisfield (1991), Non-linear Finite Element Analysis of Solids and Structure, Vol. 1, Wiley, New York.

T.J.R. Hughes (1987), *The Finite Element Method, Linear Static and Dynamic Finite Element Analysis*, Prentice-Hall, New York.

T.J.R. Hughes (1996), *personal communication*

M. Kleiber (1989), *Incremental Finite element Modeling in Non-linear Solid Mechanics*, Ellis Horwood Limited, John Wiley.

J.T. Oden (1972), *Finite elements of Nonlinear Continua*, McGraw-Hill, New York.

O.C. Zienkiewicz and R.L. Taylor (1991), *The Finite Element Method*, McGraw-Hill, New York.

Z.-H. Zhong (1993), *Finite Element Procedures for Contact-Impact Problems,* Oxford University Press, New York.

GLOSSARY. NOTATION

Voigt Notation. In finite element implementations, Voigt notation is often useful; in fact almost all linear finite element texts use Voigt notation. In Voigt notation, second order tensors such as the stress, are written as column matrices, and fourth order tensors, such as the elastic coefficient matrix, are written as square matrices. Voigt notation is quite awkward for the formulation of the equations of continuum mechanics. Therefore only those equations which are related to finite element implementations will be given in Voigt notation.

Voigt notation usually refers to the procedure for writing a symmetric tensor in column matrix form. However, we will use the term for all conversions of higher order tensor expressions to lower order matrices.

The Voigt conversion for symmetric tensors depends on whether a tensor is a kinetic quantity, such as stress, or a kinematic quantity, such as strain. We first consider Voigt notation for stresses. In Voigt notation for kinetic tensors, the second order, *symmetric tensor* $\boldsymbol{\sigma}$ is written as a column matrix:

tensor $\rightarrow$ Voigt

in two dimensions:

$$\boldsymbol{\sigma} \equiv \begin{bmatrix} \sigma_{11} & \sigma_{12} \\ \sigma_{21} & \sigma_{22} \end{bmatrix} \rightarrow \begin{Bmatrix} \sigma_{11} \\ \sigma_{22} \\ \sigma_{12} \end{Bmatrix} = \begin{Bmatrix} \sigma_1 \\ \sigma_2 \\ \sigma_3 \end{Bmatrix} \equiv \{\boldsymbol{\sigma}\} \tag{A.1.1}$$

in three dimensions:

$$\boldsymbol{\sigma} \equiv \begin{bmatrix} \sigma_{11} & \sigma_{12} & \sigma_{13} \\ \sigma_{21} & \sigma_{22} & \sigma_{23} \\ \sigma_{31} & \sigma_{32} & \sigma_{33} \end{bmatrix} \rightarrow \begin{Bmatrix} \sigma_{11} \\ \sigma_{22} \\ \sigma_{33} \\ \sigma_{23} \\ \sigma_{13} \\ \sigma_{12} \end{Bmatrix} = \begin{Bmatrix} \sigma_1 \\ \sigma_2 \\ \sigma_3 \\ \sigma_4 \\ \sigma_5 \\ \sigma_6 \end{Bmatrix} \equiv \{\boldsymbol{\sigma}\} \tag{A.1.2}$$

We will call the correspondence between the square matrix form of the tensor and the column matrix form the Voigt rule. For stresses the Voigt rule resides in the relationship between the indices of the second order tensor and the column matrix. The order of the terms in the column matrix in the Voigt rule is given by the line which first passes down the main diagonal of the tensor, then up the last column, and back across the row (if there are any elements left). As indicated in the bottom row, the square matrix form of the tensor is indicated by boldface, whereas brackets are used to distinguish the Voigt form. The correspondence is also given in Table 1.

TABLE 1

Two-Dimensional Voigt Rule

σ_{ij}		σ_a
i	*j*	*a*
1	1	1
2	2	2
3	3	3

Three-Dimensional Voigt Rule

σ_{ij}		σ_a
i	*j*	*a*
1	1	1
2	2	2
3	3	3
2	3	4
1	3	5
1	2	6

When the tensors are written in indicial notation, the difference between the Voigt and tensor form of second order tensors is indicated by the number of subscripts and the letter used. We use subscripts beginning with letters *i* to *q* for tensors, and subscripts *a* to *g* for Voigt matrix indices. Thus

σ_{ij} is replaced by σ_a

in going from tensor to Voigt notation. The correspondence between the subscripts (*i,j)* and the Voigt subscript *a* is given in Table 1 for two and three dimensions.

For a second order, symmetric kinematic tensor such as the strain ε_{ij}, the rule is almost identical: the correspondence between the tensor indices and the row numbers are identical, but the shear strains, i.e. those with indices that are not equal, are multiplied by 2. Thus the Voigt rule for the strains is

tensor $\rightarrow$ Voigt

two dimensions

$$\boldsymbol{\varepsilon} \equiv \begin{bmatrix} \varepsilon_{11} & \varepsilon_{12} \\ \varepsilon_{21} & \varepsilon_{22} \end{bmatrix} \rightarrow \begin{Bmatrix} \varepsilon_{11} \\ \varepsilon_{22} \\ 2\varepsilon_{12} \end{Bmatrix} = \begin{Bmatrix} \varepsilon_1 \\ \varepsilon_2 \\ \varepsilon_3 \end{Bmatrix} \equiv \{\boldsymbol{\varepsilon}\} \tag{A.1.3}$$

in three dimensions

$$\boldsymbol{\varepsilon} \equiv \begin{bmatrix} \varepsilon_{11} & \varepsilon_{12} & \varepsilon_{13} \\ & \varepsilon_{22} & \varepsilon_{23} \\ sym & & \varepsilon_{33} \end{bmatrix} \rightarrow \begin{Bmatrix} \varepsilon_{11} \\ \varepsilon_{22} \\ \varepsilon_{33} \\ 2\varepsilon_{23} \\ 2\varepsilon_{13} \\ 2\varepsilon_{12} \end{Bmatrix} \equiv \{\boldsymbol{\varepsilon}\} \tag{A.1.4}$$

The Voigt rule requires a factor of two in the shear strains, which can be remembered by observing that the strains in Voigt notation are the engineering shear strains.

The inclusion of the factor of 2 in the Voigt rule for strains and strain-like tensors is motivated by the requirement that the expressions for the energy be equivalent in matrix and indicial notation. It is easy to verify that an increment in energy is given by

$$\rho dw^{int} = d\varepsilon_{ij}\sigma_{ij} = d\boldsymbol{\varepsilon} : \boldsymbol{\sigma} = \{d\boldsymbol{\varepsilon}\}^T \{\boldsymbol{\sigma}\} \tag{A.1.5}$$

For these expressions to be equivalent, a factor of 2 is needed on the shear terms in the Voigt form; the factor of 2 can be added to either the stresses or the strains (or a coefficient of $\sqrt{2}$ on both the stresses and strains), but the preferred convention is to use this factor on the strains because the shear strains are then equivalent to the engineering strains.

The Voigt rule is particularly useful for converting fourth order tensors, which are awkward to implement in a computer program, to second order matrices. Thus the general linear elastic law in indicial notation involves the fourth order tensor C_{ijkl} :

$$\sigma_{ij} = C_{ijkl}\varepsilon_{kl} \qquad \text{or in tensor notation} \qquad \boldsymbol{\sigma} = \mathbf{C}\boldsymbol{\varepsilon} \tag{A.1.6}$$

The Voigt or matrix form of this law is

$$\{\boldsymbol{\sigma}\} = [\mathbf{C}]\{\boldsymbol{\varepsilon}\} \tag{A.1.7}$$

or writing the matrix expression in indicial form: $\sigma_a = C_{ab}\varepsilon_b$ (A.1.8)

and as indicated on the right, when writing the Voigt expression in matrix indicial form, indices at the beginning of the alphabet are used. The Voigt matrix form of the elastic constitutive matrix is

$$[\mathbf{C}] = \begin{bmatrix} C_{11} & C_{12} & C_{13} \\ C_{21} & C_{22} & C_{23} \\ C_{31} & C_{32} & C_{33} \end{bmatrix} = \begin{bmatrix} C_{1111} & C_{1122} & C_{1112} \\ C_{2211} & C_{2222} & C_{2212} \\ C_{1211} & C_{1222} & C_{1212} \end{bmatrix} \tag{A.1.9}$$

The first matrix refers to the elastic coefficients in in tensor notation, the second to Voigt notation; note that the number of subscripts specifies whether the matrix is expressed in Voigt or tensor notation. The above translation is completely consistent. For example, the expression for σ_{12} from (A.1.6) is

$$\sigma_{12} = C_{1211}\varepsilon_{11} + C_{1212}\varepsilon_{12} + C_{1221}\varepsilon_{21} + C_{1222}\varepsilon_{22} \tag{A.1.10}$$

The above translates to the following expression in terms of the Voigt notation

$$\sigma_3 = C_{31}\varepsilon_1 + C_{33}\varepsilon_3 + C_{32}\varepsilon_2 \tag{A.1.11}$$

which can be shown to be equivalent to (A.1.10) if we use $\varepsilon_3 = \varepsilon_{12} + \varepsilon_{21} = 2\varepsilon_{12}$ and the minor symmetry of $\mathbf{C}: C_{1212} = C_{1221}$.

It is convenient to reduce the order of the matrices in the indicial expressions when applying them in finite element methods. We will denote nodal vectors by double subscripts, such as u_{iI}, where *i* is the component index and *I* is the node number index. The component index is always lower case, the node number index is always upper case; sometimes their order is interchanged. The following rule is used for converting matrices involving node numbers and components to column matrices:

matrix u_{iI} is transformed to a column matrix $\{d\}$ by (A.1.12a)

elements of $\{d\}$ are u_a where $a = (I-1)n_{SD} + i$ (A.1.12b)

(The symbol for the column matrix associated with displacements is changed because **u** is used for the components, i.e. $\mathbf{u} = u_x,\ u_y,\ u_z$.) This rule is combined with the Voigt rule whenever a pair of indices on a term pertain to a second order symmetric tensor. For example in the higher order matrix B_{ijKk} is often used to related strains to nodal displacements by

$$\varepsilon_{ij} = B_{ijKk}u_{kK} \tag{A.1.13}$$

where

$$u_i(\mathbf{x}) = N_I(\mathbf{x})u_{iI}, \tag{A.1.14}$$

$$\varepsilon_{ij} = \tfrac{1}{2}\left(\frac{\partial u_i}{\partial x_j} + \frac{\partial u_j}{\partial x_i}\right) = \tfrac{1}{2}\left(\frac{\partial N_I}{\partial x_j}\delta_{ik} + \frac{\partial N_I}{\partial x_i}\delta_{jk}\right)u_{kI} \equiv B_{ijIk}u_{kI} \tag{A.1.15}$$

To translate this to a matrix expression in terms of column matrices for ε_{ij} and a rectangular matrix for B_{ija}, the kinematic Voigt rule is used for ε_{ij} and the first two indices of B_{ijKk} and the nodal component rule is used for the second pair of indices of B_{ijKk} and the indices of u_{kK}. Thus

elements of $[\mathbf{B}]$ are B_{ab} where $(i,j) \rightarrow a$ by the Voigt rule, (A.1.16a)

$$b = (K-1)n_{SD} + k \tag{A.1.16b}$$

The expression corresponding to (??) can then be written as

$$\varepsilon_a = B_{ab} u_b \quad \text{or} \quad \{\boldsymbol{\varepsilon}\} = [\mathbf{B}]\mathbf{d} \tag{A.1.17}$$

The correspondence of the indices depends on the dimensionally of the problem. In two dimensional problems, the matrix counterpart of B_{ijKk} is then written as

$$\mathbf{B}_K = \begin{bmatrix} B_{11xK} & B_{11yK} \\ B_{22xK} & B_{22yK} \\ 2B_{12xK} & 2B_{12xK} \end{bmatrix} \tag{A.1.18}$$

The full matrix for a 3-node triangle is

$$[\mathbf{B}] = \begin{bmatrix} B_{xx1x} & B_{xx1y} & B_{xx2x} & B_{xx2y} & B_{xx3x} & B_{xx3y} \\ B_{yy1x} & B_{yy1y} & B_{yy2x} & B_{yy2y} & B_{yy3x} & B_{yy3y} \\ 2B_{xy1x} & 2B_{xy1y} & 2B_{xy2x} & 2B_{xy2y} & 2B_{xy3x} & 2B_{xy3y} \end{bmatrix} \tag{A.1.19}$$

where the the first two indices have been replaced by the corresponding letters.

The Voigt rule is particularly useful in the implementation of stiffness matrices. In indicial notation, the stiffness matrix is written as

$$K_{IJrs} = \int_\Omega B_{ijIr} C_{ijkl} B_{klJs} d\Omega \tag{A.1.20}$$

The above stiffness is a fourth order matrix and maultiplying it with a matrix of nodal displacements is awkward. The indices in the above matrices can be converted by the Voigt rule, which gives

$$K_{ab} = \int_\Omega B_{ae} C_{ef} B_{fg} d\Omega \rightarrow [\mathbf{K}] = \int_\Omega [\mathbf{B}]^T [\mathbf{C}][\mathbf{B}] d\Omega \tag{A.1.21}$$

where the indices "*Ir*" and "*Js"* have been converted to "*a*" and "*b*" , respectively, by the column matrix rule and the indices "*ij*" and "*kl*" have been converted to "*e*" and "*f"* respectively by the Voigt rule. Another useful form of the stiffness matrix is obtained by transforming only the indices "*ij*" and "*kl*", which gives

$$[\mathbf{K}]_{IJ} = \int_\Omega [\mathbf{B}]_I^T [\mathbf{C}][\mathbf{B}]_J d\Omega \tag{A.1.22}$$

where $[\mathbf{B}]_I$ is given in Eq. (A.1.18).

4.5.3. Indicial to Voigt Notation. The above equations in Voigt notation can also be derived from the indicial equations if we start with the following expressions for the displacement and velocity fields

$$u_i = N_{ib} d_b \qquad v_i = N_{ib} \dot{d}_b \tag{4.5.20}$$

The key difference in (4.5.20) as compared to (4.4.5) is that the component index is ascribed to the shape function. In this notation, different displacement and velocity components can be approximated by different shape functions. This added generality is seldom used because it generally destroys the capability of the element to represent rigid body rotation. The gradient of the velocity field in this notation is obtained by differentiating (4.5.20):

$$\frac{\partial v_i}{\partial x_j} = \frac{\partial N_{ib}}{\partial x_j} \dot{d}_b \qquad D_{ij} = \tfrac{1}{2}\left(\frac{\partial v_i}{\partial x_j} + \frac{\partial v_j}{\partial x_i} \right) = \tfrac{1}{2}\left(\frac{\partial N_{ib}}{\partial x_j} + \frac{\partial N_{jb}}{\partial x_i} \right) \dot{d}_b = B_{ijb} \dot{d}_b \tag{4.5.21}$$

where

$$B_{ijb} = \tfrac{1}{2}\left(\frac{\partial N_{ib}}{\partial x_j} + \frac{\partial N_{jb}}{\partial x_i} \right) = sym \frac{\partial N_{ib}}{\partial x_j} \tag{4.5.22}$$

so the B_{ijb} extracts the symmetric part of the gradient of the shape functions. The rectangular **B** matrix is defined by

$B_{ab} = B_{ijb}$ where $(i, j) \rightarrow a$ by the symmetric kinematic Voigt rule, see Appendix B

and Eqs.(4.5.18) and (4.5.19) hold as before. The conversion of the internal nodal force expression to the Voigt form (4.5.19) is shown in the following

$$f_b^{int} = \int_\Omega \frac{\partial N_{ib}}{\partial x_j} \sigma_{ji} d\Omega = \int_\Omega B_{ijb} \sigma_{ji} d\Omega \rightarrow \mathbf{f}^{int} = \int_\Omega \mathbf{B}^T \{\boldsymbol{\sigma}\} d\Omega \tag{4.5.23}$$

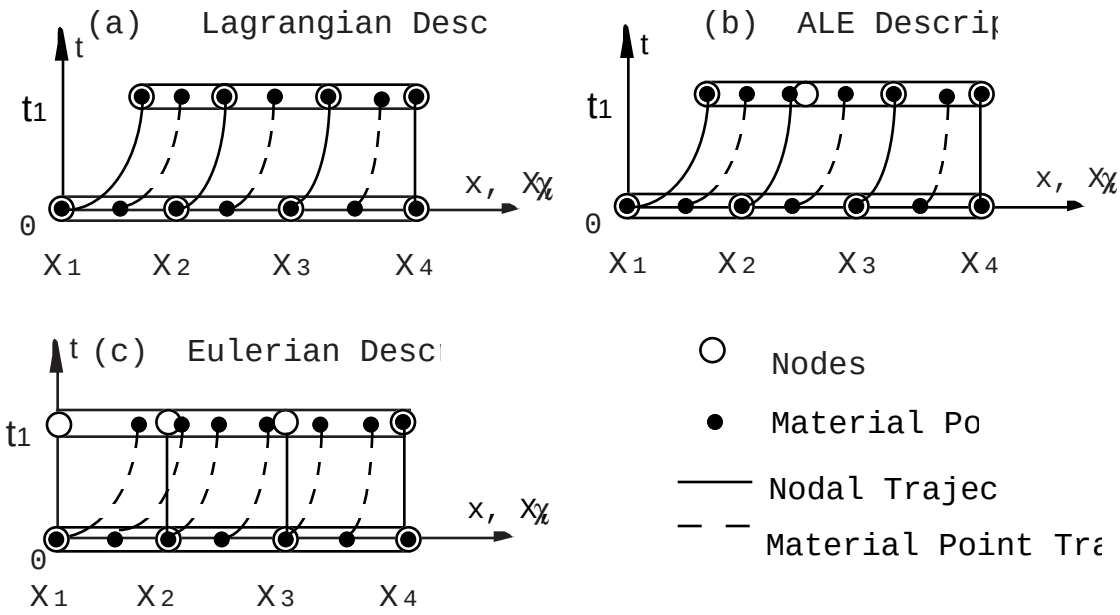
(a) Lagrangian Desc
t
t1
0
x, X
X1
X2
X3
X4
(b) ALE Descri
t
t1
0
x, X
X1
X2
X3
X4
t (c) Eulerian Desc
t1
0
x, X
X1
X2
X3
X4
Nodes
Material Po
Nodal Trajec
Material Point Tra

CHAPTER 2
LAGRANGIAN AND EULERIAN FINITE ELEMENTS IN ONE DIMENSION

by Ted Belytschko
Northwestern University

2.1 Introduction

In this chapter, the equations for one-dimensional models of nonlinear continua are described and the corresponding finite element equations are developed. The development is restricted to one dimension to simplify the mathematics so that the salient features of Lagrangian and Eulerian formulations can be demonstrated easily. These developments are applicable to nonlinear rods and one-dimensional phenomena in continua, including fluid flow. Both Lagrangian and Eulerian meshes will be considered. Two commonly used types of Lagrangian formulations will be described: updated Lagrangian and total Lagrangian. In the former, the variables are expressed in the current (or updated) configuration, whereas in the latter the variables are expressed in terms of the initial configuration. It will be seen that a variety of descriptions can be developed for large deformation problems. The appropriate description depends on the characteristics of the problem to be solved.

In addition to describing the several types of finite element formulations for nonlinear problems, this Chapter reviews some of the concepts of finite element discretization and finite element procedures. These include the weak and strong forms, the operations of assembly, gather and scatter, and the imposition of essential boundary conditions and initial conditions. Mappings between different coordinate systems are discussed along with the need for finite element mappings to be one-to-one and onto. Continuity requirements of solutions and finite element approximations are also considered. While much of this material is familiar to most who have studied linear finite elements, they are advised to at least skim this Chapter to refresh their understanding.

In solid mechanics, Lagrangian meshes are most popular. Their attractiveness stems from the ease with which they handle complicated boundaries and their ability to follow material points, so that history dependent materials can be treated accurately. In the development of Lagrangian finite elements, two approaches are commonly taken:

1. formulations in terms of the Lagrangian measures of stress and strain in which derivatives and integrals are taken with respect to the Lagrangian (material) coordinates X, called *total Lagrangian formulations*
2. formulations expressed in terms of Eulerian measures of stress and strain in which derivatives and integrals are taken with respect to the Eulerian (spatial) coordinates x, often called *updated Lagrangian formulations*.

Both formulations employ a Lagrangian mesh, which is reflected in the term *Lagrangian* in the names.

Although the total and updated Lagrangian formulations are superficially quite different, it will be shown that the underlying mechanics of the two formulations is identical; furthermore, expressions in the total Lagrangian formulation can be transformed to updated Lagrangian expressions and vice versa. The major difference between the two

formulations is in the point of view: the total Lagrangian formulation refers quantities to the original configuration, the updated Lagrangian formulation to the current configuration, often called the deformed configuration. There are also differences in the stress and deformation measures which are typically used in these two formulations. For example, the total Lagrangian formulation customarily uses a total measure of strain, whereas the updated Lagrangian formulation often uses a rate measure of strain. However these are not inherent characteristics of the formulations, for it is possible to use total measures of strain in updated Lagrangian formulations, and rate measures in total Lagrangian formulation. These attributes of the two Lagrangian formulations are discussed further in Chapter 4.

Until recently, Eulerian meshes have not been used much in solid mechanics. Eulerian meshes are most appealing in problems with very large deformations. Their advantage in these problems is a consequence of the fact that Eulerian elements do not deform with the material. Therefore, regardless of the magnitudes of the deformation in a process, Eulerian elements retain their original shape. Eulerian elements are particularly useful in modeling many manufacturing processes, where very large deformations are often encountered.

For each of the formulations, a weak form of the momentum equation, which is known as the principle of virtual work (or virtual power) will be developed. The weak form is developed by taking the product of a test function with the governing partial differential equation, the momentum equation. The integration is performed over the material coordinates for the total Lagrangian formulation, over the spatial coordinates for the Eulerian and updated Lagrangian formulation. It will also be shown how the traction boundary conditions are treated so that the approximate (trial) solutions need not satisfy these boundary conditions exactly. This procedure is identical to that in linear finite element analysis. The major difference in geometrically nonlinear formulations is the need to define the coordinates over which the integrals are evaluated and to specify the choice of stress and strain measures.

The discrete equations for a finite element approximation will then be derived. For problems in which the accelerations are important (often called dynamic problems) or those involving rate-dependent materials, the resulting discrete finite element equations are ordinary differential equations (ODEs). The process of discretizing in space is called a semidiscretization since the finite element procedure only converts the spatial differential operators to discrete form; the derivatives in time are not discretized. For static problems with rate-independent materials, the discrete equations are independent of time, so the finite element discretization results in a set of nonlinear algebraic equations.

Examples of the total and updated Lagrangian formulations are given for the 2-node, linear displacement and 3-node, quadratic displacement elements. Finally, to enable the student to solve some nonlinear problems, a central difference explicit time-integration procedures is described.

2.2 Governing Equations For Total Lagrangian Formulation

Nomenclature. Consider the rod shown in Fig. 1. The *initial configuration*, also called the *undeformed configuration* of the rod, is shown in the top of the figure. This configuration plays an important role in the large deformation analysis of solids. It is also called the *reference configuration*, since all equations in the total Lagrangian formulation are referred to this configuration. The *current or deformed configuration* is shown at the bottom of the figure. The spatial (Eulerian) coordinate is denoted by x and the coordinates in the reference configuration, or material (Lagrangian) coordinates, by X. The initial cross-sectional area of the rod is denoted by $A_0(X)$ and its initial density by $\rho_0(X)$;

variables pertaining to the reference (initial, undeformed) configuration will always be identified by a subscript or superscript nought. In this convention, we could indicate the material coordinates by x_0 since they correspond to the initial coordinates of the material points, but this is not consistent with most of the continuum mechanics literature, so we will always use X for the material coordinates.

The cross-sectional area in the deformed state is denoted by $A(X,t)$; as indicated, it is a function of space and time. The spatial dependence of this variable and all others is expressed in terms of the material coordinates. The density is denoted by $\rho(X,t)$ and the displacement by $u(X,t)$. The boundary points in the reference configuration are X_a and X_b.

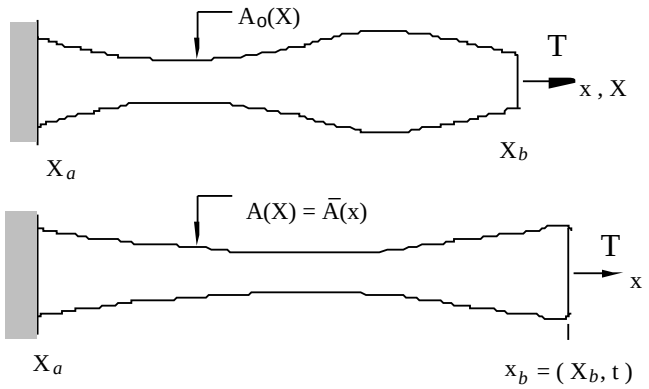

Fig. 1.1. The undeformed (reference) configuration and deformed (current) configurations for a one-dimensional rod loaded at the left end; this is the model problem for Sections 2.2 to 2.8.

Deformation and Strain Measure. The variables which specify the deformation and the stress in the body will first be described. The motion of the body is described by a function of the Lagrangian coordinates and time which specifies the position of each material point as a function of time:

$$x = \varphi(X,t) \qquad X \in [X_a, X_b] \tag{2.2.1}$$

where $\varphi(X,t)$ is called a deformation function. This function is often called a map between the initial and current domains. The material coordinates are given by the deformation function at time $t = 0$, so

$$X = \varphi(X,0) \tag{2.2.2}$$

As can be seen from the above, the deformation function at $t = 0$ is the identity map.

The displacement $u(X,t)$ is given by the difference between the current position and the original position of a material point, so

$$u(X,t) = \varphi(X,t) - X \text{ or } u = x - X \tag{2.2.3}$$

The deformation gradient is defined by

$$F = \frac{\partial \varphi}{\partial X} = \frac{\partial x}{\partial X} \tag{2.2.4}$$

The second definitions in Eq. (2.2.3) and (2.2.4) can at times be ambiguous. For example, Eq. (2.2.4) appears to involve the partial derivative of an independent variable x with respect to another independent variable X, which is meaningless. Therefore, it should be understood that whenever x appears in a context that implies it is a function, the definition $x = \varphi(X,t)$ is implied.

Let J be the Jacobian between the current and reference configurations. The Jacobian is usually defined by $J(x(X)) = \partial x / \partial X$ for one-dimensional mappings; however, to maintain consistency with multi-dimensional formulations of continuum mechanics, we will define the Jacobian as the ratio of an infinitesimal volume in the deformed body, $A\Delta x$, to the corresponding volume of the segment in the undeformed body $A_0 \Delta X$, so it is given by

$$J = \frac{\partial x}{\partial X}\frac{A}{A_0} = \frac{FA}{A_0} \tag{2.2.5}$$

The deformation gradient F is an unusual measure of strain since its value is one when the body is undeformed. We will therefore define the measure of strain by

$$\varepsilon(X,t) = F(X,t) - 1 \equiv \frac{\partial x}{\partial X} - 1 = \frac{\partial u}{\partial X} \tag{2.2.6}$$

so that it vanishes in the undeformed configuration. There are many other measures of strain, but this is the most convenient for this presentation. This measure of strain corresponds to what is known as the stretch tensor in multi-dimensional problems. In one dimension, it is equivalent to the engineering strain.

Stress Measure. The stress measure which is used in total Lagrangian formulations does not correspond to the well known physical stress. To explain the measure of stress to be used, we will first define the physical stress, which is also known as the Cauchy stress. Let the total force across a given section be denoted by T and assume that the stress is constant across the cross-section. The Cauchy stress is given by

$$\sigma = \frac{T}{A} \tag{2.2.7}$$

This measure of stress refers to the *current* area A. In the total Lagrangian formulation, we will use the nominal stress. The nominal stress will be denoted by P and is given by

$$P = \frac{T}{A_0} \tag{2.2.8}$$

It can be seen that it differs from the physical stress in that the net resultant force is divided by the *initial, or undeformed, area* A_0. This is equivalent to the definition of engineering strain; however, in multi-dimensions, the nominal stress is not equivalent to the engineering stress, this is discussed further in Chapter 3.

Comparing Eqs. (2.2.7) and (2.2.8), it can be seen that the physical and nominal stresses are related by

$$\sigma = \frac{A_0}{A} P \qquad\qquad P = \frac{A}{A_0} \sigma \tag{2.2.9}$$

Therefore, if one of the stresses is known, the other can always be computed if the current and initial cross-sectional areas are known.

Governing Equations. The nonlinear rod is governed by the following equations:

1. conservation of mass;
2. conservation of momentum;
3. conservation of energy;
4. a measure of deformation, often called a strain-displacement equation;
5. a constitutive equation, which describes material behavior and relates stress to a measure of deformation;

In addition, we require the deformation to be continuous, which is often called a compatibility requirement. The governing equations and initial and boundary conditions are summarized in Box 1.

Conservation of mass. The equation for conservation of mass for a Lagrangian formulation can be written as (see Appendix A for an engineering derivation):

$$\rho J = \rho_0 J_0 \qquad \text{or} \quad \rho(X,t) J(X,t) = \rho_0(X) J_0(X) \tag{2.2.10}$$

where the second expression is given to emphasize that the variables are treated as functions of the Lagrangian coordinates. Conservation of matter is an algebraic equation only when expressed in terms of material coordinates. Otherwise, it is a partial differential equation. For the rod, we can use Eq. (2.2.4) to write Eq. (2.2.5) as

$$\rho F A = \rho_0 A_0 \tag{2.2.11}$$

where we have used the fact that $J_0 = 1$.

Conservation of momentum. Conservation of momentum is written in terms of the nominal stress and the Lagrangian coordinates as (a derivation is given in Appendix A):

$$(A_0 P)_{,X} + \rho_0 A_0 b = \rho_0 A_0 \ddot{u} \tag{2.2.12}$$

where the superposed dots denote the material time derivative. The material time derivative of the velocity, the acceleration, is written as D^2u/Dt^2. The subscript following a comma denotes partial differentiation with respect to that variable, i.e.

$$P(X,t)_{,X} \equiv \frac{\partial P(X,t)}{\partial X} \tag{2.2.13}$$

Equation (2.2.12) is called the *momentum equation*, since it represents conservation of momentum. If the initial cross-sectional area is constant in space, the momentum equation becomes

$$P_{,X} + \rho_0 b = \rho_0 \ddot{u} \tag{2.2.14}$$

Equilibrium Equation. When the inertial term $\rho_0 \ddot{u}$ vanishes, i.e. when the problem is static, the momentum equation becomes the *equilibrium equation*

$$\left(A_0 P\right)_{,X} + \rho_0 A_0 b = 0 \tag{2.2.15}$$

Solutions of the equilibrium equations are called equilibrium solutions. Some authors call the momentum equation an equilibrium equation regardless of whether the inertial term is negligible; since equilibrium usually connotes a body at rest or moving with constant velocity, this nomenclature is avoided here.

Energy Conservation. The energy conservation equation for a rod of constant area is given by

$$\rho_0 \dot{w}^{int} = \dot{F} P - q_{x,X} + \rho_0 s \tag{2.2.16}$$

where q_X is the heat flux, s is the heat source per unit mass and $\dot{w}^{int}$ is the rate of change of internal energy per unit mass. In the absence of heat conduction or heat sources, the energy equation gives

$$\rho_0 \dot{w}^{int} = \dot{F} P \tag{2.2.17}$$

which shows that the internal work is given by the product of the rate of the deformation F and the nominal stress P. The energy conservation equation is not needed for the treatment of isothermal, adiabatic processes.

Constitutive Equations. The constitutive equations reflect the stresses which are generated in the material as a response to deformation. The constitutive equations relate the stress to the measures of strain at a material point. The constitutive equation can be written either in total form, which relates the current stress to the current deformation

$$P(X,t) = S^{PF}\left(F(X,\bar{t}),\ \dot{F}(X,\bar{t}),\ etc.,\ \bar{t} \le t\right) \tag{2.2.18}$$

or in rate form

$$\dot{P}(X,t) = S_t^{PF}\left(\dot{F}(X,\bar{t}),\ F(x,\bar{t}),\ P(X,\bar{t}),\ etc.,\ \bar{t} \le t\right) \tag{2.2.19}$$

Here S^{PF} and S_t^{PF} are functions of the deformation which give the stress and stress rate, respectively. The superscripts are here appended to the constitutive functions to indicate which measures of stress and strain they relate.

As indicated in Eq. (2.2.18), the stress can depend on both F and $\dot{F}$ and on other state variables, such as temperature, porosity; "etc." refers to these additional variables which can influence the stress. The prior history of deformation can also affect the stress, as in an elastic-plastic material; this is explicitly indicated in Eqs. (2.2.18-2.2.19) by letting the constitutive functions depend on deformations for all time prior to t. The constitutive equation of a solid is expressed in material coordinates because the stress in a solid usually

depends on the history of deformation at that material point. For example, in an elastic solid, the stress depends on strain at the material point. If there are any residual stresses, these stresses are frozen into the material and move with the material point. Therefore, constitutive equations with history dependence should track material points and are written in terms of the material coordinates. When a constitutive equation for a history dependent material is written in terms of Eulerian coordinates, the motion of the point must be accounted for in the evaluation of the stresses, which will be discussed in Chapter 7.

The above functions should be continuos functions of the independent variables. Preferably they should be continuously differentiable, for otherwise the stress is less smooth than the displacements, which can cause difficulties.

Examples of constitutive equations are:

(a) linear elastic material:

total form: $$P(X,t) = E^{PF}\varepsilon(X,t) = E^{PF}\left(F(X,t)-1\right) \tag{2.2.20}$$

rate form: $$\dot{P}(X,t) = E^{PF}\dot{\varepsilon}(X,t) = E^{PF}\dot{F}(X,t) \tag{2.2.21}$$

(b) linear viscoelastic

$$P(X,t) = E^{PF}\left[\left(F(X,t)-1\right) + \alpha\dot{F}(X,t)\right]$$

or $$P = E^{PF}(\varepsilon + \alpha\dot{\varepsilon}) \tag{2.2.22}$$

For small deformations the material parameter E^{PF} corresponds to Young's modulus; the constant α determines the magnitude of damping.

Momentum equation in terms of displacements. A single governing equation for the rod can be obtained by substituting the relevant constitutive equation, i.e. (2.2.18) or (2.2.19), into the momentum equation (2.2.12) and expressing the strain measure in terms of the displacement by (2.2.6). For the total form of the constitutive equation (2.2.18), the resulting equation can be written as

$$\left(A_0 P\left(u_{,X}, \dot{u}_{,X}, ..\right)\right)_{,X} + \rho_0 A_0 b = \rho_0 A_0 \ddot{u} \tag{2.2.23}$$

which is a nonlinear partial differential equation (PDE) in the displacement $u(X,t)$. The character of this partial differential equation is not readily apparent from the above and depends on the details of the constitutive equation. To illustrate one form of this PDE, we consider a linear elastic material. For a linear elastic material, Eq. (2.2.20), the constitutive equation and (2.2.23) yield

$$\left(A_0 E^{PF} u_{,X}\right)_{,X} + \rho_0 A_0 b = \rho_0 A_0 \ddot{u} \tag{2.2.24}$$

It can be seen that in this PDE, the highest derivatives with respect to the material coordinate X is second order, and the highest derivative with respect to time is also second order, so the PDE is second order in X and time t. If the stress in the constitutive equation only depends on the first derivatives of the displacements with respect to X and t as indicated in (2.2.18) and (2.2.19), then the momentum equation will similarly be a second order PDE in space and time.

For a rod of constant cross-section and modulus, if the body force vanishes, i.e. when $b = 0$, the momentum equation for a linear material becomes the well known linear wave equation

$$u_{,XX} = \frac{1}{c^2}\ \ddot{u} \tag{2.2.25}$$

where c is the wave speed relative to the undeformed configuration and given by

$$c^2 = \frac{E^{PF}}{\rho_0} \tag{2.2.26}$$

Boundary Conditions. The independent variables of the momentum equation are the coordinate X and the time t. It is an initial-boundary value problem (IBVP). To complete the description of the IBVP, the boundary conditions and initial conditions must be given. The boundary in a one dimensional problem consists of the two points at the ends of the domain, which in the model problem are the points X_a and X_b. From the linear form of the momentum equations, Eq. (2.2.23), it can be seen that the partial differential equation is second order in X. Therefore, at each end, either u or $u_{,X}$ must be prescribed as a boundary condition. In solid mechanics, instead of $u_{,X}$, the traction $t_x^0 = n^0 P$ is prescribed; n^0 is the unit normal to the body which is given by $n^0 = 1$ at X_a, $n^0 = -1$ at X_b. Since the stress is a function of the measure of strain, which in turn depends on the derivative of the displacement by Eq. (2.2.6), prescribing t_x^0 is equivalent to prescribing $u_{,X}$; the superscript "naught" on t indicates that the traction is defined over the undeformed area; the superscript is always explicitly included on the traction t_x^0 to distinguish it from the time t. Therefore either the traction or the displacement must be prescribed at each boundary.

A boundary is called a displacement boundary and denoted by Γ_u if the displacement is prescribed; it is called a traction boundary and denoted by Γ_t if the traction is prescribed. The prescribed values are designated by a superposed bar. The boundary conditions are

$$u = \bar{u} \quad \text{on } \Gamma_u \tag{2.2.27}$$

$$n^0 P = \bar{t}_x^0 \quad \text{on } \Gamma_t \tag{2.2.28}$$

As an example of the boundary conditions in solid mechanics, for the rod in Fig. 2.1, the boundary conditions are

$$u(X_a,t) = 0 \qquad n^0(X_b) P(X_b,t) = P(X_b,t) = \frac{T(t)}{A_0(X_b)} \tag{2.2.29}$$

The traction and displacement cannot be prescribed at the same point, but one of these must be prescribed at each boundary point; this is indicated by

$$\Gamma_u \cap \Gamma_t = 0 \qquad \Gamma_u \cup \Gamma_t = \Gamma \tag{2.2.30}$$

Thus in a one dimensional solid mechanics problem any boundary is either a traction boundary or a displacement boundary, but no boundary is both a prescribed traction and prescribed displacement boundary.

Initial Conditions. Since the governing equation for the rod is second order in time, two sets of initial conditions are needed. We will express the initial conditions in terms of the displacements and velocities:

$$u(X,0) = u_0(X) \quad \text{for } X \quad [X_a, X_b] \tag{2.2.31a}$$

$$\dot{u}(X,0) = v_0(X) \quad \text{for } X \quad [X_a, X_b] \tag{2.2.31b}$$

If the body is initially undeformed and at rest, the initial conditions can be written as

$$u(X,0) = 0 \qquad \dot{u}(X,0) = 0 \tag{2.2.32}$$

Jump Conditions. In order for the derivative in Eq.(2.2.12) to exist, the quantity A_0P must be continuous. However, neither A_0 nor P need be continuous in the entire interval. Therefore momentum balance requires that

$$\langle\!\langle A_0 P \rangle\!\rangle = 0 \tag{2.2.33}$$

where $\langle\!\langle\ \rangle\!\rangle$ designates the jump in *f(X)*, i.e.

$$\langle\!\langle f(X) \rangle\!\rangle = f(X+\varepsilon) - f(X-\varepsilon) \qquad \varepsilon \to 0 \tag{2.2.34}$$

In dynamics, it is possible to have jumps in the stress, known as shocks, which can either be stationary or moving. Moving discontinuities are governed by the Rankine-Hugoniot relations, but these are not considered in this Chapter.

2.3 Weak Form for Total Lagrangian Formulation

The momentum equation cannot be discretized directly by the finite element method. In order to discretize this equation, a weak form, often called a variational form, is needed. The principle of virtual work, or weak form, which will be developed next, is equivalent to the momentum equation and the traction boundary conditions (2.2.33). Collectively, these two equations are called the classical *strong form.* The weak form can be used to approximate the strong form by finite elements; solutions obtained by finite elements are approximate solutions to the strong form.

Strong Form to Weak Form. A weak form will now be developed for the momentum equation (2.2.23) and the traction boundary conditions. For this purpose we define trial functions $u(X,t)$ which satisfy any displacement boundary conditions and are smooth enough so that all derivatives in the momentum equation are well defined. The test functions $\delta u(X)$ are assumed to be smooth enough so that all of the following steps are well defined and to vanish on the prescribed displacement boundary. The weak form is obtained by taking the product of the momentum equation expressed in terms of the trial function with the test function. This gives

$$\int_{X_a}^{X_b} \delta u \left[\left(A_0 P \right)_{,X} + \rho_0 A_0 b - \rho_0 A_0 \ddot{u} \right] dX = 0 \tag{2.3.1}$$

Using the derivative of the product in the first term in (2.3.1) gives

$$\int_{X_a}^{X_b} \delta u (A_0 P)_{,X} dX = \int_{X_a}^{X_b} \left[\left(\delta u A_0 P \right)_{,X} - \delta u_{,X} A_0 P \right] dX \tag{2.3.2}$$

Applying the fundamental theorem of calculus to the above gives

$$\begin{aligned} \int_{X_a}^{X_b} \delta u \left(A_0 P \right)_{,X} dX &= - \int_{X_a}^{X_b} \delta u_{,X} \left(A_0 P \right) dX + \left(\delta u A_0 n^0 P \right) \Big|_{\Gamma} \\ &= - \int_{X_a}^{X_b} \delta u_{,X} \left(A_0 P \right) dX + \left(\delta u A_0 \bar{t}_x^0 \right) \Big|_{\Gamma_t} \end{aligned} \tag{2.3.3}$$

where we obtained the second line using the facts that the test function δu vanishes on the prescribed displacement boundary, the complementarity conditions on the boundaries (2.2.30) and the traction boundary conditions. Substituting (2.3.3) into the first term of Eq. (2.3.1) gives (with a change of sign)

$$\int_{X_a}^{X_b} \left[\delta u_{,X} A_0 P - \delta u \left(\rho_0 A_0 b - \rho_0 A_0 \ddot{u} \right) \right] dX - \left(\delta u A_0 \bar{t}_x^0 \right) \Big|_{\Gamma_t} = 0 \tag{2.3.4}$$

The above is the weak form of the momentum equation and the traction boundary condition for the total Lagrangian formulation.

Smoothness of Test and Trial functions; Kinematic Admissibility. We shall now investigate the smoothness required to go through the above steps more closely. For the momentum equation (2.2.12) to be well defined in a classical sense, the nominal stress and the initial area must be continuously differentiable, i.e. C^1; otherwise the first derivative would have discontinuities. If the stress is a smooth function of the derivative of the displacement as in (2.2.18), then to obtain this continuity in the stresses requires that the trial functions must be C^2. For Eq. (2.3.2) to hold, the test function $\delta u(X)$ must be C^1.

However, the weak form is well defined for test and trial functions which are far less smooth, and indeed the test and trial functions to be used in finite element methods will be rougher. The weak form (2.3.4) involves only the first derivative of the test function and the trial function appears directly or as a first derivative of the trial function through the nominal stress. Thus the integral in the weak form is integrable if both functions are C^0.

We will now define the conditions on the test and trial function more precisely. The weak form is well-defined if the trial functions *u(X,t)* are continuous functions with piecewise continuous derivatives, which is stated symbolically by $u(X,t) \quad C^0(X)$, where the X in the parenthesis following C^0 indicates that it pertains to the continuity in X; note that this definition permits discontinuities of the derivatives at discrete points. This is the same as the continuity of finite element approximations in linear finite element procedures:

the displacement is continuous and continuously differentiable within elements, but the derivative $u_{,X}$ is discontinuous across element boundaries. In addition, the trial function $u(X,t)$ must satisfy all displacement boundary conditions. These conditions on the trial displacements are indicated symbolically by

$$u(X,t) \quad U \quad \text{where} \quad U = \left\{ u(X,t) \middle| u(X,t) \quad C^0(X), \; u = \bar{u} \text{ on } \Gamma_u \right\} \tag{2.3.5}$$

Displacement fields which satisfy the above conditions, i.e. displacements which are in U, are called kinematically admissible.

The test functions are denoted by $\delta u(X)$; they are *not* functions of time. The test functions are required to be C^0 in X and to vanish on displacement boundaries, i.e.,

$$\delta u(X) \quad U_0 \quad \text{where} \quad U_0 = \left\{ \delta u(X) \middle| \delta(X) u \quad C^0(X), \; \delta u = 0 \text{ on } \Gamma_u \right\} \tag{2.3.6}$$

We will use the prefix δ for all variables which are test functions and for variables which are related to test functions. This convention originates in variational methods, where the test function emerges naturally as the difference between admissible functions. Although it is not necessary to know variational methods to understand weak forms, it provides an elegant framework for developing various aspects of the weak form. For example, in variational methods any test function is a variation and defined as the difference between two trial functions, i.e. the variation $\delta u(X) = u^a(X) - u^b(X)$, where $u^a(X)$ and $u^b(X)$ are any two functions in U. Since any function in U satisfies the displacement boundary conditions, the requirement in (2.3.6) that $\delta u(X) = 0$ on Γ_u can be seen immediately.

Weak Form to Strong Form. We will now develop the equations implied by the weak form with the less smooth trial and test functions, (2.3.5) and (2.3.6), respectively; the strong form implied with very smooth test and trial functions will also be discussed. The weak form is given by

$$\int_{X_a}^{X_b} \left[\delta u_{,X} A_0 P - \delta u \left(\rho_0 A_0 b - \rho_0 A_0 \ddot{u} \right) \right] dX - \left(\delta u A_0 \bar{t}_x^0 \right)\Big|_{\Gamma_t} = 0 \qquad \delta u(X) \quad U_0 \tag{2.3.7}$$

The displacement fields are assumed to be kinematically admissible, i.e. $u(X,t) \quad U$. The above weak form is expressed in terms of the nominal stress P, but it is assumed that this stress can always be expressed in terms of the derivatives of the displacement field through the strain measure and constitutive equation. Since $u(X,t)$ is C^0 and the strain measure involves derivatives of $u(X,t)$ with respect to X, we expect $P(X,t)$ to be C^{-1} in X if the constitutive equation is continuous: $P(X,t)$ will be discontinuous wherever the derivative of $u(X,t)$ is discontinuous.

To extract the strong form, we need to eliminate the derivative of $\delta u(X)$ from the integrand. This is accomplished by integration by parts and the fundamental theorem of calculus. Taking the derivative of the product $\delta u A_0 P$ we have

$$\int_{X_a}^{X_b} \left(\delta u A_0 P \right)_{,X} dX = \int_{X_a}^{X_b} \delta u_{,X} A_0 P \, dX + \int_{X_a}^{X_b} \delta u \left(A_0 P \right)_{,X} dX \tag{2.3.8}$$

The second term on the RHS can be converted to point values by using the fundamental theorem of calculus. Let the piecewise continuous function $(A_0P)_{,X}$ be continuous on intervals $\left[X_1^i, X_2^i \right]$, $e = 1$ to n, Then by the fundamental theorem of calculus

$$\int_{X_1^e}^{X_2^e} \left(\delta u A_0 P\right)_{,X} dX = \left(\delta u A_0 P\right)\Big|_{X_2^i} - \left(\delta u A_0 P\right)\Big|_{X_1^i} \equiv \left(\delta u A_0 n^0 P\right)\Big|_{\Gamma_i} \tag{2.3.9}$$

where n^0 is the normal to the segments are $n\left(X_1^i\right)=-1$, $n\left(X_2^i\right)=+1$, and Γ_i denotes the two boundary points of the segment i over which the function is continuously differentiable. Let $\left[X_A, X_B \right] = \sum_i \left[X_1^i, X_2^i \right]$; then applying (2.3.2) over the entire domain gives

$$\int_{X_a}^{X_b} (\delta u A_0 P)_{,X} dX = \left(\delta u A_0 n^0 P\right)\Big|_{\Gamma_t} - \sum_i \delta u \langle A_0 P \rangle_{\Gamma_i} \tag{2.3.10}$$

where Γ_i are the interfaces between the segments in which the integrand is continuously differentiable. The contributions to the boundary points on the right-hand side in the above only appear on the traction boundary Γ_t since $\delta u = 0$ on Γ_u and $\Gamma_u = \Gamma - \Gamma_t$ (see Eqs. (2.3.6) and (2.2.30)). Combining Eqs. (2.3.10) and (2.3.2) then gives

$$\int_{X_a}^{X_b} \delta u_{,X} \left(A_0 P\right) dX = -\int_{X_a}^{X_b} \delta u \left(A_0 P\right)_{,X} dX + \left(\delta u A_0 n^0 P\right)\Big|_{\Gamma_t} - \sum_i \delta u \langle A_0 P \rangle_{\Gamma_i} \tag{2.3.11}$$

Substituting the above into Eq. (2.3.7) gives

$$\int_{X_a}^{X_b} \delta u \left[\left(A_0 P\right)_{,X} + \rho_0 A_0 b - \rho_0 A_0 \ddot{u} \right] dX$$

$$+ \delta u A_0 \left(n^0 P - \dot{t}_x^0 \right)\Big|_{\Gamma_t} + \sum_i \delta u \langle A_0 P \rangle_{\Gamma_i} = 0 \qquad \delta u(X) \quad U_0 \tag{2.3.12}$$

The conversion of the weak form to a form amenable to the use of Eq. (2.3.4-5) is now complete. We can therefore deduce from the arbitrariness of the virtual displacement $\delta u(X)$ and Eqs. (2.3.4.-5) and (2.3.12) that (a more detailed derivation of this step is given in Chapter 4)

$$\left(A_0 P\right)_{,X} + \rho_0 A_0 b - \rho_0 A_0 \ddot{u} = 0 \quad \text{for } X \quad \left[X_a, X_b\right] \tag{2.3.13a}$$

$$n^0 P - \dot{t}_x^0 = 0 \quad \text{on } \Gamma_t \tag{2.3.13b}$$

$$\langle A_0 P \rangle = 0 \quad \text{on } \Gamma_i \tag{2.3.13c}$$

These are, respectively, the momentum equation, the traction boundary conditions, and the stress jump conditions. Thus when we admit the less smooth test and trial functions, we have an additional equation in the strong form, the jump condition (2.3.13c).

If the test functions and trial functions satisfy the classical smoothness conditions, the jump conditions do not appear. Thus for smooth test and trial functions, the weak form implies only the momentum equation and the traction boundary conditions.

The less smooth test and trial functions are more pertinent to finite element approximations, where these functions are only C^0. They are also needed to deal with discontinuities in the cross-sectional area and material properties. At material interfaces, the classical strong form is not applicable, since it assumes that the second derivative is uniquely defined everywhere. This is not true at material interfaces because the strains, and hence the derivatives of the displacement fields, are discontinuous. With the rougher test and trial functions, the conditions which hold at these interfaces. (2.3.13c) emerge naturally.

In the weak form for the total Lagrangian formulation, all integrations are performed over the material coordinates, i.e. the reference configuration, of the body, because total Lagrangian formulations involve derivatives with respect to the material coordinates X, so integration by parts is most conveniently performed over the domain expressed in terms of the material coordinate X. Sometimes this is referred to as integration over the undeformed, or initial, domain. The weak form is expressed in terms of the nominal stress.

Physical Names of Virtual Work Terms. For the purpose of obtaining a methodical procedure for obtaining the finite element equations, the virtual energies will be defined according to the type of work which they represent; the corresponding nodal forces will subsequently carry identical names.

Each of the terms in the weak form represents a virtual work due to the virtual displacement δu; this displacement $\delta u(X)$ is called a often "virtual" displacement to indicate that it is not the actual displacement; according to Webster's dictionary, virtual means "being in essence or effect, not in fact"; this is a rather hazy meaning and we prefer the name test function.

The virtual work of the body forces $b(X,t)$ and the prescribed tractions $\bar{t}_x^0$, which corresponds to the second and fourth terms in (2.3.4), is called the virtual external work since it results from the external loads. It is designated by the superscript *"ext"* and given by

$$\delta W^{ext} = \int_{X_a}^{X_b} \delta u \rho_0 b A_0 \, dX + \left(\delta u A_0 \bar{t}_x^0 \right) \Big|_{\Gamma_t} \tag{2.3.16}$$

The first term in (2.3.4) is the called the virtual internal work, for it arises from the stresses in the material. It can be written in two equivalent forms:

$$\delta W^{int} = \int_{X_a}^{X_b} \delta u_{,X} P A_0 \, dX = \int_{X_a}^{X_b} \delta F P A_0 \, dX \tag{2.3.17}$$

where the last form follows from (2.2.1) as follows:

$$\delta u_{,X}(X) = \delta\left(\varphi(X) - X\right)_{,X} = \delta\varphi_{,X} = \frac{\partial(\delta x)}{\partial X} = \delta F \tag{2.3.18}$$

The variation $\delta X = 0$ because the independent variable X does not change due to an incremental displacement $\delta u(X)$.

This definition of internal work in (2.3.17) is consistent with the internal work expression in the energy conservation equation, Eq. (2.2.16-2.2.17): if we change the rates in (2.2.11) to virtual increments, then $\rho_0 \delta w^{int} = \delta FP$. The virtual internal work δW^{int} is defined over the entire domain, so we have

$$\delta W^{int} = \int_{X_a}^{X_b} \delta w^{int} \rho_0 A_0 dX = \int_{X_a}^{X_b} \delta F P A_0 dX \tag{2.3.19}$$

which is the same term that appears in the weak form in (2.2.18).

The term $\rho_0 A_0 \ddot{u}$ can be considered a body force which acts in the direction opposite to the acceleration, i.e. in a d'Alembert sense. We will designate the corresponding virtual work by δW^{inert} and call it the virtual inertial work, so

$$\delta W^{inert} = \int_{X_a}^{X_b} \delta u \rho_0 A_0 \ddot{u}\, dX \tag{2.3.20}$$

This is the work by the inertial forces on the body.

Principle of Virtual Work. The principle of virtual work is now stated using these physically motivated names. By using Eqs. (2.3.16-2.3.20), Eq. (2.3.4) can then be written as

$$\delta W(\delta u, u) \equiv \delta W^{int} - \delta W^{ext} + \delta W^{inert} = 0 \qquad \delta u \quad U_0 \tag{2.3.21}$$

The above equation, with the definitions in Eqs. (2.3.16-2.3.20), is the weak form corresponding to the strong form which consists of the momentum equation, the traction boundary conditions and the stress jump conditions. The weak form implies the strong form and that the strong form implies the weak form. Thus the weak form and the strong form are equivalent. This equivalence of the strong and weak forms for the momentum equation is called the principle of virtual work.

All of the terms in the principle of virtual work δW are energies or virtual work terms, which is why it is called a virtual work principle. That the terms are energies is immediately apparent from δW^{ext} : since $\rho_0 b$ is a force per unit volume, its product with a virtual displacement δu gives a virtual work per unit volume, and the integral over the domain gives the total virtual work of the body force. Since the other terms in the weak form must be dimensionally consistent with the external work term, they must also be virtual energies. This view of the weak form as consisting of virtual work or energy terms provides a unifying perspective which is quite useful for constructing weak forms for other coordinate systems and other types of problems: it is only necessary to write an equation for the virtual energies to obtain the weak form, so the procedure we have just gone through can be avoided. The virtual work schema is also useful in memorizing the weak form. However, from a mathematical viewpoint it is not necessary to think of the test functions $\delta u(X)$ as virtual displacements: they are simply test functions which satisfy continuity conditions and vanish on the boundaries as specified by (2.3.6). This second

viewpoint becomes useful when a finite element discretization is applied to equations where the product with a test function does not have a physical meaning. The principle of virtual work is summarized in Box 2.1.

Box 2.1. Principle of Virtual Work for One Dimensional Total Lagrangian Formulation

If the trial functions $u(X,t) \in U$, then

(*Weak Form*) $\delta W = 0 \qquad \forall \delta u \in U_0$ (B2.1.1)

is equivalent to

(*Strong Form*)

the momentum equation (2.2.12): $(A_0 P)_{,X} + \rho_0 A_0 b = \rho_0 A_0 \ddot{u}$, (B2.1.2)

the traction boundary conditions (2.2.28): $n^0 P = \bar{t}_x^0 \quad$ on Γ_t, (B2.1.3)

and the jump conditions (2.2.33): $A_0 P = 0$. (B2.1.4)

Weak form definitions:

$$\delta W \equiv \delta W^{int} - \delta W^{ext} + \delta W^{inert} \tag{B2.1.5}$$

$$\delta W^{int} = \int_{X_a}^{X_b} \delta u_{,X} P A_0 \, dX = \int_{X_a}^{X_b} \delta F P A_0 \, dX , \qquad \delta W^{inert} = \int_{X_a}^{X_b} \delta u \rho_0 A_0 \ddot{u} \, dX \tag{B2.1.6}$$

$$\delta W^{ext} = \int_{X_a}^{X_b} \delta u \rho_0 b A_0 \, dX + \left(\delta u A_0 \bar{t}_x^0 \right) \Big|_{\Gamma_t} \tag{B2.1.7}$$

2.4 Finite Element Discretization In Total Lagrangian Formulation

Finite Element Approximations. The discrete equations for a finite element model are obtained from the principle of virtual work by using finite element interpolants for the test and trial functions. For the purpose of a finite element discretization, the interval $[X_a, X_b]$ is subdivided into elements e=1 to n_e with n_N nodes. The nodes are denoted by X_I, I = 1 to n_N, and the nodes of a generic element by X_I^e, I = 1 to m, where m is the number of nodes per element. The domain of each element is $\left[X_1^e, X_m^e \right]$, which is denoted by Ω_e. For simplicity, we consider a model problem in which node 1 is a prescribed displacement boundary and node n_N a prescribed traction boundary. However, to derive the governing equations we first treat the model as if there were no prescribed displacement boundaries and impose the displacement boundary conditions in the last step.

The finite element trial function $u(X,t)$ is written as

$$u(X,t) = \sum_{I=1}^{n_N} N_I(X) u_I(t) \tag{2.4.1}$$

In the above, $N_I(X)$ are C^0 interpolants, they are often called shape functions in the finite elementliterature; $u_I(t), I = 1 \text{to } n_N$, are the nodal displacements, which are functions of time, and are to be determined in the solution of the equations. The nodal displacements are considered functions of time even in static, equilibrium problems, since in nonlinear problems we must follow the evolution of the load; in many cases, t may simply be a monotonically increasing parameter. The shape functions, like all interpolants, satisfy the condition

$$N_I(X_J) = \delta_{IJ} \tag{2.4.2}$$

where δ_{IJ} is the Kronecker delta or unit matrix: $\delta_{IJ} = 1$ if $I = J$, $\delta_{IJ} = 0$ if $I \neq J$. We note here that if we set $u_1(t) = \bar{u}(0,t)$ then the trial function $u(X,t)$ U, i.e. it is kinematically admissible since it has the requisite continuity and satisfies the essential boundary conditions. Equation (2.4.1) represents a separation of variables: the spatial dependence of the solution is entirely represented by the shape functions, whereas the time dependence is ascribed to the nodal variables. This characteristic of the finite element approximation will have important ramifications in finite element solutions of wave propagation problems.

The test functions (or virtual displacements) depend only on the material coordinates

$$\delta u(X) = \sum_{I=1}^{n_N} N_I(X) \delta u_I \tag{2.4.3}$$

where δu_I are the nodal values of the test function; they are not functions of time.

Nodal Forces. To provide a systematic procedure for developing the finite element equations, nodal forces are developed for each of the virtual work terms. These nodal forces are given names which correspond to the names of the virtual work terms. Thus

$$\delta W^{int} = \sum_{I=1}^{n_N} \delta u_I \, f_I^{int} = \delta \mathbf{u}^T \mathbf{f}^{int} \tag{2.4.4a}$$

$$\delta W^{ext} = \sum_{I=1}^{n_N} \delta u_I \, f_I^{ext} = \delta \mathbf{u}^T \mathbf{f}^{ext} \tag{2.4.4b}$$

$$\delta W^{inert} = \sum_{I=1}^{n_N} \delta u_I \, f_I^{inert} = \delta \mathbf{u}^T \mathbf{f}^{inert} \tag{2.4.4c}$$

$$\delta \mathbf{u}^T = \begin{bmatrix} \delta u_1 & \delta u_2 & \ldots & \delta u_{n_N} \end{bmatrix} \qquad \mathbf{f}^T = \begin{bmatrix} f_1 & f_2 & \ldots & f_{n_N} \end{bmatrix} \tag{2.4.4d}$$

where $\mathbf{f}^{int}$ are the internal nodal forces, $\mathbf{f}^{ext}$ are the external nodal forces, and $\mathbf{f}^{inert}$ are the inertial, or d'Alembert, nodal forces. These names give a physical meaning to the nodal

forces : the internal nodal forces correspond to the stresses "in" the material, the external nodal forces correspond to the externally applied loads, while the inertial nodal forces correspond to the inertia term due to the accelerations.

Nodal forces are always defined so that they are *conjugate* to the nodal displacements in the sense of work, i.e. so the scalar product of an increment of nodal displacements with the nodal forces gives an increment of work. This rule should be observed in the construction of the discrete equations, for when it is violated many of the important symmetries, such as that of the mass and stiffness matrices, are lost.

Next we develop expressions for the various nodal forces in terms of the continuous variables in the partial differential equation by using (2.3.16-2.3.20). In developing the nodal force expressions, we continue to ignore the displacement boundary conditions and consider δu_I arbitrary at all nodes. The expressions for the nodal forces are then obtained by combining Eqs. (2.3.16) to (2.3.20) with the definitions given in Eqs. (2.4.4) and the finite element approximations for the trial and test functions. Thus to define the internal nodal forces in terms of the nominal stress, we use (2.4.4a) and Eq. (2.3.16), and use the finite element approximation of the test function (2.4.3), giving

$$\delta W^{int} \equiv \sum_I \delta u_I f_I^{int} = \int_{X_a}^{X_b} \delta u_{,X} P A_0 \, dX = \sum_I \delta u_I \int_{X_a}^{X_b} N_{I,X} P A_0 \, dX \tag{2.4.5}$$

From the above definition it follows that

$$f_I^{int} = \int_{X_a}^{X_b} N_{I,X} P A_0 dX \tag{2.4.6}$$

which gives the expression for the internal nodal forces. It can be seen that the internal nodal forces are a discrete representation of the stresses in the material. Thus they can be viewed as the nodal forces arising from the resistance of the solid to deformation.

The external and nodal forces are developed similarly. The external nodal forces are obtained by using (2.4.4b) and (2.3.17) in conjunction with the test function:

$$\begin{aligned} \delta W^{ext} &= \sum_I^N \delta u_I f_I^{ext} = \int_{X_a}^{X_b} \delta u \rho_0 b A_0 dX + \left(\delta u A_0 \bar{t}_x^0 \right)\Big|_{\Gamma_t} \\ &= \sum_I^N \delta u_I \left\{ \int_{X_a}^{X_b} N_I \rho_0 b A_0 dX + \left(N_I A_0 \bar{t}_x^0 \right)\Big|_{\Gamma_t} \ddot{u} \right\} \end{aligned} \tag{2.4.7}$$

where in the last step (2.4.3) has been used. The above give

$$f_I^{ext} = \int_{X_a}^{X_b} \rho_0 N_I b A_0 \, dX + \left(N_I A_0 \bar{t}_x^0 \right)\Big|_{\Gamma_t} \tag{2.4.8}$$

Since $N_I(X_J) = \delta_{IJ}$ the last term contributes only to those nodes which are on the prescribed traction boundary.

The inertial nodal forces are obtained from the inertial virtual work (2.4.4c) and (2.3.20):

$$\delta W^{inert} = \sum_I \delta u_I f_I^{inert} = \int_{X_a}^{X_b} \delta u \rho_0 \ddot{u} A_0 dX \tag{2.4.9}$$

Using the finite element approximation for the test functions, Eq. (2.4.3), and the trial functions, Eq. (2.4.1) gives

$$\sum_I \delta u_I f_I^{inert} = \sum_I \delta u_I \int_{X_a}^{X_b} \rho_0 N_I \sum_J N_J A_0 dX \ \ddot{u}_J \tag{2.4.10}$$

The inertial nodal force is usually expressed as a product of a mass matrix and the nodal accelerations. Therefore we define a mass matrix by

$$M_{IJ} = \int_{X_a}^{X_b} \rho_0 N_I N_J A_0 dX \quad \text{or} \quad \mathbf{M} = \int_{X_a}^{X_b} \rho_0 \mathbf{N}^T \mathbf{N} A_0 dX \tag{2.4.11}$$

Letting $\ddot{u}_I \equiv a_I$ the virtual inertial work is

$$\delta W^{inert} = \sum_I \delta u_I f_I^{inert} = \sum_I \sum_J \delta u_I M_{IJ} a_J = \delta \mathbf{u}^T \mathbf{M} \mathbf{a}, \ \mathbf{a} = \ddot{\mathbf{u}} \tag{2.4.12}$$

The definition of the inertial nodal forces then gives the following expression

$$f_I^{inert} = \sum_J M_{IJ} a_J \quad \text{or} \quad \mathbf{f}^{inert} = \mathbf{M} \mathbf{a} \tag{2.4.13}$$

Note that the mass matrix as given by Eq. (2.4.11) will not change with time, so it needs to be computed only at the beginning of the calculation. The mass matrix given by (2.4.11) is called the consistent mass matrix.

Semidiscrete Equations. We now develop the semidiscrete equations, i.e. the finite element equations for the model. At this point we will also consider the effect of the displacement boundary conditions. The displacement boundary conditions can be satisfied by the trial and test functions function by letting

$$u_1(t) = \bar{u}_1(t) \quad \text{and} \quad \delta u_1 = 0 \tag{2.4.14}$$

The trial function then meets Eq. (2.3.5). For the test function to meet the conditions of Eq. (2.3.6), it is necessary that $\delta u_1 = 0$, so the nodal values of the test function are not arbitrary at node 1. Our development here, as noted in the beginning, specifies node 1 as the prescribed displacement boundary; this is done only for convenience of notation, and in a finite element model any node can be a prescribed displacement boundary node.

We will now derive the discrete equations. It should be noted that Eqs. (2.4.4a-c) are simply definitions that are made for convenience, and do not constitute the discrete equations. Substituting the definitions (2.4.4a-c) into Eq. (2.3.21) gives

$$\sum_{I=1}^{n_N} \delta u_I \left(f_I^{int} - f_I^{ext} + f_I^{inert} \right) = 0 \tag{2.4.15}$$

Since δu_I is arbitrary at all nodes except the displacement boundary node, node 1, it follows that

$$f_I^{int} - f_I^{ext} + f_I^{inert} = 0, \quad I = 2 \text{ to } n_N \tag{2.4.16}$$

Substituting (2.4.13) into (2.4.16) gives the discrete equations, which are known as the *equations of motion*:

$$\sum_{J=1}^{n_N} M_{IJ} \frac{d^2 u_J}{dt^2} + f_I^{int} - f_I^{ext} = 0, \quad I = 2 \text{ to } n_N \tag{2.4.17}$$

The acceleration of node 1 is given in this model problem, since node 1 is a prescribed displacement node. The acceleration of the prescribed displacement node can be obtained from the prescribed nodal displacement by differentiating twice in time. Obviously, the prescribed displacement must be sufficiently smooth so that the second derivative can be taken; this requires it to be a C^1 function of time. If the mass matrix is not diagonal, then the acceleration on the prescribed displacement node, node 1, will contribute to the Eq. (2.4.17). The finite element equations can then be written as

$$\sum_{J=2}^{n_N} M_{IJ} \frac{d^2 u_J}{dt^2} + f_I^{int} - f_I^{ext} = M_{I1} \frac{d^2 \bar{u}_1}{dt^2}, \quad I = 2 \text{ to } n_N \tag{2.4.18}$$

In matrix form the equations of motion can be written as

$$\begin{aligned} &\mathbf{M a} = \mathbf{f}^{ext} - \mathbf{f}^{int} \quad \text{or} \\ &\mathbf{f} = \mathbf{M a}, \quad \mathbf{f} = \mathbf{f}^{ext} - \mathbf{f}^{int} \end{aligned} \tag{2.4.19}$$

where the matrices have been truncated so that the equations correspond to Eq. (2.4.17), i.e. $\mathbf{M}$ is a $(n_N - 1) \times n_N$ matrix and the nodal forces are column matrices of order $n_N - 1$. The effects of any nonzero nodal prescribed displacements are assumed to have been incorporated in the external nodal forces by letting

$$f_I^{ext} \leftarrow f_I^{ext} + M_{I1} \frac{d^2 \bar{u}_1}{dt^2} \tag{2.4.20}$$

Thus, when the mass matrix is consistent, prescribed velocities make contributions to nodes which are not on the boundary. For a diagonal mass matrix, the accelerations of prescribed displacement nodes have no effect on other nodes and the above modification of the external forces can be omitted.

Equations (2.4.17) and (2.4.19) are two alternate forms of the semidiscrete momentum equation, which is called the *equation of motion*. These equations are called semidiscrete because they are discrete in space but continuous in time. Sometimes they are

called discrete equations, but they are only discrete in space. The equations of motion are systems of $n_N - 1$ second-order *ordinary differential equations(ODE)*; the independent variable is the time *t*. These equations can easily be remembered by the second form in (2.4.19), $\mathbf{f} = \mathbf{M}\mathbf{a}$, which is the well known Newton's second law of motion. The mass matrix in finite element discretizations is often not diagonal, so the equations of motion differ from Newton's second law in that a force at node *I* can generate accelerations at node *J* if $M_{IJ} \neq 0$. However, in many cases a diagonal approximation to the mass matrix is used. In that case, the discrete equations of motion are identical to the Newton's equations for a system of particles interconnected by deformable elements. The force $f_I = f_I^{ext} - f_I^{int}$ is the net force on particle *I*. The negative sign appears on the internal nodal forces because these nodal forces are defined as acting on the elements; by Newton's third law, the forces on the nodes are equal and opposite, so a negative sign is needed. Viewing the semidiscrete equations of motion in terms of Newton's second law provides an intuitive feel for these equations and is useful in remembering these equations.

Initial Conditions. Since the equations of motion are second order in time, initial conditions on the displacements and velocities are needed. The continuous form of the initial conditions are given by Eqs. (2.2.22). In many cases, the initial conditions can be applied by simply setting the nodal values of the variables to the initial values, i.e. by letting

$$u_I(0) = u_0(X_I) \qquad I \qquad \text{and} \quad \dot{u}_I(0) = v_0(X_I) \qquad I \tag{2.4.21}$$

Thus the initial conditions on the nodal variables for a body which is initially at rest and undeformed are

$$u_I(0) = 0 \quad \text{and} \quad \dot{u}_I(0) = 0 \qquad I \tag{2.4.22}$$

Least Square Fit to Initial Conditions. For more complex initial conditions, the initial values of the nodal displacements and nodal velocities can be obtained by a least-square fit to the initial data. The least square fit for the initial displacements results from minimizing the square of the difference between the finite element interpolate $\sum N_I(X)u_I(0)$ and the initial data $\bar{u}(X)$. Let

$$M = \frac{1}{2}\int_{X_a}^{X_b} \left(\sum_I u_I(0) N_I(X) - u_0(X) \right)^2 \rho_0 A_0 \, dX \tag{2.4.23}$$

The density is not necessary in this expression but as will be seen, it leads to equations in terms of the mass matrix, which is quite convenient. To find the minimum set

$$0 = \frac{\partial M}{\partial u_K(0)} = \int_{X_a}^{X_b} N_K(X) \left[\sum_I u_I(0) N_I(X) - u_0(X) \right] \rho_0 A_0 \, dX \tag{2.4.24}$$

Using the definition of the mass matrix, (2.4.11), it can be seen that the above can be written as

$$\mathbf{M}\mathbf{u}(0) = \mathbf{g} \tag{2.4.25a}$$

$$g_K = \int_{X_a}^{X_b} N_K(X) u_0(X) \rho_0 A_0 \, dX \tag{2.4.25b}$$

The least square fit to the initial velocity data is obtained similarly. This method of fitting finite element approximations to functions is often called an L_2 projection.

Diagonal Mass Matrix. The mass matrix which results from a consistent derivation from the weak form is called a *consistent mass matrix*. In many applications, it is advantageous to use a diagonal mass matrix called a lumped mass matrix. Procedures for diagonalizing the mass matrix are often quite ad hoc, and there is little theory underlying these procedures. One of the most common procedures is the row-sum technique, in which the diagonal elements of the mass matrix are obtained by

$$M_{II}^D = \sum_J M_{IJ}^C \tag{2.4.26}$$

where the sum is over the entire row of the matrix, M_{IJ}^C is the consistent mass matrix and M_{IJ}^D is the diagonal or lumped, mass matrix.

The diagonal mass matrix can also be evaluated by

$$M_{II}^D = \sum_J M_{IJ}^C = \int_{X_a}^{X_b} \rho_0 N_I \left(\sum_j N_j \right) A_0 dX = \int_{X_a}^{X_b} \rho_0 N_I A_0 \, dX \tag{2.4.27}$$

where we have used the fact that the sum of the shape functions must equal one; this is a reproducing condition discussed in Chapter 8. This diagonalization procedure conserves the total momentum of a body, i.e. the momentum of the system with the diagonal mass is equivalent to that of the consistent mass, so

$$\sum_{I,J} M_{IJ}^C v_J = \sum_I M_{II}^D v_I \tag{2.4.28}$$

for any nodal velocities.

2.5 Relationships between Element and Global Matrices

In the previous section, we have developed the semidiscrete equations in terms of global shape functions, which are defined over the entire domain, although they are usually nonzero only in the elements adjacent to the node associated with the shape function. The use of global shape functions to derive the finite element equations provides little understanding of how finite element programs are actually structured. In finite element programs, the nodal forces and the mass matrix are usually first computed on an element level. The element nodal forces are combined into the global matrix by an operation called *scatter* or *vector assembly*. The mass matrix and other square matrices are combined from the element level to the global level by an operation called *matrix assembly*. When the nodal displacements are needed for computations, they are extracted from the global

matrix by an operation called *gather*. These operations are described in the following. In addition we will show that there is no need to distinguish element and global shape functions and element and global equations for the nodal forces: the expressions are identical and the element related expressions can always be obtained by limiting the integration to the domain of the element.

The relations between element matrices and the corresponding global matrices will obtained by the use of the connectivity matrices $\mathbf{L}_e$. The nodal displacements and nodal forces of element *e* are denoted by $\mathbf{u}_e$ and $\mathbf{f}_e$, respectively, and are column matrices of order *m*, where *m* is the number of nodes per element. Thus for a 2-node element, the element nodal displacement matrix is $\mathbf{u}_e^T = \left[u_1, u_2\right]_e$. The corresponding element nodal force matrix is $\mathbf{f}_e^T = \left[f_1, f_2\right]_e$. We will place the element identifier "*e*" as either a subscript or superscript, but will always use the letter "*e*" for the purpose of identifying element-related quantities.

The element and global nodal forces must be defined so that their scalar products with the corresponding nodal displacement increments gives an increment of work. This was used in defining the nodal forces in Section 2.4. In most cases, meeting this requirement entails little beyond being careful to arrange the nodal displacements and nodal forces in the same order in the corresponding matrices. This feature of the nodal force and displacement matrices is crucial to the assembly procedure and symmetry of linear and linearized equations.

The element nodal displacements are related to the global nodal displacements by

$$\mathbf{u}_e = \mathbf{L}_e\mathbf{u} \qquad \delta\mathbf{u}_e = \mathbf{L}_e\delta\mathbf{u} \tag{2.5.1}$$

The matrix $\mathbf{L}_e$ is a Boolean matrix, i.e. it consists of the integers 0 and 1. An example of the $\mathbf{L}_e$ matrix for a specific mesh is given later in this Section. The operation of extracting $\mathbf{u}_e$ from $\mathbf{u}$ is called a *gather* because in this operation the small element vectors are *gathered* from the global vector.

The element nodal forces are defined analogously to (2.4.4) as those forces which give the internal work:

$$\delta W_e^{int} = \delta\mathbf{u}_e^T\mathbf{f}_e^{int} = \int_{X_1^e}^{X_m^e} \delta u_{,X} P A_0 dX \tag{2.5.2}$$

To obtain the relations between global and local nodal forces, we use the fact that the total virtual internal energy is the sum of the element internal energies:

$$\delta W^{int} = \sum_e \delta W_e^{int} \quad \text{or} \quad \delta\mathbf{u}^T\mathbf{f}^{int} = \sum_e \delta\mathbf{u}_e^T\mathbf{f}_e^{int} \tag{2.5.3}$$

Substituting (2.5.1) into the (2.5.3) yields

$$\delta\mathbf{u}^T\mathbf{f}^{int} = \delta\mathbf{u}^T \sum_e \mathbf{L}_e^T\mathbf{f}_e^{int} \tag{2.5.4}$$

Since the above must hold for arbitrary $\delta\mathbf{u}$, it follows that

$$\mathbf{f}^{int} = \sum_e \mathbf{L}_e^T \mathbf{f}_e^{int} \tag{2.5.5}$$

which is the relationship between element nodal forces and global nodal forces. The above operation is called a *scatter*, for the small element vector is *scattered* into the global array according to the node numbers. Similar expressions can be derived for the external nodal forces and the inertial forces

$$\mathbf{f}^{ext} = \sum_e \mathbf{L}_e^T \mathbf{f}_e^{ext}, \qquad \mathbf{f}^{inert} = \sum_e \mathbf{L}_e^T \mathbf{f}_e^{inert} \tag{2.5.6}$$

The gather and scatter operations are illustrated in Fig. 2 for a one dimensional mesh of two-node elements. The sequence of gather, compute and scatter is illustrated for two elements in the mesh. As can be seen, the displacements are gathered according to the node numbers of the element. Other nodal variables, such as nodal velocities and temperatures, can be gathered similarly. In the scatter, the nodal forces are then returned to the global force matrix according to the node numbers. The scatter operation is identical for the other nodal forces.

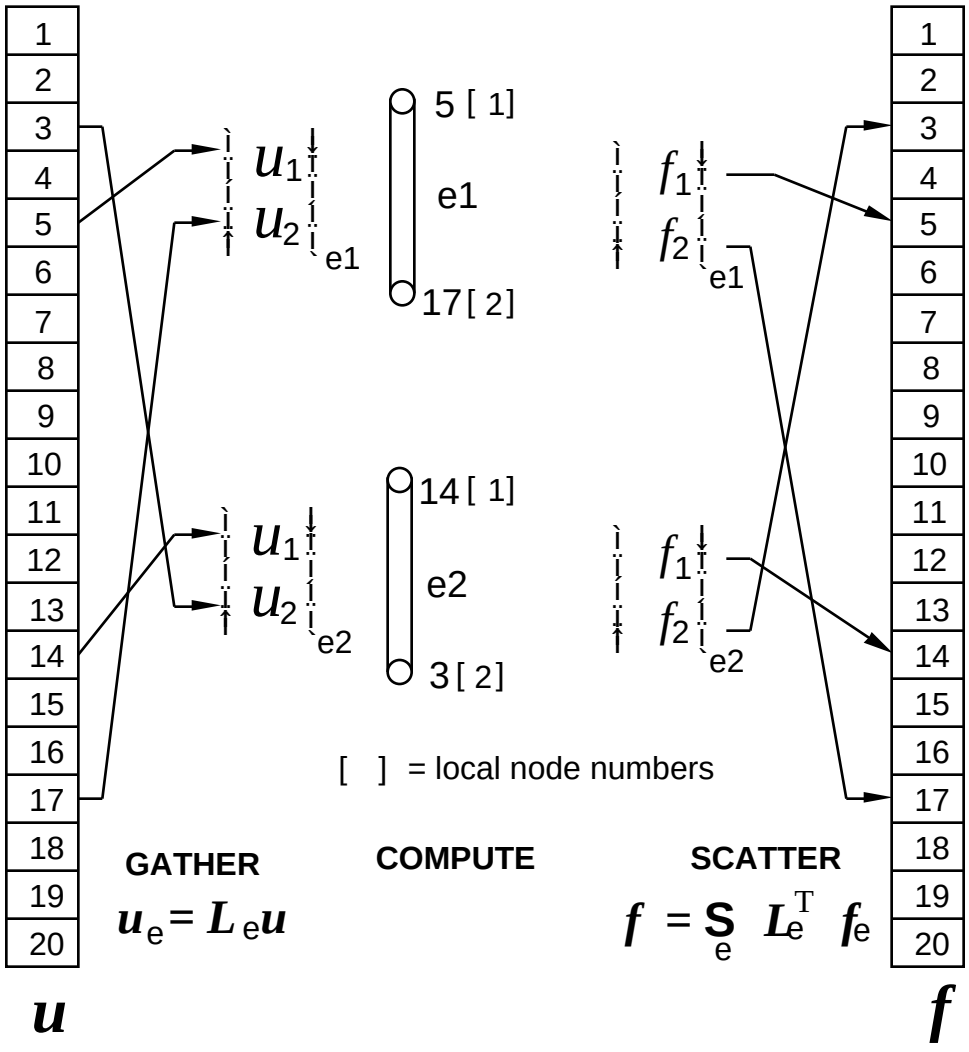

Fig. 2.2. Illustration of gather and scatter for a one-dimensional mesh of two-node elements, showing the gather of two sets of element nodal displacements and the scatter of the computed nodal forces.

In order to describe the assembly of the global mass matrix from the element mass matrices, the element inertial nodal forces are defined as a product of an element mass matrix and the element acceleration, similarly to (2.4.13):

$$\mathbf{f}_e^{inert} = \mathbf{M}_e \mathbf{a}_e \tag{2.5.7}$$

By taking time derivatives of Eq. (2.5.1), we can relate the element and global accelerations by $\mathbf{a}_e = \mathbf{L}_e \mathbf{a}$,(the connectivity matrix does not change with time) and inserting this into the above and using (2.5.6) yields

$$\mathbf{f}^{inert} = \sum_e \mathbf{L}_e^T \mathbf{M}_e \mathbf{L}_e \mathbf{a} \tag{2.5.8}$$

Comparing (2.5.8) to (2.4.13), it can be seen that the global mass matrix is given in terms of the element matrices by

$$\mathbf{M} = \sum_e \mathbf{L}_e^T \mathbf{M}_e \mathbf{L}_e \tag{2.5.9}$$

The above operation is the well known procedure of *matrix assembly*. This is the same operation which is used to assemble the stiffness matrix from element stiffnesses in linear finite element methods.

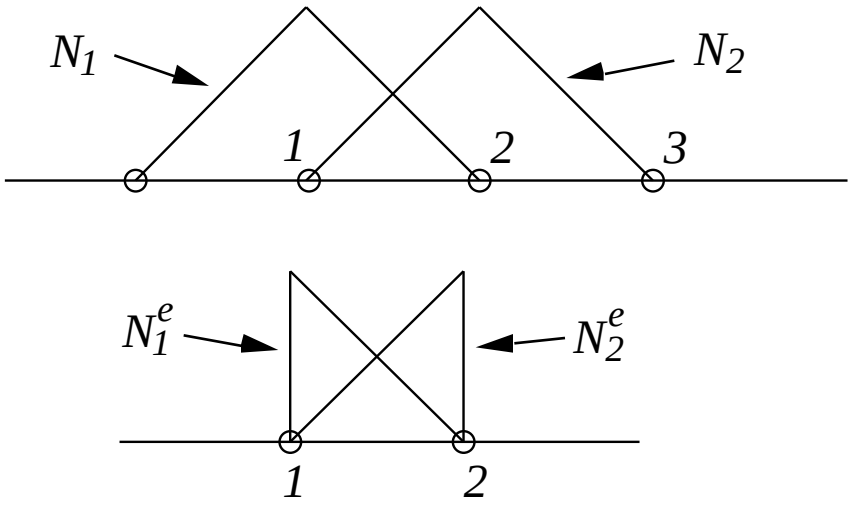

Fig. 2.3. Illustration of element $N^e(X)$ and global shape functions $N(X)$ for a one dimensional mesh of linear displacement, two-node elements.

Relations between element shape functions and global shape functions can also be developed by using the connectivity matrices. However, we shall shortly see that in most cases there is no need to distinguish them. The element shape functions are defined as the interpolants $\mathbf{N}^e(X)$, which when multiplied by the element nodal displacements, give the displacement field in the element, i.e. the displacement field in element e is given by

$$u^e(X) = \mathbf{N}^e(X)\mathbf{u}_e = \sum_{I=1}^{m} N_I^e(X) u_I^e \tag{2.5.10}$$

The global displacement field is obtained by summing the displacement fields for all elements, which gives

$$u(X) = \sum_{e=1}^{n_e} \mathbf{N}^e(X)\mathbf{L}_e\mathbf{u} = \sum_{e=1}^{n_e}\sum_{I=1}^{m}\sum_{J=1}^{n_N} N_I^e(X) L_{IJ}^e u_J \tag{2.5.11}$$

where Eq. (2.5.1) has been used in the above. Comparing the above with Eq. (2.4.1), we see that

$$\mathbf{N}(X) = \sum_{e=1}^{n_e} \mathbf{N}^e(X)\mathbf{L}_e \quad \text{or} \quad N_J(X) = \sum_{e=1}^{n_e}\sum_{I=1}^{m} N_I^e(X) L_{IJ}^e \tag{2.5.12}$$

Thus the global shape functions are obtained from the element shape functions by summing according to the node numbers of the elements. This relationship is illustrated graphically for a two-node linear displacement element in Fig. 2.3.

We will now show that the expressions for the element nodal forces are equivalent to the global nodal forces, except that the integrals are restricted to the elements. Using Eq. (2.5.2) and the element form of the displacement field, we obtain

$$\delta W_e^{int} = \delta \mathbf{u}_e^T \mathbf{f}_e^{int} = \delta \mathbf{u}_e^T \int_{X_1^e}^{X_m^e} \mathbf{N}_{,X}^e P A_0 dX \tag{2.5.13}$$

Invoking the arbitrariness of the virtual nodal displacements, we obtain

$$\mathbf{f}_e^{int} = \int_{X_1^e}^{X_m^e} \mathbf{N}_{,X} P A_0 dX \quad \text{or} \quad f_{I,e}^{int} = \int_{X_1^e}^{X_m^e} N_{I,X} P A_0 dX \tag{2.5.14}$$

where the superscript e has been removed from the last expression since in element e, $\mathbf{N}^e(X) = \mathbf{N}(X)$.

Comparing the above with (2.4.6), we can see that (2.5.14) is identical to the global expression (2.4.6) except that integrals here are limited to an element. Identical results can be obtained for the mass matrix and the external force matrix. Therefore, in subsequent derivations we will usually not distinguish element and global forms of the matrices: the element forms are identical to the global forms except that element matrices correspond to integrals over the element domain, whereas global force matrices correspond to integrals over the entire domain.

In finite element programs, global nodal forces are not computed directly but obtained from element nodal forces by assembly, i.e. the scatter operation. Furthermore, the essential boundary conditions need not be considered until the final steps of the procedure. Therefore we will usually concern ourselves only with obtaining the element equations. The assembly of the element equations for the complete model and the imposition of boundary conditions is a standard procedure.

We will often write the internal nodal force expressions for the total Lagrangian formulation in terms of a $\mathbf{B}_0$ matrix, where $\mathbf{B}_0$ is in the one-dimensional case a row matrix defined by

$$B_{0I} = N_{I,X} \tag{2.5.15}$$

The nought is specifically included to indicate that the derivatives are with respect to the initial, or material, coordinates. n The internal nodal forces (2.5.14) are then given

$$\mathbf{f}_e^{int} = \int_{\Omega_0^e} \mathbf{B}_0^T P d\Omega_0 \quad \text{or} \quad f_{I,e}^{int} = \int_{\Omega_0^e} B_{0I} P d\Omega_0 \tag{2.5.16}$$

where we have used $d\Omega_0 = A_0 dX$ and Ω_0^e is the initial domain of the element. In this notation the deformation gradient F and the one-dimensional strain are given by

$$\boldsymbol{\varepsilon} = \mathbf{B}_0 \mathbf{u}^e \tag{2.5.17}$$

Box 2.2. Discrete Equations in Total Lagrangian Formulation

$$u(X,t) = \mathbf{N}(X)\mathbf{u}_e(t) = \sum_I N_I(X) u_I^e(t)$$

(B2.2.1)

in each element

$$\boldsymbol{\varepsilon} = \sum_I \frac{\partial N_I}{\partial X} u_I^e = \mathbf{B}_0 \mathbf{u}_e \tag{B2.2.2}$$

evaluate the nominal stress P by constitutive equation

$$\mathbf{f}_e^{int} = \int_{\Omega_0^e} \frac{\partial \mathbf{N}}{\partial X} P d\Omega_0 = \int_{\Omega_0^e} \mathbf{B}_0^T P d\Omega_0 \quad \text{or} \quad f_{eI}^{int} = \int_{\Omega_0^e} \frac{\partial N_I}{\partial X} P d\Omega_0 \tag{B2.2.3}$$

$$\mathbf{f}_e^{ext} = \int_{\Omega_0^e} \rho_0 \mathbf{N}^T b d\Omega_0 + (\mathbf{N}^T A_0 \dot{t}_x^0)\Big|_{\Gamma_t^e} \tag{B2.2.4}$$

$$\mathbf{M}_e = \int_{\Omega_0^e} \rho_0 \mathbf{N}^T \mathbf{N} d\Omega_0 \tag{B2.2.5}$$

$$\mathbf{M}\ddot{\boldsymbol{u}} + \mathbf{f}^{int} = \mathbf{f}^{ext} \tag{B2.2.6}$$

Example 2.5.1. Two-Node, Linear Displacement Element. Consider a two-node element shown in Fig. 3. The element shown is initially of length ℓ_0 and constant cross-sectional area A_0 . At any subsequent time t , the length is $\ell(t)$ and the cross-sectional area is $A(t)$; the dependence ℓ and A on time t will not be explicitly noted henceforth. The cross-sectional area of the element is taken to be constant, i.e. independent of X.

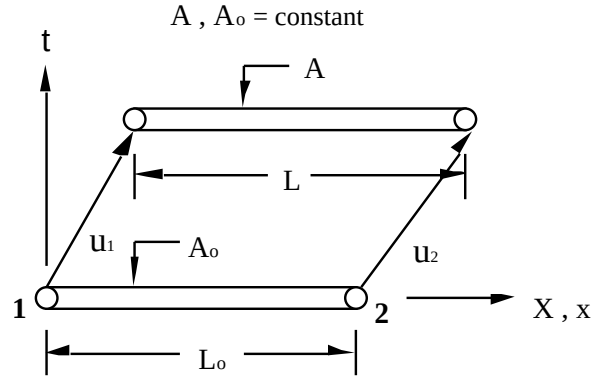

Fig. 2.3. Two node element in one dimension for total Lagrangian formulation showing the initial, undeformed (reference) configuration and the deformed (current) configuration.

Displacement field, strain, and $\mathbf{B}_0$ *matrix*. The displacement field is given by the linear Lagrange interpolant expressed in terms of the material coordinate

$$u(X,t) = \frac{1}{\ell_0}\left[X_2 - X, \quad X - X_1\right]\begin{Bmatrix} u_1(t) \\ u_2(t) \end{Bmatrix} \tag{2.5.18}$$

where $\ell_0 = X_2 - X_1$. The strain measure is evaluated in terms of the nodal displacements by using Eq. (2.5.18) with (B2.2.2):

$$\varepsilon(X,t) = u_{,X} = \frac{1}{\ell_0}\left[-1 \quad +1\right]\begin{Bmatrix} u_1(t) \\ u_2(t) \end{Bmatrix} \tag{2.5.19}$$

The above defines the $\mathbf{B}_0$ matrix to be

$$\mathbf{B}_0 = \frac{1}{\ell_0}\left[-1 \quad +1\right] \tag{2.5.20}$$

Nodal Internal Forces. The internal nodal forces are then given by (2.5.16):

$$\mathbf{f}_e^{int} = \int_{\Omega_0^e} \mathbf{B}_0^{\mathrm{T}} P \, d\Omega_X = \int_{X_1}^{X_2} \frac{1}{\ell_0}\begin{Bmatrix} -1 \\ +1 \end{Bmatrix} P A_0 \, dX \tag{2.5.21a}$$

If we assume that the cross-sectional area and the nominal stress P is constant, the integrand in (2.5.21a) is then constant, so the integral can be evaluated by taking the product of the integrand and the initial length of the element ℓ_0, which gives

$$\mathbf{f}_e^{int} = \begin{Bmatrix} f_1 \\ f_2 \end{Bmatrix}_e^{int} = A_0 P \begin{Bmatrix} -1 \\ +1 \end{Bmatrix} \tag{2.5.21b}$$

From the above, we can see that the nodal internal forces are equal and opposite, so the element internal nodal forces are in equilibrium, even in a dynamic problem. This characteristic of element nodal forces will apply to all elements for which translation results

in no deformation; it does not apply to axisymmetric elements. Since $P = T/A_0$, (see Eq. (2.1.1)) the nodal forces are equal to the load T carried by the element.

Nodal External Forces. The external nodal forces arising from the body force are given by (B2.2.3)

$$\mathbf{f}_e^{ext} = \int_{\Omega_0^e} \rho_0 \mathbf{N}^T b A_0 \, dX = \int_{X_1}^{X_2} \frac{\rho_0}{\ell_0} \begin{Bmatrix} X_2 - X \\ X - X_1 \end{Bmatrix} b A_0 \, dX \tag{2.5.22a}$$

If we approximate the body forces $b(X,t)$ by a linear Lagrange interpolant

$$b(X,t) = b_1(t) \left(\frac{X_2 - X}{\ell_0} \right) + b_2(t) \left(\frac{X - X_1}{\ell_0} \right) \tag{2.5.22b}$$

and taking A_0 to be constant, the evaluation of the integral in (2.5.22a) gives

$$\mathbf{f}_e^{ext} = \frac{\rho_0 A_0 \ell_0}{6} \begin{Bmatrix} 2b_1 + b_2 \\ b_1 + 2b_2 \end{Bmatrix} \tag{2.5.22c}$$

The evaluation of the external nodal forces is facilitated by expressing the integral in terms of a parent element coordinate

$$\xi = (X - X_1) / \ell_0 \,, \quad \xi = [0,1] \tag{2.5.23}$$

Element Mass Matrix. The element mass matrix is given by (B2.2.5):

$$\begin{aligned} \mathbf{M}_e &= \int_{\Omega_0^e} \rho_0 \mathbf{N}^T \mathbf{N} \, d\Omega_0 = \int_0^1 \rho_0 \mathbf{N}^T \mathbf{N} A_0 \ell_0 \, d\xi \\ &= \int_0^1 \rho_0 \begin{Bmatrix} 1-\xi \\ \xi \end{Bmatrix} \begin{bmatrix} 1-\xi & \xi \end{bmatrix} A_0 \ell_0 \, d\xi = \frac{\rho_0 A_0 \ell_0}{6} \begin{bmatrix} 2 & 1 \\ 1 & 2 \end{bmatrix} \end{aligned} \tag{2.5.24a}$$

It can be seen from the above that the mass matrix is independent of time, since it depends only on the initial density, cross-sectional area and length.

The diagonal mass matrix as obtained by the row-sum technique (2.4.26) is

$$\mathbf{M}_e = \frac{\rho_0 A_0 \ell_0}{2} \begin{bmatrix} 1 & 0 \\ 0 & 1 \end{bmatrix} = \frac{\rho_0 A_0 \ell_0}{2} \mathbf{I} \tag{2.5.24b}$$

As can be seen from the above, in the diagonal mass matrix for this element, half of the mass of the element is ascribed to each of the nodes. For this reason, it is often called the lumped mass matrix.

Example 2.5.2. Example of Assembled Equations. Consider a mesh of two elements as shown in Fig. 4. The body force $b(x)$ is constant, b. We will develop the governing equations for this mesh; the equation for the center node is of particular interest since it represents the typical equation for the interior node of any one-dimensional mesh.

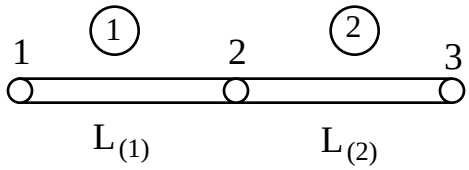

Fig. 4

The connectivity matrices $\mathbf{L}_e$ for this mesh are

$$\mathbf{L}_{(1)} = \begin{bmatrix} 1 & 0 & 0 \\ 0 & 1 & 0 \end{bmatrix} \tag{2.5.25a}$$

$$\mathbf{L}_{(2)} = \begin{bmatrix} 0 & 1 & 0 \\ 0 & 0 & 1 \end{bmatrix} \tag{2.5.25b}$$

The global internal force matrix by Eq. (2.5.5) is given in terms of the element internal forces by

$$\mathbf{f}^{int} = \mathbf{L}_{(1)}^T \mathbf{f}_{(1)}^{int} + \mathbf{L}_{(2)}^T \mathbf{f}_{(2)}^{int} = \begin{Bmatrix} f_1 \\ f_2 \\ 0 \end{Bmatrix}_{(1)}^{int} + \begin{Bmatrix} 0 \\ f_1 \\ f_2 \end{Bmatrix}_{(2)}^{int} \tag{2.5.26}$$

which from (2.5.21b) gives

$$\mathbf{f}^{\text{int}} = A_0^{(1)} P_{(1)} \begin{Bmatrix} -1 \\ +1 \\ 0 \end{Bmatrix} + A_0^{(2)} P_{(2)} \begin{Bmatrix} 0 \\ -1 \\ +1 \end{Bmatrix} \tag{2.5.27}$$

Similarly

$$\mathbf{f}^{ext} = \mathbf{L}_{(1)}^T \mathbf{f}_{(1)}^{ext} + \mathbf{L}_{(2)} \mathbf{f}_{(2)}^{ext} = \begin{Bmatrix} f_1 \\ f_2 \\ 0 \end{Bmatrix}_{(1)}^{ext} + \begin{Bmatrix} 0 \\ f_1 \\ f_2 \end{Bmatrix}_{(2)}^{ext} \tag{2.5.28}$$

and using (2.5.22c) with constant body force gives

$$\mathbf{f}^{ext} = \frac{\rho_0^{(1)} A_0^{(1)} \ell_0^{(1)}}{2} \begin{Bmatrix} b \\ b \\ 0 \end{Bmatrix} + \frac{\rho_0^{(2)} A_0^{(2)} \ell_0^{(2)}}{2} \begin{Bmatrix} 0 \\ b \\ b \end{Bmatrix} \tag{2.5.29}$$

The global, assembled mass matrix is given by (2.5.9)

$$\mathbf{M} = \mathbf{L}_{(1)}^T \mathbf{M}_{(1)} \mathbf{L}_{(1)} + \mathbf{L}_{(2)}^T \mathbf{M}_{(2)} \mathbf{L}_{(2)} \tag{2.5.30}$$

and by (2.5.24a)

$$\mathbf{M} = \mathbf{L}_{(1)}^T \frac{\rho_0^{(1)} A_0^{(1)} \ell_0^{(1)}}{6} \begin{bmatrix} 2 & 1 \\ 1 & 2 \end{bmatrix} \mathbf{L}_{(1)} + \mathbf{L}_{(2)}^T \frac{\rho_0^{(2)} A_0^{(2)} \ell_0^{(2)}}{6} \begin{bmatrix} 2 & 1 \\ 1 & 2 \end{bmatrix} \mathbf{L}_{(2)} \tag{2.5.31}$$

To simplify the form of the assembled equations, we now consider a uniform mesh with constant initial properties, so $\rho_0^{(1)} = \rho_0^{(2)} = \rho_0$, $A_0^{(1)} = A_0^{(2)} = A_0$, $\ell_0^{(1)} = \ell_0^{(2)} = \ell_0$ and we define $m_1 = \left(\rho_0^{(1)} A_0^{(1)} \ell_0^{(1)}\right)/6$, $m_2 = \left(\rho_0^{(2)} A_0^{(2)} \ell_0^{(2)}\right)/6$ so the assembled mass matrix is

$$\mathbf{M} = \begin{bmatrix} 2m_1 & m_1 & 0 \\ m_1 & 2(m_1 + m_2) & m_2 \\ 0 & m_2 & 2m_2 \end{bmatrix} \tag{2.5.32}$$

Writing out the second equation of motion for this system (which is obtained from the second row of $\mathbf{M}$, $\mathbf{f}^{ext}$ and $\mathbf{f}^{int}$) gives

$$\begin{aligned} &\tfrac{1}{6}\rho_0^{(1)} A_0^{(1)} \ell_0^{(1)} \ddot{u}_1 + \tfrac{1}{3}\left(\rho_0^{(1)} A_0^{(1)} \ell_0^{(1)} + \rho_0^{(2)} A_0^{(2)} \ell_0^{(2)}\right) \ddot{u}_2 + \tfrac{1}{6}\rho_0^{(2)} A_0^{(2)} \ell_0^{(2)} \ddot{u}_3 \\ &- A^{(1)} P^{(1)} + A^{(2)} P^{(2)} = \tfrac{b}{2}\left(\rho_0^{(1)} A_0^{(1)} \ell_0^{(1)} + \rho_0^{(2)} A_0^{(2)} \ell_0^{(2)}\right) \end{aligned} \tag{2.5.33}$$

Using uniform properties as before and dividing by $A_0 \ell_0$, we obtain the following equation of motion at node 2:

$$\rho_0\left(\tfrac{1}{6}\ddot{u}_1 + \tfrac{2}{3}\ddot{u}_2 + \tfrac{1}{6}\ddot{u}_3\right) + \frac{P^{(2)} - P^{(1)}}{\ell_0} = \rho_0 b \tag{2.5.34}$$

If the mass matrix is lumped, the corresponding expression is

$$\rho_0 \ddot{u}_2 + \frac{P^{(2)} - P^{(1)}}{\ell_0} = \rho_0 b \tag{2.5.35}$$

The above equation is equivalent to a finite difference expression for the momentum equation (2.2.4) with A_0 constant: it is only necessary to use the central difference expression $P_{,X}\left(X_2\right) = \left(P^{(2)} - P^{(1)}\right)/\ell_0$ to reveal the identity. Thus the finite element procedure appears to be a circuitous way of obtaining what follows simply and directly from a finite difference approximation. The advantage of a finite element approach is that it gives a consistent procedure for obtaining semidiscrete equations when the element lengths, cross-sectional area, and density vary. Furthermore, for linear problems, a finite element solution can be shown to provide the best approximation in the sense that the error is minimized in the energy norm (see Strang and Fix); finite difference approximations for irregular grids and varying areas and densities, on the other hand, are difficult to construct. The finite element method also gives the means of obtaining consistent mass matrices and higher order elements, which are more accurate. But the main advantage of finite element methods, which undoubtedly has been the driving force behind its popularity, is the ease with which it can model complex geometries. This of course is masked in one dimensional problems, but it will become apparent when we study multi-dimensional problems.

Example 2.5.3. Three-node quadratic displacement element. A 3-node element of length L_0 and cross-sectional area A_0 is shown in Fig. 4. Node 2 is placed between nodes 1 and 3; although in this analysis we do not assume it to be midway between the nodes, it is recommended that it be placed midway between the nodes in most models. The mapping between the material coordinates X and the referential coordinate ξ is given by

$$X(\xi) = \mathbf{N}(\xi)\mathbf{X}_e = \begin{bmatrix} \frac{1}{2}\xi(\xi-1) & 1-\xi^2 & \frac{1}{2}\xi(\xi+1) \end{bmatrix} \begin{Bmatrix} X_1 \\ X_2 \\ X_3 \end{Bmatrix} \tag{2.5.36}$$

where $\mathbf{N}(\xi)$ is the matrix of Lagrange interpolants, or shape functions, and ξ is the element coordinate. The displacement field is given by the same interpolants

$$u(\xi,t) = \mathbf{N}(\xi)\mathbf{u}_e(t) = \begin{bmatrix} \frac{1}{2}\xi(\xi-1) & 1-\xi^2 & \frac{1}{2}\xi(\xi+1) \end{bmatrix} \begin{Bmatrix} u_1(t) \\ u_2(t) \\ u_3(t) \end{Bmatrix} \tag{2.5.37}$$

By the chain rule

$$\varepsilon = F-1 = u_{,X} = u_{,\xi}\xi_{,X} = u_{,\xi}X_{,\xi}^{-1} = \frac{1}{2X_{,\xi}}\begin{bmatrix} 2\xi-1 & -4\xi & 2\xi+1 \end{bmatrix}\mathbf{u}_e \tag{2.5.38}$$

We have used the fact that in one dimension, $\xi_{,x} = X_{,\xi}^{-1}$. We can write the above as

$$\varepsilon = \mathbf{B}_0\mathbf{u}_e \text{ where } \mathbf{B}_0 = \frac{1}{2X_{,\xi}}\begin{bmatrix} 2\xi-1 & -4\xi & 2\xi+1 \end{bmatrix}\mathbf{u}_e \tag{2.5.39}$$

The internal nodal forces are given by Eq. (20):

$$\mathbf{f}_e^{int} = \int_{\Omega_0^e}\mathbf{B}_0^T P d\Omega_0 = \int_{-1}^{1}\frac{1}{2X_{,\xi}}\begin{Bmatrix} 2\xi-1 \\ -4\xi \\ 2\xi+1 \end{Bmatrix} PA_0 X_{,\xi}\, d\xi = \int_{-1}^{1}\frac{1}{2}\begin{Bmatrix} 2\xi-1 \\ -4\xi \\ 2\xi+1 \end{Bmatrix} PA_0 d\xi \tag{2.5.40}$$

The above integral is generally evaluated by numerical integration. For the purpose of examining this element further, let $P(\xi)$ be linear in ξ:

$$P(\xi) = P_1\frac{(1-\xi)}{2} + P_3\frac{(1+\xi)}{2} \tag{2.5.41}$$

where P_1 and P_3 are the values of P at nodes 1 and 3, respectively. If $X_{,\xi}$ is constant, this is an exact representation for the stress field in a material which is governed by a linear stress-strain relation in these measures, Eq. (2.2.14), since F is linear in ξ by (2.5.40). The internal forces are then given by

$$\mathbf{f}_e^{int} = \begin{Bmatrix} f_1 \\ f_2 \\ f_3 \end{Bmatrix}_e^{int} = \frac{A_0}{6} \begin{Bmatrix} -5P_1 - P_2 \\ 4P_1 - 4P_2 \\ P_1 + 5P_2 \end{Bmatrix} \tag{2.5.42}$$

When P is constant, the nodal force at the center node vanishes and the nodal forces at the end nodes are equal and opposite with magnitude $A_0 P$, as in the two node element. In addition, for any values of P_1 and P_2, the sum of the nodal forces vanishes, which can be seen by adding all the nodal forces. Thus this element is also in equilibrium.

The external nodal forces are

$$\mathbf{f}_e^{ext} = \int_{-1}^{+1} \begin{Bmatrix} \frac{1}{2}\xi(\xi-1) \\ 1-\xi^2 \\ \frac{1}{2}\xi(\xi+1) \end{Bmatrix} \rho_0 b A_0 X_{,\xi}\, d\xi + \begin{Bmatrix} \frac{1}{2}\xi(\xi-1) \\ 1-\xi^2 \\ \frac{1}{2}\xi(\xi+1) \end{Bmatrix} A_0 \bar{t}_x^0 \Big|_{\Gamma_t^e} \tag{2.5.43}$$

where the shape functions in the last term are either one or zero at a traction boundary. Using $X_{,\xi} = \xi\left(X_1 + X_3 - 2X_2\right) + \frac{1}{2}\left(X_3 - X_1\right)$, then

$$\mathbf{f}_e^{ext} = \frac{\rho_0 b A_0}{6} \begin{Bmatrix} L_0 - 2\left(X_1 + X_3 - 2X_2\right) \\ 4L_0 \\ L_0 + 2\left(X_1 + X_3 - 2X_2\right) \end{Bmatrix} + \begin{Bmatrix} \frac{1}{2}\xi(\xi-1) \\ 1-\xi^2 \\ \frac{1}{2}\xi(\xi+1) \end{Bmatrix} A_0 \bar{t}_x^0 \Big|_{\Gamma_t^e} \tag{2.5.44}$$

Element Mass Matrix. The element mass matrix is

$$\begin{aligned} \mathbf{M}_e &= \int_{-1}^{+1} \begin{Bmatrix} \frac{1}{2}\xi(\xi-1) \\ 1-\xi^2 \\ \frac{1}{2}\xi(\xi+1) \end{Bmatrix} \left[\frac{1}{2}\xi(\xi-1) \quad 1-\xi^2 \quad \frac{1}{2}\xi(\xi+1) \right] \rho_0 A_0 X_{,\xi}\, d\xi \\ &= \frac{\rho_0 A_0}{30} \begin{bmatrix} 4L_0 - 6\left(X_1 + X_3 - 2X_2\right) & 2L_0 - 4\left(X_1 + X_3 - 2X_2\right) & -L_0 \\ & 16L_0 & 2L_0 + 4\left(X_1 + X_3 - 2X_2\right) \\ sym & & 4L_0 - 6\left(X_1 + X_3 - 2X_2\right) \end{bmatrix} \end{aligned} \tag{2.5.45}$$

If the node 2 is at the midpoint of the element, i.e., $X_1 + X_3 = 2X_2$, we have

$$\mathbf{M}_e = \frac{\rho_0 A_0 L_0}{30} \begin{bmatrix} 4 & 2 & -1 \\ 2 & 16 & 2 \\ -1 & 2 & 4 \end{bmatrix} \tag{2.5.46}$$

If the mass matrix is diagonalized by the row-sum technique, we obtain

$$\mathbf{M}_e = \frac{\rho_0 A_0 L_0}{6} \begin{bmatrix} 1 & 0 & 0 \\ 0 & 4 & 0 \\ 0 & 0 & 1 \end{bmatrix} \tag{2.5.47}$$

This results displays one of the shortcomings of diagonal masses for higher order elements: most of the mass is lumped in the center node. This results in rather strange behavior when

high order modes are excited. Therefore, high order elements are usually avoided when a lumped mass matrix is necessary for efficiency.

2.6 Governing Equations for Updated Lagrangian Formulation

In the updated Lagrangian formulation, the discrete equations are formulated in the current configuration. The stress is measured by the Cauchy (physical) stress σ given by Eq. (2.1.1). In the updated Lagrangian formulation, variables need to be expressed in terms of the spatial coordinates x and the material coordinates X in different equations. The dependent variables are chosen to be the stress $\sigma(X,t)$ and the velocity $v(X,t)$. This choice differs from the total Lagrangian formulation, where we have used the displacement $u(X,t)$ as the independent variable; this is only a formal difference since the displacement and velocities are both computed in a numerical implementation.

In developing the updated Lagrangian formulation, we will need the dependent variables to be expressed in terms of the Eulerian coordinates. Conceptually this is a simple matter, for we can invert (2.2.1) to obtain

$$X = \varphi^{-1}(x,t) \equiv X(x,t) \tag{2.6.1}$$

Any variable can then be expressed in terms of the Eulerian coordinates; for example $\sigma(X,t)$ can be expressed as $\sigma(X(x,t),t)$. While the inverse of a function can easily be written in symbolic form, in practice the construction of an inverse function in closed form is difficult, if not impossible. Therefore the standard technique in finite elements is to express variables in terms of element coordinates, which are sometimes called parent coordinates or natural coordinates. By using element coordinates, we can always express a function, at least implicitly, in terms of either the Eulerian and Lagrangian coordinates.

In updated Lagrangian formulations, the strain measure is the rate-of-deformation given by

$$D_x = \frac{\partial v}{\partial x} \tag{2.6.2a}$$

This is also called the velocity-strain or stretching. It is a rate measure of strain, as indicated by two of the names. It is shown in Chapter 3 that

$$\int_0^t D_x(X,\bar{t})\,d\bar{t} = ln\ F(X,t) \tag{2.6.2b}$$

in one dimension, so the time integral of the rate-of-deformation corresponds to the "natural" or "logarithmic" strain in one dimension; as discussed in Chapter 3, this does not hold for multi-dimensional states of strain.

The governing equations for the nonlinear dimensional continuum are:

1. conservation of mass (continuity equation)

$$\rho J = \rho_0 \quad \text{or} \quad \rho F A = \rho_0 A_0 \tag{2.6.3}$$

2. conservation of momentum

$$\frac{\partial}{\partial x}(A\sigma) + \rho A b = \rho A \dot{v} \ \text{ or } \ (A\sigma)_{,x} + \rho A b = \rho A \dot{v} \tag{2.6.4}$$

3. measure of deformation

$$D_x = \frac{\partial v}{\partial x} \quad \text{or} \quad D_x = v_{,x} \tag{2.6.5}$$

4. constitutive equation
in total form

$$\sigma(X,t) = S^{\sigma D}\left(D_x(X,t)D_x(X,t),\ldots\right),\int_0^t D_x\left(X,\tilde{t}\right)d\tilde{t},\sigma\left(X,\tilde{t}\right),\tilde{t}\le t,\ etc.) \tag{2.6.6a}$$

in rate form

$$\sigma_{,t}(X,t) = S_t^{\sigma D}\left(D_x\left(X,\tilde{t}\right),\sigma\left(X,\tilde{t}\right),\ etc.,\tilde{t}\le t\right) \tag{2.6.6b}$$

energy conservation

$$\rho\dot{w}^{int} = \sigma D_x - q_{x,x} + \rho s, \quad q_x = \text{heatflux},\ s = \text{heatsource} \tag{2.6.7}$$

The mass conservation equation in the updated Lagrangian formulation is the same as in the total Lagrangian formulation. The momentum equation in the updated formulation involves derivatives with respect to the Eulerian coordinates, whereas in the total Lagrangian formulation, derivatives were with respect to Lagrangian coordinates; in addition, the nominal stress is replaced by the Cauchy stress, and that the current values of the cross-sectional area A and density ρ are used. The constitutive equation as written here relates the rate-of-deformation $D_x(X,t)$ or its integral, the logarithmic strain, to the Cauchy stress or its rate. Note that the constitutive equation is written in terms of material coordinates. The subscript "t" on (2.6.6b) indicates that the constitutive equation is a rate equation. We can also use a constitutive equation expressed in terms of the nominal stress and the stretch ε. It would then be necessary to transform the stress to the Cauchy stress before using the momentum equation and use a different measure of strain. Thus in the updated Lagrangian formulation, some of the system equations are in terms of Eulerian coordinates, while others (mass conservation and constitutive equations) are in terms of Lagrangian coordinates.

The subscripts have been appended to the constitutive function to indicate which stress and strain measures are related by the constitutive equation. The constitutive equation depends on the stress and strain measures which are involved. For example, the constitutive equation for a hypoelastic material in terms of the Cauchy stress and rate-of-deformation is

$$\sigma_{,t}(X,t) = E^{\sigma D} D_x(X,t) \tag{2.6.8}$$

where $E^{PF} \neq E^{\sigma D}$. To see the relationship between the two moduli, we use the relation

$$D_x = \frac{\partial v}{\partial x} = \frac{\partial v}{\partial X}\frac{\partial X}{\partial x} = \frac{\partial v}{\partial X}F^{-1} = \dot{F}F^{-1} \tag{2.6.9}$$

where the first equality is the definition (2.6.5), the second stems from the chain rule, and the third from the definition of F, Eq. (2.2.4). Then inserting Eqs. (2.2.9) and (2.6.9) in (2.6.8) gives

$$A_0 \frac{d}{dt}\left(\frac{P}{A}\right) = E^{\sigma D}\dot{F}F^{-1} \tag{2.6.10}$$

which after some manipulation yields

$$\dot{P} = \frac{A}{A_0 F} E^{\sigma D}\dot{F} + \frac{\sigma}{A_0}\dot{A} \tag{2.6.11}$$

In general, constitutive equations are not easily converted from one stress-strain pair to another. For the above, the cross-sectional area must be known as a function of the elongation to make the conversion.

The boundary conditions are

$$v(X,t) = \bar{v}(t) \text{ on } \Gamma_v \tag{2.6.12}$$

$$n\sigma(X,t) = \bar{t}_x(t) \text{ on } \Gamma_t \tag{2.6.13}$$

where $\bar{v}(t)$ and $\bar{t}_x(t)$ are the prescribed velocity and traction, respectively, and n is the normal to the domain. While the boundary condition is specified as applying to the velocity, any velocity boundary condition is also a displacement boundary condition. Note that the traction always carries a subscript to distinguish it from the time t. The relation between the traction and velocity boundaries is the same as in (2.2.30):

$$\Gamma_v \quad \Gamma_t = \Gamma \qquad \Gamma_v \cap \Gamma_t = 0 \tag{2.6.14}$$

The boundary over which the velocity is prescribed is denoted by Γ_v; it is an essential boundary condition and it plays the same role as Γ_u in the total Lagrangian formulation. The tractions in (2.6.13) are physical tractions, force per current area. They are related to the tractions on the undeformed area by

$$\bar{t}_x A = \bar{t}_x^0 A_0 \tag{2.6.15}$$

In addition we have the stress jump conditions, the counterpart of (2.2.33):

$$\langle \sigma A \rangle = 0 \tag{2.6.16}$$

The initial conditions are

$$\sigma(X,0) = \sigma_0(X) \tag{2.6.17}$$

$$v(X,0) = v_0(X) \tag{2.6.18}$$

Since we have chosen the velocity and the stresses as the dependent variables, the initial conditions are imposed on these variables. In most practical problems, this choice of initial conditions is more practical than conditions on velocities and displacements, as indicated in Chapter 4.

2.7 Weak Form for Updated Lagrangian Formulation

In this Section, the weak form or variational form for the momentum equation is developed. Recall that the dependent variables are the velocity $v(X,t)$ and the stress $\sigma(X,t)$.

The conditions on the trial functions $v(X,t)$ and the test functions $\delta v(X)$ are:

$$v(X,t) \quad U \qquad U = \left\{ v(X,t) \middle| v \quad C^0(X),\ v = \bar{v} \ \ on\ \Gamma_v \right\} \tag{2.7.1}$$

$$\delta v(X) \quad U_0 \qquad U_0 = \left\{ \delta v(X) \middle| \delta v \quad C^0(X),\ \delta v = 0 \ \ on\ \Gamma_v \right\} \tag{2.7.2}$$

These admissibility conditions are identical to those for the test and trial displacements in the total Lagrangian formulation. As in the total Lagrangian formulation, the stress $\sigma(X,t)$ is assumed to be a C^{-1} function in space. The current domain is $\left[x_a(t), x_b(t) \right]$, where $x_a = \varphi(X_a, t),\ x_b = \varphi(X_b, t)$.

The strong form consists of the momentum equation (2.6.4), the traction boundary conditions and the jump conditions. The weak form is developed by multiplying the momentum equation (2.6.12) by the test function $\delta v(X)$ and integrating over the current domain. The current domain of the body is appropriate, since the momentum equation involves derivatives with respect to the spatial (Eulerian) coordinates. This gives

$$\int_{x_a}^{x_b} \delta v \left((A\sigma)_{,x} + \rho A b - \rho A \frac{Dv}{Dt} \right) dx = 0 \tag{2.7.3}$$

Integration by parts is performed as in Section 2.3 (see Eqs. (2.3.2) to (2.3.4)), which gives

$$\int_{x_a}^{x_b} \delta v (A\sigma)_{,x}\, dx = \int_{x_a}^{x_b} \left[(\delta v A \sigma)_{,x} - \delta v_{,x} A \sigma \right] dx$$

$$= (\delta v A n \sigma)\big|_{\Gamma_t} - \sum_i \delta v \langle A\sigma \rangle_{\Gamma_i} - \int_{x_a}^{x_b} \delta v_{,x} A \sigma \, dx \tag{2.7.4}$$

where Γ_i are the points of discontinuity of $A\sigma$; see Eq. (2.6.16). We have used the fundamental theorem of calculus to convert a line (domain) integral to a sum of point (boundary and jump) values, with Γ changed to Γ_t because $\delta v(X) = 0$ on Γ_v; see Eq. (2.7.2). Since the strong form holds, the traction boundary condition (2.6.13) gives $n\sigma = \bar{t}_x$ and the jump condition $\langle n\sigma \rangle = 0$, which when substituted into the above give

$$\int_{x_a}^{x_b} \left(\delta v_{,x} A \sigma - \delta v \left(\rho A b - \rho A \frac{Dv}{Dt} \right) \right) dx - \left(\delta v A \bar{t}_x \right)\big|_{\Gamma_t} = 0 \tag{2.7.5}$$

This weak form is often called the principle of virtual power (or principle of virtual velocities, see Malvern (1969), p. 241). If the test function is considered a velocity, then each term in the above corresponds to a variation of power, or rate of work; for example $\rho A b dx$ is a force, and when multiplied by $\delta v(X)$ gives a variation in power. Therefore, the terms in the above weak form will be distinguished form the principle of virtual work in Section (2.3) by designating each term by P with the appropriate superscript. However, it should be stressed that this physical interpretation of the weak form is entirely a matter of choice; the test function $\delta v(X)$ need not be attributed any of the properties of a velocity; it can be any function which satisfies Eq. (2.7.2).

We define the virtual internal power by

$$\delta P^{int} = \int_{x_a}^{x_b} \delta v_{,x} \sigma A dx = \int_{x_a}^{x_b} \delta D \sigma A dx = \int_{\Omega} \delta D \sigma d\Omega \tag{2.7.6}$$

where the second equality is obtained by taking a variation of (2.6.5), i.e., $\delta D_x = \delta v_{,x}$, while the third equality results from the relation $d\Omega = A dx$ which parallels (2.5.20). The integral in Eq. (2.7.6) corresponds to the internal energy rate in the energy conservation equation (2.6.7) except that the rate-of-deformation D is replaced by δD, so designating this term as a virtual internal power is consistent with the energy equation.

The virtual powers due to external and inertial forces are defined similarly:

$$\delta P^{ext} = \int_{x_a}^{x_b} \delta v \rho b A dx + \left(\delta v A \bar{t}_x \right)\Big|_{\Gamma_t} = \int_{\Omega} \delta v \rho b d\Omega + \left(\delta v A \bar{t}_x \right)\Big|_{\Gamma_t} \tag{2.7.7}$$

$$\delta P^{inert} = \int_{x_a}^{x_b} \delta v \rho \frac{Dv}{Dt} A dx = \int_{\Omega} \delta v \rho \frac{Dv}{Dt} d\Omega \tag{2.7.8}$$

Using Eqs. (2.7.6-2.7.8). the weak form (2.7.5) can then be written as

$$\delta P = \delta P^{int} - \delta P^{ext} + \delta P^{inert} = 0 \tag{2.7.9}$$

where the terms are defined above. In summary, the principle of virtual power states that

$$\text{if } v(X,t) \in U \text{ and } \delta P = 0 \qquad \delta v(X) \in U_0 \tag{2.7.10}$$

then the momentum equation (2.6.4), the traction boundary conditions (2.6.13) and the jump conditions are satisfied. The validity of this principle can be established by simply reversing the steps used to obtain Eq. (2.7.5). All of the steps are reversible so we can deduce the strong form from the weak form.

The key difference of this weak form, as compared to the weak form for the total Lagrangian formulation, is that all integrals are over the current domain and are expressed in terms of variables which have a spatial character. However, the two weak forms are just different forms of the same principle; it is left as an Exercise to show that the principle of virtual work can be transformed to the principle of virtual power by using transformations on the integrals and the variables.

Exercise. Replace the virtual displacement in the principle of virtual work by a velocity and use the relations to show that it can be transformed into the principle of virtual power.

2.8. Element Equations for Updated Lagrangian Formulation

We will now develop the updated Lagrangian formulation. As will become clear, the updated Lagrangian formulation is simply a transformation of the total Lagrangian formulation. Numerically, the discrete equations are identical, and in fact, as we shall see, we can use the total Lagrangian formulation for some of the nodal forces and the updated for others in the same program. Students often ask why both methods are presented when they are basically identical. We must confess that the major reason for presenting both formulations today is that both are widely used, so to understand today's software and literature, a familiarity with both formulations is essential. However, in a first course, it is often useful to skip one of these Lagrangian formulations.

The domain is subdivided into elements Ω_e, so that $\Omega = \Omega_e$. The coordinates of the nodes in the initial configuration are given by $X_1, X_2, \ldots X_{n_N}$ and the positions of the nodes are given by $x_1(t), x_2(t), \ldots x_m(t)$. The m nodes of element e in the initial configuration be denoted by $X_1^e, X_2^e, \ldots X_m^e$, and the positions of these nodes in the current configuration be given by $x_1^e(t), x_2^e(t), \ldots x_m^e(t)$. The spatial coordinates of the nodes are given by the finite element approximation to the motion

$$x_I(t) = x\left(X_I, t\right) \tag{2.8.1}$$

Thus each node of the mesh remains coincident with a material point.

We will develop the equations on an element level and then obtain the global equations by assembly using the scheme described in Section 2.5. As before, the relationships between the terms of the virtual power expression and the corresponding nodal forces along with the physically motivated names will be employed to systematize the procedure.

The dependent variables in this development will be the velocity and the stress. The constitutive equation, combined with the expression for the velocity-strain, and the mass conservation equation are treated in strong form, the momentum equation in weak form. The mass conservation equation can be used to easily compute the density at any point since it is a simple algebraic equation. We develop the equations as if there were no essential boundary conditions and then impose these subsequently.

The velocity field in each element is approximated by

$$v(X,t) = \sum_{I=1}^{m} N_I(X)\, v_I^e(t) = \mathbf{N}(X)\, \mathbf{v}_e(t) \tag{2.8.2}$$

Although the shape functions are functions of the material coordinates X, they can be expressed in terms of spatial coordinates. For this purpose, the mapping $x = \varphi(X,t)$ is inverted to give $X = \varphi^{-1}(x,t)$ so the velocity field is

$$v(x,t) = \mathbf{N}\left(\varphi^{-1}(x,t)\right)\mathbf{v}^e(t) \tag{2.8.3}$$

Although developing the inverse mapping is often impossible, partial derivatives with respect to the spatial coordinates can be obtained by implicit differentiation, so the inverse mapping need never be calculated.

The acceleration field is given by taking the material time derivative of (2.8.2), which gives

$$\dot{v}(X,t) = \mathbf{N}(X)\dot{\mathbf{v}}(t) \equiv \mathbf{N}(X)\mathbf{a}(t) \tag{2.8.4}$$

It can be seen from this step that it is crucial that the shape functions be expressed as functions of the *material coordinates*. If the shape functions are expressed in terms of the Eulerian coordinates by

$$v(x,t) = \mathbf{N}(x)\,\mathbf{v}^e(t) = \mathbf{N}\left(\varphi(X,t)\right)\mathbf{v}^e(t) \tag{2.8.5}$$

then material time derivative of the shape functions does not vanish and the accelerations cannot be expressed as a product of the same shape functions and nodal accelerations. Therefore, the shape functions are considered to be functions of the material coordinates in the updated Lagrangian method. In fact, expressing the shape functions in terms of spatial coordinates is incompatible with a Lagrangian mesh, since we need to approximate the velocity in an element, which is a material subdomain.

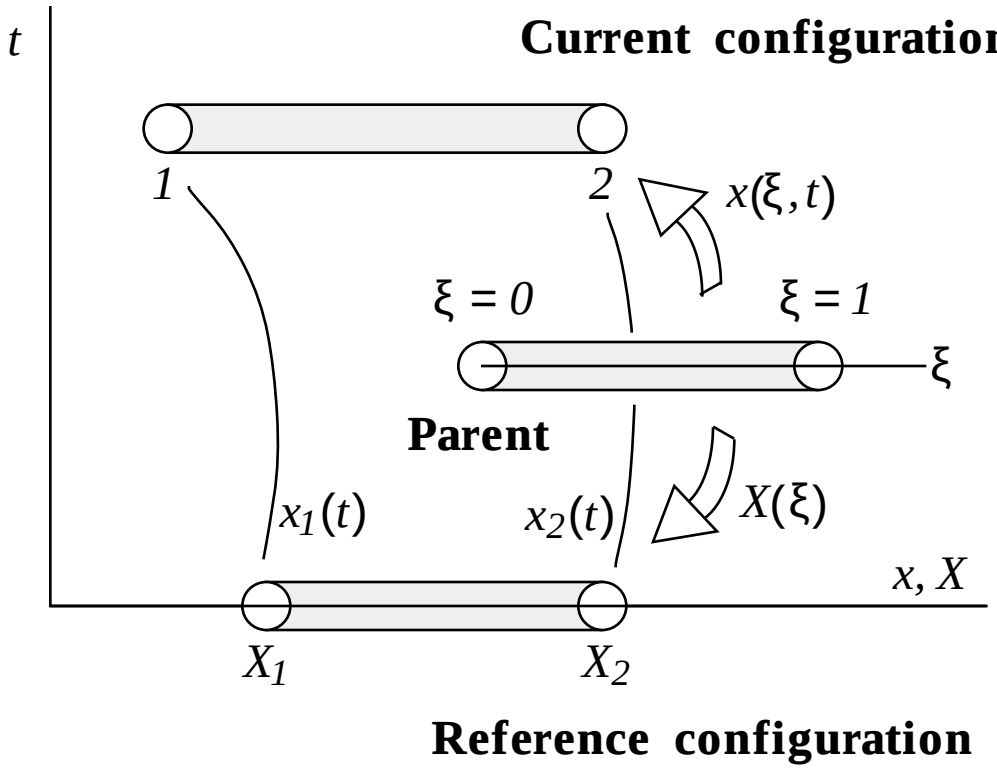

Fig. 2.5. Role of parent configuration, showing mappings to the initial, undeformed configuration and the current, deformed configuration in a Lagrangian mesh.

Element Coordinates. Calculations in the updated Lagrangian formulation are usually performed in the element coordinate system ξ in the parent domain. This is in fact simpler than working in the spatial domain. We have already used element coordinates to simplify the evaluation of element nodal forces in the examples. Element coordinates, such as triangular coordinates and isoparametric coordinates, are particularly convenient for multi-dimensional elements.

Consider Fig. 2.5, which shows a two-node element in the initial and current configurations and the parent domain, which is the interval $0 \le \xi \le 1$. The parent domain can be mapped onto the initial and current configurations as shown. For example, in the two-node element, the mapping between the element coordinates and the Eulerian coordinates is given by

$$x(\xi,t) = x_1(t)(1-\xi) + x_2(t)\xi \tag{2.8.6}$$

or for a general one dimensional element as

$$x(\xi,t) = \mathbf{N}(\xi)\mathbf{x}^e(t) \tag{2.8.7}$$

Specializing the above to the initial time gives the map between the parent domain and the initial configuration

$$X(\xi) = \sum_{I=1}^{m} N_I(\xi) X_I^e = \mathbf{N}(\xi)\mathbf{X}_e \tag{2.8.8}$$

which for the two-node element is

$$X(\xi) = X_1(1-\xi) + X_2\xi \tag{2.8.9}$$

The mapping between the Eulerian coordinates and the element coordinates, (2.8.6), changes with time, while the map between the initial configuration and the element domain is time invariant in a Lagrangian mesh. Therefore shape functions expressed in terms of the element coordinates by (2.8.8) will be independent of time. If the initial map is such that every point in the parent element ξ maps onto a unique point of the initial configuration, and for every point X there exists a point ξ, then the parent element coordinates can serve as material labels. Such a map is called one-to-one and onto. The map between the parent domain and the current configuration must be one-to-one and onto for all time; this is discussed further in Example 2.8.3 and Chapter 3.

As shown in Fig. 2.5, at any time the shape functions can be used to map between the current and parent element configurations. Thus the element coordinates provide a link between the initial configuration and the current configuration of the element which can be used in the evaluation of derivatives and integrals.

It follows from Eqs. (2.8.7) and (2.8.8) that the displacements can also be interpolated by the same shape functions since

$$u(\xi,t) = x(\xi,t) - X(\xi) = \mathbf{N}(\xi)\left(\mathbf{x}^e(t) - \mathbf{X}^e\right) = \mathbf{N}(\xi)\mathbf{u}^e(t) \tag{2.8.10}$$

The velocities and accelerations are also given by material derivatives of the displacement, while the test function is given by the same shape functions, so

$$v(\xi,t) = \mathbf{N}(\xi)\mathbf{v}_e(t) \qquad a(\xi,t) = \mathbf{N}(\xi)\ddot{\mathbf{u}}_e(t) \qquad \delta v(\xi,t) = \mathbf{N}(\xi)\delta v_e \tag{2.8.11}$$

since the shape functions are independent of time.

Using Eqs. (2.8.2) and (2.6.5) and noting Eq.(2.8.3), the rate-of-deformation can be expressed in terms of the shape functions by

$$D_x(x,t) = v_{,x}(x,t) = \mathbf{N}_{,x}\left(X(x,t)\right)\mathbf{v}^e(t) \tag{2.8.12}$$

where we have indicated the implicit dependence of the shape functions on the Eulerian coordinates. The rate-of deformation will be expressed in terms of nodal velocities via a **B** matrix by

$$D_x = v_{,x} = \mathbf{B}\mathbf{v}^e = \sum_{I=1}^{m} B_I v_I^e \tag{2.8.13}$$

where

$$\mathbf{B} = \mathbf{N}_{,x} \quad \text{or} \quad B_I = N_{I,x} \tag{2.8.14}$$

This $\mathbf{B}$ matrix differs from the $\mathbf{B}_0$ matrix used in the total Lagrangian formulation in that the derivatives are taken with respect to the Eulerian coordinates..

To compute the spatial derivative of the shape function, we use the chain rule

$$\mathbf{N}_{,\xi} = \mathbf{N}_{,x} x_{,\xi} \quad \text{so} \quad \mathbf{N}_{,x} = \mathbf{N}_{,\xi} x_{,\xi}^{-1} \tag{2.8.15}$$

From the above, it follows that

$$D_x(\xi, t) = x_{,\xi}^{-1} \mathbf{N}_{,\xi}(\xi) \mathbf{v}^e(t) = \mathbf{B}(\xi) \mathbf{v}^e(t) \qquad \mathbf{B}(\xi) = \mathbf{N}_{\xi} x_{\xi}^{-1} \tag{2.8.16}$$

Internal and External Nodal Forces. We now use the procedure given in Sections 2.4 and 2.5 to determine nodal forces corresponding to each term of the weak form on an element level. The assembled equations and essential boundary conditions are developed subsequently. The internal nodal forces will be developed from the virtual internal power. Defining the element internal nodal forces so that the scalar product with the virtual velocities gives the internal virtual power, then from (2.7.6) and (2.8.13) we can write

$$\delta P_e^{int} \equiv \delta \mathbf{v}_e^T \mathbf{f}_e^{int} = \int_{x_1^e(t)}^{x_m^e(t)} \delta v_{,x}^T \sigma A dx = \delta \mathbf{v}_e^T \int_{x_1^e(t)}^{x_m^e(t)} \mathbf{N}_{,x}^T \sigma A dx \tag{2.8.17}$$

The transpose is taken of the first term in the integrand even though it is a scalar so that the expression remains consistent when δv is replaced by a matrix product. From the arbitrariness of $\delta \mathbf{v}_e$, it follows that

$$\mathbf{f}_e^{int} = \int_{x_1^e(t)}^{x_m^e(t)} \mathbf{N}_{,x}^T \sigma A dx \equiv \int_{x_1^e(t)}^{x_m^e(t)} \mathbf{B}^T \sigma A dx \quad \text{or} \quad \mathbf{f}_e^{int} = \int_{\Omega^e(t)} \mathbf{B}^T \sigma \, d\Omega \tag{2.8.18}$$

We have explicitly indicated the time dependence of the limits of integration of the integrals to emphasize that the domain of integration varies with time. The internal nodal forces can then be evaluated in terms of element coordinates by transforming (2.8.18) to the parent domain and using the above with $dx = x_{,\xi} d\xi$, giving

$$\mathbf{f}_e^{int} = \int_{x_1^e(t)}^{x_m^e(t)} \mathbf{N}_{,x}^T \sigma A dx = \int_{\xi_1}^{\xi_m} \mathbf{N}_{,\xi}^T x_{,\xi}^{-1} \sigma A x_{,\xi} d\xi = \int_{\xi_1}^{\xi_m} \mathbf{N}_{,\xi}^T \sigma A d\xi \tag{2.8.19}$$

The last form in the above is nice, but this simplification can be made only in one dimension.

The external nodal forces are obtained from the expression for virtual external power (2.7.7):

$$\delta P_e^{ext} = \delta \mathbf{v}_e^T \mathbf{f}_e^{ext} = \int_{\Omega_t^e} \delta v^T \rho b d\Omega + \left(\delta v^T A \dot{t}_x \right) \Big|_{\Gamma_t} \tag{2.8.20}$$

Substituting (2.8.11) into the right hand side of the above and using the arbitrariness of $\delta \mathbf{v}_e$ gives

$$\mathbf{f}_e^{ext} = \int_{x_1^e}^{x_m^e} \mathbf{N}^T \rho b A dx + \left(\mathbf{N}^T A \bar{t}_x \right)\Big|_{\Gamma_t^e} = \int_{\Omega^e(t)} \mathbf{N}^T \rho b \, d\Omega + \left(\mathbf{N}^T A \bar{t}_x \right)\Big|_{\Gamma_t^e} \tag{2.8.21}$$

where the second term contributes only when the boundary coincides with a node of the element.

Mass Matrix. The inertial nodal forces and mass matrix are obtained from the virtual inertial power (2.7.8):

$$\delta P^{inert} = \delta \mathbf{v}_e^T \mathbf{f}_e^{inert} = \int_{x_1(t)}^{x_m(t)} \delta v^T \rho \frac{Dv}{Dt} A dx \tag{2.8.22}$$

Substituting (2.8.11) into the above yields

$$\mathbf{f}_e^{inert} = \int_{x_1(t)}^{x_m(t)} \rho \mathbf{N}^T \mathbf{N} A dx \, \dot{\mathbf{v}}^e = \mathbf{M}^e \dot{\mathbf{v}}^e \tag{2.8.23}$$

where the inertial force has been written as the product of a mass matrix **M** and the nodal accelerations. The mass matrix is given by

$$\mathbf{M}^e = \int_{x_1(t)}^{x_m(t)} \rho \mathbf{N}^T \mathbf{N} A \, dx = \int_{\Omega_e(t)} \rho \mathbf{N}^T \mathbf{N} \, d\Omega \tag{2.8.24}$$

The above form is inconvenient because it suggests that the mass matrix is a function of time, since the limits of integration and the cross-sectional area are functions of time. However, if we use the mass conservation equation (2.2.10) in the form $\rho_0 A_0 dX = \rho A dx$, we can obtain a time invariant form. Substituting the (2.2.10) into (2.8.24) gives

$$\mathbf{M}^e = \int_{X_1}^{X_m} \rho_0 \mathbf{N}^T \mathbf{N} A_0 dX \tag{2.8.25}$$

This formula for the mass matrix is identical to the expression developed for the total Lagrangian formulation, (2.4.11). The advantage of this expression is that it clearly shows that the mass matrix in the updated Lagrangian formulation does not change with time and therefore need not be recomputed during the simulation, which is not clear from (2.8.24). We will see shortly that any nodal force for a Lagrangian mesh can be computed by either the total or updated Lagrangian formalism. The one which is chosen is purely a matter of convenience. Since it is more convenient and illuminating to evaluate the mass matrix in the total Lagrangian form, this has been done.

Equivalence of Updated and Total Lagrangian Formulations. The internal and external nodal forces in the updated and total Lagrangian formulations can be shown to be

identical. To show the identity for the nodal internal forces, we express the spatial derivative of the shape function in terms of the material derivative by the chain rule:

$$\mathbf{N}_{,x}(X) = N_{,X}\frac{\partial X}{\partial x} = \mathbf{N}_{,X}\,F^{-1} = \mathbf{B}_0 F^{-1} \tag{2.8.26}$$

From the first equality we have $\mathbf{N}_{,x}dx = N_{,X}dX$, and substituting this into (2.8.18) gives

$$\mathbf{f}_e^{int} = \int_{x_1(t)}^{x_m(t)} \mathbf{N}_{,x}^T \sigma A dx = \int_{X_1}^{X_m} \mathbf{N}_{,X}^T \sigma A dX \tag{2.8.27}$$

where the limits of integration in the third expression have been changed to the material coordinates of the nodes since the integral has been changed to the initial configuration. If we now use the identity $\sigma A = PA_0$, Eq.(2.2.9), we obtain from the above that

$$\mathbf{f}_e^{int} = \int_{X_1}^{X_m} \mathbf{N}_{,X}^T P A_0\, dX \tag{2.8.28}$$

This expression is identical to the expression for the internal nodal forces in the total Lagrangian formulation, (2.5.14). Thus the expressions for the internal nodal forces in the updated and total Lagrangian formulations are simply two ways of expressing the same thing.

The equivalence of the external nodal forces is shown by using the conservation of mass equation, (2.2.10). Starting with (2.8.21) and using the (2.2.10) gives

$$\mathbf{f}_e^{ext} = \int_{x_1^e}^{x_m^e} \mathbf{N}^T \rho b A dx + \left(\mathbf{N}^T A \bar{t}_x\right)\Big|_{\Gamma_t^e} = \int_{X_1}^{X_m} \mathbf{N}^T \rho_0 b\, A_0 dX + \left(\mathbf{N}^T A_0 \bar{t}_x^0\right)\Big|_{\Gamma_t^e} \tag{2.8.29}$$

where we have used the identity $t_x A = t_x^0 A_0$ in the last term. The above is identical to (2.4.8), the expression in the total Lagrangian formulation.

From this and the identity of the expression for the mass matrix, it can be seen that the total and updated Lagrangian formulations simply provide alternative expressions for the same nodal force vectors. The formulation which is used is simply a matter of convenience. Moreover, it is permissible to use either of these formulations for different nodal forces in the same calculation. For example, the internal nodal forces can be evaluated by an updated Lagrangian approach and the external nodal forces by a total Lagrangian approach in the same calculation. Thus the total and updated Lagrangian formalisms simply reflect different ways of describing the stress and strain measures and different ways of evaluating derivatives and integrals. In this Chapter, we have also used different dependent variables in the two formulations, the velocity and stress in the updated formulations, the nominal stress and the displacement in the total formulation. However, this difference is not tied to the type of Lagrangian formulation, and we have done this only to illustrate how different independent variables can be used in formulating the continuum mechanics problem. We could have used the displacements as the dependent variables in the updated Lagrangian formulation just as well.

Assembly, Boundary Conditions and Initial Conditions. The assembly of the element matrices to obtain the global equations is identical to the procedure described for the total Lagrangian formulation in Section 2.5. The operations of gather are used to obtain the nodal velocities of each element, from which the strain measure, in this case the rate-of-deformation, can be computed in each element. The constitutive equation is then used to evaluate the stresses, from which the nodal internal forces can be computed by (2.8.19). The internal and external nodal forces are assembled into the global arrays by the scatter operation. Similarly, the imposition of essential boundary conditions and initial conditions is identical and described in Section 2.4. The resulting global equations are identical to (2.4.17) and (2.4.15). Initial conditions are now needed on the velocities and stresses. For an unstressed body at rest, the initial conditions are given by

$$v_I = 0,\ I = 1 \text{to } n_N \qquad \sigma_I = 0,\ I = 1 \text{ to } n_Q \tag{2.8.30}$$

That initial conditions in terms of the stresses and velocities is more appropriate for engineering problems is discussed in Section 4.2. Nonzero initial values can be fit by an L_2 projection described at the end of Section 2.4.

Box 2.3 Updated Lagrangian Formulation

$$u(X,t) = \mathbf{N}\left(X(\xi)\right)\mathbf{u}_e(t) = N_I\left(X(\xi)\right)u_I^e(t) \tag{B2.3.1}$$

$$\ldots v(X,t) = \mathbf{N}\left(X(\xi)\right)\mathbf{v}_e(t) = N_I\left(X(\xi)\right)v_I^e(t) \tag{B2.3.2}$$

note $\mathbf{N}_{,x} = \mathbf{N}_{,\xi}\, x_{,\xi}^{-1}$

in each element

$$D_x = \sum_{I=1}^{m} \frac{\partial N_I}{\partial x} v_I^e = \mathbf{B}\mathbf{v}^e \tag{B2.3.3}$$

evaluate s by constitutive equation

$$\mathbf{f}_e^{int} = \int_{\Omega_e} \frac{\partial \mathbf{N}}{\partial x}\sigma\, d\Omega \quad \text{or} \quad \mathbf{f}_e^{int} = \int_{\Omega_e} \mathbf{B}^T\sigma\, d\Omega \tag{B2.3.4}$$

$$\mathbf{f}_e^{ext} = \int_{\Omega_e} \rho\mathbf{N}^T b\, d\Omega + (\mathbf{N}^T A\dot{t}_x)\Big|_{\Gamma_t^e} \tag{B2.3.5}$$

$$\mathbf{M}_e = \int_{\Omega_e} \rho_0\mathbf{N}^T\mathbf{N}\, d\Omega \quad \text{same as total Lagrangian} \tag{B2.3.6}$$

$$\mathbf{M}\ddot{\boldsymbol{u}} + \mathbf{f}^{int} = \mathbf{f}^{ext} \tag{B2.3.7}$$

Example 2.8.1. Updated Lagrangian Form of Two-Node Linear Displacement Element. This element is the same as in Example 2.5.1, Fig. 3, except the updated Lagrangian treatment is now used. Recall that A_0 and ρ_0 are assumed to be constant in each element. The velocity field is the same as for the updated Lagrangian element, (2.5.19):

$$v(X,t) = \underbrace{\frac{1}{\ell_0}\left[X_2 - X, X - X_1\right]}_{\mathbf{N}(X)} \begin{Bmatrix} v_1(t) \\ v_2(t) \end{Bmatrix} \tag{2.8.31}$$

In terms of element coordinates, the velocity field is

$$v(\xi,t) = \underbrace{\begin{bmatrix} 1-\xi, & \xi \end{bmatrix}}_{\mathbf{N}(\xi)} \begin{Bmatrix} v_1(t) \\ v_2(t) \end{Bmatrix} \qquad \xi = \frac{X - X_1}{\ell_0} \tag{2.8.32}$$

The displacement is the time integrals of the velocity, and since ξ is independent of time

$$u(\xi,t) = \mathbf{N}(\xi)\mathbf{u}_e(t) \tag{2.8.33}$$

Therefore, since $x = X + u$

$$x(\xi,t) = \mathbf{N}(\xi)\,\mathbf{x}_e(t) = \begin{bmatrix} 1-\xi & \xi \end{bmatrix} \begin{Bmatrix} x_1(t) \\ x_2(t) \end{Bmatrix} \qquad x_{,\xi} = x_2 - x_1 = \ell \tag{2.8.34}$$

where ℓ is the current length of the element. For this element, we can express ξ in terms of the Eulerian coordinates by

$$\xi = \frac{x - x_1}{x_2 - x_1} = \frac{x - x_1}{\ell}, \quad \ell = x_2 - x_1, \quad \xi_{,x} = \frac{1}{\ell} \tag{2.8.35}$$

So $\xi_{,x}$ can be obtained directly, instead of through the inverse of $x_{,\xi}$. This is not the case for higher order elements.

The **B** matrix is obtained by the chain rule

$$\mathbf{B} = \mathbf{N}_{,x} = \mathbf{N}_{,\xi}\,\xi_{,x} = \frac{1}{\ell}\begin{bmatrix} -1, & +1 \end{bmatrix} \tag{2.8.36}$$

so the rate-of-deformation is given by

$$D_x = \mathbf{B}\mathbf{v}^e = \frac{1}{\ell}(v_2 - v_1) \tag{2.8.37}$$

Using (2.8.18) then gives

$$\mathbf{f}_e^{int} = \int_{x_1}^{x_2} \mathbf{B}^T \sigma A dx = \int_{x_1}^{x_2} \frac{1}{\ell}\begin{Bmatrix} -1 \\ +1 \end{Bmatrix} \sigma A dx \tag{2.8.38}$$

If the integrand in (2.8.38) is constant, as if often is, then (2.8.38) yields

$$\mathbf{f}_e^{int} = A\sigma \begin{Bmatrix} -1 \\ +1 \end{Bmatrix} \tag{2.8.39}$$

Thus the internal nodal forces for the element correspond to the forces resulting from the stress σ. Note that the internal nodal forces are in equilibrium.

The external nodal forces are evaluated using (2.8.21)

$$\mathbf{f}_e^{ext} = \int_{x_1}^{x_2} \begin{Bmatrix} 1-\xi \\ \xi \end{Bmatrix} \rho b A dx + \begin{Bmatrix} 1-\xi \\ \xi \end{Bmatrix} A t_x \Big|_{\Gamma_t^e} \tag{2.8.40}$$

where the last term makes a contribution only if a node of the element is on the traction boundary. Since x is a linear function of ξ and t, Eq. (2.8.16), $b(x,t)$ can always be expressed as a function of ξ and t. It is conventional to fit the data for $b(x,t)$ by linear interpolants for linear displacement elements (the information in higher order interpolations will be beyond the resolution of the mesh). So we let

$$b(\xi,t) = b_1(1-\xi) + b_2\xi \tag{2.8.41}$$

Substituting into (2.8.31) and integrating gives

$$\mathbf{f}_e^{ext} = \frac{\rho A \ell}{6} \begin{Bmatrix} 2b_1 + b_2 \\ b_1 + 2b_2 \end{Bmatrix} \tag{2.8.42}$$

Comparison to Total Lagrangian. We will now compare the nodal forces to those obtained by the total Lagrangian formulation. Replacing σ in (2.8.39) by the nominal stress using Eq. (2.1.3a), we see that (2.8.39) and (2.5.27) are equivalent. It can easily be shown that (*2.8.29*) and (*2.8.21*) lead to the same expression as (*2.8.31*).

To compare the external nodal forces, we note that by the conservation of matter, $\rho A \ell = \rho_0 A_0 \ell_0$. Using this in Eq. (2.8.42) gives (2.5.26), the total Lagrangian form of the nodal external forces. In the updated Lagrangian formulation, the mass from the total Lagrangian formulation is used, see Eq. (2.8.25), so the equivalence need not be considered.

Example 2.8.2. Updated Lagrangian of Three Node Element, Quadratic Displacement Element The 3-node element is shown in Fig. 2.7. Node 2 can be placed anywhere between the end-nodes, but we shall see there are restrictions on the placement of this node if the one-to-one condition is to be met. We will also examine the effects of *mesh distortion*.

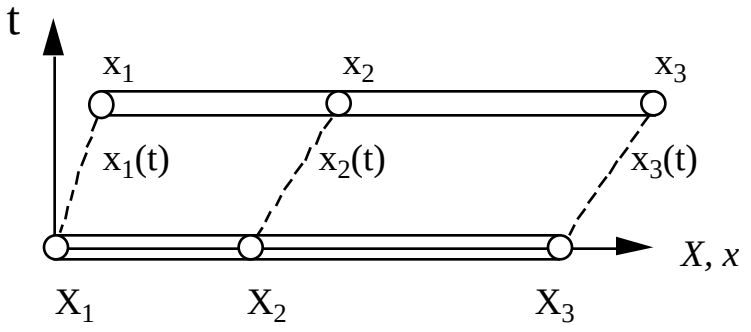

Fig. 2.7. Three node, quadratic displacement element in original and current configurations.

The displacement and velocity fields will be written in terms of the element coordinates

$$u(\xi,t)=\mathbf{N}(\xi)\,\mathbf{u}_e(t)\,,\quad v(\xi,t)=\mathbf{N}(\xi)\,\mathbf{v}_e(t)\,,\quad x(\xi,t)=\mathbf{N}(\xi)\,\mathbf{x}_e(t) \tag{2.8.43}$$

where

$$\mathbf{N}(\xi)=\left[\tfrac{1}{2}\left(\xi^2-\xi\right)\quad 1-\xi^2\quad \tfrac{1}{2}\left(\xi^2+\xi\right)\right] \tag{2.8.44}$$

and

$$\mathbf{u}_e^T=\left[u_1,u_2,u_3\right]\qquad \mathbf{v}_e^T=\left[v_1,v_2,v_3\right]\qquad \mathbf{x}_e^T=\left[x_1,x_2,x_3\right] \tag{2.8.45}$$

The **B** matrix is given by

$$\mathbf{B}=\mathbf{N}_{,x}=x_{,\xi}^{-1}\mathbf{N}_{,\xi} \tag{2.8.46}$$

$$=\frac{1}{2x_{,\xi}}\left[2\xi-1\quad -4\xi\quad 2\xi+1\right] \tag{2.8.47}$$

where

$$x_{,\xi}=\mathbf{N}_{,\xi}\,\mathbf{x}_e=\left(\xi-\tfrac{1}{2}\right)x_1-2\xi\,x_2+\left(\xi+\tfrac{1}{2}\right)x_3 \tag{2.8.48}$$

The rate of deformation is given by

$$D_x=\mathbf{N}_{,x}\,\mathbf{v}_e=\mathbf{B}\mathbf{v}_e=\frac{1}{2x_{,\xi}}\left[2\xi-1\quad -4\xi\quad 2\xi+1\right]\mathbf{v}_e \tag{2.8.49}$$

This rate-of-deformation varies linearly in the element if $x_{,\xi}$ is constant, which is the case when node 2 is midway between the other two nodes. However, when node 2 moves away from the midpoint due to element distortion, $x_{,\xi}$ becomes linear and the rate-of-deformation is a rational function. Furthermore, as node 2 moves from the center, it becomes possible for $x_{,\xi}$ to become negative or vanish. In that case, the mapping between the current spatial coordinates and the element coordinates is no longer one-to-one.

The internal forces are given by (2.8.18):

$$\mathbf{f}_e^{int}=\int_{x_1}^{x_3}\mathbf{B}^T\sigma\,A\,dx=\int_{-1}^{+1}\frac{1}{x_{,\xi}}\begin{Bmatrix}\xi-\frac{1}{2}\\ -2\xi\\ \xi+\frac{1}{2}\end{Bmatrix}\sigma\,A\,x_{,\xi}\,d\xi=\int_{-1}^{+1}\sigma\,A\begin{Bmatrix}\xi-\frac{1}{2}\\ -2\xi\\ \xi+\frac{1}{2}\end{Bmatrix}d\xi \tag{2.8.50}$$

where we have used $dx=x_{,\xi}\,d\xi$. Using (2.1.3), we can see that this expression is identical to the internal force expression for the total Lagrangian formulation.

Mesh Distortion. We will now examine the effects of mesh distortion on this element. When $x_2=\frac{1}{4}\left(x_3+3x_1\right)$, i.e. when node 2 of the element is one quarter of the element length from node 1, then $x_{,\xi}=\frac{1}{2}\left(x_3-x_1\right)\left(\xi+1\right)$, so $x_{,\xi}=0$ at $\xi=-1$. Examining the Jacobian given by Eq. (2.2.3)

$$J = \frac{A}{A_0} x_{,X} = \frac{A}{A_0} x_{,\xi} X_{,\xi}^{-1} \tag{2.8.51}$$

we see that it will also vanish. By E. (2.2.4a) this implies that the current density becomes infinite at that point. As node 2 moves closer to node 1, the Jacobian becomes negative in part of the element, which implies a negative density and a violation of the one-to-one condition. This corresponds to a violation of mass conservation and continuity of the displacement field. These situations are often masked by numerical quadrature, because the condition must be more severe to appear at Gauss quadrature points.

The failure to meet the one-to-one condition can also affect the rate-of-deformation, which is given by $D_x = \mathbf{B}\mathbf{v}_e$. From (2.8.37) we can see the potential for difficulties when the denominator $x_{,\xi}$ vanishes or becomes negative. When $x_2 = \frac{1}{4}(x_3 + x_1)$, and $x_{,\xi} = 0$ at $\xi = -1$, then the rate-of-deformation becomes infinite at node 1. This property of quadratic displacement elements has been exploited in fracture mechanics to develop elements with singular cracktip stresses called quarter-point elements, but in large displacement analysis this phenomenon can be troublesome.

In one-dimensional elements the effects of mesh distortion are not as severe as in multi-dimensional problems. In fact, the effects of mesh distortion can be alleviated somewhat in this element by using F as a measure of deformation, see Eq. (2.5.40). The deformation gradient F never becomes singular in the 3-node element if the initial position of X_2 is at the midpoint. However, any constitutive equation expressed in terms of F will differ markedly from one expressed in terms of the rate-of-deformation D_x when the strains are large.

Example 2.8.3. Axisymmetric 2-Node Element. As an example where the concept of the principle of virtual power or work becomes quite useful, we consider the analysis of an axisymmetric two dimensional disc of constant thickness, a, which is thin compared to its dimensions so $\sigma_z = 0$. The only nonzero velocity is $v_r(r)$, which as shown, is only a function of the radial coordinate in an axisymmetric problem. The nonzero Cauchy stresses and rate-of-deformations are written in cylindrical coordinates using Voigt notation

$$\{\mathbf{D}\} = \begin{Bmatrix} D_r \\ D_\theta \end{Bmatrix} \qquad \{\sigma\} = \begin{Bmatrix} \sigma_r \\ \sigma_\theta \end{Bmatrix} \tag{2.8.52}$$

The rate-of-deformations are given by

$$D_r = v_{r,r} \qquad D_\theta = \frac{v_r}{r} \tag{2.8.53}$$

and the momentum equation is

$$\frac{\partial \sigma_r}{\partial r} + \frac{\sigma_r - \sigma_\theta}{r} + \rho b_r = \rho \dot{v}_r \tag{2.8.54}$$

The boundary conditions are

$$\sigma_r(a) = \sigma_a \qquad \sigma_r(b) = \sigma_b \tag{2.8.55}$$

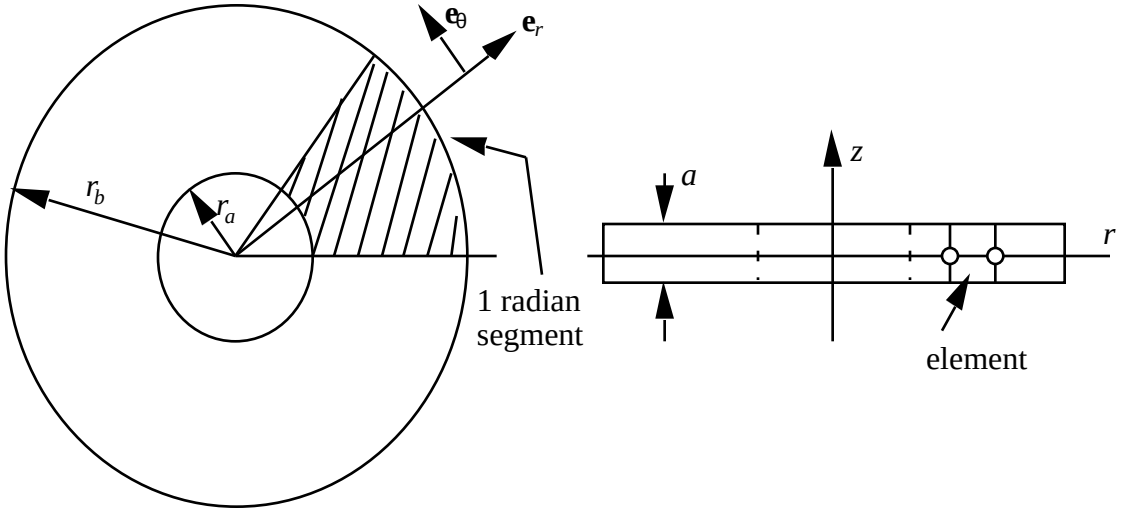

Fig. Schematic of axisymmetric disc
the shaded area is considered in work terms

It is not necessary to integrate the momentum equation to obtain its weak form. By the principle of virtual power the weak form is

$$\delta P = 0 \qquad \delta v_r \quad U_0 \tag{2.8.56}$$

The internal virtual power is obtained from the rate-of-deformation and stress

$$\delta P_e^{int} = \int_{r_1^e}^{r_2^e} \left(\delta D_r \sigma_r + \delta D_\theta \sigma_\theta\right) ar dr = \int_{\Omega_e} \{\delta \mathbf{D}\}^T \{\sigma\} d\Omega \tag{2.8.57}$$

where $d\Omega = ardr$ because a segment of one radian in the circumferential direction has been chosen to avoid the factor 2π in all terms. The external virtual power is given by

$$\delta P_e^{ext} = \int_{\Omega_e} \delta v_r \rho b_r d\Omega + \left(ar\bar{t}_r\right)\Big|_{\Gamma_t} \tag{2.8.58}$$

where ar in the last term is the area of a one radian segment. The virtual inertial power is given by

$$\delta P_e^{inert} = \int_{\Omega_e} \delta v_r \rho \dot{v}_r d\Omega \tag{2.8.59}$$

Consider a two-node finite element with a linear velocity field written in terms of element coordinates

$$v(\xi, t) = \begin{bmatrix} 1-\xi & \xi \end{bmatrix} \begin{Bmatrix} v_1(t) \\ v_2(t) \end{Bmatrix} \tag{2.8.60}$$

The rate-of-deformation is evaluated by Eq.() using the above velocity field and immediately put into matrix form

$$\mathbf{D} = \begin{Bmatrix} D_r \\ D_\theta \end{Bmatrix} = \begin{bmatrix} -\dfrac{1}{r_{21}} & \dfrac{1}{r_{21}} \\ \dfrac{1-\xi}{r} & \dfrac{\xi}{r} \end{bmatrix} \begin{Bmatrix} v_1(t) \\ v_2(t) \end{Bmatrix} = \mathbf{B}\mathbf{v}_e \tag{2.8.61}$$

The internal nodal forces are given by an expression identical to () except that the stress is replaced by the column matrix

$$\mathbf{f}_e^{int} = \int_{\Omega_e} \mathbf{B}^T \{\sigma\}\, d\Omega = \int_{r_1}^{r_2} \begin{bmatrix} -\dfrac{1}{r_{21}} & \dfrac{1}{r_{21}} \\ \dfrac{1-\xi}{r} & \dfrac{\xi}{r} \end{bmatrix} \begin{Bmatrix} \sigma_r \\ \sigma_\theta \end{Bmatrix} ar\, dr \tag{2.8.62}$$

The external nodal forces are given by

$$\mathbf{f}_e^{ext} = \int_{r_1}^{r_2} \begin{Bmatrix} 1-\xi \\ \xi \end{Bmatrix} \rho b_r ar\, dr + \left(ar\bar{t}_r \right)\Big|_{\Gamma_t} \tag{2.8.63}$$

The element mass matrix is given by

$$\begin{aligned} \mathbf{M}_e &= \int_{r_1}^{r_2} \begin{Bmatrix} 1-\xi \\ \xi \end{Bmatrix} \begin{bmatrix} 1-\xi & \xi \end{bmatrix} \rho ar\, dr \\ &= \frac{\rho a r_{21}}{12} \begin{bmatrix} 3r_1 + r_2 & r_1 + r_2 \\ r_1 + r_2 & r_1 + 3r_2 \end{bmatrix} \end{aligned} \tag{2.8.64}$$

The lumped mass matrix can be computed by the row sum technique or by lumping half the mass at each node, which gives, respectively

$$\mathbf{M}_e = \frac{\rho a r_{21}}{6} \begin{bmatrix} 2r_1 + r_2 & 0 \\ 0 & r_1 + 2r_2 \end{bmatrix}_{\text{row-sum}} \qquad \mathbf{M}_e = \frac{\rho a r_{21}(r_1 + r_2)}{4} \begin{bmatrix} 1 & 0 \\ 0 & 1 \end{bmatrix}_{\text{lump}} \tag{2.8.65}$$

As can be seen the two lumping procedures give slightly different results.

2.9. Governing Equations for Eulerian Formulation

In an Eulerian formulation, the nodes are fixed in space and the independent variables are functions of the Eulerian spatial coordinate x and the time t. The stress measure is the Cauchy (physical) stress $\sigma(x,t)$, the measure of deformation is the rate-of-deformation $D_x(x,t)$. The motion will be described by the velocity $v(x,t)$. In Eulerian formulations, the deformation is not expressed as a function of the reference coordinates since an

undeformed, initial configuration cannot be established, and no counterpart of (2.2.1) is available.

Box. 2.4. Governing Equations for Eulerian Formulation

continuity equation (mass conservation):

$$\frac{\partial \rho}{\partial t} + \frac{\partial (\rho v)}{\partial x} = 0 \qquad \text{(B2.4.1)}$$

momentum equation

$$\rho A\left(\frac{\partial v}{\partial t} + v\frac{\partial v}{\partial x}\right) = \frac{\partial (A\sigma)}{\partial x} + \rho A b \qquad \rho\left(\frac{\partial v}{\partial t} + v\frac{\partial v}{\partial x}\right) = \frac{\partial \sigma}{\partial x} + \rho b \qquad \text{(B2.4.2)}$$

strain measure (rate-of-deformation): $D_x = v_{,x}$ (B2.4.3)

constitutive equation in rate form:

$$\frac{D\sigma}{Dt} = \sigma_{,t}(x,t) + \sigma_{,x}(x,t)v(x,t) = S_t^{\sigma D}\left(D_x(X,\bar{t}), \sigma(X,\bar{t}), etc., \bar{t} \le t\right) \qquad \text{(B2.4.4)}$$

energy conservation equation
same as before

The governing equations are summarized in Box 2.4. In comparison with the updated Lagrangian formulation we have just discussed, four points are noteworthy:

1. The mass conservation equation is now written as a partial differential equation; the form used with Lagrangian meshes is not applicable because it applies only to material points.
2. The material time derivative for the velocity in the momentum equation has been written out in terms of the spatial time derivative and transport term.
3. The constitutive equation is expressed in rate form; the total form cannot be used since the stress and rate of deformation are functions of material coordinates in a history-dependent material.
4. The boundary conditions are now imposed on spatial points which do not move with time.

The continuity equation has been written as a partial differential equation because it is not possible to obtain an integral form such as Eq. (2.2.4) when the density is a function of spatial coordinates. Therefore, the continuity equation must be treated as a separate partial differential equation, although there are approximations which enable the continuity equation to be omitted when the density changes little, as for a liquid or solid; these are discussed in Chapter 7.

The constitutive equation needs to be expressed in terms of material coordinates for history-dependent materials, so it is treated in rate form in this formulation. It is thus a separate partial differential equation.

In the general case, boundary conditions are required for the density, velocity and stress. As will be seen in Chapter 7, the boundary conditions for the density and stress in an Eulerian mesh depend on whether the material is flowing in or out at the boundary. In this introductory exposition, we consider only boundaries where there is no flow. The boundary points are then Lagrangian, and the density and stress can be determined at these points by the Lagrangian mass conservation equation, Eq. (2.2.10) and the constitutive

equation, respectively. Therefore, there is no need for boundary conditions for these variables.

2.10 WEAK FORMS FOR EULERIAN MESH EQUATIONS

In the Eulerian formulation, we have 3 unknowns or dependent variables: the density $\rho(x, t)$, the velocity $v(x, t)$ and the stress $\sigma(x, t)$. The rate-of-deformation can easily be eliminated from the momentum equations by substituting (B2.4.3) into the constitutive equation (B2.4.4). Therefore, we will need three sets of discrete equations. A weak forms of the momentum equation, the mass conservation equation and the constitutive equation will be developed. We will construct continuous solutions to the governing equations. The equations given in Box 2.4 can in fact have discontinuous solutions, with discontinuities in the density, stress and velocity, as when a shock occurs in the flow. However, we will take the approach of smearing any discontinuities over several elements with a continuous function; this approach is called shock fitting or shock smearing. The trial and test functions will therefore be continuous functions of space.

We consider first the weak form of the continuity equation. The trial functions for the density are denoted by $\rho(x,t)$, the test functions by $\delta\rho(x)$ The test functions and the trial functions for the continuity equation must be piecewise continuously differentiable, so

$$\rho(x,t) \quad R, \quad R = \left\{ \rho(x,t) \middle| \rho(x,t) \quad C^0(x), \rho(x,t) = \bar{\rho} \text{ on } \Gamma_\rho \right\} \tag{2.10.1}$$

$$\delta\rho(x) \quad R_0, \quad R = \left\{ \delta\rho(x) \middle| \delta\rho(x) \quad C^0(x), \delta\rho(x_a) = 0, \delta\rho(x_b) = 0 \right\} \tag{2.10.2}$$

In this Section, we do not consider problems with prescribed densities on the boundaries.

The weak form of the continuity equation is obtained by multiplying it by the test function $\delta\rho(x)$ and integrating over the domain. This gives

$$\int_{x_a}^{x_b} \delta\rho(\rho_{,t} + (\rho v)_{,x})\, dx = 0 \qquad \delta\rho \quad R_0 \tag{2.10.3}$$

Only first derivatives with respect to the spatial variable of the density and velocity appear in the weak form, so there is no need for integration by parts. The consequence of integrating by parts are interesting and is examined in the Exercises.

The weak form of the constitutive equation is obtained the same way. We express the material derivative in terms of a spatial derivative and a transport term, giving

$$\sigma_{,t} + \sigma_{,x} v - S(v_{,x}, etc) = 0 \tag{2.10.4}$$

The test and trial functions, $\delta\sigma(x)$ and $\sigma(x,t)$, respectively, are subject to the same continuity and end conditions as for the density in the continuity equation, i.e., we let σ , $\delta\sigma$ $_0$. The weak form of the constitutive equation is then obtained by multiplying it by the test function and integrating over the domain:

$$\int_{x_a}^{x_b} \delta\sigma(\sigma_{,t} + \sigma_{,x} v - S(v_{,x}, etc))\, dx = 0 \qquad \delta\sigma \quad R_0 \tag{2.10.5}$$

As in the continuity equation, there is no benefit in integrating by parts. Neither this weak form nor the weak continuity equation have a clear physical meaning. They will be referred to as the weak continuity and constitutive equations.

The weak form of the momentum equation is obtained by integrating the test function $\delta v(x)$ over the spatial domain. The procedure is identical to that in the updated Lagrangian formulation in Section 2.7. The test and trial functions are defined by Eqs (2.7.1) and (2.7.2). The resulting weak form is

$$\int_{x_a}^{x_b} \left[\delta v_{,x} A\sigma - \delta v \left(\rho A b - \rho A \frac{Dv}{Dt} \right) \right] dx - \left(\delta v A \bar{t}_x \right)\Big|_{\Gamma_t} = 0 \tag{2.10.6}$$

or using (??)

$$\int_{x_a}^{x_b} \left[\delta v_{,x} A\sigma + \delta v \rho A \left(\frac{\partial v}{\partial t} + v_{,x} v - b \right) \right] dx - \left(\delta v A \bar{t}_x \right)\Big|_{\Gamma_t} = 0 \tag{2.10.7}$$

Note that the limits of the integration are fixed in space.

The weak form is identical to the principle of virtual power for the updated Lagrangian formulation except that the domain is fixed in space and the material time derivative is expressed in its Eulerian form. Thus the weak form of the momentum equation can be written

$$\delta P = \delta P^{int} - \delta P^{ext} + \delta P^{inert} = 0 \qquad \delta v \quad U_0 \tag{2.10.8}$$

where

$$\delta P^{int} = \int_{x_a}^{x_b} \delta v_{,x} \sigma A dx = \int_{x_a}^{x_b} \delta D_x \sigma A dx = \int_{\Omega} \delta D_x \sigma \Omega \tag{2.10.9}$$

$$\delta P^{ext} = \int_{x_a}^{x_b} \delta v \rho b A dx + \left(\delta v A \bar{t}_x \right)\Big|_{\Gamma_t} \tag{2.10.10}$$

$$\delta P^{inert} = \int_{x_a}^{x_b} \delta v \rho \left(\frac{\partial v}{\partial t} + v_{,x} v \right) A dx = \int_{\Omega} \delta v \rho \left(\frac{\partial v}{\partial t} + v_{,x} v \right) d\Omega \tag{2.10.11}$$

All of the terms are identical to the corresponding terms in the principle of virtual power for the updated Lagrangian formulation, except that the limits of integration are fixed in space and the material time derivative in the inertial virtual power has been expressed in terms of the spatial time derivative and the transport term. Similar expressions for the virtual powers also hold on the element level.

2.11. FINITE ELEMENT EQUATIONS

In a general Eulerian finite element formulation, approximations are needed for the pressure, stress and velocity. For each independent variable, test and trial functions are needed. We will develop the equations for the entire mesh. For simplicity, we consider the case where the segment is $0 \le x \le L$. As mentioned before, we consider the case where the end points are fixed in space and the velocities on these points vanish. There are then no boundary conditions on the density or stress and the boundary conditions on the velocity are

$$v(0,t) = 0, \qquad v(L,t) = 0 \tag{2.11.1}$$

The mapping between spatial and element parent coordinates is given by

$$x = N_I(\xi) x_I \tag{2.11.2}$$

In contrast to the Lagrangian formulations, this mapping is constant in time since the nodal coordinates x_I are not functions of time. The trial and test functions are given by

$$\rho(x,t) = \sum_{I=1}^{n_N} N_I^\rho(x)\rho_I(t) \qquad \delta\rho(x) = \sum_{I=1}^{n_N} N_I^\rho(x)\delta\rho_I \tag{2.11.3}$$

$$\sigma(x,t) = \sum_{I=1}^{n_N} N_I^\sigma(x)\sigma_I(t) \quad \delta\sigma(x) = \sum_{I=1}^{n_N} N_I^\sigma(x)\delta\sigma_I \tag{2.11.4}$$

$$v(x,t) = \sum_{I=2}^{n_N-1} N_I(x) v_I(t) \qquad\qquad \delta v(x) = \sum_{I=2}^{n_N-1} N_I(x)\delta v_I \tag{2.11.5}$$

The velocity trial functions have been constructed so the velocity boundary condition is automatically satisfied.

Substituting the test and trial functions for the density into the weak continuity equation gives

$$\sum_{I=1}^{n_N}\sum_{J=1}^{n_N} \delta\rho_J \int_0^L \left(N_J^\rho N_I^\rho \rho_{I,t} + N_J^\rho (\rho v)_{,x} \right) dx = 0 \tag{2.11.6}$$

Since this holds for arbitrary $\delta\rho_J$ at interior nodes, we obtain

$$\int_0^L N_I^\rho N_J^\rho dx \rho_{J,t} + \int_0^L N_I^\rho (\rho v)_{,x} dx = 0 \qquad I = 1 \text{ to } n_N \tag{2.11.7}$$

We define the following matrices

$$M_{IJ}^\rho = \int_0^L N_I^\rho N_J^\rho dx, \qquad \mathbf{M}_e^\rho = \int_{\Omega_e} \left(\mathbf{N}^\rho\right)^T \mathbf{N}^\rho dx \tag{2.11.8}$$

$$g_I^\rho = \int_0^L N_I^\rho (\rho v)_{,x} dx, \quad \mathbf{g}_e^\rho = \int_0^L \left(\mathbf{N}^\rho\right)^T (\rho v)_{,x} dx \tag{2.11.9}$$

The discrete continuity equation can be then be written as

$$\sum_J M^\rho_{IJ}\dot{\rho}_J + g^\rho_I = 0 \text{ for } I = 1 \text{ to } n_N, \text{ or } \mathbf{M}^\rho\dot{\boldsymbol{\rho}} + \mathbf{g}^\rho = 0 \tag{2.11.10}$$

The matrices $\mathbf{M}^\rho$ can be assembled from element matrices just like the mass matrix in the momentum equation. The column matrix $\mathbf{g}^\rho$ is obtained by a scatter, or vector assembly. The matrix $\mathbf{M}^\rho$ is time invariant and closely resembles the mass matrix. However, the column matrix $\mathbf{g}^\rho$ varies with time and must be computed in every time step. In most cases, the element matrices are integrated in the parent coordinate system.

The discrete form of the constitutive equation is obtained similarly. The result is

$$\sum_J M^\sigma_{IJ}\dot{\rho}_J + g^\sigma_I = h^\sigma_I \text{ for } I = 1 \text{ to } n_N, \text{ or } \mathbf{M}^\sigma\dot{\boldsymbol{\sigma}} + \mathbf{g}^\sigma = \mathbf{h} \tag{2.11.11}$$

where

$$M^\sigma_{IJ} = \int_0^L N^\sigma_I N^\sigma_J dx \quad \text{and} \quad \mathbf{M}^\sigma_e = \int_{\Omega_e} \left(\mathbf{N}^\sigma\right)^T \mathbf{N}^\sigma d\Omega \tag{2.11.12}$$

$$g^\sigma_I = \int_0^L N^\sigma_I v\sigma_{,x} dx \quad \text{and} \quad \mathbf{g}^\sigma_e = \int_{\Omega_e} \left(\mathbf{N}^\sigma\right)^T v\sigma_{,x} d\Omega \tag{2.11.13}$$

where the matrix relations on the right have been extracted from the indicial forms and immediately specialized to elements by the procedure in Section 2.8.

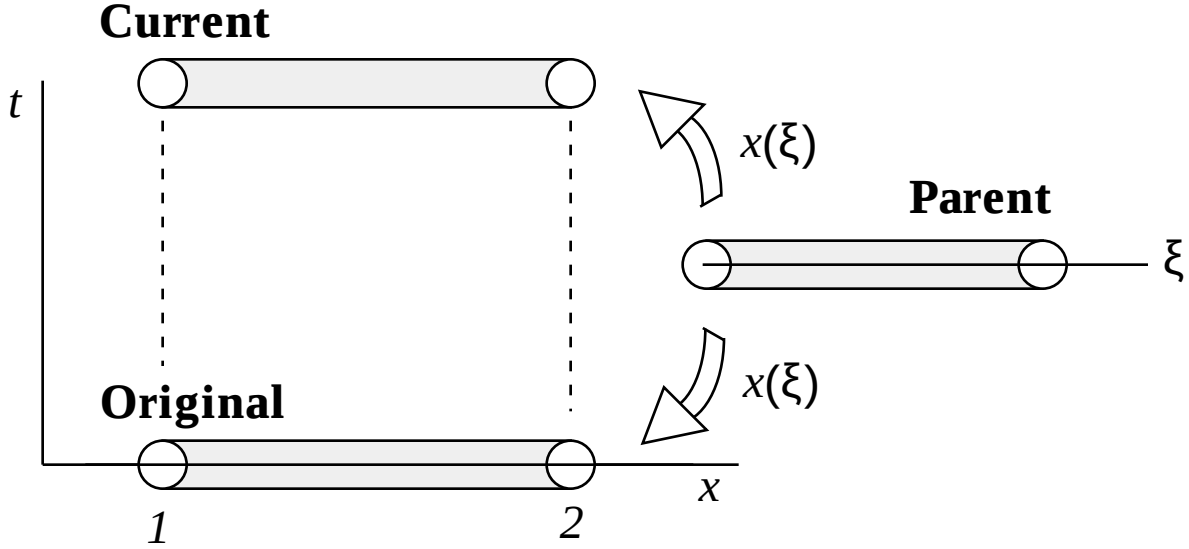

Fig. 2.8 Eulerian element in current and original configurations, which are the same, and the mapping to the parent element.

Momentum Equation. The weak form of the momentum equation is identical to the weak form for the updated Lagrangian formulation except for the inertial term. Therefore the expressions for the internal and external nodal forces are identical. The inertial nodal

forces for the Eulerian formulation are obtained in the following on an element level. We define the inertial nodal forces by Eq. (2.7.8) which gives

$$\delta P_e^{iner} = \delta \mathbf{v}_e^T \mathbf{f}_e^{inert} = \delta \mathbf{v}_e^T \int_{\Omega_e} \rho \mathbf{N}^T \left(\mathbf{N}\dot{\mathbf{v}} + v_{,x} v \right) A dx \tag{2.11.14}$$

From the above, it follows that the inertial nodal forces are given by

$$\mathbf{f}_e^{iner} = \mathbf{M}_e \dot{\mathbf{v}}_e + \mathbf{f}_e^{tran} \tag{2.11.15}$$

where

$$\mathbf{M}_e = \int_{\Omega_e} \rho \mathbf{N}^T \mathbf{N} A dx, \quad \mathbf{f}_e^{tran} = \int_{\Omega_e} \rho v_{,x} v A dx \tag{2.11.16}$$

The transport nodal forces have not been written in matrix form; they are quadratic in the nodal velocities. This term is needed in the Eulerian formulation because the nodes are fixed in space, so the time derivatives of the nodal velocities correspond to spatial derivatives. The mass matrix differs from the mass matrix in the Lagrangian meshes in that it is a function of time: as the density in the element changes, the mass matrix will change correspondingly.

Example. Two-Node Eulerian Finite Element. The finite element equations are developed for a one-dimensional, two node element with linear velocity, density and stress fields. The element, shown in Fig. 2.8, is of length $\ell = x_2 - x_1$ and unit cross-sectional area. As can be seen, the spatial configuration does not change with time since it is an Eulerian element. The map between element and spatial coordinates is given by

$$x(\xi) = \begin{bmatrix} 1-\xi & \xi \end{bmatrix} \begin{Bmatrix} x_1 \\ x_2 \end{Bmatrix}_e \equiv \mathbf{N}(\xi)\mathbf{x}_e \tag{2.11.17}$$

The density, velocity and stress are also interpolated by the same linear shape functions

$$\rho(\xi) = \mathbf{N}(\xi)\rho_e \qquad v(\xi) = \mathbf{N}(\xi)\mathbf{v}_e \qquad \sigma(\xi) = \mathbf{N}(\xi)\sigma_e \tag{2.11.18}$$

Superscripts are not appended to the shape functions because all variables are interpolated by the same shape functions.

Density Equation. The element matrices for the discrete continuity equation are given by

$$\mathbf{M}_e^\rho = \int_{x_1}^{x_2} \mathbf{N}^T \mathbf{N}\, dx = \int_0^1 \begin{Bmatrix} 1-\xi \\ \xi \end{Bmatrix} \begin{bmatrix} 1-\xi & \xi \end{bmatrix} \ell\, d\xi = \frac{\ell}{6} \begin{bmatrix} 2 & 1 \\ 1 & 2 \end{bmatrix} \tag{2.11.19}$$

$$\mathbf{g}_e^\rho = \int_{x_1}^{x_2} \mathbf{N}^T (\rho v)_{,x}\, dx = \int_0^1 \begin{Bmatrix} 1-\xi \\ \xi \end{Bmatrix} (\rho v)_{,x}\, \ell\, d\xi \tag{2.11.20}$$

The $\mathbf{g}_e^\rho$ vector is usually evaluated by numerical quadrature. For linear interpolants it is given by

$$\mathbf{g}_e^\rho = \frac{1}{6}(\rho_2 - \rho_1)\begin{bmatrix} 2v_1 + v_2 \\ v_1 + 2v_2 \end{bmatrix} + \frac{1}{6}(v_2 - v_1)\begin{bmatrix} 2\rho_1 + \rho_2 \\ \rho_1 + 2\rho_2 \end{bmatrix} \tag{2.11.21}$$

The above matrix vanishes when the density and velocity are constant in the element.

Stress Equation. The element matrix for the stresses $\mathbf{M}_e^\sigma = \mathbf{M}_e^\rho$. The vector $\mathbf{g}_e^\sigma$ is given by

$$\begin{aligned} \mathbf{g}_e^\sigma &= \int_{x_1}^{x_2} \mathbf{N}^T v\sigma_{,x}\, dx = \int_0^1 \begin{bmatrix} 1-\xi \\ \xi \end{bmatrix} (v_1(1-\xi) + v_2\xi)(\sigma_2 - \sigma_1)\, d\xi \\ &= \frac{1}{6}(\sigma_2 - \sigma_1)\begin{bmatrix} 2v_1 + v_2 \\ v_1 + 2v_2 \end{bmatrix} \end{aligned} \tag{2.11.22}$$

In summary, the finite element equations for the Eulerian formulation consists of three sets of discrete equations: the continuity equation, the constitutive equation, and the momentum equation, or equation of motion. The momentum equation is similar to the updated Lagrangian form, except that the inertial term includes a transport term and varies with time. All nodal forces are defined over fixed intervals in space. The semidiscrete forms of the continuity and constitutive equations are first order ordinary differential equations. We have only developed the discrete equations for the case where the endpoints are fixed.

2.12 Solution Methods

We have seen so far that the momentum equation can be discretized with a Lagrangian mesh in the form

$$\mathbf{M}\ddot{\mathbf{u}} = \mathbf{f}^{\text{ext}} - \mathbf{f}^{\text{int}} = \mathbf{f} \tag{2.12.1}$$

These are ordinary differential equations in time.

In order to enable some nonlinear problems to be solved at this point, we now describe the simplest solution method, explicit time integration of the equations of motion for a Lagrangian mesh. The most widely used explicit method is based on the central difference formulas. Explicit integration can be simplified further by replacing **M** by a *diagonal* or *lumped mass* matrix.

We start at time t=0 using time steps Δt, so that at time step n, $t = n\Delta t$. The value of a function at $n\Delta t$ is denoted by a superscript n, i.e., $\mathbf{u}^n \equiv \mathbf{u}(n\Delta t)$. In the central difference method, the velocities are approximated by

$$\dot{\mathbf{u}}^n = \mathbf{v}^{n+1/2} = \frac{\mathbf{u}^{n+1/2} - \mathbf{u}^{n-1/2}}{\Delta t} = \frac{\mathbf{u}(t + \Delta t/2) - \mathbf{u}(t - \Delta t/2)}{\Delta t} \tag{2.12.2}$$

where the second equality is included to clarify the notation. Half time step values are used for the velocities. The accelerations are given by

$$\ddot{\mathbf{u}}^n \equiv \mathbf{a}^n = \frac{\mathbf{v}^{n+1/2} - \mathbf{v}^{n-1/2}}{\Delta t} \tag{2.12.3}$$

In each case, the value of the derivative at the center of a time interval is obtained from the difference of the function values at the ends of the interval, hence the name *central difference* formulas. The flow chart for an explicit program is then given by the following Box.

Box 2.5 Flowchart for Explicit Time Integration of Lagrangian Mesh

1. Initial conditions and initialization: set $\mathbf{v}^0, \sigma^0$; $n = 0, t = 0$; *compute* $\mathbf{M}$
2. get $\mathbf{f}^n$
3. compute accelerations $\mathbf{a}^n = \mathbf{M}^{-1}\mathbf{f}^n$
4. update nodal velocities: $\mathbf{v}^{n+\frac{1}{2}} = \mathbf{v}^{n+\frac{1}{2}-\alpha} + \alpha \Delta t \mathbf{a}^n$: $\alpha = \begin{cases} \frac{1}{2} & \text{if } n = 0 \\ 1 & \text{if } n > 0 \end{cases}$
5. enforce essential boundary conditions: if node I on Γ_v : $v_I^n = \bar{v}(x_I, t_n)$
6. update nodal displacements: $\mathbf{u}^{n+1} = \mathbf{u}^n + \Delta t \mathbf{v}^{n+\frac{1}{2}}$
7. update counter and time: $n \leftarrow n+1$, $t \leftarrow t + \Delta t$
8. output, if simulation not complete, go to 2

Module: get $\mathbf{f}$

1. GATHER element nodal displacements $\mathbf{u}_e^n$ and velocities $\mathbf{v}_e^{n+1/2}$
2. compute measure of deformation
3. compute stress by constitutive equation σ_e^n
4. compute internal nodal forces by equation in Box.
5. compute external nodal forces on element and $\mathbf{f}_e = \mathbf{f}_e^{ext} - \mathbf{f}_e^{int}$
5. SCATTER element nodal displacements to global matrices

Updating for the displacements by Eq. (6) then does not require *any solution* of algebraic equations. Thus, in a sense, explicit integration is simpler than static linear stress analysis. As can be seen from the flowchart, most of the explicit program is a straightforward interpretation of the governing equations and the time integration formulas. The program begins with the enforcement of the initial conditions; procedures for fitting different initial conditions have already been described. The first time step is somewhat different from the others because only a half-step is taken. This enables the program to correctly account for the initial conditions on the stresses and velocities.

Most of the programming and computation time is in computing the element nodal forces, particularly the internal nodal forces. The nodal forces are computed element-by-element. Prior to starting the element computations, the element nodal velocities and displacements are gathered from the global arrays. As can be seen from the flowchart, the computation of the internal nodal forces involves the application of the equations which are left in strong form, the strain equation and the constitutive equation, followed by the evaluation of the internal nodal forces from the stress, which emanates from the weak form

of the momentum equation. When the computation of the element nodal forces is completed, they are scattered to the global array according to their node numbers.

The essential boundary conditions are enforced quite easily as shown. By setting the nodal velocities equal to the prescribed nodal velocities at all nodes on prescribed velocity boundaries, the correct displacements result, since the velocities are subsequently integrated in time. The placement of this step in the flowchart insures that the correct velocities are available in the nodal force computation. The initial velocities must be compatible with the boundary conditions; this is not checked in this flowchart but would be checked in a production program. The reaction forces can be obtained by outputting the total nodal forces at the prescribed velocity nodes.

It can be seen from the flowchart that the traction boundary conditions enter only through the external nodal forces. Therefore, for a traction-free boundary, nothing need be done: the homogeneous traction boundary condition is enforced naturally in a weak sense by the finite element solution. However, the traction boundary condition is only satisfied approximately.

Stability Criterion. The disadvantage of explicit integration is that the time step must be below a critical value or the solution "blows up" due to a numerical instability. This is described in detail in Chapter 6. Here we limit ourselves to pointing out that the critical time step for the 2-node elements described in this Chapter is given by

$$\Delta t_{crit} = \frac{\ell}{c} \tag{2.12.4}$$

where ℓ is the *current* length of the element and c is the wave speed given by

$$c^2 = E_{\sigma\eta}/\rho \tag{2.12.5}$$

where $E_{\sigma\eta}$ is the modulus in the elastic relation between Cauchy stress and rate-of-deformation. For nonlinear materials, $E_{\sigma\eta}$ is replaced by the current tangent modulus

$$E^t_{\sigma D} = \frac{\dot{\sigma}}{D_x} \tag{2.12.6}$$

A computer program for the explicit integration of the one-dimensional updated and total Lagrangian formulation is given in Appendix B.

Appendix A. Derivation of Conservation Equations in 1D.

In this Appendix, simple derivations of the conservation equations in one dimension will be given. These are "engineering" derivations which develop these equations in simplest terms, and they lack the mathematical rigor and generality associated with the derivations found in texts on continuum mechanics.

We first derive the equation of conservation of mass, also called the continuity equation. Consider a segment of the rod shown in Fig. 2.7, which in the initial, or undeformed, state is of length ΔX, cross-sectional area A_0 and density ρ_0. In the deformed state this Lagrangian segment has length Δx, area A and density ρ. The subdomain is a material, or Lagrangian subdomain, in that all material points remain in the subdomain and

the right and left end points are the same material points. No flow of material occurs in or out of the segment. Therefore, by mass conservation, the mass in the undeformed segment must equal the mass of the deformed segment:

$$\rho A \Delta x = \rho_0 A_0 \Delta X \tag{A.1}$$

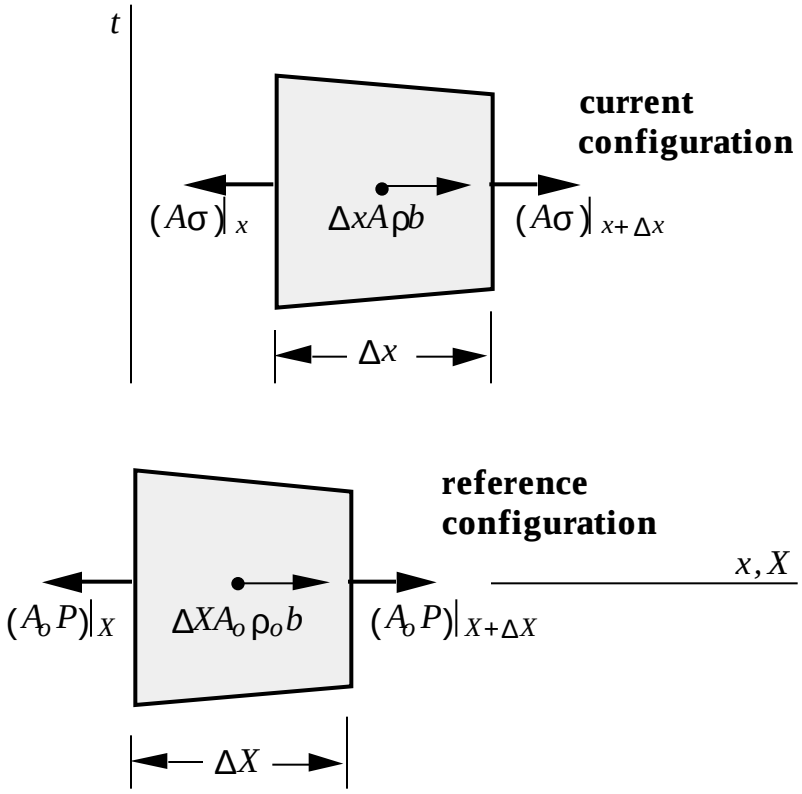

Fig. 2.9. A segment of a rod in the reference (initial, undeformed) and current configurations showing all forces acting on the segment.

Dividing by ΔX and taking the limit as $\Delta X \rightarrow 0$ gives

$$\rho_0 A_0 = \rho A \frac{\partial x}{\partial X} = \rho A F \quad \text{or} \quad \rho_0 (X) A_0 (X) = \rho(X,t) A(X,t) F(X,t) \tag{A.2}$$

The above is one form of the equation of mass conservation. On the right hand side the independent variables have been indicated to stress that this equation only holds when expressed in terms of the material coordinates; the variables on the RHS are functions of time, whereas the variables on the LHS are independent of time.

To obtain another form of this equation, we note that the volumes of the segment are related by the Jacobian by $d\Omega = J d\Omega_0$. Since $d\Omega = A dx$ and $d\Omega_0 = A_0 dX$, it follows that

$$J = \frac{A}{A_0} F \tag{A.3}$$

Substituting the above into (A.1) gives the another form of the mass conservation equation

$$\rho_0(X) = \rho(X,t)\, J(X,t) \tag{A.4}$$

The above equation also applies in multi-dimensional problems.

Momentum Equation. The momentum equation is derived by considering the segment of the rod shown in Fig. 2.9. The forces on the deformed segment are shown in Fig. 2.9 and consist of the forces arising from the stress, which act on the right and left hand end of the segment, and the body force; the body force is distributed over the entire segment and its net resultant is placed at the center of the segment. On the left hand end of the segment the force is $(A\sigma)\big|_x$, i.e. the product of the stress and the current area at the point x. The force due to the stress on the right hand end is given by $(A\sigma)\big|_{x+\Delta x}$. The resultant force due to the body force is obtained by multiplying $b\left(x+\frac{\Delta x}{2}\right)$ by the mass of the segment $\rho A\Delta x$. So if we write Newton's second law for the segment we have

$$-A\sigma\big|_x + (A\sigma)\big|_{x+\Delta x} + (\rho A b)\big|_{x+\frac{\Delta x}{2}}\Delta x = (\rho A\ddot{u})\big|_{x+\frac{\Delta x}{2}}\Delta x \tag{A.5}$$

where the LHS is the sum of the resultant forces from the stress and the body force and the RHS is the product of the mass of the segment and its acceleration.

The forces due to the stresses are now expanded by a Taylor's series about the midpoint of the segment, with the product $A\sigma$ treated as a single function, which gives

$$(A\sigma)\big|_{x+\Delta x} = (A\sigma)\big|_{x+\Delta x/2} + \left.\frac{\partial(A\sigma)}{\partial x}\right|_{x+\Delta x/2}\frac{\Delta x}{2} + O\left(\Delta x^2\right) \tag{A.6a}$$

$$(A\sigma)\big|_x = (A\sigma)\big|_{x+\Delta x/2} - \left.\frac{\partial(A\sigma)}{\partial x}\right|_{x+\Delta x/2}\frac{\Delta x}{2} + O\left(\Delta x^2\right) \tag{A.6b}$$

The use of a Taylor series expansion of course presupposes that the function is smooth enough so that the first derivative exists; this is not the case wherever the stress or the area is discontinuous. Substituting (A.6) into (A.5) and dividing by Δx gives

$$(A\sigma)_{,x} + \rho A b = \rho A\ddot{u} \tag{A.7}$$

The above is the momentum equation for a one-dimensional continuum of varying cross-section.

To derive the momentum equation in the reference configuration, we note that the forces on the sides of the segment are given by multiplying the nominal stress by the initial area, A_0P. The net force due to the body force is $\rho_0 A_0 b\Delta X$ since $\rho_0 b$ is a force per unit initial volume and the initial volume is $A_0\Delta X$. The mass of the segment is $\rho_0 A_0\Delta X$. Writing Newton's second law for the segment gives

$$(-A_0P)\big|_X + (A_0P)\big|_{X+\Delta X} + (\rho_0 A_0 b)\big|_{X+\frac{\Delta X}{2}}\Delta X = (\rho_0 A_0 b\ddot{u})\big|_{X+\frac{\Delta X}{2}}\Delta X \tag{A.8}$$

where the LHS is the sum of all forces acting on the segment and the RHS is the mass time the acceleration. Expressing the forces due to the nominal stresses by a Taylor series as in (A.6), but in terms of the material coordinate X, substituting into (A.8) and dividing by ΔX gives the momentum equation in Lagrangian form

$$\left(A_0 P\right)_{,X} + \rho_0 A_0 b = \rho_0 A_0 \ddot{u} \tag{A.9}$$

The above can easily be transformed to the Eulerian form, Eq. (A.7). By the stress transformation (2.1.2), we have $A_0 P = A\sigma$, so

$$\left(A_0 P\right)_{,x} = \left(A\sigma\right)_{,x} = \left(A\sigma\right)_{,x} x_{,X} = \left(A\sigma\right)_{,x} F \tag{A.10}$$

where the chain rule has been used in the third step, followed by the definition of F in Eq. (2.2.2). Substituting the (A.10) into (A.9) gives

$$0 = \left(A\sigma\right)_{,x} F + \rho_0 A_0 b - \rho_0 A_0 \ddot{u} = \left(A\sigma\right)_{,x} F + F\rho A b - F\rho A \ddot{u}$$

where the continuity equation (A.2) has been used in the last step. Dividing by F then gives the momentum equation in Eulerian form. Note that the body force in the Lagrangian and Eulerian momentum equations is identical. Some authors distinguish the body force in the total form by a subscript naught, i.e., Malvern (1969, p. 224), but this is superfluous if the body force is considered a force per unit mass so that ρb is a force per unit volume.

SUMMARY

The finite element equations have been developed for one-dimensional continua of varying cross-section. Two mesh descriptions have been used:

1. Lagrangian meshes, where the nodes and elements move with the material;
2. Eulerian meshes, in which nodes and elements are fixed in space.

Two formulations have been developed for Lagrangian meshes:

1. a total Lagrangian formulation, in which the strong form is expressed in spatial coordinates, i.e. the Eulerian coordinates;
2. an updated Lagrangian formulation, where the strong form is expressed in the material, i.e. the Lagrangian coordinates.

In both cases, the element formulation is most conveniently executed in terms of the element coordinates. The mapping of the element coordinates from current and original configuration for a valid finite element discretization is one-to-one and onto. Furthermore, the mapping to the original configuration is time invariant, so the element coordinates can serve as surrogate material coordinates.

It has also been shown that the updated and total Lagrangian formulations are two representations of the same mechanical behavior, and each can be transformed to the other at both the level of partial differential equations and the level of the discrete finite element equations. Thus the internal and external forces obtained by the total Lagrangian formulations are identical to those obtained by the updated formulation, and the choice of formulation is purely a matter of convenience.

The equation of motion corresponds to the momentum equation and is obtained from its weak form. As has been illustrated in the case of explicit time integration, the other equations, measure of deformation and constitutive, are used in the course of computing the internal nodal forces to update the displacements. The weak form and discrete equations have been structured so that their relationship to the corresponding terms in the partial differential equation of momentum conservation is readily apparent: the internal forces correspond to the stress terms, and the internal work (or power); the external forces correspond to the body forces and external work (or power); the terms **Ma** correspond to the inertial terms (d'Alembert) forces and the inertial work (or power). This correspondence is summarized in Fig. 8, which shows the steps which are used to convert the partial differential equation of momentum balance to a set of ordinary differential equations which are called the equations of motion. This process is called a *spatial discretization* or *semidiscretization*.

The discretization has been carried out for the general case when inertial forces are not negligible. If the inertial forces can be neglected, the term **Ma** is omitted from the discrete equations. The resulting equations are either nonlinear algebraic equations or ordinary differential equations, depending on the character of the constitutive equation.

The governing equations have been developed for a one-dimensional rod of varying cross-section and from these a weak form has been developed by integrating over the domain. When the equations are given in terms of partial derivatives with respect to the material derivatives, it is natural to develop the weak form by integrating over the undeformed domain. This leads to the *total Lagrangian formulation* where all nodal forces are obtained by integrating over the material coordinates. When the partial derivatives are with respect to the spatial coordinates, it is natural to integrate over the current configuration, which leads to the *updated Lagrangian formulation*.

The process of discretization for multidimensional problems is very similar. However, in multi-dimensional problems we will have to deal with the major consequence of geometric nonlinearities, large rotations, which are completely absent in one-dimensional problems.

Exercises

Exercise: Repeat Example 2.8.3 for spherical symmetry, where

$$\mathbf{h} = \begin{Bmatrix} \eta_r \\ \eta_\theta \\ \eta_\varphi \end{Bmatrix} \qquad \mathbf{s} = \begin{Bmatrix} \sigma_r \\ \sigma_\theta \\ \sigma_\varphi \end{Bmatrix}$$

give $\mathbf{B}$, $\mathbf{f}_e^{int}$, $\mathbf{f}_e^{ext}$, $\mathbf{M}_e$

CHAPTER 3
CONTINUUM MECHANICS

by Ted Belytschko
Northwestern University

DRAFT

3.1 INTRODUCTION

Continuum mechanics is an essential building block of nonlinear finite element analysis, and a mastery of continuum mechanics is essential for a good understanding of nonlinear finite elements. This chapter summarizes the fundamentals of nonlinear continuum mechanics which are needed for a development of nonlinear finite element methods. It is, however, insufficient for thoroughly learning continuum mechanics. Instead, it provides a review of the topics that are particularly relevant to nonlinear finite element analysis. The content of this chapter is limited to topics that are needed for the remainder of the book.

Readers who have little or no familiarity with continuum mechanics should consult texts such as Hodge (1970), Mase and Mase (1992), Fung (1994), Malvern (1969), or Chandrasekharaiah and Debnath (1994). The first three are the most elementary. Hodge (1970) is particularly useful for learning indicial notation and the fundamental topics. Mase and Mase (1992) gives a concise introduction with notation almost identical to that used here. Fung (1994) is an interesting book with many discussions of how continuum mechanics is applied. The text by Malvern (1969) has become a classic in this field for it provides a very lucid and comprehensive description of the field. Chandrasekharaiah and Debnath (1994) gives a thorough introduction with an emphasis on tensor notation. The only topic treated here which is not presented in greater depth in all of these texts is the topic of objective stress rates, which is only covered in Malvern. Monographs of a more advanced character are Marsden and Hughes (1983), Ogden (1984) and Gurtin (). Prager (1961), while an older book, still provides a useful description of continuum mechanics for the reader with an intermediate background. The classic treatise on continuum mechanics is Truesdell and Noll (1965) which discusses the fundamental issues from a very general viewpoint. The work of Eringen (1962) also provides a comprehensive description of the topic.

This Chapter begins with a description of deformation and motion, including some useful equations for characterizing deformation and the time derivatives of variables. Rigid body motion is described with an emphasis on rigid body rotation. Rigid body rotation plays a central role in nonlinear continuum mechanics, and many of the more difficult and complicated aspects of nonlinear continuum mechanics stem from rigid body rotation. The material concerning rigid body rotation should be carefully studied.

Next, the concepts of stress and strain in nonlinear continuum mechanics are described. Stress and strain can be defined in many ways in nonlinear continuum mechanics. We will confine our attention to the strain and stress

measures which are most frequently employed in nonlinear finite element programs. We cover the following kinematic measures in detail: the Green strain tensor and the rate-of-deformation. The second is actually a measure of strain rate, but these two are used in the majority of software. The stress measures treated are: the physical (Cauchy) stress, the nominal stress and the second Piola-Kirchhoff stress, which we call PK2 for brevity. There are many others, but frankly even these are too many for most beginning students. The profusion of stress and strain measures is one of the obstacles to understanding nonlinear continuum mechanics. Once one understands the field, one realizes that the large variety of measures adds nothing fundamental, and is perhaps just a manifestation of academic excess. Nonlinear continuum mechanics could be taught with just one measure of stress and strain, but additional ones need to be covered so that the literature and software can be understood.

The conservation equations, which are often called the balance equations, are derived next. These equations are common to both solid and fluid mechanics. They consist of the conservation of mass, momentum and energy. The equilibrium equation is a special case of the momentum equation which applies when there are no accelerations in the body. The conservation equations are derived both in the spatial and the material domains. In a first reading or introductory course, the derivations can be skipped, but the equations should be thoroughly known in at least one form.

The Chapter concludes with further study of the role of rotations in large deformation continuum mechanics. The polar decomposition theorem is derived and explained. Then objective rates, also called frame-invariant rates, of the Cauchy stress tensor are examined. It is shown why rate type constitutive equations in large rotation problems require objective rates and several objective rates frequently used in nonlinear finite elements are presented. Differences between objective rates are examined and some examples of the application of objective rates are illustrated.

3.2 DEFORMATION AND MOTION

3.2.1 Definitions. Continuum mechanics is concerned with models of solids and fluids in which the properties and response can be characterized by smooth functions of spatial variables, with at most a limited number of discontinuities. It ignores inhomogeneities such as molecular, grain or crystal structures. Features such as crystal structure sometimes appear in continuum models through the constitutive equations, and an example of this kind of model will be given in Chapter 5, but in all cases the response and properties are assumed to be smooth with a countable number of discontinuities. The objective of continuum mechanics is to provide a description to model the macroscopic behavior of fluids, solids and structures.

Consider a body in an initial state at a time t=0 as shown in Fig. 3.1; the domain of the body in the initial state is denoted by Ω_0 and called the *initial configuration*. In describing the motion of the body and deformation, we also need a configuration to which various equations are referred; this is called the *reference configuration*. Unless we specify otherwise, the initial configuration is used as the reference configuration. However, other configurations can also be used as the reference configuration and we will do so in some derivations. The

significance of the reference configuration lies in the fact that motion is defined with respect to this configuration.

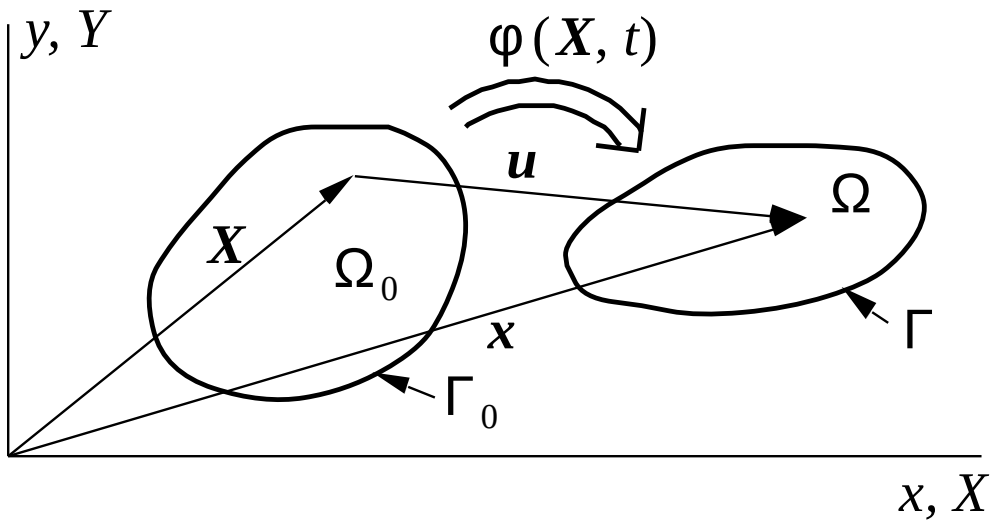

Fig. 3.1. Deformed (current) and undeformed (initial) configurations of a body.

In many cases, we will also need to specify a configuration which is considered to be an *undeformed configuration*. The notion of an "undeformed" configuration should be viewed as an idealization, since undeformed objects seldom exist in reality. Most objects previously had a different configuration and were changed by deformations: a metal pipe was once a steel ingot, a cellular telephone housing was once a vat of liquid plastic, an airport runway was once a truckload of concrete. So the term *undeformed configuration* is only relative and designates the configuration with respect to which we measure deformation. In this Chapter, the undeformed configuration is considered to be the initial configuration unless we specifically say otherwise, so it is tacitly assumed that i*n most cases the initial, reference, and undeformed configurations are identical* .

The *current configuration* of the body is denoted by Ω; this will often also be called the *deformed configuration*. The domain currently occupied by the body will also be denoted by Ω. The domain can be one, two or three dimensional; Ω then refers to a line, an area, or a volume, respectively. The boundary of the domain is denoted by Γ, and corresponds to the two end-points of a segment in one dimension, a curve in two dimensions, and a surface in three dimensions. The developments which follow hold for a model of any dimension from one to three. The dimension of a model is denoted by n_{SD}, where “SD” denotes space dimensions.

For a Lagrangian finite element mesh, the initial mesh is a discrete model of the initial, undeformed configuration, which is also the reference configuration. The configurations of the solution meshes are the current, deformed configurations. In an Eulerian mesh, the correspondence is more difficult to picture and is deferred until later.

3.2.2 Eulerian and Lagrangian Coordinates. The position vector of a material point in the reference configuration is given by **X**, where

$$\mathbf{X} = X_i \mathbf{e}_i \equiv \sum_{i=1}^{n_{SD}} X_i \mathbf{e}_i \tag{3.2.1}$$

where X_i are the components of the position vector in the reference configuration and $\mathbf{e}_i$ are the unit base vectors of a rectangular Cartesian coordinate system; indicial notation as described in Section 1.3 has been used in the second expression and will be used throughout this book. Some authors, such as Malvern (1969), also define material particles and carefully distinguish between material points and particles in a continuum. The notion of particles in a continuum is somewhat confusing, for the concept of particles to most of us is discrete rather than continuous. Therefore we will refer only to material points of the continuum.

The vector variable $\mathbf{X}$ for a given material point does not change with time; the variables $\mathbf{X}$ are called *material coordinates* or *Lagrangian coordinates* and provide labels for material points. Thus if we want to track the function $f(\mathbf{X},t)$ at a given material point, we simply track that function at a constant value of $\mathbf{X}$. The position of a point in the current configuration is given by

$$\mathbf{x} = x_i \mathbf{e}_i \equiv \sum_{i=1}^{n_{SD}} x_i \mathbf{e}_i \tag{3.2.2}$$

where x_i are the components of the position vector in the current configuration.

3.2.3 Motion. The *motion of the body* is described by

$$\mathbf{x} = \varphi(\mathbf{X},t) \qquad \text{or} \qquad x_i = \varphi_i(\mathbf{X},t) \tag{3.2.3}$$

where $\mathbf{x} = x_i \mathbf{e}_i$ is the position at time t of the material point $\mathbf{X}$. The coordinates $\mathbf{x}$ give the spatial position of a particle, and are called *spatial*, or *Eulerian coordinates*. The function $\varphi(\mathbf{X},t)$ maps the reference configuration into the current configuration at time t., and is often called a mapping or map.

When the reference configuration is identical to the initial configuration, as assumed in this Chapter, the position vector $\mathbf{x}$ of any point at time t=0 coincides with the material coordinates, so

$$\mathbf{X} = \mathbf{x}(\mathbf{X},0) \equiv \varphi(\mathbf{X},0) \qquad \text{or} \qquad X_i = x_i(\mathbf{X},0) = \varphi_i(\mathbf{X},0) \tag{3.2.4}$$

Thus the mapping $\varphi(\mathbf{X},0)$ is the identity mapping.

Lines of constant X_i, when etched into the material, behave just like a Lagrangian mesh; when viewed in the deformed configuration, these lines are no longer Cartesian. Viewed in this way, the material coordinates are often called convected coordinates. In pure shear for example, they become skewed coordinates, just like a Lagrangian mesh becomes skewed, see Fig. 1.2. However, when we view the material coordinates in the reference configuration, they are invariant with time. In the equations to be developed here, the material

coordinates are viewed in the reference configuration, so they are treated as a Cartesian coordinate system. The spatial coordinates, on the other hand, do not change with time regardless of how they are viewed.

3.2.4 Eulerian and Lagrangian Descriptions. Two approaches are used to describe the deformation and response of a continuum. In the first approach, the independent variables are the material coordinates **X** and the time *t*, as in Eq. (3.2.3); this description is called a *material description* or *Lagrangian description*. In the second approach, the independent variables are the spatial coordinates **x** and the time *t*. This is called a *spatial or Eulerian description.* The duality is similar to that in mesh descriptions, but as we have already seen in finite element formulations, not all aspects of a single formulation are exclusively Eulerian or Lagrangian; instead some finite element formulations combine Eulerian and Lagrangian descriptions as needed.

In fluid mechanics, it is often impossible and unnecessary to describe the motion with respect to a reference configuration. For example, if we consider the flow around an airfoil, a reference configuration is usually not needed for the behavior of the fluid is independent of its history. On the other hand, in solids, the stresses generally depend on the history of deformation and an undeformed configuration must be specified to define the strain. Because of the history-dependence of most solids, Lagrangian descriptions are prevalent in solid mechanics.

In the mathematics and continuum mechanics literature, cf. Marsden and Hughes (1983), different symbols are often used for the same field when it is expressed in terms of different independent variables, i.e. when the description is Eulerian or Lagrangian. In this convention, the function which in an Eulerian description is $f(\mathbf{x},t)$ is denoted by $F(\mathbf{X},t)$ in a Lagrangian description. The two functions are related by

$$F(\mathbf{X},t) = f\left(\varphi(\mathbf{X},t),t\right), \quad \text{or} \quad F = f \circ \varphi \tag{3.2.5}$$

This is called a *composition of functions*; the notation on the right is frequently used in the mathematics literature; see for example Spivak(1965, p.11). The notation for the composition of functions will be used infrequently in this book because it is unfamiliar to most engineers.

The convention of referring to different functions by different symbols is attractive and often adds clarity. However in finite element methods, because of the need to refer to three or more sets of independent variables, this convention becomes quite awkward. Therefore in this book, we associate a symbol with a field, and the specific function is defined by specifying the independent variables. Thus $f(\mathbf{x},t)$ is the function which describes the field f for the independent variables **x** and t, whereas $f(\mathbf{X},t)$ is a different function which describes the same field in terms of the material coordinates. The independent variables are always indicated near the beginning of a section or chapter, and if a change of independent variables is made, the new independent variables are noted.

3.3.5 Displacement, Velocity and Acceleration. The displacement of a material point is given by the difference between its current position and its original position (see Fig. 3.1), so

$$\mathbf{u}(\mathbf{X},t) = \varphi(\mathbf{X},t) - \varphi(\mathbf{X},0) = \varphi(\mathbf{X},t) - \mathbf{X}, \qquad u_i = \varphi_i\left(X_j,t\right) - X_i \tag{3.2.6}$$

where $\mathbf{u}(\mathbf{X},t) = u_i \mathbf{e}_i$ and we have used Eq. (3.2.4). The displacement is often written as

$$\mathbf{u} = \mathbf{x} - \mathbf{X}, \qquad u_i = x_i - X_i \tag{3.2.7}$$

where (3.2.1) has been used in (3.2.6) to replace $\varphi\left(\mathbf{X},t\right)$ by $\mathbf{x}$. Equation (3.2.7) is somewhat ambiguous since it expresses the displacement as the difference of two variables, $\mathbf{x}$ and $\mathbf{X}$, both of which are generally independent variables. The reader must keep in mind that in expressions such as (3.2.7) the variable $\mathbf{x}$ represents the motion $\mathbf{x}(\mathbf{X},t) \equiv \varphi(\mathbf{X},t)$.

The velocity $\mathbf{v}\left(\mathbf{X},t\right)$ is the rate of change of the position vector for a material point, i.e. the time derivative with $\mathbf{X}$ held constant. Time derivatives with $\mathbf{X}$ held constant are called *material time derivatives*; or sometimes *material derivatives*. Material time derivatives are also called *total derivatives*. The velocity can be written in the various forms shown below

$$\mathbf{v}(\mathbf{X},t) = \dot{\mathbf{u}} = \frac{\partial \varphi(\mathbf{X},t)}{\partial t} = \frac{\partial \mathbf{u}(\mathbf{X},t)}{\partial t} \tag{3.2.8}$$

In the above, the variable $\mathbf{x}$ is replaced by the displacement $\mathbf{u}$ in the fourth term by using (3.2.7) and the fact that $\mathbf{X}$ is independent of time. The symbol *D( )/Dt* and the superposed dot always denotes a material time derivative in this book, though the latter is often used for ordinary time derivatives when the variable is only a function of time.

The acceleration $\mathbf{a}(\mathbf{X},t)$ is the rate of change of velocity of a material point, or in other words the material time derivative of the velocity, and can be written in the forms

$$\mathbf{a}(\mathbf{X},t) = \frac{D\mathbf{v}}{Dt} \equiv \dot{\mathbf{v}} = \frac{\partial \mathbf{v}(\mathbf{X},t)}{\partial t} = \frac{\partial^2 \mathbf{u}(\mathbf{X},t)}{\partial t^2} \tag{3.2.9}$$

The above expression is called the material form of the acceleration.

When the velocity is expressed in terms of the spatial coordinates and the time, i.e. in an Eulerian description as in $\mathbf{v}(\mathbf{x},t)$, the material time derivative is obtained as follows. The spatial coordinates in $\mathbf{v}(\mathbf{x},t)$ are first expressed as a function of the material coordinates and time by using (3.2.3), giving $\mathbf{v}\left(\varphi(\mathbf{X},t),t\right)$. The material time derivative is then obtained by the chain rule:

$$\frac{Dv_i}{Dt} = \frac{\partial v_i(\mathbf{x},t)}{\partial t} + \frac{\partial v_i(\mathbf{x},t)}{\partial x_j}\frac{\partial \varphi_j(\mathbf{X},t)}{\partial t} = \frac{\partial v_i}{\partial t} + \frac{\partial v_i}{\partial x_j} v_j \tag{3.2.10}$$

where the second equality follows from (3.2.8). The second term on the RHS of (3.2.10) is the convective term, which is also called the transport term. In (3.2.10), the first partial derivative on the RHS is taken with the spatial coordinate fixed. This is called the *spatial time derivative*. It is tacitly assumed throughout this book that when neither the independent variables nor the fixed variable are explicitly indicated in a partial derivative with respect to time, then the spatial coordinate is fixed and we are referring to the spatial time derivative. On the other hand, when the independent variables are specified as in (3.2.8-9), a partial derivative can specify a material time derivative. Equation (3.2.10) is written in tensor notation as

$$\frac{D\mathbf{v}}{Dt} = \frac{\partial \mathbf{v}}{\partial t} + \mathbf{v} \quad \mathbf{v} = \frac{\partial \mathbf{v}}{\partial t} + \mathbf{v}\ grad\, \mathbf{v} \tag{3.2.11}$$

The material time derivative of any variable which is a function of the spatial variables $\mathbf{x}$ and time t can similarly be obtained by the chain rule. Thus for a scalar function $f(\mathbf{x},t)$ and a tensor function $\sigma_{ij}(\mathbf{x},t)$, the material time derivatives are given by

$$\frac{Df}{Dt} = \frac{\partial f}{\partial t} + v_i \frac{\partial f}{\partial x_i} = \frac{\partial f}{\partial t} + \mathbf{v} \quad f = \frac{\partial f}{\partial t} + \mathbf{v}\ grad\ f \tag{3.2.12}$$

$$\frac{D\sigma_{ij}}{Dt} = \frac{\partial \sigma_{ij}}{\partial t} + v_k \frac{\partial \sigma_{ij}}{\partial x_k} = \frac{\partial \sigma}{\partial t} + \mathbf{v} \quad \sigma = \frac{\partial \sigma}{\partial t} + \mathbf{v}\ grad\, \sigma \tag{3.2.13a}$$

where the first term on the RHS of each equation is the spatial time derivative and the second term is the convective term.

It should be remarked that the complete description of the motion is not needed to develop the material time derivative in an Eulerian description. In Eulerian meshes, the motion cannot be defined realistically defined as a function of the material positions in the initial configuration; see Chapter 7. In that case, variables such as the velocity can be developed by describing the motion with respect to a reference configuration that coincides with the configuration at a fixed time t.

For this purpose, let the configuration at time fixed time $t = \tau$ be the reference configuration and the position vector at that time, denoted by $\mathbf{X}^\tau$, be the reference coordinates. These reference coordinates are given by

$$\mathbf{X}^\tau = \varphi(\mathbf{X}, \tau) \tag{3.2.13b}$$

Observe we use an upper case $\mathbf{X}$ since we wish to clearly identify it as an independent variable, and we add the superscript τ to indicate that these reference coordinates are not the position vectors at the initial time. The motion can be described in terms of these reference coordinates by

$$\mathbf{x} = \varphi^{\tau}\left(\mathbf{X}^{\tau},\ t\right) \quad \text{for } t \geq \tau \tag{3.2.13c}$$

Now the arguments used to develop (3.2.10) can be repeated; noting that $\mathbf{v}(\mathbf{x},\ t) = \mathbf{v}\left(\varphi^{\tau}(\mathbf{X},\ t),\ t\right)$

$$\frac{Dv_i}{Dt} = \frac{\partial v_i(\mathbf{x},\ t)}{\partial t} + \frac{\partial v(x,\ t)}{\partial x_i}\frac{\partial \varphi_i^{\tau}}{\partial t} \tag{3.2.13d}$$

with $t = \tau$. Reference configurations coincident with a configuration other than the initial configuration will also be employed in the development of finite element equations.

3.2.6 Deformation Gradient. The description of deformation and the measure of strain are essential parts of nonlinear continuum mechanics. An important variable in the characterization of deformation is the deformation gradient. The *deformation gradient* is defined by

$$F_{ij} = \frac{\partial \varphi_i}{\partial X_j} \equiv \frac{\partial x_i}{\partial X_j} \quad \text{or} \quad \mathbf{F} = \frac{\partial \varphi}{\partial \mathbf{X}} \equiv \frac{\partial \mathbf{x}}{\partial \mathbf{X}} \equiv \left(\nabla_{\mathbf{X}}\varphi\right)^T \tag{3.2.14}$$

Note in the above that the first index of F_{ij} refers to the component of the deformation, the second to the partial derivative. The order can be remembered by noting that the indices appear in the same order in F_{ij} as in the expression for the partial derivative if it is written horizontally as $\partial\varphi_i/\partial X_j$. The operator $\nabla_{\mathbf{X}}$ is the *left gradient with respect to the material coordinates*. We will only use the left gradient in this book, but to maintain consistency with the notation of others such as Malvern, we follow his convention exactly. Therefore, the transpose of $\nabla_{\mathbf{X}}\varphi$ appears in the above because of the convention on subscripts: for the left gradient, the first subscript is the pertains to the gradient, but in F_{ij} the gradient is associated with the second index. The distinction between left and right gradients is not of importance in this book because we will always use the left gradient, but we adhere to the convention so that our equations are consistent with the continuum mechanics literature. In the terminology of mathematics, the deformation gradient is the *Jacobian matrix* of the vector function $\varphi(\mathbf{X},t)$.

If we consider an infinitesmal line segment $d\mathbf{X}$ in the reference configuration, then it follows from (3.2.14) that the corresponding line segment $d\mathbf{x}$ in the current configuration is given by

$$d\mathbf{x} = \mathbf{F}\ d\mathbf{X} \quad \text{or} \quad dx_i = F_{ij}dX_j \tag{3.2.15}$$

In the above expression, the dot could have been omitted between the $\mathbf{F}$ and $d\mathbf{X}$, since the expression is also valid as a matrix expression. We have retained it to conform to our conventionof always explicitly indicating contractions in tensor expressions.

In two dimensions, the deformation gradient in a rectangular coordinate system is given by

$$\mathbf{F} = \begin{bmatrix} \frac{\partial x_1}{\partial X_1} & \frac{\partial x_1}{\partial X_2} \\ \frac{\partial x_2}{\partial X_1} & \frac{\partial x_2}{\partial X_2} \end{bmatrix} = \begin{bmatrix} \frac{\partial x}{\partial X} & \frac{\partial x}{\partial Y} \\ \frac{\partial y}{\partial X} & \frac{\partial y}{\partial Y} \end{bmatrix} \tag{3.2.16}$$

As can be seen in the above, in writing a second-order tensor in matrix form, we use the first index for the row number, the second index for the column number.

The determinant of $\mathbf{F}$ is denoted by J and called the *Jacobian determinant* or the determinant of the deformation gradient

$$J = det(\mathbf{F}) \tag{3.2.17}$$

The Jacobian determinant can be used to relate integrals in the current and reference configurations by

$$\int_\Omega f \, d\Omega = \int_{\Omega_0} f \, J \, d\Omega_0 \quad \text{or in 2D: } \int_\Omega f(x, y) \, dxdy = \int_{\Omega_0} f(X, Y) \, J \, dXdY \tag{3.2.18}$$

The material derivative of the Jacobian determinant is given by

$$\frac{DJ}{Dt} \equiv \dot{J} = J div\mathbf{v} \equiv J\frac{\partial v_i}{\partial x_i} \tag{3.2.19}$$

The derivation of this formula is left as an exercise.

3.2.6 Conditions on Motion. The mapping $\varphi(\mathbf{X},t)$ which describes the motion and deformation of the body is assumed to satisfy the following conditions:

1. the function $\varphi(\mathbf{X},t)$ is continuous and continuously differentiable except on a finite number of sets of measure zero;
2. the function $\varphi(\mathbf{X},t)$ is one-to-one and onto;
3. the Jacobian determinant satisfies the condition $J>0$.

These conditions ensure that $\varphi(\mathbf{X},t)$ is sufficiently smooth so that compatibility is satisfied, i.e. so there are no gaps or overlaps in the deformed body. The motion and its derivatives *can be discontinuous or posses dicontinuous derivatives on sets of measure zero*; see Section 1.5, so it is characterized as piecewise continuously differentiable. Sets of measure zero are points in one dimension, lines in two dimensions and planes in three dimensions because a point has zero length, a line has zero area, and a surface has zero volume.

The deformation gradient, i.e. the derivatives of the motion, is generally discontinuous on interfaces between materials. Discontinuities in the motion itself characterize phenomena such as a growing crack. We require the number of discontinuities in a motion and its derivatives to be finite. In fact, in some

nonlinear problems, it has been found that the solutions posses an infinite number of discontinuities, see for example James () and Belytschko, et al (1986). However, these solutions are quite unusual and cannot be treated effectively by finite element methods, so we will not concern ourselves with these types of problems.

The second condition in the above list requires that for each point in the reference configuration Ω_0, there is a unique point in Ω and vice versa. This is a sufficient and necessary condition for the regularity of $\mathbf{F}$, i.e. that $\mathbf{F}$ be invertible. When the deformation gradient $\mathbf{F}$ is regular, the Jacobian determinant J must be nonzero, since the inverse of $\mathbf{F}$ exists if and only if its determinant $J \neq 0$. Thus the second and third conditions are related. We have stated a stronger condition that J be positive rather than just nonzero, which will be seen in Section 3.5.4 to follow from mass conservation.

3.2.7 Rigid Body Rotation and Coordinate Transformations. Rigid body rotation plays a crucial role in the theory of nonlinear continuum mechanics. Many of the complexities which permeate the field arise from rigid body rotation. Furthermore, the decision as to whether linear or nonlinear software is appropriate for a particular linear material problem hinges on the magnitude of rigid body rotations. When the rigid body rotations are large enough to render a linear strain measure invalid, nonlinear software must be used.

A rigid body motion consisting of a translation $\mathbf{x}_T(t)$ and a rotation about the origin is written as

$$\mathbf{x}(\mathbf{X},t) = \mathbf{R}(t)\ \mathbf{X} + \mathbf{x}_T(t) \qquad x_i(\mathbf{X},t) = R_{ij}(t)X_j + x_{Ti}(t) \tag{3.2.20}$$

where $\mathbf{R}(t)$ is the rotation tensor, also called a rotation matrix. Because rigid body rotation preserves length, and noting that $d\mathbf{x}_T = \mathbf{0}$ in rigid body motion, we have

$$d\mathbf{x}\ \ d\mathbf{x} = d\mathbf{X}\ \left(\mathbf{R}^T\ \mathbf{R}\right)\ d\mathbf{X} \qquad dx_i dx_i = R_{ij}dX_j R_{ik}\,dX_k = dX_j\left(R_{ji}^T R_{ik}\right)dX_k$$

Since the length must stay unchanged in rigid body motion, it follows that

$$\mathbf{R}^T\ \mathbf{R} = \mathbf{I} \tag{3.2.20b}$$

and its inverse is given by its transpose:

$$\mathbf{R}^{-1} = \mathbf{R}^T \qquad R_{ij}^{-1} = R_{ij}^T = R_{ji} \tag{3.2.21}$$

The rotation tensor $\mathbf{R}$ is therefore said to be an orthogonal matrix and any transformation by this matrix, such as $\mathbf{x} = \mathbf{R}\mathbf{X}$, is called an orthogonal transformation. Rotation is an example of an orthogoanl transformation.

A rigid body rotation of a Lagrangian mesh of rectangular elements is shown in Fig. 3.2. As can be seen, in the rigid body rotation, the element edges

are rotated but the angles between the edges remain right angles. The element edges are lines of constant X and Y, so when viewed in the deformed configuration, the material coordinates are rotated when the body is rotated as shown in Fig. 3.2.

Specific expressions for the rotation matrix can be obtained in various ways. We obtain it here by relating the components of the vector in $\mathbf{r}$ two different coordinate systems with orthogonal base vectors $\mathbf{e}_i$ and $\hat{\mathbf{e}}_i$; a two dimensional example is shown in Fig. 3.3. The components in the rotated coordinate system are shown in Fig. 3.3. Since the vector $\mathbf{r}$ is independent of the coordinate system

$$\mathbf{r} = r_i \mathbf{e}_i = \hat{r}_i \hat{\mathbf{e}}_i \tag{3.2.22}$$

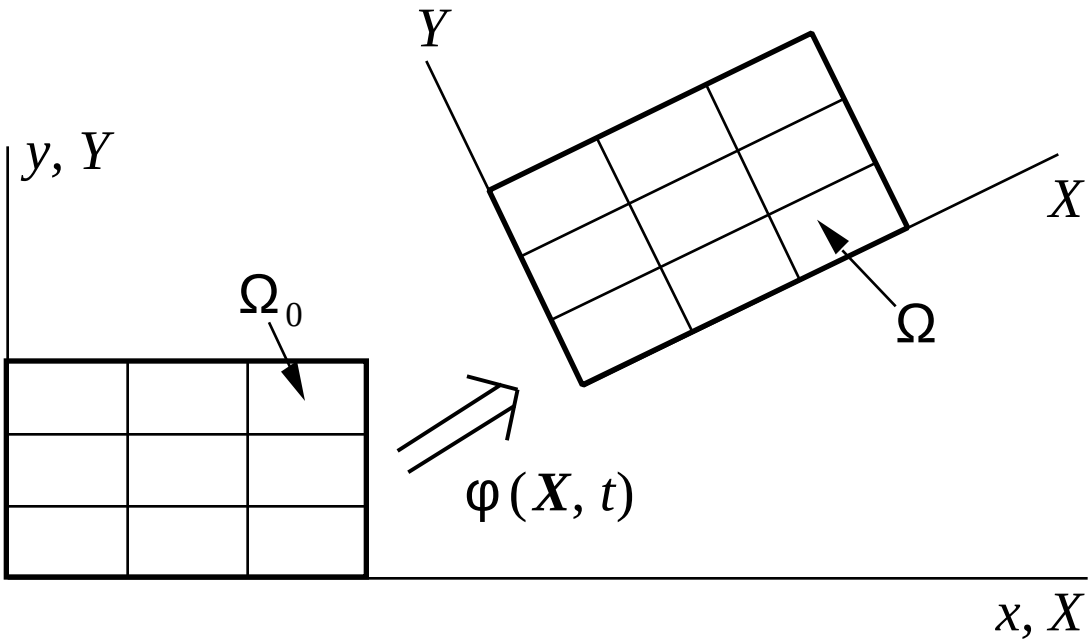

Fig. 3.2. A rigid body rotation of a Lagrangian mesh showing the material coordinates when viewed in the reference (initial, undeformed) configuration and the current configuration.

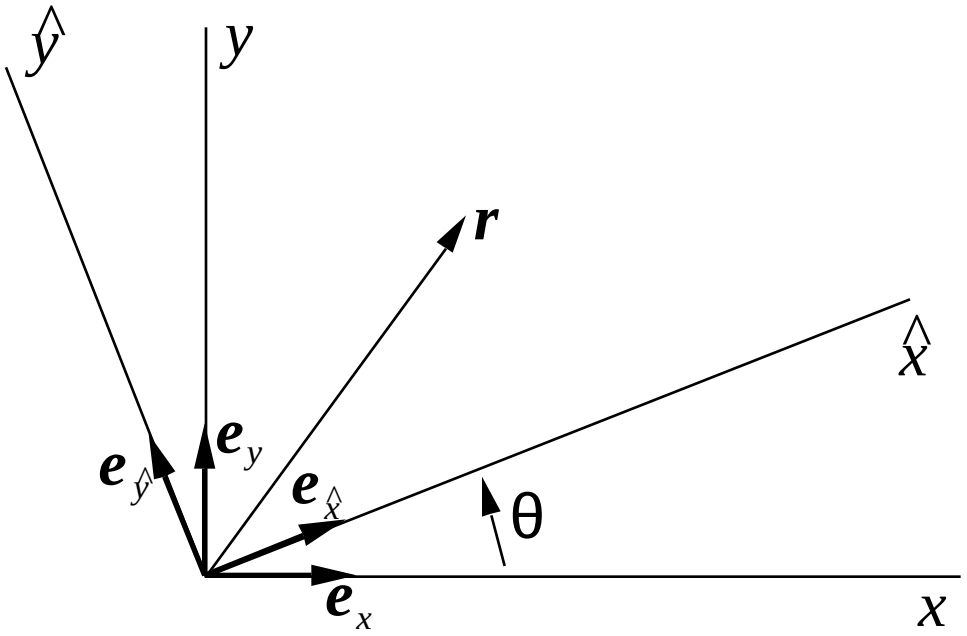

Fig. 3.3. Nomenclature for rotation transformation in two dimensions.

Taking the scalar product of the above with $\mathbf{e}_j$ gives

$$r_i \mathbf{e}_i \cdot \mathbf{e}_j = \hat{r}_i \hat{\mathbf{e}}_i \cdot \mathbf{e}_j \rightarrow r_i \delta_{ij} = \hat{r}_i \hat{\mathbf{e}}_i \cdot \mathbf{e}_j \rightarrow r_j = R_{ji} \hat{r}_i, \quad R_{ji} = \mathbf{e}_j \cdot \hat{\mathbf{e}}_i \tag{3.2.23}$$

The second equation follows from the orthogonality of the base vectors, (3.2.21).

The above shows that the elements of the rotation matrix are given by the scalar products of the corresponding base vectors; thus $R_{12} = \mathbf{e}_1 \cdot \hat{\mathbf{e}}_2$. So the transformation formulas for the components of a vector are

$$r_i = R_{ij} \hat{r}_j \equiv R_{i\hat{j}} \hat{r}_j, \quad \hat{r}_j = R^T_{ji} r_i = R_{\hat{j}i} r_i \tag{3.2.24}$$

where the equation on the right follows from (3.3.20b). In the second term of the indicial forms of the equations we have put the hat on the component associated with the hatted coordinates, but later it is often omitted. Note that the hatted index is always the second index of the rotation matrix; this convention helps in remembering the form of the transformation eqaution. In matrix form the above are written as

$$\mathbf{r} = \mathbf{R} \hat{\mathbf{r}}, \qquad \hat{\mathbf{r}} = \mathbf{R}^T \mathbf{r}$$

The above is a *matrix expression,* as indicated by the absence of dots between the terms. The column matrices of components $\mathbf{r}$ and $\hat{\mathbf{r}}$ differ, but they pertain to the same tensor. In many works, this distinction is clarified by using different symbols for matrices and tensors, but the notation we have chosen does not pemit this distinction.

Writing out the rotation transformation in two dimensions gives

$$\begin{Bmatrix} r_x \\ r_y \end{Bmatrix} = \begin{bmatrix} R_{x\hat{x}} & R_{x\hat{y}} \\ R_{y\hat{x}} & R_{y\hat{y}} \end{bmatrix} \begin{Bmatrix} \hat{r}_x \\ \hat{r}_y \end{Bmatrix} = \begin{bmatrix} \mathbf{e}_x \cdot \hat{\mathbf{e}}_{\hat{x}} & \mathbf{e}_x \cdot \hat{\mathbf{e}}_{\hat{y}} \\ \mathbf{e}_y \cdot \hat{\mathbf{e}}_{\hat{x}} & \mathbf{e}_y \cdot \hat{\mathbf{e}}_{\hat{y}} \end{bmatrix} \begin{Bmatrix} \hat{r}_x \\ \hat{r}_y \end{Bmatrix} = \begin{bmatrix} \cos\theta & -\sin\theta \\ \sin\theta & \cos\theta \end{bmatrix} \begin{Bmatrix} \hat{r}_x \\ \hat{r}_y \end{Bmatrix} \tag{3.2.25}$$

In the above, it can be seen that the subscripts of the rotation matrix correspond to the vector components which are related by that term; for example, in the expression for the x component in row 1, the $R_{x\hat{y}}$ is the coefficient of the $\hat{y}$ component of $\mathbf{r}$. The last form of the transformation in the above is obtained by evaluating the scalar products from Fig. 3.3 by inspection.

The rotation of a vector is obtained by a similar relation. If the vector $\mathbf{w}$ is obtained by a rotation of the vector $\mathbf{v}$, the two are related by

$$\mathbf{w} = \mathbf{R}\ \mathbf{v}, \quad w_i = R_{ij} v_j \tag{3.2.26}$$

The first of the above can be written as

$$\mathbf{w} = \mathbf{R}\ \left(v_j \mathbf{e}_j\right) = v_j \left(\mathbf{R}\ \mathbf{e}_j\right) = v_j \hat{\mathbf{e}}_j \tag{3.2.27}$$

where we have used the fact that the base vectors transform exactly like the components; this can easily be derived by using (3.2.23). Taking the inner product of the first and last expressions of the above with the rotated base vector $\hat{\mathbf{e}}_i$ gives

$$\hat{w}_i = \hat{\mathbf{e}}_i \cdot \mathbf{w} = v_j \left(\hat{\mathbf{e}}_i \cdot \hat{\mathbf{e}}_j\right) = v_j \delta_{ij} = v_i \tag{3.2.28}$$

This shows that the components of the rotated vector $\mathbf{w}$ in the rotated coordinate system are identical to the components of the vector $\mathbf{v}$ in the unrotated coordinate system.

The components of a second order tensor $\mathbf{D}$ are transformed between different coordinate systems by

$$\mathbf{D} = \mathbf{R}\hat{\mathbf{D}}\mathbf{R}^T \qquad D_{ij} = R_{ik} \hat{D}_{kl} R^T_{lj} \tag{3.2.30a}$$

The inverse of the above is obtained by premultiplying by $\mathbf{R}^T$, postmultiplying by $\mathbf{R}$ and using the orthogonality of $\mathbf{R}$, (3.2.20b):

$$\hat{\mathbf{D}} = \mathbf{R}^T \mathbf{D} \mathbf{R} \qquad D_{ij} = R_{ik} \hat{D}_{kl} R^T_{lj} \tag{3.2.30b}$$

Note that the above are matrix expressions which relate the components of the same tensor in two different coordinate systems.

The velocity for a rigid body motion can be obtained by taking the time derivative of Eq. (3.2.20). This gives

$$\dot{\mathbf{x}}(\mathbf{X},t) = \dot{\mathbf{R}}(t)\ \mathbf{X} + \dot{\mathbf{x}}_T(t) \quad \text{or} \quad \dot{x}_i(\mathbf{X},t) = \dot{R}_{ij}(t)X_j + \dot{x}_{Ti}(t) \tag{3.2.31}$$

The structure of rigid body rotation can be clarified by expressing the material coordinates in (3.2.31) in terms of the spatial coordinates via (3.2.20), giving

$$\mathbf{v} \equiv \dot{\mathbf{x}} = \dot{\mathbf{R}}\ \mathbf{R}^T\ \left(\mathbf{x} - \mathbf{x}_T\right) + \dot{\mathbf{x}}_T \tag{3.2.32}$$

The tensor

$$\Omega = \dot{\mathbf{R}}\ \mathbf{R}^T \tag{3.2.33}$$

is called the *angular velocity tensor* or *angular velocity matrix*, Dienes(1979, p 221). It is a skew symmetric tensor, skew symmetric tensors are also called *antisymmetric tensors*. To demonstrate the skew symmetry of the angular velocity tensor, we take the time derivative of (3.2.21) which gives

$$\frac{D}{Dt}\left(\mathbf{R}\ \mathbf{R}^T\right) = \frac{D\mathbf{I}}{Dt} = \mathbf{0} \rightarrow \dot{\mathbf{R}}\ \mathbf{R}^T + \mathbf{R}\ \dot{\mathbf{R}}^T = \mathbf{0} \rightarrow \Omega = -\Omega^T \tag{3.2.34}$$

Any skew symmetric tensor can be expressed in terms of the components of a vector, cakked the *axial vector,* and the corresponding action of that matrix on a vector can be replicated by a cross product, so if ω if the axial vector of Ω, then

$$\Omega\mathbf{r} = \omega \times \mathbf{r} \qquad \text{or} \qquad \Omega_{ij} r_j = e_{ijk}\omega_j r_k \tag{3.2.34b}$$

for any $\mathbf{r}$ and

$$e_{ijk} = \begin{cases} 1 \text{ for an even permutation of } ijk \\ -1 \text{ for an odd permutation of } ijk \\ 0 \text{ if any index is repeated} \end{cases} \tag{3.2.36}$$

The tensor e_{ijk} is called the *alternator tensor* or *permutation symbol.*

The relations between the skew symmetric tensor Ω and its axial vector ω are

$$\omega_i = \tfrac{1}{2} e_{ijk}\Omega_{jk}, \quad \Omega_{ij} = e_{ijk}\omega_k \tag{3.2.35}$$

which can be obtained by enforcing (3.2.34b) for all $\mathbf{r}$.

In two dimensions, a skew symmetric tensor has a single independent component and its axial vector is perpendicular to the two dimensional plane of the model, so

$$\Omega = \begin{bmatrix} 0 & \Omega_{12} \\ -\Omega_{12} & 0 \end{bmatrix} = \begin{bmatrix} 0 & -\omega_3 \\ \omega_3 & 0 \end{bmatrix} \tag{3.2.37a}$$

In three dimensions, a skew symmetric tensor has three independent components and which are related to the three components of its axial vector by (3.2.25) giving

$$\Omega = \begin{bmatrix} 0 & \Omega_{12} & \Omega_{13} \\ -\Omega_{12} & 0 & \Omega_{23} \\ -\Omega_{13} & -\Omega_{23} & 0 \end{bmatrix} = \begin{bmatrix} 0 & \omega_3 & -\omega_2 \\ -\omega_3 & 0 & \omega_1 \\ \omega_2 & -\omega_1 & 0 \end{bmatrix} \qquad (3.2.37b).$$

When Eq. (3.3.32) is expressed in terms of the angular velocity vector, we have

$$\begin{aligned} v_i \equiv \dot{x}_i &= \Omega_{ij}\left(x_j - x_{Tj}\right) + v_{Ti} \\ &= e_{ijk}\omega_j\left(x_k - x_{Tk}\right) + v_{Ti} \end{aligned} \quad \text{or} \quad \mathbf{v} \equiv \dot{\mathbf{x}} = \boldsymbol{\omega} \times \left(\mathbf{x} - \mathbf{x}_T\right) + \mathbf{v}_T \qquad (3.2.38)$$

where we have exchanged k and j in the second line and used $e_{kij} = e_{ijk}$. The second equation is the well known equation for rigid body motion as given in dynamics texts. The first term on the left hand side is velocity due to the rotation about the point $\mathbf{x}_T$ and the second term is the translational velocity of the point $\mathbf{x}_T$. Any rigid body velocity can be expressed by (3.2.28).

This concludes the formal discussion of rotation in this Chapter. However, the topic of rotation will reappear in many other parts of this Chapter and this book. Rotation, especially when combined with deformation, is fundamental to nonlinear continuum mechanics, and it should be thoroughly understood by a student of this field.

Corotational Rate-of-Deformation. As we shall see later, in many cases it is convenient to rotate the coordinate at each point of the material with the material. The rate-of-deformation is then expressed in terms of its corotational components $\hat{D}_{ij}$, which can be obtained from the global components by (3.2.30). These components can be obtained directly from the velocity field by

$$\hat{D}_{ij} = \frac{1}{2}\left(\frac{\partial \hat{v}_i}{\partial \hat{x}_j} + \frac{\partial \hat{v}_j}{\partial \hat{x}_i}\right) \equiv sym\left(\frac{\partial \hat{v}_i}{\partial \hat{x}_j}\right) \equiv v_{\hat{i},\hat{j}} \qquad (3.2.39)$$

where $\hat{v}_i \equiv v_{\hat{i}}$ are the components of the velocity field in the corotational system. the corotational system can be obtained from the polar decomposition theorem to be described later or by other techniques; see section 4.6.

Example 3.1 Rotation and Stretch of Triangular Element. Consider the 3-node triangular finite element shown in Fig. 3.4. Let the motion of the nodes be given by

$$
\begin{aligned}
&x_1(t) = y_1(t) = 0 \\
&x_2(t) = 2(1+at)\cos\frac{\pi t}{2}, \quad y_2(t) = 2(1+at)\sin\frac{\pi t}{2} \\
&x_3(t) = -(1+bt)\sin\frac{\pi t}{2}, \quad y_3(t) = (1+bt)\cos\frac{\pi t}{2}
\end{aligned}
\tag{E3.1.1}
$$

Find the deformation function and the Jacobian determinant as a function of time and find the values of *a(t)* and *b(t)* such that the Jacobian determinant remains constant.

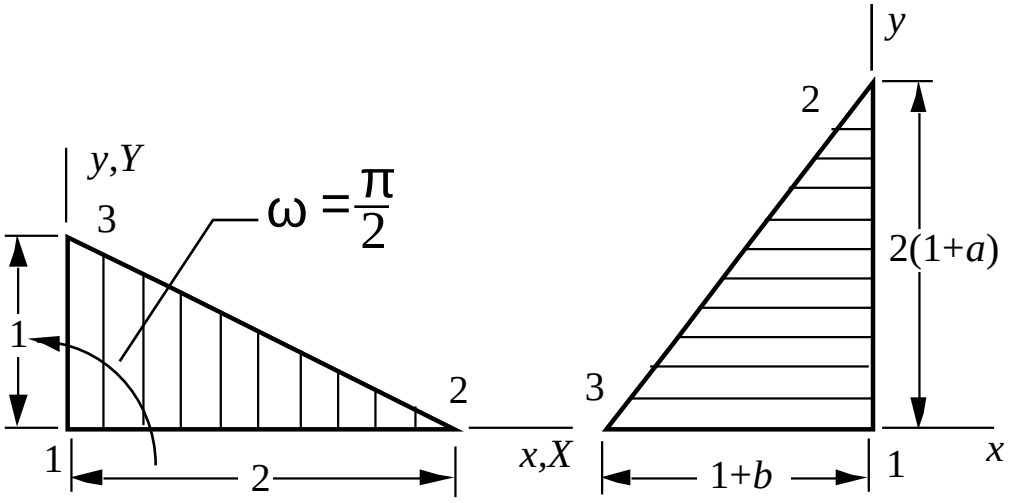

Fig. 3.4. Motion descrived by Eq. (E3.1.1) with the initial configuration at the left and the deformed configuration at t=1 shown at the right.

In terms of the triangular element coordinates ξ_I, the configuration of a triangular 3-node, linear displacement element at any time can be written as (see Appendix A if you are not familiar with triangular coordinates)

$$
\begin{aligned}
x(\xi,t) &= \sum_I x_I(t)\xi_I = x_1(t)\xi_1 + x_2(t)\xi_2 + x_3(t)\xi_3 \\
y(\xi,t) &= \sum_I y_I(t)\xi_I = y_1(t)\xi_1 + y_2(t)\xi_2 + y_3(t)\xi_3
\end{aligned}
\tag{E3.1.2}
$$

In the initial configuration, i.e. at t=0:

$$
\begin{aligned}
X &= x(\xi,0) = X_1\xi_1 + X_2\xi_2 + X_3\xi_3 \\
Y &= y(\xi,0) = Y_1\xi_1 + Y_2\xi_2 + Y_3\xi_3
\end{aligned}
\tag{E3.1.3}
$$

Substituting the coordinates of the nodes in the undeformed configuration into the above, $X_1 = X_3 = 0$, $X_2 = 2$, $Y_1 = Y_2 = 0$, $Y_3 = 1$ yields

$$
X = 2\xi_2, \quad Y = \xi_3 \tag{E3.1.4}
$$

In this case, the relations between the triangular coordinates and the material coordinates can be inverted by inspection to give

$$\xi_2 = \tfrac{1}{2} X, \qquad \xi_3 = Y \tag{E3.1.5}$$

Substituting (E3.1.1) and (E3.1.5) into (E3.1.2) gives the following expression for the motion

$$\begin{aligned} x(\mathbf{X},t) &= X(1+at)\cos\frac{\pi t}{2} - Y(1+bt)\sin\frac{\pi t}{2} \\ y(\mathbf{X},t) &= X(1+at)\sin\frac{\pi t}{2} + Y(1+bt)\cos\frac{\pi t}{2} \end{aligned} \tag{E3.1.6}$$

The deformation gradient is given by Eq.(3.2.16):

$$\mathbf{F} = \begin{bmatrix} \partial x/\partial X & \partial x/\partial Y \\ \partial y/\partial X & \partial y/\partial Y \end{bmatrix} = \begin{bmatrix} (1+at)\cos\frac{\pi t}{2} & -(1+bt)\sin\frac{\pi t}{2} \\ (1+at)\sin\frac{\pi t}{2} & (1+bt)\cos\frac{\pi t}{2} \end{bmatrix} \tag{E3.1.7}$$

The deformation gradient is a function of time only and at any time constant in the element because the displacement in this element is a linear function of the material coordinates. The determinant of the deformation gradient is given by

$$J = det(\mathbf{F}) = (1+at)(1+bt)\left(\cos^2\frac{\pi t}{2} + \sin^2\frac{\pi t}{2}\right) \tag{E3.1.8}$$

When a=b=0 the Jacobian determinant remains constant, J=1. This is a rotation without deformation. As expected, the Jacobian determinant remains constant since the volume (or area in two dimensions) of anypart of a body does not change in a rigid body motion. The second case in which the Jacobian determinant J remains constant is when $b = -a/(1+at)$, which corresponds to a deformation in which the area of the element remains constant. This is the type of deformation is called an isochoric deformation; the deformation of incompressible materials is isochoric.

Example 3.2 Consider an element which is rotating at a constant angular velocity ω about the origin. Obtain the accelerations using both the material and spatial descriptions. Fine the deformation gradient F and its rate.

The motion for a pure rotation about the origin is obtained from Eq. (3.2.20) using the rotation matrix in two dimensions (3.2.25):

$$\mathbf{x}(t) = \mathbf{R}(t)\mathbf{X} \qquad \begin{bmatrix} x \\ y \end{bmatrix} = \begin{bmatrix} \cos\omega t & -\sin\omega t \\ \sin\omega t & \cos\omega t \end{bmatrix} \begin{bmatrix} X \\ Y \end{bmatrix} \tag{E3.2.1}$$

where we have used $\theta = \omega t$ to express the motion is a function of time; ω is the angular velocity of the body. The velocity is obtained by taking the derivative of this motion with respect to time, which gives

$$\begin{bmatrix} v_x \\ v_y \end{bmatrix} = \begin{bmatrix} \dot{x} \\ \dot{y} \end{bmatrix} = \omega \begin{bmatrix} -\sin \omega t & -\cos \omega t \\ \cos \omega t & -\sin \omega t \end{bmatrix} \begin{bmatrix} X \\ Y \end{bmatrix} \tag{E3.2.2}$$

The acceleration in the material description is obtained by taking time derivatives of the velocities

$$\begin{bmatrix} a_x \\ a_y \end{bmatrix} = \begin{bmatrix} \dot{v}_x \\ \dot{v}_y \end{bmatrix} = \omega^2 \begin{bmatrix} -\cos \omega t & \sin \omega t \\ -\sin \omega t & -\cos \omega t \end{bmatrix} \begin{bmatrix} X \\ Y \end{bmatrix} \tag{E3.2.3}$$

To obtain a spatial description for the velocity, the material coordinates X and Y in (E3.2.2) are first expressed in terms of the spatial coordinates x and y by inverting (E3.2.1):

$$\begin{aligned} \begin{bmatrix} v_x \\ v_y \end{bmatrix} &= \omega \begin{bmatrix} -\sin \omega t & -\cos \omega t \\ \cos \omega t & -\sin \omega t \end{bmatrix} \begin{bmatrix} \cos \omega t & \sin \omega t \\ -\sin \omega t & \cos \omega t \end{bmatrix} \begin{bmatrix} x \\ y \end{bmatrix} \\ &= \omega \begin{bmatrix} 0 & -1 \\ 1 & 0 \end{bmatrix} \begin{bmatrix} x \\ y \end{bmatrix} = \omega \begin{bmatrix} -y \\ x \end{bmatrix} \end{aligned} \tag{E3.2.4}$$

The material time derivative the velocity field in the spatial description, Eq.(E3.2.4), is obtained via Eq.(3.2.11):

$$\begin{aligned} \frac{D\mathbf{v}}{Dt} &= \frac{\partial \mathbf{v}}{\partial t} + \mathbf{v} \quad \mathbf{v} = \begin{bmatrix} \partial v_x / \partial t \\ \partial v_y / \partial t \end{bmatrix} + \begin{bmatrix} \partial v_x / \partial x & \partial v_x / \partial y \\ \partial v_y / \partial x & \partial v_y / \partial y \end{bmatrix} \begin{bmatrix} v_x \\ v_y \end{bmatrix} \\ &= 0 + \begin{bmatrix} 0 & -\omega \\ \omega & 0 \end{bmatrix} \begin{bmatrix} v_x \\ v_y \end{bmatrix} = \omega \begin{bmatrix} -v_y \\ v_x \end{bmatrix} \end{aligned} \tag{E3.2.5}$$

If we then express the velocity field in (E3.2.5) in terms of the spatial coordinates x and y by Eq.(E3.2.4), we have

$$\begin{bmatrix} a_x \\ a_y \end{bmatrix} = \omega \begin{bmatrix} 0 & -1 \\ 1 & 0 \end{bmatrix} \omega \begin{bmatrix} 0 & -1 \\ 1 & 0 \end{bmatrix} \begin{bmatrix} x \\ y \end{bmatrix} = \omega^2 \begin{bmatrix} -1 & 0 \\ 0 & -1 \end{bmatrix} \begin{bmatrix} x \\ y \end{bmatrix} = -\omega^2 \begin{bmatrix} x \\ y \end{bmatrix} \tag{E3.2.6}$$

This is the well known result for the centrifugal acceleration: the acceleration vector points toward the center of rotation and its magnitude is $\omega^2 \left(x^2 + y^2 \right)^{\frac{1}{2}}$.

To compare the above with the material form of the acceleration (E3.2.3) we use (E3.2.1) to express the spatial coordinates in (E3.2.6) in terms of the material coordinates, which gives

$$\begin{bmatrix} \dot{v}_x \\ \dot{v}_y \end{bmatrix} = \omega^2 \begin{bmatrix} -1 & 0 \\ 0 & -1 \end{bmatrix} \begin{bmatrix} \cos \omega t & -\sin \omega t \\ \sin \omega t & \cos \omega t \end{bmatrix} \begin{bmatrix} X \\ Y \end{bmatrix} = \omega^2 \begin{bmatrix} -\cos \omega t & \sin \omega t \\ -\sin \omega t & -\cos \omega t \end{bmatrix} \begin{bmatrix} X \\ Y \end{bmatrix} \tag{E3.2.7}$$

which agrees with Eq. (E3.2.3).

The deformation gradient in obtained from its defintion (3.2.14) and (E3.2.1)

$$\mathbf{F} = \frac{\partial \mathbf{x}}{\partial \mathbf{X}} = \mathbf{R} = \begin{bmatrix} \cos\omega t & -\sin\omega t \\ \sin\omega t & \cos\omega t \end{bmatrix} \quad \mathbf{F}^{-1} = \begin{bmatrix} \cos\omega t & \sin\omega t \\ -\sin\omega t & \cos\omega t \end{bmatrix} \tag{E3.2.8}$$

Example 3.3 Consider a square 4-node element, with 3 of the nodes fixed as shown in Fig. 3.5. Find the locus of positions of node 3 which results in a vanishing Jacobian.

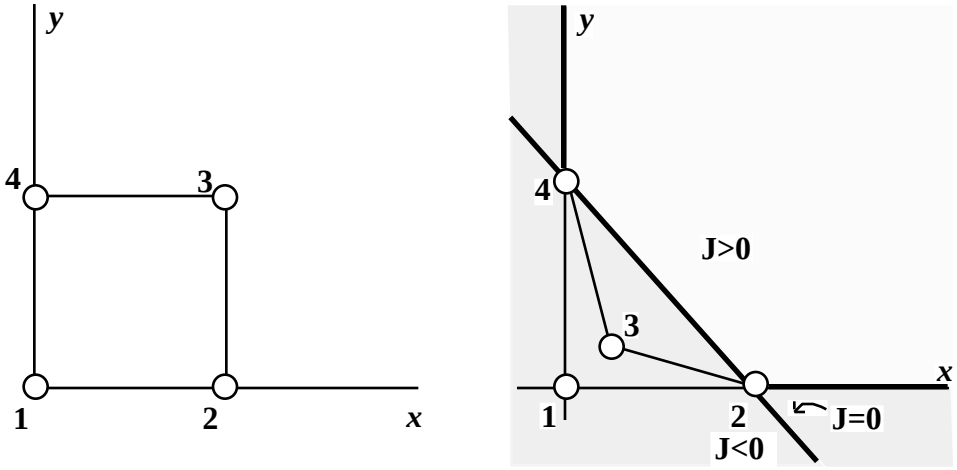

Figure 3.5. Original configuration of a square element and the locus of points for which $J = 0$; a deformed configuration with $J < 0$ is also shown.

The displacement field for the rectangular element with all nodes but node 3 fixed is given by the bilinear field

$$u_x(X,Y) = u_{3x}XY, \qquad u_y(X,Y) = u_{3y}XY \tag{E3.3.1}$$

Since this element is a square, an isoparametric mapping is not needed. This displacement field vanishes along the two shaded edges. The motion is given by

$$\begin{aligned} x &= X + u_x = X + u_{3x}XY \\ y &= Y + u_y = Y + u_{3y}XY \end{aligned} \tag{E3.3.2}$$

The deformation gradient is obtained from the above and Eq. (3.2.14):

$$\mathbf{F} = \begin{bmatrix} 1 + u_{3x}Y & u_{3x}X \\ u_{3y}Y & 1 + u_{3y}X \end{bmatrix} \tag{E3.3.3}$$

The Jacobian determinant is then

$$J = \det(\mathbf{F}) = 1 + u_{3x}Y + u_{3y}X \tag{E3.3.4}$$

We now examine when the Jacobian determinant will vanish. We need only consider the Jacobian determinant for material particles in the undeformed configuration of the element, i.e. the unit square $X \in [0,1]$, $Y \in [0,1]$. From the Eq. (E3.3.4), it is apparent that J is minimum when $u_{3x} < 0$ and $u_{3y} < 0$. Then the minimum value of J occurs at X=Y=1, so

$$J \geq 0 \qquad 1 + u_{3x} Y + u_{3y} X \geq 0 \qquad 1 + u_{3x} + u_{3y} \geq 0 \tag{E3.3.5}$$

The locus of points along which J=0 is given by a linear function of the nodal displacements shown in Fig. 3.5, which also shows one deformed configuration of the element for which $J < 0$. As can be seen, the Jacobian becomes negative when node 3 crosses the diagonal of the undeformed element.

Example 3.4. The displacement field around a growing crack is given by

$$\begin{aligned} u_x &= kf(r)\left(a + 2\sin^2\frac{\theta}{2}\right)\cos\frac{\theta}{2} \\ u_y &= kf(r)\left(b - 2\cos^2\frac{\theta}{2}\right)\sin\frac{\theta}{2} \end{aligned} \tag{E3.4.1}$$

$$r^2 = (X - ct)^2 + Y^2, \qquad \theta = \tan^{-1}(Y/X) \tag{E3.4.2}$$

where $a, b, c,$ and k are parameters which would be determined by the solution of the governing equations. This displacement field corresponds to a crack opening along the X-axis at a velocity c; the configuration of the body at two times is shown in Fig. 3.6.

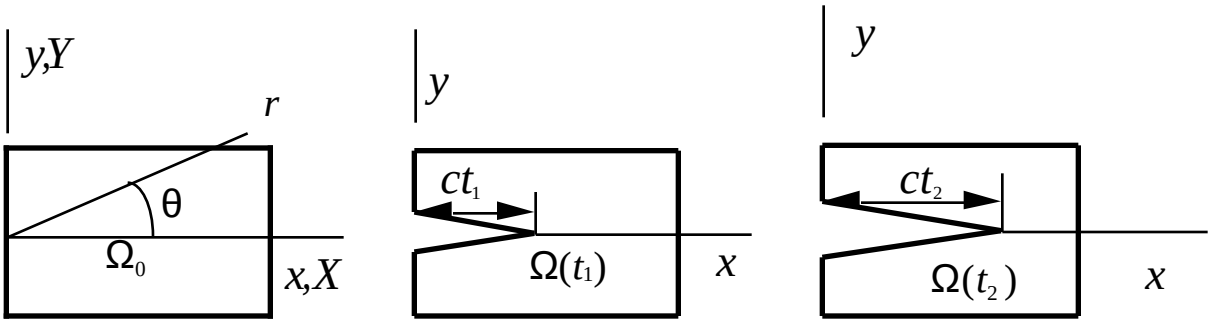

Figure 3.6. The initial uncracked configuration and two subsequent configurations for a crack growing along x-axis.

Find the discontinuity in the displacement along the line Y=0, $X \leq 0$. Does this displacement field conform with the requirements on the motion given in Section 3.2.7?

The motion is $x = X + u_x, y = Y + u_y$. The discontinuity in the displacement field is found by finding the difference in (E3.4.1) for $\theta = \pi^-$ and $\theta = \pi^+$, which gives

$$\theta = \pi^- \qquad u_x = 0,\ u_y = kf(r)b \tag{E3.4.3}$$

so the jumps, or discontinuities, in the displacement are

$$\langle u_x \rangle = 0,\ \langle u_y \rangle = 2kf(r)b \tag{E3.4.4}$$

Everywhere else the displacement field is continuous.

This deformation function meets the criteria given in Section 3.3.6 because the discontinuity occurs along only a line, which is a set of measure zero in a two dimensional problem. From Fig. 3.6 it can be seen that in this deformation, the line behind the crack tip splits into two lines. It is also possible to devise deformations where the line does not separate but a discontinuity occurs in the tangential displacement field. Both types of deformations are now common in nonlinear finite element analysis.

3.3 STRAIN MEASURES

In contrast to linear elasticity, many different measures of strain and strain rate are used in nonlinear continuum mechanics. Only two of these measures are considered here:

1. the Green (Green-Lagrange) strain **E**
2. the rate-of-deformation tensor **D**, also known as the velocity strain or rate-of-strain.

In the following, these measures are defined and some key properties are given. Many other measures of strain and strain rate appear in the continuum mechanics literature; however, the above are the most widely used in finite element methods. It is sometimes advantageous to use other measures in describing constitutive equations as discussed in Chapter 5, and these other strain measures will be introduced as needed.

A strain measure must vanish in any rigid body motion, and in particular in rigid body rotation. If a strain measure fails to meet this requirement, this strain measure will predict the developnet of nonzero strains, and in turn nonzero stresses, in an initially unstressed body due to rigid body rotation. The key reason why the usual linear strain displacement equations are abandoned in nonlinear theory is that they fail this test. This will be shown in Example 3.6. It will be shown in the following that **E** and **D** vanish in rigid body motion. A strain measure should satisfy other criteria, i.e. it should increase as the deformation increases, etc. (Hill,). However, the ability to represent rigid body motion is crucial and indicates when geometrically nonlinear theory must be used.

3.3.1 Green strain tensor. The Green strain tensor **E** is defined by

$$ds^2 - dS^2 = 2d\mathbf{X}\ \ \mathbf{E}\ \ d\mathbf{X} \quad \text{or} \quad dx_i dx_i - dX_i dX_i = 2\,dX_i E_{ij} dX_j \tag{3.3.1}$$

so it gives the change in the square of the length of the material vector $d\mathbf{X}$. Recall the vector $d\mathbf{X}$ pertains to the undeformed configuration. Therefore, the Green strain measures the difference of the square of the length of an infinitesimal segment in the current (deformed) configuration and the reference (undeformed)

configuration. To evaluate the Green strain tensor, we use (3.2.15) to rewrite the LHS of (3.3.1) as

$$d\mathbf{x}\ \ d\mathbf{x} = (d\mathbf{X}\ \ \mathbf{F})\ \ (\mathbf{F}\ \ d\mathbf{X}) = d\mathbf{X}\ \ \left(\mathbf{F}^T\ \ \mathbf{F}\right)\ \ d\mathbf{X} \tag{3.3.2}$$

The above are clearer in indicial notation

$$d\mathbf{x}\ \ d\mathbf{x} = dx_i dx_i = F_{ij} dX_j F_{ik} dX_k = dX_j F_{ji}^T F_{ik} dX_k = d\mathbf{X}\ \ \left(\mathbf{F}^T\ \ \mathbf{F}\right)\ \ d\mathbf{X}$$

Using the above with (3.3.1) and $d\mathbf{X}\ \ d\mathbf{X} = d\mathbf{X}\ \ \mathbf{I}\ \ d\mathbf{X}$ gives

$$d\mathbf{X}\ \ \mathbf{F}^T\ \ \mathbf{F}\ \ d\mathbf{X} - d\mathbf{X}\ \ \mathbf{I}\ \ d\mathbf{X} - d\mathbf{X}\ \ 2\mathbf{E}\ \ d\mathbf{X} = 0 \tag{3.3.3}$$

Factoring out the common terms then yields

$$d\mathbf{X}\ \ \left(\mathbf{F}^T\ \ \mathbf{F} - \mathbf{I} - 2\mathbf{E}\right)\ \ d\mathbf{X} = 0 \tag{3.3.4}$$

Since the above must hold for all $d\mathbf{X}$, it follows that

$$\mathbf{E} = \frac{1}{2}\left(\mathbf{F}^T\ \ \mathbf{F} - \mathbf{I}\right) \quad \text{or} \quad E_{ij} = \frac{1}{2}\left(F_{ik}^T F_{kj} - \delta_{ij}\right) \tag{3.3.5}$$

The Green strain tensor can also be expressed in terms of displacement gradients by

$$\mathbf{E} = \frac{1}{2}\left(\left(\ \ {}_X\mathbf{u}\right)^T + \ \ {}_X\mathbf{u} + \left(\ \ {}_X\mathbf{u}\right)^T\ \ \ {}_X\mathbf{u}\right), \quad E_{ij} = \frac{1}{2}\left(\frac{\partial u_i}{\partial X_j} + \frac{\partial u_j}{\partial X_i} + \frac{\partial u_k}{\partial X_i}\frac{\partial u_k}{\partial X_j}\right) \tag{3.3.6}$$

This expression is derived as follows. We first evaluate $\mathbf{F}^T\ \ \mathbf{F}$ in terms of the displacements using indicial notation.

$$F_{ik}^T F_{kj} = F_{ki} F_{kj} = \frac{\partial x_k}{\partial X_i}\frac{\partial x_k}{\partial X_j} \quad \text{(definition of transpose and Eq. (3.2.14))}$$

$$= \left(\frac{\partial u_k}{\partial X_i} + \frac{\partial X_k}{\partial X_i}\right)\left(\frac{\partial u_k}{\partial X_j} + \frac{\partial X_k}{\partial X_j}\right) \quad \text{(by Eq. (3.2.7))}$$

$$= \left(\frac{\partial u_k}{\partial X_i} + \delta_{ki}\right)\left(\frac{\partial u_k}{\partial X_j} + \delta_{kj}\right)$$

$$= \left(\frac{\partial u_i}{\partial X_j} + \frac{\partial u_j}{\partial X_i} + \frac{\partial u_k}{\partial X_i}\frac{\partial u_k}{\partial X_j} + \delta_{ij}\right)$$

Substituting the above into (3.3.5) gives (3.3.6).

To show that the Green strain vanishes in rigid body motion, we consider the deformation function for a general rigid body motion described in Eq. (3.2.20): $\mathbf{x} = \mathbf{R}\ \mathbf{X} + \mathbf{x}_T$. The deformation gradient $\mathbf{F}$ according to Eq (3.2.14) is then given by $\mathbf{F} = \mathbf{R}$. Using the expression for the Green strain, Eq. (3.3.5). gives

$$\mathbf{E} = \tfrac{1}{2}\left(\mathbf{R}^T\ \mathbf{R} - \mathbf{I}\right) = \tfrac{1}{2}\left(\mathbf{I} - \mathbf{I}\right) = \mathbf{0}$$

where the second equality follows from the orthogonality of the rotation tensor, Eq.(3.2.21). This demonstrates that the Green strain will vanish in any rigid body motion, so it meets an important requirement of a strain measure.

3.3.2 Rate-of-deformation. The second measure of strain to be considered here is the *rate-of-deformation* $\mathbf{D}$. It is also called the *velocity strain* and the *stretching* tensor. In contrast to the Green strain tensor, it is a rate measure of strain.

In order to develop an expression for the rate-of-deformation, we first define the velocity gradient $\mathbf{L}$ by

$$\mathbf{L} = \frac{\partial \mathbf{v}}{\partial \mathbf{x}} = (\ \ \mathbf{v})^T = (grad\ \mathbf{v})^T \quad \text{or} \quad L_{ij} = \frac{\partial v_i}{\partial x_j}, \qquad d\mathbf{v} = \mathbf{L}\ \ d\mathbf{x} \quad \text{or} \quad dv_i = L_{ij} dx_j \tag{3.3.7}$$

We have shown several tensor forms of the definition which are frequently seen, but we will primarily use the first or the indicial form. In the above, the symbol or the abbreviation "grad" preceding the function denotes the spatial gradient of the function, i.e., the derivatives are taken with respect to the spatial coordinates. The symbol always specifies the spatial gradient unless a different coordinate is appended as a subscript, as in $_X$, which denotes the material gradient.

The velocity gradient tensor can be decomposed into symmetric and skew symmetric parts by

$$\mathbf{L} = \frac{1}{2}\left(\mathbf{L} + \mathbf{L}^T\right) + \frac{1}{2}\left(\mathbf{L} - \mathbf{L}^T\right) \text{ or } L_{ij} = \frac{1}{2}\left(L_{ij} + L_{ji}\right) + \frac{1}{2}\left(L_{ij} - L_{ji}\right) \tag{3.3.8}$$

This is a standard decomposition of a second order tensor or square matrix: any second order tensor can be expressed as the sum of its symmetric and skew symmetric parts in the above manner; skew symmetry is also known as antisymmetry.

The rate-of-deformation $\mathbf{D}$ is defined as the symmetric part of $\mathbf{L}$, i.e. the first term on the RHS of (3.3.8) and the spin $\mathbf{W}$ is the skew symmetric part of $\mathbf{L}$, i.e. the second term on the RHS of (3.3.8). Using these definitions, we can write

$$\mathbf{L} = (\ \ \mathbf{v})^T = \mathbf{D} + \mathbf{W} \qquad \text{or} \qquad L_{ij} = v_{i,j} = D_{ij} + W_{ij} \tag{3.3.9}$$

$$\mathbf{D} = \frac{1}{2}\left(\mathbf{L} + \mathbf{L}^T\right) \quad \text{or} \quad D_{ij} = \frac{1}{2}\left(\frac{\partial v_i}{\partial x_j} + \frac{\partial v_j}{\partial x_i}\right) \tag{3.3.10}$$

$$\mathbf{W} = \frac{1}{2}\left(\mathbf{L} - \mathbf{L}^T\right) \quad \text{or} \quad W_{ij} = \frac{1}{2}\left(\frac{\partial v_i}{\partial x_j} - \frac{\partial v_j}{\partial x_i}\right) \tag{3.3.11}$$

The rate-of-deformation is a measure of the rate of change of the square of the length of infinitesimal material line segments. The definition is

$$\frac{\partial}{\partial t}\left(ds^2\right) = \frac{\partial}{\partial t}\left(d\mathbf{x}\ d\mathbf{x}\right) = 2\,d\mathbf{x}\ \mathbf{D}\ d\mathbf{x} \qquad d\mathbf{x} \tag{3.3.12}$$

The equivalence of (3.3.10) and (3.3.12) is shown as follows. The expression for the rate-of-deformation is obtained from the above as follows:

$$\begin{aligned} 2\,d\mathbf{x}\ \mathbf{D}\ d\mathbf{x} &= \frac{\partial}{\partial t}\left(d\mathbf{x}(\mathbf{X},t)\ d\mathbf{x}(\mathbf{X},t)\right) = 2\,d\mathbf{x}\ d\mathbf{v} \quad \text{(using(3.2.8))} \\ &= 2\,d\mathbf{x}\ \frac{\partial \mathbf{v}}{\partial \mathbf{x}}\ d\mathbf{x} \quad \text{by chain rule} \\ &= 2\,d\mathbf{x}\ \mathbf{L}\ d\mathbf{x} \qquad \text{(using (3.3.7))} \\ &= d\mathbf{x}\ \left(\mathbf{L} + \mathbf{L}^T + \mathbf{L} - \mathbf{L}^T\right)\ d\mathbf{x} \\ &= d\mathbf{x}\ \left(\mathbf{L} + \mathbf{L}^T\right)\ d\mathbf{x} \end{aligned} \tag{3.3.13}$$

by antisymmetry of $\mathbf{L} - \mathbf{L}^T$; (3.3.10) follows from the last line in (3.3.13) due to the arbitrariness of $d\mathbf{x}$.

In the absence of deformation, the spin tensor and angular velocity tensor are equal, $\mathbf{W} = \Omega$. This is shown as follows. In rigid body motion $\mathbf{D} = \mathbf{0}$, so $\mathbf{L} = \mathbf{W}$ and by integrating Eq. (3.3.7b) we have

$$\mathbf{v} = \mathbf{W}\ \left(\mathbf{x} - \mathbf{x}_T\right) + \mathbf{v}_T \tag{3.3.14}$$

where $\mathbf{x}_T$ and $\mathbf{v}_T$ are constants of integration. Comparison with Eq. (3.2.32) then shows that the spin and angular velocity tensors are identical in rigid body rotation. When the body undergoes deformation in addition to rotation, the spin tensor generally differs from the angular velocity tensor. This has important implications on the character of objective stress rates, which are discussed in Section 3.7.

3.3.3. Rate-of-deformation in terms of rate of Green strain. The rate-of-deformation can be related to the rate of the Green strain tensor. To obtain

this relation, we first obtain the material gradient of the velocity field, defined in Eq. (3.3.7b), in terms of the spatial gradient by the chain rule:

$$\mathbf{L} = \frac{\partial \mathbf{v}}{\partial \mathbf{x}} = \frac{\partial \mathbf{v}}{\partial \mathbf{X}} \; \frac{\partial \mathbf{X}}{\partial \mathbf{x}}, \qquad L_{ij} = \frac{\partial v_i}{\partial x_j} = \frac{\partial v_i}{\partial X_k} \frac{\partial X_k}{\partial x_j} \tag{3.3.15}$$

The definition of the deformation gradient is now recalled, Eq. (3.3.10), $F_{ij} = \partial x_i / \partial X_j$. Taking the material time derivative of the deformation gradient gives

$$\dot{\mathbf{F}} = \frac{\partial \mathbf{v}}{\partial \mathbf{X}}, \qquad \dot{F}_{ij} = \frac{\partial v_i}{\partial X_j} \tag{3.3.16}$$

By the chain rule

$$\frac{\partial x_i}{\partial X_k} \frac{\partial X_k}{\partial x_j} = \delta_{ij} \; \rightarrow F_{ik} \frac{\partial X_k}{\partial x_j} = \delta_{ij} \; \rightarrow F_{kj}^{-1} = \frac{\partial X_k}{\partial x_j}, \quad \mathbf{F}^{-1} = \frac{\partial \mathbf{X}}{\partial \mathbf{x}} \tag{3.3.17}$$

Using the above two equations, (3.3.15) can be rewritten as

$$\mathbf{L} = \dot{\mathbf{F}} \; \mathbf{F}^{-1}, \qquad L_{ij} = \dot{F}_{ik} F_{kj}^{-1} \tag{3.3.18}$$

When the deformation gradient is known, this equation can be used to obtain the rate-of-deformation and the Green strain rate. To obtain a single expression relating these two measures of strain rate, we note that from (3.3.10) and (3.3.18) we have

$$\mathbf{D} = \tfrac{1}{2}\left(\mathbf{L} + \mathbf{L}^T\right) = \tfrac{1}{2}\left(\dot{\mathbf{F}} \; \mathbf{F}^{-1} + \mathbf{F}^{-T} \; \dot{\mathbf{F}}^T\right) \tag{3.3.19}$$

Taking the time derivative of the expression for the Green strain, (3.3.5) gives

$$\dot{\mathbf{E}} = \tfrac{1}{2} \frac{D}{Dt}\left(\mathbf{F}^T \; \mathbf{F} - \mathbf{I}\right) = \tfrac{1}{2}\left(\mathbf{F}^T \; \dot{\mathbf{F}} + \dot{\mathbf{F}}^T \; \mathbf{F}\right) \tag{3.3.20}$$

Premultiplying Eq. (3.3.19) by $\mathbf{F}^T \mathbf{F}$ and postmultiplying by $\mathbf{F}$ gives

$$\mathbf{F}^T \; \mathbf{D} \; \mathbf{F} = \tfrac{1}{2}\left(\mathbf{F}^T \; \dot{\mathbf{F}} + \dot{\mathbf{F}}^T \; \mathbf{F}\right) \rightarrow \dot{\mathbf{E}} = \mathbf{F}^T \; \mathbf{D} \; \mathbf{F} \quad \text{or} \quad \dot{E}_{ij} = F_{ik}^T D_{kl} F_{lj} \tag{3.3.21}$$

where the last equality follows from Eq. (3.3.20). The above can easily be inverted to yield

$$\mathbf{D} = \mathbf{F}^{-T} \; \dot{\mathbf{E}} \; \mathbf{F}^{-1} \qquad \text{or} \qquad D_{ij} = F_{ik}^{-T} \dot{E}_{kl} F_{lj}^{-1} \tag{3.3.22}$$

As we shall see in Chapter 5, (3.3.22) is an example of a push forward operation, (3.3.21) of the pullback operation. The two measures are two ways of viewing the same tensor: the rate of Green strain is expresses in the reference configuration what the rate-of-deformation expresses in the current configuration. However, the

properties of the two forms are somewhat different. For instance, in Example 3.7 we shall see that the integral of the Green strain rate in time is path independent, whereas the integral of the rate-of-deformation is not path independent.

These formulas could be obtained more easily by starting from the definitions of the Green strain tensor and the rate-of-deformation, Eqs. (3.3.1) and (3.3.9), respectively. However, Eq. (3.3.18), which is very useful, would then be skipped. Therefore the other derivation is left as an exercise, Problem ?.

Example 3.5. Strain Measures in Combined Stretch and Rotation. Consider the motion of a body given by

$$x(\mathbf{X},t) = (1+at)X\cos\tfrac{\pi}{2}t - (1+bt)Y\sin\tfrac{\pi}{2}t \tag{E3.5.1}$$

$$y(\mathbf{X},t) = (1+at)X\sin\tfrac{\pi}{2}t + (1+bt)Y\cos\tfrac{\pi}{2}t \tag{E3.5.2}$$

where a and b are positive constants. Evaluate the deformation gradient $\mathbf{F}$, the Green strain $\mathbf{E}$ and rate-of-deformation tensor as functions of time and examine for $t = 0$ and $t = 1$.

For convenience, we define

$$A(t) \equiv (1+at),\ B(t) \equiv (1+bt),\ c \equiv \cos\tfrac{\pi}{2}t,\ s \equiv \sin\tfrac{\pi}{2}t \tag{E3.5.3}$$

The deformation gradient $\mathbf{F}$ is evaluated by Eq.(3.2.10) using (E3.5.1):

$$\mathbf{F} = \begin{bmatrix} \frac{\partial x}{\partial X} & \frac{\partial x}{\partial Y} \\ \frac{\partial y}{\partial X} & \frac{\partial y}{\partial Y} \end{bmatrix} = \begin{bmatrix} Ac & -Bs \\ As & Bc \end{bmatrix} \tag{E3.5.4}$$

The above deformation consists of the simultaneous stretching of the material lines along the X and Y axes and the rotation of the element. The deformation gradient is constant in the element at any time, and the other measures of strain will also be constant at any time. The Green strain tensor is obtained from (3.3.5), with $\mathbf{F}$ given by (E3.5.4), which gives

$$\mathbf{E} = \frac{1}{2}\left(\mathbf{F}^T\ \mathbf{F} - \mathbf{I}\right) = \frac{1}{2}\left(\begin{bmatrix} Ac & As \\ -Bs & Bc \end{bmatrix}\begin{bmatrix} Ac & -Bs \\ As & Bc \end{bmatrix} - \begin{bmatrix} 1 & 0 \\ 0 & 1 \end{bmatrix}\right)$$

$$= \frac{1}{2}\left(\begin{bmatrix} A^2 & 0 \\ 0 & B^2 \end{bmatrix} - \begin{bmatrix} 1 & 0 \\ 0 & 1 \end{bmatrix}\right) = \frac{1}{2}\begin{bmatrix} 2at + a^2t^2 & 0 \\ 0 & 2bt + b^2t^2 \end{bmatrix} \tag{E3.5.5}$$

It can be seen that the values of the Green strain tensor correspond to what would be expected from its definition: the line segments which are in the $\mathbf{X}$ and $\mathbf{Y}$ directions are extended by at and bt, respectively, so E_{11} and E_{22} are nonzero. The strain $E_{11} = E_{XX}$ is positive when a is positive because the line segment along the X axis is lengthened. The magnitudes of the components of the Green strain

correspond to the engineering measures of strain if the quadratic terms in a and b are negligible. The constants are restricted so that $at > -1$ and $bt > -1$, for otherwise the Jacobian of the deformation becomes negative. When $t = 0$, $\mathbf{x} = \mathbf{X}$ and $\mathbf{E} = \mathbf{0}$.

For the purpose of evaluating the rate-of-deformation, we first obtain the velocity, which is the material time derivative of (E3.5.1):

$$\begin{aligned} v_x &= \left(ac - \tfrac{\pi}{2} As\right)X - \left(bs + \tfrac{\pi}{2} Bc\right)Y \\ v_y &= \left(as + \tfrac{\pi}{2} Ac\right)X + \left(bc - \tfrac{\pi}{2} Bs\right)Y \end{aligned} \tag{E3.5.6}$$

The velocity gradient is given by (3.3.7b),

$$\mathbf{L} = (\nabla \mathbf{v})^T = \begin{bmatrix} \frac{\partial v_x}{\partial x} & \frac{\partial v_x}{\partial y} \\ \frac{\partial v_y}{\partial x} & \frac{\partial v_y}{\partial y} \end{bmatrix} = \begin{bmatrix} ac - \omega As & -bs - \omega Bc \\ as + \omega Ac & bc - \omega Bs \end{bmatrix} \tag{E3.5.7}$$

Since at $t = 0$, $x = X$, $y = Y$, c=1, s=0, $A = B = 1$, so the velocity gradient at $t = 0$ is given by

$$\mathbf{L} = (\nabla \mathbf{v})^T = \begin{bmatrix} a & -\frac{\pi}{2} \\ \frac{\pi}{2} & b \end{bmatrix} \rightarrow \mathbf{D} = \begin{bmatrix} a & 0 \\ 0 & b \end{bmatrix} \quad \mathbf{W} = \frac{\pi}{2} \begin{bmatrix} 0 & -1 \\ 1 & 0 \end{bmatrix} \tag{E3.5.8}$$

To determine the time history of the rate-of-deformation, we first evaluate the time derivative of the deformation tensor and the inverse of the deformation tensor. Recall that $\mathbf{F}$ is given in Eq. (E3.5.4)), from which we obtain

$$\dot{\mathbf{F}} = \begin{bmatrix} A_{,t} c - \frac{\pi}{2} As & -B_{,t} s - \frac{\pi}{2} Bc \\ A_{,t} s + \frac{\pi}{2} Ac & B_{,t} c - \frac{\pi}{2} Bs \end{bmatrix} \quad \mathbf{F}^{-1} = \frac{1}{AB} \begin{bmatrix} Bc & Bs \\ -As & Ac \end{bmatrix} \tag{E3.5.9}$$

$$\mathbf{L} = \dot{\mathbf{F}}\ \mathbf{F}^{-1} = \frac{1}{AB} \begin{bmatrix} Bac^2 + Abs^2 & cs(Ba - Ab) \\ cs(Ba - Ab) & Bas^2 + Abc^2 \end{bmatrix} + \frac{\pi}{2} \begin{bmatrix} 0 & -1 \\ 1 & 0 \end{bmatrix} \tag{E3.5.10}$$

The first term on the RHS is the rate-of-deformation since it is the ymmetric part of the velocity gradient, while the second term is the spin, which is skew symmetric. The rate-of-deformation at $t = 1$ is given by

$$\mathbf{D} = \frac{1}{AB} \begin{bmatrix} Ab & 0 \\ 0 & Ba \end{bmatrix} = \frac{1}{1 + a + b + ab} \begin{bmatrix} b + ab & 0 \\ 0 & a + ab \end{bmatrix} \tag{E3.5.11}$$

Thus, while in the intermediate stages, the shear velocity-strains are nonzero, in the configuration at $t = 1$ only the elongational velocity-strains are nonzero. For comparison, the rate of the Green strain at $t = 1$ is given by

$$\dot{\mathbf{E}} = \begin{bmatrix} Aa & 0 \\ 0 & Bb \end{bmatrix} = \begin{bmatrix} a + a^2 & 0 \\ 0 & b + b^2 \end{bmatrix} \tag{E3.5.12}$$

Example 3.6 An element is rotated by an angle θ about the origin. Evaluate the infinitesimal strain (often called the linear strain).

For a pure rotation, the motion is given by (3.2.20), $\mathbf{x} = \mathbf{R}\ \mathbf{X}$, where the translation has been dropped and $\mathbf{R}$ is given in Eq.(3.2.25), so

$$\begin{bmatrix} x \\ y \end{bmatrix} = \begin{bmatrix} \cos\theta & -\sin\theta \\ \sin\theta & \cos\theta \end{bmatrix} \begin{bmatrix} X \\ Y \end{bmatrix} \qquad \begin{bmatrix} u_x \\ u_y \end{bmatrix} = \begin{bmatrix} \cos\theta - 1 & -\sin\theta \\ \sin\theta & \cos\theta - 1 \end{bmatrix} \begin{bmatrix} X \\ Y \end{bmatrix} \tag{E3.6.1}$$

In the definition of the linear strain tensor, the spatial coordinates with respect to which the derivatives are taken are not specified. We take them with respect to the material coordinates (the result is the same if we choose the spatial coordinates). The infinitesimal strains are then given by

$$\varepsilon_x = \frac{\partial u_x}{\partial X} = \cos\theta - 1, \quad \varepsilon_y = \frac{\partial u_y}{\partial Y} = \cos\theta - 1, \quad 2\varepsilon_{xy} = \frac{\partial u_x}{\partial Y} + \frac{\partial u_y}{\partial X} = 0 \tag{E3.6.2}$$

Thus, if θ is large, the extensional strains do not vanish. Therefore, the linear strain tensor cannot be used for large deformation problems, i.e. in geometrically nonlinear problems.

A question that often arises is how large the rotations can be before a nonlinear analysis is required. The previous example provides some guidance to this choice. The magnitude of the strains predicted in (E3.6.2) are an indication of the error due to the small strain assumption. To get a better handle on this error, we expand $\cos\theta$ in a Taylor's series and substitute into (E3.6.2), which gives

$$\varepsilon_x = \cos\theta - 1 = 1 - \frac{\theta^2}{2} + O\left(\theta^4\right) - 1 \approx -\frac{\theta^2}{2} \tag{3.3.23}$$

This shows that the error in the linear strain is second order in the rotation. The adequacy of a linear analysis then hinges on how large an error can be tolerated and the magnitudes of the strains of interest. If the strains of interest are of order 10^{-2}, and 1% error is acceptable (it almost always is) then the rotations can be of order 10^{-2}, since the error due to the small strain assumption is of order 10^{-4}. If the strains of interest are smaller, the acceptable rotations are smaller: for strains of order 10^{-4}, the rotations should be of order 10^{-3} for 1% error. These guidelines assume that the equilibrium solution is stable, i.e. that buckling is not possible. When buckling is possible, measures which can properly account for large deformations should be used or a stability analysis as described in Chapter 6 should be performed.

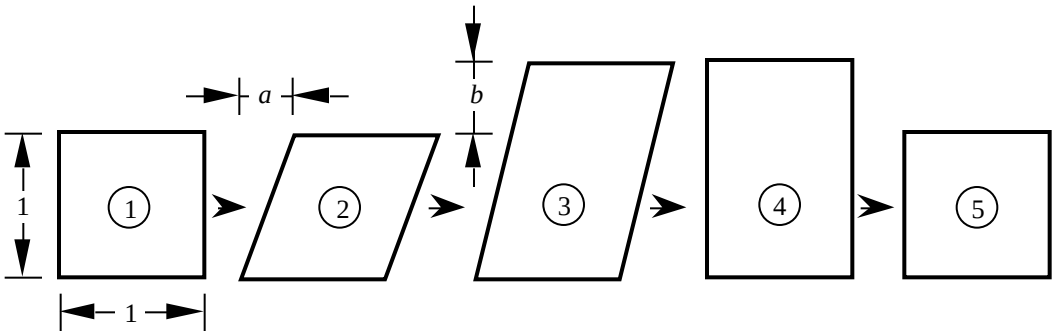

Fig. 3.7. An element which is sheared, followed by an extension in the y-direction and then subjected to deformations so that it is returned to its initial configuration.

Example 3.7 An element is deformed through the stages shown in Fig. 3.7. The deformations between these stages are linear functions of time. Evaluate the rate-of-deformation tensor **D** in each of these stages and obtain the time integral of the rate-of-deformation for the complete cycle of deformation ending in the undeformed configuration.

Each stage of the deformation is assumed to occur over a unit time interval, so for stage n, $t = n-1$. The time scaling is irrelevant to the results, and we adopt this particular scaling to simplify the algebra. The results would be identical with any other scaling. The deformation function that takes state 1 to state 2 is

$$x(\mathbf{X},t) = X + atY, \quad y(\mathbf{X},t) = Y \quad 0 \le t \le 1 \tag{E3.7.1}$$

To determine the rate-of-deformation, we will use Eq. (3.3.18), $\mathbf{L} = \dot{\mathbf{F}}\ \mathbf{F}^{-1}$ so we first have to determine $\mathbf{F}, \dot{\mathbf{F}}$ and $\mathbf{F}^{-1}$. These are

$$\mathbf{F} = \begin{bmatrix} 1 & at \\ 0 & 1 \end{bmatrix} \quad \dot{\mathbf{F}} = \begin{bmatrix} 0 & a \\ 0 & 0 \end{bmatrix} \quad \mathbf{F}^{-1} = \begin{bmatrix} 1 & -at \\ 0 & 1 \end{bmatrix} \tag{E3.7.2}$$

The velocity gradient and rate of deformation are then given by (3.3.10):

$$\mathbf{L} = \dot{\mathbf{F}}\ \mathbf{F}^{-1} = \begin{bmatrix} 0 & a \\ 0 & 0 \end{bmatrix} \begin{bmatrix} 1 & -at \\ 0 & 1 \end{bmatrix} = \begin{bmatrix} 0 & a \\ 0 & 0 \end{bmatrix} \quad \mathbf{D} = \tfrac{1}{2}\left(\mathbf{L} + \mathbf{L}^T\right) = \tfrac{1}{2}\begin{bmatrix} 0 & a \\ a & 0 \end{bmatrix} \tag{E3.7.3}$$

Thus the rate-of-deformation is a pure shear, for both elongational components vanish. The Green strain is obtained by Eq. (3.3.5), its rate by taking the time derivative

$$\mathbf{E} = \tfrac{1}{2}\left(\mathbf{F}^T\ \mathbf{F} - \mathbf{I}\right) = \tfrac{1}{2}\begin{bmatrix} 0 & at \\ at & a^2t^2 \end{bmatrix} \quad \dot{\mathbf{E}} = \tfrac{1}{2}\begin{bmatrix} 0 & a \\ a & 2a^2t \end{bmatrix} \tag{E3.7.4}$$

The Green strain and its rate include an elongational component, E_{22} which is absent in the rate-of-deformation tensor. This component is small when the constant a, and hence the magnitude of the shear, is small.

For the subsequent stages of deformation, we only give the motion, the deformation gradient, its inverse and rate and the rate-of-deformation and Green strain tensors.

configuration 2 to configuration 3

$$x(\mathbf{X},t) = X + aY, \quad y(\mathbf{X},t) = (1+bt)Y, \quad 1 \le \bar{t} \le 2, \quad t = \bar{t} - 1 \tag{E3.7.5a}$$

$$\mathbf{F} = \begin{bmatrix} 1 & a \\ 0 & 1+bt \end{bmatrix}, \quad \dot{\mathbf{F}} = \begin{bmatrix} 0 & 0 \\ 0 & b \end{bmatrix}, \quad \mathbf{F}^{-1} = \frac{1}{1+bt}\begin{bmatrix} 1+bt & -a \\ 0 & 1 \end{bmatrix} \tag{E3.7.5b}$$

$$\mathbf{L} = \dot{\mathbf{F}}\ \mathbf{F}^{-1} = \frac{1}{1+bt}\begin{bmatrix} 0 & 0 \\ 0 & b \end{bmatrix} \quad \mathbf{D} = \tfrac{1}{2}\left(\mathbf{L}+\mathbf{L}^T\right) = \frac{1}{1+bt}\begin{bmatrix} 0 & 0 \\ 0 & b \end{bmatrix} \tag{E3.7.5c}$$

$$\mathbf{E} = \tfrac{1}{2}\left(\mathbf{F}^T\ \mathbf{F} - \mathbf{I}\right) = \tfrac{1}{2}\begin{bmatrix} 0 & a \\ a & a^2 + bt(bt+2) \end{bmatrix}, \quad \dot{\mathbf{E}} = \tfrac{1}{2}\begin{bmatrix} 0 & 0 \\ 0 & 2b(bt+1) \end{bmatrix} \tag{E3.7.5d}$$

configuration 3 to configuration 4:

$$x(\mathbf{X},t) = X + a(1-t)Y, \quad y(\mathbf{X},t) = (1+b)Y, \quad 2 \le \bar{t} \le 3, \quad t = \bar{t} - 2 \tag{E3.7.6a}$$

$$\mathbf{F} = \begin{bmatrix} 1 & a(1-t) \\ 0 & 1+b \end{bmatrix}, \quad \dot{\mathbf{F}} = \begin{bmatrix} 0 & -a \\ 0 & 0 \end{bmatrix}, \quad \mathbf{F}^{-1} = \frac{1}{1+b}\begin{bmatrix} 1+b & a(t-1) \\ 0 & 1 \end{bmatrix} \tag{E3.7.6b}$$

$$\mathbf{L} = \dot{\mathbf{F}}\ \mathbf{F}^{-1} = \frac{1}{1+b}\begin{bmatrix} 0 & -a \\ 0 & 0 \end{bmatrix}, \quad \mathbf{D} = \tfrac{1}{2}\left(\mathbf{L}+\mathbf{L}^T\right) = \frac{1}{2(1+b)}\begin{bmatrix} 0 & -a \\ -a & 0 \end{bmatrix} \tag{E3.7.6c}$$

configuration 4 to configuration 5:

$$x(\mathbf{X},t) = X, \quad y(\mathbf{X},t) = (1+b-bt)Y, \quad 3 \le \bar{t} \le 4, \quad t = \bar{t} - 3 \tag{E3.7.7a}$$

$$\mathbf{F} = \begin{bmatrix} 1 & 0 \\ 0 & 1+b-bt \end{bmatrix}, \quad \dot{\mathbf{F}} = \begin{bmatrix} 0 & 0 \\ 0 & -b \end{bmatrix}, \quad \mathbf{F}^{-1} = \frac{1}{1+b-bt}\begin{bmatrix} 1+b-bt & 0 \\ 0 & 1 \end{bmatrix} \tag{E3.7.7b}$$

$$\mathbf{L} = \dot{\mathbf{F}}\ \mathbf{F}^{-1} = \frac{1}{1+b-bt}\begin{bmatrix} 0 & 0 \\ 0 & -b \end{bmatrix}, \quad \mathbf{D} = \mathbf{L} \tag{E3.7.7c}$$

The Green strain in configuration 5 vanishes, since at $\bar{t} = 4$ the deformation gradient is the unit tensor, $\mathbf{F} = \mathbf{I}$. The time integral of the rate-of-deformation is given by

$$\int_0^4 \mathbf{D}(t)\,dt = \tfrac{1}{2}\begin{bmatrix} 0 & a \\ a & 0 \end{bmatrix} + \begin{bmatrix} 0 & 0 \\ 0 & ln(1+b) \end{bmatrix} + \frac{1}{2(1+b)}\begin{bmatrix} 0 & -a \\ -a & 0 \end{bmatrix} + \begin{bmatrix} 0 & 0 \\ 0 & -ln(1+b) \end{bmatrix} \tag{E3.7.8a}$$

$$= \frac{ab}{2(1+b)} \begin{bmatrix} 0 & 1 \\ 1 & 0 \end{bmatrix} \qquad \text{(E3.7.8b)}$$

Thus the integral of the rate-of-deformation over a cycle ending in the initial configuration does not vanish. In other words, while the final configuration in this problem is the undeformed configuration so that a measure of strain should vanish, the integral of the rate-of-deformation is nonzero. This has significant repercussions on the range of applicability of hypoelastic formulations to be described in Sections 5? and 5?. It also means that the integral of the rate-of deformation is not a good measure of total strain. It should be noted the integral over the cycle is close enough to zero for engineering purposes whenever *a* or *b* are small. The error in the strain is second order in the deformation, which means it is negligible as long as the strains are of order 10^{-2}. The integral of the Green strain rate, on the other hand, will vanish in this cycle, since it is the time derivative of the Green strain **E**, which vanishes in the final undeformed state.

3 .4 STRESS MEASURES

3.4.1 Definitions of Stresses. In nonlinear problems, various stress measures can be defined. We will consider three measures of stress:

1. the Cauchy stress σ,
2. the nominal stress tensor **P**;
3. the second Piola-Kirchhoff (PK2) stress tensor **S**.

The definitions of the first three stress tensors are given in Box 3.1.

Box 3.1
Definition of Stress Measures

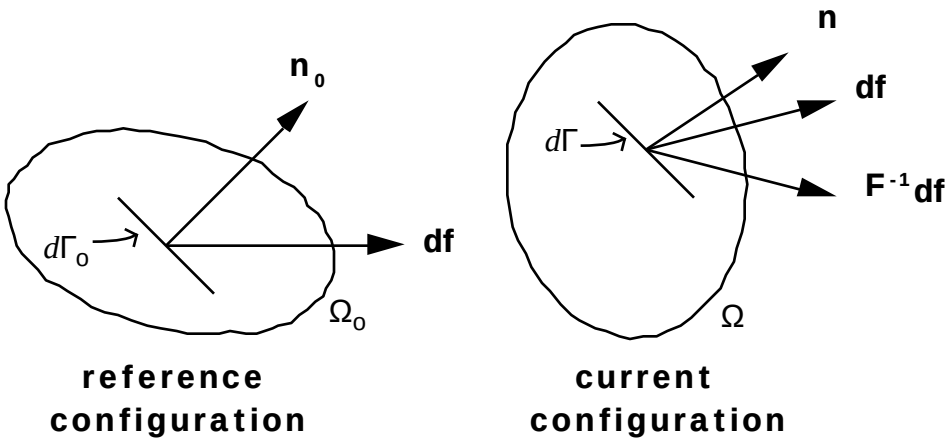

Cauchy stress: $\mathbf{n}\ \sigma d\Gamma = d\mathbf{f} = \mathbf{t}d\Gamma$ (3.4.1)

Nominal stress: $\mathbf{n}_0\ \mathbf{P}d\Gamma_0 = d\mathbf{f} = \mathbf{t}_0 d\Gamma_0$ (3.4.2)

2nd Piola-Kirchhoff stress: $\mathbf{n}_0\ \mathbf{S}d\Gamma_0 = \mathbf{F}^{-1}\ d\mathbf{f} = \mathbf{F}^{-1}\ \mathbf{t}_0 d\Gamma_0$ (3.4.3)

$d\mathbf{f} = \mathbf{t}d\Gamma = \mathbf{t}_0 d\Gamma_0$ (3.4.4)

The expression for the traction in terms of the Cauchy stress, Eq. (3.4.1), is called Cauchy's law or sometimes the Cauchy hypothesis. It involves the normal to the current surface and the traction (force/unit area) on the current surface. For this reason, the Cauchy stress is often called the physical stress or true stress. For example, the trace of the Cauchy stress, $trace(\sigma) = -p\mathbf{I}$, gives the true pressure p commonly used in fluid mechanics. The traces of the stress measures **P** and **S** do not give the true pressure because they are referred to the undeformed area. We will use the convention that the normal components of the Cauchy stress are positive in tension. The Cauchy stress tensor is symmetric, i.e. $\sigma^T = \sigma$, which we shall see follows from the conservation of angular momentum.

The definition of the nominal stress **P** is similar to that of the Cauchy stress except that it is expressed in terms of the area and normal of the reference surface, i.e. the underformed surface. It will be shown in Section 3.6.3 that the nominal stress is not symmetric. The transpose of the nominal stress is called the first Piola-Kirchhoff stress. (The nomenclature used by different authors for nominal stress and first Piola-Kirchhoff stress is contradictory; Truesdell and Noll (1965), Ogden (1984), Marsden and Hughes (1983) use the definition given here, Malvern (1969) calls **P** the first Piola-Kirchhoff stress.) Since **P** is not symmetric, it is important to note that in the definition given in Eq. (3.4.2), the normal is to the left of the tensor **P**.

The second Piola-Kirchhoff stress is defined by Eq. (3.4.3). It differs from $\mathbf{P}$ in that the force is shifted by $\mathbf{F}^{-1}$. This shift has a definite purpose: it makes the second Piola-Kirchhoff stress symmetric and as we shall see, conjugate to the rate of the Green strain in the sense of power. This stress measure is widely used for path-independent materials such as rubber. We will use the abbreviations PK1 and PK2 stress for the first and second Piola-Kirchhoff stress, respectively.

3.4.2 Transformation Between Stresses. The different stress tensors are interrelated by functions of the deformation. The relations between the stresses are given in Box 3.2. These relations can be obtained by using Eqs. (1-3) along with Nanson's relation (p.169, Malvern(1969)) which relates the current normal to the reference normal by

$$\mathbf{n}d\Gamma = J\mathbf{n}_0 \cdot \mathbf{F}^{-1}d\Gamma_0 \qquad n_i d\Gamma = Jn_j^0 F_{ji}^{-1}d\Gamma_0 \tag{3.4.5}$$

Note that the nought is placed wherever it is convenient: "0" and "*e*" have invariant meaning in this book and can appear as subscripts or superscripts!

To illustrate how the transformations between different stress measures are obtained, we will develop an expression for the nominal stress in terms of the Cauchy stress. To begin, we equate $d\mathbf{f}$ written in terms of the Cauchy stress and the nominal stress, Eqs. (3.4.2) and (3.4.3), giving

$$d\mathbf{f} = \mathbf{n} \cdot \sigma d\Gamma = \mathbf{n}_0 \cdot \mathbf{P}d\Gamma_0 \tag{3.4.6}$$

Substituting the expression for normal $\mathbf{n}$ given by Nanson's relation, (3.4.5) into (3.4.6) gives

$$J\mathbf{n}_0 \cdot \mathbf{F}^{-1} \cdot \sigma d\Gamma_0 = \mathbf{n}_0 \cdot \mathbf{P}d\Gamma_0 \tag{3.4.7}$$

Since the above holds for all $\mathbf{n}_0$, it follows that

$$\mathbf{P} = J\mathbf{F}^{-1} \cdot \sigma \quad \text{or} \quad P_{ij} = JF_{ik}^{-1}\sigma_{kj} \quad \text{or} \quad P_{ij} = J\frac{\partial X_i}{\partial x_k}\sigma_{kj} \tag{3.4.8a}$$

$$J\sigma = \mathbf{F} \cdot \mathbf{P} \quad \text{or} \quad J\sigma_{ij} = F_{ik}P_{kj} \tag{3.4.8b}$$

It can be seen immediately from (3.4.8a) that $\mathbf{P} \neq \mathbf{P}^T$, i.e. the nominal stress tensor is not symmetric. The balance of angular momentum, which gives the Cauchy stress tensor to be symmetric, $\sigma = \sigma^T$, is expressed as

$$\mathbf{F} \cdot \mathbf{P} = \mathbf{P}^T \cdot \mathbf{F}^T \tag{3.4.9}$$

The nominal stress can be related to the PK2 stress by multiplying Eq. (3.4.3) by $\mathbf{F}$ giving

$$d\mathbf{f} = \mathbf{F} \cdot (\mathbf{n}_0 \cdot \mathbf{S})d\Gamma_0 = \mathbf{F} \cdot \left(\mathbf{S}^T \cdot \mathbf{n}_0\right)d\Gamma_0 = \mathbf{F} \cdot \mathbf{S}^T \cdot \mathbf{n}_0 d\Gamma_0 \tag{3.4.10}$$

The above is somewhat confusing in tensor notation, so it is rewritten below in indicial notation

$$df_i = F_{ik}\left(n_j^0 S_{jk}\right)d\Gamma_0 = F_{ik}S_{kj}^T n_j^0 d\Gamma_0 \tag{3.4.11}$$

The force $d\mathbf{f}$ in the above is now written in terms of the nominal stress using (3.4.2):

$$d\mathbf{f} = \mathbf{n}_0 \ \mathbf{P} d\Gamma_0 = \mathbf{P}^T \ \mathbf{n}_0 d\Gamma_0 = \mathbf{F}\ \mathbf{S}^T \ \mathbf{n}_0 d\Gamma_0 \tag{3.4.12}$$

where the last equality is Eq. (3.4.10) repeated. Since the above holds for all $\mathbf{n}_0$, we have

$$\mathbf{P} = \mathbf{S}\ \mathbf{F}^T \qquad \text{or} \qquad P_{ij} = S_{ik}F_{kj}^T = S_{ik}F_{jk} \tag{3.4.13}$$

Taking the inverse transformation of (3.4.8a) and substituting into (3.4.13) gives

$$\sigma = J^{-1}\mathbf{F}\ \mathbf{S}\ \mathbf{F}^T \quad \text{or} \quad \sigma_{ij} = J^{-1}F_{ik}S_{kl}F_{lj}^T \tag{3.4.14a}$$

The above relation can be inverted to express the PK2 stress in terms of the Cauchy stress:

$$\mathbf{S} = J\mathbf{F}^{-1}\ \sigma\ \mathbf{F}^{-T} \quad \text{or} \quad S_{ij} = JF_{ik}^{-1}\sigma_{kl}F_{lj}^{-T} \tag{3.4.14b}$$

The above relations between the PK2 stress and the Cauchy stress, like (3.4.8), depend only on the deformation gradient $\mathbf{F}$ and the Jacobian determinant $J = det(\mathbf{F})$. Thus, if the deformation is known, the state of stress can always be expressed in terms of either the Cauchy stress σ, the nominal stress $\mathbf{P}$ or the PK2 stress $\mathbf{S}$. It can be seen from (3.4.14b) that if the Cauchy stress is symmetric, then $\mathbf{S}$ is also symmetric: $\mathbf{S} = \mathbf{S}^T$. The inverse relationships to (3.4.8) and (3.4.14) are easily obtained by matrix manipulations.

3.4.3. Corotational Stress and Rate-of-Deformation. In some elements, particularly structural elements such as beams and shells, it is convenient to use the Cauchy stress and rate-of-deformation in corotational form, in which all components are expressed in a coordinate system that rotates with the material. The corotational Cauchy stress, denoted by $\hat{\sigma}$, is also called the rotated-stress tensor (Dill p. 245). We will defer the details of how the rotation and the rotation matrix $\mathbf{R}$ is obtained until we consider specific elements in Chapters 4 and 9. For the present, we assume that we can somehow find a coordinate system that rotates with the material.

The corotational components of the Cauchy stress and the corotational rate-of-deformation are obtained by the standard transformation rule for second order tensors, Eq.(3.2.30):

$$\hat{\sigma} = \mathbf{R}^T \ \sigma\ \mathbf{R} \quad \text{or} \quad \hat{\sigma}_{ij} = R_{ik}^T\sigma_{kl}R_{lj} \tag{3.4.15a}$$

$$\hat{\mathbf{D}} = \mathbf{R}^T \ \mathbf{D} \ \mathbf{R} \quad \text{or} \quad \hat{D}_{ij} = R^T_{ik} D_{kl} R_{lj} \tag{3.4.15b}$$

The corotational Cauchy stress tensor is the same tensor as the Cauchy stress, but it is expressed in terms of components in a coordinate system that rotates with the material. Strictly speaking, from a theoretical viewpoint, a tensor is independent of the coordinate system in which its components are expressed. However, such a fundamentasl view can get quite confusing in an introductory text, so we will superpose hats on the tensor whenever we are referring to its corotational components. The corotational rate-of-deformation is similarly related to the rate-of-deformation.

By expressing these tensors in a coordinate system that rotates with the material, it is easier to deal with structural elements and anisotropic materials. The corotational stress is sometimes called the *unrotated stress*, which seems like a contradictory name: the difference arises as to whether you consider the hatted coordinate system to be moving with the material (or element) or whether you consider it to be a fixed independent entity. Both viewpoints are valid and the choice is just a matter of preference. We prefer the corotational viewpoint because it is easier to picture, see Example 4.?.

Box 3.2
Transformations of Stresses

	Cauchy Stress σ	Nominal Stress $\mathbf{P}$	2nd Piola-Kirchhoff Stress $\mathbf{S}$	Corotational Cauchy Stress $\hat{\sigma}$
σ		$J^{-1}\mathbf{F}\ \mathbf{P}$	$J^{-1}\mathbf{F}\ \mathbf{S}\ \mathbf{F}^T$	$\mathbf{R}\ \hat{\sigma}\ \mathbf{R}^T$
$\mathbf{P}$	$J\mathbf{F}^{-1}\ \sigma$		$\mathbf{S}\ \mathbf{F}^T$	$J\mathbf{U}^{-1}\ \hat{\sigma}\ \mathbf{R}^T$
$\mathbf{S}$	$J\mathbf{F}^{-1}\ \sigma\ \mathbf{F}^{-T}$	$\mathbf{P}\ \mathbf{F}^{-T}$		$J\mathbf{U}^{-1}\ \hat{\sigma}\ \mathbf{U}^{-1}$
$\hat{\sigma}$	$\mathbf{R}^T\ \sigma\ \mathbf{R}$	$J^{-1}\mathbf{U}\ \mathbf{P}\ \mathbf{R}$	$J^{-1}\mathbf{U}\ \mathbf{S}\ \mathbf{U}$	

Note: $d\mathbf{x} = \mathbf{F}\ d\mathbf{X} = \mathbf{R}\ \mathbf{U}\ d\mathbf{X}$ in deformation,
$\mathbf{U}$ is the strectch tensor, see Sec.5?
$d\mathbf{x} = \mathbf{R}\ d\mathbf{X} = \mathbf{R}\ d\hat{\mathbf{x}}$ in rotation

Example 3.8 Consider the deformation given in Example 3.2, Eq. (E3.2.1). Let the Cauchy stress in the initial state be given by

$$\sigma(t=0) = \begin{bmatrix} \sigma_x^0 & 0 \\ 0 & \sigma_y^0 \end{bmatrix} \tag{E3.8.1}$$

Consider the stress to be frozen into the material, so as the body rotates, the initial stress rotates also, as shown in Fig. 3.8.

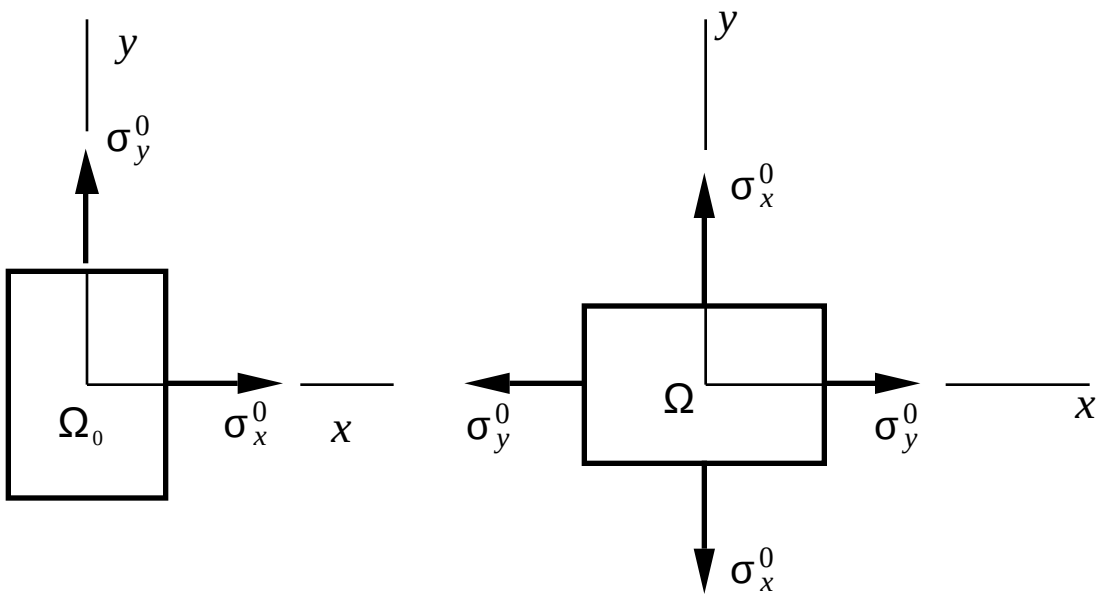

Figure 3.8. Prestressed body rotated by 90˚.

This corresponds to the behavior of an initial state of stress in a rotating solid, which will be explored further in Section 3.6 Evaluate the PK2 stress, the nominal stress and the corotational stress in the initial configuration and the configuration at $t = \pi/2\omega$.

In the initial state, $\mathbf{F} = \mathbf{I}$, so

$$\mathbf{S} = \mathbf{P} = \hat{\sigma} = \sigma = \begin{bmatrix} \sigma_x^0 & 0 \\ 0 & \sigma_y^0 \end{bmatrix} \tag{E3.8.2}$$

In the deformed configuration at $t = \dfrac{\pi}{2\omega}$, the deformation gradient is given by

$$\mathbf{F} = \begin{bmatrix} \cos\pi/2 & -\sin\pi/2 \\ \sin\pi/2 & \cos\pi/2 \end{bmatrix} = \begin{bmatrix} 0 & -1 \\ 1 & 0 \end{bmatrix}, \qquad J = det(\mathbf{F}) = 1 \tag{E3.8.3}$$

Since the stress is considered frozen in the material, the stress state in the rotated configuration is given by

$$\sigma = \begin{bmatrix} \sigma_y^0 & 0 \\ 0 & \sigma_x^0 \end{bmatrix} \tag{E3.8.4}$$

The nominal stress in the configuration is given by Box 3.2:

$$\mathbf{P} = J\mathbf{F}^{-1}\sigma = \begin{bmatrix} 0 & 1 \\ -1 & 0 \end{bmatrix} \begin{bmatrix} \sigma_y^0 & 0 \\ 0 & \sigma_x^0 \end{bmatrix} = \begin{bmatrix} 0 & \sigma_x^0 \\ -\sigma_y^0 & 0 \end{bmatrix} \tag{E3.8.5}$$

Note that the nominal stress is not symmetric. The 2nd Piola-Kirchhoff stress can be expressed in terms of the nominal stress **P** by Box 3.2 as follows:

$$\mathbf{S} = \mathbf{P}\ \mathbf{F}^{-T} = \begin{bmatrix} 0 & \sigma_x^0 \\ -\sigma_y^0 & 0 \end{bmatrix} \begin{bmatrix} 0 & -1 \\ 1 & 0 \end{bmatrix} = \begin{bmatrix} \sigma_x^0 & 0 \\ 0 & \sigma_y^0 \end{bmatrix} \tag{E3.8.6}$$

Since the mapping in this case is a pure rotation, $\mathbf{R} = \mathbf{F}$, so when $t = \frac{\pi}{2\omega}$, $\hat{\sigma} = \mathbf{S}$.

This example used the notion that an initial state of stress can be considered in a solid is frozen into the material and rotates with the solid. It showed that in a pure rotation, the PK2 stress is unchanged; thus the PK2 stress behaves as if it were frozen into the material. This can also be explained by noting that the material coordinates rotate with the material and the components of the PK2 stress are related to the orientation of the material coordiantes. Thus in the previous example, the component S_{11}, which is associated with X-components, corresponds to the σ_{22} components of physical stress in the final configuration and the components σ_{11} in the initial configuration. The corotational components of the Cauchy stress $\hat{\sigma}$ are also unchanged by the rotation of the material, and in the absence of deformation equal the components of the PK2 stress. If the motion were not a pure rotation, the corotational Cauchy stress components would differ from the components of the PK2 stress in the final configuration.

The nominal stress at $t = 1$ is more difficult to interpret physically. This stress is kind of an expatriate, living partially in the current configuration and partially in the reference configuration. For this reason, it is often described as a two-point tensor, with a leg in each configuration, the reference configuration and the current configuration. The left leg is associated with the normal in the reference configuration, the right leg with a force on a surface element in the current configuration, as seen from in its defintion, Eq. (3.4.2). For this reason and the lack of symmetry of the nominal stress **P**, it is seldom used in constitutive equations. Its attractiveness lies in the simplicity of the momentum and finite element equations when expressed in terms of **P**.

Example 3.9 Uniaxial Stress.

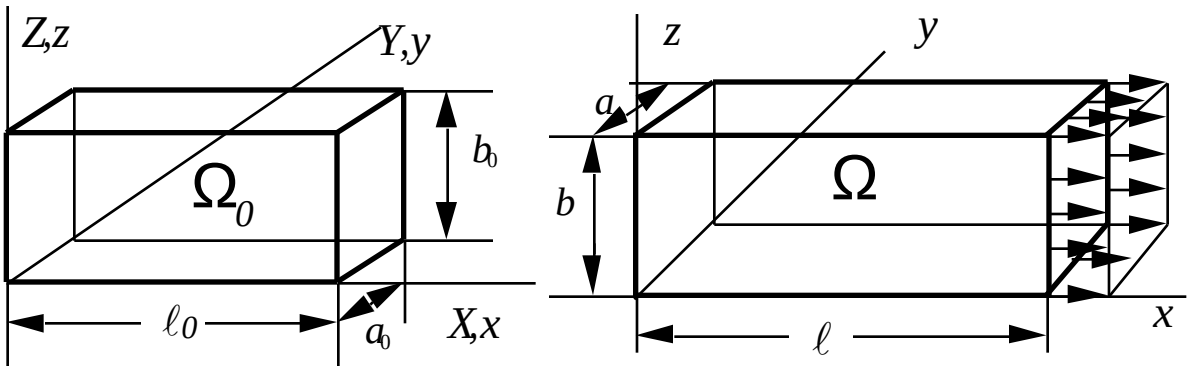

Figure 3.9. Undeformed and current configurations of a body in a uniaxial state of stress.

Consider a bar in a state of uniaxial stress as shown in Fig. 3.9. Relate the nominal stress and the PK2 stress to the uniaxial Cauchy stress. The initial dimensions (the dimensions of the bar in the reference configuration) are l_0, a_0 and b_0, and the current dimensions are l, a so

$$x = \frac{\ell}{\ell_0} X, \quad y = \frac{a}{a_0} Y, \quad z = \frac{b}{b_0} Z \tag{E3.9.1}$$

Therefore

$$\mathbf{F} = \begin{bmatrix} \partial x/\partial X & \partial x/\partial Y & \partial x/\partial Z \\ \partial y/\partial X & \partial y/\partial Y & \partial y/\partial Z \\ \partial z/\partial X & \partial z/\partial Y & \partial z/\partial Z \end{bmatrix} = \begin{bmatrix} \ell/\ell_0 & 0 & 0 \\ 0 & a/a_0 & 0 \\ 0 & 0 & b/b_0 \end{bmatrix} \tag{E3.9.2}$$

$$J = det(\mathbf{F}) = \frac{ab\ell}{a_0 b_0 \ell_0} \tag{E3.9.3}$$

$$\mathbf{F}^{-1} = \begin{bmatrix} \ell_0/\ell & 0 & 0 \\ 0 & a_0/a & 0 \\ 0 & 0 & b_0/b \end{bmatrix} \tag{E3.9.4}$$

The state of stress is uniaxial with the x-component the only nonzero component, so

$$\sigma = \begin{bmatrix} \sigma_x & 0 & 0 \\ 0 & 0 & 0 \\ 0 & 0 & 0 \end{bmatrix} \tag{E3.9.5}$$

Evaluating $\mathbf{P}$ as given by Box 3.2 using Eqs. (E3.9.3-E3.9.5) then gives

$$\mathbf{P} = \frac{ab\ell}{a_0 b_0 \ell_0} \begin{bmatrix} \ell_0/\ell & 0 & 0 \\ 0 & a_0/a & 0 \\ 0 & 0 & b_0/b \end{bmatrix} \begin{bmatrix} \sigma_x & 0 & 0 \\ 0 & 0 & 0 \\ 0 & 0 & 0 \end{bmatrix} = \begin{bmatrix} \frac{ab\sigma_x}{a_0 b_0} & 0 & 0 \\ 0 & 0 & 0 \\ 0 & 0 & 0 \end{bmatrix} \tag{E3.9.6}$$

Thus the only nonzero component of the nominal stress is

$$P_{11} = \frac{ab}{a_0 b_0} \sigma_x = \frac{A\sigma_x}{A_0} \tag{E3.9.7}$$

where the last equality is based on the formulas for the cross-sectional area, $A=ab$ and $A_0 = a_0 b_0$; Eq. (E3.9.7) agrees with Eq. (2.2.7). Thus, in a state of uniaxial stress, P_{11} corresponds to the engineering stress.

The relationship between the PK2 stress and Cauchy stress for a uniaxial state of stress is obtained by using Eqs. (E3.9.3-E3.9.5) with Eq. (3.4.14), which gives

$$S_{11} = \frac{\ell_0}{\ell}\left(\frac{A}{A_o}\sigma_x\right) \tag{E3.9.8}$$

where the quantity in the parenthesis can be recognized as the nominal stress. It can be seen from the above that it is difficult to ascribe a physical meaning to the PK2 stress. This, as will be seen in Chapter 5, influences the selection of stress measures for plasticity theories, since yield functions must be described in terms of physical stresses. Because of the nonphysical nature of the nominal and PK2 stresses, it is awkward to formulate plasticity in terms of these stresses.

3.5 CONSERVATION EQUATIONS

3.5.1 Conservation Laws. One group of the fundamental equations of continuum mechanics arises from the conservation laws. These equations must always be satisfied by physical systems. Four conservation laws relevant to thermomechanical systems are considered here:

1. conservation of mass
2. conservation of linear momentum, often called conservation of momentum
3. conservation of energy
4. conservation of angular momentum

The conservation laws are also known as balance laws, e.g. the conservation of energy is often called the balance of energy.

The conservation laws are usually expressed as partial differential equations (PDEs). These PDEs are derived by applying the conservation laws to a domain of the body, which leads to an integral equation. The following relationship is used to extract the PDEs from the integral equation:

if $f(\mathbf{x},t)$ is C^{-1} and $\int_\Omega f(\mathbf{x},t)d\Omega = 0$ for any subdomain Ω of $\overline{\Omega}$

and time $t \in [0,\bar{t}]$, then

$$f(\mathbf{x},t) = 0 \text{ in } \Omega \text{ for } t \in [0,\bar{t}] \tag{3.5.1}$$

In the following, Ω is an *arbitrary subdomain* of the body under consideration. Prior to deriving the balance equations, several theorems useful for this purpose are derived.

3.5.2 Gauss's Theorem. In the derivation of the governing equations, Gauss's theorem is frequently used. This theorem relates integrals of different dimensions: it can be used to relate a contour integral to an area integral or a surface integral to a volume integral. The one dimensional form of Gauss's theorem is the fundamental theorem of calculus, which we used in Chapter 2.

Gauss's theorem states that when $f(\mathbf{x})$ is a piecewise continuously diffrentiable, i.e. C^1 function, then

$$\int_\Omega \frac{\partial f(\mathbf{x})}{\partial x_i} d\Omega = \int_\Gamma f(\mathbf{x}) n_i d\Gamma \qquad \text{or} \qquad \int_\Omega f(\mathbf{x}) d\Omega = \int_\Gamma f(\mathbf{x}) \mathbf{n} d\Gamma \tag{3.5.2a}$$

$$\int_{\Omega_0} \frac{\partial f(\mathbf{X})}{\partial X_i} d\Omega_0 = \int_{\Gamma_0} f(\mathbf{X}) n_i^0 d\Gamma_0 \quad \text{or} \quad \int_{\Omega_0} \mathbf{X} f(\mathbf{X}) d\Omega_0 = \int_{\Gamma_0} f(\mathbf{X}) \mathbf{n}_0 d\Gamma_0 \tag{3.5.2b}$$

As seen in the above, Gauss's theorem applies to integrals in both the current and reference configurations.

The above theorem holds for a tensor of any order; for example if $f(\mathbf{x})$ is replaced by a tensor of first order, then

$$\int_\Omega \frac{\partial g_i(\mathbf{x})}{\partial x_i} d\Omega = \int_\Gamma g_i(\mathbf{x}) n_i d\Gamma \qquad \text{or} \qquad \int_\Omega \mathbf{g}(\mathbf{x}) d\Omega = \int_\Gamma \mathbf{n}\ \mathbf{g}(\mathbf{x}) d\Gamma \tag{3.5.3}$$

which is often known as the divergence theorem. The theorem also holds for gradients of the vector field:

$$\int_\Omega \frac{\partial g_i(\mathbf{x})}{\partial x_j} d\Omega = \int_\Gamma g_i(\mathbf{x}) n_j d\Gamma \qquad \text{or} \qquad \int_\Omega \mathbf{g}(\mathbf{x}) d\Omega = \int_\Gamma \mathbf{n} \quad \mathbf{g}(\mathbf{x}) d\Gamma \tag{3.5.3b}$$

and to tensors of arbitrary order.

If the function $f(\mathbf{x})$ is not continuously differentiable, i.e. if its derivatives are discontinuous along a finite number of lines in two dimensions or on surfaces in three dimensions, then Ω must be subdivided into subdomains so that the function is C^1 within each subdomain. Discontinuities in the derivatives of the function will then occur only on the interfaces between the subdomains. Gauss's theorem is applied to each of the subdomains, and summing the results yields the following counterparts of (3.5.2) and (3.5.3):

$$\int_\Omega \frac{\partial f}{\partial x_i} d\Omega = \int_\Gamma f n_i d\Gamma + \int_{\Gamma_{int}} \langle f n_i \rangle d\Gamma \qquad \int_\Omega \frac{\partial g_i}{\partial x_i} d\Omega = \int_\Gamma g_i n_i d\Gamma + \int_{\Gamma_{int}} \langle g_i n_i \rangle d\Gamma \tag{3.5.4}$$

where Γ_{int} is the set of all interfaces between these subdomains and $\langle f \rangle$ and $\langle \mathbf{n}\ \mathbf{g} \rangle$ are the jumps defined by

$$\langle f \rangle = f^A - f^B \tag{3.5.5a}$$

$$\langle \mathbf{n}\ \mathbf{g} \rangle = \langle g_i n_i \rangle = g_i^A n_i^A + g_i^B n_i^B = \left(g_i^A - g_i^B \right) n_i^A = \left(g_i^B - g_i^A \right) n_i^B \tag{3.5.5b}$$

where A and B are a pair of subdomains which border on the interface Γ_{int}, $\mathbf{n}^A$ and $\mathbf{n}^B$ are the outward normals for the two subdomains and f^A and f^B are the function values at the points adjacent to the interface in subdomains A and B, respectively. All the forms in (3.5.5b) are equivalent and make use of the fact that on the interface, $\mathbf{n}^A = -\mathbf{n}^B$. The first of the formulas is the easiest to remember because of its symmetry with respect to A and B.

3.5.3 Material Time Derivative of an Integral and Reynold's Transport Theorem. The material time derivative of an integral is the rate of change of an integral on a material domain. A material domain moves with the material, so that the material points on the boundary remain on the boundary and no flux occurs across the boundaries. A material domain is analogous to a Lagrangian mesh; a Lagrangian element or group of Lagrangian elements is a nice example of a material domain. The various forms for material time derivatives of integrals are called Reynold;s transport theorem, which is employed in the development of conservation laws.

The material time derivative of an integral is defined by

$$\frac{D}{Dt}\int_\Omega f\, d\Omega = \lim_{\Delta t\to 0}\frac{1}{\Delta t}\Big(\int_{\Omega_{\tau+\Delta t}} f(\mathbf{x},\tau+\Delta t)\, d\Omega_{\mathbf{x}} - \int_{\Omega_\tau} f(\mathbf{x},\tau)\, d\Omega_{\mathbf{x}}\Big) \tag{3.5.6}$$

where Ω_τ is the spatial domain at time τ and $\Omega_{\tau+\Delta t}$ the spatial domain occupied by the same material points at time $\tau+\Delta t$. The notation on the left hand side is a little confusing because it appears to refer to a single spatial domain. However, in this notation, which is standard, the material derivative on the integral implies that the domain refers to a material domain. We now transform both integrals on the right hand side to the reference domain using (3.2.18) and change the independent variables to the material coordinates, which gives

$$\frac{D}{Dt}\int_\Omega f\, d\Omega = \lim_{\Delta t\to 0}\frac{1}{\Delta t}\Big(\int_{\Omega_0} f(\mathbf{X},\tau+\Delta t) J(\mathbf{X},\tau+\Delta t)\, d\Omega_0 - \int_{\Omega_0} f(\mathbf{X},\tau) J(\mathbf{X},\tau)\, d\Omega_0\Big) \tag{3.5.7}$$

The function is now $f\big(\varphi(\mathbf{X},t),t\big) \equiv f\circ\varphi$, but we adhere to our convention that the symbol represents the field and leave the symbol unchanged.

Since the domain of integration is now independent of time, we can pull the limit operation inside the integral and take the limit, which yields

$$\frac{D}{Dt}\int_\Omega f\, d\Omega = \int_{\Omega_0}\frac{\partial}{\partial t}\big(f(\mathbf{X},t)J(\mathbf{X},t)\big)\, d\Omega_0 \tag{3.5.9}$$

The partial derivative with respect to time in the integrand is a material time derivative since the independent space variables are the material coordinates. We next use the product rule for derivatives on the above:

$$\frac{D}{Dt}\int_\Omega f\, d\Omega = \int_{\Omega_0}\frac{\partial}{\partial t}\big(f(\mathbf{X},t)J(\mathbf{X},t)\big)\, d\Omega_0 = \int_{\Omega_0}\left(\frac{\partial f}{\partial t}J + f\frac{\partial J}{\partial t}\right) d\Omega_0$$

Bearing in mind that the partial time derivatives are material time derivatives because the independent variables are the material coordinates and time, we can use (3.2.19) to obtain

$$\frac{D}{Dt}\int_{\Omega} f\, d\Omega = \int_{\Omega_0} \left(\frac{\partial f(\mathbf{X},t)}{\partial t} J + f J \frac{\partial v_i}{\partial x_i} \right) d\Omega_0 \tag{3.5.12}$$

We can now transform the RHS integral to the current domain using (3.2.18) and change the independent variables to an Eulerian description, which gives

$$\frac{D}{Dt}\int_{\Omega} f(\mathbf{x},t) d\Omega = \int_{\Omega} \left(\frac{Df(\mathbf{x},t)}{Dt} + f \frac{\partial v_i}{\partial x_i} \right) d\Omega \tag{3.5.11}$$

where the partial time derivative has been changed to a material time derivative because of the change of independent variables; the material time derivative symbol has been changed with the change of independent variables, since $Df(\mathbf{x},t)/Dt \equiv \partial f(\mathbf{X},t)/\partial t$ as indicated in (3.2.8).

An alternate form of Reynold's transport theorem can be obtained by using the definition of the material time derivative, Eq. (3.2.12) in (3.5.11). This gives

$$\frac{D}{Dt}\int_{\Omega} f\, d\Omega = \int_{\Omega} \left(\frac{\partial f}{\partial t} + v_i \frac{\partial f}{\partial x_i} + \frac{\partial v_i}{\partial x_i} f \right) d\Omega = \int_{\Omega} \left(\frac{\partial f}{\partial t} + \frac{\partial (v_i f)}{\partial x_i} \right) d\Omega \tag{3.5.13}$$

which can be written in tensor form as

$$\frac{D}{Dt}\int_{\Omega} f\, d\Omega = \int_{\Omega} \left(\frac{\partial f}{\partial t} + div(\mathbf{v} f) \right) d\Omega \tag{3.5.14}$$

Equation (3.5.14) can be put into another form by using Gauss's theorem on the second term of the RHS, which gives

$$\frac{D}{Dt}\int_{\Omega} f\, d\Omega = \int_{\Omega} \frac{\partial f}{\partial t} d\Omega + \int_{\Gamma} f v_i n_i d\Gamma \quad \text{or} \quad \frac{D}{Dt}\int_{\Omega} f\, d\Omega = \int_{\Omega} \frac{\partial f}{\partial t} d\Omega + \int_{\Gamma} f \mathbf{v}\cdot\mathbf{n} d\Gamma \tag{3.5.15}$$

where the product $f\mathbf{v}$ is assumed to be C^1 in Ω. Reynold's transport theorem, which in the above has been given for a scalar, applies to a tensor of any order. Thus to apply it to a first order tensor (vector) g_k, replace f by g_k in Eq. (3.5.14), which gives

$$\frac{D}{Dt}\int_{\Omega} g_k\, d\Omega = \int_{\Omega} \left(\frac{\partial g_k}{\partial t} + \frac{\partial (v_i g_k)}{\partial x_i} \right) d\Omega \tag{3.5.16}$$

3.5.5 Mass Conservation. The mass $m(\Omega)$ of a material domain Ω is given by

$$m(\Omega) = \int_{\Omega} \rho(\mathbf{X}, t)\, d\Omega \tag{3.5.17}$$

where $\rho(\mathbf{X}, t)$ is the density. Mass conservation requires that the mass of a material subdomain be constant, since no material flows through the boundaries of a material subdomain and we are not considering mass to energy conversion. Therefore, according to the principle of mass conservation, the material time derivative of $m(\Omega)$ vanishes, i.e.

$$\frac{Dm}{Dt} = \frac{D}{Dt}\int_{\Omega} \rho\, d\Omega = 0 \tag{3.5.18}$$

Applying Reynold's theorem, Eq. (3.5.11), to the above yields

$$\int_{\Omega} \left(\frac{D\rho}{Dt} + \rho\, div(\mathbf{v}) \right) d\Omega = 0 \tag{3.5.19}$$

Since the above holds for any subdomain Ω, it follows from Eq.(3.5.1) that

$$\frac{D\rho}{Dt} + \rho\, div(\mathbf{v}) = 0 \quad \text{or} \quad \frac{D\rho}{Dt} + \rho v_{i,i} = 0 \quad \text{or} \quad \dot{\rho} + \rho v_{i,i} = 0 \tag{3.5.20}$$

The above is the equation of *mass conservation*, often called *the continuity equation*. It is a first order partial differential equation.

Several special forms of the mass conservation equation are of interest. When a material is incompressible, the material time derivative of the density vanishes, and it can be seen from equation (3.5.20) that the mass conservation equation becomes:

$$div(\mathbf{v}) = 0 \qquad v_{i,i} = 0 \tag{3.5.21}$$

In other words, mass conservation requires the divergence of the velocity field of an incompressible material to vanish.

If the definition of a material time derivative, (3.2.12) is invoked in (3.5.20), then the continuity equation can be written in the form

$$\frac{\partial \rho}{\partial t} + \rho_{,i} v_i + \rho v_{i,i} = \frac{\partial \rho}{\partial t} + (\rho v_i)_{,i} = 0 \tag{3.5.22}$$

This is called the *conservative form* of the mass conservation equation. It is often preferred in computational fluid dynamics because discretizations of the above form are thouught to more accurately enforce mass conservation.

For Lagrangian descriptions, the rate form of the mass conservation equation, Eq. (3.5.18), can be integrated in time to obtain an algebraic equation for the density. Integrating Eq. (3.5.18) in time gives

$$\int_{\Omega} \rho \, d\Omega = \text{constant} = \int_{\Omega_0} \rho_0 \, d\Omega_0 \tag{3.5.23}$$

Transforming the left hand integral in the above to the reference domain by (3.2.18) gives

$$\int_{\Omega_0} \left(\rho J - \rho_0 \right) d\Omega_o = 0 \tag{3.5.24}$$

Then invoking the smoothness of the integrand and Eq. (3.5.1) gives the following equation for mass conservation

$$\rho(\mathbf{X},t) J(\mathbf{X},t) = \rho_0(\mathbf{X}) \qquad \text{or} \qquad \rho J = \rho_0 \tag{3.5.25}$$

We have explicitly indicated the independent variables on the left to emphasize that this equation only holds for material points; the fact that the independent variables must be the material coordinates in these equations follows from the fact that the integrand and domain of integration in (3.5.24) must be expressed for a material coordinate and material subdomain, respectively.

As a consequence of the integrability of the mass conservation equation in Lagrangian descriptions, the algebraic equation (3.5.25) are used to enforce mass conservation in Lagrangian meshes. In Eulerian meshes, the algebraic form of mass conservation, Eq. (3.5.25), cannot be used, and mass conservation is imposed by the partial differential equation, (3.5.20) or (3.5.22), i.e. the continuity equation.

3.5.5 Conservation of Linear Momentum. The equation emanating from the principle of momentum conservation is a key equation in nonlinear finite element procedures. Momentum conservation is a statement of Newton's second law of motion, which relates the forces acting on a body to its acceleration. We consider an arbitrary subdomain of the body Ω with boundary Γ. The body is subjected to body forces $\rho\mathbf{b}$ and to surface tractions $\mathbf{t}$, where $\mathbf{b}$ is a force per unit mass and $\mathbf{t}$ is a force per unit area. The total force on the body is given by

$$\mathbf{f}(t) = \int_{\Omega} \rho \mathbf{b}(\mathbf{x},t) \, d\Omega + \int_{\Gamma} \mathbf{t}(\mathbf{x},t) d\Gamma \tag{3.5.26}$$

The linear momentum of the body is given by

$$\mathbf{p}(t) = \int_{\Omega} \rho \mathbf{v}(\mathbf{x},t) d\Omega \tag{3.5.27}$$

where $\rho\mathbf{v}$ is the linear momentum per unit volume.

Newton's second law of motion for a continuum states that the material time derivative of the linear momentum equals the net force. Using (3.5.26) and (3.5.27), this gives

$$\frac{D\mathbf{p}}{Dt} = \mathbf{f} \qquad \frac{D}{Dt}\int_\Omega \rho \mathbf{v}\, d\Omega = \int_\Omega \rho \mathbf{b}\, d\Omega + \int_\Gamma \mathbf{t}\, d\Gamma \tag{3.5.28}$$

We now convert the first and third integrals in the above to obtain a single domain integral so Eq. (3.5.1) can be applied. Reynold's Transport Theorem applied to the first integral in the above gives

$$\frac{D}{Dt}\int_\Omega \rho \mathbf{v}\, d\Omega = \int_\Omega \left(\frac{D}{Dt}(\rho \mathbf{v}) + div(\mathbf{v})\rho \mathbf{v}\right) d\Omega = \int_\Omega \left(\rho \frac{D\mathbf{v}}{Dt} + \mathbf{v}\left(\frac{D\rho}{Dt} + \rho\, div(\mathbf{v})\right)\right) d\Omega \tag{3.5.29}$$

where the second equality is obtained by using the product rule of derivatives for the first term of the integrand and rearranging terms.

The term multiplying the velocity in the RHS of the above can be recognized as the continuity equation, which vanishes, giving

$$\frac{D}{Dt}\int_\Omega \rho \mathbf{v}\, d\Omega = \int_\Omega \rho \frac{D\mathbf{v}}{Dt} d\Omega \tag{3.5.30}$$

To convert the last term in Eq. (3.5.28) to a domain integral, we invoke Cauchy's relation and Gauss's theorem in sequence, giving

$$\int_\Gamma \mathbf{t}\, d\Gamma = \int_\Gamma \mathbf{n}\ \sigma\, d\Gamma = \int_\Omega \quad \sigma d\Omega \quad \text{or} \quad \int_\Gamma t_j d\Gamma = \int_\Gamma n_i \sigma_{ij}\, d\Gamma = \int_\Omega \frac{\partial \sigma_{ij}}{\partial x_i} d\Omega \tag{3.5.31}$$

Note that since the normal is *to the left* on the boundary integral, the divergence is *to the left* and contracts with the first index on the stress tensor. When the divergence operator acts on the first index of the stress tensor it is called the left divergence operator and is placed to the left of operand. When it acts on the second index, it is placed to the right and call the right divergence. Since the Cauchy stress is symmetric, the left and right divergence operators have the same effect. However, in contrast to linear continuum mechanics, in nonlinear continuum mechanics it is important to become accustomed to placing the divergence operator where it belongs because some stress tensors, such as the nominal stress, are not symmetric. When the stress is not symmetric, the left and right divergence operators lead to different results. When Gauss's theorem is used, the divergence on the stress tensor is on the same side as the normal in Cauchy's relation. In this book we will use the convention that the *normal and divergence are always placed on the left.*

Substituting (3.5.30) and (3.5.31) into (3.5.28) gives

$$\int_\Omega \left(\rho \frac{D\mathbf{v}}{Dt} - \rho \mathbf{b} - \quad \sigma\right) d\Omega = 0 \tag{3.5.32}$$

Therefore, if the integrand is C^{-1}, since (3.5.32) holds for an arbitrary domain, applying (3.5.1) yields

$$\rho \frac{D\mathbf{v}}{Dt} = \quad \sigma + \rho\mathbf{b} \equiv div\sigma + \rho\mathbf{b} \qquad \text{or} \qquad \rho \frac{Dv_i}{Dt} = \frac{\partial \sigma_{ji}}{\partial x_j} + \rho b_i \qquad (3.5.33)$$

This is called the *momentum equation* or the *equation of motion*; it is also called the balance of linear momentum equation. The LHS term represents the change in momentum, since it is a product of the acceleration and the density; it is also called the inertial term. The first term on the RHS is the net resultant internal force per unit volume due to divergence of the stress field.

This form of the momentum equation is applicable to both Lagrangian and Eulerian descriptions. In a Lagrangian description, the dependent variables are assumed to be functions of the Lagrangian coordinates $\mathbf{X}$ and time t, so the momentum equation is

$$\rho(\mathbf{X},t)\frac{\partial \mathbf{v}(\mathbf{X},t)}{\partial t} = div\sigma\left(\varphi^{-1}(\mathbf{x},t),t\right) + \rho(\mathbf{X},t)\mathbf{b}(\mathbf{X},t) \qquad (3.5.34)$$

Note that the stress must be expressed as a function of the Eulerian coordinates through the motion $\varphi^{-1}(\mathbf{X},t)$ so that the spatial divergence of the stress field can be evaluated; the total derivative of the velocity with respect to time in (3.5.33) becomes a partial derivative with respect to time when the independent variables are changed from the Eulerian coordinates $\mathbf{x}$ to the Lagrangian coordinates $\mathbf{X}$.

In an Eulerian description, the material derivative of the velocity is written out by (3.2.9) and all variables are considered functions of the Eulerian coordinates. Equation (3.5.33) becomes

$$\rho(\mathbf{x},t)\left(\frac{\partial \mathbf{v}(\mathbf{x},t)}{\partial t} + (\mathbf{v}(\mathbf{x},t)\ grad)\mathbf{v}(\mathbf{x},t)\right) = div\sigma(\mathbf{x},t) + \rho(\mathbf{x},t)\mathbf{b}(\mathbf{x},t) \qquad (3.5.35)$$

$$\text{or} \quad \rho\left(\frac{\partial v_i}{\partial t} + v_{i,j}v_j\right) = \frac{\partial \sigma_{ji}}{\partial x_j} + \rho b_i$$

As can be seen from the above, when the independent variables are all explicitly written out the equations are quite awkward, so we will usually drop the independent variables. The independent variables are specified wherever the dependent variables are first defined, when they first appear in a section or chapter, or when they are changed. So if the independent variables are not clear, the reader should look back to where the independent variables were last specified.

In computational fluid dynamics, the momentum equation is sometimes used without the changes made by Eqs. (3.5.13-3.5.30). The resulting equation is

$$\frac{D(\rho\mathbf{v})}{Dt} \equiv \frac{\partial(\rho\mathbf{v})}{\partial t} + \mathbf{v}\ grad(\rho\mathbf{v}) = div\sigma + \rho\mathbf{b} \qquad (3.5.36)$$

This is called the conservative form of the momentum equation with considered $\rho\mathbf{v}$ as one of the unknowns. Treating the equation in this form leads to better observance of momentum conservation.

3.5.7 Equilibrium Equation. In many problems, the loads are applied slowly and the inertial forces are very small and can be neglected. In that case, the acceleration in the momentum equation (3.5.35) can be dropped and we have

$$\nabla\cdot\boldsymbol{\sigma} + \rho\mathbf{b} = 0 \quad \text{or} \quad \frac{\partial \sigma_{ji}}{\partial x_j} + \rho b_i = 0 \tag{3.5.37}$$

The above equation is called the *equilibrium equation*. Problems to which the equilibrium equation is applicable are often called static problems. The equilibrium equation should be carefully distinguished from the momentum equation: equilibrium processes are static and do not include acceleration. The momentum and equilibrium equations are tensor equations, and the tensor forms (3.5.33) and (3.5.37) represent n_{SD} scalar equations.

3.5.8 Reynold's Theorem for a Density-Weighted Integrand. Equation (3.5.30) is a special case of a general result: the material time derivative of an integral in which the integrand is a product of the density and the function f is given by

$$\frac{D}{Dt}\int_\Omega \rho f\, d\Omega = \int_\Omega \rho \frac{Df}{Dt} d\Omega \tag{3.5.38}$$

This holds for a tensor of any order and is a consequence of Reynold's theorem and mass conservation; thus, it can be called another form of Reynold's theorem. It can be verified by repeating the steps in Eqs. (3.5.29) to (3.5.30) with a tensor of any order.

3.5.9 Conservation of Angular Momentum. The conservation of angular momentum provides additional equations which govern the stress tensors. The integral form of the conservation of angular momentum is obtained by taking the cross-product of each term in the corresponding linear momentum principle with the position vector $\mathbf{x}$, giving

$$\frac{D}{Dt}\int_\Omega \mathbf{x}\times\rho\mathbf{v}\, d\Omega = \int_\Omega \mathbf{x}\times\rho\mathbf{b}\, d\Omega + \int_\Gamma \mathbf{x}\times\mathbf{t}\, d\Gamma \tag{3.5.39}$$

We will leave the derivation of the conditions which follow from (3.5.39) as an exercise and only state them:

$$\boldsymbol{\sigma} = \boldsymbol{\sigma}^T \qquad \text{or} \qquad \sigma_{ij} = \sigma_{ji} \tag{3.5.40}$$

In other words, conservation of angular momentum requires that the Cauchy stress be a symmetric tensor. Therefore, the Cauchy stress tensor represents 3 distinct dependent variables in two-dimensional problems, 6 in three-dimensional problems. The conservation of angular momentum does not result in any additional partial differential equations when the Cauchy stress is used.

3.5.10 Conservation of Energy. We consider thermomechanical processes where the only sources of energy are mechanical work and heat. The principle of conservation of energy, i.e. the energy balance principle, states that the rate of change of total energy is equal to the work done by the body forces and surface tractions plus the heat energy delivered to the body by the heat flux and other sources of heat. The internal energy per unit volume is denoted by ρw^{int} where w^{int} is the internal energy per unit mass. The heat flux per unit area is denoted by a vector **q**, in units of power per area and the heat source per unit volume is denoted by ρs. The conservation of energy then requires that the rate of change of the total energy in the body, which includes both internal energy and kinetic energy, equal the power of the applied forces and the energy added to the body by heat conduction and any heat sources.

The rate of change of the total energy in the body is given by

$$P^{tot} = P^{int} + P^{kin}, \quad P^{int} = \frac{D}{Dt}\int_\Omega \rho w^{int} d\Omega, \quad P^{kin} = \frac{D}{Dt}\int_\Omega \tfrac{1}{2}\rho \mathbf{v}\cdot\mathbf{v} d\Omega \tag{3.5.41}$$

where P^{int} denotes the rate of change of internal energy and P^{kin} the rate of change of the kinetic energy. The rate of the work by the body forces in the domain and the tractions on the surface is

$$P^{ext} = \int_\Omega \mathbf{v}\cdot\rho\mathbf{b} d\Omega + \int_\Gamma \mathbf{v}\cdot\mathbf{t} d\Gamma = \int_\Omega v_i \rho b_i d\Omega + \int_\Gamma v_i t_i d\Gamma \tag{3.5.42}$$

The power supplied by heat sources s and the heat flux **q** is

$$P^{heat} = \int_\Omega \rho s d\Omega - \int_\Gamma \mathbf{n}\cdot\mathbf{q} d\Gamma = \int_\Omega \rho s d\Omega - \int_\Gamma n_i q_i d\Gamma \tag{3.5.43}$$

where the sign of the heat flux term is negative since positive heat flow is out of the body.

The statement of the conservation of energy is written

$$P^{tot} = P^{ext} + P^{heat} \tag{3.5.44}$$

i.e. the rate of change of the total energy in the body (consisting of the internal and kinetic energies) is equal to the rate of work by the external forces and rate of work provided by heat flux and energy sources. This is known as the *first law of thermodynamics.* The disposition of the internal work depends on the material. In an elastic material, it is stored as elastic internal energy and fully recoverable upon unloading. In an elastic-plastic material, some of it is converted to heat, whereas some of the energy is irretrievably dissipated in changes of the internal structure of the material.

Substituting Eqs. (3.5.41) to (3.5.43) into (3.5.44) gives the full statement of the conservation of energy

$$\frac{D}{Dt}\int_\Omega \left(\rho w^{int} + \tfrac{1}{2}\rho \mathbf{v}\ \mathbf{v}\right) d\Omega = \int_\Omega \mathbf{v}\ \rho\mathbf{b}\, d\Omega + \int_\Gamma \mathbf{v}\ \mathbf{t}\, d\Gamma + \int_\Omega \rho s\, d\Omega - \int_\Gamma \mathbf{n}\ \mathbf{q}\, d\Gamma \tag{3.5.45}$$

We will now derive the equation which emerges from the above integral statement using the same procedure as before: we use Reynolds's theorem to bring the total derivative inside the integral and convert all surface integrals to domain integrals. Using Reynold's Theorem, (3.5.38) on the first integral in Eq. (3.5.45) gives

$$\begin{aligned}\frac{D}{Dt}\int_\Omega \left(\rho w^{int} + \tfrac{1}{2}\rho \mathbf{v}\ \mathbf{v}\right) d\Omega &= \int_\Omega \left(\rho \frac{Dw^{int}}{Dt} + \tfrac{1}{2}\rho \frac{D(\mathbf{v}\ \mathbf{v})}{Dt}\right) d\Omega \\ &= \int_\Omega \left(\rho \frac{Dw^{int}}{Dt} + \rho \mathbf{v}\ \frac{D\mathbf{v}}{Dt}\right) d\Omega\end{aligned} \tag{3.5.46}$$

We will use commas in the following to denote spatial derivatives. Applying Cauchy's law (3.4.1) and Gauss's theorem (3.5.12) to the traction boundary integrals on the RHS of (3.5.45) yields:

$$\int_\Gamma \mathbf{v}\ \mathbf{t}\, d\Gamma = \int_\Gamma \mathbf{n}\ \sigma\ \mathbf{v}\, d\Gamma = \int_\Omega \left(v_i \sigma_{ji}\right)_{,j} d\Omega = \int_\Omega \left(v_{i,j}\sigma_{ji} + v_i \sigma_{ji,j}\right) d\Omega$$

$$= \int_\Omega \left(D_{ji}\sigma_{ji} + W_{ji}\sigma_{ji} + v_i \sigma_{ji,j}\right) d\Omega \quad \text{using (3.3.9)}$$

$$= \int_\Omega \left(D_{ji}\sigma_{ji} + v_i \sigma_{ji,j}\right) d\Omega \qquad \begin{array}{l}\text{symmetry of } \sigma \text{ and} \\ \text{skew symmetry of } \mathbf{W}\end{array}$$

$$= \int_\Omega \left(\mathbf{D} : \sigma + (\quad \sigma)\ \mathbf{v}\right) d\Omega \tag{3.5.47}$$

Inserting these results into (3.5.44) or (3.5.45), application of Gauss's theorem to the heat flux integral and rearrangement of terms yields

$$\int_\Omega \left(\rho \frac{Dw^{int}}{Dt} - \mathbf{D} : \sigma + \quad \mathbf{q} - \rho s + \mathbf{v}\ \left(\rho \frac{D\mathbf{v}}{Dt} - \quad \sigma - \rho\mathbf{b}\right)\right) d\Omega = 0 \tag{3.5.48}$$

The last term in the integral can be recognized as the momentum equation, Eq. (3.5.33), so it vanishes. Then invoking the arbitrariness of the domain gives:

$$\rho \frac{Dw^{int}}{Dt} = \mathbf{D} : \sigma - \quad \mathbf{q} + \rho s \tag{3.5.49}$$

When the heat flux and heat sources vanish, i.e. in a purely mechanical process, the energy equation becomes

$$\rho \frac{Dw^{int}}{Dt} = \mathbf{D} : \sigma = \sigma : \mathbf{D} = \sigma_{ij} D_{ij} \tag{3.5.50}$$

The above defines the rate of internal energy or internal power in terms of the measures of stress and strain. It shows that the internal power is given by the contraction of the rate-of-deformation and the Cauchy stress. We therefore say that the rate-of-deformation and the Cauchy stress are *conjugate in power*. As we shall see, conjugacy in power is helpful in the development of weak forms: measures of stress and strain rate which are conjugate in power can be used to construct principles of virtual work or power, which are the weak forms for finite element approximations of the momentum equation. Variables which are conjugate in power are also said to be *conjugate in work or energy*, but we will use the phrase conjugate in power because it is more accurate.

The rate of change of the internal energy of the system is obtained by integrating (3.5.50) over the domain of the body, which gives

$$\frac{DW^{int}}{Dt} = \int_\Omega \rho \frac{Dw^{int}}{Dt}\, d\Omega = \int_\Omega \mathbf{D}:\sigma\, d\Omega = \int_\Omega D_{ij}\sigma_{ij} d\Omega = \int_\Omega \frac{\partial v_i}{\partial x_j}\sigma_{ij} d\Omega \qquad (3.5.51)$$

where the last expression follows from the symmetry of the Cauchy stress tensor.

The conservation equations are summarized in Box 3.3 in both tensor and indicial form. The equations are written without specifying the independent variables; they can be expressed in terms of either the spatial coordinates or the material coordinates, and as we shall see later, they can be written in terms of other coordinate systems which are neither fixed in space nor coincident with material points. The equations are not expressed in conservative form because this does not seem to be as useful in solid mechanics as it is in fluid mechanics. The reasons for this are not explored in the literature, but it appears to be related to the mauch smaller changes in density which occur in solid mechanics problems.

Box 3.3
Conservation Equations

Eulerian description

Mass

$$\frac{D\rho}{Dt} + \rho\, div(\mathbf{v}) = 0 \quad \text{or} \quad \frac{D\rho}{Dt} + \rho v_{i,i} = 0 \quad \text{or} \quad \dot{\rho} + \rho v_{i,i} = 0 \qquad (B3.3.1)$$

Linear Motion

$$\rho\frac{D\mathbf{v}}{Dt} = \quad \sigma + \rho\mathbf{b} \equiv div\sigma + \rho\mathbf{b} \qquad \text{or} \qquad \rho\frac{Dv_i}{Dt} = \frac{\partial\sigma_{ji}}{\partial x_j} + \rho b_i \qquad (B3.3.2)$$

Angular Momentum

$$\sigma = \sigma^T \quad \text{or} \quad \sigma_{ij} = \sigma_{ji} \qquad (B3.3.3)$$

Energy

$$\rho\frac{Dw^{int}}{Dt} = \mathbf{D}:\sigma - \quad \mathbf{q} + \rho s \qquad (B3.3.4)$$

Lagrangian Description

Mass

$$\rho(\mathbf{X},t)J(\mathbf{X},t) = \rho_0(\mathbf{X}) \qquad \text{or} \qquad \rho J = \rho_0 \qquad (B3.3.5)$$

Linear Momentum

$$\rho_0 \frac{\partial \mathbf{v}(\mathbf{X},t)}{\partial t} = \quad_{\mathbf{X}} \mathbf{P} + \rho_0 \mathbf{b} \qquad \text{or} \qquad \rho_0 \frac{\partial v_i(\mathbf{X},t)}{\partial t} = \frac{\partial P_{ji}}{\partial X_j} + \rho_0 b_i \tag{B3.3.6}$$

Angular Momentum

$$\mathbf{F} \quad \mathbf{P} = \mathbf{P}^T \quad \mathbf{F}^T \qquad F_{ik}P_{kj} = P_{ik}^T F_{kj}^T = F_{jk}P_{ki} \tag{B3.3.7}$$

$$\mathbf{S} = \mathbf{S}^T \tag{B3.3.8}$$

Energy

$$\rho_0 \dot{w}^{int} = \rho_0 \frac{\partial w^{int}(\mathbf{X},t)}{\partial t} = \dot{\mathbf{F}}^T : \mathbf{P} - \quad_X \tilde{\mathbf{q}} + \rho_0 s \tag{B3.3.9}$$

3.5.11 System Equations. The number of dependent variables depends on the number of space dimensions in the model. If we denote the number of space dimensions by n_{SD}, then for a purely mechanical problem, the following unknowns occur in the equations for a purely mechanical process (a process without heat transfer, so the energy equation is not used):

ρ, the density	1 unknown
$\mathbf{v}$, the velocity	n_{SD} unknowns
σ, the stresses	$n_\sigma = n_{SD}*(n_{SD}+1)/2$ unknowns

In counting the number of unknowns attributed to the stress tensor, we have exploited its symmetry, which results from the conservation of angular momentum. The combination of the mass conservation (1 equation), and the momentum conservation (n_{SD} equations) gives a total of $n_{SD}+1$ equations. Thus we are left with n_σ extra unknowns. These are provided by the constitutive equations, which relate the stresses to a measure of deformation. This equation introduces n_σ additional unknowns, the components of the symmetric rate-of-deformation tensor. However, these unknowns can immediately be expressed in terms of the velocities by Eq. (3.3.10), so they need not be counted as additional unknowns.

The displacements are not counted as unknowns. The displacements are considered secondary dependent variables since they can be obtained by integrating the velocities in time using Eq. (3.2.8) at any material point. The displacements are considered secondary dependent variables, just like the position vectors. This choice of dependent variables is a matter of preference. We could just as easily have chosen the displacement as a primary dependent variable and the velocity as a secondary dependent variable.

3.6. LAGRANGIAN CONSERVATION EQUATIONS

3.6.1 Introduction and Definitions. For solid mechanics applications, it is instructive to directly develop the conservation equations in terms of the Lagrangian measures of stress and strain in the reference configuration. In the continuum mechanics literature such formulations are called Lagrangian, whereas in the finite element literature these formulations are called *total Lagrangian formulations*. For a total Lagrangian formulation, a Lagrangian mesh is always used. The conservation equations in a Lagrangian framework are fundamentally identical to those which have just been developed, they are just expressed in terms

of different variables. In fact, as we shall show, they can be obtained by the transformations in Box 3.2 and the chain rule. This Section can be skipped in a first reading. It is included here because much of the finite element literature for nonlinear mechanics employs total Lagrangian formulations, so it is essential for a serious student of the field.

The independent variables in the total Lagrangian formulation are the Lagrangian (material) coordinates $\mathbf{X}$ and the time t. The major dependent variables are the initial density $\rho_0(\mathbf{X},t)$ the displacement $\mathbf{u}(\mathbf{X},t)$ and the Lagrangian measures of stress and strain. We will use the nominal stress $\mathbf{P}(\mathbf{X},t)$ as the measure of stress. This leads to a momentum equation which is strikingly similar to the momentum equation in the Eulerian description, Eq. (3.5.33), so it is easy to remember. The deformation will be described by the deformation gradient $\mathbf{F}(\mathbf{X},t)$. The pair $\mathbf{P}$ and $\mathbf{F}$ is not especially useful for constructing constitutive equations, since $\mathbf{F}$ does not vanish in rigid body motion and $\mathbf{P}$ is not symmetric. Therefore constitutive equations are usually formulated in terms of the of the PK2 stress $\mathbf{S}$ and the Green strain $\mathbf{E}$. However, keep in mind that relations between $\mathbf{S}$ and $\mathbf{E}$ can easily be transformed to relations between $\mathbf{P}$ and $\mathbf{E}$ or $\mathbf{F}$ by use of the relations in Boxes 3.2.

The applied loads are defined on the reference configuration. The traction $\mathbf{t}_0$ is defined in Eq. (3.4.2); $\mathbf{t}_0$ is in units of force per unit initial area. As mentioned in Chapter 1, we place the noughts, which indicate that the variables pertain to the reference configuration, either as subscripts or superscripts, whichever is convenient. The body force is denoted by $\mathbf{b}$, which is in units of force per unit mass; the body force per initial unit volume is given by $\rho_0\mathbf{b}$, which is equivalent to the force per unit current volume $\rho\mathbf{b}$. This equivalence is shown in the following

$$d\mathbf{f} = \rho\mathbf{b}\,d\Omega = \rho\mathbf{b}J d\Omega_0 = \rho_0\mathbf{b}\,d\Omega_0 \tag{3.6.1}$$

where the second equality follows from the conservation of mass, Eq. (3.5.25). Many authors, including Malvern(1969) use different symbols for the body forces in the two formulations; but this is not necessary with our convention of associating symbols with fields.

The conservation of mass has already been developed in a form that applies to the total Lagrangian formulation, Eq.(3.5.25). Therefore we develop only the conservation of momentum and energy.

3.6.2 Conservation of Linear Momentum. In a Lagrangian description, the linear momentum of a body is given in terms of an integral over the reference configuration by

$$\mathbf{p}_0(t) = \int_{\Omega_0} \rho_0 \mathbf{v}(\mathbf{X},t)\, d\Omega_0 \tag{3.6.2}$$

The total force on the body is given by integrating the body forces over the reference domain and the traction over the reference boundaries:

$$\mathbf{f}_0(t) = \int_{\Omega_0} \rho_0 \mathbf{b}(\mathbf{X}, t)\, d\Omega_0 + \int_{\Gamma_0} \mathbf{t}_0(\mathbf{X}, t) d\Gamma_0 \tag{3.6.3}$$

Newton's second law then gives

$$\frac{d\mathbf{p}_0}{dt} = \mathbf{f}_0 \tag{3.6.4}$$

Substituting (3.6.2) and (3.6.3) into the above gives

$$\frac{d}{dt} \int_{\Omega_0} \rho_0 \mathbf{v}\, d\Omega_0 = \int_{\Omega_0} \rho_0 \mathbf{b} d\Omega_0 + \int_{\Gamma_0} \mathbf{t}_0\, d\Gamma_0 \tag{3.6.5}$$

On the LHS, the material derivative can be taken inside the integral because the reference domain is constant in time, so

$$\frac{d}{dt} \int_{\Omega_0} \rho_0 \mathbf{v}\, d\Omega_0 = \int_{\Omega_0} \rho_0 \frac{\partial \mathbf{v}(\mathbf{X}, t)}{\partial t} d\Omega_0 \tag{3.6.6}$$

Using Cauchy's law (3.4.2) and Gauss' theorem in sequence gives

$$\int_{\Gamma_0} \mathbf{t}_0\, d\Gamma_0 = \int_{\Gamma_0} \mathbf{n}_0 \cdot \mathbf{P}\, d\Gamma_0 = \int_{\Omega_0} \nabla_{\mathbf{X}} \cdot \mathbf{P}\, d\Omega_0 \quad \text{or}$$

$$\int_{\Gamma_0} t_i^0\, d\Gamma_0 = \int_{\Gamma_0} n_j^0 P_{ji}\, d\Gamma_0 = \int_{\Omega_0} \frac{\partial P_{ji}}{\partial X_j} d\Omega_0 \tag{3.6.7}$$

Note that in tensor notation, the left gradient appears in the domain integral because the nominal stress is defined with the normal on the left side. The definition of the material gradient, which is distinguished with the subscript $\mathbf{X}$, should be clear from the indicial expression. The index on the material coordinate is the same as the first index on the nominal stress: the order is important because the nominal stress is not symmetric.

Substituting (3.6.6) and (3.6.7) into (3.6.5) gives

$$\int_{\Omega_0} \left(\rho_0 \frac{\partial \mathbf{v}(\mathbf{X}, t)}{\partial t} - \rho_0 \mathbf{b} - \nabla_{\mathbf{X}} \cdot \mathbf{P} \right) d\Omega_0 = 0 \tag{3.6.8}$$

which, because of the arbitrariness of Ω_0 gives

$$\rho_0 \frac{\partial \mathbf{v}(\mathbf{X}, t)}{\partial t} = \nabla_{\mathbf{X}} \cdot \mathbf{P} + \rho_0 \mathbf{b} \qquad \text{or} \qquad \rho_0 \frac{\partial v_i(\mathbf{X}, t)}{\partial t} = \frac{\partial P_{ji}}{\partial X_j} + \rho_0 b_i \tag{3.6.9}$$

Comparing the above with the momentum equation in the Eulerian description, Eq.(3.5.33), we can see that they are quite similar: in the Lagrangian form of the

momentum equation the Cauchy stress is replaced by the nominal stress and the density is replaced by the density in the reference configuration.

The above form of the momentum equation can also be obtained directly by transforming all of the terms in Eq.(3.5.33) using the chain rule and Box 3.2. Actually, this is somewhat difficult, particularly for the gradient term. Using the transformation from Box 3.2 and the chain rule gives

$$\frac{\partial \sigma_{ji}}{\partial x_j} = \frac{\partial \left(J^{-1} F_{jk} P_{ki} \right)}{\partial x_j} = P_{ki} \frac{\partial}{\partial x_j} \left(J^{-1} F_{jk} \right) + J^{-1} F_{jk} \frac{\partial P_{ki}}{\partial x_j} = J^{-1} \frac{\partial x_j}{\partial X_k} \frac{\partial P_{ki}}{\partial x_j} \quad (3.6.10)$$

In the above we have used the definition of the deformation gradient $\mathbf{F}$, Eq. (3.2.14) and $\partial (J^{-1} F_{jk}) / \partial x_j = 0$,(see Ogden(1984)). Thus (3.5.33) becomes

$$\rho \frac{\partial v_i}{\partial t} = J^{-1} \frac{\partial x_j}{\partial X_k} \frac{\partial P_{ki}}{\partial x_j} + \rho b_i \quad (3.6.11)$$

By the chain rule, the first term on the RHS is $J^{-1} \partial P_{ki} / \partial X_k$. Multiplying the equation by J and using mass conservation, $\rho J = \rho_0$ then gives Eq. (3.6.9).

3.6.3 Conservation of Angular Momentum. The balance equations for angular momentum will not be rederived in the total Lagrangian framework. We will use the consequence of angular momentum balance in Eq. (3.5.40) in conjunction with the stress transformations in Box 3.2 to derive the consequences for the Lagrangian measures of stress. Substituting the transformation expression from Box 3.2 into (3.5.40) gives

$$J^{-1} \mathbf{F} \cdot \mathbf{P} = \left(J^{-1} \mathbf{F} \cdot \mathbf{P} \right)^T \quad (3.6.12)$$

Multiplying both sides of the above by J and taking the transpose inside the parenthesis then gives

$$\mathbf{F} \cdot \mathbf{P} = \mathbf{P}^T \cdot \mathbf{F}^T \qquad F_{ik} P_{kj} = P_{ik}^T F_{kj}^T = F_{jk} P_{ki} \quad (3.6.13)$$

The above equations are nontrivial only when $i \neq j$. Thus the above gives one nontrivial equation in two dimensions, three nontrivial equations in three dimensions. So, while the nominal stress is not symmetric, the number of conditions imposed by angular momentum balance equals the number of symmetry conditions on the Cauchy stress, Eq. (3.5.40). In two dimensions, the angular momentum equation is

$$F_{11} P_{12} + F_{12} P_{22} = F_{21} P_{11} + F_{22} P_{21} \quad (3.6.14)$$

These conditions are usually imposed directly on the constitutive equation, as will be seen in Chapter 5.

For the PK2 stress, the conditions emanating from conservation of angular momentum can be obtained by expressing **P** in terms of **S** in Eq. (3.6.13), (the same equations are obtained if σ is replaced by **S** in the symmetry conditions (3.5.40)), which gives

$$\mathbf{F}\ \mathbf{S}\ \mathbf{F}^T = \mathbf{F}\ \mathbf{S}^T\ \mathbf{F}^T \tag{3.6.15}$$

Since **F** must be a regular (nonsingular) matrix, its inverse exists and we can premultiply by $\mathbf{F}^{-1}$ and postmultiply by $\mathbf{F}^{-T} \equiv \left(\mathbf{F}^{-1}\right)^T$ the above to obtain

$$\mathbf{S} = \mathbf{S}^T \tag{3.6.16}$$

So the conservation of angular momentum requires the PK2 stress to be symmetric.

3.6.4 Conservation of Energy in Lagrangian Description. The counterpart of Eq. (3.5.45) in the reference configuration can be written as

$$\begin{aligned} &\frac{d}{dt}\int_{\Omega_0}\left(\rho_0 w^{int} + \tfrac{1}{2}\rho_0 \mathbf{v}\ \mathbf{v}\right)d\Omega_0 = \\ &\qquad \int_{\Omega_0}\mathbf{v}\ \rho_0\mathbf{b}\,d\Omega_0 + \int_{\Gamma_0}\mathbf{v}\ \mathbf{t}_0\,d\Gamma_0 + \int_{\Omega_0}\rho_0 s\,d\Omega_0 - \int_{\Gamma_0}\mathbf{n}_0\ \tilde{\mathbf{q}}\,d\Gamma_0 \end{aligned} \tag{3.6.17}$$

The heat flux in a total Lagrangian formulation is defined as energy per unit reference area and therefore is denoted by $\tilde{\mathbf{q}}$ to distinguish it from the heat flux per unit current area $\mathbf{q}$, which are related by

$$\tilde{\mathbf{q}} = J^{-1}\mathbf{F}^T\ \mathbf{q} \tag{3.6.17b}$$

The above follows from Nanson's law (3.4.5) and the equivalence

$$\int_{\Gamma}\mathbf{n}\ \mathbf{q}\,d\Gamma = \int_{\Gamma_0}\mathbf{n}_0\ \tilde{\mathbf{q}}\,d\Gamma_0$$

Substituting (3.4.5) for $\mathbf{n}$ into the above gives (3.6.17b).

The internal energy per unit initial volume in the above is related to the internal energy per unit current volume in (3.5.45) as follows

$$\rho_0 w^{int} d\Omega_0 = \rho_0 w^{int} J^{-1} d\Omega = \rho w^{int} d\Omega \tag{3.6.18}$$

where the last step follows from the mass conservation equation (3.5.9). On the LHS, the time derivative can be taken inside the integral since the domain is fixed, giving

$$\frac{d}{dt}\int_{\Omega_0}(\rho_0 w^{int}+\frac{1}{2}\rho_0\mathbf{v}\ \mathbf{v})d\Omega_0=\int_{\Omega_0}(\rho_0\frac{\partial w^{int}(\mathbf{X},t)}{\partial t}+\rho_0\mathbf{v}\ \frac{\partial\mathbf{v}(\mathbf{X},t)}{\partial t})d\Omega_0 \quad (3.6.19)$$

The second term on the RHS can be modified as follows by using Eq. (3.4.2) and Gauss's theorem

$$\begin{aligned}\int_{\Gamma_0}\mathbf{v}\ \mathbf{t}_0 d\Gamma_0&=\int_{\Gamma_0}v_j t_j^0 d\Gamma_0=\int_{\Gamma_0}v_j n_i^0 P_{ij}\,d\Gamma_0\\&=\int_{\Omega_0}\frac{\partial}{\partial X_i}\left(v_j P_{ij}\right)d\Omega_0=\int_{\Omega_0}\left(\frac{\partial v_j}{\partial X_i}P_{ij}+v_j\frac{\partial P_{ij}}{\partial X_i}\right)d\Omega_0\\&=\int_{\Omega_0}\left(\frac{\partial F_{ji}}{\partial t}P_{ij}+\frac{\partial P_{ij}}{\partial X_i}v_j\right)d\Omega_0=\int_{\Omega_0}\left(\frac{\partial\mathbf{F}^T}{\partial t}:\mathbf{P}+(\ _X\ \mathbf{P})\ \mathbf{v}\right)d\Omega_0\end{aligned} \quad (3.6.20)$$

Gauss's theorem on the fourth term of the LHS and some manipulation gives

$$\int_{\Omega_0}\left(\rho_0\frac{\partial w^{int}}{\partial t}-\frac{\partial\mathbf{F}^T}{\partial t}:\mathbf{P}+\ _X\ \tilde{\mathbf{q}}-\rho_0 s+\left(\rho_0\frac{\partial\mathbf{v}(\mathbf{X},t)}{\partial t}-\ _X\ \mathbf{P}-\rho_0\mathbf{b}\right)\mathbf{v}\right)d\Omega_0=0 \quad (3.6.21)$$

The term inside the parenthesis of the integrand is the total Lagrangian form of the momentum equation, (3.6.30), so it vanishes. Then because of the arbitrariness of the domain, the integrand vanishes, giving

$$\rho_0\dot{w}^{int}=\rho_0\frac{\partial w^{int}(\mathbf{X},t)}{\partial t}=\dot{\mathbf{F}}^T:\mathbf{P}-\ _X\ \tilde{\mathbf{q}}+\rho_0 s \quad (3.6.22)$$

In the absence of heat conduction or heat sources, the above gives

$$\rho_0\dot{w}^{int}=\dot{F}_{ji}P_{ij}=\dot{\mathbf{F}}^T:\mathbf{P}=\mathbf{P}:\dot{\mathbf{F}} \quad (3.6.23)$$

This is the Lagrangian counterpart of Eq. (3.5.50). It shows that the *nominal stress is conjugate in power to the material time derivative of the deformation gradient*.

These energy conservation equations could also be obtained directly from Eq. (3.5.50) by transformations. This is most easily done in indicial notation.

$$\rho D_{ij}\sigma_{ij}=\rho\frac{\partial v_i}{\partial x_j}\sigma_{ij}\qquad\text{by definition of }\mathbf{D}\text{ and symmetry of stress }\sigma$$

$$=\rho\frac{\partial v_i}{\partial X_k}\frac{\partial X_k}{\partial x_j}\sigma_{ij}\qquad\text{by chain rule}$$

$$= \rho \dot{F}_{ik} \frac{\partial X_k}{\partial x_j} \sigma_{ij} \qquad \text{by definition of } \mathbf{F}\text{, Eq. (3.2.10)} \tag{3.6.24}$$

$$= \rho \dot{F}_{ik} P_{ki} J^{-1} = \rho_0 \dot{F}_{ik} P_{ki} \qquad \text{by Box 3.2 and mass conservation}$$

3.6.5 Power in terms of PK2 stress. The stress transformations in Box 3.2 can also be used to express the internal energy in terms of the PK2 stress.

$$\dot{\mathbf{F}}^T : \mathbf{P} \equiv \dot{F}_{ik} P_{ki} = \dot{F}_{ik} S_{kr} F^T_{ri} \qquad \text{by Box 3.2}$$

$$= F^T_{ri} \dot{F}_{ik} S_{rk} = \left(\mathbf{F}^{\mathbf{T}} \dot{\mathbf{F}} \right) : \mathbf{S} \qquad \text{by symmetry of } \mathbf{S} \tag{3.6.25}$$

$$= \left(\tfrac{1}{2} \left(\mathbf{F}^{\mathbf{T}} \dot{\mathbf{F}} + \dot{\mathbf{F}}^{\mathbf{T}} \mathbf{F} \right) + \tfrac{1}{2} \left(\mathbf{F}^{\mathbf{T}} \dot{\mathbf{F}} - \dot{\mathbf{F}}^{\mathbf{T}} \mathbf{F} \right) \right) : \mathbf{S} \qquad \text{decomposing tensor into symmetric and antisymmetric parts}$$

$$= \tfrac{1}{2} (\mathbf{F}^{\mathbf{T}} \dot{\mathbf{F}} + \dot{\mathbf{F}}^{\mathbf{T}} \mathbf{F}) : \mathbf{S} \qquad \text{since contraction of symmetric and antisymmetric tensors vanishes}$$

Then, using the time derivative of $\mathbf{E}$ as defined in Eq.(3.3.20) gives

$$\rho_0 \dot{w}^{int} = \dot{\mathbf{E}} : \mathbf{S} = \mathbf{S} : \dot{\mathbf{E}} = \dot{E}_{ij} S_{ij} \tag{3.6.26}$$

This shows that the *rate of the Green strain tensor is conjugate in power (or energy) to the PK2 stress*.

Thus we have identified three stress and strain rate measures which are conjugate in the sense of power. These conjugate measures are listed in Box 3.4 along with the corresponding expressions for the power. Box 3.4 also includes a fourth conjugate pair, the corotational Cauchy stress and corotational rate-of-deformation. Its equivalence to the power in terms of the unrotated Cauchy stress and rate-of-deformation is easily demonstrated by (3.4.15) and thhe orthgonality of the rotation matrix.

Conjugate stress and strain rate measures are useful in developing weak forms of the momentum equation, i.e. the principles of virtual work and power. The conjugate pairs presented here just scratch the surface: many other conjugate pairs have been developed in continuum mechanics, {Ogden(1984), Hill()}. However, those presented here are the most frequently used in nonlinear finite element methods.

Box 3.4

Stress-deformation (strain) rate pairs conjugate in power

Cauchy stress/rate-of deformation: $\rho \dot{w}^{int} = \mathbf{D} : \sigma = \sigma : \mathbf{D} = D_{ij} \sigma_{ij}$

Nominal stress/rate of deformation gradient: $\rho_0 \dot{w}^{int} = \dot{\mathbf{F}} : \mathbf{P}^T = \mathbf{P} : \dot{\mathbf{F}}^T = \dot{F}_{ij} P_{ji}$
PK2 stress/rate of Green strain: $\rho_0 \dot{w}^{int} = \dot{\mathbf{E}} : \mathbf{S} = \mathbf{S} : \dot{\mathbf{E}} = \dot{E}_{ij} S_{ij}$
Corotational Cauchy stress/rate-of-deformation: $\rho \dot{w}^{int} = \hat{\mathbf{D}} : \hat{\sigma} = \hat{\sigma} : \hat{\mathbf{D}} = \hat{D}_{ij} \hat{\sigma}_{ij}$

3.7 POLAR DECOMPOSITION AND FRAME-INVARIANCE

In this Section, the role of rigid body rotation is explored. First, a theorem known as the polar decomposition theorem is presented. This theorem enables the rigid body rotation to be obtained for any deformation. Next, we consider the effect of rigid body rotations on constitutive equations. We show that for the Cauchy stress, a modification of the time derivatives is needed to formulate rate constitutive equations. This is known as a *frame-invariant or objective rate of stress*. Three frame-invariant rates are presented: the Jaumann rate, the Truesdell rate and the Green-Naghdi rate. Some startling differences in hypoelastic constitutive equations with these various rates are then demonstrated.

3.7.1 Polar Decomposition Theorem. A fundamental theorem which elucidates the role of rotation in large deformation problems is the polar decomposition theorem. In continuum mechanics, this theorem states that any deformation gradient tensor $\mathbf{F}$ can be multiplicatively decomposed into the product of an orthogonal matrix $\mathbf{R}$ and a symmetric tensor $\mathbf{U}$, called the right stretch tensor (the adjective right is often omitted):

$$\mathbf{F} = \mathbf{R}\ \mathbf{U} \qquad \text{or} \qquad F_{ij} = \frac{\partial x_i}{\partial X_j} = R_{ik} U_{kj} \qquad \text{where} \tag{3.7.1}$$

$$\mathbf{R}^{-1} = \mathbf{R}^T \qquad \text{and} \qquad \mathbf{U} = \mathbf{U}^T \tag{3.7.2}$$

Rewriting the above with Eq. (3.2.15) gives

$$d\mathbf{x} = \mathbf{R}\ \mathbf{U}\ \ d\mathbf{X} \tag{3.7.3}$$

The above shows that any motion of a body consists of a deformation, which is represented by the symmetric mapping $\mathbf{U}$, and a rigid body rotation $\mathbf{R}$; $\mathbf{R}$ can be recognized as a rigid-body rotation because all proper orthogonal transformations are rotations. Rigid body translation does not appear in this equation because $d\mathbf{x}$ and $d\mathbf{X}$ are differential line segments in the current and reference configurations, respectively, and the differential line segments are not affected by translation. If Eq. (3.7.3) were integrated to obtain the deformation function, $\mathbf{x} = \varphi(\mathbf{X}, t)$, then the rigid body translation would appear as a constant of integration. In a translation, $\mathbf{F} = \mathbf{I}$, and $d\mathbf{x} = d\mathbf{X}$.

The polar decomposition theorem is proven in the following. To simplify the proof, we treat the tensors as matrices. Premultiplying both sides of Eq. (3.7.1) by its transpose gives

$$\mathbf{F}^T\ \mathbf{F} = (\mathbf{RU})^T(\mathbf{RU}) = \mathbf{U}^T\mathbf{R}^T\mathbf{RU} = \mathbf{U}^T\mathbf{U} = \mathbf{UU} \tag{3.7.4}$$

where (3.7.2) is used to obtain the third and fourth equalities. The last term is the square of the $\mathbf{U}$ matrix. It follows that

$$\mathbf{U} = \left(\mathbf{F}^T\ \mathbf{F}\right)^{1/2} \tag{3.7.5}$$

The fractional power of a matrix is defined in terms of its spectral representation, see e.g. Chandrasekharaiah and Debnath (1994, p96). It is computed by first transforming the matrix to its principal coordinates, where the matrix becomes a diagonal matrix with the eigenvalues on the diagonal. The fractional power is then applied to all of the diagonal terms, and the matrix is transformed back. This is illustrated in the following examples. The matrix $\mathbf{F}^T\ \mathbf{F}$ is positive definite, so all of its eigenvalues are positive. Consequently the matrix $\mathbf{U}$ is always real.

The rotation part of the deformation, $\mathbf{R}$, can then be found by applying Eq. (3.7.1), which gives

$$\mathbf{R} = \mathbf{F}\ \mathbf{U}^{-1} \tag{3.7.6}$$

The existence of the inverse of $\mathbf{U}$ follows from the fact that all of its eigenvalues are always positive, since the right hand side of Eq. (3.7.5) is always a positive matrix.

The matrix $\mathbf{U}$ is closely related to an engineering definition of strain. Its principal values represent the elongations of line segments in the principal directions of $\mathbf{U}$. Therefore, many researchers have found this tensor to be appealing for developing constitutive equations. The tensor $\mathbf{U} - \mathbf{I}$ is called the Biot strain tensor.

A deformation can also be decomposed in terms of a left stretch tensor and a rotation according to

$$\mathbf{F} = \mathbf{V}\ \mathbf{R} \tag{3.7.7}$$

This form of the polar decomposition is used less frequently and we only note it in passing here. It will play a role in discussions of material symmetry for elastic materials at finite strain. The polar decomposition theorem, which is usually applied to the deformation tensor, applies to any invertible square matrix: any square matrix can be multiplicatively decomposed into a rotation matrix and a symmetric matrix, see Chandrasekharaiah and Debnath (1994, p97).

It is emphasized that the rotations of different line segments at the same point depend on the orientation of the line segment. In a three dimensional body, only three line segments are rotated exactly by $\mathbf{R}(\mathbf{X},t)$ at any point $\mathbf{X}$. These are the line segments corresponding to the principal directions of the stretch tensor $\mathbf{U}$. It can be shown that these are also the principal directions of the Green strain tensor. The rotations of line segments which are oriented in directions other than the principal directions of $\mathbf{E}$ are not given by $\mathbf{R}$.

Example 3.10 Consider the motion of a triangular element in which the nodal coordinates $x_I(t)$ and $y_I(t)$ are given by

$$\begin{aligned} x_1(t) &= a + 2at \qquad & y_1(t) &= 2at \\ x_2(t) &= 2at & y_2(t) &= 2a - 2at \\ x_3(t) &= 3at & y_3(t) &= 0 \end{aligned} \tag{E3.10.1}$$

Find the rigid body rotation and the stretch tensors by the polar decomposition theorem at t=1.0 and at t=0.5.

The motion of a triangular domain can most easily be expressed by using the shape functions for triangular elements, i.e. the area coordinates. In terms of the triangular coordinates, the motion is given by

$$x(\xi,t) = x_1(t)\xi_1 + x_2(t)\xi_2 + x_3(t)\xi_3 \tag{E3.10.2}$$

$$y(\xi,t) = y_1(t)\xi_1 + y_2(t)\xi_2 + y_3(t)\xi_3 \tag{E3.10.3}$$

where ξ_I are the triangular, or area, coordinates; see Appendix A; the material coordinates appear implicitly in the RHS of the above through the relationship between the area coordinates and the coordinates at time t=0. To extract those relationships we write the above at time t=0, which gives

$$x(\xi,0) = X = X_1\xi_1 + X_2\xi_2 + X_3\xi_3 = a\xi_1 \tag{E3.10.4}$$

$$y(\xi,0) = Y = Y_1\xi_1 + Y_2\xi_2 + Y_3\xi_3 = 2a\xi_2 \tag{E3.10.5}$$

In this case, the relations between the triangular coordinates are particularly simple because most of the nodal coordinates vanish in the initial configuration, so the relations developed above could be obtained by inspection.

Using Eq. (E3.10.5) to express the triangular coordinates in terms of the material coordinates, Eq (E3.10.1) can be written

$$\begin{aligned} x(\mathbf{X},1) &= 3a\xi_1 + 2a\xi_2 + 3a\xi_3 \\ &= 3X + Y + 3a\left(1 - \frac{X}{a} - \frac{Y}{2a}\right) = 3a - \frac{Y}{2} \end{aligned} \tag{E3.10.6}$$

$$\begin{aligned} y(\mathbf{X},1) &= 2a\xi_1 + 0\xi_2 + 0\xi_3 \\ &= 2X \end{aligned} \tag{E3.10.7}$$

The deformation gradient is then obtained by evaluating the derivatives of the above motion using Eq. (3.2.16)

$$\mathbf{F} = \begin{bmatrix} \frac{\partial x}{\partial X} & \frac{\partial x}{\partial Y} \\ \frac{\partial y}{\partial X} & \frac{\partial y}{\partial Y} \end{bmatrix} = \begin{bmatrix} 0 & -0.5 \\ 2 & 0 \end{bmatrix} \tag{E3.10.8}$$

The stretch tensor $\mathbf{U}$ is then evaluated by Eq. (3.7.5):

$$\mathbf{U} = (\mathbf{F}^T\mathbf{F})^{1/2} = \begin{bmatrix} 4 & 0 \\ 0 & 0.25 \end{bmatrix}^{1/2} = \begin{bmatrix} 2 & 0 \\ 0 & 0.5 \end{bmatrix} \tag{E3.10.9}$$

In this case the $\mathbf{U}$ matrix is diagonal, so the principal values are simply the diagonal terms. The positive square roots are chosen in evaluating the square root of the matrix because the principal stretches must be positive; otherwise the Jacobian determinant would be negative since according to Eq. (3.7.1), $J = det(\mathbf{R})\,det(\mathbf{U})$ and $det(\mathbf{R}) = 1$, so $det(\mathbf{U}) < 0$ implies $J < 0$. The rotation matrix $\mathbf{R}$ is then given by Eq. (3.7.6):

$$\mathbf{R} = \mathbf{F}\mathbf{U}^{-1} = \begin{bmatrix} 0 & -0.5 \\ 2 & 0 \end{bmatrix}\begin{bmatrix} 0.5 & 0 \\ 0 & 2 \end{bmatrix} = \begin{bmatrix} 0 & -1 \\ 1 & 0 \end{bmatrix} \tag{E3.10.10}$$

Comparing the above rotation matrix $\mathbf{R}$ and Eq. (3.2.25), it can be seen that the rotation is a counterclockwise 90 degree rotation. This is also readily apparent from Fig. 3.9. The deformation consists of an elongation of the line segment between nodes 1 and 3, i.e. dX, by a factor of 2, (see $\mathbf{U}_{11}$ in Eq. (E3.10.9)) and a contraction of the line segment between nodes 3 and 2, i.e. dY, by a factor of 0.5, (see $\mathbf{U}_{22}$ in Eq. (E3.10.9)), followed by a translation of $3a$ in the x-direction and a 90 degree rotation. Since the original line segments along the x and y directions correspond to the principal directions, or eigenvectors, of $\mathbf{U}$, the rotations of these line segments correspond to the rotation of the body in the polar decomposition theorem.

The configuration at t=0.5 is given by evaluating Eq. (E3.10.1) at that time, giving:

$$\begin{aligned} x(\mathbf{X}, 0.5) &= 2a\xi_1 + a\xi_2 + 1.5a\xi_3 \\ &= 2a\frac{X}{a} + a\frac{Y}{2a} + 1.5a\left(1 - \frac{X}{a} - \frac{Y}{2a}\right) = 1.5a + 0.5X - 0.25Y \end{aligned} \tag{E3.10.11a}$$

$$\begin{aligned} y(\mathbf{X}, 0.5) &= a\xi_1 + a\xi_2 + 0\xi_3 \\ &= a\frac{X}{a} + a\frac{Y}{2a} = X + 0.5Y \end{aligned} \tag{E3.10.11b}$$

The deformation gradient $\mathbf{F}$ is then given by

$$\mathbf{F} = \begin{bmatrix} \frac{\partial x}{\partial X} & \frac{\partial x}{\partial Y} \\ \frac{\partial y}{\partial X} & \frac{\partial y}{\partial Y} \end{bmatrix} = \begin{bmatrix} 0.5 & -0.25 \\ 1 & 0.5 \end{bmatrix} \tag{E3.10.12}$$

and the stretch tensor **U** is given by Eq. (3.7.6):

$$\mathbf{U} = (\mathbf{F}^T\mathbf{F})^{1/2} = \begin{bmatrix} 1.25 & 0.375 \\ 0.375 & 0.3125 \end{bmatrix}^{1/2} = \begin{bmatrix} 1.0932 & 0.2343 \\ 0.2343 & 0.5076 \end{bmatrix} \tag{E3.10.13}$$

The last matrix in the above is obtained by finding the eigenvalues λ_i of $\mathbf{F}^T\mathbf{F}$, taking their positive square roots, and placing them on a diagonal matrix called $\mathbf{H} = diag\left(\sqrt{\lambda_1}, \sqrt{\lambda_2}\right)$. The matrix **H** transformed back to the global components by $\mathbf{U} = \mathbf{A}^T\mathbf{H}\mathbf{A}$ where **A** is the matrix whose columns are the eigenvectors of $\mathbf{F}^T\mathbf{F}$. These matrices are:

$$\mathbf{A} = \begin{bmatrix} -0.9436 & 0.3310 \\ -0.3310 & -0.9436 \end{bmatrix} \qquad \mathbf{H} = \begin{bmatrix} 1.3815 & 0 \\ 0 & 0.1810 \end{bmatrix} \tag{E3.10.14}$$

The rotation matrix **R** is then found by

$$\mathbf{R} = \mathbf{F}\mathbf{U}^{-1} = \begin{bmatrix} 0.5 & -0.25 \\ 1 & 0.5 \end{bmatrix} \begin{bmatrix} 1.0932 & 0.2343 \\ 0.2343 & 0.5076 \end{bmatrix}^{-1} = \begin{bmatrix} 0.6247 & -0.7809 \\ 0.7809 & 0.6247 \end{bmatrix} \tag{E3.10.15}$$

Example 3.11 Consider the deformation for which the deformation gradient is

$$\mathbf{F} = \begin{bmatrix} c - as & ac - s \\ s + ac & as + c \end{bmatrix} \qquad c = \cos\theta, \quad s = \sin\theta \tag{E3.11.1}$$

where a is a constant. Find the stretch tensor and the rotation matrix when $a = \frac{1}{2}$, $\theta = \frac{\pi}{2}$.

For the particular values given

$$\mathbf{F} = \begin{bmatrix} -\frac{1}{2} & -1 \\ 1 & \frac{1}{2} \end{bmatrix} \qquad \mathbf{C} = \mathbf{F}^T\mathbf{F} = \begin{bmatrix} 1.25 & 1 \\ 1 & 1.25 \end{bmatrix} \tag{E3.11.2}$$

The eigenvalues and corresponding eigenvectors of **C** are

$$\lambda_1 = 0.25 \qquad \mathbf{y}_1^T = \tfrac{1}{\sqrt{2}}\begin{bmatrix} 1 & -1 \end{bmatrix}$$

$$\lambda_2 = 2.25 \qquad \mathbf{y}_2^T = \tfrac{1}{\sqrt{2}}\begin{bmatrix} 1 & 1 \end{bmatrix} \tag{E3.11.3}$$

The diagonal form of $\mathbf{C}$, diag($\mathbf{C}$), consists of these eigenvalues and the square root of diag($\mathbf{C}$) is obtained by taking the positive square roots of these eigenvalues

$$\text{diag}(\mathbf{C}) = \begin{bmatrix} \frac{1}{4} & 0 \\ 0 & \frac{9}{4} \end{bmatrix} \qquad \text{diag}(\mathbf{C}^{1/2}) = \begin{bmatrix} \frac{1}{2} & 0 \\ 0 & \frac{3}{2} \end{bmatrix} \tag{E3.11.4}$$

The $\mathbf{U}$ matrix is then obtained by transforming diag($\mathbf{C}$) back to the *x*-*y* coordinate system

$$\mathbf{U} = \mathbf{Y}\ \text{diag}(\mathbf{C}^{1/2})\ \mathbf{Y}^T = \frac{1}{\sqrt{2}} \begin{bmatrix} 1 & 1 \\ -1 & 1 \end{bmatrix} \begin{bmatrix} \frac{1}{2} & 0 \\ 0 & \frac{3}{2} \end{bmatrix} \frac{1}{\sqrt{2}} \begin{bmatrix} 1 & -1 \\ 1 & 1 \end{bmatrix} = \frac{1}{2} \begin{bmatrix} 2 & 1 \\ 1 & 2 \end{bmatrix} \tag{E3.11.5}$$

The rotation matrix is obtained by Eq. (3.7.6):

$$\mathbf{R} = \mathbf{F}\mathbf{U}^{-1} = \begin{bmatrix} -\frac{1}{2} & -1 \\ 1 & \frac{1}{2} \end{bmatrix} \frac{1}{3} \begin{bmatrix} 2 & -1 \\ -1 & 2 \end{bmatrix} = \begin{bmatrix} 0 & -1 \\ 1 & 0 \end{bmatrix} \tag{E3.11.6}$$

3.7.2 Objective Rates in Constitutive Equations. To explain why objective rates are needed for the Cauchy stress tensor, we consider the rod shown in Fig. 3.10. Suppose the simplest example of a rate constitutive equation is used, known as a hypoelastic law, where the stress rate is linearly related to the rate-of-deformation:

$$\frac{D\sigma_{ij}}{Dt} = C_{ijkl} D_{kl} \qquad \text{or} \qquad \frac{D\sigma}{Dt} = \mathbf{C} : \mathbf{D} \tag{3.7.8}$$

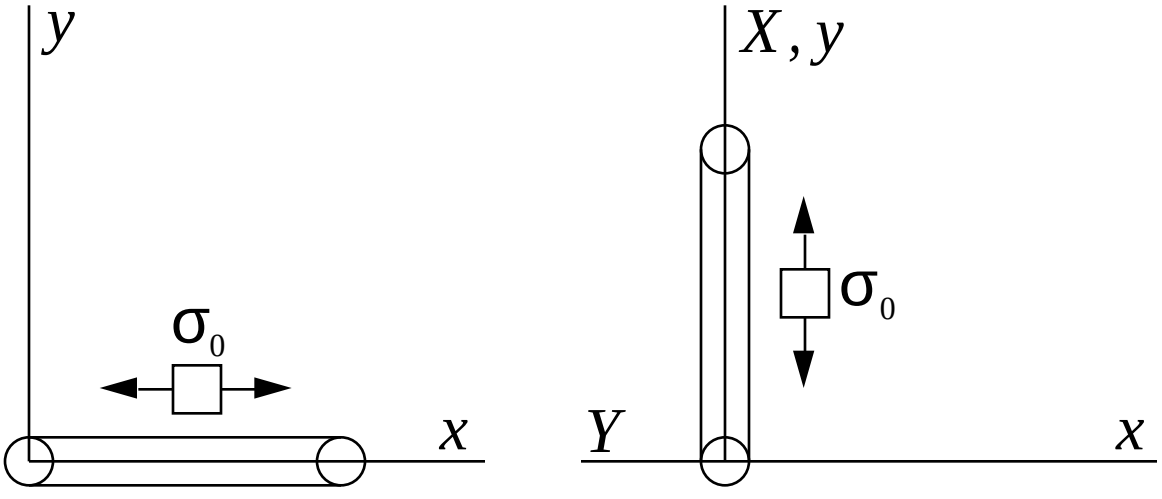

$\sigma_x = \sigma_0, \sigma_y = 0$ $\qquad$ $\sigma_x = 0, \sigma_y = \sigma_0$

Fig. 3.10. Rotation of a bar under initial stress showing the change of Cauchy stress which occurs without any deformation.

The question posed here is: are the above valid constitutive equations?

The answer is negative, and can be explained as follows. Consider a solid, such as the bar in Fig. 3.10, which is stressed in its initial configuration with $\sigma_x = \sigma_0$. Now assume that the bar rotates as shown at constant length, so there is no deformation, i.e. $\mathbf{D}$=0. Recall that in rigid body motion a state of initial stress (or prestress) is frozen in the body in a solid, i.e. since the deformation does not change in a rigid body rotation, the stress as viewed by an observer riding with the body should not change. Therefore the Cauchy stress expressed in a fixed coordinate system will change during the rotation, so the material derivative of the stress must be nonzero. However, in a pure rigid body rotation, the right hand side of Eq. (3.7.8) will vanish throughout the motion, for we have already shown that the rate-of-deformation vanishes in rigid body motion. Therefore, something must be missing in Eq. (3.7.8).

The situation explained in the previous paragraph is not just hypothetical; it is representative of what happens in real situations and simulations. A body may be in a state of stress due to thermal stresses or prestressing; an example is the stress in prestressed reinforcement bars. Large rotations of an element may occur due to actual rigid body motions of the body, as in a space vehicle or a moving car, or large local large rotations, as in a buckling beam. The rotation need not be as large as 90 degrees for the same effect; we have chosen 90 degrees to simplify the numbers.

The missing factor in Eq. (3.7.8) is that it does not account for the rotation of the material. The material rotation can be accounted for correctly be using an objective rate of the stress tensor; it is also called a frame-invariant rate. We will consider three objective rates, the Jaumann rate, the Truesdell rate and the Green-Nagdi rate. All of these are used in current finite element software. There are many other objective rates, some of which will be discussed in Chapter 9.

3.7.3 Jaumann rate. The Jaumann rate of the Cauchy stress is given by

$$\boldsymbol{\sigma}^{J} = \frac{D\boldsymbol{\sigma}}{Dt} - \mathbf{W}\,\boldsymbol{\sigma} - \boldsymbol{\sigma}\,\mathbf{W}^T \quad \text{or} \quad \sigma_{ij}{}^{J} = \frac{D\sigma_{ij}}{Dt} - W_{ik}\sigma_{kj} - \sigma_{ik}W_{kj}^T \tag{3.7.9}$$

where $\mathbf{W}$ is the spin tensor given by Eq. (3.3.11). The superscript " ^{J} " here designates an objective rate; the Jaumann rate is designated by the subsequent superscript "*J*". One appropriate hypoelastic constitutive equation is given by

$$\boldsymbol{\sigma}^{J} = \mathbf{C}^{J} : \mathbf{D} \quad \text{or} \quad \sigma_{ij}{}^{J} = C_{ijkl}^{J} D_{kl} \tag{3.7.10}$$

The material rate for the Cauchy stress tensor, i.e. the correct equation corresponding to (3.7.8), is then

$$\frac{D\boldsymbol{\sigma}}{Dt} = \boldsymbol{\sigma}^{J} + \mathbf{W}\,\boldsymbol{\sigma} + \boldsymbol{\sigma}\,\mathbf{W}^T = \mathbf{C}^{J} : \mathbf{D} + \mathbf{W}\,\boldsymbol{\sigma} + \boldsymbol{\sigma}\,\mathbf{W}^T \tag{3.7.11}$$

where the first equality is just a rearrangement of Eq. (3.7.9) and the second equality follows from (3.7.10). We see in the above that the objective rate is a function of material response. The material derivative of the Cauchy stress then depends on two parts: the rate of change due to material response, which is reflected in the objective rate, and the change of stress due to rotation, which corresponds to the last two terms in Eq. (3.7.11).

Truesdell Rate. The Truesdell rate and Green-Naghdi rates are given in Box 3.5. The Green-Naghdi rate differs from the Jaunmann rate only in using a different measure of the rotation of the material. In the Green-Nagdi rate, the angular velocity defined in Eq. (3.2.23b) is used.

Box 3.5 Objective Rates

Jaumann rate

$$\boldsymbol{\sigma}^{J} = \frac{D\boldsymbol{\sigma}}{Dt} - \mathbf{W}\ \boldsymbol{\sigma} - \boldsymbol{\sigma}\ \mathbf{W}^T \qquad \sigma_{ij}{}^{J} = \frac{D\sigma_{ij}}{Dt} - W_{ik}\sigma_{kj} - \sigma_{ik}W_{kj}^T$$

Truesdell rate (3.2.23)

$$\boldsymbol{\sigma}^{T} = \frac{D\boldsymbol{\sigma}}{Dt} + div(\mathbf{v})\boldsymbol{\sigma} - \mathbf{L}\ \boldsymbol{\sigma} - \boldsymbol{\sigma}\ \mathbf{L}^T$$

$$\sigma_{ij}{}^{T} = \frac{D\sigma_{ij}}{Dt} + \frac{\partial v_k}{\partial x_k}\sigma_{ij} - \frac{\partial v_i}{\partial x_k}\sigma_{kj} - \sigma_{ik}\frac{\partial v_j}{\partial x_k}$$

Green-Naghdi rate (3.2.24)

$$\boldsymbol{\sigma}^{G} = \frac{D\boldsymbol{\sigma}}{Dt} - \Omega\ \boldsymbol{\sigma} - \boldsymbol{\sigma}\ \Omega^T \qquad \sigma_{ij}{}^{G} = \frac{D\sigma_{ij}}{Dt} - \Omega_{ik}\sigma_{kj} - \sigma_{ik}\Omega_{kj}^T$$

$$\Omega = \dot{\mathbf{R}}\ \mathbf{R}^T, \quad \mathbf{L} = \frac{\partial \mathbf{v}}{\partial \mathbf{x}} = \mathbf{D} + \mathbf{W} \qquad L_{ij} = \frac{\partial v_i}{\partial x_j} = D_{ij} + W_{ij}$$

The relationship between the Truesdell rate and the Jaumann rate can be examined by replacing the velocity gradient in Eq. (3.7.23) by its symmetric and antisymmetric parts, i.e. Eq. (3.3.9):

$$\boldsymbol{\sigma}^{T} = \frac{D\boldsymbol{\sigma}}{Dt} + div(\mathbf{v})\boldsymbol{\sigma} - (\mathbf{D}+\mathbf{W})\ \boldsymbol{\sigma} - \boldsymbol{\sigma}\ (\mathbf{D}+\mathbf{W})^T \tag{3.7.12}$$

A comparison of Eqs. (3.7.9) and (3.7.12) then shows that the Truesdell rate includes the same spin-related terms as the Jaumann rate, but also includes additional terms which depend on the rate of deformation. To examine the relationship further, we consider a rigid body rotation for the Truesdell rate and find that

$$\text{when } \mathbf{D} = \mathbf{0}, \quad \boldsymbol{\sigma}^{T} = \frac{D\boldsymbol{\sigma}}{Dt} - \mathbf{W}\ \boldsymbol{\sigma} - \boldsymbol{\sigma}\ \mathbf{W}^T \tag{3.7.13}$$

Comparison of the above with Eq. (3.7.9) shows that the Truesdell rate is equivalent to the Jaumann rate in the absence of deformation, i.e. in a rigid body rotation. However, when the Jaumann rate is used in a constitutive equation, it will give a different material rate of stress unless the constitutive equation is changed appropriately. Thus if we write the constitutive equation in the form

$$\sigma^{T} = \mathbf{C}^{T} : \mathbf{D} \tag{3.7.14}$$

then the material response tensor $\mathbf{C}^T$ will differ from the material response tensor associated with the Jaumann rate form of the material law in Eq. (3.7.11). For this reason, whenever the material response matrix can refer to different rates, we will often add the superscripts to specify which objective rate is used by the material law. The hypoelastic relations (3.7.11) and (3.7.14) represent the same material response if the material response tensors $\mathbf{C}^T$ and $\mathbf{C}^J$ are related as follows:

$$\sigma^{T} = \mathbf{C}^{J} : \mathbf{D} = \left(\mathbf{C}^{T} + \mathbf{C}^{\sigma} \right) : \mathbf{D} \tag{3.7.15}$$

where from (3.7.12)

$$\mathbf{C}^{\sigma} : \mathbf{D} = \left(div \mathbf{v} \right) \sigma - \mathbf{D}\ \sigma - \sigma\ \mathbf{D}^{T} = \left(tr \mathbf{D} \right) \sigma - \mathbf{D}\ \sigma - \sigma\ \mathbf{D}^{T} \tag{3.7.16}$$

The components of $\mathbf{C}^{\sigma}$ are given by

$$C^{\sigma}_{ijkl} = \sigma_{ij}\delta_{kl} - \delta_{ik}\sigma_{jl} - \sigma_{il}\delta_{jk} \tag{3.7.17}$$

With these relations, the hypoelastic relations can be modified for a Truesdell rate to match the behavior of a constitutive eqaution expressed in terms of the Jaumann rate. The correspondence to the Green-Naghdi rate depends on the difference between the angular velocity and the spin and is more difficult to adjust for.

Example 3.12 Consider a body rotating in the *x*-*y* plane about the origin with an angular velocity ω ; the original configuration is prestressed as shown in Fig. 3.11. The motion is rigid body rotation and the related tensors are given in Example 3.2. Evaluate the material time derivative of the Cauchy stress using the Jaumann rate and integrate it to obtain the Cauchy stress as a function of time.

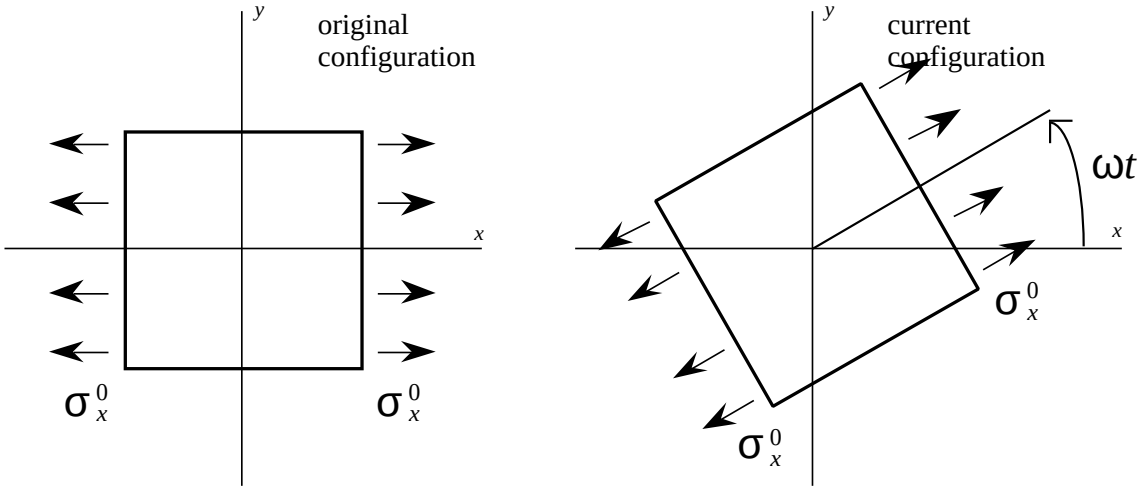

Figure 3.11. Rotation of a prestressed element with no deformation.

From Example 3.2, Eq. (E3.2.8) we note that

$$\mathbf{F} = \mathbf{R} = \begin{bmatrix} c & -s \\ s & c \end{bmatrix}, \quad \dot{\mathbf{F}} = \omega \begin{bmatrix} -s & -c \\ c & -s \end{bmatrix}, \quad \mathbf{F}^{-1} = \begin{bmatrix} c & s \\ -s & c \end{bmatrix} \tag{E3.12.1a}$$

where $s = \sin\omega t$, $c = \cos\omega t$. The spin is evaluated in terms of the velocity gradient $\mathbf{L}$, which is given for this case by Eq. (3.3.18) and then using (E3.12.1a) :

$$\mathbf{L} = \dot{\mathbf{F}}\ \mathbf{F}^{-1} = \omega \begin{bmatrix} -s & -c \\ c & -s \end{bmatrix} \begin{bmatrix} c & s \\ -s & c \end{bmatrix} = \omega \begin{bmatrix} 0 & -1 \\ 1 & 0 \end{bmatrix}$$

$$\mathbf{W} = \tfrac{1}{2}\left(\mathbf{L} - \mathbf{L}^T\right) = \omega \begin{bmatrix} 0 & -1 \\ 1 & 0 \end{bmatrix} \tag{E3.12.1b}$$

The material time derivative based on the Jaumann rate is then given by specializing (3.7.9) to the case when there is no deformation:

$$\frac{D\sigma}{Dt} = \mathbf{W}\ \sigma + \sigma\ \mathbf{W}^T \tag{E3.12.1.c}$$

($\mathbf{D}$=0, since there is no deformation; this is easily verified by noting that the symmetric part of $\mathbf{L}$ vanishes). We now change the material time derivative to an ordinary derivative since the stress is constant in space and write out the matrices in (E3.12.1c):

$$\frac{d\sigma}{dt} = \omega \begin{bmatrix} 0 & -1 \\ 1 & 0 \end{bmatrix} \begin{bmatrix} \sigma_x & \sigma_{xy} \\ \sigma_{xy} & \sigma_y \end{bmatrix} + \begin{bmatrix} \sigma_x & \sigma_{xy} \\ \sigma_{xy} & \sigma_y \end{bmatrix} \omega \begin{bmatrix} 0 & 1 \\ -1 & 0 \end{bmatrix} \tag{E3.12.2}$$

$$\frac{d\sigma}{dt} = \omega \begin{bmatrix} -2\sigma_{xy} & \sigma_x - \sigma_y \\ \sigma_x - \sigma_y & 2\sigma_{xy} \end{bmatrix} \tag{E3.12.3}$$

It can be seen that the the material time derivative of the Cauchy stress is symmetric. We now write out the three scalar ordinary differential equations in three unknowns, $\sigma_x, \sigma_y,$ and σ_{xy} corresponding to (E3.12.3) (the fourth scalar equation of the above tensor equation is omitted because of symmetry):

$$\frac{d\sigma_x}{dt} = -2\omega\sigma_{xy} \tag{E3.12.4a}$$

$$\frac{d\sigma_y}{dt} = 2\omega\sigma_{xy} \tag{E3.12.4b}$$

$$\frac{d\sigma_{xy}}{dt} = \omega\left(\sigma_x - \sigma_y\right) \tag{E3.12.4c}$$

The initial conditions are

$$\sigma_x(0) = \sigma_x^0, \quad \sigma_y(0) = 0, \quad \sigma_{xy}(0) = 0 \tag{E3.12.5}$$

It can be shown that the solution to the above differential equations is

$$\sigma = \sigma_x^0 \begin{bmatrix} c^2 & cs \\ cs & s^2 \end{bmatrix} \tag{E3.12.6}$$

We only verify the solution for $\sigma_x(t)$:

$$\frac{d\sigma_x}{dt} = \sigma_x^0 \frac{d\left(cos^2 \omega t\right)}{dt} = \sigma_x^0 \omega(-2 cos\omega t \, sin\omega t) = -2\omega\sigma_{xy} \tag{E3.12.7}$$

where the last step follows from the solution for $\sigma_{xy}(t)$ as given in Eq. (E3.12.7); comparing with (E3.14.4a) we see that the differential equation is satisfied.

Examining Eq. (E3.12.6) we can see that the solution corresponds to a constant state of the corotational stress $\hat{\sigma}$, i.e. if we let the corotational stress be given by

$$\hat{\sigma} = \begin{bmatrix} \sigma_x^0 & 0 \\ 0 & 0 \end{bmatrix}$$

then the Cauchy stress components in the global coordinate system are given by (e3.12.6) by $\sigma = \mathbf{R}\ \hat{\sigma}\ \mathbf{R}^T$ according to Box 3.2 with (E3.12.1a) gives the result (E3.12.6).

We leave as an exercise to show that when all of the initial stresses are nonzero, then the solution to Eqs. (E3.12.4) is

$$\sigma = \begin{bmatrix} c & -s \\ s & c \end{bmatrix} \begin{bmatrix} \sigma_x^0 & \sigma_{xy}^0 \\ \sigma_{xy}^0 & \sigma_y^0 \end{bmatrix} \begin{bmatrix} c & s \\ -s & c \end{bmatrix} \tag{E3.12.8}$$

Thus in rigid body rotation, the Jaumann rate changes the Cauchy stress so that the corotational stress is constant. Therefore, the Jaumann rate is often called the corotational rate of the Cauchy stress. Since the Truesdell and Green-Naghdi rates are identical to the Jaumann rate in rigid body rotation, they also correspond to the corotational Cauchy stress in rigid body rotation.

Example 3.13 Consider an element in shear as shown in Fig. 3.12. Find the shear stress using the Jaumann, Truesdell and Green-Naghdi rates for a hypoelastic, isotropic material.

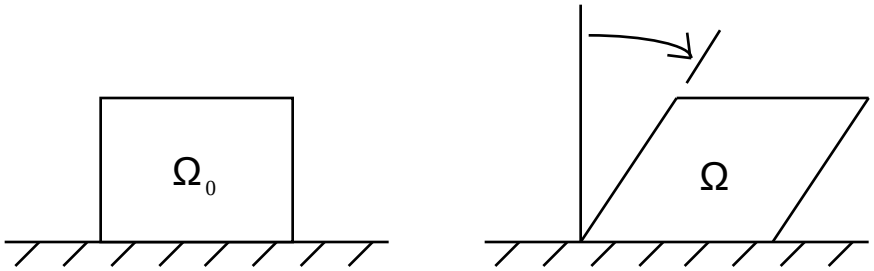

Figure 3.12.

The motion of the element is given by

$$\begin{aligned} x &= X + tY \\ y &= Y \end{aligned} \tag{E3.13.1}$$

The deformation gradient is given by Eq. (3.2.16), so

$$\mathbf{F} = \begin{bmatrix} 1 & t \\ 0 & 1 \end{bmatrix} \qquad \dot{\mathbf{F}} = \begin{bmatrix} 0 & 1 \\ 0 & 0 \end{bmatrix} \qquad \mathbf{F}^{-1} = \begin{bmatrix} 1 & -t \\ 0 & 1 \end{bmatrix} \tag{E3.13.2}$$

The velocity gradient is given by Eq. (E3.12.1), and the rate-of-deformation and spin are its symmetric and skew symmetric parts so

$$\mathbf{L} = \dot{\mathbf{F}}\mathbf{F}^{-1} = \begin{bmatrix} 0 & 1 \\ 0 & 0 \end{bmatrix} \qquad \mathbf{D} = \frac{1}{2}\begin{bmatrix} 0 & 1 \\ 1 & 0 \end{bmatrix} \qquad \mathbf{W} = \frac{1}{2}\begin{bmatrix} 0 & 1 \\ -1 & 0 \end{bmatrix} \tag{E3.13.3}$$

The hypoelastic, isotropic constitutive equation in terms of the Jaumann rate is given by

$$\dot{\sigma} = \left(\lambda^J \, trace\mathbf{D}\right)\mathbf{I} + 2\mu^J \mathbf{D} + \mathbf{W}\,\sigma + \sigma\,\mathbf{W}^T \tag{E3.13.4}$$

We have placed the superscripts on the material constants to distinguish the material constants which are used with different objective rates. Writing out the matrices in the above gives

$$\begin{aligned} &\begin{bmatrix} \dot{\sigma}_x & \dot{\sigma}_{xy} \\ \dot{\sigma}_{xy} & \dot{\sigma}_y \end{bmatrix} = \mu^J \begin{bmatrix} 0 & 1 \\ 1 & 0 \end{bmatrix} \\ &+ \frac{1}{2}\begin{bmatrix} 0 & 1 \\ -1 & 0 \end{bmatrix}\begin{bmatrix} \sigma_x & \sigma_{xy} \\ \sigma_{xy} & \sigma_y \end{bmatrix} + \frac{1}{2}\begin{bmatrix} \sigma_x & \sigma_{xy} \\ \sigma_{xy} & \sigma_y \end{bmatrix}\begin{bmatrix} 0 & -1 \\ 1 & 0 \end{bmatrix} \end{aligned} \tag{E3.13.5}$$

so

$$\dot{\sigma}_x = \sigma_{xy}, \qquad \dot{\sigma}_y = -\sigma_{xy}, \qquad \dot{\sigma}_{xy} = \mu^J + \frac{1}{2}\left(\sigma_y - \sigma_x\right) \tag{E3.13.6}$$

The solution to the above differential equations is

$$\sigma_x = -\sigma_y = \mu^J (1 - \cos t), \quad \sigma_{xy} = \mu^J \sin t \tag{E3.13.7}$$

For the Truesdell rate, the constitutive equation is

$$\overset{\circ}{\sigma} = \lambda^T tr\mathbf{D} + 2\mu^T \mathbf{D} + \mathbf{L}\,\sigma + \sigma\,\mathbf{L}^T - (tr\,\mathbf{D})\sigma \tag{E3.13.8}$$

This gives

$$\begin{bmatrix} \overset{\circ}{\sigma}_x & \overset{\circ}{\sigma}_{xy} \\ \overset{\circ}{\sigma}_{xy} & \overset{\circ}{\sigma}_y \end{bmatrix} = \mu^T \begin{bmatrix} 0 & 1 \\ 1 & 0 \end{bmatrix} + \begin{bmatrix} 0 & 1 \\ 0 & 0 \end{bmatrix} \begin{bmatrix} \sigma_x & \sigma_{xy} \\ \sigma_{xy} & \sigma_y \end{bmatrix} + \begin{bmatrix} \sigma_x & \sigma_{xy} \\ \sigma_{xy} & \sigma_y \end{bmatrix} \begin{bmatrix} 0 & 0 \\ 1 & 0 \end{bmatrix} \tag{E3.13.9}$$

where we have used the results $trace\,\mathbf{D} = 0$, see Eq. (E3.13.3). The differential equations for the stresses are

$$\overset{\circ}{\sigma}_x = 2\sigma_{xy}, \quad \overset{\circ}{\sigma}_y = 0, \quad \overset{\circ}{\sigma}_{xy} = \mu^T + \sigma_y \tag{E3.13.10}$$

and the solution is

$$\sigma_x = \mu^T t^2, \quad \sigma_y = 0, \quad \sigma_{xy} = \mu^T t \tag{E3.13.11}$$

To obtain the solution for the Cauchy stress by means of the Green-Nagdhi rate, we need to find the rotation matrix $\mathbf{R}$ by the polar decomposition theorem. To obtain the rotation, we diagonalize $\mathbf{F}^T\mathbf{F}$

$$\mathbf{F}^T\mathbf{F} = \begin{bmatrix} 1 & t \\ t & 1 + t^2 \end{bmatrix} \quad \text{eigenvalues} \quad \bar{\lambda}_i = \frac{2 + t^2 \pm t\sqrt{4 + t^2}}{2} \tag{E3.13.12}$$

The closed form solution by hand is quite involved and we recommend a computer solution. A closed form solution has been given by Dienes (1979):

$$\sigma_x = -\sigma_y = 4\mu^G \left(\cos 2\beta \ln \cos\beta + \beta \sin 2\beta - \sin^2 \beta\right), \tag{E3.13.13}$$

$$\sigma_{xy} = 2\mu^G \cos 2\beta \left(2\beta - 2\tan 2\beta \ln \cos\beta - \tan\beta\right), \quad \tan\beta = \frac{t}{2} \tag{E.13.14}$$

The results are shown in Fig. 3.13.

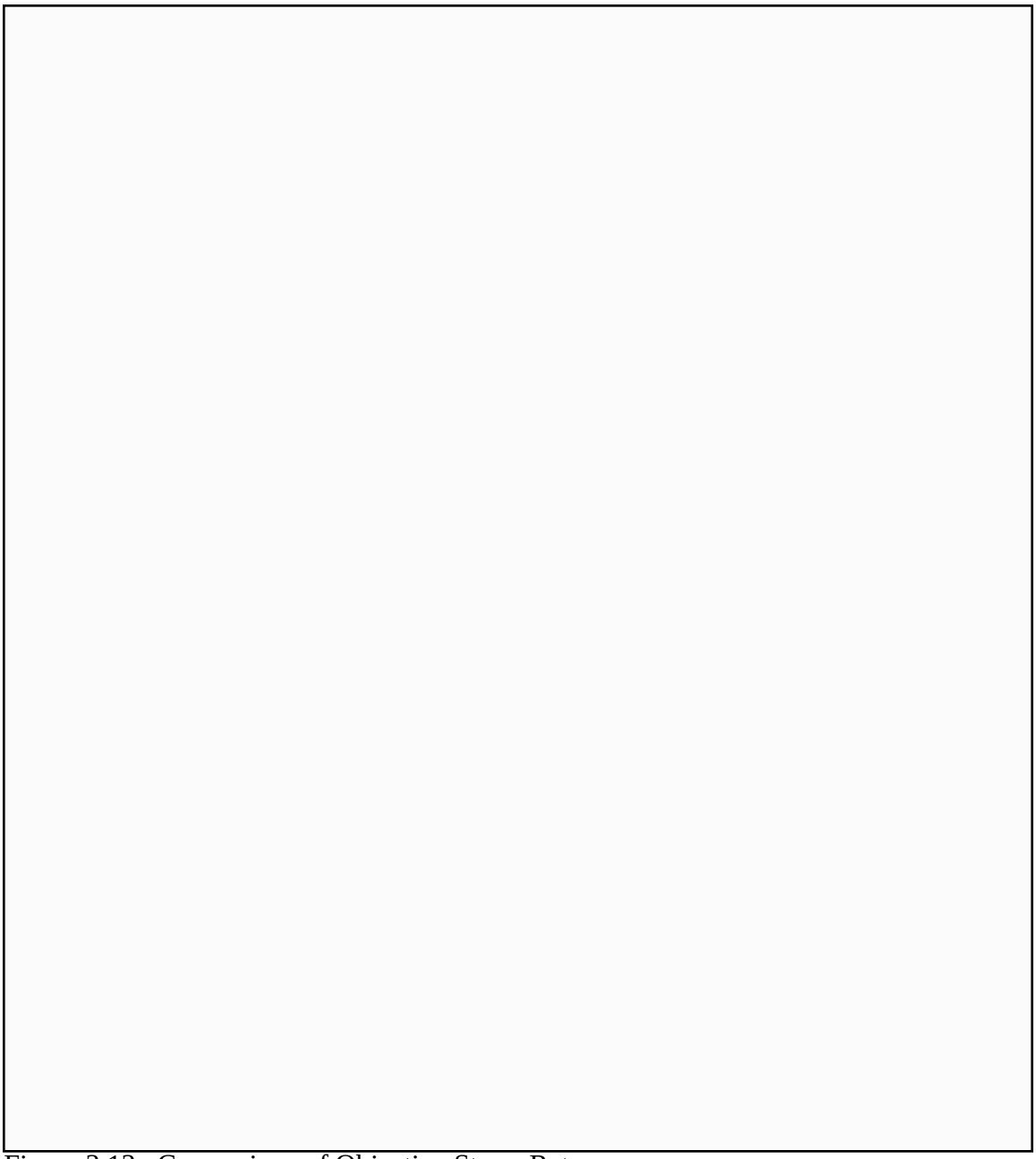

Figure 3.13. Comparison of Objective Stress Rates

Explanation of Objective Rates. One underlying characteristic of objective rates can be gleaned from the previous example: an objective rate of the Cauchy stress instantaneously coincides with the rate of a stress field whose material rate already accounts for rotation correctly. Therefore, if we take a stress measure which rotates with the material, such as the corotational stress or the PK2 stress, and add the additional terms in its rate, then we can obtain an objective stress rate. This is not the most general framework for developing objective rates. A general framework is provided by using objectivity in the sense that the stress rate should be invariant for observers who are rotating with respect to each other. A derivation based on these principles may be found in Malvern (1969) and Truesdell and Noll (????).

To illustrate the first approach, we develop an objective rate from the corotational Cauchy stress $\hat{\sigma}$. Its material rate is given by

$$\frac{D\hat{\sigma}}{Dt} = \frac{D\left(\mathbf{R}^T\sigma\mathbf{R}\right)}{Dt} = \frac{D\mathbf{R}^T}{Dt}\sigma\mathbf{R} + \mathbf{R}^T\frac{D\sigma}{Dt}\mathbf{R} + \mathbf{R}^T\sigma\frac{D\mathbf{R}}{Dt} \tag{3.7.18}$$

where the first equality follows from the stress transformation in Box 3.2 and the second equality is based on the derivative of a product. If we now consider the corotational coordinate system coincident with the reference coordinates but rotating with a spin $\mathbf{W}$ then

$$\mathbf{R} = \mathbf{I} \qquad \frac{D\mathbf{R}}{Dt} = \mathbf{W} = \Omega \tag{3.7.19}$$

Inserting the above into Eq. (3.7.18), it follows that at the instant that the corotational coordinate system coincides with the global system, the rate of the Cauchy stress in rigid body rotation is given by

$$\frac{D\hat{\sigma}}{Dt} = \mathbf{W}^T\ \sigma + \frac{D\sigma}{Dt} + \sigma\ \mathbf{W} \tag{3.7.20}$$

The RHS of this expression can be seen to be identical to the correction terms in the expression for the Jaumann rate. For this reason, the Jaumann rate is often called the corotational rate of the Cauchy stress.

The Truesdell rate is derived similarly by considering the time derivative of the PK2 stress when the reference coordinates instantaneously coincide with the spatial coordinates. However, to simplify the derivation, we reverse the expressions and extract the rate corresponding to the Truesdell rate.

Readers familiar with fluid mechanics may wonder why frame-invariant rates are rarely discussed in introductory courses in fluids, since the Cauchy stress is widely used in fluid mechanics. The reason for this lies in the structure of constitutive equations which are used in fluid mechanics and in introductory fluid courses. For a Newtonian fluid, for example, $\sigma = 2\mu\mathbf{D}' - p\mathbf{I}$, where μ is the viscosity and $\mathbf{D}'$ is the deviatoric part of the rate-of-deformation tensor. A major difference between this constitutive equation for a Newtonian fluid and the hypoelastic law (3.7.14) can be seen immediately: the hypoelastic law gives the stress rate, whereas in the Newtonian consititutive equation gives the stress. The stress transforms in a rigid body rotation exactly like the tensors on the RHS of the equation, so this constitutive equation behaves properly in a rigid body rotation. In other words, the Newtonian fluid is objective or frame-invariant.

REFERENCES

T. Belytschko, Z.P. Bazant, Y-W Hyun and T.-P. Chang, "Strain Softening Materials and Finite Element Solutions," Computers and Structures, Vol 23(2), 163-180 (1986).

D.D. Chandrasekharaiah and L. Debnath (1994), *Continuum Mechanics*, Academic Press, Boston.

J.K. Dienes (1979), On the Analysis of Rotation and Stress Rate in Deforming Bodies, Acta Mechanica, 32, 217-232.

A.C. Eringen (1962), *Nonlinear Theory of Continuous Media*, Mc-Graw-Hill, New York.

P.G. Hodge, *Continuum Mechanics*, Mc-Graw-Hill, New York.

L.E. Malvern (1969), *Introduction to the Mechanics of a Continuous Medium*, Prentice-Hall, New York.

J.E. Marsden and T.J.R. Hughes (1983), *Mathematical Foundations of Elasticity*, Prentice-Hall, Englewood Cliffs, New Jersey.

G.F. Mase and G.T. Mase (1992), *Continuum Mechanics for Engineers*, CRC Press, Boca Raton, Florida.

R.W. Ogden (1984), *Non-linear Elastic Deformations*, Ellis Horwood Limited, Chichester.

W. Prager (1961), *Introduction to Mechanics of Continua*, Ginn and Company, Boston.

M. Spivak (1965), *Calculus on Manifolds*, W.A. Benjamin, Inc., New York.

C, Truesdell and W. Noll, *The non-linear field theories of mechanics*, Springer-Verlag, New York.

LIST OF FIGURES

LIST OF BOXES

Exercise ??. Consider the same rigid body rotation as in Example ??>. Find the Truesdell stress and the Green-Naghdi stress rates and compare to the Jaumann stress rate.

Starting from Eqs. (3.3.4) and (3.3.12), show that

$$2d\mathbf{x}\ \mathbf{D}\ d\mathbf{x} = 2d\mathbf{x}F^{-T}\dot{E}\dot{F}^{-1}d\mathbf{x}$$

and hence that Eq. (3.3.22) holds.

Using the transformation law for a second order tensor, show that $\mathbf{R} = \hat{\mathbf{R}}$.

Using the statement of the conservation of momentum in the Lagrangian description in the initial configuration, show that it implies

$$\mathbf{P}\mathbf{F}^T = \mathbf{F}\mathbf{P}^T$$

Extend Example 3.3 by finding the conditions at which the Jacobian becomes negative at the Gauss quadrature points for 2×2 quadrature when the initial element is rectangular with dimension $a\times b$. Repeat for one-point quadrature, with the quadrature point at the center of the element.

Kinematic Jump Condition. The kinematic jump conditions are derived from the restriction that displacement remains continuous across a moving singular surface. The surface is called singular because ???. Consider a singular surface in one dimension.

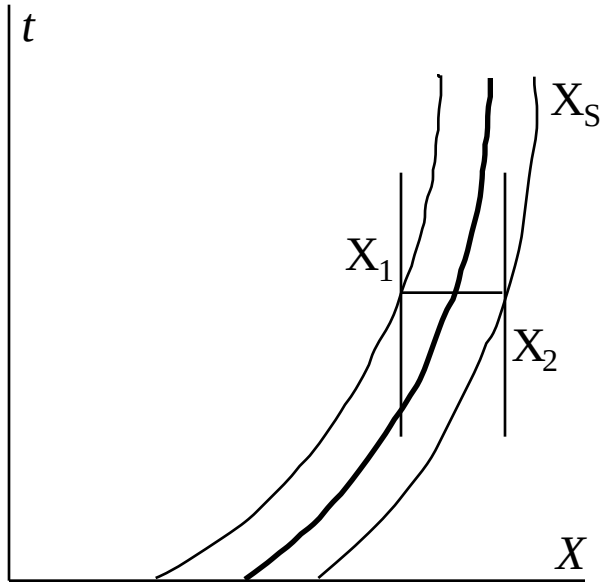

Figure 3.?

Its material description is given by

$$X = X_S(t)$$

We consider a narrow band about the singular surface defined by

CHAPTER 4
LAGRANGIAN MESHES

by Ted Belytschko
Departments of Civil and Mechanical Engineering
Northwestern University
Evanston, IL 60208

4.1 INTRODUCTION

In Lagrangian meshes, the nodes and elements move with the material. Boundaries and interfaces remain coincident with element edges, so that their treatment is simplified. Quadrature points also move with the material, so constitutive equations are always evaluated at the same material points, which is advantageous for history dependent materials. For these reasons, Lagrangian meshes are widely used for solid mechanics.

The formulations described in this Chapter apply to large deformations and nonlinear materials, i.e. they consider both geometric and material nonlinearities. They are only limited by the element's capabilities to deal with large distortions. The limited distortions most elements can sustain without degradation in performance or failure is an important factor in nonlinear analysis with Lagrangian meshes and is considered for several elements in the examples.

Finite element discretizations with Lagrangian meshes are commonly classified as updated Lagrangian formulations and total Lagrangian formulations. Both formulations use Lagrangian descriptions, i.e. the dependent variables are functions of the material (Lagrangian) coordinates and time. In the updated Lagrangian formulation, the derivatives are with respect to the spatial (Eulerian) coordinates; the weak form involves integrals over the deformed (or current) configuration. In the total Lagrangian formulation, the weak form involves integrals over the initial (reference) configuration and derivatives are taken with respect to the material coordinates.

This Chapter begins with the development of the updated Lagrangian formulation. The key equation to be discretized is the momentum equation, which is expressed in terms of the Eulerian (spatial) coordinates and the Cauchy (physical) stress. A weak form for the momentum equation is then developed, which is known as the principle of virtual power. The momentum equation in the updated Lagrangian formulation employs derivatives with respect to the spatial coordinates, so it is natural that the weak form involves integrals taken with respect to the spatial coordinates, i.e. on the current configuration. It is common practice to use the rate-of-deformation as a measure of strain rate, but other measures of strain or strain-rate can be used in an updated Lagrangian formulation. For many applications, the updated Lagrangian formulation provides the most efficient formulation.

The total Lagrangian formulation is developed next. In the total Lagrangian formulation, we will use the nominal stress, although the second Piola-Kirchhoff stress is also used in the formulations presented here. As a measure of strain we will use the Green strain tensor in the total Lagrangian formulation. A weak form of the momentum equation is developed, which is known as the principle of virtual work. The development of the toal Lagrangian formulation closely parallels the updated Lagrangian formulation, and it is stressed that the two are basically identical. Any of the expressions in the updated Lagrangian formulation can be transformed to the total Lagrangian formulation by transformations of tensors and mappings of configurations. However, the total Lagrangian formulation is often used in practice, so to understand the literature, an

advanced student must be familiar with it. In introductory courses one of the formulations can be skipped.

Implementations of the updated and total Lagrangian formulations are given for several elements. In this Chapter, only the expressions for the nodal forces are developed. It is stressed that the nodal forces represent the discretization of the momentum equation. The tangential stiffness matrices, which are emphasized in many texts, are simply a means to solving the equations for certain solution procedures. They are not central to the finite element discretization. Stiffness matrices are developed in Chapter 6.

For the total Lagrangian formulation, a variational principle is presented. This principle is only applicable to static problems with conservative loads and hyperelastic materials, i.e. materials which are described by a path-independent, rate-independent elastic constitutive law. The variational principle is of value in interpreting and understanding numerical solutions and the stability of nonlinear solutions. It can also sometimes be used to develop numerical procedures.

4.2 GOVERNING EQUATIONS

We consider a body which occupies a domain Ω with a boundary Γ. The governing equations for the mechanical behavior of a continuous body are:

1. conservation of mass (or matter)
2. conservation of linear momentum and angular momentum
3. conservation of energy, often called the first law of thermodynamics
4. constitutive equations
5. strain-displacement equations

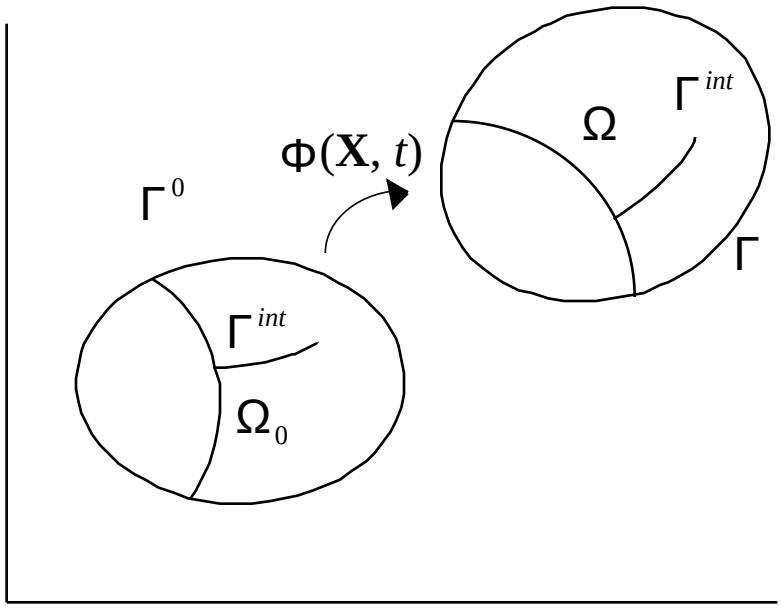

Figure 4.0. Deformed and undeformed body showing a set of admissible lines of interwoven discontinuities Γ^{int} and the notation.

We will first develop the updated Lagrangian formulation. The conservation equations have been developed in Chapter 3 and are given in both tensor form and indicial form in Box 4.1. As can be

seen, the dependent variables in the conservation equations are written in terms of material coordinates but are expressed in terms of what are classically Eulerian variables, such as the Cauchy stress and the rate-of-deformation.

We next give a count of the number of equations and unknowns. The conservation of mass and conservation of energy equations are scalar equations. The equation for the conservation of linear momentum, or momentum equation for short, is a tensor equation which consists of n_{SD} partial differential equations, where n_{SD} is the number of space dimensions. The constitutive equation relates the stress to the strain or strain-rate measure. Both the strain measure and the stress are symmetric tensors, so this provides n_σ equations where

$$n_\sigma \equiv n_{SD}\left(n_{SD}+1\right)/2 \tag{4.2.1}$$

In addition, we have the n_σ equations which express the rate-of-deformation **D** in terms of the velocities or displacements. Thus we have a total of $2n_\sigma + n_{SD} + 1$ equations and unknowns. For example, in two-dimensional problems ($n_{SD} = 2$) without energy transfer, so we have nine partial differential equations in nine unknowns: the two momentum equations, the three constitutive equations, the three equations relating **D** to the velocity and the mass conservation equation. The unknowns are the three stress components (we assume symmetry of the stress), the three components of **D**, the two velocity components, and the density ρ, for a total of 9 unknowns. Additional unknown stresses (plane strain) and strains (plane stress) are evaluated using the plane strain and plane stress conditions, respectively. In three dimensions ($n_{SD} = 3,\ n_\sigma = 6$), we have 16 equations in 16 unknowns.

When a process is neither adiabatic nor isothermal, the energy equation must be appended to the system. This adds one equation and n_{SD} unknowns, the heat flux vector q_i. However, the heat flux vector can be determined from a single scalar, the temperature, so only one unknown is added; the heat flux is related to the temperature by a type of constitutive law which depends on the material. Usually a simple linear relation, Fourier's law, is used. This then completes the system of equations, although often a law is needed for conversion of some of the mechanical energy to thermal energy; this is discussed in detail in Section 4.10.

The dependent variables are the velocity $\mathbf{v}(\mathbf{X},t)$, the Cauchy stress $\sigma(\mathbf{X},t)$, the rate-of-deformation $\mathbf{D}(\mathbf{X},t)$ and the density $\rho(\mathbf{X},t)$. As seen from the preceding a Lagrangian description is used: the dependent variables are functions of the material (Lagrangian) coordinates. The expression of all functions in terms of material coordinates is intrinsic in any treatment by a Lagrangian mesh. In principle, the functions can be expressed in terms of the spatial coordinates at any time t by using the inverse of the map $\mathbf{x} = \varphi(\mathbf{X},t)$. However, inverting this map is quite difficult. In the formulation, we shall see that it is only necessary to obtain derivatives with respect to the spatial coordinates. This is accomplished by implicit differentiation, so the map corresponding to the motion is never explicitly inverted.

In Lagrangian meshes, the mass conservation equation is used in its integrated form (B4.1.1) rather than as a partial diffrential equation. This eliminates the need to treat the continuity equation, (3.5.20). Although the continuity equation can be used to obtain the density in a Lagrangian mesh, it is simpler and more accurate to use the integrated form (B4.1.1)

The constitutive equation (Eq. B4.1.5), when expressed in rate form in terms of a rate of Cauchy stress, requires a frame invariant rate. For this purpose, any of the frame-invariant rates,

such as the Jaumann or the Truesdell rate, can be used as described in Chapter 3. It is not necessary for the constitutive equation in the updated Lagrangian formulation to be expressed in terms of the Cauchy stress or its frame invariant rate. It is also possible to use constitutive equations expressed in terms of the PK2 stress and then to convert the PK2 stress to a Cauchy stress using the transformations developed in Chapter 3 prior to computing the internal forces.

The rate-of-deformation is used as the measure of strain rate in Eq. (B4.1.5). However, other measures of strain or strain-rate can also be used in an updated Lagrangian formulation. For example, the Green strain can be used in updated Lagrangian formulations. As indicated in Chapter 3, simple hypoelastic laws in terms of the rate-of-deformation can cause difficulties in the simulation of cyclic loading because its integral is not path independent. However, for many simulations, such as the single application of a large load, the errors due to the path-dependence of the integral of the rate-of-deformation are insignificant compared to other sources of error, such as inaccuracies and uncertainties in the material data and material model. The appropriate selection of stress and strain measures depends on the constitutive equation, i.e. whether the material response is reversible or not, time dependence, and the load history under consideration.

The boundary conditions are summarized in Eq. (B4.1.7). In two dimensional problems, each component of the traction or velocity must be prescribed on the entire boundary; however the same component of the traction and velocity cannot not be prescribed on any point of the boundary as indicated by Eq. (B.4.1.8). Traction and velocity components can also be specified in local coordinate systems which differ from the global system. An identical rule holds: the same components of traction and velocity cannot be prescribed on any point of the boundary. A velocity boundary condition is equivalent to a displacement boundary condition: if a displacement is specified as a function of time, then the prescribed velocity can be obtained by time differentiation; if a velocity is specified, then the displacement can be obtained by time integration. Thus a velocity boundary condition will sometimes be called a displacement boundary condition, or vice versa.

The initial conditions can be applied either to the velocities and the stresses or to the displacements and velocities. The first set of initial conditions are more suitable for most engineering problems, since it is usually difficult to determine the initial displacement of a body. On the other hand, initial stresses, often known as residual stresses, can sometimes be measured or estimated by equilibrium solutions. For example, it is almost impossible to determine the displacements of a steel part after it has been formed from an ingot. On the other hand, good estimates of the residual stress field in the engineering component can often be made. Similarly, in a buried tunnel, the notion of initial displacements of the soil or rock enclosing the tunnel is quite meaningless, whereas the initial stress field can be estimated by equilibrium analysis. Therefore, initial conditions in terms of the stresses are more useful.

BOX 4.1
Governing Equations for Updated Lagrangian Formulation

conservation of mass

$$\rho(\mathbf{X})J(\mathbf{X}) = \rho_0(\mathbf{X})J_0(\mathbf{X}) = \rho_0(\mathbf{X}) \tag{B4.1.1}$$

conservation of linear momentum

$$\sigma + \rho\mathbf{b} = \rho\dot{\mathbf{v}} \equiv \rho\frac{D\mathbf{v}}{Dt} \quad \text{or} \quad \frac{\partial\sigma_{ji}}{\partial x_j} + \rho b_i = \rho\dot{v}_i \equiv \rho\frac{Dv_i}{Dt} \tag{B4.1.2}$$

conservation of angular momentum: $\sigma = \sigma^T$ or $\sigma_{ij} = \sigma_{ji}$ (B4.1.3)

conservation of energy:

$$\rho \dot{w}^{int} = \mathbf{D}:\sigma - \quad \mathbf{q} + \rho s \quad \text{or} \quad \rho \dot{w}^{int} = D_{ij}\sigma_{ji} - \frac{\partial q_i}{\partial x_i} + \rho s \tag{B4.1.4}$$

constitutive equation: $\sigma = S_t^{\sigma D}(\mathbf{D}, \sigma, \text{etc.})$ (B4.1.5)

rate-of-deformation: $\mathbf{D} = sym(\mathbf{v})$ $\qquad D_{ij} = \frac{1}{2}\left(\frac{\partial v_i}{\partial x_j} + \frac{\partial v_j}{\partial x_i}\right)$ (B4.1.6)

boundary conditions

$$n_j\sigma_{ji} = \bar{t}_i \quad \text{on} \quad \Gamma_{t_i} \qquad v_i = \bar{v}_i \quad \text{on} \quad \Gamma_{v_i} \tag{B4.1.7}$$

$$\Gamma_{t_i} \cap \Gamma_{v_i} = 0 \qquad \Gamma_{t_i} \quad \Gamma_{v_i} = \Gamma \qquad i = 1 \text{ to } n_{SD} \tag{B4.1.8}$$

initial conditions

$$\mathbf{v}(\mathbf{x},0) = \mathbf{v}_0(\mathbf{x}) \qquad \sigma(\mathbf{x},0) = \sigma_0(\mathbf{x}) \tag{B4.1.9}$$

or

$$\mathbf{v}(\mathbf{x},0) = \mathbf{v}_0(\mathbf{x}) \qquad \mathbf{u}(\mathbf{x},0) = \mathbf{u}_0(\mathbf{x}) \tag{B4.1.10}$$

interior continuity conditions (stationary)

$$\text{on } \Gamma_{int}: \ \langle \mathbf{n}\ \sigma \rangle = 0 \qquad \text{or} \qquad \langle n_i \sigma_{ij} \rangle \equiv n_i^A \sigma_{ij}^A + n_i^B \sigma_{ij}^B = 0 \tag{B4.1.11}$$

We have also included the interior continuity conditions on the stresses in Box 4.1as Eq. (B4.1.11). In this equation, superscripts A and B refer to the stresses and normal on two sides of the discontinuity: see Section 3.5.10. These continuity conditions must be met by the tractions wherever stationary discontinuites in certain stress and strain components are possible, such as at material interfaces. They must hold for bodies in equilibrium and in transient problems. As mentioned in Chapter 2, in transient problems, moving discontinuities are also possible; however, moving discontinuities are treated in Lagrangian meshes by smearing them over several elements. Thus the moving discontinuity conditions need not be explicitly stated. Only the stationary continuity conditions are imposed explicitly by a finite element approximation.

4.3 WEAK FORM: PRINCIPLE OF VIRTUAL POWER

In this section, the principle of virtual power, is developed for the updated Lagrangian formulation. The principle of virtual power is the weak form for the momentum equation, the traction boundary conditions and the interior traction continuity conditions. These three are collectively called generalized momentum balance. The relationship of the principle of virtual power to the momentum equations will be described in two parts:

1. The principle of virtual power (weak form) will be developed from the generalized momentum balance (strong form), i.e. strong form to weak form.
2. The principle of virtual power (weak form) will be shown to imply the generalized momentum balance (strong form), i.e. weak form to strong form.

We first define the spaces for the test functions and trial functions. We will consider the minimum smoothness required for the functions to be defined in the sense of distributions, i.e. we allow Dirac delta functions to be derivatives of functions. Thus, the derivatives will not be defined

according to classical definitions of derivatives; instead, we will admit derivatives of piecewise continuous functions, where the derivatives include Dirac delta functions; this generalization was discussed in Chapter 2.

The space of test functions is defined by:

$$\delta v_j(\mathbf{X}) \quad U_0 \qquad U_0 = \left\{ \delta v_i | \delta v_i \quad C^0(\mathbf{X}), \delta v_i = 0 \text{ on } \Gamma_{v_i} \right\} \tag{4.3.1}$$

This selection of the space for the test functions $\delta\mathbf{v}$ is dictated by foresight from what will ensue in the development of the weak form; with this construction, only prescribed tractions are left in the final expression of the weak form. The test functions $\delta\mathbf{v}$ are sometimes called the virtual velocities.

The velocity trial functions live in the space given by

$$v_i(\mathbf{X}, t) \quad U \qquad U = \left\{ v_i | v_i \quad C^0(\mathbf{X}), v_i = \bar{v}_i \text{ on } \Gamma_{v_i} \right\} \tag{4.3.2}$$

The space of displacements in U is often called kinematically admissible displacements or compatible displacements; they satisfy the continuity conditions required for compatibility and the velocity boundary conditions. Note that the space of test functions is identical to the space of trial functions except that the virtual velocities vanish wherever the trial velocities are prescribed. We have selected a specific class of test and trial spaces that are applicable to finite elements; the weak form holds also for more general spaces, which is the space of functions with square integrable derivatives, called a Hilbert space.

Since the displacement $u_i(\mathbf{X}, t)$ is the time integral of the velocity, the displacement field can also be considered to be the trial function. We shall see that the constitutive equation can be expressed in terms of the displacements or velocities. Whether the displacements or velocities are considered the trial functions is a matter of taste.

4.3.1 Strong Form to Weak Form. As we have already noted, the strong form, or generalized momentum balance, consists of the momentum equation, the traction boundary conditions and the traction continuity conditions, which are respectively:

$$\frac{\partial \sigma_{ji}}{\partial x_j} + \rho b_i = \rho \dot{v}_i \quad \text{in } \Omega \tag{4.3.3a}$$

$$n_j \sigma_{ji} = \bar{t}_i \quad \text{on } \Gamma_{t_i} \tag{4.3.3b}$$

$$\langle n_j \sigma_{ji} \rangle = 0 \quad \text{on } \Gamma_{int} \tag{4.3.3c}$$

where Γ_{int} is the union of all surfaces (lines in two dimensions) on which the stresses are discontinuous in the body.

Since the velocities are $C^0(\mathbf{X})$, the displacements are similarly $C^0(\mathbf{X})$; the rate-of-deformation and the rate of Green strain will then be $C^{-1}(\mathbf{X})$ since they are related to spatial derivatives of the velocity. The stress σ is a function of the velocities via the constitutive equation (B4.1.4relates the rate-of-deformation to the velocities) and Eq. (B4.1.5), which or the Green

strain to the displacement. It is assumed that the constitutive equation leads to a *stress that is a well-behaved function of the Green strain tensor,* so that the stresses will also be $C^{-1}(\mathbf{X})$. Note that the stress rate is often not a continuous function of the rate-of-deformation; for example, it is discontinuous at the transition between plastic behavior and elastic unloading.

The first step in the development of the weak form, as in the one-dimensional case in Chapter 2, consists of taking the product of a test function δv_i with the momentum equation and integrating over the *current configuration*:

$$\int_\Omega \delta v_i \left(\frac{\partial \sigma_{ji}}{\partial x_j} + \rho b_i - \rho \dot{v}_i \right) d\Omega = 0 \tag{4.3.4}$$

In the intergral, all variables must be implicitly transformed to be functions of the Eulerian coordinates by (???). However, this transformation is never needed in the implementation. The first term in (4.3.4) is next expanded by the product rule, which gives

$$\int_\Omega \delta v_i \frac{\partial \sigma_{ji}}{\partial x_j} d\Omega = \int_\Omega \left[\frac{\partial}{\partial x_j} \left(\delta v_i \sigma_{ji} \right) - \frac{\partial \left(\delta v_i \right)}{\partial x_j} \sigma_{ji} \right] d\Omega \tag{4.3.5}$$

Since the velocities are C^0 and the stresses are C^{-1}, the term $\delta v_i \sigma_{ji}$ on the RHS of the above is C^{-1}. We assume that the discontinuities occur over a finite set of surfaces Γ_{int}, so Gauss's theorem, Eq. (3.5.4) gives

$$\int_\Omega \frac{\partial}{\partial x_j} \left(\delta v_i \sigma_{ji} \right) d\Omega = \int_{\Gamma_{int}} \delta v_i \left\langle n_j \sigma_{ji} \right\rangle d\Gamma + \int_\Gamma \delta v_i n_j \sigma_{ji} d\Gamma \tag{4.3.6}$$

From the strong form (4.3.3c), the first integral on the RHS vanishes. For the second integral on the RHS we can use another part of the strong form, the traction boundary conditions (4.3.3b) on the prescribed traction boundaries. Since the test function vanishes on the complement of the traction boundaries, (4.3.6) gives

$$\int_\Omega \frac{\partial}{\partial x_j} \left(\delta v_i \sigma_{ji} \right) d\Omega = \sum_{i=1}^{n_{SD}} \int_{\Gamma_{t_i}} \delta v_i \bar{t}_i d\Gamma \tag{4.3.7}$$

The summation sign is included on the RHS to avoid any confusion arising from the presence of a third index i in Γ_{t_i}; if this index is ignored in the summation convention then there is no need for a summation sign.

If (4.3.7) is substituted into (4.3.4) we obtain

$$\int_\Omega \delta v_i \frac{\partial \sigma_{ji}}{\partial x_j} d\Omega = \sum_{i=1}^{n_{SD}} \int_{\Gamma_{t_i}} \delta v_i \bar{t}_i d\Gamma - \int_\Omega \frac{\partial \left(\delta v_i \right)}{\partial x_j} \sigma_{ji} \, d\Omega \tag{4.3.8}$$

The process of obtaining the above is called integration by parts. If Eq. (4.3.8) is then substituted into (4.3.4), we obtain

$$\int_\Omega \frac{\partial(\delta v_i)}{\partial x_j}\sigma_{ji}\,d\Omega - \int_\Omega \delta v_i \rho b_i\,d\Omega - \sum_{i=1}^{n_{SD}} \int_{\Gamma_{t_i}} \delta v_i \bar{t}_i\,d\Gamma + \int_\Omega \delta v_i \rho \dot{v}_i\,d\Omega = 0 \tag{4.3.9}$$

The above is the weak form for the momentum equation, the traction boundary conditions and the interior continuity conditions. It is known as the principle of virtual power, see Malvern (1969), for each of the terms in the weak form is a virtual power; see Section 2.5.

4.3.2. Weak Form to Strong Form. It will now be shown that the weak form (4.3.9) implies the strong form or generalized momentum balance: the momentum equation, the traction boundary conditions and the interior continuity conditions, Eqs. (4.3.3). To obtain the strong form, the derivative of the test function must be eliminated from (4.3.9). This is accomplished by using the derivative product rule on the first term, which gives

$$\int_\Omega \frac{\partial(\delta v_i)}{\partial x_j}\sigma_{ji}\,d\Omega = \int_\Omega \frac{\partial(\delta v_i \sigma_{ji})}{\partial x_j}\,d\Omega - \int_\Omega \delta v_i \frac{\partial \sigma_{ji}}{\partial x_j}\,d\Omega \tag{4.3.10}$$

We now apply Gauss's theorem, see Section 3.5.2, to the first term on the RHS of the above

$$\begin{aligned}\int_\Omega \frac{\partial(\delta v_i \sigma_{ji})}{\partial x_j}\,d\Omega &= \int_\Gamma \delta v_i n_j \sigma_{ji}\,d\Gamma + \int_{\Gamma_{int}} \delta v_i \langle n_j \sigma_{ji} \rangle\,d\Gamma = \\ &\sum_{i=1}^{n_{SD}} \int_{\Gamma_{t_i}} \delta v_i n_j \sigma_{ji}\,d\Gamma + \int_{\Gamma_{int}} \delta v_i \langle n_j \sigma_{ji} \rangle\,d\Gamma\end{aligned} \tag{4.3.11}$$

where the second equality follows because $\delta v_i = 0$ on Γ_{v_i}, (see Eq. (4.3.1) and Eq. (B4.1.7)). Substituting Eq. (4.3.11) into Eq. (4.3.10) and in turn to (4.3.9), we obtain

$$\int_\Omega \delta v_i \left(\frac{\partial \sigma_{ji}}{\partial x_j} + \rho b_i - \rho \dot{v}_i \right) d\Omega - \sum_{i=1}^{n_{SD}} \int_{\Gamma_{t_i}} \delta v_i \left(n_j \sigma_{ji} - \bar{t}_i \right) d\Gamma - \int_{\Gamma_{int}} \delta v_i \langle n_j \sigma_{ji} \rangle\,d\Gamma = 0 \tag{4.3.12}$$

We will now prove that the coefficients of the test functions in the above integrals must vanish. For this purpose, we prove the following theorem

$$\begin{aligned}&\text{if } \alpha_i(\mathbf{X}), \beta_i(\mathbf{X}), \gamma_i(\mathbf{X}) \in C^{-1} \text{ and } \delta v_i(\mathbf{X}) \in U_0 \\ &\text{and } \int_\Omega \delta v_i \alpha_i\,d\Omega + \sum_{i=1}^{n_{SD}} \int_{\Gamma_{t_i}} \delta v_i \beta_i\,d\Gamma + \int_{\Gamma_{int}} \delta v_i \gamma_i\,d\Gamma = 0 \quad \forall \delta v_i(\mathbf{X}) \\ &\text{then } \alpha_i(\mathbf{X}) = 0 \text{ in } \Omega,\ \beta_i(\mathbf{X}) = 0 \text{ on } \Gamma_{t_i}, \gamma_i(\mathbf{X}) = 0 \text{ on } \Gamma_{int}\end{aligned} \tag{4.3.13}$$

where the integral is either transformed to the reference configuration or the variables are expressed in terms of the Eulerian coordinates by the inverse map prior to evaluation of the integrals.

In functional analysis, the statement in (4.3.13) is called the *density theorem*, Oden and Reddy (1976, p.19). It is also called the *fundamental theorem of variational calculus;* sometimes we call it the *function scalar product theorem* since it is the counterpart of the scalar product theorem given in Chapter 2. We follow Hughes [1987, p.80] in proving (4.3.13). As a first step we show that $\alpha_i(\mathbf{X}) = 0$ in Ω. For this purpose, we assume that

$$\delta v_i(\mathbf{X}) = \alpha_i(\mathbf{X}) f(\mathbf{X}) \tag{4.3.14}$$

where

1. $f(\mathbf{X}) > 0$ on Ω but $f(\mathbf{X}) = 0$ on Γ_{int} and $f(\mathbf{X}) = 0$ on Γ_{t_i}
2. $f(\mathbf{X})$ is C^{-1}

Substituting the above expression for δv_i into (4.3.13) gives

$$\int_\Omega \alpha_i(\mathbf{X}) \alpha_i(\mathbf{X}) f(\mathbf{X}) d\Omega = 0 \tag{4.3.15}$$

The integrals over the boundary and interior surfaces of discontinuity vanish because the arbitrary function $f(\mathbf{X})$ has been chosen to vanish on these surfaces. Since $f(\mathbf{X}) > 0$, and the functions $f(\mathbf{X})$ and $\alpha_i(\mathbf{X})$ are sufficiently smooth, Equation (4.3.15) implies $\alpha_i(\mathbf{X}) = 0$ in Ω for $i = 1$ to n_{SD}

To show that the $\gamma_i(\mathbf{X}) = 0$, let

$$\delta v_i(\mathbf{X}) = \gamma_i(\mathbf{X}) f(\mathbf{X}) \tag{4.3.16}$$

where

1. $f(\mathbf{x}) > 0$ on Γ_{int} ; $f(\mathbf{x}) = 0$ on Γ_{t_i} ;
2. $f(\mathbf{x})$ is C^{-1}

Substituting (4.3.16) into (4.3.13) gives

$$\int_{\Gamma_{int}} \gamma_i(\mathbf{x}) \gamma_i(\mathbf{x}) f(\mathbf{x}) d\Gamma = 0 \tag{4.3.17}$$

which implies $\gamma_i(\mathbf{x}) = 0$ on Γ_{int} (since $f(\mathbf{x}) > 0$).

The final step in the proof, showing that $\beta_i(\mathbf{x}) = 0$ is accomplished by using a function $f(\mathbf{x}) > 0$ on Γ_{t_i}. The steps are exactly as before. Thus each of the $\alpha_i(\mathbf{x})$, $\beta_i(\mathbf{x})$, and $\gamma_i(\mathbf{x})$ must vanish on the relevant domain or surface. Thus Eq. (4.3.12) implies the strong form: the momentum equation, the traction boundary conditions, and the interior continuity conditions, Eqs. (4.3.3).

Let us now recapitulate what has been accomplished so far in this Section. We first developed a weak form, called the principle of virtual power, from the strong form. The strong form consists of the momentum equation, the traction boundary conditions and jump conditions.

The weak form was obtained by multiplying the momentum equation by a test function and integrating over the *current configuration*. A key step in obtaining the weak form is the elimination of the derivatives of the stresses, Eq. (4.3.5-6). This step is crucial since as a result, the stresses can be C^{-1} functions. As a consequence, if the constitutive equation is smooth, the velocities need only be C^0.

Equation (4.3.4) could also be used as the weak form. However, since the derivatives of the stresses would appear in this alternate weak form, the displacements and velocities would have to be C^1 functions (see Chapter 2); C^1 functions are difficult to construct in more than one dimension. Furthermore, the trial functions would then have to be constructed so as to satisfy the traction boundary conditions, which would be very difficult. The removal of the derivative of the stresses through integration by parts also leads to certain symmetries in the linearized equations, as will be seen in Chapter 6. Thus the integration by parts is a key step in the development of the weak form.

Next we started with the weak form and showed that it implies the strong form. This, combined with the development of the weak form from the strong form, shows that the weak and strong forms are equivalent. Therefore, if the space of test functions is infinite dimensional, a solution to the weak form is a solution of the strong form. However, the test functions used in computational procedures must be finite dimensional. Therefore, satisfying the weak form in a computation only leads to an approximate solution of the strong form. In linear finite element analysis, it has been shown that the solution of the weak form is the best solution in the sense that it minimizes the error in energy, Strang and Fix (1973). In nonlinear problems, such optimality results are not available in general.

4.3.3. Physical Names of Virtual Power Terms. We will next ascribe a physical name to each of the terms in the virtual power equation. This will be useful in systematizing the development of finite element equations. The nodal forces in the finite element discretization will be identified according to the same physical names.

To identify the first integrand in (4.3.9), note that it can be written as

$$\frac{\partial(\delta v_i)}{\partial x_j}\sigma_{ji} = \delta L_{ij}\sigma_{ji} = (\delta D_{ij} + \delta W_{ij})\sigma_{ji} = \delta D_{ij}\sigma_{ji} = \delta \mathbf{D} : \sigma \tag{4.3.18}$$

Here we have used the decomposition of the velocity gradient into its symmetric and skew symmetric parts and that $\delta W_{ij}\sigma_{ij} = 0$ since δW_{ij} is skew symmetric while σ_{ij} is symmetric. Comparison with (B4.1.4) then indicates that we can interpret $\delta D_{ij}\sigma_{ij}$ as the rate of virtual internal work, or the *virtual internal power*, per unit volume. Observe that $\dot{w}^{int}$ in (B4.1.4) is power per unit mass, so $\rho\dot{w}^{int} = \mathbf{D} : \sigma$ is the power per unit volume. The total virtual internal power δP^{int} is defined by the integral of $\delta D_{ij}\sigma_{ij}$ over the domain, i.e.

$$\delta P^{int} = \int_\Omega \delta D_{ij}\sigma_{ij} d\Omega = \int_\Omega \frac{\partial(\delta v_i)}{\partial x_j}\sigma_{ij} d\Omega \equiv \int_\Omega \delta L_{ij}\sigma_{ij} d\Omega = \int_\Omega \delta \mathbf{D} : \sigma d\Omega \tag{4.3.19}$$

where the third and fourth terms have been added to remind us that they are equivalent to the second term because of the symmetry of the Cauchy stress tensor.

The second and third terms in (4.3.9) are the *virtual external power:*

$$\delta P^{ext} = \int_\Omega \delta v_i \rho b_i d\Omega + \sum_{j=1}^{n_{SD}} \int_{\Gamma_{tj}} \delta v_j \bar{t}_j d\Gamma = \int_\Omega \delta \mathbf{v} \cdot \rho \mathbf{b} d\Omega + \sum_{j=1}^{n_{SD}} \int_{\Gamma_{t_j}} \delta v_j \mathbf{e}_j \cdot \bar{\mathbf{t}} d\Gamma \tag{4.3.20}$$

This name is selected because the virtual external power arises from the external body forces $\mathbf{b}(\mathbf{x}, t)$ and prescribed tractions $\bar{\mathbf{t}}(x,t)$.

The last term in (4.3.9) is the *virtual inertial power*

$$\delta P^{inert} = \int_\Omega \delta v_i \rho \dot{v}_i d\Omega \tag{4.3.21}$$

which is the power corresponding to the inertial force. The inertial force can be considered a body force in the d'Alembert sense.

Inserting Eqs. (4.3.19-4.3.21) into (4.3.9), we can write the principle of virtual power as

$$\delta P = \delta P^{int} - \delta P^{ext} + \delta P^{inert} = 0 \qquad \delta v_i \quad U_0 \tag{4.3.22}$$

which is the weak form for the momentum equation. The physical meanings help in remembering the weak form and in the derivation of the finite element equations. The weak form is summarized in Box 4.2.

BOX 4.2
Weak Form in Updated Lagrangian Formulation:
Principle of Virtual Power

If σ_{ij} is a smooth function of the displacements and velocities and $v_i \quad U$, then if

$$\delta P^{int} - \delta P^{ext} + \delta P^{inert} = 0 \qquad \delta v_i \quad U_0 \tag{B4.2.1}$$

then

$$\frac{\partial \sigma_{ji}}{\partial x_j} + \rho b_i = \rho \dot{v}_i \quad \text{in} \quad \Omega \tag{B4.2.2}$$

$$n_j \sigma_{ji} = \bar{t}_i \quad \text{on} \quad \Gamma_{ti} \tag{B4.2.3}$$

$$\langle n_j \sigma_{ji} \rangle = 0 \quad \text{on} \quad \Gamma_{int} \tag{B4.2.4}$$

where

$$\delta P^{int} = \int_\Omega \delta \mathbf{D} : \boldsymbol{\sigma} d\Omega = \int_\Omega \delta D_{ij} \sigma_{ij} d\Omega = \int_\Omega \frac{\partial (\delta v_i)}{\partial x_j} \sigma_{ij} d\Omega \tag{B4.2.5}$$

$$\delta P^{ext} = \int_\Omega \delta \mathbf{v}\, \rho \mathbf{b}\, d\Omega + \sum_{j=1}^{n_{SD}} \int_{\Gamma_{t_j}} \left(\delta \mathbf{v}\ \mathbf{e}_j\right) \bar{\mathbf{t}}\ \mathbf{e}_j\, d\Gamma = \int_\Omega \delta v_i \rho b_i\, d\Omega + \sum_{j=1}^{n_{SD}} \int_{\Gamma_{t_j}} \delta v_j \bar{t}_j\, d\Gamma \tag{B4.2.6}$$

$$\delta P^{inert} = \int_\Omega \delta \mathbf{v}\ \rho \dot{\mathbf{v}}\, d\Omega = \int_\Omega \delta v_i \rho \dot{v}_i\, d\Omega \tag{B4.2.7}$$

4.4 UPDATED LAGRANGIAN FINITE ELEMENT DISCRETIZATION

4.4.1 Finite Element Approximation. In this section, the finite element equations for the updated Lagrangian formulation are developed by means of the principle of virtual power. For this purpose the current domain Ω is subdivided into elements Ω_e so that the union of the elements comprises the total domain, $\Omega = \bigcup_e \Omega_e$. The nodal coordinates in the current configuration are denoted by x_{iI}, $I = 1$ to n_N. Lower case subscripts are used for components, upper case subscripts for nodal values. In two dimensions, $x_{iI} = [x_I, y_I]$, in three dimensions $x_{iI} = [x_I, y_I, z_I]$. The nodal coordinates in the undeformed configuration are X_{iI}.

In the finite element method, the motion $\mathbf{x}(\mathbf{X}, t)$ is approximated by

$$x_i(\mathbf{X}, t) = N_I(\mathbf{X}) x_{iI}(t) \quad \text{or} \quad \mathbf{x}(\mathbf{X}, t) = N_I(\mathbf{X}) \mathbf{x}_I(t) \tag{4.4.1}$$

where $N_I(\mathbf{X})$ are the interpolation (shape) functions and $\mathbf{x}_I$ is the position vector of node I. Summation over repeated indices is implied; in the case of lower case indices, the sum is over the number of space dimensions, while for upper case indices the sum is over the number of nodes. The nodes in the sum depends on the entity considered: when the total domain is considered, the sum is over all nodes in the domain, whereas when an element is considered, the sum is over the nodes of the element.

Writing (4.4.1) at a node with initial position $\mathbf{X}_J$ we have

$$\mathbf{x}(\mathbf{X}_J, t) = \mathbf{x}_I(t) N_I(\mathbf{X}_J) = \mathbf{x}_I(t) \delta_{IJ} = \mathbf{x}_J(t) \tag{4.4.3}$$

where we have used the interpolation property of the shape functions in the third term. Interpreting this equation, we see that node J always corresponds to the same material point $\mathbf{X}_J$: in a Lagrangian mesh, nodes remain coincident with material points.

We define the nodal displacements by using Eq. (3.2.7) at the nodes

$$u_{iI}(t) = x_{iI}(t) - X_{iI} \qquad \text{or} \qquad \mathbf{u}_I(t) = \mathbf{x}_I(t) - \mathbf{X}_I \tag{4.4.4a}$$

The displacement field is

$$u_i(\mathbf{X}, t) = x_i(\mathbf{X}, t) - X_i = u_{iI}(t) N_I(\mathbf{X}) \quad \text{or} \quad \mathbf{u}(\mathbf{X}, t) = \mathbf{u}_I(t) N_I(\mathbf{X}) \tag{4.4.4b}$$

which follows from (4.4.1), (4.4.2) and (4.4.3).

The velocities are obtained by taking the material time derivative of the displacements, giving

$$v_i(\mathbf{X},t) = \frac{\partial u_i(\mathbf{X},t)}{\partial t} = \dot{u}_{iI}(t) N_I(\mathbf{X}) = v_{iI}(t) N_I(\mathbf{X}) \quad \text{or} \quad \mathbf{v}(\mathbf{X},t) = \dot{\mathbf{u}}_I(t) N_I(\mathbf{X}) \tag{4.4.5}$$

where we have written out the derivative of the displacement on the left hand side to stress that the velocity is a material time derivative of the displacement, i.e., the partial derivative with respect to time with the material coordinate fixed. Note the velocities are given by the same shape function since the shape functions are constant in time. The superposed dot on the nodal displacements is an ordinary derivative, since the nodal displacements are only functions of time.

The accelerations are similarly given by the material time derivative of the velocities

$$\dot{v}_i(\mathbf{X},t) = \ddot{u}_{iI}(t) N_I(\mathbf{X}) \qquad \text{or} \qquad \dot{\mathbf{v}}(\mathbf{X},t) = \ddot{\mathbf{u}}_I(t) N_I(\mathbf{X}) \tag{4.4.6}$$

It is emphasized that the shape functions are expressed in terms of the material coordinates in the updated Lagrangian formulation even though we will use the weak form in the current configuration. As pointed out in Section 2.8, it is crucial to express the shape functions in terms of material coordinates when a Lagrangian mesh is used because we want the time dependence in the finite element approximation of the motion to reside entirely in the nodal variables.

The velocity gradient is obtained by substituting Eq. (4.4.5) into Eq. (3.3.7), which yields

$$L_{ij} = v_{i,j} = v_{iI} \frac{\partial N_I}{\partial x_j} = v_{iI} N_{I,j} \qquad \text{or} \qquad \mathbf{L} = \mathbf{v}_I N_{I,j} \tag{4.4.7}$$

and the rate-of-deformation is given by

$$D_{ij} = \tfrac{1}{2}\left(L_{ij} + L_{ji}\right) = \tfrac{1}{2}\left(v_{iI} N_{I,j} + v_{jI} N_{I,i}\right) \tag{4.4.7b}$$

In the construction of the finite element approximation to the motion, Eq. (4.4.1), we have ignored the velocity boundary conditions, i.e. the velocities given by Eq. (4.4.5) are not in the space defined by Eq. (4.3.2). We will first develop the equations for an unconstrained body with no velocity boundary conditions, and then modify the discrete equations to account for the velocity boundary conditions.

In Eq. (4.4.1), all components of the motion are approximated by the same shape functions. This construction of the motion facilitates the representation of rigid body rotation, which is an essential requirement for convergence. This is discussed further in Chapter 8.

The test function, or variation, is not a function of time, so we approximate the test function as

$$\delta v_i(\mathbf{X}) = \delta v_{iI} N_I(\mathbf{X}) \qquad \text{or} \qquad \delta \mathbf{v}(\mathbf{X}) = \delta \mathbf{v}_I N_I(\mathbf{X}) \tag{4.4.8}$$

where δv_{iI} are the virtual nodal velocities.

As a first step in the construction of the discrete finite element equations, the test function is substituted into principle of virtual power giving

$$\delta v_{iI}\int_\Omega \frac{\partial N_I}{\partial x_j}\sigma_{ji}d\Omega - \delta v_{iI}\int_\Omega N_I\rho b_i d\Omega - \sum_{i=1}^{n_{SD}}\delta v_{iI}\int_{\Gamma_{t_i}} N_I\bar{t}_i d\Gamma + \delta v_{iI}\int_\Omega N_I\rho\dot{v}_i d\Omega = 0 \tag{4.4.9a}$$

The stresses in (4.4.9a) are functions of the trial velocities and trial displacements. From the definition of the test space, (4.3.4), the virtual velocities must vanish wherever the velocities are prescribed, i.e. $\delta v_i = 0$ on Γ_{v_i} and therefore only the virtual nodal velocities for nodes not on Γ_{v_i} are arbitrary, as indicated above. Using the arbitrariness of the virtual nodal velocities everywhere except on Γ_{v_i}, it then follows that the weak form of the momentum equation is

$$\int_\Omega \frac{\partial N_I}{\partial x_j}\sigma_{ji}d\Omega - \int_\Omega N_I\rho b_i d\Omega - \sum_{j=1}^{n_{SD}}\int_{\Gamma_{t_j}} N_I\bar{t}_i d\Gamma + \int_\Omega N_I\rho\dot{v}_i d\Omega = 0 \qquad I,i \quad \Gamma_{v_i} \tag{4.4.9b}$$

However, the above form is difficult to remember. For purposes of convenience and for a better physical interpretation, it is worthwhile to ascribe physical names to each of the terms in the above equation.

4.4.2. Internal and External Nodal Forces. We define the nodal forces corresponding to each term in the virtual power equation. This helps in remembering the equation and also provides a systematic procedure which is found in most finite element software. The internal nodal forces are defined by

$$\delta P^{int} = \delta v_{iI} f_{iI}^{int} = \int_\Omega \frac{\partial(\delta v_i)}{\partial x_j}\sigma_{ji}d\Omega = \delta v_{iI}\int_\Omega \frac{\partial N_I}{\partial x_j}\sigma_{ji}d\Omega \tag{4.4.10}$$

where the third term is the definition of internal virtual power as given in Eqs. (B4.2.5) and (4.4.8) has been used in the last term. From the above it can be seen that the internal nodal forces are given by

$$\boxed{f_{iI}^{int} = \int_\Omega \frac{\partial N_I}{\partial x_j}\sigma_{ji}d\Omega} \tag{4.4.11}$$

These nodal forces are called internal because they represent the *stresses in the body*. These expressions apply to both a complete mesh and to any element or group of elements, as has been described in Chapter 2. Note that this expression involves derivatives of the shape functions with respect to spatial coordinates and integration over the current configuration. Equation (4.4.11) is a key equation in nonlinear finite element methods for updated Lagrangian meshes; it applies also to Eulerian and ALE meshes.

The external nodal forces are defined similarly in terms of the virtual external power

$$\delta P^{ext} = \delta v_{iI} f_{iI}^{ext} = \int_\Omega \delta v_i \rho b_i d\Omega + \sum_{i=1}^{n_{SD}} \int_{\Gamma_{t_i}} \delta v_i \bar{t}_i d\Gamma$$
$$= \delta v_{iI} \int_\Omega N_I \rho b_i d\Omega + \sum_{i=1}^{n_{SD}} \delta v_{iI} \int_{\Gamma_{t_i}} N_I \bar{t}_i d\Gamma \tag{4.4.12}$$

so the external nodal forces are given by

$$f_{iI}^{ext} = \int_\Omega N_I \rho b_i d\Omega + \int_{\Gamma_{t_i}} N_I \bar{t}_i d\Gamma \quad \text{or} \quad \mathbf{f}_I^{ext} = \int_\Omega N_I \rho \mathbf{b} d\Omega + \int_{\Gamma_{t_i}} N_I \mathbf{e}_i \, \bar{\mathbf{t}} d\Gamma \tag{4.4.13}$$

4.4.3. Mass Matrix and Inertial Forces. The inertial nodal forces are defined by

$$\delta P^{inert} = \delta v_{iI} f_{iI}^{inert} = \int_\Omega \delta v_i \rho \dot{v}_i d\Omega = \delta v_{iI} \int_\Omega N_I \rho \dot{v}_i d\Omega \tag{4.4.14}$$

so

$$f_{iI}^{inert} = \int_\Omega \rho N_I \dot{v}_i d\Omega \quad \text{or} \quad \mathbf{f}_I^{inert} = \int_\Omega \rho N_I \dot{\mathbf{v}} d\Omega \tag{4.4.15}$$

Using the expression (4.4.6) for the accelerations in the above gives

$$f_{iI}^{inert} = \int_\Omega \rho N_I N_J d\Omega \, \dot{v}_{iJ} \tag{4.4.16}$$

It is convenient to define these nodal forces as a product of a mass matrix and the nodal accelerations. Defining the mass matrix by

$$M_{ijIJ} = \delta_{ij} \int_\Omega \rho N_I N_J d\Omega \tag{4.4.17}$$

it follows from (4.4.16) and (4.4.17) that the inertial forces are given by

$$f_{iI}^{inert} = M_{ijIJ} \dot{v}_{jJ} \quad \text{or} \quad \mathbf{f}_I^{inert} = \mathbf{M}_{IJ} \dot{\mathbf{v}}_J \tag{4.4.18}$$

4.4.4. Discrete Equations. With the definitions of the internal, external and inertial nodal forces, Eqs. (4.4.10), (4.4.12) and (4.4.17), we can concisely write the discrete approximation to the weak form (4.4.9a) as

$$\delta v_{iI} \left(f_{iI}^{int} - f_{iI}^{ext} + M_{ijIJ} \dot{v}_{jJ} \right) = 0 \quad \text{for} \quad \delta v_{iI} \quad \Gamma_{v_i} \tag{4.4.19}$$

Invoking the arbitrariness of the unconstrained, virtual nodal velocities gives

$$M_{ijIJ} \dot{v}_{jJ} + f_{iI}^{int} = f_{iI}^{ext} \qquad I, i \quad \Gamma_{v_i} \quad \text{or} \quad \mathbf{M}_{IJ} \dot{\mathbf{v}}_J + \mathbf{f}_I^{int} = \mathbf{f}_I^{ext} \tag{4.4.20}$$

The above are the *discrete momentum equations* or *the equations of motion*; they are also called the *semidiscrete momentum equations* since they have not been discretized in time. The implicit sums are over all components and all nodes of the mesh; any prescribed velocity component that appears in the above is not an unknown. The matrix form on the left depends on the interpretation of the indices: this is discussed further in Section 4.5.

The semidiscrete momentum equations are a system of n_{DOF} ordinary differential equations in the nodal velocities, where n_{DOF} is the number of nodal velocity components which are unconstrained; n_{DOF} is often called the number of degrees of freedom. To complete the system of equations, we append the constitutive equations at the element quadrature points and the expression for the rate-of-deformation in terms of the nodal velocities. Let the n_Q quadrature points in the mesh be denoted by

$$\mathbf{x}_Q(t) = N_I\left(\mathbf{X}_Q\right)\mathbf{x}_I(t) \tag{4.4.21}$$

Note that the quadrature points are coincident with material points. Let n_σ be the number of independent components of the stress tensor: in a two dimensional plane stress problem, $n_\sigma = 3$, since the stress tensor σ is symmetric; in three-dimensional problems, $n_\sigma = 6$.

The semidiscrete equations for the finite element approximation then consist of the following ordinary differential equations in time:

$$M_{ijIJ}\dot{v}_{jJ} + f_{iI}^{int} = f_{iI}^{ext} \quad \text{for} \quad (I,i) \quad \Gamma_{v_i} \tag{4.4.22}$$

$$\sigma_{ij}\left(\mathbf{X}_Q\right) = S_{ij}\left(D_{kl}\left(\mathbf{X}_Q\right), \text{ etc}\right) \qquad \mathbf{X}_Q \tag{4.4.23}$$

$$\text{where } D_{ij}\left(\mathbf{X}_Q\right) = \tfrac{1}{2}\left(L_{ij} + L_{ji}\right) \quad \text{and} \quad L_{ij} = N_{I,j}\left(\mathbf{X}_Q\right)v_{iI} \tag{4.4.24}$$

This is a standard initial value problem, consisting of first-order ordinary differential equations in the velocities $v_{iI}(t)$ and the stresses $\sigma_{ij}\left(\mathbf{X}_Q, t\right)$. If we substitute (4.4.24) into (4.4.23) to eliminate the rate-of-deformation from the equations, the total number of unknowns is $n_{DOF} + n_\sigma n_Q$. This system of ordinary differential equations can be integrated in time by any of the methods for integrating ordinary differential equations, such as Runge-Kutta methods or the central difference method; this is discussed in Chapter 6.

The nodal velocities on prescribed velocity boundaries, v_{iI}, $(I,i) \quad \Gamma_{v_i}$, are obtained from the boundary conditions, Eq. (B4.1.7b). The initial conditions (B4.1.9) are applied at the nodes and quadrature points

$$v_{iI}(0) = v_{iI}^0 \tag{4.4.25}$$

$$\sigma_{ij}\left(\mathbf{X}_Q, 0\right) = \sigma_{ij}^0\left(\mathbf{X}_Q\right) \tag{4.4.26}$$

where v_{iI}^0 and σ_{ij}^0 are initial data at the nodes and quadrature points. If data for the initial conditions are given at a different set of points, the values at the nodes and quadrature points can be estimated by least square fits, as in Section 2.4.5.

For an equilibrium problem, the accelerations vanish and the governing equations are

$$f_{iI}^{int} = f_{iI}^{ext} \quad \text{for} \quad (I,i) \quad \Gamma_{v_i} \qquad \text{or} \qquad \mathbf{f}^{int} = \mathbf{f}^{ext} \tag{4.4.27}$$

along with (4.4.23) and (4.4.24). The above are called the discrete *equilibrium equations*. If the constitutive equations are rate-independent, then the discrete equilibrium equations are a set of nonlinear algebraic equations in the stresses and nodal displacements. For rate-dependent materials, any rate terms must be discretized in time to obtain a set of nonlinear algebraic equations; this is further discussed in Chapter 6.

4.4.5. Element Coordinates. Finite elements are usually developed with shape functions expressed in terms of parent element coordinates, which we will often call element coordinates for brevity. Examples of element coordinates are triangular coordinates and isoparametric coordinates. We will next describe the use of shape functions expressed in terms of element coordinates. As part of this description, we will show that the element coordinates can be considered an alternative set of material coordinates in a Lagrangian mesh. Therefore, expressing the shape functions in terms of element coordinates is intrinsically equivalent to expressing them in terms of material coordinates. We denote the parent element coordinates by ξ_i^e, or ξ^e in tensor notation, and the parent domain by Δ; the superscript *e* will only be carried in the beginning of this description. The shape of the parent domain depends on the type of element and the dimension of the problem; it may be a biunit square, a triangle, or a cube, for example. Specific parent domains are given in the examples which follow.

When a Lagrangian element is treated in terms of element coordinates, we are concerned with three domains that correspond to an element:

1. the parent element domain Δ;
2. the current element domain $\Omega^e = \Omega^e(t)$;
3. the initial (reference) element domain Ω_0^e

The following maps are pertinent:

1. parent domain to current configuration: $\mathbf{x} = \mathbf{x}\left(\xi^e, t\right)$
2. parent domain to initial configuration: $\mathbf{X} = \mathbf{X}\left(\xi^e\right)$
3. initial configuration to the current configuration, i.e. the motion $\mathbf{x} = \mathbf{x}\left(\mathbf{X}, t\right) \equiv \varphi\left(\mathbf{X}, t\right)$

The map $\mathbf{X} = \mathbf{X}\left(\xi^e\right)$ corresponds to $\mathbf{x} = \mathbf{x}\left(\xi^e, 0\right)$. These maps are illustrated in Fig. 4.1 for a triangular element where a space-time plot of a two-dimensional triangular element is shown.

The motion in each element is described by a composition of these maps

$$\mathbf{x} = \mathbf{x}\left(\mathbf{X}, t\right) = \mathbf{x}\left(\xi^e\left(\mathbf{X}\right), t\right) \qquad \mathbf{x}\left(\mathbf{X}, t\right) = \mathbf{x}\left(\xi^e, t\right) \circ \xi^e\left(\mathbf{X}\right) \quad \text{in } \Omega_e \tag{4.4.28}$$

where $\xi^e(\mathbf{X}) = \mathbf{X}^{-1}\left(\xi^e\right)$. For the motion to be well defined and smooth, the inverse map $\mathbf{X}^{-1}\left(\xi^e\right)$ must exist and the function $\mathbf{x} = \mathbf{x}\left(\xi^e, t\right)$ must be sufficiently smooth and meet certain conditions of regularity so that $\mathbf{x}^{-1}\left(\xi^e, t\right)$ exists; these conditions are given in Section 4.4.8. The inverse map $\mathbf{x}^{-1}\left(\xi^e, t\right)$ is usually not constructed because in most cases it cannot be obtained explicitly, so instead the derivatives with respect to the spatial coordinates are obtained in terms of the derivatives with respect to the parent coordinates by implicit differentiation.

The motion is approximated by

$$x_i(\xi, t) = x_{iI}(t) N_I(\xi) \qquad \text{or} \qquad \mathbf{x}(\xi, t) = \mathbf{x}_I(t) N_I(\xi) \tag{4.4.29}$$

where we have dropped the supercript *e* on the element coordinates. As can be seen in the above, the shape functions $N_I(\xi)$ are only functions of the parent element coordinates; the time dependence of the motion resides entirely in the nodal coordinates. The above represents a time dependent mapping between the parent domain and the current configuration of the element.

Writing this map at time $t = 0$ we obtain

$$X_i(\xi) = x_i(\xi, 0) = x_{iI}(0) N_I(\xi) = X_{iI} N_I(\xi) \quad \text{or} \quad \mathbf{X}(\xi) = \mathbf{X}_I N_I(\xi) \tag{4.4.30}$$

It can be seen from (4.4.30) that the map between the material coordinates and the element coordinates is time invariant in a Lagrangian element. If this map is one-to-one and onto, then *the element coordinates can in fact be considered surrogate material coordinates in a Lagrangian mesh*, since each material point in an element then has a unique element coordinate label. To establish a unique correspondence between element coordinates and the material coordinates in Ω_0, the element number must be part of the label. This does not apply to meshes which are not Lagrangian, as will be seen in Chapter 7. The use of the initial coordinates **X** as material coordinates in fact originates mainly in analysis; in finite element methods, the use of element coordinates as material labels is more natural.

As before, since the element coordinates are time invariant, we can express the displacements, velocities and accelerations in terms of the same shape functions

$$u_i(\xi, t) = u_{iI}(t) N_I(\xi) \qquad \mathbf{u}(\xi, t) = \mathbf{u}_I(t) N_I(\xi) \tag{4.4.31}$$

$$\dot{u}_i(\xi, t) = v_i(\xi, t) = v_{iI}(t) N_I(\xi) \qquad \mathbf{u}(\xi, t) = \mathbf{v}(\xi, t) = \mathbf{v}_I(t) N_I(\xi) \tag{4.4.32}$$

$$\dot{v}(\xi, t) = \dot{v}_{iI}(t) N_I(\xi) \qquad \dot{\mathbf{v}}(\xi, t) = \dot{\mathbf{v}}_I(t) N_I(\xi) \tag{4.4.33}$$

where we have obtained (4.4.32) by taking material time derivative of (4.4.31) and we have obtained (4.4.33) by taking the material time derivative of (4.4.32). The time dependence, as before, resides entirely in the nodal variables, since the element coordinates are independent of time.

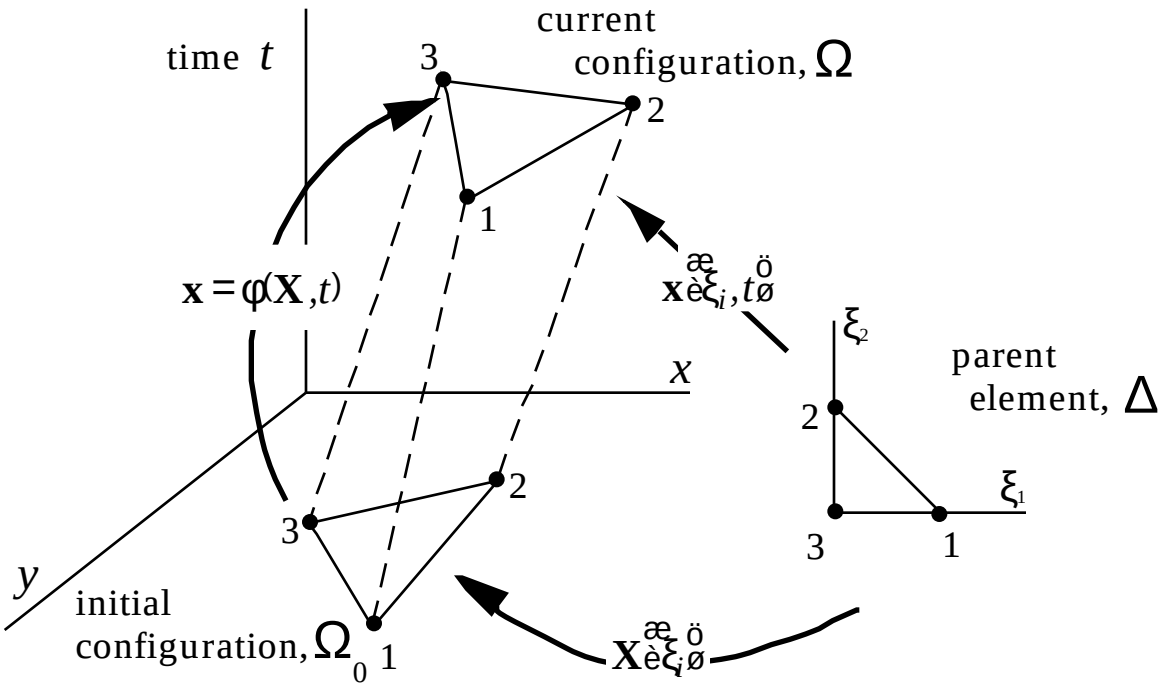

Fig. 4.1. Initial and current configurations of an element and their relationships to the parent element.

4.4.6. Derivatives of Functions. The spatial derivatives of the velocity field are obtained by implicit differentiation because the function $\mathbf{x}(\xi,t)$ is generally not explicitly invertible; i.e. it is not possible to write closed-form expressions for ξ in terms of $\mathbf{x}$. By the chain rule,

$$\frac{\partial v_i}{\partial \xi_j} = \frac{\partial v_i}{\partial x_k}\frac{\partial x_k}{\partial \xi_j} \quad \text{or} \quad \mathbf{v}_{,\xi} = \mathbf{v}_{,\mathbf{x}}\mathbf{x}_{,\xi} \tag{4.4.34}$$

The matrix $\partial x_k / \partial \xi_j$ is the Jacobian of the map between the current configuration of the element and the parent element configuration. We will use two symbols for this matrix: $\mathbf{x}_{,\xi}$ and $\mathbf{F}_\xi$, where $F^{\xi}_{ij} = \partial x_i / \partial \xi_j$. The second symbol is used to convey the notion that the Jacobian with respect to the element coordinates can be viewed as a deformation gradient with respect to the parent element configuration. In two dimensions

$$\mathbf{x}_{,\xi}(\xi,t) \equiv \mathbf{F}_\xi(\xi,t) = \begin{bmatrix} x_{,\xi_1} & x_{,\xi_2} \\ y_{,\xi_1} & y_{,\xi_2} \end{bmatrix} \tag{4.4.35}$$

As indicated in (4.4.35), the Jacobian of the map between the current and parent configurations is a function of time.

Inverting (4.4.34), we obtain

$$L_{ij} = \frac{\partial v_i}{\partial \xi_k} F^{-1}_{\xi kj} = \left(\frac{\partial v_i}{\partial \xi_k}\right)\left(\frac{\partial \xi_k}{\partial x_j}\right) \quad \text{or} \quad \mathbf{L} = \mathbf{v}_{,\mathbf{x}} = \mathbf{v}_{,\xi}\ \mathbf{x}^{-1}_{,\xi} = \mathbf{v}_{,\xi}\ \mathbf{F}^{-1}_{\xi} \tag{4.4.36}$$

Thus computation the derivatives with respect to ξ involves finding the inverse of the Jacobian between the current and parent element coordinates; the matrix to be inverted in the two dimensional case is given in (4.4.35). Similarly for the shape functions N_I, we have

$$N^T_{I,\mathbf{x}} = N^T_{I,\xi}\mathbf{x}^{-1}_{,\xi} = N^T_{I,\xi}\mathbf{F}^{-1}_{\xi} \tag{4.4.37}$$

where the transpose appears in the matrix expressions because we consider $N_{I,\mathbf{x}}$ and $N_{I,\xi}$ to be column matrices and the matrix on the RHS of the above must be a row matrix. The determinant of the element Jacobian $\mathbf{F}_\xi$,

$$J_\xi = det\left(\mathbf{x}_{,\xi}\right) \tag{4.4.38}$$

is called the *element Jacobian determinant*; we append the subscript to distinguish it from the determinant of the deformation gradient, *J*. Substituting (4.4.37) into (4.4.36) gives

$$L_{ij} = v_{iI}\frac{\partial N_I}{\partial \xi_k} F^{-1}_{\xi kj} \quad \text{or} \quad \mathbf{L} = \mathbf{v}_I N^T_{I,\xi}\mathbf{x}^{-1}_{,\xi} \tag{4.4.39}$$

The rate-of-deformation is obtained from the velocity gradient by using (3.3.10).

4.4.7. Integration and Nodal Forces. Integrals on the current configuration are related to integrals over the reference domain and the parent domain by

$$\int_{\Omega^e} g(\mathbf{x})d\Omega = \int_{\Omega^e_0} g(\mathbf{X})Jd\Omega_0 = \int_\Delta g(\xi)J_\xi d\Delta \quad \text{and} \quad \int_{\Omega^e_0} g(\mathbf{X})d\Omega_0 = \int_\Delta g(\xi)J^0_\xi d\Delta \tag{4.4.40}$$

where J and J_ξ are the determinants of the Jacobians between the current configurations and the reference and parent element configurations, respectively. Part of equations is identical to (3.2.18). The other part is obtained in the same way by using the map between the current and parent configurations. The above is consitent with our convention

When the internal nodal forces are computed by integration over the parent domain, (4.4.11) is tranformed to the parent element domain by (4.4.40), giving

$$f^{int}_{iI} = \int_{\Omega^e}\frac{\partial N_I}{\partial x_j}\sigma_{ji}d\Omega = \int_\Delta \frac{\partial N_I}{\partial x_j}\sigma_{ji}J_\xi d\Delta \tag{4.4.41}$$

The external nodal forces and the mass matrix can similarly be integrated over the parent domain.

4.4.8. Conditions on Parent to Current Map. The finite element approximation to the motion $\mathbf{x}(\xi,t)$, which maps the parent domain of an element onto the current domain of the

element, is subject to the same conditions as $\varphi(\mathbf{X},t)$, as given in Section 3.3.6, except that no discontinuities are allowed. These conditions are:

1. $\mathbf{x}(\xi,t)$ must be one-to-one and onto;
2. $\mathbf{x}(\xi,t)$ must be at least C^0 in space;
3. the element Jacobian determinant must be positive, i.e.

$$J_\xi \equiv \det(\mathbf{x}_{,\xi}) > 0 \,. \tag{4.4.43}$$

These conditions insure that $\mathbf{x}(\xi,t)$ is invertible.

We now explain why the condition $det(\mathbf{x}_{,\xi}) > 0$ is necessary. We first use the chain rule to express $\mathbf{x}_{,\xi}$ in terms of $\mathbf{F}$ and $\mathbf{X}_{,\xi}$:

$$\frac{\partial x_i}{\partial \xi_j} = \frac{\partial x_i}{\partial X_k}\frac{\partial X_k}{\partial \xi_j} = F_{ik}\frac{\partial X_k}{\partial \xi_j} \qquad \text{or} \qquad \mathbf{x}_{,\xi} = \mathbf{x}_{,\mathbf{X}}\mathbf{X}_{,\xi} = \mathbf{F}\mathbf{X}_{,\xi} \tag{4.4.44a}$$

We can also write the above as

$$\mathbf{F}_\xi = \mathbf{F}\ \mathbf{F}_\xi^0 \tag{4.4.44b}$$

which highlights the fact that the deformation gradient with respect to the parent element coordinates is the product of the standard deformation gradient and the initial deformation gradient with respect to the parent element coordinates. The determinant of the product of two matrices is equal to the product of the determinants, so

$$det\,(\mathbf{x}_{,\xi}) = det\,(\mathbf{F})\,det(\mathbf{X}_{,\xi}) \equiv JJ_\xi^0 \tag{4.4.45}$$

We assume that the elements in the initial mesh are properly constructed so that $J_\xi^0 = J_\xi(0) > 0$ for all elements; otherwise the initial mapping would not be one-to-one. If $J_\xi(t) \le 0$ at any time then by (4.4.45), $J \le 0$. By the conservation of matter $\rho = \rho_0/J$ so $J \le 0$ implies $\rho \le 0$, which is physically impossible. Therefore it is necessary that $J_\xi(t) > 0$ for all time. In some calculations, excessive mesh distortion can result in severely deformed meshes in which $J_\xi \le 0$. This implies a negative density, so such calculations violate the physical principle that mass is always positive.

4.4.9. Simplifications of Mass Matrix. When the same shape functions are used for all components, it is convenient to take advantage of the form of the mass matrix (4.4.20) by writing it as

$$M_{ijIJ} = \delta_{ij}\tilde{M}_{IJ} \tag{4.4.46}$$

where

$$\tilde{M}_{IJ} = \int_\Omega \rho N_I N_J d\Omega \qquad \tilde{\mathbf{M}} = \int_\Omega \rho \mathbf{N}^T \mathbf{N} d\Omega \tag{4.4.47}$$

Then the equations of motion (4.4.22) become

$$\tilde{M}_{IJ} \dot{v}_{iJ} + f_{iI}^{int} = f_{iI}^{ext} \tag{4.4.48}$$

This form is advantageous when the consistent mass matrix is used with explicit time integration, since the order of the matrix which needs to be inverted is reduced by a factor of n_{SD}.

We next show that the mass matrix for a Lagrangian mesh is constant in time. If the shape functions are expressed in terms of parent element coordinates, then

$$M_{ijIJ} = \delta_{ij} \int_\Delta \rho N_I N_J \, det\left(\mathbf{x}, \xi\right) d\Delta = \delta_{ij} \int_\Omega \rho N_I N_J d\Omega \tag{4.4.49}$$

Since $det\left(\mathbf{x}_{,\xi}\right)$ and the density are time dependent, this mass matrix appears to be time dependent. To show that the matrix is in fact time independent, we transform the above integral to the undeformed configuration by (3.2.18), giving

$$M_{ijIJ} = \delta_{ij} \int_{\Omega_0} \rho N_I N_J J d\Omega_0 \tag{4.4.50}$$

From mass conservation, (B4.1.1) it follows that $\rho J = \rho_0$. Hence (4.4.50) becomes

$$M_{ijIJ} = \delta_{ij} \int_{\Omega_0} \rho_0 N_I N_J \, d\Omega_0 \quad \text{or} \quad M_{ijIJ} = \delta_{ij} \int_\Delta \rho_0 N_I N_J J_\xi^0 \, d\Delta \tag{4.4.51}$$

The compact form of the mass matrix, (4.4.47) can similarly be written as

$$\tilde{M}_{IJ} = \int_{\Omega_0} \rho_0 N_I N_J \, d\Omega_0 \quad \text{and} \quad \mathbf{M}_{IJ} = \mathbf{I} \tilde{M}_{IJ} = \mathbf{I} \int_{\Omega_0} \rho_0 N_I N_J \, d\Omega_0 \tag{4.4.52}$$

In the above integrals, the integrand is independent of time, so the mass matrix is constant in time. It needs to be evaluated only at the beginning of a computation. The same result could be obtained by computing the mass matrix by (4.4.49) at the initial time, i.e. in the intial configuration. The mass matrix in (4.4.52) can be called *total Lagrangian* since it is evaluated in the reference (undeformed) configuration. We take the view here and subsequently that the discrete equations should be evaluated in whatever configuration is most convenient.

4.5. IMPLEMENTATION

In the implementation of the finite element equations developed in the previous Section, two approaches are popular:

1. the indicial expressions are directly treated as matrix equations;
2. Voigt notation is used, as in linear finite element methods, so the square stress and strain matrices are converted to column matrices.

Box 4.3
Discrete Equations and Internal Nodal Force Algorithm for the Updated Lagrangian Formulation

Equations of Motion (discrete momentum equation)

$$M_{ijIJ}\dot{v}_{jJ} + f_{iI}^{int} = f_{iI}^{ext} \quad \text{for} \quad (I,i) \quad \Gamma_{v_i} \tag{B4.8.1}$$

Internal Nodal Forces

$$f_{iI}^{int} = \int_\Omega B_{Ij}\sigma_{ji}d\Omega = \int_\Omega \frac{\partial N_I}{\partial x_j}\sigma_{ji}d\Omega \quad \text{or} \quad \left(\mathbf{f}_I^{int}\right)^T = \int_\Omega B_I^T \sigma d\Omega \tag{B4.8.2}$$

$$\mathbf{f}_I^{int} = \int_\Omega \mathbf{B}_I^T\{\sigma\}d\Omega \quad \text{in Voigt notation}$$

External Nodal Forces

$$f_{iI}^{ext} = \int_\Omega N_I \rho b_i d\Omega + \int_{\Gamma_{t_i}} N_I \bar{t}_i d\Gamma \quad \text{or} \quad \mathbf{f}_I^{ext} = \int_\Omega N_I \rho \mathbf{b} d\Omega + \int_{\Gamma_{t_i}} N_I \mathbf{e}_i\ \bar{\mathbf{t}} d\Gamma \tag{B4.8.3}$$

Mass Matrix (total Lagrangian)

$$M_{ijIJ} = \delta_{ij}\int_{\Omega_0}\rho_0 N_I N_J d\Omega_0 = \delta_{ij}\int_\Delta \rho_0 N_I N_J J_\xi^0 d\Delta \tag{B4.8.4}$$

$$\mathbf{M}_{IJ} = \mathbf{I}\tilde{M}_{IJ} = \mathbf{I}\int_{\Omega_0}\rho_0 N_I N_J\, d\Omega_0 \tag{B4.8.5}$$

Internal nodal force computation for element

1. $\mathbf{f}^{int} = 0$

2. for all quadrature points ξ_Q

   i. compute $\left[B_{Ij}\right] = \left[\partial N_I\left(\xi_Q\right)/\partial x_j\right]$ for all I

   ii. $\mathbf{L} = \left[L_{ij}\right] = \left[v_{iI}B_{Ij}\right] = \mathbf{v}_I B_I^T; \quad L_{ij} = \dfrac{\partial N_I}{\partial x_j}\ v_{iI}$

   iii. $\mathbf{D} = \frac{1}{2}\left(\mathbf{L}^T + \mathbf{L}\right)$

   iv. if needed compute $\mathbf{F}$ and $\mathbf{E}$ by procedures in Box 4.7

   v. compute the Cauchy stress σ or the PK2 stress $\mathbf{S}$ or by constitutive equation

   vi. if $\mathbf{S}$ computed, compute σ by $\sigma = J^{-1}\mathbf{F}\mathbf{S}\mathbf{F}^T$

   vii. $\mathbf{f}_I^{int} \leftarrow \mathbf{f}_I^{int} + B_I^T \sigma J_\xi \bar{w}_Q$ for all I

end loop

$\bar{w}_Q$ are quadrature weights

Each of these methods has advantages, so both methods will be described. In Box 4.8 the discrete eqautions are summarized in both forms. The internal force computations is then given for the matrix-indicial form.

4.5.1. Indicial to Matrix Expressions. The conversion of indicial expressions to matrix frorm is somewhat arbitrary and depends on individual preferences. In this book, we have tried to interpret single-index variables as column matrices in most cases; the details are somewhat different when there is a preference for row matrices. To illustrate this procedure, consider the expression for the velocity gradient, Eq. (3.3.7) and (4.4.5):

$$L_{ij} = \frac{\partial v_i}{\partial x_j} = v_{iI} \frac{\partial N_I}{\partial x_j} \tag{4.5.1}$$

The above expression can be put into the form of a matrix product if we associate the index I with a column number in v and a row number in $\partial N_I / \partial x_j$. To simplify the writing of a matrix expression, we define a matrix B by

$$B_{jI} = \frac{\partial N_I}{\partial x_j} \quad \text{or} \quad \boldsymbol{B} = \left[B_{jI} \right] = \left[\partial N_I / \partial x_j \right] \tag{4.5.2}$$

where j is the row number in the matrix. The velocity gradient can then be expressed in terms of the nodal displacements by (4.5.1) and (4.5.2) by

$$\left[L_{ij} \right] = \left[v_{iI} \right] \left[B_{Ij} \right] = \left[v_{iI} \right] \left[B_{jI} \right]^T \qquad \text{or} \qquad \mathbf{L} = \mathbf{v} \boldsymbol{B}^T \tag{4.5.3}$$

so, because of the implicit sum on I, the indicial expression corresponds to a matrix product.

We can also often write the expression (4.5.1) without expressing the sum on I in matrix form. The B matrix is then subdivided into B_I matrices, each associated with node I:

$$B = \left[B_1, B_2, B_3, \ldots, B_m \right] \quad \text{where} \quad \boldsymbol{B}_I^T = \left\{ B_j \right\}_I = N_{I,\mathbf{x}} \tag{4.5.3b}$$

For each node I, the B_I matrix is a column matrix. Then the expression for the velocity gradient can be written as a sum of tensor products, a product of a column matrix with a row matrix, as shown below

$$\mathbf{L} = \mathbf{v}_I B_I^T = \begin{bmatrix} v_{xI} \\ v_{yI} \end{bmatrix} \begin{bmatrix} N_{I,x} & N_{I,y} \end{bmatrix} = \begin{bmatrix} v_{xI} N_{I,x} & v_{xI} N_{I,y} \\ v_{yI} N_{I,x} & v_{yI} N_{I,y} \end{bmatrix} \tag{4.5.4}$$

To put the internal force expression (4.4.11) in matrix form, we first rearrange the terms so that adjacent terms correspond to matrix products. This entails interchanging the row and column number on the internal forces a shown below

$$\left(f_{iI}^{int} \right)^T = f_{Ii}^{int} = \int_\Omega \frac{\partial N_I}{\partial x_j} \sigma_{ji} \, d\Omega = \int_\Omega B_{Ij}^T \sigma_{ji} \, d\Omega \tag{4.5.5}$$

The above can be put in the following matrix form

$$\left[f_{iI}^{int} \right]^T = \left[f_{Ii}^{int} \right] = \int_\Omega \left[\partial N_I / \partial x_j \right] \left[\sigma_{ji} \right] d\Omega = \int_\Omega \left[B_{jI} \right]^T \left[\sigma_{ji} \right] d\Omega \qquad \left(\mathbf{f}_I^{int} \right)^T = \int_\Omega B_I^T \sigma d\Omega \tag{4.5.6}$$

For example, in two dimensions this gives

$$\left[f_{xI} \quad f_{yI} \right]^{int} = \int_\Omega \left[N_{I,x} \quad N_{I,y} \right] \begin{bmatrix} \sigma_{xx} & \sigma_{xy} \\ \sigma_{xy} & \sigma_{yy} \end{bmatrix} d\Omega \tag{4.5.7}$$

There are many other ways of converting indicial expressions to matrix form but the above is convenient because it adheres to the convention of treating single index matrices as column matrices, which is customary in the finite element literature. The expression for all nodal forces can be obtained by using the B matrix as defined in (4.5.3b), which gives

$$\left(\mathbf{f}^{int} \right)^T = \int_\Omega \boldsymbol{B}^T \sigma d\Omega$$

4.5.2. Voigt notation. An alternate implementation which is widely used in linear finite element analysis is based on Voigt notation, see Appendix B. Voigt notation is useful for computing tangent stiffness matrices in Newton methods, See Chapter 6. In Voigt notation the stresses and rate-of-deformation are expressed in column vectors, so in two dimensions

$$\{\mathbf{D}\}^T = \begin{bmatrix} D_x & D_y & 2D_{xy} \end{bmatrix} \qquad \{\sigma\}^T = \begin{bmatrix} \sigma_x & \sigma_y & \sigma_{xy} \end{bmatrix} \tag{4.5.11}$$

We define the $\mathbf{B}_I$ matrix so it relates the rate-of-deformation to the nodal velocities by

$$\{\mathbf{D}\} = \mathbf{B}_I \mathbf{v}_I \qquad \{\delta\mathbf{D}\} = \mathbf{B}_I \delta\mathbf{v}_I \tag{4.5.12}$$

where the summation convention as usual applies to repeated indices. The elements of the $\mathbf{B}_I$ matrix are obtained so as to meet the definition (4.5.12); this is illustrated in the following examples. Note that a matrix is enclosed in brackets only when this is needed to distinguish a matrix from its usual form as a square matrix; matrices and tensors of third order or higher which become square matrices are written simply as boldface.

The expression for the internal force vector can be derived in this notation by using the definition of the virtual internal power in terms of the nodal forces and nodal velocities and in terms of the stresses and rate of deformation, Eq. (4.3.19). Since $\{\mathbf{D}\}^T\{\sigma\}$ gives the internal power per unit volume (the column matrices were designed with this in mind), it follows that

$$\delta P^{int} = \delta\mathbf{v}_I^T \mathbf{f}_I^{int} = \int_\Omega \{\delta\mathbf{D}\}^T \{\sigma\} d\Omega \tag{4.5.13}$$

Substituting (4.5.12) into the above and invoking the arbitrariness of $\{\delta\mathbf{v}\}$ gives

$$\mathbf{f}_I^{int} = \int_\Omega \mathbf{B}_I^T \{\sigma\} d\Omega \tag{4.5.14}$$

As will be shown in the examples, Eq. (4.5.14) gives the same expression for the internal nodal forces as Eq. (4.5.6): Eq. (4.5.14) uses the symmetric part of the velocity gradient, whereas the complete velocity gradient has been used in Eq. (4.5.6). However, since the Cauchy stress is symmetric, the two expression are equivalent; this is verified in the following examples.

It is sometimes convenient to place the displacement, velocities and nodal forces for an element or a complete mesh in a single column matrix. We will then use the symbol $\mathbf{d}$ for the column matrix of all nodal displacements, $\dot{\mathbf{d}}$ for the column matrix of nodal velocities and $\{\mathbf{f}\}$ for the column matrix of nodal forces, i.e.

$$\mathbf{d} = \begin{Bmatrix} \mathbf{u}_1 \\ \mathbf{u}_2 \\ \cdot \\ \mathbf{u}_m \end{Bmatrix} \qquad \dot{\mathbf{d}} = \begin{Bmatrix} \mathbf{v}_1 \\ \mathbf{v}_2 \\ \cdot \\ \mathbf{v}_m \end{Bmatrix} \qquad \mathbf{f} = \begin{Bmatrix} \mathbf{f}_1 \\ \mathbf{f}_2 \\ \cdot \\ \mathbf{f}_m \end{Bmatrix} \tag{4.5.15}$$

where m is the number of nodes. The correspondence between the two matrices is given by

$$d_a = u_{iI} \quad \text{where } a = (I-1)^* n_{SD} + i \tag{4.5.16}$$

Note that we use a different symbol for the column matrix of all nodal displacements and nodal velocities because the symbols $\mathbf{u}$ and $\mathbf{v}$ refer to the displacement and velocity vector fields in the continuum mechanics description.

In this notation, we can write the counterpart of Eq. (4.5.12) as

$$\{\mathbf{D}\} = \mathbf{B}\dot{\mathbf{d}} \qquad \text{where } \mathbf{B} = \left[\mathbf{B}_1, \mathbf{B}_2, ..., \mathbf{B}_m\right] \tag{4.5.18}$$

where the brackets around $\mathbf{D}$ indicate that the tensor is stored in colum matrix form; we do not put brackets around $\mathbf{B}$ because this is always a rectangular matrix. The nodal forces are given by the counterpart of Eq. (4.5.14):

$$\{\mathbf{f}\}^{int} = \int_\Omega \mathbf{B}^T \{\sigma\}\, d\Omega \tag{4.5.19}$$

Often we omit the brackets on the nodal force, since the presence of a single term in Voigt notation always indicates that the entire equation is in Voigt notation. The Voigt form can also be obtained by rewriting (4.5.5) as

$$f_{Ir}^{int} = \int_\Omega \frac{\partial N_I}{\partial x_j} \delta_{ri} \sigma_{ji}\, d\Omega \tag{4.5.20}$$

Then defining the $\mathbf{B}$ matrix by

$$B_{ijIr} = \frac{\partial N_I}{\partial x_j} \delta_{ri} \tag{4.5.21}$$

and converting the indices (*i*,*j*) by the kinematic Voigt rule to a and the indices (*I.r*) by the matrix-column vector rule gives

$$f_a^{int} = \int_\Omega B_{ba}^T \sigma_b d\Omega \quad or \quad \mathbf{f}^{int} = \int_\Omega \mathbf{B}^{\mathbf{T}}\{\sigma\}\sigma d\Omega \tag{4.5.22}$$

More detail and techniques for translating indicial notation to Voigt notation can be found in Appendix B.

4.5.4. Numerical Quadrature. The integrals for the nodal forces, mass matrix and other element matrices can generally not be evaluated in closed form, and are instead integrated numerically (often called numerical quadrature). The most widely used procedure for numerical integration in finite elements is Gauss quadrature. The Gauss quadrature formulas are, see for example Dhatt and Touzot (1984, p.240), Hughes (1977, p. 137)

$$\int_{-1}^{1} f(\xi) d\xi = \sum_{Q=1}^{n_Q} w_Q f(\xi_Q) \tag{4.5.24}$$

where the weights w_Q and coordinates ξ_Q of the n_Q quadrature points are available in tables; a short table is given in Appendix C. Equation (4.5.24) integrates $f(\xi)$ exactly if it is a polynomial of order $m \le 2n_Q - 1$. Equation (4.5.24) is tailored to quadrature over the parent element domains, since it is over the interval [-1, 1].

To integrate over a two dimensional element, the procedure is repeated over the second direction, yielding the following

$$\int_\Delta f(\xi) d\Delta = \int_{-1}^{1}\int_{-1}^{1} f(\xi,\eta) d\xi d\eta = \sum_{Q_1=1}^{n_{Q_1}} \sum_{Q_2=1}^{n_{Q_2}} w_{Q_1} w_{Q_2} f(\xi_{Q_1}, \eta_{Q_2}) \tag{4.5.25}$$

In three dimensions, the Gauss quadrature formula is

$$\int_\Delta f(\xi) d\Delta = \int_{-1}^{1}\int_{-1}^{1}\int_{-1}^{1} f(\xi) d\xi d\eta d\zeta = \sum_{Q_1=1}^{n_{Q_1}} \sum_{Q_2=1}^{n_{Q_2}} \sum_{Q_3=1}^{n_{Q_3}} w_{Q_1} w_{Q_2} w_{Q_3} f(\xi_{Q_1}, \eta_{Q_2}, \zeta_{Q_3}) \tag{4.5.26}$$

For example, in integrating the expression for the internal nodal forces over the biunit square parent element in two dimensions, we use

$$\begin{aligned} \mathbf{f}^{int} &= \int_\Delta \mathbf{B}^T \{\sigma\} J_\xi \, d\Delta = \int_{-1}^{1}\int_{-1}^{1} \mathbf{B}^T \{\sigma\} J_\xi \, d\xi d\eta \\ &= \sum_{Q_1=1}^{n_{Q_1}} \sum_{Q_2=1}^{n_{Q_2}} w_{Q_1} w_{Q_2} \mathbf{B}^T(\xi_{Q_1}, \eta_{Q_2}) \{\sigma(\xi_{Q_1}, \eta_{Q_2})\} J_\xi(\xi_{Q_1}, \eta_{Q_2}) \end{aligned} \tag{4.5.27}$$

To simplify the notation for multi-dimensional quadrature, we often combine the weights into a single weight and write the quadrature formula in any dimension as

$$\int_{\Delta} f(\xi) d\Delta = \sum_{Q} \overline{w}_Q f(\xi_Q) \tag{4.5.28}$$

where $\overline{w}_Q$ is a products of the weights for one-dimensional quadrature w_Q.

The number of quadrature points used in nonlinear analysis is generally based on the same rules as for linear analysis; the number of quadrature points is chosen to exactly integrate the nodal internal forces for a regular element. A regular form of an element is one that can be obtained by only stretching but not shearing the parent element; for example, a rectangle for two-dimensional isoparametric elements. To choose the number of quadrature points for the internal nodal forces for a 4-node quadrilateral, we use the following argument. The rate-of-deformation and the **B**-matrix are linear in this element since the velocities are bilinear. If the stress is linearly related to the rate-of-deformation, it will vary linearly within the quadrilateral element. The integrand for the internal nodal forces is approximately quadratic, since it is a product of the **B**-matrix and the stresses. By the above rule for Gauss quadrature, two quadrature points are then needed in each direction for exact quadrature of a quadratic function, so 2x2 quadrature on a quadrilateral integrates the internal nodal forces exactly on a regular element. Quadrature formulas which integrate the nodal internal forces almost exactly for a linear constitutive equation are called *full quadrature*.

Gauss quadrature is very powerful for smooth functions which are polynomials or nearly polynomials. In linear finite element analysis, the integrand in the expression for the stiffness matrix consists of polynomials for rectangular elements and is smooth and nearly a polynomial for isoparametric elements. In nonlinear analysis, the integrand is not always smooth. For example, for an elastic-plastic material, the stress may have a discontinuous derivative in space at the surface separating elastic and plastic material. Even if the stress-strain law is smooth for an elastic-plastic material, the derivative of the stress with respect to the strain changes drastically when the response changes from elastic to plastic, so the effect is the same. Therefore, the errors in Gauss quadrature of an element that contains an elastic-plastic interface are likely to be large. However, higher order quadrature is not recommended for circumventing these errors, since it often leads to stiff behavior or locking of elements.

4.5.5. Selective-Reduced Integration. For incompressible or nearly incompressible materials, full quadrature of the nodal internal forces may cause an element to lock, i.e. the displacements are very small and do not converge or converge very slowly. The easiest way to circumvent this difficulty is to use selective-reduced integration.

In selective-reduced integration, the pressure is underintegrated, whereas the remainder of the stress matrix is fully integrated. For this purpose, the stress tensor is decomposed into the hydrostatic component or pressure *p*, which is the trace of the stress tensor

$$\sigma_{ij}^{dil} = p\delta_{ij} = \frac{1}{3}\sigma_{kk}\delta_{ij} \tag{4.5.29a}$$

and the deviatoric components:

$$\sigma_{ij}^{dev} = \sigma_{ij} - p\delta_{ij} \tag{4.5.29b}$$

The rate-of-deformation is similarly split into dilatational and deviatoric components which are defined by

$$D_{ij}^{dev} = D_{ij} - \frac{1}{3} D_{kk}\delta_{ij} \qquad D_{ij}^{dil} = \frac{1}{3} D_{kk}\delta_{ij} \tag{4.5.30}$$

It is noted that the dilatational and deviatoric components are orthogonal to each other so that the total virtual internal power as defined in Eq. (4.3.19) becomes:

$$\delta P^{int} = \int_\Omega \delta D_{ij}\sigma_{ij}\, d\Omega = \tfrac{1}{3}\int_\Omega \delta D_{ii}\, p\, d\Omega + \int_\Omega \delta D_{ij}^{dev}\sigma_{ij}^{dev}\, d\Omega \tag{4.5.31}$$

After expressing the rate-of-deformation in terms of the shape functions by (4.4.7b) and (4.5.30), the dilatational and deviatoric integrands become:

$$\delta D_{ii}\, p = \delta v_{iI} N_{I,i}\, p \tag{4.5.32a}$$

and

$$\delta D_{ij}^{dev}\sigma_{ij}^{dev} = \frac{1}{2}\left(N_{I,j}\delta v_{iI} + N_{I,i}\delta v_{jI}\right)\sigma_{ij}^{dev} - \frac{1}{3} N_{I,k}\delta v_{kI}\delta_{ij}\sigma_{ij}^{dev} \tag{4.5.32b}$$

Using the symmetry of σ_{ij}^{dev} and the fact that the trace of σ_{ij}^{dev} vanishes, the deviatoric integrand simplifies to:

$$\delta D_{ij}^{dev}\sigma_{ij}^{dev} = \delta v_{iI} N_{I,j}\sigma_{ij}^{dev} \tag{4.5.33}$$

Selective-reduced integration consists of full integration on the deviatoric term and reduced integration on the dilatational term on δP^{int}. Thus, for a four-node quadrilateral, selective-reduced integration gives:

$$\delta P^{int} = \delta v_{iI}\left[\frac{1}{3} J_\xi(\mathbf{0}) N_{I,i}(\mathbf{0}) p(\mathbf{0}) + \sum_{Q=1}^{4} \overline{w}_Q J_\xi\left(\xi_Q\right) N_{I,j}\left(\xi_Q\right)\sigma_{ji}^{dev}\left(\xi_Q\right)\right] \tag{4.3.34a}$$

Hence the selective-reduced integration internal force expression is:

$$\left(f_{iI}^{int}\right)^T = f_{Ii}^{int} = \left[\frac{1}{3} J_\xi(\mathbf{0}) N_{I,i}(\mathbf{0}) p(\mathbf{0}) + \sum_{Q=1}^{4} \overline{w}_Q J_\xi\left(\xi_Q\right) N_{I,j}\left(\xi_Q\right)\sigma_{ji}^{dev}\left(\xi_Q\right)\right] \tag{4.3.34b}$$

where, as indicated in the above, the single quadrature point for the reduced quadrature is the centroid of the parent element. The deviatoric part is integrated by full quadrature using two points in each direction, for a total of four quadrature points; this is called 2x2 quadrature. This scheme is similar to the scheme used in linear analysis of incompressible materials. Selective-reduced schemes for other elements can be developed by similarly modifying selective-reduced integration schemes given linear finite element texts; see Hughes(1979) for selective-reduced integration procedures for linear problems.

4.5.6. Element Force and Matrix Transformations. Often element nodal forces and element matrices must be expressed which in terms of alternate degrees of freedom, i.e. for a

different set of nodal displacements. In the following, transformations are developed for nodal forces and element matrices.

Consider an element or assemblage of elements with nodal displacements $\hat{\mathbf{d}}$. We wish to express the nodal forces for the nodal displacements $\mathbf{d}$ which are related to $\hat{\mathbf{d}}$ by

$$\frac{d\hat{\mathbf{d}}}{dt} = \mathbf{T}\frac{d\mathbf{d}}{dt} \qquad \text{or} \qquad \delta\hat{\mathbf{d}} = \mathbf{T}\delta\mathbf{d} \tag{4.5.35}$$

The nodal forces associated with $\mathbf{d}$ are then given by

$$\mathbf{f} = \mathbf{T}^T\hat{\mathbf{f}} \tag{4.5.36}$$

This transformation holds because the nodal foces and velocities are assumed to be conjugate in power, see Section 2.4.2. It is proven as follows. An increment of work is given by

$$\delta W = \delta\mathbf{d}^T\mathbf{f} = \delta\hat{\mathbf{d}}^T\hat{\mathbf{f}} \qquad \delta\mathbf{d} \tag{4.5.37}$$

Either set of nodal forces and virtual displacements must give an increment in work, since work is a scalar independent of the coordinate system or choice of generalized displacements. Substituting (4.5.35) into (4.5.37) gives

$$\delta\mathbf{d}^T\mathbf{f} = \delta\mathbf{d}^T\mathbf{T}^T\hat{\mathbf{f}} \qquad \delta\mathbf{d} \tag{4.5.38}$$

Since (4.5.38) holds for all $\delta\mathbf{d}$, Eq.(4.5.36) follows.

The mass matrix can be transformed similarly. We first consider the case where $\mathbf{T}$ is independent of time. then the mass matrix for the two set of degrees of freedom is related by

$$\mathbf{M} = \mathbf{T}^T\hat{\mathbf{M}}\mathbf{T} \tag{4.5.39}$$

This is shown as follows. By Eq.(4.5.36)

$$\mathbf{f}^{inert} = \mathbf{T}^T\hat{\mathbf{f}}^{inert} \tag{4.5.40}$$

and using (4.4.18) for the two sets of degrees of freedom, we have

$$\mathbf{M}\dot{\mathbf{v}} = \mathbf{T}^T\hat{\mathbf{M}}\dot{\hat{\mathbf{v}}} \tag{4.5.41}$$

If $\mathbf{T}$ is independent of time, from (4.5.35), $\dot{\hat{\mathbf{v}}} = \mathbf{T}\dot{\mathbf{v}}$, and substituting this into the above and using the fact that this must hold for the arbitrary nodal accelerations, we obtain (4.5.39). If the $\mathbf{T}$ matrix is time dependent, then $\dot{\hat{\mathbf{v}}} = \mathbf{T}\dot{\mathbf{v}} + \dot{\mathbf{T}}\mathbf{v}$, so

$$\mathbf{f}^{inert} = \mathbf{T}^T\hat{\mathbf{M}}\mathbf{T}\ddot{\mathbf{d}} + \mathbf{T}^T\hat{\mathbf{M}}\dot{\mathbf{T}}\dot{\mathbf{d}} \tag{4.5.42}$$

The matrix $\dot{\mathbf{T}}$ usually depends on the nodal velocities, so in this case terms which are not linear in the velocities occur in the equations of motion.

A transformation similar to (4.3.39) holds for the linear stiffness matrix and the tangent stiffness discussed in Chapter 6:

$$\mathbf{K} = \mathbf{T}^T \hat{\mathbf{K}} \mathbf{T}, \qquad \mathbf{K}^{tan} = \mathbf{T}^T \hat{\mathbf{K}}^{tan} \mathbf{T} \tag{4.5.43}$$

These transformations enable us to evaluate element matrices in coordinate systems which simplify the procedure as in example 4.6. They are also useful for treating slave nodes, see example 4.5

Example 4.1. Triangular 3-node element. The triangular element will be developed using triangular coordinates (also called area coordinates and barycentric coordinates). The element is shown in Figure 4.2. It is a 3-node element with a linear displacement field; the thickness of the element is *a*. The nodes are numbered counterclockwise in the parent element, and they must be numbered counterclockwise in the initial configuration, otherwise the determinant of the map between the initial and parent domains will be negative.

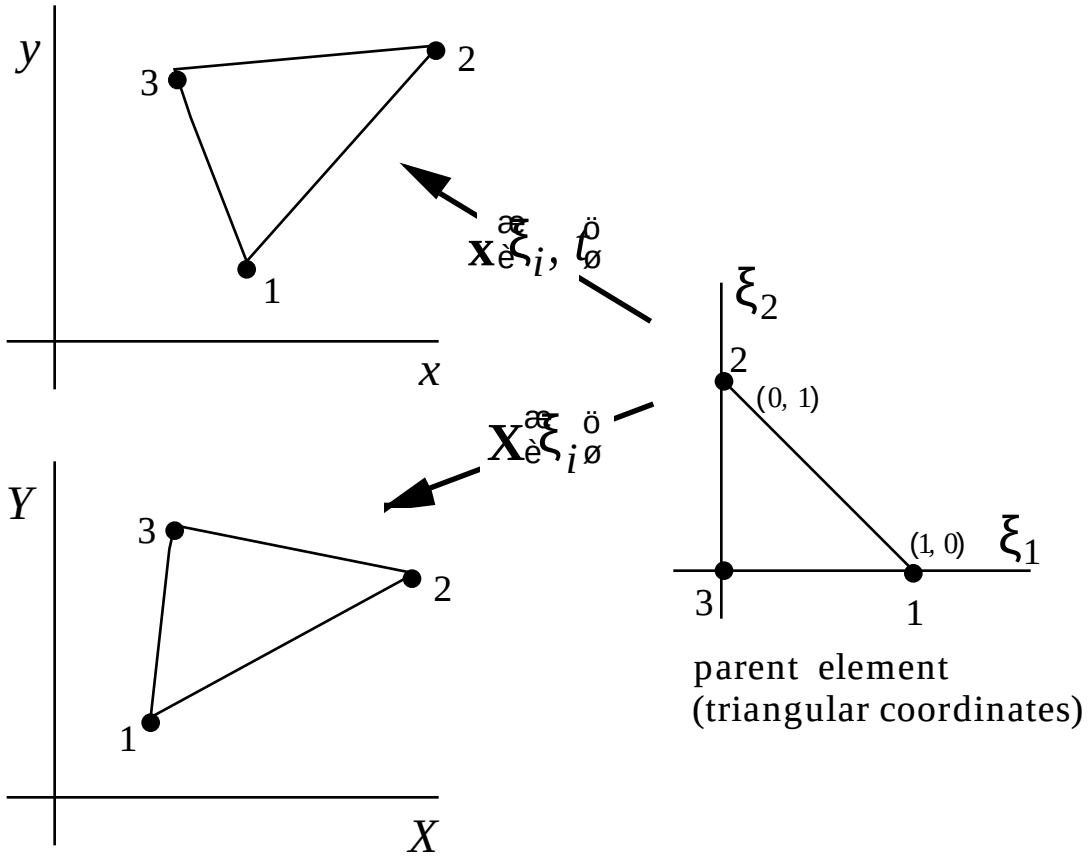

Fig. 4.2. Triangular element showing node numbers and the mappings of the initial and current configurations to the parent element.

The shape functions for the linear displacement triangle are the triangular coordinates, so $N_I = \xi_I$. The spatial coordinates are expressed in terms of the triangular coordinates ξ_I by

$$\begin{Bmatrix} x \\ y \\ 1 \end{Bmatrix} = \begin{bmatrix} x_1 & x_2 & x_3 \\ y_1 & y_2 & y_3 \\ 1 & 1 & 1 \end{bmatrix} \begin{Bmatrix} \xi_1 \\ \xi_2 \\ \xi_3 \end{Bmatrix} \tag{E4.1.2}$$

where we have appended the condition that the sum of the triangular element coordinates is one. The inverse of Eq. (E4.1.2) is given by

$$\begin{Bmatrix} \xi_1 \\ \xi_2 \\ \xi_3 \end{Bmatrix} = \frac{1}{2A} \begin{bmatrix} y_{23} & x_{32} & x_2 y_3 - x_3 y_2 \\ y_{31} & x_{13} & x_3 y_1 - x_1 y_3 \\ y_{12} & x_{21} & x_1 y_2 - x_2 y_1 \end{bmatrix} \begin{Bmatrix} x \\ y \\ 1 \end{Bmatrix} \tag{E4.1.4a}$$

where we have used the notation

$$x_{IJ} = x_I - x_J \qquad y_{IJ} = y_I - y_J \tag{E4.1.3}$$

and

$$2A = x_{32} y_{12} - x_{12} y_{32} \tag{E4.1.4b}$$

where A is the current area of the element. As can be seen from the above, in the triangular three-node element, the parent to current map (E4.1.2) can be inverted explicitly. This unusual circumstance is due to the fact that the map for this element is linear. However, the parent to current map is nonlinear for most other elements, so for most elements it cannot be inverted.

The derivatives of the shape functions can be determined directly from (E4.1.4a) by inspection:

$$\left[N_{I,j} \right] = \left[\xi_{I,j} \right] = \begin{bmatrix} \xi_{1,x} & \xi_{1,y} \\ \xi_{2,x} & \xi_{2,y} \\ \xi_{3,x} & \xi_{3,y} \end{bmatrix} = \frac{1}{2A} \begin{bmatrix} y_{23} & x_{32} \\ y_{31} & x_{13} \\ y_{12} & x_{21} \end{bmatrix} \tag{E4.1.5}$$

We can obtain the map between the parent element and the initial configuration by writing Eq. (E4.1.2) at time $t = 0$, which gives

$$\begin{Bmatrix} X \\ Y \\ 1 \end{Bmatrix} = \begin{bmatrix} X_1 & X_2 & X_3 \\ Y_1 & Y_2 & Y_3 \\ 1 & 1 & 1 \end{bmatrix} \begin{Bmatrix} \xi_1 \\ \xi_2 \\ \xi_3 \end{Bmatrix} \tag{E4.1.6}$$

The inverse of this relation is identical to (E4.1.4) except that it is in terms of the initial coordinates

$$\begin{Bmatrix} \xi_1 \\ \xi_2 \\ \xi_3 \end{Bmatrix} = \frac{1}{2A_0} \begin{bmatrix} Y_{23} & X_{32} & X_2 Y_3 - X_3 Y_2 \\ Y_{31} & X_{13} & X_3 Y_1 - X_1 Y_3 \\ Y_{12} & X_{21} & X_1 Y_2 - X_2 Y_1 \end{bmatrix} \begin{Bmatrix} x \\ y \\ 1 \end{Bmatrix} \tag{E4.1.7a}$$

$$2A_0 = X_{32} Y_{12} - X_{12} Y_{32} \tag{E4.1.7b}$$

where A_0 is the initial area of the element.

Voigt Notation. We first develop the element equations in Voigt notation, which should be familiar to those who have studied linear finite elements. Those who like more condensed matrix notation can skip directly to that form. In Voigt notation, the displacement field is often written in terms of triangular coordinates as

$$\begin{Bmatrix} u_x \\ u_y \end{Bmatrix} = \begin{bmatrix} \xi_1 & 0 & \xi_2 & 0 & \xi_3 & 0 \\ 0 & \xi_1 & 0 & \xi_2 & 0 & \xi_3 \end{bmatrix} \mathbf{d} = \mathbf{N}\mathbf{d} \tag{E4.1.8}$$

where **d** is the column matrix of nodal displacements, which is given by

$$\mathbf{d}^T = \left[u_{x1}, u_{y1}, u_{x2}, u_{y2}, u_{x3}, u_{y3}\right] \tag{E4.1.9}$$

We will generally not use this form, since it includes many zeroes and write the displacement in a form similar to (E4.4.1). The velocities are obtained by taking the material time derivatives of the displacements, giving

$$\begin{Bmatrix} v_x \\ v_y \end{Bmatrix} = \begin{bmatrix} \xi_1 & 0 & \xi_2 & 0 & \xi_3 & 0 \\ 0 & \xi_1 & 0 & \xi_2 & 0 & \xi_3 \end{bmatrix} \dot{\mathbf{d}} \tag{E4.1.10}$$

$$\dot{\mathbf{d}}^T = \left[v_{x1}, v_{y1}, v_{x2}, v_{y2}, v_{x3}, v_{y3}\right] \tag{E4.1.11}$$

The nodal velocities and nodal forces of the element are shown in Fig. 4.3.

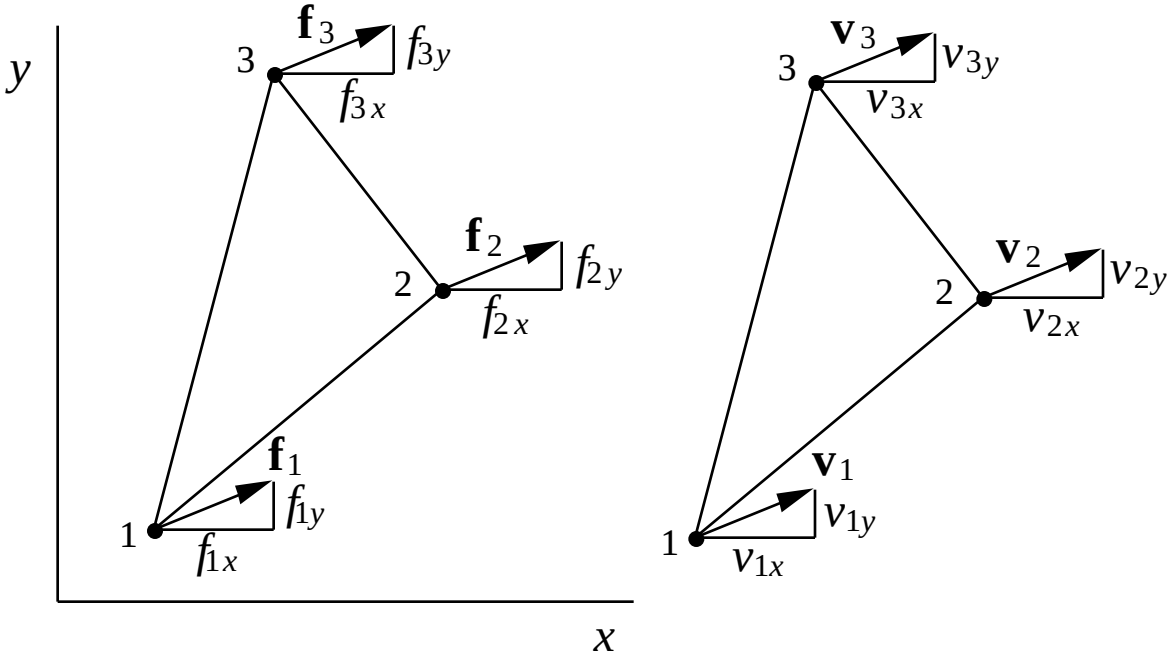

Fig. 4.3. Triangular element showing the nodal force and velocity components.

The rate-of-deformation and stress column matrices in Voigt form are

$$\{\mathbf{D}\} = \begin{Bmatrix} D_{xx} \\ D_{yy} \\ 2D_{xy} \end{Bmatrix} \qquad \{\sigma\} = \begin{Bmatrix} \sigma_{xx} \\ \sigma_{yy} \\ \sigma_{xy} \end{Bmatrix} \tag{E4.1.12}$$

where the factor of 2 on the shear velocity strain is needed in Voigt notation; see the Appendix B. Only the in-plane stresses are needed in either plane stress or plain strain, since $\sigma_{zz} = 0$ in plane stress whereas $D_{zz} = 0$ in plane strain, so $D_{zz}\sigma_{zz}$ makes no contribution to the power in either case. The transverse shear stresses, σ_{xz} and σ_{yz}, and the corresponding components of the rate-of-deformation, D_{xz} and D_{yz}, vanish in both plane stress and plane strain problems.

By the definition of the rate-of-deformation, Equations (3.3.10) and the velocity approximation, we have

$$\begin{aligned} D_{xx} &= \frac{\partial v_x}{\partial x} = \frac{\partial N_I}{\partial x} v_{Ix} \\ D_{yy} &= \frac{\partial v_y}{\partial y} = \frac{\partial N_I}{\partial y} v_{Iy} \\ 2D_{xy} &= \frac{\partial v_x}{\partial y} + \frac{\partial v_y}{\partial x} = \frac{\partial N_I}{\partial y} v_{Ix} + \frac{\partial N_I}{\partial x} v_{Iy} \end{aligned} \tag{E4.1.13}$$

In Voigt notation, the **B** matrix is developed so it relates the rate-of-deformation to the nodal velocities by $\{\mathbf{D}\} = \mathbf{B}\dot{\mathbf{d}}$, so using (E4.1.13) and the formulas for the derivatives of the triangular coordinates (E4.1.5), we have

$$\mathbf{B}_I = \begin{bmatrix} N_{I,x} & 0 \\ 0 & N_{I,y} \\ N_{I,y} & N_{I,x} \end{bmatrix} \qquad [\mathbf{B}] = [\mathbf{B}_1 \quad \mathbf{B}_2 \quad \mathbf{B}_3] = \frac{1}{2A} \begin{bmatrix} y_{23} & 0 & y_{31} & 0 & y_{12} & 0 \\ 0 & x_{32} & 0 & x_{13} & 0 & x_{21} \\ x_{32} & y_{23} & x_{13} & y_{31} & x_{21} & y_{12} \end{bmatrix} \tag{E4.1.14}$$

The internal nodal forces are then given by (4.5.14):

$$\begin{Bmatrix} f_{x1} \\ f_{y1} \\ f_{x2} \\ f_{y2} \\ f_{x3} \\ f_{y3} \end{Bmatrix} = \int_\Omega \mathbf{B}^T \{\sigma\} d\Omega = \int_\Omega \frac{a}{2A} \begin{bmatrix} y_{23} & 0 & x_{32} \\ 0 & x_{32} & y_{23} \\ y_{31} & 0 & x_{13} \\ 0 & x_{13} & y_{31} \\ y_{12} & 0 & x_{21} \\ 0 & x_{21} & y_{12} \end{bmatrix} \begin{Bmatrix} \sigma_{xx} \\ \sigma_{yy} \\ \sigma_{xy} \end{Bmatrix} dA \tag{E4.1.15}$$

where a is the thickness and we have used $d\Omega = a dA$; if we assume that the stresses and thickness a are constant in the element, we obtain

$$\begin{Bmatrix} f_{x1}^{int} \\ f_{y1} \\ f_{x2} \\ f_{y2} \\ f_{x3} \\ f_{y3} \end{Bmatrix} = \frac{a}{2} \begin{bmatrix} y_{23} & 0 & x_{32} \\ 0 & x_{32} & y_{23} \\ y_{31} & 0 & x_{13} \\ 0 & x_{13} & y_{31} \\ y_{12} & 0 & x_{21} \\ 0 & x_{21} & y_{12} \end{bmatrix} \begin{Bmatrix} \sigma_{xx} \\ \sigma_{yy} \\ \sigma_{xy} \end{Bmatrix} \tag{E4.1.16}$$

In the 3-node triangle, the stresses are sometimes not constant within the element; for example, when thermal stresses are included for a linear temperature field, the stresses are linear. In this case, or when the thickness a varies in the element, one-point quadrature is usually adequate. One-point quadrature is equivalent to (E4.1.16) with the stresses and thickness evaluated at the centroid of the element.

Matrix Form based on Indicial Notation. In the following, the expressions for the element are developed using a direct translation of the indicial expression to matrix form. The equations are more compact but not in the form commonly seen in linear finite element analysis.

Rate-of-Deformation. The velocity gradient is given by a matrix form of (4.4.7)

$$\mathbf{L} = \left[L_{ij}\right] = \left[v_{iI}\right]\left[N_{I,j}\right] = \begin{bmatrix} v_{x1} & v_{x2} & v_{x3} \\ v_{y1} & v_{y2} & v_{y3} \end{bmatrix} \frac{1}{2A} \begin{bmatrix} y_{23} & x_{32} \\ y_{31} & x_{13} \\ y_{12} & x_{21} \end{bmatrix} =$$

$$= \frac{1}{2A} \begin{bmatrix} y_{23}v_{x1} + y_{31}v_{x2} + y_{12}v_{x3} & x_{32}v_{x1} + x_{13}v_{x2} + x_{21}v_{x3} \\ y_{23}v_{y1} + y_{31}v_{y2} + y_{12}v_{y3} & x_{32}v_{y1} + x_{13}v_{y2} + x_{21}v_{y3} \end{bmatrix} \tag{E4.1.19}$$

The rate-of-deformation is obtained from the above by (3.3.10):

$$\mathbf{D} = \frac{1}{2}\left(\mathbf{L} + \mathbf{L}^T\right) \tag{E4.1.20}$$

As can be seen from (E4.1.19) and (E4.1.20), the rate-of-deformation is constant in the element; the terms x_{IJ} and y_{IJ} are differences in nodal coordinates, not functions of spatial coordinates.

Internal Nodal Forces. The internal forces are given by (4.5.10) using (E4.1.5) for the derivatives of the shape functions:

$$\mathbf{f}_{int}^T = \left[f_{Ii}\right]^{int} = \begin{bmatrix} f_{1x} & f_{1y} \\ f_{2x} & f_{2y} \\ f_{3x} & f_{3y} \end{bmatrix}^{int} = \int_\Omega \left[N_{I,j}\right]\left[\sigma_{ji}\right] d\Omega = \int_A \frac{1}{2A} \begin{bmatrix} y_{23} & x_{32} \\ y_{31} & x_{13} \\ y_{12} & x_{21} \end{bmatrix} \begin{bmatrix} \sigma_{xx} & \sigma_{xy} \\ \sigma_{xy} & \sigma_{yy} \end{bmatrix} a \, dA \tag{E4.1.21}$$

where a is the thickness. If the stresses and thickness are constant within the element, the integrand is constant and the integral can be evaluated by multiplying the integrand by the volume aA, giving

$$\mathbf{f}_{int}^T = \frac{a}{2}\begin{bmatrix} y_{23} & x_{32} \\ y_{31} & x_{13} \\ y_{12} & x_{21} \end{bmatrix}\begin{bmatrix} \sigma_{xx} & \sigma_{xy} \\ \sigma_{xy} & \sigma_{yy} \end{bmatrix} = \frac{a}{2}\begin{bmatrix} y_{23}\sigma_{xx} + x_{32}\sigma_{xy} & y_{23}\sigma_{xy} + x_{32}\sigma_{yy} \\ y_{31}\sigma_{xx} + x_{13}\sigma_{xy} & y_{31}\sigma_{xy} + x_{13}\sigma_{yy} \\ y_{12}\sigma_{xx} + x_{21}\sigma_{xy} & y_{12}\sigma_{xy} + x_{21}\sigma_{yy} \end{bmatrix} \tag{E4.1.22}$$

This expression gives the same result as Eq. (E4.1.16). It is easy to show that the sums of each of the components of the nodal forces vanish, i.e. the element is in equilibrium. Comparing (E4.1.21) with (E4.1.16), we see that the matrix form of the indicial expression involves fewer multiplications. In evaluating the Voigt form (E4.1.16) involves many multiplications with zero, which slows computations, particularly in the three-dimensional counterparts of these equations. However, the matrix indicial form is difficult to extend to the computation of stiffness matrices, so as will be seen in Chapter 6, the Voigt form is indispensible when stiffness matrices are needed.

Mass Matrix. The mass matrix is evaluated in the undeformed configuration by (4.4.52). The mass matrix is given by

$$\tilde{M}_{IJ} = \int_{\Omega_0} \rho_0 N_I N_J d\Omega_0 = \int_{\Delta} a_0 \rho_0 \xi_I \xi_J J_\xi^0 d\Delta \tag{E4.1.23}$$

where we have used $d\Omega_0 = a_0 J_\xi^0 d\Delta$; the quadrature in the far right expression is over the parent element domain. Putting this in matrix form gives

$$\tilde{\mathbf{M}} = \int_{\Delta} a_0 \rho_0 \begin{bmatrix} \xi_1 \\ \xi_2 \\ \xi_3 \end{bmatrix}\begin{bmatrix} \xi_1 & \xi_2 & \xi_3 \end{bmatrix} J_\xi^0 d\Delta \tag{E4.1.24}$$

where the element Jacobian determinant for the initial configuration of the triangular element is given by $J_\xi^0 = 2A_0$, where A_0 is the initial area. Using the quadrature rule for triangular coordinates, the consistent mass matrix is:

$$\tilde{\mathbf{M}} = \frac{\rho_0 A_0 a_0}{12}\begin{bmatrix} 2 & 1 & 1 \\ 1 & 2 & 1 \\ 1 & 1 & 2 \end{bmatrix} \tag{E4.1.25}$$

The mass matrix can be expanded to full size by using Eq. (4.4.46), $M_{iIjJ} = \delta_{ij}\tilde{M}_{IJ}$ and then using the rule of Eq. (1.4.26), which gives

$$\mathbf{M} = \frac{\rho_0 A_0 a_0}{12}\begin{bmatrix} 2 & 0 & 1 & 0 & 1 & 0 \\ 0 & 2 & 0 & 1 & 0 & 1 \\ 1 & 0 & 2 & 0 & 1 & 0 \\ 0 & 1 & 0 & 2 & 0 & 1 \\ 1 & 0 & 1 & 0 & 2 & 0 \\ 0 & 1 & 0 & 1 & 0 & 2 \end{bmatrix} \tag{E4.1.26}$$

The diagonal or lumped mass matrix can be obtained by the row-sum technique, giving

$$\tilde{\mathbf{M}} = \frac{\rho_0 A_0 a_0}{3}\begin{bmatrix} 1 & 0 & 0 \\ 0 & 1 & 0 \\ 0 & 0 & 1 \end{bmatrix} \tag{E4.1.27}$$

This matrix could also be obtained by simply assigning one third of the mass of the element to each of the nodes.

External Nodal Forces. To evaluate the external forces, an interpolation of these forces is needed. Let the body forces be approximated by linear interpolants expressed in terms of the triangular coordinates as

$$\begin{Bmatrix} b_x \\ b_y \end{Bmatrix} = \begin{bmatrix} b_{x1} & b_{x2} & b_{x3} \\ b_{y1} & b_{y2} & b_{y3} \end{bmatrix}\begin{Bmatrix} \xi_1 \\ \xi_2 \\ \xi_3 \end{Bmatrix} \tag{E4.1.28}$$

Interpretation of Equation (4.4.13) in matrix form then gives

$$\mathbf{f}_{ext}^T = \begin{bmatrix} f_{x1} & f_{x2} & f_{x3} \\ f_{y1} & f_{y2} & f_{y3} \end{bmatrix}^{ext} = \begin{bmatrix} b_{x1} & b_{x2} & b_{x3} \\ b_{y1} & b_{y2} & b_{y3} \end{bmatrix}\int_\Omega \begin{Bmatrix} \xi_1 \\ \xi_2 \\ \xi_3 \end{Bmatrix}\begin{bmatrix} \xi_1 & \xi_2 & \xi_3 \end{bmatrix}\rho a dA \tag{E4.1.29}$$

Using the integration rule for triangular coordinates with the thickness and density considered constant then gives

$$\mathbf{f}_{ext}^T = \frac{\rho A a}{12}\begin{bmatrix} b_{x1} & b_{x2} & b_{x3} \\ b_{y1} & b_{y2} & b_{y3} \end{bmatrix}\begin{bmatrix} 2 & 1 & 1 \\ 1 & 2 & 1 \\ 1 & 1 & 2 \end{bmatrix} \tag{E4.1.30}$$

To illustrate the formula for the computation of the external forces due to a prescribed traction, consider component *i* of the traction to be prescribed between nodes 1 and 2. If we approximate the traction by a linear interpolation, then

$$\bar{t}_i = \bar{t}_{i1}\xi_1 + \bar{t}_{i2}\xi_2 \tag{E4.1.31}$$

The external nodal forces are given by Eq. (4.4.13). We develop a row of the matrix:

$$\begin{bmatrix} f_{i1} & f_{i2} & f_{i3} \end{bmatrix}^{ext} = \int_{\Gamma_{12}} \bar{t}_i N_I d\Gamma = \int_0^1 \left(\bar{t}_{i1}\xi_1 + \bar{t}_{i2}\xi_2\right)\begin{bmatrix} \xi_1 & \xi_2 & \xi_3 \end{bmatrix} a\ell_{12} d\xi_1 \tag{E4.1.32}$$

where we have used $ds = \ell_{12} d\xi_1$; ℓ_{12} is the current length of the side connecting nodes 1 and 2. Along this side, $\xi_2 = 1 - \xi_1$, $\xi_3 = 0$ and evaluation of the integral in (E4.1.32) gives

$$\begin{bmatrix} f_{i1} & f_{i2} & f_{i3} \end{bmatrix}^{ext} = \frac{a\ell_{12}}{6}\begin{bmatrix} 2\bar{t}_{i1}+\bar{t}_{i2} & \bar{t}_{i1}+2\bar{t}_{i2} & 0 \end{bmatrix} \tag{E4.1.33}$$

The nodal forces are nonzero only on the nodes of the side to which the traction is applied. This equation holds for an arbitrary local coordinate system. For an applied pressure, the above would be evaluated with a local coordinate system with one coordinate along the element edge.

Example 4.2. Quadrilateral Element and other Isoparametric 2D Elements. Develop the expressions for the deformation gradient, the rate-of-deformation, the nodal forces and the mass matrix for two-dimensional isoparametric elements. Detailed expressions are given for the 4-node quadrilateral. Expressions for the nodal internal forces are given in matrix form.

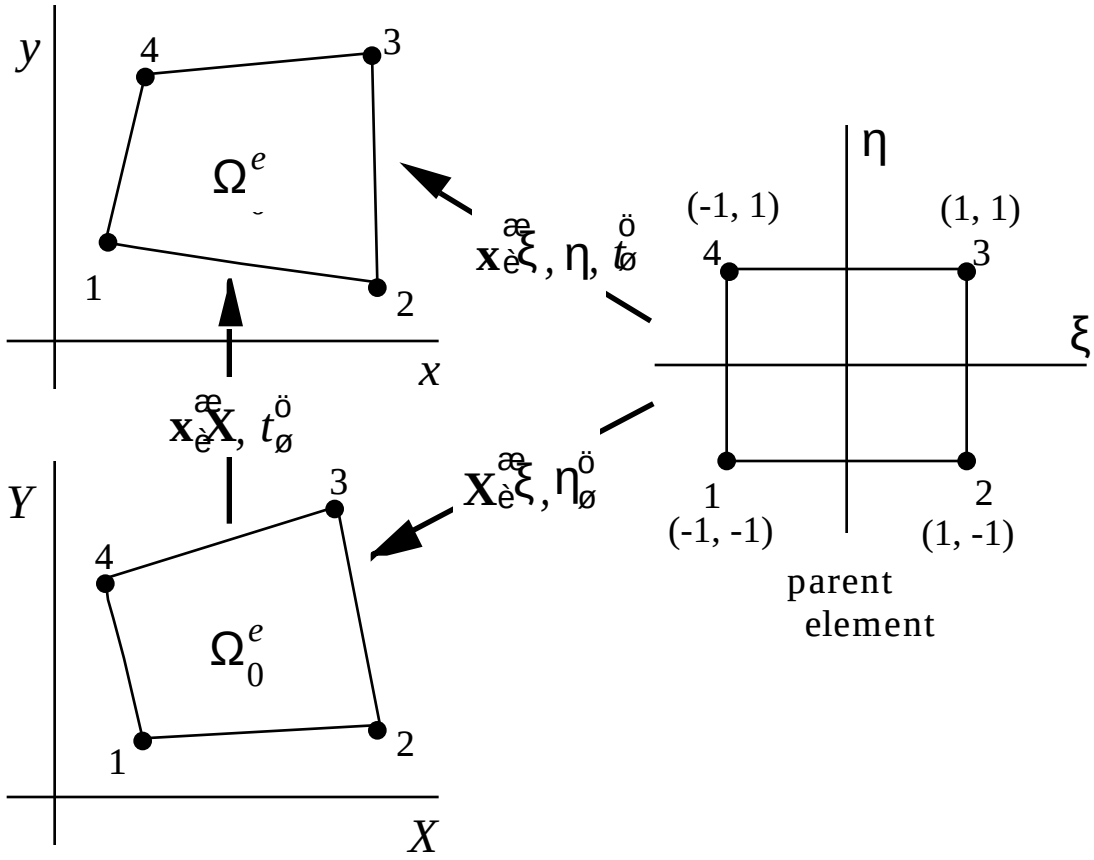

Fig. 4.4. Quadrilateral element in current and initial configurations and the parent domain.

Shape Functions and Nodal Variables. The element shape functions are expressed in terms of the element coordinates (ξ,η). At any time *t*, the spatial coordinates can be expressed in terms of the shape functions and nodal coordinates by

$$\begin{Bmatrix} x(\xi,t) \\ y(\xi,t) \end{Bmatrix} = N_I(\xi)\begin{Bmatrix} x_I(t) \\ y_I(t) \end{Bmatrix}, \quad \xi = \begin{Bmatrix} \xi \\ \eta \end{Bmatrix} \tag{E4.2.1}$$

For the quadrilateral, the isoparametric shape functions are

$$N_I(\xi) = \frac{1}{4}(1+\xi_I\xi)(1+\eta_I\eta) \tag{E4.2.2}$$

where (ξ_I, η_I), I= 1 to 4, are the nodal coordinates of the parent element shown in Fig. 4.4. They are given by

$$[\xi_{iI}] = \begin{bmatrix} \xi_I \\ \eta_I \end{bmatrix} = \begin{bmatrix} -1 & 1 & 1 & -1 \\ -1 & -1 & 1 & 1 \end{bmatrix} \tag{E4.2.3}$$

Since (E4.2.1) also holds for t=0, we can write

$$\begin{Bmatrix} X(\xi) \\ Y(\xi) \end{Bmatrix} = \begin{Bmatrix} X_I \\ Y_I \end{Bmatrix} N_I(\xi) \tag{E4.2.4}$$

where X_I, Y_I are the coordinates in the undeformed configuration. The nodal velocities are given by

$$\begin{Bmatrix} v_x(\xi,t) \\ v_y(\xi,t) \end{Bmatrix} = \begin{Bmatrix} v_{xI}(t) \\ v_{yI}(t) \end{Bmatrix} N_I(\xi) \tag{E4.2.5}$$

which is the material time derivative of the expression for the displacement.

Rate-of-Deformation and Internal Nodal Forces. The map (E4.2.1) is not invertible for the shape functions given by (E4.2.2). Therefore it is impossible to write explicit expressions for the element coordinates in terms of x and y, and the derivatives of the shape functions are evaluated by using implicit differentiation. Referring to (4.4.47) we have

$$N_{I,\mathbf{x}}^T = \begin{bmatrix} N_{I,x} & N_{I,y} \end{bmatrix} = N_{I,\xi}^T \mathbf{x}_{,\xi}^{-1} = \begin{bmatrix} N_{I,\xi} & N_{I,\eta} \end{bmatrix} \begin{bmatrix} \xi_{,x} & \xi_{,y} \\ \eta_{,x} & \eta_{,y} \end{bmatrix} \tag{E4.2.6}$$

The Jacobian of the current configuration with respect to the element coordinates is given by

$$\mathbf{x}_{,\xi} = \begin{bmatrix} x_{,\xi} & x_{,\eta} \\ y_{,\xi} & y_{,\eta} \end{bmatrix} = [x_{iI}][\partial N_I/\partial \xi_j] = \begin{Bmatrix} x_I \\ y_I \end{Bmatrix} \begin{bmatrix} N_{I,\xi} & N_{I,\eta} \end{bmatrix} = \begin{bmatrix} x_I N_{I,\xi} & x_I N_{I,\eta} \\ y_I N_{I,\xi} & y_I N_{I,\eta} \end{bmatrix} \tag{E4.2.7a}$$

For the 4-node quadrilateral the above is

$$\mathbf{x}_{,\xi} = \sum_{I=1}^{4} \begin{bmatrix} x_I(t)\xi_I(1+\eta_I\eta) & x_I(t)\eta_I(1+\xi_I\xi) \\ y_I(t)\xi_I(1+\eta_I\eta) & y_I(t)\eta_I(1+\xi_I\xi) \end{bmatrix} \tag{E4.2.7b}$$

In the above, the summation has been indicated explicitly because the index I appears three times. As can be seen from the RHS, the Jacobian matrix is a function of time. The inverse of $\mathbf{F}_\xi$ is given by

$$\mathbf{x}_{,\xi}^{-1} = \frac{1}{J_\xi}\begin{bmatrix} y_{,\eta} & -x_{,\eta} \\ -y_{,\xi} & x_{,\xi} \end{bmatrix} \quad J_\xi = x_{,\xi}y_{,\eta} - x_{,\eta}y_{,\xi} \tag{E4.2.7c}$$

The gradients of the shape functions for the 4-node quadrilateral with respect to the element coordinates are given by

$$\mathbf{N}_{,\xi}^T = \left[\partial N_I/\partial\xi_i\right] = \begin{bmatrix} \partial N_1/\partial\xi & \partial N_1/\partial\eta \\ \partial N_2/\partial\xi & \partial N_2/\partial\eta \\ \partial N_3/\partial\xi & \partial N_3/\partial\eta \\ \partial N_4/\partial\xi & \partial N_4/\partial\eta \end{bmatrix} = \frac{1}{4}\begin{bmatrix} \xi_1(1+\eta_1\eta) & \eta_1(1+\xi_1\xi) \\ \xi_2(1+\eta_2\eta) & \eta_2(1+\xi_2\xi) \\ \xi_3(1+\eta_3\eta) & \eta_3(1+\xi_3\xi) \\ \xi_4(1+\eta_4\eta) & \eta_4(1+\xi_4\xi) \end{bmatrix}$$

The gradients of the shape functions with respect to the spatial coordinates can then be computed by

$$B_I = N_{I,\mathbf{x}}^T = N_{I,\xi}^T\mathbf{x}_{,\xi}^{-1} = \begin{bmatrix} \xi_1(1+\eta_1\eta) & \eta_1(1+\xi_1\xi) \\ \xi_2(1+\eta_2\eta) & \eta_2(1+\xi_2\xi) \\ \xi_3(1+\eta_3\eta) & \eta_3(1+\xi_3\xi) \\ \xi_4(1+\eta_4\eta) & \eta_4(1+\xi_4\xi) \end{bmatrix}\frac{1}{J_\xi}\begin{bmatrix} y_{,\eta} & -y_{,\xi} \\ -x_{,\eta} & x_{,\xi} \end{bmatrix} \tag{E4.2.8a}$$

and the velocity gradient is given by Eq. (4.5.3)

$$\mathbf{L} = \mathbf{v}_I B_I^T = \mathbf{v}_I N_{I,\mathbf{x}}^T \tag{E4.2.8b}$$

For a 4-node quadrilateral which is not rectangular, the velocity gradient, and hence the rate-of-deformation, is a rational function because $J_\xi = det\left(\mathbf{x}_{,\xi}\right)$ appears in the denominator of $\mathbf{x}_{,\xi}$ and hence in $\mathbf{L}$. The determinant J_ξ is a linear function in (ξ,η).

The nodal internal forces are obtained by (4.5.6), which gives

$$\left(\mathbf{f}_I^{int}\right)^T = \begin{bmatrix} f_{xI} & f_{yI} \end{bmatrix}^{int} = \int_\Omega B_I^T\sigma d\Omega = \int_\Omega \begin{bmatrix} N_{I,x} & N_{I,y} \end{bmatrix}\begin{bmatrix} \sigma_{xx} & \sigma_{xy} \\ \sigma_{xy} & \sigma_{yy} \end{bmatrix} d\Omega \tag{E4.2.9}$$

The integration is performed over the parent domain. For this purpose, we use

$$d\Omega = J_\xi a d\xi d\eta \tag{E4.2.10}$$

where a is the thickness. The internal forces are then given by (4.4.11), which when written out for two dimensions gives:

$$\left(\mathbf{f}_I^{int}\right)^T = \begin{bmatrix} f_{xI} & f_{yI} \end{bmatrix}^{int} = \int_\Delta \begin{bmatrix} N_{I,x} & N_{I,y} \end{bmatrix}\begin{bmatrix} \sigma_{xx} & \sigma_{xy} \\ \sigma_{xy} & \sigma_{yy} \end{bmatrix} a J_\xi d\Delta \tag{E4.2.11}$$

where $N_{I,i}$ is given in Eq. (E4.2.8a). Equation (E4.2.14) applies to any isoparametric element in two dimensions. The integrand is a rational function of the element coordinates, since J_ξ appears in the denominator (see Eq. (4.2.8a)), so analytic quadrature of the above is not feasible. Therefore numerical quadrature is generally used. For the 4-node quadrilateral, 2x2 Gauss quadrature is full quadrature. However, for full quadrature, as discussed in Chapter 8, the element locks for incompressible and nearly incompressible materials in plane strain problems. Therefore, selective-reduced quadrature as described in Section 4.5.4, in which the volumetric stress is underintegrated, must be used for the four-node quadrilateral for plane strain problems when the material response is nearly incompressible, as in elastic-plastic materials.

The displacement for a 4-node quadrilateral is linear along each edge. Therefore, the external nodal forces are identical to those for the 3-node triangle, see Eqs. (E4.1.29-E4.1.33).

Mass Matrix. The consistent mass matrix is obtained by using (4.4.52), which gives

$$\tilde{\mathbf{M}} = \int_{\Omega_0} \begin{bmatrix} N_1 \\ N_2 \\ N_3 \\ N_4 \end{bmatrix} \begin{bmatrix} N_1 & N_2 & N_3 & N_4 \end{bmatrix} \rho_0 \, d\Omega_0 \tag{E4.2.12}$$

We use

$$d\Omega_0 = J_\xi^0(\xi,\eta) a_0 \, d\xi \, d\eta \tag{E4.2.13}$$

where $J_\xi^0(\xi,\eta)$ is the determinant of the Jacobian of the transformation of the parent element to the initial configuration a_0 is the thickness of the undeformed element. The expression for $\tilde{\mathbf{M}}$ when evaluated in the parent domain is given by

$$\tilde{\mathbf{M}} = \int_{-1}^{+1}\int_{-1}^{+1} \begin{bmatrix} N_1^2 & N_1N_2 & N_1N_3 & N_1N_4 \\ & N_2^2 & N_2N_3 & N_2N_4 \\ \textit{symmetric} & & N_3^2 & N_3N_4 \\ & & & N_4^2 \end{bmatrix} \rho_0 a_0 J_\xi^0(\xi,\eta) \, d\xi \, d\eta \tag{E4.2.14}$$

The matrix is evaluated by numerical quadrature. This mass matrix can be expanded to an 8x8 matrix using the same procedure described for the triangle in the previous example.

A lumped, diagonal mass matrix can be obtained by using Lobatto quadrature with the quadrature points coincident with the nodes. If we denote the integrand of Eq. (E4.2.14) by $\mathbf{m}(\xi_I,\eta_I)$, then Lobatto quadrature gives

$$\overline{\mathbf{M}} = \sum_{I=1}^{4} \mathbf{m}(\xi_I,\eta_I) \tag{E4.2.15}$$

Alternatively, the lumped mass matrix can be obtained by apportioning the total mass of the element equally among the four nodes. The total mass is $\rho_0 A_0 a_0$ when a_0 is constant, so dividing it among the four nodes gives

$$\overline{\mathbf{M}} = \frac{1}{4}\rho_0 A_0 a_0 \mathbf{I}_4 \tag{E4.2.16}$$

where $\mathbf{I}_4$ is the unit matrix of order 4.

Example 4.3. Three Dimensional Isoparametric Element. Develop the expressions for the rate-of-deformation, the nodal forces and the mass matrix for three dimensional isoparametric elements. An example of this class of elements, the eight-node hexahedron, is shown in Fig. 4.5.

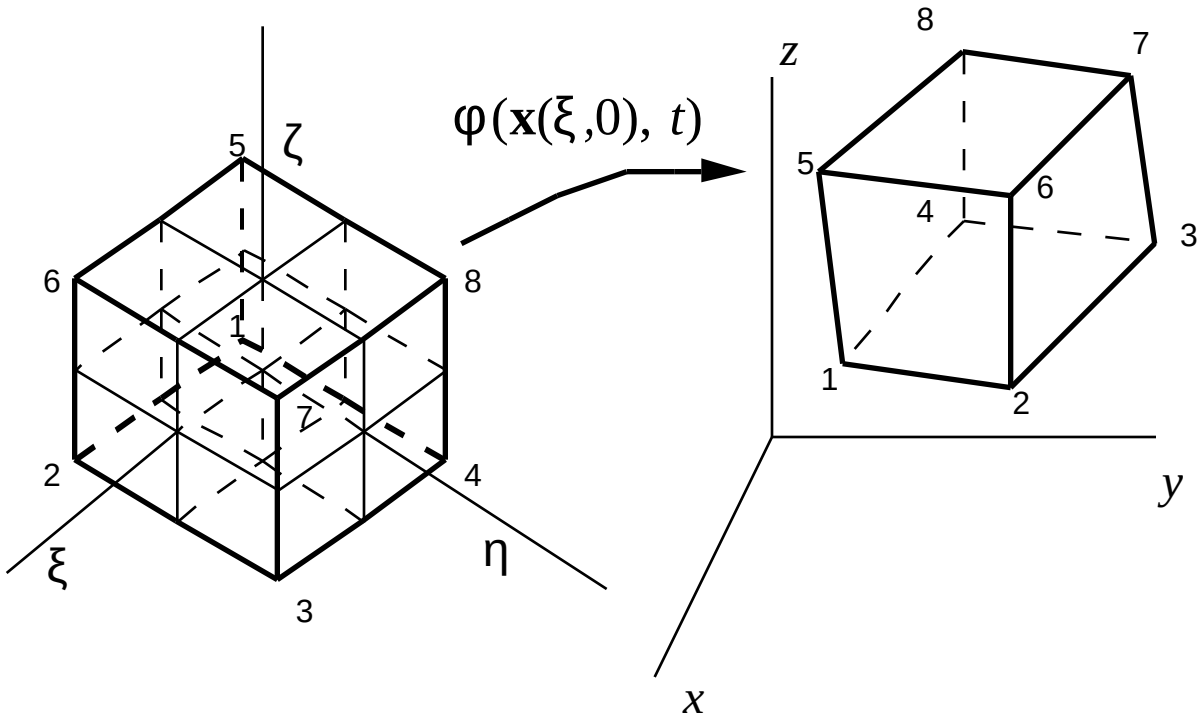

Fig. 4.5. Parent element and current configuration for an 8-node hexahedral element.

Motion and Strain Measures. The motion of the element is given by

$$\begin{bmatrix} x \\ y \\ z \end{bmatrix} = N_I(\xi) \begin{bmatrix} x_I(t) \\ y_I(t) \\ z_I(t) \end{bmatrix} \qquad \xi = (\xi, \eta, \zeta) \tag{E4.3.1}$$

where the shape functions for particular elements are given in Appendix C. Equation (E4.3.1) also holds at time t=0, so

$$\begin{Bmatrix} X \\ Y \\ Z \end{Bmatrix} = N_I(\xi) \begin{Bmatrix} X_I \\ Y_I \\ Z_I \end{Bmatrix} \tag{E4.3.2}$$

The velocity field is given by

$$\begin{Bmatrix} v_x \\ v_y \\ v_z \end{Bmatrix} = N_I(\xi) \begin{Bmatrix} v_{xI} \\ v_{yI} \\ v_{zI} \end{Bmatrix} \tag{E4.3.3}$$

The velocity gradient is obtained from Eq. (4.5.3), giving

$$B_I^T = \begin{bmatrix} N_{I,x} & N_{I,y} & N_{I,z} \end{bmatrix} \tag{E4.3.4}$$

$$\mathbf{L} = \mathbf{v}_I B_I^T = \begin{Bmatrix} v_{xI} \\ v_{yI} \\ v_{zI} \end{Bmatrix} \begin{bmatrix} N_{I,x} & N_{I,y} & N_{I,z} \end{bmatrix} \tag{E4.3.5}$$

$$= \begin{bmatrix} v_{xI}N_{I,x} & v_{xI}N_{I,y} & v_{xI}N_{I,z} \\ v_{yI}N_{I,x} & v_{yI}N_{I,y} & v_{yI}N_{I,z} \\ v_{zI}N_{I,x} & v_{zI}N_{I,y} & v_{zI}N_{I,z} \end{bmatrix} \tag{E4.3.6}$$

The derivatives with respect to spatial coordinates are obtained in terms of derivatives with respect to the element coordinates by Eq. (4.4.37).

$$N_{I,\mathbf{x}}^T = N_{I,\xi}^T \mathbf{x}_{,\xi}^{-1} \tag{E4.3.7}$$

$$\mathbf{x}_{,\xi} \equiv \mathbf{F}_\xi \, \mathbf{x}_{,\xi} = \mathbf{x}_I N_{I,\xi}^T = \begin{Bmatrix} x_I \\ y_I \\ z_I \end{Bmatrix} \begin{bmatrix} N_{I,\xi} & N_{I,\eta} & N_{I,\zeta} \end{bmatrix} \tag{E4.3.8}$$

The deformation gradient can be computed by Eqs. (3.2.10), (E4.3.1) and (E4.3.7):

$$\mathbf{F} = \frac{\partial \mathbf{x}}{\partial \mathbf{X}} = \mathbf{x}_I N_{I,\mathbf{X}} = \mathbf{x}_I N_{I,\xi}^T \mathbf{X}_{,\xi}^{-1} \equiv \mathbf{x}_I N_{I,\xi}^T \left(\mathbf{F}_\xi^0 \right)^{-1} \tag{E4.3.9}$$

where

$$\mathbf{X}_{,\xi} \equiv \mathbf{F}_\xi^0 = \mathbf{X}_I N_{I,\xi}^T \tag{E4.3.10}$$

The Green strain is then computed by Eq. (3.3.5); a more accurate procedure is described in Example 4.12.

Internal Nodal Forces. The internal nodal forces are obtained by Eq. (4.5.6):

$$\left(\mathbf{f}_I^{int}\right)^T = \left[f_{xI},\, f_{yI},\, f_{zI} \right]^{int} = \int_\Omega B_I^T \sigma \, d\Omega = \int_\Delta \begin{bmatrix} N_{I,x} & & \\ & N_{I,y} & \\ & & N_{I,z} \\ N_{I,y} & N_{I,x} & \\ & N_{I,z} & N_{I,y} \\ N_{I,z} & & N_{I,x} \end{bmatrix} \begin{Bmatrix} \sigma_{xx} \\ \sigma_{yy} \\ \sigma_{zz} \\ \sigma_{xy} \\ \sigma_{yz} \\ \sigma_{xz} \end{Bmatrix} J_\xi \, d\Delta \qquad \text{(E4.3.11)}$$

The integral is evaluated by numerical quadrature, using the quadrature formula (4.5.26).

External Nodal Forces. We consider first the nodal forces due to the body force. By Eq. (4.4.13), we have

$$f_{iI}^{ext} = \int_\Omega N_I \rho b_i \, d\Omega = \int_\Delta N_I(\xi) \rho(\xi) b_i(\xi) J_\xi \, d\Delta \qquad \text{(E4.3.12a)}$$

$$\begin{Bmatrix} f_{xI} \\ f_{yI} \\ f_{zI} \end{Bmatrix}^{ext} = \int_{-1}^{1}\int_{-1}^{1}\int_{-1}^{1} N_I(\xi) \rho(\xi) \begin{Bmatrix} b_x(\xi) \\ b_y(\xi) \\ b_z(\xi) \end{Bmatrix} J_\xi \, d\xi \, d\eta \, d\zeta \qquad \text{(E4.3.12b)}$$

where we have transformed the integral to the parent domain. The integral over the parent domain is evaluated by numerical quadrature.

To obtain the external nodal forces due to an applied pressure $\mathbf{t} = -p\mathbf{n}$, we consider a surface of the element. For example, consider the external surface corresponding with the parent element surface $\zeta = -1$; see Fig. 4.6. The nodal forces for any other surface are constructed similarly.

On any surface, any dependent variable can be expressed as a function of two parent coordinates, in this case they are ξ and η. The vectors $\mathbf{x}_{,\xi}$ and $\mathbf{x}_{,\eta}$ are tangent to the surface. The vector $\mathbf{x}_{,\xi} \times \mathbf{x}_{,\eta}$ is in the direction of the normal $\mathbf{n}$ and as shown in any advanced calculus text, its magnitude is the surface Jacobian, so we can write

$$p\mathbf{n}\, d\Gamma = p\left(\mathbf{x}_{,\xi} \times \mathbf{x}_{,\eta}\right) d\xi \, d\eta \qquad \text{(E4.3.13)}$$

For a pressure load, only the normal component of the traction is nonzero. The nodal external forces are then given by

$$f_{iI}^{ext} = \int_\Gamma t_i N_I \, d\Gamma = -\int_\Gamma p n_i N_I \, d\Gamma = -\int_{-1}^{1}\int_{-1}^{1} p \, e_{ijk} x_{j,\xi} x_{k,\eta} N_I \, d\xi \, d\eta \qquad \text{(E4.3.14)}$$

where we have used (E4.3.13) in indicial form in the last step. In matrix form the above is

$$\mathbf{f}_I^{ext} = -\int_\Gamma p N_I \mathbf{x}_{,\xi} \times \mathbf{x}_{,\eta} \, d\Gamma \qquad \text{(E4.3.16)}$$

We have used the convention that the pressure is positive in compression. We can expand the above by using Eq. (4.4.1) to express the tangent vectors in terms of the shape functions and writing the cross product in determinant form, giving

$$\mathbf{f}_I^{ext} = f_{xI}\mathbf{e}_x + f_{yI}\mathbf{e}_y + f_{zI}\mathbf{e}_z = -\int_{-1}^{1}\int_{-1}^{1} pN_I \det \begin{bmatrix} \mathbf{e}_x & \mathbf{e}_y & \mathbf{e}_z \\ x_J N_{J,\xi} & y_J N_{J,\xi} & z_J N_{J,\xi} \\ x_K N_{K,\eta} & y_K N_{K,\eta} & z_K N_{K,\eta} \end{bmatrix} d\xi d\eta \qquad \text{(E4.3.17)}$$

This integral can readily be evaluated by numerical quadrature over the loaded surfaces of the parent element.

Example 4.4. Axisymmetric Quadrilateral. The expressions for the rate-of-deformation and the nodal forces for the axisymmetric quadrilateral element are developed. The element is shown in Fig. 4.7. The domain of the element is the volume swept out by rotating the quadrilateral 2π radians about the axis of symmetry, the z-axis. The expressions in indicial notation, Eqs. (4.5.3) and (4.5.6), are not directly applicable since they do not apply to curvilinear coordinates.

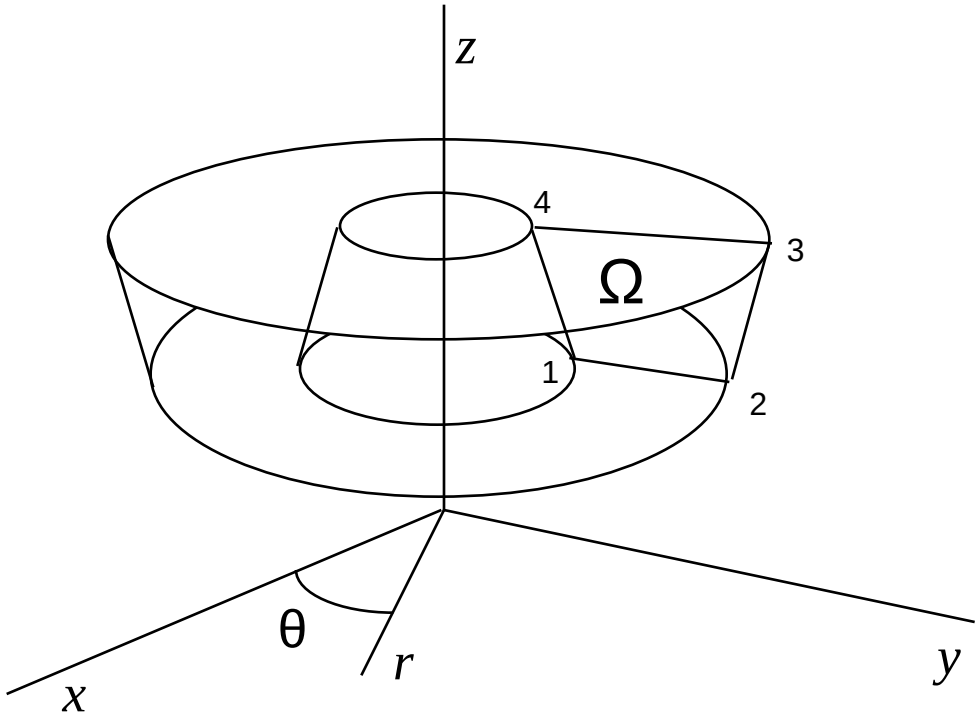

Fig. 4.7. Current configuration of quadrilateral axisymmetric element; the element consists of the volume generated by rotating the quadrilateral 2π radians about the z-axis.

In this case, the isoparametric map relates the cylindrical coordinates $[r,\ z]$ to the parent element coordinates $[\xi,\ \eta]$:

$$\begin{Bmatrix} r(\xi,\eta,t) \\ z(\xi,\eta,t) \end{Bmatrix} = \begin{Bmatrix} r_I(t) \\ z_I(t) \end{Bmatrix} N_I(\xi,\eta) \qquad \text{(E4.4.1)}$$

where the shape functions N_I are given in (E4.2.20. The expression for the rate-of-deformation is based on standard expressions of the gradient in cylindrical coordinates (the expression are identical to the expressions for the linear strain):

$$\begin{Bmatrix} D_r \\ D_z \\ D_\theta \\ 2D_{rz} \end{Bmatrix} = \begin{bmatrix} \frac{\partial}{\partial r} & 0 \\ 0 & \frac{\partial}{\partial z} \\ \frac{1}{r} & 0 \\ \frac{\partial}{\partial z} & \frac{\partial}{\partial r} \end{bmatrix} \begin{Bmatrix} v_r \\ v_z \end{Bmatrix} = \begin{bmatrix} \frac{\partial v_r}{\partial r} \\ \frac{\partial v_z}{\partial z} \\ \frac{v_r}{r} \\ \frac{\partial v_r}{\partial z} + \frac{\partial v_z}{\partial r} \end{bmatrix} \tag{E4.4.2}$$

The conjugate stress is

$$\{\sigma\}^T = [\sigma_r, \sigma_z, \sigma_\theta, \sigma_{rz}] \tag{E4.4.3}$$

The velocity field is given by

$$\begin{Bmatrix} v_r \\ v_z \end{Bmatrix} = N_I(\xi,\eta) \begin{Bmatrix} v_{rI} \\ v_{zI} \end{Bmatrix} = \begin{bmatrix} N_1 & 0 & N_2 & 0 & N_3 & 0 & N_4 & 0 \\ 0 & N_1 & 0 & N_2 & 0 & N_3 & 0 & N_4 \end{bmatrix} \dot{\mathbf{d}} \tag{E4.4.4}$$

$$\dot{\mathbf{d}}^T = [v_{r1}, v_{z1}, v_{r2}, v_{z2}, v_{r3}, v_{z3}, v_{r4}, v_{z4}] \tag{E4.4.5}$$

The submatrices of the **B** matrix are given from Eq. (E4.4.2) by

$$[B]_I = \begin{bmatrix} \frac{\partial N_I}{\partial r} & 0 \\ 0 & \frac{\partial N_I}{\partial z} \\ \frac{N_I}{r} & 0 \\ \frac{\partial N_I}{\partial z} & \frac{\partial N_I}{\partial r} \end{bmatrix} \tag{E4.4.6}$$

The derivatives in (E4.4.6) now have to be expressed in terms of derivates with respect to the parent element coordinates. Rather than obtaining these with a matrix product, we just write out the expressions using (E4.2.7c) with *x,y* replaced by *r,z,* which gives

$$\frac{\partial N_I}{\partial r} = \frac{1}{J_\xi}\left(\frac{\partial z}{\partial \eta}\frac{\partial N_I}{\partial \xi} - \frac{\partial r}{\partial \eta}\frac{\partial N_I}{\partial \eta}\right) \tag{E4.4.7a}$$

$$\frac{\partial N_I}{\partial z} = \frac{1}{J_\xi}\left(\frac{\partial r}{\partial \xi}\frac{\partial N_I}{\partial \eta} - \frac{\partial z}{\partial \xi}\frac{\partial N_I}{\partial \xi}\right) \tag{E4.4.7b}$$

where

$$\frac{\partial z}{\partial \eta} = z_I \frac{\partial N_I}{\partial \eta} \qquad \frac{\partial z}{\partial \xi} = z_I \frac{\partial N_I}{\partial \xi} \tag{E4.4.8a}$$

$$\frac{\partial r}{\partial \eta} = r_I \frac{\partial N_I}{\partial \eta} \qquad \frac{\partial r}{\partial \xi} = r_I \frac{\partial N_I}{\partial \xi} \tag{E4.4.8b}$$

The nodal forces are obtained from (4.5.14), which yields

$$\mathbf{f}_I^{int} = \int_\Omega \mathbf{B}_I^T \{\sigma\}\, d\Omega = 2\pi \int_\Delta \mathbf{B}_I^T \{\sigma\}\, J_\xi r\, d\Delta \tag{E4.4.9}$$

where $\mathbf{B}_I$ is given by (E4.4.6) and we have used $d\Omega = 2\pi r J_\xi d\Delta$ where r is given by Eq. (E4.4.1). The factor 2π is often omitted from all nodal forces, i.e. the element is taken to be the volume generated by sweeping the quadrilateral by one radian about the z-axis in Fig. 4.7.

Example 4.5. Master-Slave Tieline. A master slave tieline is shown in Figure 4.5. Tielines are frequently used to connect parts of the mesh which use different element sizes, for they are more convenient than connecting the elements of different sizes by triangles or tetrahedra. Continuity of the motion across the tieline is enforced by constraining the motion of the slave nodes to the linear field of the adjacent edge connecting the master nodes. In the following, the resulting nodal forces and mass matrix are developed by the transformation rules of Section 4.5.5.

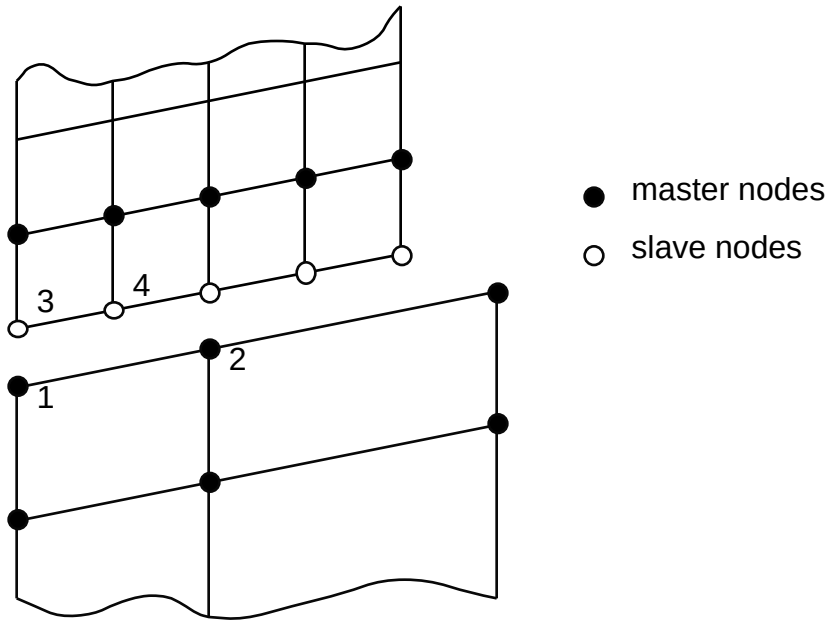

Fig. 4.8. Exploded view of a tieline; when joined together, the velocites of nodes 3 and 5 equal the nodal velocities of nodes 1 and 2 and the velocity of node 4 is given in terms of nodes 1 and 2 by a linear constraint.

The slave node velocities are given by the kinematic constraint that the velocities along the two sides of the tieline must remain compatible, i.e. C^0. This constraint can be expressed as a linear relation in the nodal velocities, so the relation corresponding to Eq. (4.5.35) can be written as

$$\begin{Bmatrix} \hat{\mathbf{v}}_M \\ \hat{\mathbf{v}}_S \end{Bmatrix} = \begin{bmatrix} \mathbf{I} \\ \mathbf{A} \end{bmatrix} \{\mathbf{v}_M\} \qquad \text{so} \qquad \mathbf{T} = \begin{bmatrix} \mathbf{I} \\ \mathbf{A} \end{bmatrix} \tag{E4.5.1}$$

where the matrix $\mathbf{A}$ is obtained from the linear constraint and the superposed hats indicate the velocities of the disjoint model before the two sides are tied together. We denote the nodal forces of the disjoint model at the slave nodes and master nodes by $\hat{\mathbf{f}}_S$ and $\hat{\mathbf{f}}_M$, respectively. Thus, $\hat{\mathbf{f}}_S$ is the matrix of nodal forces assembled from the elements on the slave side of the tieline and $\hat{\mathbf{f}}_M$ is the matrix of nodal forces assembled from the elements on the master side of the tieline. The nodal forces for the joined model are then given by Eq. (4.5.36):

$$\{\mathbf{f}_M\} = \mathbf{T}^T \begin{Bmatrix} \hat{\mathbf{f}}_M \\ \hat{\mathbf{f}}_S \end{Bmatrix} = \begin{bmatrix} \mathbf{I} & \mathbf{A}^T \end{bmatrix} \begin{Bmatrix} \hat{\mathbf{f}}_M \\ \hat{\mathbf{f}}_S \end{Bmatrix} \tag{E4.5.2}$$

where $\mathbf{T}$ is given by (E4.5.1). As can be seen from the above, the master nodal forces are the sum of the master nodal forces for the disjoint model and the transformed slave node forces. These formulas apply to both the external and internal nodal forces.

The consistent mass matrix is given by Eq. (4.5.39):

$$\mathbf{M} = \mathbf{T}^T \mathbf{M} \mathbf{T} = \begin{bmatrix} \mathbf{I} & \mathbf{A}^T \end{bmatrix} \begin{bmatrix} \mathbf{M}_M & 0 \\ 0 & \mathbf{M}_s \end{bmatrix} \begin{bmatrix} \mathbf{I} \\ \mathbf{A} \end{bmatrix} = \mathbf{M}_M + \mathbf{A}^T \mathbf{M}_s \mathbf{A} \tag{E4.5.3}$$

We illustrate these transformations in more detail for the 5 nodes which are numbered in Fig. 4.8. The elements are 4-node quadrilaterals, so the velocity along any edge is linear. Slave nodes 3 and 5 are coincident with master nodes 1 and 2, and slave node 4 is at a distance $\xi\ell$ from node 1, where $\ell = \|\mathbf{x}_2 - \mathbf{x}_1\|$. Therefore,

$$\mathbf{v}_3 = \mathbf{v}_1, \quad \mathbf{v}_5 = \mathbf{v}_2, \quad \mathbf{v}_4 = \xi \mathbf{v}_2 + (1-\xi)\mathbf{v}_1 \tag{E4.5.4}$$

and Eq. (E4.5.1) can be written as

$$\begin{Bmatrix} \mathbf{v}_1 \\ \mathbf{v}_2 \\ \mathbf{v}_3 \\ \mathbf{v}_4 \\ \mathbf{v}_5 \end{Bmatrix} = \begin{bmatrix} \mathbf{I} & \mathbf{0} \\ \mathbf{0} & \mathbf{I} \\ \mathbf{I} & 0 \\ (1-\xi)\mathbf{I} & \xi\mathbf{I} \\ 0 & \mathbf{I} \end{bmatrix} \begin{Bmatrix} \mathbf{v}_1 \\ \mathbf{v}_2 \end{Bmatrix} \qquad \mathbf{T} = \begin{bmatrix} \mathbf{I} & \mathbf{0} \\ \mathbf{0} & \mathbf{I} \\ \mathbf{I} & 0 \\ (1-\xi)\mathbf{I} & \xi\mathbf{I} \\ 0 & \mathbf{I} \end{bmatrix} \tag{E4.5.5}$$

The nodal forces are then given by

$$\begin{bmatrix}\mathbf{f}_1\\ \mathbf{f}_2\end{bmatrix} = \begin{bmatrix}\mathbf{I} & \mathbf{0} & \mathbf{I} & (1-\xi)\mathbf{I} & \mathbf{0}\\ \mathbf{0} & \mathbf{I} & \mathbf{0} & \xi\mathbf{I} & \mathbf{I}\end{bmatrix}\begin{Bmatrix}\hat{\mathbf{f}}_1\\ \hat{\mathbf{f}}_2\\ \hat{\mathbf{f}}_3\\ \hat{\mathbf{f}}_4\\ \hat{\mathbf{f}}_5\end{Bmatrix} \tag{E4.5.6}$$

The force for master node 1 is

$$\mathbf{f}_1 = \hat{\mathbf{f}}_1 + \hat{\mathbf{f}}_3 + (1-\xi)\hat{\mathbf{f}}_5 \tag{E4.5.7}$$

Both components of the nodal force transform identically; the transformation applies to both internal and external nodal forces. The mass matrix is transformed by Eq. (4.5.39) using **T** as given in Eq. (E4.5.1).

If the two lines are only tied in the normal direction, a local coordinate system needs to be set up at the nodes to write the linear constraint. The normal components of the nodal forces are then related by a relation similar to Eq. (4.5.7), whereas the tangential components remain independent.

4.6 COROTATIONAL FORMULATIONS

In structural elements such as bars, beams and shells, it is awkward to deal with fixed coordinate systems. Consider for example a rotating rod such as shown in Fig. 3.6. Initially, the only nonzero stress is σ_x, whereas σ_y vanishes. Subsequently, as the rod rotates it is awkward to express the state of uniaxial stress in a simple way in terms of the global components of the stress tensor.

A natural approach to overcoming this difficulty is to embed a coordinate system in the bar and rotate the embedded system with the rod. Such coordinate systems are known as *corotational coordinates*. For example, consider a coordinate system, $\hat{\mathbf{x}} = [\hat{x}, \hat{y}]$ for a rod so that $\hat{x}$ always connects nodes 1 and 2, as shown in Fig. 4.9. A uniaxial state of stress can then always be described by the condition that $\hat{\sigma}_y = \hat{\sigma}_{xy} = 0$ and that $\hat{\sigma}_x$ is nonzero. Similarly the rate-of-deformation of the rod is described by the component $\hat{D}_x$.

There are two approaches to corotational finite element formulations:

1. a coordinate system is embedded at each quadrature point and rotated with material in some sense.
2. a coordinate system is embedded in an element and rotated with the element.

The first procedure is valid for arbitrarily large strains and large rotations. A major consideration in corotational formulations lies in defining the rotation of the material. The polar decomposition theorem can be used to define a rotation which is independent of the coordinate system. However, when particular directions of the material have a large stiffness which must be represented accurately, the rotation provided by a polar decomposition does not necessarily provide the best rotation for a Cartesian coordinate system; this is illustrated in Chapter 5.

A remarkable aspect of corotational theories is that although the corotational coordinate is defined only at discrete points and is Cartesian at these points, the resulting finite element

formulation accurately reproduces the behavior of shells and other complex structures. Thus, by using a corotational formulation in conjunction with a "degenerated continuum" approximation, the complexities of curvilinear coordinate formulations of shells can be avoided. This is further discussed in Chapter 9, since this is particularly attractive for the nonlinear analysis of shells.

For some elements, such as a rod or the constant strain triangle, the rigid body rotation is the same throughout the element. It is then sufficient to embed a single coordinate system in the element. For higher order elements, if the strains are small, the coordinate system can be embedded so that it does not rotate exactly with the material as described later. For example, the corotational coordinate system can be defined to be coincident to one side of the element. If the rotations relative to the embedded coordinate system are of order θ, then the error in the strains is of order θ^2. Therefore, as long as θ^2 is small compared to the strains, a single embedded coordinate system is adequate. These applications are often known as *small-strain, large rotation* problems; see Wempner (1969) and Belytschko and Hsieh(1972).

The components of a vector $\mathbf{v}$ in the corotational system are related to the global components by

$$\hat{v}_i = R_{ji} v_j \quad \text{or} \quad \hat{\mathbf{v}} = \mathbf{R}^{\mathrm{T}}\mathbf{v} \quad \text{and} \quad \mathbf{v} = \mathbf{R}\hat{\mathbf{v}} \tag{4.6.1}$$

where $\mathbf{R}$ is an orthogonal transformation matrix defined in Eqs. (3.2.24-25) and the superposed "^" indicates the corotational components.

The corotational components of the finite element approximation to the velocity field can be written as

$$\hat{v}_i(\xi, t) = N_I(\xi)\hat{v}_{iI}(t) \tag{4.6.2}$$

This expression is identical to (4.4.32) except that it pertains to the corotational components. Equation (4.6.2) can be obtained from (4.4.32) by multiplying both sides by $\mathbf{R}^T$.

The corotational components of the velocity gradient tensor are given by

$$\hat{L}_{ij} = \frac{\partial \hat{v}_i}{\partial \hat{x}_j} = \frac{\partial N_I(\xi)}{\partial \hat{x}_j}\hat{v}_{iI}(t) = \hat{B}_{jI}\hat{v}_{iI} \quad \text{or} \quad \hat{\mathbf{L}} = \hat{\mathbf{v}}_I \frac{\partial N_I}{\partial \hat{\mathbf{x}}} = \hat{\mathbf{v}}_I N_{I,\hat{\mathbf{x}}}^T = \hat{\mathbf{v}}_I \hat{B}_I^T \tag{4.6.3}$$

where

$$\hat{B}_{jI} = \frac{\partial N_I}{\partial \hat{x}_j} \tag{4.6.4}$$

The corotational rate-of-deformation tensor is then given by

$$\hat{D}_{ij} = \frac{1}{2}\left(\hat{L}_{ij} + \hat{L}_{ji}\right) = \frac{1}{2}\left(\frac{\partial \hat{v}_i}{\partial \hat{x}_j} + \frac{\partial \hat{v}_j}{\partial \hat{x}_i}\right) \tag{4.6.5}$$

The corotational formulation is used only for the evaluation of internal nodal forces. The external nodal forces and the mass matrix are sually evaluated in the global system as before. The

the semi-discrete equations of motion are treated in terms of global components. We therefore concern ourselves only with the evaluation of the internal nodal forces in the corotational formulation.

The expression for $\hat{\mathbf{f}}_I^{int}$ in terms of corotational components is developed as follows. We start with the standard expression for the nodal internal forces, Eq. (4.5.5):

$$f_{iI}^{int} = \int_\Omega \frac{\partial N_I}{\partial x_j}\sigma_{ji}\, d\Omega \qquad \text{or} \qquad \left(\mathbf{f}_I^{int}\right)^T = \int_\Omega N_{I,\mathbf{x}}^T \sigma\, d\Omega \tag{4.6.6}$$

By the chain rule and Eq. (4.6.1)

$$\frac{\partial N_I}{\partial x_j} = \frac{\partial N_I}{\partial \hat{x}_k}\frac{\partial \hat{x}_k}{\partial x_j} = \frac{\partial N_I}{\partial \hat{x}_k} R_{jk} \qquad \text{or} \qquad N_{I,\mathbf{x}} = \mathbf{R} N_{I,\hat{\mathbf{x}}} \tag{4.6.7}$$

Substituting the transformation for the Cauchy stress into the corotational stress, Box 3.2, and Eq. (4.6.7) into Eq. (4.6.6), we obtain

$$\left(\mathbf{f}_I^{int}\right)^T = \int_\Omega N_{I,\hat{\mathbf{x}}}^T \mathbf{R}^T \mathbf{R}\hat{\sigma}\mathbf{R}^T d\Omega \tag{4.6.8}$$

and using the orthogonality of **R**, we have

$$\left(\mathbf{f}_I^{int}\right)^T = \int_\Omega N_{I,\hat{\mathbf{x}}}^T \hat{\sigma}\mathbf{R}^T d\Omega \qquad \text{or} \qquad \left[\, f_{iI}^{int}\right]^T = f_{Ii}^{int} = \int_\Omega \frac{\partial N_I}{\partial \hat{x}_j}\hat{\sigma}_{jk} R_{ki}^T d\Omega \tag{4.6.9}$$

Comparing the above to the standard expression for the nodal internal forces, (4.6.5), we can see that the expressions are similar, but the stress is expressed in the corotational system and the rotation matrix **R** now appears. In the expression on the right, the indices on $\mathbf{f}^{int}$ have been exchanged so that the expression can be converted to matrix form.

If we use the $\hat{B}$ matrix defined by Eq. (4.6.4) we can write

$$\left(\mathbf{f}_I^{int}\right)^T = \int_\Omega \hat{B}_I^T \hat{\sigma}\mathbf{R}^T d\Omega \qquad\qquad \mathbf{f}_{int}^T = \int B^T \hat{\sigma}\mathbf{R}^T d\Omega \tag{4.6.10}$$

Corresponding relations for the internal nodal forces can be developed in Voigt notation:

$$\mathbf{f}_I^{int} = \int_\Omega \mathbf{R}^T \hat{\mathbf{B}}_I^T \left\{\hat{\sigma}\right\} d\Omega \qquad \text{where} \qquad \left\{\hat{\mathbf{D}}\right\} = \hat{\mathbf{B}}_I \hat{\mathbf{v}}_I \tag{4.6.11}$$

and $\hat{\mathbf{B}}_I$ is obtained from $\hat{\boldsymbol{B}}_I$ by the Voigt rule.

The rate of the corotational Cauchy stress is objective (frame-invariant), so the constitutive equation can be expressed directly as a relationship between the rate of the corotational Cauchy stress and the corotational rate-of-deformation

$$\frac{D\hat{\sigma}}{Dt} = S^{\hat{\sigma}\hat{D}}\left(\hat{\mathbf{D}}, \hat{\sigma}, \, etc\right) \tag{4.6.12}$$

In particular, for hypoelastic material,

$$\frac{D\hat{\sigma}}{Dt} = \hat{\mathbf{C}} : \hat{\mathbf{D}} \qquad \text{or} \qquad \frac{D\hat{\sigma}_{ij}}{Dt} = \hat{C}_{ijkl}\hat{D}_{kl} \tag{4.6.13}$$

where the elastic response matrix is also expressed in terms of the corotational components. An attractive feature of the above relation is that the $\hat{\mathbf{C}}$ matrix for anisotropic materials need not be changed to reflect rotations. Since the coordinate system rotates with the material, material rotation has no effect on $\hat{\mathbf{C}}$. On the other hand, for an anisotropic material, the $\mathbf{C}$ matrix changes as the material rotates.

Example 4.6. Rods in Two Dimensions. A two-node element is shown in Fig. 4.9. The element uses linear displacement and velocity fields. The corotational coordinate $\hat{x}$ is chosen to coincide with the axis of the element at all times as shown. Obtain an expression for the corotational rate-of-deformation and the internal nodal forces. Then the methodology is extended to a three-node rod.

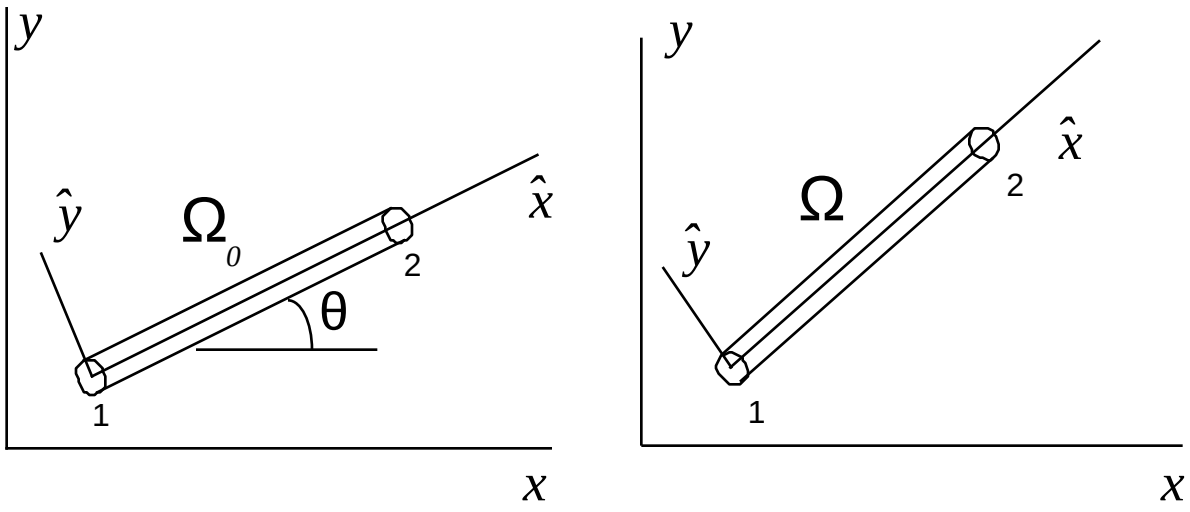

Fig. 4.9. Two-node rod element showing initial configuration and current configuration and the corotational coordinate.

The displacement and velocity fields are linear in $\hat{x}$ and given by

$$\begin{bmatrix} x \\ y \end{bmatrix} = \begin{bmatrix} x_1 & x_2 \\ y_1 & y_2 \end{bmatrix} \begin{bmatrix} 1-\xi \\ \xi \end{bmatrix}$$

$$\begin{bmatrix} \hat{v}_x \\ \hat{v}_y \end{bmatrix} = \begin{bmatrix} \hat{v}_{x1} & \hat{v}_{x2} \\ \hat{v}_{y1} & \hat{v}_{y2} \end{bmatrix} \begin{bmatrix} 1-\xi \\ \xi \end{bmatrix} \tag{E4.6.1}$$

$$\xi = \frac{\hat{x}}{\ell}$$

where ℓ is the current length of the element. The corotational velocities are related to the global components by the vector transformation Eq. (E4.6.1):

$$\begin{bmatrix} v_{xI} \\ v_{yI} \end{bmatrix} = \mathbf{R} \begin{bmatrix} \hat{v}_{xI} \\ \hat{v}_{yI} \end{bmatrix}, \quad \mathbf{R} = \begin{bmatrix} R_{x\hat{x}} & R_{x\hat{y}} \\ R_{y\hat{x}} & R_{y\hat{y}} \end{bmatrix} = \begin{bmatrix} \cos\theta & -\sin\theta \\ \sin\theta & \cos\theta \end{bmatrix} \frac{1}{\ell} \begin{bmatrix} x_{21} & -y_{21} \\ y_{21} & x_{21} \end{bmatrix} \tag{E4.6.2}$$

A state of uniaxial stress is assumed; the only nonzero stress is $\hat{\sigma}_x$ which is the stress along the axis of the bar element. Since $\hat{x}$ rotates with the bar element, $\hat{\sigma}_x$ is the axial stress for any orientation of the element. Only the axial component of the rate-of-deformation tensor, $\hat{D}_x$, contributes to the internal power. It is given the derivative of the velocity field (E4.6.1):

$$\hat{D}_x = \frac{\partial \hat{v}_x}{\partial \hat{x}} = \left[N_{I,\hat{x}} \right] \begin{bmatrix} \hat{v}_{x1} \\ \hat{v}_{x2} \end{bmatrix} = \frac{1}{\ell} \left[-1 \quad +1 \right] \begin{bmatrix} \hat{v}_{x1} \\ \hat{v}_{x2} \end{bmatrix} = \hat{\mathbf{B}} \hat{\mathbf{v}} \qquad \hat{\mathbf{B}} = \left[N_{I,\hat{x}} \right] = \frac{1}{\ell} \left[-1 \quad +1 \right] \tag{E4.6.3}$$

Nodal Internal Forces. The nodal internal forces are obtained from Eq. (4.6.8), which can be rewritten as

$$\left[\mathbf{f}_{Ii} \right]^{int} = \int_\Omega \frac{\partial N_I}{\partial \hat{x}_j} \hat{\sigma}_{jk} R^T_{ki} \, d\Omega = \int_\Omega \frac{\partial N_I}{\partial \hat{x}} \hat{\sigma}_{xx} R^T_{\hat{x}i} \, d\Omega = \int_\Omega \hat{\mathbf{B}}^T \hat{\sigma}_{xx} R^T_{\hat{x}i} \, d\Omega \tag{E4.6.4}$$

where the second expression omits the many zeros which appear in the more general expression; the subscripts on the internal nodal forces have been interchanged. Substituting (E4.6.2) and (E4.6.3) into the above gives

$$\left[f_{Ii} \right]^{int} = \int \frac{1}{\ell} \begin{bmatrix} -1 \\ +1 \end{bmatrix} \hat{\sigma}_x \left[\cos\theta \quad \sin\theta \right] d\Omega \tag{E4.6.6}$$

If we assume the stress is constant in the element, we can evaluate the integral by multiplying the integral by the volume of the element, $V = A\ell$, which gives

$$\left[f_{Ii} \right]^{int} = \begin{bmatrix} f_{1x} & f_{1y} \\ f_{2x} & f_{2y} \end{bmatrix} = A \hat{\sigma}_x \begin{bmatrix} -\cos\theta & -\sin\theta \\ \cos\theta & \sin\theta \end{bmatrix} \tag{E4.6.7}$$

The above result shows that the nodal forces are along the axis of the rod and equal and opposite at the two nodes.

The stress-strain law in this element is computed in the corotational system. Thus, the rate form of the hypoelastic law is

$$\frac{D\hat{\sigma}_x}{Dt} = E\hat{D}_x \tag{E4.6.8}$$

where E is a tangent modulus in uniaxial stress. The rotation terms which appear in the objective rates are not needed, since the coordinate system is corotational.

To evaluate the nodal forces, the current cross-sectional area A must be known. The change in area can then be expressed in terms of the transverse strains; the exact formula depends on the shape of the cross-section. For a rectangular cross-section

$$\dot{A} = A\left(\hat{D}_y + \hat{D}_z\right) \tag{E4.6.9a}$$

Computation of internal nodal forces from one-dimensional rod. The internal nodal forces can also be obtained by computing the corotational components as in Example 2.8.1, Eq. (E2.2.8) and then transforming by Eq. (4.5.40). In the corotational system, the nodal forces are given by Eq. (E2.8.8), so we write this equation in the corotational system:

$$\hat{\mathbf{f}}^{int} = \begin{Bmatrix} \hat{f}_{x1} \\ \hat{f}_{x2} \end{Bmatrix}^{int} = \int_\Omega \frac{1}{l}\begin{bmatrix} -1 \\ +1 \end{bmatrix} \hat{\sigma}_x A dx \tag{E4.6.10}$$

Since the we are considering a slender rod with no stiffness normal to its axis, the transverse snodal forces vanish, i.e. $\hat{f}_{y1} = \hat{f}_{y2} = 0$.

Voigt notation. In Voigt procedures, the element equations are usually developed by starting with the equations in the local, corotational cooordinates. The global components of the nodal forces can then be obtained by the transformation equations, (4.5.40). We first define $\mathbf{T}$ by relating the local degrees-of-freedom (which are conjugate to $\hat{\mathbf{f}}^{int}$) to the four degrees-of-freedom of the element:

$$\begin{Bmatrix} \hat{v}_{x1} \\ \hat{v}_{x2} \end{Bmatrix} = \begin{bmatrix} \cos\theta & \sin\theta & 0 & 0 \\ 0 & 0 & \cos\theta & \sin\theta \end{bmatrix} \begin{Bmatrix} v_{x1} \\ v_{y1} \\ v_{x2} \\ v_{y2} \end{Bmatrix} \quad \text{so} \quad \mathbf{T} = \begin{bmatrix} \cos\theta & \sin\theta & 0 & 0 \\ 0 & 0 & \cos\theta & \sin\theta \end{bmatrix} \tag{E4.6.11}$$

which defines the $\mathbf{T}$ matrix. Using Eq. (4.5.36), $\mathbf{f} = \mathbf{T}^T\hat{\mathbf{f}}$, and assuming the stress is constant in the element then gives

$$\mathbf{f}^{int} = \begin{Bmatrix} f_{x1} \\ f_{y1} \\ f_{x2} \\ f_{y2} \end{Bmatrix}^{int} = \mathbf{T}^T\mathbf{f}^{int} = \begin{bmatrix} \cos\theta & 0 \\ \sin\theta & 0 \\ 0 & \cos\theta \\ 0 & \sin\theta \end{bmatrix} A\hat{\sigma}_x \begin{Bmatrix} -1 \\ 1 \end{Bmatrix} = A\hat{\sigma}_x \begin{Bmatrix} -\cos\theta \\ -\sin\theta \\ \cos\theta \\ \sin\theta \end{Bmatrix} \tag{E4.6.12}$$

which is identical to (E4.6.7).

Three-Node Element. We consider the three-node curved rod element shown in Fig. 4.10. The configurations, displacement, and velocity are given by quadratic fields. The expression for the nodal internal forces will be developed by the corotational approach.

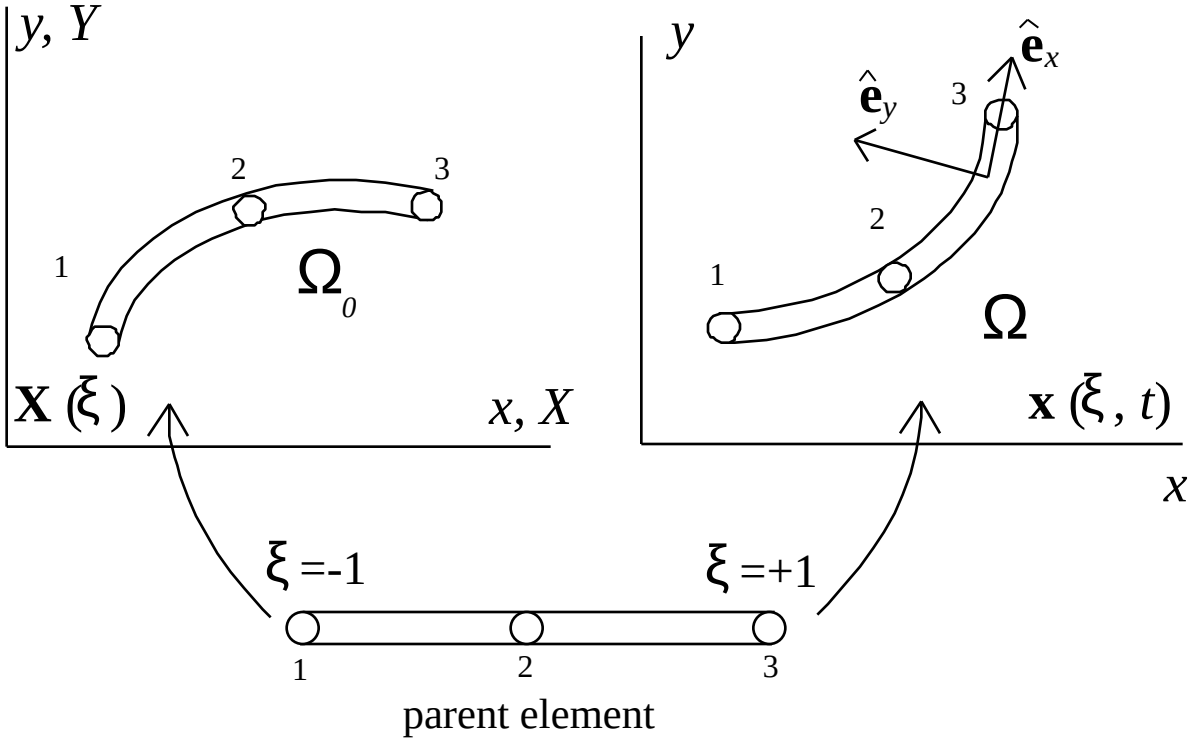

Fig. 4.10. Initial, current, and parent elements for a three-node rod; the corotational base vector $\hat{\mathbf{e}}_x$ is tangent to the current configuration.

The initial and current configurations are given by

$$\mathbf{X}(\xi,t)=\mathbf{X}_I(t)N_I(\xi) \qquad \mathbf{x}(\xi,t)=\mathbf{x}_I(t)N_I(\xi) \tag{E4.6.13}$$

where

$$[N_I]=\begin{bmatrix}\frac{1}{2}\xi(\xi-1) & 1-\xi^2 & \frac{1}{2}\xi(\xi+1)\end{bmatrix} \tag{E4.6.14}$$

The displacement and velocity are given by

$$\mathbf{u}(\xi,t)=\mathbf{u}_I(t)N_I(\xi) \qquad \mathbf{v}(\xi,t)=\mathbf{v}_I(t)N_I(\xi) \tag{E4.6.15}$$

The corotational system is defined at each point of the rod (in practice it is needed only at the quadrature points). Let $\hat{\mathbf{e}}_x$ be tangent to the rod, so

$$\hat{e}_x = \frac{\mathbf{x}_{,\xi}}{\left\|\mathbf{x}_{,\xi}\right\|} \text{ where } \mathbf{x}_{,\xi} = \mathbf{x}_I N_{I,\xi}(\xi) \tag{E4.6.16}$$

The normal to the element is given by

$$\hat{\mathbf{e}}_y = \mathbf{e}_z \times \hat{\mathbf{e}}_x \text{ where } \mathbf{e}_z = [0,\ 0,\ 1] \tag{E4.6.17}$$

The rate of deformation is given by

$$\hat{D}_x = \frac{\partial \hat{v}_x}{\partial \hat{x}} = \frac{\partial \hat{v}_x}{\partial \xi}\frac{\partial \xi}{\partial \hat{x}} = \frac{1}{\left\|\mathbf{x}_{,\xi}\right\|}\frac{\partial \hat{v}_x}{\partial \xi} \quad \textit{must be explained-may be wrong} \tag{E4.6.18}$$

From Eq. (E4.6.15) and Eq. (E4.6.18)

$$\hat{v}_x = N_I(\xi)\left(R_{x\hat{x}} v_{xI} + R_{y\hat{x}} v_{yI}\right) \tag{E4.6.19}$$

the rate-of-deformation is given by

$$\hat{D}_x = \frac{1}{\left\|\mathbf{x}_{,\xi}\right\|} N_{I\xi}(\xi) \begin{Bmatrix} v_{xI} \\ v_{yI} \end{Bmatrix} \tag{E4.6.20}$$

The above shows the $\hat{B}_I$ matrix to be

$$\hat{B}_I = \frac{1}{\left\|\mathbf{x}_{,\xi}\right\|} N_{I\xi} \tag{E4.6.21}$$

The nodal internal forces are then given by

$$\left(\mathbf{f}_I^{int}\right)^T = \left[f_{xI} \quad f_{yI}\right]^{int} = \int_{-1}^{1} A\hat{B}_I \hat{\sigma}_x \left\|\mathbf{x}_{,\xi}\right\| \left[R_{x\hat{x}} \quad R_{y\hat{x}}\right] d\xi \tag{E4.6.22}$$

An interesting feature of the above development is that it avoids curvilinear tensors completely. However, the rate-of-deformation as computed here is correct; Exercize ?? shows how Eq. (E4.6.20) reproduces the correct result for a curved bar.

Example 4.7. Triangular Element. Develop the expression for the velocity strain and the nodal internal forces for a three-node triangle using the corotational approach.

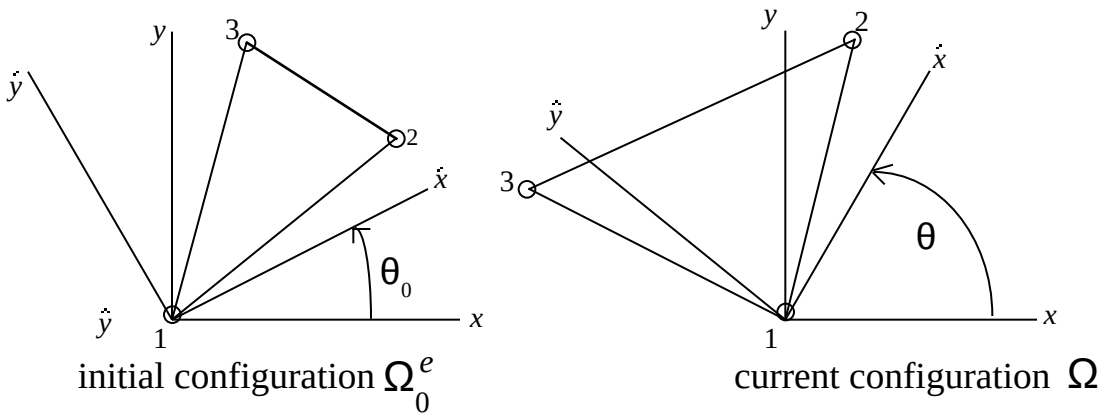

Fig. 4.11 Triangular three-node element treated by corotational coordinate system.

The element in its initial and current configurations is shown in Fig. 4.11. The corotational system is initially at an angle of θ_0 with the global coordinate system; in the following, θ_0 is often chosen to vanish, but for an anistropic material it may be desirable to orient the initial $\hat{x}$-axis in a direction of anisotropy, for example, in a composite material it may be useful to orient $\hat{x}$ in a fiber direction. The current angle of the corotational coordinate system is θ. We discuss how to compute this angle subsequently.

The motion can be expressed in terms of the triangular coordinates, as in Example 4.1.

$$\begin{Bmatrix} x \\ y \end{Bmatrix} = \begin{bmatrix} x_1 & x_2 & x_3 \\ y_1 & y_2 & y_3 \end{bmatrix} \begin{Bmatrix} \xi_1 \\ \xi_2 \\ \xi_3 \end{Bmatrix} \tag{E4.7.1}$$

The displacement and velocity fields in the element are then given by

$$\begin{Bmatrix} \hat{u}_x \\ \hat{u}_y \end{Bmatrix} = \begin{bmatrix} \hat{u}_{x1} & \hat{u}_{x2} & \hat{u}_{x3} \\ \hat{u}_{y1} & \hat{u}_{y2} & \hat{u}_{y3} \end{bmatrix} \begin{Bmatrix} \xi_1 \\ \xi_2 \\ \xi_3 \end{Bmatrix} \tag{E4.7.2}$$

$$\begin{Bmatrix} \hat{v}_x \\ \hat{v}_y \end{Bmatrix} = \begin{bmatrix} \hat{v}_{x1} & \hat{v}_{x2} & \hat{v}_{x3} \\ \hat{v}_{y1} & \hat{v}_{y2} & \hat{v}_{y3} \end{bmatrix} \begin{Bmatrix} \xi_1 \\ \xi_2 \\ \xi_3 \end{Bmatrix} \tag{E4.7.3}$$

The derivatives of the shape functions with respect to the corotational coordinate system are given by the counterpart of (E4.1.5):

$$\left[\partial N_I / \partial \hat{x}_j\right] \equiv \left[\partial \xi_I / \partial \hat{x}_j\right] = \frac{1}{2A} \begin{bmatrix} \hat{y}_{23} & \hat{x}_{32} \\ \hat{y}_{31} & \hat{x}_{13} \\ \hat{y}_{12} & \hat{x}_{21} \end{bmatrix} \equiv \hat{B} \tag{E4.7.4}$$

The corotational components of the rate-of-deformation are given by

$$\hat{\mathbf{D}} = \tfrac{1}{2}\left(\hat{B}_I \mathbf{v}_I^T + \mathbf{v}_I \hat{B}_I^T\right) \tag{E4.7.5}$$

The nodal internal forces are given by Eq. (4.6.10):

$$\left[f_{Ii} \right]^{int} = \int_\Omega \hat{B}_{Ij}\, \hat{\sigma}_{jk} R_{ki}^T d\Omega = \int_\Omega \frac{\partial \xi_I}{\partial \hat{x}_j} \hat{\sigma}_{jk} R_{ki}^T d\Omega \tag{E4.7.6}$$

Writing out the matrices using (E4.6.2) and (E4.7.4) gives

$$\begin{bmatrix} f_{1x} & f_{1y} \\ f_{2x} & f_{2y} \\ f_{3x} & f_{3y} \end{bmatrix}^{int} = \int_A \frac{1}{2A} \begin{bmatrix} \hat{y}_{23} & \hat{x}_{32} \\ \hat{y}_{31} & \hat{x}_{13} \\ \hat{y}_{12} & \hat{x}_{21} \end{bmatrix} \begin{bmatrix} \hat{\sigma}_x & \hat{\sigma}_{xy} \\ \hat{\sigma}_{xy} & \hat{\sigma}_y \end{bmatrix} \begin{bmatrix} \cos\theta & \sin\theta \\ -\sin\theta & \cos\theta \end{bmatrix} a\, dA \tag{E4.7.7}$$

The rotation of the coordinate system can be obtained in several ways:

1. by polar decomposition;
2. by rotating the corotational coordinate system with a material line in the element, e.g. a preferred direction in a composite;
3. by rotating the corotational coordinate system with a side of the element (this is only correct for small strain problems).

To use polar decomposition, the same approach as described in Section 3, Example ?? is used.

4.7. TOTAL LAGRANGIAN FORMULATION

4.7.1. Governing Equations. The physical principles which govern the total Lagrangian formulation are the same as those for the updated Lagrangian formulation, which were given in Section 4.2. The form of the governing equations is different, but as has been seen in Chapter 3, they express the same physical principles and can be obtained by transforming the associated conservation equations from Eulerian to Lagrangian form.

Similarly, the finite element equations for the total Lagrangian formulation can be obtained by transforming the equations for the updated Lagrangian formulation. It is only necessary to transform the integrals to the reference (undeformed) domain and transform the stress and strain measures to the Lagrangian type. This approach is used in Section 4.7.2, and for most readers Section 4.7.2 and the following examples will suffice as an introduction to the total Lagrangian formulation. However, for readers who would like to see the entire structure of the total Lagrangian formulation or prefer to learn it first, Section 4.8 gives a development of the weak form in the total Lagrangian description, followed by the direct derivation of the finite element equations from this weak form.

The governing equations are given in both tensor form and indicial form in Box 4.5. We have chosen to use the nominal stress **P** in the momentum equation, because the resulting momentum equation and its weak form are simpler than for the PK2 stress. However, the nominal stress is awkward in constitutive equations because of its lack of symmetry, so we have used the PK2 stress for constitutive equations. Once the PK2 stress has been evaluated by the constitutive

equations, the nominal stress stress can then easily be obtained by a transformation given in Box 3.2, Eq. (B4.5.5). The constitutive equation can relate the Cauchy stress σ to the rate-of-deformation **D**. The stress would then be converted to the nominal stress **P** prior to evaluation of the nodal forces. However, this entails additional transformations and hence additional computational expense, so when the constitutive equations are expressed in terms of σ it is advantageous to use the updated Lagrangian formulation.

Box 4.5
Governing Equations For Total Lagrangian Formulation

conservation of mass

$$\rho J = \rho_0 J_0 = \rho_0 \tag{B4.5.1}$$

conservation of linear momentum

$$_X \ \mathbf{P} + \rho_0 \mathbf{b} = \rho_0 \ddot{\mathbf{u}} \quad \text{or} \quad \frac{\partial P_{ji}}{\partial X_j} + \rho_0 b_i = \rho_0 \ddot{u}_i \tag{B4.5.2}$$

conservation of angular momentum:

$$\mathbf{F} \ \mathbf{P} = \mathbf{P}^T \ \mathbf{F}^T \quad \text{or} \quad F_{ij} P_{jk} = F_{kj} P_{ji} \tag{B4.5.3}$$

conservation of energy

$$\rho_0 \dot{w}^{int} = \dot{\mathbf{F}}^T : \mathbf{P} - \ _X \ \bar{\mathbf{q}} + \rho_0 s \quad \text{or} \quad \rho_0 \dot{w}^{int} = \dot{F}_{ij} P_{ji} - \frac{\partial \bar{q}_i}{\partial X_i} + \rho_0 s \tag{B4.5.4}$$

where $\bar{\mathbf{q}} = J\mathbf{F}^{-1}\mathbf{q}$

constitutive equation

$$\mathbf{S} = \boldsymbol{S}(\mathbf{E}, .. etc) \qquad \mathbf{P} = \mathbf{S} \ \mathbf{F}^T \tag{B4.5.5}$$

measure of strain

$$\mathbf{E} = \frac{1}{2}\left(\mathbf{F}^T \ \mathbf{F} - \mathbf{I}\right) \quad \text{or} \quad E_{ij} = \frac{1}{2}\left(F_{ki} F_{kj} - \delta_{ij}\right) \tag{B4.5.6}$$

boundary conditions

$$n_j^0 P_{ji} = \bar{t}_i^0 \quad \text{or} \quad \mathbf{e}_i \ \mathbf{n}^0 \ \mathbf{P} = \mathbf{e}_i \ \bar{\mathbf{t}}_0 \quad \text{on} \quad \Gamma_{t_i}^0, \quad u_i = \bar{u}_i \quad \text{on} \quad \Gamma_{u_i}^0 \tag{B4.5.7}$$

$$\Gamma_{t_i}^0 \quad \Gamma_{u_i}^0 = \Gamma^0 \quad \Gamma_{t_i}^0 \cap \Gamma_{u_i}^0 = 0 \quad \text{for i = 1 to } n_s \tag{B4.5.8}$$

initial conditions

$$\mathbf{P}(\mathbf{X},0) = \mathbf{P}_0(\mathbf{X}) \quad \text{in} \tag{B4.5.9}$$

$$\mathbf{u}(\mathbf{X},0) = \mathbf{u}_0(\mathbf{X}) \tag{B4.5.10}$$

internal continuity conditions

$$\langle n_j^0 P_{ji} \rangle = 0 \quad \text{on } \Gamma_{int}^0 \tag{B4.5.11}$$

The nominal stress is conjugate to the material time derivative of the deformation tensor, $\dot{\mathbf{F}}$, see Box 3.4. Thus in (B4.5.4) the internal work is expressed in terms of these two tensors. Note that we have used the left divergence of $\mathbf{P}$ (see (B.5.1.2)), so $\mathbf{n}^0$ appears before $\mathbf{P}$ in the traction expression; if the order is reversed the resulting matrix corresponds to the transpose of $\mathbf{P}$, which is the PK1 stress; see Section 3.4.1. The PK1 stress is also frequently used, so it is important to note the distinction between these two stress tensors. The traction is obtained in terms of the nominal stress by putting the initial normal to the left, and the left divergence operator is used in the momentum equation. For the PK1 stress, the normal appears to the right and the right divergence is used in the momentum equation.

The deformation tensor $\mathbf{F}$ is not suitable as a measure of strain in constitutive equations since it does not vanish in rigid body rotation. Therefore constitutive equations in total Lagrangian formulations are usually formulated in terms of the Green strain tensor $\mathbf{E}$, which can be obtained from $\mathbf{F}$. In the continuum mechanics literature, one often sees constitutive equations expressed as $\mathbf{P} = \mathbf{P}(\mathbf{F})$, which gives the impression that the constitutive equation uses $\mathbf{F}$ as a measure of strain. In fact, when writing $\mathbf{P(F)}$, it is implicit that the constitutive stress depends on $\mathbf{F}^T\mathbf{F}$ (i.e., $\mathbf{E} + \mathbf{I}$, where the unit matrix $\mathbf{I}$ makes no difference) or some other measure of deformation which is independent of rigid body rotation. Similarly, the nominal stress $\mathbf{P}$ in constitutive equations is incorporated so it satisfies conservation of angular momentum, Eq. (B4.5.3).

As in any mechanical system, the same component of traction and displacement cannot be prescribed at any point of a boundary, but one of these must be prescribed; see Eqs. (B4.5.7-B4.5.8). In the Lagrangian formulation, tractions are prescribed in units of force per undeformed area.

The total Lagrangian formulation can be obtained in two ways:

1. transforming the finite element equations for the updated Lagrangian fomulation to the initial (reference) configuration and expressing it in terms of Lagrangian variables.
2. by developing the weak form in terms of the initial configuration and Lagrangian variables and then using this weak form to obtain discrete equations.

We will begin with the first approach since it is quicker and more convenient. The second approach is only recommended for intensive courses or for those who prefer the total Lagrangian formulation.

4.7.2. Total Lagrangian Finite Element Equations by Transformation. To obtain the discrete finite element equations for total Lagrangian formulation, we will transform each of the

nodal force expressions in the updated Lagrangian formulation, beginning with the internal nodal forces. The mass conservation equation (B4.5.1), $\rho J = \rho_0$, and the relation

$$d\Omega = J d\Omega_0 \tag{4.7.1}$$

will also be used. The internal nodal forces are given in the updated Lagrangian formulation by Eq. (4.4.10)

$$f_{iI}^{int} = \int_\Omega \frac{\partial N_I}{\partial x_j} \sigma_{ji} d\Omega \tag{4.7.2}$$

Using the transformation from Box 3.2, $J\sigma_{ji} = F_{jk} P_{ki} = \dfrac{\partial x_j}{\partial X_k} P_{ki}$, we convert (4.7.2) to:

$$f_{iI}^{int} = \int_\Omega \frac{\partial N_I}{\partial x_j} \frac{\partial x_j}{\partial X_k} P_{ki} J^{-1} d\Omega \tag{4.7.3}$$

Recognizing that the product of the first two terms is a chain rule expression of $\partial N_I / \partial X_k$ and using Eq. (4.7.1), we get

$$f_{iI}^{int} = \int_{\Omega_0} \frac{\partial N_I}{\partial X_k} P_{ki} d\Omega_0 = \int_{\Omega_0} B_{0Ik} P_{ki} d\Omega_0 \tag{4.7.4}$$

where

$$B_{0kI} = \frac{\partial N_I}{\partial X_k} \tag{4.7.5}$$

In matrix form, the above can be written as

$$\left(\mathbf{f}_I^{int}\right)^T = \int_{\Omega_0} B_0^T \mathbf{P} d\Omega_0 \tag{4.7.6}$$

The expression has been written in the above form to stress the analogy to the updated Lagrangian form: if B is replaced by B_0, Ω by Ω_0, and σ by $\mathbf{P}$, we obtain the updated Lagrangian form from the above.

The external nodal forces are next obtained by transforming the updated Lagrangian expression to the total Lagrangian form. We start with Eq. (4.4.13)

$$f_{iI}^{ext} = \int_\Omega N_I \rho b_i d\Omega + \int_{\Gamma_{t_i}} N_I \bar{t}_i d\Gamma \tag{4.7.7}$$

Substituting Eq. (3.6.1), $\rho \mathbf{b} d\Omega = \rho_0 \mathbf{b} d\Omega_0$, and Eq. (3.4.4), $\bar{\mathbf{t}} d\Gamma = \mathbf{t}_0 d\Gamma_0$, into Eq. (4.7.7) gives

$$f_{iI}^{ext} = \int_{\Omega_0} N_I \rho_0 b_i d\Omega_0 + \int_{\Gamma_{t_i}^0} N_I \bar{t}_i^0 d\Gamma_0 \tag{4.7.8}$$

which is the total Lagrangian form of the external nodal forces. The two integrals are over the intial (reference) domain and boundary; note that $\rho_0 \mathbf{b}$ is the body force per unit of the reference volume, see (3.6.1). This can be written in matrix form as:

$$\mathbf{f}_I^{ext} = \int_{\Omega_0} N_I \rho_0 \mathbf{b} d\Omega_0 + \int_{\Gamma_{t_i}^0} N_I \mathbf{e}_i \, \bar{\mathbf{t}}_0 d\Gamma \tag{4.7.9}$$

The inertial nodal forces and the mass matrix were expressed in terms of the initial configuration in the development of the updated Lagrangian form, Eq. (4.4.50). Thus, all of the nodal forces can be expressed in terms of Lagrangian variables on the initial (reference) configuration by the transformations. The equations of motion for the total Lagrangian discretization are identical to that of the updated Lagrangian discretization, Eq. (4.4.48).

4.8 TOTAL LAGRANGIAN WEAK FORM

In this Section, we develop the weak form from the strong form in a total Lagrangian format. Subsequently, we will show that the weak form implies the strong form. The strong form consists of the momentum equation, Eq. (B4.5.2), the traction boundary condition, Eq. (B4.5.7), and the interior continuity conditions, Eq. (B4.5.11). We define the spaces for the test and trial functions as in Section 4.3:

$$\delta\mathbf{u}(\mathbf{X}) \in U_0, \mathbf{u}(\mathbf{X}, t) \in U \tag{4.8.1}$$

where U is the space of kinematically admissible displacements and U_0 is the same space with the additional requirement that the displacements vanish on displacement boundaries.

Strong Form to Weak Form. To develop the weak form, we multiply the momentum equation (B4.5.3) by the test function and integrate over the *initial (reference) configuration:*

$$\int_{\Omega_0} \delta u_i \left(\frac{\partial P_{ji}}{\partial X_j} + \rho_0 b_i - \rho_0 \ddot{u}_i \right) d\Omega_0 = 0 \tag{4.8.2}$$

In the above, the nominal stress is a function of the trial displacements via the consitutive equation and the strain-displacement equation. This weak form is not useful because it requires the trial displacements to be C^1, since a derivative of the nominal stress appears in (4.8.2); see Sections 4.3.1-2.

To eliminate the derivative of the nominal stress from Eq. (4.8.2), the derivative product formula is used:

$$\int_{\Omega_0} \delta u_i \frac{\partial P_{ji}}{\partial X_j} d\Omega_0 = \int_{\Omega_0} \frac{\partial}{\partial X_j} \left(\delta u_i P_{ji} \right) d\Omega_0 - \int_{\Omega_0} \frac{\partial \left(\delta u_i \right)}{\partial X_j} P_{ji} d\Omega_0 \tag{4.8.3}$$

The first term of the RHS of the above can be expressed as a boundary integral by Gauss's theorem (3.5.6):

$$\int_{\Omega_0} \frac{\partial}{\partial X_j}\left(\delta u_i P_{ji}\right) d\Omega_0 = -\int_{\Gamma_0} \delta u_i n_j^0 P_{ji}\, d\Gamma_0 + \int_{\Gamma_{int}^0} \delta u_i \left\langle n_j^0 P_{ji} \right\rangle d\Gamma_0 \tag{4.8.4}$$

From the strong form Eq. (B4.5.11), the last term vanishes. The first term on the RHS can be reduced to the traction boundary since $\delta u_i = 0$ on $\Gamma_{u_i}^0$ and $\Gamma_{t_i}^0 = \Gamma_0 - \Gamma_{u_i}^0$, so

$$\int_{\Omega_0} \frac{\partial}{\partial X_j}\left(\delta u_i P_{ji}\right) d\Omega_0 = \int_{\Gamma_0} \delta u_i n_j^0 P_{ji}\, d\Gamma_0 = \sum_{i=1}^{n_{SD}} \int_{\Gamma_{t_i}^0} \delta u_i \bar{t}_i^{\,0}\, d\Gamma_0 \tag{4.8.5}$$

where the last equality follows from the strong form. From Eq. (3.2.14)we note that

$$\delta F_{ij} = \delta\left(\frac{\partial u_i}{\partial X_j}\right) \tag{4.8.6}$$

Substituting Eq. (4.8.5) into (4.8.3) and the result into (4.8.2) gives, after a change of sign and using (4.8.6):

$$\int_{\Omega_0} \left(\delta F_{ij} P_{ji} - \delta u_i \rho_0 b_i + \delta u_i \rho_0 \ddot{u}_i\right) d\Omega_0 - \sum_{i=1}^{n_{SD}} \int_{\Gamma_{t_i}^0} \delta u_i \bar{t}_i^{\,0}\, d\Gamma_0 = 0 \tag{4.8.7}$$

or

$$\int_{\Omega_0} \left(\delta \mathbf{F}^T : \mathbf{P} - \rho_0 \delta \mathbf{u}\ \mathbf{b} + \rho_0 \delta \mathbf{u}\ \ddot{\mathbf{u}}\right) d\Omega_0 - \sum_{i=1}^{n_{SD}} \int_{\Gamma_{t_i}^0} \left(\delta \mathbf{u}\ \mathbf{e}_i\right)\left(\mathbf{e}_i\ \bar{\mathbf{t}}_i^{\,0}\right) d\Gamma_0 = 0 \tag{4.8.8}$$

The above is the weak form of the momentum equation, traction boundary conditions, and interior continuity conditions. It is called the *principle of virtual work*, since each of the terms in Eq. (4.8.7) is a virtual work increment. The weak form is summarized in Box 4.6, in which physical names are ascribed to each of the terms.

This weak form can also be developed by replacing the test velocity by a test displacement in Eq. (4.3.9) and transforming each term to the reference configuration. The total Lagrangian weak form, Eq. (4.8.8), is thus simply a transformation of the updated Lagrangian weak form.

Box 4.6
Weak Form for Total Lagrangian Formulation:
Principle of Virtual Work

WEAK FORM: if $u \quad U$ and

$$\delta W^{int}(\delta\mathbf{u},\mathbf{u}) - \delta W^{ext}(\delta\mathbf{u},\mathbf{u}) + \delta W^{inert}(\delta\mathbf{u},\mathbf{u}) = 0 \qquad \delta\mathbf{u} \quad U_0 \tag{B4.6.1}$$

then equilibrium, the traction boundary conditions and internal continuity conditions are satisfied.
In the above

$$\delta W^{int} = \int_{\Omega_0} \delta\mathbf{F}^T : \mathbf{P}\, d\Omega_0 = \int_{\Omega_0} \delta F_{ij} P_{ji}\, d\Omega_0 \tag{B4.6.2}$$

$$\delta W^{ext} = \int_{\Omega_0} \rho_0 \delta\mathbf{u} \quad \mathbf{b}\, d\Omega_0 + \sum_{i=1}^{n_{SD}} \int_{\Gamma_{t_i}^0} (\delta\mathbf{u} \quad \mathbf{e}_i)(\mathbf{e}_i \quad \bar{\mathbf{t}}_i^0)\, d\Gamma_0 = 0$$

$$= \int_{\Omega_0} \delta u_i \rho_0 b_i\, d\Omega_0 + \sum_{i=1}^{n_{SD}} \int_{\Gamma_{t_i}^0} \delta u_i \bar{t}_i^0\, d\Gamma_0 \tag{B4.6.3}$$

$$\delta W^{inert} = \int_{\Omega_0} \delta\mathbf{u} \quad \rho_0 \ddot{\mathbf{u}}\, d\Omega_0 = \int_{\Omega_0} \delta u_i \rho_0 \ddot{u}_i\, d\Omega_0 \tag{B4.6.4}$$

Weak Form to Strong Form. Next we deduce the strong form from the weak form. To avoid writing summations, we shall assume that on any part of the boundary, all traction or displacement components are prescribed; the reader can easily generalize the proof to mixed boundary conditions where for each component, either the displacement or traction component is prescribed. Substituting (B4.8.6) into the first term of (B4.8.7) and the derivative product rule gives

$$\int_{\Omega_0} \frac{\partial(\delta u_i)}{\partial X_j} P_{ji}\, d\Omega_0 = \int_{\Omega_0} \left\{ \frac{\partial}{\partial X_j}(\delta u_i P_{ji}) - \delta u_i \frac{\partial P_{ji}}{\partial X_j} \right\} d\Omega_0 \tag{4.8.9}$$

Gauss's theorem on the first term on the RHS then yields:

$$\int_{\Omega_0} \frac{\partial(\delta u_i)}{\partial X_j} P_{ji}\, d\Omega_0 = \sum_{i=1}^{n_{SD}} \int_{\Gamma_{t_i}^0} \delta u_i n_j^0 P_{ji}\, d\Gamma_0 + \int_{\Gamma_{int}^0} \delta u_i \langle n_j^0 P_{ji} \rangle\, d\Gamma_0 - \int_{\Omega_0} \delta u_i \frac{\partial P_{ji}}{\partial X_j}\, d\Omega_0$$

where the surface integral is changed to the traction boundary because $\delta u_i = 0$ on $\Gamma_{u_i}^0$ and $\Gamma_{t_i}^0 = \Gamma^0 - \Gamma_{u_i}^0$.

Substituting (4.8.9) into (4.8.7) and collecting terms gives

$$0 = \int_{\Omega_0} \delta u_i \left(\frac{\partial P_{ji}}{\partial X_j} + \rho_0 b_i - \rho_0 \ddot{u}_i \right) d\Omega_0 + \sum_{i=1}^{n_{SD}} \int_{\Gamma_{t_i}^0} \delta u_i \left(n_j^0 P_{ji} - \bar{t}_i^0 \right) d\Gamma_0 + \int_{\Gamma_{int}^0} \delta u_i \left\langle n_j^0 P_{ji} \right\rangle d\Gamma_0 = 0 \quad (4.8.10)$$

Since the above holds for all $\delta \mathbf{u} \quad U_0$, it follows by the density theorem given in Section 4.3.2 that the momentum equation (B4.5.2) holds on Ω_0, the traction boundary conditions (B4.5.8) hold on Γ_t^0, and the interior continuity conditions (B4.5.11) hold on Γ_{int}^0. Thus the weak form implies the momentum equation, the traction boundary conditions, and the interior continuity conditions.

4.9 FINITE ELEMENT SEMIDISCRETIZATION

4.9.1. Discrete Equations. We consider a Lagrangian mesh with the same properties as described in Section 4.4.1. The finite element approximation to the motion is given by

$$x_i(\mathbf{X}, t) = x_{iI}(t) N_I(\mathbf{X}) \quad (4.9.5)$$

where $N_I(\mathbf{X})$ are the shape functions; as in the updated Lagrangian formulation, the shpae functions are functions of the material (Lagrangian) coordinates. The trial displacement field is given by

$$u_i(\mathbf{X}, t) = u_{iI}(t) N_I(\mathbf{X}) \qquad \text{or} \qquad \mathbf{u}(X, t) = \mathbf{u}_I(t) N_I(\mathbf{X}) \quad (4.9.1)$$

The test functions, or variations, are not functions of time, so

$$\delta u_i(\mathbf{X}) = \delta u_{iI} N_I(\mathbf{X}) \qquad \text{or} \qquad \delta \mathbf{u}(\mathbf{X}) = \delta \mathbf{u}_I N_I(\mathbf{X}) \quad (4.9.2)$$

As before, we will use indicial notation where *all* repeated indices are summed; upper case indices pertain to nodes and are summed over all relevant nodes and lower case indices pertain to components and are summed over the number of dimensions.

Taking material time derivatives of (4.9.1) gives the velocity and acceleration

$$\dot{u}_i(\mathbf{X}, t) = \dot{u}_{iI}(t) N_I(\mathbf{X}) \quad (4.9.3)$$

$$\ddot{u}_i(\mathbf{X}, t) = \ddot{u}_{iI}(t) N_I(\mathbf{X}) \quad (4.9.4)$$

The deformation gradient is then given by

$$F_{ij} = \frac{\partial x_i}{\partial X_j} = \frac{\partial N_I}{\partial X_j} x_{iI} \quad (4.9.6)$$

It is sometimes convenient to write the above as

$$F_{ij} = B_{jI}^0 u_{iI} \quad \text{where} \quad B_{jI}^0 = \frac{\partial N_I}{\partial X_j} \quad \text{so} \quad \mathbf{F} = \mathbf{x} B_0^T \quad (4.9.7)$$

$$\delta F_{ij} = \frac{\partial N_I}{\partial X_j}\delta x_{iI} = \frac{\partial N_I}{\partial X_j}\delta u_{iI} \quad \text{so} \quad \delta \mathbf{F} = \delta \mathbf{u} B_0^T \tag{4.9.8}$$

where we have used $\delta x_{iI} = \delta\left(X_{iI} + u_{iI}\right) = \delta u_{iI}$. Nodal forces will now be developed for each of the virtual weak terms.

Internal nodal forces. The internal nodal forces are defined in terms of the internal virtual work using

$$\delta W^{int} = \delta u_{iI} f_{iI}^{int} = \int_{\Omega_0} \delta F_{ij} P_{ji} d\Omega_0 = \delta u_{iI} \int_{\Omega_0} \frac{\partial N_I}{\partial X_j} P_{ji} d\Omega_0 \tag{4.9.9}$$

where Eq. (4.9.7) has been used in the last step. Then the arbitrariness of δu_{iI} yields

$$f_{iI}^{int} = \int_{\Omega_0} \frac{\partial N_I}{\partial X_j} P_{ji} d\Omega_0 \quad \text{or} \quad f_{iI}^{int} = \int_{\Omega_0} B_{jI}^0 P_{ji} d\Omega_0 \quad \text{or} \quad f_{iI}^{int} = \int_{\Omega_0} B_{jI}^0 P_{ji} d\Omega_0 \tag{4.9.10}$$

which is identical to (4.7.6), the expression developed by transformation.

External Nodal Forces. The external nodal forces are defined by equating the virtual external work (B4.6.3) to the virtual work of the external nodal forces:

$$\delta W^{ext} = \delta u_{iI} f_{iI}^{ext} = \int_{\Omega_0} \delta u_i \rho_0 b_i d\Omega_0 + \int_{\Gamma_{t_i}^0} \delta u_i \bar{t}_i^0 d\Gamma_0 = \delta u_{iI} \left[\int_{\Omega_0} N_I \rho_0 b_i d\Omega_0 + \int_{\Gamma_{t_i}^0} N_I \bar{t}_i^0 d\Gamma_0 \right] \tag{4.9.12a}$$

This gives

$$f_{iI}^{ext} = \int_{\Omega_0} N_I \rho_0 b_i d\Omega_0 + \int_{\Gamma_t^0} N_I \bar{t}_i^0 d\Gamma_0 \tag{4.9.12b}$$

Mass Matrix: Using the inertial force (B4.6.4) and defining an equivalent nodal force gives

$$\delta M = \delta u_{iI} f_{iI}^{inert} = \int_{\Omega_0} \delta u_i \rho_0 \ddot{u}_i d\Omega_0 \tag{4.9.13}$$

Substituting Eq. (4.9.2) and (4.9.4) in the right hand side of the above gives

$$\delta u_{iI} f_{iI}^{inert} = \delta u_{iI} \int_{\Omega_0} \rho_0 N_I N_J d\Omega_0 \ddot{u}_{jJ} = \delta u_{iI} M_{ijIJ} \ddot{u}_{jJ} \tag{4.9.14}$$

Since the above holds for arbitrary $\delta \mathbf{u}$ and $\ddot{\mathbf{u}}$, it follows that the mass matrix is given by

$$M_{ijIJ} = \delta_{ij} \int_{\Omega_0} \rho_0 N_I N_J \, d\Omega_0 \tag{4.9.15}$$

Comparing this mass matrix **M** to that used for the updated Lagrangian formulation, Eq. (4.4.51), we see that they are identical, which is expected since we transformed the mass to the reference configuration to highlight its time invariance for a Lagrangian mesh.

Substituting the above expressions into the weak form, (B4.6.1), we have

$$\delta u_{iI} \left(f_{iI}^{int} - f_{iI}^{ext} + M_{ijIJ} \ddot{u}_{jJ} \right) = 0 \qquad I, i \quad \Gamma_{u_i} \tag{4.9.16}$$

Since the above for arbitrary values of all nodal displacement components that are not constrained by displacement boundary conditions, it follows that

$$M_{ijIJ} \ddot{u}_{jJ} + f_{iI}^{int} = f_{iI}^{ext} \qquad I, i \quad \Gamma_{u_i} \tag{4.9.17}$$

The above equations are identical to the governing equations for the updated Lagrangian formulation, as given in Box 5.5. The nodal forces in the updated and total Lagrangian formulations are expressed in terms of different variables and integrated over different domains, but from a fundamental viewpoint the updated Lagrangian formulation and the total Lagrangian formulation are identical. The numerical values for the nodal forces obtained by either formulation are also identical. Each of these formulations can be advantageous for certain constitutive equations or loadings by reducing the number of transformations which are needed.

4.9.2. Implementation. The procedure for the computation of the internal nodal forces is given in Box 4.7. In the procedure shown, the nodal forces are evaluated by numerical quadrature.

Box 4.7
Discrete Equations and Internal Force Computation in Total Lagrangian Formulation

Equations of Motion (discrete momentum equation)

$$M_{ijIJ}\dot{v}_{jJ} + f_{iI}^{int} = f_{iI}^{ext} \quad \text{for} \quad (I,i) \quad \Gamma_{v_i} \tag{B4.8.1}$$

Internal Nodal Forces

$$f_{iI}^{int} = \int_{\Omega_0} B_{0Ij} P_{ji} d\Omega_0 = \int_{\Omega_0} \frac{\partial N_I}{\partial X_j} P_{ji} d\Omega_0 \quad \text{or} \quad \left(\mathbf{f}_I^{int}\right)^T = \int_{\Omega_0} B_{0I}^T \mathbf{P} d\Omega_0 \tag{B4.8.2}$$

$$\mathbf{f}_I^{int} = \int_{\Omega_0} \mathbf{B}_{0I}^T \{\mathbf{S}\} d\Omega_0 \quad \text{in Voigt notation}$$

External Nodal Forces

$$f_{iI}^{ext} = \int_{\Omega_0} N_I \rho_0 b_i d\Omega_0 + \int_{\Gamma_{t_i}^0} N_I \bar{t}_i^0 d\Gamma_0 \quad \text{or} \quad \mathbf{f}_I^{ext} = \int_{\Omega_0} N_I \rho_0 \mathbf{b} d\Omega_0 + \int_{\Gamma_{t_i}^0} N_I \mathbf{e}_i \ \bar{\mathbf{t}}^0 d\Gamma_0 \tag{B4.8.3}$$

Mass Matrix (total Lagrangian)

$$M_{ijIJ} = \delta_{ij} \int_{\Omega_0} \rho_0 N_I N_J d\Omega_0 = \delta_{ij} \int_{\Delta} \rho_0 N_I N_J J_\xi^0 d\Delta \tag{B4.8.4}$$

$$\mathbf{M}_{IJ} = \mathbf{I}\tilde{M}_{IJ} = \mathbf{I} \int_{\Omega_0} \rho_0 N_I N_J \, d\Omega_0 \tag{B4.8.5}$$

Internal nodal force computation for element

1. $\mathbf{f}^{int} = 0$
2. for all quadrature points ξ_Q
   - i. compute $\left[B_{Ij}^0\right] = \left[\partial N_I\left(\xi_Q\right)/\partial X_j\right]$ for all I
   - ii. $\mathbf{H} = \sum_I \mathbf{B}_{0I}\mathbf{u}_I; \quad H_{ij} = \dfrac{\partial N_I}{\partial X_j} \ u_{iI}$ (B4.7.6)
   - iii. $\mathbf{F} = \mathbf{I} + \mathbf{H}, \quad J = det(\mathbf{F})$
   - iv. $\mathbf{E} = \dfrac{1}{2}\left(\mathbf{H} + \mathbf{H}^T + \mathbf{H}^T\mathbf{H}\right)$ (B4.7.7)
   - v. if needed, compute $\dot{\mathbf{E}} = \Delta\mathbf{E}/\Delta t, \quad \dot{\mathbf{F}} = \Delta\mathbf{F}/\Delta t, \quad \mathbf{D} = sym\left(\dot{\mathbf{F}}\mathbf{F}^{-1}\right)$
   - vi. compute the PK2 stress $\mathbf{S}$ or Cauchy stress σ by constitutive equation
   - vii. $\mathbf{P} = \mathbf{S}\mathbf{F}^T$ or $\mathbf{P} = J\mathbf{F}^{-1}\sigma$
   - viii. $\mathbf{f}_I^{int} \leftarrow \mathbf{f}_I^{int} + B_{OI}^T \mathbf{P} J_\xi^0 \overline{w}_Q$ for all nodes I

end loop

$\overline{w}_Q$ are quadrature weights

Usually the shape functions are expressed in terms of element coordinates ξ, such as the area coordinates in triangular elements or reference coordinates in isoparametric elements. The derivatives with respect to the material coordinates are then found by

$$\mathbf{N}_{I,\mathbf{X}} \equiv B_I^0 = \mathbf{N}_{,\xi}\, \mathbf{X}_{,\xi}^{-1} = \mathbf{N}_{,\xi}\left(\mathbf{F}_\xi^0\right)^{-1} \tag{4.9.18}$$

where $\mathbf{F}_\xi^0$ is the Jacobian between the material and intrinsic coordinates. As shown in Box 4.7, the Green strain tensor is usually not computed in terms of the deformation gradient $\mathbf{F}$, because the resulting computation is susceptible to round-off errors for small strains. Therefore the procedure shown in Eqs. (B4.7.6-7) is used. The total Lagrangian formulation can easily be adapted to constitutive equations expressed in terms of the Cauchy stress: it is only necessary to introduce the transormations shown in steps 2.vi-vii.

Voigt Form. It is of little use to write the nodal forces in terms of $\mathbf{P}$ using Voigt notation since $\mathbf{P}$ is not symmetric. Therefore, we will write the Voigt form in terms of the PK2 stress $\mathbf{S}$. Using the transformation $\mathbf{P} = \mathbf{S}\ \mathbf{F}^T$, the expression for the internal nodal forces becomes

$$f_{jI}^{int} = \int_{\Omega_0} \frac{\partial N_I}{\partial X_i} F_{jk} S_{ik}\, d\Omega_0 \quad \text{or} \quad \left(\mathbf{f}_I^{int}\right)^T = \int_{\Omega_0} \frac{\partial N_I}{\partial \mathbf{X}} \mathbf{S}\mathbf{F}^T d\Omega_0 \tag{4.9.19}$$

We define a $\mathbf{B}_0$ matrix by

$$B_{ikIj}^0 = \mathrm{sym}_{(i,k)}\left(\frac{\partial N_I}{\partial X_i} F_{jk}\right) \tag{4.9.20}$$

Note that the above specializes to the updated form (4.5.21) where the current configuration and the reference configuration coincide, so that $F_{ij} \to \delta_{ij}$. The Voigt form of this matrix (see Appendix A) is

$$B_{ikIj}^0 \to B_{ab}^0 \qquad \begin{array}{l} (i,\ k) \to a \text{ by the Voigt kinematic rule} \\ (I,\ j) \to b \text{ by the rectangular to column matrix rule} \end{array} \tag{4.9.21}$$

Similarly, S_{ik} is converted to S_b by the kinetic Voigt rule. Then

$$f_a^{int} = \int_{\Omega_0} \left(B_{ab}^0\right)^T S_b\, d\Omega_0 \quad \text{or} \quad \mathbf{f} = \int_{\Omega_0} \mathbf{B}_0^T \{\mathbf{S}\}\, d\Omega_0 \quad \text{or} \quad \mathbf{f}_I = \int_{\Omega_0} \mathbf{B}_{0\,I}^T \{\mathbf{S}\}\, d\Omega_0 \tag{4.9.22}$$

The construction of the $\mathbf{B}_0$ matrix hinges on the correspondence between the index a and the i and k indices given in Table A.?. Using this correspondence for a two-dimensional element, we obtain:

$$
\begin{aligned}
&B_{0ikIj} \;\rightarrow\; B_{0aIj} \\
&\quad i=1,\ k=1 \rightarrow a=1 \quad \left[B_{0aj}\right]_I = \frac{\partial N_I}{\partial X} F_{j1} = \frac{\partial N_I}{\partial X}\frac{\partial x_j}{\partial X} \\
&\quad i=2,\ k=2 \rightarrow a=2 \quad \left[B_{0aj}\right]_I = \frac{\partial N_I}{\partial Y} F_{j2} = \frac{\partial N_I}{\partial Y}\frac{\partial x_j}{\partial Y} \\
&\quad i=1,\ k=2 \rightarrow a=3 \quad \left[B_{0aj}\right]_I = \frac{\partial N_I}{\partial X} F_{j2} + \frac{\partial N_I}{\partial Y} F_{j1} = \frac{\partial N_I}{\partial X}\frac{\partial x_j}{\partial Y} + \frac{\partial N_I}{\partial Y}\frac{\partial x_j}{\partial X}
\end{aligned}
\tag{4.9.23}
$$

The $\mathbf{B}_{0I}$ matrix is then written out by letting j=1 and 2 correspond to columns 1 and 2 of the matrix, respectively:

$$
\mathbf{B}_{0I} = \begin{bmatrix}
\dfrac{\partial N_I}{\partial X}\dfrac{\partial x}{\partial X} & \dfrac{\partial N_I}{\partial X}\dfrac{\partial y}{\partial X} \\
\dfrac{\partial N_I}{\partial Y}\dfrac{\partial x}{\partial Y} & \dfrac{\partial N_I}{\partial Y}\dfrac{\partial y}{\partial Y} \\
\dfrac{\partial N_I}{\partial X}\dfrac{\partial x}{\partial Y} + \dfrac{\partial N_I}{\partial Y}\dfrac{\partial x}{\partial X} & \dfrac{\partial N_I}{\partial X}\dfrac{\partial y}{\partial Y} + \dfrac{\partial N_I}{\partial Y}\dfrac{\partial y}{\partial X}
\end{bmatrix}
\tag{4.9.24}
$$

In three dimensions, a similar procedure yields

$$
\mathbf{B}_{0I} = \begin{bmatrix}
\dfrac{\partial N_I}{\partial X}\dfrac{\partial x}{\partial X} & \dfrac{\partial N_I}{\partial X}\dfrac{\partial y}{\partial X} & \dfrac{\partial N_I}{\partial X}\dfrac{\partial z}{\partial X} \\
\dfrac{\partial N_I}{\partial Y}\dfrac{\partial x}{\partial Y} & \dfrac{\partial N_I}{\partial Y}\dfrac{\partial y}{\partial Y} & \dfrac{\partial N_I}{\partial Y}\dfrac{\partial z}{\partial Y} \\
\dfrac{\partial N_I}{\partial Z}\dfrac{\partial x}{\partial Z} & \dfrac{\partial N_I}{\partial Z}\dfrac{\partial y}{\partial Z} & \dfrac{\partial N_I}{\partial Z}\dfrac{\partial z}{\partial Z} \\
\dfrac{\partial N_I}{\partial Y}\dfrac{\partial x}{\partial Z} + \dfrac{\partial N_I}{\partial Z}\dfrac{\partial x}{\partial Y} & \dfrac{\partial N_I}{\partial Y}\dfrac{\partial y}{\partial Z} + \dfrac{\partial N_I}{\partial Z}\dfrac{\partial y}{\partial Y} & \dfrac{\partial N_I}{\partial Y}\dfrac{\partial z}{\partial Z} + \dfrac{\partial N_I}{\partial Z}\dfrac{\partial z}{\partial Y} \\
\dfrac{\partial N_I}{\partial X}\dfrac{\partial x}{\partial Z} + \dfrac{\partial N_I}{\partial Z}\dfrac{\partial x}{\partial X} & \dfrac{\partial N_I}{\partial X}\dfrac{\partial y}{\partial Z} + \dfrac{\partial N_I}{\partial Z}\dfrac{\partial y}{\partial X} & \dfrac{\partial N_I}{\partial X}\dfrac{\partial z}{\partial Z} + \dfrac{\partial N_I}{\partial Z}\dfrac{\partial z}{\partial X} \\
\dfrac{\partial N_I}{\partial X}\dfrac{\partial x}{\partial Y} + \dfrac{\partial N_I}{\partial Y}\dfrac{\partial x}{\partial X} & \dfrac{\partial N_I}{\partial X}\dfrac{\partial y}{\partial Y} + \dfrac{\partial N_I}{\partial Y}\dfrac{\partial y}{\partial X} & \dfrac{\partial N_I}{\partial X}\dfrac{\partial z}{\partial Y} + \dfrac{\partial N_I}{\partial Y}\dfrac{\partial z}{\partial X}
\end{bmatrix}
\tag{4.9.25}
$$

Many writers construct the $\mathbf{B}_{0I}$ matrix through a sequence of multiplications by Boolean matrices. The procedure shown here can easily be coded and is much faster.

It can be easily shown that $\mathbf{B}_0$ relates the rate of Green strain $\dot{\mathbf{E}}$ to the node velocities by

$$
\left\{\dot{\mathbf{E}}\right\} = \mathbf{B}_{0I}\mathbf{v}_I = \mathbf{B}_0\dot{\mathbf{d}}
\tag{4.9.27}
$$

The reader should be cautioned about one characteristic of the $\mathbf{B}_0$ matrix: although it carries a subscript nought, the matrix $\mathbf{B}_0$ is not time invariant. This can easily be seen from Eqs. (4.9.20) or (4.9.24-25), which show that the $\mathbf{B}_0$ matrix depends on $\mathbf{F}$, which varies with time.

The total Lagrangian equation for internal nodal forces, (4.9.22) can easily be reduced to the updated Lagrangian form, Eq. (4.5.14) without any transformations. This is accomplished by letting the configuration at a fixed time t be the reference configuration. We then use the total Lagrangian formulation with this new reference configuration. It is immediately clear that

$$\mathbf{F} = \mathbf{I} \qquad \text{or} \qquad F_{ij} = \frac{\partial x_i}{\partial X_j} = \delta_{ij} \tag{4.9.28}$$

since the two coordinates systems are now coincident at time t. There are several consequences of this:

$$\mathbf{B}_0 = \mathbf{B} \qquad \mathbf{S} = \sigma \qquad \Omega_0 = \Omega \qquad J=1 \qquad d\Omega_0 = d\Omega \tag{4.9.29}$$

to verify this, compare (4.9.20) and (??); from Box 3.2 it follows that since $\mathbf{F} = \mathbf{I}$ and $\mathbf{S} = \sigma$. Then Eq. (4.9.22) becomes

$$\mathbf{f}_I = \int_\Omega \mathbf{B}_I^T \{\sigma\} \, d\Omega \tag{4.9.30}$$

which agrees with Eq. (4.5.14). This process of instantenously making the current configuration the reference configuration is a helpful trick which we will again use later.

Example 4.8. Rod in Two Dimensions. Develop the internal nodal forces for a two-node rod element in two-dimensions. The bar element is shown in Fig. 4.12. It is in a uniaxial state of stress with the only nonzero stress along the axis of the bar.

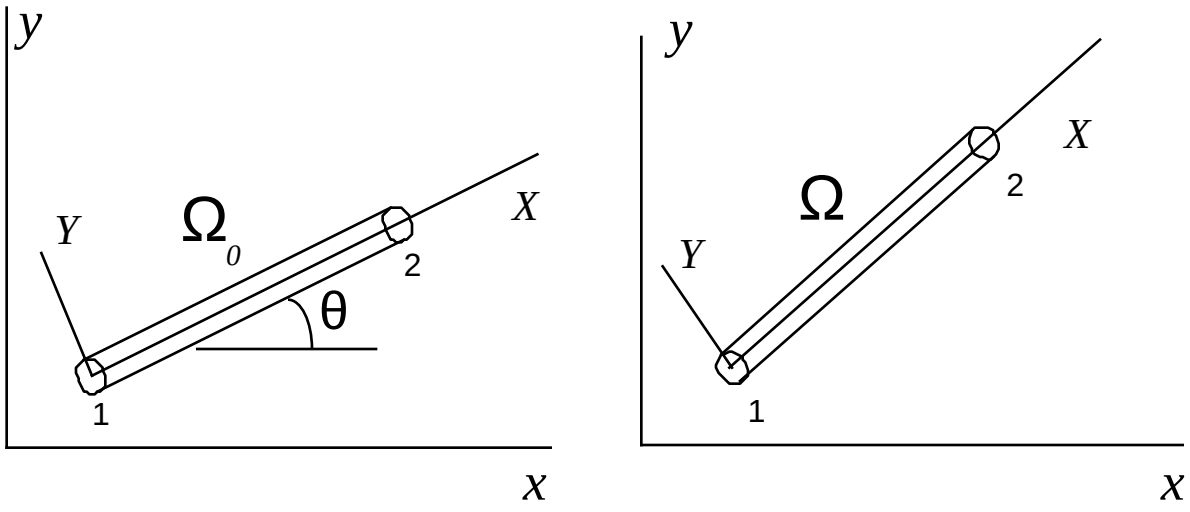

Fig. 4.12. Rod element in rwo dimensions in total Lagrangian formulation

To simplify the formulation, we place the material coordinate system so that the X-axis coincides with the axis of the rod, as shown in Fig. 4.12, with the origin of the material coordinates at node 1. The parent element coordinate is ξ, $\xi \in [0,1]$. The material coordinates are then related to the element coordinates by

$$X = X_2\xi = \ell_0\xi \tag{E4.8.1}$$

where ℓ_0 is the initial length of the element. In this example, the coordinates X, Y are used in a somewhat different sense than before: it is no longer true that $\mathbf{x}(t=0) = \mathbf{X}$. However, the definition used here corresponds to a rotation and translation of $\mathbf{x}(t=0)$. Since neither rotation nor translation effects $\mathbf{E}$ or any strain measure, this choice of an X, Y coordinate system is perfectly acceptable. We could have used the element coordinates ξ as material coordinates, but this complicates the definition of physical strain components.

The spatial coordinates are given in terms of the element coordinates by

$$\begin{aligned} x &= x_1(1-\xi) + x_2\xi \\ y &= y_1(1-\xi) + y_2\xi \end{aligned} \quad \text{or} \quad \begin{bmatrix} x \\ y \end{bmatrix} = \begin{bmatrix} x_1 & x_2 \\ y_1 & y_2 \end{bmatrix} \begin{bmatrix} 1-\xi \\ \xi \end{bmatrix} \tag{E4.8.2}$$

or

$$\mathbf{x}(\xi, t) = \mathbf{x}_I(t) N_I(\xi) \tag{E4.8.3}$$

where

$$\left\{ N_I(\xi) \right\}^T = \begin{bmatrix} (1-\xi) & \xi \end{bmatrix} = \begin{bmatrix} 1 - \dfrac{X}{\ell_0} & \dfrac{X}{\ell_0} \end{bmatrix} \tag{E4.8.4}$$

The $\boldsymbol{B}_0$ matrix as defined in (4.9.7) is given by

$$\left[B_{0iI} \right] \equiv \left[\partial N_I / \partial X_i \right]^T = \begin{bmatrix} \dfrac{\partial N_1}{\partial X} & \dfrac{\partial N_2}{\partial X} \end{bmatrix} = \frac{1}{\ell_0} \begin{bmatrix} -1 & +1 \end{bmatrix} \tag{E4.8.5}$$

where Eq. (4.8.1) has been used to give $\dfrac{\partial N_I}{\partial X} = \dfrac{1}{\ell_0} \dfrac{\partial N_I}{\partial \xi}$. The deformation gradient is given by (4.9.7):

$$\mathbf{F} = \mathbf{x}_I \left(\boldsymbol{B}_I^0 \right)^T = \begin{bmatrix} x_1 & x_2 \\ y_1 & y_2 \end{bmatrix} \frac{1}{\ell_0} \begin{bmatrix} -1 \\ 1 \end{bmatrix} = \frac{1}{\ell_0} \begin{bmatrix} x_2 - x_1 & y_2 - y_1 \end{bmatrix} \equiv \frac{1}{\ell_0} \begin{bmatrix} x_{21} & y_{21} \end{bmatrix} \tag{E4.8.6}$$

The deformation gradient $\mathbf{F}$ is not a square matrix for the rod since there are two space dimensions but only one independent variable describes the motion, (E4.8.2).

The only nonzero stress is along the axis of the rod. To take advantage of this, we use the nodal force formula in terms of the PK2 stress, since S_{11} is the only nonzero component of this stress. For the nominal stress, P_{11} is not the only nonzero component. The X axis as defined here is corotational with the axis of the rod, so S_{11} is always the stress component along the axis of the rod. Substituting (E4.8.5) and (E4.8.6) into Eq. (4.9.19) then gives the following expression for the internal nodal forces:

$$\mathbf{f}_{int}^T = \int_{\Omega_0} \boldsymbol{B}_0^T \mathbf{S}\mathbf{F}^T d\Omega_0 = \int_{\Omega_0} N_{,\mathbf{X}} \mathbf{S}\mathbf{F}^T d\Omega_0 = \int_{\Omega_0} \frac{1}{\ell_0}\begin{bmatrix}-1\\+1\end{bmatrix} [S_{11}] \frac{1}{\ell_0}\begin{bmatrix} x_{21} & y_{21}\end{bmatrix} d\Omega_0 \qquad \text{(E4.8.7)}$$

Since the deformation is constant in the element, we can assume the integrand is constant, so multiplying the integrand by the volume $A_0\ell_0$ we have

$$\begin{bmatrix} f_{1x} & f_{1y}\\ f_{2x} & f_{2y}\end{bmatrix}^{int} = \frac{A_0 S_{11}}{\ell_0}\begin{bmatrix}-x_{21} & -y_{21}\\ x_{21} & y_{21}\end{bmatrix} \qquad \text{(E4.8.9)}$$

This result can be transformed to the result for the corotational formulation if we use Eq. (E3.9.8) and note that $cos\,\theta = \frac{x_{21}}{\ell}$ and $sin\,\theta = \frac{y_{21}}{\ell}$.

In Voigt notation, the nonzero entries of the $\mathbf{B}_0$ matrix are the first row of (4.9.24), so

$$\mathbf{B}_{0I} = \begin{bmatrix} x_{,X}N_{I,X} & y_{,X}N_{I,X}\end{bmatrix} = \begin{bmatrix} cos\,\theta\, N_{I,X} & sin\,\theta\, N_{I,X}\end{bmatrix}$$

Noting that $N_{1,X} = -1/\ell_0$, $N_{2,X} = 1/\ell_0$, we have that

$$\mathbf{B}_0 = \begin{bmatrix}\mathbf{B}_1^0 & \mathbf{B}_2^0\end{bmatrix} = \frac{1}{\ell_0}\begin{bmatrix} -cos\,\theta & -sin\,\theta & cos\,\theta & sin\,\theta\end{bmatrix}$$

The expression for the nodal forces, (4.5.19) then becomes

$$\mathbf{f}^{int} \equiv \begin{Bmatrix} f_{x1}\\ f_{y1}\\ f_{x2}\\ f_{y2}\end{Bmatrix}^{int} = \int_{\Omega_0} \mathbf{B}_0^T \{\mathbf{S}\}\, d\Omega_0 = \int_{\Omega_0} \frac{1}{\ell_0}\begin{Bmatrix} -cos\,\theta\\ -sin\,\theta\\ cos\,\theta\\ sin\,\theta\end{Bmatrix} \{S_{11}\}\, d\Omega_0$$

Example 4.9. Triangular Element. Develop expressions for the deformation gradient, nodal internal forces and nodal external forces for the 3-node, linear displacement triangle. The element was developed in the updated Lagrangian formulation in Example 4.1; the element is shown in Fig. 4.2.

The motion of the element is given by the same linear map as in Example 4.1, Eq. (E4.1.2) in terms of the triangular coordinates ξ_I. The B_0 matrix is given by (4.9.7):

$$B_{0I} = \left[B^0_{jI}\right] = \left[\partial N_I / \partial X_j\right], \quad B_0 = \begin{bmatrix} B_{01} & B_{02} & B_{03} \end{bmatrix} = \begin{bmatrix} \dfrac{\partial N_1}{\partial X} & \dfrac{\partial N_2}{\partial X} & \dfrac{\partial N_3}{\partial X} \\ \dfrac{\partial N_1}{\partial Y} & \dfrac{\partial N_2}{\partial Y} & \dfrac{\partial N_3}{\partial X} \end{bmatrix}$$

$$= \frac{1}{2A_0} \begin{bmatrix} Y_{23} & Y_{31} & Y_{12} \\ X_{32} & X_{13} & X_{21} \end{bmatrix} \tag{E4.9.1}$$

$$A_0 = \frac{1}{2}\left(X_{32}Y_{12} - X_{12}Y_{32}\right)$$

where A_0 is the area of the undeformed element and $X_{IJ} = X_I - X_J, Y_{IJ} = Y_I - Y_J$. These equations are identical to those given in the updated Lagrangian formulation except that the initial nodal coordinates and initial area are used. The internal forces are then given by (4.9.11b):

$$\mathbf{f}^T_{int} = \left[f_{iI}\right] = \begin{bmatrix} f_{1x} & f_{1y} \\ f_{2x} & f_{2y} \\ f_{3x} & f_{3y} \end{bmatrix}^{int} = \int_{\Omega_0} B_0^T \mathbf{P}\, d\Omega_0$$

$$= \int_{A_0} \frac{1}{2A_0} \begin{bmatrix} Y_{23} & X_{32} \\ Y_{31} & X_{13} \\ Y_{12} & X_{21} \end{bmatrix} \begin{bmatrix} P_{11} & P_{12} \\ P_{21} & P_{22} \end{bmatrix} a_0\, dA_0 = \frac{a_0}{2} \begin{bmatrix} Y_{23} & X_{32} \\ Y_{31} & X_{13} \\ Y_{12} & X_{21} \end{bmatrix} \begin{bmatrix} P_{11} & P_{12} \\ P_{21} & P_{22} \end{bmatrix} \tag{E4.9.2}$$

Voigt Notation. The expression for the internal nodal forces in Voigt notation requires the $\mathbf{B}_0$ matrix. Using Eq. (4.9.24) and the derivatives of the shape functions in Eq. (E4.9.1) gives

$$\mathbf{B}_0 = \begin{bmatrix} Y_{23}x_{,X} & Y_{23}y_{,X} & Y_{31}x_{,X} & Y_{31}y_{,X} & Y_{12}x_{,X} & Y_{12}y_{,X} \\ X_{32}x_{,Y} & X_{32}y_{,Y} & X_{13}x_{,Y} & X_{13}y_{,Y} & X_{21}x_{,Y} & X_{21}y_{,Y} \\ Y_{23}x_{,Y} + X_{32}x_{,X} & Y_{23}y_{,Y} + X_{32}y_{,X} & Y_{31}x_{,Y} + X_{13}x_{,X} & Y_{31}y_{,Y} + X_{13}y_{,X} & Y_{12}x_{,Y} + X_{21}x_{,X} & Y_{12}y_{,Y} + X_{21}y_{,X} \end{bmatrix} \tag{E4.9.3}$$

The terms of the **F** matrix, $x_{,X}$, $y_{,X}$, etc., are evaluated by Eq. (4.9.6); for example:

$$x_{,X} = N_{I,X} x_I = \frac{1}{2A_0}\left(Y_{23}x_1 + Y_{31}x_2 + Y_{12}x_3\right) \tag{E4.9.4}$$

Note that the **F** matrix is constant in the element, and so is $\mathbf{B}_0$. The nodal forces are then given by Eq. (4.9.22):

$$\mathbf{f}^{int} = \{f_a\} = \begin{Bmatrix} f_{1x} \\ f_{1y} \\ f_{2x} \\ f_{2y} \\ f_{3x} \\ f_{3y} \end{Bmatrix}^{int} = \int_{\Omega_0} \mathbf{B}_0^T \begin{Bmatrix} S_{11} \\ S_{22} \\ S_{12} \end{Bmatrix} d\Omega_0 \tag{E4.9.5}$$

Example 4.10. Two-Dimensional Isoparametric Element. Construct the discrete equations for two- and three-dimensional isoparametric elements in indicial matrix notation and Voigt notation. The element is shown in Fig. 4.4; the same element in the updated Lagrangian form was considered in Example 4.2.

The motion of the element is given in Eq. (E4.2.1), followed by the shape functions and their derivatives with respect to the spatial coordinates. The key difference in the formulation of the isoparametric element in the total Lagrangian formulation is that the matrix of derivatives of the shape functions with respect to the material coordinates must be found. By implicit differentiation

$$\begin{Bmatrix} N_{I,X} \\ N_{I,Y} \end{Bmatrix} = \mathbf{X}_{,\xi}^{-1} \begin{Bmatrix} N_{I,\xi} \\ N_{I,\eta} \end{Bmatrix} = \left(\mathbf{F}_\xi^0\right)^{-1} \begin{Bmatrix} N_{I,\xi} \\ N_{I,\eta} \end{Bmatrix} \tag{E4.10.1}$$

where

$$\mathbf{X}_{,\xi} = \mathbf{X}_I N_{I,\xi} \quad \text{or} \quad \frac{\partial X_i}{\partial \xi_j} = X_{iI} \frac{\partial N_I}{\partial \xi_j} \tag{E4.10.2}$$

Writing out the above gives

$$\begin{bmatrix} X_{,\xi} & X_{,\eta} \\ Y_{,\xi} & Y_{,\eta} \end{bmatrix} = \begin{Bmatrix} X_I \\ Y_I \end{Bmatrix} \begin{bmatrix} N_{I,\xi} & N_{I,\eta} \end{bmatrix} \tag{E4.10.3}$$

which can be evaluated from the shape functions and nodal coordinates; details are given for the 4-node quadrilateral in Eqs. (E4.2.7-8) in terms of the updated coordinates and the formulas for the material coordinates can be obtained by replacing (x_I, y_I) by (X_I, Y_I). The inverse of $\mathbf{X}_{,\xi}$ is then given by

$$\mathbf{X}_{,\xi}^{-1} = \begin{bmatrix} X_{,\xi} & X_{,\eta} \\ Y_{,\xi} & Y_{,\eta} \end{bmatrix}^{-1} = \frac{1}{J_0^\xi} \begin{bmatrix} Y_{,\eta} & -X_{,\eta} \\ -Y_{,\xi} & X_{,\xi} \end{bmatrix} = \begin{bmatrix} \xi_{,X} & \eta_{,X} \\ \xi_{,Y} & \eta_{,Y} \end{bmatrix}$$

where the determinant of the Jacobian between the parent and reference configurations is given by

$$J_0^\xi = X_{,\xi} Y_{,\eta} - Y_{,\xi} X_{,\eta}$$

The B_{0I} matrices are given by

$$B_{0I}^T = \begin{bmatrix} N_{I,X} & N_{I,Y} \end{bmatrix} = \begin{bmatrix} N_{I,\xi} & N_{I,\eta} \end{bmatrix} \mathbf{X}_{,\xi}^{-1} = \begin{bmatrix} N_{I,\xi} & N_{I,\eta} \end{bmatrix} \begin{bmatrix} \xi_{,X} & \eta_{,X} \\ \xi_{,Y} & \eta_{,Y} \end{bmatrix} \tag{E4.10.4}$$

The gradient of the displacement field **H** is given by

$$\mathbf{H} = \mathbf{u}_I B_{0I}^T = \begin{bmatrix} \mathbf{u}_{xI} \\ \mathbf{u}_{yI} \end{bmatrix} \begin{bmatrix} N_{I,X} & N_{I,Y} \end{bmatrix} \tag{E4.10.5}$$

The deformation gradient is then given by

$$\mathbf{F} = \mathbf{I} + \mathbf{H} \tag{E4.10.6}$$

The Green strain **E** is obtained from (B4.7.4) and the the stress **S** is evaluated by the constitutive equation; the nominal stress **P** can then be computed by $\mathbf{P} = \mathbf{S}\mathbf{F}^T$; see Box 3.2.

The internal nodal forces are given by Eq. (4.9.11b):

$$\left(\mathbf{f}_I^{int}\right)^T = \int_{\Omega_0} B_{0I}^T \mathbf{P} d\Omega_0 = \int_{-1}^{1}\int_{-1}^{1} \begin{bmatrix} N_{I,X} & N_{I,Y} \end{bmatrix} \begin{bmatrix} P_{11} & P_{12} \\ P_{21} & P_{22} \end{bmatrix} J_0^{\xi} d\xi d\eta \tag{E4.10.7}$$

where

$$J_0^{\xi} = det\left(\mathbf{X}_{,\xi}\right) = det\left(\mathbf{F}_{\xi}^0\right) \tag{E4.10.8}$$

If the Voigt form is used, the internal forces are computed by Eq. (4.9.22) in terms of **S**. The external nodal forces, particularly those due to pressure, are usually best computed in the updated form. The mass matrix was computed in the total Lagrangian form in Example 4.2.

Example 4.12. Three-Dimensional Element. Develop the strain and nodal force equations for a general three-dimensional element in the total Lagrangian format. The element is shown in Figure 4.5. The parent element coordinates are $\xi = (\xi_1, \xi_2, \xi_3) \equiv (\xi, \eta, \zeta)$ for an isoparametric element, $\xi = (\xi_1, \xi_2, \xi_3)$ for a tetrahedral element, where for the latter ξ_i are the volume (barycentric) coordinates.

Matrix Form. The standard expressions for the motion, Eqs. (4.9.1-5) are used. The deformation gradient is given by Eq. (4.9.6). The Jacobian matrix relating the reference configuration to the parent is

$$\mathbf{X}_{,\xi} = \begin{bmatrix} X_{,\xi} & X_{,\eta} & X_{,\xi} \\ Y_{,\xi} & Y_{,\eta} & Y_{,\xi} \\ Z_{,\xi} & Z_{,\eta} & Z_{,\xi} \end{bmatrix} = \mathbf{X}_I \mathbf{B}_{0I}^T = \{X_I\}\left[\partial N_I / \partial \xi_j\right] = \begin{bmatrix} X_I \\ Y_I \\ Z_I \end{bmatrix} \begin{bmatrix} N_{I,\xi} & N_{I,\eta} & N_{I,\xi} \end{bmatrix} \tag{E4.12.1}$$

The deformation gradient is given by

$$\left[F_{ij}\right]=\left[x_{iI}\right]\left[\frac{\partial N_I}{\partial X_J}\right]=\begin{bmatrix} x_1, \ldots, x_N \\ y_1, \ldots, y_N \\ z_1, \ldots, z_N \end{bmatrix}\begin{bmatrix} N_{I,X} \\ N_{I,Y} \\ N_{I,Z} \end{bmatrix} \tag{E4.12.2}$$

where

$$\begin{Bmatrix} \frac{\partial N_I}{\partial X_j} \end{Bmatrix}=\begin{Bmatrix} N_{I,X} \\ N_{I,Y} \\ N_{I,Z} \end{Bmatrix}=\begin{bmatrix} \frac{\partial N_I}{\partial \xi_k} \end{bmatrix}\begin{bmatrix} \frac{\partial \xi_k}{\partial X_j} \end{bmatrix}=\begin{bmatrix} \frac{\partial N_I}{\partial \xi_k} \end{bmatrix}\mathbf{X}_{,\xi}^{-1} \tag{E4.12.3}$$

where $\mathbf{X}_{,\xi}^{-1}$ is evaluated numerically from Eq. (E4.12.1). The Green-strain tensor can be computed directly from $\mathbf{F}$, but to avoid round-off errors, it is better to compute

$$\left[H_{ij}\right]=\left[u_{iI}\right]\begin{Bmatrix} \frac{\partial N_I}{\partial X_j} \end{Bmatrix}=\begin{bmatrix} u_{x1}, \ldots, u_{xn} \\ u_{y1}, \ldots, u_{yn} \\ u_{z1}, \ldots, u_{zn} \end{bmatrix}\begin{bmatrix} \partial N_{I,X} \\ \partial N_{I,Y} \\ \partial N_{I,Z} \end{bmatrix} \tag{E4.12.4}$$

The Green-strain tensor is then given by Eq. (???).

If the constitutive law relates the PK2 stress $\mathbf{S}$ to $\mathbf{E}$, the nominal stress is then computed by $\mathbf{P}=\mathbf{S}\mathbf{F}^T$, using $\mathbf{F}$ from Eq. (??.2). The nodal internal forces are then given by

$$\begin{Bmatrix} f_{xI}^{int} \\ f_{yI} \\ f_{zI} \end{Bmatrix}=\int_\Delta \begin{Bmatrix} N_{I,X} \\ N_{I,Y} \\ N_{I,Z} \end{Bmatrix}\begin{bmatrix} P_{11} & P_{12} & P_{13} \\ P_{21} & P_{22} & P_{23} \\ P_{31} & P_{32} & P_{33} \end{bmatrix} J_\xi^0 \, d\Delta \tag{E4.12.5}$$

where $J_\xi^0=det\left(\mathbf{X}_{,\xi}\right)$.

Voigt Form. All of the variables needed for the evaluation of the B_0 matrix given in Eq. (???) can be obtained from Eq. (E???). In Voigt form

$$\begin{aligned} \{\mathbf{E}\}^T &=\left[E_{11},\ E_{22},\ E_{33},\ 2E_{23},\ 2E_{13},\ 2E_{12}\right] \\ \{\mathbf{S}\}^T &=\left[S_{11},\ S_{22},\ S_{33},\ S_{23},\ S_{13},\ S_{12}\right] \end{aligned} \tag{E4.12.6}$$

The rate of Green-strain can be computed by Eq. (???):

$$\begin{aligned} \dot{\mathbf{E}} &= \mathbf{B}_0\dot{\mathbf{d}} \\ \dot{\mathbf{d}} &= \left[u_{x1},\ u_{y1},\ u_{z1},\ \ldots\ u_{xn},\ u_{yn},\ u_{zn}\right] \end{aligned} \tag{E4.12.7}$$

The Green strain is computed by the procedure in Eq. (???). The nodal forces are given by

$$\mathbf{f}_I^{int} = \int_{\Delta} \boldsymbol{B}_{0I}^T \{\mathbf{S}\} J_0^{\xi} d\Delta \tag{E4.12.8}$$

4.9.3. Variational Principle. For static problems, weak forms for nonlinear analysis with path-independent materials can be obtained from variational principles. For many nonlinear problems, variational principles can not be formulated. However, when constitutive equations and loads are path-independent and nondissipative, a variational priniciple can be written because the stress and load can be obtained from potentials. The materials for which stress is derivable from a potential are called hyperelastic materials, see Section 5.4. In a hyperelastic material, the nominal stress is given in terms of a potential by Eq (5.4.113) which is rewritten here

$$\mathbf{P}^T = \frac{\partial w}{\partial \mathbf{F}}, \text{ or } P_{ji} = \frac{\partial w}{\partial F_{ij}}, \quad \text{where } w = \rho w^{int}, \quad W^{int} = \int_{\Omega_0} w d\Omega_0 \tag{4.9.28}$$

Note the order of the subscripts on the stress, which follows from the definition.

For the existence of a variational principle, the loads must also be conservative, i.e. they must be independent of the deformation path. Such loads are also derivable from a potential, i.e. the loads must be related to a potential so that

$$W^{ext}(\mathbf{u}) = \int_{\Omega_0} w_b^{ext}(\mathbf{u}) d\Omega_0 + \int_{\Gamma_t} w_t^{ext}(\mathbf{u}) d\Gamma_0$$

$$b_i = \frac{\partial w_b^{ext}}{\partial u_i} \quad \bar{t}_i^0 = \frac{\partial w_t^{ext}}{\partial u_i} \tag{4.9.29b}$$

Theoem of Stationary Potential Energy. When the loads and constitutive equations posses potentials, then the stationary points of

$$W(\mathbf{u}) = W^{int}(\mathbf{u}) - W^{ext}(\mathbf{u}), \quad \mathbf{u}(\mathbf{X},t) \quad U \tag{4.9.30}$$

satisfies the strong form of the equilibrium equation (B4.5.2b). The equilibrium equation which emanates from this statienary principle is written in terms of the displacements by incorporating the constitutive equation and strain-displacement equation. This stationary principle applies only to static problems.

The theorem is proven by showing the equivalence of the stationary principle to the weak form for equilibrium, traction boundary conditions and the interior continuity conditions. We first write the stationary condition of (4.9.30), which gives

$$0 = \delta W(\mathbf{u}) = \int_{\Omega_0} \left(\frac{\partial w}{\partial F_{ij}} \delta F_{ij} d\Omega - \frac{\partial w_b^{ext}}{\partial u_i} \delta u_i \right) d\Omega_0 - \int_{\Gamma_0} \frac{\partial w_t^{ext}}{\partial u_i} \delta u_i d\Gamma_0 \tag{4.9.31}$$

Substituting Eqs. (4.9.28) and (4.9.29) into the above gives

$$0 = \int_{\Omega_0} \left(P_{ji} \delta F_{ij} - \rho_0 b_i \delta u_i \right) d\Omega_0 - \int_{\Gamma_0} t_i^0 \delta u_i d\Gamma_0 \tag{4.9.32}$$

which is the weak form given in Eq. (4.8.7) for the case when the accelerations vanish. The same steps given in Section 4.8 can then be used to establish the equivalence of Eq. (4.8.7) to the strong form of the equilibrium equation.

Stationary principles are thus in a sense more restrictive weak forms: they apply only to conservative, static problems. However they can improve our understanding of stability problems and are used in the study of the existence and uniqueness of solutions.

The discrete equations are obtained from the stationary principle by using the usual finite element approximation to motion with a Lagrangian mesh, Eqs. (4.12) to (4.9.5), which we write in the form

$$\mathbf{u}(\mathbf{X},t) = \mathbf{N}(\mathbf{X})\mathbf{d}(t) \tag{4.9.33}$$

The potential energy can then be expressed in terms of the nodal displacements, giving

$$W(\mathbf{d}) = W^{int}(\mathbf{d}) - W^{ext}(\mathbf{d}) \tag{4.9.34}$$

The solutions to the above correspond to the stationary points of this function, so the discrete eqautions are

$$0 = \frac{\partial W(\mathbf{d})}{\partial \mathbf{d}} = \frac{\partial W^{int}(\mathbf{d})}{\partial \mathbf{d}} - \frac{\partial W^{ext}(\mathbf{d})}{\partial \mathbf{d}} \equiv \mathbf{f}^{int} - \mathbf{f}^{ext} \tag{4.9.35}$$

It will be shown in Chapter 6, that when the equilibrium point is stable, the potential energy is a minimum.

Example 4.11. Rod Element by Stationary Principle. Consider a structural model consisting of two-node rod elements in three dimensions. Let the internal potential energy be given by

$$w = \frac{1}{2} C^{SE} E_{11}^2 \tag{E4.11.1}$$

and let the only load on the structure be gravity, for which the external potential is

$$w^{ext} = -\rho_0 g z \tag{E4.11.2}$$

where g is the acceleration of gravity. Find expressions for the internal and external nodal forces of an element.

From Eqs. (4.9.28) and (E4.11.1), the total internal potential is given by

$$w^{int} = \sum_e W_e^{int}, \quad W_e^{int} = \frac{1}{2} \int_{\Omega_0^e} C^{SE} E_{11}^2 d\Omega_0 \tag{E4.11.3}$$

For the two-node element, the displacement field is linear and the Green strain is constant, so Eq. (E4.11.3) can be simplified by multiplying the integrand by the initial volume of the element $A_0 \ell_0$:

$$W_e^{int} = \frac{1}{2} A_0 \ell_0 C^{SE} E_{11}^2 \tag{E4.11.4}$$

To develop the internal nodal forces, we will need the derivatives of the Green strain with respect to the nodal displacements. Since the strain is constant in the element, Eq. (3.3.1) (also see Eq. (??)) gives:

$$E_{11} = \frac{\ell^2 - \ell_0^2}{2\ell_0^2} = \frac{\mathbf{x}_{21} \ \mathbf{x}_{21} - \mathbf{X}_{21} \ \mathbf{X}_{21}}{2\ell_0^2} \tag{E4.11.5}$$

where $\mathbf{x}_{IJ} \equiv \mathbf{x}_I - \mathbf{x}_J$, $\mathbf{X}_{IJ} \equiv \mathbf{X}_I - \mathbf{X}_J$. Noting that

$$\mathbf{x}_{IJ} \equiv \mathbf{X}_{IJ} + \mathbf{u}_{IJ} \tag{E4.11.6}$$

where $\mathbf{u}_{IJ} \equiv \mathbf{u}_I - \mathbf{u}_J$ are the nodal displacements and substituting Eq. (E4.11.6) into Eq. (4.11.5) gives, after some algebra,

$$E_{11} = \frac{2\mathbf{X}_{21} \ \mathbf{u}_{21} + \mathbf{u}_{21} \ \mathbf{u}_{21}}{2\ell_0^2} \tag{E4.11.7}$$

The derivatives of E_x^2 with respect to the nodal displacements are then given by

$$\frac{\partial \left(E_x^2\right)}{\partial \mathbf{u}_2} = \frac{\mathbf{X}_{21} + \mathbf{u}_{21}}{\ell_0^2} = \frac{\mathbf{x}_{21}}{\ell_0^2}, \quad \frac{\partial \left(E_x^2\right)}{\partial \mathbf{u}_1} = -\frac{\mathbf{X}_{21} + \mathbf{u}_{21}}{\ell_0^2} = -\frac{\mathbf{x}_{21}}{\ell_0^2} \tag{E4.11.8}$$

Using the definition for internal nodal forces in conjunction with Eqs. (E4.11.4) and (E4.11.8) gives

$$\mathbf{f}_2^{int} = -\mathbf{f}_1^{int} = \frac{A_0 C^{SE} E_x \mathbf{x}_{21}}{\ell_0} \tag{E4.11.9}$$

By using the fact that $S_x = C^{SE} E_x$, it follows that

$$\left(\mathbf{f}_2^{int}\right)^T = -\left(\mathbf{f}_1^{int}\right)^T = \frac{A_0 S_x}{\ell_0} \begin{bmatrix} x_{21} & y_{21} & z_{21} \end{bmatrix} \tag{E4.11.10}$$

This result, as expected, is identical to the result obtained for the bar by the principle of virtual work, Eq. (E4.8.9). The external potential for a gravity load is given by

$$W^{ext} = -\int_{\Omega_0} \rho_0 g z d\Omega_0 \tag{E4.11.11}$$

The external potential is independent of x or y, and $W,_z^{ext} = W,_{u_z}^{ext}$. If we make the finite element approximation $z = z_I N_I$, where N_I are the shape functions given in Eq. (E4.8.4) then

$$W^{ext} = -\int_{\Omega_0} \rho_0 g z_I N_I d\Omega_0 \tag{E4.11.12}$$

and

$$f_{zI}^{ext} = \frac{\partial W^{ext}}{\partial u_{zI}} = -\int_0^1 \rho_0 g z_I N_I(\xi) \ell_0 A_0 d\xi = -\frac{1}{2} A_0 \ell_0 \rho_0 g \tag{E4.11.13}$$

so the external nodal force on each node is half the force on the rod element due to gravity.

REFERENCES

T. Belytschko and B.J. Hsieh, "Nonlinear Transient Finite Element Analysis with Convected Coordinates," *International Journal for Numerical Methods in Eng.*, **7**, pp. 255-271, 1973.

T.J.R. Hughes (1997), *The Finite Element Method*, Prentice-Hall, Englewood Cliffs, New Jersey.

L.E. Malvern (1969), *Introduction to the Mechanics of a Continuous Medium*, Prentice-Hall, Englewood Cliffs, New Jersey.

J.T. Oden and J.N. Reddy (1976), *An Introduction to the Mathematical Theory of Finite Elements*, John Wiley & Sons, New York.

G. Strang and G.J. Fix (1973), *An Analysis of the Finite Element Method*, Prentice Hall, New York.

G.A. Wempner (1969), "Finite elements, finite rotations and small strains," *Int. J. Solids and Structures*, **5**, 117-153.

LIST OF FIGURES

LIST OF BOXES

CHAPTER 5
CONSTITUTIVE MODELS

By Brian Moran
Northwestern University
Department of Civil Engineering
Evanston, IL 60208

In the mathematical description of material behavior, the response of the material is characterized by a constitutive equation which gives the stress as a function of the deformation history of the body. Different constitutive relations allow us to distinguish between a viscous fluid and rubber or concrete, for example. In one-dimensional applications in solid mechanics, the constitutive relation is often referred to as the stress-strain law for the material. In this chapter, some of the most common constitutive models used in solid mechanics applications are described. Constitutive equations for different classes of materials are first presented for the one-dimensional case and are then generalized to multiaxial stress states. Special emphasis is placed on the elastic-plastic constitutive equations for both small and large strains. Some fundamental properties such as reversibility, stability and smoothness are also dsicussed. An extensive body of theory exists on the thermodynamic foundations of constituive equations at finite strains and the interested reader is referred to Noll (1973), Truesdell and Noll (1965) and Truesdell (1969). In the present discussion, emphasis is on the mechanical response, although coupling to energy equations and thermal effects are considered.

The implementation of the constitutive relation in a finite element code requires a procedure for the evaluation of the stress given the deformation (or an increment of deformation from a previous state). This may be a straightforward function evaluation as in hyperelasticity or it may require the integration of the rate or incremental form of the constitutive equations. The algorithm for the integration of the rate form of the constitutive relation is called a *stress update algorithm*. Several stress update algorithms are presented and discussed along with their numerical accuracy and stability. The concept of stress rates arises naturally in the specification of the incremental or rate forms of constitutive equations and this lays the framework for the discussion of linearization of the governing equations in Chapter 6.

In the following Section, the tensile test is introduced and discussed and used to motivate different classes of material behavior. One-dimensional constitutive relations for elastic materials are then discussed in detail in Section 5.2. The special and practically important case of linear elasticity is considered in Section 5.3. In this section, the constitutive relation for general anisotropic linear elasticity is developed. The case of linear isotropic elasticity is obtained by taking account of material symmetry. It is also shown how the isotropic linear elastic constitutive relation may be developed by a generalization of the one-dimensional behavior observed in a tensile test.

Multixial constitutive equations for large deformation elasticity are given in Section 5.4. The special cases of hypoelasticity (which often plays an important role in large deformation elastic-plastic constitutive relations) and hyperelasticity are considered. Well-known constitutive models such as Neo-Hookean, Saint Venant Kirchhoff and Mooney-Rivlin material models are given as examples of hyperleastic constitutive relations.

In Section 5.5, constitutive relations for elastic-plastic material behavior for multiaxial stress states for both rate-independent and rate-dependent materials are presented for the case of small deformations. The commonly used von Mises J_2-flow theory plasticity models (representative of the behavior of metals) for rate-independent and rate-dependent plastic deformation and the Mohr-Coulomb relation (for the deformation of soils and rock) are presented. The constitutive behavior of elastic-plastic materials undergoing large deformations is presented in Section 5.6.

Well-established extensions of J_2-flow theory constituve equations to finite strain resulting in hypoelastic-plastic constitutive relations are discussed in detail in Section 5.7. The Gurson constitutive model which accounts for void-growth and coalescence is given as an illustration of a constitutive relation for modeling material deformation together with damage and failure. The constitutive modeling of single crystals (metal) is presented as an illustration of a set of micromechanically motivated constitutive equation which has proven very successful in capturing the essential features of the mechanical response of metal single crystals. Single crystal plasticity models have also provided a basis for large deformation constitutive models for polycrstalline metals and for other classes of material undergoing large deformation. Hyperelastic-plastic constitutive equations are also considered. In these models, the elastic response is modeled as hyperelastic (rather than hypoelastic) as a means of circumventing some of the difficulties associated with rotations in problems involving geometric nonlinearity.

Constitutive models for the viscoelastic response of polymeric materials are described in section 5.8. Straightforward generalizations of one-dimensional viscoelastic models to multixial stress states are presented for the cases of small and large deformations.

Stress update algorithms for the integration of constitutive relations are presented in section 5.9. The radial return and associated so-called return-mappng algorithms for rate-independent materials are presented first. Stress-update schemes for rate dependentmaterial are then presented and the concept of algorithmic tangent modulus is introduced. Issues of accuracy and stability of the various schemes are introduced and discussed.

5.1. The Stress-Strain Curve

The relationship between stress and deformation is represented by a constitutve equation. In a displacement based finite element formulation, the constitutive relation is used to represent stress or stress increments in terms of displacment or displacement increments respectively. Consequently, a constitutve equation for general states of stress and stress and deformation histories is required for the material. The purpose of this chapter is to present the theory and development of constitutive equations for the most commonly observed classes of material behavior. To the product designer or analyst, the choice of material model is very important and may not always be obvious. Often the only information available is general knowledge and experience about the material behavior along with perhaps a few stress strain curves. It is the analyst's task to choose the appropriate constitutive model from available libraries in the finite element code or to develop a user supplied constitutive routine if no suitable constitutive equation is available. It is important for the engineer to understand what the key features of the constitutive model for the material are, what assumptions have gone into the development of the model, how suitable the model is for the material in question, how appropriate the model is for the expected load and deformation regime and what numerical issues are involved in the implentation of the model to assure accuracy and stability of the numerical procedure. As will be seen below, the analyst needs to have a broad understanding of relevant areas of mechanics of materials, continuum mechanics and numerical methods.

Many of the essential features of the stress-strain behavior of a material can be obtained from a set of stress-strain curves for the material response in a state of one-dimensional stress. Both the physical and mathematical descriptions of the material behavior are often easier to describe for one-dimensional stress states than for any other. Also, as mentioned above, often the only quantitative information the analyst has about the material is a set of stress strain curves. It is essential for the analyst to know how to characterize the material behavior on the basis of such stress-strain curves and to know what additional tests, if any, are required so that a judicious choice of constitutive equation can be made. For these reasons, we begin our treatment of constitutive models and their implementation in finite element codes with a discussion of the tensile test. As will be seen, constitutive equations for multixial states are often based on simple generalizations of the one-dimensional behavior observed in tensile tests.

5.1.1. The Tensile Test

The stress strain behavior of a material in a state of uniaxial (one-dimensional) stress can be obtained by performing a tensile test (Figure 5.1). In the tensile test, a specimen is gripped at each end in a testing machine and elongated at a prescribe rate. The elongation δ of the gage section and the force T required to produce the elongation are measured. A plot of load versus elongation (for a typical metal) is shown in Figure 5.1. This plot represents the response of the specimen as a structure. In order to extract meaningful information about the material behavior from this plot, the contributions of the specimen geometry must be removed. To do this, we plot load per unit area (or stress) of the gage cross-section versus elongation per unit length (or strain). Even at this stage, decisions need to be made: Do we use the the original area and length or the instantaneous ones? Another way of stating this question is what stress and strain measures should we use? If the deformations are sufficently small that distinctions between original and current geometries are negligible for the purposes of computing stress and strain, a small strain theory is used and a small strain constitutive relation developed. Otherwise, full nonlinear kinematics are used and a large strain (or finite deformation) constitutive relation is developed. From Chapter 3 (Box 3.2), it can be seen that we can always transform from one stress or strain measure to another but it is important to know precisely how the original stress-strain relation is specified. A typical procedure is as follows:

Define the stretch $\lambda = L/L_0$ where $L = L_0 + \delta$ is the length of the gage section associated with elongation δ. Note that $\lambda = F_{11}$ where $\mathbf{F}$ is the deformation gradient. The nominal (or engineering stress) is given by

$$P = \frac{T}{A_0} \tag{5.1.1}$$

where A_0 is the original cross-sectional area. The engineering strain is given by

$$\varepsilon = \frac{\delta}{L_0} = \lambda - 1 \tag{5.1.2}$$

A plot of engineering stress versus engineering strain for a typical metal is given in Figure 5.2.

Alternatively, the stress strain response may be given in terms of true stress. The Cauchy (or true) stress is given by

$$\sigma = \frac{T}{A} \tag{5.1.3}$$

where A is the current (instantaneous) area of the cross-section. A measure of true strain is derived by considering an increment of true strain as change in length per unit current length, i.e., $d\varepsilon^{true} = dL/L$. Integrating this relation from the initial length L_0 to the current length L gives

$$\varepsilon^{true} = \int_{L_0}^{L} \frac{dL}{L} = ln\left(L/L_0\right) = ln\,\lambda \tag{5.1.4}$$

Taking the material time derivative of this expression gives

$$\varepsilon^{true} = \frac{\dot{\lambda}}{\lambda} = D_{11} \tag{5.1.5}$$

i.e., in the one-dimensional case, the time-derivative of the true strain is equal to the rate of deformation given by Eq. (3.3.19). This is not true in general unless the principal axes of the deformation are fixed.

To plot true stress versus true strain, we need to know the cross-sectional area A as a function of the deformation and this can be measured during the test. If the material is incompressible, then the volume remains constant and we have $A_0L_0 = AL$ which can be written as

$$A = A_0/\lambda \tag{5.1.6}$$

and therefore the Cauchy stress is given by

$$\sigma = \frac{T}{A} = \lambda \frac{T}{A_0} = \lambda P \tag{5.1.7}$$

A plot of true stress versus true strain is given in Figure 5.3.

The nominal or engineering stress is written in tensorial form as $\mathbf{P} = P_{11}\mathbf{e}_1 \quad \mathbf{e}_1$ where $P_{11} = P = T/A_0$. From Box 3.2, the Cauchy (or true) stress is given by

$$\sigma = J^{-1}\mathbf{F}^T \ \mathbf{P} \tag{5.1.8}$$

where $J = det\,\mathbf{F}$ and it follows that

$$\sigma = \sigma_{11}\mathbf{e}_1 \quad \mathbf{e}_1 = J^{-1}\lambda P_{11}\mathbf{e}_1 \quad \mathbf{e}_1 \tag{5.1.9}$$

For the special case of an incompressible material $J = 1$ and Eq. (5.1.9) is equivalent to Eq. (5.1.7).

Prior to the development of instabilities (such as the well known phenomenon of necking) the deformation in the gage section of the bar can be taken to be homogeneous. The deformation gradient, Eq. (3.2.14), is written as

$$\mathbf{F} = \lambda_1 \mathbf{e}_1 \quad \mathbf{e}_1 + \lambda_2 \mathbf{e}_2 \quad \mathbf{e}_2 + \lambda_3 \mathbf{e}_3 \quad \mathbf{e}_1 3 \tag{5.1.10}$$

where $\lambda_1 = \lambda$ is the stretch in the axial direction (taken to be aligned with the x_1-axis of a rectangular Cartesian coordinate system) and $\lambda_2 = \lambda_3$ are the stretches in the lateral directions. For an incompressible material $J = det\,\mathbf{F} = \lambda_1 \lambda_2 \lambda_3 = 1$ and thus $\lambda_2 = \lambda_3 = \lambda^{-1/2}$.

Now assume that we can represent the relationship between nominal stress and

engineering strain in the form of a function

$$P_{11} = s_0(\varepsilon_{11}) \tag{5.1.11}$$

where $\varepsilon_{11} = \lambda - 1$ is the engineering strain. We can regard (5.1.11) as a stress-strain equation for the material undergoing uniaxial stressing at a given rate of deformation. At this stage we have not introduced unloading or made any assumptions about the material response. From equation (5.1.9), the true stress (for an incompressible material) can be written as

$$\sigma_{11} = \lambda s_0(\varepsilon_{11}) = s(\lambda) \tag{5.1.12}$$

where the relation between the functions is $s(\lambda) = \lambda s_0(\lambda - 1)$. This is an illustration of how we obtain different functional representations of the constitutive relation for the same material depending on what measures of stress and deformation are used. It is especially important to keep this in mind when dealing with multiaxial constitutive relations at large strains.

A material for which the stress-strain response is independent of the rate of deformation is said to be *rate-independent*; otherwise it is *rate-dependent*. In Figures 5.4 a,b, the one-dimensional response of a rate-independent and a rate-dependent material are shown respectively for different nominal strain rates. The nominal strain rate is defined as $\dot{\varepsilon} = \dot{\delta}/L_0$. Using the result $\dot{\delta} = \dot{L}$ and therefore $\dot{\delta}/L_0 = \dot{L}/L_0 = \dot{\lambda}$ it follows that the nominal strain rate is equivalent to the rate of stretching, i.e., $\dot{\varepsilon} = \dot{\lambda} = \dot{F}_{11}$. As can be seen, the stress-strain curve for the rate-independent material is independent of the strain rate while for the rate-dependent material the stress strain curve is elevated at higher rates. The elevation of stress at the higher strain rate is the typical behavior observed in most materials (such as metals and polymers). A material for which an increase in strain rate gives rise to a decrease in the stress strain curve is said to exhibit anomolous rate-dependent behavior.

In the description of the tensile test given above no unloading was considered. In Figure 5.5 unloading behaviors for different types of material are illustrated. For elastic materials, the unloading stress strain curve simply retraces the loading one. Upon complete unloading, the material returns to its inital unstretched state. For elastic-plastic materials, however, the unloading curve is different from the loading curve. The slope of the unloading curve is typically that of the elastic (initial) portion of the stress strain curve. This

results in permanent strains upon unloading as shown in Figure 5.5b. Other materials exhibit behaviors between these two extremes. For example, the unloading behavior for a brittle material which develops damage (in the form of microcracks) upon loading exhibits the unloading behavior shown in Figure 5.5c. In this case the elastic strains are recovered when the microcracks close upon removal of the load. The initial slope of the unloading curve gives information about the extent of damage due to microcracking.

In the following section, constitutive relations for one-dimensional linear and nonlinear elasticity are introduced. Multixial consitutive relations for elastic materials are discussed in section 9.3 and for elastic-plastic and viscoelastic materials in the remaining sections of the chapter.

5.2. One-Dimensional Elasticity

A fundamental property of elasticity is that the stress depends only on the current level of the strain. This implies that the loading and unloading stress strain curves are identical and that the strains are recovered upon unloading. In this case the strains are said to be *reversible*. Furthermore, an elastic material is rate-independent (no dependence on strain rate). It follows that, for an elastic material, there is a one-to-one correspondence between stress and strain. (We do not consider a class of nonlinearly elastic materials which exhibit phase transformations and for which the stress strain curve is not one-to-one. For a detailed discussion of the treatment of phase transformations within the framework of nonlinear elasticity see (Knowles,).)

We focus initially on elastic behavior in the small strain regime. When strains and rotations are small, a small strain theory (kinematics, equations of motion and constitutive equation) is often used. In this case we make no distinction between the various measures of stress and strain. We also confine our attention to a purely mechanical theory in which thermodyanamics effects (such as heat conduction) are not considered.For a nonlinear elastic material (small strains) the relation between stress and strain can be written as

$$\sigma_x = s(\varepsilon_x) \tag{5.2.1}$$

where σ_x is the Cauchy stress and $\varepsilon_x = \delta / L_0$ is the linear strain, often known as the engineering strain. Here $s(\varepsilon_x)$ is assumed to be a monotonically increasing function. The assumption that the function $s(\varepsilon_x)$ is monotonically increasing is crucial to the stability of the material: if at any strain ε_x, the slope of the stress strain curve is negative, i.e., $ds/d\varepsilon_x < 0$ then the material response is unstable. Such behavior can occur in constitutive models for materials which exhibit phase transformations (Knowles). Note that reversibility and path-independence are implied by the structure of (5.2.1): the stress σ_x for any strain ε_x is uniquely given by (5.2.1). It does not matter how the strain reaches the value ε_x. The generalization of (5.2.1) to multixial large strains is a formidable mathematical problem which has been addressed by some of the keenest minds in the 20th century and still enocmpasses open questions (see Ogden, 1984, and references therein). The extension of (5.2.1) to large strain uniaxial behaior is presented later in this Section. Some of the most common multiaxial generalizations to large strain are discussed in Section 5.3.

In a purely mechanical theory, reversibility and path-independence also imply the absence of energy dissipation in deformation. In other words, in an elastic material, deformation is not accompanied by any dissipation of energy and all energy expended in deformation is stored in the body and can be recovered upon unloading. This implies that there exists a potential function $\rho w^{int}(\varepsilon_x)$ such that

$$\sigma_x = s(\varepsilon_x) = \frac{\rho dw^{int}(\varepsilon_x)}{d\varepsilon_x} \tag{5.2.2}$$

where $\rho w^{int}(\varepsilon_x)$ is the strain energy density per unit volume. From Eq. (5.2.2) it follows that

$$\rho dw^{int}(\varepsilon_x) = \sigma_x d\varepsilon_x \tag{5.2.3}$$

which when integrated gives

$$\rho w^{int} = \int_0^{\varepsilon_x} \sigma_x d\varepsilon_x \tag{5.2.4}$$

This can also be seen by noting that $\sigma_x d\varepsilon_x = \sigma_x \dot{\varepsilon}_x dt$ is the one-dimensional form of $\sigma_{ij} D_{ij} dt$ for small strains.

One of the most obvious characteristics of a stress-strain curve is the degree of nonlinearity it exhibits. For many materials, the stress strain curve consists of an initial linear portion followed by a nonlinear regime. Also typical is that the material behaves elastically in the initial linear portion. The material behvior in this regime is then said to be linearly elastic. The regime of linear elastic behavior is typically confined to strains of no more than a few percent and consequently, small strain theory is used to describe linear elastic materials or other materials in the linear elastic regime.

For a linear elastic material, the stress strain curve is linear and can be written as

$$\sigma_x = E\varepsilon_x \tag{5.2.5}$$

where the constant of proportionality is Young's modulus, E. This relation is often referred to as Hooke's law. From Eq. (5.2.4) the strain energy density is therefore given by

$$pw^{int} = \frac{1}{2} E\varepsilon_x^2 \tag{5.2.6}$$

which is a qudratic function of strains. To avoid confusion of Young's modulus with the Green strain, note that the Green (Lagrange) strain is *always* subscripted or in boldface.

Because energy is expended in deforming the body, the strain energy w^{int} is assumed to be a convex function of strain, i.e., $\left(w^{int}\left(\varepsilon_x^1\right) - w^{\int}\left(\varepsilon_x^2\right)\right)\left(\varepsilon_x^1 - \varepsilon_x^2\right) \geq 0$, equality

if $\varepsilon_x^1 = \varepsilon_x^2$. If w^{int} is non-convex function, this implies that energy is released by the body as it deforms, which can only occur if a source of energy other than mechanical is present and is converted to mechanical energy. This is the case for materials which exhibit phase transformations. Schematics of convex and non-convex energy functions along with the corresponding stress strain curves given by (5.2.2) are shown in Figure 5.6.

In summary, the one-dimensional behavior of an elastic material is characterized by three properties which are all interrelated

$$\text{path} - \text{independence} \Leftrightarrow \text{reversible} \Leftrightarrow \text{nondissipative}$$

These properties can be embodied in a material model by modeling the material response by an elastic potential.

The extension of elasticity to large strains in one dimension is rather straightforward: it is only necessary to choose a measure of strain and define an elastic potential for the (work conjugate) stress. Keep in mind that the existence of a potential implies reversibility, path-independence and absence of dissipation in the deformation process. We can choose the Green strain as a measure of strain E_x and write

$$S_X = \frac{d\Psi}{dE_X} \tag{5.2.7}$$

The fact that the corresponding stress is the second Piola-Kirchhoff stress follows from the work (power) conjugacy of the second Piola-Kirchhoff stress and the Green strain, i.e., recalling Box 3.4 and, specializing to one dimension, the stress power per unit reference volume is given by $\dot{\Psi} = S_X \dot{E}_X$.

The potential Ψ in (5.2.7) reduces to the potential (5.2.2) as the strains become small. Elastic stress-strain relationships in which the stress can be obtained from a potential function of the strains are called hyperelastic.

The simplest hyperelastic relation (for large deformation problems in one dimension) results from a potential which is quadratic in the Green strain:

$$\Psi = \frac{1}{2} E E_X^2 \tag{5.2.8}$$

Then,

$$S_X = E E_X \tag{5.2.9}$$

by equation (5.2.7), so the relation between these stress and strain measures is linear. At small strains, the relation reduces to Hooke's Law (5.2.5).

We could also express the elastic potential in terms of any other conjugate stress and strain measures. For example, it was pointed out in Chapter 3 that the quantity $\bar{\mathbf{U}} = \mathbf{U} - \mathbf{I}$ is a valid strain measure (called the Biot strain), and that in *one-dimension* the conjugate stress is the nominal stress P_X, so

$$P_X = \frac{d\Psi}{d\bar{U}_X} = \frac{d\Psi}{dU_X} \tag{5.2.10}$$

We can write the second form in (5.2.10) because the unit tensor **I** is constant and hence $d\bar{U}_X = dU_X$. It is interesting to observe that linearity in the relationship between a certain pair of stress and strain measures does not imply linearity in other conjugate pairs. For example if $S_X = EE_X$ it follows that $P_X = E\left(U_X^2 + 2U_X\right)\Big/2$.

A material for which the rate of Cauchy stress is related to the rate of deformation is said to be *hypoelastic*. The relation is generally nonlinear and is given by

$$\dot{\sigma} = f(\sigma_x, D_x) \tag{5.2.11}$$

where a superposed dot denotes the material time derivative and D_x is the rate of deformation. A particular linear hypoelastic relation is given by

$$\dot{\sigma}_x = ED_x = E\frac{\dot{\lambda}_x}{\lambda_x} \tag{5.2.12}$$

where E is Young's modulus and λ_x is the stretch. Integrating, this relation we obtain

$$\sigma_x = E\,ln\,\lambda_x \tag{5.2.13}$$

or

$$\sigma_x = \frac{d}{d\lambda_x}\int_1^{\lambda_x} E\,ln\,\xi\,d\xi \tag{5.2.14}$$

which is a *hyperelastic* relation and thus path-independent. However, for multiaxial problems, hypoelastic relations can not in general be transformed to hyperelastic. Multixial constitutive models for hypoelastic, elastic and hyperelastic materials are described in Sections 5.3 and 5.4 below.

A hypoelastic material is, in general, strictly path-independent only in the one-dimensional case. ($\cdot$ check). However, if the elastic strains are small, the behavior is close enough to path-independent to model elastic behavior. Because of the simplicity of hypoelastic laws, a muti-axial generalization of (5.2.11) is often used in finite element software to model the elastic response of materials in large strain elastic-plastic problems (see Section 5.7 below).

For the case of small strains, equation (9.2.12) above can be written as

$$\dot{\sigma}_x = E\dot{\varepsilon}_x \tag{5.2.15}$$

which is the rate form (material time derivative) of Hooke's law (5.2.5).

For the general elastic relation (5.2.1) above, the function $s(\varepsilon_x)$ was assumed to be monotonically increasing. The corresponding strain energy is shown in Figure 5.6b and can be seen to be a convex function of strain. Materials for which $s(\varepsilon_x)$ first increases and then decreases exhibit *strain-softening* or unstable material response (i.e., $ds/d\varepsilon_x < 0$). A special form of non-monotonic response is illustrated in Figure 5.7a. Here, the function $s(\varepsilon_x)$ increases monotonically again after the strain-softening stage. The corresponding energy is shown in Figure 5.7b. This type of non-convex strain energy has been used in nonlienar elastic models of phase transformations (Knowles). At a given stress σ below σ_M the material may exist in either of the two strained states ε_a or ε_b as depicted in the figure. The reader is referred to (Knowles) for further details including such concepts as the energetic force on a phase boundary (interface driving traction) and constitutive relations for interface mobility.

5.3. Multiaxial Linear Elasticity

In many engineering applications involving small strains and rotations, the response of the material may be considered to be linearly elastic. The most general way to represent a {\em linear} relation between the stress and strain tensors is given by

$$\sigma_{ij} = C_{ijkl}\varepsilon_{kl} \qquad \sigma = C:\varepsilon \tag{5.3.1}$$

where C_{ijkl} are components of the 4th-order tensor of elastic moduli. This represents the generalization of (5.2.5) to multiaxial states of stress and strain and is often referred to as the generalized Hooke's law which incorporates fully anisotropic material response.

The strain energy per unit volume, often called the elastic potential., as given by (5.2.4) is generalized to multixial states by:

$$W = \int \sigma_{ij} d\varepsilon_{ij} = \frac{1}{2} C_{ijkl}\varepsilon_{ij}\varepsilon_{kl} = \frac{1}{2}\varepsilon : C : \varepsilon \tag{5.3.2}$$

The stress is then given by

$$\sigma_{ij} = \frac{\partial w}{\partial \varepsilon_{ij}}, \qquad \sigma = \frac{\partial w}{\partial \varepsilon} \tag{5.3.3}$$

which is the tensor equivalent of (5.2.2). The strain energy is assumed to be positive-definite, i.e.,

$$W = \frac{1}{2} C_{ijkl}\varepsilon_{ij}\varepsilon_{kl} \equiv \frac{1}{2}\varepsilon : C : \varepsilon \geq 0 \tag{5.3.4}$$

with equality if and only if $\varepsilon_{ij} = 0$ which implies that C is a positive-definite fourth-order tensor. From the symmetries of the stress and strain tensors, the material coefficients have the so-called minor symmetries

$$C_{ijkl} = C_{jikl} = C_{ijlk} \tag{5.3.5}$$

and from the existence of a strain energy potential (5.3.2) it follows that

$$C_{ijkl} = \frac{\partial^2 W}{\partial \varepsilon_{ij} \partial \varepsilon_{kl}}, \qquad C = \frac{\partial^2 W}{\partial \varepsilon \partial \varepsilon} \tag{5.3.6}$$

If W is a smooth $\left(C^1\right)$ function of ε, Eq. (5.3.6) implies a property called major symmetry:

$$C_{ijkl} = C_{klij} \tag{5.3.7}$$

since smoothness implies

$$\frac{\partial^2 W}{\partial \varepsilon_{ij} \varepsilon_{kl}} = \frac{\partial^2 W}{\partial \varepsilon_{kl} \varepsilon_{ij}} \tag{5.3.8}$$

The general fourth-order tensor C_{ijkl} has $3^4 = 81$ independent constants. These 81 constants may also be interpreted as arising from the necessity to relate 9 components of the complete stress tensor to 9 components of the complete strain tensor, i.e., $81 = 9 \times 9$. The symmetries of the stress and strain tensors require only that 6 independent components of stress be related to 6 independent components of strain. The resulting minor symmetries of the elastic moduli therefore reduce the number of independent constants to $6 \times 6 = 36$. Major symmetry of the moduli, expressed through Eq. (5.3.7) reduces the number of independent elastic constants to $n\left(n+1\right)/2 = 21$, for $n = 6$, i.e., the number of independent components of a 6×6 matrix.

Considerations of material symmetry further reduce the number of independent material constants. This will be discussed below after the introduction of Voigt notation. An isotropic material is one which has no preferred orientations or directions, so that the stress-strain relation is identical when expressed in component form in any recatngular Cartesion coordinate system. The most general constant isotropic fourth-order tensor can be shown to be a linear combination of terms comprised of Kronecker deltas, i.e., for an isotropic linearly elastic material

$$C_{ijkl} = \lambda \delta_{ij} \delta_{kl} + \mu\left(\delta_{ik}\delta_{jl} + \delta_{il}\delta_{jk}\right) + \mu'\left(\delta_{ik}\delta_{jl} + \delta_{il}\delta_{jk}\right) \tag{5.3.9}$$

Because of the symmetry of the strain and the associated minor symmetry $C_{ijkl} = C_{ijlk}$ it follows that $\mu' = 0$. Thus Eq. (6.3.9) is written

$$C_{ijkl} = \lambda \delta_{ij} \delta_{kl} + \mu\left(\delta_{ik}\delta_{jl} + \delta_{il}\delta_{jk}\right), \qquad C = \lambda \mathbf{I} \quad \mathbf{I} + 2\mu I \tag{5.3.10}$$

and the two independent material constants λ and μ are called the Lamé constants.

The stress strain relation for an isotropic linear elastic material may therefore be written as

$$\sigma_{ij} = \lambda \varepsilon_{kk} \delta_{ij} + 2\mu \varepsilon_{ij} = C_{ijkl} \varepsilon_{kl}, \qquad \sigma = \lambda trace(\varepsilon)\mathbf{I} + 2\mu\varepsilon \tag{5.3.11}$$

Voigt Notation

Voigt notation employs the following mapping of indices to represent the components of stress, strain and the elastic moduli in convenient matrix form:

$$\begin{array}{lll} 11 \to 1 & 22 \to 2 & 33 \to 3 \\ 23 \to 4 & 13 \to 5 & 12 \to 6 \end{array} \tag{5.3.12}$$

Thus, stress can be written as a column matrix $\{\sigma\}$ with

$$\begin{bmatrix} \sigma_{11} & \sigma_{12} & \sigma_{13} \\ & \sigma_{22} & \sigma_{23} \\ sym & & \sigma_{33} \end{bmatrix} \to \begin{Bmatrix} \sigma_{11} \\ \sigma_{22} \\ \sigma_{33} \\ \sigma_{23} \\ \sigma_{13} \\ \sigma_{12} \end{Bmatrix} \tag{5.3.13}$$

or

$$\begin{aligned} \{\sigma\}^T &= [\sigma_1, \ \sigma_2, \ \sigma_3, \ \sigma_4, \ \sigma_5, \ \sigma_6] \\ &= [\sigma_1, \ \sigma_{22}, \ \sigma_{33}, \ \sigma_{23}, \ \sigma_{13}, \ \sigma_{12}] \end{aligned} \tag{5.3.14}$$

Strain is

similarly written in matrix form with the exception that a factor of 2 is introduced on the shear terms, i.e.,

$$\begin{aligned} \{\varepsilon\}^T &= [\varepsilon_1, \ \varepsilon_2, \ \varepsilon_3, \ \varepsilon_4, \ \varepsilon_5, \ \varepsilon_6] \\ &= [\varepsilon_1, \ \varepsilon_{22}, \ \varepsilon_{33}, \ 2\varepsilon_{23}, \ 2\varepsilon_{13}, \ 2\varepsilon_{12}] \end{aligned} \tag{5.3.15}$$

The factor of 2 is included in the shear strain terms to render the stress and strain column matrices work conjugates, i.e.,

$$W = \frac{1}{2}\sigma^T \varepsilon = \frac{1}{2}\sigma_{ij}\varepsilon_{ij} = \frac{1}{2}\sigma : \varepsilon \tag{5.3.16}$$

The matrix of elastic constants is obtained from the tensor components by mapping the first and second pairs of indices according to (5.3.12). For example, $C_{11} = C_{1111}$, $C_{12} = C_{1122}$, $C_{14} = C_{1123} C_{56} = C_{1312}$ etc. For example, the stress strain relation for σ_{11} is given by

$$
\begin{aligned}
\sigma_{11} &= C_{1111}\varepsilon_{11} + C_{1112}\varepsilon_{12} + C_{1113}\varepsilon_{13} \\
&\quad + C_{1121}\varepsilon_{21} + C_{1122}\varepsilon_{22} + C_{1123}\varepsilon_{23} \\
&\quad + C_{1131}\varepsilon_{31} + C_{1132}\varepsilon_{32} + C_{11331}\varepsilon_{33} \\
&= C_{11}\varepsilon_1 + \frac{1}{2}C_{16}\varepsilon_6 + \frac{1}{2}C_{15}\varepsilon_5 + \frac{1}{2}C_{16}\varepsilon_6 \\
&\quad + \frac{1}{2}C_{12}\varepsilon_2 + \frac{1}{2}C_{14}\varepsilon_4 + \frac{1}{2}C_{15}\varepsilon_5 + \frac{1}{2}C_{14}\varepsilon_4 + \frac{1}{2}C_{13}\varepsilon_3 \\
&= C_{11}\varepsilon_1 + C_{12}\varepsilon_2 + C_{13}\varepsilon_3 + C_{14}\varepsilon_4 + C_{15}\varepsilon_5 + C_{16}\varepsilon_6 \\
&= C_{1j}\varepsilon_j
\end{aligned}
\tag{5.3.17}
$$

and similarly for the remaining components of stress. The constitutive relation may then be written in matrix form as

$$
\sigma = C\varepsilon, \qquad \sigma_i = C_{ij}\varepsilon_j \tag{5.3.18}
$$

Major symmetry (5.3.7) implies that the matrix [*C*], of elastic constants is symmetric with 21 independent entries, i.e.,

$$
\begin{Bmatrix} \sigma_1 \\ \sigma_2 \\ \sigma_3 \\ \sigma_4 \\ \sigma_5 \\ \sigma_6 \end{Bmatrix} =
\begin{bmatrix}
C_{11} & C_{12} & C_{13} & C_{14} & C_{15} & C_{16} \\
 & C_{22} & C_{23} & C_{24} & C_{25} & C_{26} \\
 & & C_{33} & C_{34} & C_{35} & C_{36} \\
 & & & C_{44} & C_{45} & C_{46} \\
 & & sym & & C_{55} & C_{56} \\
 & & & & & C_{66}
\end{bmatrix}
\begin{Bmatrix} \varepsilon_1 \\ \varepsilon_2 \\ \varepsilon_3 \\ \varepsilon_4 \\ \varepsilon_5 \\ \varepsilon_6 \end{Bmatrix}
\tag{5.3.19}
$$

The relation (5.3.19) holds for arbitrary anisotropic linearly elastic materials. The number of independent material constants is further reduced by considerations of material symmetry (see Nye (1985) for example). For example, if the material has a plane of symmetry, say the x_1-plane, the elastic moduli must remain unchanged when the coordinate system is changed to one in which the x_1-axis is reflected through the x_1-plane. Such a reflection introduces a factor of -1 for each term in the moduli C_{ijkl} in which the index 1 appears. Because the x_1 plane is a plane of symmetry, the moduli must remain unchanged under this reflection and therefore any term in which the index 1 appears an odd number of times must vanish. This occurs for the terms $C_{\alpha 5}$ and $C_{\alpha 6}$ for α =1,2,3. For an orthotropic material (e.g., wood or aligned fiber reinforced composites) for which there are three mutually orthogonal planes of symmetry, this procedure can be repated for all three planes to show that there are only 9 independent elastic constants and the constitutive matrix is written as

$$\begin{bmatrix}\sigma_1\\ \sigma_2\\ \sigma_3\\ \sigma_4\\ \sigma_5\\ \sigma_6\end{bmatrix} = \begin{bmatrix} C_{11} & C_{12} & C_{13} & 0 & 0 & 0\\ & C_{22} & C_{23} & 0 & 0 & 0\\ & & C_{33} & 0 & 0 & 0\\ & & & C_{44} & 0 & 0\\ & & sym & & C_{55} & 0\\ & & & & & C_{66}\end{bmatrix} \begin{bmatrix}\varepsilon_1\\ \varepsilon_2\\ \varepsilon_3\\ \varepsilon_4\\ \varepsilon_5\\ \varepsilon_6\end{bmatrix} \tag{5.3.20}$$

An isotropic material is one for which there are no preferred orientations. Recall that an isotropic tensor is one which has the same components in any (rectangular Cartesian) coordinate system. Many materials (such as metals and ceramics) can be modeled as isotropic in the linear elastic range and the linear isotropic elastic constitutive relation is perhaps the most widely used material model in solid mechanics. There are many excellent treatises on the theroy of elasticity and the reader is referred to (Timoshenko and Goodier, 1975; Love, and Green and Zerna,) for more a more detailed description than that given here. As in equation (5.3.10) above the number of independent elastic constants for an isotropic linearly elastic material reduces to 2. The isotropic linear elastic law is written in Voigt notation as

$$\begin{bmatrix}\sigma_1\\ \sigma_2\\ \sigma_3\\ \sigma_4\\ \sigma_5\\ \sigma_6\end{bmatrix} = \begin{bmatrix} \lambda+2\mu & \lambda & \lambda & 0 & 0 & 0\\ & \lambda+2\mu & \lambda & 0 & 0 & 0\\ & & \lambda+2\mu & 0 & 0 & 0\\ & & & \mu & 0 & 0\\ & & sym & & \mu & 0\\ & & & & & \mu\end{bmatrix} \begin{bmatrix}\varepsilon_1\\ \varepsilon_2\\ \varepsilon_3\\ \varepsilon_4\\ \varepsilon_5\\ \varepsilon_6\end{bmatrix} \tag{5.3.21}$$

where λ and μ are the Lamé constants.

The isotropic linear elastic relation (5.3.21) has been derived from the general anisotropic material model (5.3.19) by considering material symmetry. It is instructive to see also how the relation (5.3.21) may be generalized from the particular by starting with the case of a linearly elastic isotropic bar under uniaxial stress. For small strains, the axial strain in the bar is given by the elongation per unit original length, i.e., $\varepsilon_{11} = \delta / L_0$ and from Hooke's law (5.2.5)

$$\varepsilon_{11} = \frac{\sigma_{11}}{E} \tag{5.3.22}$$

The lateral strain in the bar is given by $\varepsilon_{22} = \varepsilon_{33} = \Delta D / D_0$ where ΔD is the change in the original diameter D_0. For an isotropic material, the lateral strain is related to the axial strain by

$$\varepsilon_{22} = \varepsilon_{33} = -\nu\varepsilon_{11} = -\nu\frac{\sigma_{11}}{E} \tag{5.3.23}$$

where ν is Poisson's ratio. To generalize these relations to multiaxial stress states, consider the stress state shown in Figure 5.8 where the primed coordinate axes are aligned with the directions of principal stress. Because of the linearity of the material repsonse, the strains due to the indiviudal stresses may be superposed to give

$$\begin{aligned}
\varepsilon'_{11} &= \frac{\sigma'_{11}}{E} - \nu\left(\sigma'_{22} + \sigma'_{33}\right) \\
\varepsilon'_{22} &= \frac{\sigma'_{22}}{E} - \nu\left(\sigma'_{11} + \sigma'_{33}\right) \\
\varepsilon'_{33} &= \frac{\sigma'_{33}}{E} - \nu\left(\sigma'_{11} + \sigma'_{22}\right)
\end{aligned} \tag{5.3.24}$$

Referring the stresses and strains to an arbitrary set of (rectangular Cartesian) axes by using the relation (3.2.30) for transformation of tensor components gives

$$\varepsilon_{ij} = \frac{(1+\nu)}{E}\sigma_{ij} - \frac{\nu}{E}\sigma_{kk}\delta_{ij} \tag{5.3.25}$$

Exercise 5.1. Derive Eq. (5.3.25) from (5.3.24) and (3.2.30).

The relation between shear stress and shear strain is given by (for example) $\sigma_{12} = 2\mu\varepsilon_{12}$ where the shear modulus (or modulus of rigidity) μ is defined as

$$\mu = \frac{E}{2(1+\nu)} \tag{E5.1.1}$$

From Eq.(5.3.25) it follows that

$$\varepsilon_{kk} = \frac{(1-2\nu)}{E}\sigma_{kk} = \frac{\sigma_{kk}}{3K} \tag{E5.1.2}$$

where

$$K = \frac{E}{3(1-2\nu)} = \lambda + \frac{2\mu}{3} \tag{E5.1.3}$$

is the bulk modulus. Introducing the Lamé constant λ, given by

$$\lambda = \frac{\nu E}{(1+\nu)(1-2\nu)} \tag{E5.1.4}$$

the bulk modulus is wrtten as

$$K = \lambda + \frac{2\mu}{3} \tag{E5.1.5}$$

From (5.3.29) and (5.3.26), the quantity we obtain the relation $\nu/E = \lambda/2\mu$. Using this result and (5.3.26) in (5.3.25), the stress strain relation is given by

$$\varepsilon_{ij} = \frac{\sigma_{ij}}{2\mu} - \frac{\lambda}{2\mu(3\lambda + 2\mu)}\sigma_{kk}\delta_{ij} \tag{E5.1.6}$$

Using (5.3.27) this expression may be inverted to give Eq.(5.3.11), the generalized Hooke's law.

Writing the stress and strain tensors as the sum of deviatoric and hydrostatic or volumetric parts, i.e.,

$$\begin{aligned} \sigma_{ij} &= s_{ij} + \frac{1}{3}\sigma_{kk}\delta_{ij} \\ \varepsilon_{ij} &= e_{ij} + \frac{1}{3}\varepsilon_{kk}\delta_{ij} \end{aligned} \tag{E5.1.7}$$

then using (5.3.11) and (5.3.26-27) the constitutive relation for an isotropic linearly elastic material can be written as

$$\sigma_{ij} = 2\mu e_{ij} + K\varepsilon_{kk}\delta_{ij} \tag{E5.1.8}$$

The strain energy (5.3.16) for an isotropic material is given by

$$\begin{aligned} W &= \frac{1}{2}\sigma_{ij}\varepsilon_{ij} \\ &= \frac{1}{2}\left(s_{ij} + \frac{1}{3}\sigma_{kk}\delta_{ij}\right)\left(e_{ij} + \frac{1}{3}\varepsilon_{mm}\delta_{ij}\right) \\ &= \mu e_{ij}e_{ij} + \frac{1}{2}K(\varepsilon_{kk})^2 \end{aligned} \tag{E5.1.9}$$

Positive definiteness of the strain energy $W \geq 0$, equality iff $\varepsilon = 0$ imposes restrictions on the elastic moduli (see Malvern, for example). For the case of isotropic linear elasticity positive definitness of *W* requires

$$\begin{aligned} &K > 0 \quad \text{and} \quad \mu > 0 \quad \text{or} \\ &E > 0 \quad \text{and} \quad -1 < \nu < \frac{1}{2} \end{aligned} \tag{E5.1.10}$$

Exercise 5.2. Derive these conditions by considering appropriate deformations. For example, to derive the condition on the shear modulus, μ, consider a purely deviatoric deformation and the positive definiteness requirement.

Incompressibility.

The particular case of $\nu = 1/2$ $(K = \infty)$ corresponds to an incompressible material. In an incompressible material in small deformations, the trace of the strain tensor must vanish,

i.e., $\varepsilon_{kk} = 0$. Deformations for which this constraint is observed are called isochoric. From (5.3.33) it can be seen that, for an incompressible material, the pressure can not be determined from the constitutive relation. Rather, it is determined from the momentum equation. Thus, the constitutive relation for an incompressible, isotropic linear elastic material is written as

$$\sigma_{ij} = -p\delta_{ij} + 2\mu\varepsilon_{ij} \tag{5.3.26}$$

where the pressure $p = -\sigma_{kk}/3$ is unspecified and is determined as part of the solution.

Plane Strain

For plane problems, the stress-strain relation (5.3.21) can be even further simplified. In plane strain, $\varepsilon_{i3} = 0$, i.e., $\varepsilon_3 = \varepsilon_4 = \varepsilon_5 = 0$. In finite element coding, the standard Voigt notation used above is often modified to accommodate a reduction in dimension of the matrices. Letting $12 \rightarrow 3$, the stress-strain relation for plane strain is written as

$$\begin{Bmatrix} \sigma_{11} \\ \sigma_{22} \\ \sigma_{12} \end{Bmatrix} = \begin{bmatrix} \lambda+2\mu & \lambda & 0 \\ \lambda & \lambda+2\mu & 0 \\ 0 & 0 & \mu \end{bmatrix} \begin{Bmatrix} \varepsilon_{11} \\ \varepsilon_{22} \\ 2\varepsilon_{12} \end{Bmatrix}$$

$$= \frac{E(1-\nu)}{(1+\nu)(1-2\nu)} \begin{bmatrix} 1 & \frac{\nu}{1-\nu} & 0 \\ \frac{\nu}{1-\nu} & 1 & 0 \\ 0 & 0 & \frac{1-2\nu}{2(1-\nu)} \end{bmatrix} \begin{Bmatrix} \varepsilon_{11} \\ \varepsilon_{22} \\ 2\varepsilon_{12} \end{Bmatrix} \tag{5.3.27}$$

and in addition

$$\sigma_{33} = \lambda(\varepsilon_{11} + \varepsilon_{22}) = \nu(\sigma_{11} + \sigma_{22}) \tag{5.3.28}$$

Plane Stress

For plane stress, $\sigma_{i3} = 0$. The condition $\sigma_{33} = 0$ gives the relation

$$\varepsilon_{33} = -\frac{\lambda}{\lambda+2\mu}(\varepsilon_{11} + \varepsilon_{22}) = -\nu(\varepsilon_{11} + \varepsilon_{22}) \tag{5.3.29}$$

Letting $\bar{\lambda} = 2\mu\lambda/(\lambda+2\mu)$ and using (5.3.21), the stress-strain relation for plane stress is given by

$$\begin{Bmatrix}\sigma_{11}\\ \sigma_{22}\\ \sigma_{12}\end{Bmatrix}=\begin{bmatrix}\bar{\lambda}+2\mu & \bar{\lambda} & 0\\ \bar{\lambda} & \bar{\lambda}+2\mu & 0\\ 0 & 0 & \mu\end{bmatrix}\begin{Bmatrix}\varepsilon_{11}\\ \varepsilon_{22}\\ 2\varepsilon_{12}\end{Bmatrix}=\frac{E}{1-\nu^2}\begin{bmatrix}1 & \nu & 0\\ \nu & 1 & 0\\ 0 & 0 & \frac{1-\nu}{2}\end{bmatrix}\begin{Bmatrix}\varepsilon_{11}\\ \varepsilon_{22}\\ 2\varepsilon_{12}\end{Bmatrix} \tag{5.3.30}$$

Axisymmetry

For problems with an axis of symmetry (using a cylindrical polar coordinate system) the constitutive relation is given by

$$\begin{Bmatrix}\sigma_{rr}\\ \sigma_{\theta\theta}\\ \sigma_{zz}\\ \sigma_{rz}\end{Bmatrix}=\begin{bmatrix}\lambda+2\mu & \lambda & \lambda & 0\\ \lambda & \lambda+2\mu & \lambda & 0\\ \lambda & \lambda & \lambda+2\mu & 0\\ 0 & 0 & 0 & \mu\end{bmatrix}\begin{Bmatrix}\varepsilon_{rr}\\ \varepsilon_{\theta\theta}\\ \varepsilon_{zz}\\ 2\varepsilon_{rz}\end{Bmatrix}$$

$$=\frac{E(1-\nu)}{(1+\nu)(1-2\nu)}\begin{bmatrix}1 & \frac{\nu}{1-\nu} & \frac{\nu}{1-\nu} & 0\\ \frac{\nu}{1-\nu} & 1 & \frac{\nu}{1-\nu} & 0\\ \frac{\nu}{1-\nu} & \frac{\nu}{1-\nu} & 1 & 0\\ 0 & 0 & 0 & \frac{1-2\nu}{2(1-\nu)}\end{bmatrix}\begin{Bmatrix}\varepsilon_{rr}\\ \varepsilon_{\theta\theta}\\ \varepsilon_{zz}\\ 2\varepsilon_{rz}\end{Bmatrix} \tag{5.3.31}$$

where

$$\varepsilon_{rr}=\frac{\partial u_r}{\partial r},\quad \varepsilon_{\theta\theta}=\frac{u_r}{r},\quad \varepsilon_{zz}=\frac{\partial u_z}{\partial z},\quad \varepsilon_{rz}=\left(\frac{\partial u_r}{\partial z}+\frac{\partial u_z}{\partial r}\right) \tag{5.3.32}$$

5.4. Multiaxial Nonlinear Elasticity

In this section, the small strain linear elasticity constitutive relations presented above will be extended to the case of finite strain. As will be seen, the extension to finite strains can be carried out in different ways andmany different constitutive relations can be developed for multiaxial elasticity at large strains. In addition, because of the many different stress and deformation measures for finite strain, the same constitutive relation can be written in several different ways. It is important to distinguish between these two situations. The first case gives different material models while in the second, the same material model is represented by different mathematical expressions. In the latter, it is always possible to mathematically transform from one form of the constitutive relation to another.

The constitutive models for large strain elasticity are presented in order of increasing degree of what is commonly thought of as *elasticity*, i.e., hypoleasticity is presented first, followed by elasticity and finally hyperelasticity.

5.4.1 Hypoelasticity. One of the simplest ways to represent elasticity at large strains, is to write the increments in stress as a function of the incremental deformation. As discussed in Section 3.7.2, in order to satisify the principle of material fame indifference,

the stress increments (or stress rate) should be objective and should be related to an objective measure of the increment in deformation. A more detailed treatment of material frame indifference is given in the Appendix to this chapter and we will draw on that material as needed in the remainder of the chapter. Truesdell [ ] presented a general hypoelastic relation of the form

$$\sigma = \mathbf{f}(\sigma, \mathbf{D}) \tag{5.4.1}$$

where σ represents any objective rate of the Cauchy stress and $\mathbf{D}$ is the rate of deformation tensor which is an objective tensor (see Equation (A.x)).

A large class of hypoelastic constitutive relations can be written in the form of a linear relation between the objective measure of stress and the rate of deformation tensor, i.e.,

$$\sigma = \boldsymbol{C} : \boldsymbol{D} \tag{5.4.2}$$

In general, the fourth order tensor $\boldsymbol{C}$ is a function of the stress state. As noted by Prager ( ), the relation (5.4.2) is rate-independent and incrementally linear and reversible. This means that for small increments about a finitely deformed state, the increments in stress and strain are linearly related and are recovered upon unloading. However, for large deformations, energy is not necessarily conserved and the work done in a closed deformation path is not-necessarily zero. It should be noted that the primary use of hypoelastic constitutive relations is in the representation of the elastic response in phenomenological elastic-plastic constitutive relations where the elastic deformations are smaal. In this case, dissipative effects are usually small also.

Some commonly used forms of hypoelastic constitutive relations are

$$\overset{J}{\sigma} = \boldsymbol{C}^{J} : \boldsymbol{D} \tag{5.4.3}$$

where $\overset{J}{\sigma}$ is the Jaumann rate of Cauchy stress given in equation (3.7.9) and

$$L_v \tau = J\boldsymbol{C}^{T} : \boldsymbol{D} \tag{5.4.4}$$

where $L_v \tau$ is the Lie-Derivative of the Kirchhoff stress. Note that

$$\begin{aligned} L_v \tau &= \dot{\tau} - \mathbf{L}\ \tau - \tau\ \mathbf{L}^T \\ &= J\left(\dot{\sigma} - \mathbf{L}\ \sigma - \sigma\ \mathbf{L}^T + (\text{trace}\ \mathbf{L})\sigma\right) \\ &= J\ \overset{T}{\sigma} \end{aligned} \tag{5.4.5}$$

where $J = det\ \mathbf{F}$ and $\overset{T}{\sigma}$ is the Truesdell rate of Cauchy stress. Thus the Lie-derivative of the Kirchoff stress is simply the weighted Truesdell rate of the Cauchy stress. A more detailed discussion of Lie derivatives in the context of pull-back and push-forard operations

is given in the Appendix. We will use the concept of the Lie derivatives more extensively in our treatment of hyperelasticity (Section 5.4.3) and hyperelastic-plastic constitutive relations (Section 5.7.4).

Other forms of hypoelastic relations are based on the Green-Nagdhi (also called the Dienes) rate which is denoted here by $\overset{G}{\sigma}$ and is given by

$$\begin{aligned}\overset{G}{\sigma} &= \dot{\sigma} - \dot{\Omega}\ \sigma - \sigma\ \Omega^T \\ &= \mathbf{R}\ \frac{d}{dt}\left(\mathbf{R}^T\ \sigma\ \mathbf{R}\right)\ \mathbf{R}^T\end{aligned} \tag{5.4.6}$$

where

$$\Omega = \dot{\mathbf{R}}\ \mathbf{R}^T \tag{5.4.7}$$

is the spin associated with the rotation tensor **R**. The hypoelastic relation is given by

$$\overset{G}{\sigma} = \boldsymbol{C}^G : \boldsymbol{D} \tag{5.4.8}$$

Note that the Green-Naghdi rate is a form of Lie Derivative (Appendix A.x) in that the Cauchy stress is pulled back by the rotation **R** to the unrotated configuration where the material time derivative is taken with impunity and the result pushed forward by **R** again to the current configuration. The quantity

$$\sigma = \mathbf{R}^T\ \sigma\ \mathbf{R} \tag{5.4.9}$$

is the co-rotational Cauchy stress (Equation 3.7.18) discussed in Chapter 3.

In the consitutive equations (5.4.3), (5.4.4) and (5.4.11) above, the fourth-order tensors of elastic moduli $\boldsymbol{C}^J$, $\boldsymbol{C}^T$ and $\boldsymbol{C}^G$ are often taken to be constant and isotropic, e.g.,

$$C^J_{ijkl} = \lambda\delta_{ij}\delta_{kl} + \mu\left(\delta_{ik}\delta_{jl} + \delta_{il}\delta_{jk}\right), \qquad \boldsymbol{C}^J = \lambda\mathbf{I}\quad\mathbf{I} + 2\mu\boldsymbol{I} \tag{5.4.10}$$

Given a constitutive equation

$$\overset{J}{\sigma} = \boldsymbol{C}^J : \boldsymbol{D} \tag{5.4.11}$$

with constant moduli $\boldsymbol{C}^J$ then, using the defintion of the Jaumann stress rate (3.7.9) and the co-rotational rate (6.4.6), this relation can be written as

$$\overset{R}{\sigma} = \boldsymbol{C}^J : \boldsymbol{D} + (\Omega - W)\ \sigma + \sigma\ (\Omega - W)^T \tag{5.4.12}$$

which is a different constitutive equation to (5.4.8) with constant moduli $\boldsymbol{C}^G$.

5.4.2. Cauchy Elastic Material. As previously mentioned, an elastic material may be characterized as one which has no dependence on the history of the motion. The constitutive relation for a Cauchy elastic material is given by a special form of (A.y) written as

$$\sigma = \boldsymbol{G}(\mathbf{F}) \tag{5.4.13}$$

where $\boldsymbol{G}$ is called the material response function and the explicit dependence on position $\mathbf{X}$ and time t has been suppressed for notational convenience. Applying the restriction (A.z) due to material objectivity gives the form

$$\sigma = \mathbf{R}\ \boldsymbol{G}(\mathbf{U})\ \mathbf{R}^T \tag{5.4.14}$$

Alternative forms of the same constitutive relation for other representations of stress and strain follow from the stress transformation relations in Box (3.2), e.g., the first Piola-Kirchhoff stress for a Cauchy elastic material is given by

$$\begin{aligned} \mathbf{P} &= J^{-1}\sigma\ \mathbf{F}^{-T} \\ &= J^{-1}\mathbf{R}\ \boldsymbol{G}(\mathbf{U})\ \mathbf{R}^T\ \mathbf{R}\ \mathbf{U}^{-1} \\ &= J^{-1}\mathbf{R}\ \mathbf{G}(\mathbf{U})\ \mathbf{U}^{-1} \end{aligned} \tag{5.4.15}$$

while the relationship for the second Piola-Kirchhoff stress takes the form

$$\begin{aligned} S &= J^{-1}\mathbf{F}^{-1}\ \sigma\ \mathbf{F}^{-T} \\ &= J^{-1}\mathbf{U}^{-1}\ \mathbf{R}^T\ \mathbf{R}\ \boldsymbol{G}(\mathbf{U})\ \mathbf{R}^T\ \mathbf{R}\ \mathbf{U}^{-1} \\ &= J^{-1}\mathbf{U}^{-1}\ \mathbf{R}^T\ \mathbf{G}(\mathbf{U})\ \mathbf{U}^{-1} = \mathbf{h}(\mathbf{U}) = \tilde{\mathbf{h}}(\mathbf{C}) \end{aligned} \tag{5.4.16}$$

where $\mathbf{C} = \mathbf{F}^T\ \mathbf{F} = \mathbf{U}^2$ is the right Cauchy Green deformation tensor. For a given the motion, the deformation gradient is always known by its definition $\mathbf{F} = \partial x / \partial \mathbf{X}$ (Equation 3.2.14). The stresses can therefore be computed for a Cauchy elastic material by (5.4.13) or one of the specialized forms (5.4.14-5.4.16) independent of the history of the deformation. However, the work done may depend on the deformation history or load path. Thus, while the material is history independent, it is in a sense*path* dependent. This apparent anomaly arises from the complications of large strain theory (see Example 5.1) below. In material models for small deformations, the work done in history-independent materials is always path-independent.

To account for material symmetry, we note that following Noll ( ) (see Appendix for further discussions of material symmetry) the stress field remains unchanged if the material is initially rotated by a rotation which belongs to the symmetry group of the material, i.e., if the deformation gradient, $\mathbf{F}$ is replaced by $\mathbf{F}\ \mathbf{Q}$ where $\mathbf{Q}$ is an element of the symmetry group. Thus (5.4.13) is written as

$$\sigma = \boldsymbol{G}(\mathbf{F}\ \mathbf{Q}) \tag{5.4.17}$$

For an initially isotropic material, all rotations belong to the symmetry group (5.4.17) must therefore hold for the special case $\mathbf{Q} = \mathbf{R}^T$, i.e.,

$$\sigma = \boldsymbol{G}\left(\mathbf{F}\ \mathbf{R}^T\right) = \boldsymbol{G}(\mathbf{V}) \tag{5.4.18}$$

where the right polar decomposition (3.7.7) of the deformation gradient has been used.

It can be shown (Malvern,) that for an initially isotropic material, the Cauchy stress for a Cauchy elastic material is given by

$$\sigma = \alpha_0 \mathbf{I} + \alpha_1 \mathbf{V} + \alpha_2 \mathbf{V}^2 \tag{5.4.19}$$

where α_0, α_1, and α_2 are functions of the scalar invariants of $\mathbf{V}$. For further discussion of the invariants of a second order tensor, see Box 5.x below. The expression (5.4.19) is a special case of the general relation for an isotropic material given in (5.4.18).

Example 5.1. Consider a Cauchy Elastic material with consitutive relation given by

$$\sigma = \alpha(\mathbf{V} - \mathbf{I}), \quad \alpha = \alpha_0 J, \quad J = det\ \mathbf{V} \tag{E5.1.1}$$

Let the motion be given by

$$\mathbf{R} = \mathbf{I}, \quad \mathbf{F} = \mathbf{V} = \sum_{i=1}^{3} \lambda_i \mathbf{e}_i \quad \mathbf{e}_i \tag{E5.1.2}$$

with $\lambda_3 = 1$ and $\lambda_1 = \lambda_1(t),\ \lambda_2 = \lambda_2(t)$.

The principle stretches for two deformation paths $0AB$ and $0B$ are shown in Figure 5.y below:

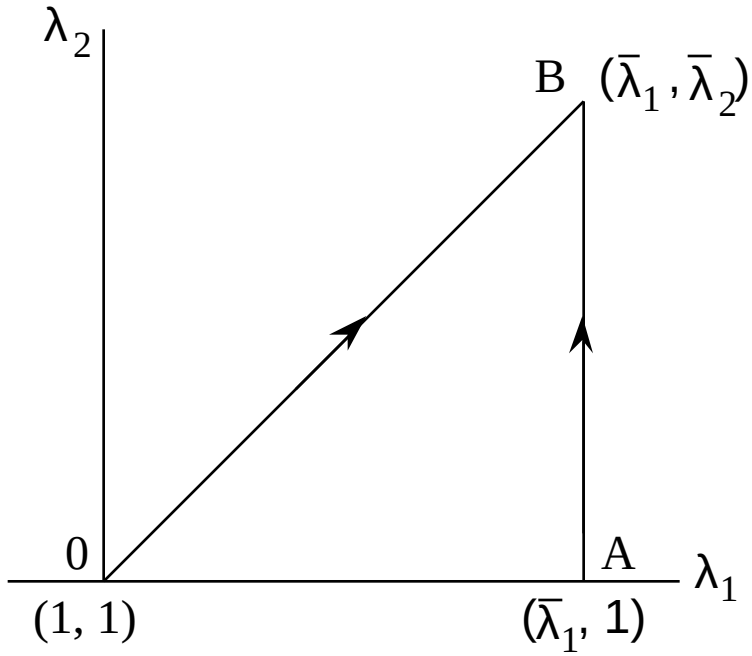

Figure 5.y. Deformation paths 0*AB* and 0*B*.

Show thatthe work done in deforming the material along paths 0*AB* and 0*B* is different, i.e., path-dependent.

$$\mathbf{V} = \begin{bmatrix} \lambda_1 & & \\ & \lambda_2 & \\ & & 1 \end{bmatrix} \qquad \sigma = \alpha \begin{bmatrix} \lambda_1 - 1 & & \\ & \lambda_2 - 1 & \\ & & 1 \end{bmatrix} \tag{E5.1.3}$$

Here,

$$\mathbf{D} = \dot{\mathbf{V}}\mathbf{V}^{-1} = \begin{bmatrix} \dot{\lambda}_1/\lambda_1 & & \\ & \dot{\lambda}_2/\lambda_2 & \\ & & 0 \end{bmatrix} \tag{E5.1.4}$$

$$J = det\ \mathbf{V} = \lambda_1\lambda_2\lambda_3 = \lambda_1\lambda_2 \tag{E5.1.5}$$

The stress power is given by

$$\begin{aligned} \dot{W} &= \sigma : \mathbf{D} \\ &= \alpha_0\lambda_1\lambda_2(\lambda_1 - 1)\frac{\dot{\lambda}_1}{\lambda_1} + \alpha_0\lambda_1\lambda_2(\lambda_2 - 1)\frac{\dot{\lambda}_2}{\lambda_2} \\ &= \alpha_0\lambda_2(\lambda_1 - 1)\dot{\lambda}_1 + \alpha_0\lambda_1(\lambda_2 - 1)\dot{\lambda}_2 \end{aligned} \tag{E5.1.6}$$

Path 0*AB*:

$$dW = \alpha_0 \lambda_2 (\lambda_1 - 1) d\lambda_1 + \alpha_0 \lambda_1 (\lambda_2 - 1) d\lambda_2 \tag{E5.1.7}$$

On $0A$, $\lambda_2 = 1$, constant. On AB $\lambda_1 = \bar{\lambda}_1$, constant. Thus

$$W = \alpha_0 \bar{\lambda}_1 \bar{\lambda}_2 \left(\frac{\lambda_1}{2} - 1 \right) + \alpha_0 \bar{\lambda}_1 \bar{\lambda} \left(\frac{\lambda_2}{2} - 1 \right) \tag{E5.1.8}$$

Path $0AB$:

$$\lambda_2 = m\lambda_1 \qquad m = \bar{\lambda}_2 / \bar{\lambda}_1 \tag{E5.1.9}$$

$$dW = \alpha m \lambda_1 (\lambda_1 - 1) d\lambda_1 + \alpha \frac{1}{m} \lambda_2 (\lambda_2 - 1) d\lambda_2 \tag{E5.1.10}$$

$$\begin{aligned} W &= \alpha m \left(\frac{\bar{\lambda}_1^3}{3} - \frac{\bar{\lambda}_1^2}{2} \right) + \alpha \frac{1}{m} \left(\frac{\bar{\lambda}_2^3}{3} - \frac{\bar{\lambda}_2^2}{2} \right) d\lambda_2 \\ &= \alpha_0 \bar{\lambda}_1 \bar{\lambda}_2 \left(\frac{\bar{\lambda}_1}{3} - \frac{1}{2} \right) + \alpha_0 \bar{\lambda}_1 \bar{\lambda}_2 \left(\frac{\bar{\lambda}_2}{3} - \frac{1}{2} \right) \end{aligned} \tag{E5.1.11}$$

which differs from Eq. (E5.1.8), i.e., the work done is path-dependent.

Exercise 5.2. Show that the consitutive relation $\sigma = \alpha_0 (\mathbf{V} - \mathbf{I})$ gives a path-independent result for the two paths considered in Example 5.1 above.

Rate (or incremental) forms of the constitutive relation are required in the treatment of linearization (Chapter 6). A useful starting point for derivation of the rate form of the constitutive relation is, where possible, to take the material time derivative of the expression for the second Piola-Kirchhoff stress $\mathbf{S}$. Thus, for a Cauchy elastic material

$$\dot{\mathbf{S}} = \frac{\partial \tilde{\mathbf{h}}(\mathbf{C})}{\partial \mathbf{C}} : \dot{\mathbf{C}} \tag{5.4.20}$$

The fourth order tensor $\boldsymbol{C}^{SC} = \partial \tilde{\mathbf{h}}(\mathbf{C}) / \partial (\mathbf{C})$ is called the instantaneous tangent modulus. From the symmetries of $\mathbf{S}$ and $\mathbf{C}$, the tangent modulus possesses the minor symmetries, i.e, $C^{SC}_{ijkl} = C^{SC}_{jikl} = C^{SC}_{ijlk}$.

5.4.3. Hyperelastic Materials

Elastic materials for which the work done on the material is independent of the load path are said to be *hyperelastic* (or Green elastic materials). In this section, some general features of hyperelastic materials are considered and then examples of hyperelastic constitutive models which are widely used in practice are given. Hyperelastic materials are characterized by the existence of a stored (or strain) energy function which is a potential for the stress. Note that from Eq. (5.4.16) the second Piola-Kirchhoff stress for a Cauchy elastic material can be written as

$$\dot{\mathbf{S}} = \tilde{\mathbf{h}}(\mathbf{C}) \tag{5.4.21}$$

where $\mathbf{C} = \mathbf{F}^T \mathbf{F} = \mathbf{U}^2$ is the right Cauchy Green deformation tensor. For the case of a hyperelastic material, the second-order tensor $\tilde{\mathbf{h}}$ is derived from a potential, i.e.,

$$\mathbf{S} = \tilde{\mathbf{h}}(\mathbf{C}) = 2\frac{\partial \Psi(\mathbf{C})}{\partial \mathbf{C}} \tag{5.4.22}$$

where Ψ is called the stored energy function. Expressions for different stress measures are obtained through the appropriate transformations (given in Box (3.2)), e.g.,

$$\tau = J\sigma = \mathbf{F}\ \mathbf{S}\ \mathbf{F}^T = 2\mathbf{F}\ \frac{\partial \Psi(\mathbf{C})}{\partial \mathbf{C}}\ \mathbf{F}^T \tag{5.4.23}$$

It can be shown (Marsden and Huges) that, given (5.4.22), the Kirchhoff stress is also derivable from a potential, i.e.,

$$\tau = 2\frac{\partial \Psi(\mathbf{g})}{\partial \mathbf{g}} \tag{5.4.24}$$

where $\mathbf{g}$ is the spatial metric tensor (which is equivalent to the identity tensor for Euclidean spaces).

A consequence of the existence of a stored energy function is that the work done on a hyperelastic material is independent of the deformation path. This behavior is approximately observed in many rubber-like materials. To illustrate the independence of work on deformation path, consider the stored energy per unit reference volume in going from deformation state $\mathbf{C}_1$ to $\mathbf{C}_2$. Since the second Piola-Kirchhoff stress tensor $\mathbf{S}$ and the Green strain $\mathbf{E} = \frac{(\mathbf{C} - \mathbf{I})}{2}$ are work conjugates,

$$\frac{1}{2}\int_{\mathbf{C}_1}^{\mathbf{C}_2} \mathbf{S}: d\mathbf{C} = \Psi(\mathbf{C}_1) - \Psi(\mathbf{C}_2) \tag{5.4.25}$$

which depends only on the initial and final states of deformation and is therefore independent of the deformation (or load) path. (Contrast this with the behavior of the Cauchy elastic material in Example 5.1 above.)

The rate forms of consitutive equations for hyperelastic materials and the corresponding moduli can be obtained by taking the material time derivative of Eq. (5.4.22) as follows:

$$\begin{aligned}\dot{\mathbf{S}} &= \frac{\partial \tilde{\mathbf{h}}(\mathbf{C})}{\partial \mathbf{C}} : \dot{\mathbf{C}} \\ &= 4\frac{\partial^2 \Psi(\mathbf{C})}{\partial \mathbf{C} \partial \mathbf{C}} : \dot{\mathbf{C}} \\ &= \boldsymbol{C}^{SC} : \frac{\dot{\mathbf{C}}}{2}\end{aligned} \tag{5.4.26}$$

where

$$\boldsymbol{C} = 4\frac{\partial^2 \Psi(\mathbf{C})}{\partial \mathbf{C} \partial \mathbf{C}} \tag{5.4.27}$$

is the tangent modulus. It follows that the tangent modulus for a hyperelastic material has the major symmetry $\boldsymbol{C}^{SC}_{ijkl} = \boldsymbol{C}^{SC}_{klij}$, in addition to the minor symmetries shown already for the Cauchy elastic material.

It is often desirable (particularly in the linearization of the weak form of the governing equations (Chapter 6) to express the stress rate in terms of an Eulerian stress tensor such as the Kirchhoff stress. To this end we recall the Lie Derivative (also referred to as the convected rate) of the Kirchhoff stress introduced earlier in this Chapter, i.e.,

$$\begin{aligned}L_{\mathbf{v}}\tau &= \mathbf{F}\ \frac{d}{dt}\left(\mathbf{F}^{-1}\ \tau\ \mathbf{F}^{-T}\right)\ \mathbf{F}^{T} = \mathbf{F}\ \dot{\mathbf{S}}\ \mathbf{F}^{T} \\ &= \dot{\tau} - \mathbf{L}\ \tau - \tau\ \mathbf{L}^{T} \\ &= \varphi_{x}\left(\frac{d}{dt}\varphi_{x}^{*}(\tau)\right)\end{aligned} \tag{5.4.28}$$

Note that the right Cauchy Green deformation tensor can be written as $\mathbf{C} = \mathbf{F}^{T}\ \mathbf{F} = \mathbf{F}^{T}\ \mathbf{g}\ \mathbf{F}$ where $\mathbf{g}$ is the spatial metric tensor. In Euclidean space, we have $\mathbf{g} = \mathbf{I}$ the identity tensor. Noting also that $\dot{\mathbf{C}}/2 = \mathbf{F}^{T}\ \mathbf{D}\ \mathbf{F}$ it follows that the rate of deformation tensor can be written as

$$\mathbf{D} = \mathbf{F}^{-T}\ \frac{d}{dt}\left(\mathbf{F}^{T}\ \mathbf{g}\ \mathbf{F}\right)\ \mathbf{F}^{-1} = \frac{1}{2}\boldsymbol{L}_{\mathbf{v}}\mathbf{g} = \varphi_{x}\left(\frac{d}{dt}\varphi_{x}^{*}\left(\frac{\mathbf{g}}{2}\right)\right) \tag{5.4.29}$$

where $\boldsymbol{L}_{\mathbf{v}}\mathbf{g}$ is the Lie derivative of the spatial metric tensor. Using Eqs. (5.4.29) and (5.4.26) in (5.4.28) gives

$$\boldsymbol{L}_{\mathbf{v}}\tau = \boldsymbol{C}^{\tau D} : \mathbf{D} \tag{5.4.30}$$

where

$$\boldsymbol{C}^{\tau D}_{ijkl} = F_{im}F_{jn}F_{kp}F_{lq}\boldsymbol{C}^{SC}_{mnpq}$$

are referred to as the spatial tangent moduli. It can be seen from the above that the Lie derivative of the Kirchhoff stress arises naturally as a stress rate in finite strain elasticity.

- Issues of uniqueness and stability of solutions in finite strain elasticity are mathematically complex. The reader is referred to [Ogden] and [Marsden and Hughes] for a detailed description.

It can be shown that, using the representation theorem (Malvern, 1969), the stored (strain) energy for a hyperelastic material which is isotropic with respect to the initial, unstressed configuration, can be written as a function of the principal invariants (I_1, I_2, I_3) of the right Cauchy-Green deformation tensor, i.e., $W = W(\mathbf{C})$. The principal invariants of a second order tensor and their derivatives figure prominently in elastic and elastic-plastic constitutive relations. For reference, Box 5.1 summarizes key relations involving princpal invariants.

Box 5.1
Principal Invariants

The principal invariants of a second order tensor **A** are given by

$$I_1(\mathbf{A}) = Trace\ \mathbf{A}$$

$$I_2(\mathbf{A}) = \frac{1}{2}\left\{(Trace\ \mathbf{A})^2 - Trace\ \mathbf{A}^2\right\} \qquad \text{(B5.1.1)}$$

$$I_3(\mathbf{A}) = det\ \mathbf{A}$$

When the tensor in question is clear from the context, the argument **A** is omitted and the principal invariants denoted simply as I_1, I_2, and I_3.

If **A** is symmetric, then $\mathbf{A} = \mathbf{A}^T$ and a set of 3 real eigenvalues (or principal values) of **A** may be formed and written as $\lambda_1, \lambda_2, \lambda_3$. Then

$$I_1 = \lambda_1 + \lambda_2 + \lambda_3$$

$$I_2 = \lambda_1\lambda_2 + \lambda_2\lambda_3 + \lambda_3\lambda_1 \qquad \text{(B5.1.2)}$$

$$I_3 = \lambda_1\lambda_2\lambda_3$$

The derivatives of the principal invariants of a second order tensor with respect to the tensor itself are often required in constitutive equations and in the linearization of the weak form (Chapter 6). For reference:

$$\frac{\partial I_1}{\partial \mathbf{A}} = \mathbf{I}; \qquad \frac{\partial I_1}{\partial \mathbf{A}_{ij}} = \delta_{ij} \qquad \text{(B5.1.3)}$$

$$\frac{\partial I_2}{\partial \mathbf{A}} = I_1\mathbf{I} - \mathbf{A}^T; \qquad \frac{\partial I_2}{\partial \mathbf{A}_{ij}} = \mathbf{A}_{kk}\delta_{ij} - \mathbf{A}_{ji} \qquad \text{(B5.1.4)}$$

$$\frac{\partial I_3}{\partial \mathbf{A}} = I_3\mathbf{A}^{-T}; \qquad \frac{\partial I_3}{\partial \mathbf{A}_{ij}} = \mathbf{I}_3\mathbf{A}^{-1}_{ji} \qquad \text{(B5.1.5)}$$

The second Piola-Kirchhoff stress tensor is given by ( ). Thus, for an isotropic material we have

$$\mathbf{S} = 2\frac{\partial w}{\partial \mathbf{C}} = 2\left(\frac{\partial w}{\partial I_1} + I_1\frac{\partial w}{\partial I_2}\right)\mathbf{I} - 2\frac{\partial w}{\partial I_2}\mathbf{C} + 2I_3\frac{\partial w}{I_3}\mathbf{C}^{-1} \qquad \text{(5.4.32)}$$

The Kirchhoff stress tensor is given by

$$\tau = \mathbf{F}\ \mathbf{S}\ \mathbf{F}^T = 2\left(\frac{\partial w}{\partial I_1} + I_1 \frac{\partial w}{\partial I_2}\right)\mathbf{B} - 2\frac{\partial w}{\partial I_2}\mathbf{B}^2 + 2I_3 \frac{\partial w}{I_3}\mathbf{I}$$

where $\mathbf{B} = \mathbf{F}\ \mathbf{F}^T$ is the left Cauchy-Green deformation tensor. Note that $\mathbf{S}$ is co-axial has the same principal directions) with $\mathbf{C}$ while τ is co-axial with $\mathbf{B}$. These results will be used below in deriving expressions for the stress tensors for specific hyperelastic models.

In the remainder of this section, examples of hyperelastic materials which are frequently used to model the behavior of rubber-like materials are presented.

Neo-Hookean Material. The stored energy function for a compressible Neo-Hookean material [Ref] (isotropic with respect to the initial, unstressed configuration) is written as

$$w(\mathbf{C}) = \frac{1}{2}\lambda_0(log\ J)^2 - \mu_0\ log\ J + \frac{1}{2}\mu_0(trace\ \mathbf{C} - 3) \tag{5.4.34}$$

From Eq. (5.4.32), the stresses are given by

$$\begin{aligned} \mathbf{S} &= \lambda_0\ log\ J\mathbf{C}^{-1} + \mu_0\left(\mathbf{I} - \mathbf{C}^{-1}\right) \\ \tau &= \lambda_0\ log\ J\mathbf{I} + \mu_0(\mathbf{B} - \mathbf{I}) \end{aligned} \tag{5.4.35}$$

Letting

$$\lambda = \lambda_0, \quad \mu = \mu_0 - \lambda\ log\ J \tag{5.4.36}$$

and using Eqs. (5.4.27) and (5.4.31), the elasticity tensors (tangent moduli) are written in component form on Ω_0 as

$$C^{SC}_{ijkl} = \lambda C^{-1}_{ij}C^{-1}_{kl} + \mu\left(C^{-1}_{ik}C^{-1}_{jl} + C^{-1}_{il}C^{-1}_{kj}\right) \tag{5.4.37}$$

and on Ω as

$$C^{\tau D}_{ijkl} = \lambda\delta_{ij}\delta_{kl} + \mu\left(\delta_{ik}\delta_{jl} + \delta_{il}\delta_{kj}\right) \tag{5.4.38}$$

The elasticity tensor in Eq. (5.4.38) has the same form as in Hooke's Law for small strain elasticity, except for the dependence of the shear modulus μ on the deformation (see Eq. 5.4.36). Here λ_0 and μ_0 are the Lamé constants of the linearized theory. Near incompressible behavior is obtained for $\lambda_0 >> \mu_0$.

Saint Venant - Kirchhoff Model. A wide class of engineering problems can be studied by linear elastic material behavior. If the effects of large deformation are primarily due to rotations (such as in the bending of a marine riser or a fishing rod, for example) a straightforward generalization of Hooke's law to finite strains is often adequate. The Saint Venant-Kirchhoff model accomplishes this through the use of the Green strain measure **E** as follows. Let

$$w(\mathbf{C}) = W(\mathbf{E}) = \frac{1}{2}\mathbf{E}:\mathbf{C}^{SE}:\mathbf{E} \tag{5.4.39}$$

where

$$C_{ijkl}^{SE} = \lambda_0 \delta_{ij}\delta_{kl} + \mu_0\left(\delta_{ik}\delta_{jl} + \delta_{il}\delta_{kj}\right) \tag{5.4.40}$$

and where λ_0 and μ_0 are Lamé constants. Noting that

μ_0

and that

\begin{equation}

{\bf S} = 2{\partial \Psi({\bf C})\over \partial {\bf C}} =

{\partial W({\bf E})\over\partial {\bf E}}

\end{equation}

the components S_{ij} of the second Piola-Kirchhoff stress are given by

\begin{equation}

S_{ij} = \lambda_0 E_{kk}\delta_{ij} +

2\mu_0 E_{ij}

\end{equation}

or

\begin{equation}

{\bf S}=\lambda_0\, {\rm trace}\,({\bf E}){\bf I}

+ 2\mu_0 {\bf E} = \mbox{\boldmath ${\cal D}$}:{\bf E}

\end{equation}

Because the Green strain tensor is symmetric, it follows that the

stress tensor ${\bf S}$ is also symmetric. From Eq. () it is apparent that

the

fourth order material response tensor possesses major and minor

symmetries. Because ${\bf E}$, ${\bf F}$

and ${\bf C}$ are related ( ), it can also be shown that the components of the nominal stress tensor is given by

\begin{equation}
{\bf P} = {\partial W\over \partial {\bf F}^T}, \qquad
P_{ij} = {\partial W\over \partial F_{ji}}
\end{equation}

As the deformation gradient tensor ${\bf F}$ is not necessarily symmetric, the 9 components
of the nominal stress tensor ${\bf P}$ do not necessarily possess symmetry. Employing Eq. ( ), the Cauchy stress tensor $\mbox{\boldmath ${\sigma}$}$ is related to W by:

\begin{equation}
\mbox{\boldmath ${\sigma}$} = {1\over J} {\bf F}\cdot{\partial W\over
\partial {\bf F}^T} = {1\over J} {\bf F}\cdot {\partial W\over \partial
{\bf E}}\cdot {\bf
F}^T
\end{equation}

(Exercise: Show this.)

\noindent {\bf Modified Mooney-Rivlin Material}\par

In 1951, Rivlin and Saunders [ ] published their experimental results on the large elastic deformations of vulcanized rubber - an incompressible homogeneous isotropic elastic solid, in the Journal of Phil. Trans. A., Vol. 243, pp. 251-288. This material model with a few refinements is still the most commonly used model for rubber materials. It is assumed

in the model that behavior of the material is initially isotropic and path-independent, i.e., a stored energy function exists. The stored energy function is written

$$\Psi = \Psi({\bf C}) = W(I_1, I_2, I_3)$$

where I_1, I_2 and I_3 are the three scalar invariants of ${\bf C}$. Rivlin and Saunders considered an initially isotropic nonlinear elastic incompressible material ($I_3=1$) then

$$\Psi = \Psi(I_1,I_2) = \sum_{i=0}^\infty\sum_{j=0}^\infty \bar{c}_{ij}(I_1-3)^i(I_2-3)^j,\qquad \bar{c}_{00}=0$$

where $\bar{c}_{ij}$ are constants.
They performed a number of experiments on different types of rubbers and discovered that Eq. ( ) may be reduced to

$$\Psi = c(I_1 - 3) + f(I_2 - 3)$$

where c is a constant and
f is a function of $I_2 - 3$. For a Mooney-Rivlin material, W can be reduced further to

$$\Psi = \Psi(I_1, I_2) = c_1 (I_1 - 3) + c_2 (I_2 - 3)$$

An example of the set of c_1 and c_2 is: $c_1 = 18.35 {\rm psi}$ and
$ c_2 = 1.468 {\rm psi}.$ Equation ( ) is also an example of a
Neo-Hookean material, and the components of the second Piola-Kirchhoff stress
 can be obtained by
differentiating Eq. ( ) with respect to the components of the right
Cauchy Green deformation tensor
tensor; however, the deformation is constrained such that
\begin{equation}
{\bf S} = 2{\partial \Psi\over \partial {\bf C}}, \qquad{\rm with}\
I_3 =
{\rm det}\,{\bf C} = 1
\end{equation}

The condition $I_3 = 1$ simply implies that $J=1$ and there is no volume
change. The condition can be written as
\begin{equation}
 {\rm ln}I_3 = 0
 \end{equation}
 which represents a constraint on the deformation. One way in which the
 constraint ( ) can be enforced is through the use of a constrained
 potential, or stored energy, function [Ref]. Alternatively, a penalty
 function formulation (Hughes, 1987) can be used. In this case,
 the modified strain energy function
and the constitutive equation become:
\begin{eqnarray}
\bar{\Psi} &=& \Psi + p_0\,{\rm ln}I_3 + {1\over 2} \lambda({\rm ln}I_3)^2 \\
{\bf S} &=& 2{\partial \Psi\over \partial {\bf C}} + 2(p_0 + \lambda({\rm

ln}I_3)){\bf C}^{-1}

\end{eqnarray}

respectively. The penalty parameter λ must be large enough so that the

compressibility error is negligible (i.e., I_3 is approximately equal

to 1), yet not so large that numerical ill-conditioning occurs.

Numerical experiments reveal that $\lambda = 10^3\times {\rm max}(C_1,

C_2)$ to $\lambda = 10^7\times {\rm max}(C_1,

C_2)$ is adequate for floating-point

word length of 64 bits. The constant p_o is chosen so that the components

of ${\bf S}$ are all zero in the initial configuration, i.e,

\begin{equation}

po = -(C_1 + 2 C_2)

\end{equation}

$\bullet$ Exercises

\setcounter{equation}{0}

\subsection {Plasticity in One Dimension}

Materials for which permanent strains are developed upon unloading are called plastic materials. Many materials (such as metals) exhibit elastic (often linear) behavior up tp a well defined stress levlel called the yeild strength. Onec loaded beyond the initial yield strength, plastic strains are developed. Elastic plastic materials are further subdivided into rate-independent materials, where the stress is independent of the strain rate, i.e., the rate of loading has no effect on the stresses and rate-dependent materials , in which the stress depends on the strain

rate; such materials are often called strain rate-sensitive.

The major ingredients of the theory of
plasticity are

\begin{enumerate}
\item A decomposition of each increment of strain into an elastic,
reversible component $d\varepsilon^e$ and an irreversible plastic part
$d\varepsilon^p$.

\item A yield function f which governs the onset and continuance of
plastic deformation.

\item A flow rule which governs the plastic flow, i.e., determines the
plastic strain increments.

\item A hardening relation which governs the evolution of the yield function.
\end{enumerate}

There are two classes of elastic-plastic laws:

\begin{itemize}
\item Associative models, where the yield function and the potential
function are identical

\item Nonassociative models where the yield function and flow potential are
different.

\end{itemize}

Elastic-plastic laws are path-dependent and dissipative. A large part of the work expended in deforming the solid is irreversibly converted to other forms of energy, particularly heat, which can not be converted to mechanical work. The stress depends on the entire history of the deformation, and can not
be written as a single valued function of the strain as in ( ) and ( ).
The stress is path-dependent and dependes on the history of the deformation. We cannot therefore write an explicit relation for the stress in terms
of strain, but only as a relation between rates of stress and strain

The constitutive relations for rate-independent and rate-dependent plasticity in one-dimension are given in the following sections.

\subsubsection{\bf Rate-Independent Plasticity in One-Dimension}
A typical stress-strain curve for a metal under uniaxial stress is shown in Figure~\ref{fig:stress-strain}. Upon initial loading, the material behaves elastically (usually assumed linear) until the initial yield stress is attained. The elastic regime is followed by an elastic-plastic regime where permanent irreversible plastic strains are induced upon further loading.
Reversal of the stress is called unlaoding. In unloading, the
stress-strain response is typically
assumed to be governed by the elastic modulus and the strains
which remain after complete unloading are called

the plastic strains. The increments in strain are
assumed to be additively decomposed into elastic and plastic parts. Thus
we write

$$d\varepsilon = d\varepsilon^e + d\varepsilon^p$$

Dividing both sides of this equation by a differential time increment
dt gives the rate form

$$\dot{\varepsilon} = \dot{\varepsilon}^e + \dot{\varepsilon}^p$$

The stress increment (rate) is related to the increment (rate) of
elastic strain. Thus

$$d\sigma = Ed\varepsilon^e, \quad \dot\sigma = E\dot\varepsilon^e$$

relates the increment in stress to the increment in elastic strain.

In the nonlinear
elastic-plastic regime, the stress-strain relation is given by
(see Figure ( ))

$$d\sigma = Ed\varepsilon^e = E^{\rm tan} d\varepsilon$$

where the elastic-plastic tangent modulus, $E^{\rm tan}$, is the slope of the

stress-strain curve. In rate form, the relation is written as

\begin{equation}

\dot{\sigma} = E\dot{\varepsilon^e} = E^{\rm tan}\dot{\varepsilon}

\end{equation}

The above relations are homogeneous in the rates of stress and strain which means that if time
is scaled by an arbitrary factor, the constitutive relation remains
unchanged and therefore the material response is {\em rate-independent}
even though it is expressed in terms of a strain rate. In the sequel,
the rate form of the constitutive relations will be used as the notation
because the incremental form can get cumbersome especially for large strain formulations.

$\bullet$ kinematic hardening

The increase of stress after initial yield is called work or strain
hardening. The hardening behavior of the material is generally a
function of the prior history of plastic deformation.
In metal plasticity, the history of plastic deformation is often
charcterized by a
single quantitiy $\bar{\varepsilon}$ called the accumulated plastic strain
which is given by

\begin{equation}

\bar{\varepsilon} = \int\dot{{\bar\varepsilon}}dt

\end{equation}

where

\begin{equation}

\dot{\bar{\varepsilon}} = \sqrt{\dot{\varepsilon}^p\dot{\varepsilon}^p}

\end{equation}

is the effective plastic strain rate. The plastic strain rate is given by

\begin{equation}

\dot{\varepsilon}^p = \dot{\lambda}{\rm sgn}(\sigma)

\end{equation}

where

\begin{equation}

{\rm sign}(\sigma) = \left\{\begin{array}{cc} 1 & {\mbox{if $\sigma>0$}} \\

-1 & {\mbox{if $\sigma <0$}}

\end{array}

\right.

\end{equation}

>From ( ) it follows that

\begin{equation}

\dot{\lambda} = \dot{\bar{\varepsilon}}

\end{equation}

The accumulated

plastic strain $\bar{\varepsilon}$, is

an example of an internal variable used to characterize the inelastic

response of the material. An alternative, internal variable used in the

representation of hardening is the plastic work which is given by (Hill,

1958)

\begin{equation}

W^P = \int \sigma\dot{\varepsilon}^p dt

\end{equation}

The hardening behavior is often expressed through the dependence of the yield stress, Y, on the accumulated plastic strain, i.e., $Y = Y(\bar{\varepsilon})$. More general constitutive relations use additional internal variables.

A typical hardening curve is shown in Figure ( ). The slope of this curve is the plastic modulus, H, i.e.,

$$H = {dY(\bar{\varepsilon})\over d\bar{\varepsilon}}$$

The effective stress is defined as

$$\bar{\sigma} = \sqrt{\sigma^2}\equiv |\sigma | = \sigma {\rm sgn}(\sigma)$$

The yield condition is written as

$$f = \bar{\sigma} - Y(\bar{\varepsilon}) = 0$$

which is regarded as the equation for the yield point (or surface when multiaxial stress states are considered). Note that the plastic strain rate can be written as

$$\dot{\varepsilon}^p = \dot{\bar{\varepsilon}}{\rm sign}(\sigma) = \dot{\bar{\varepsilon}}{\partial f\over \partial \sigma}$$

where the result $\partial \bar{\sigma}/\partial \sigma = {\rm sign}(\sigma)$ has been used. For plasticity in one-dimension (uniaxial stress), the distinction between associated and non-associated plasticity is nost possible. Also, the lateral strain which accompanies the axial strain has both elastic and plastic parts. This point will be addressed further in Section X on multiaxial plasticity.

Plastic deformation occurs only when the yield condition is met. Upon plastic loading, the stress must remain at yield, which is called the {\em consistency} condition, and is given by

\begin{equation}
\dot{f} = \dot{\bar{\sigma}} - \dot{Y}(\bar{\varepsilon}) = 0.
\end{equation}

>From ( ) it follows that, during plastic loading,

\begin{equation}
\dot{\bar{\sigma}} = {dY(\bar{\varepsilon})\over d\bar{\varepsilon}}\dot{\bar{\varepsilon}} = H\dot{\bar{\varepsilon}}
\end{equation}

Using ( ), ( ) and ( ) in ( ) gives

\begin{equation}
{1\over E^{\rm tan}} = {1\over E} + {1\over H}
\end{equation}

or

\begin{equation}
E^{\rm tan} = {EH\over E + H} = E - {E^2\over E + H}
\end{equation}

The plastic switch parameter α is introduced with $\alpha=1$ corresponding to plastic
loading and $\alpha=0$ corresponding to purely elastic response (loading or unlaoding). Thus the tangent modulus is written

\begin{equation}
E^{\rm tan} = E - \alpha{E^2\over E + H}
\end{equation}

An alternative way of writing the laoding-unlaoding conditions without using the switch parameter α is through the use of the Kuhn-Tucker conditions, which play an important role in mathematical programming theory [Ref?]
For plasticity, the conditions are:
\begin{equation}
\dot{\lambda}\dot{f}=0,\quad \dot{\lambda}\ge 0, \quad \dot{f}\le 0
\end{equation}
Thus for plastic loading, $\dot{\lambda}\ge 0$ and the consistency condition $\dot{f}=0$ is satisfied. For purely elastic loading or unloading, $\dot{f}\ne 0$ and it follows that $\dot{\lambda}=0$.

The constitutive relations for rate-independent plasticity in 1D are summarized in Box 9.1.

\subsubsection{Rate-Dependent Plasticity in One Dimension}

In rate dependent plasticity, the plastic response of the material depends on the rate of loading. The elastic response is given as before (in rate form) as

$$\dot{\sigma} = E\dot{\varepsilon}^e$$

which may be written using the elastic-plastic decomposition of the total strain rate (Equation) as

$$\dot{\sigma}=E(\dot{\varepsilon}-\dot{\varepsilon}^p).$$

For plastic deformation to occur the yield condition must be met or exceeded. This differs from the rate-independent case in that in rate-dependent plasticity the stress can exceed the yield stress.

The plastic strain rate is given by

$$\dot\varepsilon^p = \dot{\bar\varepsilon} {\rm sgn}\sigma$$

For many rate-dependent materials, the plastic response is characterized by an overstress model of the form

$$\dot{\bar{\varepsilon}} = {\phi (\sigma, \bar{\varepsilon})\over \eta}$$

where, ϕ is the overstress and η is the viscosity.

For example, the overstress model introduced by Perzyna (19xx) is given by

\begin{equation}

\phi = Y\bigl({\bar{\sigma}\over Y}-1\bigr)^n

\end{equation}

where n is called the rate-sensivity

exponent. Using ( ) and ( ) the expression for the stress rate is given by

\begin{equation}

\dot{\sigma}=E\biggl(\dot{\varepsilon} - {\phi(\sigma, \bar{\varepsilon})

\over \eta}{\rm sgn}(\sigma)\biggr).

\end{equation}

which is a differential equation for the evolution of the stress.

Comparing this expression to ( ), it can be seen that ( ) is

inhomogeneous in the rates and therefore the material response is

{\em rate-dependent}. Models of this type are often used to model the

strain-rate dependence observed in materials. More elaborate models with

additional internal variables and perhaps different response in different

strain-rate regimes have been developed (see for examplethe unified creep

plasticity model [Ref]). Nevertheless, the simple overstress model ( )

has been very successful in capturing the strain rate dependence of

metals over a large range of strain rates [Refs].

An alternative form of rate-dependent plasticity that has been used with

considerable success by Needleman ( ) and others is given by

\begin{equation}

\dot{\bar{\varepsilon}}^p = \dot{\varepsilon_0}\biggl({\bar{\sigma}\over

Y}\biggr)^{1/m}

\end{equation}

without any explicit yield surface. For plastic straining at the rate $\dot{\varepsilon_0}$, the response $\bar{\sigma}=Y$ is obtained. This response is called the reference response and can be obtained by performing a unixial stress test with a plastic strain rate $\dot{\varepsilon}_0$. In the case of small elastic strain rates, the test can be run at total strain rate of $\dot{\epsilon}_0$ without significant error (Check!). For rates which exceed $\dot{\varepsilon}_0$ the stress is elevated above the reference stress while for lower rates the stress falls below this value. A case of particular interest is the near rate-independent limit when the rate-sensitivity exponent $m\to 0$. It can be seen from ( ) that, for $\bar{\sigma}<Y$, the effective plastic strain rate is negligible while for a finite plastic strain rate the effective stress is approximately equal to the reference stress, Y. In this way, the model exhibits an effective yield limit together with near elastic unloading and rate-independent response.

The constitutive relations for rate-dependent plasticity in 1D are summarized in Box 9.2

CHAPTER 6
SOLUTION METHODS AND STABILITY

Very Rough Draft-use equations at your own peril

by Ted Belytschko and Brian Moran
Northwestern University

6.1 INTRODUCTION

This Chapter describes solution procedures for nonlinear finite element discretizations. In addition, methods for examining the physical stability of solutions and the stability of solution procedures are described.

The first part of the chapter describes time integration, the procedures used for integrating the discrete momemtum equation and other time dependent equations in the system, such as the constitutive equation. We begin with the simplest of methods, the central difference method for explicit time integration. Next the family of Newmark β-methods, which encompass both explicit and implicit methods, are described. Explicit and implicit methods are compared and their relative advantages described. As part of implicit methods, the solution of equilibrium equations is also examined.

A critical step in the solution of implicit systems and equilibrium problems is the linearization of the governing equations. Linearization procedures for the equations of motion, and as a special case, the equilibrium equations are described.

6.2 EXPLICIT METHODS

In this Section the major features of explicit and implicit time integration methods for the discretized momentum equation and solution methods for the discrete equilibrium equations are described. The methods are described in the context of Lagrangian meshes, but can be extended to Eulerian and ALE meshes with some techniques described in Chapter 7. The description of the solution procedures of equilibrium problems is combined with the description of implicit procedures for dynamic problems, because, as we show later, the methodologies are almost identical; the solution of a static problem by an implicit method only requires that the inertial term be dropped.

To illustrate the major features of explicit and implicit methods for time integration, the solution of the equations of motion is first considered for rate-independent materials. In this class of equations, we can avoid some of the complications that arise in the treatment of rate-dependent materials but still illustrate the most important properties of explicit and implicit methods. We will first describe explicit and implicit methods using only a single time integration formula: the central difference method for explicit time integration and the

Newmark β-methods for implicit integration. In Section X, other time integration formulas are considered.

6.2.1. Central Difference Method. The central difference method is among the most popular of the explicit methods in computational mechanics and physics. It has already been discussed in Chapter 2, where it was chosen to demonstrate some nonlinear solutions in one dimension. The central difference method is developed from central difference formulas for the velocity and acceleration. We consider here its application to Lagrangian meshes with rate-independent materials. Geometric and material nonlinearites are included, and in fact have little effect on the time integration algorithm.

For the purpose of developing this and other time integrators we will use the following notation. Let the time of the simulation $0 \le t \le t_E$ be subdivided into time intervals, or time steps, Δt^n, $n = 1$ to n_{TS} where n_{TS} is the number of time steps and t_E is the end-time of the simulation; Δt^n is also called the nth time increment. The variables at any time step are indicated by a superscript; thus t^n is the time at time step n, $t^0 = 0$ is the beginning of the simulation and $\mathbf{d}^n \equiv \mathbf{d}\left(t^n\right)$ is the matrix of nodal displacements at time step n. Time increment n is given by

$$\Delta t^n = t^n - t^{n-1} \qquad \Delta t^{n+\frac{1}{2}} = \tfrac{1}{2}\left(\Delta t^n + \Delta t^{n+1}\right) \tag{6.2.1}$$

where the second equation gives the midpoint time step.

The central difference formula for the velocity is

$$\dot{\mathbf{d}}^{n+\frac{1}{2}} \equiv \mathbf{v}^{n+\frac{1}{2}} = \frac{1}{\Delta t^{n+\frac{1}{2}}}\left(\mathbf{d}^{n+1} - \mathbf{d}^n\right), \quad \mathbf{d}^{n+1} = \mathbf{d}^n + \Delta t^{n+\frac{1}{2}}\mathbf{v}^{n+\frac{1}{2}} \tag{6.2.2}$$

where the second equation gives the corresponding integration equation which is obtained by a rearrangement of the first. The acceleration is given by

$$\ddot{\mathbf{d}}^n \equiv \mathbf{a}^n = \frac{1}{\Delta t^n}\left(\mathbf{v}^{n+\frac{1}{2}} - \mathbf{v}^{n-\frac{1}{2}}\right) \qquad \mathbf{v}^{n+\frac{1}{2}} = \mathbf{v}^{n-\frac{1}{2}} + \Delta t^n \mathbf{a}^n \tag{6.2.3a}$$

As can be seen from the above, the velocities are defined at the midpoints of the time intervals, or at half-steps. By substituting (6.2.2a) and its counterpart for the previous time step into (6.2.3), the acceleration can be expressed directly in terms of the displacements

$$\ddot{\mathbf{d}}^n \equiv \mathbf{a}^n = \frac{\Delta t^{n-\frac{1}{2}}\left(\mathbf{d}^{n+1} - \mathbf{d}^n\right) - \Delta t^{n+\frac{1}{2}}\left(\mathbf{d}^n - \mathbf{d}^{n-1}\right)}{\Delta t^n \Delta t^{n-\frac{1}{2}} \Delta t^{n+\frac{1}{2}}} \tag{6.2.3b}$$

For the case of equal time steps the above reduces to

$$\ddot{\mathbf{d}}^n \equiv \mathbf{a}^n = \frac{\left(\mathbf{d}^{n+1} - 2\mathbf{d}^n + \mathbf{d}^{n-1}\right)}{\left(\Delta t^n\right)^2} \tag{6.2.3c}$$

This is the well known central difference formula for the second derivative of a function.

We now consider the time integration of the undamped equations of motion for rate-independent materials, Eq. (4.x.x.), which at time step *n* are given by

$$\mathbf{M}\mathbf{a}^n = \mathbf{f}^n = \mathbf{f}^{ext}\left(\mathbf{d}^n, t^n\right) - \mathbf{f}^{int}\left(\mathbf{d}^n, t^n\right) \tag{6.2.4a}$$

$$\text{subject to } g_I\left(\mathbf{d}^n\right) = 0, \quad I = 1 \text{to } n_c \tag{6.2.4b}$$

where (6.2.4b) is a generalized representation of the n_c displacement boundary conditions; constraints may also arise from other conditions on the model. The mass matrix in this expression is considered constant because as noted in Section X, it is time independent for a Lagrangian mesh. Methods for Eulerian meshes are discussed in Chapter 7. The internal and external nodal forces are functions of the nodal displacements and the time. The external loads are usually prescribed as functions of time; they may also be functions of the nodal displacements because they may depend on the configuration of the structure, as when pressures are applied to the surfaces which undergo large deformations. The dependence of the internal nodal forces on displacements is quite obvious: the nodal displacements determine the strains, which in turn determine the stresses and hence the nodal internal forces by Eq. (4.4.11). Internal nodal forces are generally not directly dependent on time, but there are situations of engineering relevance when this is the case; for example, when the temperature is prescribed as a function of time, the stresses and hence the internal nodal forces depend directly on time.

The equations for updating the nodal velocities and displacements are obtained as follows. Substituting Eq. (6.2.4a) into (6.2.3b) gives

$$\mathbf{v}^{n+\frac{1}{2}} = \Delta t^n \mathbf{M}^{-1}\mathbf{f}^n + \mathbf{v}^{n-\frac{1}{2}} \tag{6.2.5}$$

which provides an update for the nodal velocities; the displacements are then updated by (6.2.2).

At any time step *n*, the displacements $\mathbf{d}^n$ will be known. The nodal forces $\mathbf{f}^n$ can be determined by using in sequence the strain-displacement equations, the constitutive equation and the relation for the nodal internal forces. Thus the entire right hand side of (6.2.5) can be evaluated, which gives $\upsilon^{n+1/2}$, and the displacements $\mathbf{d}^{n+1}$ at time step $n+1$ can be determined by (6.2.2b). The entire update can be accomplished without solving any system equations provided that the mass matrix $\mathbf{M}$ is diagonal. This is the salient characteristic of an explicit method:

in an explicit method, the time integration of the discrete momentum equations for a finite element model does not require the solution of any equations.

In numerical analysis, integration methods are classified according to the structure of the time difference equation. The difference equations for first and second derivatives are written in the general forms

$$\sum_{n=0}^{n_S}\left(\alpha_n \mathbf{d}^{n_S-n} - \Delta t \beta_n \dot{\mathbf{d}}^n\right) = 0 \qquad \sum_{n=0}^{n_S}\left(\bar{\alpha}_n \mathbf{d}^{n_S-n} - \Delta t^2 \bar{\beta}_n \ddot{\mathbf{d}}^n\right) = 0 \tag{6.2.6}$$

where n_S is the number of steps in the difference equation. The difference formula for the first or second derivatives is called explicit if $\beta_0 = 0$ or $\bar{\beta}_0 = 0$, respectively. From (6.2.3c) it can be seen that $\bar{\beta}_0 = 0, \bar{\beta}_1 = 1, \bar{\beta}_2 = 0$, so the formula is explicit. Thus the difference formula is called explicit if the equation for the function at time step *n* only involves the derivatives at previous time steps. Difference equations which are explicit according to this classification generally lead to solution schemes which require no solution of equations. In most cases there is no benefit in using explicit schemes which involve the solution of equations, so the use of such explicit schemes is rare. There are a few exceptions. For example, if the consistent mass is used with the central difference method, even though the difference equation is classified as explicit, system equations still need to be solved in the update.

6.2.2. Implementation. A flow chart for explicit time integration of a finite element model with rate-independent materials is shown in Box 6.1. This flowchart generalizes the flowchart given in Chapter 2 by considering nonzero initial conditions, a variable time step and including elements which require more than one-point quadrature. The primary dependent variables in this flowchart are the velocities and the Cauchy stresses. Initial conditions must be given for the velocitites, the Cauchy stresses, and all state variables of the materials in the model. The displacements are initially considered to vanish.

Flowchart inorrect, half missing on time steps, not n order

Box 6.1
Flowchart for Explicit Time Integration

1. Initial conditions and initialization:

   set $\mathbf{v}^0, \sigma^0$, and other material state variables;

   $\mathbf{d}^0 = 0, n = 0, t = 0$; compute $\mathbf{M}$

2. *getf* $\left(\mathbf{f}^n, \Delta t_{crit}\right)$
3. compute accelerations $\mathbf{a}^n = \mathbf{M}^{-1}\mathbf{f}^n$
4. compute kinetic energy and check energy balance, see Section ??
5. update nodal velocities: $\mathbf{v}^{n+\frac{1}{2}} = \mathbf{v}^n + \frac{1}{2}\Delta t^n \mathbf{a}^n$

6. enforce velocity boundary conditions:

   if node I on Γ_{v_i}: $v_{iI}^{n+\frac{1}{2}} = \bar{v}_i\left(\mathbf{x}_I, t_{n+\frac{1}{2}}\right)$

7. update nodal displacements: $\mathbf{d}^{n+1} = \mathbf{d}^n + \Delta t^{n+\frac{1}{2}} \mathbf{v}^{n+\frac{1}{2}}$
8. update counter and time: $n \leftarrow n+1,\ t \leftarrow t + \Delta t$
9. update nodal velocities: $\mathbf{v}^{n+1} = \mathbf{v}^{n+\frac{1}{2}} + \frac{1}{2}\Delta t^n \mathbf{a}^n$
10. output, if simulation not complete, go to 2

Subroutine *getf* $\left(\mathbf{f}^n, \Delta t_{crit}\right)$

0. initialization: $\mathbf{f}^n = 0,\ \Delta t_{crit} = \infty$
1. compute external nodal forces $\mathbf{f}^{ext,n}$ which are global
2. loop over elements e
   - i. GATHER element nodal displacements and velocities
   - ii. $\mathbf{f}_e^{int,n} = 0$
   - iii. loop over quadrature points ξ_Q
     1. if n=0, go to 8
     2. compute measures of deformation: $\mathbf{D}^{n-\frac{1}{2}}\left(\xi_Q\right), \mathbf{F}^n\left(\xi_Q\right), \mathbf{E}^n\left(\xi_Q\right)$
     3. compute stress $\sigma^n\left(\xi_Q\right)$ by constitutive equation
     4. $\mathbf{f}_e^{int,n} \leftarrow \mathbf{f}_e^{int,n} + \mathcal{B}^T \sigma^n \bar{w}_Q J\Big|_{\xi_Q}$

     END quadrature point loop
   - iv. compute external nodal forces on element, $\mathbf{f}_e^{ext,n}$
   - v. $\mathbf{f}_e^n = \mathbf{f}_e^{ext,n} - \mathbf{f}_e^{int,n}$
   - vi. compute Δt_{crit}^e, if $\Delta t_{crit}^e < \Delta t_{crit}$ then $\Delta t_{crit} = \Delta t_{crit}^e$
   - vii. SCATTER $\mathbf{f}_e^n$ to global $\mathbf{f}^n$
3. END loop over elements

In this algorithm, the accelerations are first integrated to obtain the velocities. The integration of the velocities is broken into two half-steps so that the velocities are available at an integer step in the computation of the energy balance. The displacements are computed in each time step by integrating the velocities.

The main part of the procedure is the calculation of the nodal forces from the nodal displacements at a given time step, which is performed in *getf*. In this subroutine, the equations governing a continuum are used along with the gather/scatter procedures:

1. the nodal displacements of the element are extracted from the global matrix of nodal displacements by the "gather " operation;
2. the strain measures are computed at each quadrature point of the element;
3. the stresses are computed by the constitutive equation at each quadrature point;
4. the internal nodal forces are computed by integrating the product of the $\boldsymbol{B}$ matrix and the stresses over the domain of the element with the Cauchy stress;
5. the nodal forces of the element are scattered into the global array.

In the first time step, the strain measures and the stress are not computed. Instead, as shown in the flowchart, the initial stresses are used to obtain the internal nodal forces.

The flowchart shows the algorithm with the matrix form of the internal force computation, in which the stress tensor is stored as a square matrix and the $\boldsymbol{B}$ matrix is used. The change to the Voigt form only requires the use of a column matrix for the stresses and the $\mathbf{B}$ matrix, (4.5.14). Similarly, the internal force computation can be changed to the total Lagrangian format by replacing the discrete values of the integrand in step 10 by the integrands of (B4.8.2).

Most essential boundary conditions are easily handled in explicit methods. For example, if the velocities or displacements are prescribed as functions of time along any boundary, then the velocity/displacement boundary conditions can be enforced by setting the nodal velocities according to the data:

$$v_{iI}^n = \bar{v}_i\left(\mathbf{x}_I, t^n\right) \tag{6.2.7}$$

If the data is not available on the nodes, the least square procedure given in Section 2.4.5 can be used to fit the nodal values.

The velocity boundary conditions can also be enforced in local coordinate systems as shown in the Box 6.1. In that case, the equations of motion at these nodes must be expressed in the local coordinate system, so the nodal force components must be expressed in the local coordinate systems before assembly and time integration. The boundary condition is also enforced in the local coordinate system. The orientation of the local coordinate system may vary with time but the time integration formulas must then be modified to account for the additional terms in the equations of motion.

When essential boundary conditions are given as linear or nonlinear algebraic equations relating the displacements, the implementation is more complicated. One approach is to use a linearization of the constraint. Consider for example the nonlinear constraint

$$\mathbf{g}\left(\mathbf{d}(t)\right) = 0 \tag{6.2.8}$$

where $\mathbf{g}\left(\mathbf{d}(t)\right)$ is a linear or nonlinear algebraic function of the nodal displacements. If the constraint involves integral or differential relationships, such as a dependence on the velocities, it can be put in the above form by using

difference equations or a numerical approximation of the integral. The above can be linearized as follows:

$$\left(\frac{\partial G\left(\mathbf{d}^n\right)}{\partial d_a} + \frac{\partial G\left(\mathbf{d}^{n+1}\right)}{\partial d_a} \right) v_a^{n+1/2} = 0 \tag{6.2.9}$$

After a large number of time steps, linearizations such as the above combined with a central difference update of the displacements may substantially violate the constraint. This drift in the enforcement of the constraint can be avoided by correcting the linearized update so that the constraint is enforced exactly at the next time step, n+1. When accurate treatment of the constraints is important, techniques for differential-algebraic equations should be used, Petzold (??).

As can be seen from the flowchart, an explicit method is easily implemented. Furthermore, explicit time integration is very robust, by which we mean that the explicit procedure seldom aborts due to failure of the numerical algorithm. The salient disadvantage of explicit integration, the price you pay for the simplicity of the method and its avoidance of the solution of equations, is *the conditional stability of explicit methods.* If the time step exceeds a critical value Δt_{crit}, the solution may grow unboundedly and will in any case be erroneous.

The *critical time step* is also called the *stable time step.* The critical time step for a model depends on the mesh and the material properties. For low order elements, we will show in Section X that the critical time step for linear response is given by

$$\Delta t_{crit} = \min \frac{\ell_e}{c_e} \tag{6.2.10}$$

where ℓ_e is a characteristic length of element e and c_e the wavespeed of element e. Thus the critical time step decreases with mesh refinement and increasing stiffness of the material. The cost of an explicit simulation is independent of the frequency content which is of interest and depends only on the size of the model and the time of the simulation relative to the critical time step given by (6.2.10).

The time step is calculated in the flowchart on an element basis. For each element, a critical time step is calculated, and if it is smaller than that calculated for all previous elements in that time step, it is reset. The theoretical justification for setting the critical time step on an element basis and other approaches are described in Section 6.??.

6.3 EQUILIBRIUM SOLUTIONS AND IMPLICIT TIME INTEGRATION.

6.3.1. Equilibrium and Transient Problems. We will combine the description of the solution of the equilibrium equations with time integration by implicit methods because they share many common features. To begin, we write

the discrete momentum equation at time step *n+1* in a form applicable to both equilibrium and dynamic problems:

$$0 = \mathbf{r}\left(\mathbf{d}^{n+1}, t^{n+1}\right) = s_D \mathbf{M}\ddot{\mathbf{d}}^{n+1} - \mathbf{f}^{n+1} = s_D \mathbf{M}\mathbf{a}^{n+1} - \mathbf{f}^{ext}\left(\mathbf{d}^{n+1}, t^{n+1}\right) + \mathbf{f}^{int}\left(\mathbf{d}^{n+1}\right) \quad (6.3.1)$$

where s_D is a switch which is set by:

$$s_D = \begin{cases} 0 & \text{for a static(equilibrium)problem} \\ 1 & \text{for a dynamic(transient) problem} \end{cases} \quad (6.3.2)$$

The column matrix $\mathbf{r}(\mathbf{d}^{n+1}, t^{n+1})$ is called a residual. When $s_D = 0$, the above are the equilibrium equations at the next step. In addition, the displacement boundary conditions must be met; these can be written as a set of n_c nonlinear algebaric equations

$$G_i\left(\mathbf{d}^{n+1}\right) = g_i, \quad i = 1 \text{ to } n_c \quad (6.3.2b)$$

Differential and integral constraints are put in discrete form by using discretizations of the derivatives and integrals, respectively. In most cases the displacement boundary conditions are linear algebraic equations, but we have written the general form (6.3.2b) because complex boundary conditions are often needed in nonlinear problems.

When the accelerations vanish or are negligible, a system is in equilibrium and the solution of the resulting equations is called an *equilibrium solution*. The equilibrium equations are given by (6.3.1) with $s_D = 0$:

$$0 = \mathbf{r}\left(\mathbf{d}^{n+1}, t^{n+1}\right) = \mathbf{f}^{int}\left(\mathbf{d}^{n+1}, t^{n+1}\right) - \mathbf{f}^{ext}\left(\mathbf{d}^{n+1}, t^{n+1}\right) \quad (6.3.3)$$

In equilibrium problems, the residuals correspond to the out-of-balance forces; problems in which the accelerations can be neglected are called static problems.

The governing equations for both the implicit update of the equations of motion and the equilibrium equations are a set of nonlinear algebraic equations in the nodal displacements, $\mathbf{d}^{n+1}$. In equilibrium problems with rate-independent materials, t need not be the real time. Instead it can be any monotonically increasing parameter which describes the changing load. If the constitutive equation is a differential or integral equation, it must also be discretized in time to obtain a set of algebraic equations for the system.

6.3.2a. Newmark β-equations. We will now show that the discrete equations obtained with an implicit time integrator are nonlinear algebraic equations in the unknowns $\mathbf{d}^{n+1}$. For this purpose we consider a popular class of time integrators called the Newmark β-method. In this time integration formula, the updated displacements and velocities are given by

$$\mathbf{d}^{n+1} = \tilde{\mathbf{d}}^{n} + \beta \Delta t^2 \mathbf{a}^{n+1} \quad (6.3.4)$$

$$\tilde{\mathbf{d}}^n = \mathbf{d}^n + \Delta t \mathbf{v}^n + \tfrac{\Delta t^2}{2}(1-2\beta)\mathbf{a}^n \tag{6.3.5}$$

$$\mathbf{v}^{n+1} = \tilde{\mathbf{v}}^n + \gamma \Delta t \mathbf{a}^{n+1} \tag{6.3.6}$$

$$\tilde{\mathbf{v}}^n = \mathbf{v}^n + (1-\gamma)\Delta t \mathbf{a}^n \tag{6.3.7}$$

Here β and γ are parameters whose useful values are summarized in Box 6.2. In writing the time integration formulas, we have segregated the historical values of the nodal variables, i.e. those pertaining to time step *n*, in $\tilde{\mathbf{v}}^n$ and $\tilde{\mathbf{d}}^n$. The resulting formulas correspond to the predictor-corrector form given by Hughes and Liu( ). This segregation of the historical terms is convenient for the algebraic operations which follow and for the construction of explicit-implicit time integration procedures.

Equation (6.3.4) can be solved for the updated accelerations for $\beta > 0$, giving

$$\mathbf{a}^{n+1} = \tfrac{1}{\beta \Delta t^2}\left(\mathbf{d}^{n+1} - \tilde{\mathbf{d}}^{n+1}\right) \tag{6.3.8}$$

Substituting (6.3.8) into (6.3.1) gives

$$0 = \mathbf{r} = \tfrac{s_D}{\beta \Delta t^2}\mathbf{M}(\mathbf{d}^{n+1} - \tilde{\mathbf{d}}^n) - \mathbf{f}^{ext}\left(\mathbf{d}^{n+1}, t^{n+1}\right) + \mathbf{f}^{int}\left(\mathbf{d}^{n+1}, t^{n+1}\right) \tag{6.3.9}$$

which is a set of nonlinear algebraic equations in the nodal displacements $\mathbf{d}^{n+1}$. Eq.(6.3.9) applies to both the static and dynamic problems. Therefore, in both cases we consider the discrete problem to be

$$\text{find } \mathbf{d}^{n+1} \text{ so that } \mathbf{r}\left(\mathbf{d}^{n+1}\right) = \mathbf{0} \text{ subject to } \mathbf{g}\left(\mathbf{d}^{n+1}\right) = 0 \tag{6.3.10}$$

where $\mathbf{r}\left(\mathbf{d}^{n+1}\right)$ is given by Eq. (6.3.9).

6.3.3. Newton's Method. The most widely used and most robust method for the solution of the nonlinear algebraic equations (6.3.9) is Newton's method. The method is often called the Newton-Raphson method in computational mechanics. It is identical to the Newton method taught in introductory calculus courses.

We first illustrate the Newton method for one equation in one unknown *d* without a displacement boundary condition. It is then generalized to an arbitrary number of unknowns. For the case of one unknown, (6.3.9) reduces to a single nonlinear algebraic equation

$$r\left(d^{n+1}, t^{n+1}\right) = \tfrac{s_D}{\beta \Delta t^2} M\left(d^{n+1} - \tilde{d}^n\right) - f\left(d^{n+1}, t^{n+1}\right) = 0 \tag{6.3.11}$$

The solution of (6.3.11) by Newton's method is an iterative procedure. The iteration number is indicated by Greek subsript: d_υ^{n+1} is the υth iteration at time step n+1; when there is no chance for confusion, the time step number will be omitted.

To begin the iterative procedure, a starting value for the unknown must be chosen; usually the value of the solution d^n from the last time step is used, so $d_0^{n+1} \equiv d^n$ Taking a Taylor expansion of the residual about the current value of the nodal displacement, d_υ and setting the resulting residual equal to zero:

$$0 = r\left(d_{\upsilon+1}, t^{n+1}\right) = r\left(d_\upsilon, t^{n+1}\right) + \frac{\partial r\left(d_\upsilon, t^{n+1}\right)}{\partial d}\Delta d + O\left(\Delta d^2\right) \tag{6.3.12}$$

where

$$\Delta d = d_{\upsilon+1} - d_\upsilon, \tag{6.3.12b}$$

$$r\left(d_\upsilon, t^{n+1}\right) = Ma\left(d_\upsilon\right) + f^{int}\left(d_\upsilon, t^{n+1}\right) - f^{ext}\left(d_\upsilon, t^{n+1}\right) \tag{6.3.13}$$

If the terms which are higher order in Δd than linear are dropped, then (6.3.12) gives a linear equation for Δd:

$$0 = r\left(d_\upsilon, t^{n+1}\right) + \frac{\partial r\left(d_\upsilon, t^{n+1}\right)}{\partial d}\Delta d \tag{6.3.14}$$

Note that in the Taylor expansion, the residual is written in terms of the time t^{n+1}. The time-dependence of the residual at constant nodal displacements is usually known. For example, if the tractions and body forces are given as functions of time, then the time dependent part of the nodal forces is known at time t^{n+1} at the beginning of the iterations. Therefore the residual is always computed at time t^{n+1}. The above is called a linear model of the nonlinear equations. The linear model is the tangent to the nonlinear residual function; the process of obtaining the linear model is called *linearization.*

Equation (6.3.14) is often called a linear model of the nonlinear equations, Schnabel (?). Solving this linear model for the incremental displacements gives

$$\Delta d = -\left(\frac{\partial r(d_\upsilon)}{\partial d}\right)^{-1} r(d_\upsilon) \tag{6.3.15}$$

In the Newton procedure, the solution to the nonlinear equation is obtained by iteratively solving a sequence of linear models (6.3.15). The new value for the unknown in each step of the iteration is obtained by rewriting Eq. (6.3.12b) as

$$d_{\upsilon+1} = d_\upsilon + \Delta d \tag{6.3.16}$$

The procedure is illustrated in Fig. 6.1. The process is continued until the solution is obtained with the desired level of accuracy.

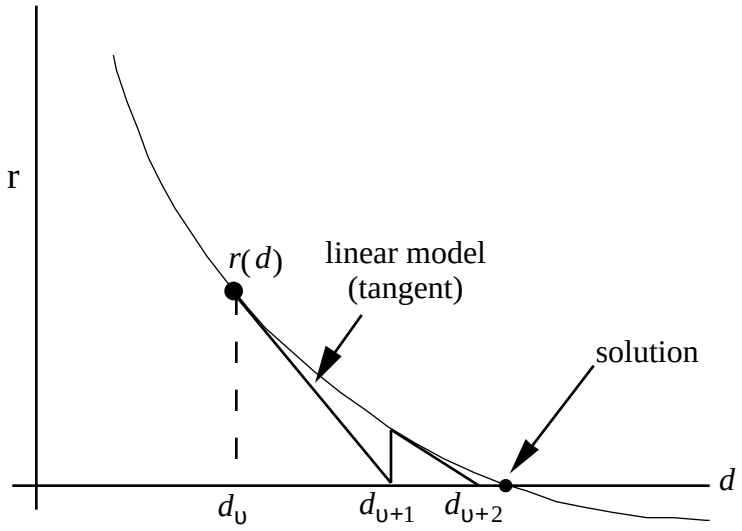

Fig. 6.1. Linear models for a nonlinear equation $r(d) = 0$.

6.3.4. Newton's Method for *n* Unknowns. The generalization of this procedure to n_{DOF} unknowns is accomplished by replacing the above scalar equations by matrix equations. The counterpart of Eq. (6.3.12) becomes

$$\mathbf{r}(\mathbf{d}_\upsilon) + \frac{\partial \mathbf{r}(\mathbf{d}_\upsilon)}{\partial \mathbf{d}} \Delta\mathbf{d} + O\left(\Delta\mathbf{d}^2\right) = 0$$

or

$$r_a\left(\mathbf{d}_\upsilon\right) + \sum_{b=1}^{n_{DOF}} \frac{\partial r_a\left(\mathbf{d}_\upsilon\right)}{\partial d_b} \Delta d_b + O\left(\Delta d_b\right)^2 = 0 \tag{6.3.17}$$

The matrix $\partial \mathbf{r} / \partial \mathbf{d}$ is called the Jacobian matrix and will be denoted by **A:**

$$\mathbf{A} = \frac{\partial \mathbf{r}}{\partial \mathbf{d}}, \quad \text{or} \quad A_{ab} = \frac{\partial r_a}{\partial d_b} \tag{6.3.18}$$

Using (6.3.17) and dropping terms in higher order than linear, Eqs. (6.3.16) can be rewritten as

$$\mathbf{r} + \mathbf{A}\Delta\mathbf{d} = \mathbf{0} \tag{6.3.19}$$

which is the linear model of the nonlinear equations. The linear model is difficult to picture for problems with more than one unknown, since $\mathbf{r}(\mathbf{d})$ maps ^{n} to ^{n}, Figure 6.2 shows the first component of the residual for a function of two unknowns. The linear model is a plane tangent to the nonlinear function $r_1(d_1, d_2)$. The other residual component is another nonlinear function $r_2(d_1, d_2)$, which is not drawn.

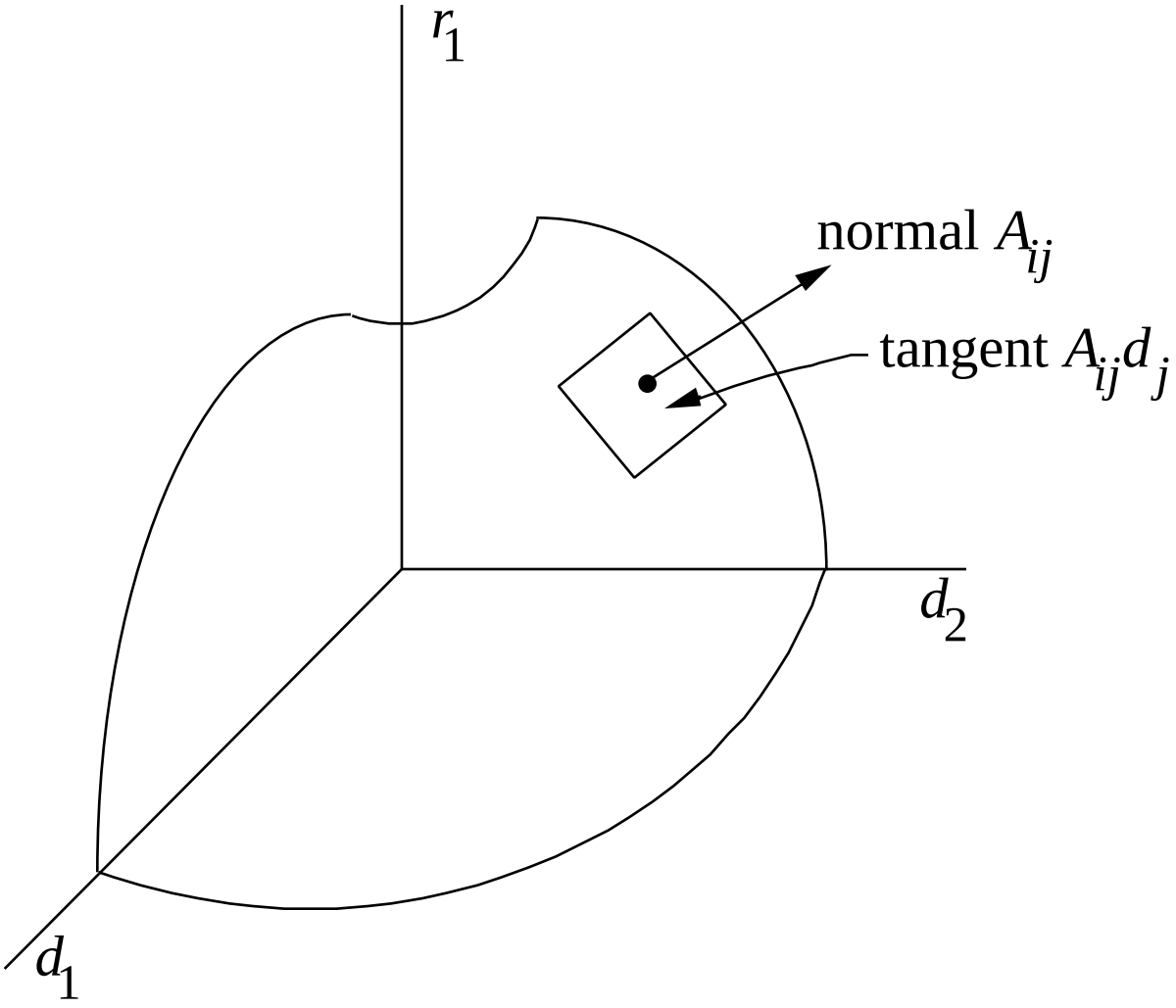

Figure 6.2. Depiction of a residual component r_1 as a function of d_1 and d_2 and the tangent plane.

The increment in the nodal displacements in the Newton iterative procedure is obtained by solving (6.3.18), which gives

$$\Delta\mathbf{d} = -\mathbf{A}^{-1}\mathbf{r}\left(\mathbf{d}_\upsilon, t^{n+1}\right) \tag{6.3.20}$$

The increment in the nodal displacements is obtained from this system of linear algebraic equations. The solution of these equations is discussed in Section X. Once the increments in nodal displacements have been obtained, the new values of the nodal displacements are obtained by

$$\mathbf{d}_{\upsilon+1} = \mathbf{d}_{\upsilon} + \Delta\mathbf{d} \tag{6.3.21}$$

The new displacement is checked for convergence, see Section 6.3.7. If the convergence criterion is not met, a new linear model is constructed and used to find another increment in the nodal displacements. The procedure is repeated until the convergence criterion is satisfied.

In computational mechanics, the Jacobian is called the *effective tangent stiffness matrix* and the contributions of the inertial, internal and external nodal forces are linearized separately. From (6.3.9) we can write

$$\mathbf{A} = \frac{\partial \mathbf{r}}{\partial \mathbf{d}} = \frac{s_D}{\beta \Delta t^2}\mathbf{M} + \frac{\partial \mathbf{f}^{int}}{\partial \mathbf{d}} - \frac{\partial \mathbf{f}^{ext}}{\partial \mathbf{d}} \tag{6.3.22}$$

where we have used the fact that the mass matrix in a Lagrangian mesh is constant in time and (6.3.4). The Jacobian of the internal nodal forces is called the *tangent stiffness matrix* and will be denoted by $\mathbf{K}^{int}$:

$$K_{ab}^{int} = \frac{\partial f_a^{int}}{\partial d_b} \qquad K_{iIjJ}^{int} = \frac{\partial f_{iI}^{int}}{\partial u_{jJ}} \qquad \mathbf{K}^{int} = \frac{\partial \mathbf{f}^{int}}{\partial \mathbf{d}} \tag{6.3.23}$$

The tangent stiffness matrix is shown above in three forms. The Jacobian matrix of the external nodal forces is called the *load stiffness matrix* and denoted by

$$K_{ab}^{ext} = \frac{\partial f_a^{ext}}{\partial d_b} \qquad K_{iIjJ}^{ext} = \frac{\partial f_{iI}^{ext}}{\partial u_{jJ}} \qquad \mathbf{K}^{ext} = \frac{\partial \mathbf{f}^{ext}}{\partial \mathbf{d}} \tag{6.3.24}$$

The development of these matrices is the topic of linearization and is treated in Sections 6.4 and 6.5. Using these definitions, the Jacobian matrix (6.3.22) can be written as

$$\mathbf{A} = \frac{s_D}{\beta \Delta t^2}\mathbf{M} + \mathbf{K}^{int} - \mathbf{K}^{ext} \tag{6.3.25}$$

This Jacobian matrix applies to both dynamic and equilibrium problems with the dynamic switch s_D set by (6.3.2).

The Jacobians in (6.3.23-24) can be used to relate differentials of the nodal forces to differentials of the nodal displacements by

$$d\mathbf{f}^{int} = \mathbf{K}^{int} d\mathbf{d} \qquad d\mathbf{f}^{ext} = \mathbf{K}^{ext} d\mathbf{d} \qquad d\mathbf{r} = \mathbf{A}\, d\mathbf{d} \tag{6.3.26}$$

The matrices which relate finite increments of nodal displacements to increments of nodal forces differ from the above. We will use a

$$\Delta\mathbf{f}^{int} = \mathbf{K}_{\Delta}^{int} \Delta\mathbf{d} \qquad \Delta\mathbf{f}^{ext} = \mathbf{K}_{\Delta}^{ext} \Delta\mathbf{d} \qquad \Delta\mathbf{r} = \mathbf{A}_{\Delta}\, \Delta\mathbf{d} \tag{6.3.27}$$

The matrix $\mathbf{K}_\Delta^{int}$ is called a secant stiffness and $\mathbf{A}_\Delta$ the secant Jacobian. The secant stiffnes and secant Jacobian depend on the magnitude and direction of $\Delta\mathbf{d}$. This can easily be seen in one dimension as illustrated in Fig. 6.3, which shows secants for various stepsizes and two directions (there are only two in a function of a single variable). The tangent and secant Jacobians are identical only in the limit as $\Delta\mathbf{d} \rightarrow 0$; for finite increments, the secant stiffness in (6.3.27) differs from the tangent stiffness in (6.3.23).

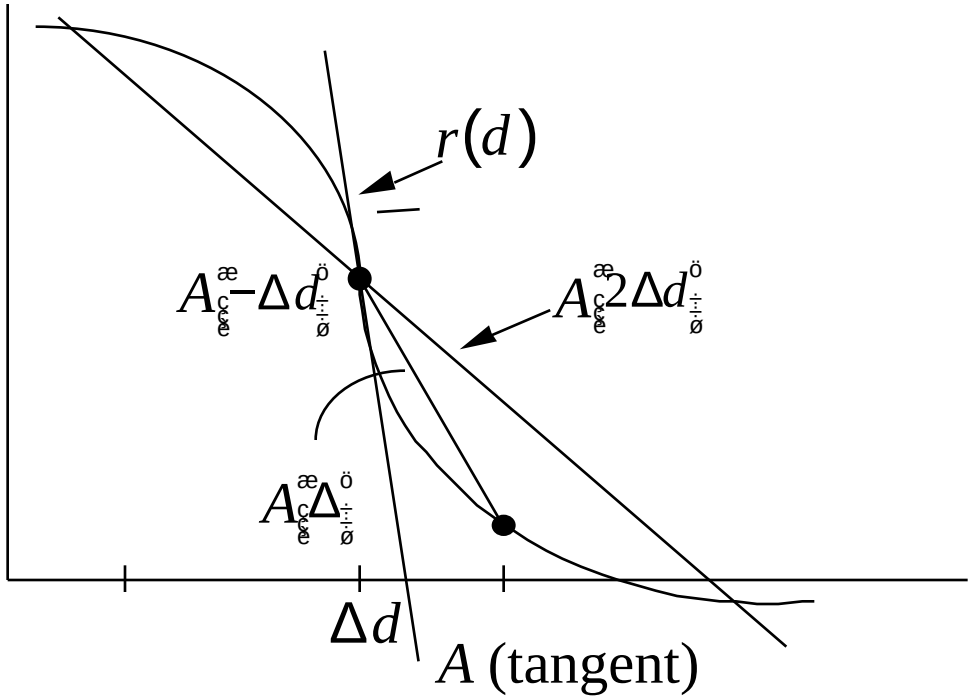

Figure 6.3. Secant Jacobians for various step sizes and directions.

Conservative Problems (Stationary Points). It is useful at this point to examine the discrete problem corresponding to the stationary principle described in Section 4.9.3. This stationary principle only applies to conservative equilibrium problems, but it is nevertheless provides insight into the character of nonlinear problems. An equilibrium solution is a stationary point of the potential, so by enforcing the conditions that the derivative of the potential vanish and using (4.9.29-30) and the definition of the residual (6.3.3) we have

$$0 = \mathbf{r} = -\frac{\partial W}{\partial \mathbf{d}} = \frac{\partial W^{int}}{\partial \mathbf{d}} - \frac{\partial W^{ext}}{\partial \mathbf{d}} = \mathbf{f}^{int} - \mathbf{f}^{ext} \tag{6.3.28}$$

A solution is a stable equilibrium solution if it corresponds to a minimum of the potential energy. Thus stable equilibrium solutions can be found by minimizing the potential *W*. The situation is depicted in Fig. 6.3, which shows the local behavior of a potential of two generalized displacements and the contours for this potential. The residual is the negative of the gradient of the potential (note the sign in the above.)

The linear model for (6.3.28) is (see 6.3.17-18)

$$-\mathbf{r}_\nu = \frac{\partial \mathbf{r}}{\partial \mathbf{d}} \Delta\mathbf{d} = -\frac{\partial^2 W}{\partial \mathbf{d}\partial \mathbf{d}} \Delta\mathbf{d} = \mathbf{A}\Delta\mathbf{d} \text{ where } A_{ab} = \frac{\partial^2 W}{\partial d_a \partial d_b} \text{ or } \mathbf{A} = \frac{\partial^2 W}{\partial \mathbf{d}\partial \mathbf{d}}$$

$$-r_{a_\upsilon} = \frac{\partial r_a}{\partial d_b} \Delta d_b = -\frac{\partial^2 W}{\partial d_a \partial d_b} \Delta d_b = A_{ab}\Delta d_b \text{ where } A_{ab} = \frac{\partial^2 W}{\partial d_a \partial d_b} \tag{6.3.29}$$

The matrix $\mathbf{A}$ when it arises from the second derivatives of a potential is called a Hessian matrix. It is identical to the Jacobian, so

$$\mathbf{A} = \mathbf{K}^{int} - \mathbf{K}^{ext} \tag{6.3.30}$$

The linearized equations for a conservative system are

$$\left(\mathbf{K}^{int} - \mathbf{K}^{ext}\right)\Delta\mathbf{d} = -\mathbf{r}$$

The above are identical to Eq. (6.3.19) except that the mass matrix is omitted, since dynamic effects cannot be included in a conservative problem. However, when the problem is posed as a minimization problem, many techniques not directly applicable to linear models, such as the method of steepest descent, can be applied to the problem. Thus, viewing the solution of the residual equations as a minimization problem is helpful in many cases.

6.3.2b. α-METHOD EQUATIONS

The α-method, also known as Hilber-Hughes-Taylor (HHT) method [??], was introduced to improve numerical dissipation for high frequencies in the Newmark-β method. The Newmark-β formulas, Eqs. (6.3.4) - (6.3.7), remain the same, wheras the time-discrete equation of motion is modified as follows (cf Eq. 6.3.1)

$$0 = \mathbf{r}\left(\mathbf{d}^{n+1},\ t^{n+1}\right) = s_D \mathbf{M}\mathbf{a}^{n+1} - \mathbf{f}^{ext}\left(\mathbf{d}^{n+\alpha},\ t^{n+1}\right) + \mathbf{f}^{int}\left(\mathbf{d}^{n+\alpha}\right) \tag{6.6.1}$$

where

$$\mathbf{d}^{n+\alpha} = (1+\alpha)\mathbf{d}^{n+1} - \alpha\mathbf{d}^{n} \tag{6.6.2}$$

It is noted that in the case of a linear analysis, the internal force vector becomes:

$$\mathbf{f}^{int}\left(\mathbf{d}^{n+\alpha}\right) = \mathbf{K}\mathbf{d}^{n+\alpha} = (1+\alpha)\mathbf{K}\mathbf{d}^{n+1} - \alpha\mathbf{K}\mathbf{d}^{n} \tag{6.6.3}$$

which is exactly the HHT method presented in [??]. Follow the α-method stability analysis, unconditional stability is achieved by setting the following parameters:

$$\alpha \in \left[-\frac{1}{3},\ 0\right] \quad \gamma = \frac{(1-2\alpha)}{2}; \text{ and } \beta = \frac{(1-\alpha)^2}{4} \tag{6.6.4}$$

If $\alpha = 0$, the trapezoidal rule is obtained.

Remark: Although there is no stability analysis in the literature for a nonlinear setting (i.e., with Eq. (6.6.1)), a linearized stability analysis will yield the same stability result as in Eq. (6.6.4).

Following the same procedure given in Section 6.3.2, the discrete problem as stated in Eq. (6.3.10) is revised as:

find $\mathbf{d}^{n+1}$ so that $\mathbf{r}\left(\mathbf{d}^{n+1}\right) = 0$ as shown in Eqs. (6.6.1) - (6.6.2), subject to $\mathbf{g}\left(\mathbf{d}^{n+1}\right) = 0$.

In order to define the Jacobian matrices and incremental nodal displacements given in Eqs. (6.3.18) through (6.3.25), the following linearized displacement equations are defined (cf. Eq. (6.3.21)):

$$\mathbf{d}_{v+1}^{n+\alpha} \overset{def}{=} (1+\alpha)\left(\mathbf{d}_v^{n+1} + \Delta\mathbf{d}\right) - \alpha\mathbf{d}^n = \mathbf{d}_v^{n+\alpha} + \Delta\tilde{\mathbf{d}} \tag{6.6.5a}$$

where

$$\mathbf{d}_{v+1}^{n+\alpha} = (1+\alpha)\mathbf{d}_v^{n+1} - \alpha\mathbf{d}^n \tag{6.6.5b}$$

and

$$\Delta\tilde{\mathbf{d}} = (1+\alpha)\Delta\mathbf{d} \qquad \begin{array}{l} \text{for } \upsilon = 0 \\ \mathbf{a}_0^{n+1} = \mathbf{0},\ \mathbf{d}_0^{n+1} = d^n + \Delta t\upsilon^n + \dfrac{\Delta t^2}{2}(1-2\beta)\mathbf{a} \end{array} \tag{6.6.5c}$$

With the above definitions, the linearized Jacobian matrix equations becomes: (cf. Eq. (6.3.17))

$$\mathbf{r}\left(\mathbf{d}_v^{n+\alpha}\right) + \frac{\partial\mathbf{r}\left(\mathbf{d}_v^{n+\alpha}\right)}{\partial\mathbf{d}}\Delta\mathbf{d} + 0\left(\Delta\mathbf{d}^2\right) = 0 \tag{6.6.6}$$

The Jacobian matrix or the effective tangent stiffness matrix (cf. Eq. (6.3.22)) can be shown to be

$$\mathbf{A} = \frac{\partial\mathbf{r}\left(\mathbf{d}_v^{n+\alpha}\right)}{\partial\mathbf{d}} = \frac{s_D}{\beta\Delta t^2}\mathbf{M} + (1+\alpha)\frac{\partial\mathbf{f}^{int}\left(\mathbf{d}_v^{n+\alpha}\right)}{\partial\mathbf{d}} - (1+\alpha)\frac{\partial\mathbf{f}^{ext}\left(\mathbf{d}_v^{n+\alpha}\right)}{\partial\mathbf{d}} \tag{6.6.8}$$

The rest of the formulation remains the same.

6.3.5. Implementation of Newton Method. Flowcharts for implicit integration and equilibrium solutions are given in Boxes 6.3 and 6.4. Both the dynamic problem and the equilibrium problem are solved by time-stepping: the external loads and other conditions are described as functions of time, which is incremented over the range of interest. In equilibrium problems, the time is often

replaced by a monotonically increasing parameter. Solutions of equilibrium processes obtained in this manner are called *incremental solutions*.

The flowchart shows a procedure often called a full Newton algorithm, where the Jacobian matrix is inverted in every iteration of the procedure. Many programs use a modified Newton algorithm, in which the Jacobian is only triangulated at the beginning of the iterations or intermittently during the iteration. For, example, in a modified Newton procedure the Jacobian may be triangulated only when the ietrative procedure does not seem to be converging well. These modified schemes are faster but less robust.

The flowcharts begin with the imposition of the intial conditions. The initial conditions can be handled exactly as in explicit methods. The initial displacements are considered to be zero. The initial accelerations are computed as shown in steps 2 and 3.

The displacements $\mathbf{d}^{n+1}$ for each time step are obtained by the iterative Newton procedure. To begin the iterative procedure, a starting value of $\mathbf{d}$ is needed; usually the solution from the preceding step is used. The residual is then calculated for this starting value. In an equilibrium solution, the residual depends only on the internal and external nodal forces. and is obtained in the module *getf*. This module, *getf*, is the same as in the explicit procedure, Box 6.1, except that the calculation of the stable time step is omitted, so it is not repeated. In transient implicit solutions, the residuals also depend on the accelerations.

Box 6.3
Flowchart for Implicit Time Integration

1. Initial conditions & initialization of parameters:
   set $\mathbf{v}^0, \sigma^0; \mathbf{d}^0 = \mathbf{0}, n = 0, t = 0;$ compute $\mathbf{M}$
2. get $\mathbf{f}^0 = \mathbf{f}\left(\mathbf{d}^0, 0\right)$
3. compute initial accelerations $\mathbf{a}^n = \mathbf{M}^{-1}\mathbf{f}^n$
4. estimate next solution $\mathbf{d}$: $\mathbf{d} = \mathbf{d}^n$
5. Newton iterations for time step $n+1$
   a. *get f* computes $\mathbf{f}\left(\mathbf{d}, t^{n+1}\right)$
   b. $\mathbf{a}^{n+1} = \frac{1}{\beta \Delta t^2}\left(\mathbf{d} - \tilde{\mathbf{d}}^n\right), \quad \mathbf{v}^{n+1} = \tilde{\mathbf{v}}^n + \gamma \Delta t \mathbf{a}^{n+1}$, see Eqs. (6.3.4 - 6.3.7)
   c. $\mathbf{r} = \mathbf{M}\mathbf{a}^{n+1} - \mathbf{f}$
   d. compute Jacobian $\mathbf{A}(\mathbf{d})$
   e. modify $\mathbf{A}(\mathbf{d})$ for essential boundary conditions
   f. solve linear equations $\Delta \mathbf{d} = \mathbf{A}^{-1}\mathbf{r}$
   g. $\mathbf{d} \leftarrow \mathbf{d} + \Delta \mathbf{d}$
   h. check error criterion; if not met, go to step 5a
6. update displacements, counter and time: $\mathbf{d}^{n+1} = \mathbf{d}, n \leftarrow n+1, t \leftarrow t + \Delta t$
7. check energy balance
8. output, if simulation not complete, go to 3

Box 6.4
Flowchart for Equilibrium Solution

1. Initial conditions and initialization: set $\mathbf{u}^0 = \mathbf{0}$; σ^0; $n = 0$;
2. Newton iterations for load increment $n+1$
   a. *getf* computes $\mathbf{f}\left(\mathbf{d}, t^{n+1}\right)$; $\mathbf{r} = \mathbf{f}\left(\mathbf{d}, t^{n+1}\right)$
   b. compute $\mathbf{A}(\mathbf{d})$
   c. modify $\mathbf{A}(\mathbf{d})$ for essential boundary conditions
   d. solve linear equations $\Delta\mathbf{d} = \mathbf{A}^{-1}\mathbf{r}$
   e. $\mathbf{d} \leftarrow \mathbf{d} + \Delta\mathbf{d}$
   f. check error criterion; if not met, go to 2a
3. update displacements, counter and time: $\mathbf{d}^{n+1} = \mathbf{d}$, $n \leftarrow n+1$, $t \leftarrow t + \Delta t$
4. output, if simulation not complete, go to 2

The Jacobian matrix in this algorithm is then calculated based on the latest state of the body. In some algorithms, the Jacobian for the last converged solution is used for all the iterations or the Jacobian is only recomputed intermittenly during the iterations; these are known as *modified Newton methods*. Simple essential boundary conditions, such as homogeneous displacement conditions, can be enforced by modifying the Jacobian matrix. The equation corresponding to the vanishing displacement component is either omitted or replaced by a dummy equation that the component vanishes by zeroing the cooresponding row and column and putting a one on the diagonal of the Jacobian. For more complex algebraic constraints, Lagrange multipliers methods or penalty methods are used: these are described in Section 6.?.

6.3.6. Equilibrium Solutions Based on Stationary Potential Energy. In Chapter 4 we saw that when the system is conservative, i.e. when the stresses and external loads are derivable from a potential, then the equilibrium problem can be posed as the determination of the stationary points of the energy. Such problems are called *conservative*. Stable equilibrium solutions correspond to local minima of the potential energy.

Consequently, stable solutions for conservative problems can be found by minimization techniques. The discrete problem is then: for any time t (the time parametrizes the external load):

$$\min\ W(\mathbf{d}, t) \text{ subject to } g_I(\mathbf{d}) = 0 \quad I = 1 \text{ to } n_c \tag{6.3.31}$$

where $g_I(\mathbf{d}) = 0$ are n_c discrete constraints on the system. These must be linear algebraic constraints. If they involve differentials or integrals, they must be converted to algebraic from by time discretization. Displacement boundary conditions are often imposed as auxiliary consraints of this type. Often the essential boundary conditions can be met by simply eliminating nodal displacements from the unknowns. If both linear stable and linear unstable

solutions are desired, then the the stationary points of $W(\mathbf{d},t)$ must be found. The discrete problem is then

$$\text{find } \mathbf{d} \text{ so that } \frac{\partial W(\mathbf{d})}{\partial \mathbf{d}} = -\mathbf{f} = \mathbf{r} = \mathbf{0} \text{ subject to } g_I(\mathbf{d}) = 0 \quad I = 1 \text{ to } n_c \tag{6.3.32}$$

Solutions to these equations for loads which vary as a function of the parameter t, which could be time but need not be, appear as branches (lines) in the space of the nodal displacement components. Some examples are given in Section 6.??.

In the above we have indicated that the derivatives of the potential with respect to the nodal displacements is the negative of the nodal forces, which are in turn equal to the residuals. Viewing an equilibrium solution as the determination of the stationary points of a potential provides substantial insight, particularly when the stability of a solution is of interest. This is pursued further in Section ??. As can be seen from a comparison of Eqs. (6.3.1) and (6.3.27) , the equations for a stationary point are identical to the discrete equations derived previously. These methods are not applicable to dynamic problems.

6.3.8 Convergence Criteria. The termination of the iterative procedure in implicit and equilibrium solutions by the Newton method is determined by convergence criteria. These criteria pertain to the convergence of the discrete solution to the equations $\mathbf{r}\left(\mathbf{d}^n, t^n\right) = 0$, not the convergence of the discrete solution to the solution of the partial differential equations. Three types of convergence criteria are used to control the iterations:

1. criteria based on the magnitude of the residual $\mathbf{r}$;
2. criteria based on the magnitude of the displacement increments $\Delta\mathbf{d}$;
3. energy error criteria.

Usually an ℓ_2 norm of the vectors is used for the first two criteria. The criteria then are:

residual error criterion:

$$\|\mathbf{r}\|_{\ell_2} = \left(\sum_{a=1}^{DOF} r_a^2\right)^{\frac{1}{2}} \le \varepsilon \, max\left(\|\mathbf{f}^{ext}\|_{\ell_2}, \|\mathbf{f}^{int}\|_{\ell_2}, \|\mathbf{M}\mathbf{a}\|_{\ell_2}\right) \tag{6.3.28}$$

displacement increment error criterion:

$$\|\Delta\mathbf{d}\|_{\ell_2} = \left(\sum_{a=1}^{DOF} \Delta d_a^2\right)^{\frac{1}{2}} \le \varepsilon \|\mathbf{d}\|_{\ell_2} \tag{6.3.29}$$

The ℓ_2 norm, which has been indicated in the above, is the probably most suitable when the mean error over all degrees of freedom is to be controlled, but a maximum norm can also be used. A maximum norm would limit the maximum error at any node. The terms on the right-hand side of Eqs. (6.3.28) and (6.3.29) are scaling factors. Without these, the criterion would depend on the parameters

of the problem. The error tolerance ε determines the precision with which the displacements are calculated before terminating the iterative procedure; when $\varepsilon = 10^{-3}$, the mean accuracy of the nodal displacements is in the third significant digit when the ℓ_2 norm is used. The convergence tolerance determines the speed and accuracy of a calculation. If the criterion is too coarse, the solution may be quite inaccurate. On the other hand, a criterion which is too tight results in unnecessary computations.

The energy convergence criterion measures the energy flow to the system resulting from the residual, which is like an error in energy. It is given by

$$\Delta \mathbf{d}^T \mathbf{r} = \Delta d_a r_a \le \varepsilon \max\left(W^{ext}, W^{int}, W^{kin}\right) \tag{6.3.30}$$

where the computation of the energies used for scaling the criterion is described in Section 6.?. The left hand side in the above represents an error in the energy, since a nonzero residual is an error in the forces on the system.

6.3.7. Convergence and Robustness of Newton Iteration. The rate of the convergence of the iterations in the Newton method is quadratic when the Jacobian matrix $\mathbf{A}$ satisfies certain conditions. These conditions may roughly be described as follows**:**

1. the Jacobian $\mathbf{A}$ should be a sufficiently smooth function of $\mathbf{d}$;

2. the Jacobian $\mathbf{A}$ should be regular (invertable) and well-conditioned in the entire domain in the displacement space that the iterative procedure traverses.

Quadratic convergence means that the ℓ_2 norm of the difference between the solution and the iterate $\mathbf{d}_\upsilon$ decreases quadratically in each iteration:

$$\left\|\mathbf{d}_{\upsilon+1} - \mathbf{d}\right\| \le c\left\|\mathbf{d}_\upsilon - \mathbf{d}\right\|^2 \tag{6.3.31}$$

where c is a constant that depends on the nonlinearity of the problem and $\mathbf{d}$ is the solution to the nonlinear algebraic equations. Thus the convergence of the Newton algorithm is quite rapid when $\mathbf{A}$ meets the above conditions. The above gives the requirements for convergence only in broad terms and convergence has been proven for various conditions on $\mathbf{A}$. One set of conditions for quadratic convergence are: the residual must be continuously differentiable and the inverse of the Jacobian matrix must exist and be uniformly bounded in the neighborhood of the solution, Dennis and Schnabel (1983, p 90).

These conditions are usually not satisfied by nonlinear finite element problems. For example, in an elastic-plastic material, the residual is not continuously differentiable when a discrete point changes from elastic to plastic or vice versa; therefore, the Jacobian is discontinuous. In a two degree of freedom problem, the discontinuities in the Jacobian appear as kinks in the contour plots for the residual components. This is illustrated in Example X. In the solution of contact-impact problems with Lagrange multiplier methods, the residual often lacks smoothness, as illustrated by Chapter 10. Thus the conditions for quadratic convergence of the Newton method are often not satisfied in engineering

problems. Yet, Newton's method is remarkably effective in engineering problems, although the rate of convergence often deteriorates. At this time, more robust methods are not available. In many problems, the conditions for quadratic convergence are satisfied; for example, the above conditions are satisfied in the response of a model with a Mooney-Rivlin material when the load is small enough so that the equilibirium solutions are stable.

Newton's method fails particularly often when applied to equilibrium problems. Since Eq. (6.3.3) are nonlinear algebraic equations, they can have multiple solutions and solutions in which are unstable. When the equilibrium path is unstable, the inverse of the Jacobian matrix is no longer regular at all points and the proof of quadratic convergence does not apply. The convergence of the Newton method often fails in the vicinity of unstable states. These types of problems are considered in the next Section.

In summary, Newton's method sometimes lacks robustness when applied to engineering problems. The robustness decreases as we increase the time step and appears more often in equilibrium solutions, since in the latter we lose the effect of the mass matrix. The mass matrix improves the conditioning of the Jacobian matrix because it is always positive definite, see Exercise X. As the time step increases, the beneficial effects of the mass matrix decrease since the coefficient of the mass matrix is inversely proportional to the square of the time step, as can be seen from Eq. (6.3.9). For many problems, a straightforward application of the Newton method will sometimes fail completely, and enhancements of the Newton method such as the arc length method, line search, and augmented Lagrangian, which are described in Section ?, are needed to solve the nonlinear algebraic equations.

6.3.8. Line Search. An effective way to increase the robustness of Newton methods when convergence is slow is to use the line search technique. The rationale behind line search is that the direction $\Delta\mathbf{d}$ found by the Newton method is often a good direction, but the step size is not optimal. It is cheaper to find the best point along this direction by several computations of the residual than to get a new direction by using a new Jacobian. Therefore, before proceeding to the next direction, the residual is minimized along the line $\mathbf{d}_{old} + \xi\Delta\mathbf{d}$ where $\mathbf{d}_{old}$ is the last iterate and $\xi > 0$ is a parameter. In other words, we find the parameter ξ so that $\mathbf{d}_{old} + \xi\Delta\mathbf{d}$ minimizes some measure of the residual. We can use as a measure of the measure of the residual its ℓ_2 norm, as defined in Eq. (6.3.28), the maximum norm, i.e. the maximum absolute value of any component of the residual, or some other measure. Line search then involves the calculation of two or more residuals along the line and an interpolation of a measure of the residual. For example, if the ℓ_2 norm is used, then

A measure for the residual which is frequently used in line search is based on the existence of a potential for the problem, i.e. on the solution by the stationary energy principle, Sections 4.9.3 and 6.3.6. For a conservative problem, the minimizer of the potential $W(\mathbf{d})$, along the line $\Delta\mathbf{d}$ is the point where the gradient of the function is orthogonal to the line. The residual is given in terms of a potential by

$$\frac{\partial W}{\partial \mathbf{d}} = \frac{\partial W^{int}}{\partial \mathbf{d}} - \frac{\partial W^{ext}}{\partial \mathbf{d}} = \mathbf{f}^{int} - \mathbf{f}^{ext} = \mathbf{r} \tag{6.3.32}$$

where the above follows from Eqs. (4.9.34) and (6.3.3). When the residual is orthogonal to the incremental displacement

$$\Delta \mathbf{d}^T \mathbf{r} = 0 \qquad \Delta \mathbf{d}^T \frac{\partial W}{\partial \mathbf{d}} = 0 \tag{6.3.33}$$

the potential must be minimum (or be stationary) at that point. This is illustrated in Fig. 6.1, which shows the contours of the potential energy for a two degree-of-freedom system and the residual of the nodal forces for several points along the line $\mathbf{d}_{old} + \xi \Delta \mathbf{d}$. As can be seen, the potential is minimum when the residual, i.e. the gradient of the potential, is normal to the line. The line search can then be conducted by minimizing $\Delta \mathbf{d}^T \mathbf{r}$.

This criterion can also be used for systems that are not conservative, since $\Delta \mathbf{d}^T \mathbf{r}$ does not involve the potential. Note that this measure of the residual is equivalent to the criterion for error in energy, Eq. (6.3.30).

Equation (6.3.33a) can also be derived directly by using the chain rule to expand the potential energy in the parameter ξ. This gives

$$\frac{dW(\xi)}{d\xi} = \frac{\partial W}{\partial \mathbf{d}} \frac{d\mathbf{d}}{d\xi} = 0 \qquad \mathbf{r}^T \Delta \mathbf{d} = 0 \tag{6.3.34}$$

where we have set the derivative of the potential energy with respect to the parameter ξ equal to zero, since we are looking for the minimum of the potential along the line $\Delta \mathbf{d}$ parametrized by ξ. The second equation follows from (6.3.32) and

$$\frac{d\mathbf{d}}{d\xi} = \frac{d(\mathbf{d}_{old} + \xi \Delta \mathbf{d})}{d\xi} = \Delta \mathbf{d} \tag{6.3.35}$$

Once a measure of the residual has been chosen, the line search can be made with any of the methods for minimizing a function of a single parameter. The method of bisection or searches based on interpolation or combinations thereof can be used. Once the residual has been evaluated at two points, a quadratic fit can be made to the residual measure, since its value at $\xi = 0$ is known to vanish. This quadratic fit can then be used to estimate the position of the minimum. The iteration along the line is terminated when the measure has been minimized to a suitable precision. Note that when the orthogonality condition (6.3.29) is used, it should be normalized like the error energy criterion is in Eq. (6.3.26).

6.3.9. Secant Methods *to be inserted*

6.3.10. Stability of Implicit methods. The advantage of an implicit method over an explicit method is that *for linear transient, problems, suitable implicit integrators are unconditionally stable*. The unconditional stability of implicit integrators has not been proven for all nonlinear systems, although results which deal with specific situations indicate that unconditional stability holds at least for certain nonlinear systems. In any case, experience indicates that the time steps which can be used with implicit integrators are much larger than those for explicit integration in many problems.

The major restrictions on the size of time steps in implicit methods arise from accuracy requirements and the decreasing robustness of the Newton procedure as the time step increases. The latter is particularly pronounced in problems with very rough response, such as contact-impact. With a large time step, the starting iterate may be far from the solution, so the possibility of failure of the Newton method to converge increases. Therefore small time steps are often used to improve the robustness of the Newton algorithm.

In return for their enhanced stability, implicit methods exact a significant price: implicit methods require the solution of nonlinear algebraic equations in each time step. The construction of the linearized algebraic equations for the Newton procedure is often quite involved. Furthermore, the storage of these equations requires significant amounts of memory. The memory requirements can be reduced substantially by iterative linear equation solvers (an iterative method within an iterative Newton method). In recent research, iterative solvers have been improved dramatically, so implicit solutions are feasible in many problems where they were prohibitive before, see Section ?. The robustness and speed of Newton methods has increased markedly over the past two decades, and we are certain that further improvements are imminent. Nevertheless, high cost and lack of robustness are still plague many implicit and equilibrium solutions.

6.4 LINEARIZATION

There are several different ways to linearize the discrete equations. In discussing the various linearization procedures, it is useful to keep in mind that the order in which linearization and spatial discretization are carried out does not matter (in mathematical terminology, the operations of linearization and spatial discretization are said to *commute*). This means that linearization of the semi-discrete equations of motion (6.2.x) gives rise to the same finite element equations as does the semi-discretization of a linearized weak form (we have not yet developed such forms, but they appear frequently in the literature). The choice between these two approaches is a matter of style. For completeness, we will consider both approaches.

In the linearization procedure, there are several possibilities:

1. Linearization is carried out before the stress-update algorithm (integration algorithm for the constitutive equation) is introduced; this gives rise to the so-called continuum tangent moduli which will be discussed below.
2. Linearization is carried out after the stress-update algorithm is introduced; this gives rise to the so-called algorithmic moduli.

These two distinct approaches yield different tangent stiffness matrices. The choice of which approach to use rests on practical considerations related to ease of implementation and on convergence of the iterative scheme. The first

approach, based on the continuum tangent modulus, is straightforward to implement. However, it can run into convergence difficulties, especially for elastic-plastic materials where the slope discontinuity at the yield point on the stress-strain curve requires small steps to assure convergence and to preserve accuracy.

The second approach, based on the algorithmic moduli, exhibits better convergence because, through linearization of the stress-update algorithm, it accounts for the change in slope associated with a finite increment of strain. One drawback of the method is that it is not always possible to derive explicit forms for the algorithmic moduli for complex constitutive relations. Numerical differentiation schemes are sometimes used to obtain the algorithmic moduli, and they introduce additional inaccuracies.

We first consider linearization of the discrete equations based on the continuum tangent moduli, which relate a stress rate to a strain rate. The resulting material tangent stiffness matrix is called the *continuum tangent stiffness matrix*.

A somewhat more mathematical approach to linearization based on directional derivatives is then presented and it is shown how the resulting expressions are equivalent to those obtained by using the procedure based on the material time derivative. This linearization procedure based on the directional derivative is then used to develop the linearized equations for the second approach discussed above, i.e, linearization of the weak form after introduction of the stress-update algorithm. Because the stress-update algorithm is introduced prior to linearization, the expression for the stress increment that appears in the linearization of the weak form is based on the linearized constitutive integration scheme and not on the continuum rate form of the constitutive relation. As a result, the material tangent stiffness differs from the continuum tangent stiffness and is referred to as the algorithmic modulus (sometimes referred to as the consistent tangent modulus because of the consistent linearization of the weak form and the stress-update algorithm). Examples of the algorithmic modulus for the 2-node bar element and the 3-node triangle are also given.

6.4.1 Linearization of the Discrete Equations

In the following, we derive expressions for the continuum tangent stiffness matrix $\mathbf{K}^{int}$. As will be seen, part of the expression can be derived independently of the material response. These expressions are completed upon introduction of the constitutive relation. The continuum rate form of the constitutive relation will be used, i.e., linearization is carried out prior to introduction of the stress-update algorithm. Specific examples for the continuum tangent matrices for hyperelastic materials and elastic-plastic materials are presented in Section 6.4.2.

For notational convenience, we will develop the tangential stiffness matrix by relating rates of the internal nodal forces $\dot{\mathbf{f}}^{int}$ to the nodal velocities $\dot{\mathbf{d}}$. Thus the stiffness matrices $\mathbf{K}^{int}$ can be derived by taking the material time-derivative of the nodal internal forces. The procedure is identical to relating an infinitesmal increment of nodal displacements $d\mathbf{f}^{int}$ to an infinitesmal increment of nodal displacements $d\mathbf{d}$, and we will occasionally recast the equations in that form; the dot notation is chosen for convenience. The derivation is perfectly rigorous for

any continuously differentiable residual; for rougher residuals, directional derivatives are needed and are described later.

By (4.9.10-11), the internal nodal forces in the total Lagrangian form are given by,

$$\mathbf{f}^{int} = \int_{\Omega_o} B_0^T \mathbf{P} d\Omega_0, \qquad f_{Ii}^{int} = \int_{\Omega_o} \frac{\partial N_I}{\partial X_j} P_{ji} d\Omega_0 \tag{6.4.1}$$

where $\mathbf{P}$ is the nominal stress tensor with components P_{ji}, N_I are the nodal shape functions and $\left(B_0^T\right)_{jI} = \partial N_I / \partial X_j$. We have chosen the total Lagrangian form because this leads to the simplest derivation. In the total Lagrangian form, (6.4.1), only the nominal stress is a function of time, i.e. it is the only variable which varies with deformation. In the updated Lagrangian form, (4.5.5) the domain of the element (or body), the spatial derivatives $\partial N_I / \partial x_j$ and the Cauchy stress depend on the deformation, and hence on time.

Taking the material time-derivative of (6.4.7) gives

$$\dot{\mathbf{f}}^{int} = \int_{\Omega_o} B_0^T \dot{\mathbf{P}} d\Omega_0, \qquad \dot{f}_{Ii}^{int} = \int_{\Omega_o} \frac{\partial N_I}{\partial X_j} \dot{P}_{ji} d\Omega_0 \tag{6.4.2}$$

since B_0 and $d\Omega_0$ are independent of the deformation, which varies with time. To obtain the stiffness matrix $\mathbf{K}^{int}$ it is now necessary to express the stress rate $\dot{\mathbf{P}}$ in terms of nodal velocities. However, constitutive equations are not expressed in terms of $\dot{\mathbf{P}}$ because this stress rate is not objective. So we work in terms of the material time derivative of the PK2 stress, which we have seen is objective.

The material time derivative of the PK2 stress is then related to the material time derivative of the nominal stress by Box 3.2, which gives $\mathbf{P} = \mathbf{S}\ \mathbf{F}^T$, so

$$\dot{\mathbf{P}} = \dot{\mathbf{S}}\ \mathbf{F}^T + \mathbf{S}\ \dot{\mathbf{F}}^T \quad \text{or} \quad \dot{P}_{ij} = \dot{S}_{ir} F_{rj}^T + S_{ir} \dot{F}_{rj}^T \tag{6.4.3}$$

Substituting (6.4.3) into (6.4.2) yields

$$\dot{f}_{iI}^{int} = \int_{\Omega_0} \frac{\partial N_I}{\partial X_j} \left(\dot{S}_{jr} F_{ir} + S_{jr} \dot{F}_{ir} \right) d\Omega_0 \ \text{ or } \ df_{iI} = \int_{\Omega_0} \frac{\partial N_I}{\partial X_j} \left(dS_{ir} F_{ir} + S_{jr} dF_{ir} \right) d\Omega_0 \tag{6.4.4}$$

The above shows that the rate (or increment) of the internal nodal forces consists of two distinct parts:

1. The first term involves the rate of stress ($\dot{\mathbf{S}}$) and thus depends on the material response and leads to what is called the material tangent stiffness matrix which we denote by $\mathbf{K}_{mat}$. Note that although this

term reflects material response, it changes with deformation since $\boldsymbol{B}_0$ depends on $\mathbf{F}$.

2. The second term involves the current state of stress, $\mathbf{S}$ and accounts for rotation of the stress with the motion. This term is called the geometric stiffness because it represents for geometric nonlinearities associated with rotation of the stress. It is also called the initial stress matrix to indicate the role of the existing state of stress. It is denoted by $\mathbf{K}_{geo}$.

Therefore we write Eq. (6.4.4) as

$$\dot{\mathbf{f}}^{int} = \dot{\mathbf{f}}^{mat} + \dot{\mathbf{f}}^{geo} \quad \text{or} \quad \dot{f}_{iI}^{int} = \dot{f}_{iI}^{mat} + \dot{f}_{iI}^{geo} \tag{6.4.5}$$

where

$$\dot{f}_{iI}^{mat} = \int_{\Omega_0} \frac{\partial N_I}{\partial Xj} F_{ir} \dot{S}_{jr} d\Omega_0, \qquad \dot{f}_{iI}^{geo} = \int_{\Omega_0} \frac{\partial N_I}{\partial Xj} S_{jr} \dot{F}_{ir} d\Omega_0 \tag{6.4.6}$$

To simplify the remaining development, we put the above expression into Voigt form. Voigt form is convenient in developing the material stiffness matrices because the tensor of material coefficients, $C_{ijk\ell}$, which which relates the stress rate to the strain rate is a fourth order tensor; this tensor cannot be handled by readily standard matrix operations. Therefore, the stiffness matrix is conventionally handled in Voigt notation; other ways of handling the fourth order stiffness matrices are discussed later.

We consider the material and geometric effects on the nodal forces one at a time. Referring to Eq. (??), we can see that with the definition of (??), which is

$$B_{jrIi}^0 = sym\left(_{j,r}\right)\left[\frac{\partial N_I}{\partial Xj} F_{ir}\right] \tag{6.4.7}$$

we can rewrite the material increment in the nodal forces, Eq. (6.4.4), in Voigt notation as

$$\dot{\mathbf{f}}_{mat}^{int} = \int_{\Omega_0} \mathbf{B}_0^T \left\{\dot{\mathbf{S}}\right\} d\Omega_0 \tag{6.4.8}$$

where $\mathbf{S}$ is now a column matrix arranged according to the Voigt kinetic rule, Appendix A. It should be stressed that Eq. (6.4.6) is identical to Eq. (6.4.5). We now consider the consitutive equation in the following rate form

$$\dot{S}_{ij} = C_{ijkl}^S \dot{E}_{kl} \quad \text{or} \quad \left\{\dot{\mathbf{S}}\right\} = \mathbf{C}^S \left\{\dot{\mathbf{E}}\right\} \tag{6.4.9}$$

Recall (4.9.27), which gives the following relation in Voigt notation

$$\left\{\dot{\mathbf{E}}\right\} = \mathbf{B}_0 \dot{\mathbf{d}} \tag{6.4.10}$$

Substituting Eqs. (6.4.9) and (6.4.10) into Eq. (6.4.8) gives

$$\dot{\mathbf{f}}^{int}_{mat} = \int_{\Omega_0} \mathbf{B}_0^T \mathbf{C}^S \mathbf{B}_0 \, d\Omega_0 \, \dot{\mathbf{d}} \quad \text{or} \quad d\mathbf{f}^{int}_{mat} = \int_{\Omega_0} \mathbf{B}_0^T \mathbf{C}^S \mathbf{B}_0 \, d\Omega_0 \, d\mathbf{d} \tag{6.4.11}$$

So the material tangent stiffness matrix is given by

$$\mathbf{K}^{mat} = \int_{\Omega_0} \mathbf{B}_0^T \mathbf{C}^S \mathbf{B}_0 \, d\Omega_0 \qquad \textbf{or } \mathbf{K}^{mat}_{IJ} = \int_{\Omega_0} \mathbf{B}_{0I}^T \mathbf{C}^S \mathbf{B}_{0J} \, d\Omega_0 \tag{6.4.12}$$

The material tangent stiffness relates the increment (or rate) in internal nodal forces to the increment (or rate) of displacement due to material response, which is reflected in the material response matrix $\mathbf{C}^S$.

The geometric effect on the nodal forces is obtained as follows. From the definition $B^0_{iI} = \dfrac{\partial N_I}{\partial X_i}$ and Eq. (6.4.4), we can write

$$\dot{f}^{geo}_{iI} = \int_{\Omega_0} \left(B^0_{jI}\right)^T S_{jr} \dot{F}_{ir} \, d\Omega_0 = \int_{\Omega_0} \left(B^0_{jI}\right)^T S_{jr} B^0_{rJ} \, d\Omega_0 \dot{u}_{iJ} \tag{6.4.13}$$

$$= \int_{\Omega_0} \left(B^0_{jI}\right)^T S_{jr} B^0_{rJ} \, d\Omega_0 \delta_{ij} \dot{u}_{jJ} \tag{6.4.14}$$

where in the second step we have used (4.9.7), $\dot{F}_{ir} = B^0_{rI} \dot{u}_{iI}$, and in the third step we have added a dummy unit matrix so that the component indices in $\dot{f}^{geo}_{iI}$ and $\dot{u}_{iJ}$ are not the same. Writing the resulting expression for the geometric stiffness gives

$$\mathbf{f}_I = \mathbf{K}^{geo}_{IJ} \dot{\mathbf{u}}_J \text{ where } \mathbf{K}^{geo}_{IJ} = \int_{\Omega_0} \boldsymbol{B}^T_{0I} \mathbf{S} \boldsymbol{B}_{0J} \, d\Omega_0 \mathbf{I} \tag{6.4.15}$$

Note that the PK2 stress in the above is a square matrix. Each submatrix of the geometric stiffness matrix is a unit matrix; therefore, it follows that the geometric stiffness matrix, like the unit matrix, is invariant with rotation, i.e.

$$\hat{\mathbf{K}}^{geo}_{IJ} = \mathbf{K}^{geo}_{IJ} \tag{6.4.16}$$

where $\hat{\mathbf{K}}^{geo}_{IJ}$ relates nodal forces to nodal velocities expressed in any alternate set of Cartesian coordinates.

To summarize

$$d\mathbf{f}^{int} = \mathbf{K}^{int} d\mathbf{d} \quad \text{or} \quad \dot{\mathbf{f}}^{int} = \mathbf{K}^{int} \dot{\mathbf{d}} \quad \text{where} \quad \mathbf{K}^{int} = \mathbf{K}^{mat} + \mathbf{K}^{geo} \tag{6.4.17}$$

where the material tangent stiffness and the geometric stiffness are given by Eqs. (6.4.12) and 6.4.15), respectively. The material tangent stiffness reflects the effect on the nodal internal forces of the deformation of the material. The geometric stiffness reflects the effects of the rotation and deformation on the current state of stress.

The above forms are easily converted to updated Lagrangian forms by letting the current configuration be a reference configuration, as in Section 4.??. From Eqs. (4.9.29), we recall that taking the current configuration as the reference configuration gives

$$\mathbf{B}_0 \rightarrow \mathbf{B} \quad \boldsymbol{B}_0 \rightarrow \boldsymbol{B} \quad \mathbf{S} \rightarrow \sigma \quad d\Omega_0 \rightarrow d\Omega \tag{6.4.18}$$

Also, referring to Section 4.??, we note that when a fixed current configuration becomes the reference configuration, then

$$\mathbf{F} \rightarrow \mathbf{I} \tag{6.4.19}$$

In Section (???), we have seen that the relationship rate of the PK2 stress to the given strain is equivalent to that of the Truesdell rate of the Cauchy stress to the rate-of-deformation in the current configuration, so

$$\mathbf{C}^S \rightarrow \mathbf{C}^{\sigma T} \tag{6.4.20}$$

Thus, Eqs. (6.4.13) and (6.4.16) become

$$\begin{aligned} &\mathbf{K}_{IJ}^{mat} = \int_\Omega \mathbf{B}_I^T \mathbf{C}^{\sigma T} \mathbf{B}_J \, d\Omega \qquad \mathbf{K}^{mat} = \int_\Omega \mathbf{B}^T \mathbf{C}^{\sigma T} \mathbf{B} d\Omega \\ &\mathbf{K}_{IJ}^{geo} = \mathbf{I} \int_\Omega \boldsymbol{B}_I^T \sigma \boldsymbol{B}_J d\Omega \end{aligned} \tag{6.4.21}$$

These forms are generally easier to use than the total Lagrangian forms, since **B** is more easily constructed than B_0 and many material laws are developed in terms of Cauchy stress. It is not possible to write a convenient expression for the entire geometric stiffness matrix in this notation. Note that either the material or geometric stiffness can be used in total Lagrangian form with the other in updated Lagrangian form. The numerical values of the matrices in total and updated lagrangian form are identical, and the choice is a matter of convenience.

The integrand in the geometric stiffness is a scalar for given values of *I* and *J*, so Eq. (6.4.21) can be written as

$$\mathbf{K}_{IJ}^{geo} = \mathbf{I} H_{IJ} \quad \text{where} \quad H_{IJ} = \int_\Omega \boldsymbol{B}_I^T \mathbf{S} \boldsymbol{B}_J \, d\Omega \tag{6.4.22}$$

Alternate Derivations. In this Section the tangent stiffness matrix is derived in terms of the convected rate of the Kirchhoff stress. Many of the relations in nonlinear mechanics take on a particular elegance and simplicity when expressed in terms of the Kirchhoff stress. In addition, the following development relies

more on indicial notation and the shift to Voigt notation is not made until the last steps.

Noting that the Kirchhoff stress $\boldsymbol{\tau}$ is related to the nominal stress by (???), $\mathbf{P} = \mathbf{F}^{-1}\ \boldsymbol{\tau}$, the rate form of the relation between the nominal stress and the Kirchhoff stress is obtained by taking the material time derivative

$$\dot{\mathbf{P}} = \mathbf{F}^{-1}\ \dot{\boldsymbol{\tau}} + \dot{\mathbf{F}}^{-1}\ \boldsymbol{\tau} \tag{6.4.24}$$

Using the result $\dfrac{D\left(\mathbf{F}^{-1}\ \mathbf{F}\right)}{Dt} = 0$, it is straightforward to show that

$$\left(\mathbf{F}^{-1}\right)^{\cdot} = -\mathbf{F}^{-1}\ \dot{\mathbf{F}}\ \left(\mathbf{F}^{-1}\right) = -\mathbf{F}^{-1}\ \mathbf{L} \tag{6.4.25}$$

where the second relation follows from (???). Thus the expression (6.4.24) for the nominal stress rate is written as

$$\dot{\mathbf{P}} = \mathbf{F}^{-1}\left(\dot{\boldsymbol{\tau}} - \mathbf{L}\ \boldsymbol{\tau}\right) \tag{6.4.26}$$

Using (5. ????) to relate the material rate of theKirchhoff stress to its convected rate, $\boldsymbol{\tau}^{c} = \dot{\boldsymbol{\tau}} - \mathbf{L}\ \boldsymbol{\tau} - \boldsymbol{\tau}\ \mathbf{L}^{T}$, (6.4.26) is written as

$$\dot{\mathbf{P}} = \mathbf{F}^{-1}\left(\dot{\boldsymbol{\tau}}^{c} + \boldsymbol{\tau}\ \mathbf{L}^{T}\right) \tag{6.4.27}$$

Writing (6.4.27) in indicial notation, we obtain

$$\dot{P}_{ji} = F^{-1}\left(\tau_{ki}{}^{c} + \tau_{kl} L_{il}\right) = \frac{\partial X_j}{\partial x_k}\left(\tau_{ki}{}^{c} + \tau_{kl} L_{il}\right) \tag{6.4.28}$$

Substituitng the above into (6.4.2) gives

$$\begin{aligned} \dot{f}_{iI}^{int} &= \int_{\Omega_o} \frac{\partial N_I}{\partial X_j}\frac{\partial X_j}{\partial x_k}\left(\tau_{ki}{}^{c} + \tau_{kl} L_{il}\right) d\Omega_0 \\ &= \int_{\Omega_o} \frac{\partial N_I}{\partial x_k}\left(\tau_{ki}{}^{c} + \tau_{kl} L_{il}\right) d\Omega_0 \\ &= \int_{\Omega_o} N_{I,k}\left(\tau_{ki}{}^{c} + \tau_{kl} L_{il}\right) d\Omega_0 \end{aligned} \tag{6.4.29}$$

where the second expression follows from the first by the chain rule; in the third expression we have used the notation $N_{I,k} = \partial N_I / \partial x_k$. This is the counterpart of (6.4.4) in terms of the Kirchhoff stress.

This result can easily be transformed to an updated Lagrangian form with the integral over the current domain. Using (3.2.18, $d\Omega = Jd\Omega_0$ and the relation (5.???) between the convected rate of Kirchhoff stress and the Truesdell rate of Cauchy stress ($\tau^c = J\sigma^T$) the expression (6.4.29) yields

$$\dot{f}_{iI} = \int_\Omega N_{I,k}\left(\sigma_{ki}{}^T + \sigma_{kl} L_{il}\right) d\Omega \tag{6.4.30}$$

which is the updated Lagrangian counterpart of Eq. (6.4.4); (6.4.30) could also be obtained by making the current configuration the reference configuration EXERCISE

An alternative derivation of (6.4.29) is given as follows. Recall Eq. (6.4.3):

$$\dot{\mathbf{P}} = \dot{\mathbf{S}}\ \mathbf{F}^T + \mathbf{S}\ \dot{\mathbf{F}}^T \tag{6.4.33}$$

Now note that this relation can be written as

$$\dot{\mathbf{P}} = \mathbf{F}^{-1}\ \mathbf{F}\ \dot{\mathbf{S}}\ \mathbf{F}^T + \mathbf{F}^{-1}\ \mathbf{F}\ \mathbf{S}\ \mathbf{F}^T\ \mathbf{F}^{-T}\ \dot{\mathbf{F}}^T \tag{6.3.34}$$

Using the push-forward relation (5????) for the convected rate of Kirchhoff stress in terms of the rate of the PK2 stress, $\tau^c = \mathbf{F}\ \dot{\mathbf{S}}\ \mathbf{F}^T$, and (3.3.18), $\mathbf{L}^T = \mathbf{F}^{-T}\ \dot{\mathbf{F}}^T$, (6.4.34) can be written as

$$\dot{\mathbf{P}} = \mathbf{F}^{-1}\left(\tau^c + \tau\ \mathbf{L}^T\right) \tag{6.4.35}$$

which is the same as (6.4.27). The tangent stiffness expression (6.4.29) follows in an identical fashion.

To complete the derivation of the material tangent stiffness matrix (6.4.29), it is necessary to introduce the constitutive relation to relate the convected stress rate to the nodal velocities. We write the constitutive relation (rate-independent material response) in the form

$$\tau_{ij}{}^c = C^\tau_{ijkl} D_{kl} \tag{6.4.38}$$

where the superscript τ on the tangent modulus C^τ_{ijkl} indicates that it relates the Kirchoff stress rate to the rate-of-deformation. This tangent modulus possesses the minor symmetries, i.e., $C^\tau_{ijkl} = C^\tau_{jikl} = C^\tau_{ijlk}$. For some materials, this tangent modulus tensor also has major symmetry, i.e, $C^\tau_{ijkl} = C^\tau_{klij}$, i.e. for hyperelastic materials and for associated rate-independent plasticity based on the Kirchhoff stress; see Chapter 5. This tangent modulus tensor for non-associated rate-independent plasticity is not symmetric. We will also show in the following that the tangent modulus for associated plasticity based on the Jaumann rate of the Cauchy stress also does not have major symmetry.

An expression for the material tangent stiffness matrix is now derived using the general form (6.4.38) of the constitutive relation for a rate-independent material. Specific examples of this relation and the associated tangent moduli are given at the end of this subsection. In this derivation, instead of immediately changing to Voigt notation, we will continue with indicial notation to the final expression and then translate that to Voigt notation.

Substituting (6.4.38) into (6.4.32) gives

$$K^{mat}_{IJij}\dot{d}_{Jj} = \int_{\Omega_o} \frac{\partial N_I}{\partial x_k} C^{\tau}_{kijl} D_{jl}\, d\Omega_o \tag{6.4.39}$$

Recall from (4.4.7b), that the rate of deformation tensor is the symmetric part of the spatial velocity gradient, $D_{k\ell} = v_{(k,\ell)} = sym\left(v_{kI} N_{I,\ell}\right)$. Substituting this and the rate form of the constitutive equation (6.4.38) into (6.4.39) we obtain

$$\begin{aligned} K^{tan}_{IJij}\dot{d}_{Jj} &== \int_{\Omega_o} N_{I,k} C^{\tau}_{kijl} v_{j,l}\, d\Omega_o \\ &= \int_{\Omega_o} N_{I,k} C^{\tau}_{kijl} N_{J,l} \dot{u}_{jJ}\, d\Omega_o \\ &= \int_{\Omega_o} N_{I,k} C^{\tau}_{kijl} N_{J,l}\, d\Omega_o \dot{u}_{jJ} \end{aligned} \tag{6.4.41}$$

where in the second of the above we have used the result $C^{\tau}_{kijl} D_{jl} = C^{\tau}_{kijl} v_{j\,l}$ which follows the minor symmetry of the tangent modulus matrix, $C^{\tau}_{kijl} = C^{\tau}_{kijl}$. From (6.4.41), the material tangent stiffness matrix is defined by

$$K^{mat}_{IJij} = \int_{\Omega_o} N_{I,k} C^{\tau}_{kijl} N_{J,l}\, d\Omega_o \tag{6.4.42}$$

This expression can also be written as an integral over the current domain, i.e.,

$$K^{mat}_{IJij} = \int_{\Omega_o} N_{I,k} \frac{1}{J} C^{\tau}_{kijl} N_{J,l}\, d\Omega = \int_{\Omega} N_{I,k} C^{\sigma T}_{kijl}\, N_{J,l}\, d\Omega \tag{6.4.43}$$

where we have used (????) to write the second expression.

We now convert the above to Voigt notation. Equation (6.4.43) is now written as

$$K^{mat}_{IJrs} = \int_{\Omega} N_{A,k} \delta_{ri} C^{\sigma\, T}_{kijl} N_{B,l} \delta_{sj}\, d\Omega \tag{6.4.46}$$

Noting that $C^{\tau}_{kijl} = C^{\tau}_{ikjl} = C^{\tau}_{kilj}$, (6.4.46) and using (4.5.19b), the above can be written as

$$K^{mat}_{IJrs} = \int_\Omega B_{ikAr} \frac{1}{J} C^{\tau}_{kijl} B_{jlBs} d\Omega \tag{6.4.47}$$

which is given in matrix form as

$$\mathbf{K}^{mat}_{IJ} = \int_\Omega \mathbf{B}^T_I C^{\sigma T} \mathbf{B}_J d\Omega = \int_\Omega J^{-1} \mathbf{B}^T_I C^{\tau} \mathbf{B}_J d\Omega \tag{6.4.49)\}$$

This form is identical to the linear stiffness matrix except that the material response matrix $J^{-1}\mathbf{C}^{\tau}$ relates the convected rate of Kirchhoff stress to the rate-of-deformation (or alternatively the response matrix $\mathbf{C}^{\sigma T}$ relates the Truesdell rate of Cauchy stress to the rate-of-deformation).

Some examples of tangent moduli for different materials are given in the following. Detailed derivations of the tangent material stiffness matrices for specific finite elements are given in Section 6.4.2 below.

Tangent Modulus for Hyperelastic Material The rate form of the constitutive relation for a hyperelastic material is given by (5.x), i.e,

$$\tau^{c} = C_{ijkl} D_{kl} \quad \text{or} \quad \sigma^{T} = C_{ijkl} D_{kl} \tag{6.4.50}$$

Thus from (6.4.50), the tangent modulus for a hyperelastic material is given by

$$C^{\tau}_{ijkl} = J C^{\sigma T}_{ijkl} = F_{im} F_{jn} F_{kp} F_{lq} C^{SE}_{mnpq} \tag{6.4.51}$$

where from (5.y) $\overline{C}_{mnpq}$ is derived from the hyperelastic potential, i.e.,

$$C^{SE}_{mnpq} = \frac{\partial S_{mn}}{\partial E_{pq}} = 2 \frac{\partial S_{mn}}{\partial C_{pq}} = 2 \frac{\partial^2 W(C)}{\partial C_{mn} \partial C_{pq}} \tag{6.4.52}$$

An interesting feature of the expression (6.4.51) is that for a hyperelastic material the rate form of the material response is expressed naturally in terms of the convected rate of Kirchhoff stress. The expression (6.4.51) contains no geometric terms consisting of the product of the current stress the spatial velocity gradient (or its symmetric or antisymmetric parts)??????MORAN???. In many materials, (including the elastic-plastic material considered in the following) the tangent moduli are functions of the initial stresses.

Tangent Modulus for Hypoelastic-Plastic Material We will now develop the tangent modulus for hypoelastic-plastic materials based on i) the Kirchhoff stress and ii) the Cauchy stress. The elastic response is assumed to be given by relating the Jaumann rate of stress to the elastic part of the rate of deformation tensor.

i) Kirchhoff Stress Formulation Recalling the relation ( ) which relates the Jaumann rate of Kirchhoff stress to the rate of deformation tensor, we have

$$\tau_{ij}{}^{c} = C^{\tau}_{ijkl} D_{kl} \tag{6.4.53}$$

where C^{τ}_{ijkl} is the elastic-plastic tangent modulus given in (5.??) Using the relationship (5.???) between the convected rate and the Jaumann rate gives

$$\begin{aligned}\tau_{ij}{}^{c} &= \tau_{ij}{}^{J} - D_{ik}\tau_{kj} - \tau_{ik}D_{kj} \\ &= C^{ep}_{ijkl}D_{kl} - D_{ik}\tau_{kj} - \tau_{ik}D_{kj} \\ &= \left(C^{ep}_{ijkl} - \delta_{il}\tau_{kj} - \tau_{ik}\delta_{jl}\right)D_{kl}\end{aligned} \tag{6.4.54}$$

The terms involving the stress tensor are a result of the use of the Jaumann rate in the hypoelastic relation and the difference between the Jaumann rate and the convected rate which appears in the expression for the tangent stiffness matrix. These are traditionally interpreted as part of the material tangent stiffness matrix although they can also be regarded as geometric terms due to the convection of the stress.

Because of the symmetry of D_{kl}, the last expression can be written as

$$\begin{aligned}\tau_{ij}{}^{c} &= \left(C^{\tau}_{ijkl} - \frac{1}{2}\left(\delta_{il}\tau_{kj} + \tau_{ik}\delta_{jl} + \delta_{ik}\tau_{lj} + \tau_{il}\delta_{jk}\right)\right)D_{kl} \\ &= C^{tan}_{ijkl}D_{kl}\end{aligned} \tag{6.4.43}$$

where

$$C^{tan}_{ijkl} = C^{ep}_{ijkl} - \frac{1}{2}\left(\delta_{il}\tau_{kj} + \tau_{ik}\delta_{jl} + \delta_{ik}\tau_{lj} + \tau_{il}\delta_{jk}\right) \tag{6.4.55}$$

is the tangent modulus. Note that this tangent modulus has major and minor symmetries for an associated law, so the tangent stiffness is symmetric.

ii) Cauchy Stress Formulation We will now develop the tangent stiffness for a hypoelastic-plastic material based on the Cauchy stress and we will show that the resulting stiffness is not symmetric. The constitutive relation in elasto-plasticity relates the Jaumann rate of the Cauchy stress to the rate-of-deformation:

$$\sigma_{ij}{}^{J} = C^{\sigma J}_{ijkl}D_{kl} \tag{6.4.56}$$

where $C^{\sigma J}_{ijkl}$ is the elastic-plastic tangent modulus. The Jaumann rate is used because the invariants of the Cauchy stress tensor remain constant when the Jaumann rate vanishes, see section 5.??. Using the relationship (5.??) between the Jaumann rates of Kirchhoff and Cauchy stresses, the convected rate is written as

$$\tau_{ij}{}^{c} = \tau_{ij}{}^{J} - D_{ik}\tau_{kj} - \tau_{ik}D_{kj}$$

$$= J\sigma_{ij} + D_{kk}\tau_{ij} - D_{ik}\tau_{kj} - \tau_{ik}D_{kj} \tag{6.4.57}$$

Linearization with Directional Derivatives

Three difficulties arise in applying the traditional Newton-Raphson method to solid mechanics problems:

1. the nodal forces are not continuously differentiable functions of the nodal displacements for materials such as elastic-plastic materials;
2. for path-dependent materials, the classical Newton method pollutes the constitutive models since the intermediate solutions to the linear problem in the iterative procedure, $\mathbf{d}_\nu$, are not part of the actual load path;
3. for large incremental rotations and deformation, the linearized increments introduce a substantial error

In order to overcome these difficulties, the Newton-Raphson method is often modified as follows:

1. directional derivatives, also called Frechet derivatives, are used to develop the tangent stiffness;
2. a secant method is used instead of a tangent method and the last converged solution is used as the iteration point.
3. formulas depending on increment size are used to relate the increments forces and displacements.

It should be pointed out that the third difficulty only arises when the secant method is used to circumvent the second difficulty. If a tangent Newton method is used for a smooth material, there is no advantage to carrying higher order terms in the geometric terms.

To illustrate the need for directional derivatives with elastic-plastic materials, consider the following example. The two-bar truss shown in Fig. 6.??? has been loaded so that the stresses in both bars are compressive and equal, and both bars are at the compressive yield stress. For simplicity, we consider only material nonlinearities and neglect geometric nonlinearities. If an arbitrary load increment $\Delta\mathbf{f}_1^{ext}$ is now applied to node 1, the tangent stiffness matrix will depend on the incremental displacement $\Delta\mathbf{u}_1$ because the derivatives of the internal nodal displacements depend on the direction of the displacement increment. The residual is not a continuoiusly differentiable function of the incremental nodal displacments at this point, because the change in nodal internal forces depends on whether the response of the either rod is elastic or plastic. In this case, there are four lines of discontinuity for the derivatives, as shown in Figure ???. These result from the fact that if the displacment increment results in a tensile strain increment, then the bar unloads elastically, so the tangent modulus changes from the elastic modulus E to the plastic modulus H_p.

The internal nodal forces in the current configuration are

$$\begin{Bmatrix} f_{x1} \\ f_{y1} \end{Bmatrix}^{int} = A \begin{Bmatrix} \sigma_0 \cos\theta - \sigma_0 \cos\theta \\ \sigma_0 \sin\theta + \sigma_0 \sin\theta \end{Bmatrix} \tag{6.4.58}$$

where σ_0 is the current yield stress; the above is obtained by assembling the internal nodal forces for rod elements as given by Eq. (E.4.6.7). For each rod element, there are two possibilities depending on the direction of the force: either the rod continues to load witha plastic modulus, or it unloads with an elastic modulus. As a result, the tangent stiffness in this configuration can take on four different values.

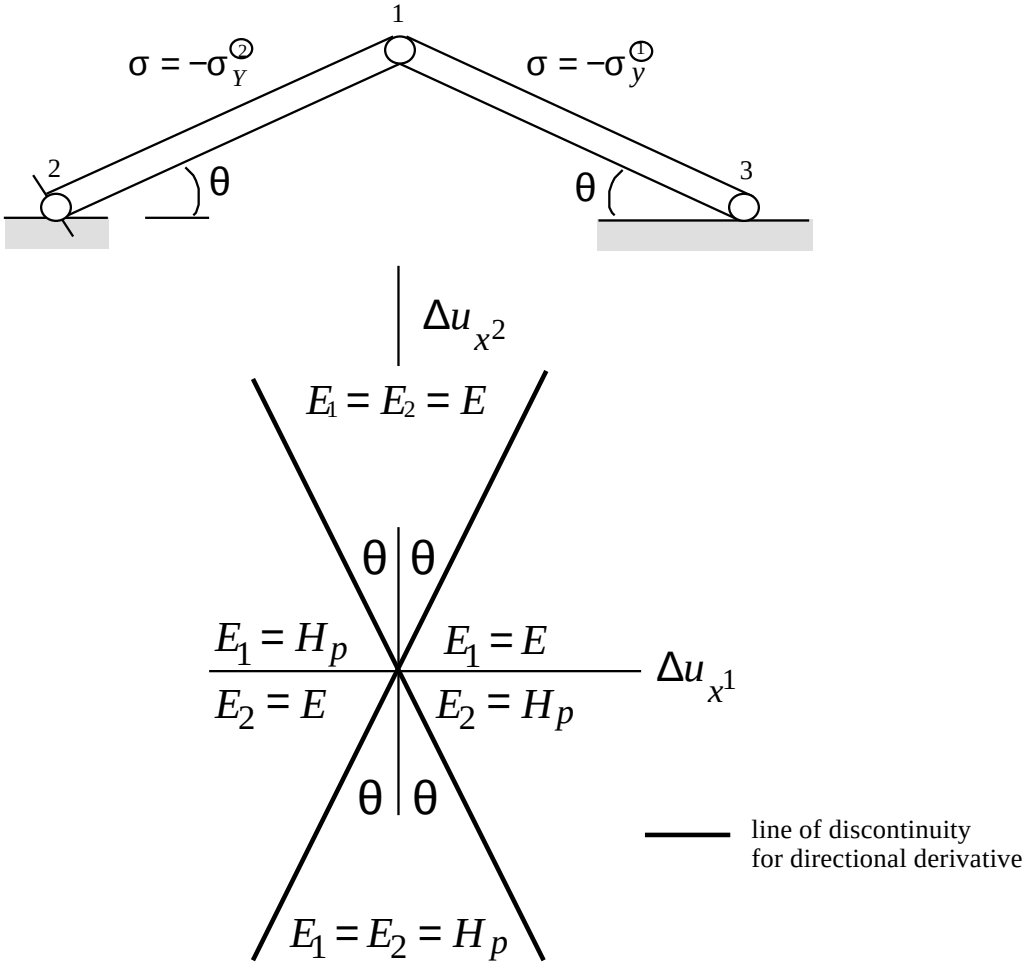

Figure ??. A two-bar truss in a state with both bars in compressive yield and the four quadrants of directional derivatives.

The nodal force f_{1x} is shown as a function of the two components of the nodal displacement increment in Figure ???, where the discontinuity in the derivatives is clearly apparent. Obviously, a standard derivative cannot be evaluated since it has four different values.

These regimes of the four different responses are illustrated in Fig. 6.??, which shows the four quadrants in the space of the components of the nodal

displacement. The tangent stiffness for dkisplacement increments in the four quadrants is given by the following:

in quadrant 1:

$$\mathbf{K}^{int} = \frac{AE}{\ell} \begin{bmatrix} 2\cos^2\theta & 0 \\ 0 & 2\sin^2\theta \end{bmatrix} \tag{6.4.59a}$$

in quadrant 2:

$$\mathbf{K}^{int} = \frac{A}{\ell} \begin{bmatrix} \left(E + H_p\right)\cos^2\theta & \left(E - H_p\right)\sin\theta\cos\theta \\ \left(E - H_p\right)\sin\theta\cos\theta & \left(E + H_p\right)\sin^2\theta \end{bmatrix} \tag{6.5.59b}$$

in quadrant 3:

$$\mathbf{K}^{int} = \frac{AH_p}{\ell} \begin{bmatrix} 2\cos^2\theta & 0 \\ 0 & 2\sin^2\theta \end{bmatrix} \tag{6.5.59c}$$

in quadrant 4:

$$\mathbf{K}^{int} = \frac{A}{\ell} \begin{bmatrix} \left(E + H_p\right)\cos^2\theta & \left(H_p - E\right)\sin\theta\cos\theta \\ \left(H_p - E\right)\sin\theta\cos\theta & \left(E + H_p\right)\sin^2\theta \end{bmatrix} \tag{6.5.59d}$$

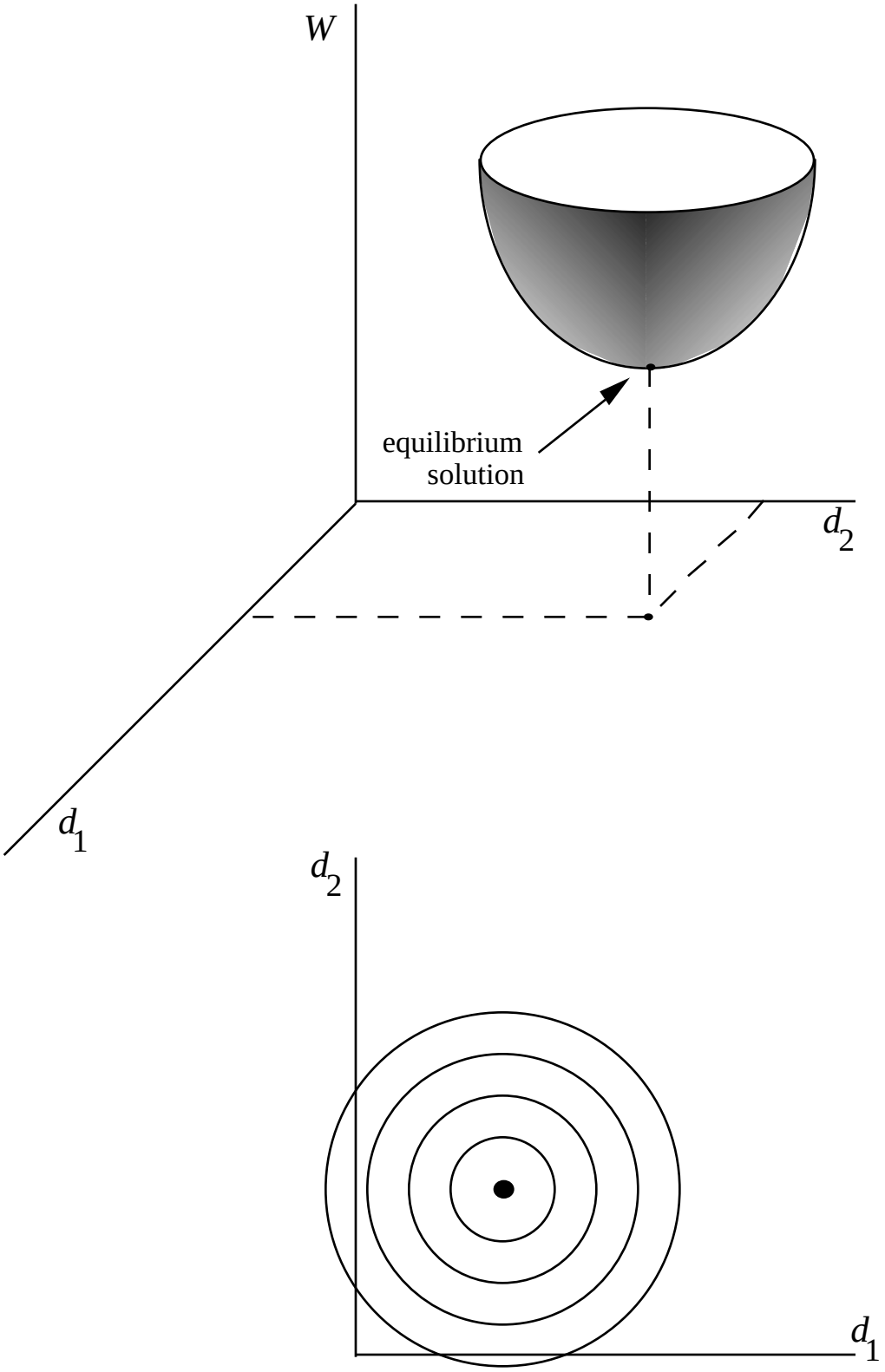

Figure 6.4. Schematic of potential energy, a stable equilibrium solution, and the contours for the potential with their gradient $-\mathbf{r}$.

To deal with this type of behavior in a methodical manner, a Frechet derivative, often called a directional derivative, must be used. The Frechet derivative is defined by

$$\frac{df(\mathbf{d})}{d\mathbf{d}_{[\Delta\mathbf{d}]}} = \lim_{\varepsilon \to 0} \frac{d}{d\varepsilon} f(\mathbf{d} + \varepsilon \Delta\mathbf{d})\Big|_{\varepsilon=0} \tag{6.4.60}$$

The subcript on the lower term gives the direction in which the derivative is taken. The notation $Df(\mathbf{d})\,[\Delta\mathbf{d}]$ is often used for the directional derivative in the finite element literature..

The value of directional derivative depends on the direction of the increment of the independent variable. The tangent stiffnesses in (??) are based on directional derivatives for the nodal forces have been given in (???).

In the computation of the tangent stiffness matrix, and in particular the material tangent stiffness, directional derivatives are used for elastic-plastic materials. The direction is based on the last displacement increment in the iterative procedure. If the load increment suddenly reverses, the last increment is not in the direction of the next solution increment, and the directional derivative may be quite erroneous,. However, after several iterations, the correct direction is determined for the displacement increment and the directional derivative gives the correct rate of change of the nodal forces.

Since the directional derivative to a specific value of the nodal displacements, this approach cannot be used with the standard tangent Newton described in Box ???. Instead, a secant Newton method must be used. The secant Newton method is given in Box ???.

External Load Stiffness. An important class of loads are follower loads, which change with the configuration of the body. Examples of follower forces are shown in Figure ??. Pressure loading is a common example of a follower load. Since a pressure loading is always normal to the surface, as the surface moves, the nodal external forces change even if the pressure is constant. These effects are accounted for in the Jacobian matrix $\mathbf{K}^{ext}$, which is also called the load stiffness.

The load stiffness $\mathbf{K}^{ext}$ is obtained by relatinng the time derivative (or increment) of the external nodal forces to the time derivative (or increment) of nodal displacements. We first consider loading by pressure, $p(\mathbf{x}, t)$. The external nodal forces on a surface of element *e* are given by letting $\mathbf{t} = -p\mathbf{n}$ in Eq. (4.9.13):

$$\mathbf{f}_I^{ext} = -\int_\Gamma N_I p\mathbf{n} d\Gamma \tag{6.4.61}$$

Let the surface Γ be described in terms of two variables ξ and η. For a quadrilateral surface element, these independent variables are the parent element coordinates on the biunit square. As in Eq. (E4.3.1b), since $\mathbf{n}d\Gamma = \mathbf{x}_{,\xi} \times \mathbf{x}_{,\eta}\, d\xi d\eta$ becomes

$$\mathbf{f}_I^{ext} = \int_{-1}^{1}\int_{-1}^{1} pN_I \mathbf{x}_{,\xi} \times \mathbf{x}_{,\eta}\, d\xi d\eta \tag{6.4.62}$$

Taking the time derivative of the above gives

$$\dot{f}_I^{ext} = \int_{-1}^{1}\int_{-1}^{1} N_I \left(\dot{p}\mathbf{x}_{,\xi} \times \mathbf{x}_{,\eta} + p\mathbf{v}_{,\xi} \times \mathbf{x}_{,\eta} + p\mathbf{x}_{,\xi} \times \mathbf{v}_{,\eta} \right) d\xi d\eta \tag{6.4.63}$$

The first term is the rate of change of the external forces due to the rate of change of the pressure. In many problems the rate of change of pressure is prescribed as part of the problem. In some problems, such as in fluid-structure interaction problems, the pressure may arise from changes of the geometry; these effects must then be linearized and added to the load stiffness. The second two terms represent the changes in the external nodal forces due to the change in the direction of the surface and the area of the surface. These are the terms which are reflected in the external load stiffness, so

$$\mathbf{K}_{IK}^{ext}\mathbf{v}_K = \int_{-1}^{1}\int_{-1}^{1} pN_I \left(\mathbf{v}_{,\xi} \times \mathbf{x}_{,\eta} + \mathbf{x}_{,\xi} \times \mathbf{v}_{,\eta} \right) d\xi d\eta \tag{6.4.64}$$

At this point, it is convenient to switch partially to indicial notation. Taking the dot product of the above with the unit vector $\mathbf{e}_i$ gives

$$\begin{aligned} \mathbf{e}_i \cdot \mathbf{K}_{IK}^{ext}\mathbf{v}_K &\equiv K_{ijIK}^{ext} v_{jK} \\ &\equiv \int_{-1}^{1}\int_{-1}^{1} pN_I \left[N_{J,\xi}\mathbf{e}_i \cdot \left(\mathbf{e}_k \times \mathbf{x}_{,\eta} \right) + N_{J,\eta}\mathbf{e}_i \cdot \left(\mathbf{x}_{,\xi} \times \mathbf{e}_k \right) \right] d\xi d\eta \end{aligned} \tag{6.4.65}$$

where we have expanded the velocity field in terms of the shape functions by $\mathbf{v}_{,\xi} = \mathbf{v}_K N_{K,\xi}$. We now define

$$H_{ik}^{\eta} \equiv e_{ik\ell} x_{\ell,\eta} \qquad H_{ik}^{\xi} = e_{ik\ell} x_{\ell,\xi} \tag{6.4.66}$$

Using these definitions and Eq. (6.4.65), we obtain

$$K_{ijIJ}^{ext} = \int_{-1}^{1}\int_{-1}^{1} pN_I \left(N_{J,\xi} H_{ij}^{\eta} - N_{J,\eta} H_{ij}^{\xi} \right) d\xi d\eta \tag{6.4.67}$$

or

$$\mathbf{K}_{IJ}^{ext} = \int_{-1}^{1}\int_{-1}^{1} pN_I \left(N_{J,\xi}\mathbf{H}^{\eta} - N_{J,\eta}\mathbf{H}^{\xi} \right) d\xi d\eta$$

If we write out the matrices $\mathbf{H}^{\xi}$ and $\mathbf{H}^{\eta}$ we have

$$\mathbf{K}_{IJ}^{ext} = \int_{-1}^{1}\int_{-1}^{1} pN_I \left(N_{J,\xi} \begin{bmatrix} 0 & z_{,\eta} & -y_{,\eta} \\ -z_{,\eta} & 0 & x_{,\eta} \\ y_{,\eta} & -x_{,\eta} & 0 \end{bmatrix} - N_{J,\eta} \begin{bmatrix} 0 & z_{,\xi} & -y_{,\xi} \\ -z_{,\xi} & 0 & x_{,\xi} \\ y_{,\xi} & -x_{,\xi} & 0 \end{bmatrix} \right) d\xi d\eta \tag{6.4.68}$$

which is the load stiffness of any surface which is generated from a biunit square in the parent element loaded by a pressure p. The load surface for a surface originating can be similarly expressed in terms of the area coordinates, although the limits of integration need to be changed. This load stiffness reflects the effect of the change in geometry on the nodal forces: both alterations in the direction of the loaded surfaces and size of the surface will changes in the nodal forces. It is immediately apparent from (6.4.68) that the submatrices of the load stiffness matrix are not symmetric, so the complete matrix is not symmetric. However, it can be shown that for a closed structure in a constant pressure field, the assembled external load stiffness is symmetric.

Example 6.1. Three-Node Triangle Element.

We first consider the three-node triangle element in two dimensions as in Example 4.1. The tangent stiffness matrix is derived and explicit forms for hyperelastic and rate-independent hypoelastic-plastic materials are given. The geometric tangent stiffness matrix, which is independent of material response, is then derived. Finally, the external load matrices are derived for a pressure load along any edge.

Material Tangent Stiffness Matrix. We consider the case of plane strain deformation (using the x-y plane). The only velocity components are v_x and v_y and derivatives with respect to z vanish. The tangent stiffness matrix for a rate-independent material given by Eq. (6.3.36):

$$K^{tan} = \int \mathbf{B}^T [C] \mathbf{B} dA \tag{E6.1.1}$$

where A is the current area of the element and we have assumed a unit thickness (see Eq. (4.??)).

$$\left[C_{ab}^{tan} \right] = \begin{bmatrix} C_{1111}^{\sigma T} & C_{1122}^{\sigma T} & C_{1112}^{\sigma T} \\ C_{2211}^{\sigma T} & C_{2222}^{\sigma T} & C_{2212}^{\sigma T} \\ C_{1211}^{\sigma T} & C_{1222}^{\sigma T} & C_{1212}^{\sigma T} \end{bmatrix} \tag{E6.1.2}$$

The **B** matrix is given by Eq. (E4.1.45):

$$\mathbf{B} = \frac{1}{2A}\begin{bmatrix} y_{23} & 0 & y_{31} & 0 & y_{12} & 0 \\ 0 & x_{32} & 0 & x_{13} & 0 & x_{21} \\ x_{32} & y_{23} & x_{13} & y_{31} & x_{21} & y_{12} \end{bmatrix} \tag{E6.1.3}$$

The material tangent stiffness matrix, Eq. (6.4.81), is rewritten, using Eqs. (6.4.82 - 6.4.84) as

$$\mathbf{K}^{tan} = \int_{A_0} \left(\frac{1}{2A}\right)^2 \begin{bmatrix} y_{23} & 0 & x_{32} \\ 0 & x_{32} & y_{23} \\ y_{31} & 0 & x_{13} \\ 0 & x_{13} & y_{31} \\ y_{12} & 0 & x_{21} \\ 0 & x_{21} & y_{12} \end{bmatrix} \begin{bmatrix} C^{\sigma T}_{1111} & C^{\sigma T}_{1122} & C^{\sigma T}_{1112} \\ C^{\sigma T}_{2211} & C^{\sigma T}_{2222} & C^{\sigma T}_{2212} \\ C^{\sigma T}_{1211} & C^{\sigma T}_{1222} & C^{\sigma T}_{1212} \end{bmatrix} \begin{bmatrix} y_{23} & 0 & y_{31} & 0 & y_{12} & 0 \\ 0 & x_{32} & 0 & x_{13} & 0 & x_{21} \\ x_{32} & y_{23} & x_{13} & y_{31} & x_{21} & y_{12} \end{bmatrix} dA_0 \tag{E6.1.4}$$

Assuming the integrand to be constant, we obtain, by multiplying the integrand by the element area A_0 (note that, for plane strain, a unit thickness is assumed and the element volume is given by $V_0 = A_0(1) = A_0$).

$$K^{tan}_{AB} = \frac{A_0}{4A^2} \begin{bmatrix} y_{23} & 0 & x_{32} \\ 0 & x_{32} & y_{23} \\ y_{31} & 0 & x_{13} \\ 0 & x_{13} & y_{31} \\ y_{12} & 0 & x_{21} \\ 0 & x_{21} & y_{12} \end{bmatrix} \begin{bmatrix} C^{\sigma T}_{1111} & C^{\sigma T}_{1122} & C^{\sigma T}_{1112} \\ C^{\sigma T}_{2211} & C^{\sigma T}_{2222} & C^{\sigma T}_{2212} \\ C^{\sigma T}_{1211} & C^{\sigma T}_{1222} & C^{\sigma T}_{1212} \end{bmatrix} \begin{bmatrix} y_{23} & 0 & y_{31} & 0 & y_{12} & 0 \\ 0 & x_{32} & 0 & x_{13} & 0 & x_{21} \\ x_{32} & y_{23} & x_{13} & y_{31} & x_{21} & y_{12} \end{bmatrix} \tag{E6.1.5}$$

Neo-Hookean Material. For a Neo-Hookean material (see Section 5.??),

$$C^{\sigma T}_{ijkl} = \lambda \delta_{ij}\delta_{kl} + \mu(J)\left(\delta_{ik}\delta_{jl} + \delta_{il}\delta_{jk}\right) \tag{E6.1.6}$$

where

$$J = det\ \mathbf{F}, \qquad \mu(J) = \mu_0 - \lambda\ log\ J, \tag{E6.1.7}$$

and Eq. (6.4.88) is written in Voigt notation as

$$\left[C_{ab}^{tan}\right] = \begin{bmatrix} \lambda+2\mu & \lambda & 0 \\ \lambda & \lambda+2\mu & 0 \\ 0 & 0 & \mu \end{bmatrix} \tag{E6.1.8}$$

Thus, for a Neo-Hookean material, the material tangent stiffness matrix has the same form as the stiffness matrix for small strain linear elasticity except for the dependence of the moduli on the deformation (through Eq. (6.4.90)) and the geometry factor $A_0/\Delta A$.

Rate-Independent Elastoplasticity. For a rate-independent elastic-plastic model in terms of the Kirchoff stress, with associated plastic flow and a von-Mises yield condition, the tangent modulus is given by Eq. (5.??)

$$C_{ijkl}^{tan} = C_{ijkl}^{ep} - \frac{1}{2}\left(\delta_{il}\tau_{jk} + \tau_{ik}\delta_{jl} + \delta_{ik}\tau_{jl} + \tau_{il}\delta_{jk}\right) \tag{E6.1.9}$$

The elastoplastic tangent modulus is given by

$$C_{ijkl}^{ep} = C_{ijkl} - \frac{C_{ijmn}p_{mn}C_{klrs}p_{rs}}{h + p_{mn}C_{mnrs}p_{rs}} \tag{E6.1.10}$$

where h is the plastic modulus, $p_{ij} = \dfrac{3\tau'_{ij}}{2\bar{\sigma}}$ is the plastic flow direction, τ'_{ij} is the deviatoric part of the Kirchoff stress and $\bar{\sigma}$ is the effective stress defined by (??). Assuming constant isotropic elastic moduli, Eq. (6.4.92) is written as

$$C_{ijkl}^{ep} = \lambda\delta_{ij}\delta_{kl} + \mu\left(\delta_{ik}\delta_{jl} + \delta_{il}\delta_{jk}\right) - \frac{4\mu^2}{h+3\mu}\,p_{ij}p_{kl} \tag{E6.1.11}$$

Using Voigt notation and letting $\gamma = \dfrac{2\mu}{\left(h+3\mu\right)}$, $p_1 = p_{11}$, $p_2 = p_{22}$, $p_3 = p_{12}$ and $\tau_1 = \tau_{11}$, $\tau_2 = \tau_{22}$, $\tau_3 = \tau_{12}$, the tangent stiffness matrix is obtained as

$$\left[C_{ab}^{tan}\right] = \begin{bmatrix} \lambda+2\mu & \lambda & 0 \\ \lambda & \lambda+2\mu & 0 \\ 0 & 0 & \mu \end{bmatrix} - 2\mu\gamma \begin{bmatrix} p_1^2 & p_1p_2 & p_1p_3 \\ p_2p_1 & p_2^2 & p_2p_3 \\ p_3p_1 & p_3p_2 & p_3^2 \end{bmatrix} - \frac{1}{2}\begin{bmatrix} 4\tau_1 & 0 & 2\tau_3 \\ 0 & 4\tau_2 & 2\tau_3 \\ 2\tau_3 & 2\tau_3 & \tau_1+\tau_2 \end{bmatrix} \tag{E6.1.12}$$

Geometric Stiffness Matrix. The geometric stiffness matrix is given by Eq. (6.3.55), i.e.,

$$\mathbf{K}_{IJ}^{geo} = \mathbf{I}_{2\times 2}\int_{A_0} \mathcal{B}_I^T \sigma \mathcal{B}_J \, dA = \mathbf{I}_{2\times 2} H_{IJ} \tag{E6.1.13}$$

From Eq. (E4.1.18)

$$\mathcal{B} = \frac{1}{2A}\begin{bmatrix} y_{23} & y_{31} & y_{12} \\ x_{32} & x_{13} & x_{21} \end{bmatrix} \tag{E6.1.15}$$

Substituting Eq. (E6.1.15) into Eq. (E6.1.16) gives

$$\mathbf{H} = \frac{1}{2A}\begin{bmatrix} y_{23} & x_{32} \\ y_{31} & x_{13} \\ y_{12} & x_{21} \end{bmatrix}\begin{bmatrix} \sigma_{xx} & \sigma_{xy} \\ \sigma_{xy} & \sigma_{yy} \end{bmatrix}\frac{1}{2A}\begin{bmatrix} y_{23} & y_{31} & y_{12} \\ x_{32} & x_{13} & x_{21} \end{bmatrix} \tag{E6.1.18}$$

Assuming the integrand to be constant, the geometric stiffness matrix is obtained by multiplying the integrand in Eq. (E6.1.13) by A to give

$$\mathbf{K}_{IJ}^{geo} = \frac{1}{4A} H_{IJ}\mathbf{I}_{2\times 2}$$

$$\mathbf{K}^{geo} = \frac{1}{4A}\begin{bmatrix} H_{11} & 0 & H_{12} & 0 & H_{13} & 0 \\ 0 & H_{11} & 0 & H_{12} & 0 & H_{13} \\ H_{21} & 0 & H_{22} & 0 & H_{23} & 0 \\ 0 & H_{21} & 0 & H_{22} & 0 & H_{23} \\ H_{31} & 0 & H_{32} & 0 & H_{33} & 0 \\ 0 & H_{31} & 0 & H_{32} & 0 & H_{33} \end{bmatrix} \tag{E6.1.19}$$

The geometric stiffness matrix is independent of material response and as can be seen from Eqs. (E6.1.18 - E6.1.19) depends only on the current stress rate and the geometry of the element. The load stiffness matrix is given by the same equation as described for the rod.

Example 6.2. Two-Node Rod Element.

We now consider the two-node rod element under a state of uniaxial stress. The rod is assumed to lie along the $\hat{x}-$axis. The only non-zero Cauchy stress component is $\hat{\sigma}_{11} \equiv \hat{\sigma}_x$. The tangent stiffness and the external load matrices are derived in the updated Lagrangian form, i.e. in the current configuration. We first reconsider the constitutive relation for the special case of uniaxial stress. The superscript hats are dropped in the following for convenience.

The Truesdell rate of the Cauchy stress is assumed to be given by Eq. (6.3.??)

$$\sigma_{ij}^{\nabla J} = C_{ijk\ell} D_{k\ell} \tag{E6.2.1}$$

For the case of uniaxial stress, the only non-zero components of the rate of deformation tensor are D_{11}, D_{22}, and D_{33}.

The uniaxial stress rate is therefore given by

$$\sigma_{11}^{\nabla J} = C_{1111}^{\sigma J} D_{11} + C_{1122}^{\sigma J} D_{22} + C_{1133}^{\sigma J} D_{33} \tag{E6.2.2}$$

The traction-free condition on the surface of the rod can be stated as

$$\begin{aligned} \sigma_{22}^{\nabla c} &= C_{2211}^{\sigma J} D_{11} + C_{2222}^{\sigma J} D_{22} + C_{2233}^{\sigma J} D_{33} = 0 \\ \sigma_{33}^{\nabla c} &= C_{3311}^{\sigma J} D_{11} + C_{3333}^{\sigma J} D_{22} + C_{3333}^{\sigma J} D_{33} = 0 \end{aligned} \tag{E6.2.3}$$

If the rod is initially transversely isotropic (with the axis of symmetry coincident with the x_1-axis) the tangent moduli are related by $C_{1133}^{\sigma J} = C_{1122}^{\sigma J}$ and $C_{2222}^{\sigma J} = C_{3333}^{\sigma J}$. Furthermore, uniaxial stressing in the direction of the axis of isotropy preserves the transverse isotropy and these relations hold throughout the deformation. Solving Eq. (6.2.3), with these assumptions we obtain *S*

$$D_{22} = D_{33}, \qquad D_{22} = -\frac{C_{2211}^{\sigma J}}{C_{2222}^{\sigma J} + C_{2233}^{\sigma J}} D_{11} \tag{E6.2.4}$$

Using Eq. (6.2.4) for D_{22} and D_{23} in Eq. (E6.2.3) gives the uniaxial relation

$$\sigma_{11}^{\nabla J} = E^{\sigma T} D_{11} \quad \text{or} \quad \left[C^{\sigma\tau}\right] = \left[E^{\sigma\tau}\right] \tag{E6.2.5}$$

where E^{tan} is the tangent modulus associated with the state of uniaxial stress and is given by

$$E^{\sigma T} = C_{1111}^{\sigma T} - \frac{2C_{2211}^{\sigma T} C_{1122}^{\sigma T}}{C_{2233}^{\sigma T} + C_{2222}^{\sigma T}} \tag{E6.2.6}$$

Material Tangent Stiffness Matrix. The tangent stiffness matrix for a rate-independent material is given by Eq. (6.4.18) in the current configuration which we write in the local coordinate system as

$$\hat{\mathbf{K}}^{mat} = \int_{\Omega} \hat{\mathbf{B}}^T \hat{\mathbf{C}}^{\sigma T} \hat{\mathbf{B}} \, d\Omega \tag{E6.2.7}$$

Using the **B** matrix from Eq. (E4.6.3) and $\mathbf{C}^{\sigma J}$ as given by Eq. (E6.2.5), we obtain

$$\hat{K}^{mat} = \int_0^1 \frac{1}{\ell} \begin{Bmatrix} -1 \\ 0 \\ 1 \\ 0 \end{Bmatrix} \left[E^{\sigma T}\right] \frac{1}{\ell} \begin{bmatrix} -1 & 0 & +1 & 0 \end{bmatrix} A\ell \, d\xi \tag{E6.2.8}$$

Here, the **B** matrix has been expanded to a 4×1 matrix by adding zeros to reflect that the $\hat{x}$-component of the rate-of-deformation is independent of the transverse velocities. If we assume $E^{\sigma T}$ is constant in the element, then

$$\hat{\mathbf{K}}^{mat} = \frac{AE^{\sigma T}}{\ell} \begin{bmatrix} +1 & 0 & -1 & 0 \\ 0 & 0 & 0 & 0 \\ -1 & 0 & +1 & 0 \\ 0 & 0 & 0 & 0 \end{bmatrix} \tag{E6.2.9}$$

This is identical to the linear stiffness matrix for a rod if $E^{\sigma T}$ is replaced by Young's modulus *E*. The global stiffness is given by Eq. (4.5.42):

$$\mathbf{K}^{mat} = \mathbf{T}^T \hat{\mathbf{K}}^{mat} \mathbf{T} \tag{E6.2.10a}$$

where **T** is given by

$$\mathbf{T} = \begin{bmatrix} \cos\theta & \sin\theta & 0 & 0 \\ -\sin\theta & \cos\theta & 0 & 0 \\ 0 & 0 & \cos\theta & \sin\theta \\ 0 & 0 & -\sin\theta & \cos\theta \end{bmatrix} \tag{E6.2.10b}$$

so

$$\mathbf{K}^{mat} = \frac{AE^{\sigma T}}{\ell} \begin{bmatrix} \cos^2\theta & \cos\theta\sin\theta & -\cos^2\theta & -\cos\theta\sin\theta \\ & \sin^2\theta & -\cos\theta\sin\theta & -\sin^2\theta \\ & & \cos^2\theta & \cos\theta\sin\theta \\ & \text{symmetric} & & \sin^2\theta \end{bmatrix} \tag{E6.2.11}$$

where the material constant $E^{\sigma T}$ relates the Truesdell rate of the Cauchy stress to the rate-of-deformation in a uniaxial state of stress.

Geometric Stiffness Matrix. The geometric stiffness is developed in a coordinate system that at time *t* coincides with the axis of the bar but is fixed in time. Note that since the coordinate system is fixed in the orientation shown in Fig. ??, it is not a true corotational coordinate system, so the rotation corrections of an objective rate must be considered. We will use the Truesdell rate. We could also consider the $\hat{x}$, $\hat{y}$ coordinate system corotational and derive the geometric stiffness by accounting for the channge of the transformation matrix **T** in (E4.6.11) . Many such derivations are given in Crisfield. The result should be identical, since the same mechanical effect is represented, but the derivation is generally more difficult. The geometric stiffness matrix is given by Eq. (6.4.18):.

$$\hat{\mathbf{K}}_{IJ} = \hat{H}_{IJ}\mathbf{I} \qquad \hat{\mathbf{H}} = \int_\Omega \hat{\boldsymbol{B}}^T \sigma \hat{\boldsymbol{B}}\, d\Omega \tag{E6.2.12}$$

where the geometric stiffness has been expressed in the local coordinate system for simplicity. Using the B matrix from Eq. (4.6.3), it follows that

$$\mathbf{H} = \int_\Omega \frac{1}{\ell}\begin{bmatrix}-1\\+1\end{bmatrix}[\hat{\sigma}_x]\frac{1}{\ell}\begin{bmatrix}-1 & +1\end{bmatrix} d\Omega \tag{E6.2.13}$$

Assuming that the stress is constant gives

$$\hat{\mathbf{H}} = \frac{\hat{\sigma}_x A}{\ell}\begin{bmatrix}+1 & -1\\ -1 & +1\end{bmatrix} \tag{E6.2.14}$$

Expanding the above, we obtain the geometric stiffness as given by Eq. (E6.2.12)

$$\hat{\mathbf{K}}^{geo} = \frac{A\hat{\sigma}_x}{\ell}\begin{bmatrix}+1 & 0 & -1 & 0\\ 0 & +1 & 0 & -1\\ -1 & 0 & +1 & 0\\ 0 & -1 & 0 & +1\end{bmatrix} \tag{E6.2.15}$$

Use of the transformation formula, Eq. (4.5.42), shows that the geometric stiffness is independent of the orientation of the beam.

$$\mathbf{K}^{geo} = \mathbf{T}^T\hat{\mathbf{K}}^{geo}\mathbf{T} = \hat{\mathbf{K}}^{geo} \tag{E6.2.16}$$

The total tangent stiffness is then given by the sum of the material and geometric stiffnesses

$$\mathbf{K}^{int} = \mathbf{K}^{mat} + \mathbf{K}^{geo} \tag{E6.2.17}$$

The matrix is symmetric, which is a consequence of choosing a constitutive equation in terms of the Truesdell rate of the convected rate of the Kirchhoff stress. The matrix is positive definite as long as the initial stress is small compared to the tangent modulus. THE STIFFNESS FOR JAUMANN RATE AND THE EIGENVALUES OF K ARE LEFT AS EXERCIZES.

Load Stiffness. The load stiffness for the rod is given by Eq. (??). We write only the nonzero terms noting $N_{,i\eta} = 0$ and that $x_{,\eta} = y_{,\eta} = 0$, since the shape function is only a function of ξ. For simplicity, we first evaluate it in the corotational system, which gives

$$\hat{\mathbf{K}}_{IJ} = \int_0^1 pN_I N_{J,\xi}\begin{bmatrix}0 & z_{,\eta}\\ -z_{,\eta} & 0\end{bmatrix} d\xi \tag{E6.2.18}$$

In the above, $z_{,\eta}$ can be taken to the width of the element a. Using (???) gives

$$\hat{\mathbf{K}}_{IJ} = \int_0^1 pN_I N_{J,\xi}\,\ell\begin{bmatrix}0 & 1\\ -1 & 0\end{bmatrix} a\,d\xi \tag{E6.2.19}$$

Let

$$H_{IJ} = \int_0^1 N_I N_{J,\xi} d\xi = \int_0^1 \begin{bmatrix} -1+\xi \\ 1 \end{bmatrix} \frac{1}{\ell} \begin{bmatrix} -1 & +1 \end{bmatrix} d\xi \tag{E6.2.20}$$

$$= \frac{1}{2\ell} \begin{bmatrix} -1 & 1 \\ -1 & 1 \end{bmatrix} \tag{E6.2.21}$$

Then

$$\hat{K}_{IJ}^{ext} = p\ell a H_{IJ} \tag{E6.2.22}$$

Taking the shape functions (???) and substituting into the above gives

$$\hat{\mathbf{K}}^{ext} = \frac{pa}{2} \begin{bmatrix} 0 & -1 & 0 & 1 \\ 1 & 0 & -1 & 0 \\ 0 & -1 & 0 & 1 \\ 1 & 0 & -1 & 0 \end{bmatrix} \tag{E6.2.23}$$

The above matrix is also invariant with rotation, i.e.,

$$\mathbf{K}^{ext} = \mathbf{T}^T \hat{\mathbf{K}}^{ext} \mathbf{T} = \hat{\mathbf{K}}^{ext} \tag{E6.2.24}$$

for forces and velocities expressed in any other Cartesian coordinate system.

Material Tangent Stiffness Matrix in Total Lagrangian Form. The material tangent stiffness matrix for a rate-independent material is given by Eq. (6.4.18) in the reference configuration

$$\mathbf{K}^{mat} = \int_{\Omega_0} \mathbf{B}^T \mathbf{C}^{SE} \mathbf{B} d\Omega_0 \tag{E6.2.25}$$

Using the **B** matrix from Eq. (E4.???) and $\mathbf{C}^{SE}$ as given by Eq. (E6.2.5), we obtain

$$K^{mat} = \int_0^1 \frac{1}{\ell_0} \begin{bmatrix} -\cos\theta \\ -\sin\theta \\ \cos\theta \\ \sin\theta \end{bmatrix} \left[E^{SE} \right] \frac{1}{\ell_0} \begin{bmatrix} -\cos\theta & -\sin\theta & \cos\theta & \sin\theta \end{bmatrix} A_0 \ell_0 d\xi \tag{E6.2.26}$$

If we assume E^{SE} is constant in the element, then

$$\mathbf{K}^{mat} = \frac{A_0 E^{SE}}{\ell_0} \begin{bmatrix} \cos^2\theta & \cos\theta\sin\theta & -\cos^2\theta & -\cos\theta\sin\theta \\ & \sin^2\theta & -\cos\theta\sin\theta & -\sin^2\theta \\ & & \cos^2\theta & \cos\theta\sin\theta \\ \text{symmetric} & & & \sin^2\theta \end{bmatrix} \tag{E6.2.27}$$

where the material constant E^{SE} relates the Truesdell rate of the Cauchy stress to the rate-of-deformation in a uniaxial state of stress. It can easily be shown via (???) that the above is identical to (E6.2.12).

Geometric Stiffness Matrix in Total Lagrangian Form. The geometric stiffness is developed from (6.4.15):

$$\mathbf{K}_{IJ} = H_{IJ}\mathbf{I} \qquad \mathbf{H} = \int_{\Omega_0} \boldsymbol{B}_0^T \mathbf{S} \boldsymbol{B}_0 \, d\Omega_0 \tag{E6.2.28}$$

where the $\boldsymbol{B}_0$ matrix is given in (4.6.3), so

$$\mathbf{H} = \int_{\Omega_0} \frac{1}{\ell_0} \begin{bmatrix} -1 \\ +1 \end{bmatrix} [S_{11}] \frac{1}{\ell_0} \begin{bmatrix} -1 & +1 \end{bmatrix} d\Omega_0 \tag{E6.2.29}$$

Assuming that the stress is constant gives

$$\hat{\mathbf{H}} = \frac{S_{11} A_0}{\ell_0} \begin{bmatrix} +1 & -1 \\ -1 & +1 \end{bmatrix} \tag{E6.2.30}$$

Expanding the above, we obtain the geometric stiffness

$$\mathbf{K}^{geo} = \frac{A_0 S_{11}}{\ell_0} \begin{bmatrix} +1 & 0 & -1 & 0 \\ 0 & +1 & 0 & -1 \\ -1 & 0 & +1 & 0 \\ 0 & -1 & 0 & +1 \end{bmatrix} \tag{E6.2.31}$$

The total tangent stiffness is then given by the sum of the material and geometric stiffnesses, (E6.2.17).

6.3.7. Constraints. Three types of methods are frequently used for treating the constraint Eq. (6.3.10). They are:

1. penalty methods
2. Lagrangian multiple methods
3. augmented Lagrangian methods

These methods originate in constrained optimization theory. As will be seen, they can readily be adapted to the solution of the nonlinear algebraic equations that correpond to the momentum or equilibrium equations, Eq. (6.3.10). To motivate these methods, we begin with a description of how they are applied to the nonlinear minimization problem, Eq. (6.3.27) (note that while Eq. (6.3.27)

[...] the stationary prints are determined in the problem is often called a minimization problem because often only the stable equilibrium solutions are of interest).

The problem then is to solve:

$$\mathbf{r}(\mathbf{d}) = 0 \quad \text{subject to } g_I(\mathbf{d}) = 0,\ I = 1 \text{ to } n_c$$

where $\mathbf{r} \quad R^n$, $\mathbf{d} \quad R^n$. The following notation is used

$$W_{,a} = \frac{\partial W}{\partial d_a} \qquad G_{Ia} = \frac{\partial g_I}{\partial d_a} = g_{I,\,a} \qquad G_{Ia} = \frac{\partial g_I}{\partial d_a} = g_{I,\,a}$$

$$r_{a,\,b} = A_{ab} \qquad \text{or} \qquad \frac{\partial \mathbf{r}}{\partial \mathbf{d}} = \mathbf{A} = \mathbf{M}\ddot{\mathbf{d}} + \mathbf{f}^{int} - \mathbf{f}^{ext}$$

We will use the conventions $G_I = \left[G_{I1},\ G_{I2},\ \ldots,\ G_{In_c} \right]$ and $\mathbf{H}_I \quad R^{n_c} \times R^{n_c}$, as before. Recall that

$$W_{,a} = r_a = f_a^{int} - f_a^{ext} \tag{6.3.40d}$$

in a conservation problem and that $W_{,ab}$, the Jacobian

$$W_{,ab} = A_{ab} \tag{6.3.40e}$$

matrix of the system.

We will also examine the less general problem of finding stationary the points of

$$W(\mathbf{d}) = 0 \text{ subject to } g_I(\mathbf{d}) = 0 \tag{6.3.41}$$

Lagrange Multiplier Method. In the Lagrange method, the constraints are appended to the objective function with the Lagrangian multipliers. The minimization Eq. (6.3.41) becomes equivalent to finding the stationary points of

$$W + \lambda_I g_I \equiv W + \lambda^T \mathbf{g} \tag{6.3.42}$$

Note that at a minimum of W, the augmented function given above has a saddle point.

The stationary points are found by setting to zero the derivatives of the above with respect to d_a and λ_I :

$$W_{,a} + \lambda_I g_{I,\,a} \equiv r_a + \lambda_I g_{I,\,a} = 0 \tag{6.3.43a}$$

$$g_I = 0 \tag{6.3.43b}$$

The above is the system of equations for the constrained problem. The constraint introduces extra forces $\lambda_I g_{I,a}$, which are linear combinations of the Lagrange multipliers.

The linear model of (6.3.43) is the first two terms of a Taylor expansion of (6.3.43), giving

$$r_a + \lambda_I g_{I,a} + r_{a,b}\Delta d_b + \lambda_I g_{I,a} + \lambda_I g_{I,ab}\Delta d_b = 0 \tag{6.3.44a}$$

$$g_I + g_{I,a}\Delta d_a = 0 \tag{6.3.44b}$$

Using matrix notation we can write the above as

$$\begin{bmatrix} \mathbf{A} + \lambda_I \mathbf{H}_I & \mathbf{G}^T \\ \mathbf{G} & \mathbf{0} \end{bmatrix} \begin{Bmatrix} \Delta \mathbf{d} \\ \Delta\lambda \end{Bmatrix} = \begin{Bmatrix} -\mathbf{r} - \lambda^T \mathbf{G} \\ -\mathbf{g} \end{Bmatrix} \tag{6.3.45}$$

So the linear model has n_c additional equations due to the constraint. Even when the **A** is positive definite, the augmented system of equations will not be positive definite because of the zeroes on the diagonal in the lower right hand corner of the matrix. For a linear statics problem with a linear constraints $\mathbf{G}\mathbf{d} = \mathbf{g}$, the above becomes

$$\begin{bmatrix} \mathbf{K} & \mathbf{G}^T \\ \mathbf{G} & \mathbf{0} \end{bmatrix} \begin{Bmatrix} \mathbf{d} \\ \lambda \end{Bmatrix} = \begin{Bmatrix} \mathbf{f}^{ext} \\ \mathbf{g} \end{Bmatrix} \tag{6.3.46}$$

since

1. $\mathbf{A} = \mathbf{K}$ for linear statics;
2. $\mathbf{H}_I = 0$ for linear constraints, see Eq. (6.3.40c);
3. the starting value is zero and $\Delta\mathbf{d} = \mathbf{d}$, $\Delta\lambda = \lambda$, and the constraint is $\mathbf{G}\mathbf{d} = \mathbf{0}$.

For the general problem with nonconservative materials, dynamics, etc., the Lagrangian multiplier method is formulated as follows. The stationary condition Eq. (6.3.43) can be written

$$\delta W + \delta\left(\lambda_I g_I\right) = 0 \tag{6.3.47}$$

From Eq. (B4.6.1) and Eq. (6.3.1)

$$\begin{aligned}\delta W &= \delta W^{ext} - \delta W^{int} + \delta W^{inert} \\ &= \delta \mathbf{d}^T \left(-\mathbf{f}^{ext} + \mathbf{f}^{int} + s_D \mathbf{M} \ddot{\mathbf{d}} \right) \\ &= \delta \mathbf{d}^T \mathbf{r} = \delta d_a r_a\end{aligned} \tag{6.3.48}$$

Substituting Eq. (6.3.48) into Eq. (6.3.47) and writing out the differentials on the second term gives

$$\delta \mathbf{d}_a r_a + \delta \lambda_I^T g_I + \lambda_I^T g_{I,\,a} \delta d_a = 0 \qquad \delta d_a \delta \lambda_I \tag{6.3.49}$$

Using the arbitrariness of the differentials in the above implies Eq. (4.3.44-45). Thus the same structure is obtained for a nonconservative dynamic problem. The linearization procedure leads to the same equations, Eq. (6.3.45). While the development has been given for the virtual work δW, it applies identically to virtual power.

Penalty Method. Again, we first consider conservative problems where the solution is determined by minimization. In the penalty method, the constraint is enforced by adding the square of the constraints to the poential, so we minimize as modified potential

$$\overline{W}(\mathbf{d}) = W(\mathbf{d}) + \frac{1}{2} \beta g_I(\mathbf{d}) g_I(\mathbf{d}) \tag{6.3.50}$$

where β is a penalty parameter. The penalty parameter is generally orders of magnitude greater than other parameters of the problem. The idea is that if β is large enough, the minimum of $\overline{W}(\mathbf{d})$ cannot be attained without satisfying the constraints.

The stationary (or minimum) conditions give

$$\overline{W}_{,a} = W_{,a} + \beta g_I g_{I,\,a} = 0 \quad \text{or} \quad \mathbf{r} + \beta \mathbf{g}^T \mathbf{G} = 0 \tag{6.3.51}$$

The linear model is

$$\left(r_{a,\,b} + \beta g_{I,\,b} g_{I,\,a} + g_I g_{I,\,ab} \right) d_b = 1 \left(r_a + \beta g_I g_{Ia} \right) \tag{6.3.52}$$

or in matrix form

$$\bar{A} \Delta \mathbf{d} = \left(\mathbf{A} + \beta \mathbf{G}^T \mathbf{G} + g_I \mathbf{H}_I \right) \Delta \mathbf{d}_b = -\mathbf{r} + \beta \mathbf{g}^T \mathbf{G} \tag{6.3.53}$$

The size of this system is not increased over the unconstrained system. For linear constraints, if $\mathbf{A} > 0$, $\bar{A} > 0$, i.e. the augmented system if positive definite if the original Jacobian matrix is positive definite. The major drawback of penalty methods is that they impair the conditioning of the equations.

The discrete equations for nonconservative systems are obtained by the same procedure as for the Lagrange multipliers. Write the stationary conditions in differential form

$$0 = \delta \overline{W} = \delta W + \frac{1}{2}\beta\delta\left(g_I g_I\right) \tag{6.3.54}$$

Now apply Eq. (6.3.48) to replace δW in the above. The discrete equations and linear model are then given by Eqs. (6.3.51) and (6.3.52), respectively.

6.5. STABILITY: CONTINUATION AND ARCLENGTH METHODS

Stability. In nonlinear problems, stability of solutions is of considerable interest. There are many definitions of stability: stability is a concept that depends on the beholder and his objectives. However, some general definitions are widely accepted. We will here describe a theory of stability that originates from Liapunov(??) and is widely used throughout mathematical analysis, see Saybol(??) for a very lucid account of its compuuttional application to a variety of problems. We will focus on its application to finite element methods.

We will first give a definition of stability and explore its implications. Consider a process that is governed by an evolution equation such as the equation of motion or the heat conduction equations. Let the solution for the initial conditions $\mathbf{d}_A\left(0\right) = \mathbf{d}_A^0$ be denoted by $\mathbf{d}_A\left(t\right)$. Now consider additional solutions for initial conditions $\mathbf{d}_B\left(0\right) = \mathbf{d}_B^0$, where $\mathbf{d}_B^0$ are small perturbation of $\mathbf{d}_A^0$. This means that $\mathbf{d}_B^0$ is close to $\mathbf{d}_A^0$ in some norm, i.e.

$$\left\| \mathbf{d}_A^0 - \mathbf{d}_B^0 \right\| \le \varepsilon \tag{6.5.1}$$

A solution is stable when for all initial conditions that satisfy (6.5.1), the solution satisfies

$$\left\| \mathbf{d}_A\left(t\right) - \mathbf{d}_B\left(t\right) \right\| \le C\varepsilon \qquad t > 0 \tag{6.5.2}$$

To explain this definition, we specify the norm to be the ℓ_2 norm. Note that all initial conditions which satisfy (6.5.1) lie in a neighborhood of $\mathbf{d}_A^0$. It is often said that the initial conditions lie in a ball around $\mathbf{d}_A^0$. The definition then states that for all initial conditions which lie in the ball around $\mathbf{d}_A^0$, the solutions $\mathbf{d}_B\left(t\right)$ must lie in a ball around the solution $\mathbf{d}_A\left(t\right)$ for all time. This definition is illustrated for a system with two dependent variables in Fig. 6.7. The right-hand

side shows the behavior of a stable system. Here we have only shown two solutions resulting from perturbations of the initial data, since it is impossible to show an infinite number of solutions. The leftr hand side shows an unstable system. It suffices for a single solution starting in the ball about $\mathbf{d}_A^0$ to diverge to indicate an unstable solution.

The applicability of this definition to processes we intuitively consider stable and unstable can be seen by the following examples. Consider a beam a beam loaded axially by a vertical load as shown in Fig. 6.8. We first consider the numerical response when the beam is perfectly straight. The lateral response in this case is the path is denoted by $d_A\left(t\right)$, and as can be seen, the lateral displacement is zero even though the load eventually exceeds the buckling load. If you don't believe this, try it. The beam will usually not buckle in an incremental solution or a dynamic solution with explicit or implicit integration. Only if roundoff error introduces a "numerical imperfection" will the perfectly straight beam buckle. We then plot the lateral displacement of the beam as we perturb the location of node 2, which can be considered an initial condition on the displacement of that node. The resulting paths are also shown in Fig. 6.8. It can be seen that when the load is below the buckling load, the paths for different initial conditions remain in a ball about the $d_A\left(t\right)$. However, when the load exceeds the buckling load, the solutions for different initial conditions in the location of point A diverge drastically. Therefore any process in which the load exceeds the buckling load is unstable. Note that the direction of the divergence depends on the sign of the initial imperfection.

Another example is the flow of a liquid in a pipe. When the flow velocity is below a critical Reynold's number, the flow is stable. A perturbation of the state leads to small changes in the evolution of the system. On the other hand, when the flow is above the critical Reynold's number, a small perturbation leads to large changes because the flow changes from laminar to turbulent.

Stability is usually ascribed to a state, rather than a process. The definition is then identical: a state is stable if a small perturbation of that state results in a small differences for all time. When perturbations lead to large differences in the subsequent states of the system, the state is unstable. This concept fits within the framework of the definition of stability given by Eq. (6.5.1) with the state considered as the initial condition.

A common example of stable and unstable states often given in introductory dynamics texts is shown in Fig. 6.9. It is clear that state *A* is stable, since small perturbations of the positionn of the ball will not significantly change the evolution of the system. State *B* is unstable, small perturbations will lead to large changes: the ball can roll either to the right or to the left. State *C* is often called neutral stability in introductory texts. According to the definition of Eq. (6.5.1), state *C* is an unstable state, since small changes in the velocity will lead to large changes in the position as large times. Thus the definition of stability given in introductory texts does not completely conform to the one given here.

Stability of Equilibrium Solutions. To obtain a good understanding oof the behavior of a system, its equilibrium paths, or branches, and their stability

must be determined. It is often argued among structural mechanicians that the difficulties associated with unstable behavior can be circumvented by simply obtaining a dynamic solution. When a structure is loaded above its limit point or a bifurcation point in a dynamic simulation, the structure passes dynamically to the vicinity of the next stable branch and the instability is not apparent except for the onset of a different mode of deformation, such as the lateral deformation in a beam. However, to understand the behavior of a structure or process thoroughly, its static equilibrium behavior should be carefully examined. Many vagaries of structural behavior may be hidden by dynamic simulations. For example, when the fundamental path bifurcates with an asymmetric branch as shown in Fig. 6.10, the structure becomes very sensitive to imperfections. The theoretical bifurcation point is not a realistic measure of the strength; an actual structure will buckle at a much lower load than the theoretical value because imperfections are unavoidable. A single numerical simulation could miss this sennsitivity completelly. This sensitivity to imperfections for cylindrical shells was analyzed by Koiter(??) and is a classical example of imperfection sensitivity.

As a first step in studying the equilibrium behavior of a system, the load and any other parameters of interest, such as the temperature or an active control, must be parametrized. Up to now we have parametrized the load by the time *t,* which is convenient in many practical problems. However, a single parameter does not always suffice in the study of equilibrium problems. We will now parametrize the load by n_γ parameters γ_a, so the load is then given by $\gamma_a q_a$, where q_a represent a distributed loading such as a pressure or concentrated loads. We use the convention that repeated indices are summed over the range, in this case n_γ. For distributed loads, the parameter γ_a should not be applied directly to the external nodal forces, since the external nodal forces will depend on the nodal displacements. The discrete loads can be parametrized by $\gamma_a \mathbf{f}_a^{ext}$, where $\mathbf{f}_a^{ext}$ are column matrices of nodal external forces associated with a loading mode *a*.

Our intention is to trace the equilibrium behavior of the model as a function of the parameters γ_α The problem then is then is to find $\mathbf{d}(\gamma_a)$ such that

$$\mathbf{r}\Big(\mathbf{d}(\gamma_a)\Big) = \mathbf{0} \tag{6.5.2b}$$

For purposes of characterizing the nonlinear system, the solutions are usually grouped into branches, which are continuous lines describing the response for one change of one parameter. Branches along which the solution is in equilibrium, i.e. satisfies Eq(6.5.2b), are called equilibrium branches, regardless of whether they are stable or unstable.

Nonlinear systems exhibit three types of branching behavior:

1. turning points, usually called limit points in structural analysis, in which the slope of the branch changes sign;
2. stationary bifurcations, often called simply bifurcations, in which two equilibrium branches intersect.

3. Hopf bifurcations, in which an equilibrium branch intersects with a branch on which there is periodic motion.

The behavior of the shallow truss exhibits a limit (or turning) point, as can be seen from Fig. 6.11. Subsequent to a turning point, a branch can be either stable or stable. In this case, as shown in the analysis of the problem in Example 6.4, the branch after the first limit point, point *a*, is unstable, while the branch after thhe second limit point, point *b*, is stable.

The beam problem shown in Fig. 6.12 is a classical example of a bifurcation. The point *b* where the two branches intersect is the point of bifurcation. Subsequent to the bifurcation point, the continuation of the fundamental branch *ab*, becomes unstable. Point *b*, the bifurcation point, corresponds to the classical buckling load of the Euler beam. This type of branching is often called a pitchfork, (do you see the hay on the end?)

Hopf bifurcations are quite uncommon in passive structures. They are found in general nonlinear behavior and can be seen in structures under active control. In a Hopf bifurcation, stable equilibtrium solutions become impossible at the end of a branch. Instead, there are two branches with periodic solutions. An example of a Hopf bifurcation is given in Example ??.

Methods of continuation and arclength methods. The tracing of branches is called a *continuation method*. The tracing of equilibrium branches is often quite difficult and robust, automatic procedures for continuation are not available. In the following, we describe continuation methods base on parametrization, such as the arc length method. In the arc length method, the arc length along the equilibrium path replaces the load as the incremental parameter. It enables branches to be followed around turning points, which is critical to the succesful continuation of equilibrium branches..

We first consider continuation with the arc length method for the case of a single load parameter. In tracing the branches in a model with a single load parameter, the load parameter is usually started at zero and incremented. For each load increment, an equilibrium solution is computed, i.e. we find $\mathbf{d}^{n+1}$, a solution to

$$\mathbf{r}\left(\mathbf{d}^{n+1}, \gamma^{n+1}\right) = 0 \quad \text{or} \qquad \mathbf{f}^{int}\left(\mathbf{d}^{n+1}\right) - \gamma^{n+1}\mathbf{f}^{ext} = 0 \tag{6.5.3}$$

where n is the step number and $\mathbf{f}^{ext}$ is the load distribution chosen for tracing the branch. We assume that the loads are prescribed discretely so that the distribution of nodal external forces does not change with the deformation of the model. The inertial term is not included in the above because continuation methods are applicable only to equilibrium problems. One of the most widely used continuation methods in structural mechanics is the arc length method. Instead of incrementing the load parameter γ to trace the branch, a measure of the arclength is incremented. This is accomplished by adding a parametrization equation to the equilibrium equations

$$p\left(\mathbf{d},\Delta\mathbf{d},\gamma\right)=\Delta s^2,\quad \Delta\gamma=\gamma^{n+1}-\gamma^n,\ \ \Delta\mathbf{d}=\mathbf{d}^{n+1}-\mathbf{d}^n \tag{6.5.4}$$

The parametrization equations may be written in terms of the displacements or increments in the displacements or both. For example, in the arclength method the parametrizationn equations are written directly in terms of the displacement increments

$$\Delta\mathbf{d}^T\Delta\mathbf{d}+\Delta\gamma^2=\Delta s^2 \tag{6.5.4b}$$

Many other types of parametrization equations can be devised, and some are described at the end of this section. DEESCRIBED FISH PARAMETRIZATION LATER WHEN SCALINNG IS DESCRIBED

The total system of equations then consists of the equilibrium equations and the parametrization equation, so we have

$$\begin{bmatrix}\mathbf{r}\left(\mathbf{d},\gamma\right)\\ p\left(\mathbf{d},\Delta\mathbf{d},\gamma\right)\end{bmatrix}=\begin{bmatrix}\mathbf{0}\\ \Delta s^2\end{bmatrix} \tag{6.5.5}$$

The load parameter γ is now treated as an additional unknown of the system and the arclength s is now incremented instead of the parameter γ.

This procedure is most easily explained for a one degree-of-freedom problem such as the shallow truss shown in Fig. 6.13. The fundamental branch is shown in Fig. 6.13 and we assume that a solution has been obtained at point *n*. The arclength equation when viewed in the γ, d_y is the circle about point *n;* in the 3-space $\left(\gamma, d_x, d_y\right)$ it would be a sphere about the point. In solving the parametrized equations, (6.5.5), we seek a solution which is the intersection of the equilibrium branch with the circle about the last solution point, which gives the solution shown as point *n*+1 in Fig. 6.13. Thus, while incrementing the load parameter would be fruitless at point *n*, the problem has been restated in terms of the arclength along the branch so that a solution with a lower load can be found.

The parametrized equations for the truss with symmetry can then be posed as follows: find a solution to

$$r_1(d_1,\gamma)=-f_1(d_1,\gamma)=0\quad\text{subject to}\quad\left(\gamma(s)-\gamma^n\right)^2+\left(d_1(s)-d_1^n\right)^2=\Delta s^2 \tag{6.5.6}$$

Alternatively, we can write the above in terms of increments in the displacements and the load parameters as: find a solution to

$$f_1=0\quad\text{subject to}\quad\Delta\gamma^2+\left(\Delta d_1\right)^2=\Delta s^2 \tag{6.5.7}$$

Thus the problem with one unknown is augmented by a second equation, which leads to two nonlinear algeraic equations in two unknowns. The load need not increase in the step, and may in fact decrease. It is only necessary for the arclength parameter to increase, which is a perfectly natural way of tracing the branch.

To describe the method in a more general case, we consider the problem with n_γ load parameters γ_a. For each load parameter, a parametrization equation must be added:

$$p_a\left(\mathbf{d},\gamma_b\right) = \Delta s_a^2 \qquad \text{or} \quad \mathbf{p}\left(\mathbf{d},\gamma\right) = \Delta\mathbf{s} \tag{6.5.8}$$

where

$$\mathbf{p} = \begin{bmatrix} p_1 & \cdots & p_{n_\gamma} \end{bmatrix}, \quad \Delta\mathbf{s} = \begin{bmatrix} \Delta s_1^2 & \cdots & \Delta s_{n_\gamma}^2 \end{bmatrix}, \quad \gamma = \begin{bmatrix} \gamma_1 & \cdots & \gamma_{n_\gamma} \end{bmatrix}$$

The resulting augmented equations for the equilibrium path are then

$$\begin{bmatrix} \mathbf{f}\left(\mathbf{d},\gamma\right) \\ \mathbf{p}\left(\mathbf{d},\gamma\right) \end{bmatrix} = \begin{bmatrix} \mathbf{0} \\ \Delta\mathbf{s} \end{bmatrix} \tag{6.5.9}$$

Thus for a system with n_{DOF} degrees of freedom, we obtain an augmented system of $n_{DOF} + n_\gamma$ equations in the same number of unknowns.

The resulting equations can be solved by the standard Newton methods we have described. The linearized equations for the Newton method are given by

$$\begin{bmatrix} \partial\mathbf{f}/\partial\mathbf{d} & \partial\mathbf{f}/\partial\gamma \\ \partial p/\partial\mathbf{d} & \partial\mathbf{p}/\partial\gamma \end{bmatrix} \begin{bmatrix} \Delta\mathbf{d} \\ \Delta\gamma \end{bmatrix} = \begin{bmatrix} \mathbf{0} \\ \Delta\mathbf{s} \end{bmatrix}$$

$$\begin{bmatrix} \mathbf{K}^{int} - \gamma_a \mathbf{K}_a^{ext} & \partial\mathbf{p}/\partial\gamma \\ \partial\mathbf{p}/\partial\mathbf{d} & \partial\mathbf{p}/\partial\gamma \end{bmatrix} \begin{bmatrix} \Delta\mathbf{d} \\ \Delta\gamma \end{bmatrix} = \begin{bmatrix} \mathbf{0} \\ \Delta\mathbf{s} \end{bmatrix} \tag{6.5.10}$$

where the Jacobians of the nodal forces have been expressed in terms of the internal tangent stiffness and the load stiffness on the LHS. A subscript has been added to the load stiffness because the Jacobian for each group of external loads must be considered separately. At times the internal tangent stiffness must also be subdivided into terms associated with different parameters, as when the temperature changes and causes buckling.

The parametrization equations need not be arclength equations: any parametrization which leads to a regular set of Newton equations is a candidate.

A major difficulty in all branch continuation techniques is setting the increment size and in the scaling of the parametrization equations. If the increment size is too small, considerable effort is wasted in determining unnecessary equilibrium points. On the other hand, if the increment size is too large, the convergence of the Newton procedure can fail or too many iterations are needed. The selection of an appropriate stepsize can be aided by an estimate of the location of the next turning point or bifurcation point. The step size can then be set so that a reasonable fraction of that distance is covered in the next increment. It is stressed however that bifurcation paths can appear out of nowhere, so if a good knowledge of the branches is essential, branch continuations should be repeated with different stepsizes.

Scaling of Arclength Equation. The arclength equation, when posed in terms of force parameters and displacement increments is often poorly scaled. We summarize in the following some of the scaling methods which have been proposed that appear to be effective in structural mechanics problems.

The simplest method is to introduce a scaling factor between the increments in load and the increments in displacements. The parametrization then is

$$p(\mathbf{d},\gamma) = \Delta\gamma^2 \left(\Delta\mathbf{f}_0^T \Delta\mathbf{f}_0\right) + \alpha\, \Delta\mathbf{d}^T \Delta\mathbf{d} = \Delta s^2 \tag{6.5.11}$$

where α is a scaling factor. A candidate for a scaling factor is the square of the average diagonal of the initial stiffness matrix.

Bifurcations. We consider first equilibrium bifurcations, i.e. we ignore Hopf bifurcations. The bifurcation then consists of the intersection of two equilibrium branches. If we are tracing a given equilibrium branch, such as AB in Fig. ?, then it is very easy to miss the intersecting branch and end up on an unstable branch. The objective of this Section is to describe some methods for detecting the crossing of a bifurcation point and anticipating when a bifurcation point will come up along thhe branch.

The classical method for detecting bifurcations in structural mechanics is an eigenvalue analysis. In an eigenvalue approach, we exploit the fact that the linearized equations for the increment, Eqs. () are singular at the bifurcation point.

Linear Stability. In Example 1, we have employed a technique which is frequently used to examine the stability of an equilibrium solution: a dynamic solution to a perturbation of the equilibrium solution. The dynamic equations are linear because the perturbations are small, so this is called a *linearized model*. If the dynamic solution grows, then it is said that the equilibrium solution is *linear unstable*. Otherwise, it is *linear stable*. In the following, we develop a general procedure for examining the linear stability of an equilibrium solution by examining the characteristics of the Jacobian matrix.

We consider an equilibrium point $\mathbf{d}^{eq}$ associated with a parametrized load, $\lambda\mathbf{f}^{ext}$ of a rate-independent system. A Taylor series expansion of the residual about the equilibrium solution gives

$$\mathbf{f}\left(\mathbf{d}^{eq}+\bar{\mathbf{d}}\right)=\mathbf{f}\left(\mathbf{d}^{eq}\right)+\frac{\partial\mathbf{f}}{\partial\mathbf{d}}\left(\mathbf{d}^{eq}\right)\bar{\mathbf{d}}+\text{higher order terms} \tag{6.5.12}$$

The first term on the RHS vanishes because $\mathbf{d}^{eq}$ is an equilibrium solution. From Eq. () we can see that the second term can be linearized as follows:

$$\frac{\partial\mathbf{f}}{\partial\mathbf{d}}\left(\mathbf{d}^{eq}\right)=\mathbf{K}^{ext}\left(\mathbf{d}^{eq}\right)-\mathbf{K}^{int}\left(\mathbf{d}^{eq}\right)=-\bar{\mathbf{A}}\left(\mathbf{d}^{eq}\right) \tag{6.5.13}$$

We now add the inertial forces to the system. Since the mass matrix does not change with displacements, we can then write the equations of motion for a small perturbations about the equilibrium point as

$$\mathbf{M}\frac{d^2\bar{\mathbf{d}}}{dt^2}+\bar{\mathbf{A}}\bar{\mathbf{d}}=0 \tag{6.5.14}$$

Note, that in contrast to Section ??, we do not include the mass matrix in the Jacobian matrix $\bar{\mathbf{A}}$. The above is a set of linear ordinary differential equations in $\bar{\mathbf{d}}$. Since the solutions to such linear ordinary differential equations are exponential, we take solutions of the form

$$\bar{\mathbf{d}}=\mathbf{y}e^{\mu t}\qquad \bar{d}_i=y_a e^{\mu t} \tag{6.5.15}$$

Substituting the above into Eq. (6.5.14) gives

$$\left(\mathbf{A}+\mu^2\mathbf{M}\right)\mathbf{y}e^{\mu t}=0 \tag{6.5.16}$$

The characteristic values μ_i of this system can be obtained from the eigenvalue problem

$$\mathbf{A}\mathbf{y}_i=-\lambda_i\mathbf{M}\mathbf{y}_i,\quad \lambda_i=\mu_i^2 \tag{6.5.17}$$

where λ_i, $i=1$ to n are the n eigenvalues and y_i are the n eigenvectors. The linear stability of the system then revolves around the character and magnitudes of the eigenvalues μ_i. The eigenvalues will generally be complex. If the real part of the eigenvalue is positive the solution will grow, i.e. if

$$\text{if for any } i,\ \text{Real}\left(\mu_i\right)>0,\ \text{ the equilibrium point is linearly unstable} \tag{6.5.18}$$

Here $\bar{\mu}_i$ is the complex conjugate of μ_i. On the other hand, if the real parts of all eigenvalues are negative, then the linearized solutions about the equilibrium point do not grow and we can say that

$$\text{if for all } i, \text{ Real}\left(\mu_i\right) \le 0, \text{ equilibrium point is linearly stable} \qquad (6.5.19)$$

When the linearized equations are symmetric, then the eigenvalues must be real. We can then see that if the matrix **A** is positive definite, then the eigenvalues must be negative, and consequently the parameters μ_i are strictly complex. Therefore, when μ are complexthe perturbated solutions are harmonic and of the same magnitude as the perturbation and the *equilibrium points is linear stable*.

This result has important ramifications for many structural systems. If the system has a potential, i.e. if the system is conservative, then the matrix **A** is symmetric and corresponds to the Hessian of the potential energy, i.e., $A_{ab} = \partial^2 W \big/ \partial d_a \partial d_b$ by Eq. ???. Recall that an equilibrium solution is a stationary point of the potential. Since **A** is the matrix of second derivatives, the positive definiteness of **A** implies that the stationary point is a local minimum. Thus an equilibrium point is linear stable if and only if the potential at the equilibrium point is a local minimum, which implies that the Jacobian and Hessian matrices are positive definite. In other words, if

$$\Delta d_a \frac{\partial^2 W\left(\mathbf{d}^{eq}\right)}{\partial d_a \partial d_b} \Delta d_b = A_{ab}\left(\mathbf{d}^{eq}\right)\Delta d_a \Delta d_b = \Delta \mathbf{d}^T \mathbf{A} \Delta \mathbf{d} > 0 \qquad \Delta \mathbf{d} \quad (6.5.20)$$

then the equilibrium point $\mathbf{d}^{eq}$ must be linear stable. On the other hand, if there exists a $\Delta \mathbf{d}$ for which the above inequality is violated, then the stationary point must be a saddle point, and the equilibrium solution is not linear stable.

To summarize, an equilibrium solution for a conservative system is linear stable if it corresponds to a local minimum of the potential energy, which requires the positive definiteness of the Hessian or Jacobian matrices (they are the same in that case). If the equilibrium solution is a saddle point, then the equilibrium solution is unstable.

For nonconservative systems, an equilibrium solution is also linear stable if the Jacobian matrix is symmetric and positive definite. If the Jacobian is not positive definite, it is not linear stable. Any system is linear stable if all real parts of the eigenvalues of the system (6.5.17) are negative.

The information provided by a linear stability analysis is not conclusive from an engineering viewpoint. Since linear stability analysis assumes the linearity of the response in the vicinity of the equilibrium point, perturbations must be small enough so that the response can be predicted by a linear model. Linear stability of an equilibrium point does not preclude the possibility that a physically realistic perturbation will grow. If the system is highly nonlinear in the

neighborhood of the equilibrium point, moderate perturbations of the system may lead to unstable growth. A linear stability analysis only reveals how a system with properties obtained by a linearization of the system about the equilibrium point behaves. Nevertheless, it gives information which is useful in engineering and scientific analysis of systems.

Estimates of Bifurcation Points. It is often desirable to determine the location of bifurcation points as the equilibrium path is generated. Both bifurcation points which may have been passed or which are upcoming are of interest. Whether a bifuraction point has been passed can be determined by checking when the determinant of the Jacobian changes sign. A change of sign in the determinant of the Jacobian is an indication of the change of sign of an eigenvalue. The determinant of the Jacobian vanishes at a critical point and will often change sign when the critical point is passed. It would appear at first that the sign of the Jacobiann determinant would always change when passing a bifurcation but things are not that simple: sometimes, two eigenvalues change sign at a bifurcation point and then the Jacobian determinant does not change sign, so the determinant test is not conclusive. Thus tracking the determinant provides some guidance in finding bifurcation points, but it is not foolproof.

Bifurcation points can also be estimated by tracking the eigenvalues of the system. The estimation of eigenvalues is simplified in solid mechanics because the stress appears linearly in the geometric stiffness and varies approximately in proportion with the load. As we have seen from Example 6.?, the stability of an equilibrium path chamges when the lowest eigenvalue of the system changes sign. Thus the critical points can be located by an eigenvalue problem. There are several ways to do this:

1. interpolate the Jacobian matrix of the system by a linear relationship.
2. assume that the geometric and load stiffness are linearly proportional to the load parameter in the neighborhood under consideration;

Both methods can be applied with only a single load parameter. In the first method, we assume that the Jacobian **A,** is a linear function of the load parameter γ. The Jacobian matrix in the vicinity of the state *n* can then be written in terms of the states around *n-1* and *n* by

$$\mathbf{A}(\mathbf{d},\gamma) = (1-\xi)\mathbf{A}(\mathbf{d}_{n-1},\gamma_{n-1}) + \xi\mathbf{A}(\mathbf{d}_n,\gamma_n) \equiv (1-\xi)\mathbf{A}^- + \xi\mathbf{A}^0 \qquad (6.5.21)$$

$$\gamma = (1-\xi)\gamma_{n-1} + \xi\gamma_n \qquad (6.5.21b)$$

where the last term in the above defines a more compact notation we will use in the following. At the critical point, the determinant of the Jacobian matrix **A** vanishes, so

$$\det \mathbf{A}(\mathbf{d},\gamma_{crit}) = 0 \qquad (6.5.22)$$

From (6.5.21) and the fact that a ystem with a zero determinant has a nontrivial homogenrous soloution, we deduce that there exists a ξ such that

$$(1-\xi)\mathbf{A}^{-}\mathbf{y}+\xi\mathbf{A}^{0}\mathbf{y}=0 \tag{6.5.23}$$

This can be put in the standard form of the generalized eigenvalue problem by the following rearrangement of terms:

$$\mathbf{A}^{0}\mathbf{y}=\xi\left(\mathbf{A}^{0}-\mathbf{A}^{-}\right)\mathbf{y} \tag{6.5.24}$$

The solution of this eigenvalue problem then gives an estimate of the critical load by (6.5.21b).

The lowest eigenvalues of (6.5.24) can be either positive or negative. Negative eigenvalues indicate critical points which have been passed and are known about, or they may indicate critical values which have inadvertently been passed. In the latter case, state *n* may no longer be on a stable equilibrium path.

For many structural problems, the eigenvalue problem may be simplified by taking advantage of the following:

1. the material stiffness in a linear material will not change significantly if the displacements prior to the critical point are small;

2. the geometric stiffness depends linearly on the load parameter, since it depends almost linearly on the stresses if the displacements are small (see the geometric stiffness for the bending and axial response in Eqs. ());

3. the load is independent of the displacements, so the load stiffness vanishes.

Since the geometric stiffness varies linearly with the load, if the above three conditions are met we can then write

$$\mathbf{A}^{0}=\mathbf{K}^{mat}+\mathbf{K}^{geo}\left(\lambda^{0}\right),\quad \mathbf{A}^{-}=\mathbf{K}^{mat}+\mathbf{K}^{geo}\left(\lambda^{-}\right) \tag{6.5.25}$$

where $\mathbf{K}^{geo}$ is the geometric stiffness for a unit value of the load parameter. Substituting into () then gives

$$\mathbf{K}^{mat}\mathbf{y}=\xi\left(\mathbf{K}^{geo}\left(\lambda^{0}\right)-\mathbf{K}^{geo}\left(-\lambda^{-}\right)\right)\mathbf{y} \tag{6.5.26}$$

The critical load is then given by

$$\lambda_{crit}=\xi\left(\lambda^{0}-\lambda^{-}\right) \tag{6.5.27}$$

The procedure of determining the location of a nearly critical point then consists of storing the following and they geometric stiffness is saved from the last step, and using the current geometric and material stiffness, the eigenvalues are obtained. The eigenvalue which leads to the smallest critical load is the one of interest. When the parameter $0\le\xi\le 1$, the critical point has been passed in the last step. When $\xi>1$, the critical point is estimated to be further ahead in the branch.

In analyzing structures, it is often desirable to estimate the first bifurcation point along the fundamental equilibrium path after a single load increment λ_1 has been applied. An initial estimate of the bifurcation point can be found in terms of the geometric stiffness computed after one load increment. We assume that $\mathbf{K}^{geo}\left(\lambda^{-}\right) = \mathbf{0}$ since the first step is stress-free. Then Eq () gives

$$\mathbf{K}^{mat}\mathbf{y} = \xi\mathbf{K}^{geo}\left(\lambda^{0}\right)\mathbf{y} \tag{6.5.28}$$

The critical value of the load parameter is then $\lambda_{crit} = \xi\lambda^0$, where λ^0 is the load parameter for the first load increment. this is the formula commonly cited in matrix structural texts for obtaining the buckling load of a structure. Note that it assumes that the geometry of the structure changes so little with increasing load that the first estimate of the geometric stiffness suffices for extrapolating the critical point. It is effective primarily for bifurcation points. Prior to reaching a limit point, the geometric stiffness changes significantly, so an estimate based on () is quite erroneous.

The study of **s**ystems stability has in the past two decades become a rich science known as dynamical systems theory. It includes topics such as chaos, fractals, attractors, repellors. These topics are beyond the scope of this book; some good references are Argyris and Melenk (), Moon () and Temam ().

Example 6.4. A simple example of a problem with stable and unstable paths connected by a turning point is the shallow truss shown in Fig. 6.11. The initial cross sectional areas of the elements are A_0 and the initial lengths of the two elements are ℓ_0, which is given by $\ell_0^2 = a^2 + b^2$. A vertical load *f* is applied as shown, and since this is the only load we consider *f* to be the load parameter. The material is governed by a Kirchhoff law, (see Eq. ())

$$S = CE_x \tag{E6.1.1}$$

where *C*; as pointed out in Section ??, for a small strain, large-displacement problem such as this, this constitutive equation is almost to a small-strain elastic, linear law. We will determine the equilibrium path as a function of the load and determine which branches are stable.

The deformation of the truss in is described by the variable *y*, the current vertical coordinate of the centerpoint, which leads to simpler equations than using the displacement. Since this material is path-independent, we can use the theorem of minimum potential energy to develop the discrete equations. The potential energy, Eq.(), in this case is given by

$$W = W^{int} - W^{ext}, \quad W^{int} = \tfrac{1}{2}\sum_{e=1}^{2}\int_{\Omega_0^e} C\hat{E}_{xx}^2 d\Omega, \quad W^{ext} = f\left(b - y\right) \tag{E6.1.2}$$

where the Green strain is uniaxial with a only component along the axes of the bars contributing to the internal energy. The Green strain in for both elements is most easily evaluated by Eq.(), which gives

$$\hat{E}_{xx} = \tfrac{1}{2}\left(\ell^2 - \ell_0^2\right) = \tfrac{1}{2}\left(a^2 + y^2 - a^2 - b^2\right) = \tfrac{1}{2}\left(y^2 - b^2\right) \tag{E6.1.3}$$

so the internal energy is given by

$$W^{int} = k\left(y^2 - b^2\right)^2 \quad \text{where } k = \tfrac{1}{4} CA_0\ell_0 \tag{E6.1.4}$$

Combining the above with the potential of the external forces gives the total potential

$$W = k\left(y^2 - b^2\right)^2 - f\left(b - y\right) \tag{E6.1.5}$$

The equilibrium equation is now obtained by applying the theorem of minimum potential energy, which states that the equilibrium equation is given by the stationary points of the potential W given above, so the equilibrium equation is

$$0 = \frac{dW}{dy} = 4k\left(y^2 - b^2\right)y + f \tag{E6.1.6}$$

As can be seen from the above, the force is a cubic function of the vertical position of the centerpoint, which is shown in Fig. ?. The equilibrium path has two turning points, usually called limit points in structural mechanics, and three branches, denoted by AB, BC and CD in Fig. ?.

We will now examine the stability of the branches of the equilibrium path. The dynamic response is examined at a position y_0 subject to a perturbation. A solution to the linearized equations is considered, so

$$y = y_0 + \bar{y} \quad \text{where} \quad \bar{y} = \varepsilon e^{\mu t} \tag{E6.1.7}$$

where ε is a small parameter. The equations of motion for this problem are given by

$$M\frac{d^2y}{dt^2} = f^{ext} - f^{int} = f_0 - 4k\left(y^2 - b^2\right)y \tag{E6.1.8}$$

where M is the mass of the node. Substituting () into () gives

$$f_0 - 4k\left(\left(y_0 + \bar{y}\right)^2 - b^2\right)\left(y_0 + \bar{y}\right) = M\frac{d^2\bar{y}}{dt^2} \tag{E6.1.9}$$

Expanding the above and dropping all terms which are higher order than linear in $\bar{y}$, gives (it is expressed in terms of

$$f_0 - 4k\left[y_0\left(y_0^2 - b^2\right) + \bar{y}\left(3y_0^2 - b^2\right)\right] = M\frac{d^2\bar{y}}{dt^2} \tag{E6.1.10}$$

The load cancels the first term in the brackets, so the equations of motion become

$$M\frac{d^2\bar{y}}{dt^2}+4k\bar{y}\left(3y_0^2-b^2\right)=0\rightarrow \alpha=\pm i\left(3y_0^2-b^2\right)^{\frac{1}{2}} \qquad \text{(E6.1.11)}$$

where the (b)follows from substituting () into (a). It can then be seen that the perturbation solution () is real with one positive exponential whenever $3y_0^2-b^2<0$. So the branch defined by

$$-b/\sqrt{3}<y_0<b/\sqrt{3} \quad \text{isunstable} \qquad \text{(E6.1.12)}$$

The results of the above stability analysis can be obtained directly be examining the second derivative of the potential energy function, which from () is given by

$$\frac{d^2W}{dy^2}=4k\left(3y^2-b^2\right),\ \ \frac{d^2W}{dy^2}<0 \text{ when } -b<\sqrt{3}y<b,\ \frac{d^2W}{dy^2}>0 \text{ otherwise} \qquad \text{(E6.1.13)}$$

So in the unstable equilibrium branches of a conservative system, the second derivative of the potential energy changes sign. The results of () and () are in fact identical: for a system which has no velocity dependent terms, the perturbation analysis is identical to taking a derivative of the forces, and the stability of the result of the perturbation analysis simply depends on the sign of the derivative of the forces, which is the second derivative of the work potential.

The linearized test for stability used in Example 8.?.1 is not a foolproof test for stability. For example, if $y_0=-0.99b$, the test indicates that the equilibrium point is unstable. However, a numerical dynamics solution when started at tat point, will only oscillate with an amplitude of 0.002, which to most engineers would not be an instability. The test as posed in Example 1 checks whether any perturbation will grow at all and conform to the criterion () based on a linearized analysis, which need not conform to any physical notion of instability. In contrast to the exponential instabilities seen in stability analysis of numerical methods, the instabilities in physical systems will not exhibit continuing growth. What it is does predict accurately is that when the dynamics is added to the system, the system will not oscillate about the unstable equilibrium point in response to a perturbation but move to oscillating about a nearby point on a stable equilibrium path.

Example 6.5. Consider a linear stability analysis of the beam element shown in Fig. 6.5E. Node 2 is clamped, node 1 is free to rotate and move in the *x*-direction. Find the equilibrium equation and the equilibrium branches of the system.

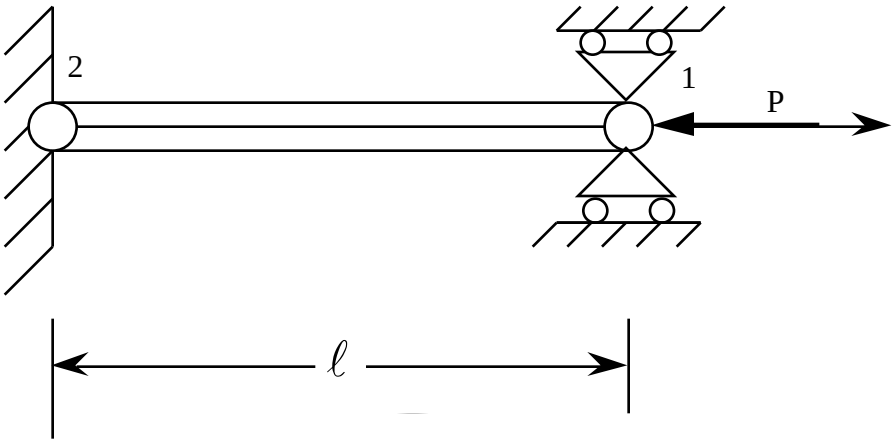

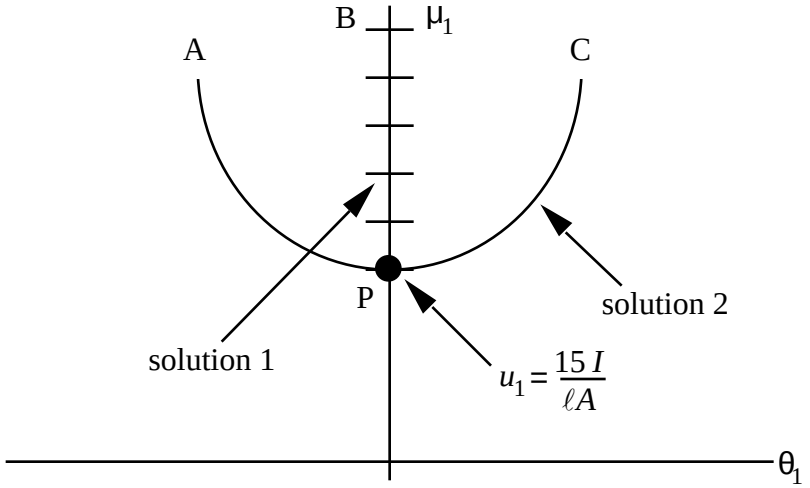

Figure 6.5E. Beam model used for stability analysis and equilibrium paths.

The displacement boundary conditions imply that

$$u_{x1} = u_{y1} = \theta_1 = u_{y2} = 0 \tag{E6.5.1}$$

Therefore, the only nonzero degrees-of-freedom are $u_{y1} \equiv u_1$ and θ_1. The equations of equilibrium can be deduced from Example ??? to be

$$\frac{EA}{\ell} u_1 - \frac{2EA}{15}\theta_1^2 = F \tag{E6.5.2}$$

$$-\frac{2EA}{15}\theta_1 u_1 + \left(\frac{4EI}{\ell} - \frac{2EA}{15} u_1 + \frac{3EAP}{35}\right)\theta_1 = 0 \tag{E6.5.3}$$

The above system of two nonlinear algebraic equations in two unknowns possesses two solutions:

$$\text{Solution 1:} \quad \theta_1 = 0, \; u_1 = \frac{P\ell}{EA} \tag{E6.5.4}$$

$$\text{Solution 2:} \quad u_1 = \frac{2\ell}{15}\theta_1^2 + \frac{P\ell}{EA} \tag{E6.5.5}$$

$$u_1 = \frac{P\ell}{28}\theta_1^2 + \frac{15I}{A\ell} \tag{E6.5.6}$$

These two curves are plotted in Figure 6. It can be seen a pitchfork bifurcation occurs at

$$u_1 = \frac{15I}{A\ell} \tag{E6.5.7}$$

This is the critical point for this beam. The corresponding load can be found by substituting (???) and $\theta_1 = 0$ into Eq. (E6.5.2), which gives

$$F_{crit} = \frac{15EI}{\ell^2} \tag{E6.5.8}$$

The linearized stability of any of the equilibrium paths can be examined by considering the linearized equations of motion about a point on the path:

$$\mathbf{M}\Delta\ddot{\mathbf{d}} + \left(\mathbf{K}_{mat} + \mathbf{K}_{geo}\right)\Delta\mathbf{d} = 0 \tag{E6.5.9}$$

where $\Delta\mathbf{d}$ here is the displacement from the path. The equations can be written out by using the mass matrix given in Eq. (9.3.18) and the material and tangent stiffnesses given in Eqs. (???) and (???). The resulting equations are

$$\frac{\rho_0 \ell_0 A_0}{420}\begin{bmatrix} 210 & 0 \\ 0 & \alpha\ell^2 \end{bmatrix}\begin{bmatrix} \Delta\ddot{u}_1 \\ \Delta\ddot{\theta}_1 \end{bmatrix} + \begin{bmatrix} \frac{AE}{\ell} & \\ & \frac{4EI}{\ell} \end{bmatrix}\begin{bmatrix} \Delta u_1 \\ \Delta\theta_1 \end{bmatrix} = 0 \tag{E6.5.10}$$

We will examine the stability of two of the paths for $u_1 > 15I/A\ell$; the path *PA* and the path *PC*.

The problem parameters are Young's modulus E, the moment of the cross-section I, and the original length of the beam ℓ_o. The beam is modeled by a single element with a linear axial displacement field and a cubic transverse displacement field. This is a standard beam element described in Chapter 9. The unknowns are $\mathbf{d}^T = \begin{bmatrix} u_x & u_y & \theta \end{bmatrix}$, where θ is the rotation of the node; nodal subscripts have been dropped because they all refer to node 1.

NUMERICAL STABILITY

At this point it is worthwhile to comment on the differences between physical stability and numerical stability. Physical stability pertains to the stability of an solution of a model, whereas numerical stability pertains to the stability of the numerical solution. Numerical instabilities arise from the discretization of the model equations, whereas physical instabilities are instabilities in the solutions of the model equations independent of the numerical discretization. Numerical stability is usually only examined for processes which are physically stable. Very little is known how a "stable" numerical procedures behave in physically unstable processes. This shortcoming has important practical ramifications, because many computations today simulate physical instabilities, and if we cannot guarantee that our methods track these instabilities accurately, then these simulations may be suspect.

Numerical stability of a time integration procedure is defined in analogously to stability of solutions, Eq. (6.5.1-2). A numerical procedure is stable if small perturbations of initial data result in small changes in the numerical response. More formally, the numerical procedure is stable if

$$\left\| \mathbf{u}_A^n - \mathbf{u}_B^n \right\| \le C\varepsilon \qquad n > 0 \tag{6.5.29}$$

when

$$\left\| \mathbf{u}_A^0 - \mathbf{u}_B^0 \right\| \le \varepsilon \tag{6.5.30}$$

LATERIt is of interest to note that numerical stability of a process that is physically unstable cannot be examined by this definition, i.e. we cannot say anything about the stability of a numerical procedure when applied an equation that exhibits unstable response. The reason can be seen as follows. If a system is unstable, then the solution to the system will not satisfy (). Therefore, even if the numerical solution procedure is stable, it will not satisfy ().

General results for numerical stability of time integrators are largely based on the analysis of linear systems. These results are extrapolated to nonlinear systems by applying them to the linearized equations. Therefore, we will first describe the stability theory which is used to obtain critical time steps for linear systems. Next we described the procedures for applying these results to nonlinear systems. In conclusion, we will describe some results on stability of time integrators which apply directly to nonlinear systems. However, we stress that at the present time there is no stability theory which encompasses the nonlinear problems which are routinely solved by nonlinear finite element methods, and most of our insight into stability stems from the analysis of linear models.

Numerical Stability of Linear Systems. Most of the theory of stability of numerical methods is concerned with linear systems. The idea is that if a numerical method is unstable for linear systems, it will of course be unstable for nonlinear systems also, since linear systems are a subset of nonlinear systems. Luckily, the converse has also turned out to be true: numerical methods which are stable for linear systems in almost all cases turn out to be stable for nonlinear systems. Therefore, the stability of numerical procedures for linear systems provides a useful guide to their behavior in both linear and nonlinear systems.

To begin our exploration of stability of numerical procedures, and in particular the stability of time integrators, we first consider the equations of heat conduction:

$$\mathbf{M}\dot{\mathbf{u}} + \mathbf{K}\mathbf{u} = \mathbf{f} \tag{6.5.31}$$

where M is the capacitance matrix, K is the conductance matrix, f is the forcing term and u is a matrix of nodal temperatures. This system is chosen as a starting point because it is a first order system of ordinary differential equations, while the equations of motion are second order in time.

To apply the definition of stability, we consider two solutions for the same system with the same discrete forcing function but slightly different initial data. The two solutions satisfy the same equation with the same $\mathbf{f}$, so

$$\mathbf{M}\dot{\mathbf{u}}_A + \mathbf{K}\mathbf{u}_A = \mathbf{f} \qquad \mathbf{M}\dot{\mathbf{u}}_B + \mathbf{K}\mathbf{u}_B = \mathbf{f} \tag{6.5.32}$$

If we now take the difference of the two equations, we obtain

$$\mathbf{M}\dot{\mathbf{d}} + \mathbf{K}\mathbf{d} = 0 \qquad \mathbf{d} = \mathbf{u}_A - \mathbf{u}_B \tag{6.5.33}$$

We now consider a two-step family of time integrators:

$$\mathbf{d}_{n+1} = \mathbf{d}_n + (1-\alpha)\Delta t\dot{\mathbf{d}}_n + \alpha\Delta t\dot{\mathbf{d}}_{n+1} \tag{6.5.34}$$

Since (6.5.33) holds at time steps n and $n+1$, we can multiply them respectively by $\left(1-\alpha\right)\Delta t$ and $\alpha\Delta t$, respectively

$$(1-\alpha)\Delta t\mathbf{M}\dot{\mathbf{d}}_n + (1-\alpha)\Delta t\mathbf{K}\mathbf{d}_n = 0, \qquad \alpha\Delta t\mathbf{M}\dot{\mathbf{d}}_{n+1} + \alpha\Delta t\mathbf{K}\mathbf{d}_{n+1} = 0 \tag{6.5.35}$$

Adding the above two equations and using (6.5.34) to eliminate the derivatives, we obtain

$$(\mathbf{M} + \alpha\Delta t\mathbf{K})\mathbf{d}_{n+1} = \left(\mathbf{M} + (1-\alpha)\Delta t\right)\mathbf{K}\mathbf{d}_n \tag{6.5.36}$$

This equation is in general amplification matrix form: it gives the numerical solution at times step $n+1$ in terms of the solution at time step n. An amplification matrix $\mathbf{A}$ is a matrix which gives the solution at time step $n+1$ in of the solution at time step n by

$$\mathbf{d}_{n+1} = \mathbf{A}\mathbf{d}_n \tag{6.5.37}$$

The generalized amplification matrix form is

$$\mathbf{B}\mathbf{d}_{n+1} = \mathbf{A}\mathbf{d}_n \tag{6.5.38}$$

We shall now show that the time integrator is stable if the eigenvalues of the generalized amplification matrix form lie within the unit circle in the complex plane.

For this purpose, we need to recall the eigenvalue problem associated with (6.5.33):

$$\mathbf{K}\mathbf{y}_i = \lambda_i \mathbf{M}\mathbf{y}_i \tag{6.5.39}$$

where λ_i are the eigenvalues and $\mathbf{y}_i$ the eigenvectors of the system. We recall that the matrix $\mathbf{M}$ is positive definite and symmetric, whereas the matrix $\mathbf{K}$ is positive semidefinite and symmetric. Because of the symmetry of the matrices, the eigenvectors of (6.5.39) are orthogonal with respect to $\mathbf{M}$ and $\mathbf{K}$, which can be written as

$$\mathbf{y}_j \mathbf{M}\mathbf{y}_i = \delta_{ij}, \qquad \mathbf{y}_j \mathbf{K}\mathbf{y}_i = \lambda_i \delta_{ij} \ \ (\text{nosumon } i) \tag{6.5.40}$$

and from the positiveness of the matrices the eigenvalues are nonnegative. The generalized amplification equation is associated the generalized eigenvalue problem

$$\mathbf{A}\mathbf{z}_i = \mu_i \mathbf{B}\mathbf{z}_i \tag{6.5.41}$$

The eigenvalues of the above system will be shown to control the stability of the time integrator. In general, these eigenvalues may be complex. Stability then requires that the moduli of all of the eigenvalues be less or equal to 1. Otherwise at least one component of the solution grows exponenetially like z^n, so the solution is unstable. In other words, if we consider the complex plane as shown in Fig, X, then the eigenvalues must lie within or on the unit circle for the numerical method to be stable.

The eigenvectors span the space R^n, so any vector $\mathbf{d}$ R^{n_D} can be written as a linear combination of the eigenvalues, see XXX,. The eigenvectors of (6.5.41) and are identical to the eigenvectors of the (6.5.39) and the eigenvalues are related by the following:

$$\text{if } \mathbf{A} = a_1\mathbf{M} + a_2\mathbf{K} \text{ and } \mathbf{B} = b_1\mathbf{M} + b_2\mathbf{K} \text{ then } \mu = \frac{a_1 + a_2\lambda_i}{b_1 + b_2\lambda_i} \tag{6.5.42}$$

This is shown as follows. Since the eigenvectors $\mathbf{y}_i$ span the space, we can expand the eigenvectors $\mathbf{z}_i$ in terms of $\mathbf{y}_i$ by

$$\mathbf{z}_i = c_i \mathbf{y}_i \tag{6.5.43}$$

Substituting the above into (6.5.41), premultiplying by $\mathbf{y}_j$ and using the orthogonality relations (6.5.40) gives

$$a_1 + a_2\lambda_i = \mu_i (b_1 + b_2\lambda_i) \tag{6.5.44}$$

from which the last equation in (6.5.42) follows immediately.

We now ascertain the conditions under which the eigenvalues μ_i fall within the unit circle, which corresponds to a stable numerical integration. Using again the fact that the eigenvectors $\mathbf{y}_i$ span the space, expand the initial solution vector at $t = 0$ in terms of the eigenvectors by

$$\mathbf{d}_0 = \sum_{i=1}^{n_D} r_0^i \mathbf{y}_i \tag{6.5.45}$$

where r_0^i is determined by the initial conditions. Substituting the above into () and using the fact that $\mathbf{y}_i$ are also eigenvectors of () with eigenvalues μ_i, we obtain that

$$\mathbf{d}_1 = \sum_{i=1}^{n_D} \mu_i r_0^i \mathbf{y}_i \ , \quad \mathbf{d}_2 = \sum_{i=1}^{n_D} (\mu_i)^2 r_0^i \mathbf{y}_i , \quad \mathbf{d}_n = \sum_{i=1}^{n_D} (\mu_i)^n r_0^i \mathbf{y}_i \tag{6.5.46}$$

where the second equation follows by repeating the process and the last equation can be obtained by induction. We can see immediately from the above that if any of the eigenvalues of the generalized amplification matrix μ_i is greater than one, the solution will grow exponentially. Since we are examining the behavior of the difference of two solutions, this indicates that the procedure is unstable. Although some readers will advance the counterargument that this unstable growth will occur only if the initial data contains the eigenvector associated with μ_i, in fact, due to roundoff error, the constant r_i^0 will be initially be nonzero or become nonzero later in the calculation. No matter how small the constant, the exponenetial growth will dominate ina very few time steps.

Using Eqs. (6.5.42) and (6.5.36) it follows that

$$\mu_i = \frac{1-\alpha \Delta t \lambda_i}{1+\alpha \Delta t \lambda_i} \tag{6.5.47}$$

Since this eigenvalue is always real, the stability condition can be written as $|\mu_i| \le 1$. We consider eigenvalues $|\mu_i| = 1$ to lead to stable solutions at this point, but this is not always the case. From the preceding we deduce the conditions on the time step necessary for numerical stability as follows:

$$\mu_i \le 1 \rightarrow \frac{1-(1-\alpha)\Delta t \lambda_i}{1-\alpha \Delta t \lambda_i} \le 1 \ \rightarrow \text{ always met} \tag{6.5.48}$$

$$\mu_i \ge -1 \rightarrow \frac{1-(1-\alpha)\Delta t \lambda_i}{1-\alpha \Delta t \lambda_i} \ge -1 \ \rightarrow (1-2\alpha)\Delta t \lambda_i \le 2 \tag{6.5.49}$$

There are two distinct consequences of Eq.(). If $1-2\alpha \ge 0$, *i.e.* $\alpha \ge 0.5$, then the condition of stability is met regardless of the size of the time step. The method is

then called *unconditionally stable*. When $1-2\alpha<0$, *i.e.* $\alpha<0.5$, Eq (6.5.49) yields the requirement that

$$\Delta t \le \frac{2}{(1-2\alpha)\lambda_i} \quad i \tag{6.5.50}$$

where we have indicated that the condition on the eigenvalue μ_i must be met for all i. The maximum eigenvalue then sets the time step, so the critical time step is given by

$$\Delta t \le \max_i \frac{2}{(1-2\alpha)\lambda_i} \quad \text{or} \quad \Delta t_{crit} = \frac{2}{(1-2\alpha)\lambda_{max}} \tag{6.5.51}$$

A method which is stable only for time steps below a critical value is called conditionally stable. If we consider the explicit form of this generalized update equation, i.e. $\alpha = 0$, then the above gives

$$\Delta t_{crit} = \frac{2}{\lambda_{max}} \tag{6.5.52}$$

Thus the stable time step is inversely proportional to the maximum eigenvalue of the system. The stiffer the system, the smaller the stable time step. For the trapezoidal rule, $\alpha = 0.5$, and for any $0.5<\alpha\le 1$ the method is unconditionally stable. For $0\le\alpha<0.5$, the integrator is implicit but conditionally stable, so these values of α are of little practical value.

To give the reader a appreciation of the explosive growth of an exponential instability, Table ? shows the results for exponential growth for several values of the eigenvalue μ_i. Exponential growth is truly startling. It is also the reason why compound interest can make you very rich if you live long enough and start saving early.

In summary, we have shown that the determination of the stability of an integration formula for the semidiscrete initial value problem () can be reduced to examining the eigenvalues of the generalized amplification matrix (). If any eigenvalue lies outside the unit circle in the complex plane, the perturbation grows exponentially so the solution is numerically unstable. Otherwise, the method is stable.

Stability of thhe Central Difference Method. We now use the same techniques to examine the stability of the central difference method for the equations of motion.

MATERIAL STABILITY

An important issue in modern computational mechanics is the stability of the material models. The issue has already been discussed on several occasions in Chapter 5, cf...In this Section, we examine the implications of material instability on computational procedures and provide some remedies for the major difficulties.

As pointed out in Chapter 5, material instability results from the loss of positive definiteness in the tangent modulus tensor relating the Truesdell rate of the Cauchy stress to the rate of deformation. The name material instability is a slight misnomer because the occurrence of this phenomenon does not lead automatically to the violation of stability definitions such as (6.5.1). Instead, an unstable material is characterized by the possibility of unbounded spectral growth for a body in a homogeneous state of stress. When a material fails to meet the stability criteria for a subdomain of the problem, unbounded growth of the solution does not necessarily occur.

Nevertheless, the consequences in a computation of the failure to meet material stability criteria are dramatic: for rate-independent materials, loss of material stability changes the PDE locally from hyperbolic to elliptic in dynamic problems and vice versa in static problems. Furthermore, in rate indenpendent materials this is accompanied by a phenomenon called *localization* to a set of measure zero: the domain in which material instability occurs in a three dimensional problem will localize to a surface. On that surface in the domain, the strains will be infinite and the motion will be discontinuous. Although this ostensibly looks like a good way to model fracture and failure of materials, because of the localization to a set of measure zero, the dissipation associated with this process vanishes, so that the model is inappropriate for any realistic physical model of fracture or shear banding.

The literature on material instability goes back at least as far as Hadamard (1906). I haven't read the literature of that time, and even my knowledge of Hadamard is second-hand, so there could be earlier studies. Hadamard examined the question of what happens when the tangent modulus in a small deformation problem is negative. He concluded that according to the wave equation and the formula for the wavespeed, (???), that the wavespeed is then imaginary (the square root of a negative number), so such materials could not exist.

The next major milestone in the study of unstable materials is the work of Hill (??), who examined the conditions under which materials are unstable. His methodology was to consider the momentum equation for a homogeneous state of initial stress in terms of the displacements. The momentum equation is then

$$C_{ijkl} v_{k,l} = \rho \ddot{v}_i \quad \text{wrong eqn unless v=displ}$$

Using the technique of linear stability analysis, he examined the growth and decay of solutions of the form

$$u_i = A_i e^{\kappa\left(x - ct\right)}$$

The solution grows exponentially if any of the eigenvalues of the problem

$$u_i = A_i e^{\kappa\left(x - ct\right)}$$

are negative. He also showed that equivalently one could examine the material instability through the possibility of acceleration waves. This technique is now classical and is used in finite elements to detect the possibility of material instability> It goes as follows:

Hill() also examined material instabilities for large deformation problems and the question of which rate is appropriate for ascertaining unstable behavior. he concluded that

Another milestone paper in this stream is the work of Rudnicki and Rice(??), who showed that material instabilities can occur even in the presence of strain hardening when the plasticity is nonassociative. The argument has been given in Section 5.?

Thus when computers came on the scene for nonlinear analysis in the 1970's there were two known causes of material instability: a negative modulus (or a negative eigenvalue of the tangent modulus matrix) and a nonassociative plasticity law. Computational analysts soon began to include material models which included either or both of these and they discovered many difficulties. In fact it was argued by many, including Drucker and Sandler(), that material models that violate the stability postulates should never be used in computational methods. Their arguments proved fruitless since there is no way to replicate observed phenomena such as shear banding without a model that exhibits strain softening, although the models which were first used to examine shear bands, Clifton and Milliner(), are viscoplastic and satisfy the stability postulates.

Zdenek Bazant and I started studying the problem in 197? and based on some computational results of Hyun we surmised that the closed form solution for a rate-independent material model must exhibit an infinite strain. We were able to construct a one-dimensional solution of this behavior, albeit quite inelegant in retrospect, and learned that for these materials the unstable behavio must localize to a set of measure zero and that the dissipation would then vanish.

This led to the search for a regularization of the governing equations, which we called a localization limiter at the time. We soon discovered that both gradient models and nonlocal models regularize the solution, Bazant, Chang and Belytschko and Lasry and Belytschko(). This solution of remedying the difficulties associated with negative moduli had already occurred in another context, the heat equation, where Kahn and Hilliard() circumvented the difficulty by a gradient theory, which came to be known as the Kahn-Hilliard theory. Hilliard was incidentally also at Northwestern but we were unaware of his work until later. Aifantis(??) had proposed gradient regularization in solid mechaincs before us.

Subsequently a plethora of work emerged in this area, with two goals: to obtain physical ustifications for the regularization procedure and to simplify the treatment of nonlocal and gradient models. Schreyer et al (), introduced gradient theories based on the gradient of the plasticity parameter lambda in Eq.(5.??), Pijaudier-Cabot and Bazant(??) introduced the gradient on the damage parameter. These are important because introducing nonlocality in the 6 strain components is awkward indeed. Mulhaus and Vardoulakis showed that a coupled stress theory also regularizes the equations, and Needleman showed that viscoplasticity regularizes the equations. an important recent work is Triantifyllides and ?, who proposed a technique for relating unit cell models to the parameters in a nonlocal theory. deBorst et al (??) further investigated the Schreyer et al approach and showed that that consistency (5.??) requirement then intdroduces another partial differential equation into the system; the boundary conditions for these partial differential equations are still an enigma. Hutchinson and Fleck() showed

expreimentally that metal plasticity depends on scale and developed a gradient plasticity theory motivated by dislocation movement.

Regularization Techniques. There are thus four regularization techniques that are under study for unstable materials:

1. gradient regularization, in which a gradient of a field variable is introduced in the constitutive equation
2. integral, or nonlocal, regularization, in which the the constitutive equation is a function of a nonlocal variable, such as nonlocal damage, a nonlocal invariant of a strain, or a nonlocal strain.
3. coupled stress regularizaztion
4, regularization by introducing time dependence into the material

All of these are except the last are still in an embryonic state of development. Little is known about the material constants and the associated material length scales which are required.

Regularization by introducing time dependence has progressed faster than the others because viscoplastic material laws has achieved a stat e of maturity by the time that localization became a hot area of research. However, viscoplastic regularization has some notable peculiarites: there is no constant length scale in the viscoplastic maodel and the solution in the presence of matrial instability is characterized by exponential growth. Therefore, although a discontinuity does not develop in te displacement as in the rate-independent strain-softening material, the gradient in thhe displacement increases unboundedly with time. Wright and Walter have shown that this anomaly can be rectified by coupling the momentum equation to heat conduction via the energy conservation equation. the length scales then computed agree well with observed shear band widths in metals.

The computational meodeling of localization still poses substantial difficulties. for most materials, the length scales of shear bands are much smaller than those of the body. Therefore tremendous resolution is required to obtain a reasonably accdurate solution to these problems, see Belytschko et al for some high resolution computations. Solutions converge very slowly with mesh refinement. This behavior of numerical solutions is often called mesh sensitivity or lack of objectivity, though it has nothing to do with objectivity or its absence: it is simply a consequence of the inabiloity of coarse meshes to resolves high gradient in viscopladtic materials or discontinuites in rate-independent solutions.

Several techniques have evolved to improve the coarse-mesh accuracy of finite element models for unstable materials. The first of these involve the embedment of discontinuities in the element. Ortiz ewt al were the first to do this: theyembedded discontinuites in the strain field of the 4-node quadrilateral when the acoustic trensor indicated a material instability in the element. Belytschko, Fish and Engleman attempted to embed a displacement discontinuity by enriching the strain field with a narrow band where the unstable material behavior occurs. In the band, the material behavior was considered homogeneous, which is ridiculous since an unstable material cannot remain ina homogenous state of stress: any perturbation will trigger a growth on the scale of the perturbation. Such is hindsight. Nevertheless these models were able to capture the evolving discontinuity in displacement more effectively. Sime and ??? invoked the theory oof distributions to justify such techniques. They also categorized discontinuities as strong (in the displacements) and weak (in the strains). This categorization

incidentally is at odds with the widely used categorization in shocks in fluid dynamics, where discontinuites in occur in the velocity and the motion is continuous, see Section ??. These techniques have recently been further explored by Armero et al () and Garipakti ad Hughes (??).

Shear bands are closely related to fracture: a shear band can be viewed as a discontinuity in the tangential displacement,a fracture as a discopntinuity in all components of the displacement, see Chapter 3, Example ??. Just as shear bands can be viewed as the outcome of a material instability in the shear component, the development of a fracture can be viewed numerically as the outcome of a material instability in the directions normal (and tangential in the case of mode 2 fracture)to the discontinuity. The relationship of damage and fracture has long been noted, see LeMaitre and Chab oche (??), where a fracture is assumed to occur when the damage variable reaches 0.7. the origin of the number 0,7 is quite hazy in most works on damage mechanics, but it can be seen to arise from the phase transition point based on percolation theory is 0.59275, Taylor and Francis (1985). The modeling of fracture by dmage poses some of the same difficulties encountered in shear band modeling, since the material law becomesunstable when the damage excdeeds a threshold value. All of the phenomena found in shear banding then occur: localization to a set of measure zero for rate-independent models, exponential growth for simple rate-dependent models, zero dissipation in failure and absence of a length scale.

These difficulties were grasped and resolved in a novel way early in the evolution of fintie elements by Hillerborg et al (??), Basant (??) and Willam(??) have also contributed to this approach. The idea is to match the energy of fracture to the energy dissipated by the element in which the localization occurs.

[??] H.M. Hiller, T.J.R. Hughes, and R.L. Taylor, "Improved Numerical Dissipation for Time Integration Algorithms in Structural Dynamics," *Earthquake Engineering and Structural Dyanmics*, Vol. 5, 282-292, 1977.

The tangent moduli are denoted by C^{SE} and a general constitutive equation can be written as

$$\dot{\mathbf{S}} = C^{SE} : \dot{\mathbf{E}} \quad \text{or} \quad \dot{S}_{ir} = C^{SE}_{irkl} \dot{E}_{kl}$$

$$P_{ij} = C_{irkl} \dot{E}_{kl} F^T_{rj} + S_{ir} \dot{F}^T_{rj}$$

Now using (3.3.20) to express $\dot{\mathbf{E}}$ in terms of $\dot{\mathbf{F}}$ and noting the minor symmetry of the tangent modulus marix (see Section 5.?) gives

$$P_{ij} = C_{irkl} F_{km} \dot{F}_{lm} F^T_{rj} + S_{ir} \dot{F}^T_{rj}$$

(6.4.3)

Norms.

Norms are used in this book primarily for simplifying the notation. No proofs are given that rely on the properties of normed spaces so the student need only learn the definitions of the norms as given below. It is also worthwhile to learn an interpretation of a norm as a distance. This is easily grasped by first learning the norms in the space ℓ_n, which is a norm in the space of vectors of real numbers. The extension to function spaces such as the Hilbert spaces and the space of Lebesque integrable functions, $\mathcal{L}_2$, (often named el-two) is then straightforward.

The norms on ℓ_n are defined by the following. We begin with the norm ℓ_2, which is simply Euclidan distance. If we consider an *n*-dimensional vector $\mathbf{a}$, often written as $\mathbf{a} \quad R_n$, then the ℓ_2 norm is given by

$$\left\| \mathbf{a} \right\|_2 = \left(\sum_{i=1}^{n} a_i^2 \right)^{\frac{1}{2}}$$

In the above, the symbol $\| \quad \|$ indicates a norm and the subscript 2 in combination with the fact that the enclosed variable is a vector indicates that we are referring to the ℓ_2 norm. For $n = 2$ or 3, respectively, the ℓ_2 norm is simply the length of the enclosed vector. The distance between two points, or the difference between two vectors, is written as

$$\left\| \mathbf{a} - \mathbf{b} \right\|_2 = \left(\sum_{i=1}^{n} \left(a_i - b_i \right)^2 \right)^{\frac{1}{2}}$$

Fundamental properties of the ℓ_2 norm are that:

1. it is positive,

2. it satisfies the triangle inequality

3. it is linear

The ℓ_k norms are generalizations for the above definition to arbitrary $k > 1$ as follows:

$$\left\| \mathbf{a} \right\|_k = \left(\sum_{i=1}^{n} \left| a_i \right|^k \right)^{\frac{1}{k}}$$

Norms for $k \neq 2$ are seldom used except for $k = \infty$, which is called the infinity norm. The infinity norm gives the component of the vector with the maximum absolute value, which can easily be figured out by thinking about (??) a little bit. Thus we can write that

$$\left\| \mathbf{a} \right\|_\infty = \max_i \left| a_i \right|$$

One of the principal applications of these norms is to define the error in a vector. Thus if we have a approximate solution to a set of discrete equations $\mathbf{d}^{app}$ and the exact solution is $\mathbf{d}^{exact}$, then a measure of the error is

$$\text{error} = \left\| \mathbf{d}^{app} - \mathbf{d}^{exact} \right\|_2$$

If you are concerned with the maximum error in any component of the solution, then you should select the infinity norm. When the concern is with the error over a selected number of components, then the norm can be restricted to those components. The idea is that you use norms to achieve what you need: they are not immutable. In using norms to asses errors in solutions, it is recommended that the error be normalized, e.g.

$$\text{error} = \frac{\left\| \mathbf{d}^{app} - \mathbf{d}^{exact} \right\|_2}{\left\| \mathbf{d}^{app} \right\|}$$

because absolute errors are very difficult to interprete and are meaningless unless the approximate magnitude of the solution is reported.

Norms of functions are defined analogously to the above. The relationship between functions and vectors is that a function can be thought of as an infinte dimensional vector. Thus the norm in function space that corresponds to ℓ_2 is given by

$$\left\| a\left(x\right) \right\|_{\mathcal{L}_2} = \left(\sum_{i=1}^{n} a^2\left(x_i\right) \Delta x \right)^{\frac{1}{2}} = \left(\int_0^1 a^2\left(x\right) dx \right)^{\frac{1}{2}}$$

This norm is called the $\mathcal{L}_2$, and the space of functions for which this norm is well-defined and bounded is called the $\mathcal{L}_2$ space; usually just the number is indicated This space is the set of all functions which are square integrable, and it includes the space of all functions which are piecewise continuous.

The Dirac delta function $\delta\left(x-y\right)$ is defined by

$$f\left(x\right) = \int_{-\infty}^{+\infty} f\left(y\right)\delta\left(x-y\right)dy$$

is not square integrable. It can be thought of as a function which is infinite at x=y but vanishes everywhere else. The mathematical definition of this function is the topic of the theory of Schwartz distributions, which is needed for a good understanding of convergence theory but not for nonlinear finite element analysis.

The exact delineation of the space $\mathcal{L}_2$ can get quite technical, since mathematicians are concerned with questions such as whether the function $f\left(x\right) = 1$ when x is rational, $f\left(x\right) = 0$ otherwise, is square integrable (it is not). But for engineers concerned with the finite element method, it is sufficient to know that any function mentioned in this book except the Dirac delta function posseses an $\mathcal{L}_2$ norm.

The space of functions $\mathcal{L}_2$ is a special case of a more general group of spaces called Hilbert spaces. The norm in the Hilbert space $\mathcal{H}_1$ is defined by

$$\left\|a\left(x\right)\right\|_{\mathcal{H}_1} = \left(\int_0^1 \left(a^2\left(x\right) + a_{,x}^2\left(x\right)\right)dx\right)^{\frac{1}{2}}$$

Just as for vector norms, the major utility of these norms is in measuring errors in functions. Thus if the finite element solution for the displacement in a one dimensional problem is denoted by $u^h(x)$ and the exact solution is $u(x)$, then the error in the displacement can be measured by

$$\text{error}=\left\|u^h(x)-u(x)\right\|_{\mathcal{L}_2}$$

The error in the strain, i.e. the first derivative of the displacement, can be measured by the $\mathcal{H}_1$ norm. While this norm also includes the error in the function itself, the error in the derivative almost always dominates. On the other hand, you could measure the error in the strain by the $\mathcal{L}_2$ norm of the first

derivative. This is not a valid norm in mathematics, because it can vanish for a nonzero function (just take a constant), so it is called a seminorm.

These norms can be generalized to arbitrary domains in multi-dimensional space and to vector and tensors by just changing the integrals and integrands. Thus the

$\mathcal{L}_2$ norm of the displacement on a domain is given by

$$\left\| \mathbf{u}\left(\mathbf{x}\right) \right\|_{\mathcal{L}_2} = \left(\int_\Omega u_i\left(\mathbf{x}\right) u_i\left(\mathbf{x}\right) d\Omega \right)^{\frac{1}{2}}$$

The definition of the $\mathcal{H}_1$ norm is somewhat more puzzling??? since as given in mathematical tests it is not a true scalar (it is not invariant with rotation):

$$\left\| \mathbf{u}\left(\mathbf{x}\right) \right\|_{\mathcal{H}_1} = \left(\int_\Omega u_i\left(\mathbf{x}\right) u_i\left(\mathbf{x}\right) + u_{i,j}\left(\mathbf{x}\right) u_{i,j}\left(\mathbf{x}\right) d\Omega \right)^{\frac{1}{2}}$$

In general, the precise space to which a norm pertains is not given. Usually only a number, or even nothing is given by the norm sign. The norm must then be inferred from the context.

In linear stress analysis, the energy norm is often used to measure error. It is given by

$$\text{energy norm} = \left(\int_\Omega \varepsilon_{ij}\left(\mathbf{x}\right) C_{ijkl} \varepsilon_{kl}\left(\mathbf{x}\right) d\Omega \right)^{\frac{1}{2}}$$

Its behavior is similar to that of the $\mathcal{H}_1$ norm.

CHAPTER 7
Arbitrary Lagrangian Eulerian Formulations

by W.K.Liu
Northwestern University

7.1 Introduction

In Chapter 3, the classical Lagrangian and Eulerian approaches to the description of motion in continuum mechanics were presented. In the Lagrangian approach, the independent variables are taken to be the initial position, $\mathbf{X}$, of a material point and time, t. Thus the motion is given by

$$\mathbf{x} = \mathbf{f}(\mathbf{X}, t) \tag{7.1.1}$$

In this expression, the quantity $\mathbf{x}$ is the position occupied at time t by the material point which occupied the position $\mathbf{X}$ at time $t=0$. The quantity $\mathbf{f}$ is a mapping which describes the motion in terms of the independent variables $\mathbf{X}$ and t, and $\mathbf{x}$ is the value of the mapping for the values $\mathbf{X}$ and t. Recall that, in the Lagrangian description, the distinction between the value $\mathbf{x}$ and the mapping $\mathbf{f}$ is often ignored and we write $\mathbf{x} = \mathbf{x}(\mathbf{X}, t)$. A scalar field F, for example, may be represented by

$$F = F(\mathbf{X}, t) \tag{7.1.2}$$

In the Eulerian description, the independent variables are spatial position $\mathbf{x}$ and time t. A scalar field in the Eulerian description may then be given by

$$f = f(\mathbf{x}, t) \tag{7.1.4}$$

The field can be represented in terms of either the Eulerian or Lagrangian coordinates as follows

$$f(\mathbf{x}, t) = f(\mathbf{f}(\mathbf{X}, t), t) = F(\mathbf{X}, t) \tag{7.1.5}$$

but in fluid mechanics, the mapping $\mathbf{f}$ may not be known and this interpretation is not particularly useful.

In Chapter 4, Lagrangian finite elements were discussed. In Lagrangian finite element implementations, the finite element mesh convects with the material. The advantages of Lagrangian finite elements include the ease of tracking material interfaces and boundaries as well as the more straight-forward treatment of constitutive equations. Among the disadvantages of a Lagrangian formultation include the severe distortions that the elements may undergo as they deform with the material resulting in a deterioration of performance due to ill-conditioning. Nevertheless, Lagrangian finite elements prove extremely useful in large deformation problems in solid mechanics and are most widely used in solid mechanics. Eulerian finite elements are most often used in fluid mechanics for the same reasons that Eulerian representations of the equations of continuum mechanics are used,

i.e., there is often no well-defined reference configuration and the motion from a reference configuration is often not known explicitly. In Eulerian finite elements, the elements are fixed in space and material convects through the elements. Eulerian finite elements thus undergo no distortion due to material motion; however the treatment of constitutive equations and updates is complicated due to the convection of material through the elements. Eulerian elements may also lack resolution in the most highly deforming regions of the body.

The aim of ALE finite element formulations is to capture the advantages of both Lagrangian and Eulerian finite elements while minimizing the disadvantages. As the name suggests, ALE formulations are based on a description of the equations of continuum mechanics which is an arbitrary combination of the Lagrangian and Eulerian descriptions. The word *arbitrary* here means that the description (or specific combination of Lagrangian and Eulerian character) may be specified freely by the user. Of course, a judicious choice of the ALE motion is required if severe mesh distortions are to be eliminated. Suitable choices of the ALE motion will be discussed. Before introducing the ALE finite element formulation, it is useful to first consider some preliminary topics in continuum mechanics which were not covered in Chapter 3 and which provide the basis for the subsequent finite element implementation of the ALE methodology.

7.2 ALE Continuum Mechanics

7.2.1 Mesh Displacement, Mesh Velocity, and Mesh Acceleration

In figure (7.1), the motion $\mathbf{x} = \mathbf{f}(\mathbf{X}, t)$ is indicated as a mapping of the body from the reference configuration Ω_0 to the current or spatial configuration Ω. To introduce the ALE formulation, we now consider an alternative reference region $\hat{\Omega}$ as shown. We note that this region need not be an actual configuration of the body. Our objective is to show how the governing equations and kinematics for the body may be referred to this reference configuration and then how to use this description to formulate the ALE finite elements.

Points $\mathbf{c}$ in the reference region, $\hat{\Omega}$, are mapped to points $\mathbf{x}$ in the spatial region, Ω via the mapping

$$\mathbf{x} = \hat{\mathbf{f}}(\mathbf{c}, t) \tag{7.2.6}$$

This mapping $\hat{\mathbf{f}}$ will ultimately play an important role in the ALE finite element formulation. At this point, it is regarded as an arbitrary mapping (although it will be assumed to be invertible) of the region $\hat{\Omega}$ to the region Ω. The left hand side of (7.2.6) gives the mapping $\hat{\mathbf{f}}$ as a function of $\mathbf{c}$ and t. By virtue of (7.2.6), and (7.1.1), we have

$$\mathbf{x} = \hat{\mathbf{f}}(\mathbf{c}, t) = \mathbf{f}(\mathbf{X}, t) \tag{7.2.7}$$

which states that $\mathbf{x}$ in the Eulerian representation, $\mathbf{c}$ in the ALE representation, and $\mathbf{X}$ in the Lagrangian representation are mapped into $\mathbf{x}$(spatial coordinates) at time t. It is noted that even though the ALE mapping $\hat{\mathbf{f}}$ is different from the material mapping $\mathbf{f}$, the spatial coordinates $\mathbf{x}$ are the same.

In particular, if $\mathbf{c}$ is chosen to be the Lagrangian coordinate $\mathbf{X}$, $\hat{\mathbf{f}}$ becomes the material mapping $\mathbf{f}$ so that Eq.(7.2.7) becomes Eq.(7.1.1). A natural question arises: what is the ALE mapping $\hat{\mathbf{f}}$ if $\mathbf{c}$ is chosen to be the spatial coordinate $\mathbf{x}$? In this situation it is intuitive to think that Eq.(7.2.6) becomes:

$$\mathbf{x} = \hat{\mathbf{f}}(\mathbf{x}, t) \tag{7.2.8}$$

Therefore, $\hat{\mathbf{f}}$ is an identity mapping and it is not a function of time. As a result, we may define the material and mesh velocities in the spatial coordinate form:

$$\mathbf{v}(\mathbf{x}, t) = \left.\frac{\partial \mathbf{f}(\mathbf{X}, t)}{\partial t}\right|_{\mathbf{X}} \tag{7.2.9a}$$

and

$$\bar{\mathbf{v}}(\mathbf{x}, t) = \left.\frac{\partial \hat{\mathbf{f}}(\mathbf{c}, t)}{\partial t}\right|_{\mathbf{c}} \tag{7.2.9b}$$

It is noted that the right hand sides of Eqs.(7.2.9) are simply the definitions of material and mesh velocities, whereas the complete knowledge of the functions of the material and mesh velocites are often the solutions to the ALE continuum conservation equations. It is also understood that the mesh velocity, $\bar{\mathbf{v}}(\mathbf{x}, t)$, is equal to zero for an Eulerian description. We now assume that the two velocity equations are given so that with the definitions of the material motion, Eq.(7.1.1), and the mesh motion, Eq.(7.2.6), a set of first order boundary value equations are obtained:

$$\left.\frac{\partial \mathbf{f}(\mathbf{X}, t)}{\partial t}\right|_{\mathbf{X}} = \mathbf{v}(\mathbf{f}(\mathbf{X}, t), t) \tag{7.2.10a}$$

and

$$\left.\frac{\partial \hat{\mathbf{f}}(\mathbf{c}, t)}{\partial t}\right|_{\chi} = \bar{\mathbf{v}}(\hat{\mathbf{f}}(\mathbf{c}, t), t) \tag{7.2.10b}$$

The objective of Eqs.(7.2.10) is: given the material velocity function $\mathbf{v}(\mathbf{x}, t)$, and the mesh velocity function $\bar{\mathbf{v}}(\mathbf{x}, t)$, find the material mapping $\mathbf{f}(\mathbf{X}, t)$ and the ALE mapping $\hat{\mathbf{f}}(\mathbf{c}, t)$ such that Eqs.(7.2.10) are satisfied with the following initial conditions:

$$\mathbf{f}(\mathbf{X}, 0) = \mathbf{X}_0 \tag{7.2.11a}$$

and

$$\hat{\mathbf{f}}(\mathbf{c}, 0) = \mathbf{X}_0 \tag{7.2.11b}$$

With the stated initial boundary value problem, the above raised questions regarding the ALE mapping $\hat{\mathbf{f}}$ when $\mathbf{c}$ is chosen to be $\mathbf{x}$ can be answered by choosing $\mathbf{c} = \mathbf{x}$ (an Eulerian description, implying $\bar{\mathbf{v}}(\mathbf{x}, t) = \mathbf{0}$), so that

$$\bar{\mathbf{v}}(\hat{\mathbf{f}}(\mathbf{c},t),t) = \left.\frac{\partial \hat{\mathbf{f}}(\mathbf{x},t)}{\partial t}\right|_{\mathbf{x}} = \left.\frac{\partial \mathbf{I}(\mathbf{x})}{\partial t}\right|_{\mathbf{x}} = \mathbf{0} \tag{7.2.12}$$

Hence, Eq.(7.2.10b) becomes

$$\left.\frac{\partial \hat{\mathbf{f}}(\mathbf{c},t)}{\partial t}\right|_{\mathbf{c}} = \left.\frac{\partial \hat{\mathbf{f}}(\mathbf{x},t)}{\partial t}\right|_{\mathbf{x}} = \mathbf{0} \tag{7.2.13}$$

and therefore,

$$\hat{\mathbf{f}}(\chi,t) = \text{constant},$$

is determined from the initial conditions. By choosing $\mathbf{x} = \mathbf{X}_0$, Eq.(7.2.8) becomes the identity mapping so that

$$\mathbf{x} = \hat{\mathbf{f}}(\mathbf{x},t) = \mathbf{I}(\mathbf{x}) \tag{7.2.14}$$

Thus $\hat{\mathbf{f}}$ is indeed an identity mapping when $\mathbf{c} = \mathbf{x}$.

In the finite element implementation of the ALE formulation, a mesh is defined with respect to the configuration $\hat{\Omega}$. The motion $\hat{\mathbf{f}}(\mathbf{c},t)$ is used to describe the motion of the mesh and, as mentioned earlier, is chosen so as to reduce the effects of mesh distortion. For this reason, we also refer to $\hat{\mathbf{f}}(\mathbf{c},t)$ as the mesh motion. In this sense, we introduce the mesh displacement, $\hat{\mathbf{u}}$, for points in $\hat{\Omega}$ through

$$\mathbf{x} = \hat{\mathbf{f}}(\mathbf{c},t) = \mathbf{c} + \hat{\mathbf{u}}(\mathbf{c},t) \tag{7.2.8}$$

Consistent with this terminology, we also introduce the mesh velocity and acceleration fields for points in $\hat{\Omega}$ as follows

$$\hat{\mathbf{v}} = \left.\frac{\partial \hat{\mathbf{f}}(\mathbf{c},t)}{\partial t}\right|_{[\mathbf{c}]} = \left.\frac{\partial \hat{\mathbf{u}}(\mathbf{c},t)}{\partial t}\right|_{[\mathbf{c}]} \tag{7.2.9}$$

and

$$\hat{\mathbf{a}} = \left.\frac{\partial \hat{\mathbf{v}}(\mathbf{c},t)}{\partial t}\right|_{[\mathbf{c}]} = \left.\frac{\partial^2 \hat{\mathbf{u}}(\mathbf{c},t)}{\partial t^2}\right|_{[\mathbf{c}]} \tag{7.2.10}$$

This expression for velocity could be written as

$$\hat{\mathbf{v}} = \left.\frac{\partial \mathbf{x}}{\partial t}\right|_{[\mathbf{c}]} \tag{7.2.11}$$

However, in the interest of clarity in the ALE formulation, we refrain from this notation as it eliminates the distinction between the mapping or motion (in this case $\hat{\mathbf{f}}$) and the value

of the mapping, $\mathbf{x}$. For purely Eulerian or Lagrangian descriptions, however, this distinction in notation can be dropped with little loss of clarity.

Referring to (7.2.7), it can be seen that points in the reference configuration can be identified as

$$\mathbf{c} = \mathbf{y}(\mathbf{X}, t) = \hat{\mathbf{f}}^{-1} \circ \mathbf{f}(\mathbf{X}, t) \tag{7.2.12}$$

although we will have little occasion to use this relation. Instead, we will make use of the previously defined mappings and the chain rule where necessary. A schematic diagram representing these descriptions is shown in Fig. 7.1 and a summary of the kinematics for a general ALE formulation with Lagrangian and Eulerian formulations shown as special cases is given in Table 7.1.

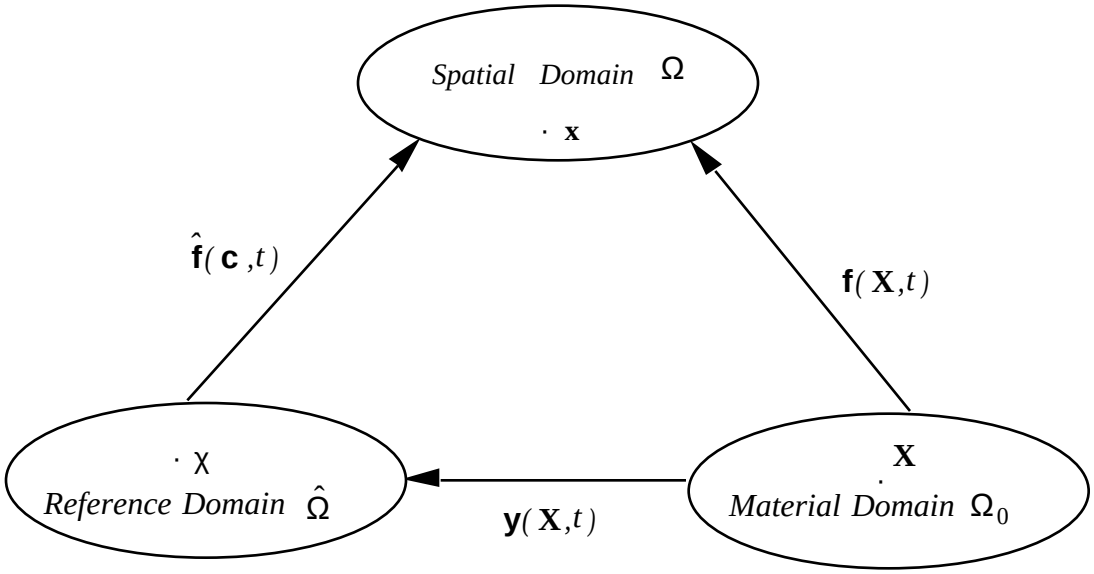

Fig 7.1 Mappings between Lagrangian, Eulerian, ALE descriptions

Description		General ALE	Lagrangian	Eulerian
Motion	Material	$\mathbf{x} = \mathbf{f}(\mathbf{X}, t)$	$\mathbf{x} = \mathbf{f}(\mathbf{X}, t)$	$\mathbf{x} = \mathbf{f}(\mathbf{X}, t)$
	Mesh	$\mathbf{x} = \hat{\mathbf{f}}(\mathbf{c}, t)$	$\mathbf{x} = \mathbf{f}(\mathbf{X}, t)$ $(\mathbf{c} = \mathbf{X},\ \hat{\mathbf{f}} = \mathbf{f})$	$\mathbf{x} = I(\mathbf{x})$ $(\mathbf{c} = \mathbf{x},\ \hat{\mathbf{f}} = \mathbf{I})$
Displacement	Material	$\mathbf{u} = \mathbf{x} - \mathbf{X}$	$\mathbf{u} = \mathbf{x} - \mathbf{X}$	$\mathbf{u} = \mathbf{x} - \mathbf{X}$
	Mesh	$\hat{\mathbf{u}} = \mathbf{x} - \mathbf{c}$	$\hat{\mathbf{u}} = \mathbf{x} - \mathbf{X} = \mathbf{u}$	$\hat{\mathbf{u}} = \mathbf{x} - \mathbf{x} = \mathbf{0}$
Velocity	Material	$\mathbf{v} = \mathbf{u}_{,t[X]}$	$\mathbf{v} = \mathbf{u}_{,t[X]}$	$\mathbf{v} = \mathbf{u}_{,t[X]}$
	Mesh	$\hat{\mathbf{v}} = \hat{\mathbf{u}}_{,t[\chi]}$	$\hat{\mathbf{v}} = \hat{\mathbf{u}}_{,t[\mathbf{X}]} = \mathbf{v}$	$\hat{\mathbf{v}} = \hat{\mathbf{u}}_{,t[\mathbf{x}]} = \mathbf{0}$
Acceleration	Material	$\mathbf{a} = \mathbf{v}_{,t[X]}$	$\mathbf{a} = \mathbf{v}_{,t[X]}$	$\mathbf{a} = \mathbf{v}_{,t[X]}$

	Mesh	$\hat{\mathbf{a}} = \hat{\mathbf{v}}_{,t[\chi]}$	$\hat{\mathbf{a}} = \hat{\mathbf{v}}_{,t[X]} = \mathbf{a}$	$\hat{\mathbf{a}} = \hat{\mathbf{v}}_{,t[\mathbf{x}]} = \mathbf{0}$

Table 7.1 Kinematics for a general ALE formulation with Lagrangian and Eulerian formulations shown as special cases.

7.2.2 Time Derivatives

In the balance laws, the material time derivative of a function appears. For a given scalar function, $f = f(\mathbf{x},t) = F(\mathbf{X},t)$, the *material time derivative*, and the *spatial derivative* or spatial gradient of f which appears in continuum conservation laws are defined as:

$$\dot{f} = \frac{D}{Dt} F(\mathbf{X},t) = \left.\frac{\partial F(\mathbf{X},t)}{\partial t}\right|_{[X]} = f(\mathbf{x}(\mathbf{X},t),t)_{,t[X]} \tag{7.2.14a}$$

and

$$\frac{\partial f}{\partial x_i} \equiv f_{,i} \quad \text{or} \quad grad_x\ f \equiv grad\ f \tag{7.2.14b}$$

respectively. The subscript x denotes partial differentiation with respect to x. These two important shorthand notations will be used subsequently.

7.2.3 Convective Velocity

Although functions $f(\mathbf{x}, t)$ are usually given in terms of $\mathbf{x}$ and t, it is convenient in ALE mechanics to express the function f in terms of $\boldsymbol{\chi}$ in the finite element formulation since the initial input coordinates $\boldsymbol{\chi}$ are fixed in the finite element mesh.

In general, by composition of mapping, f can be expressed as a function of $\mathbf{X}$ and t, denoted by F; a function of $\mathbf{x}$ and t, denoted by f; or a function of $\boldsymbol{\chi}$ and t, denoted by $\hat{f}$. That is

$$f = F(\mathbf{X},t) = f(\mathbf{x},t) = \hat{f}(\boldsymbol{\chi},t) \tag{7.2.15}$$

These are different functions, which represent the same field. The material time derivative can be expressed for the different descriptions as follow:

$$\frac{Df}{Dt} = \dot{F} = \text{material time derivative} = F_{,t[\mathbf{X}]}(\mathbf{X},t) \qquad (\mathbf{X},\ t) \tag{7.2.16a}$$

$$= f_{,t[x]} + \left.\frac{\partial f}{\partial x_i}\frac{\partial x_i}{\partial t}\right|_{[X]} = f_{,t[x]} + f_{,i} v_i \qquad (\mathbf{x},\ t) \tag{7.2.16b}$$

$$= \hat{f}_{,t[\chi]} + \left.\frac{\partial \hat{f}}{\partial \chi_i}\frac{\partial \chi_i}{\partial t}\right|_{[X]} = \hat{f}_{,t[\chi]} + \frac{\partial \hat{f}}{\partial \chi_i} w_i \qquad (\mathbf{c}, t) \tag{7.2.16c}$$

where w_i is the particle velocity in the referential coordinates and may be defined explicitely as

$$w_i = \left.\frac{\partial \chi_i}{\partial t}\right|_{[X]} \tag{7.2.16d}$$

. In Eq. (7.2.16c), the variable $\mathbf{c}$ is not defined explicitly in terms of $\mathbf{X}$ and t through the components of $\mathbf{x}$, but is given in terms of the material motion $\mathbf{f}$ and also of the mesh motion $\hat{\mathbf{f}}$. That is:

$$x_j = \varphi_j(\mathbf{X}, t) = \hat{\varphi}_j(\mathbf{c}, t) \tag{7.2.17}$$

Differentiating with respect to time while holding $\boldsymbol{X}$ fixed gives:

$$x_{j,t[\mathbf{X}]} = v_j = \left.\frac{\partial \hat{\varphi}_j}{\partial t}\right|_{[\chi]} + \left.\frac{\partial \hat{\varphi}_j}{\partial \chi_i}\frac{\partial \chi_i}{\partial t}\right|_{[\mathbf{X}]} = \hat{v}_j + \left.\frac{\partial x_j}{\partial \chi_i}\frac{\partial \chi_i}{\partial t}\right|_{[\mathbf{X}]} \tag{7.2.18}$$

The second term on the right hand side can be rearranged to yield:

$$\left.\frac{\partial x_j}{\partial \chi_i}\frac{\partial \chi_i}{\partial t}\right|_{[\mathbf{X}]} = \frac{\partial x_j}{\partial \chi_i} w_i = v_j - \hat{v}_j \equiv c_j \tag{7.2.19}$$

where c_j are the components of the *convective velocity* $\mathbf{c}$. Applying the chain rule to Eq. (7.2.16c) and employing Eq. (7.2.19) yields:

$$\frac{Df}{Dt} = \dot{F} = \hat{f}_{,t[\chi]} + \left.\frac{\partial f}{\partial x_j}\frac{\partial x_j}{\partial \chi_i}\frac{\partial \chi_i}{\partial t}\right|_{[X]} = \hat{f}_{,t[\chi]} + f_{,j} c_j \tag{7.2.20a}$$

or in vector notation:

$$\frac{Df}{Dt} = \hat{f}_{,t[\chi]} + \mathbf{c} \cdot \mathrm{grad}\, f = \hat{f}_{,t[\chi]} + \mathbf{c} \cdot {}_x f \tag{7.2.20b}$$

It can be shown that Eq. (7.2.20a) reduces to Eqs. (7.2.16a) and (7.2.16b) when $\mathbf{c} = \mathbf{X}(\mathbf{c} = \mathbf{0})$ and $\mathbf{c} = \mathbf{x}(\mathbf{c} = \mathbf{v})$, respectively. The former is known as the Lagrangian description, whereas the latter is the Eulerian description. Equation (7.2.20) is the material time derivative of f in a referential (i.e., ALE) description.

Example

The comparison of the Lagrangian, Eulerian, and ALE descriptions is pictorially depicted in Fig. 7.2 by a 4-node one dimensional finite element mesh. The finite element nodes and the material points are denoted by circles(○) and solid dots(●), respectively. The normalized coordinates are: $X_1 = 0$, $X_2 = 1$, $X_3 = 2$, and $X_4 = 3$; and normalied time is between 0 and 1. In Chapter 3, the Lagrangian and Eulerian descriptions were described as shown in Figs. 7.2(a) and (c). To illustrate the ALE description, as shown in Fig. 7.2(b), the motion of the material points is described by:

$$x = \varphi(X,t) = (1 - X^2)t + X t^2 + X \tag{7.2.13a}$$

In order to regulate the mesh motion, the four mesh nodes are spaced uniformly based on the end points of the material motion, that is, $\varphi(X_1,t)$ and $\varphi(X_4,t)$. Therefore, the mesh motion can be described by a linear Lagrange polynomial:

$$x = \hat{\varphi}(\chi,t) = \frac{\chi - \chi_1}{\chi_4 - \chi_1}\varphi(X_1,t) + \frac{\chi - \chi_4}{\chi_1 - \chi_4}\varphi(X_4,t) \tag{7.2.13b}$$

Combining Eqs. (7.2.13a) and (b) yields :

$$x = \frac{\chi - \chi_1}{\chi_4 - \chi_1}\left[(1 - X_1^2)t + X_1(t^2 + 1)\right] + \frac{\chi - \chi_4}{\chi_1 - \chi_4}\left[(1 - X_4^2)t + X_4(t^2 + 1)\right]$$

Therefore, we have:

material displacement:

$$u = x - X = (1 - X^2)t + Xt^2 + X - X = (1 + X - X^2)t$$

material velocity:

$$v = \left.\frac{\partial u}{\partial t}\right|_X = (1 + X - X^2)$$

material acceleration:

$$a = \left.\frac{\partial v}{\partial t}\right|_X = 0$$

mesh displacement:

$$\hat{u} = x - \chi = \frac{\chi - \chi_1}{\chi_4 - \chi_1}\left[(1 - X_1^2)t + X_1(t^2 + 1)\right] + \frac{\chi - \chi_4}{\chi_1 - \chi_4}\left[(1 - X_4^2)t + X_4(t^2 + 1)\right] - \chi$$

mesh velocity:

$$\hat{v} = \left.\frac{\partial \hat{u}}{\partial t}\right|_\chi = \frac{\chi - \chi_1}{\chi_4 - \chi_1}\left[(1 - X_1^2) + 2X_1 t\right] + \frac{\chi - \chi_4}{\chi_1 - \chi_4}\left[(1 - X_4^2) + 2X_4 t\right]$$

mesh acceleration:

$$\hat{a} = \left.\frac{\partial \hat{v}}{\partial t}\right|_{\chi} = \frac{2X_1(\chi - \chi_1)}{\chi_4 - \chi_1} + \frac{2X_4(\chi - \chi_4)}{\chi_1 - \chi_4}$$

The ALE mapping from the material domain to the reference domain is given by:

$$\chi = \psi(X,t) = \frac{[(1-X^2)t + X(t^2+1)](\chi_4 - \chi_1) + \chi_1\varphi(X_1,t) - \chi_4\varphi(X_4,t)}{\varphi(X_1,t) - \varphi(X_4,t)}$$

The particle velocity and acceleration in the referential coordinates may then be computed using Eq. (7.2.16d) and its time deravitive, respectively.

Comparing the two motions above, even though both motions give the same range of x, the two mappings are quite different as shown in Eqs. (7.2.13a,b) and Fig.7.2b.

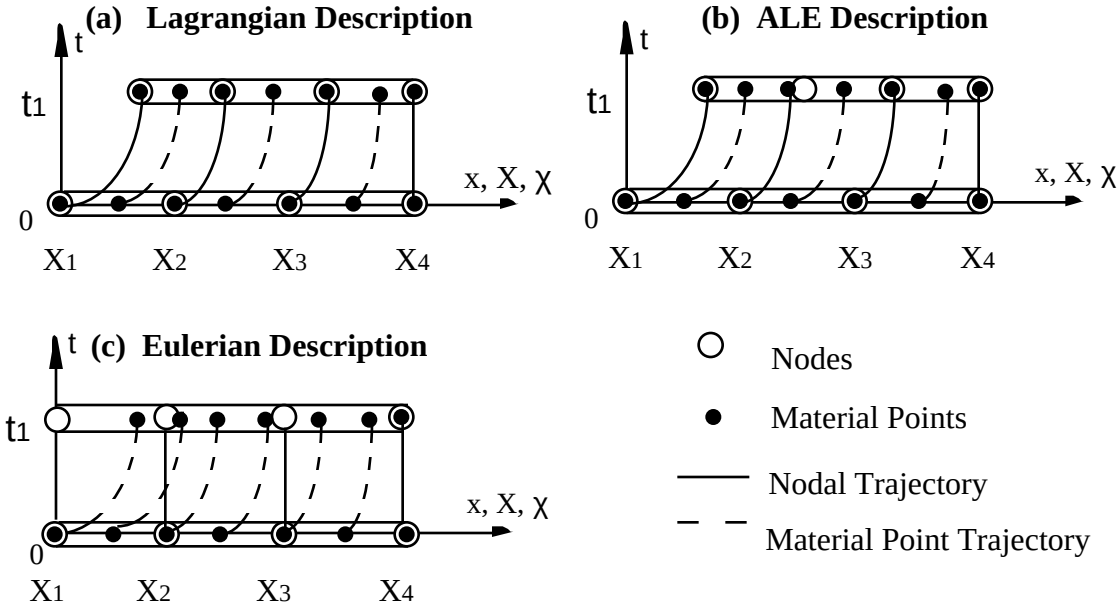

Fig 7.2 Comparison of Lagrangian, Eulerian, and ALE descriptions

7.4 Updated ALE Balance Laws in Referential Description

To derive the updated ALE balance laws analogous to those of the Lagrangian description, it is convenient to first use the Lagrangian equations given in Chapter 3 and then apply Eq. (7.2.20) to the material time derivatives to obtain the ALE conservation laws. Consequently, the *only* difference between the updated Lagrangian and updated ALE formulations is in the material time derivative terms. For completeness, the total ALE formulations are given in Appendix 7.1.

7.4.1 Conservation of Mass (Equation of Continuity) in ALE

The continuity equation is given by:

$$\dot{\rho} + \rho v_{j,j} = 0 \tag{7.4.1}$$

Applying the material time derivative operator Eqs. (7.2.20) to Eq. (7.4.1), the continuity equation becomes:

$$\rho_{,t[\chi]} + \rho_{,j} c_j + \rho v_{j,j} = 0 \tag{7.4.2a}$$

or in vector form:

$$\rho_{,t[\chi]} + \mathbf{c} \cdot \mathit{grad}\, \rho + \rho \nabla \cdot \mathbf{v} = 0 \tag{7.4.2b}$$

where $\nabla \cdot \mathbf{v}$ is the divergence of $\mathbf{v}$ in index free notation.

An alternate way of deriving the continuity equation is to employ the Reynolds transport theorem (given in Chapter 3) and using the divergence theorem to give:

$$\int_\Omega \left(\left. \frac{\partial \rho}{\partial t} \right|_x + \frac{\partial (\rho v_i)}{\partial x_i} \right) d\Omega = 0 \tag{7.7.14b}$$

Assuming there are no discontinuities in the linear momentum, an application of the chain rule yields

$$\int_\Omega \left(\left. \frac{\partial \rho}{\partial t} \right|_x + v_i \frac{\partial \rho}{\partial x_i} + \rho \frac{\partial v_i}{\partial x_i} \right) d\Omega = 0 \tag{7.7.14c}$$

Observing that the first two terms yield the material time derivative of ρ and hence using Eq. (7.2.20), Eq. (7.7.14c) becomes:

$$\int_\Omega \left(\left. \frac{\partial \rho}{\partial t} \right|_\chi + c_i \frac{\partial \rho}{\partial x_i} + \rho \frac{\partial v_i}{\partial x_i} \right) d\Omega = 0 \tag{7.7.14d}$$

and since Ω is arbitrarily chosen, it follows that:

$$\left. \frac{\partial \rho}{\partial t} \right|_\chi + c_i \frac{\partial \rho}{\partial x_i} + \rho \frac{\partial v_i}{\partial x_i} = 0 \qquad \text{in } \Omega \tag{7.7.15}$$

which is identical to Eq.(7.4.2). It is noted that if there is a discontinuity, we cannot apply the chain rule to the linear momentum since there is a jump in ρv_i hence we have to employ the conservative form, Eq.(7.7.14b) instead of the non-conservative form, Eq.(7.4.1)

7.4.2 Conservation of Linear Momentum in ALE

The conservative form of the momentum equation is given as:

$$\frac{D}{Dt}(\rho\, v_i) + (\rho\, v_i)v_{j,j} = \sigma_{ji,j} + \rho b_i \tag{7.4.6a}$$

It was shown in Chapter 3 that if there are no discontinuities, then the non-conservative form of the momentum equation can be obtained by applying the chain rule to ρv_i. With the help of the continuity equation, Eq (7.4.1), we obtain

$$\rho\, \dot{v}_i = \sigma_{ji,j} + \rho b_i$$

Similarly, after applying the material time derivative operator Eqs.(7.2.20) to Eq.(7.4.6a), the momentum equation becomes:

$$\rho\left\{v_{i,t[\chi]} + c_j v_{i,j}\right\} = \sigma_{ji,j} + \rho b_i \tag{7.4.8a}$$

or, in index free notation:

$$\rho\left\{\mathbf{v}_{,t[\chi]} + \mathbf{c}\ grad\,\mathbf{v}\right\} = div(\sigma) + \rho\mathbf{b} \tag{7.4.8b}$$

It is a simple exercise that by applying the material time derivative operator to the energy equation derived in Chapter 3, and show that the non-conservative form of the energy equation is:

$$\rho\dot{E} = (v_i\sigma_{ij})_{,j} + b_i v_i + (k_{ij}\theta_{,j})_{,i} + \rho s$$

7.5 Formal Statement of the Updated ALE Governing Equations in Non-Conservative Form (Strong Form) in Referential Description

In the equations given below, (7.6.2), k_{ij} and v_i are the components of the thermal conductivity matrix and convective heat transfer coefficients, respectively; θ_0 is the ambient temperature; b_i are the components of the body force; and s is the heat source. The objective of the initial/boundary-value problem is to find the following functions:

$\mathbf{u}(\mathbf{X}, t)$ material displacement (7.6.1a)

$\sigma(\mathbf{x}, t)$ Cauchy stress tensor (7.6.1b)

$\theta(\mathbf{x}, t)$ thermodynamic temperature (7.6.1c)

$\hat{\mathbf{u}}(\mathbf{c}, t)$ mesh displacement (7.6.1d)

and

$\rho(\mathbf{x}, t)$ density (7.6.1e)

such that they satisfy the following field and state equations shown in Box 7.1:

Strong Form of Updated ALE Governing Equations in Referential Description

Continuity Equation

$$\dot{\rho} + \rho v_{k,k} = 0 \quad \text{or} \quad \rho_{,t[\chi]} + \rho_{,i} c_i + \rho v_{k,k} = 0 \tag{7.6.2a}$$

Momentum Equations

$$\rho \dot{v}_i = \sigma_{ji,j} + \rho b_i \quad \text{or} \quad \rho\,(v_{i,t[\chi]} + v_{i,j} c_j) = \sigma_{ji,j} + \rho b_i \tag{7.6.2b}$$

Energy Equation

$$\rho \dot{E} = (v_i \sigma_{ij})_{,j} + b_i v_i + (k_{ij} \theta_{,j})_{,i} + \rho s \quad \text{or}$$

$$\rho(E_{,t[\chi]} + E_{,i} c_i) = (v_i \sigma_{ij})_{,j} + b_i v_i + (k_{ij} \theta_{,j})_{,i} + \rho s \tag{7.6.2c}$$

Equations of State

supplemented by the constitutive equations given in Chapter 6.

Natural Boundary Conditions

$$t_i(\mathbf{x}, t) = n_j(\mathbf{x}, t) \sigma_{ji}(\mathbf{x}, t) \quad \text{on } \partial\Gamma_x^t \tag{7.6.2g}$$

$$q_i(\mathbf{x}, t) = -k_{ij}(\theta, \mathbf{x}, t) \theta_{,j}(\mathbf{x}, t) + v_i(\theta, t)(\theta - \theta_0) \quad \text{on } \partial\Gamma_x^{t\theta} \tag{7.6.2h}$$

Essential Boundary Conditions

$$u_i(\mathbf{x}, t) = \bar{u}_i(\mathbf{x}, t) \quad \text{on } \partial\Gamma_x^g \tag{7.6.2i}$$

$$\theta(\mathbf{x}, t) = \bar{\theta}(\mathbf{x}, t) \quad \text{on } \partial\Gamma_x^{g\theta} \tag{7.6.2j}$$

Initial Conditions

$$\mathbf{u}(\mathbf{X}, 0) = \mathbf{u}_0, \quad \hat{\mathbf{u}}(\mathbf{c}, 0) = \hat{\mathbf{u}}_0 \tag{7.6.2k}$$

$$\mathbf{v}(\mathbf{X}, 0) = \mathbf{v}_0, \quad \hat{\mathbf{v}}(\mathbf{c}, 0) = \hat{\mathbf{v}}_0 \tag{7.6.2l}$$

Mesh Motion

$\hat{\mathbf{u}}(\mathbf{c}, t)$ = a given representation except, perhaps, on part of the boundary.

(7.6.2m)

Box 7.1 Strong Form of Updated ALE Governing Equations in Referential Description

Prior to developing the weak form and Petrov-Galerkin finite element discretization of the ALE continuity and momentum equations outlined above, it is most instructive to digress briefly and formally acquaint the reader with the general Petrov-Galerkin method. In doing so, it hoped that the necessity and power of such an approach will become apparent and that an intuitive feeling for the physics involved will be brought to light. The following section is designed to fulfill this requirement after which our development of the ALE equations will resume.

7.14 Introduction to the Petrov-Galerkin Method

In this section, streamline upwinding by a Petrov Galerkin method(SUPG) is formulated. Prior to the development of this method, the need for an upwinding scheme was motivated by an examination of the classical advection-diffusion equation. The advection-diffusion equation is a useful model for studying the momentum since it corresponds to a linearization of the transport equation. A closed form solution for the discrete steady-state advection diffusion equation will be obtained. It will be shown that the solution is oscillatory when a parameter of the mesh, known as the Peclet number, exceeds a critical value. Next, a Petrov Galerkin method will be developed which eliminates these oscillations.

Consider the linear advection-diffusion equation:

$$\frac{\partial \varphi}{\partial t} + \mathbf{u} \quad \varphi - \upsilon \quad ^2\varphi = 0 \tag{7.14.1}$$

where φ is the dependent variable, υ is the kinematic viscosity, and $\mathbf{u}$ is a given velocity field. For the steady state case, $\frac{\partial \varphi}{\partial t} = 0$. So, the steady state equation is:

$$\mathbf{u} \quad \varphi - \upsilon \quad ^2\varphi = 0 \tag{7.14.2}$$

For the study of special numerical instabilities, we restrict Eq. (7.14.2) to one dimension so that:

$$u\frac{d\varphi}{dx} = \upsilon \frac{d^2\varphi}{dx^2} \tag{7.14.3}$$

Equation (7.14.3) with boundary conditions:

$$\varphi(0) = 0 \text{ and } \varphi(L) = 1 \tag{7.14.4}$$

is a two-point boundary value problem on the domain $0 \le x \le L$.

It is easy to verify that the exact solution to Eqs. (7.14.3) and (7.14.4) is:

$$\varphi(x) = \frac{1 - e^{ux/\upsilon}}{1 - e^{uL/\upsilon}} \tag{7.14.5}$$

7.14.1 The Galerkin Finite Element Approximation of the Advection-Diffusion Equation

Letting the test function be w(x), multiplying Eq. (7.14.3) by w, and integrating over the domain gives

$$\int_\Omega w\left(u\frac{d\varphi}{dx} - \upsilon\frac{d^2\varphi}{dx^2}\right)dx = 0 \tag{7.14.6}$$

Integrating by parts and making use of the divergence theorem, the weak form of the one dimensional advection-diffusion equation, Eq. (7.14.3), is

$$\int_\Omega w u\frac{d\varphi}{dx}\,dx + \int_\Omega \upsilon\, w_{,x}\varphi_{,x}\,dx = 0 \tag{7.14.7}$$

with $w \quad U_0$. The domain (0, L) is then divided into equally sized linear finite elements, Ω^e, on which the finite element approximation is given by:

$$\left(\int_{\Omega^e} u N_a N_{b,x}\,dx\right)\varphi_b + \left(\int_{\Omega^e} \upsilon\, N_{a,x}N_{b,x}\,dx\right)\varphi_b = 0 \qquad a, b = 1, 2 \tag{7.14.8}$$

where N_a and N_b are the linear finite elements shape functions. This can be written in matrix component form as

$$N_{ab}\,\varphi_b + K_{ab}\,\varphi_b = 0 \qquad a, b = 1, 2 \tag{7.14.9a}$$

where the convective matrix is given as:

$$N_{ab} = \int_{x_e}^{x_{e+1}} u N_a N_{b,x}\,dx \tag{7.14.9b}$$

and the diffusion matrix is:

$$K_{ab} = \int_{x_e}^{x_{e+1}} \upsilon\, N_{a,x}N_{b,x}\,dx \tag{7.14.9c}$$

It is a simple exercise to show that, when using linear finite element shape functions,

$$\mathbf{N} = \frac{u}{2}\begin{bmatrix} -1 & 1 \\ -1 & 1 \end{bmatrix} \qquad \mathbf{K} = \frac{\upsilon}{\Delta x}\begin{bmatrix} 1 & -1 \\ -1 & 1 \end{bmatrix} \tag{7.14.10}$$

After assembly, the equation for the jth node is :

$$u\left(\frac{\varphi_{j+1}-\varphi_{j-1}}{2\Delta x}\right)-\upsilon\left(\frac{\varphi_{j+1}-2\varphi_j+\varphi_{j-1}}{\Delta x^2}\right)=0 \tag{7.14.11a}$$

which is exactly the central difference approximation. It is convenient to normalize the above equation, so that:

$$\frac{u\Delta x}{2\upsilon}\left(\varphi_{j+1}-\varphi_{j-1}\right)-\left(\varphi_{j+1}-2\varphi_j+\varphi_{j-1}\right)=0 \tag{7.14.11b}$$

The Peclet number, P_e, may then be defined as:

$$P_e=\frac{u\Delta x}{2\upsilon} \tag{7.14.12}$$

In terms of the Peclet number, Eq. (7.14.11b) then becomes:

$$P_e\left(\varphi_{j+1}-\varphi_{j-1}\right)-\left(\varphi_{j+1}-2\varphi_j+\varphi_{j-1}\right)=0 \tag{7.14.13a}$$

$$\left(P_e-1\right)\varphi_{j+1}+2\varphi_j-\left(P_e+1\right)\varphi_{j-1}=0 \tag{7.14.13b}$$

Ignoring the boundary conditions, Eq. (7.14.13) can be put into the standard matrix notation by expanding the jth term in Eq. (7.14.13):

$$\boxed{P_e\begin{bmatrix}\cdots & & & & \cdots\end{bmatrix}\begin{Bmatrix}\vdots\\ \varphi_{j-1}\\ \varphi_j\\ \varphi_{j+1}\\ \vdots\end{Bmatrix}+\begin{bmatrix}\cdots & & & & \cdots\end{bmatrix}\begin{Bmatrix}\vdots\\ \varphi_{j-1}\\ \varphi_j\\ \varphi_{j+1}\\ \vdots\end{Bmatrix}=\begin{Bmatrix}\vdots\\ 0\\ 0\\ 0\\ \vdots\end{Bmatrix}} \tag{7.14.14}$$

$$\begin{bmatrix}\cdots & & & & \cdots\end{bmatrix}=\begin{bmatrix}\cdots & -1 & 0 & 1 & \cdots\end{bmatrix}\quad\begin{bmatrix}\cdots & -1 & 2 & -1 & \cdots\end{bmatrix}$$

convective term diffusion term

The solution to the discrete finite difference Eq. (7.14.13) can be obtained by assuming:

$$\varphi(x_j)\equiv\varphi_j=e^{ax_j}=e^{a(j\Delta x)}=e^{(a\Delta x)j}\equiv z^j \tag{7.14.15}$$

Where $z=e^{a\Delta x}$ and a is an unknown coefficient to be determined. By the definition in Eq. (7.14.15), the j+1th and j-1th terms of φ are:

$$\varphi_{j+1}=e^{a(j+1)\Delta x}=e^{aj\Delta x}e^{a\Delta x}=z^{j+1} \tag{7.14.16a}$$

$$\varphi_{j-1}=e^{a(j-1)\Delta x}=e^{aj\Delta x}e^{-a\Delta x}=z^{j-1} \tag{7.14.16b}$$

Substituting Eqs. (7.14.16) into Eq. (7.14.13) yields:

$$\left(P_e - 1\right)z^{j+1} + 2z^j - \left(P_e + 1\right)z^{j-1} = 0 \tag{7.14.17}$$

Assuming that $z^{j-1} \neq 0$ and dividing the above equation by z^{j-1}, Eq. (7.14.17) becomes:

$$\left(P_e - 1\right)z^2 + 2z - \left(P_e + 1\right) = 0 \tag{7.14.18}$$

The roots for Eq. (7.14.18) are:

$$z = 1 \text{ or } z = \frac{1 + P_e}{1 - P_e} \tag{7.14.19}$$

Recalling that $\varphi_j = z^j$, the solution to Eq. (7.14.13) takes the form:

$$\varphi_j = c_1 + c_2\left(\frac{1 + P_e}{1 - P_e}\right)^j \tag{7.14.20}$$

where c_1 and c_2 are coefficients to be determined from the boundary conditions. Since the exact solution to Eq. (7.14.3) is given by Eq. (7.14.5), the exact solution of φ, evaluated at $x = x_j$, has the form of:

$$\varphi(x_j) = \frac{1}{1 - e^{uL/\upsilon}}\left[1 - e^{ux_j/\upsilon}\right] = c_1 + c_2 e^{\frac{u}{\upsilon} j\Delta x} \tag{7.14.21}$$

Comparing the finite difference solution Eq. (7.14.20) with the exact solution, Eq. (7.14.21), it can be concluded that:

(i) If the Peclet number is less than one, i.e., $|P_e| < 1$, then the discrete solution will have a solution similar to the exponential solution as given in the exact solution since $\left(\frac{1 + P_e}{1 - P_e}\right)^j > 0$.

(ii) If the Peclet number is greater than one, i.e., $P_e > 1$, then the discrete solution becomes:

$$\left(\frac{1 + P_e}{1 - P_e}\right)^j = (-m)^j \quad \text{with } m > 0$$

Hence nodal oscillations occur because φ_j is positive or negative depending on whether j is even or odd, respectively. To illustrate these nodal oscillations, we consider the one

dimensional advection-diffusion equation as given in Eq.(7.14.3) with boundary conditions (7.14.4). The plots below compare the exact solution with finite element solutions for the cases of both no upwinding and full upwinding. In all cases, 80 elements were used with an element Peclet number of 300.

7.14.2 Ramification of Nodal Oscillation by the Petrov-Galerkin Formulation

Recall the weak form of Eq. (7.14.3):

$$\int_\Omega w(u\frac{d\varphi}{dx} - \upsilon\frac{d^2\varphi}{dx^2})dx = 0 \tag{7.14.27}$$

The Petrov-Galerkin formulation for Eq. (7.14.3) is obtained by replacing the test function w by $\tilde{w}$, where $\tilde{w}$ is defined as:

$$w \to \tilde{w} \equiv \underbrace{w}_{Galerkin test function} + \underbrace{\alpha\frac{\Delta x}{2}\frac{dw}{dx}(\text{sign}\,u)}_{discontinuous test function} \tag{7.14.28}$$

Replacing w by $\tilde{w}$, Eq. (7.14.27) becomes:

$$\int_\Omega \tilde{w}(u\frac{d\varphi}{dx} - \upsilon\frac{d^2\varphi}{dx^2})dx = 0 \tag{7.14.29}$$

Note that $w \quad U_0$ and $\tilde{w} \quad U_0$. The parameter α is to be determined so as to eliminate oscillations for $P_e > 1$ and hopefully get accurate solutions; in one dimension, it is possible to select α so as to obtain exact values of the solution at the nodes. Substituting the definition of $\tilde{w}$, Eq. (7.14.28), into Eq. (7.14.29) yields:

$$0 = \int_\Omega \tilde{w}(u\frac{d\varphi}{dx} - \upsilon\frac{d^2\varphi}{dx^2})dx = \underbrace{\int_\Omega w(u\frac{d\varphi}{dx} - \upsilon\frac{d^2\varphi}{dx^2})dx}_{GalerkinTerm}$$

$$+ \underbrace{\sum_{e=1}^{N_e}\int_{\Omega^e}\alpha\frac{\Delta x}{2}\frac{dw}{dx}(\text{sign}\,u)(u\frac{d\varphi}{dx} - \upsilon\frac{d^2\varphi}{dx^2})dx}_{Upwind\ Petrov-Galerkin\ Term} \tag{7.14.30}$$

After integrating by parts (and using $w(0)=w(L)=0$ be construction), Eq. (7.14.30) becomes:

$$0 = \int_\Omega wu\frac{d\varphi}{dx}dx + \int_\Omega \upsilon\frac{dw}{dx}\frac{d\varphi}{dx}dx$$

$$+\sum_{e=1}^{N_e}\int_{\Omega^e} u\frac{\alpha\Delta x}{2}(\operatorname{sign} u)\frac{dw}{dx}\frac{d\varphi}{dx}\,dx-\sum_{e=1}^{N_e}\int_{\Omega^e}\upsilon\frac{\alpha\Delta x}{2}(\operatorname{sign} u)\frac{dw}{dx}\frac{d^2\varphi}{dx^2}\,dx \tag{7.14.31}$$

The above equation is known as upwinding Petrov-Galerkin formulation(Brooks & Hughes, 1978). It is noted that in this formulation the second derivative of φ is required. Further, the free parameter α is determined in the following section after the presentation of an alternative formulation which only requires the first derivative of φ.

7.14.3 An Alternative Derivation of the Upwind/Petrov-Galerkin Formulation

This section outlines an alternative derivation of the upwind formulation. Motivated by a desire to necessitate low order continuity restrictions on the trial functions, we begin by starting with the one dimensional advection-diffusion equation as before. The equation is then multiplied by a test function $\tilde{w}$ and integrated over the domain Ω (following the traditional weak form development) thereby yielding

$$\int_\Omega \tilde{w}\left(u\frac{d\varphi}{dx}-\upsilon\frac{d^2\varphi}{dx^2}\right)dx=0$$

Examining the second term on the left hand side in more detail, our goal is to remove one derivative from the trial function and place it on the test function, $\tilde{w}$, thereby relaxing trial function continuity requirements. To this end, we integrate by parts in the familiar manner as follows:

$$I\equiv\int_\Omega \tilde{w}\upsilon\frac{d^2\varphi}{dx^2}\,dx=\int_\Omega\left(\tilde{w}\upsilon\frac{d\varphi}{dx}\right)_{,x}dx-\int_\Omega\frac{d\tilde{w}}{dx}\upsilon\frac{d\varphi}{dx}\,dx$$

Applying the divergence theorem and the substituting in the definition of $\tilde{w}$ gives:

$$I=\tilde{w}\upsilon\frac{d\varphi}{dx}\bigg|_o^L-\int_\Omega\frac{d\tilde{w}}{dx}\upsilon\frac{d\varphi}{dx}\,dx=\left[w+\alpha\frac{\Delta x}{2}\frac{dw}{dx}(\operatorname{sign} u)\right]\upsilon\frac{d\varphi}{dx}\bigg|_0^L-\int_\Omega\frac{d\tilde{w}}{dx}\upsilon\frac{d\varphi}{dx}\,dx$$

$$=\alpha\frac{\Delta x}{2}\frac{dw}{dx}(\operatorname{sign} u)\upsilon\frac{d\varphi}{dx}\bigg|_0^L-\int_\Omega\frac{d\tilde{w}}{dx}\upsilon\frac{d\varphi}{dx}\,dx\qquad(\text{since } w(o)=0 \text{ and } w(L)=0)$$

Combining the above results with the advection term yields the following alternative weak form:

$$\int_\Omega\left[\tilde{w}u\frac{d\varphi}{dx}+\frac{d\tilde{w}}{dx}\upsilon\frac{d\varphi}{dx}\right]dx-\alpha\frac{\Delta x}{2}\frac{dw}{dx}(\operatorname{sign} u)\upsilon\frac{d\varphi}{dx}\bigg|_0^L=0$$

Now it is apparent that removal of a trial function derivative gives rise to a boundary integral term which was not present in the Petrov-Galerkin formulation presented earlier. In the particular case when $\tilde{w}$ is defined as in Eq. (7.14.28), it is straightforward to show that this alternative formulation yields the same results as the formulation presented in the previous section. To see this, substitute the explicit expression for $\tilde{w}$ into the equation giving

$$\int_\Omega \left[w + \alpha \frac{\Delta x}{2} \frac{dw}{dx}(sign\, u) u \right] \frac{d\varphi}{dx} dx + \int_\Omega \left[\frac{dw}{dx} + \alpha \frac{\Delta x}{2} \frac{d^2 w}{dx^2}(sign\, u) v \right] \frac{d\varphi}{dx} dx$$
$$- \alpha \frac{\Delta x}{2} \frac{dw}{dx}(sign\, u) \upsilon \frac{d\varphi}{dx}\Big|_0^L = 0$$

Using integrating by parts on the fourth term gives

$$\int_\Omega \left[\alpha \frac{\Delta x}{2} \frac{d^2 w}{dx^2}(sign\, u) v \right] \frac{d\varphi}{dx} dx = \alpha \frac{\Delta x}{2}(sign\, u) v \frac{dw}{dx} \frac{d\varphi}{dx}\Big|_0^L - \int_\Omega \alpha \frac{\Delta x}{2}(sign\, u) v \frac{dw}{dx} \frac{d^2\varphi}{dx^2} dx$$

which, upon rearrangement of the terms, yields the expression resulting from the previously presented Petrov-Galerkin formulation:

$$\int_\Omega wu \frac{d\varphi}{dx} dx + \int_\Omega v \frac{dw}{dx} \frac{d\varphi}{dx} dx + \sum_{e=1}^{N_e} \int_{\Omega^e} \alpha \frac{\Delta x}{2}(sign\, u) u \frac{dw}{dx} \frac{d\varphi}{dx} dx$$
$$- \sum_{e=1}^{N_e} \int_{\Omega^e} \alpha \frac{\Delta x}{2}(sign\, u) v \frac{dw}{dx} \frac{d^2\varphi}{dx^2} dx + \alpha \frac{\Delta x}{2}(sign\, u) v \frac{dw}{dx} \frac{d\varphi}{dx}\Big|_0^L -$$
$$\alpha \frac{\Delta x}{2}(sign\, u) v \frac{dw}{dx} \frac{d\varphi}{dx}\Big|_0^L = 0$$

Following the cancelation of the last two terms, this equation is identical to that of the previous formulation, Eq.(7.14.31). As a result, we may select either formulation depending on which is more convenient computationally for the problem at hand.

Finally, it can be noted that when linear elements are used, $\frac{d^2\varphi}{dx^2} = 0$, so all terms involving second derivatitves vanish. Consequently, Eq. (7.14.31) may be written as:

$$0 = \sum_e \int_{\Omega^e} \left[wu \frac{d\varphi}{dx} + v \frac{dw}{dx} \frac{d\varphi}{dx} \right] dx \tag{7.14.32}$$

where, υ^* ,which may be thought of as a sum of two viscosities will be defined below.

7.14.4 Parameter Determination and Further Analysis

To begin, we wish to shed additional light on the physical interpretation of Eq. (7.14.32). As a result, we make the following definitions:

$$\upsilon^* = \upsilon + \bar{\upsilon} \text{ = total viscosity} \tag{7.14.33a}$$

and

$$\bar{\upsilon} = \alpha u \frac{\Delta x}{2} \text{sign}(u), \ \alpha \geq 0 \tag{7.14.33b}$$

It then becomes clear that $\bar{\upsilon}$ may be thought of as an artificial viscosity which must be added to the "normal" flow viscosity, υ, to ensure stability. That is, without this superficial damping which does not correspond to the physics of the problem, our numerical solution oscillates wildly thereby leading to physically meaningless results.

To define these viscosities in terms of various Peclet numbers, consider the following relationships:

$$\upsilon \qquad P_e = \frac{u\Delta x}{2\upsilon} \tag{7.14.34a}$$

$$\bar{\upsilon} \qquad \overline{P_e} = \frac{u\Delta x}{2\bar{\upsilon}} \tag{7.14.34b}$$

$$\upsilon^* \qquad P_e^* = \frac{u\Delta x}{2\upsilon^*} \tag{7.14.34c}$$

The relationships between Eq. (7.14.34a-c) can be expressed as:

$$\frac{1}{P_e^*} = \frac{2\upsilon^*}{u\Delta x} = \frac{2\upsilon}{u\Delta x} + \frac{2\bar{\upsilon}}{u\Delta x} = \frac{1}{P_e} + \frac{1}{\overline{P_e}} \tag{7.14.35}$$

In Eq. (7.14.35), if $P_e^* < 1$, then

$$\frac{2\upsilon}{u\Delta x} + \frac{2\bar{\upsilon}}{u\Delta x} > 1 \text{ or } \frac{1}{\overline{P_e}} > 1 - \frac{1}{P_e} \tag{7.14.36}$$

and the solution will not be oscillatory. From Eq. (7.14.13), the discrete equation in terms of P_e^* can be written as:

$$(P_e^* - 1)\varphi_{j+1} + 2\varphi_j - (P_e^* + 1)\varphi_{j-1} = 0 \tag{7.14.37}$$

Recall that the discrete solution is oscillatory when $\varphi_N = z^N$, the roots of Eq. (7.14.37) are :

$$z^N = c_1, c_2 \left(\frac{1 + P_e^*}{1 - P_e^*}\right)^N \tag{7.14.38}$$

From Eq. (7.14.21) and Eq. (7.14.38), we can solve P_e^*. That is,

$$\left(\frac{1 + P_e^*}{1 - P_e^*}\right)^j = e^{(\frac{u}{\upsilon}\Delta x) j} \tag{7.14.39}$$

The RHS of Eq. (7.14.39) can be expressed in terms of P_e. That is:

$$\frac{1+P_e^*}{1-P_e^*} = e^{\frac{u}{\upsilon}\Delta x} = e^{2(\frac{u\Delta x}{2\upsilon})} = e^{2P_e} \tag{7.14.40a}$$

or

$$1 - e^{2P_e} = -P_e^*(1+e^{2P_e}) \tag{7.14.40b}$$

Therefore,

$$P_e^* = \frac{e^{2P_e}-1}{e^{2P_e}+1} = \frac{e^{P_e}-e^{-P_e}}{e^{P_e}+e^{-P_e}} \tag{7.14.41a}$$

or

$$P_e^* = \tanh(P_e) \tag{7.14.41b}$$

Substituting Eq. (7.14.41b) into Eq. (7.14.35) yields:

$$\frac{1}{\tanh(P_e)} = \frac{1}{P_e} + \frac{1}{\overline{\overline{P_e}}} \tag{7.14.42a}$$

or

$$\frac{1}{\overline{\overline{P_e}}} = \coth(P_e) - \frac{1}{P_e} \tag{7.14.42b}$$

Together, Eq. (7.14.34b) and Eq. (7.14.42b) may be combined to give:

$$\overline{P}_e = \frac{u\Delta x}{2\overline{\upsilon}} = \left[\coth(P_e) - \frac{1}{P_e}\right]^{-1} \tag{7.14.43}$$

Using Eq. (7.14.43), we can also express $\overline{\upsilon}$ in terms of P_e:

$$\overline{\upsilon} = \frac{1}{2}u\Delta x\left[\coth(P_e) - \frac{1}{P_e}\right] = \alpha\frac{u\Delta x}{2}\,\mathrm{sign}(u) \tag{7.14.44a}$$

so therefore,

$$\bar{\upsilon} = \frac{1}{2} u\Delta x \left[\coth(P_e) - \frac{1}{P_e} \right] = \alpha \frac{u\Delta x}{2} \text{sign}(u) \tag{7.14.44b}$$

Finally, it becomes apparent that we may define the parameter α as:

$$\alpha = sign(u)\,[\coth(P_e) - \frac{1}{P_e}] \tag{7.14.45}$$

Note that when $\alpha = 0$, Eq. (7.14.29) is simply like a central difference method and when $\alpha = 1$, it is a full upwind Petrov-Galerkin formulation.

7.14.5 Streamline-Upwind/Petrov-Galerkin Formulation for Multiple Dimensions

The advection-diffusion equation in multiple dimension is:

$$\mathbf{u} \quad \varphi - \mathbf{v} \quad ^2\varphi = 0 \qquad \text{in } \Omega \tag{7.14.45a}$$

where the boundary conditions are:

$$\varphi = g \qquad \text{on } \partial\Omega_g \tag{7.14.45b}$$

$$\mathbf{v} \quad \varphi \quad \mathbf{n} = 0 \qquad \text{on } \partial\Omega_t \tag{7.14.45c}$$

The weak form of the advection-diffusion equation for a streamline-upwind/Petrov-Galerkin formulation of Eq. (7.14.45a) is obtained by multiplying Eq. (7.14.45a) by the test function w and integrating over the domain Ω

$$\int w(\mathbf{u} \quad \varphi - \mathbf{v} \quad ^2\varphi) = 0$$

Similar to the one-dimensional formulation presented above, let the Petrov-Galerkin test functions be defined by

$$w \to \tilde{w} \equiv \underbrace{\underset{\sim}{w}}_{Galerkin test function} + \underbrace{\tau \mathbf{u} \quad w}_{discontinuous test function} \tag{7.14.45d}$$

thus giving

$$0 = \int_\Omega (w + \tau \mathbf{u} \quad w)(\mathbf{u} \quad \varphi - \upsilon \quad ^2\varphi)\, d\Omega \tag{7.14.46a}$$

where the stabilization parameter is now given by

$$\tau = |\alpha| \frac{h}{2\|u\|} \text{ and } h \equiv \Delta x \tag{7.14.45b}$$

where α is given by Eq.(7.14.33c). For a time dependent problem, the stabilization parameter can be set by:

$$\tau = |\alpha| \frac{\Delta t}{2} \tag{7.14.45c}$$

Note that $w \quad U_0$ and $\tilde{w} \quad U_0$ as in the one dimensional case. Applying integration by parts and the divergence theorem, the weak form of Eq. (7.14.46a) can be shown to be:

$$0 = \underbrace{\int_\Omega \; w\mathbf{u} \quad \varphi \, d\Omega + \int_\Omega \upsilon \quad w \quad \varphi d\Omega}_{Galerkin \quad terms}$$

$$\underbrace{+\sum_{e=1}^{N_e} \int_{\Omega^e} \tau (\mathbf{u} \quad w)(\mathbf{u} \quad \varphi) \, d\Omega - \sum_{e=1}^{N_e} \int_{\Omega^e} \tau (\mathbf{u} \quad w) \upsilon \quad {}^2 \varphi d\Omega}_{streamlineupwind \; stabilization \quad terms} \tag{7.14.46}$$

As can be seen from the above equation, the Petrov-Galerkin terms are simply the sum of the standard Galerkin terms plus the streamline upwind stabilization terms. Namely,

Petrov / Galerkin = Galerkin + Streamline Upwind Stabilization

The third term of Eq. (7.14.46) can be rewritten as:

$$\int_{\Omega^e} \tau (\mathbf{u} \quad w)(\mathbf{u} \quad \varphi) \, d\Omega$$

$$= \int_{\Omega^e} \tau \begin{bmatrix} w_{,1} & w_{,2} & w_{,3} \end{bmatrix} \begin{bmatrix} u_1 \\ u_2 \\ u_3 \end{bmatrix} \begin{bmatrix} u_1 & u_2 & u_3 \end{bmatrix} \begin{bmatrix} \varphi_{,1} \\ \varphi_{,2} \\ \varphi_{,3} \end{bmatrix} d\Omega$$

$$= \int_{\Omega^e} \tau \begin{bmatrix} w_{,1} & w_{,2} & w_{,3} \end{bmatrix} \begin{bmatrix} u_1 u_1 & u_1 u_2 & u_1 u_3 \\ u_2 u_1 & u_2 u_2 & u_2 u_3 \\ u_3 u_1 & u_3 u_2 & u_3 u_3 \end{bmatrix} \begin{bmatrix} \varphi_{,1} \\ \varphi_{,2} \\ \varphi_{,3} \end{bmatrix} d\Omega$$

$$= \int_{\Omega^e} \quad w \quad (\tilde{\upsilon} \quad \varphi) \, d\Omega \tag{7.14.47a}$$

where

$$\tilde{\upsilon} = \tau \begin{bmatrix} u_1u_1 & u_1u_2 & u_1u_3 \\ u_2u_1 & u_2u_2 & u_2u_3 \\ u_3u_1 & u_3u_2 & u_3u_3 \end{bmatrix} \qquad (7.14.47b)$$

Substituting Eq. (7.14.47a) into Eq. (7.14.46) and ignoring the last second order term, Eq. (7.14.46) becomes:

$$0 = \underbrace{\int_\Omega w\,\mathbf{u} \quad \varphi\, d\Omega + \sum_{e=1}^{N_e} \int_{\Omega^e} \quad w(\upsilon \mathbf{1} + \quad \tilde{\upsilon} \quad)}_{\text{Galerkin Term}} \quad \varphi\, d\Omega \qquad (7.14.48)$$

artifical viscosity

The artificial viscosity acts as a stabilization term which eliminates the oscillations resulting from a standard Galerkin formulation.

7.14.6 An Alternative Derivation of the Multiple Dimensional Streamline-Upwind/Petrov-Galerkin Formulation

Paralleling section 7.14.3, this section outlines an alternative derivation of the multidimensional streamline-upwind/Petrov-Galerkine formulation presented above. To this end, we begin by starting with the multiple dimensional advection-diffusion equation as before. The equation is then multiplied by a test function $\tilde{w}$ and integrated over the domain Ω (following the traditional weak form development) thereby yielding

$$\int \tilde{w}(\mathbf{u} \quad \varphi - \mathbf{v} \quad ^2\varphi) = 0$$

Examining the second term on the left hand side in more detail, our goal is to remove one derivative from the trial function and place it on the test function, $\tilde{w}$, thereby relaxing trial function continuity requirements. To this end, we integrate by parts in the familiar manner as follows:

$$I \equiv \int_\Omega \tilde{w}\mathbf{v} \quad ^2\varphi d\Omega = \int_\Omega \quad (\tilde{w}\mathbf{v} \quad \varphi)\, d\Omega - \int_\Omega \quad \tilde{w}\mathbf{v} \quad \varphi d\Omega$$

Applying the divergence theorem and the substituting in the definition of $\tilde{w}$ gives:

$$I = \tilde{w}\mathbf{v} \quad \varphi|_\Gamma - \int_\Omega \quad \tilde{w}\mathbf{v} \quad \varphi d\Omega = [w + \tau\mathbf{u} \quad w]\mathbf{v} \quad \varphi|_\Gamma - \int_\Omega \quad \tilde{w}\mathbf{v} \quad \varphi d\Omega$$

$$= \tau\mathbf{u} \quad w\mathbf{v} \quad \varphi|_\Gamma - \int_\Omega \quad \tilde{w}\mathbf{v} \quad \varphi d\Omega$$

where the last line has been obtained by using the fact that $w \quad U_0$. Combining the above results with the advection term yields the following alternative weak form:

$$\int_\Omega [\tilde{w}\mathbf{u} \quad w + \quad \tilde{w}\mathbf{v} \quad \varphi] d\Omega - \tau\mathbf{u} \quad w\mathbf{v} \quad \varphi|_\Gamma = 0$$

Now it is apparent that removal of a trial function derivative gives rise to a boundary integral term which was not present in the streamline-upwind/Petrov-Galerkin formulation

presented earlier. In the particular case when $\tilde{w}$ is defined as in Eq. (7.14.28), it is straightforward to show that this alternative formulation yields the same results as the formulation presented in the previous section.

Example Petrov-Galerkin formulation of the ALE momentum equation for a 1D 2-node linear displacement element may be done as follows.
The test function is chosen to be:

$$\bar{N}_I = N_I + \alpha \frac{h}{2} \frac{dN_I}{dx} sign(c)$$

where α is the viscosity constant, c is the convective velocity, h is the element size, and N_I is the shape function of the usual Galerkin form. If constant density is assumed, we obtain the Petrov-Galerkin form of the mass matrix in the ALE formulation, as:

$$\mathbf{M} = \rho h \begin{bmatrix} \frac{1}{3} - \frac{\alpha}{2}(K_2 - K_1) & \frac{1}{6} - \frac{\alpha}{2} K_1 \\ \frac{1}{6} + \frac{\alpha}{2}(K_2 - K_1) & \frac{1}{3} + \frac{\alpha}{2} K_1 \end{bmatrix}$$

where

$$K_1 = \begin{cases} \frac{1}{2} sign(c_1) & if\ (c_1 = c_2) \\ \frac{1}{2}\left[sign(c_1) - sign(c_2)\right]\left(\frac{c_1}{c_1 - c_2}\right)^2 + \frac{1}{2} sign(c_2) & if\ (c_1 \neq c_2) \end{cases}$$

$$K_2 = \begin{cases} sign(c_1) & if\ (c_1 = c_2) \\ \left[sign(c_1) - sign(c_2)\right]\left(\frac{c_1}{c_1 - c_2}\right) + sign(c_2) & if\ (c_1 \neq c_2) \end{cases}$$

and c_1 and c_2 are the convective velocities at the 2 nodes.

Similar to that for convective-advective equation, we can rewrite the mass matrix as:

$$\mathbf{M} = \underbrace{\rho h \begin{bmatrix} \frac{1}{3} & \frac{1}{6} \\ \frac{1}{6} & \frac{1}{3} \end{bmatrix}}_{Galerkin\ terms} + \underbrace{\rho h \begin{bmatrix} -\frac{\alpha}{2}(K_2 - K_1) & -\frac{\alpha}{2} K_1 \\ +\frac{\alpha}{2}(K_2 - K_1) & +\frac{\alpha}{2} K_1 \end{bmatrix}}_{streamline\ upwind\ stabilization\ terms}$$

namely, the Petrov-Galerkin terms can be split into the sum of Galerkin terms and the streamline upwind stabilization terms.

7.3 Weak Form and Petrov-Galerkin Finite Element Discretization of the ALE Continuity and Momentum Equations:

As can be seen from Box 7.1, the only difference between the updated Lagrangian equations and the updated ALE equations is the interpretation of the material time derivative. Hence the weak form, and subsequently the Galerkin finite element

formulations, are identical to those derived in Chapter 4. However, note that the spatial domain now depends on how the mesh motion is updated, which is one of the key ingredients in the updated ALE formulation.

The variational equations corresponding to the conservation equations of Box 7.1 are obtained by multiplying by the test functions, $\delta\rho$ and δv_i, integrating over the spatial domain Ω and employing the divergence theorem to embed the traction force vector $\boldsymbol{t}$ on the boundary Γ^t. Following the same procedures as in Chapter 4, we can achieve the following weak forms:

Continuity Equation:

$$\int_\Omega \delta\rho\dot{\rho} d\Omega = \int_\Omega \delta\rho\rho_{,t[\chi]} d\Omega + \int_\Omega \delta\rho c_i \rho_{,i} d\Omega = -\int_\Omega \delta\rho\rho v_{i,i} d\Omega \tag{7.16.2a}$$

Momentum Equation:

$$\begin{aligned} &\int_\Omega \delta v_i \rho \dot{v}_i d\Omega \\ &= \int_\Omega \delta v_i \rho v_{i,t[\chi]} d\Omega + \int_\Omega \delta v_i \rho c_j v_{i,j} d\Omega \\ &= -\int_\Omega \delta v_{i,j} \sigma_{ij} d\Omega + \int_\Omega \delta v_i \rho b_i d\Omega_x + \int_{\Gamma^t} \delta v_i \bar{t}_i d\Gamma \end{aligned} \tag{7.16.2b}$$

It is noted that because convective terms ($\rho_{,i} c_i$ and $v_{i,j} c_j$) appeared in the continuity and momentum equations, a Galerkin finite element formulation will give rise to numerical difficulties. Therefore, in this section, the Petrov-Galerkin formulation will be employed to alleviate some of these difficulties. In a Petrov Galerkin finite element discretization, the current domain Ω is subdivided into elements. However, different sets of shape functions, $\boldsymbol{N}$ and $\boldsymbol{N}^\rho$ for the trial functions, and $\bar{\mathbf{N}}$ and $\bar{\mathbf{N}}^\rho$ for the test functions, will be used to interpolate the velocity and density, respectively. If $\bar{\mathbf{N}} = \mathbf{N}$, the Galerkin ALE formulations will be obtained. The choice of $\bar{\mathbf{N}}$ and $\bar{\mathbf{N}}^\rho$ to eliminate numerical oscillations will be described in section ????.

The finite element matrix equations corresponding to Eq.(7.16.2a,b) are :

Continuity equation:

$$\mathbf{M}^\rho \rho_{,t[\chi]} + \mathbf{L}^\rho \rho + \mathbf{K}^\rho \rho = 0 \tag{7.16.3a}$$

where $\mathbf{M}^\rho$, $\mathbf{L}^\rho$, $\mathbf{K}^\rho$ are generalized mass, convective, and stiffness matrices, respectively, for density under a reference description such that:

$$\mathbf{M}^\rho = [M^\rho_{IJ}] = \int_\Omega \bar{N}^\rho_I N^\rho_J d\Omega \tag{7.16.3b}$$

$$\mathbf{L}^\rho = [L^\rho_{IJ}] = \int_\Omega \bar{N}^\rho_I c_i N^\rho_{J,i} d\Omega \tag{7.16.3c}$$

$$\mathbf{K}^{\rho} = [K_{IJ}^{\rho}] = \int_{\Omega} \overline{N}_I^{\rho} v_{i,i} N_J^{\rho} d\Omega \tag{7.16.3d}$$

Momentum Equation:

$$\mathbf{M}\mathbf{v}_{,t[\chi]} + \mathbf{L}\mathbf{v} + \mathbf{f}^{int} = \mathbf{f}^{ext} \tag{7.16.4a}$$

where $\mathbf{M}$ and $\mathbf{L}$ are generalized mass and convective matrices, respectively, for velocity under a reference description; while $\mathbf{f}^{int}$ and $\mathbf{f}^{ext}$ are the internal and external force vectors respectively, such that:

$$\mathbf{M} = [M_{IJ}] = \int_{\Omega} \rho \overline{N}_I N_J d\Omega \tag{7.16.4b}$$

$$\mathbf{L} = [L_{IJ}] = \int_{\Omega} \rho \overline{N}_I c_i N_{J,i} d\Omega \tag{7.16.4c}$$

$$\mathbf{f}^{int} = [f_{iI}^{int}] = \int_{\Omega} \overline{N}_{I,j} \sigma_{ij} d\Omega \tag{7.16.4d}$$

$$\mathbf{f}^{ext} = [f_{iI}^{ext}] = \int_{\Omega} \rho \overline{N}_I b_i d\Omega + \int_{\Gamma_t} \overline{N}_I \bar{t}_i d\Gamma \tag{7.16.4e}$$

REMARK 7.16.1.4 The nonself-adjoint and nonlinear convective terms, $\mathbf{L}^{\rho}$ and $\mathbf{L}$, which appear in Eqs.(7.16.3c) and (7.16.4c) and characterize the ALE method, will inevitably pose difficulties.

REMARK 7.16.1.5 All the matrices and vectors defined in Eqs(7.16.3)-(7.16.6) are integrated over the spatial domain Ω. Unlike the Lagrangian formulations, the spatial domain changes continuously throughout the computation. The mesh update procedure will be described in section ????.

In the subsequent development of this chapter, we shall divide the discussion of ALE formulations into four parts:
1) Updated ALE formulations for continuum material models *without* memory, that is, the evaluation of constitutive laws is independent of the strain history. A simple example of this kind of materials is a slightly compressible Newtonian fluid which will be discussed in section ???
2) Updated ALE formulations of continuum material models *with* memory, that is, the evaluation of constitutive laws is strain history dependent. This will be described in section ???.
3) The Petrov-Galerkin finite element method, of which the discretization of the transport term requires special treatment. For high velocities, if the mesh is not sufficiently refined, the Galerkin method gives rise to oscillatory solutions. To overcome this difficulty, various schemes, collectively known as upwinding, will be described in section ????.
4) The mesh update procedure, which is described in section ????.

The reason for the distinction between ALE formulations with and without memory is due to the difference between ALE material update procedures. Recall that the material time

derivative of a given function f can be related to the referential time derivative by Eq.(7.2.20), that is

$$\dot{f} = \frac{Df}{Dt} = \hat{f}_{,t[\chi]} + c_j f_{,j}$$

It is noted that f can represent density ρ, velocity $\mathbf{v}$, energy E, Cauchy stress σ, etc., as appearing in the governing equations Box 7.1.

The next section will illustrate the difference between Lagrangian and ALE material update procedures.

7.3 ALE Material Updates

In the Lagrangian description, the updating of any material-related state variable is simple. Since the Lagrangian coordinate is always associated with the same material point, a Taylor series expansion in time may be used. Using first order accuracy gives:

$$F(\mathbf{X}, t+dt) = F(\mathbf{X}, t) + dt \frac{\partial F}{\partial t}(\mathbf{X}, t)\Big|_{\mathbf{X}} + \ldots \tag{7.3.1}$$

However, in a referential description, updating of a material state variable introduces complicates. To illustrate this, we expand a state variable $\hat{f}(\chi, t)$ in a Taylor series:

$$\hat{f}(\chi, t+dt) = \hat{f}(\chi, t) + dt \frac{\partial \hat{f}}{\partial t}(\chi, t)\Big|_{\chi} + \ldots \tag{7.3.2}$$

or, by referring everything to the particle $\mathbf{X}$ at time t (see Eq. (7.2.10)), as:

$$\hat{f}\left[\psi(\mathbf{X}, t+dt), t+dt\right] = \hat{f}\left[\psi(\mathbf{X}, t), t\right] + dt \frac{\partial \hat{f}}{\partial t}\left[\psi(\mathbf{X}, t), t\right]\Big|_{\chi=\psi(\mathbf{X},t)} + \ldots \tag{7.3.3}$$

which is equivalent to

$$F(\overline{\mathbf{X}}, t+dt) = F(\mathbf{X}, t) + dt \frac{\partial F}{\partial t}(\mathbf{X}, t)\Big|_{\mathbf{X}=\psi^{-1}(\chi,t)} + \ldots \tag{7.3.4a}$$

where

$$\overline{\mathbf{X}} = \psi^{-1}(\chi, t+dt) \quad \text{and} \quad \mathbf{X} = \psi^{-1}(\chi, t) \tag{7.3.4b}$$

Comparing Eq. (7.3.4a) with Eq. (7.3.1), even though the terms in the right hand side of the equations are the same , shows that $\mathbf{X}$ and $\overline{\mathbf{X}}$ are two different material particles, which

at t and $t + dt$, respectively, have the same referential coordinates. Therefore, in a referential description, a simple updating technique, such as Eq. (7.3.2) cannot be used for material point-related variables, such as state variables in path-dependent materials; however, for homogeneous materials with no memory, such as the generalized Newtonian fluids, Eq. (7.3.2) can be implemented with no further complications. Further detail will be given on this subject later.

7.16 ALE Finite Element Method for Path-Dependent Materials

The purpose of this section is to provide a general formulation and an explicit computational procedure for nonlinear ALE finite element analyses. Emphasis is placed on the stress update procedure for path-dependent materials. First, after the general formulations for the ALE description are reviewed, according to strong form, weak form and finite element form, the most important part of the ALE application for path-dependent materials, the stress update procedure, is studied in detail. Formulations for regular Galerkin method, Streamline-upwind/Petrov-Galerkin(SUPG) method and operator split method are derived respectively. All the path-dependent state variables are updated with a similar procedure. Further, the stress update procedures are specified in 1-D case. And the matrices corresponding to these three methods are listed. Then, an explicit computational method and a flowchart are presented. Finally, elastic and elastic-plastic wave propagation examples are given.

7.16.1 Formulations for Updated ALE:

7.16.1.1 Strong Form Formulations for ALE:

In addition to continuity and momentum equations given in section ????, for the purpose of introducing path-dependent material model, the Cauchy stress may be decomposed into the deviatoric stress tensor s_{ij} and the hydrostatic pressure p such that

$$\sigma_{ij} = s_{ij} - p\delta_{ij} \tag{7.16.1c}$$

and the components of the deviatoric stress term are given by the Jaumann rate constitutive equation

$$s_{ij,t[\chi]} + c_k s_{ij,k} = C_{ijkl} D_{kl} + s_{kj} W_{ik} + s_{ki} W_{jk} \tag{7.16.1d}$$

Similarly the rate from of the equation of state is given by:

$$p_{,t[\chi]} + c_i p_{,i} = p(\rho) \tag{7.16.1e}$$

In the above equations, D_{ij} and W_{ij} are of deformation tensor and the spin tensor, respectively; such that

$$D_{ij} = \frac{1}{2}(v_{i,j} + v_{j,i}) \tag{7.16.1f}$$

$$W_{ij} = \frac{1}{2}(v_{i,j} - v_{j,i}) \tag{7.16.1g}$$

and C_{ijkl} is the material response tensor which relates any frame-invariant rate of the Cauchy stress to the velocity strain. Both geometric and material nonlinearities are included in the setting of Eqs. (7.16.1a-g).

REMARK 7.16.1.1 The right-hand sides of Eqs. (7.16.1a,b,d and e) remain the same for all descriptions.
REMARK 7.16.1.2. Eqs. (7.16.1a,b,d and e) are referred to as the "quasi-Eulerian" description (Belytschko and Kennedy, 1978) because these equations have a strong resemblance to the Eulerian equations. In particular, the Eulerian equations can be readily obtained by choosing $\mathbf{c} = \mathbf{v}$, i.e., $\chi = \mathbf{x}$.
REMARK 7.16.1.3. With the help of integration by part, Eq.(7.16.1d) is equivalent to the following equations:

$$s_{ij,t[\chi]} + y_{ijk,k} - c_{k,k}s_{ij} = C_{ijkl}D_{kl} + s_{kj}W_{ik} + s_{ki}W_{jk} \tag{7.16.1h}$$

and

$$y_{ijk} = s_{ij}c_k \tag{7.16.1i}$$

where y_{ijk} is the stress-velocity product. In the following finite element computation, these two equations will replace Eq.(7.16.1d) in the weak form.

7.16.1.2 Weak Form of the ALE Equations:

Similar to the case for continuity and momentum equations, we may obtain the weak form of the constitutive equations:

$$\begin{aligned}&\int_\Omega \delta s_{ij} s_{ij,t[\chi]} d\Omega + \int_\Omega \delta s_{ij} y_{ijk,k} d\Omega - \int_\Omega \delta s_{ij} c_{k,k} s_{ij} d\Omega \\ &= \int_\Omega \delta s_{ij} C_{ijkl} D_{kl} d\Omega + \int_\Omega \delta s_{ij} \{s_{kj} W_{ik} + s_{ki} W_{jk}\} d\Omega\end{aligned} \tag{7.16.2c}$$

and

$$\int_\Omega \delta y_{ijk} y_{ijk} d\Omega = \int_\Omega \delta y_{ijk} s_{ij} c_k d\Omega \tag{7.16.2d}$$

Equation of state

$$\int_\Omega \delta p p_{t,[\chi]} d\Omega + \int_\Omega \delta p c_i p_{,i} d\Omega = \int_\Omega \delta p p(\rho) d\Omega \tag{7.16.2e}$$

Eq.(7.16.2a) represents the control volume form of material conservation. Eq.(7.16.2b) is a generalization of the principle of virtual work to the control volume form with the first integral brought in as d'Alembert forces.

7.16.1.3 Finite Element Discretization:

Similar to the finite element discretization for continuity and momentum equations, we can obtain the finite element form for constitutive equations by employing $\boldsymbol{N}^s$, $\boldsymbol{N}^y$ and $\boldsymbol{N}^p$ as

sets of shape functions, and $\bar{\boldsymbol{N}}^s$, $\bar{\boldsymbol{N}}^y$ and $\bar{\boldsymbol{N}}^p$ as corresponding sets of test functions to interpolate the deviatoric stress, stress-velocity product, and hydrostatic pressure respectively. Note that the test functions and the shape functions for deviatoric stresses are used only in the constitutive equations.

Constitutive Equations:

$$\mathbf{M}^s\mathbf{s}_{,t[\chi]} + \mathbf{G}^T\mathbf{y} - \mathbf{D}\mathbf{s} = \mathbf{z} \tag{7.16.5a}$$

$$\mathbf{M}^y\mathbf{y} = \mathbf{L}^y\mathbf{s} \tag{7.16.5b}$$

where the superscript T denotes matrix transpose, $\mathbf{M}^s$ and $\mathbf{D}$ are the generalized mass and diffusion matrices for deviatoric stress respectively; $\mathbf{G}^T\mathbf{y}$ corresponds to the generalized convective term; $\mathbf{M}^y$ and $\mathbf{L}^y$ are the generalized mass and convective matrices for stress-velocity product respectively; and $\mathbf{z}$ is the generalized deviatoric stress vector such that

$$\mathbf{M}^s = [M^s_{IJ}] = \int_\Omega \bar{N}^s_I N^s_J d\Omega \tag{7.16.5c}$$

$$\mathbf{G}^T = [G^T_{IJ}] = \int_\Omega \bar{N}^s_I N^y_{J,x} d\Omega \tag{7.16.5d}$$

$$\mathbf{D} = [D_{IJ}] = \int_\Omega \bar{N}^s_I c_{k,k} N^s_J d\Omega \tag{7.16.5e}$$

$$\mathbf{z} = [z_{ijI}] = \int_\Omega \bar{N}^s_I C_{ijkl} D_{kl} d\Omega + \int_\Omega \bar{N}^s_I \{s_{kj} W_{ik} + s_{ki} W_{jk}\} d\Omega \tag{7.16.5f}$$

$$\mathbf{M}^y = [M^y_{IJ}] = \int_\Omega \bar{N}^y_I N^y_J d\Omega \tag{7.16.5g}$$

$$\mathbf{L}^y = [L^y_{IJ}] = \int_\Omega \bar{N}^s_I c N^s_J d\Omega \tag{7.16.5h}$$

Equation of State:

$$\mathbf{M}^p\mathbf{p}_{,t[\chi]} + \mathbf{L}^p\mathbf{p} = \mathbf{u} \tag{7.16.6a}$$

where $\mathbf{M}^p$ and $\mathbf{L}^p$ are the generalized mass and convective matrices for pressure respectively; and $\mathbf{u}$ is the generalized pressure vector, such that

$$\mathbf{M}^p = [M^p_{IJ}] = \int_\Omega \bar{N}^p_I N^p_J d\Omega \tag{7.16.6b}$$

$$\mathbf{L}^p = [L^p_{IJ}] = \int_\Omega \bar{N}^p_I c_i N^p_{J,i} d\Omega \tag{7.16.6c}$$

$$\mathbf{u} = [u_I] = \int_\Omega \bar{N}^p_I p(\rho) d\Omega \tag{7.16.6d}$$

REMARK 7.16.1.6 The stress-velocity product $\mathbf{y}$ is stored at each node as a vector with a dimension of (number of space dimensions) × (number of stress components). The diagonal form for $\mathbf{M}^y$ is considered by location the numerical integration points at nodes.

REMARK 7.16.1.7 The numerical integration of (7.16.3) and (7.16.4) has been discussed by Liu & Belytschko(1983), Liu(1981) and Liu & Ma(1982). A procedure for the stress update Eqs. (7.16.5a) and (7.16.5b) is presented in the next section to clarify the temporal integration for path-dependent materials. All the path-dependent quantities are updated analogous to Eqs(7.16.5a) and (7.16.5b). The Petrov-Galerkin formulation of the continuity and momentum equation derived in section 7.14 can be adopted here.

7.16.2 Stress Update Procedures:

7.16.2.1 Stress Update Procedure for Galerkin Method

The stress state in a path-dependent material depends on the stress history of the material point. A stress history can be readily treated in Lagrangian description because elements contain the same material points regardless of the deformation of the continuum; similarly, quadrature points at which stresses are computed in Lagrangian elements coincide with material points throughout the deformation. On the other hand, in an ALE description, a mesh point does not coincide with a material point so that the stress history needs to be convected by the relative velocity $\mathbf{c}$, as indicated in Eq.(7.16.1d). Note that the spatial derivatives of the deviatoric stress are involved in the convection term.

When $\mathbf{C}^{-1}$ functions are used to interpolate the element stresses, the ambiguity of the stress derivatives at the element interface renders the calculation of the spatial derivatives of stress a difficult task. As mentioned in Remark 7.16.1.3, this is remedied by replacing Eq.(7.16.1d) by a set of coupled equations, Eqs.(7.16.1h) and (7.16.1i), and the corresponding matrix equations have been given in Eqs.(7.16.5a) and (7.16.5b). The stress-velocity product $\mathbf{y}$ can be eliminated by inverting $\mathbf{M}^y$ in Eq(7.16.5b) and substituting into Eq(7.16.5a):

$$\mathbf{M}^s\mathbf{s}_{,t[\chi]} + \mathbf{G}^T(\mathbf{M}^y)^{-1}\mathbf{L}^y\mathbf{s} - \mathbf{D}\mathbf{s} = \mathbf{z} \tag{7.16.7a}$$

where $\mathbf{G}^T(\mathbf{M}^y)^{-1}\mathbf{L}^y\mathbf{s}$ can be identified as the convective term, and the upwind techniques mentioned in Remark 7.16.1.4 should be applied to evaluate $\mathbf{L}^y\mathbf{s}$. When $\mathbf{c} = 0$, i.e., $\chi = \mathbf{x}$, Eq.(7.16.7a) degenerates to the usual stress updating formula in the Lagrangian description,

$$\mathbf{M}^s\mathbf{s}_{,t[\chi]} = \mathbf{z} \tag{7.16.7b}$$

REMARK 7.16.2.1. The conservation equations are listed here to show the similarity among the equations:

$$\mathbf{M}^\rho\rho_{,t[\chi]} + \mathbf{L}^\rho\rho + \mathbf{K}^\rho\rho = 0 \tag{7.16.7c}$$

$$\mathbf{M}\mathbf{v}_{,t[\chi]} + \mathbf{L}\mathbf{v} + \mathbf{f}^{int} = \mathbf{f}^{ext} \tag{7.16.7d}$$

$$\mathbf{M}^{s}\mathbf{s}_{,t[\chi]} + \mathbf{G}^{T}(\mathbf{M}^{y})^{-1}\mathbf{L}^{y}\mathbf{s} - \mathbf{D}\mathbf{s} = \mathbf{z} \tag{7.16.7e}$$

REMARK 7.16.2.2. In the above, Eq.(7.16.5b) is eliminated because it can be incorporated in Eq.(7.16.7e). This procedure is analogous to that by Liu & Chang(1985) where a fluid-structure interaction algorithm is described.

REMARK 7.16.2.3. All the path-dependent material properties, such as yield strains, effective plastic strains, yield stresses, and back stresses, should be convected via Eq.(7.16.7e) with **s** replaced by these properties, respectively, and with **z** appropriately modified.

7.16.2.2 Stress Update Procedure for SUPG Method:

In a nonlinear displacement finite element formulation, when applied to elastic-plastic materials with kinematic hardening, the velocities are stored at nodes while the stress histories, back stresses, and yield radii are available only at quadrature points. In order to establish the nodal values for the stress-velocity product, a weak formulation is a logical necessity. In addition, based on the one-dimensional study(Liu et. al. 1986), in which the upwind procedure is used to define this intermediate variable, the artificial viscosity technique(streamline upwind) is considered here as a generalization of this upwind procedure to multi-dimensional cases.
The relation for the stresses-velocity product of Eq.(7.16.1i), is modified to accommodate the artificial viscosity tensor A_{ijkm} by

$$y_{ijk} = s_{ij}c_k - A_{ijkm,m} \tag{7.16.8a}$$

The ingredients of the artificial viscosity tensor consist of a tensorial coefficient multiplied by the stress:

$$A_{ijkm} = \mu_{km}s_{ij} \tag{7.16.8b}$$

where the tensorial coefficient is constructed to act only in the flow direction (streamline upwind effect)

$$\mu_{km} = \bar{\mu}c_k c_m / c_n c_n \tag{7.16.8c}$$

and the scalar $\bar{\mu}$ is given by

$$\bar{\mu} = \sum_{i=1}^{NSD} \alpha_i c_i h_i / NSD \tag{7.16.8d}$$

Here h_i is the element length in the i-direction; NSD designates the number of space dimensions; and α_i is the artificial viscosity parameter given by

$$\alpha_i = \begin{cases} \frac{1}{2} & for \quad c_i > 0 \\ -\frac{1}{2} & for \quad c_i < 0 \end{cases} \tag{7.16.8e}$$

The weak form corresponding to Eq. (7.16.8a) can be obtained by multiplying by test function for the stress-velocity product and integrating over the spatial domain Ω:

$$\int_\Omega \delta y_{ijk} y_{ijk} d\Omega = \int_\Omega \delta y_{ijk} s_{ij} c_k d\Omega - \int_\Omega \delta y_{ijk} A_{ijkm,m} d\Omega \tag{7.16.9a}$$

This equation may be written as

$$\int_\Omega \delta y_{ijk} y_{ijk} d\Omega = \int_\Omega \delta y_{ijk} s_{ij} c_k d\Omega + \int_\Omega \delta y_{ijk,m} A_{ijkm} d\Omega \tag{7.16.9b}$$

by applying the divergence theorem and by assuming no traction associated with the artificial viscosity on the boundary. The expression for A_{ijkm}, Eq. (7.16.8b and c), can be substituted into this equation to yield

$$\int_\Omega \delta y_{ijk} y_{ijk} d\Omega = \int_\Omega (\delta y_{ijk} + \delta \bar{y}_{ijk}) s_{ij} c_k d\Omega \tag{7.16.9c}$$

where

$$\delta \bar{y}_{ijk} = \delta y_{ijk,m} \bar{\mu} c_m / c_n c_n \tag{7.16.9d}$$

can be viewed as a modification of the Galerkin finite element method because of the transport nature of the stress-velocity product.

The shape functions for the stress-velocity product can be chosen to be the standard C^0 functions. The number and position of quadrature points for Eq.(7.16.9c and d) should be selected to be the Gauss quadrature points, since the stress histories in Eq.(7.16.9c) are only available at these points.

Following the procedures given above, the stress-velocity product can be defined at each nodal point and it can be substituted into the constitutive equation of Eq.(7.16.5a) to calculate the rate of change of stresses with the same procedure as that of without artificial viscosity. Note that the interpolation functions for stresses are integrated over the spatial element domain. The task of selecting the number of quadrature points for the displacement finite element poses another important issue. For example, the locking phenomenon for fully integrated elements arises when the material becomes incompressible(Liu, et.al., 1985). While selective reduced integration can overcome this difficulty, it is just as costly as full quadrature. To alleviate this computational hurdle, the use of one-point quadrature combined with hourglass control is developed by Belytschko et.al. (1984). In addition, the nonlinear two-quadrature point element (Liu et.al., 1988) appears to be another candidate for large-scale computations because it exhibits nearly the same accuracy as the selective reduced integration element while with only one-third of the cost. These two kind of elements, as well as the other displacement elements, can be readily adopted in the ALE computations.

Following the procedure described by Liu et.al(1986), the displacement element is divided into M sub-domain, where M denotes the number of quadrature points. Each sub-domain is designated by Ω_I (I=1,...,M), which contains the quadrature points $\mathbf{x}_I$, and no two sub-domains overlap. Associated with Ω_I, a stress interpolation function N_I^s is assigned and its value is prescribed to be unity only at the quadrature point $\mathbf{x} = \mathbf{x}_I$ such that

$$N_I^s(\mathbf{x} = \mathbf{x}_I) = 1 \tag{7.16.10a}$$

The test function in Ω_I is chosen to be the Dirac delta function

$$\bar{N}_I^s = \delta(\mathbf{x} - \mathbf{x}_I) \tag{7.16.10b}$$

Substitution of these functions into the constitutive equation represents a mathematical requirement that the residual of the weal from vanishes at each collocative quadrature point. Because the collocation point is located right at the quadrature point, the algebraic equations resulting from Eq.(7.16.5a) can be easily worked out without numerical integration and given as below:
General mass matrix is

$$M_{IJ}^s = \int_\Omega \bar{N}_I^s N_J^s d\Omega_x = \mathbf{I}_{M\times M} \tag{7.16.11a}$$

where the subscripts I and J range from 1 to M, the number of stress quadrature points per element. The transpose of the divergence operator matrix reads,

$$G_{IJ}^T = \int_\Omega \bar{N}_I^s N_{J,x}^y d\Omega$$

For 2D 4-node element, it will be:

$$\mathbf{G}^T = \begin{bmatrix} N_{1,x}(\xi_1) & N_{1,y}(\xi_1) & N_{2,x}(\xi_1) & N_{2,y}(\xi_1) \\ N_{1,x}(\xi_2) & N_{1,y}(\xi_2) & N_{2,x}(\xi_2) & N_{2,y}(\xi_2) \\ \vdots & \vdots & \vdots & \vdots \\ N_{1,x}(\xi_M) & N_{1,y}(\xi_M) & N_{2,x}(\xi_M) & N_{2,y}(\xi_M) \end{bmatrix}$$

$$\begin{bmatrix} N_{3,x}(\xi_1) & N_{3,y}(\xi_1) & N_{4,x}(\xi_1) & N_{4,x}(\xi_1) \\ N_{3,x}(\xi_2) & N_{3,y}(\xi_2) & N_{4,x}(\xi_2) & N_{4,y}(\xi_2) \\ \vdots & \vdots & \vdots & \vdots \\ N_{3,x}(\xi_M) & N_{3,y}(\xi_M) & N_{4,x}(\xi_M) & N_{4,y}(\xi_M) \end{bmatrix}_{M\times 8} \tag{7.16.11b}$$

The generalized diffusion matrix for stress is

$$D_{IJ} = \int_\Omega \bar{N}_I^s c_{k,k} N_J^s d\Omega$$

or

$$\mathbf{D} = \begin{bmatrix} c_{k,k}(\xi_1) & & & \\ & c_{k,k}(\xi_2) & & \\ & & \ddots & \\ & & & c_{k,k}(\xi_M) \end{bmatrix}_{M\times M} \tag{7.16.11c}$$

The generalized stress vector is

$$z_{ijI} = \int_\Omega \bar{N}_I^s \{C_{ijkl} D_{kl} + \tau_{kj} W_{ik} + \tau_{ki} W_{jk}\} d\Omega$$

or

$$\mathbf{z} = \begin{bmatrix} (C_{ijkl}D_{kl} + \tau_{kj}W_{ik} + \tau_{ki}W_{jk})_{\xi_1} \\ (C_{ijkl}D_{kl} + \tau_{kj}W_{ik} + \tau_{ki}W_{jk})_{\xi_2} \\ \vdots \\ (C_{ijkl}D_{kl} + \tau_{kj}W_{ik} + \tau_{ki}W_{jk})_{\xi_M} \end{bmatrix}_{M\times 1} \tag{7.16.11d}$$

7.16.2.3. Stress Update Procedure for Operator Split Method:

In addition to the methods shown in the last section to solve the fully coupled equations, another approach referred to as an operator split is an alternative way to apply FEM to solve this problem numerically(Benson, 1989). Conceptually, the approach is simple. "Splitting" stands for "decomposing" a set of PDE operators into several sets of simple PDE operators which will be solved sequentially. An operator split decouples the various physical phenomena in the governing equations to obtain simpler equations to be solved more easily. In exchange of certain loss of accuracy, the operator split offers a generic advantage: simpler equations leads to simpler and stable algorithms, specifically designed for each decoupled equation according to the different physical characteristics.

To illustrate the operator split concept, we consider the transport equation of one component of the Cauchy stress by:

$$\sigma_{,t[\mathbf{X}]} = \sigma_{,t[\chi]} + c_i\sigma_{,i} = q \tag{7.16.12}$$

where the expression of q will be determined by the constitutive law. An example of q is the right hand of Eq.(7.16.1h).
The operator split technique is to split Eq.(7.16.12) into 2 phases. The first phase of the operator split is to solve a Lagrangian step without considering the convective effect as below:

$$\sigma_{,t[\chi]} = q \tag{7.16.13}$$

In this Lagrangian phase, it is integrated in time to update stresses from $\sigma^{(t)}$ (stress at time t) to $\sigma^{(L)}$ (denotation of the Lagrangian updated stress), neglecting the convective terms which is equivalent to assuming that mesh points χ move with material particles $\mathbf{X}$, that is $\chi = \mathbf{X}$. Thus this Lagrangian phase can proceed in the same way as the usual Updated Lagrangian procedure. In addition, it is well known that the stresses are obtained at Gauss points.
The second phase is to deal with the convective term that has not been taken into account during the Lagrangian phase, where the governing PDE is :

$$\sigma_{,t[\chi]} + c_i\sigma_{,i} = 0 \tag{7.16.14}$$

and during which phase, the stresses are updated from $\sigma^{(L)}$ to $\sigma^{(t+\Delta t)}$.
According to the two phases strategy above, the constitutive equation is split into the parabolic equation of the Lagrangian phase and the hyperbolic equation of the convection phase.
Here, we follow [12] to apply explicit methods to integrate the convection equation. To compute gradients of the stress fields on the surface of elements, two different approaches

have been taken: i) use an explicit smoothing procedure (Lax-Wendroff update); or (ii) use an algorithm that circumvents the computation of the stress gradient (Godunov-like technique).

(1) Lax-Wendroff update:
The key point of the Lax-Wendroff method is to replace the time derivatives of depending variables with spatial derivatives using the governing equations. For the partial differential equations of Eq.(7.16.14), we have:

$$\sigma^{(L)}_{,t[\chi]} = -c_i^{(t+\Delta t/2)}\sigma^{(L)}_{,i} \tag{7.16.15a}$$

and

$$\begin{aligned}\sigma^{(L)}_{,tt[\chi]} &= (\sigma^{(L)}_{,t[\chi]})_{,t} = -(c_i^{(t+\Delta t/2)}\sigma^{(L)}_{,i})_{,t} = -c_i^{(t+\Delta t/2)}(\sigma^{(L)}_{,t[\chi]})_{,i} \\ &= -c_i^{(t+\Delta t/2)}(-c_j^{(t+\Delta t/2)}\sigma^{(L)}_{,j})_{,i} = c_i^{(t+\Delta t/2)}c_j^{(t+\Delta t/2)}\sigma^{(L)}_{,ij}\end{aligned} \tag{7.16.15b}$$

After substituting the above two equations into the Taylor series expansion of $\sigma^{(t+\Delta t)}$ with respect to the time:

$$\sigma^{(t+\Delta t)} = \sigma^{t} + \sigma^{(L)}_{,t[\chi]}\Delta t + \frac{1}{2}\sigma^{(L)}_{,tt[\chi]}\Delta t^2 \tag{7.16.16a}$$

we obtain the update equation of the Lax-Wendroff method as:

$$\sigma^{(t+\Delta t)} = \sigma^{t} - c_i^{(t+\Delta t/2)}\sigma_i^{(L)}\Delta t + \frac{1}{2}c_i^{(t+\Delta t/2)}c_j^{(t+\Delta t/2)}\sigma^{(L)}_{,ij}\Delta t^2 \tag{7.16.16b}$$

where $c_i^{(t+\Delta t/2)}$ is the convective velocity evaluated at the mid-step.
In Eq. (7.16.16b), both the stress gradient, which will be denoted by γ, and its spatial derivatives are required. To obtain the gradient in Eq.(7.16.16b), a classical least-squares project is employed to obtain a smoothed field of stress gradient. Via divergence theorem, we have

$$\int_\Omega N^\gamma \gamma d\Omega = -\int_\Omega \sigma \quad N^\gamma d\Omega + \int_\Gamma N^\gamma \sigma n d\Gamma \tag{7.16.17}$$

where n is the outward unit normal in the current configuration. After the regular assembling procedure, we obtain the linear set of equations:

$$\mathbf{M}^\gamma \gamma = \Phi \tag{7.16.18}$$

where $\mathbf{M}^\gamma$ is a consistent pseudo-mass matrix defined as:

$$\mathbf{M}^\gamma = [M^\gamma_{IJ}] = \int_\Omega N^\gamma_I N^\gamma_J d\Omega \tag{7.16.19a}$$

γ is the vector of nodal smoothed values of the stress gradient, and the vector Φ is defined as:

$$\Phi = [\Phi_I] = \sum_e \left[-\int_\Omega \sigma \quad \mathbf{N}^\gamma_I d\Omega + \int_\Gamma \mathbf{N}^\gamma_I \sigma \mathbf{n} d\Gamma \right] \tag{7.16.19b}$$

To make the algorithm explicit, the lumped mass matrix is preferred instead of consistent one. After doing so, the solution of stress gradient of γ can be achieved straightforward. Then Eq.(7.16.16) can be solved. To obtain the stress value at Gauss points, the collocation technique can be applied to handle the weak form of Eq.(7.16.16).

(2) Godunov-like update:
In this phase, the convection equation of :

$$\sigma_{,t[\chi]} + c_i \sigma_{,i} = 0 \tag{7.16.20}$$

will be solved. With the help of the stress-velocity product $Y = \sigma c$, Eq.(7.16.20) can be rewritten as:

$$\sigma_{,t[\chi]} + Y_{i,i} = \sigma c_{i,i} \tag{7.16.21}$$

To apply Godunov method, the weak form is presented

$$\int_\Omega \delta\sigma \sigma_{,t[\chi]} d\Omega = \int_\Omega \delta\sigma \sigma c_{i,i} d\Omega - \int_{\Gamma^t} \delta\sigma Y_i n_i d\Gamma \tag{7.16.22}$$

where the test functions $\delta\sigma$ are constant within any single element. Since both σ and $\delta\sigma$ are constants within an element e , Eq.(7.16.22) results in

$$\sigma_{,t[\chi]} = -\frac{1}{2\Omega} \sum_{s=1}^{N_s} f_s (\sigma_s^c - \sigma)[1 - sign(f_s)] \tag{7.16.23}$$

with the upwind consideration, where the element e has volume Ω and N_s faces, σ_s^c is the stress component in the contiguous element across face s, and f_s is the flux of convective velocity c across face s,

$$f_s = \int_s c_i n_i ds . \tag{7.16.24}$$

To apply the Godunov update to the situation of multi-point quadrature, we can divide every finite element into various subelements, each of them corresponding to the influence domain of a Gauss point. In every subelement, σ is assumed to be constant, and represented by the Gauss-point value. Because of this , σ is a piece wise constant filed with respect to the mesh of subelements, and Eq.(7.16.24) can be integrated to update the value of σ for each subelement.

7.16.3 Stress Update Procedures in 1-D Case:

In this section, we will compare the performance of different update procedure. Below, we will emphasize on the stress update. For illustrative purposes, we consider one-dimensional(1-D) case. In a 1-D case, the shape functions and the corresponding test functions for density, velocity, energy and stress-velocity product may be chosen to be the piecewise linear C^0 functions such that

$$N_1 = \frac{1}{2}(1 - \xi) \tag{7.16.25a}$$

$$N_2 = \frac{1}{2}(1 + \xi) \tag{7.16.25b}$$

where $\xi \in [-1,1]$, while the functions for deviatoric stress and pressure can be C^{-1}, or in particular, constant in each element. The test and trial functions for all variables are identical. The full upwind method can be applied for all the matrices involving convection effects.
For a uniform mesh when the 1-D rod is divided into M segments of equal size of h, where the elements and the nodes are numbered sequentially from *1* to M and $M+1$, respectively. Let c_m designate the convective velocity at node m and s_m the stress in element m. For simplicity, all the nodal convective velocities are considered to be positive.

7.16.3.1 Application of SUPG in 1-D Case:

The stress update is according to Eq.(7.16.7e). The matrices and vectors appeared in Eq.(7.16.7e) are as the following.

The generalized mass matrix is:

$$\mathbf{M}^s = h\begin{bmatrix} 1 & & & \\ & \ddots & & \\ & & 1 & \\ & & & 1 \end{bmatrix}_{M\times M} \tag{7.16.26a}$$

The transpose of the divergence operator matrix is

$$\mathbf{G}^T = \begin{bmatrix} -1 & 1 & & & \\ & \ddots & \ddots & & \\ & & -1 & 1 & \\ & & & -1 & 1 \end{bmatrix}_{M\times(M+1)} \tag{7.16.26b}$$

The matrix $\mathbf{M}^y$ is diagonal by locating the integration points at the nodes

$$diag(\mathbf{M}^y) = h\{\tfrac{1}{2},1,\cdots,1,\cdots 1,\tfrac{1}{2}\}^T_{(M+1)\times 1} \tag{7.16.26c}$$

The transport of stress vector is

$$\mathbf{L}^y\mathbf{s} = \tfrac{1}{6}h\{(2c_1+c_2)s_1,\cdots,(c_{m-1}+2c_m)s_{m-1}+(2c_m+c_{m+1})s_m,\cdots, (c_M+2c_{M+1})s_M\}^T_{(M+1)\times 1} \tag{7.16.26d}$$

if exact integration is used;
or

$$\mathbf{L}^y\mathbf{s} = \tfrac{1}{2}h\{0,\cdots,(c_m+c_{m+1})s_m,\cdots,(c_M+c_{M+1})s_M\}^T_{(M+1)\times 1} \tag{7.16.26e}$$

if full upwind is used, where $1 < m < M$ hereafter.

The generalized diffusion vector is

$$\mathbf{Ds} = \{(-c_1 + c_2)s_1, \cdots, (-c_m + c_{m+1})s_m, \cdots, (-c_M + c_{M+1})s_M\}^T_{M\times 1} \tag{7.16.26f}$$

and the rate of change of stress due to material deformation (the rotation of stress vanishes in 1-D case) is

$$\mathbf{z} = h\{\dot{s}_1, \cdots, \dot{s}_m, \cdots, \dot{s}_M\}^T_{M\times 1} \tag{7.16.26g}$$

where $\dot{s} = C_{1111}v_{(1,1)}$

By substituting Eqs.(7.16.12a-g) into Eq.(7.16.7e), the rate of change of stress in ALE description can be shown to be:

$$\begin{Bmatrix} s_{1,[\chi]} \\ \vdots \\ s_{m,[\chi]} \\ \vdots \\ s_{M,[\chi]} \end{Bmatrix}_{t,[\chi]=} = \frac{1}{h}\begin{Bmatrix} (-c_1 + c_2)s_1 \\ \vdots \\ (-c_m + c_{m+1})s_m \\ \vdots \\ (-c_M + c_{M+1})s_M \end{Bmatrix} - \frac{1}{6h}\begin{Bmatrix} (-3c_1)s_1 + (2c_2 + c_3)s_2 \\ \vdots \\ -(c_{m-1} + 2c_m)s_{m-1} \\ -(c_m - c_{m+1})s_m \\ +(2c_{m+1} + c_{m+2})s_{m+1} \\ \vdots \\ -(c_{M-1} + 2c_M)s_{M-1} \\ +3c_{M+1}s_M \end{Bmatrix} + \begin{Bmatrix} s_{1,[\mathbf{x}]} \\ \vdots \\ s_{m,[\mathbf{x}]} \\ \vdots \\ s_{M,[\mathbf{x}]} \end{Bmatrix}$$

(7.16.27a)

if exact integration is used;
or

$$\begin{Bmatrix} s_{1,[\chi]} \\ \vdots \\ s_{m,[\chi]} \\ \vdots \\ s_{M,[\chi]} \end{Bmatrix}_{t,[\chi]=} = \frac{1}{h}\begin{Bmatrix} (-c_1 + c_2)s_1 \\ \vdots \\ (-c_m + c_{m+1})s_m \\ \vdots \\ (-c_M + c_{M+1})s_M \end{Bmatrix} - \frac{1}{2h}\begin{Bmatrix} (-c_1 + c_2)s_1 \\ \vdots \\ (-c_{m-1} + c_m)s_{m-1} \\ +(c_m + c_{m+1})s_m \\ \vdots \\ -(c_{M-1} + c_M)s_{M-1} \\ +2(c_M + c_{M+1})s_M \end{Bmatrix} + \begin{Bmatrix} s_{1,[\mathbf{x}]} \\ \vdots \\ s_{m,[\mathbf{x}]} \\ \vdots \\ s_{M,[\mathbf{x}]} \end{Bmatrix} \tag{7.16.27b}$$

if full upwind is used to evaluate $\mathbf{L}^y\mathbf{s}$.

The second bracket on the right-hand side of Eq.(7.16.27a) shows the central differencing (or simple averaging) effects for the transport of stresses, while Eq.(7.16.27b) exhibits the donor-cell differencing. This can be further clarified by letting

$$c_1 = \cdots = c_m = \cdots = c_{M+1} = c(constant),$$

then

$$\mathbf{s}_{t,[\chi]=}\begin{Bmatrix} s_{1,[\chi]} \\ \vdots \\ s_{m,[\chi]} \\ \vdots \\ s_{M,[\chi]} \end{Bmatrix}_{M\times 1} = -\frac{c}{2h}\begin{Bmatrix} -s_1 + s_2 \\ \vdots \\ -s_{m-1} + s_{m+1} \\ \vdots \\ -s_{M-1} + s_M \end{Bmatrix} + \begin{Bmatrix} s_{1,[\mathbf{x}]} \\ \vdots \\ s_{m,[\mathbf{x}]} \\ \vdots \\ s_{M,[\mathbf{x}]} \end{Bmatrix} \tag{7.16.28a}$$

if exact integration is used; and

$$\mathbf{s}_{t,[\chi]=}\begin{Bmatrix} s_{1,[\chi]} \\ \vdots \\ s_{m,[\chi]} \\ \vdots \\ s_{M,[\chi]} \end{Bmatrix}_{M\times 1} = -\frac{c}{h}\begin{Bmatrix} s_1 \\ \vdots \\ -s_{m-1} + s_m \\ \vdots \\ -s_{M-1} + 2s_M \end{Bmatrix} + \begin{Bmatrix} s_{1,[\mathbf{x}]} \\ \vdots \\ s_{m,[\mathbf{x}]} \\ \vdots \\ s_{M,[\mathbf{x}]} \end{Bmatrix} \tag{7.16.28b}$$

if full upwind is used.
Eq.(7.16.28a) shows that the transport of the stresses at odd and even elements tends to be decoupled, therefore physically unrealistic oscillations would be expected when the simple averaging method is employed to evaluate the spatial derivatives of stresses.

7.16.3.2. Application of Operator Split in 1D Case:

Also, for illustrative purposes, a 1D rod is considered which is divided into M segments of equal size of h and assume:

$$c_1 = \cdots = c_m = \cdots c_{M+1} = c(constant) > 0\,,$$

(1) Lax-Wendroff update:

We can see that this procedure of update will not work for constant stress and linear shape function since the RHS of Eq.(7.16.19) will be zero. In addition, we can see that for Lax-Wendroff update, the shape function of $\mathbf{s}$, $\mathbf{N}^s$, must be in the same order as $\mathbf{N}^y$. Assuming both of them are linear shape functions, we can obtain:

$$diag(\mathbf{M}^y) = h\{\tfrac{1}{2},1,\cdots,1,\cdots 1,\tfrac{1}{2}\}^T_{(M+1)\times 1} \tag{7.16.29a}$$

$$\Phi = \frac{1}{2}[-s_1 + s_2, -s_1 + s_3, -s_2 + s_4, \cdots, -s_{m-1} + s_{m+1}, \cdots -s_{M-1} + s_{M+1}]^T_{(M+1)\times 1}$$

(7.16.29b)

(2) Godunov-like update:
For constant stress and linear shape function, it is easy to obtain the update equation for element *n*

$$s_n^{(t+\Delta t)} = s_n^{(t)} - \frac{c\Delta t}{h}(s_n^{(t)} - s_{n-1}^{(t)}) + \Delta t \dot{s}_n^{(t+\Delta t/2)} \tag{7.16.30}$$

7.16.4 Explicit Time Integration Algorithm:

For simplicity, the coupled equations (7.16.7c-e) will be integrated by an explicit scheme. Lumped mass matrices are used to enhance the computational efficiency. Both predictor-corrector method(Hughes & Liu, 1978) and standard central difference(Huerta & Casadei, 1994) method can be applied here for explicit time integration. Below, $(\,)_n$ and $(\,)_{n+1}$ will denote the matrices at times $t_n = n\Delta t$ and $t_{n+1} = (n+1)\Delta t$ respectively, where Δt is the time increment.

(1) Predictor-corrector method
This kind of predictor-corrector method is similar to the Newmark algorithm. The major difference is that the former algorithm is explicit, while the latter is implicit.

Mass equations:

$$\rho_{,t[\chi]_{n+1}} = -(\mathbf{M}_n^{\rho})^{-1}(\mathbf{L}_n^{\rho}\tilde{\rho}_{n+1} + \mathbf{K}_n^{\rho}\tilde{\rho}_{n+1}) \tag{7.16.31a}$$

$$\tilde{\rho}_{n+1} = \rho_n + (1-\alpha)\Delta t \rho_{,t[\chi]_n} \tag{7.16.31b}$$

$$\rho_{n+1} = \tilde{\rho}_{n+1} + \alpha\Delta t \rho_{,t[\chi]_{n+1}} \tag{7.16.31c}$$

Momentum equations:

$$\mathbf{v}_{,t[\chi]_{n+1}} = (\mathbf{M}_n)^{-1}(\mathbf{f}_{n+1}^{ext} - \mathbf{f}_n^{int} - \mathbf{L}_n\tilde{\mathbf{v}}_{n+1}) \tag{7.16.32a}$$

$$\tilde{\mathbf{v}}_{n+1} = \mathbf{v}_n + (1-\gamma)\Delta t \mathbf{v}_{,t[\chi]_n} \tag{7.16.32b}$$

$$\mathbf{v}_{n+1} = \tilde{\mathbf{v}}_{n+1} + \gamma\Delta t \mathbf{v}_{,t[\chi]_{n+1}} \tag{7.16.32c}$$

Eq.(7.16.32a) needs to be used in conjunction with

$$\tilde{\mathbf{d}}_{n+1} = \mathbf{d}_n + \Delta t \mathbf{v}_n + (\frac{1}{2} - \beta)\Delta t^2 \mathbf{v}_{,t[\chi]_n} \tag{7.16.32d}$$

$$\mathbf{d}_{n+1} = \tilde{\mathbf{d}}_{n+1} + \beta\Delta t^2 \mathbf{v}_{,t[\chi]_{n+1}} \tag{7.16.32e}$$

to calculate the $\mathbf{f}_n^{int}$.
In the above equations, α, β and γ are the computational parameters. For explicit calculations, the following constraints on the parameters are used:

$$\alpha = 0 \tag{7.16.33a}$$

$$\beta = 0 \tag{7.16.33b}$$

$$\gamma \geq \frac{1}{2} \tag{7.16.33c}$$

The flowchart of the computational procedure for the class of pressure-insensitive materials is as follows:

Step 1. Initialization. Set *n=0*, input initial conditions.

Step 2. Time stepping loop, $t \quad [0, t_{\max}]$.

Step 3. Integrate the mesh velocity to obtain the mesh displacement and spatial coordinates.

Step 4. Calculate incremental hydrostatic pressure by integration Eq.(7.16.7e) with $\boldsymbol{s}$ and $\boldsymbol{z}$ replaced by $\boldsymbol{p}$ and $\boldsymbol{u}$ respectively:

(a) the rate of pressure due to convection,

(b) the rate of pressure due to deformation.

Step 5. Calculate incremental deviatoric stresses, yield stresses, and back stresses by integration Eq.(7.16.7e) which stress update procedures have been discussed in detail in last section:

(a) the rate of stresses due to convection,

(b) the rate of stresses due to rotation,

(c) the rate of stresses due to deformation.

Step 6. Compute the internal force vector.

Step 7. Compute the acceleration by the equations of motion, Eq.(7.16.32a).

Step 8. Compute the density by the equation of mass conservation, Eq.(7.16.31a).

Step.7. Integrate the acceleration to obtain the velocity.

Step 10. If $(n+1)\Delta t > t_{\max}$, stop; otherwise, replace *n* by *n+1* and go to Step 2

(2) Central difference method

The central difference can also be applied for the time integration. Same as the standard central difference procedure, we can obtain displacement and acceleration vectors at each *i* time step, while get velocity vector at each $i+\frac{1}{2}$ time step. The momentum equation will be integrated as an example to illustrate this explicit scheme.

After obtaining the velocity vector at $(n-\frac{1}{2})\Delta t$ and the displacement vector at $n\Delta t$, the acceleration vector at $n\Delta t$ is :

$$\mathbf{v}_{,t[\chi]_n} = (\mathbf{M}_n)^{-1}(\mathbf{f}_n^{ext} - \mathbf{f}_n^{int} - \mathbf{L}_{n-\frac{1}{2}}\mathbf{v}_{n-\frac{1}{2}})$$

With central difference scheme, the velocity and displacement of next time step are:

$$\mathbf{v}_{n+\frac{1}{2}} = \mathbf{v}_{n-\frac{1}{2}} + \Delta t \mathbf{v}_{,t[\chi]_n}$$

and

$$\mathbf{d}_{n+1} = \mathbf{d}_n + \Delta t \mathbf{v}_{n+\frac{1}{2}}$$

For operator splitting update, the Lagrangian part for strains is calculated with a usual central difference scheme as:

$$\varepsilon(t\ ) = \varepsilon_n + \Delta t \dot{\varepsilon}^{(L)}_{,t[\mathbf{x}]_{n+\frac{1}{2}}}$$

where

$$\dot{\varepsilon}^{(L)}_{,t[\mathbf{x}]_{n+\frac{1}{2}}} = (\mathbf{v}_{,x})_{n+\frac{1}{2}}$$

After considering the Godunov scheme for the convect part, the full upwind integration for 1D 2-node element can be written as:

$$\varepsilon_{n+1} = \varepsilon(t\ ) - \frac{\Delta t}{h}[c_1 \frac{1+sign(c_1)}{2}(\varepsilon_e - \varepsilon_{e-1}) + c_2 \frac{1-sign(c_2)}{2}(\varepsilon_{e+1} - \varepsilon_e)]$$

For elastic-plastic problem, the radial return method can be used to determine the correct states of stress and strain.

7.10 ALE Governing Equation

7.10.1 Slightly Compressible Viscous Flow with Moving Boundary Problem

In this section, we develop the governing equations for a slightly compressible Newtonian fluid. In a generalized Newtonian fluid, the stress is a function of the rate-of-deformation. Therefore, the stress is independent of the history of deformation. The most well known case is a linear Newtonian fluid, where the stress is a linear function of the rate-of-deformation.

This class of materials simplifies the implementation since the constitutive equation is independent of the strain history. Therefore, the constitutive equation can be used in its strong form.

The formulation is restricted to isothermal processes; therefore energy equation is not needed. The continuity equation (7.7.15), momentum equation (7.7.25) and the mesh update equation (7.2.19) in ALE description are:

$$\left.\frac{\partial \rho}{\partial t}\right|_{\chi} + c_i \frac{\partial \rho}{\partial x_i} + \rho \frac{\partial v_i}{\partial x_i} = 0 \tag{7.10.1a}$$

$$\rho \left.\frac{\partial v_i}{\partial t}\right|_{\chi} + \rho c_j \frac{\partial v_i}{\partial x_j} = \frac{\partial \sigma_{ij}}{\partial x_j} + \rho b_i \tag{7.10.1b}$$

$$\frac{\partial x_i}{\partial \chi_j} w_j = c_i \tag{7.10.1c}$$

In the constitutive equation, the hydrostatic stress is independent of deformation while the shear stress, which depend on the rate of deformation.

$$\sigma_{ij} = -p\delta_{ij} + 2\mu D_{ij} \tag{7.10.1d}$$

where

$$D_{ij} = \frac{1}{2}\left(\frac{\partial v_i}{\partial x_j} + \frac{\partial v_j}{\partial x_i}\right) \text{ and } \mu = \mu(D_{ij}) \tag{7.10.1e}$$

where μ is the dynamic viscosity which is shear rate dependent. The functions μ for generalized Newtonian models are presented in Table 7.2.

Model	1-D Viscosity	3-D Generalization
Newtonian	$\mu_0 = constant$	$\mathbf{s} = 2\mu_0 \mathbf{D}$
Power Law	$\mu = mD^{n-1}$	$\mathbf{s} = 2m\left[\sqrt{2tr(\mathbf{D})^2}\right]^{n-1}\mathbf{D}$

Truncated Power Law	if $D \le D_0$
	$\mu = \mu_0$
	if $D \ge D_0$
	$\mu = \mu_0 (\frac{D}{D_0})^{n-1}$
		if $\sqrt{2tr(\mathbf{D})^2} \le D_0$:
		$\mathbf{s} = 2\mu_0 \mathbf{D}$
		if $\sqrt{2tr(\mathbf{D})^2} \ge D_0$:
		$\mathbf{s} = 2\mu_0 \left[\frac{\sqrt{2tr(\mathbf{D})^2}}{\dot{\gamma}_0}\right]^{n-1}\mathbf{D}$

Carreau	$\frac{\mu - \mu_\infty}{\mu_0 - \mu_\infty} = \left[1 + (\lambda D)^2\right]^{(n-1)/2}$	$\mathbf{s} = 2\mu_\infty \mathbf{D}$ $+2(\mu_0 - \mu_\infty)\left[1 + 2\lambda^2 tr(\mathbf{D})^2\right]^{(n-1)/2}\mathbf{D}$
Carreau-A	$\mu_\infty = 0$	$\mathbf{s} = 2\mu_0 \left[1 + 2\lambda^2 tr(\mathbf{D})^2\right]^{(n-1)/2}\mathbf{D}$
Bingham	$\mu = \infty \quad \tau \le \tau_0$ $\mu = \mu_p + \frac{\tau_0}{D} \quad \tau \ge \tau_0$	if $\frac{1}{2}tr(\mathbf{s})^2 \le \tau_0^2$ $\mathbf{s} = \mathbf{0}$ if $\frac{1}{2}tr(\mathbf{s})^2 \ge \tau_0^2$ $\mathbf{s} = 2\mu_p \left[1 + \frac{\tau_0}{\sqrt{2tr(\mathbf{D})^2}}\right]\mathbf{D}$
where $\mathbf{s}$ and $\mathbf{D}$ are the deviatoric part of the stress and stretch tensors, respectively		

Table 7.2

We will first consider a viscous, barotropic fluid, so that the pressure depends only on the density, $p = p(\rho)$. The material time derivative of the pressure p gives:

$$\dot{p} = \frac{\partial p}{\partial \rho}\dot{\rho} \tag{7.10.2a}$$

Now we can define the bulk modules B by:

$$\frac{B}{\rho} = \frac{\partial p}{\partial \rho} \tag{7.10.2b}$$

Using this definition in Eq. (7.10.2a) yields:

$$\dot{p} = \frac{B}{\rho}\dot{\rho} \text{ or } \frac{\dot{\rho}}{\rho} = \frac{\dot{p}}{B} \tag{7.10.2c}$$

Substituting Eq. (7.10.2c) into Eq. (7.10.1a), the continuity equation may be rewritten as (Liu and Ma, 1982):

$$\frac{1}{B}\frac{Dp}{Dt} + \frac{\partial v_i}{\partial x_i} = 0 \tag{7.10.3a}$$

or, by introducing Eq. (7.2.20b) in (7.10.3a), as:

$$\frac{1}{B}\frac{\partial p}{\partial t}\bigg|_{\chi} + \frac{1}{B}c_i\frac{\partial p}{\partial x_i} + \frac{\partial v_i}{\partial x_i} = 0 \tag{7.10.3b}$$

The objective here is to find the density, the material velocity and the mesh velocity by solving Eqs. (7.10.1a-e). Prior to presenting the strong from of the governing equations and boundary conditions, the finite element mesh updating procedure will first be discussed in the next section.

In each Eq (7.10.1) a convective term is present; thus, one of the drawbacks of an Eulerian formulation is retained in the ALE methods. The major advantage of an ALE approach is that it simplifies the treatment moving boundaries and interfaces.

7.11 Mesh Update Equations

7.11.1 Introduction

The option of arbitrarily moving the mesh in the ALE description offers interesting possibilities. By means of ALE, moving boundaries (which are material surfaces) can be tracked with the accuracy characteristic of Lagrangian methods and the interior mesh can be moved so as to avoid excessive element distortion and entanglement. However, this requires that an effective algorithm for updating the mesh, i.e. the mesh velocities $\hat{\mathbf{v}}$, must

be prescribed. The mesh should be prescribed so that mesh distortion is avoided and so that boundaries and interfaces remain at least partially Lagrangian.

In this section, we will describe several procedures for updating the mesh. The material and mesh velocities are related by Eq. (7.2.19); hence, once one of them is determined, the other is automatically fixed. It is important to note that, if $\hat{\mathbf{v}}$ is given, $\hat{\mathbf{d}}$ and $\hat{\mathbf{a}}$ can be computed and there is no need to evaluate **w.** On the other hand, if $\hat{\mathbf{v}}$ is considered the unknown but **w** is given, Eq. (7.2.19) must be solved to evaluate $\hat{\mathbf{v}}$ before updating the mesh. Finally, mixed reference velocities can be given (i.e. a component of $\hat{\mathbf{v}}$ can be prescribed and **w** in the other(s)). Finding the *best* choice for these velocities and an algorithm for updating the mesh constitutes one of the major hurdles in developing an effective implementation the ALE description. Depending on which velocity ($\hat{\mathbf{v}}$ or **w** or mixed) is prescribed, three different cases may be studied.

7.11.2 Mesh Motion Prescribed a Priori

The case where the mesh motion $\hat{\mathbf{v}}$ is given corresponds to an analysis where the domain boundaries are known at every instant. When the boundaries of the fluid domain have a known motion, the mesh movement along this boundary can be prescribed a priori.

7.11.3 Lagrange-Euler Matrix Method

The case where the relative velocity **w** is arbitrarily defined is a format for apropos by Hughes et al (1981). Let **w** be:

$$w_i = \left.\frac{\partial \chi_i}{\partial t}\right|_X = \left(\delta_{ij} - \alpha_{ij}\right) v_j \tag{7.11.1}$$

where δ_{ij} is the Kroneker delta and α_{ij} is the Lagrange-Euler parameter matrix such that $\alpha_{ij} = 0$ if $i \neq j$ and $\alpha_{\underline{ii}}$ is real (underlined indices meaning no sum on them). In general, the α's can vary in space and be time-dependent; however α_{ij} is usually taken as time-independent. According to Eq. (7.11.1) the relative velocity **w** becomes a linear function of the material velocity and it was chosen because, if $\alpha_{ij} = \delta_{ij}$, **w** = **0** and the Lagrangian description is obtained, whereas, if $\alpha_{ij} = 0$, **w** = **v** and the Eulerian formulation is used. The Lagrange-Euler matrix needs to be given once and for all at each grid point.

Since **w** is defined by Eq. (7.11.1), the other velocities are determined by Eq. (7.2.19), which become, respectively.

$$c_i = \frac{\partial x_i}{\partial \chi_j}\left(\delta_{jk} - \alpha_{jk}\right) v_k \tag{7.11.2a}$$

and

$$\hat{v}_i = v_i - \left(\delta_{jk} - \alpha_{jk}\right) v_k \frac{\partial x_i}{\partial \chi_j} \tag{7.11.2b}$$

The latter equations must be satisfied in the referential domain along its boundaries. Substituting Eq. (7.2.8a) into (7.11.2b) yields a basic equation for mesh rezoning:

$$\left.\frac{\partial x_i}{\partial t}\right|_{\chi} + \left(\delta_{jk} - \alpha_{jk}\right) v_k \frac{\partial x_i}{\partial \chi_j} - v_i = 0 \tag{7.11.3}$$

The explicit form of Eq. (7.11.3) in 1D, 2D and 3D are listed:

1D Form

$$\left.\frac{\partial x}{\partial t}\right|_{\chi} + (1-\alpha) v \frac{\partial x}{\partial \chi} - v = 0 \tag{7.11.4}$$

2D Form

$$\left.\frac{\partial x_1}{\partial t}\right|_{\chi} + (1-\alpha_{11}) v_1 \frac{\partial x_1}{\partial \chi_1} + (1-\alpha_{22}) v_2 \frac{\partial x_1}{\partial \chi_2} - v_1 = 0 \tag{7.11.5a}$$

$$\left.\frac{\partial x_2}{\partial t}\right|_{\chi} + (1-\alpha_{11}) v_1 \frac{\partial x_2}{\partial \chi_1} + (1-\alpha_{22}) v_2 \frac{\partial x_2}{\partial \chi_2} - v_2 = 0 \tag{7.11.5b}$$

3D Form

$$\left.\frac{\partial x_1}{\partial t}\right|_{\chi} + (1-\alpha_{11}) v_1 \frac{\partial x_1}{\partial \chi_1} + (1-\alpha_{22}) v_2 \frac{\partial x_1}{\partial \chi_2} + (1-\alpha_{33}) v_3 \frac{\partial x_1}{\partial \chi_3} - v_1 = 0 \tag{7.11.6a}$$

$$\left.\frac{\partial x_2}{\partial t}\right|_{\chi} + (1-\alpha_{11}) v_1 \frac{\partial x_2}{\partial \chi_1} + (1-\alpha_{22}) v_2 \frac{\partial x_2}{\partial \chi_2} + (1-\alpha_{33}) v_3 \frac{\partial x_2}{\partial \chi_3} - v_2 = 0 \tag{7.11.6b}$$

$$\left.\frac{\partial x_3}{\partial t}\right|_{\chi} + (1-\alpha_{11}) v_1 \frac{\partial x_3}{\partial \chi_1} + (1-\alpha_{22}) v_2 \frac{\partial x_3}{\partial \chi_2} + (1-\alpha_{33}) v_3 \frac{\partial x_3}{\partial \chi_3} - v_3 = 0 \tag{7.11.6c}$$

Remark 1:

Equation (7.11.3) differs only in its last term from the one proposed by Hughes et al (1981). This difference is not noticeable if the Lagrange-Euler parameters α_{ij} are chosen equal to zero or one. Moreover, Eq. (7.11.3) includes the Jacobian matrix (i.e. $\partial x_i / \partial \chi_j$) that is missing in the Liu and Ma (1982) formulation. Finally, Eq. (7.11.3) is a transport equation without any diffusion so the classic numerical difficulties associated with transport equations are expected.

The ALE technique with a mesh update based on the Lagrange-Euler parameters is very useful in surface wave problems. We assume that the free surface is oriented relative to the global coordinates so that it can be written as $x_{3s} = x_{3s}(x_1, x_2, t)$. An Eulerian description used in the x_1 and x_2 directions (i.e. $x_1 = \chi_1$ and $x_2 = \chi_2$). The free surface is defined by one spatial coordinate which is a continuous and differentiable function of the other two spatial coordinates and time. In this case the Lagrange Euler matrix has only one non-zero term, α_{33} (usually equal to 1), and the only non-trivial equation in (7.11.3) is:

$$\left.\frac{\partial x_{3s}}{\partial t}\right|_{\chi} + v_1 \frac{\partial x_{3s}}{\partial \chi_1} + v_2 \frac{\partial x_{3s}}{\partial \chi_2} - v_3 = (\alpha_{33} - 1) v_3 \frac{\partial x_{3s}}{\partial \chi_3} \tag{7.11.7}$$

The above equation is easily recognized as the kinematics equation of the surface and may be written as:

$$\left.\frac{\partial x_{3s}}{\partial t}\right|_{\chi} + v_i n_i N_s = a(x_1, x_2, x_{3s}, t) \tag{7.11.8}$$

where the components of **n** is the unit normal pointing out from the surface. The components of the normal vector are given by:

$$\frac{1}{N_s}\left(\frac{\partial x_{3s}}{\partial \chi_1}, \frac{\partial x_{3s}}{\partial \chi_2}, -1\right) \tag{7.11.9a}$$

with N_s given by:

$$N_s = \left[1 + \left(\frac{\partial x_{3s}}{\partial \chi_1}\right)^2 + \left(\frac{\partial x_{3s}}{\partial \chi_2}\right)^2\right]^{1/2} = \left[1 + \left(\frac{\partial x_{3s}}{\partial x_1}\right)^2 + \left(\frac{\partial x_{3s}}{\partial x_2}\right)^2\right]^{1/2} \tag{7.11.9b}$$

where $a(x_1, x_2, x_{3s}, t)$ is the so-called accumulation rate function expressing the gain or loss of mass under the free surface (Hutter and Vulliet, 1985). It can be seen by comparing Eq. (7.11.7) and Eq. (7.11.8) that the accumulation rate function is:

$$a(x_1, x_2, x_{3s}, t) = (\alpha_{33} - 1) v_3 \frac{\partial x_{3s}}{\partial \chi_3} = w_3 \frac{\partial x_{3s}}{\partial \chi_2} \tag{7.11.10}$$

The free surface is a material surface; along the free surface the accumulation rate must be zero, and consequently α_{33} has to be taken equal to one. This can also be deduced by noticing that no particles can cross the free surface, so w_3 must be zero. Although Eq. (7.11.3) can be applied to problems where x_1 and/or x_2 are not Eulerian by prescribing non zero α's in these directions, controlling the element shapes by adjusting the α's is very difficult**.**

Control of the mesh by Eq. (7.11.1) has some disadvantages; for instance, while $\hat{\mathbf{v}}$ has a clear physical interpretation (i.e. the mesh velocity), $\mathbf{w}$ is much more difficult to visualize (except in the direction perpendicular to material surfaces, where it is identically zero) and therefore it is very difficult to maintain regular shaped elements inside the fluid domain by just prescribing the α's. Because of this important drawback the mixed formulation introduced by Huerta and Liu, called deformation gradient method, was developed, it is discussed next.

7.11.4 Deformation Gradient Formulations

Noticing the restrictions of the α's scheme, a mixed formulation is developed for the resolution of Eq. (7.2.19). One of the goals of the ALE method is the accurate tracking of the moving boundaries which are usually material surfaces. Hence, along these surfaces we enforce $\mathbf{w} \cdot \mathbf{n} = 0$ where $\mathbf{n}$ is the exterior normal. The other goal of the ALE technique is to avoid element entanglement and this is better achieved, once the boundaries are known, by prescribing the mesh displacements independently (through the potential equations, for instance) or velocities, because both $\hat{\mathbf{d}}$ and $\hat{\mathbf{v}}$ govern directly the element shape. Therefore, one can prescribe $\mathbf{w} \cdot \mathbf{n} = 0$ along the domain boundaries while defining the $\hat{\mathbf{d}}$'s or $\hat{\mathbf{v}}$'s in the interior.

The system of differential equations defined in Eq. (7.2.19) has to be solved along the moving boundaries. Notice first that solving for w_i in terms of $(v_i - \hat{v}_i)$, Eq. (7.2.19) can be rewritten as:

$$c_j \equiv v_j - \hat{v}_j = F^{\chi}_{ji} w_i \tag{7.11.11}$$

Define the Jacobian matrix of the map between the spatial and ALE coordinates by

$$F^{\chi}_{ij} \equiv \frac{\partial x_i}{\partial \chi_j} \tag{7.11.12}$$

Its inverse is:

$$\left(\mathbf{F}^{\chi}\right)^{-1} = \frac{1}{\hat{J}} \begin{bmatrix} \hat{J}_{11} & -\hat{J}_{12} & \hat{J}_{13} \\ -\hat{J}_{21} & \hat{J}_{22} & -\hat{J}_{23} \\ \hat{J}_{31} & -\hat{J}_{32} & \hat{J}_{33} \end{bmatrix} \equiv \frac{\hat{J}_{ij}}{\hat{J}} \tag{7.11.13a}$$

where $\hat{J}_{ij}$ are the cofactors of F^{χ}_{ij}, $\hat{J}$ is the Jacobian already defined in Eq. (7.7.4b) and $\hat{J}^{ij}$ are the minors of the Jacobian matrix F^{χ}_{ij}. Multiplying the inverse Jacobian matrix on both sides of Eq. (7.11.11) and substituting Eq. (7.11.13) into Eq. (7.11.11), yields:

$$\frac{\hat{J}_{ij}}{\hat{J}} v_j - \hat{v}_j = w_i \text{ or } \hat{J}^{ji}(v_j - \hat{v}_j) = \hat{J}\, w_i \tag{7.11.14}$$

Dividing $\hat{J}^{\underline{ii}}$ on both sides of Eqs. (7.11.14), gives:

$$\frac{\hat{J}^{ji}}{\hat{J}^{\underline{ii}}}(v_j - \hat{v}_j) = \frac{\hat{J}}{\hat{J}^{\underline{ii}}} w_i = \begin{cases} \left.\dfrac{\partial x_i}{\partial t}\right|_\chi - v_i & i = j \\ \displaystyle\sum_{\substack{j=1 \\ j\neq i}}^{nsd} \frac{v_j - \hat{v}_j}{\hat{J}^{\underline{ii}}} \hat{J}^{ji} & i \neq j \end{cases} \tag{7.11.15}$$

When the LHS of Eq. (7.11.15) has been simplified using by the definition of $\hat{v}_j$, Eq. (7.2.8a). Substituting Eq. (7.11.16) into Eq. (7.11.15) yields:

$$\left.\frac{\partial x_i}{\partial t}\right|_\chi - v_i - \sum_{\substack{j=1 \\ j\neq i}}^{NSD} \frac{v_j - \hat{v}_j}{\hat{J}^{\underline{ii}}} \hat{J}^{ji} = -\frac{\hat{J}}{\hat{J}^{\underline{ii}}} w_i \tag{7.11.17}$$

Notice that the cofactor $\hat{J}^{\underline{ii}}$ appears in the denominator to account for the motion of the mesh in the plane perpendicular to χ_i because Eqs. (7.11.17) are verified in the reference domain $\hat{\Omega}$, not in the actual deformed domain Ω.

Examples for Eq. (7.11.17) in 1D, 2D and 3D are:

1D

$$\left.\frac{\partial x_1}{\partial t}\right|_{\chi} - v_1 = -\frac{\hat{J}}{\hat{J}^{11}} w_1 \tag{7.11.18}$$

where $\hat{J}^{11} = 1$.

2D

$$\left.\frac{\partial x_1}{\partial t}\right|_{\chi} - v_1 - \frac{v_2 - \hat{v}_2}{\hat{J}^{11}} \hat{J}^{21} = -\frac{\hat{J}}{\hat{J}^{11}} w_1 \tag{7.11.19a}$$

$$\left.\frac{\partial x_2}{\partial t}\right|_{\chi} - v_2 - \frac{v_1 - \hat{v}_1}{\hat{J}^{22}} \hat{J}^{12} = -\frac{\hat{J}}{\hat{J}^{22}} w_2 \tag{7.11.19b}$$

where $\hat{J}^{11} = \dfrac{\partial x_2}{\partial \chi_2}$ and $\hat{J}^{22} = \dfrac{\partial x_1}{\partial \chi_1}$.

3D

$$\left.\frac{\partial x_1}{\partial t}\right|_{\chi} - v_1 - \frac{v_2 - \hat{v}_2}{\hat{J}^{11}} \hat{J}^{21} - \frac{v_3 - \hat{v}_3}{\hat{J}^{11}} \hat{J}^{31} = -\frac{\hat{J}}{\hat{J}^{11}} w_1 \tag{7.11.20a}$$

$$\left.\frac{\partial x_2}{\partial t}\right|_{\chi} - v_2 - \frac{v_1 - \hat{v}_1}{\hat{J}^{22}} \hat{J}^{12} - \frac{v_3 - \hat{v}_3}{\hat{J}^{22}} \hat{J}^{32} = -\frac{\hat{J}}{\hat{J}^{22}} w_2 \tag{7.11.20b}$$

$$\left.\frac{\partial x_3}{\partial t}\right|_{\chi} - v_3 - \frac{v_1 - \hat{v}_1}{\hat{J}^{33}} \hat{J}^{13} - \frac{v_2 - \hat{v}_2}{\hat{J}^{33}} \hat{J}^{23} = -\frac{\hat{J}}{\hat{J}^{33}} w_3 \tag{7.11.20c}$$

For purposes of simplification and without any loss of generality, assume that the moving boundaries are perpendicular to one coordinate axis in the reference domain. Let the free surface be perpendicular to χ_3, the first two equations in Eq. (7.11.17) are trivial because in the direction of χ_1 and χ_2 the mesh velocity is prescribed and therefore the mesh motion is known, but the third one must be solved for $\hat{v}_3$ given w_3, $\hat{v}_1$, and $\hat{v}_2$, it may be written explicitly as:

$$\hat{v}_3 - \frac{\hat{J}^{13}}{\hat{J}^{33}}(v_1 - \hat{v}_1) - \frac{\hat{J}^{23}}{\hat{J}^{33}}(v_2 - \hat{v}_2) - v_3 = -\frac{\hat{J}}{\hat{J}^{33}} w_3 \tag{7.11.21a}$$

or

$$\left.\frac{\partial x_{3s}}{\partial t}\right|_{\chi} - \frac{v_1 - \hat{v}_1}{\hat{J}^{33}}\hat{J}^{13}\left(\frac{\partial x_{3s}}{\partial \chi_1}, \frac{\partial x_{3s}}{\partial \chi_2}\right) - \frac{v_2 - \hat{v}_2}{\hat{J}^{33}}\hat{J}^{23}\left(\frac{\partial x_{3s}}{\partial \chi_1}, \frac{\partial x_{3s}}{\partial \chi_2}\right) - v_3$$

$$= -\frac{w_3}{\hat{J}^{33}}\hat{J}\left(\frac{\partial x_{3s}}{\partial \chi_1}, \frac{\partial x_{3s}}{\partial \chi_2}\right) \tag{7.11.22b}$$

where $\hat{v}_3$ has been substituted by $\left.\frac{\partial x_{3s}}{\partial t}\right|_{\chi}$, $\hat{J}^{13}$, $\hat{J}^{23}$, and the Jacobian $\hat{J}$ are function of $\frac{\partial x_{3s}}{\partial \chi_1}$ and $\frac{\partial x_{3s}}{\partial \chi_2}$: $\hat{J}^{33}$ is not dependent on x_{3s}: and x_{3s} is the free surface equation. In Eq. (7.11.22b) x_{3s} is the unknown function, while $\hat{v}_1$, $\hat{v}_2$ and w_3 are known. If $\hat{v}_1 = \hat{v}_2 = 0$ (i.e. the Eulerian description is used in χ_1 and χ_2), the kinematic surface equation, Eq. (7.11.8), is again obtained. However, with the mixed formulation $\hat{v}_1$ and $\hat{v}_2$ can be prescribed (as a percentage of the wave celerity, for instance) and therefore better numerical results are obtained than by defining in Eq. (7.11.7) α_{11} and α_{22}, whose physical interpretation is much more obscure.

7.11.5 Automatic Mesh Generation

The Laplacian method for remeshing is based on mapping the new position of the nodes by solutions of the Laplace equation space (I, J) into real space (x, y) through solving the Laplace differential equation is the most commonly use one.

The determination of the nodes is posed as finding $x(I, J)$ and $y(I, J)$, such that they satisfy the following equations

$$L^2(x) = \frac{\partial^2 x}{\partial I^2} + \frac{\partial^2 x}{\partial J^2} = 0;\ L^2(y) = \frac{\partial^2 y}{\partial I^2} + \frac{\partial^2 y}{\partial J^2} = 0 \qquad \text{in } \Omega_x \tag{7.11.23a}$$

The boundary conditions in two dimension are

$$x(I, J) = \bar{x}(I, J);\ y(I, J) = \bar{y}(I, J) \qquad \text{in } \Gamma_x \tag{7.11.23b}$$

Here $x(I)$ and $y(J)$ are the coordinates of nodes I and J when I and J take on integer values. Ω and Γ are the domain and boundary of the remesh region and L^2 is the second-order differential operator.

Another useful mesh generation scheme is by solving a fourth order differential equation

$$L^4(x) = \frac{\partial^4 x}{\partial I^2 \partial J^2};\ L^4(y) = \frac{\partial^4 x}{\partial I^2 \partial J^2} \tag{7.11.24}$$

Eqs. (7.11.23) and (7.11.24) can be solved by the finite difference method with a Gauss-Seidel iteration scheme. Meshes generated by the Laplace equation are distorted near the boundary where a high curvature occurs. However, the fourth-order equation gives a better mesh shape, because a higher differentiation is employed. An equipotential method regards the mesh lines as two intersecting sets of equipotentials, with each set satisfying Laplace's equation in the interior with adequate boundary condition.

7.12 Strong Form, Governing Equations of Slightly Compressible Viscous Flow with Moving Boundary Problem

The object here is to find the following functions:

$v(x,t)$ = velocity, $p(x,t)$ = pressure fields, $\hat{x}(x,t)$ = mesh displacement (7.12.1c)

such that they satisfy the following state and field equations:

Continuity Equation [Eq. (7.10.3b)]

$$\frac{1}{B}\frac{\partial p}{\partial t}\bigg|_{\chi} + \frac{1}{B}c_i\frac{\partial p}{\partial x_i} + \frac{\partial v_i}{\partial x_i} = 0 \tag{7.12.2a}$$

Momentum Equation [Eq. (7.10.1b)]

$$\rho\frac{\partial v_i}{\partial t}\bigg|_{\chi} + \rho c_j\frac{\partial v_i}{\partial x_j} = \frac{\partial \sigma_{ij}}{\partial x_j} + \rho g_i \tag{7.12.2b}$$

Free Surface Update Equation

We can employ either mesh rezoning equation [Eq. (7.11.3)]:

$$\frac{\partial x_i}{\partial t}\bigg|_{\chi} + \left(\delta_{jk} - \alpha_{jk}\right)v_k\frac{\partial x_i}{\partial \chi_j} - v_i = 0 \tag{7.12.2c}$$

or the mesh updating equation [Eq. (7.11.17)]:

$$\frac{\partial x_i}{\partial t}\bigg|_{\chi} - v_i - \sum_{\substack{j=1\\ j\neq 1}}^{NSD}\frac{v_j - \hat{v}_j}{\hat{J}^{ii}}\hat{J}^{ji} = -\frac{\hat{J}}{\hat{J}^{ii}}w_i \tag{7.12.2d}$$

The boundary conditions are as follows. It is required that:

$$v_i = \bar{v}_i \qquad \text{on } \Gamma_i^v \tag{7.12.3}$$

$$\sigma_{ij}n_j = \bar{t}_i \qquad \text{on } \Gamma_i^t \tag{7.12.4}$$

where b and h are the prescribed boundary velocities and tractions, respectively; n is the outward normal to Γ_i^v, and Γ_i^v is the piecewise smooth boundary of the spatial domain, Ω and the decomposition of Γ is given in Chapter 3.

Constitutive Equation

$$\sigma_{ij} = -p\delta_{ij} + 2\mu D_{ij} \tag{7.12.5a}$$

where

$$D_{ij} = \frac{1}{2}\left(\frac{\partial v_i}{\partial x_j} + \frac{\partial v_j}{\partial x_i}\right) \quad \text{and} \quad \mu = \mu(D_{ij}) \tag{7.12.5b}$$

μ is the dynamic viscosity which is shear rate dependent. In Table 7.2 several Generalized Newtonian models (see e.g. Bird et al, 1977) are presented. The finite element method presented here is independent of the particular Generalized Newtonian model chosen.

7.13 Weak Form of Slightly Compressible Viscous Flow with Moving Boundary Problem

We denote the spaces of the test function and trial functions by:

$$\delta v_i \quad U_0^v \quad U_0^v = \left\{\delta v_i | \delta v_i \quad C^0, \delta v_i = 0 \text{ on } \Gamma_i^v\right\} \qquad \text{(test function)} \tag{7.13.1a}$$

$$v_i \quad U^v \quad U^v = \left\{v_i | v_i \quad C^0, v_i = \bar{v}_i \text{ on } \Gamma_i^v\right\} \qquad \text{(trial function)} \tag{7.13.1b}$$

To establish the weak form of the momentum equation, Eq. (7.12.2b), we take the inner product of the momentum equation, Eq. (7.12.2b), with a test function δv_i and integrate over the spatial region, that is:

$$\int_\Omega \delta v_i \rho \left.\frac{\partial v_i}{\partial t}\right|_\chi d\Omega + \int_\Omega \delta v_i \rho c_j \frac{\partial v_i}{\partial x_j} d\Omega - \int_\Omega \delta v_i \frac{\partial \sigma_{ij}}{\partial x_j} d\Omega - \int_\Omega \delta v_i \rho g_i d\Omega = 0 \tag{7.13.2}$$

It is noticed that the stresses in Eq. (7.13.2) are functions of the velocities. Applying integration by parts on the stress term yields:

$$\int_\Omega \delta v_i \frac{\partial \sigma_{ij}}{\partial x_j} d\Omega = \int_\Omega \frac{\partial}{\partial x_j}(\delta v_i \sigma_{ij}) d\Omega - \int_\Omega \frac{\partial(\delta v_i)}{\partial x_j} \sigma_{ij} d\Omega \tag{7.13.3}$$

By the Gauss divergence theorem, the first term in the RHS of Eq. (7.13.3) can be written as a boundary integral, which is:

$$\int_\Omega \frac{\partial}{\partial x_j}(\delta v_i \sigma_{ij})\, d\Omega = \int_{\Gamma^t} \delta v_i\, (n_j \sigma_{ij})\, d\Gamma \tag{7.13.4}$$

Substituting the specified boundary condition defined in Eq. (7.12.3b) into Eq. (7.13.4) gives:

$$\int_{\Gamma^t} \delta v_i\, (n_j \sigma_{ij})\, d\Gamma = \int_{\Gamma^t} \delta v_i \bar{t}_j\, d\Gamma \tag{7.13.5}$$

The second term in the RHS of Eq. (7.13.3) can be further expressed by using the definition of the constitutive equation, Eq. (7.12.5a). That gives:

$$\int_\Omega \frac{\partial(\delta v_i)}{\partial x_j}\sigma_{ij}\, d\Omega = \int_\Omega \frac{\partial(\delta v_i)}{\partial x_j}\left[-p\delta_{ij} + 2\mu D_{ij}\right] d\Omega$$

$$= -\int_\Omega \frac{\partial(\delta v_i)}{\partial x_i}\, p\, d\Omega + \int_\Omega \frac{\partial(\delta v_i)}{\partial x_i}\, 2\mu D_{ij}\, d\Omega \tag{7.13.6}$$

We now may use the decomposition of the velocity gradient in Eq. (7.13.6) into symmetric and antisymmetric parts:

$$\frac{\partial(\delta v_i)}{\partial x_i} = \delta L_{ij} = \delta D_{ij} + \delta\omega_{ij} \tag{7.13.7a}$$

where

$$\delta D_{ij} = \frac{1}{2}\left[\frac{\partial(\delta v_i)}{\partial x_j} + \frac{\partial(\delta v_j)}{\partial x_i}\right] \text{ and } \delta\omega_{ij} = \frac{1}{2}\left[\frac{\partial(\delta v_i)}{\partial x_j} - \frac{\partial(\delta v_j)}{\partial x_i}\right] \tag{7.13.7b}$$

Since ω_{ij} is antisymmetric and D_{ij} is symmetric, it leads to $\omega_{ij}D_{ij} = 0$. Therefore, together with the constitutive equation, Eq. (7.12.5b), and Eq. (7.13.7a) , we can express Eq. (7.13.6) as:

$$-\int_\Omega \frac{\partial(\delta v_i)}{\partial x_i} P\, d\Omega + \int_\Omega \frac{\mu}{2}\left[\frac{\partial(\delta v_i)}{\partial x_j} + \frac{\partial(\delta v_j)}{\partial x_i}\right]\left[\frac{\partial v_i}{\partial x_j} + \frac{\partial v_j}{\partial x_i}\right] d\Omega \tag{7.13.8}$$

Now, substitute Eqs. (7.13.5) and (7.13.8) into (7.13.2), the weak form for the momentum equation and associated boundary condition is obtained:

$$\int_\Omega \delta v_i \rho \left.\frac{\partial v_i}{\partial t}\right|_\chi d\Omega + \int_\Omega \delta v_i \rho c_j \frac{\partial v_i}{\partial x_j}\, d\Omega$$

$$-\int_\Omega \frac{\partial(\delta v_i)}{\partial x_i} P d\Omega + \int_\Omega \frac{\mu}{2}\left[\frac{\partial(\delta v_i)}{\partial x_j} + \frac{\partial(\delta v_j)}{\partial x_i}\right]\left[\frac{\partial v_i}{\partial x_j} + \frac{\partial v_j}{\partial x_i}\right] d\Omega$$

$$-\int_\Omega \delta v_i \rho g_i d\Omega - \int_{\Gamma^t} \delta v_i \bar{t}_j \, d\Gamma = 0 \qquad (7.13.9)$$

The weak forms for the continuity equation and the free surface update equation are simply obtained by taking the inner product with δp and δx_i, respectively.

We may now state a suitable weak form for the momentum equation.

Weak Form for Newtonian Fluid

Given density, ρ, bulk modules, B, and Cauchy stress function, σ, defined in Table 7.2, respectively, find $v \in U^v$, $p \in U^p$ and $x \in U^x$ such that for every $\delta v \in U_0^v$, $\delta p \in U_0^p$ and $\delta x \in U_0^x$:

Continuity Equation [Eq. (7.12.2a)]

$$\int_\Omega \delta p \frac{1}{B}\frac{\partial p}{\partial t}\bigg|_\chi d\Omega + \int_\Omega \delta p \frac{1}{B} c_i \frac{\partial p}{\partial x_i} d\Omega + \int_\Omega \delta p \frac{\partial v_i}{\partial x_i} d\Omega = 0 \qquad (7.13.10a)$$

Momentum Equation [Eq. (7.12.2b)]

$$\int_\Omega \delta v_i \rho \frac{\partial v_i}{\partial t}\bigg|_\chi d\Omega + \int_\Omega \delta v_i \rho c_j \frac{\partial v_i}{\partial x_j} d\Omega - \int_\Omega \frac{\partial(\delta v_i)}{\partial x_i} p d\Omega$$

$$+ \int_\Omega \frac{\mu}{2}\left(\frac{\partial(\delta v_i)}{\partial x_j} + \frac{\partial(\delta v_j)}{\partial x_i}\right)\left(\frac{\partial v_i}{\partial x_j} + \frac{\partial v_j}{\partial x_i}\right) d\Omega - \int_\Omega \delta v_i \rho g_i d\Omega - \int_{\Gamma_t} \delta v_i \bar{t}_j d\Gamma = 0$$

(7.13.10b)

Free Surface Update Equation

The mesh rezoning equation [Eq. (7.12.2c)]:

$$\int_{\hat\Omega} \delta x_i \frac{\partial x_i}{\partial t}\bigg|_\chi d\hat\Omega + \int_{\hat\Omega} \left(\delta_{jk} - \alpha_{jk}\right) v_k \delta x_i \frac{\partial x_i}{\partial \chi_j} d\hat\Omega - \int_{\hat\Omega} \delta x_i v_i d\hat\Omega = 0 \qquad (7.13.10c)$$

or the mesh updating equation [Eq. (7.12.2d)]:

$$\int_{\hat\Omega} \delta x_i \frac{\partial x_i}{\partial t}\bigg|_\chi d\hat\Omega - \int_{\hat\Omega} \delta x_i \sum_{\substack{j=1 \\ j\neq 1}}^{NSD} \frac{v_j - \hat v_j}{\hat J^{ii}} \hat J^{ji} d\hat\Omega - \int_{\hat\Omega} \delta x_i \left(v_i - \frac{\hat J}{\hat J^{ii}} w_i\right) d\hat\Omega = 0 \qquad (7.13.10d)$$

Constitutive Equation

$$\sigma_{ij} = -p\delta_{ij} + 2\mu D_{ij} \qquad (7.13.11e)$$

Table 7.3 Weak Form of Slightly Compressible Viscous Flow with Moving Boundary Problem

7.13.1 Galerkin Approximation of Slightly Compressible Viscous Flow with Moving Boundaries

To obtain the semidiscrete equations by the Galerkin approximation, Eq. (7.13.10a) through (7.13.10d) is replaced by the finite functions p^h, $\mathbf{v}^h$ and $\mathbf{x}^h$. That is:

$$p \to p^h,\ \mathbf{x} \to \mathbf{x}^h \text{ and } \mathbf{v} \to \mathbf{v}^h \tag{7.13.11}$$

In particular, we wish to separate these functions into two parts, the unknown parts $w_{\mathbf{x}}^h$, w_p^h and $w_{\mathbf{v}}^h$ and the prescribed boundary parts (essential boundary conditions) $\bar{\mathbf{x}}^h$, $\bar{p}^h$ and $\bar{\mathbf{v}}^h$, so that:

$$p^h = w_p^h + \bar{p}^h \tag{7.13.12a}$$

$$\mathbf{v}^h = w_{\mathbf{v}}^h + \bar{\mathbf{v}}^h \tag{7.13.12b}$$

$$\mathbf{x}^h = w_{\mathbf{x}}^h + \bar{\mathbf{x}}^h \tag{7.13.12c}$$

Given ρ, B, σ as before, find $v_i^h = w_{v_i}^h + \bar{v}_i^h$, $p^h = w_p^h + \bar{p}^h$ and $x_i^h = w_{x_i}^h + \bar{x}_i^h$, where $w_v^h \quad U_0^{v^h}$, $w_p^h \quad U_0^{p^h}$ and $w_x^h \quad U_0^{x^h}$, such that for every $\delta v^h \quad U_0^{v^h}$, $\delta p^h \quad U_0^{p^h}$ and $\delta x^h \quad U_0^{x^h}$:

Galerkin Form of Continuity Equation

$$\int_\Omega \delta p^h \frac{1}{B}\frac{\partial w_p^h}{\partial t}\bigg|_\chi d\Omega + \int_\Omega \delta p^h \frac{1}{B} c_i \frac{\partial w_p^h}{\partial x_i} d\Omega + \int_\Omega \delta p^h \frac{\partial v_i}{\partial x_i} d\Omega$$

$$= -\int_\Omega \delta p^h \frac{1}{B}\frac{\partial \bar{p}^h}{\partial t}\bigg|_\chi d\Omega - \int_\Omega \delta p^h \frac{1}{B} c_i \frac{\partial \bar{p}^h}{\partial x_i} d\Omega \tag{7.13.13a}$$

Galerkin Form of Momentum Equation

$$\int_\Omega \delta v_i^h \rho \frac{\partial w_{v_i}^h}{\partial t}\bigg|_\chi d\Omega + \int_\Omega \delta v_i^h \rho c_j \frac{\partial w_{v_i}^h}{\partial x_j} d\Omega - \int_\Omega \frac{\partial(\delta v_i^h)}{\partial x_i} P d\Omega$$

$$+\int_\Omega \frac{\mu}{2}\left[\frac{\partial(\delta v_i^h)}{\partial x_j}+\frac{\partial(\delta v_j^h)}{\partial x_i}\right]\left[\frac{\partial w_{v_i}^h}{\partial x_j}+\frac{\partial w_{v_j}^h}{\partial x_i}\right]d\Omega-\int_\Omega \delta v_i^h \rho g_i\, d\Omega$$

$$=\int_\Gamma \delta v_i^h h_j\, d\Gamma-\int_\Omega \delta v_i^h \rho\left.\frac{\partial \bar{v}_i^h}{\partial t}\right|_\chi d\Omega-\int_\Omega \delta v_i^h \rho c_j \frac{\partial \bar{v}_i^h}{\partial x_j}\, d\Omega$$

$$-\int_\Omega \frac{\mu}{2}\left[\frac{\partial(\delta v_i^h)}{\partial x_j}+\frac{\partial(\delta v_j^h)}{\partial x_i}\right]\left[\frac{\partial \bar{v}_i^h}{\partial x_j}+\frac{\partial \bar{v}_j^h}{\partial x_i}\right]d\Omega \qquad (7.13.13b)$$

Galerkin Form of Free Surface Update Equation
The mesh rezoning equation:

$$\int_{\hat{\Omega}} \delta x_i^h \left.\frac{\partial w_{x_i}^h}{\partial t}\right|_\chi d\hat{\Omega}+\int_{\hat{\Omega}} \left(\delta_{jk}-\alpha_{jk}\right)v_k \delta x_i^h \frac{\partial w_{x_i}^h}{\partial \chi_j}\, d\hat{\Omega}-\int_{\hat{\Omega}} \delta x_i^h v_i d\hat{\Omega}$$

$$=\int_{\hat{\Omega}} \delta x_i^h \left.\frac{\partial \bar{x}_i^h}{\partial t}\right|_\chi d\hat{\Omega}+\int_{\hat{\Omega}} \left(\delta_{jk}-\alpha_{jk}\right)v_k \delta x_i^h \frac{\partial \bar{x}_i^h}{\partial \chi_j}\, d\hat{\Omega} \qquad (7.13.13c)$$

or the mesh updating equation:

$$\int_{\hat{\Omega}} \delta x_i^h \left.\frac{\partial w_{x_i}^h}{\partial t}\right|_\chi d\hat{\Omega}-\int_{\hat{\Omega}} \delta x_i^h \sum_{\substack{j=1\\ j\neq 1}}^{NSD} \frac{v_j-\hat{v}_j}{\hat{J}^{ji}}\hat{J}^{ji} d\hat{\Omega}-\int_{\hat{\Omega}} \delta x_i^h \left[v_i-\frac{\hat{J}}{\hat{J}^{ii}}w_i\right]d\hat{\Omega}$$

$$=-\int_{\hat{\Omega}} \delta x_i^h \left.\frac{\partial \bar{x}_i^h}{\partial t}\right|_\chi d\hat{\Omega} \qquad (7.13.13d)$$

7.13.2 Element Matrices for Slightly Compressible Viscous Flow with Moving Boundaries

The discrete forms of the continuity, momentum and mesh updating equations are presented next. First, we define:

$$v^h = w_v^h+\bar{v}^h=\sum_{A=1}^{NEQv} N_A^v(\mathbf{x})v_A(t)+\sum_{A=NEQv+1}^{NUMNPv} N_A^v(\mathbf{x})\bar{v}_A^h(t) \qquad (7.13.14a)$$

$$p^h = w_p^h + \bar{p}^h = \sum_{A=1}^{NEQp} N_A^p(\mathbf{x})\, p_A(t) + \sum_{A=NEQp+1}^{NUMNPp} N_A^p(\mathbf{x})\, \bar{p}_A^h(t) \tag{7.13.14b}$$

$$\hat{v}^h = w_{\hat{v}}^h + \bar{\hat{v}}^h = \sum_{A=1}^{NEQ\hat{v}} N_A^{\hat{v}}(\mathbf{x})\, \hat{v}_A(t) + \sum_{A=NEQ\hat{v}+1}^{NUMNP\hat{v}} N_A^{\hat{v}}(\mathbf{x})\, \bar{\hat{v}}_A^h(t) \tag{7.13.14c}$$

$$\delta\hat{v}^h = \sum_{A=1}^{NEQ\hat{v}} N_A^{\hat{v}}(\mathbf{X})\, c_A^{\hat{v}}(t) \tag{7.13.14d}$$

$$\delta p^h = \sum_{A=1}^{NEQp} N_A^p(\mathbf{X})\, c_A^p(t) \tag{7.13.14e}$$

$$\delta v^h = \sum_{A=1}^{NEQv} N_A^v(\mathbf{X})\, c_A^v(t) \tag{7.13.14f}$$

where N_A^p, N_A^v and $N_A^{\hat{v}}$ are the continuous element shape function for pressure, velocity and mesh velocity, respectively.

(ii) Mixed Formulation:
Without any loss of generality, the free surface is assumed perpendicular to the χ_3 direction. The cofactors are

$$\hat{J}^{13} = \frac{\partial x_2}{\partial \chi_1}\frac{\partial x_3}{\partial \chi_2} - \frac{\partial x_2}{\partial \chi_2}\frac{\partial x_3}{\partial \chi_1} \tag{7.13.20a}$$

$$\hat{J}^{23} = \frac{\partial x_1}{\partial \chi_2}\frac{\partial x_3}{\partial \chi_1} - \frac{\partial x_1}{\partial \chi_1}\frac{\partial x_3}{\partial \chi_2} \tag{7.13.20b}$$

$$\hat{J}^{33} = \frac{\partial x_1}{\partial \chi_2}\frac{\partial x_1}{\partial \chi_2} - \frac{\partial x_1}{\partial \chi_2}\frac{\partial x_2}{\partial \chi_1} \tag{7.13.20c}$$

It should be noted that x_3 is the only unknown that defines the free surface which is assumed material (i.e. $w_3 = 0$).

(8d) Show that by substituting Eqs. (7.13.20) into Eq. (7.11.22b) yields:

$$\left.\frac{\partial x_3}{\partial t}\right|_{\chi} + \frac{1}{\hat{J}^{33}}\left[(v_1 - \hat{v}_1)\frac{\partial x_2}{\partial \chi_2} - (v_2 - \hat{v}_2)\frac{\partial x_1}{\partial \chi_2}\right]\frac{\partial x_3}{\partial \chi_1}$$

$$+\frac{1}{\hat{J}^{33}}\left[-(v_1-\hat{v}_1)\frac{\partial x_2}{\partial \chi_1}+(v_2-\hat{v}_2)\frac{\partial x_1}{\partial \chi_1}\right]\frac{\partial x_3}{\partial \chi_2}=0 \tag{7.13.21}$$

(8e) Show that the convective term is:

$$\hat{L}_A=\int_{\Omega_\chi^e}\hat{N}_A\hat{c}_m\frac{\partial x_i}{\partial \chi_m}\,d\Omega_\chi \tag{7.13.22a}$$

by defining:

$$\hat{c}_1=\frac{1}{\hat{J}^{33}}\left[(v_1-\hat{v}_1)\frac{\partial x_2}{\partial \chi_2}-(v_2-\hat{v}_2)\frac{\partial x_1}{\partial \chi_2}\right] \tag{7.13.22b}$$

$$\hat{c}_2=\frac{1}{\hat{J}^{33}}\left[-(v_1-\hat{v}_1)\frac{\partial x_2}{\partial \chi_1}+(v_2-\hat{v}_2)\frac{\partial x_1}{\partial \chi_1}\right] \tag{7.13.22c}$$

$$\hat{c}_3=0 \tag{7.13.22d}$$

7.15. Numerical Example

7.15.1 Elastic-plastic wave propagation problem

An elastic-plastic wave propagation problem is used to assess the ALE approach in conjunction with the regular fixed mesh method. The problem statement, given in Fig.1, represents a 1-D infinitely long, elastic-plastic hardening rod. Constant density and isothermal conditions are assumed to simplify the problem. Thus only the momentum equation and constitutive equation are considered for this problem. It should be noted that this elastic-plastic wave propagation problem does not require an ALE mesh and the problem was selected because it provides a severe test of the stress update procedure and because of the availability of an analytic solution. The problem is solved using 400 elements which are uniformly spaced with a mesh size of 0.1. The mesh is arranged so that no reflected wave will occur during the time interval under consideration. Material properties and computational parameters are also depicted in Fig.7.16.1. Four stages are involved in this problem:

(1) $t \in [0,\ t_1]$, the mesh is fixed, and a square wave is generated at the origin;

(2) $t \in [t_1, t_2]$, the mesh is fixed and the wave travels along the bar;

(3) $t \in [t_2, t_3]$, two cases are studied:

case A: the mesh is moved uniformly to the left-hand side with a constant speed $-\hat{v}$;
case B: same as Case A except the mesh is moved to the right;

(4) $t = t_3$, the stress is reported as a function of spatial coordinates in Figs. 7.16.2 and 7.16.3 for Case A and Case B, respectively.

For both cases, the momentum and stress transport are taken into account by employing the full upwind method for elastic and elastic-plastic materials. The results are compared to :
(1) Regular Galerkin method runs, in which all of the transport items are handled by the exact integration;
(2) Fixed mesh runs, in which the finite element mesh is fixed in space and the results are pretty close to the analytic solutions.

The results according to several time step size are reported in Table 7.16.1. The wave arrival time for both methods, with or without upwinding technique, agree well with the fixed mesh runs. However, the scheme without upwinding technique causes severe unrealistic spatial oscillations in Case A because of the significant transport effects. The new method proposed here eliminates these oscillations completely. Base on these studies, it is found that the transport of stresses as well as yield stress (and back stresses if kinematic hardening) plays an important role in ALE computations for path-dependent materials, and the proposed update procedure is quite accurate and effective.

$\rho = 1 \quad E = 10^4 \quad E / E_T = 3 \quad \sigma_{y0} = 75 \quad \sigma_0 = -100$

$\Delta x = \Delta\chi = 0.1 \quad \hat{v} = 0.25\sqrt{E/\rho} \quad t_1 = 45 \quad t_2 = 240 \quad t_3 = 320(\times 10^{-3})$

1. $t \in [0, t_1]$ *mesh fixed, wave generated*

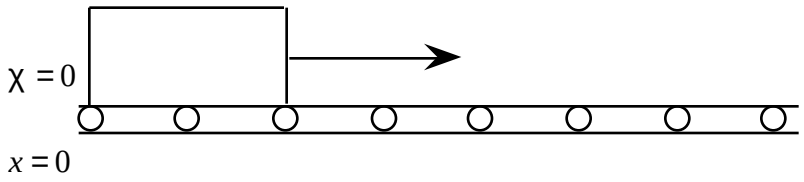

2. $t \in [t_1, t_2]$ *mesh fixed, wave travelling*

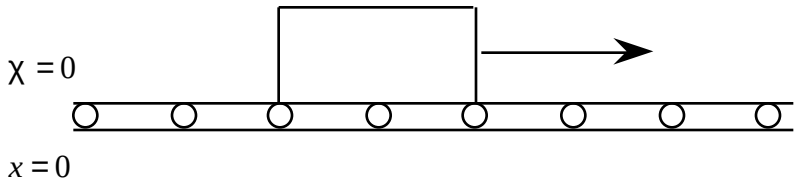

3A. $t \in [t_2, t_3]$ *Case A: mesh moving with* $\hat{v} = -\hat{v}$

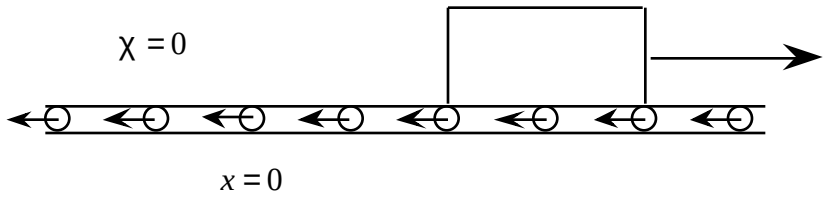

3B. $t \in [t_2, t_3]$ *Case B: mesh moving with* $\hat{v} = +\hat{v}$

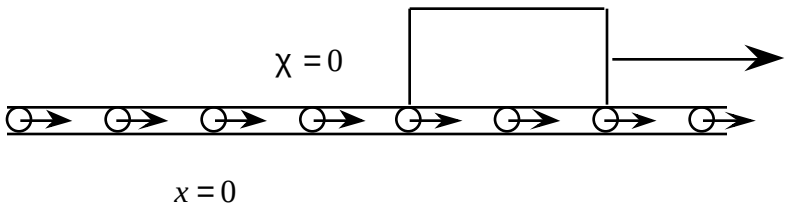

4. $t = t_3$ *report stress vs. spatial coordinate*

Fig 7.16.1 Problem statement and computational parameters for wave propagation

Table 7.16.1 Time step sizes and numbers of time steps for elliptic-plastic wave propagation example:

Time Step (Δt)	$\Delta t / Cr^a$	Number of time steps
0.040×10^{-2}	0.5	400
0.056×10^{-2}	0.7	286
0.072×10^{-2}	0.9	222

$^a Cr = \Delta x / \sqrt{E/\rho} + |c|$

7.15.2 Breaking of a dam

This example is an attempt to model the breaking of a dam or more generally a flow with large free surface motion by the ALE formulations described in the previous sections. This problem, which has an approximate solution for an inviscid fluid flowing over a perfect frictionless bed, presents a formidable challenge when this solution is applied to mine tailings embankments. A detailed description of this problem can be found in Huerta & Liu(1988).

The problem is solved without the restraints imposed by shallow water theory and only the case of flow over a still fluid (FSF) is considered. Study on another case of flow over a dry bed (FDB) can be found in the paper of Huerta & Liu(1988). The accuracy of the ALE finite element approach is checked by solving the inviscid case, which has an analytical solution in shallow water theory; then, other viscous cases are studied and discussed.

Figure 7.8 shows a schematic representation of the flow over a still fluid The dimensionless problem is defined by employing the following characteristic dimensions: the length scale is the height of the dam, H, over the surface of the downstream still fluid; the characteristic velocity, $\sqrt{gH}$,is chosen to scale velocities; and ρgH is the pressure scale. The characteristic time is arbitrarily taken as the length scale over the velocity scale, i.e. $\sqrt{H/g}$. Consequently, if the fluid is Newtonian, the only dimensionless parameter associated with the field equations is the Reynolds number, $R_e = H\sqrt{gH}/\nu$, where ν is the kinematics viscosity. A complete parametric analysis may be found in Huerta (1987). Since the problem is studied in its dimensionless form, H is always set equal to one.

Along the upstream and downstream boundaries a frictionless condition is assumed, whereas on the bed perfect sliding is only imposed in the inviscid case (for viscous flows the velocities are set equal to zero). In the horizontal direction 41 elements of unit length are usually employed, while in the vertical direction one, three, five, or seven layers are taken. depending on the particular case (see Figure 7.9). For the inviscid analysis, $\Delta H = H = 1$, as in Lohner et al (1984). In this problem both the Lagrange-Euler matrix method and the mixed formulation are equivalent because an Eulerian description is taken in the horizontal direction; in the vertical direction a Lagrangian description is used along the free surface while an Eulerian description is employed everywhere else.

Figure 7.10 compares the shallow water solution with the numerical results obtained by the one and three layers of elements meshes. Notice how the full integration of the Navier-Stokes equations smoothes the surface wave and slows down the initial motion of the flooding wave (recall that the Saint Venant equations predict a constant wave celerity, $\sqrt{gH}$, from $t = 0$). No important differences exists between the two discretizations (i.e. one or three elements in depth); both present a smooth downstream surface and a clearly separate peak at the tip of the wave. It is believed that this peak is produced in large part by the sudden change in the vertical component of the particle velocity between still conditions and the arrival of the wave, instead of numerical oscillations only. Figure 7.11 shows the

difference between a Galerkin formulation of the rezoning equation, where numerical node to node oscillations are clear, and a Petrov-Galerkin integration of the free surface equation (i.e. the previous 4lx3 element solution). The temporal criterion (Hughes and Tezduyar, 1984) is selected for the perturbation of the weighting functions, and, as expected (Hughes and Tezduyar, 1984; Hughes and Mallet, 1986), better results are obtained if the Courant number is equal to one. In the inviscid dam-break problem over a still fluid, the second-order accurate Newmark scheme (Hughes and Liu, 1978) is used (i.e. γ = 0.5 and β = 0.25), while in all of the following cases numerical damping is necessary (i.e. γ > 0.5) because of the small values of ΔH; this numerical instability is discussed later

The computed free surfaces for different times and the previous Generalized Newtonian fluids are shown in Figures 7.14 and 7.15. It is important to point out that the results obtained with the Carreau-A model and n = 0.2 are very similar to those of the Newtonian case with $R_e = 300$, whereas for the Bingham material with $\mu_p = 1\times 10^2 P_a \cdot s$ the free surface shapes resemble more closely those associated with R_e = 3000; this is expected because the range of shear rate for this problem is from 0 up to 20-30 s^{-1} It should also be noticed that both Bingham cases present larger oscillations at the free surface and that even for the $\mu_p = 1\times 10^3 P_a \cdot s$ case the flooding wave moves faster than that for the Carreau models. Two main reasons can explain such behavior; first, unless uneconomical time-steps are chosen, oscillations appear in the areas where the fluid is at rest because of the extremely high initial viscosity (1000 μ_p); second, the larger shear rates occur at the tip of the wave, and it is in this area that the viscosity suddenly drops at least two orders of magnitude, creating numerical oscillations.

Exercise 7.1

Observe that if the Jacobian described in Eq. (7.4.3a) is:

$$J = \det\left(\frac{\partial \mathbf{x}}{\partial \mathbf{X}}\right) = \varepsilon_{ijk}\frac{\partial x_i}{\partial X_1}\frac{\partial x_j}{\partial X_2}\frac{\partial x_k}{\partial X_3} \tag{7.4.11a}$$

where ε_{ijk} is the permutation symbol, then $\dot{J}$ becomes:

$$\dot{J} = \frac{\partial(v_1, x_2, x_3)}{\partial(X_1, X_2, X_3)} + \frac{\partial(x_1, v_2, x_3)}{\partial(X_1, X_2, X_3)} + \frac{\partial(x_1, x_2, v_3)}{\partial(X_1, X_2, X_3)} \tag{7.4.11b}$$

where

$$\frac{\partial(a,b,c)}{\partial(X_1,X_2,X_3)} = \begin{vmatrix} \dfrac{\partial a}{\partial X_1} & \dfrac{\partial a}{\partial X_2} & \dfrac{\partial a}{\partial X_3} \\ \dfrac{\partial b}{\partial X_1} & \dfrac{\partial b}{\partial X_2} & \dfrac{\partial b}{\partial X_3} \\ \dfrac{\partial c}{\partial X_1} & \dfrac{\partial c}{\partial X_2} & \dfrac{\partial c}{\partial X_3} \end{vmatrix} \tag{7.4.11c}$$

for arbitrary scalars a, b, and c, and $v_i = \dot{x}_i$.

Using the chain rule on $\dfrac{\partial v_1}{\partial X_j}$, show that:

$$\frac{\partial(v_1,v_2,v_3)}{\partial(X_1,X_2,X_3)} = \sum_{m=1}^{3} \frac{\partial v_1}{\partial x_m} \frac{\partial(x_m,x_2,v_3)}{\partial(X_1,X_2,X_3)} = \frac{\partial v_1}{\partial x_1} J \tag{7.4.12a}$$

Similarly, show that:

$$\dot{J} = J\, v_{k,k} \tag{7.4.12b}$$

Exercise 7.2 Updated ALE Conservation of Angular Momentum

The principle of conservation of angular momentum states that the time rate of change of the angular momentum of a given mass with respect to a given point, say the origin of the reference frame, is equal to the applied torque referred to the same point. That is:

$$\frac{D}{Dt}\int_\Omega \mathbf{x}\times\rho(\mathbf{x},t)\mathbf{v}(\mathbf{x},t)d\Omega = \int_\Omega \mathbf{x}\times\mathbf{b}(\mathbf{x},t)d\Omega + \int_\Gamma \mathbf{x}\times\mathbf{t}(\mathbf{x},t)d\Gamma \tag{7.4.13a}$$

It should be noticed that the left hand side of Eq. (7.4.13a) is simply $\dot{\mathbf{H}}$.

(2a) Show that:

$$\dot{\mathbf{H}} = \int_{\Omega_0} \frac{D}{Dt}(\mathbf{x})\times(\rho\mathbf{v})Jd\Omega_0 + \int_{\Omega_0} \mathbf{x}\times\frac{D}{Dt}(\rho\,\mathbf{v}\,J)d\Omega_0 \tag{7.4.13b}$$

$$= \int_\Omega \mathbf{x}\times\left[\frac{D}{Dt}(\rho\mathbf{v}) + (\rho\mathbf{v})div(\mathbf{v})\right]d\Omega$$

Hint, in deriving the above equation, the following pieces of information have been used of (1) $\mathbf{x}_{,t[\mathbf{X}]} = \mathbf{v}$; (2) $\mathbf{v}\times(\rho\,\mathbf{v}) = \mathbf{0}$ and (3) Eq. (7.3.6b).

Now, show that substituting Eqs. (7.4.13b) into Eq. (7.4.13a) yields:

$$\int_\Omega \mathbf{x} \times \left\{ \frac{D}{Dt}(\rho \mathbf{v}) + (\rho \mathbf{v}) div(\mathbf{v}) \right\} d\Omega \tag{7.4.14}$$

$$= \int_\Omega \mathbf{x} \times \mathbf{b}(\mathbf{x},t) d\Omega + \int_\Gamma \mathbf{x} \times (\mathbf{n} \cdot \sigma) d\Gamma$$

(2b) Show that by employing the divergence theorem and the momentum equations given in Eq. (7.4.6), the component form of Eq. (7.4.14) is:

$$\int_\Omega \varepsilon_{ijk} \sigma_{jk} d\Omega = 0 \tag{7.4.15}$$

(2c) If the Cauchy stress tensor, σ, is *smooth* within Ω, then the conservation of angular momentum leads to the symmetry condition of the Cauchy (true) stress via Eq. (7.4.15) and is given as:

$$\sigma_{ij} = \sigma_{ji} \tag{7.4.16}$$

Exercise 7.3 Updated ALE Conservation of Energy

Energy conservation is expressed as (see chapter 3):

$$\frac{D}{Dt}\int_\Omega \rho E d\Omega = \int_\Gamma \sigma_{ji} n_j v_i \, d\Gamma + \int_\Omega \rho b_i v_i \, d\Omega - \int_\Gamma q_i n_i \, d\Gamma + \int_\Omega \rho s d\Omega \tag{7.4.17}$$

where q_i is the heat flux leaving the boundary $\partial\Omega_x$. Recall that E is the specific total energy density and is related to the specific internal energy e, by:

$$E = e + \frac{V^2}{2} \tag{7.4.18a}$$

where $e = e(\theta, \rho)$ with θ being the thermodynamic temperature and ρs is the specific heat source, i.e. the heat source per unit spatial volume and $V^2 = v_i v_i$. The Fourier law of heat conduction is:

$$q_i = -k_{ij} \theta_{,j} \tag{7.4.18b}$$

(3a) Show that the energy equation is (hint, use integration by parts and the divergence theorem):

$$(\rho E)_{,t[\chi]} + (\rho E c_j)_{,j} + \rho E \hat{v}_{j,j} = (\sigma_{ij} v_i)_{,j} + b_j v_j + (k_{ij} \theta_{,j})_{,i} + \rho s \tag{7.4.19a}$$

(3b) If there is sufficient smoothness, time differentiate Eq. (7.4.19a) via the chain rule and make use of the continuity equation to show that Eq. (7.4.19a) reduces to:

$$\rho\left\{E_{,t[\chi]} + E_{,j}c_j\right\} = (\sigma_{ij}v_i)_{,j} + b_j v_j + (k_{ij}\theta_{,j})_{,i} + \rho s \tag{7.4.19b}$$

or, in index free notation:

$$\rho\left\{E_{,t[\chi]} + \mathbf{c}\ \ grad\ E\right\} = div(\mathbf{v}\ \ \sigma) + \mathbf{v}\ \ \mathbf{b} + div(\mathbf{k}\ \ grad\,\theta) + \rho s \tag{7.4.19c}$$

(3c) Show that the above equations can be specified in the Lagrangian description by choosing:

$$\chi = \mathbf{X};\quad \hat{\varphi} = \varphi;\quad \mathbf{c} = \mathbf{0};\quad J = \det\left[\frac{\partial \mathbf{x}}{\partial \mathbf{X}}\right] \tag{7.4.20a}$$

and they are given by:

$$\rho E_{,t[\chi]} = (\sigma_{ij}v_i)_{,j} + b_j v_j + (k_{ij}\theta_{,j})_{,i} + \rho s \tag{7.4.20b}$$

or, in index free notation:

$$\rho E_{,t[\chi]} = div(\mathbf{v}\ \ \sigma) + \mathbf{v}\ \ \mathbf{b} + div(\mathbf{k}\ \ grad\ \theta) + \rho s \tag{7.4.20c}$$

(3d) Similarly, show that the Eulerian energy equation is obtained by choosing:

$$\chi = \mathbf{x};\quad \hat{\varphi} = \mathbf{1};\quad \mathbf{c} = \mathbf{v};\quad \hat{\mathbf{v}} = \mathbf{0};\quad J = \det\left[\frac{\partial \mathbf{x}}{\partial \mathbf{X}}\right] = 1 \tag{7.4.21a}$$

and they are given by:

$$\rho\left\{E_{,t[\chi]} + E_{,j}v_j\right\} = (\sigma_{ij}v_i)_{,j} + b_j v_j + (k_{ij}\theta_{,j})_{,i} + \rho s \tag{7.4.21b}$$

or

$$\rho\left\{E_{,t[\chi]} + \mathbf{v}\ \ grad\ E\right\} = div(\mathbf{v}\ \ \sigma) + \mathbf{v}\ \ \mathbf{b} + div(\mathbf{k}\ \ grad\,\theta) + \rho s \tag{7.4.21c}$$

Exercise 7.4
Show Eqs (7.13.10a), (7.13.10c), and (7.13.10d).

Exercise 7.5 Galerkin Approximation
Show the following Galerkin approximation by substituting these approximation functions, Eqs (7.13.12), into Eqs. (7.13.10).

Exercise 7.6 The Continuity Equation
(6a) Show that:

$$\mathbf{M}^p\dot{\mathbf{P}} + \mathbf{L}^p(\mathbf{P}) + \mathbf{G}^T\mathbf{v} = f^{extp} \tag{7.13.15a}$$

where $\mathbf{M}^p$ is the generalized mass matrices for pressure; $\mathbf{L}^p$ is the generalized convective terms for pressure; **G** is the divergence operator matrix; f^{extp} is the external load vector; **P** and **v** are the vectors of unknown nodal values for pressure and velocity, respectively; and $\dot{\mathbf{P}}$ is the time derivative of the pressure.

(6b) Show that:

$$M_{AB}^P = \int_{\Omega^e} \frac{1}{B} N_A^p N_B^p \, d\Omega \tag{7.13.15b}$$

$$L_A^P = \int_{\Omega^e} \frac{1}{B} N_A^p c_k \frac{\partial p}{\partial x_k} \, d\Omega \tag{7.13.15c}$$

$$G_{AB}^P = \int_{\Omega^e} N_A^p \frac{\partial N_B}{\partial x_m} \, d\Omega \tag{7.13.15d}$$

Example 7.2 1D Advection-Diffusion Equation

$$2P_e \, \varphi_{,x} - \varphi_{,xx} = 0$$

$P_e = 1.5 \quad \tau = 0.438 \quad \Delta x = 1$

Exercise 7.7 The Momentum Equation

(7a) Show that:

$$\mathbf{Ma} + \mathbf{L}(\mathbf{v}) + \mathbf{K}_\mu \mathbf{v} - \mathbf{GP} = f^{extv} \tag{7.13.16a}$$

where **M** is the generalized mass matrices for velocity; **L** is the generalized convective terms for velocity; **G** is the divergence operator matrix; f^{extv} is the external load vector applied on the fluid; $\mathbf{K}_\mu$ is the fluid viscosity matrix; **P** and **v** are the vectors of unknown nodal values for pressure and velocity, respectively; and $\dot{\mathbf{P}}$ and **a** are the time derivative of the pressure, and the material velocity, holding the reference fixed.

(7b) Show that:

$$M_{AB} = \int_{\Omega^e} \rho N_A N_B \, d\Omega \tag{7.13.16b}$$

$$L_A = \int_{\Omega^e} \rho N_A c_m \frac{\partial v_i}{\partial x_m} \, d\Omega \tag{7.13.16c}$$

$$\mathbf{K}_{\mu} = \int_{\Omega^e} \mathbf{B}^T \mathbf{D} \mathbf{B}\, d\Omega \tag{7.13.16d}$$

where

$$\mathbf{B} = \left[\mathbf{B}_1 \cdots \mathbf{B}_a \cdots \mathbf{B}_{\mathrm{NEN}} \right] \tag{7.13.17a}$$

$$\mathbf{B}_a^T = \begin{bmatrix} \frac{\partial N_a}{\partial x_1} & \frac{\partial N_a}{\partial x_2} & 0 & 0 & 0 & \frac{\partial N_a}{\partial x_3} \\ 0 & \frac{\partial N_a}{\partial x_1} & \frac{\partial N_a}{\partial x_2} & 0 & \frac{\partial N_a}{\partial x_3} & 0 \\ 0 & 0 & 0 & \frac{\partial N_a}{\partial x_3} & \frac{\partial N_a}{\partial x_2} & \frac{\partial N_a}{\partial x_1} \end{bmatrix} \tag{7.13.17b}$$

$$\mathbf{D} = \begin{bmatrix} 2\mu & 0 & 0 & 0 & 0 & 0 \\ 0 & \mu & 0 & 0 & 0 & 0 \\ 0 & 0 & 2\mu & 0 & 0 & 0 \\ 0 & 0 & 0 & 2\mu & 0 & 0 \\ 0 & 0 & 0 & 0 & \mu & 0 \\ 0 & 0 & 0 & 0 & 0 & \mu \end{bmatrix} \tag{7.13.17c}$$

Exercise 7.8 The Mesh Updating Equation

(8a) Show that:

$$\hat{\mathbf{M}}\hat{\mathbf{v}} + \hat{\mathbf{L}}(\mathbf{x}) - \hat{\mathbf{M}}\mathbf{v} = f^{extx} \tag{7.13.18a}$$

where $\hat{\mathbf{M}}$ is the generalized mass matrices for mesh velocity; $\hat{\mathbf{L}}$ is the generalized convective terms for mesh velocity; f^{extx} is the external load vector; and $\hat{\mathbf{v}}$ is the vectors of unknown nodal values for mesh velocity.

(8b) Show that:

$$\hat{M}_{AB} = \int_{\hat{\Omega}^e} \rho \hat{N}_A \hat{N}_B \, d\hat{\Omega} \tag{7.13.18b}$$

The convective term is defined as follows:

(i) Lagrangian-Eulerian Matrix Method:

Define:

$$\hat{c}_i = (\delta_{ij} - \alpha_{ij}) v_j \tag{7.13.19a}$$

(8c) Show that the convective term is:

$$\hat{L}_A = \int_{\hat{\Omega}^e} \hat{N}_A \hat{c}_m \frac{\partial x_i}{\partial \chi_m} \, d\hat{\Omega} \tag{7.13.19b}$$

Exercise 6

Replacing the test function δv_i by $\delta v_i + \tau \rho c_j \frac{\delta v_i}{\delta x_j}$, show that the streamline-upwind/Petrov-Galerkin formulation for the momentum equation is:

$$0 = \int_\Omega \delta v_i \rho \left. \frac{\partial v_i}{\partial t} \right|_\chi d\Omega + \int_\Omega \delta v_i \rho c_j \frac{\partial v_i}{\partial x_j} d\Omega - \int_\Omega \frac{\partial (\delta v_i)}{\partial x_i} P d\Omega - \int_{\Omega_x} \delta v_i \rho g_i d\Omega$$

$$+ \int_\Omega \frac{\mu}{2} \left[\frac{\partial (\delta v_i)}{\partial x_j} + \frac{\partial (\delta v_j)}{\partial x_i} \right] \left[\frac{\partial v_i}{\partial x_j} + \frac{\partial v_j}{\partial x_i} \right] d\Omega - \int_\Gamma \delta v_i h_j \, d\Gamma \qquad \textit{Galerkin}$$

$$+ \sum_{e=1}^{NUMEL} \int_{\Omega^e} \tau \rho c_j \frac{\delta v_i}{\delta x_j} \left[\rho \left. \frac{\partial v_i}{\partial t} \right|_\chi + \rho c_j \frac{\partial v_i}{\partial x_j} - \frac{\partial \sigma_{ij}}{\partial x_j} - \rho g_i \right] d\Omega \qquad \textit{StreamlineUpwind}$$

References:

Belytschko, T. and Liu, W.K. (1985), "Computer Methods for Transient Fluid-Structure Analysis of Nuclear Reactors," *Nuclear Safety*, Volume 26, pp. 14-31.

Bird, R.B., Amstrong, R.C., and Hassager, 0. (1977), *Dynamics of Polymeric Liquids, Volume 1: Fluid Mechanics*, John Wiley and Sons, 458 pages.

Huerta, A. (1987), Numerical Modeling of Slurry Mechanics Problems. Ph.D Dissertation of Northwestern University.

Hughes, T.J.R., Liu, W.K., and Zimmerman, T.K. (1981), "LagrangianEulerian Finite Element Formulation for Incompressible Viscous Flows", *Computer Methods in Applied Mechanics and Engineering*, Volume 29, pp. 329-349.

Hughes, T.J.R., and Mallet, M. (1986), "A New Finite Element Formulation for Computational Fluid Dynamics: III. The Generalized Streamline Operator for Multidimensional AdvectiveDiffusive Systems," *Computer Methods in Applied Mechanics and Engineering*, Volume 58, pp. 305-328.

Hughes, T.J.R., and Tezduyar, T.E. (1984), "Finite Element Methods for First-Order Hyperbolic Systems with Particular Emphasis on the Compressible Euler Equations", *Computer Methods in Applied Mechanics and Engineering*, Volume 45, pp. 217-284.

Hutter, K., and Vulliet, L. (1985), 'Gravity-Driven Slow Creeping Flow of a Thermoviscous Body at Elevated Temperatures," *Journal of Thermal Stresses*, Volume 8, pp. 99-138.

Liu, W.K., and Chang, H. G. (1984), "Efficient Computational Procedures for Long-Time Duration Fluid-Structure Interaction Problems," *Journal of Pressure Vessel Technology*, Volume 106, pp. 317-322.

Liu, W.K., Lam, D., and Belytschko, T. (1984), "Finite Element Method for Hydrodynamic Mass with Nonstationary Fluid," *Computer Methods in Applied Mechanics and Engineering*, Volume 44, pp. 177-211.

Lohner, R., Morgan, K., and Zienkiewicz, O.C. (1984), "The Solution of Nonlinear Hyperbolic Equations Systems by the Finite Element Method," *International Journal for Numerical Methods in Fluids*, Volume 4, pp. 1043-1063.

Belytschko, T. and Kennedy, J.M.(1978), 'Computer models for subassembly simulation', *Nucl. Engrg. Design*, **49**, 17-38.

Liu, W.K. and Ma, D.C.(1982), 'Computer implementation aspects for fluid-structure interaction problems', *Comput. Methos. Appl. Mech. Engrg.*, **31**, 129-148.

Brooks, A.N. and Hughes, T.J.R.(1982), 'Streamline upwind/Petrov-Galerkin formulations for convection dominated flows with particular emphasis on the incompressible Navier-Stokes equations', *Comput. Meths. Appl. Mech. Engrg.*, **32**, 199-259.

Lohner, R., Morgan, K. and Zienkiewicz, O.C.(1984), 'The solution of non-linear hyperbolic equations systems by the finite element method', Int. J. Numer. Meths. Fluids, **4**, 1043-1063.

Liu, W.K.(1981) 'Finite element procedures for fluid-structure interactions with application to liquid storage tanks', *Nucl. Engrg. Design*, **65**, 221-238.

Liu, W.K. and Chang, H.(1985), 'A method of computation for fluid structure interactions', *Comput. & Structures*, **20**, 311-320.

Hughes, T.J.R., and Liu, W.K.(1978), 'Implicit-explicit finite elements in transient analysis', *J. Appl.Mech.*, **45**, 371-378.

Liu, W.K., Belytschko, T. And Chang, H.(1986), 'An arbitrary Lagrangian-Eulerian finite element method for path-dependent materials', *Comput. Meths. Appl. Mech. Engrg.*, **58**, 227-246.

Liu, W.K., Ong, J.S., and Uras, R.A.(1985), 'Finite element stabilization matrices¾a unification approach', *Comput. Meths. Appl. Mech. Engrg.*, **53**, 13-46.

Belytschko, T., Ong,S.-J, Liu, W.K., and Kennedy, J.M.(1984), 'Hourglass control in linear and nonlinear problems', *Comput. Meths. Appl. Mech. Engrg.*, **43**, 251-276.

Liu, W.K., Chang, H, Chen, J-S, and Belytschko, T.(1988), 'Arbitrary Lagrangian-Eulerian Petrov-Galerkin finite elements for nonlinear continua', *Comput. Meths. Appl. Mech. Engrg.*, **68**, 259-310.

Benson, D.J.,*(1989),* 'An efficient, accurate simple ALE method for nonlinear finite element programs', *Comput. Meths. Appl. Mech. Engrg, **72** 205-350.*

Huerta, A. & Casadei, F.(1994), "New ALE applications in non-linear fast-transient solid dynamics", *Engineering Computations*, **11**, 317-345.

Huerta, A. & Liu, W.K. (1988), "Viscous flow with large free surface motion", *Computer Methods in Applied Mechanis and Engineering*, **69**, 277-324.

---------- Backup of the previous version ----------

In section 7.1, a brief introduction of the ALE is given. In section 7.2, the kinematics in ALE formulation is described. In section 7.3, the Lagrangian versus referential updates is given. In section 7.4, the updated ALE balance laws in referential description is described. In section 7.5, the strong form of updated ALE conservation laws in referenctial description is derived. In section 7.6, an example of dam-break is used to show the application of updated ALE. In section 7.7, the updated ALE is applied to the path-dependent materials extensively where the strong form, the weak form and the finite element decretization are derived. In this section, emphasize is focused on the stress update procedure. Formulations for regular Galerkin method, Streamline-upwind/Petrov-Galerkin(SUPG) method and operator splitting method are derived respectively. All the path-dependent state variables are updated with a similar procedure. In addition, the stress update procedures in 1D case are specified with the elastic and elastic-plastic wave propagation examples to demonstrate the effectiveness of the ALE method. In section 7.8, the total ALE method, the counterpart of updated ALE method, is studied.

7.1 Introduction

The theory of continuum mechanics (Malvern [1969], Oden [1972]) serves to establish an idealization and a *mathematical* formulation for the physical responses of a material body which is subjected to a variety of external conditions such as thermal and mechanical loads. Since a material body *B* defined as a *continuum* is a collection of material particles *p*, the purpose of continuum mechanics is to provide governing equations which describe the *deformations* and *motions* of a continuum in space and time under thermal and mechanical disturbances.

The mathematical model is achieved by labelling the points in the material body *B* by the real number planes Ω, where Ω is the region (or domain) of the Euclidean space. Henceforth, the material body B is replaced by an idealized mathematical body, namely, the region Ω. Instead of being interested in the atomistic view of the particles *p*, the description of the behavior of the body *B* will only pertain to the regions of Euclidean space .

Equations describing the behavior of a continuum can generally be divided into four major categories: (1) kinematic, (2) kinetic (balance laws), (3) thermodynamic, and (4) constitutive. Detailed treatments of these subjects can be found in many standard texts.

The two classical descriptions of motion, are the Lagrangian and Eulerian descriptions. Neither is adequate for many engineering problems involving finite deformation especially when using finite element methods. Typical examples of these are fluid-structure-solid interaction problems, free-surface flow and moving boundary problems, metal forming processes and penetration mechanics, among others.

Therefore, one of the important ingredients in the development of finite element methods for nonlinear mechanics involves the choice of a suitable kinematic description for each particular problem. In solid mechanics, the Lagrangian description is employed extensively for finite deformation and finite rotation analyses. In this description, the calculations follow the motion of the material and the finite element mesh coincides with the

same set of material points throughout the computation. Consequently, there is no material motion relative to the convected mesh. This method has its popularity because
(1) the governing equations are simple due to the absence of convective effects, and
(2) the material properties, boundary conditions, stress and strain states can be accurately defined since the material points coincide with finite element mesh and quadrature points throughout the deformation. However, when large distortions occur, there are disadvantages such as:

(1) the meshes become entangled and the resulting shapes may yield negative volumes, and

(2) the time step size is progressively reduced for explicit time-stepping calculations.

On the other hand, the Eulerian description is preferred when it is convenient to model a fixed region in space for situations which may involve large flows, large distortions, and mixing of materials. However, convective effects arise because of the relative motion between the flow of material and the fixed mesh, and these introduce numerical difficulties. Furthermore, the material interfaces and boundaries may move through the mesh which requires special attention.

In this chapter, a general theory of the Arbitrary Lagrangian-Eulerian (ALE) description is derived. The theory can be used to develop an Eulerian description also. The definitions of convective velocity and referential or mesh time derivatives are given. The balance laws, such as conservation of mass, balances of linear and angular momentum and conservation of energy are derived within the *mixed* Lagrangian-Eulerian concept. The degenerations of the mixed description to the two classical descriptions, Lagrangian and Eulerian, are emphasized. The formal statement of the initial/boundary-value problem for the ALE description is also discussed.

7.2 Kinematics in ALE formulation

7.2.1 Mesh Displacement, Mesh Velocity and Mesh Acceleration

In order to complete the *referential* description, it is necessary to define the *referential* motion; this motion is called the *mesh* motion in the finite element formulation.

The *motion* of the body *B*, which occupies a reference region Ω_χ, is given by

$$\mathbf{x} = \hat{\varphi}(\chi, t) = \chi + \hat{\mathbf{u}}(\chi, t) = \varphi(\mathbf{X}, t) \tag{7.2.7}$$

This ALE referential(mesh) region Ω_χ is specified throughout and its motion is defined by the mapping function $\hat{\varphi}$ such that the motion of $\chi \quad \Omega_\chi$ at time *t* is denoted by $\chi \quad \Omega_\chi$ and $\hat{\mathbf{u}}(\chi, t)$ is the *mesh* displacement in the finite element formulation. It is noted that even thought in general the mesh function $\hat{\varphi}$ is different from the material function φ, the two motions are the same as given in Eq.(7.2.7). The corresponding velocity (*mesh* velocity) and acceleration (*mesh* acceleration) are defined as :

$$\hat{\mathbf{v}} = \left.\frac{\partial \mathbf{x}}{\partial t}\right|_{[\chi]} = \mathbf{x}_{,t[\chi]} = \hat{\mathbf{u}}_{,t[\chi]} \qquad \text{mesh velocity} \tag{7.2.8a}$$

and

$$\hat{\mathbf{a}} = \left.\frac{\partial \hat{\mathbf{v}}}{\partial t}\right|_{[\chi]} = \hat{\mathbf{v}}_{,t[\chi]} \qquad \text{mesh acceleration} \qquad (7.2.8b)$$

The motion $\hat{\varphi}$ is arbitrary and the usefulness of the referential description will depend on how this motion is chosen.

Depending on the choice of χ, we can obtain the Lagranginan description by setting $\chi = \mathbf{X}$ and $\hat{\varphi} = \varphi$, the Eulerian description by setting $\chi = \mathbf{x}$, and the ALE description by setting $\hat{\varphi} \neq \varphi$. The *general* referential description is referred to as Arbitrary Lagrangian-Eulerian (ALE) in the finite element formulation. In this description, the function $\hat{\varphi}$ must be specified such that the mapping between $\mathbf{x}$ and χ is one to one. With this assumption and by the composition of the mapping (denoted by a circle), a third mapping is defined such that

$$\chi = \psi(\mathbf{X}, t) = \hat{\varphi}^{-1} \circ \varphi(\mathbf{X}, t) \qquad (7.2.10)$$

Similarly, for this motion *displacement*, *velocity* and *acceleration* variables can be defined.

However, this is not necessary. These displacement, velocity and acceleration variables can instead be defined with the aid of the chain rule and the appropriate mappings.

The schematic set up of these descriptions in one-dimension is shown in Fig. 1, and a summary of the three descriptions is given in Table 7.1.

Fig.7.2 is shown to compare the three descriptions further, where the 1D motion of the material is specified as:

$$x = (1 - X^2)t + X\,t^2 + X$$

Fig 7.2 Comparsion of Lagranian, Eulerian, ALE description

References:

Fried, I., and Johnson, A. R., [1988]. "A Note on Elastic Energy Density Function for Largely Deformed Compressible Rubber Solids," Computer Methods in Applied Mechanics and Engineering, 69, pp. 53-64.

Hughes, T. J. R., [1987]. The Finite Element Method, Linear Static and Dynamic Finite Element Analysis, Prentice-Hall.

Malvern, L. E., [1969]. Introduction to the Mechanics of a Continuous Medium, Prentice-Hall.

Noble, B., [1969]. Applied Linear Algebra, Prentice-Hall.

Oden, J. T., [1972]. Finite Elements of Nonlinear Continua, McGraw Hill.

REFERENCES

Belytschko, T., and Kennedy, J.M. (1978), "Computer Models for Subassembly Simulation," Nuclear Engineering Design, Volume 49, pp. 17-38.

Belytschko, T., Kennedy, J.M., and Schoeberie, D.F. (1980), 'QuasiEulerian Finite Element Formulation for Fluid Structure Interaction, 11 Journal of Pressure Vessel Technology, American Society of Mechanical Engineers, Volume 102, pp. 62-69.

Belytschko, T. and Liu, W.K. (1985), "Computer Methods for Transient Fluid-Structure Analysis of Nuclear Reactors," Nuclear Safety, Volume 26, pp. 14-31.

Bird, R.B., Amstrong, R.C., and Hassager, 0. (1977), Dynamics of Polymeric Liquids, Volume 1: Fluid Mechanics, John Wiley and Sons, 458 pages.

Brugnot, G., and Pochet, R. (1981), "Numerical Simulation Study of Avalanches," Journal of Glaciology, Volume 27, Number 95, pp. 7788.

Brooks, A.N., and Hughes, T.J.R. (1982), "Streamline Upwind/PetrovGalerkin Formulations for Convection Dominated Flows with Particular Emphasis on the Incompressible Navier-Stokes Equations, " Computer Methods in Applied Mechanics and Engineering-, Volume 32, pp. 199-259.

Carey, G.F., and Oden, J.T. (1986), Finite Elements: Fluid Mechanics, Volume VI of the Texas Finite Element Series, Prentice Hall, 323 pages.

Chen, C., and Armbruster, J.T. (1980), "Dam-Break Wave Model: Formulation and Verification," Journal of the Hydraulics Division,

American Society of Civil Engineers, Volume 106, Number HY5, pp.747-767.

Donea, J. (1983), "Arbitrary Lagrangian-Eulerian Finite Element Methods," Computational Methods for Transient Analysis, Edited by T. Belytschko and T.J.R. Hughes, Elvesier Science Publishers, pp. 473-516.

Donea, J. (1984), "A Taylor-Galerkin Method for Convective Transport Problems," International Journal for Numerical Methods in Engineering, Volume 20, pp. 101-119.

Donea, J., Fasoli-Stella, P., and Giuliani, S. (1977), "Lagrangian and Eulerian Finite Element Techniques for Transient Fluid Structure Interaction Problems," Transactions of the 4th International Conference on Structural Mechanics in Reactor Technology, Paper Bl/2.

Dressler, R.F. (1952), "Hydraulic Resistance Effect Upon the Dam-Break Functions,' Journal of Research of the National Bureau of Standards, Volume 49, Number 3, pp. 217-225.

Goring, D.G. (1978), Tsunamis-The Propagation of Long Waves onto a Shelf, Dissertation submitted to the California Institute of Technology in partial fulfillment of the requirements for the degree of Doctor of Philosophy, 337 pages.

Heinrich, J.C., Huyakorn, P.S., Zienkiewicz, O.C., and Mitchell, A.R. (1977), "An Upwind Finite Element Scheme for Two-Dimensional Convective Transport,' International Journal for Numerical Methods in Engineering, Volume 11, pp. 131-145.

Heinrich, J.C., and Zienkiewicz, O.C. (1979), "The Finite Element Method and "Upwinding" Techniques in the Numerical Solution of Convection Dominated Flow Problems,' in Finite Elements for-Convection Dominated Flow, Edited by T.H.R. Hughes, American Society of Mechanical Engineers, Volume 34, pp. 105-136.

Hirt, C.W., Amsden, A.A., and Cook, J.L. (1974), " An Arbitrary Lagrangian Eulerian Computing Method for All Flow Speeds,' Journal of Computational Physics, Volume 14, pp. 227-253.

Huerta, A. (1987), Numerical Modeling of Slurry Mechanics Problems. Dissertation submitted to Northwestern University in partial fulfillment of the requirements for the degree of Doctor of Philosophy, 187 pages.

Huerta, A., and Liu, W.K. (1987), "Viscous Flow Structure Interaction," to appear in Journal of Pressure Vessel Technology, American Society of Mechanical Engineers.

Hughes, T.J.R. (1978), 'A Simple Scheme for Developing Upwind Finite Elements,' International Journal of Numerical Methods in Engineering, Volume 12, pp. 1359-1365.

Hughes, T.J.R., and Brooks, A.N. (1982), 'A Theoretical Framework for Petrov-Galerkin Methods with Discontinuous Weighting Functions: Application to the Streamline-Upwind Procedure," Finite Elements in Fluids, Edited by R.H. Gallagher et al, John Wiley and Sons Ltd., Volume 4, pp. 47-65.

Hughes, T.J.R., and Liu, W.K. (1978), 'Implicit-Explicit Finite Elements in Transient Analysis' Journal of Applied Mechanics, Volume 45, pp. 371-378.

Hughes, T.J.R., Liu, W.K., and Zimmerman, T.K. (1981), "LagrangianEulerian Finite Element Formulation for Incompressible Viscous Flows", Computer Methods in Applied Mechanics and Engineering, Volume 29, pp. 329-349.

Hughes, T.J.R., and Mallet, M. (1986), "A New Finite Element Formulation for Computational Fluid Dynamics: III. The Generalized Streamline Operator for Multidimensional AdvectiveDiffusive Systems," Computer Methods in Applied Mechanics and Engineering" , Volume 58, pp. 305-328.

Hughes, T.J.R., and Tezduyar, T.E. (1984), "Finite Element Methods for First-Order Hyperbolic Systems with Particular Emphasis on the Compressible Euler Equations", Computer Methods in Applied Mechanics and Engineering, Volume 45, pp. 217-284.

Hutter, K., and Vulliet, L. (1985), 'Gravity-Driven Slow Creeping Flow of a Thermoviscous Body at Elevated Temperatures," Journal of Thermal Stresses, Volume 8, pp. 99-138.

Jeyapalan, J.K. (1980), Analysis of Flow Failures of Mine Tailings Impoundements, Dissertation submitted to the University of California, Berkeley, in partial fulfillment of the requirements for the degree of Doctor of Philosophy, 298 pages.

Keentok, M., Milthorpe, J.F., and O'Donovan, E. (1985), "On the Shearing Zone Around Rotating Vanes in Plastic Liquids: Theory and Experiment," Journal of Non-Newtonian Fluid Mechanics, Volume 17, pp. 23-35.

Liu, W.K., Belytschko, T., and Chang, H. (1986), "An Arbitrary Lagrangian-Eulerian Finite Element Method for Path Dependent Materials," Computer Methods in Applied Mechanics and Engineering, Volume 58, pp. 227-246.

Liu, W.K., and Chang, H. G. (1984), "Efficient Computational Procedures for Long-Time Duration Fluid-Structure Interaction Problems," Journal of Pressure Vessel Technology, American Society of Mechanical Engineers, Volume 106, pp. 317-322.

Liu, W.K., and Chang, H. G. (1985), "A Method of Computation for Fluid Structure Interaction," Journal of Computers and Structures", Volume 20, Number 1-3, pp. 311-320.

Liu, W.K., Chang, H., and Belytschko, T. (1987), "Arbitrary Lagrangian-Eulerian Petrov-Galerkin Finite Elements for Nonlinear Continua," to appear in Computer Methods in Applied Mechanics and Engineering.

Liu, W.K., and Gvildys, J. (1986), 'Fluid Structure Interactions of Tanks with and Eccentric Core Barrel," Computer Methods in-Applied Mechanics and Engineering, Volume 58, pp. 51-57.

Liu, W.K., Lam, D., and Belytschko, T. (1984), "Finite Element Method for Hydrodynamic Mass with Nonstationary Fluid," Computer Methods in Applied Mechanics and Engineering, Volume 44, pp. 177-211.

Liu, W.K., and Ma, D. (1982), "Computer Implementation Aspects for Fluid Structure Interaction Problems," Computer Methods in Applied Mechanics and Engineering, Volume 31, pp. 129-148.

Lohner, R., Morgan, K., and Zienkiewicz, O.C. (1984), "The Solution of Nonlinear Hyperbolic Equations Systems by the Finite Element Method," International Journal for Numerical Methods in Fluids, Volume 4, pp. 1043-1063.

Ma, D.C., Gvildys, J., Chang, Y.W. , and Liu, W.K. (1982), "Seismic Behavior of Liquid-Filled Shells," Nuclear Engineering- and Design, Volume 72, pp. 437-455.

Malvern, L.E. (1965), Introduction to the Mechanics of a Continuous Medium. Prentice Hall, Engelwood Cliffs, New Jersey.

Muto, K., Kasai, Y., Nakahara, M., and Ishida, Y. (1985), "Experimental Tests on Sloshing Response of a Water Pool with Submerged Blocks," Proceedings of the 1985 Pressure Vessels and Piping Conference, Volume 98-7 (Fluid-Structure Dynamics), Edited by S.J. Brown, American Society of Mechanical Engineers, pp. 209214.

Noh, W.F. (1964), "CEL: A Time-Dependent- Two-Space.-Dimensional Coupled Eulerian-Lagrangian Code,' in Methods in Computational Physics, Volume 3, Edited by B. Alder, S. Fernbach and M. Rotenberg, Academic Press, New York.

O'Donovan, E.J., and Tanner, R.I. (1984), "Numerical Study of the Bingham Squeeze Film Problem,' Journal of Non-Newtonian FluidMechanics, Volume 15, pp. 75-83.

Ramaswamy, B., Kawahara, M., and Nakayama, T. (1986), "Lagrangian Finite Element Method for the Analysis of Two-Dimensional Sloshing Problems," International Journal for Numerical Methods in Fluids, Volume 6, pp. 659-670.

Ritchmyer, R.D., and Morton, K.W. (1967), Difference Methods for 56 Initial-Value Problems, Interscience, New York, 2nd edition.

Sakkas, J.G., and Strelkoff, T. (1976), 'Dimensionless Solution of Dam-Break Flood Waves," Journal of the Hydraulics Division, American Society of Civil Engineers, Volume 102, Number HY2, pp. 171-184.

Strelkoff, T. (1969), "One Dimensional Equations for Open Channel Flow," Journal of the Hydraulics Division, American Society of Civil Engineers, Volume 95, Number HY3, pp. 861-876.

Tangy, P., Fortin, M., and Choplin, L. (1984), 'Finite Element Simulation of Dip Coating, II: Non-Newtonian Fluids," International Journal for Numerical Methods in Fluids, Volume 4, pp. 459-475.

Whitham, G.B. (1955), "The Effects of Hydraulic Resistance in the DamBreak Problem," Proceeding-s of the Royal Society of London, Series A, Volume 227, pp. 399-407.

Zienkiewicz, O.C., and Bettess, P. (1978), "Fluid-Structure Dynamic Interaction and Wave Forces. An Introduction to Numerical Treatment," International Journal of Numerical Methods in Engineering, Volume 13, pp. 1-16.

1. Belytschko, T. and Kennedy, J.M., 'Computer models for subassembly simulation', *Nucl. Engrg. Design,* **49** (1978), 17-38.
2. Liu, W.K. and Ma, D.C., 'Computer implementation aspects for fluid-structure interaction problems', *Comput. Methos. Appl. Mech. Engrg.*, **31**(1982), 129-148.
3. Brooks, A.N. and Hughes, T.J.R., 'Streamline upwind/Petrov-Galerkin formulations for convection dominated flows with particular emphasis on the incompressible Navier-Stokes equations', *Comput. Meths. Appl. Mech. Engrg.*, **32**(1982), 199-259.
4. Lohner, R., Morgan, K. and Zienkiewicz, O.C., 'The solution of non-linear hyperbolic equations systems by the finite element method', Int. J. Numer. Meths. Fluids, 4(1984), 1043-1063.
5. Liu, W.K. 'Finite element procedures for fluid-structure interactions with application to liquid storage tanks', *Nucl. Engrg. Design,* **65**(1981), 221-238.
6. Liu, W.K. and Chang, H., 'A method of computation for fluid structure interactions', *Comput. & Structures*, **20**(1985), 311-320.
7. Hughes, T.J.R., and Liu, W.K., 'Implicit-explicit finite elements in transient analysis', *J. Appl.Mech.*, **45**(1978), 371-378.
8. Liu, W.K., Belytschko, T. And Chang, H., 'An arbitrary Lagrangian-Eulerian finite element method for path-dependent materials', *Comput. Meths. Appl. Mech. Engrg.*, **58**(1986), 227-246.
9. Liu, W.K., Ong, J.S., and Uras, R.A., 'Finite element stabilization matrices¾ a unification approach', *Comput. Meths. Appl. Mech. Engrg.*, **53**(1985), 13-46.
10. Belytschko, T., Ong,S.-J, Liu, W.K., and Kennedy, J.M., 'Hourglass control in linear and nonlinear problems', *Comput. Meths. Appl. Mech. Engrg.*, **43**(1984), 251-276.
11. Liu, W.K., Chang, H, Chen, J-S, and Belytschko, T., 'Arbitrary Lagrangian-Eulerian Petrov-Galerkin finite elements for nonlinear continua', *Comput. Meths. Appl. Mech. Engrg.*, **68**(1988), 259-310.

12. Benson, D.J., 'An efficient, accurate simple ALE method for nonlinear finite element programs', *Comput. Meths. Appl. Mech. Engrg,* ***72****(1989), 205-350.*

CHAPTER 8
ELEMENT TECHNOLOGY

by Ted Belytschko
Northwestern University

8.1 Introduction

Element technology is concerned with obtaining elements with better performance, particularly for large-scale calculations and for incompressible materials. For large-scale calculations, element technology has focused primarily on underintegration to achieve faster elements. For three dimensions, cost reductions on the order of 8 have been achieved through underintegration. However, underintegration requires the stabilization of the element. Although stabilization has not been too popular in the academic literature, it is ubiquitous in large scale calculations in industry. As shown in this chapter, it has a firm theoretical basis and can be combined with multi-field weak forms to obtain elements which are of high accuracy.

The second major thrust of element technology in continuum elements has been to eliminate the difficulties associated with the treatment of incompressible materials. Low-order elements, when applied to incompressible materials, tend to exhibit volumetric locking. In volumetric locking, the displacements are underpredicted by large factors, 5 to 10 is not uncommon for otherwise reasonable meshes. Although incompressible materials are quite rare in linear stress analysis, in the nonlinear regime many materials behave in a nearly incompressible manner. For example, Mises elastic-plastic materials are incompressible in their plastic behavior. Though the elastic behavior may be compressible, the overall behavior is nearly incompressible, and an element that locks volumetrically will not perform well for Mises elastic-plastic materials. Rubbers are also incompressible in large deformations. To be applicable to a large class of nonlinear materials, an element must be able to treat incompressible materials effectively. However, most elements have shortcomings in their performance when applied to incompressible or nearly incompressible materials. An understanding of these shortcomings are crucial in the selection of elements for nonlinear analysis.

To eliminate volumetric locking, two classes of techniques have evolved:

1. multi-field elements in which the pressures or complete stress and strain fields are also considered as dependent variables;
2. reduced integration procedures in which certain terms of the weak form for the internal forces are underintegrated.

Multi-field elements are based on multi-field weak forms or variational principles; these are also known as mixed variational principles. In multi-field elements, additional variables, such as the stresses or strains, are considered as dependent, at least on the element level, and interpolated independently of the displacements. This enables the strain or stress fields to be designed so as to avoid volumetric locking. In many cases, the strain or stress fields are also designed to achieve better accuracy for beam bending problems. These methods cannot improve the performance of an element in general when there are no constraints

such as incompressibility. In fact, for a 4-node quadrilateral, only a 3 parameter family of elements is convergent and the rate of convergence can never exceed that of the 4-node quadrilateral. Thus the only goals that can be achieved by mixed elements is to avoid locking and to improve behavior in a selected class of problems, such as beam bending.

The unfortunate byproduct of using multi-field variational principles is that in many cases the resulting elements posses instabilities in the additonal fields. Thus most 4-node quadrilaterals based on multi-field weak forms are subject to a pressure instability. This requires another fix, so that the resulting element can be quite complex. The developemnt of truly robust elements is not easy, particularly for low order elements. For this reason, an understanding of element technology is useful to anyone engaged in finite element analysis.

Elements developed by means of underintegration in its various forms are quite similar from a fundamental and practical viewpoint to elements based on multi-field variational principles, and the equivalence was proven by Malkus and Hughes() for certain classes of elements. Therefore, while underintegration is more easily understood than multi-field approaches, the methods suffer from the same shortcomings as multi-field elements: pressure instabilities. Nevertheless, they provide a straightforward way to overcome locking in certain classes of elements.

We will begin the chapter with an overview of element performance in Section 8.1. This Section describes the characteristics of many of the most widely used elements for continuum analysis. The description is limited to elements which are based on polynomials of quadratic order or lower, since elements of higher order are seldom used in nonlinear analysis at this time. This will set the stage for the material that follows. Many readers may want to skip the remainder of the Chapter or only read selected parts based on what they have learned from this Section.

Although the techniques introduced in this Chapter are primarily useful for controlling volumetric locking for incompressible and nearly incompressible materials, they apply more generally to what can collectively be called constrained media problems. Another important class of such problems are structural problems, such as thin-walled shells and beams. The same techniques described in this Chapter will be used in Chapter 9 to develop beam and shell elements.

Section 8.3 describes the patch tests. These are important, useful tests for the performance of an element. Patch tests can be used to examine whether an element is convergent, whether it avoids locking and whether it is stable. Various forms of the patch test are described which are applicable to both static programs and programs with explicit time integration. They test both the underlying soundness of the approximations used in the elements and the correctness of the implementation.

Section 8.4 describes some of the major multi-field weak forms and their application to element development. Although the first major multi-field variational principle to be discovered for elasticity was the Hellinger-Reissner variational principle, it is not considered because it can not be readily used with strain-driven constitutive equations in nonlinear analysis. Therefore, we will confine ourselves to various forms of the Hu-Washizu principles and some simplifications that are useful in the design of new elements.

We will also describe some limitation principles and stability issues which pertain to mixed elements.

To illustrate the application of element technology, we will focus on the 4-node isoparametric quadrilateral element (QUAD4). This element is convergent for compressible material without any modifications, so none of the techniques described in this Chapter are needed if this element is to be used for compressible materials. On the other hand, for incompressible or nearly incompressible materials, this element locks. We will illustrate two classes of techniques to eliminate volumetric locking: reduced integration and multi-field elements. We then show that reduced integration by one-point quadrature is rank deficient, which leads to spurious singular modes. To stabilize these modes, we first consider perturbation hourglass stabilization of Flanagan and Belytschko (1981). We then derive mixed methods for stabilization of Belytschko and Bachrach (1986), and assumed strain stabilization of Belytschko and Bindeman (1991). We show that assumed strain stabilization can be used with multiple-point quadrature to obtain better results when the material response is nonlinear without great increases in cost. The elements of Pian and Sumihara() and Simo and Rifai() are also described and compared. Numerical results are also presented to demonstrate the performance of various implementations of this element. Finally, the extension of these results to the 8-node hexhedron is sketched.

8.2. Overview of Element Performance

In this Section, we will provide an overview of characteristics of various widely-used elements with the aim of giving the reader a general idea of how these elements perform, their advantages and their major difficulties. This will provide the reader with an understanding of the consequences of the theoretical results and procedures which are described later in this Chapter. We will concentrate on elements in two dimensions, since the properties of these elements parallel those in three dimensions; the corresponding elements in three dimension will be specified and briefly discussed. The overview is limited to continuum elements; the properties of shell elements are described in Chapter 9.

In choosing elements, the ease of mesh generation for a particular element should be borne in mind. Triangles and tetrahedral elements are very attractive because the most powerful mesh generators today are only applicable to these elements. Mesh generators for quadrilateral elements tend to be less robust and more time consuming. Therefore, triangular and tetrahedral elements are preferable when all other performance characteristics are the same for general purpose analysis.

The most frequently used low-order elements are the three-node triangle and the four-node quadrilateral. The corresponding three dimensional elements are the 4-node tetrahedron and the 8-node hexahedron. The detailed displacement and strain fields are given later, but as is well-known to anyone familiar with linear finite element theory, the displacement fields of the triangle and tetrahedron are linear and the strains are constant. The displacement fields of the quadrilateral and hexahedron are bilinear and trilinear, respectively. All of these elements can represent a linear displacement field and constant strain field exactly. Consequently they satisfy the standard patch test, which is described in Section 8.3. The satisfaction of the standard patch test insures that the elements converge

in linear analysis, and provide a good guarantee for convergent behavior in nonlinear problems also, although there are no theoretical proofs of this statement.

We will first discuss the simplest elements, the three-node triangle in two dimensions, the four-node tetrahedron in three dimensions. These are also known as simplex elements because a simplex is a set of $n+1$ points in n dimensions. Neither simplex element performs very well for incompressible materials. Constant-strain triangular and tetrahedral elements are characterized by severe *volumetric locking in two-dimensional plane strain problems and in three dimensions*. They also manifest stiff behavior in many other cases, such as beam bending. For arbitrary arrangements of these elements, volumetric locking is very pronounced for materials such as Mises plasticity. The proviso plane strain is added here because volumetric locking will not occur in plane stress problems, for in plane stress the thickness of the element can change to accommodate incompressible materials. The consequences of volumetric locking are almost a complete lack of convergence. In the presence of volumetric locking, displacements are underpredicted by factors of 5 or more, so the results are completely worthless.

Volumetric locking does not preclude the use of simplex elements for incompressible materials completely, for locking can be avoided by using special arrangements of the elements. For example, the cross-diagonal arrangement of triangles shown in Fig.?? eliminates locking, Naagtegal et al. However, meshing in this arrangement is similar to meshing quadrilaterals, so the benefits arising from triangular and tetrahedral meshing are lost. In addition, this arrangement results in pressure oscillations, such as those described subsequently for quadrilaterals.

When fully integrated, i.e. 2x2 Gauss quadrature for the quadrilateral, both the 4-node quadrilateral and the hexahedron lock for incompressible materials. Volumetric locking can be eliminated in these elements by using reduced integration, namely one-point quadrature, or selective-reduced integration, which consists of one-point quadrature on the volumetric terms and 2x2 quadrature on the deviatoric terms; this is described in detail later. The resulting quadrilateral will then exhibit good convergence properties in the displacements. However, the element still is plagued by one flaw: it exhibits pressure oscillations due to the failure of the quadrilateral with modified quadrature to satisfy the BB-condition, which is described later. As a consequence, the pressure field will often be oscillatory, with a pattern of pressures as shown in fig, ??. This oscillatory pattern in the pressures is often known as checkerboarding. Checkerboarding is sometimes harmless: for example, in materials governed by the Mises law the response is independent of pressure, so pressure oscillations are not very harmful, although they lead to errors in the elastic strains. Checkerboarding can also be eliminated by filtering procedures. Nevertheless it is undesirable, and a user of finite elements should at least be aware of its possibility with these elements. Pressure oscillations also occur for the mixed elements based on multi-field variational principles. In fact mixed elements are in many cases identical or very similar in performance to selective reduced integration elements, since theoretically they are in many cases equivalent, Malkus and Hughes(). Some stabilization procedures for BB oscillations have been developed; they are described and discussed in Section ??.

In large scale computations, the fastest form of the quadrilateral and hexahedron is the one-point quadrature element: it is often 3 to 4 times as fast as the selective-reduced quadrature quadrilateral element. In three dimensions, the speedup is of the order of 6 to 8.

The one-point quadrature element also suffers from pressure oscillations, and in addition possess instabilities in the displacement field. These instabilities are shown in Fig. ??, and have various names: hourglassing, keystoning, kinematic modes, spurious zero energy modes and chickenwiring are some of the appellations for these modes. The control of these modes has been the topic of considerable research, and they can be controlled quite effectively. In fact, the rate of convergence is not decreased by a consistent control of these modes, so for many large scale calculations, one-point quadrature with hourglass control are very effective. Hourglass control is described in Sections ???.

The next highest order elements are the 6-node triangle and the 8 and 9 node quadrilaterals. The counterparts in three dimensions are the 10 node tetrahedron and the 20 and 27 node quadrilaterals. The 6-node triangle and 9-node quadrilateral have a complete quadratic displacement field and complete linear strain field when the edges of the element are straight. Ciarlet and Raviart() in a landmark paper proved that the convergence of these elements is quadratic when the displacement of the midside nodes is small compared to the length of the elements; whether the distortions introduced by a mesh in normal mesh generation are small is often an open question. These elements satisfy the quadratic and linear patch tests when the element sides are straight, but only the linear patch test when the element sides are curved. In other words, these elements cannot reproduce a quadratic displacement field exactly when the sides are not straight. Of course, curved sides are an intrinsic advantage of finite elements, for they enable boundary conditions to be met for higher order elements, but curved sides should only be used for exterior surfaces, since their presence decreases the accuracy of the element. In nonlinear problems with large deformations, the performance of these elements degrades when the midside nodes move substantially; this had already been discussed in the one-dimensional context in Example 2.8.2. Element distortion is a pervasive difficulty in the use of higher order elements for large-deformation analysis: the convergence rate of higher order elements degrades significantly as they are distorted, and in addition solution procedures often fail when distortion becomes excessive.

The 6-node triangle does not lock for incompressible materials, but it fails the BB pressure stability test for incompressible materials. The 9-node quadrilateral when developed appropriately by a mixed variational principle with a linear pressure field satisfies the pressure stability test and does not lock. It is the only element we have discussed so far which has flawless behavior for incompressible materials.

In summary, element technology deals with two major quirks:

1. volumetric locking, which prevents convergence for incompressible and nearly incompressible materials;
2. pressure oscillations which result from the failure to meet the BB condition.

For low-order elements, the presence of one of these flaws is nearly unavoidable. The quadrilateral with reduced integration and a pressure stabilization or pressure filter appears to be the best of the low-order elements. When speed of computation is a consideration, a stabilized quadrilateral with one-point quadrature appears to be optimal. Only the 9-node quadrilateral and 27-node hexahedral are flawless elements for imcompressible materials, and the fact that no flaws have been discovered so far does not preclude that none will ever be discovered. Almost all of these difficulties are driven by incompressibility, and persist

for near-incompressiblity. When the material is compressible, or when considering two dimensional plane stress, standard element procedure can be used.

Error Norms. In order to compare these elements further, it is worthwhile to study a convergence theorem which has been proven for linear problems. Although this theorem has not been proven for the nonlinear regime, it provides insight into element accuracy. For the purpose of studying this convergence theorem, we will first define some norms frequently used in error analysis of finite elements. These will also be used to evaluate some of the element technology developed later in this Chapter.

Errors in finite element analysis are measured by norms. A norm in functional analysis is just a way of measuring the distance between two functions. A norm of the difference between a finite element solution and the exact solution to a problem is a measure of the error in the solution. The most common norms for the evaluating the error in a finite element solution are the L_2 norm and the error in energy. The L_2 norm of a vector function $f_i(\mathbf{x})$ is defined by

$$\left\| f_i(\mathbf{x}) \right\|_0 = \left(\int_\Omega f_i(\mathbf{x})\, f_i(\mathbf{x})\, d\Omega \right)^{\frac{1}{2}} \tag{8.2.1}$$

where the subscript nought on the symbol for the norm designates the L_2 norm. It can be seen that the L_2 norm is always positive, and measures an average or mean value of the function. To use the L_2 norm for a measure of error for a finite element solution, we denote the finite element solution for the displacement by $\mathbf{u}^h(\mathbf{x})$ and the exact solution by $\mathbf{u}(\mathbf{x})$. The error in the finite element solution at any point can then be expressed by the vector $\mathbf{e}(\mathbf{x}) = \mathbf{u}^h(\mathbf{x}) - \mathbf{u}(\mathbf{x})$. Since we seek a single number for the error, we will use the magnitude of the vector $\mathbf{e}(\mathbf{x})$. which is $\mathbf{e}(\mathbf{x})\ \mathbf{e}(\mathbf{x})$. Thus we can define the error in the displacements by the L_2 norm as

$$\left\| \mathbf{e}(\mathbf{x}) \right\|_0 = \left(\int_\Omega \mathbf{e}(\mathbf{x})\ \mathbf{e}(\mathbf{x})\, d\Omega \right)^{\frac{1}{2}} \quad \text{or} \quad \left\| \mathbf{u} - \mathbf{u}^h \right\|_0 = \left(\int_\Omega \left(\mathbf{u} - \mathbf{u}^h\right) \left(\mathbf{u} - \mathbf{u}^h\right) d\Omega \right)^{\frac{1}{2}} \tag{8.2.2}$$

This error norm measures the average error in the displacements over the domain of the problem. There are many other error norms. We have chosen to use this one because the most powerful and most well known results are expressed in terms of this norm. Furthermore, it gives a measure of error which is useful for engineering purposes.

The second norm we will consider are the norms in Hilbert space. The H_1 norm of a vector function is defined by

$$\left\| f_i(\mathbf{x}) \right\|_1 = \left(\int_\Omega f_i(\mathbf{x}) f_i(\mathbf{x}) + f_{i,j}(\mathbf{x}) f_{i,j}(\mathbf{x}) d\Omega \right)^{\frac{1}{2}} \tag{8.2.3}$$

This norm is a good measure of the error in the derivatives of a function. It includes the terms from the L_2 norm given in Eq. (1), but when applied to real approximations, the errors in the derivatives dwarf the errors in the function itself, so they play an insignificant role. If we take the H_1 norm of the error in the displacements, i.e. by letting $f_i(\mathbf{x}) = u_i^h(\mathbf{x}) - u_i(\mathbf{x})$ we otain a useful measure of the error in strains. The errors in norm, incidentally, are usually similar to the error in energy, Hughes(,p.273) which is defined by

$$\left\| a(\mathbf{u}, \mathbf{u}) \right\|_1 = \left(\int_\Omega e_{ij} C_{ijkl} e_{kl} d\Omega \right)^{\frac{1}{2}} \qquad e_{ij} = \varepsilon_{ij} - \varepsilon_{ij}^h \tag{8.2.4}$$

Note the similarity of this form to the strain energy defined in Eq. (). In the above expression, the error in strain replaces the strain in Eq.(), hence the name energy error in strain.

We conclude with a few more facts on norms. The H_r norm is generated in terms of the *r*th derivatives of the function. Thus the H_0 norm is equivalent to the L_2 norm, Eq (1), whereas the H_2 norm would involve the squares of the second derivatives. These norms exist, i.e. the integral corresponding to the norms H_r, is integrable, when the function is of continuity C^{r-1}. This can be seen quite easily for the H_1 norm: if the function $f_i(\mathbf{x})$ is not $C^{0,}$ i.e. if it is discontinuious, then the derivatives will be Dirac delta functions at the points of the discontinuity. The square of a Dirac delta function cannot be integrated, so the norm can not be evaluated. The kinematic admissibility conditions () are often stated in terms of Hilbert spaces, so in Eq () the requirement could be replaced by . The latter is often found in the literature, but we used the simpler concept since we were not concerned with convergence proofs. For more on norms, seminorms, and other good stuff of this type see Hughes(), Oden and Reddy() or Strang().

Convergence Results for Linear Problems. The fundamental convergence results for linear finite elements is given in the following. If the finite element solution is generated by elements which can reproduce polynomials of order *k*, and if the solution $\mathbf{u}(\mathbf{x})$ is sufficiently smooth for the Hilbert norm H_r to exist, then

$$\left\| \mathbf{u} - \mathbf{u}^h \right\|_m \le C h^\alpha \left\| u \right\|_r, \quad \alpha = min(k+1-m, r-m) \tag{8.2.5}$$

where *h* is a measure of element size and C is an arbitrary constant which is independent of *h* and varies from problem to problem.

We will now examine the implications of this theorem for various elements. The parameter α indicates the rate of convergence of the finite element solution: the greater the value of α, the faster the finite element solution converges to the exact solution and therefore the more accurate the element. It is important to note that the rate of convergence is limited by the smoothness of the solution in space. An elastic solution is analytic, i.e. infinitely smooth, if there are no acute corners or cracks, so in that case r tends toward infinity. Therefore, the second term in the definition for α, $r - m$, plays no role for smooth solutions. However, if the solution is not very smooth, i.e. if there are discontinuities in the derivatives or higher order derivatives, then r is finite. For example, if there are discontinuities in the second derivatives, then r is at most 2, and the second term plays a role.

We first examine what Eq. (5) means for smooth elastic solutions for various elements for the error in displacements. In that case, we consider the H_0 norm, which is equivalent to the L_2 norm, so $m = 0$. The 3-node triangle, the 4-node quadrilateral, the 4-node tetrahedron and the 8-node hexahedron all reproduce in linear polynomials exactly; this result is proven for the isoparametric elements in Section 8.?; therefore $k = 1$. Therefore, for the elements with linear completeness just listed we obtain that

$$\alpha = min(k + 1 - m, r - m) = min(1 + 1 - 0, \infty - 0) = 2$$

This result is illustrated in Fig. (), which shows a log-log plot of the error for the plate with a hole; details of this problem are given in Section ??. In a log-log plot, the graph of error in displacements versus element size according to Eq. (5) is given by a straight line with a slope $\alpha = 2$. The solution in this case is said to converge quadratically. The actual numerical results compare with this theoretical result quite closely, although the slope deviates 5% or so from the theoretical result. Equation 5 is an aymptotic result which should hold only as the element size goes to zero, but remarkably it agrees very well with numerical experiments with realistic meshes.

We next consider the higher order elements, namely the 6-node triangle, the 9-node quadrilateral, the tetrahedron and the 27-node hexahedron with straight edges. In this case $k = 2$, and for an elastic solution the remaining constants are unchanged. We find then that $\alpha = 3$, so the rate of convergence is cubic in the displacements. This increase of one order in convergence is quite significant, as illustrated in the results shown in Fig. ??. In effect, the choice of a higher order element here buys a tremendous amount of accuracy.

The results for the strains, i.e. the derivatives of the displacement field, are similar. In this case $m = 1$ since the error in strains is indicated by the H1-norm. The rates of convergence are then one order lower, $\alpha = 1$ for elements with linear completeness, $k = 1$, and $\alpha = 2$ for elements with quadratic completeness, $k = 2$. the results are illustrated for a plate with a hole in fig. ??.

Convergence in Nonlinear Problems. The behavior of elements for nonlinear problems according to this theorem, Eq (), will depend on the smoothness of the constitutive equation. If the constitutive equation is very smooth, such as hyperelastic models for rubber, then the rate of convergence are expected to be the same as for elastic, linear

materials. However, for constitutive equations which are not smooth, such as elastic-plastic materials, the second term in the definition of α governs the accuracy. For example in an elastic-plastic material, the relation between stress and strain is C0. Therefore the displacements are at most C1, and $r = 2$. It can now be seen that the rate of convergence of the displacements now is at most of order 2, i.e. $\alpha = 2$, regardless of whether the completeness of the element is as indicated by k is linear or quadratic. Thus there appears to be no benefit in going to a higher order element for these materials. Similarly, the rate of convergence in the strains is at most of order $\alpha = 1$. Thus, if the constitutive equation is not very smooth, the benefits of a higher order element can be lost.

In summary, for smooth constitutive equations, higher order elements are advantageous because of their higher rate of convergence. If the constitutive equation lacks sufficient smoothness, then there is no advantage in going to higher order elements. These results also are relevant for dynamic problems: when the signals are very smooth, there is some benefit in going to higher order elements, provided that a consistent mass matrix is used. For signals which lack smoothness, there is little advantage to higher order elements.

These statements do not take cognizance of the deterioration of element performance with large deformations. When the deformations are so large that the elements are highly distorted, then the accuracy of the higher order elements also decreases. These provisos pertain to both total and updated Lagrangian meshes, but not to Eulerian meshes. Thus, the amount of element distortion expected should also be considered in the choice of an element for nonlinear analysis.

It could be argued that even elastic problems in practical situations have discontinuities in derivatives due to different materials. However, in linear problems, the element edges are usually aligned with the material interfaces. In that case, the full accuracy of higher order elements can be retained since they can model discontinuities in derivatives effectively along element edges. In elastic-plastic problems, on the other hand, discontinuities float through the model and as the problem evolves, they proliferate. Thus their effects in nonlinear problems are more devastating to accuracy.

It should be stressed that the convergence results (5) has only been proven for linear problems. However, the major impediment to obtaining such convergence results for nonlinear problems is probably the lack of stability of nonlinear solutions. It is likely that the estimates given above, which are based on interpolation error estimates, play a similar role in nonlinear problems. This conjecture appears to be verified by numerical convergence studies which have verified that the estimates () apply in nonlinear problems quite well.

8.3. The Patch Tests

The patch tests are an extremely useful for examining the soundness of element formulations, for examining their stability and convergence behavior, and checking the proper implementation of an element in a compute program. The patch test was first conceived by Irons() to examine the soundness of a nonconforming plate element. In this original form, the patch test was primarily a test for polynomial completeness, i.e. the ability to reproduce exactly a polynomial of order k. It has been proposed by Strang() that

the patch test is necessary and sufficient for convergence. Subsequently, the patch test has been generalized and modified so that it can test also for stability in pressures and displacements, simo(), bathe(). Methods for implementing the patch test in explicit programs have also been developed, Belytschko(). Special versions of the patch test to test performance in large displacement analysis can also be constructed. In the following we describe these various forms of the patch test.

Before describing the patch test, it is worthwhile to define a few terms and point out a few overlaps in terms which are at times confusing. In functional analysis, the term completeness refers to the ability of an approximation to approximate a function arbitrarily closely. A sequence of functions $\varphi_I(\mathbf{x})$ is complete in H_r if for any function $f(\mathbf{x}) \quad H_r$,

$$\left\| f(\mathbf{x}) - \sum_{I=1}^{n} a_I \varphi_I(\mathbf{x}) \right\|_r \rightarrow 0 \quad \text{as } n \rightarrow \infty \tag{8.2.3}$$

Thus any set of functions is complete if it can approximate any function of a specified continuity arbitrarily closely, when the error is measured by an appropriate norm. The appropriate norm is any norm which exists or a lower order norm.

In the preceding we have referred to polynomial completeness. A better terms which has emerged in wavelet thoery is the reproducing condition. The reproducing condition is defined by the ability of an approximation to reproduce a function exactly. Thus for an interpolant such as a finite element shape function, the reproducing conditions state that if the nodal values of an element are given by $p_i(\mathbf{x}_J)$ where $p_i(\mathbf{x})$ is an arbitrary function, then

$$\sum_{J=1}^{m} N_J(\mathbf{x}) p_i(\mathbf{x}_J) = p_i(\mathbf{x}) \tag{8.3.4}$$

This equation is quite subtle and contains more than first meets the eye. It states that when the reproducing condition holds, the shape functions or interpolants are able to exactly reproduce the given function $p_i(\mathbf{x})$. For example, if the shape functions are able to reproduce the constant and linear functions, then we have

$$\sum_{J=1}^{m} N_J(\mathbf{x}) = 1, \quad \sum_{J=1}^{m} N_J(\mathbf{x}) x_{jJ} = x_j \tag{8.3.5}$$

This is called linear completeness by Hughes(), but the term reproducing condition seems more appropriate, since completeness refers to a more general condition described by (4). Therefore, when using completeness in the sense of Hughes we will use the term polynomial completeness.

Any approximation which satisfies the linear reproducing conditions can be shown to be complete. On the other hand, the converse does not hold. Consider for example the Fourier series: they are complete, but they cannot reproduce a linear polynomial.

A third definition pertinent to convergence is the defintion of consistency. Consistency is usually defined in the context of finite difference methods. According to the standard definitions of consiostency, a discretization in space $D(u)$ is a consistent approximation of a partial differential equation $L(u)=0$ if the error is on the order of the meshsize, i.e. if

$$L(u)-D(u)=o\left(h^n\right), \qquad n \geq 1$$

The above states that the truncation error must tend to zero as the nodal spacing, i.e. the element size tends to zero. For time dependent problems, the disretization error will be a function of the time step and the element size h, and the truncation error will depend on both. For a time-independent problem in one dimension

Standard Patch Test. We first describe the standard patch test which checks for polynomial completeness of the displacement field, i.e. the ability of the element to reproduce polynomilas of a specified order. In addition, the test can be used to check the overall implementation of the element in the program; sometimes the shape functions are correct, but the element in a program fails the patch test anyway because of faulty programming.

In the standard patch test, a patch of elements such as shown in Fig.?? is used. The elements should be distorted as shown because the behavior of distorted elements is important and can differ from that of regular elements. No body forces should be applied, and the material properties should be uniform and linear elastic in the patch. The displacements of the nodes on the periphery of the patch are then prescribed according to the order of the patch test. For a linear patch test in two dimensions, the displacement field is given by

$$u_x = a_{1x} + a_{2x}x + a_{3x}y$$
$$u_y = a_{1y} + a_{2y}x + a_{3y}y$$

where a_{Ii} are constants set by the user; they should all be nonzero to test the reproducing condition completely. This displacement field is used to set the prescribed displacements of the nodes on the periphery of the patch, so the prescribed displacements are

$$u_{Ix} = a_{1x} + a_{2x}x_I + a_{3x}y_I$$
$$u_{Iy} = a_{1y} + a_{2y}x_I + a_{3y}y_I$$

To satisfy the patch test, the finite element solution should be given by () throughout the patch: the nodal displacements at the interior nodes should be given by () and the strains should be constant and given by the application of the strain-displacement equations to the displacement in ():

$$\varepsilon_x = u_{x,x} = a_{2x}, \quad \varepsilon_y = u_{y,y} = a_{3y}$$
$$2\varepsilon_{xy} = u_{x,y} + u_{y,x} = a_{3x} + a_{2y}$$

The stresses should similarly be constant and correspond to what would be obtained by multiplying the above strains in the elastic, linear law used in the program. All of these conditions should be met to a high degree of precision, on the order of the precision in the computer used.

That rationale for the standard patch test are the reproducing condition and the fact that () corresponds to an exact solution to the governing equations for linear elasticity. It can easily be seen that () is an exact solution to the elastic problem. Since the strains are constant, and the material properties uniform, the stresses are constant. Therefore, since there are no body forces, the equilibrium equation () is satisfied exactly. Since linear elastic solutions are unique, Eq. () then represents a unique solution to the equations. If the finite element procedure is able to reproduce the linear field, it should be able to replicate this solution exactly because the trial functions include this solution!

When the patch test fails, then the finite element is either not complete, i.e. it can not reproduce the linear field exactly, or there is an error in the program in developing the discrete equations or in the solution of the discrete equations. Whether the reproducing conditions are satisfied can be checked independently by setting the nodal displacements according to () at all nodes and then checking the strains at all quadrature points. This test in fact suffices as a test of the reproducing conditions, and hence of convergence of the element. Going through the solution procedure is primarily a check on the program.

Patch Test in Explicit Programs. The patch test as applied above is not readily applicable to explicit programs because these program do not have a means for solving the linear static equations. However, the patch test can be modified for use in explicit programs as described in elytschko and Chiang(). The basic idea is to prescribe the intial velocities by a linear field identical to Eq.(), so

Here aij are arbitrary constant values, but they should be very small because in most programs the geometric nonlinearities will be triggered otherwise. The program is then used to integrate the equations of motion one time step; no extrenal forces should be applied and a linear, hypoelastic material model such as Eq. () should be used. The rate-of-deformation or the strains and the accelerations at the end of time step are then checked. The rate-of-deformation should have the correct constant values in all of the elements and the accelerations should vanish at all of the interior nodes. The accelerations should vanish because the stresses should aslo be constant and according to the momentum equation, in the absence of body forces, the accelerations should vanish.

The test should be met to a high degree of precision if the constants aij are small enough. For example, when the constants aij are of order , the accelerations should not be larger than order .

Patch Tests for Stability. Simo, Taylor and Z have devised a modified patch test with the aim of checking for stability, primarily in the stability of the displacement field rather than the instability of the pressures. It can also test whether the program treats traction boundary conditions exactly. The main difference from the standard patch test is that the displacements are not prescribed at all nodes. Instead, displacement boundary conditions

are prescribed only for the minimal number of components needed to prevent rigid body rotation. An example of the test is shown in Fig. ??.

This test is not an infallible test for detecting instabilities. Furthermore, it can only detect displacement instabilities, not pressure instabilities. To thoroughly check an element for displacement instabilities, it is also worthwhile to to an eigenvalue analysis on a single free element, i.e. a completely unconstrained element. The number of zero eigenvalues should be equal to the number of rigid body modes. For example, in two dimensional analysis, an element or a patch of elements should posess three zero eigenvalues, which are arise forom two translations and on erotation, whereas in three dimensions, an element should posses six zero eigenvalues, three translational and three rotational rigid body modes. If there are more zero eigenvalues, this indicates an element which may exhibit displacement instabilities; this characteristic is also called rank deficiency of the stiffness matrix, as discussed in Sectiopn 8.?.

8.6. Isoparametric Element 4-Node Quadrilateral

In this Section, the isoparametric elements are developed in two dimensions, with an emphasis on the 4-node quadrilateral. The objective is to present a setting in which we can explain some of the concepts described in the preceding Sections. The displacement field for QUAD4 is given by

$$u_x(\xi,\eta) = \sum_{I=1}^{4} N_I(\xi,\eta)\, u_{xI} \qquad u_y(\xi,\eta) = \sum_{I=1}^{4} N_I(\xi,\eta)\, u_{yI} \tag{8.2.1}$$

where N_I is the isoparametric shape function for node I given by

$$N_I(\xi,\eta) = \frac{1}{4}(1 + \xi_I\xi)(1 + \eta_I\eta) \tag{1.2.2}$$

u_{xI} and u_{yI} are the displacements at node I, and $u_x(\xi,\eta)$ and $u_y(\xi,\eta)$ give the displacement field within the element domain. The displacement field is written in terms of a reference coordinate system (ξ,η). Within the reference system, the element domain is a bi-unit square as shown in Fig. 8.6.1.

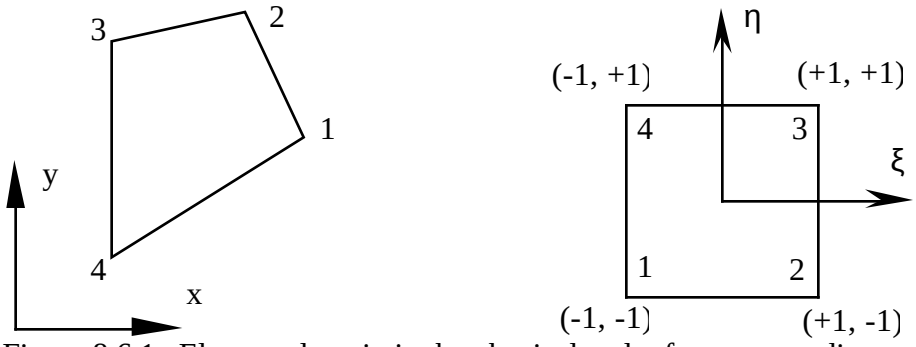

Figure 8.6.1. Element domain in the physical and reference coordinate systems

The transformation (or mapping) between the physical domain and element or parent domain is given by

$$x(\xi,\eta) = \sum_{I=1}^{4} N_I(\xi,\eta)\, x_I \qquad (1.2.3a)$$

$$y(\xi,\eta) = \sum_{I=1}^{4} N_I(\xi,\eta)\, y_I \qquad (1.2.3b)$$

where x_I and y_I are the nodal coordinates. Equations (3a) and (3b) can also be written in the form

$$x_i = \sum_{I=1}^{4} N_I x_{iI} = \mathbf{N}\mathbf{x}_i \qquad (1.2.3c)$$

where $\mathbf{N}$ is a row matrix consisting of the 4 shape functions

$$\mathbf{N} = (N_1, N_2, N_3, N_4)$$

and

$$\mathbf{x}_1^t = \mathbf{x}^t = (x_1, x_2, x_3, x_4)$$

$$\mathbf{x}_2^t = \mathbf{y}^t = (y_1, y_2, y_3, y_4)$$

Because the same shape functions are used for both the mapping and the displacement interpolation, this element is called an <u>iso</u>parametric element.

The interpolants and mapping, Eq. (2), are bilinear in (ξ,η), that is, they contain the following monomials: $(1, \xi, \eta, \xi\eta)$; the last term is called the bilinear term. Thus u_x can be written as

$$u_x(\xi,\eta) = \alpha_{0x} + \alpha_{1x}\xi + \alpha_{2x}\eta + \alpha_{3x}\xi\eta \qquad (1.2.4)$$

where α_{ix} are constants. It can easily be verified that the interpolants are <u>linear</u> along each of the edges of the element as follows. Along any of the edges, either ξ or η is constant, so the monomial $\xi\eta$ is linear along the edges. Therefore, while the bilinear term is nonlinear within the element, it is linear on the edges. Therefore compatibility, or continuity, of the displacement is assured when elements share two nodes along any edge. QUAD4 can be mixed with linear displacement triangles without any discontinuities.

1.2.1 <u>Strain Field</u>. The strain field is obtained by using Eq. (1). Implicit differentiation is used to evaluate the derivatives because the shape functions are functions of ξ and η and the relation (3) can not be inverted explicitly to obtain ξ and η in terms of x and y. Writing the chain-rule for a shape function in matrix form gives:

$$\mathbf{J}\begin{Bmatrix} \frac{\partial N_I}{\partial x} \\ \frac{\partial N_I}{\partial y} \end{Bmatrix} = \begin{Bmatrix} \frac{\partial N_I}{\partial \xi} \\ \frac{\partial N_I}{\partial \eta} \end{Bmatrix} \tag{1.2.5a}$$

where **J** is the Jacobian matrix given by

$$\mathbf{J} = \begin{bmatrix} \frac{\partial x}{\partial \xi} & \frac{\partial y}{\partial \xi} \\ \frac{\partial x}{\partial \eta} & \frac{\partial y}{\partial \eta} \end{bmatrix} \tag{1.2.5b}$$

Its determinant is denoted by J, i.e.

$$J = \det(\mathbf{J}) \tag{1.2.6}$$

If we invert (5b), and multiply both sides of (5a) by the inverse, we obtain

$$\begin{Bmatrix} \frac{\partial N_I}{\partial x} \\ \frac{\partial N_I}{\partial y} \end{Bmatrix} = \frac{1}{J}\begin{bmatrix} \frac{\partial y}{\partial \eta} & \frac{-\partial y}{\partial \xi} \\ \frac{-\partial x}{\partial \eta} & \frac{\partial x}{\partial \xi} \end{bmatrix}\begin{Bmatrix} \frac{\partial N_I}{\partial \xi} \\ \frac{\partial N_I}{\partial \eta} \end{Bmatrix} \tag{1.2.7a}$$

from which we see by the chain rule that

$$\begin{bmatrix} \frac{\partial \xi}{\partial x} & \frac{\partial \eta}{\partial x} \\ \frac{\partial \eta}{\partial x} & \frac{\partial \eta}{\partial y} \end{bmatrix} = \frac{1}{J}\begin{bmatrix} \frac{\partial y}{\partial \eta} & \frac{-\partial y}{\partial \xi} \\ \frac{-\partial x}{\partial \eta} & \frac{\partial x}{\partial \xi} \end{bmatrix} \tag{1.2.7b}$$

The derivatives of the spatial coordinates with respect to ξ and η can be obtained from (3) and (2). First

$$\frac{\partial x}{\partial \xi} = \frac{1}{4}\sum_{I=1}^{4} x_I \xi_I (1 + \eta_I \eta) \tag{1.2.8a}$$

$$\frac{\partial x}{\partial \eta} = \frac{1}{4}\sum_{I=1}^{4} x_I \eta_I (1 + \xi_I \xi) \tag{1.2.8b}$$

$$\frac{\partial y}{\partial \xi} = \frac{1}{4}\sum_{I=1}^{4} y_I \xi_I (1 + \eta_I \eta) \tag{1.2.8c}$$

$$\frac{\partial y}{\partial \eta} = \frac{1}{4}\sum_{I=1}^{4} y_I \eta_I (1 + \xi_I \xi) \tag{1.2.8d}$$

Using the definitions of **J** and J given in Eqs. (5) and (6), respectively, then gives

$$J = \frac{1}{8}[x_{24}y_{31} + x_{31}y_{42} + (x_{21}y_{34} + x_{34}y_{12})\xi + (x_{14}y_{32} + x_{32}y_{41})\eta] \tag{1.2.9a}$$

$$x_{IJ} \equiv x_I - x_J \tag{1.2.9b}$$

$$y_{IJ} \equiv y_I - y_J \tag{1.2.9c}$$

Note that the bilinear term is absent in J.

Using the definition of the linear strain gives the following

$$\begin{Bmatrix} \varepsilon_x \\ \varepsilon_y \\ 2\varepsilon_{xy} \end{Bmatrix} = \sum_{I=1}^{4} \begin{bmatrix} \frac{\partial N_I}{\partial x} & 0 \\ 0 & \frac{\partial N_I}{\partial y} \\ \frac{\partial N_I}{\partial y} & \frac{\partial N_I}{\partial x} \end{bmatrix} \begin{Bmatrix} u_{xI} \\ u_{yI} \end{Bmatrix} = \begin{bmatrix} \frac{\partial \mathbf{N}}{\partial x} & \mathbf{0} \\ \mathbf{0} & \frac{\partial \mathbf{N}}{\partial y} \\ \frac{\partial \mathbf{N}}{\partial y} & \frac{\partial \mathbf{N}}{\partial x} \end{bmatrix} \begin{Bmatrix} \mathbf{u}_x \\ \mathbf{u}_y \end{Bmatrix} \equiv \mathbf{B}\mathbf{d} \tag{1.2.10}$$

$$\mathbf{u}_x^t = [u_{x1}, u_{x2}, u_{x3}, u_{x4}]$$
$$\mathbf{u}_y^t = [u_{y1}, u_{y2}, u_{y3}, u_{y4}]$$

1.2.2 Linear Reproducing Conditions of Isoparametric Elements. It will now be shown that isoparametric elements of any order reproduce the complete linear velocity (displacement) field. This property is called linear completeness. It guarantees that the element will pass the linear patch test and is essential for the element to be convergent.

A general isoparametric element with n_N^e nodes is considered because it is easy to demonstrate this property for any isoparametric element. The number of spatial dimensions denoted by n_D^e. The isoparametric transformation is

$$x_i = \sum_{I=1}^{n_N^e} N_I(\mathbf{x}) x_{iI} \tag{1.2.11}$$

where i = 1 to n_D^e. The dependent variable is denoted by u. In the case of two or three dimensional solids, u may refer to any displacement component. For an isoparametric

element, the displacement field is interpolated by the same shape functions used in the mapping (12), so

$$u = \sum_{I=1}^{n_N^e} N_I(\mathbf{x}) u_I \tag{1.2.12}$$

Consider the situation where the displacement field is linear

$$u = \alpha_o + \sum_{i=1}^{n_D^e} \alpha_i x_i \tag{1.2.13}$$

so the nodal displacements are given by

$$u_I = \alpha_o + \sum_{i=1}^{n_D^e} \alpha_i x_{iI} \tag{1.2.14}$$

where α_o and α_i are constants. This can also be written as

$$u_I = \alpha_o s_I + \sum_{i=1}^{n_D^e} \alpha_i x_{iI} \tag{1.2.15a}$$

or

$$\mathbf{u} = \alpha_o \mathbf{s} + \sum_{i=1}^{n_D^e} \alpha_i \mathbf{x}_i \tag{1.2.15b}$$

where $\mathbf{u}$ and $\mathbf{x}_i$ are column vectors of the nodal unknowns and coordinates; $\mathbf{s}$ is a column vector of the same dimension consisting of all 1's. Substituting (14) into (12) yields

$$u = \sum_{I=1}^{n_N^e} \left(\alpha_o s_I + \sum_{i=1}^{n_D^e} \alpha_i x_{iI} \right) N_I(\mathbf{x}) \tag{1.2.16}$$

and rearranging the terms

$$u = \alpha_o \sum_{I=1}^{n_N^e} s_I N_I(\mathbf{x}) + \sum_{i=1}^{n_D^e} \left(\alpha_i \sum_{I=1}^{n_N^e} x_{iI} N_I(\mathbf{x}) \right) \tag{1.2.17}$$

It is recognized from (11) that the coefficients of α_i on the right hand side of Eq (17) correspond to x_i so

$$u = \alpha_o \sum_{I=1}^{n_N^e} s_I N_I(\mathbf{x}) + \sum_{i=1}^{n_D^e} \alpha_i x_i \tag{1.2.18}$$

We now make use of the fact that

$$\sum_{I=1}^{n_N^e} s_I N_I = \sum_{I=1}^{n_N^e} N_I(\mathbf{x}) = 1 \tag{1.2.19}$$

The first equality is obvious since $s_I=1$. To obtain the second equality consider an element whose nodes are coincident: $x_{iI} = x_{io}$ for I = 1 to n_N^e. The mapping (11) must then yield

$$x_{io} = \sum_{I=1}^{n_N^e} N_I(\mathbf{x})\, x_{io} \tag{1.2.20a}$$

$$= x_{io} \sum_{I=1}^{n_N^e} N_I(\mathbf{x}) \tag{1.2.20b}$$

Since the above must hold for arbitrary x_{io}, the second equality in (19) follows.

Making use of (19) then reduces (18) to

$$u = \alpha_o + \sum_{i=1}^{n_D^e} \alpha_i x_i \tag{1.2.21}$$

which is precisely the linear field (13) from which the nodal values u_I were defined in Eq. (15). Thus any isoparametric element contains the linear field and will exhibit constant strain fields when the nodal displacements emanate from a linear field. As a consequence, it satisfies the linear patch test exactly.

Although this attribute of isoparametric elements appears at first somewhat trivial, its subtlety can be appreciated by noting that the bilinear terms *xy* will not be represented exactly in a 4-node isoparametric element. Consider for example the case when the nodal displacements are obtained from the bilinear field u(x,y)=xy:

$$u(x,y) = \sum_{I=1}^{4} u_I N_I(\xi,\eta) = \sum_{I=1}^{4} x_I y_I N_I(\xi,\eta) \tag{1.2.22}$$

It is impossible to extricate xy from the right hand side of Eq. (22) unless $\mathbf{x}^t$ = a(-1, +1, +1, -1), $\mathbf{y}^t$ = b(-1, -1, +1, +1) where a and b are constants, i.e. when the element is rectangular. Therefore, for an arbitrary quadrilateral, the displacement field is not bilinear when the nodal values are determined from a bilinear field, i.e., when $u_I = x_I y_I$, $u(x,y) \neq xy$.

Similarly, for higher order isoparametrics, such as the 9-node Lagrange element, the distribution within the element is not quadratic when the nodal values of u are obtained from a quadratic field unless the element is rectangular with equispaced nodes. For curved edges, the deviation of the field from quadratic is substantial, and the accuracy diminishes. The convergence proofs of Ciarlet and Raviart (1972) show that the order of convergence for the 9-node element is better than the 4-node quadrilateral only when the element midpoint nodes are displaced from the midpoint of the side by a small amount.

The linear completeness of subparametric elements can be shown analogously. In a subparametric element, the mapping is of lower order than the interpolation of the dependent variable. For example, consider the element in Fig. 2 that has a 4-node bilinear mapping with a 9-node interpolation for u(x,y). This is written

$$u(x,y) = \sum_{I=1}^{9} u_I \bar{N}_I(\xi,\eta) \tag{1.2.23}$$

$$\begin{Bmatrix} x \\ y \end{Bmatrix} = \sum_{I=1}^{4} \begin{Bmatrix} x_I \\ y_I \end{Bmatrix} N_I(\xi,\eta) \tag{1.2.24}$$

The 9-node Lagrange interpolant for the dependent variable u is distinguished from the 4-node interpolant used for the element mapping by a superposed bar. We now define a set of 9 nodes $(\bar{x}_I, \bar{y}_I)$, I = 1 to 9, which are obtained by evaluating (x,y) at the 9-nodes used for interpolating u(x,y) by Eq. (24). Then the mapping can be expressed as

$$\begin{Bmatrix} x \\ y \end{Bmatrix} = \sum_{I=1}^{9} \begin{Bmatrix} \bar{x}_I \\ \bar{y}_I \end{Bmatrix} \bar{N}_I(\xi,\eta) \tag{1.2.25}$$

Using (23) and (25), the arguments invoked in going from Eqs. (13) to (21) can be repeated to establish the linear completeness of the subparametric element.

Superparametric elements, in which the mapping is of higher order than the interpolation of the dependent variable, are not complete. This can by shown by considering the element in Fig. 2 with 9-node mapping and 4-node bilinear interpolation for u(x,y). In order to use the previous argument, we would have to use the 4 nodes used for interpolation to do a bilinear mapping, but such a mapping would be unable to reproduce the domain of the element unless it has straight edges with the nodes at the midpoints of the nodes.

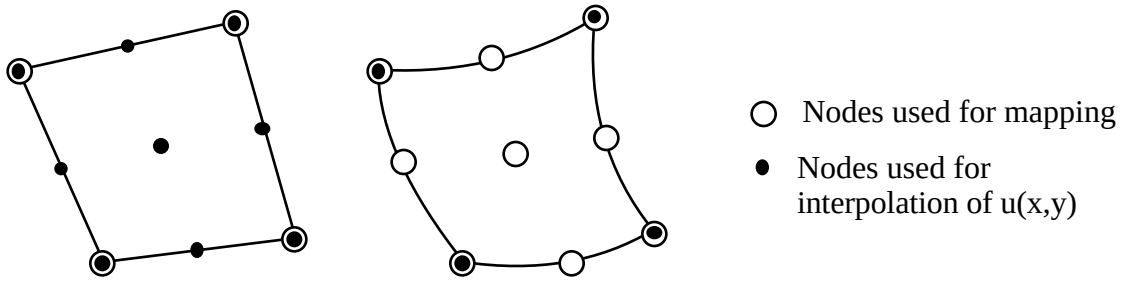

Figure 2. Examples of subparametric and superparametric elements

In summary, it has been shown that isoparametric and subparametric elements are linearly complete and consistent in that they represent linear fields exactly. This implies that when the nodal values are prescribed by a linear field, the interpolant is an identical linear field and the derivative of the interpolant has the correct constant value throughout the element. Therefore, for these elements, the correct constant strain state is obtained for a linear displacement field, and the patch test will be satisfied. The element will also represent rigid body translation and rotation exactly. The 4-node quadrilateral considered here is isoparametric, so it possesses these necessary features. A superparametric element does not have linear completeness, and will therefore fail the patch test.

1.2.3 Element Rank and Rank Deficiency. In order to perform reliably, an element must have the proper rank. If its rank is too small, the global stiffness may be singular or near singular; in the latter case, it will exhibit spurious singular modes. If the rank of an element is too large, it will strain in rigid body motion and either fail to converge or converge very slowly.

The proper rank of an element stiffness is given by

$$\text{proper rank}\,(\mathbf{K}_e) = \dim(\mathbf{K}_e) - n_{RB} \tag{1.2.26a}$$

$$\text{rank deficiency}(\mathbf{K}_e) = \text{proper rank}(\mathbf{K}_e) - \text{rank}(\mathbf{K}_e) \tag{1.2.26b}$$

where n_{RB} is the number of rigid body modes. Another way of expressing this is that if the element is of proper rank, then

$$\dim(\ker(\mathbf{K}_e)) = n_{RB}$$

where the kernel of $\mathbf{K}_e$ is defined by

$$\mathbf{x} \quad \ker(\mathbf{K}_e) \text{ if } \mathbf{K}_e\mathbf{x} = 0 \tag{1.2.27}$$

To determine the rank of an element stiffness which is evaluated by numerical quadrature, consider the quadrature formula

$$\mathbf{K}_e = \int_{\Omega_e} \mathbf{B}^t\mathbf{C}\mathbf{B}\, d\Omega = \int_{-1}^{+1}\int_{-1}^{+1} \mathbf{B}^t\mathbf{C}\mathbf{B}\, J d\xi d\eta$$

$$= \sum_{\alpha=1}^{n_Q} w_\alpha\, J(\xi_\alpha)\, \mathbf{B}^t(\xi_\alpha)\, \mathbf{C}(\xi_\alpha)\, \mathbf{B}(\xi_\alpha) \tag{1.2.28}$$

where $\mathbf{C}$ is a constitutive matrix, Ω_e is the element domain, w_α are the quadrature weights, and ξ_α are the n_Q quadrature points. In Gauss quadrature, w_α correspond to the products of the one-dimensional weight factors and ξ_α are the quadrature points in the reference coordinates. The element domain in (28) and throughout this discussion is assumed to have unit thickness. The above form can be written as

$$\mathbf{K}_e = \overset{o}{\mathbf{B}}{}^t \overset{o}{\mathbf{C}}\overset{o}{\mathbf{B}} \tag{1.2.29a}$$

where

$$\overset{o}{\mathbf{B}} = \begin{bmatrix} \mathbf{B}(\mathbf{x}_1) \\ \mathbf{B}(\mathbf{x}_2) \\ \vdots \\ \mathbf{B}(\mathbf{x}_{n_Q}) \end{bmatrix} \tag{1.2.29b}$$

$$\overset{o}{\mathbf{C}} = \begin{bmatrix} w_1 J(\mathbf{x}_1)\mathbf{C}(\mathbf{x}_1) & \mathbf{0} & \cdots & \mathbf{0} \\ \mathbf{0} & w_2 J(\mathbf{x}_2)\mathbf{C}(\mathbf{x}_2) & & \mathbf{0} \\ \vdots & & \ddots & \vdots \\ \mathbf{0} & \mathbf{0} & \cdots & w_{n_Q} J(\mathbf{x}_{n_Q})\mathbf{C}(\mathbf{x}_{n_Q}) \end{bmatrix} \tag{1.2.29c}$$

A special form of the product-rank theorem is now used, which states that when $\overset{o}{\mathbf{C}}$ is positive definite

$$\text{rank } \mathbf{K}_e = \text{rank } \left(\overset{o}{\mathbf{B}}\right) \tag{1.2.30}$$

Note that $\overset{o}{\mathbf{C}}$ is positive definite if and only if J and **C** are positive definite at all quadrature points. If a material loses ellipticity, as for example in strain softening or non-associative plastic materials, Eq. (30) no longer holds. Similarly, if the element is so distorted that J < 0, the above may not hold.

Assuming an element domain of unit thickness, the nodal forces are obtained directly from stress field by

$$\mathbf{f}_e^{int} = \begin{Bmatrix} \mathbf{f}_x^{int} \\ \mathbf{f}_y^{int} \end{Bmatrix} = \int_{\Omega_e} \mathbf{B}^t \mathbf{s}\, d\Omega = \int_{-1}^{+1}\int_{-1}^{+1} \mathbf{B}^t \mathbf{s}\, J\, d\xi d\eta \tag{1.2.31a}$$

where the stress is written as

$$\mathbf{s} = \begin{Bmatrix} \sigma_x \\ \sigma_y \\ \sigma_{xy} \end{Bmatrix}$$

and

$$\left(\mathbf{f}_x^{int}\right)^t = \left[f_{x1}, f_{x2}, f_{x2}, f_{x4} \right]^{int}$$

$$\left(\mathbf{f}_y^{int}\right)^t = \left[f_{y1}, f_{y2}, f_{y2}, f_{y4} \right]^{int}$$

Applying numerical quadrature, this becomes

$$\mathbf{f}_e^{int} = \sum_{\alpha=1}^{n_Q} w_\alpha\, J(\mathbf{x}_\alpha)\, \mathbf{B}^t(\mathbf{x}_\alpha)\mathbf{s}(\mathbf{x}_\alpha) \tag{1.2.31b}$$

$$= \overset{o}{\mathbf{B}}{}^t \overset{o}{\mathbf{s}} \tag{1.2.31c}$$

where

$$\overset{o}{\mathbf{s}}{}^{t} = \left[w_1 J(\mathbf{x}_1)\mathbf{s}(\mathbf{x}_1), \quad w_2 J(\mathbf{x}_2)\mathbf{s}(\mathbf{x}_2), \quad \cdots \quad w_{n_Q} J(\mathbf{x}_{n_Q})\mathbf{s}(\mathbf{x}_{n_Q}) \right] \tag{1.2.31d}$$

The rank of $\overset{o}{\mathbf{B}}$ can be estimated by the following

$$\text{rank}\,\overset{o}{\mathbf{B}} \le \min(\text{rows in}\,\overset{o}{\mathbf{B}}, \dim D\mathbf{u}) \tag{1.2.32}$$

where D is the symmetric gradient operator given by

$$D = \begin{bmatrix} \dfrac{\partial}{\partial x} & 0 \\ 0 & \dfrac{\partial}{\partial y} \\ \dfrac{\partial}{\partial y} & \dfrac{\partial}{\partial x} \end{bmatrix}$$

and the dimension of $D\mathbf{u}$ (or $\dim D\mathbf{u}$) is equal to the number of independent functions in $D\mathbf{u}$. In most cases, the above is an equality, but it is possible, even with regular quadrature schemes and undistorted elements, to lose the equality, i.e. to have linearly dependent rows in the **B** matrix.

The rank-sufficiency of QUAD4 will now be examined for various quadrature schemes. The element has 4 nodes with 2 degrees of freedom at each node, so dim ($\mathbf{K}_e$) = 8. The number of rigid body modes is 3: translation in the x and y directions and rotation in the (x,y) plane. By Eq. (26a), the proper rank of $\mathbf{K}_e$ = 5.

The most widely used quadrature scheme is 2x2 Gauss quadrature. The number of quadrature points n_Q=4, the number of rows in each $\mathbf{B}(\mathbf{x}_\alpha)$=3, so the number of rows in $\overset{o}{\mathbf{B}}$=12 This exceeds the proper rank. However, based on the linear completeness of the quadrilateral, it will be shown later that (see Section 1.4)

$$u_x(x,y) = \alpha_{ox} + \alpha_{1x}x + \alpha_{2x}y + \alpha_{3x}h \tag{1.2.33a}$$

$$u_y(x,y) = \alpha_{oy} + \alpha_{1y}x + \alpha_{2y}y + \alpha_{3y}h \tag{1.2.33b}$$

$$h \equiv \xi\eta$$

Then

$$\overset{o}{\mathbf{e}} = D\mathbf{u} = \begin{bmatrix} \alpha_{1x} + \alpha_{3x}\dfrac{\partial h}{\partial x} \\ \alpha_{2y} + \alpha_{3y}\dfrac{\partial h}{\partial y} \\ \alpha_{2x} + \alpha_{1y} + \alpha_{3x}\dfrac{\partial h}{\partial y} + \alpha_{3y}\dfrac{\partial h}{\partial x} \end{bmatrix} \tag{1.2.34}$$

Examination of the above shows that the strain-rate field contains 5 linearly independent functions: α_{1x}, α_{2y}, $\alpha_{3x}\partial h/\partial x$, $\alpha_{3y}\partial h/\partial y$, and $\alpha_{2x} + \alpha_{1y}$. Note that the two constants in the shear strain field must be considered as a single independent field and the function $\alpha_{3x}\partial h/\partial y + \alpha_{3y}\partial h/\partial x$ cannot be considered linearly independent because it is a combination of the two functions that have already been included in the list. Thus dim $D\mathbf{u}$ = 5 and since rows in $\overset{o}{\mathbf{B}}$ = 12, it follows from (32) that

$$\text{rank}(\overset{o}{\mathbf{B}})=5$$

It may be concluded that for any quadrature scheme the rank of $\overset{o}{\mathbf{B}}$ for QUAD4 cannot exceed 5.

The rank of the element stiffness of QUAD4 for one-point quadrature can be ascertained similarly. In one-point quadrature, $\overset{o}{\mathbf{B}}$ consists of $\mathbf{B}$ evaluated at a single point, so its rank is 3. Therefore rank $\mathbf{K}_e$ is 3 by Eq. (30), and Eq. (26b) indicates that the element has a rank deficiency of 2. This rank deficiency can cause serious difficulties unless it is corrected. Such corrective procedures are described later.

1.2.4. Nodal Forces and B-Matrix for One-Point Quadrature Element. Prior to describing procedures for correcting the rank deficiency of QUAD4 with one point quadrature, it is worthwhile to develop the one-point quadrature formulas in detail. These formulas will then provide the framework for the development of the rank correction procedures, which in QUAD4 are often called hourglass control.

The internal nodal forces are given by (31b). When one-point quadrature is used, the quadrature point is selected to be the origin of the coordinate system in the reference plane: $\xi = \eta = 0$. Evaluating the Jacobian at this point yields (see Eq. (9)) gives

$$J(\mathbf{0}) = \frac{1}{8}(x_{31}\, y_{42} + x_{24}\, y_{31}) = \frac{A}{4} \tag{1.2.35}$$

where A is the area of the element. The expression for the internal nodal forces now becomes

$$\mathbf{f}^{\text{int}} = 4\mathbf{B}^t(\mathbf{0})\mathbf{s}(\mathbf{0})J(\mathbf{0}) = A\mathbf{B}^t(\mathbf{0})\mathbf{s}(\mathbf{0}) \tag{1.2.36}$$

Evaluating the $\mathbf{B}$ matrix from Eq. (10) at $\xi = \eta = 0$ is a simple algebraic process which gives

$$\mathbf{B}(\mathbf{0}) = \begin{bmatrix} \mathbf{b}_x^t & 0 \\ 0 & \mathbf{b}_y^t \\ \mathbf{b}_y^t & \mathbf{b}_x^t \end{bmatrix} \tag{1.2.37}$$

where

$$\mathbf{b}_x^t \equiv \mathbf{b}_1^t = \frac{1}{2A}\,[y_{24},\, y_{31},\, y_{42},\, y_{13}]$$
$$\mathbf{b}_y^t \equiv \mathbf{b}_2^t = \frac{1}{2A}\,[x_{42},\, x_{13},\, x_{24},\, x_{31}] \tag{1.2.38}$$

Since one-point quadrature is used, the nodal forces are simply the product of the area and the integrand evaluated at $\xi = \eta = 0$, which using (37) and (39) gives

$$\mathbf{f}^{\text{int}} = A\begin{bmatrix} \mathbf{b}_x & \mathbf{0} & \mathbf{b}_y \\ \mathbf{0} & \mathbf{b}_y & \mathbf{b}_x \end{bmatrix}\begin{Bmatrix} \sigma_x \\ \sigma_y \\ \sigma_{xy} \end{Bmatrix} = A\mathbf{B}^t(\mathbf{0})\mathbf{s}(\mathbf{0}) \tag{1.2.39}$$

The element stiffness matrix for the underintegrated element can be obtained by using the stress-strain law

$$\mathbf{s} = \mathbf{C}\mathbf{e} \tag{1.2.40}$$

in conjunction with Eqs. (37), (39) and $\mathbf{e}=\mathbf{B}\mathbf{d}$. This gives

$$\mathbf{f}^{\text{int}} = \mathbf{K}_e\mathbf{d} \tag{1.2.41}$$

where

$$\mathbf{K}_e = A\mathbf{B}^t(\mathbf{0})\mathbf{C}\mathbf{B}(\mathbf{0}) \tag{1.2.42}$$

The element stiffness matrix could also be obtained from (28) by using one-point quadrature and the values of **B** and **C** at the quadrature point.

1.2.5 Spurious Singular Modes (Hourglass) The presence and shape of the spurious singular modes of the one-point quadrature QUAD4 element will now be demonstrated. Any nodal displacement $\mathbf{d}^H$ that is not a rigid body motion but results in no straining of the element is a spurious singular mode. From (43) it can be seen that such nodal displacements will not generate any nodal forces, i.e. they will not be resisted by the element, since in the absence of strains, the stresses will also vanish, so $\mathbf{f}^{\text{int}} = 0$.

Consider the nodal displacements

$$\mathbf{d}^{Hx} = \begin{Bmatrix} \mathbf{h} \\ \mathbf{0} \end{Bmatrix} \qquad \mathbf{d}^{Hy} = \begin{Bmatrix} \mathbf{0} \\ \mathbf{h} \end{Bmatrix} \tag{1.2.43}$$

$$\mathbf{h}^t = [+1,\, -1,\, +1,\, -1]$$

It can easily be verified that

$$\mathbf{b}_x^t\,\mathbf{h} = 0 \qquad \mathbf{b}_y^t\,\mathbf{h} = 0 \tag{1.2.44}$$

Therefore, it follows from Eqs. (37), (43) and (44) that

$$\mathbf{B}(\mathbf{0})\mathbf{d}^{Hx} = \mathbf{0} \tag{1.2.45a}$$

$$\mathbf{B}(\mathbf{0})\mathbf{d}^{Hy} = \mathbf{0} \tag{1.2.45b}$$

Fig. 3 shows rectangular elements with the spurious singular modes of deformation $\mathbf{d}^{Hx}$ and $\mathbf{d}^{Hy}$, and also both modes simultaneously. In the rectangle, it can be seen that the hourglass modes are associated with the bilinear term in the displacement field. The deformed configuration of the mesh in the spurious singular modes is shown in Fig. 4. A vertical pair of elements in this x-mode looks like an hourglass, an ancient device for measuring time by the flow of sand from the top element to the bottom. For this reason, this spurious singular mode is often called hourglassing or the hourglass mode. Because each element is in an hourglass mode, the entire mesh can deform as shown without any resisting forces from the element.

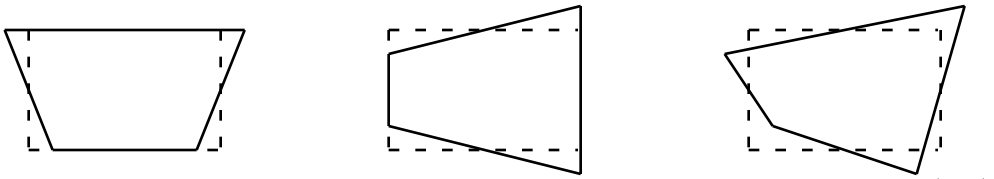

Figure 3. Hourglass modes of deformation

The problem of hourglassing first appeared in finite difference hydrodynamics programs in which the derivatives were evaluated by transforming them to contour integrals by means of the divergence theorem; see for example Wilkins and Blum (1975). This procedure tacitly assumed that the derivatives are constant in the domain enclosed by each contour. This assumption is equivalent to the constant strain (and stress) assumption which is associated with one-point quadrature. The equivalence of these contour-integral finite difference methods was demonstrated by Belytschko et al. (1975); also see Belytschko (1983). Many ad hoc procedures for hourglass control were developed by finite difference workers. The procedures focused on controlling the relative rotations of element sides; no consideration was given to maintaining consistency.

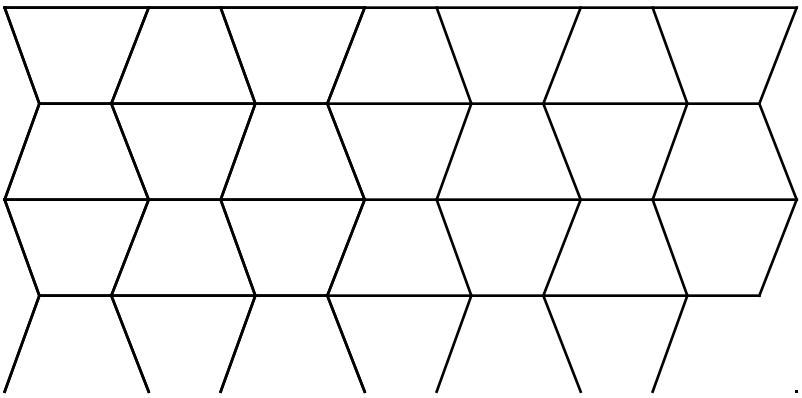

Figure 4. Mesh in hourglass mode of deformation

This phenomenon occurs in many other settings, so a variety of names have evolved. For example, they occur frequently in mixed or hybrid elements, where they are called zero-energy modes or spurious zero-energy modes. Hourglass modes are zero-energy modes, since they don't result in any strain at the points in the element which are sampled. Therefore they do no work and $(\mathbf{d}^{Hx})^t\mathbf{f}^{int} = (\mathbf{d}^{Hy})^t\mathbf{f}^{int} = 0$

In structural analysis, spurious singular modes arise when there is insufficient redundancy, i.e. the number of structural members is insufficient to preclude rigid body motion of part of the structure. Such modes often occur in three dimensional truss structures. In structural analysis, they are called kinematic modes, and because of the close relationship between the structural analysis and finite element communities, this name has also been applied to spurious singular modes. Other names which have been applied to this phenomenon are: keystoning (Key et al. (1978)), chickenwiring, and mesh instability.

For finite element discretizations of partial differential equations, spurious singular modes appears to be the most accurate term for this phenomenon, so we shall use that name. For example, the terms kinematic modes or zero-energy modes are not appropriate for the Laplace equation. In elements where the spurious singular mode has a distinctive appearance, such as the hourglass pattern in QUAD4, we shall also use that name. The condition which leads to spurious singular modes is rank deficiency of the element stiffness matrix.

When rank deficient elements are assembled, the system stiffness will often be singular or nearly singular. Therefore, in matrix methods, the presence of spurious singular modes can be detected by the presence of zero or very small pivots in the total stiffness. If the pivots are zero, the stiffness will be singular and not invertible. If the pivots are very small, the total stiffness is near-singular, and the displacement solutions will be oscillatory in space, i.e., they will exhibit the hourglass mode.

Because a system stiffness matrix is never assembled in explicit methods, the singularity cannot be readily detected. In iterative solvers, the presence of spurious singular modes will often lead to divergence of the solution. With explicit integrators, singular modes are not readily detectable without plots of the deformed configuration. This is also true for matrix dynamic methods, since the mass matrix then renders the system matrix nonsingular even when the stiffness matrix is singular.

The evolution of an hourglass mode in a transient problem is shown in Fig. 5. In this problem, the beam was supported at a single node to facilitate the appearance of the hourglass mode. If all nodes at the left-hand end of the beam were fixed to simulate a clamped support condition, the hourglass mode would not appear. Althoughrank-deficient elements may sometimes appear to work, they should not be used without an appropriate correction.

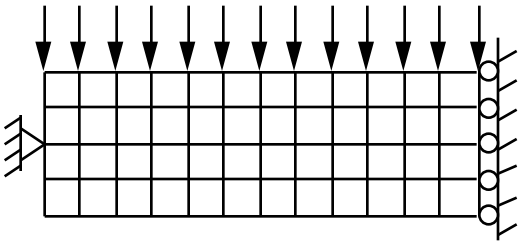

Figure 5. Four views of a simply supported beam showing the evolution of the hourglass mode (due to symmetry, only half the beam was modeled)

1.3 Perturbation Hourglass Stabilization

The simplest way to control spurious singular modes without impairing convergence is to augment the rank of the element stiffness without disturbing the linear completeness (consistency) of the isoparametric element. One approach to this task is to augment the $\mathbf{B}(\mathbf{0})$ matrix of the one-point quadrature element by two rows which are linearly independent of the other three. These additional two rows consist of a $\mathbf{g}$ vector that will be derived subsequently. Adding these two rows corresponds to adding 2 generalized strains. The matrices for the one-point quadrature QUAD4 are then

$$\widetilde{\mathbf{B}} = \begin{bmatrix} \mathbf{b}_x^T & 0 \\ 0 & \mathbf{b}_y^T \\ \mathbf{b}_y^T & \mathbf{b}_x^T \\ \mathbf{g}^T & 0 \\ 0 & \mathbf{g}^T \end{bmatrix} \qquad \widetilde{\mathbf{C}} = \begin{bmatrix} C_{11} & C_{12} & C_{13} & 0 & 0 \\ C_{11} & C_{22} & C_{23} & 0 & 0 \\ C_{13} & C_{23} & C_{33} & 0 & 0 \\ 0 & 0 & 0 & C^Q & 0 \\ 0 & 0 & 0 & 0 & C^Q \end{bmatrix} \tag{1.3.1a}$$

$$\widetilde{\mathbf{s}}^T = [\sigma_x, \sigma_y, \sigma_{xy}, Q_x, Q_y] \tag{1.3.1b}$$

$$\widetilde{\mathbf{e}}^T = [\varepsilon_x, \varepsilon_y, 2\varepsilon_{xy}, q_x, q_y] \tag{1.3.1c}$$

where $\widetilde{\mathbf{C}}$ is the constitutive matrix augmented by two rows and columns in terms of a constant to be determined (C^Q); $\widetilde{\mathbf{s}}$ and $\widetilde{\mathbf{e}}$ are the stress and strain matrices augmented by the generalized stresses and strains (Q_x, Q_y) and (q_x, q_y), respectively.

To maintain linear consistency for the element, these additional generalized strains should vanish when the nodal displacements (or velocities) emanate from linear fields. Consistency and stability (rank sufficiency) are essential requirements for a sound numerical method.

The requirement that $q_x = q_y = 0$ for linear fields implies

$$\mathbf{g}^T\mathbf{u}^{Lin} = \mathbf{g}^T(\alpha_0\mathbf{s} + \alpha_1\mathbf{x} + \alpha_2\mathbf{y}) = 0 \qquad \alpha_i \tag{1.3.2}$$

The above must be satisfied for both $\mathbf{u}_x$ and $\mathbf{u}_y$ so we have not specified the component; $\mathbf{u}^{Lin}$ is taken from Eq. (1.2.15b). The above can be interpreted as an orthogonality condition: $\mathbf{g}$ must be orthogonal to all linear fields.

1.3.1 The Gamma Vector. We first define a set of four vectors, $\mathbf{b}^*$.

$$\mathbf{b}^* \equiv \left(\mathbf{b}_x,\ \mathbf{b}_y,\ \mathbf{s},\ \mathbf{h}\right) \tag{1.3.3}$$

To obtain $\mathbf{g}$, two properties of $\mathbf{b}^*$ are used:

1. the vectors $\mathbf{b}_i$ are biorthogonal to $\mathbf{x}_j$
2. the vectors $\mathbf{b}_i^*$ are linearly independent.

The biorthogonality property, given by

$$\mathbf{b}_i^t\mathbf{x}_j = \delta_{ij} \qquad (i, j) = 1 \text{ to } 2 \tag{1.3.4}$$

is an identity which holds for all isoparametric elements:

$$\frac{\partial \mathbf{N}}{\partial x_i}\mathbf{x}_j = \delta_{ij} \tag{1.3.5}$$

The demonstration of this identity is based on the isoparametric mapping, Eq. (1.2.3c), which when combined with (5) gives

$$\frac{\partial \mathbf{N}}{\partial x_i}\mathbf{x}_j = \frac{\partial x_j}{\partial x_i} = \delta_{ij} \tag{1.3.6}$$

where the last equality expresses the fact that in two dimensions, for example, $\partial x/\partial x=\partial y/\partial y=1$, $\partial x/\partial y=\partial y/\partial x=0$. Eq. (5) holds for the derivatives of the shape functions at any point. In particular, it also holds for the point $\xi = \eta = 0$ in QUAD4. Additional orthogonality conditions,

$$\mathbf{b}_i^t\mathbf{s} = 0 \qquad \mathbf{b}_i^t\mathbf{h} = 0 \qquad \mathbf{h}^t\mathbf{s} = 0 \qquad i=1 \text{ to } 2 \tag{1.3.7}$$

can easily be verified by arithmetic using the definitions of these vectors.

The linear independence of the 4 $\mathbf{b}_i^*$ vectors is demonstrated as follows. Assume $\mathbf{b}_i^*$ are linearly dependent. Then it follows that there exists $\alpha_i \neq 0$ such that

$$\alpha_1 \mathbf{b}_x + \alpha_2 \mathbf{b}_y + \alpha_3 \mathbf{s} + \alpha_4 \mathbf{h} = 0 \tag{1.3.8}$$

Premultiplying the above by $\mathbf{s}^t$, and using (7) yields $\alpha_3 = 0$. Similarly premultiplying by $\mathbf{h}^t$ yields $\alpha_4 = 0$. Then premultiplying $\mathbf{x}^t$ yields

$$\alpha_1 + \alpha_3 \mathbf{x}^t\mathbf{s} + \alpha_4 \mathbf{x}^t\mathbf{h} = 0 \tag{1.3.9}$$

and since it has just been determined that $\alpha_3 = \alpha_4 = 0$, it follows that $\alpha_1 = 0$. Similarly, premultiplying by $\mathbf{y}^t$ shows that $\alpha_2 = 0$. Thus $\alpha_i = 0$, for i = 1 to 4, and it follows that the vectors $\mathbf{b}_i^*$ are linearly independent.

The preceding developments are now used as tools for the construction of $\mathbf{g}$, via the consistency requirement (2). Since the vectors $\mathbf{b}_i^*$ are linearly independent, they span R^4. It follows that any vector in R^4, including $\mathbf{g}$ can be expressed as a linear combination of $\mathbf{b}_i^*$:

$$\mathbf{g} = \beta_1 \mathbf{b}_x + \beta_2 \mathbf{b}_y + \beta_3 \mathbf{h} + \beta_4 \mathbf{s} \tag{1.3.10}$$

where β_i are constants to be determined by the linear consistency requirement (2). Substituting (10) into (2) and collecting the coefficients of α_i yields

$$\begin{aligned} &\alpha_o\left(\beta_1 \mathbf{b}_x^t\mathbf{s} + \beta_2 \mathbf{b}_y^t\mathbf{s} + \beta_3 \mathbf{h}^t\mathbf{s} + \beta_4 \mathbf{s}^t\mathbf{s}\right) \\ &+ \alpha_1\left(\beta_1 \mathbf{b}_x^t\mathbf{x} + \beta_2 \mathbf{b}_y^t\mathbf{x} + \beta_3 \mathbf{h}^t\mathbf{x} + \beta_4 \mathbf{s}^t\mathbf{x}\right) \\ &+ \alpha_2\left(\beta_1 \mathbf{b}_x^t\mathbf{y} + \beta_2 \mathbf{b}_y^t\mathbf{y} + \beta_3 \mathbf{h}^t\mathbf{y} + \beta_4 \mathbf{s}^t\mathbf{y}\right) = 0 \end{aligned} \tag{1.3.11}$$

Since the above must vanish for all α_i, each coefficient of α_i must vanish. Taking the coefficient of α_o and simplifying by means of Eqs. (4) and (7) gives

$$\beta_4 \mathbf{s}^t\mathbf{s} = 4\beta_4 = 0 \tag{1.3.12}$$

Using (12) and (6) to simplify the coefficient of α_1 in (11) gives

$$\beta_1 + \beta_3 \mathbf{h}^t\mathbf{x} = 0 \tag{1.3.13}$$

and a similar procedure for the coefficient of α_2 gives

$$\beta_2 + \beta_3 \mathbf{h}^t\mathbf{y} = 0 \tag{1.3.14}$$

Using Eqs. (13) and (14) in (10) to express β_1 and β_2 in terms of β_3 and using (12) yields

$$\mathbf{g} = \beta_3\left[\mathbf{h} - \left(\mathbf{h}^t\mathbf{x}\right)\mathbf{b}_x - \left(\mathbf{h}^t\mathbf{y}\right)\mathbf{b}_y\right] \tag{1.3.15}$$

The constant β_3 remains undetermined, since for any value of β_3 the vector $\mathbf{g}$ is orthogonal to all linear fields. It will be convenient later to have $\mathbf{g}^t\mathbf{h}$=1, so we set $\beta_3 = 1/4$. The value of $\beta_3 = 1$ was used in Flanagan and Belytschko (1981) because the reference element was a unit square; this changes some of the subsequent constants but not the substance of the development. In this description we choose $\beta_3 = 1/4$, which gives

$$\mathbf{g} = \frac{1}{4}\left[\mathbf{h} - \left(\mathbf{h}^t\mathbf{x}\right)\mathbf{b}_x - \left(\mathbf{h}^t\mathbf{y}\right)\mathbf{b}_y\right] \tag{1.3.16a}$$

The above expression can be written in indicial notation as

$$\mathbf{g} = \frac{1}{4}\left[\mathbf{h} - \left(\mathbf{h}^t\mathbf{x}_i\right)\mathbf{b}_i\right] \tag{1.3.16b}$$

or

$$\gamma_I = \frac{1}{4}\left[h_I - (h_J x_{iJ})b_{iI}\right] \tag{1.3.16c}$$

Using (4), (7), and (16a) the following are easily verified by:

$$\mathbf{g}^t\mathbf{x} = \mathbf{g}^t\mathbf{y} = \mathbf{g}^t\mathbf{s} = 0 \qquad \mathbf{g}^t\mathbf{h} = 1 \tag{1.3.17}$$

1.3.2 Stabilization Forces and Stiffness Matrix. Replacing $\mathbf{B}(\mathbf{0})$ and $\mathbf{s}(\mathbf{0})$ in Eq. (1.2.39) by the augmented matrices $\widetilde{\mathbf{B}}$ and $\widetilde{\mathbf{s}}$ gives the nodal forces

$$\mathbf{f}^{\text{int}} = A\begin{bmatrix} \mathbf{b}_x & \mathbf{0} & \mathbf{b}_y \\ \mathbf{0} & \mathbf{b}_y & \mathbf{b}_x \end{bmatrix}\begin{Bmatrix} \sigma_x \\ \sigma_y \\ \sigma_{xy} \end{Bmatrix} + A\begin{Bmatrix} Q_x\mathbf{g} \\ Q_y\mathbf{g} \end{Bmatrix} \tag{1.3.18}$$

$$= A\mathbf{B}^T(\mathbf{0})\mathbf{s}(\mathbf{0}) + \mathbf{f}^{\text{stab}} \tag{1.3.19}$$

The first term in the internal force is obtained by one-point quadrature. The generalized stresses and are strains are obtained by the stress-strain law, $\widetilde{\mathbf{s}} = \widetilde{\mathbf{C}}\widetilde{\mathbf{e}}$, and the strain-displacement equation $\widetilde{\mathbf{e}} = \widetilde{\mathbf{B}}\mathbf{d}$:

$$Q_x = C^Q q_x \qquad Q_y = C^Q q_y$$
$$q_x = \mathbf{g}^t\mathbf{u}_x \quad q_y = \mathbf{g}^t\mathbf{u}_y \tag{1.3.20}$$

The stiffness matrix is obtained by substituting replacing $\mathbf{B}(\mathbf{0})$ and $\mathbf{C}$ in (1.2.42) by the augmented matrices $\widetilde{\mathbf{B}}$ and $\widetilde{\mathbf{C}}$ which gives

$$\mathbf{K}_e = \mathbf{K}_e^{1pt} + \mathbf{K}_e^{\text{stab}} \tag{1.3.21a}$$

where

$$\mathbf{K}_e^{1pt} = A\mathbf{B}^t(\mathbf{0})\mathbf{C}\mathbf{B}(\mathbf{0}) \tag{1.3.21b}$$

$$\mathbf{K}_e^{\text{stab}} = AC^Q\begin{bmatrix} \mathbf{g}\mathbf{g}^t & \mathbf{0} \\ \mathbf{0} & \mathbf{g}\mathbf{g}^t \end{bmatrix} \tag{1.3.21c}$$

$\mathbf{K}_e^{1pt}$ is the stiffness matrix obtained from one-point quadrature. $\mathbf{K}_e^{\text{stab}}$ is obtained from the additional generalized strains which were introduced to stabilize the element and is often called a stabilization matrix. The stabilization matrix is of rank 2. Combined with the one-point quadrature stiffness, it yields a matrix of rank 5, which is the correct rank for the QUAD4.

This form of the linearly consistent generalized strains occurs in many stabilization procedures for underintegrated elements, and will be designated as the $\mathbf{g}$ vector. Note that the vector is not completely determined by linear consistency: an unspecified constant β_3 remains. This vector is orthogonal to the nodal displacements which emanate from a linear

field for arbitrarily shaped quadrilaterals. When the element is rectangular, $\mathbf{h}^t\mathbf{x} = \mathbf{h}^t\mathbf{y} = 0$ and $\mathbf{g} = \beta_3\mathbf{h}$.

1.3.3 Scaling the Stabilization Forces. Since the constants C^Q in Eq. (1) are not true material constants, it is important to provide formulas for these constants which provide approximately the same degree of stabilization regardless of the geometry and material properties of the element. The basic objective is to obtain a scaling which perturbs the element sufficiently to insure the correct rank but not to overwhelm the one-point quadrature stiffness.

One procedure for selecting C^Q is to scale the maximum eigenvalue of the stabilization stiffness to the maximum eigenvalue of the underintegrated stiffness. In fact, it would be desirable to shift eigenvalues associated with hourglass modes out of the spectrum that is of interest in the response. The hourglass modes in a fully integrated element are smaller than the 1-point quadrature element eigenvalues. To avoid locking, the stabilization should be a small fraction of the one point quadrature eigenvalue.

According to Flanagan and Belytschko (1981), the maximum eigenvalue for the 1-point quadrature version of QUAD4 for an isotropic material is bounded by

$$\frac{1}{2}Ac^2b \le \lambda_{max} \le Ac^2b \tag{1.3.22a}$$

$$b = \sum_{i=1}^{2} \mathbf{b}_i^T\mathbf{b}_i \qquad\qquad c^2 = \lambda + 2\mu \tag{1.3.22b}$$

The eigenvalues of $\mathbf{K}_e$ are given by the eigenvalue problem

$$\mathbf{K}\mathbf{x}=\lambda\mathbf{x} \tag{1.3.23}$$

The eigenvalue associated with the stabilization can be estimated by letting $\mathbf{x} = \mathbf{d}^{Hx}$ in the Rayleigh quotient, which with (20) and the orthogonality properties (4) and (7) gives

$$\lambda = \frac{\mathbf{x}^t\mathbf{K}\mathbf{x}}{\mathbf{x}^t\mathbf{x}} = \frac{AC^Q\mathbf{h}^t\mathbf{g}\mathbf{g}^t\mathbf{h}}{\mathbf{h}^t\mathbf{h}} \tag{1.3.24}$$

where the second equality follows because $\mathbf{K}_e^{1pt}\mathbf{h} = \mathbf{0}$. Using Eq. (17), it can be seen that

$$\lambda = AC^Q/4 \tag{1.3.25}$$

Using Eqs. (22) and (25) it follows that the eigenvalue associated with the stabilization is scaled to the lower bound on the maximum eigenvalue of the element if

$$C^Q = 2\alpha_s c^2 b = 2\alpha_s(\lambda+2\mu)\sum_{i=1}^{2}\mathbf{b}_i^t\mathbf{b}_i \tag{1.3.26}$$

where α_s is a scaling parameter.

In Flanagan and Belytschko (1981), the hourglass control parameter was scaled by the dynamic eigenvalue, i.e., the frequency, of the element. However, since the hourglass control is strictly an element-stiffness related stress, this seems inconsistent and a pure stiffness scaling is more appropriate.

1.4 Mixed Method Hourglass Stabilization

The mixed variational principles are another vehicle for developing four-node quadrilaterals which do not lock. Furthermore, they can be used to develop rank-compensation procedures for underintegrated elements (stabilization matrices) which do not involve any arbitrary perturbation parameters and are based on the material properties and geometry of the element.

1.4.1 Displacement Field of QUAD4 in Terms of Biorthogonal Basis. Before developing elements based on a mixed method, the displacement field in the element is expressed in a form in which the parts which cause locking can easily be identified and corrected. Furthermore, when this expression for the displacement field is used, the stiffness matrix can be obtained in closed form without any numerical integration. This is useful for understanding its properties and for implementation in vector method programs.

The procedure described here is based on Belytschko and Bachrach (1986). As a preliminary to developing this expression (which will be called the Belytschko-Bachrach form), the basis vectors $\mathbf{b}^{**}$ and $\mathbf{x}^{*}$ are defined so they are biorthogonal in R^4:

$$\left(\mathbf{x}_\beta^*\right)^t \mathbf{b}_\alpha^{**} = \delta_{\alpha\beta} \qquad (\alpha,\beta) = 1 \text{ to } 4 \tag{1.4.1}$$

$$\mathbf{b}^{**} = \left(\mathbf{b}_x, \mathbf{b}_y, \mathbf{g}, \mathbf{s}^*\right) \tag{1.4.2a}$$

$$\mathbf{x}^{*} = \left(\mathbf{x}, \mathbf{y}, \mathbf{h}, \mathbf{s}\right) \tag{1.4.2b}$$

where

$$\mathbf{s}^* = \frac{1}{4}\left[\mathbf{s} - \left(\mathbf{s}^t\mathbf{x}\right)\mathbf{b}_x - \left(\mathbf{s}^t\mathbf{y}\right)\mathbf{b}_y\right] \tag{1.4.3}$$

The vector $\mathbf{s}^*$ is obtained by orthogonalizing $\mathbf{s}$ to $\mathbf{x}$ and $\mathbf{y}$. The arbitrary constant which emerges is chosen to be 1/4 so that $\mathbf{s}^t\mathbf{s}^* = 1$. Most of the identities involved in (1) have already been proven; see Eqs. (1.3.4-7); the remaining ones are easily verified using (3) and (1.3.7).

To develop the Belytschko-Bachrach form, we start by expressing the displacement field as

$$u(x,y) = \alpha_o + \alpha_1 x + \alpha_2 y + \alpha_3 \xi\eta \tag{1.4.4}$$

Only a single component is considered since the procedure for both components is identical. Evaluating the above at the 4 nodes gives

$$u_I = u(x_I,y_I) = \alpha_o + \alpha_1 x_I + \alpha_2 y_I + \alpha_3 \xi_I\eta_I \tag{1.4.5}$$

It is easily shown that $\xi_I\eta_I = h_I$, so writing the above in matrix form gives

$$\mathbf{u} = \alpha_o\mathbf{s} + \alpha_1\mathbf{x} + \alpha_2\mathbf{y} + \alpha_3\mathbf{h} \tag{1.4.6}$$

which is a linear combination of the linearly independent $\mathbf{x}^*$ vectors. Linear independence of $\mathbf{x}^*$ follows from the biorthogonality of $\mathbf{x}^*$ and $\mathbf{b}^{**}$.

We now exploit this biorthogonality to evaluate α_i. Premultiplying (6) by $\mathbf{s}^{*t}$ and invoking the orthogonality conditions, $\mathbf{s}^{*t}\mathbf{x} = \mathbf{s}^{*t}\mathbf{y} = \mathbf{s}^{*t}\mathbf{h} = 0$ yields

$$\alpha_o = \mathbf{s}^{*t}\mathbf{u} \tag{1.4.7}$$

Similarly premultiplying respectively by $\mathbf{b}_x^t$, $\mathbf{b}_y^t$ and $\mathbf{g}^t$ and using the biorthogonality (4) yields

$$\alpha_1 = \mathbf{b}_x^t\mathbf{u} \tag{1.4.8a}$$

$$\alpha_2 = \mathbf{b}_y^t\mathbf{u} \tag{1.4.8b}$$

$$\alpha_3 = \mathbf{g}^t\mathbf{u} \tag{1.4.8c}$$

Substituting the above into (4) yields

$$u(x,y) = \left(\mathbf{s}^{*t} + x\mathbf{b}_x^t + y\mathbf{b}_y^t + \xi\eta\mathbf{g}^t\right)\mathbf{u} \tag{1.4.9a}$$

The two components of the displacement field can be expressed in the same form

$$u_x(x,y) = \left(\mathbf{s}^t + x\mathbf{b}_x^t + y\mathbf{b}_y^t + h\mathbf{g}^t\right)\mathbf{u_x} \tag{1.4.9b}$$

$$u_y(x,y) = \left(\mathbf{s}^t + x\mathbf{b}_x^t + y\mathbf{b}_y^t + h\mathbf{g}^t\right)\mathbf{u_y} \tag{1.4.9c}$$

$$h=\xi\eta \tag{1.4.9d}$$

This is the same interpolation as the standard isoparametric form (1.2.1), however, this expression will more clearly reveal what causes locking and how to eliminate it.

1.4.2 Volumetric Locking. The four node quadrilateral locks in plane strain for incompressible materials when it is fully integrated. The cause of volumetric locking can be explained by considering a mesh of elements in plane strain with fixed boundaries on two sides as shown in Fig. 6. Consider the element in the lower left-hand corner, element 1. The nodal displacements of the element for an incompressible material must preserve the total volume of the element (or to be specific, the area in plane strain, since constant volume implies that the area be constant). If we consider small displacements, the only displacements of node 3 which maintain constant area are

$$\begin{aligned} u_{x3} &= -\alpha a \\ u_{y3} &= +\alpha b \end{aligned} \tag{1.4.10}$$

where α is an arbitrary parameter; all other nodal displacements of element 1 are zero due to the boundary conditions. Differentiating (9b) and (9c), we obtain the dilatation throughout the element.

$$\Delta = u_{x,x} + u_{y,y} = \mathbf{b}_x^t\mathbf{u}_x + \mathbf{b}_y^t\mathbf{u}_y + \frac{\partial h}{\partial x}\mathbf{g}^t\mathbf{u}_x + \frac{\partial h}{\partial y}\mathbf{g}^t\mathbf{u}_y \tag{1.4.11a}$$

Substituting Eq. (10) into (11a), the constant part of the dilatation drops out leaving

$$\Delta = \frac{1}{4}\alpha\left(b\frac{\partial h}{\partial y} - a\frac{\partial h}{\partial x}\right) \qquad (1.4.11b)$$

which only vanishes everywhere except along a line that passes through the origin.

For rectangular elements as in Fig. 7, Eq. (11b) simplifies to

$$\Delta = \frac{\alpha}{ab}(b\bar{x} - a\bar{y}) \qquad (1.4.12)$$

where $(\bar{x}, \bar{y})$ is a local coordinate system. The volumetric strain is non zero everywhere except along the line $\bar{y} = (b/a)\bar{x}$; therefore, for an incompressible material the volumetric energy will be infinite if the strain energy is evaluated exactly as is the case in a fully integrated element. Thus node 3 will not be able to move; nodes 2 and 3 then provide a rigid boundary for the left hand side of element 2, and it can similarly be shown that by using these arguments for element 2 that node 6 cannot move. This argument can then be repeated for all nodes of the mesh to show that deformation of the mesh is impossible. This argument also applies to meshes of skewed elements as in Fig. 6.

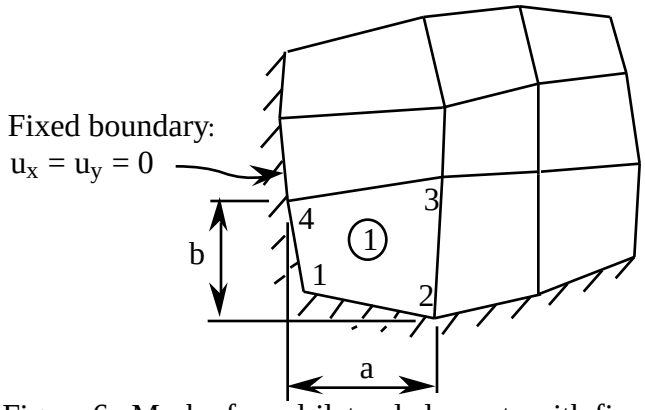

Figure 6. Mesh of quadrilateral elements with fixed boundaries on two sides

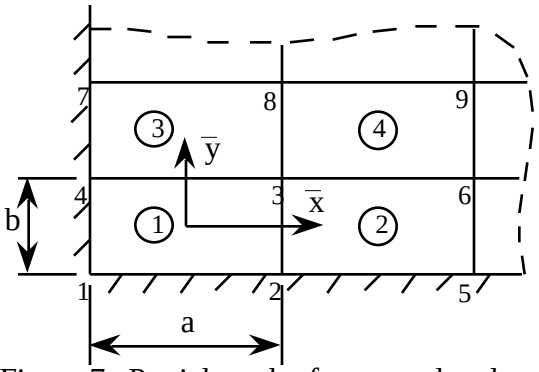

Figure 7. Partial mesh of rectangular elements fixed on two sides

Another way to examine this behavior is consider an arbitrary element deformation as expressed by Eq. (4).

$$u_x = \alpha_{0x} + \alpha_{1x}x + \alpha_{2x}y + \alpha_{3x}h$$

(1.4.13)

$$u_y = \alpha_{0y} + \alpha_{1y}x + \alpha_{2y}y + \alpha_{3y}h$$

The dilatation can be evaluated by differentiating.

$$\Delta = u_{x,x} + u_{y,y} = \alpha_{1x} + \alpha_{2y} + \alpha_{3x}\frac{\partial h}{\partial x} + \alpha_{3y}\frac{\partial h}{\partial y} \tag{1.4.14}$$

We can evaluate the change in area of the element by integrating the dilatation over the element domain.

$$\int_{\Omega_e}\Delta dA = \int_{\Omega_e}(\alpha_{1x} + \alpha_{2y} + \alpha_{3x}\frac{\partial h}{\partial x} + \alpha_{3y}\frac{\partial h}{\partial y})dA \tag{1.4.15}$$

We can show algebraically using (1.2.7b) and (1.2.8a-d) an important property of $h(\xi,\eta)$:

$$\int_{\Omega_e}\frac{\partial h}{\partial x}d\Omega = \int_{\Omega_e}\frac{\partial h}{\partial y}d\Omega = 0 \tag{1.4.16}$$

Therefore (15) is trivial to integrate and the change in element area is

$$\int_{\Omega_e}\Delta dA = (\alpha_{1x} + \alpha_{2y})A \tag{1.4.17}$$

which is zero only for $\alpha_{2y} = -\alpha_{1x}$. If we now consider volume preserving element deformation, i.e. $\alpha_{2y} = -\alpha_{1x}$, the dilatation is

$$\Delta = \alpha_{3x}\frac{\partial h}{\partial x} + \alpha_{3y}\frac{\partial h}{\partial y} \tag{1.4.18}$$

This dilatation will be non zero everywhere within the element except along the curve $\alpha_{3x}\partial h/\partial x = -\alpha_{3y}\partial h/\partial y$, even though the overall element deformation is volume preserving. Thus it becomes apparent that locking arises from the inability of the element to represent the isochoric field associated with the hourglass mode, as reflected by α_{3x} and α_{3y} in the above equations. To eliminate locking, the strain field must be designed, or projected, so that in the hourglass mode the dilatation in the projected strain field vanishes throughout the element. *In more general terms this may be stated as follows: to avoid locking, the strain field must be isochoric throughout the element for any displacement field which preserves the total volume of the element.* In particular, in the quadrilateral, the dilatation must vanish in the entire element for the hourglass mode, because this displacement mode is equivoluminal.

1.4.3 Variational principle The weak form corresponding to the Hu-Washizu variational principle is given for a single element domain by

$$0 = \delta\pi(\mathbf{u},\mathbf{e},\mathbf{s}) = \int_{\Omega_e}\delta\mathbf{e}^t\mathbf{C}\mathbf{e}d\Omega + \delta\int_{\Omega_e}\mathbf{s}^t(\mathbf{e} - D\mathbf{u})d\Omega - \delta W^{ext}$$

$$= \int_{\Omega_e} [\delta \mathbf{e}^t(\mathbf{C}\mathbf{e}-\mathbf{s}) - \delta \mathbf{s}^t(\mathbf{e}-D\mathbf{u}) + \delta(D\mathbf{u})^t\mathbf{s}]d\Omega - \delta \mathbf{d}^t\mathbf{f}^{ext} \quad (1.4.19)$$

where δ denotes a variation, $\mathbf{e}$ is the interpolated strain, and $\mathbf{s}$ the interpolated stress. $D\mathbf{u}$ is the symmetric displacement gradient which would be equivalent to the strain in a displacement method. In mixed elements that are derived from the Hu-Washizu variational principle, the displacement gradient is projected on a smaller space to avoid locking. The term δW^{ext} designates the external work, $\mathbf{f}^{ext}$ the external nodal forces. The domain chosen for (19) is a single element, but an arbitrary domain can also be assumed if connectivity is introduced into the subsequent development.

The isoparametric shape functions are used to interpolate the displacement field, which when integrated, gives the symmetric displacement gradient as

$$D\mathbf{u} = \mathbf{B}\mathbf{d} \quad (1.4.20)$$

We introduce additional interpolants for the strains and stresses.

$$\mathbf{e} = \mathbf{E}\mathbf{e} \quad (1.4.21)$$

$$\mathbf{s} = \mathbf{S}\mathbf{s} \quad (1.4.22)$$

where the interpolation matrices, $\mathbf{E}$ and $\mathbf{S}$, and the augmented strains and stresses, $\mathbf{e}$ and $\mathbf{s}$ will be defined subsequently. Substituting (20), (21), and (22) into (19), we obtain

$$0 = \int_{\Omega_e} [\delta \mathbf{e}^t\mathbf{E}^t(\mathbf{C}\mathbf{E}\mathbf{e}-\mathbf{S}\mathbf{s}) - \delta \mathbf{s}^t\mathbf{S}^t(\mathbf{E}\mathbf{e}-\mathbf{B}\mathbf{d}) + \delta \mathbf{d}^t\mathbf{B}^t\mathbf{S}\mathbf{s}]d\Omega - \delta \mathbf{d}^t\mathbf{f}_{ext} \quad (1.4.23)$$

By invoking the stationary condition on (19), we obtain

$$\tilde{\mathbf{C}}\mathbf{e} = \tilde{\mathbf{E}}^t\mathbf{s} \quad (1.4.24a)$$

$$\tilde{\mathbf{E}}\mathbf{e} = \tilde{\mathbf{B}}\mathbf{d} \quad (1.4.24b)$$

$$\tilde{\mathbf{B}}^t\mathbf{s} = \mathbf{f}^{ext} \quad (1.4.24c)$$

where

$$\tilde{\mathbf{C}} \equiv \int_{\Omega_e} \mathbf{E}^t\mathbf{C}\mathbf{E}\, d\Omega \quad (1.4.25a)$$

$$\tilde{\mathbf{E}} \equiv \int_{\Omega_e} \mathbf{S}^t\mathbf{E}\, d\Omega \quad (1.4.25b)$$

$$\tilde{\mathbf{B}} \equiv \int_{\Omega_e} \mathbf{S}^t\mathbf{B}\, d\Omega \quad (1.4.25c)$$

We obtain expressions for $\mathbf{e}$, $\mathbf{s}$, and the stiffness matrix from (24a-c).

$$\mathbf{e} = \tilde{\mathbf{E}}^{-1}\tilde{\mathbf{B}}\mathbf{d} \quad (1.4.26a)$$

$$\mathbf{s} = \tilde{\mathbf{E}}^{-1t}\tilde{\mathbf{C}}\mathbf{e} \quad (1.4.26b)$$

$$\mathbf{f}^{ext} = \tilde{\mathbf{B}}^t\mathbf{s} = \tilde{\mathbf{B}}^t\tilde{\mathbf{E}}^{-1t}\tilde{\mathbf{C}}\tilde{\mathbf{E}}^{-1}\tilde{\mathbf{B}}\mathbf{d} \equiv \mathbf{K}_e\mathbf{d} \tag{1.4.26c}$$

1.4.4 Strain Interpolations to Avoid Locking. The strain-field associated with the displacement field (9) can be obtained by straightforward differentiation which gives:

$$D\mathbf{u} = \begin{Bmatrix} \dfrac{\partial u_x}{\partial x} \\ \dfrac{\partial u_y}{\partial y} \\ \dfrac{\partial u_x}{\partial y} + \dfrac{\partial u_y}{\partial x} \end{Bmatrix} = \begin{bmatrix} \mathbf{b}_x^t + \dfrac{\partial h}{\partial x}\mathbf{g}^t & 0 \\ 0 & \mathbf{b}_y^t + \dfrac{\partial h}{\partial y}\mathbf{g}^t \\ \mathbf{b}_y^t + \dfrac{\partial h}{\partial y}\mathbf{g}^t & \mathbf{b}_x^t + \dfrac{\partial h}{\partial x}\mathbf{g}^t \end{bmatrix} \begin{Bmatrix} \mathbf{u}_x \\ \mathbf{u}_y \end{Bmatrix} = \mathbf{B}\mathbf{d} \tag{1.4.27a}$$

$$= \begin{Bmatrix} \varepsilon_x^o + q_x\dfrac{\partial h}{\partial x} \\ \varepsilon_y^o + q_y\dfrac{\partial h}{\partial y} \\ 2\varepsilon_{xy}^o + q_x\dfrac{\partial h}{\partial y} + q_y\dfrac{\partial h}{\partial x} \end{Bmatrix} \tag{1.4.27b}$$

where the naughts indicate the constant part of the strain field.

In Section 1.4.2, it was demonstrated that QUAD4 elements of incompressible material can lock when the dilatational energy at any point other than the origin is included in the stiffness matrix. It was also shown that this is caused by the dilatational field associated with the hourglass modes, $\mathbf{d}^{Hx}$ and $\mathbf{d}^{Hy}$, which in a fully integrated element always leads to non-vanishing dilatation. From Eq. (27b), it can be seen that the hourglass modes generate the nonconstant part of the volumetric field.

In constructing a strain interpolant which will not lock volumetrically, we then have two alternatives:

1. the nonconstant terms of the first two rows of Eq. (27b) can be dropped
2. the first two rows can be modified so that no volumetric strains occur in the hourglass modes.

The first alternative leads to the strain field

$$\mathbf{e} = \begin{Bmatrix} \varepsilon_x^o \\ \varepsilon_y^o \\ 2\varepsilon_{xy}^o + q_x\partial h/\partial y + q_y\partial h/\partial x \end{Bmatrix} \tag{1.4.28a}$$

This can be written in the form of Eq. (17) by letting

$$\mathbf{E} = \begin{bmatrix} 1 & 0 & 0 & 0 & 0 \\ 0 & 1 & 0 & 0 & 0 \\ 0 & 0 & 1 & \partial h/\partial y & \partial h/\partial x \end{bmatrix} \tag{1.4.28b}$$

$$\mathbf{e}^t = \begin{bmatrix} \varepsilon_x^o, & \varepsilon_y^o, & 2\varepsilon_{xy}^o, & q_x, & q_y \end{bmatrix} \tag{1.4.28c}$$

The second alternative is to define the strain field by

$$\mathbf{e} = \begin{Bmatrix} \varepsilon_x^o + q_x \partial h/\partial x - q_y \partial h/\partial y \\ \varepsilon_y^o + q_y \partial h/\partial y - q_x \partial h/\partial x \\ 2\varepsilon_{xy}^o + q_x \partial h/\partial y + q_y \partial h/\partial x \end{Bmatrix} \tag{1.4.29}$$

In Eq. (29), the dilatation $\varepsilon_x + \varepsilon_y$ still vanishes in the hourglass mode, since regardless of the value of q_x and q_y, Eq. (29) yields

$$\varepsilon_x + \varepsilon_y = \varepsilon_x^o + \varepsilon_y^o \tag{1.4.30}$$

The question then arises as to which of the two alternatives, (28) or (29), is preferable. The field in (29) is frame invariant whereas (28) is not. However, the computations associated with (28) are simpler. However, neither of these are particularly attractive for most problems from the viewpoints of accuracy and efficiency.

For elements which involve beam bending, the performance of the element can be improved strikingly by omitting the nonconstant part of the shear field. This shear strain field cannot be combined with the extensional strains in (28) because the strain field would then only contain three independent functions, and the element would be rank deficient. Therefore this shear strain field is combined with the extensional strains in (29), which gives

$$\mathbf{e} = \begin{Bmatrix} \varepsilon_x^o + q_x \partial h/\partial x - q_y \partial h/\partial y \\ \varepsilon_y^o + q_y \partial h/\partial y - q_x \partial h/\partial x \\ \varepsilon_{xy}^o \end{Bmatrix} \tag{1.4.31a}$$

For this element

$$\mathbf{E} = \begin{bmatrix} 1 & 0 & 0 & \partial h/\partial x & -\partial h/\partial y \\ 0 & 1 & 0 & -\partial h/\partial x & \partial h/\partial y \\ 0 & 0 & 1 & 0 & 0 \end{bmatrix} \tag{1.4.31b}$$

with **e** given in (28c). The strain field (31) leads to the "Optimal Incompressible" or OI element in Belytschko and Bachrach. This element performs well in beam bending problems when one set of element sides are parallel to the axis of the beam and the elements are not too distorted.

The performance of QUAD4 in bending can be enhanced even further for isotropic, elastic problems by using a strain field which depends on Poisson's ratio as follows:

$$\mathbf{e} = \begin{Bmatrix} \varepsilon_x^o + q_x \dfrac{\partial h}{\partial x} - \bar{\nu} q_y \dfrac{\partial h}{\partial y} \\ \varepsilon_y^o + q_y \dfrac{\partial h}{\partial y} - \bar{\nu} q_x \dfrac{\partial h}{\partial x} \\ 2\varepsilon_{xy}^o \end{Bmatrix} \tag{1.4.32}$$

$$\text{where } \bar{\nu} \equiv \begin{cases} \nu & \text{for plane stress} \\ \nu/(1-\nu) & \text{for plane strain} \end{cases}$$

This is the field called "Quintessential Bending and Incompressible" or QBI in Belytschko and Bachrach (1986), which has great accuracy in bending with linear elastic material. For a rectangle, as shown by Fröier et al. (1974), this element corresponds to the incompatible quadrilateral of Wilson et al. (1973).

1.4.5 Stiffness Matrix for OI Element. In order to gain more insight into these mixed elements and to see how they are used to construct stabilization (rank-compensating) matrices which do not involve arbitrary parameters, the stiffness matrix for the OI element, which is based on the strain field (31b) will be developed.

The stress field is chosen to be

$$\mathbf{s} = \begin{bmatrix} 1 & 0 & 0 & \partial h/\partial x & 0 \\ 0 & 1 & 0 & 0 & \partial h/\partial y \\ 0 & 0 & 1 & 0 & 0 \end{bmatrix} \mathbf{s} \equiv \mathbf{S}\,\mathbf{s} \tag{1.4.33.a}$$

$$\mathbf{s}^t = \begin{bmatrix} \sigma_x^o, & \sigma_y^o, & \sigma_{xy}^o, & Q_x & Q_y \end{bmatrix} \tag{1.4.33b}$$

Using (16), and integrating (25b) and (25c), we obtain $\tilde{\mathbf{E}}$ and $\tilde{\mathbf{B}}$ as follows:

$$\tilde{\mathbf{E}} = \begin{bmatrix} A\mathbf{I}_{3x3} & \mathbf{0}_{3x2} \\ \mathbf{0}_{2x3} & \begin{bmatrix} H_{xx} & -H_{xy} \\ -H_{xy} & H_{yy} \end{bmatrix} \end{bmatrix} \tag{1.4.34}$$

where A is the area of the element, and

$$H_{ij} = \int_{\Omega_e} (\partial h/\partial x_i)(\partial h/\partial x_j) d\Omega \tag{1.4.35}$$

The $\tilde{\mathbf{B}}$ matrix is given by

$$\tilde{\mathbf{B}} = \begin{bmatrix} A\mathbf{b}_x^t & \mathbf{0} \\ \mathbf{0} & A\mathbf{b}_y^t \\ A\mathbf{b}_y^t & A\mathbf{b}_x^t \\ H_{xx}\mathbf{g}^t & \mathbf{0} \\ \mathbf{0} & H_{yy}\mathbf{g}^t \end{bmatrix} \tag{1.4.36}$$

The inverse of $\tilde{\mathbf{E}}$ is given by

$$\tilde{\mathbf{E}}^{-1} = \begin{bmatrix} \frac{1}{A}\mathbf{I}_{3x3} & \mathbf{0}_{3x2} \\ \mathbf{0}_{2x3} & \frac{1}{H}\begin{bmatrix} H_{yy} & H_{xy} \\ H_{xy} & H_{xx} \end{bmatrix} \end{bmatrix} \tag{1.4.37}$$

where

$$H = H_{xx} H_{yy} - H_{xy}^2 \tag{1.4.38}$$

Using (26a), (36) and (37), we can evaluate $\mathbf{e}$ to be

$$\begin{aligned} \varepsilon_x^o &= \mathbf{b}_x^t \mathbf{u}_x \\ \varepsilon_y^o &= \mathbf{b}_y^t \mathbf{u}_y \\ 2\varepsilon_y^o &= \mathbf{b}_x^t \mathbf{u}_y + \mathbf{b}_y^t \mathbf{u}_x \\ q_x &= \frac{1}{H}\left(H_{xx}H_{yy}\mathbf{g}^t\mathbf{u}_x + H_{xy}H_{yy}\mathbf{g}^t\mathbf{u}_y\right) \\ q_y &= \frac{1}{H}\left(H_{xy}H_{xx}\mathbf{g}^t\mathbf{u}_x + H_{xx}H_{yy}\mathbf{g}^t\mathbf{u}_y\right) \end{aligned} \tag{1.4.39}$$

From (39) we can see that in the mixed element, the constant parts of the strain field corresponds exactly to the constant part which emanates from the displacement field $D\mathbf{u}$ given in (27). The nonconstant part depends strictly on the hourglass mode (any component of $\mathbf{u}_x$ or $\mathbf{u}_y$ which is not orthogonal to $\mathbf{g}$). The effect of the projection is to modify this part of the strain field so that the volumetric strains vanish.

To complete the evaluation of the element stiffness, we obtain $\widetilde{\mathbf{C}}$ by integrating (25a).

$$\widetilde{\mathbf{C}} = \begin{bmatrix} A\mathbf{C}_{3x3} & \mathbf{0}_{3x2} \\ \mathbf{0}_{2x3} & \begin{bmatrix} 4\mu H_{xx} & -4\mu H_{xy} \\ -4\mu H_{xy} & 4\mu H_{yy} \end{bmatrix} \end{bmatrix} \tag{1.4.40a}$$

For a linear isotropic material, $\mathbf{C}$ is given by

$$\mathbf{C} = \begin{bmatrix} \bar{\lambda}+2\mu & \bar{\lambda} & 0 \\ \bar{\lambda} & \bar{\lambda}+2\mu & 0 \\ 0 & 0 & \mu \end{bmatrix} \tag{1.4.40b}$$

For plane strain, $\bar{\lambda}=\lambda=2\mu\nu/(1-2\nu)$; for plane stress $\bar{\lambda}=2\mu\nu/(1-\nu)$. Substituting (28c), (37), and (40a) into (26b), we obtain

$$\begin{Bmatrix} Q_x \\ Q_y \end{Bmatrix} = 4\mu \begin{Bmatrix} q_x \\ q_y \end{Bmatrix} \tag{1.4.41}$$

It can be seen already that because of the way the assumed strain field was designed, the nonconstant part depends only on the shear modulus μ and is independent of the bulk modulus.

Evaluating the stiffness by (26c),

$$\mathbf{K}_e = \mathbf{B}^t(\mathbf{0})\,\mathbf{C}\mathbf{B}(\mathbf{0}) + \mathbf{K}_e^{stab} \tag{1.4.42a}$$

$$\mathbf{K}_e^{stab} = \begin{bmatrix} c_1\mathbf{g}\mathbf{g}^t & c_2\mathbf{g}\mathbf{g}^t \\ c_2\mathbf{g}\mathbf{g}^t & c_3\mathbf{g}\mathbf{g}^t \end{bmatrix} \tag{1.4.42b}$$

$\mathbf{B}(\mathbf{0})$ is given by (1.2.39). Constants for OI stabilization as well as those for QBI are given in Table 1. QBI stabilization is derived in the same way as OI with $\mathbf{E}$ given by (32).

Table 1. Constants for the mixed method stabilization matrix

Stabilization	c_1	c_2	c_3
OI	$4\mu H_{xx}H^*$	$4\mu H_{xy}H^*$	$4\mu H_{yy}H^*$
QBI	$2\mu(1+\bar{\nu})H_{xx}H^{**}$	$2\mu\bar{\nu}(1+\bar{\nu})H_{xy}H^{**}$	$2\mu(1+\bar{\nu})H_{yy}H^{**}$

Note. $\bar{\nu} \equiv \nu$ for plane stress and $\bar{\nu} \equiv \nu/(1-\nu)$ for plane strain;

$$H^* \equiv \frac{H_{xx}H_{yy}}{H_{xx}H_{yy} - H_{xy}^2} \qquad H^{**} \equiv \frac{H_{xx}H_{yy}}{H_{xx}H_{yy} - \bar{\nu}H_{xy}^2}$$

Explicit approximate expressions for H_{ij} can be obtained by integrating (28) in closed form assuming the Jacobian to be constant within the element domain.

$$H_{xx} = \frac{\left(\mathbf{L}_1^t\mathbf{y}\right)^2 + \left(\mathbf{L}_2^t\mathbf{y}\right)^2}{3A}$$

$$H_{yy} = \frac{\left(\mathbf{L}_1^t\mathbf{x}\right)^2 + \left(\mathbf{L}_2^t\mathbf{x}\right)^2}{3A} \tag{1.4.43}$$

$$H_{xy} = \frac{-\left(\mathbf{L}_1^t\mathbf{x}\right)\left(\mathbf{L}_1^t\mathbf{y}\right) - \left(\mathbf{L}_2^t\mathbf{x}\right)\left(\mathbf{L}_2^t\mathbf{y}\right)}{3A}$$

where

$$\mathbf{L}_1^t = (-1, +1, +1, -1)$$
$$\mathbf{L}_2^t = (-1, -1, +1, +1). \tag{1.4.44}$$

The quantities used to evaluate H_{ij} can also be used to evaluate the element area by

$$A = \frac{1}{4}\left[(\mathbf{L}_1^t\mathbf{x})(\mathbf{L}_2^t\mathbf{y}) - (\mathbf{L}_1^t\mathbf{y})(\mathbf{L}_2^t\mathbf{x})\right] \tag{1.4.45}$$

The first part of the stiffness corresponds to the one-point quadrature stiffness. The second part is the stabilization or rank compensating stiffness, which is of rank 2 and thus increases the rank of the total stiffness from 3 (rank of one-point quadrature stiffness) to 5. This is the correct rank of QUAD4 according to Eq. (1.2.26a).

The form given in (35) can be considered a canonical form for the stiffness matrix of QUAD4 if the constants c_i are arbitrary. For any c_i, this element stiffness will satisfy the patch test. The constants c_i can be varied to improve the performance of the element for specific problem classes, but as shown by numerical studies in Belytschko and Bachrach (1986), the rate of convergence will always be the same, provided the element does not lock. When the stabilization matrix is independent of the bulk modulus $\lambda + \frac{2}{3}\mu$, the element will not lock volumetrically.

This development also provides guidance about the design of stabilization procedures in nonlinear problems which are based on material properties. If the current linearized value of μ can be estimated, then (34) provides a stress-strain relation between $\dot{Q}_i$ and $\dot{q}_i$.

1.4.6 Frame Invariance. The elimination of the nonconstant part of the shear strain as is done with the OI and QBI elements improves their performance in bending problems. The cantilever test problems of the next section demonstrates the excellent coarse mesh bending accuracy of QBI; however, elimination of the nonconstant shear strain also causes the element to lose frame invariance. For most problems, the effect is negligible, but for coarse mesh bending, the effect can be significant.

Elements based on the OI or QBI assumed strain field can be made frame invariant by evaluating the stabilization matrix using an orthogonal, local coordinate system that is aligned with the element. The local coordinate system, called the $(\hat{x}, \hat{y})$ system, is related to the global coordinate system by a rotation matrix **R**.

The nodal coordinates, **x** and **y**, evaluated in the local $(\hat{x}, \hat{y})$ coordinate system, are renamed $\hat{\mathbf{x}}$ and $\hat{\mathbf{y}}$. They are obtained by

$$\begin{Bmatrix} \hat{\mathbf{x}} \\ \hat{\mathbf{y}} \end{Bmatrix} = \mathbf{R} \begin{Bmatrix} \mathbf{x} \\ \mathbf{y} \end{Bmatrix} \tag{1.4.46}$$

where **R** consists of the standard two dimensional rotation matrix arranged in an 8x8 matrix to transform each pair of nodal coordinates, x_I and y_I.

$$\mathbf{R} = \begin{bmatrix} \cos\theta \mathbf{I}_{4x4} & \sin\theta \mathbf{I}_{4x4} \\ -\sin\theta \mathbf{I}_{4x4} & \cos\theta \mathbf{I}_{4x4} \end{bmatrix} \tag{1.4.47}$$

where $\mathbf{I}_{4x4}$ is a rank 4 identity matrix.

The angle between the global and local coordinate system can be defined by

$$\tan\theta = \mathbf{L}_1^t \mathbf{y} \Big/ \mathbf{L}_1^t \mathbf{x} \tag{1.4.48}$$

This definition aligns the $\hat{x}$ axis with the referential ξ axis of the element as shown in Fig. 8. This definition may not be appropriate for anisotropic material. This point is discussed further in the explicit formulation that follows.

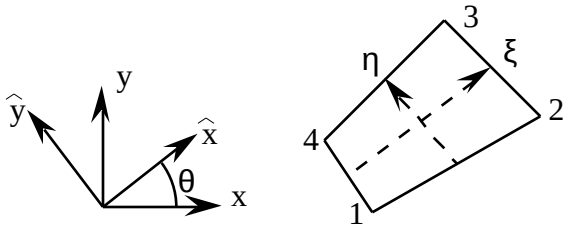

Figure 8. Local $(\hat{x}, \hat{y})$ coordinate system aligned with ξ axis of an element

We evaluate $\hat{\mathbf{b}}_x$, $\hat{\mathbf{b}}_y$, and $\hat{\mathbf{g}}$ by substituting $\hat{\mathbf{x}}$ and $\hat{\mathbf{y}}$ for **x** and **y** in (1.2.40) and (1.3.15).

$$\hat{\mathbf{b}}_x^t = \frac{1}{2A} \left[\hat{y}_{24}, \hat{y}_{31}, \hat{y}_{42}, \hat{y}_{13}\right] \tag{1.4.49a}$$

$$\hat{\mathbf{b}}_y^t = \frac{1}{2A} \left[\hat{x}_{42}, \hat{x}_{13}, \hat{x}_{24}, \hat{x}_{31}\right] \tag{1.4.49b}$$

$$\hat{y}_{IJ} = \hat{y}_I - \hat{y}_J \quad \hat{x}_{IJ} = \hat{x}_I - \hat{x}_J \tag{1.4.49c}$$

$$\hat{\mathbf{g}} = \frac{1}{4}\left[\mathbf{h} + \left(\mathbf{h}^t \hat{\mathbf{x}}\right)\hat{\mathbf{b}}_x + \left(\mathbf{h}^t \hat{\mathbf{y}}\right)\hat{\mathbf{b}}_y\right] \tag{1.4.50}$$

Hats are added to terms to indicate that local coordinates are used in their evaluation. $\widehat{H}_{xx}$, $\widehat{H}_{yy}$, and $\widehat{H}_{xy}$, are evaluated by Eq. (44) with $\widehat{\mathbf{x}}$ and $\widehat{\mathbf{y}}$ substituted for $\mathbf{x}$ and $\mathbf{y}$. Likewise, the constants in Table 1 are evaluated in terms of $\widehat{H}_{xx}$, $\widehat{H}_{yy}$, and $\widehat{H}_{xy}$ and are renamed $\hat{c}_1$, $\hat{c}_2$, and $\hat{c}_3$. The stabilization matrix is analogous to (42b) and is given by

$$\widehat{\mathbf{K}}_e^{stab} = \begin{bmatrix} \hat{c}_1 \widetilde{\mathbf{gg}}^t & \hat{c}_2 \widetilde{\mathbf{gg}}^t \\ \hat{c}_2 \widetilde{\mathbf{gg}}^t & \hat{c}_3 \widetilde{\mathbf{gg}}^t \end{bmatrix} \tag{1.4.51}$$

In order to add the element stabilization matrix to the global stiffness matrix, it must be transformed back to the global coordinate system by

$$\mathbf{K}_e^{stab} = \mathbf{R}^t \widehat{\mathbf{K}}_e^{stab} \mathbf{R} \tag{1.4.52}$$

It is simple enough to evaluate $\mathbf{K}_e^{stab}$ in closed form as

$$\mathbf{K}_e^{stab} = \begin{bmatrix} \hat{c}_1^* \widetilde{\mathbf{gg}}^t & \hat{c}_2^* \widetilde{\mathbf{gg}}^t \\ \hat{c}_2^* \widetilde{\mathbf{gg}}^t & \hat{c}_3^* \widetilde{\mathbf{gg}}^t \end{bmatrix} \tag{1.4.53}$$

where

$$\begin{aligned} \hat{c}_1^* &= \hat{c}_1 \cos^2\theta + \hat{c}_3 \sin^2\theta - 2\hat{c}_2 \sin\theta\cos\theta \\ \hat{c}_2^* &= \hat{c}_2 \left(\cos^2\theta - \sin^2\theta\right) + \left(\hat{c}_1 - \hat{c}_3\right) \sin\theta\cos\theta \\ \hat{c}_3^* &= \hat{c}_3 \cos^2\theta + \hat{c}_1 \sin^2\theta + 2\hat{c}_2 \sin\theta\cos\theta \end{aligned} \tag{1.4.54}$$

1.4.7 Hourglass Control Procedure. We seek to evaluate internal forces directly by the first equality in Eq. (26c) which in corotational coordinates is

$$\hat{\mathbf{f}}^{int} = \widehat{\widetilde{\mathbf{B}}}^t \hat{\mathbf{s}} \tag{1.4.55}$$

For the OI and QBI strain and stress fields, Eq. (55) can be shown to take the form of a one-point element plus stabilization forces:

$$\hat{\mathbf{f}}^{int} = A \widehat{\mathbf{B}}^t(\mathbf{0}) \widehat{\mathbf{s}}(\mathbf{0}) + \hat{\mathbf{f}}^{stab} \tag{1.4.56}$$

A procedure for large deformation, nonlinear problems based on the previous analysis of the mixed element is described. The mixed field OI given in Section 1.4.5 will be used for this purpose. Implementations based on other assumed strain fields can be developed similarly.

The development hinges on the fact that the linear theory developed in Section 1.4.5 is identical to the nonlinear theory if all variables are interpreted as rates. Thus components of the generalized hourglass strain rates can be obtained by Eq. (26a) written in the form

$$\dot{\hat{q}}_x = \frac{1}{\hat{H}}\left(\hat{H}_{xx}\hat{H}_{yy}\,\hat{\mathbf{g}}^t\hat{\mathbf{v}}_x + \hat{H}_{xy}\hat{H}_{yy}\hat{\mathbf{g}}^t\hat{\mathbf{v}}_y\right)$$
$$\dot{\hat{q}}_y = \frac{1}{\hat{H}}\left(\hat{H}_{xy}\hat{H}_{xx}\,\hat{\mathbf{g}}^t\hat{\mathbf{v}}_x + \hat{H}_{xx}\hat{H}_{yy}\hat{\mathbf{g}}^t\hat{\mathbf{v}}_y\right) \qquad (1.4.57)$$

where the superposed carets indicate that the quantities are evaluated using a corotational coordinate system. This formulation results in a frame invariant element. The corotational coordinate system is equivalent to the local coordinate system presented in the previous section, however it is embedded in the element and rotates with the element as the element deforms. The corotational coordinate system can be embedded by various techniques, and for anisotropic materials, it is advantageous to embed the coordinate system so that it coincides with axes of orthotropy or other directional features of the material.

The corotational coordinate system can also be used to evaluate the rate-of-deformation and update the stress at the quadrature point. An advantage of the corotational system is that a frame invariant stress rate is not needed for large deformation problems.

The stress-strain law for the generalized hourglass strain rates and stress rates is given by

$$\dot{\hat{Q}}_i = 4\mu\dot{\hat{q}}_i \qquad (1.4.58)$$

This relation involves the shear modulus μ and assumes an isotropic material response. The shear modulus, μ is obtained by taking the ratio of the effective deviatoric stress rates and strain rates.

$$2\mu = \left(\frac{\dot{\hat{s}}_{ij}\dot{\hat{s}}_{ij}}{\dot{\hat{e}}_{ij}\dot{\hat{e}}_{ij}}\right)^{\frac{1}{2}} \qquad (1.4.59a)$$

$$\dot{\hat{s}}_{ij} = \dot{\hat{\sigma}}_{ij} - \frac{1}{3}\dot{p}\delta_{ij} \qquad (1.4.59b)$$

$$\dot{\hat{e}}_{ij} = \dot{\hat{\varepsilon}}_{ij} - \frac{1}{3}\dot{\hat{\varepsilon}}_{kk}\delta_{ij} \qquad (1.4.59c)$$

In two-dimensional plane stress problems

$$\dot{\hat{s}}_{ij}\dot{\hat{s}}_{ij} = \dot{\hat{\sigma}}_x^2 - \dot{\hat{\sigma}}_x\dot{\hat{\sigma}}_y + \dot{\hat{\sigma}}_x^2 + 3\dot{\hat{\sigma}}_{xy}^2 \qquad (1.4.60a)$$

$$\dot{\hat{e}}_{ij}\dot{\hat{e}}_{ij} = \dot{\hat{\varepsilon}}_x^2 - \dot{\hat{\varepsilon}}_x\dot{\hat{\varepsilon}}_y + \dot{\hat{\varepsilon}}_x^2 + 3\dot{\hat{\varepsilon}}_{xy}^2 \qquad (1.4.60b)$$

The stabilization stresses are then updated by

$$\hat{Q}_i^{n+1} = \hat{Q}_i^n + \int_{t^n}^{t^{n+1}} \dot{\hat{Q}}_i dt \tag{1.4.61a}$$

which for the central difference method gives

$$\hat{Q}_i^{n+1} = \hat{Q}_i^n + \Delta t \dot{\hat{Q}}_i^{n+1/2} \tag{1.4.61b}$$

The stabilization internal forces, evaluated by (26b), are then given by

$$\hat{\mathbf{f}}_x^{stab} = (\hat{H}_{xx}\hat{Q}_x - \hat{H}_{xy}\hat{Q}_y)\hat{\mathbf{g}} \tag{1.4.62a}$$

$$\hat{\mathbf{f}}_y^{stab} = (\hat{H}_{yy}\hat{Q}_y - \hat{H}_{xy}\hat{Q}_x)\hat{\mathbf{g}} \tag{1.4.62b}$$

Not that the stress and strain which is used to evaluate the shear modulus is marked with hats to indicate that these are corotational quantities. This is not necessary since the shear modulus is an invariant quantity for isotropic material.

The assumptions made in this development is that the material response is uniform over the element and the deviatoric response is isotropic. The second assumption can be avoided by using a $\tilde{\mathbf{C}}$ matrix based on a fully anisotropic $\mathbf{C}$. However, this entails availability of $\mathbf{C}$ in the computational process, and in procedures such as radial return for elastoplasticity, $\mathbf{C}$ is not available. The first assumption is more troublesome; as the elastic-plastic front passes across an element, one-point quadrature is not as effective in resolving the behavior along the boundary. This effect has been noted in Liu et al. (1988). Usually, however, the substantially reduced cost of one-point quadrature elements allows more elements to compensate for this effect. Adaptive schemes with automatic mesh refinement in zones of rapidly varying material behavior are also effective. To avoid these difficulties, assumed strain methods with 2 or more quadrature points as described in Section 1.5.6 can be used.

1.5 Assumed Strain Hourglass Stabilization

In this section, the stabilization procedure for the quadrilateral will be developed by means of the assumed strain methodology. The arguments used in constructing the assumed strain field for this procedure are identical to those used with the Hu-Washizu principle. However, the implementation is much simpler because many of the intermediate matrices which are required in the Hu-Washizu approach can be bypassed. Nevertheless, the results obtained by the assumed strain procedure differ very little from the results obtained by the corresponding Hu-Washizu elements.

The assumed strain approach can also be used in conjunction with quadrature schemes which use more than one point. This avoids the use of stabilization schemes, but does require substantially more effort if the constitutive equations are complex.

In addition to describing the assumed strain method, the notion of projection of strains is examined further in this section. It is shown that the assumed strain fields which eliminate volumetric locking and excessive stiffness in bending problems correspond to projections of the higher order terms in the strain field.

1.5.1 Variational principle Assumed strain elements herein are based on a simplified form of the Hu-Washizu variational principle as described by Simo and Hughes (1986) in which the interpolated stress is assumed to be orthogonal to the difference between the symmetric part of the velocity gradient and the interpolated rate-of-deformation. Therefore, the second term of (1.4.19) drops out leaving

$$0 = \delta\pi(\mathbf{e}) = \int_{\Omega_e} \delta\mathbf{e}^t \mathbf{C}\mathbf{e}\, d\Omega - \delta\mathbf{d}^t \mathbf{f}^{ext} \tag{1.5.1}$$

In this form, the interpolated stress does not need to be defined since it no longer appears in the variational principle.

The discrete equations then require only the interpolation of the strain, which we relate to the nodal displacements by $\bar{\mathbf{B}}$ which will be defined later.

$$\mathbf{e}(\mathbf{x}) \equiv \bar{\mathbf{B}}(\mathbf{x})\mathbf{d} \tag{1.5.2}$$

Substituting (2) into (1) gives

$$0 = \delta\mathbf{d}^t \int_{\Omega_e} \bar{\mathbf{B}}^t \mathbf{C} \bar{\mathbf{B}}\, d\Omega\, \mathbf{d} - \delta\mathbf{d}^t \mathbf{f}^{ext} \tag{1.5.3}$$

so the arbitrariness of $\delta\mathbf{d}$ leads to

$$\mathbf{f}^{int} = \mathbf{f}^{ext} \tag{1.5.4}$$

where

$$\mathbf{f}^{int} = \mathbf{K}_e \mathbf{d} \tag{1.5.5}$$

and

$$\mathbf{K}_e = \int_{\Omega_e} \bar{\mathbf{B}}^t \mathbf{C} \bar{\mathbf{B}}\, d\Omega \tag{1.5.6}$$

The stiffness matrix of the fully integrated isoparametric element is found by (1.2.28). The application of the assumed strain method to the development of a stabilization procedure for an underintegrated element then involves the construction of an appropriate form for the $\bar{\mathbf{B}}$ matrix which avoids locking.

1.5.2 Elimination of Volumetric Locking. To eliminate volumetric locking, the strain field must be projected so that the volumetric strain energy always vanishes in the hourglass mode. For this purpose, we consider a general form of the assumed strain

$$\mathbf{e} = \begin{Bmatrix} \varepsilon_x^o + q_x e_1 h_{,x} + q_y e_2 h_{,y} \\ \varepsilon_y^o + q_x e_2 h_{,x} + q_y e_1 h_{,y} \\ 2\varepsilon_{xy}^o + q_x e_3 h_{,y} + q_y e_3 h_{,x} \end{Bmatrix} \equiv \begin{Bmatrix} \varepsilon_x^o + \tilde{\varepsilon}_x \\ \varepsilon_y^o + \tilde{\varepsilon}_y \\ 2\varepsilon_{xy}^o + 2\tilde{\varepsilon}_{xy} \end{Bmatrix} \tag{1.5.7a}$$

$$q_x = \mathbf{g}^t \mathbf{u}_x \qquad q_y = \mathbf{g}^t \mathbf{u}_y \tag{1.5.7b}$$

where e_1, e_2, and e_3 are arbitrary constants, and q_x and q_y are the magnitudes of the hourglass modes, which vanish except when the element is in the hourglass mode. In (7a) and subsequent equations, commas denote derivatives with respect to the variables that follow. Substituting (1.4.39) and (7b) into (7a), the assumed strain field is put into $\bar{\mathbf{B}}$ form as follows:

$$\mathbf{e} = \bar{\mathbf{B}}\mathbf{d}$$

$$\bar{\mathbf{B}} = \begin{bmatrix} \mathbf{b}_x^t + e_1 h_{,x}\mathbf{g}^t & e_2 h_{,y}\mathbf{g}^t \\ e_2 h_{,x}\mathbf{g}^t & \mathbf{b}_y^T + e_1 h_{,y}\mathbf{g}^t \\ \mathbf{b}_y^T + e_3 h_{,y}\mathbf{g}^t & \mathbf{b}_x^T + e_3 h_{,x}\mathbf{g}^t \end{bmatrix} \tag{1.5.8}$$

For the purpose of illustrating the projections, the symmetric displacement gradient (1.4.27b) is written as

$$D\mathbf{u} = \begin{bmatrix} u^o_{x,x} + \tilde{u}_{x,x} \\ u^o_{y,y} + \tilde{u}_{y,y} \\ u^o_{x,y} + \tilde{u}_{x,y} + u^o_{y,x} + \tilde{u}_{y,x} \end{bmatrix} = \begin{bmatrix} \varepsilon^o_x + q_x h_{,x} \\ \varepsilon^o_y + q_y h_{,y} \\ 2\varepsilon^o_{xy} + q_x h_{,y} + q_y h_{,x} \end{bmatrix} \tag{1.5.9}$$

The dilatation of the assumed strain field given by Eq. (2a), which is denoted by $\bar{\Delta}$, vanishes in the hourglass mode if $e_1 = -e_2$. This is shown as follows. Consider the nodal displacements that correspond to the hourglass mode of deformation.

$$\mathbf{u}_x = \alpha_{3x}\mathbf{h} \qquad \mathbf{u}_y = \alpha_{3y}\mathbf{h} \tag{1.5.10}$$

Evaluating the strain by (2), we obtain the dilatation as

$$\bar{\Delta} = \varepsilon_x + \varepsilon_y = (e_1 + e_2)(\alpha_{3x} h_{,x} + \alpha_{3y} h_{,y}) \tag{1.5.11}$$

So for $e_1 = -e_2$, $\bar{\Delta} = 0$. Thus, with this projected strain, the dilatation vanishes throughout the element in the hourglass mode. Furthermore, it can easily be shown that for the meshes in Figs. 6 and 7 with the nodal displacements given by (1.4.10), the dilatation $\bar{\Delta}$ vanishes throughout the element.

For linear elastic material with a constitutive matrix given by (1.4.40b), and the nodal displacements given in Eq. (10), the strain energy of the assumed strain element with $e_2 = -e_1$ is

$$U = \tfrac{1}{2}\int_{\Omega_e} \mathbf{e}^t \mathbf{C} \mathbf{e}\, d\Omega \tag{1.5.12}$$

$$= \mu e_1^2 (\alpha_{3x}^2 H_{xx} + \alpha_{3x}\alpha_{3y} H_{xy} + \alpha_{3y}^2 H_{yy}) + \tfrac{1}{2}\mu e_3^2 (\alpha_{3y}^2 H_{xx} + \alpha_{3x}\alpha_{3y} H_{xy} + \alpha_{3x}^2 H_{yy})$$

which is independent of the bulk modulus. Thus the volumetric energy in this element is always finite and the element will not be subject to volumetric locking.

The portion of the volumetric strain which has been eliminated by this projection is often called "spurious" or "parasitic" volumetric strain. Whatever the name, it is certainly undesirable for the treatment of incompressible materials. Since in the nonlinear range, many materials are incompressible, its elimination from the element is crucial.

The character of this projection for various values of e_1 (when $e_1 = -e_2$) is shown in Fig. 9. The two axes represent the nonconstant terms in $u_{x,x}$ and $u_{y,y}$, which are denoted by $\tilde{u}_{x,x}$ and $\tilde{u}_{y,y}$, and the corresponding terms in the assumed strain (compare Eqs. (8) and (9)) $\tilde{\varepsilon}_x$ and $\tilde{\varepsilon}_y$ respectively. The square represents an example of a point in ($\tilde{u}_{x,x}$, $\tilde{u}_{y,y}$)

space, while the circles represent corresponding points in ($\tilde{\varepsilon}_x$, $\tilde{\varepsilon}_y$) space. From the formula relating these quantities, namely

$$\tilde{\varepsilon}_x = e_1(\tilde{u}_{x,x} - \tilde{u}_{y,y}) \qquad (1.5.13a)$$

$$\tilde{\varepsilon}_y = e_1(\tilde{u}_{y,y} - \tilde{u}_{x,x}) \qquad (1.5.13b)$$

it can be seen the $e_1=\frac{1}{2}$ corresponds to a normal projection of the functions $\tilde{u}_{x,x}$, $\tilde{u}_{y,y}$ onto the line $\tilde{\varepsilon}_x + \tilde{\varepsilon}_y = 0$, which is the line on which the higher order terms in the assumed strain field posses no dilatation. Other values of e_1 shift the higher order terms of the assumed strain along the same line.

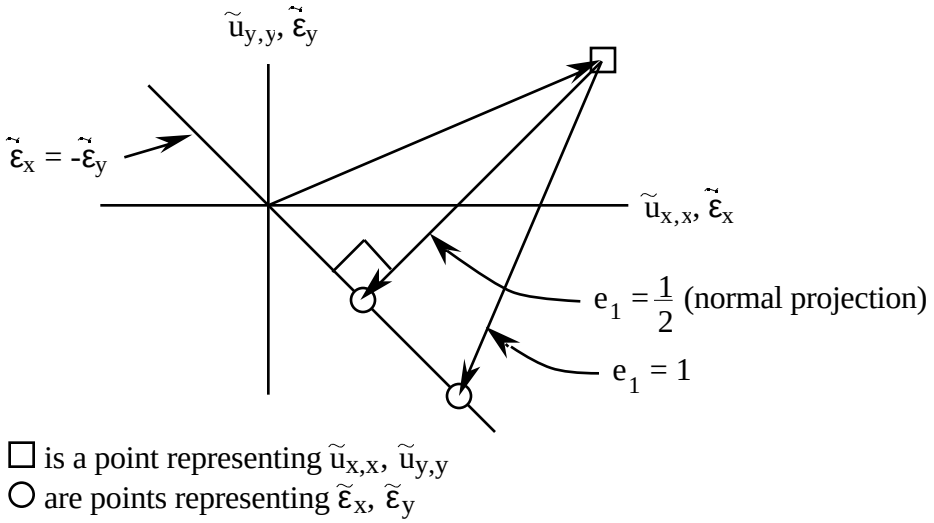

Figure 9. Depiction of projection of nonconstant part of displacement gradient $\tilde{u}_{x,x}$, $\tilde{u}_{y,y}$ onto isochoric assumed strain fields

1.5.3 Shear Locking and its Elimination. Shear locking in the four-node quadrilateral may be explained and eliminated by projection in a similar manner. It should be mentioned, and this will become clear from the results, that the effect of "spurious" shear is somewhat different than that of "spurious" strains in volumetric locking. In volumetric locking, the results completely fail to converge; with spurious shear, the solutions converge but rather slowly. Thus the term "excessive shear stiffness" is probably more precise, but the term shear locking is also a useful description.

To understand shear locking and its elimination, consider a beam represented by a single row of elements which is in pure bending as shown in Fig. 10. In pure bending, the moment field is constant and as is well known to structural engineers, the shear must vanish, since the shear is the derivative of the moment with respect to x: $s=m_{,x}$.

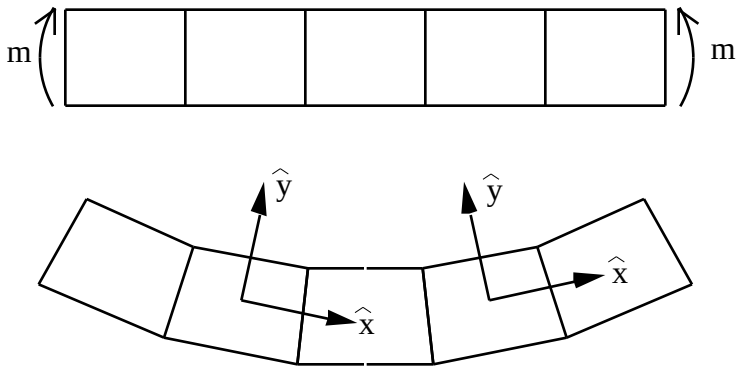

Figure 10. A beam in pure bending showing that the deformation is primarily into the hourglass mode

To eliminate shear locking, the portion of the shear field which is triggered by any nodal displacements which are not orthogonal to **g** must be eliminated. Since only **h** is not orthogonal to **g**, this is another way of saying that the shear associated with the hourglass mode must be eliminated. This can be accomplished by letting e_3=0 in Eq. (8). In pure bending, the nodal displacements in the local coordinate system of the element defined as shown in Fig. 10 are given by

$$\hat{\mathbf{u}}_x = c\hat{\mathbf{h}} \qquad \hat{\mathbf{u}}_y = \mathbf{0} \tag{1.5.14}$$

where c is an arbitrary constant. If the strain energy is computed using Eq. (8) for arbitrary e_3, we find that the shear strain energy

$$U_{shear} = \tfrac{1}{2}\mu e_3^2 c^2 H_{yy} = 0 \tag{1.5.15}$$

so it vanishes as expected when e_3=0; parasitic shear in bending is thus eliminated. This corresponds to the projection illustrated in Fig. 11. The shear field emanating from the displacement field can be written in terms of the 3 parameters ε_{xy}^{o}, q_x, and q_y. The second and third parameters are associated with the parts of the shear which are triggered only by the hourglass mode of deformation. The assumed shear strain field, ε_{xy}, is the projection of the strain field emanating from the displacement field onto the line of constant shear strain fields, as shown in Fig. 11.

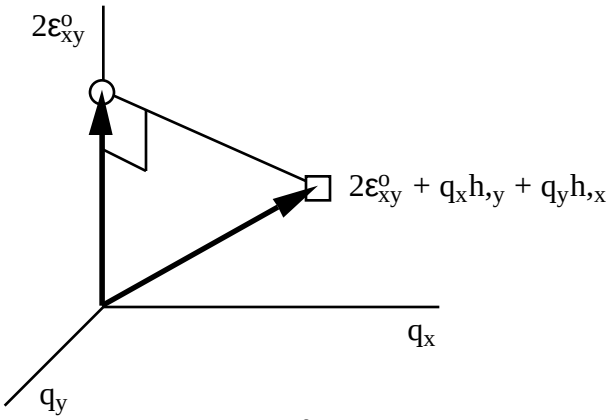

Figure 11. Projection of higher order shear terms in assumed strain elements

Table 2 lists the arbitrary constants for Eq. (8) for the assumed strain elements considered in this paper. Note that the fully integrated QUAD4 element can be obtained by stabilization with one point quadrature for linear materials. It can be shown that ASMD stabilization is identical to the mean dilatation approach of Nagtegaal et al. (1974) for linear materials. ASQBI and ASOI are identical to the mixed method QBI and OI stabilization of Belytschko and Bachrach (1986) for rectangular elements.

Table 2. Constants to define the assumed strain field

Element	e_1	e_2	e_3
QUAD4	1	0	1
ASMD	$\frac{1}{2}$	$-\frac{1}{2}$	1
ASQBI	1	$-\bar{\nu}$	0
ASOI	1	-1	0
ADS	$\frac{1}{2}$	$-\frac{1}{2}$	0

1.5.4 Stiffness Matrices for Assumed Strain Elements. The stiffness matrix for all of the assumed strain elements can be obtained by (16). If we take advantage of (1.4.16), then

$$\mathbf{K}_e = \mathbf{K}_e^{1\ pt} + \mathbf{K}_e^{stab} \tag{1.5.16}$$

where $\mathbf{K}_e^{1\ pt}$ is the stiffness obtained by one-point quadrature with the quadrature point $\xi=\eta=0$, and $\mathbf{K}_e^{stab}$ is the rank 2 stabilization stiffness, which is given by

$$\mathbf{K}_e^{stab} = 2\mu \begin{bmatrix} (c_1H_{xx}+c_2H_{yy})\gamma\gamma^t & c_3H_{xy}\gamma\gamma^t \\ c_3H_{xy}\gamma\gamma^t & (c_1H_{yy}+c_2H_{xx})\gamma\gamma^t \end{bmatrix} \tag{1.5.17}$$

where the constants c_1, c_2, and c_3 are given by Table 3. Constants are given not only for the elements listed in Table 2, but also for the ASSRI stabilization which behaves like the

SRI element of Hughes (1987) with elastic material. SRI stabilization cannot be derived by the assumed strain approach. It is obvious that the plane strain QUAD4 element will lock for nearly incompressible materials since c_1 and c_3 get very large. The projection to eliminate excessive shear stiffness corresponds to $c_2=0$. When both projections are made, then $c_1=-c_3$.

Table 3. Constants for assumed strain stabilization

Element	c_1	c_2	c_3
QUAD4 (plane strain)	$\frac{1-\nu}{1-2\nu}$	$1/2$	$\frac{1}{2(1-2\nu)}$
QUAD4 (plane stress)	$\frac{1}{1-\nu}$	$1/2$	$\frac{1+\nu}{2(1-\nu)}$
ASSRI	1	$1/2$	$1/2$
ASMD	$1/2$	$1/2$	0
ASQBI	$1+\bar{\nu}$	0	$-\bar{\nu}(1+\bar{\nu})$
ASOI	2	0	-2
ADS	$1/2$	0	$-1/2$

1.5.5 Nonlinear Hourglass Control. The nonlinear counterpart of the Simo-Hughes (1986) principle has been given by Fish and Belytschko (1988) as the following weak form:

$$0 = \delta\Pi = \int_{\Omega_e} \delta\mathring{\mathbf{e}}^t \mathbf{s}(\mathring{\mathbf{e}}, \mathbf{s}, \ldots) d\Omega + \delta \int_{\Omega_e} \mathbf{t}^t (D\mathbf{v} - \mathring{\mathbf{e}}) d\Omega - \delta \mathbf{v}^t \mathbf{f}^{ext} \qquad (1.5.18)$$

where $\mathring{\mathbf{e}}$ is the interpolated velocity strain (rate-of-deformation), $\mathbf{s}$ the Cauchy stress which is computed from the velocity strain and other state variables by the constitutive equation, $\mathbf{t}$ the interpolated Cauchy stress, and $D\mathbf{v}$ is the symmetric part of the velocity gradient; the latter would be equivalent to the rate-of-deformation in a standard displacement method, but in mixed methods, the velocity gradient is projected on a smaller space to avoid locking. Note that $\mathbf{s}$ was the symbol for the interpolated stress in Section 1.4, but has a new meaning here. The superposed circle on the symbol for the rate of deformation, $\mathring{\mathbf{e}}$ does not indicate a time derivative.

The velocity and strain-rate (rate-of-deformation) are interpolated by

$$\mathbf{v} = \sum_{I=1}^{n_N^e} \mathbf{N}_I(\xi,\eta)\mathbf{v}_I \equiv \mathbf{N}\mathbf{v} \qquad (1.5.19)$$

$$\mathring{\mathbf{e}} = \sum_{I=1}^{n_N^e} \bar{\mathbf{B}}_I(\xi,\eta)\mathbf{v}_I \equiv \bar{\mathbf{B}}\mathbf{v} \qquad (1.5.20)$$

where n_N^e is the number of nodes per element. In addition, we define the standard $\mathbf{B}$ matrix by

$$D\mathbf{v} = \sum_{I=1}^{n_N^e} D(\mathbf{N}_I \mathbf{v}_I) \equiv \mathbf{B}\mathbf{v} \tag{1.5.21}$$

Substituting Eqs. (20) into (18) and using the orthogonality condition for **t** as before gives

$$0 = \delta\Pi = \delta\mathbf{v}^T \int_\Omega \overline{\mathbf{B}}^T \mathbf{s}\, d\Omega - \delta\mathbf{v}^T \mathbf{f}^{ext} \tag{1.5.22}$$

Exploiting the arbitrariness of $\delta\mathbf{v}$ we obtain the discrete equilibrium equations

$$\mathbf{f}^{int} - \mathbf{f}^{ext} = 0 \tag{1.5.23}$$

$$\mathbf{f}^{int} = \int_\Omega \overline{\mathbf{B}}^t \mathbf{s}\, d\Omega \tag{1.5.24}$$

where the stress is given by some nonlinear constitutive equation

$$\mathbf{s} = \mathcal{S}(\mathring{\mathbf{e}}, \mathbf{s}, \ldots) = \mathcal{S}(\overline{\mathbf{B}}\mathbf{v}, \mathbf{s}, \ldots) \tag{1.5.25}$$

The above formulation is applicable to problems with both material and geometric nonlinearities. In applying the assumed strain stabilization procedure, it is convenient to use a corotational formulation as discussed in Section 1.4.7, where the Cauchy stresses and velocity strains are expressed in terms of a coordinate system $(\hat{x}, \hat{y})$ which rotates with the element. As with mixed method stabilization of Section 1.4, a corotational coordinate system also assure that the element is frame invariant.

The internal forces in a corotational formulation are given by

$$\hat{\mathbf{f}}^{int} = \int_\Omega \hat{\overline{\mathbf{B}}}^t \hat{\mathbf{s}}\, d\Omega \tag{1.5.26}$$

where the superposed tildes indicate quantities expressed in terms of the corotational coordinates. The counterpart of (20) is

$$\hat{\mathring{\mathbf{e}}} = \hat{\overline{\mathbf{B}}}\hat{\mathbf{v}} \tag{1.5.27}$$

and the rate form of the constitutive equation can be written

$$\hat{\dot{\mathbf{s}}} = \hat{\mathbf{C}}\hat{\mathring{\mathbf{e}}} \tag{1.5.28}$$

where $\hat{\mathbf{C}}$ is a matrix which depends on the stress and other state variables; for an incrementally isotropic hypoelastic material, $\hat{\mathbf{C}}$ is given by (1.4.40b).

The above form of a stress-strain law is objective (frame-invariant). The spin is then given by

$$\omega = \frac{1}{2}\left(\frac{\partial \hat{v}_y}{\partial \hat{x}} - \frac{\partial \hat{v}_x}{\partial \hat{y}} \right) \tag{1.5.29}$$

In developing the hourglass resistance based on physical parameters, two assumptions must be made:

1. the spin is constant within the element
2. the material response tensor $\hat{\mathbf{C}}$ is constant within the element.

The velocity for the 4 node quadrilateral is given by a form identical to (1.4.9b)

$$v_i = (\mathbf{s}^t + x\hat{\mathbf{b}}_x^t + y\hat{\mathbf{b}}_y^t + h\hat{\mathbf{g}}^t)\hat{\mathbf{v}}_i \tag{1.5.30}$$

The spin (29) is then given by

$$\omega = \tfrac{1}{2}(\hat{\mathbf{b}}_x^t \hat{\mathbf{v}}_y - \hat{\mathbf{b}}_y^t \hat{\mathbf{v}}_x + \dot{\hat{q}}_y \hat{h}_{,x} - \dot{\hat{q}}_x \hat{h}_{,y})) \tag{1.5.31}$$

$$\dot{\hat{q}}_x = \hat{\mathbf{g}}^t \hat{\mathbf{v}}_x \qquad \dot{\hat{q}}_y = \hat{\mathbf{g}}^t \hat{\mathbf{v}}_y \tag{1.5.32}$$

Because of the orthogonality property (1.4.16), the average spin is given by

$$\omega^o = \frac{1}{A}\int_{\Omega_e} \omega d\Omega = \tfrac{1}{2}(\hat{\mathbf{b}}_x^t \hat{\mathbf{v}}_y - \hat{\mathbf{b}}_y^t \hat{\mathbf{v}}_x) \tag{1.5.33}$$

This corresponds to the spin at the center of the element. It can be seen from (31) that the stronger the hourglass mode, the more assumption 1 is violated.

To illustrate the remainder of the development, the special case, $e_2=-e_1$, $e_3=0$ is considered. The corotational components of the velocity strain are then given by the counterpart of (8).

$$\begin{Bmatrix} \mathring{\hat{\varepsilon}}_x \\ \mathring{\hat{\varepsilon}}_y \\ 2\mathring{\hat{\varepsilon}}_{xy} \end{Bmatrix} = \begin{bmatrix} \hat{\mathbf{b}}_x^t + e_1 \hat{h}_{,x} \hat{\mathbf{g}}^t & -e_1 \hat{h}_{,y} \hat{\mathbf{g}}^t \\ -e_1 \hat{h}_{,x} \hat{\mathbf{g}}^t & \hat{\mathbf{b}}_y^t + e_1 \hat{h}_{,y} \hat{\mathbf{g}}^t \\ \hat{\mathbf{b}}_y^t & \hat{\mathbf{b}}_x^t \end{bmatrix} \begin{Bmatrix} \hat{v}_x \\ \hat{v}_y \end{Bmatrix} = \hat{\bar{\mathbf{B}}} \hat{\mathbf{v}} \tag{1.5.34}$$

For an anisotropic material, the stress rate is then given by

$$\dot{\hat{\mathbf{s}}} = \dot{\hat{\mathbf{s}}}^o + \dot{\hat{\mathbf{s}}}^1 = \hat{\mathbf{C}} \mathring{\hat{\mathbf{e}}}^o + e_1 \begin{Bmatrix} (\hat{C}_{11}-\hat{C}_{12})(\dot{\hat{q}}_x \hat{h}_{,x} - \dot{\hat{q}}_y \hat{h}_{,y}) \\ (\hat{C}_{22}-\hat{C}_{21})(\dot{\hat{q}}_y \hat{h}_{,y} - \dot{\hat{q}}_x \hat{h}_{,x}) \\ 0 \end{Bmatrix} \tag{1.5.35}$$

It can be seen that the corotational stress rate always has the same distribution within the element, so the stress also has the same form; at any point in time, $\hat{\mathbf{s}}^o$ is the constant part of the element stress field evaluated at the quadrature point, and $\hat{\mathbf{s}}^1$ is the nonconstant part.

Taking advantage of this form of the stress field, and inserting (34) and (35) into (26), and taking advantage of the orthogonality properties of $\hat{h}_x$ and $\hat{h}_y$ (1.4.16) and the fact that **C** is constant in the element, gives

$$\hat{\mathbf{f}}^{int} = A\hat{\mathbf{B}}^{ot}\hat{\mathbf{s}}^o + \hat{\mathbf{f}}^{stab} \tag{1.5.36}$$

where $\hat{\mathbf{f}}^{stab}$ are the hourglass (stabilization) nodal forces, which are given by

$$\hat{\mathbf{f}}^{stab} = \begin{Bmatrix} \hat{Q}_x \hat{\mathbf{g}} \\ \hat{Q}_y \hat{\mathbf{g}} \end{Bmatrix} \tag{1.5.37}$$

where

$$\begin{Bmatrix} \dot{\hat{Q}}_x \\ \dot{\hat{Q}}_y \end{Bmatrix} = e_1^2(\hat{C}_{11}-\hat{C}_{12}-\hat{C}_{21}+\hat{C}_{22}) \begin{Bmatrix} \hat{H}_{xx}\dot{\hat{q}}_x - \hat{H}_{xy}\dot{\hat{q}}_y \\ \hat{H}_{yy}\dot{\hat{q}}_y - \hat{H}_{xy}\dot{\hat{q}}_x \end{Bmatrix} \tag{1.5.38}$$

and $\hat{\mathbf{B}}^o$ is the constant part of $\hat{\mathbf{B}}$ which is given by

$$\hat{\mathbf{B}}^o = \begin{bmatrix} \hat{\mathbf{b}}_x^t & \mathbf{0} \\ \mathbf{0} & \hat{\mathbf{b}}_y^t \\ \hat{\mathbf{b}}_y^t & \hat{\mathbf{b}}_x^t \end{bmatrix} \tag{1.5.39a}$$

$$\hat{\mathbf{b}}_x^t = \frac{1}{2A}[\hat{y}_{24}, \hat{y}_{31}, \hat{y}_{42}, \hat{y}_{13}] \qquad \hat{\mathbf{b}}_y^t = \frac{1}{2A}[\hat{x}_{42}, \hat{x}_{13}, \hat{x}_{24}, \hat{x}_{31}] \tag{1.5.39b}$$

The nodal force vector is arranged by components:

$$\mathbf{f}^t = [\mathbf{f}_x^t, \mathbf{f}_y^t] \qquad \mathbf{f}_x^t = [f_{x1}, f_{x2}, f_{x3}, f_{x4}] \quad \mathbf{f}_y^t = [f_{y1}, f_{y2}, f_{y3}, f_{y4}] \tag{1.5.40}$$

For an isotropic material, $\dot{\hat{Q}}_x$ and $\dot{\hat{Q}}_y$ can be written in terms of the constants given in Table 3.

$$\begin{Bmatrix} \dot{\hat{Q}}_x \\ \dot{\hat{Q}}_y \end{Bmatrix} = 2\mu \begin{Bmatrix} (c_1\hat{H}_{xx}+c_2\hat{H}_{yy})\dot{\hat{q}}_x + c_3\hat{H}_{xy}\dot{\hat{q}}_y \\ (c_1\hat{H}_{yy}+c_2\hat{H}_{xx})\dot{\hat{q}}_y + c_3\hat{H}_{xy}\dot{\hat{q}}_x \end{Bmatrix} \tag{1.5.41}$$

As with mixed method stabilization, the shear modulus in a nonlinear isotropic process is given by (1.4.9a).

Table 4 is a flowchart outlining the procedure to evaluate nodal forces in an explicit program with time step Δt. Implementation in a static program simply requires the replacement of the products of rates and Δt by an increment in the corresponding integral; for example, $\Delta\hat{\mathbf{s}}$ replaces $\dot{\hat{\mathbf{s}}}\Delta t$.

Table 4. Element nodal force calculation

1. update corotational coordinate system
2. transform nodal velocities $\mathbf{v}$ and coordinates $\mathbf{x}$ to corotational coordinate system
3. compute strain-rate at quadrature the point by $\dot{\hat{\mathbf{e}}}=\hat{\mathbf{B}}^o\hat{\mathbf{v}}$ (Eq. (39) gives $\hat{\mathbf{B}}^o$)
4. compute stress-rate by constitutive law and update stress (note: $\dot{\hat{\mathbf{s}}}=\Delta\hat{\mathbf{s}}/\Delta t$)
5. compute generalized hourglass strain rates by Eq. (32)
6. compute the generalized hourglass stresses rates by (38) and update the generalized hourglass stresses
7. compute $\hat{\mathbf{f}}^{int}$ by Eqs. (36) and (37)
8. transform $\hat{\mathbf{f}}^{int}$ to global system and assemble

Remark 3.1 The stress rate in (36) corresponds to the Green-Naghdi rate if the corotational coordinate system is rotated by $\omega\Delta t$ in each time step.
Remark 3.2 If the Jaumann rate is used in conjunction with a fixed coordinate system, the stress field loses the form of (35) and other approximations are needed.
Remark 3.3 Because of the assumption of a constant spin and material response in the element, deviations from this assumption are directly proportional to the strength of the hourglass modes (see for example (31-33)); thus in h-adaptive methods, it is advantageous to refine by fission those elements which exhibit substantial hourglass energy, as advocated in Belytschko, Wong, and Plaskacz (1989).
Remark 3.4 If a Jaumann rate is used in a fixed coordinate system, the stress field does not maintain the distribution (35) This is one reason that the corotational form is preferred.

1.5.6 Assumed Strain with Multiple Integration Points. In the development above, stabilization forces are obtained for a reduced one-point integration element. One-point integration was chosen because it is usually advantageous to keep the number of stress evaluations to a minimum; however, there is a correlation between the number of integration points needed in a mesh and the nonlinearity of the stress field. An example of this is the dynamic cantilever beam of Section 1.6.3. For elastic material, a very accurate solution can be obtained with only one element through the depth of the beam, because the axial stress varies linearly through the depth. For elastic-plastic material, many elements are need through the depth to obtain a reasonably accurate solution, because the axial stress varies nonlinearly through the depth. The number of integration points can be increased by refining the mesh, or by increasing the number of integration points in each element. The latter method has the advantage of being able to increase the number of quadrature points without reducing the stable time step of an explicit method.

The assumed strain fields developed above can be used with any number of integration points without encountering locking since the strain fields have zero dilatational strain throughout the element domain for incompressible material. The element force vector for multi-point integration using an assumed strain field is analogous to (1.2.31b) and is given by

$$\hat{\mathbf{f}}_e^{int} = \sum_{\alpha=1}^{n_Q} w_\alpha J(\mathbf{x}_\alpha)\, \hat{\bar{\mathbf{B}}}^t(\mathbf{x}_\alpha)\hat{\mathbf{s}}(\mathbf{x}_\alpha) \tag{1.5.42}$$

where $\hat{\bar{\mathbf{B}}}(\mathbf{x}_\alpha)$ and $\hat{\mathbf{s}}(\mathbf{x}_\alpha)$ are the corotational counterparts of (8) and (25) evaluated at a quadrature point, $\mathbf{x}_\alpha$. Stabilization forces, may or may not be necessary with (42) depending on the location of the integration points.

The $\mathbf{g}$ terms in (8) assure rank sufficiency, as long as $\hat{h}_{,x}$ and $\hat{h}_{,y}$ are not too small. If we consider the rectangular element in Fig. 12 with a corotational coordinate system, the referential axes are parallel to the corotational axes, so

$$\hat{\xi}_{,x} = \frac{1}{a} \qquad \hat{\eta}_{,y} = \frac{1}{b} \qquad \hat{\eta}_{,x} = \hat{\xi}_{,y} = 0 \tag{1.5.43a}$$

$$\hat{h}_{,x} = \frac{1}{a}\eta \qquad \hat{h}_{,y} = \frac{1}{b}\xi \tag{1.5.43b}$$

From (43b), it is apparent that $\hat{h}_{,x} = 0$ along the η axis and $\hat{h}_{,y} = 0$ along the ξ axis. Therefore if the integration points are all located on one of the referential axes, stabilization forces will be needed in either the $\hat{x}$ or $\hat{y}$ directions to maintain rank sufficiency.

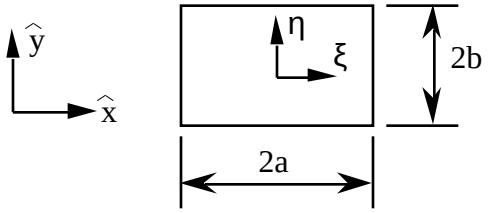

Figure 12. A rectangular element in the corotational coordinate system

Full 2x2 integration using Eq. (42) is rank sufficient, but nearly the same results are obtained with two integration points using a modified form of Eq. (42) given by

$$\hat{\mathbf{f}}_e^{int} = 2J(\mathbf{0}) \sum_{\alpha=1}^{2} \hat{\bar{\mathbf{B}}}^t(\mathbf{x}_\alpha)\hat{\mathbf{s}}(\mathbf{x}_\alpha) \tag{1.5.44}$$

In Eq. (44), $J(\mathbf{0})$ is the Jacobian evaluated at the origin of the referential coordinate system, and the two integration points are either $\mathbf{x}_1 = (-1/\sqrt{3}, -1/\sqrt{3})$, $\mathbf{x}_2 = (+1/\sqrt{3}, +1/\sqrt{3})$, or else $\mathbf{x}_1 = (-1/\sqrt{3}, +1/\sqrt{3})$, $\mathbf{x}_2 = (+1/\sqrt{3}, -1/\sqrt{3})$. The choice of the pair of integration points makes little difference in the solution. This 2-point integration scheme is similar to the IPS2 element reported in Liu et al. (1988). The formulation here differs by using an assumed strain field is used to improve accuracy. Using, the QBI strain field, a flexural-superconvergent 2-point element is obtained.

In Section 1.6.3, we observe that the ASQBI element with 1-point integration provides an accurate coarse mesh solution with elastic material; however, with elastic-plastic material, the coarse mesh solution is poor. We can therefore attribute the error in the elastic-plastic solution to an insufficient number of integration points. This large error is not surprising if we consider the nature of the solution. The plastic deformation of a beam in bending initiates at the top and bottom surfaces of a beam where the axial stress is greatest. With 1-point integration, the only stress evaluation is at the center of the element, so while the stress state at the integration point remains within the yield surface, the stress state may be outside the yield surface at other points in the element domain. For coarse mesh bending, the error is large, resulting in too little plastic deformation.

The 2-point integration scheme of Eq. (44), and 2x2 integration by Eq. (42) improve on 1-point integration by placing integration points nearer the edge of the element. In Section 1.6.3, the effect of multiple stress evaluations is demonstrated by the solution of an elastic-plastic cantilever beam. Results for the 2 and 4-point integration schemes are given in Tables 11a through 11d. Both use the QBI strain field, so the 2 point scheme is called ASQBI(2 pt), and 2x2 integration is called ASQBI(2x2). Both of these elements have flexural-superconvergence as does the 1-point element with ASQBI stabilization, so the elastic part of the solution is solved very accurately. Therefore, the difference in the solutions of these three elements with elastic-plastic material can be attributed to the effect of multiple stress evaluations on the nonlinear part of the solution.

1.6 Numerical Results

The numerical examples reported here include linear and nonlinear problems. The linear problems were studied to examine the convergence rate of various forms of these and competing elements. Table 5 gives a complete listing of the names associated with the elements tested in this section. All use 1-point integration in the nonlinear problems except for QUAD4, ASQBI(2pt), ASQBI(2x2).

Table 5. Names and descriptions of elements tested in this section

Name	Section	Description
QUAD4	1.2	Standard isoparametric element with full 2x2 integration.
FB (0.1)	1.3	Perturbation hourglass stabilization with the hourglass control factor, $\alpha_s = 0.1$. (Flanagan and Belytschko (1981))
FB (0.3)	1.3	Same as FB (0.1), except with $\alpha_s = 0.3$
OI	1.4	Mixed method Optimal Incompressible stabilization (Belytschko and Bachrach (1986)).
QBI	1.4	Mixed method Quintessential Bending and Incompressible stabilization (Belytschko and Bachrach).
ASOI	1.5	Assumed strain stabilization using the OI strain field
ASQBI	1.5	Assumed strain stabilization using the QBI strain filed
ADS	1.5	Assumed deviatoric strain stabilization
ASMD	1.5	Assumed strain stabilization using the strain field associated with the mean dilatation element (Nagtegaal et al.(1974)).
ASSRI	1.5	Assumed strain stabilization using the strain field associated with selective reduced integration (Hughes(1980))
ASQBI(2 pt)	1.5.6	The QBI strain field is used with two stress evaluations per element
ASQBI(2x2)	1.5.6	The QBI strain filed is used with four stress evaluations per element
Pian-Sumihara		The Pian-Sumihara (1984) hybrid element (the formulation does not appear in this paper)

1.6.1 Static Beam. A linear, elastic cantilever with a load at its end is shown in Fig. 13. M and P at the left end of the cantilever are reactions at the support.

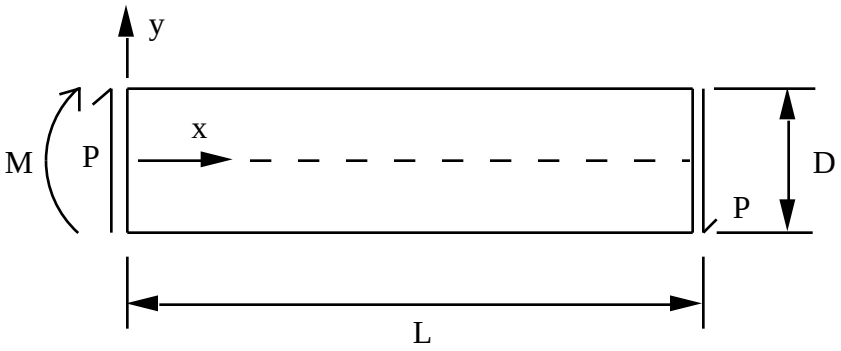

Figure 13. Static cantilever beam

This problem is identical to that used by Belytschko and Bachrach (1986). The analytical solution from Timoshenko and Goodier (1970) is

$$u_x(x,y) = \frac{-Py}{6\bar{E}I}[(6L-3x)x + (2+\bar{\nu})(y^2 - \tfrac{1}{4}D^2)] \tag{1.5.44a}$$

$$u_y(x,y) = \frac{P}{6\bar{E}I}[3\bar{\nu}y^2(L-x) + \tfrac{1}{4}(4+5\bar{\nu})D^2x + (3L-x)x^2] \tag{1.5.44b}$$

where $I = \frac{1}{12}D^3$

$$\bar{E} = \begin{cases} E & \text{for plane stress} \\ E/(1-\nu^2) & \text{for plane strain} \end{cases} \tag{1.5.45a}$$

$$\bar{\nu} = \begin{cases} \nu & \text{for plane stress} \\ \nu/(1-\nu) & \text{for plane strain} \end{cases} \tag{1.5.45b}$$

The displacements at the support end, x=0, $-\frac{1}{2}D \le y \le \frac{1}{2}D$ are nonzero except at the top, bottom, and midline (as shown in Fig. 14). Reaction forces are applied at the support based on the stresses corresponding to (1.5.46) at x=0, which are

$$\sigma_x = -\frac{Py}{I}(L-x) \tag{1.5.46a}$$

$$\sigma_y = 0. \tag{1.5.46b}$$

$$\tau_{xy} = \frac{P}{2I}(\tfrac{1}{4}D^2 - y^2) \tag{1.5.46c}$$

The distribution of applied load to the nodes at x=L is also obtained from the closed-form stress fields. The coarsest mesh used is shown in Fig. 14. This problem is symmetric, so only half the cantilever is modeled.

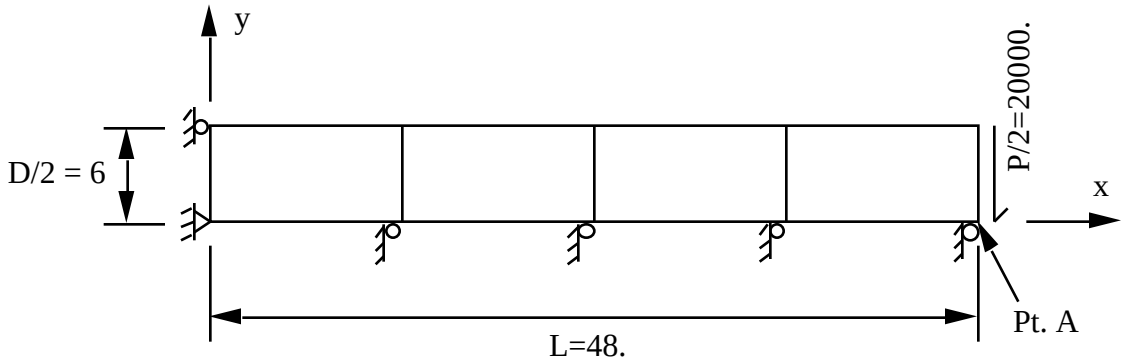

Figure 14. Coarse mesh of rectangular elements

All meshes use elements with an aspect ratio of 2. Only the top half of the cantilever is modeled since the problem is antisymmetric. The following isotropic elastic materials were used:

1. Plane stress, $\nu = 0.25$
2. Plane strain, $\nu = 0.4999$

The displacement and energy error norms are plotted in Figs. 15 and 16. for $\nu=0.25$, the rate of convergence of the displacement error norm is around 1.8 for all of the elements except for QBI, ASQBI and Pian-Sumihara which converge at a rate of 2. All have a rate of convergence of the energy error norm of 1. For $\nu=0.4999$, the rate of convergence of the displacement error norms is around 1.7 to 1.8 and the and rate of convergence of the energy error norms is 1.0 for all elements except QUAD4 which locks as expected and exhibits very slow convergence. For incompressible material, QBI and ASQBI are almost identical to OI and ASOI, whereas ASMD has less absolute accuracy. For rectangular elements and any linear material, OI and ASOI are identical. Likewise, the Pian and Sumihara (1984) element is identical to QBI and ASQBI.

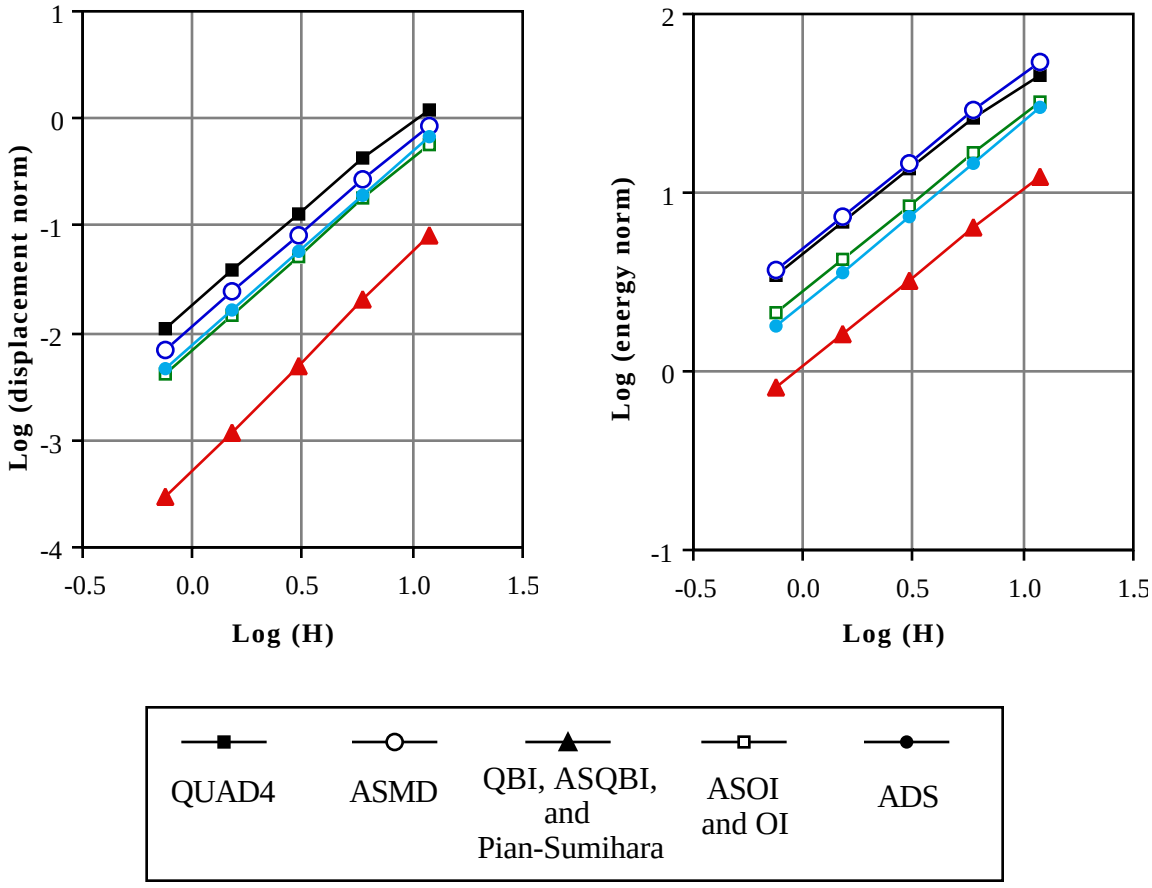

Figure 15. Convergence of displacement and energy error norms; ν=0.25, plane stress

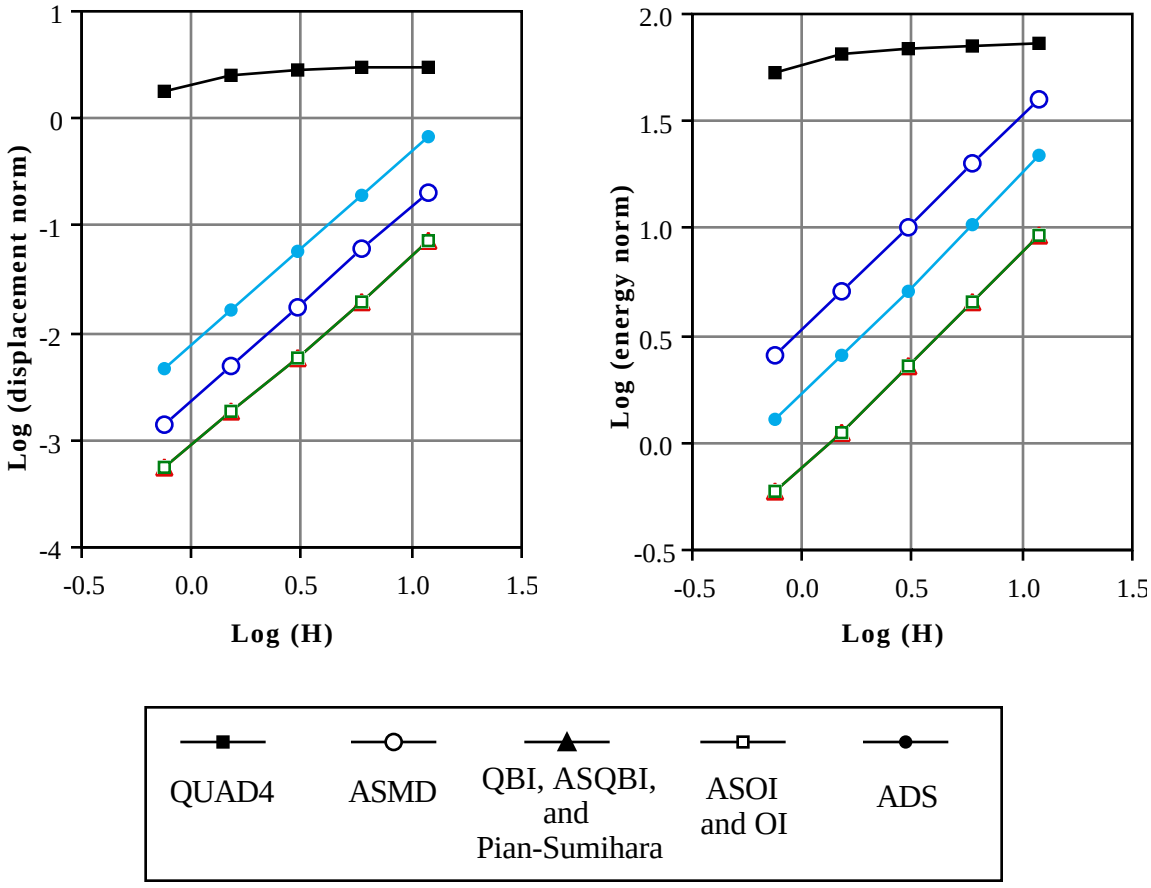

Figure 16. Convergence of displacement and energy error norms; ν=0.4999, plane strain

To assess the coarse mesh accuracy of the elements, the normalized end displacements (point A if Fig. 14) for the 1x4 element mesh are shown in Table 6. A coarse 1x4 element mesh of skewed elements was also run and the normalized end displacements (point A in Fig. 17) are shown in Table 7. Pian-Sumihara is slightly better than ASQBI for the skewed elements, but the difference is minor.

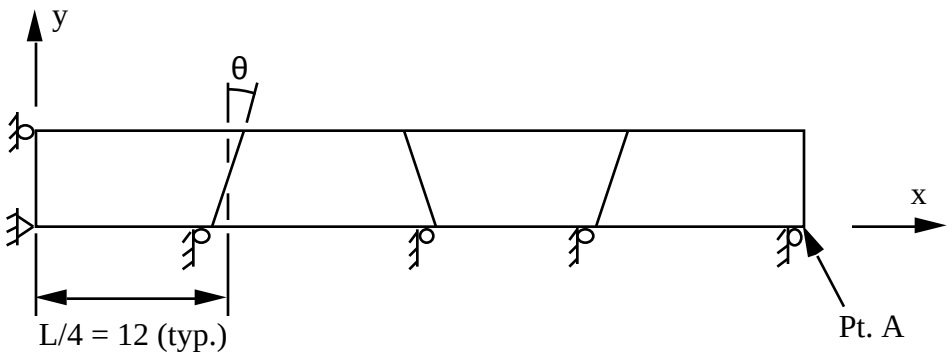

Figure 17. Skewed coarse mesh with $\theta = 9.462°$

Table 6. $d_{yFEM} / d_{yAnalytical}$ at point A of mesh in Fig. 14 (rectangular elements)

Material	QUAD4	ASMD	QBI, ASQBI, and Pian-Sumihara	OI and ASOI	ADS
1	0.708	0.797	0.986	0.862	1.155
2	0.061	0.935	0.982	0.982	1.205

Table 7. $d_{yFEM} / d_{yAnalytical}$ at point A of mesh in Fig. 17 (skewed elements)

Material	QUAD4	ASMD	ASQBI	Pian-Sumihara	ASOI	ADS
1	0.689	0.776	0.948	0.955	0.834	1.112
2	0.061	0.915	0.957	0.960	0.957	1.170

1.6.2 Circular Hole in Plate. This problem was considered to evaluate the performance of these elements in a different setting. A plate with a hole, solved by R. C. J. Howland (1930) is shown in Fig. 18. The solution is in the form of an infinite series and gives the stress field around the circular hole in the center of an axially loaded plane stress plate of finite width and of infinite length. The series converges only within a circular region around the hole. The diameter of this circular area is equal to the plate width. The displacement field is not given so convergence of the displacement norm could not be checked.

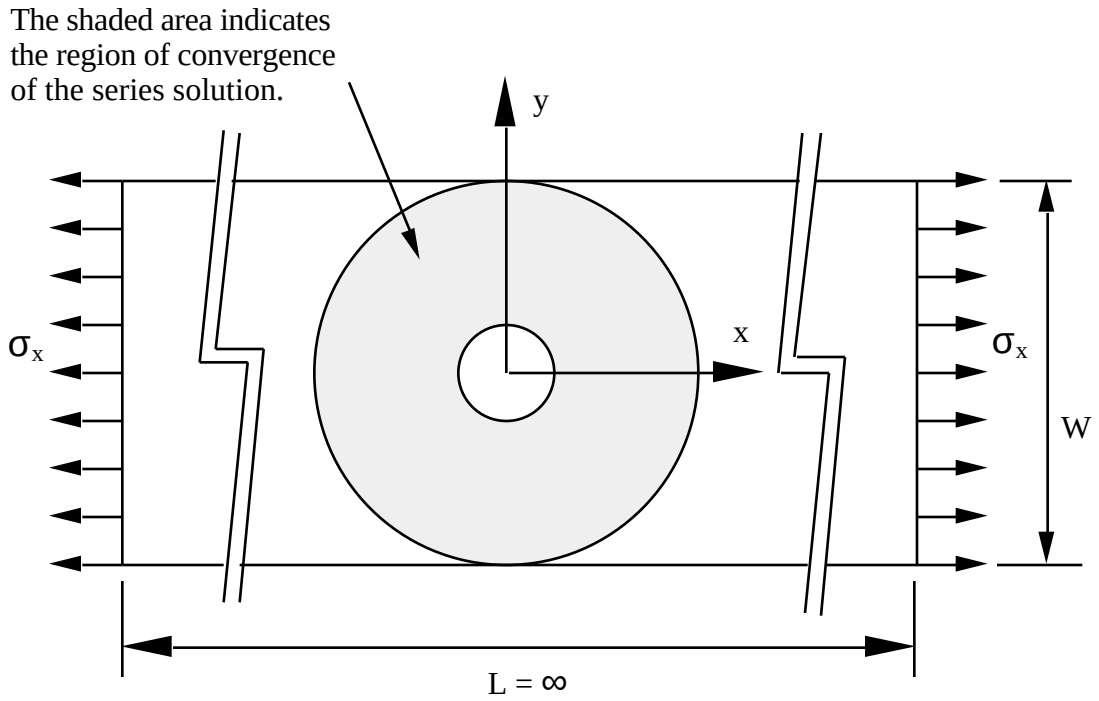

Figure 18. Plate of finite width with a circular hole

For the finite element meshes, the plate length was taken to be twice the plate width. The nodes at which the load is applied are outside the region in which the analytical solution converges, so the analytical solution could not be used to determine the load distribution on the end of the plate. The nodal forces were therefore calculated by assuming the analytical stress field at infinity, which is uniaxial. The error due to the finite length was checked by running meshes with lengths of 2 and 5 times the plate width. The difference between these solutions was found to be negligible. Four different meshes were used which are summarized in Table 8. Fig. 19 shows the dimensions and boundary conditions of the finite element model, and Fig. 20 shows the discretization for mesh 3 with 320 elements. The problem is symmetric, so only one fourth of the plate was modeled.

Table 8. Meshes used for Howland plate with hole problem

Mesh number	Number of elements	
	Total in mesh	In portion of mesh used to calculate the energy norm
1	20	12
2	80	48
3	320	192
4	1280	768

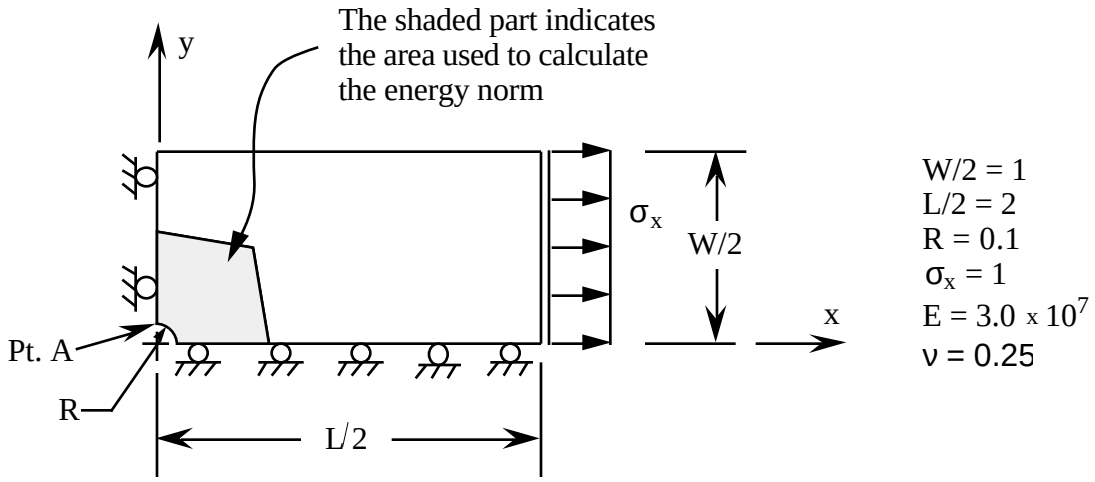

Figure 19. Finite element model of plate with a circular hole

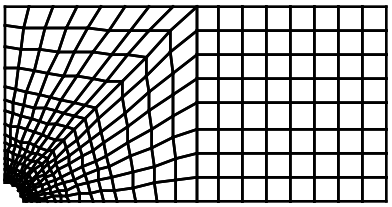

Figure 20. Mesh 3 discretization

The circular hole is approximated by elements with straight edges, so the hole is actually a polygon. As the number of elements is increased, the shape and area of the hole changes slightly.

Because the analytical solution only converges in a region around the hole, a subset of the total number of elements in the mesh was used to calculate the energy norm. This area, shaded in Fig. 19, was held constant as the mesh was refined, except for the change in the area of the hole.

Table 9 shows the calculated stress concentration factor at point A on Fig. 19 normalized by the analytical solution. At point A, $\sigma_x = 3.0361$ according to the analytical solution. The stress concentration factor depends on both the constant and non-constant part of the stress field. None of the elements can represent exactly the nonlinear stress field in the area near the hole; however, some are better than others. The ASQBI element was shown earlier to represent the pure bending mode of deformation better than the ASOI elements. This ability seems to help also in the calculation of the stress concentration factor at point A. For the ASMD and ADS elements ($e_1 = 1/2$), the non-constant part of the strain is only half the magnitude that of the ASOI element ($e_1 = 1$), so the stress concentration factor is lower.

Table 9. $\sigma_{xFEM}/\sigma_{xAnalytical}$ at point A in Fig. 19

Mesh	QUAD4	ASMD	ASQBI	Pian-S	ASOI	ADS
1	0.888	0.721	0.885	0.778	0.772	0.733
2	0.973	0.838	0.961	0.914	0.874	0.831
3	0.994	0.900	0.988	0.971	0.926	0.902
4	1.000	0.946	0.997	0.993	0.963	0.947

Table 10 shows the normalized x-component of stress at the center of the element that is nearest to the point of maximum stress (point A on Fig. 19). This value is independent of the nonconstant part of the stress field, so there is much less variation between the elements. The coordinates of the element center change as the mesh is refined, so the analytical stress used to normalize the solutions is included in Table 10.

Table 10. $\sigma_{xFEM}/\sigma_{xAnalytical}$ at the center of the element nearest point A in Fig. 19

Mesh	Analytical stress	QUAD4	ASMD	ASQBI	Pian-S	ASOI	ADS
1	1.671	1.000	1.031	1.009	1.056	.982	1.040
2	2.089	1.010	1.029	1.013	1.038	.995	1.031
3	2.462	1.005	1.015	1.006	1.016	.997	1.012
4	2.717	1.002	1.007	1.003	1.007	.999	1.008

Fig. 21 shows the convergence of the error in the energy norm. All elements were found to have convergence rates ranging from 0.92 to 0.98. Theoretically, the convergence rate of the energy norm should go to 1 as the element size $H \rightarrow 0$. Note that the differences in the errors for the various elements are much smaller than in the beam problem. This is expected, since the nonconstant mode of deformation in this problem is much less significant than it is in bending.

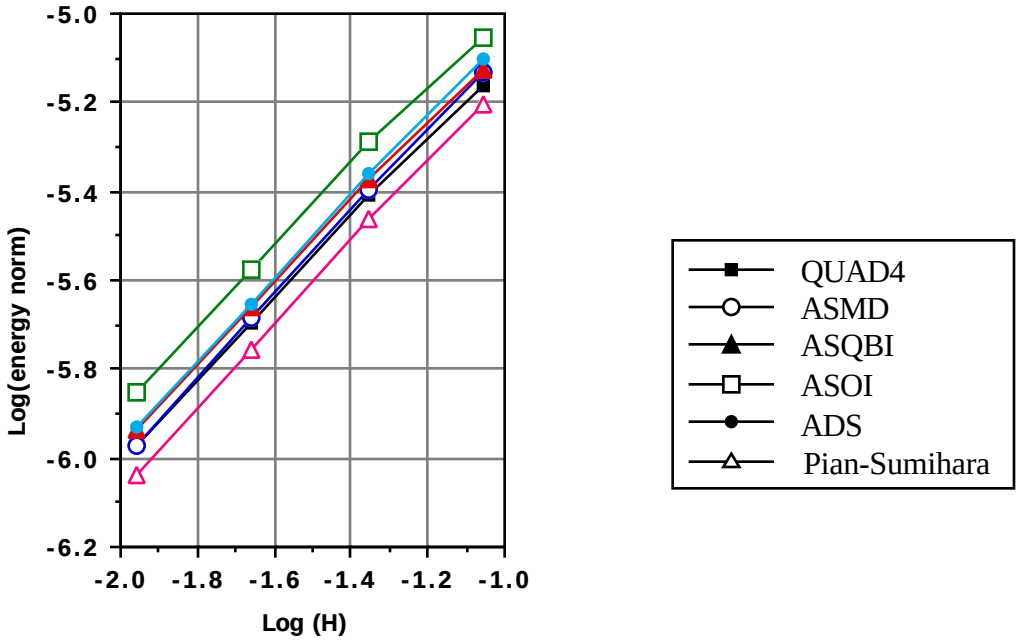

Figure 21. Convergence of the error in the energy norm

1.6.3 Dynamic Cantilever The rate form of stabilization was implemented in the two dimensional version of WHAMS (Belytschko and Mullen (1978)). An end loaded cantilever was modeled with both elastic and elastic-plastic materials as shown in Fig. 22. A similar problem is reported in Liu et al. (1988). Two plane-strain isotropic materials were used with ν=0.25, E=1x10^4, and the material density, ρ=1.

(1) elastic

(2) elastic-plastic with 1 plastic segment (σ_y = 300; E_t=0.01E)

where σ_y is the yield stress, E_t is the plastic hardening modulus; a Mises yield surface and isotropic hardening were used.

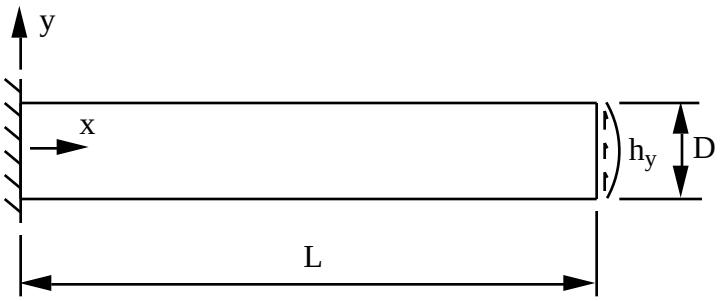

L = 25
D = 4
$h_y = 15\left(1-y^2/4\right)$ applied as a step function at time T=0.
d = 1 (out of plane thickness)

Figure 22. Dynamic cantilever beam

Ten meshes were considered. Six of them are composed of rectangular elements, while the other four are skewed. A coarse mesh called the 1x6 mesh has one element through the beam depth and 6 along the length. The aspect ratio of these elements is nearly 1. Meshes of 2x12, 4x24, and 8x48 elements are generated from the 1x6 mesh by

subsequent divisions of each element into 4 smaller elements. Two meshes of elongated elements, 2x6(E) and 4x12(E) were made of elements with aspect ratios of slightly more than 2. Finally four meshes are made up of skewed elements. Two of them, 2x12(S) and 4x24(S), are formed by skewing 2x12 and 4x24; the other two, 2x6(ES) and 4x12(ES), are formed by skewing 2x6(E) and 4x12(E). Figures (23a-g) show 7 of the meshes.

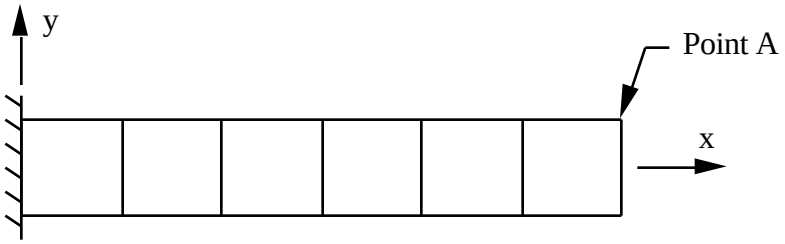

Figure 23a. 1x6 mesh

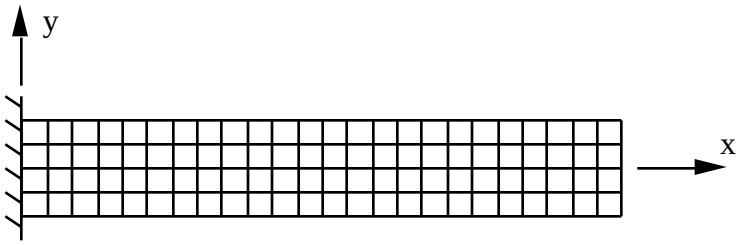

Figure 23b. 4x24 mesh

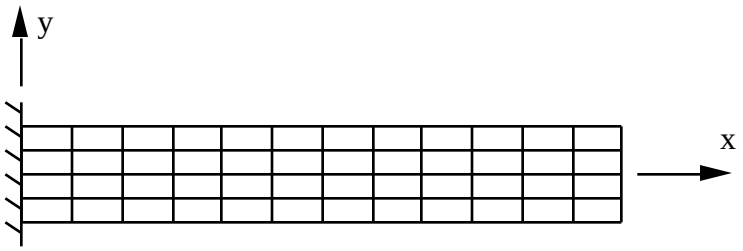

Figure 23c. 4x12(E) mesh

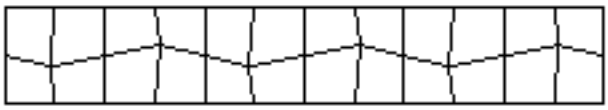

Figure 23d. 2x12(S) mesh

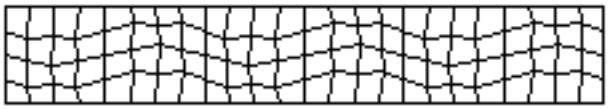

Figure 23e. 4x24(S) mesh

Figure 23f. 2x6(ES) mesh

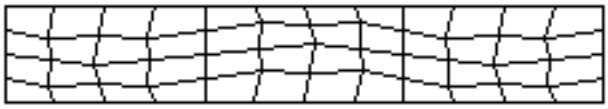

Figure 23g. 4x12(ES) mesh

The problem involves very large displacement (of order one third the length of the beam). No analytical solutions is available, so the results are not normalized; however, a more refined meshes of 32x192 elements were run using a 1-point element with ADS stabilization in an attempt to find a converged solution. The end displacements at point A in Fig. 23(a) are listed in Tables 11a through 11d. Fig. 24 is a typical deformed mesh which shows the large strain and rotation that occurs. Figs. (25a-e) are time plots of the y-component of the displacement at the end of the cantilever. The first three demonstrate the convergence of the elastic-plastic solution with mesh refinement for ASQBI and ADS stabilization, and for the ASQBI(2pt) element. These plots also include the elastic solution and the 32x192 element elastic-plastic solution using ADS stabilization for comparison. The last two time plots each show a solution of a single mesh by ADS and ASQBI stabilization, and the ASQBI (2pt) and ASQBI (2x2) elements. These plots also include the elastic and 32x192 element solution for comparison.

Table 12 lists the percentage of the strain energy that is associated with the hourglass mode of deformation at the time of maximum end displacement for some of the runs with elastic-plastic material. As expected, nearly all the strain energy is in the hourglass mode for the coarse (1x6) mesh. As the mesh is refined, the percentage of strain energy in the hourglass mode decreases rapidly, so the importance of accurately calculating the hourglass strains also decreases.

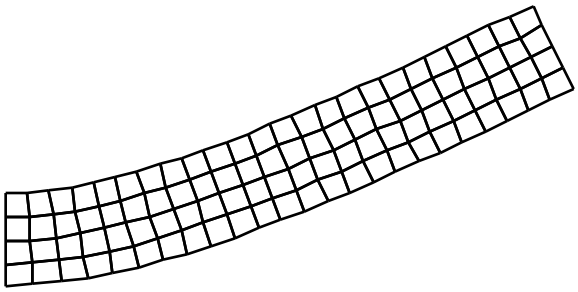

Figure 24. Deformed 4x24 mesh showing maximum end displacement (elastic-plastic material)

With all of the elements, the onset of plastic deformation is significantly retarded when the mesh is too coarse. This is most evident in the QBI elements which are flexural-superconvergent for elastic material. The ADS or FB (0.1) elastic solutions are too flexible, which tends to mask the error caused by too few integration points. The only sure way to reduce the error in solutions that involve elastic-plastic bending is to increase the number of integration points. This can be accomplished by mesh refinement or by using multiple integration points in each element, as with the 2 point and 2x2 integration. If the mesh is refined, not only are the number of integration points increased, but the amount of strain energy that is in the hourglass mode of deformation decreases (Table 12), so the accuracy of the coarse mesh solution becomes less relevant. When multiple integration points are used, the energy in the nonconstant modes of deformation remains significant, so an accurate strain field such as ASQBI is more important.

With two and four stress evaluations per element respectively, ASQBI(2 pt) and ASQBI(2x2) give similar results to ADS stabilization when the mesh is refined to 8x48 elements. These elements are also have flexural-superconvergence with elastic material. The improvement over a 1-point element with ASQBI stabilization is similar to the improvement obtained by one level of mesh refinement, and it is significantly less computationally expensive. Each level of mesh refinement slows the run by a factor of 8, while additional integration points slow it by less than 2 for ASQBI (2 pt) and 4 for ASQBI (2x2). For this problem with a fairly simple constitutive relationship, the additional c.p.u time needed for an a second stress evaluation is largely offset by the elimination of the need for stabilization, so ASQBI(2 pt) solutions are less than 10% slower than the stabilized 1-point element.

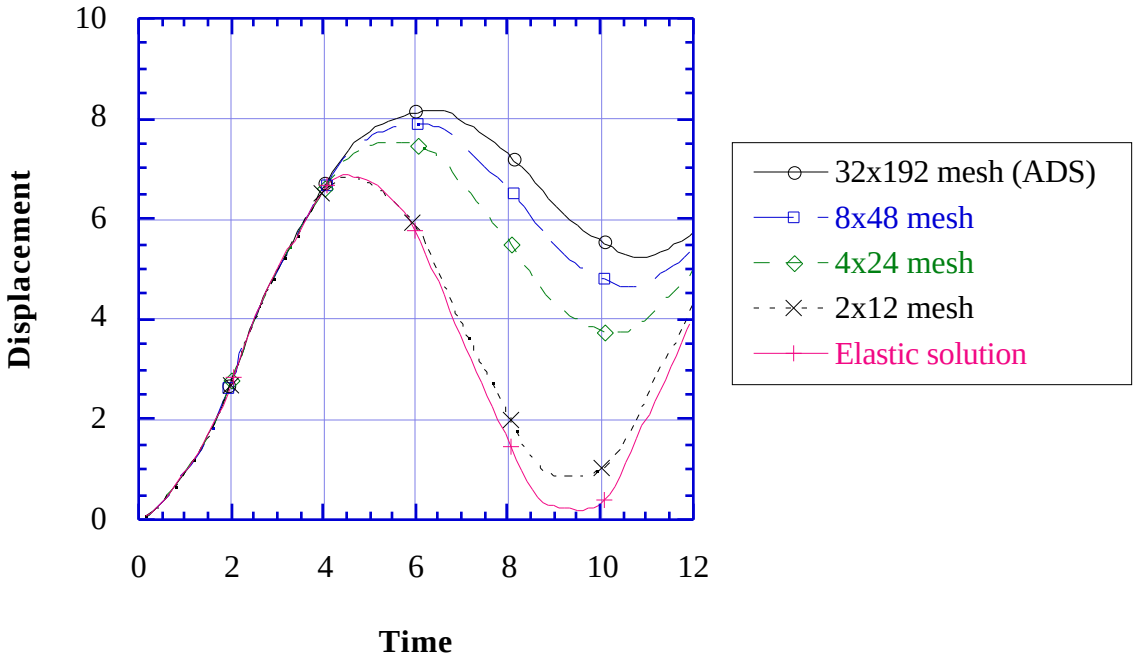

Figure 25a. End displacement of elastic-plastic cantilever; ASQBI stabilization

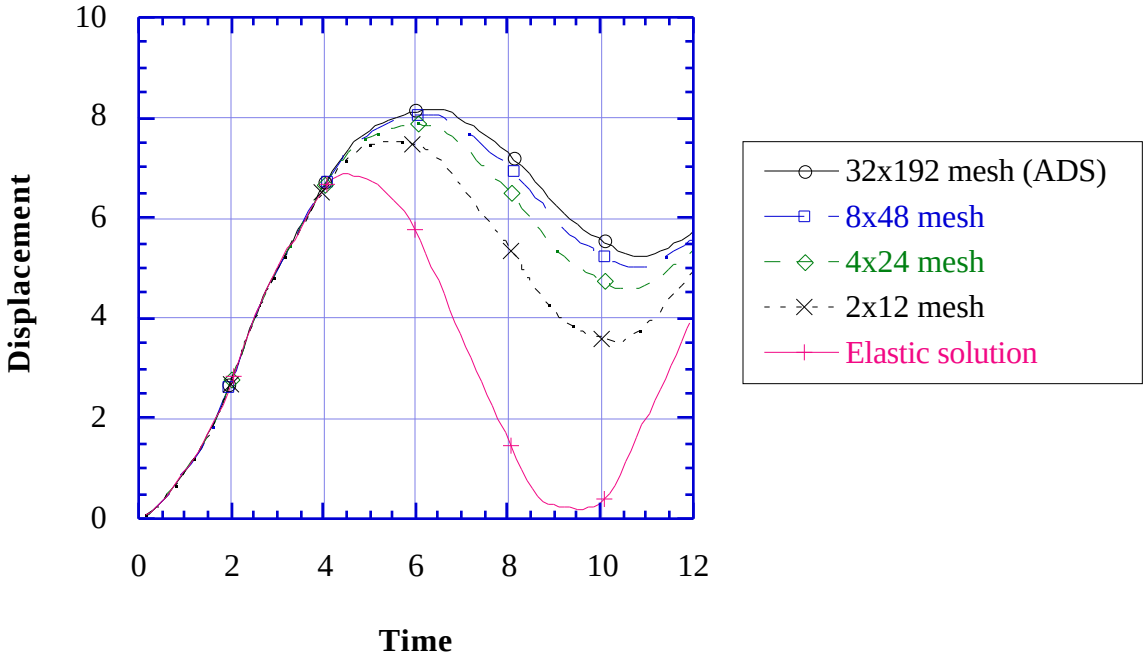

Figure 25b. End displacement of elastic-plastic cantilever; ASQBI (2 pt) element

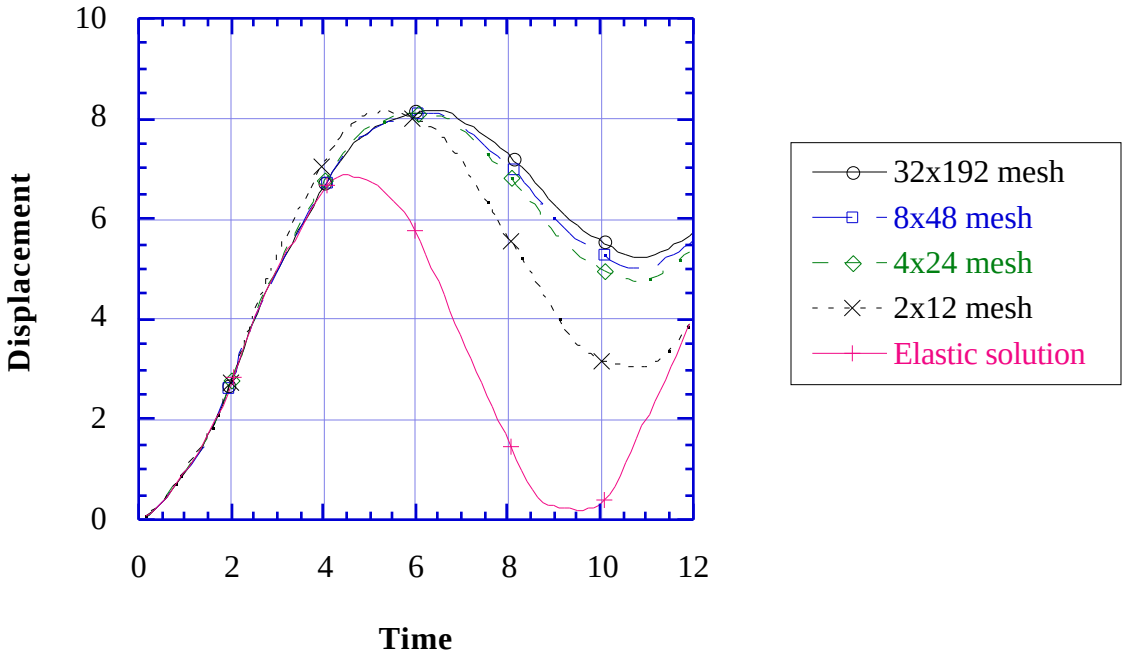

Figure 25c. End displacement for elastic-plastic cantilever; ADS stabilization

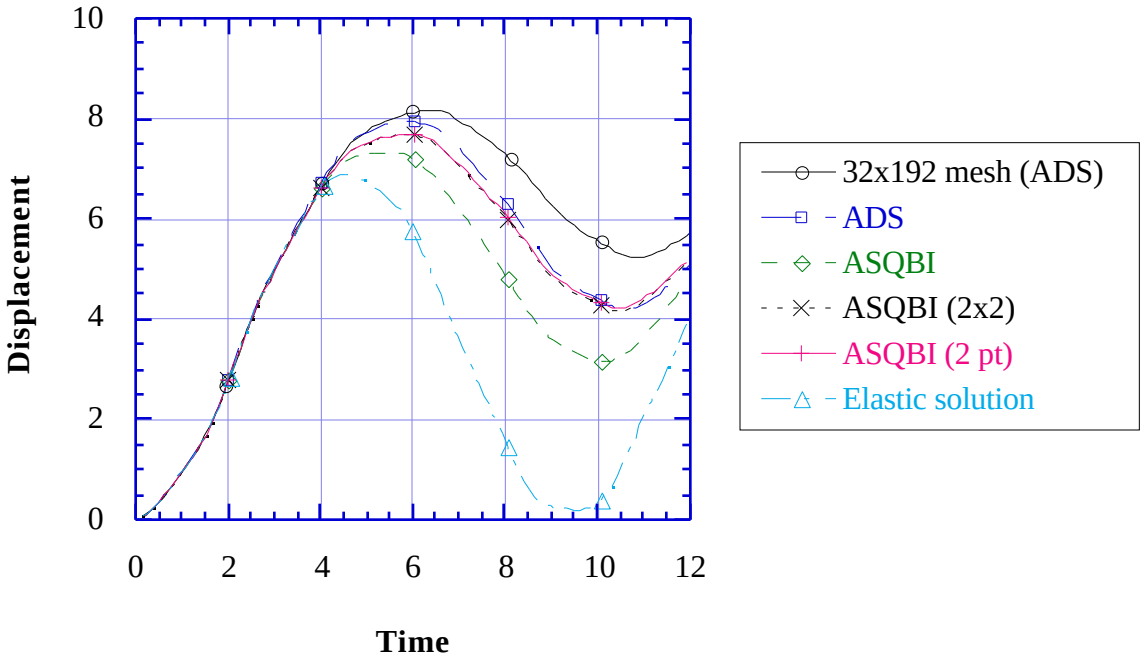

Figure 25d. End displacement for 4x12(E) mesh (elastic-plastic)

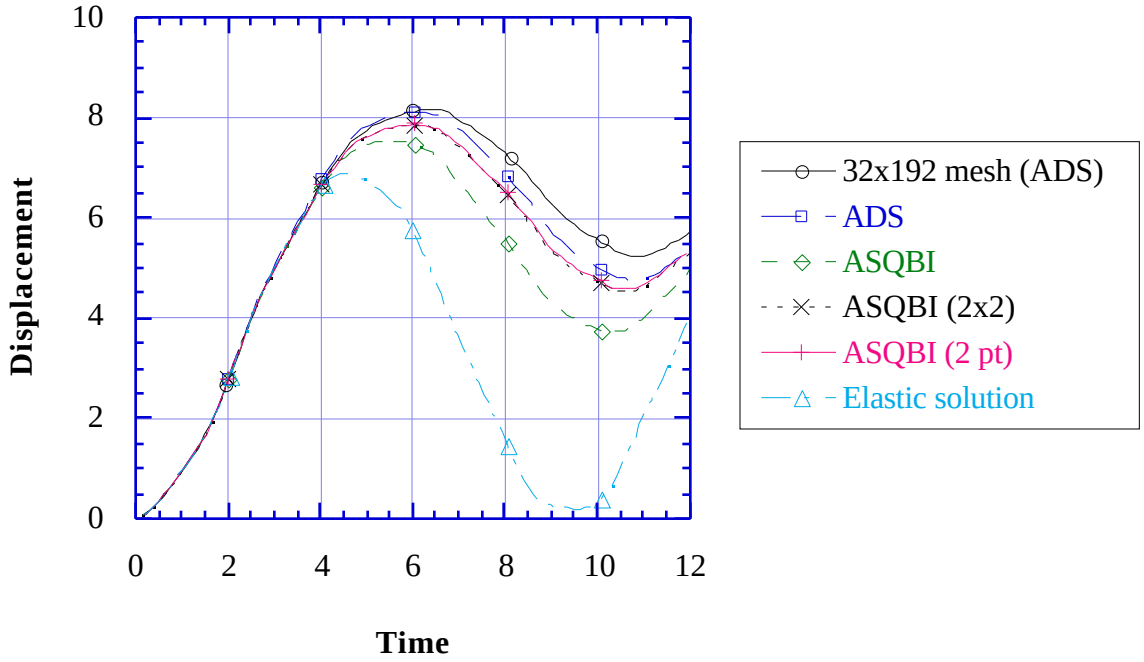

Figure 25e. End displacement for 4x24 element mesh (elastic-plastic)

Table 11a. Maximum end displacement of elastic cantilever

Element	1x6	2x12	4x24	8x48	2x6(E)	4x12(E)
QUAD4 (2x2)	4.69	6.14	6.68	6.84	4.92	6.25
FB (0.1)	15.9	8.12	7.17	6.97	7.22	6.97
FB (0.3)	7.68	7.04	6.93	6.91	5.35	6.432
OI	4.78	6.17	6.70	6.85	6.11	6.66
ASOI	4.78	6.17	6.70	6.85	6.11	6.66
QBI	6.89	6.86	6.88	6.90	6.79	6.86
ASQBI	6.89	6.86	6.88	6.90	6.79	6.86
ASQBI (2x2)	6.89	6.86	6.88	6.90	6.79	6.86
ASQBI (2 pt)	6.89	6.85	6.88	6.90	6.78	6.85
ADS	14.2	7.95	7.13	6.96	7.87	7.11
ASMD	8.49	7.20	6.97	6.92	5.59	6.51
ASSRI	6.05	6.63	6.82	6.88	5.23	6.38

Table 11b. Maximum end displacement of elastic cantilever for the meshes of skewed elements; solutions are normalized by the solutions from Table 11a for the corresponding meshes of rectangular elements

Element	2x12(S)	4x24(S)	2x6(ES)	4x12(ES)
QUAD4 (2X2)	0.99	0.99	0.97	0.98
FB (0.1)	1.01	1.00	0.99	0.99
FB (0.3)	0.99	1.00	0.99	0.99
OI	0.99	0.99	0.97	0.98
ASOI	1.00	1.00	0.98	0.99
QBI	0.99	0.99	0.97	0.98
ASQBI	0.99	0.99	0.97	0.98
ASQBI (2x2)	0.99	0.99	0.97	0.98
ASQBI (2 pt)	0.99	0.99	0.96	0.98
ADS	1.00	1.00	0.99	0.99
ASMD	1.00	1.00	0.99	0.99
ASSRI	0.99	1.00	0.99	0.99

Table 11c. Maximum end displacement and residual displacement (in parentheses) of elastic-plastic cantilever; a solution by ADS stabilization with a 32x192 element mesh gives a maximum displacement of 8.17, and a residual displacement of 5.24.

Element	1x6	2x12	4x24	8x48	2x6(E)	4x12(E)
QUAD4 (2x2)	4.69 (0.11)	6.30 (1.79)	7.31 (3.69)	7.85 (4.65)	4.94 (0.78)	6.61 (2.76)
FB (0.1)	15.9 (0.00)	8.39 (3.40)	8.18 (4.88)	8.14 (5.04)	7.22 (1.05)	7.67 (3.82)
FB (0.3)	7.68 (0.12)	7.05 (1.15)	7.59 (3.74)	7.92 (4.67)	5.35 (0.13)	6.69 (2.41)
OI	4.78 (0.05)	6.17 (0.20)	7.17 (3.13)	7.76 (4.41)	6.11 (0.16)	7.00 (2.63)
ASOI	4.78 (0.05)	6.17 (0.20)	7.17 (3.16)	7.76 (4.40)	6.11 (0.16)	7.00 (2.63)
QBI	6.89 (0.11)	6.86 (0.89)	7.53 (3.69)	7.90 (4.64)	6.79 (0.34)	7.34 (3.16)
ASQBI	6.89 (0.11)	6.86 (0.87)	7.54 (3.72)	7.90 (4.64)	6.79 (0.34)	7.34 (3.16)
ASQBI (2x2)	6.98 (1.79)	7.52 (3.62)	7.86 (4.53)	8.05 (4.99)	7.27 (3.10)	7.68 (4.17)
ASQBI (2 pt)	7.00 (1.75)	7.53 (3.54)	7.87 (4.57)	8.06 (5.01)	7.28 (3.14)	7.69 (4.21)
ADS	14.2 (0.00)	8.15 (3.03)	8.12 (4.77)	8.12 (5.01)	7.94 (1.89)	7.94 (4.19)
ASMD	8.49 (0.13)	7.21 (1.38)	7.73 (4.05)	7.97 (4.77)	5.59 (0.14)	6.83 (2.58)
ASSRI	6.05 (0.09)	6.63 (0.60)	7.42 (3.54)	7.86 (4.57)	5.23 (0.12)	6.60 (2.21)

Table 11d. Maximum end displacement and residual end displacement (in parentheses) of elastic-plastic cantilever for the meshes of skewed elements; solutions are normalized by the solutions from Table 11c for the corresponding meshes of rectangular elements

Element	2x12(S)	4x24(S)	2x6(ES)	4x12(ES)
QUAD4 (2x2)	1.08	0.98	0.98	0.98
	(0.62)	(0.96)	(1.21)	(1.02)
	1.04	0.99	1.02	0.99
FB (0.1)	(1.18)	(0.99)	(1.78)	(1.05)
	1.00	0.99	0.99	0.99
FB (0.3)	(1.23)	(0.99)	(2.28)	(1.04)
	0.99	0.98	0.97	0.98
OI	(2.40)	(0.98)	(3.61)	(0.97)
	1.00	0.99	0.98	0.98
ASOI	(2.45)	(0.98)	(3.66)	(0.96)
	0.99	0.98	0.98	0.98
QBI	(1.21)	(0.99)	(3.07)	(0.97)
	0.99	0.98	0.98	0.98
ASQBI	(1.28)	(0.97)	(3.12)	(0.98)
	0.98	0.98	0.98	0.98
ASQBI (2x2)	(0.96)	(0.97)	(1.03)	(0.98)
	0.98	0.98	0.96	0.98
ASQBI (2 pt)	(1.03)	(0.97)	(0.96)	(0.97)
	1.03	0.99	1.03	0.99
ADS	(1.17)	(0.99)	(1.48)	(1.02)
	1.00	0.98	0.99	0.99
ASMD	(1.30)	(0.98)	(3.15)	(1.04)
	0.99	0.98	0.99	0.99
ASSRI	(1.62)	(0.97)	(1.53)	(1.05)

Table 12. Hourglass energy in the mesh when the end displacements maximum (normalized by total strain energy)

Mesh	FB (0.1)	ASOI	ASQBI	ADS	ASMD
1x6	0.982	0.975	0.981	0.988	0.984
2x12	0.108	0.327	0.247	0.124	0.207
4x24	0.033	0.110	0.079	0.036	0.065
8x48	0.011	0.035	0.026	0.012	0.021

REMARK 6.1 The QUAD4 element performs no better that the stabilized one-point elements

REMARK 6.2 The value of α_s has a significant effect on the solution of bending problems using perturbation stabilization (FB) when the mesh is coarse

REMARK 6.3 Those elements that do not project out the nonconstant part of the strain field, (QUAD4, ASMD, and ASSRI) stiffen significantly more than the others when the elements are elongated as with 2x6(E) and 4x12(E) solutions. Perturbation stabilization (FB) is also sensitive since it is not responsive to the element aspect ratio.

REMARK 6.4 Skewing the elements seems to have little effect on any of the elements. This may be a little deceptive since this is a large deformation problem. The elements of all the meshes skew noticeably when deformed (Fig. 24) so the initially skewed meshes only introduce additional skewing. The elastic-plastic 2x6(ES) results are of dubious significance, since the elastic-plastic 2x6(E) solutions are quite inaccurate.
REMARK 6.5 Another set of runs was made using an elastic-plastic material with a larger plastic modulus (E_t=0.1E). The results were similar to those for (E_t=0.01E) and are not shown.

1.6.4 Cylindrical Stress Wave. A two dimensional domain with a circular hole at its center was modeled with 4876 quadrilateral elements as shown in Figs 26 and 27. A compressive load with the time history shown in Fig. 28 was applied to the hole and the dynamic evolution was obtained until t=0.09. The domain is large enough to prevent the wave from reflecting from the outer boundary. Elastic and elastic plastic materials were used.

To provide an estimate of the error in the 2D results, solutions were obtained for the same domain and load history using 3600 axisymmetric, 1D elements. The radial strain ε_{rr} for the elastic and elastic-plastic solutions at t=0.09 is shown in Fig. 29. The normalized L_2 norms of the error in displacements at time t=0.09 along the radial lines at θ=0 and $\theta=\pi/4$ are given in Tables 13a and 13b. All of the elements have the same magnitude of error.

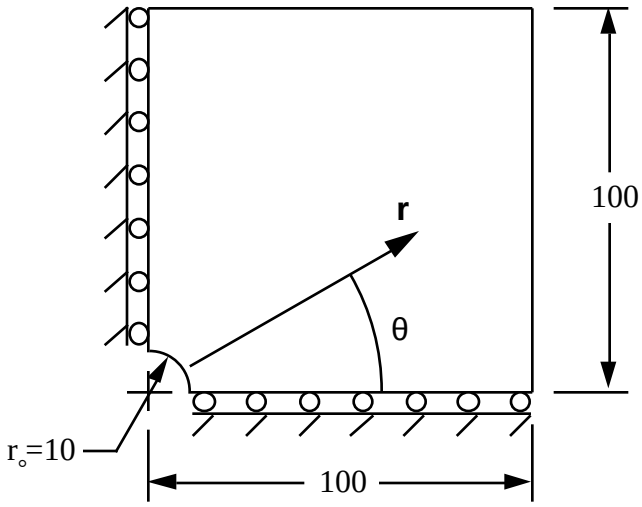

Elastic material:
Young's modulus, E=1x 10^6
Density, ρ=1.0

Elastic-plastic material:
Young's modulus, E=1x 10^6
Density, ρ=1.0
Yield stress, σ_y=1x10^4
Plastic modulus, E_t = E/ 16

Figure 26. 4 node quad. mesh dimensions

Figure 27. Discretization of infinite domain with a hole

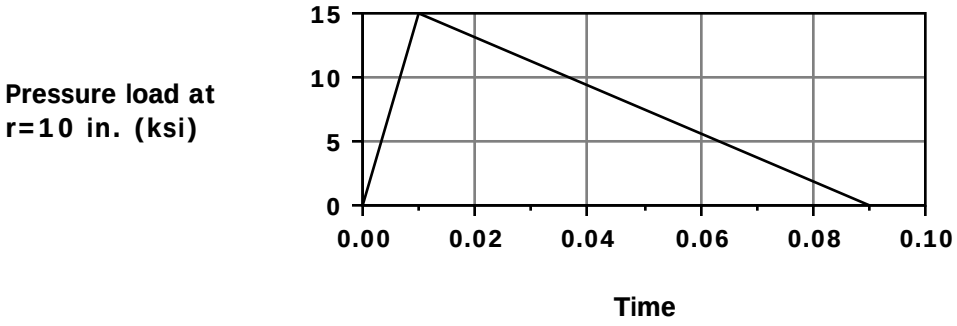

Figure 28. Load history

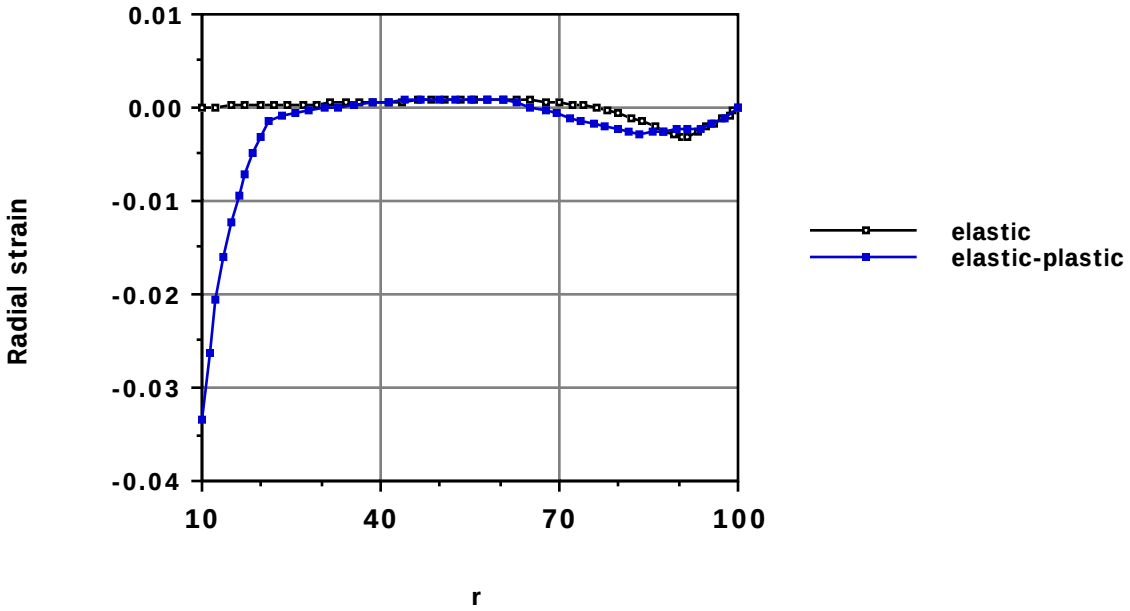

Figure 29. Radial strain at t=0.09

Table 13a. Normalized L_2 norms of error in displacements for material 1 (elastic)

θ	QUAD4	FB (0.1)	ASMD	ASQBI	ASOI	ADS
0°	.014	.014	.014	.014	.013	.014
45°	.022	.022	.019	.019	.012	.021

Table 13b. Normalized L_2 norms of error in displacements for material 2 (elastic-plastic)

θ	QUAD4	FB (0.1)	ASMD	ASQBI	ASOI	ADS
0°	.0063	.0063	.0061	.0061	.0061	.0063
45°	.0069	.0069	.0086	.0088	.0073	.0088

1.6.5 Static Cantilever. The solutions to the test problems of Sections 1.6.1 and 1.6.2 were obtained using a local coordinate formulation of the stabilization matrix: Likewise, the solutions to the test problems of Sections 1.6.3 and 1.6.4 were obtained using a corotational coordinate formulation. The need for these local and corotational formulations to obtain a frame invariant element is discussed in Section 1.4.6. The following solutions to a static cantilever demonstrate this need.

A cantilever with a shear load at its end was solved by two versions of the linear static finite element code using QBI stabilization. One version had a local coordinate formulation, and the other did not. These are called the "local" and "global" formulations respectively. A total of seven solutions were obtained with three meshes as shown in Figs. (30a-c). Each was solved with the longitudinal axis of the undeformed beam aligned with the global x axis, and also with the beam initially rotated before applying the load.

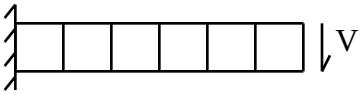

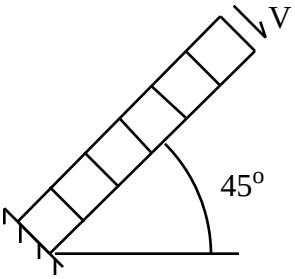

Figure 30a. 1x6 element mesh

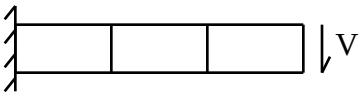

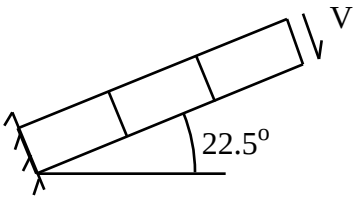

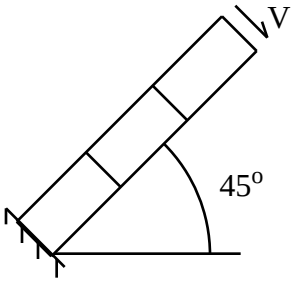

Figure 30b. 1x3 element mesh

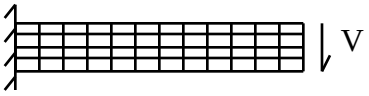

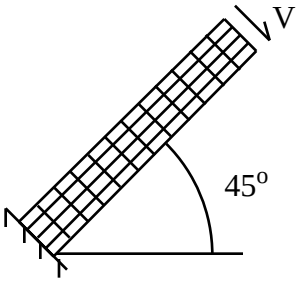

Figure 30c. 4x12 element mesh

Table 14 lists the end displacement in the direction of the load for the seven solutions normalized by the solutions of the unrotated meshes. Therefore, these numbers do not demonstrate absolute accuracy, but the variation in the element stiffness that occurs with rigid body rotation. The results show that the global formulation is sensitive to rigid body rotation when the elements are elongated and the mesh is coarse. When the aspect ratio 1, both formulations are frame invariant. Also, when the mesh is refined, the lack of frame invariance is less noticeable. The local formulation is always frame invariant.

Table 14. End displacements in the direction of the applied load normalized by the 0° solution

Mesh	Initial rotation (degrees)	Global	Local
1x6	0	1.00	1.00
	45	1.00	1.00
1x3	0	1.00	1.00
	22.5	0.71	1.00
	45	0.49	1.00
4x12	0	1.00	1.00
	45	0.94	1.00

1.7 Discussion and Conclusions

The bilinear quadrilateral element is a good choice for solving two dimensional continuum problems with explicit methods, because the mass matrix can be lumped with little loss of accuracy. There are two major benefits to 1-point integration with the quadrilateral. The first is the elimination of volumetric locking which plagues the fully integrated element. The second is a reduction in the computational effort for such elements. A drawback of 1-point integration is that spurious modes will occur if they are not stabilized. We have examined some ways of stabilizing the spurious modes in this chapter.

With all the methods considered, the stabilization forces are proportional to a **g** vector which is orthogonal to the constant strain modes of deformation, so the stabilization forces do not contribute to the constant strain field. Therefore, all have a quadratic rate of convergence in the displacement error norm. The major difference between the methods is in the way the evaluation of the magnitude of the stabilization forces.

Flanagan and Belytschko (1981) were motivated by the desire to keep the stabilization forces small so they would not interfere with the solution or cause locking. This stabilization has the drawback of requiring a user specified parameter. A bending dominated solution can depend significantly on the value of the parameter which is undesirable.

Using mixed methods, Belytschko and Bachrach (1986) chose strain and stress fields that more closely resemble the strength of materials solution of elastic deformation. Thus, they were able to use stabilization to improve to the accuracy of bending solutions. They obtain very accurate bending solutions with very few elements with elastic material. Mixed method stabilization is dependent only on material properties and element geometry; no user specified parameter is needed.

The Simo-Hughes form of the assumed strain method has also been used to develop stabilization. The assumed strain fields are motivated in the same way as the mixed method elements, and the resulting stabilization is nearly the same. As with mixed method stabilization, no user specified parameter is needed. The most noticeable difference between assumed strain and mixed-method stabilization is in the derivation. Assumed strain stabilization is much simpler. As we will see in Chapter 2, a major benefit of this simplification is the ability to derive stabilization for the three dimensional 8 node hexahedral element.

The relative performance of these elements is problem dependent; thus QBI and ASQBI are very accurate for elastic bending, but they do not perform as well for elastic-

plastic problems. Although it is not so accurate for elastic bending, ADS may be a good choice since it is very simple to implement and does not require knowledge of the material's Poisson's ratio. It's performance should exceed that of the other 1-point elements for elastic-plastic solutions. If the Poisson's ratio of the material is known, the ASQBI strain field with 2-point integration will provide both accurate elastic bending and reasonable elastic-plastic performance at a slightly higher cost.

CHAPTER 9
SHELLS AND STRUCTURES

DRAFT

by Ted Belytschko
Northwestern University

9.1 INTRODUCTION

Shell elements and other structural elements are invaluable in the modeling of many engineered components and natural structures. Thin shells appear in many products, such as the sheet metal in an automobile, the fuselage, wings and rudder of an airplane, the housings of products such as cell phones, washing machines, computers. Modeling these items with continuum elements would require a huge number of elements and lead to extremely expensive computations. As we have seen in Chapter 8, modeling a beam with hexahedral continuum elements requires a minimum of about 5 elements through the thickness. Thus even a low order shell element can replace 5 or more continuum elements, which improves computational efficiency immensely. Furthermore, modeling thin structures with continuum elements often leads to elements with high aspect ratios, which degrades the conditioning of the equations and the accuracy of the solution. In explicit methods, continuum element models of shells are restricited to very small stable time steps. Thus it can be seen that structural elements are very useful in engineering analysis.

Structural elements are classified as:
1. beams, in which the motion is described as the function of a single independent variable;
2. shells, where the motion is described as a function of two independent variables;
3. plates, which are flat shells.

Plates are usually modeled by shell elements in computer software. Since they are just flat shells, we will not consider plate elements separately. Beams on the other hand, require some additional theoretical considerations and provide simple models for learning the fundamentals of structural elements, so we will devote a substantial part of this chapter to beams.

There are two approaches to developing shell finite elements:
1. develop the formulation for shell elements by using classical strain-displacement and momentum (or equilibrium) equations for shells to develop a weak form of the momentum (or equilibrium) equations;
2. develop the element directly from a continuum element by imposing the structural assumptions on the weak form or on the discrete equation; this is called the continuum based (CB) approach.

The first approach is difficult, particularly for nonlinear shells, since the governing equations for nonlinear shells are very complex and awkward to deal with; they are usually formulated in terms of curvilinear components of tensors, and features such as

variations in thickness, junctions and stiffeners are generally difficult to incorporate. There is still disagreement as to what are the best nonlinear classical shell equations. The CB (continuum-based) approach, on the other hand, is straightforward, yields excellent results, is applicable to arbitrarily llarge deformations and is widely used in commercial software and research. Therefore we will concentrate on the CB methodology. It is also called the degenerated continuum approach; we prefer the appellation continuum based, coined by Stanley(1985), since there is nothing degenerate about it.

The CB methodology is not only simpler, but intellectually a more appealing appraoch than classical shell theories for developing shell elements. In most plate and shell theories, the equilibrium or momentum equations are developed by imposing the structural assumptions on the motion and then using the principle of virtual work to develop the partial differential equations for momentum balance or equilibrium. The development of a weak form for these shell momentum equations than entails going back to the principle of virtual work. In the CB approach, the kinematic assumptions are either

1. imposed on the motion in the weak form of the momentum equations for continua or
2. imposed directly on the discrete equations for continua.

Thus the CB shell formulation is a more straightforward way of obtaining the discrete equations for shells and structures.

We will begin with a description of beams in two dimensions. This will provide a setting for clearly and easily describing the assumptions of various structural theories and comparing them with CB beam elements. In contrast to the schema in previous Chapters, we will begin with the implementation, for in the implementation the simplicity and key features of the CB approach are most transparent. We will then examine CB beam elements more thoroughly from a theoretical viewpoint.

The CB approach is subsequently employed for the development of shell elements. Again, we begin with the implementation, illustrating how many of the techniques developed for continuum elements in the previous chapters can be applied directly to shells. The CB shell theory developed here is a synthesis of various approaches reported in the literature but also incorporates a new treatment of changes in thickness due to large deformations and conservation of matter. As part of this treatment, the methodologies for describing large rotations in three dimensions are described.

Two of the pitfalls of CB shell elements are then examined: shear and membrane locking. These phenomena are examined in the context of beams but the insights gained are applicable to shell elements. Methods for circumventing these difficulties by means of assumed strain fields are described and examples of elements which alleviate shear and membrane locking are given.

We conclude with a description of 4-node quadrilateral shell elements that evaluate the internal nodal forces with one stack of quadrature points, often called one-point quadrature elements. These elements are widely used in explicit methods and large scale analysis. Several elements of this genre are reviewed and compared and the techniques for consistently controlling the hourglass modes which result from the underintegration are described.

9.2 TWO DIMENSIONAL BEAMS

9.2.1. Governing Equations and Assumptions. In this Section the CB theory is developed for beams. In addition, we develop a beam element based on classical beam theory.

The governing equations for structures are identical to those for continua:

1. conservation of matter
2. conservation of linear and angular momentum
3. conservation of energy
4. constitutive equations
5. strain-displacement equations

The key feature which distinguishes structures from continua is that assumptions are made about the motion and the state of stress in the element. In other words, the motion is constrained so that it satisfies certain hypothesis which are based on experimental observations on the motion of thin structures and shells. The assumptions on the motion are called kinematic assumptions, the assumptions on the stress field are called kinetic assumptions.

The major kinematic assumption concerns the motion of the normals to the midline (also called reference line) of the beam. In linear structural theory, the midline is usually chosen to be the loci of the centroids of the cross-sections of the beam. However, the selection of a reference line has no effect on the response of a CB element: any line which corresponds approximately to the shape of the beam may be chosen as the reference line. The choice of reference line only effects the values of the resultant moments; the stresses and the overall response are not affected. We will use the terms reference line and midline interchangeably, noting that even when the term midline is used the precise location of this line relative to the cross-section of the beam is irrelevant in a CB element. The plane defined by the normals to the midline is called the normal plane. Fig. 9.2 shows the reference line and normal plane for a beam.

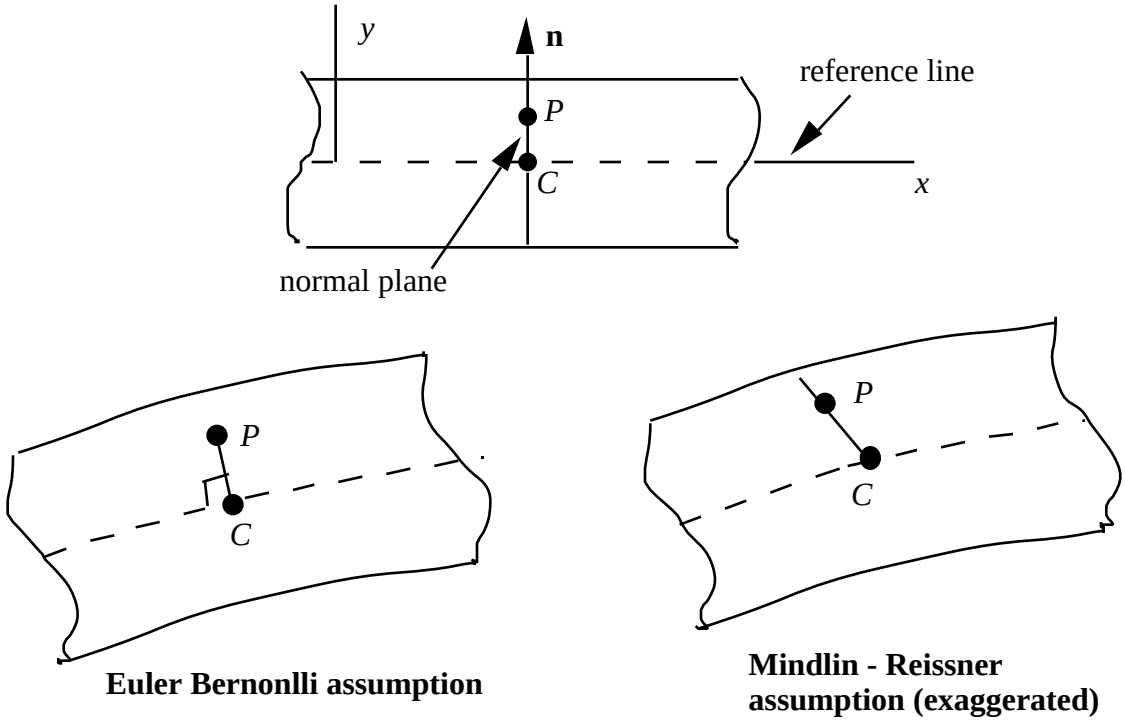

Figure 9.2. Motion in an Euler-Bernoulli bean and a shear (Mindlin-Reissner) beam; in the Euler-Bernoulli beam, the normal plane remains plane and normal, whereas in the shear beam the normal plane remains plane but not normal.

Two types of beam theory are widely used: Euler-Bernoulli beam theory and shear beam theory. The kinematic assumptions of these theories are:

1. in Euler-Bernoulli beam theory the planes normal to the midline are assumed to remain plane and normal; this is also called engineering beam theory while the corresponding shell theory is called the Kirchhoff-Love shell theory;
2. in shear beam theory the planes normal to the midline are assumed to remain plane; this is also called Timoshenko beam theory, and the corresponding shell theory is called the Mindlin-Reissner shell theory;

Euler-Bernoulli beams, as we shall see shortly, do not admit any transverse shear, whereas beams governed by the second assumption do admit transverse shear. The motions of an Euler-Bernoulli beam are a subset of the motions encompassed by shear beam theory.

For the purpose of describing the consequences of these kinematic assumptions, we consider a straight beam along the *x*-axis in two dimensions as shown in Fig. 9.2. Let the *x*-axis coincide with the midline and the *y*-axis with the normal to the midline. We consider only the instant when the beam is in the configuration described, so the following equations do not constitute a nonlinear theory. We will first express the kinematic assumptions mathematically and develop the rate-of-deformation tensor; the rate-of-deformation will have the same properties as the linear strain since the equations for the rate-of-deformation can be obtained by replacing velocities by displacements in the linear strain equations. The aim of the following is to illustrate the consequences of the kinematic assumptions on the strain field, not to construct a theory which is worth implementing.

9.9.2. Timoshenko (Shear Beam) Theory. We first describe the shear beam theory. This beam thoery is usually called Timoshenko beam theory. The major assumption of this theory is that the normal planes are assumed to remain plane, i.e. flat. Thus the planes normal to the midline rotate as rigid bodies. Consider the motion of a point *P* whose orthogonal projection on the midline is point *C*. If the normal plane rotates as a rigid body, the velocity of point *P* relative to the velocity of point *C* is given by

$$\mathbf{v}_{CP} = \omega \times \mathbf{r} \tag{9.2.1a}$$

where ω is the angular velocity of the plane and $\mathbf{r}$ is the vector from *C* to *P*. In two dimensions, the only nonzero component of the angular velocity vector of the plane is the z-component, so $\omega = \dot{\theta}\mathbf{e}_z \equiv \omega \mathbf{e}_z$. Since $\mathbf{r} = y\mathbf{e}_y$, the relative velocity is

$$\mathbf{v}_{CP} = \omega \times \mathbf{r} = -y\omega \mathbf{e}_x . \tag{9.2.1b}$$

The velocity of any point along the midline is only a function of *x*, so

$$\mathbf{v}^M(x) = v_x^M(x)\mathbf{e}_x + v_y^M(x)\mathbf{e}_y \tag{9.2.1c}$$

The velocity of any point in the beam is then given by adding the relative velocity (9.2.1b) to the midline velocity

$$\mathbf{v} = \mathbf{v}^M(x) + \omega \times \mathbf{r} = \mathbf{v}^M(x) - y\omega \mathbf{e}_x \tag{9.2.1d}$$

The x-component of the total velocity is obtained form the above:

$$v_x(x, y) = v_x^M(x) - y\omega(x) \tag{9.2.2}$$

where $v_x^M(x)$ is the x-component of the velocity of the midline and $\dot{\theta}(x)$ is the angular velocity of the normal to the midline. The y-component of the velocity is equivalent to that of the midline through the depth of the beam, so

$$v_y(x, y) = v_y^M(x) \tag{9.2.3}$$

Applying the definition of the rate-of-deformation $D_{ij} = sym(v_{i,j})$, see Section 3.3.2, shows that the rate-of-deformation for a Timoshenko beam is given by

$$D_{xx} = v_{x,x}^M - y\omega_{,x}, \; D_{yy} = 0, \; D_{xy} = \frac{1}{2}\left(v_{y,x}^M - \omega\right) \tag{9.2.4a-c}$$

It can be seen that the only nonzero components of the rate-of-deformation are the axial component, D_{xx}, and the shear component, D_{xy}, the latter is called the *transverse shear*.

It can be seen immediately from (9.2.2) and (9.2.3) that the dependent variables $v_i^M(x)$ and $\theta(x)$ need only be C^0 for the rate-of-deformation to be finite throughout the beam. Thus the standard isoparametric shape functions can be used in the construction of shear beam finite elements. Theories for which the interpolants need only be C^0 are often called C^0 structural theories.

9.2.3. Euler-Bernoulli Theory. In the Euler-Bernoulli or engineering beam theories, the kinematic assumption is that the normal remains normal and straight. Therefore the angular velocity of the normal is given by the rate of change of the slope of the midline

$$\omega = v_{y,x}^M$$

By examining Eq. (9.2.4c) it can be seen that the above is equivalent to requiring the shear rate-of-deformation D_{xy} to vanish, which implies that the angle between the normal and the midline does not change, i.e. the normal remains normal. The axial displacement is then given by

$$v_x(x, y) = v_x^M(x) - yv_{y,x}^M(x)$$

The rate-of-deformation in Euler-Bernoulli (or engineering) beam theory is given by

$$D_{xx} = v^M_{x,x} - yv^M_{y,xx}, \;\; D_{yy} = 0, \;\; D_{xy} = 0$$

Two features are noteworthy in the above:

1. the transverse shear vanishes;
2. the second derivative of the velocity appears in the expression for the rate-of-deformation tensor, so the velocity field must be C^1 for the rate-of-deformation to be well-defined.

Whereas in the Timoshenko beam, two dependent variables are needed, only a single dependent variable is needed for the Euler-Bernoulli beam. Similar reductions in the number of unknowns take place in the corresponding shell theories: a Kirchhoff-Love shell theory only has three dependent variables, whereas a Mindlin-Reissner theory has five dependent variables (six are often used in practice; this is discussed in Section 9.4. This type of structural theory is often called a C^1 theory because of the need for C^1 approximations. The requirement for C^1 approximations is the biggest disadvantage of Euler-Bernoulli and Kirchhoff-Love theories, since C^1 approximations are difficult to construct in more than one dimension. For this reason, C^1 structural theories are seldom used in software except for beams. Beam elements are often based on Euler-Bernoulli theory because C^1 interpolants are easily constructed in one dimension. Theories which require C^1 interpolants are often called C^1 structural theories.

Transverse shear is of significance only in thick beams. However Timoshenko beams Mindlin-Reissner shells are frequently used even when transverse shear is not physically important. For thin beams, the transverse shears in Timoshenko beams also go to zero in well-behaved elements. Thuis the normality hypothesis, which implies that transverse shear vanishes for thim beams, is a trend also observed in numerical solutions and analytic solutions as the thickness decreases.

9.2.4. Discrete Kirchhoff and Mindlin-Reissner Theories. A third approach, which is only used in numerical method, are the discrete theories. In the discrete Kirchhoff theory, the Kirchhoff-Love assumption is only applied discretely, i.e. at a finite number of points, usually the quadrature points. Transverse shear then develops at other points in the element but it is ignored. Similarly, discrete Mindlin-Reissner elements can be formulated by imposing these assumptions discretely.

9.3 DEGENERATED CONTINUUM BEAM.

In the following, the continuum based (CB) formulation for a beam in two dimensions is developed. In this development we will impose the kinematic assumptions on the discrete equations, i.e. the continuum finite element will be modified so that it behaves like a shell. In the next Section, we will develop the CB beam by imposing the kinematic assumption on the motion before writing the weak form. These two sections will introduce many of the concepts and techniques which are used in the development of CB shell elements. The elements to be developed are applicable to nonlinear materials and geometrical nonlinearities. Either an updated Lagrangian or a total Lagrangian approach can be used. However, Lagrangian elements are almost always used for shells and structures because they consist of closely separated surfaces which are difficult to treat with Eulerian elements.

We will not go through the steps followed in Chapters 2, 4, and 7 of developing a weak form for the momentum equation and showing the equivalence to the strong form, since we will use the discrete equations for continua. The essence of the CB beam

approach is to impose the kinematic assumption on the motion of continuum elements. We will first describe how this is done directly on the discrete continuum equations.

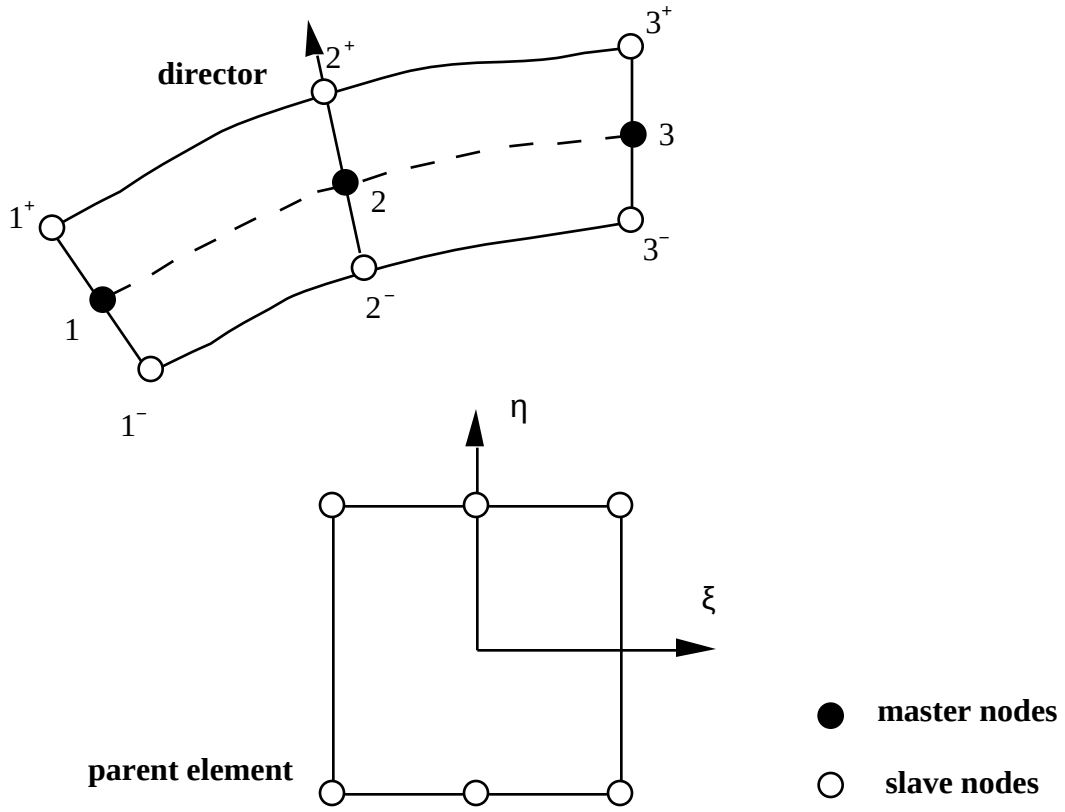

Figure 9.3. A three-node CB beam element and the underlying 6-node continuum element; the two notations for slave nodes of the underlying continuum element by two conventions are shown with the initial and current configurations.

9.3.1. Definitions and Nomenclature. A finite element model of a CB beam is shown in Figure 9.3; a 6-node quadrilateral is shown here as the underlying continuum element, but any other contiuum element with n_N nodes on the top and bottom surfaces can also be used. The parent element for the continuum element is also shown. As can be seen in Fig. 9.3, the continuum element only has nodes on the top and bottom surfaces (the surfaces are lines in two dimensional elements), for as will become clear, the motion must be linear in η. The reference line may be placed anywhere, but we will place it on the line $\eta = 0$ for convenience.

The lines of constant ξ are called *fibers* (they are also called pseudonormals), the unit vector along each fiber is called a *director*, which is denoted by $\mathbf{p}$. The directors play the same role in the CB theory as normals in the classical Mindlin-Reissner theory, hence the alternate name pseudonormals. Lines of constant η are called *lamina.*

Master nodes are introduced at the intersections of the fibers connecting nodes of the continuum element with the reference line. The degrees-of-freedom of these nodes describe the motion of the beam, and the equations of motion will be formulated in terms of generalized forces and velocities at these nodes. The original nodes of the continuum element on the top and bottom surfaces are designated as *slave nodes*. Each master node is associated with a pair of slave nodes along a common fiber, see Fig. 9.3. The slave

nodes are indicated either by superposed bars or by superscript plus and minus signs on the node numbers: thus node I^+ and I^- are slave nodes associated with master node I and lie on the top (+) and bottom (-) surfaces of the beam; I^* are alternate node numbers of the continuum element. Each triplet of nodes I^-, I, and I^+ is collinear and lie on the same fiber. The appellations "top" and "bottom" have no exact definition; either surface of the beam can be designated as the "top" surface.

The two sets of node numbers for the continuum element are related by.

$$\begin{aligned} I^* &= I^+ \qquad & I^+ &= I^* \quad \text{for } I^* \le n_N \\ I^* &= I^- + n_N \qquad & I^- &= I^* - n_N \quad \text{for } I^* > n_N \end{aligned} \tag{9.3.0}$$

For each point in the beam, a corotational coordinate system is defined with x tangent to the lamina; y then corresponds to the normal direction.

9.3.2. Assumptions. The following assumptions are made:

1. the fibers remain straight;
2. the element is in a state plane stress, so

$$\hat{\sigma}_{yy} = 0 \tag{9.3.1}$$

3. the elongation of fibers is governed by conservation of matter and/or the constitutive eqaution

The first assumption will be called the *modified Mindlin-Reissner assumption* in this book. It differs from what we call the classical Mindlin-Reissner assumption, which requires the normal to remain straight; the fibers are not initially normal to the midline. The resulting theory is similar to a single director Cosserat theory. Although the shear beam theory is called a Timoshenko beam theory, we will use the appellation modified Mindlin-Reissner for this assumptions for both beams and shells.

For the CB beam element to satisfy the classical Mindlin-Reissner assumptions, it is necessary for the fibers be aligned as closely as possible with the normal to the midline. This can be accomplished by placing the slave nodes so that the fibers are as close to normal to the midline as possible in the initial configuration. Otherwise the behavior of the degenerated beam element may deviate substantially from classical Mindlin-Reissner theory and may not agree with the physical behavior of beams. From exercise, it can be seen that it is impossible to align the fibers with the normal exactly along the entire length of the element when the motion of the continuum element is C^0.

Instead of the third assumption, many authors assume that the fibers are insxtensible. Inextensibility contradicts the plane stress assumption: the fibers are usually close to the $\hat{y}$ direction and so if $\hat{\sigma}_{yy} = 0$, the velocity strain in the $\hat{y}$ direction generally can not vanish. The contradiction is reconciled by not using the continuum displacement field to compute $\hat{D}_{yy}$; instead, $\hat{D}_{yy}$ is computed by the constitutive eqaution from the requirement that $\hat{\sigma}_{yy} = 0$.

The assumption of constant fiber length is inconsistent with the conservation of matter: if the beam element is stretched, it must become thinner to conserve matter. Conservation of matter is usually imposed through the constitutive equation. For

example, in plasticity, conservation of matter is reflected in the isochoric character of the plastic strains, see Chapter 5. Therefore, if the thickness strain is calculated through the constitutive equation via the plane stress requirement, conservation of matter is enforced. The important feature of the third assumption is that the extension of the fibers is not governed by the equations of motion or equilibrium. From the third assumption, it follows automatically that the equations of motion or equilibrium associated with the thickness modes are eliminated from the system.

The third assumption can be replaced by an inextensibility assumption if the change is thickness is small. In that case, the thickness velocity strain $\hat{D}_{yy}$ is still computed by the constitutive equation, but the effect of the thickness strain on the position of the slave nodes is neglected, so that the nodal internal forces do not reflect changes in the thickness. The theory is then applicable only to problems with moderate strains (on the oder of 0.01). This approach is taken in the following description of beam motion. In Section 9.5 we describe a methodlogy that completely accounts for thickness strains.

We have not given the plane stress condition in terms of the PK2 stress or nominal stress, for unless simplifying assumptions are made, they are more complex than (9.3.1): the plane stress condition requires that the $\hat{y}$-component of the physical stress vanish, which is not equivalent to requiring $\hat{S}_{22}$ to vanish. However, since the plane stress requirement is only an assumption which is almost never satisfied exactly in physical beams, the use of the slightly different condition $\hat{S}_{22} = 0$ is often acceptable, particularly for thin beams where **p** and $\hat{y}$ are collinear. This is examined further in Exercise 9.?.

9.4.3. Motion. The motion of the beam is described by translations of the master nodes, $x_I(t), y_I(t)$ and rotations of the nodal fibers, which are denoted by $\theta_I(t)$. To develop this form of the motion, we begin with the motion of the element in terms of the slave node (the nodes of the underlying continuum element) position vectors by

$$\mathbf{x}(\xi, t) = \sum_{I^+=1}^{n_N} \mathbf{x}_{I^+}(t) N_{I^+}(\xi,\eta) + \sum_{I^-=1}^{n_N} \mathbf{x}_{I^-}(t) N_{I^-}(\xi,\eta) = \sum_{I^*=1}^{2n_N} \mathbf{x}_{I^*}(t) N_{I^*}(\xi,\eta) \qquad (9.3.2)$$

In the above $\mathbf{x}^T = [x, y]$, $N_{I^*}(\xi,\eta)$ are the *standard shape functions for continua* (indicated by asterisks or superscripts "+" and "-" signs on nodal index) and n_N is the number of nodes along the top or bottom surface.

The *shape functions of the underlying continuum must be linear in* η for the above motion to be consistent with the modified Mindlin-Reissner assumption. Therefore the parent element can only have two nodes along the η direction, i.e. there can be only two slave nodes along a fiber. The velocity field is obtained by taking the material time derivative of the above, which gives

$$\mathbf{v}(\xi, t) = \sum_{I^+=1}^{n_N} \mathbf{v}_{I^+}(t) N_{I^+}(\xi,\eta) + \sum_{I^-=1}^{n_N} \mathbf{v}_{I^-}(t) N_{I^-}(\xi,\eta) = \sum_{I^*=1}^{2n_N} \mathbf{v}_{I^*}(t) N_{I^*}(\xi,\eta) \qquad (9.3.2b)$$

We now impose the inextensibility assumption and the modified Mindlin-Reissner assumptions on the motion of the slave nodes

$$\mathbf{x}_{I^+}(t) = \mathbf{x}_I(t) + \tfrac{1}{2} h_I^0 \mathbf{p}_I(t) \qquad \mathbf{x}_{I^-}(t) = \mathbf{x}_I(t) - \tfrac{1}{2} h_I^0 \mathbf{p}_I(t) \tag{9.3.3}$$

where $\mathbf{p}_I(t)$ is the director at master node *I*, and h_I^0 is the initial thickness of the beam at node *I* (or more precisely a pseudo-thickness since it is the distance between the top to bottom surfaces along a fiber, not along the normal). The director at node *I* is a unit vector along the fiber $\left(I^-, I, I^+\right)$, so the current nodal directors are given by

$$\mathbf{p}_I(t) = \frac{1}{h_I^0}\left(\mathbf{x}_{I^+}(t) - \mathbf{x}_{I^-}(t)\right) = \mathbf{e}_x \cos\theta_I + \mathbf{e}_y \sin\theta_I \tag{9.3.4a}$$

where $\mathbf{e}_x$ and $\mathbf{e}_y$ are the global base vectors. The above can also be derived by subtracting (9.3.3b) from (9.3.3a). The initial nodal directors are

$$\mathbf{p}_I^0(t) = \frac{1}{h_I^0}\left(\mathbf{X}_{I^+} - \mathbf{X}_{I^-}\right) = \mathbf{e}_x \cos\theta_I^0 + \mathbf{e}_y \sin\theta_I^0$$

The initial thickness is given by

$$h_I^0 = \left\| \mathbf{x}_{I+}(0) - \mathbf{x}_{I-}(0) \right\| \tag{9.3.4c}$$

From. (9.3.3) it can be shown that if $h_I = h_I^0$, then the fiber through node *I* is inextensible, i.e. $\left\| x_{I^+} - x_{I^-} \right\|$ is constant during the motion; it will be shown in Section 9.4 that all fibers of the element remain constant in length when the nodal fibers remain constant in length.

The velocities of the slave nodes are obtained by taking the material time derivative of (9.3.3), yielding

$$\mathbf{v}_{I+}(t) = \mathbf{v}_I(t) + \tfrac{1}{2} h_I^0 \omega_I(t) \times \mathbf{p}_I(t) \qquad \mathbf{v}_{I-}(t) = \mathbf{v}_I(t) - \tfrac{1}{2} h_I^0 \omega_I(t) \times \mathbf{p}_I(t) \tag{9.3.5}$$

where we have used (9.2.1) to express the nodal velocities in terms of the angular velocities, noting that the vectors from the master node to the slave nodes are $\frac{1}{2} h_I^0 \mathbf{p}_I(t)$ and $-\frac{1}{2} h_I^0 \mathbf{p}_I(t)$ for the top and bottom slave nodes, respectively. Since the model is two-dimensional, $\omega = \omega_z \mathbf{e}_z \equiv \dot{\theta} \mathbf{e}_z$ and the slave node velocity can be written by using (9.3.4a), (9.3.4b), and (9.3.5) as:

$$\mathbf{v}_{I^+} = \mathbf{v}_I - \omega_z \left(\left(y_{I^+} - y_I \right) \mathbf{e}_x - \left(x_{I^+} - x_I \right) \mathbf{e}_y \right) = \mathbf{v}_I - \tfrac{1}{2} \omega_z h_I^0 \left(\mathbf{e}_x \sin\theta - \mathbf{e}_y \cos\theta \right) \tag{9.3.6a}$$

$$\mathbf{v}_{I^-} = \mathbf{v}_I - \omega_z \left(\left(y_{I^-} - y_I \right) \mathbf{e}_x - \left(x_{I^-} - x_I \right) \mathbf{e}_y \right) = \mathbf{v}_I - \tfrac{1}{2} \omega_z h_I^0 \left(\mathbf{e}_x \sin\theta - \mathbf{e}_y \cos\theta \right) \tag{9.3.6b}$$

The motion of the master nodes is described by three degrees of freedom per node

$$\mathbf{d}_I(t) = \begin{bmatrix} u_{xI}^M & u_{yI}^M & \theta_I \end{bmatrix}^T \qquad \dot{\mathbf{d}}_I(t) = \begin{bmatrix} v_{xI}^M & v_{yI}^M & \omega_I \end{bmatrix}^T \tag{9.3.6}$$

Equation (9.3.6) can be written in matrix form as

$$\begin{Bmatrix} \mathbf{v}_{I^+} \\ \mathbf{v}_{I^-} \end{Bmatrix}^{slave} = \begin{Bmatrix} v_{xI^+} \\ v_{yI^+} \\ v_{xI^-} \\ v_{yI^-} \end{Bmatrix} = \mathbf{T}_I \dot{\mathbf{d}}_I \tag{9.3.7a}$$

Recall that we are not using the summation convention on nodal indices in this Chapter. From a comparison of (9.3.7a) and (9.3.6) we can see that

$$\mathbf{T}_I = \begin{bmatrix} 1 & 0 & y_I - y_{I^+} \\ 0 & 1 & x_{I^+} - x_I \\ 1 & 0 & y_I - y_{I^-} \\ 0 & 1 & x_{I^-} - x_I \end{bmatrix} \qquad \dot{\mathbf{d}}_I = \begin{Bmatrix} v_{xI} \\ v_{yI} \\ \omega_I \end{Bmatrix} \tag{9.3.7b}$$

The velocities of the master nodes are the degrees of freedom of the discrete model. We can see from the above that the discrete variables characterizing the motion of the beam are the two components of the velocity of the midline and the angular velocity of the node.

9.2.4.3. Nodal Forces. The procedure for calculating the internal nodal forces at the slave nodes in the CB approach is almost identical to that of the continuum element. The nodal velocities of the underlying continuum element are obtained from the master nodal velocities by (9.3.7). The continuum element procedures as described in Chapter 4 are then used to obtain the nodal internal forces at the slave nodes via the strain-displacement and constitutive equations.

The master nodal internal forces are related to the slave nodal internal forces by the transformation rule given in Section 4.5.6, Eq. (4.5.36). Since the slave nodal velocities are related to the master nodal velocities by (9.3.7), the nodal forces are related by

$$\mathbf{f}_I^{mast} = \begin{Bmatrix} f_{xI} \\ f_{yI} \\ m_I \end{Bmatrix} = \mathbf{T}_I^T \begin{Bmatrix} \mathbf{f}_{I+} \\ \mathbf{f}_{I-} \end{Bmatrix}^{slave} = \begin{bmatrix} 1 & 0 & 1 & 0 \\ 0 & 1 & 0 & 1 \\ y_I - y_{I^+} & x_{I^+} - x_I & y_I - y_{I^-} & x_{I^-} - x_I \end{bmatrix} \begin{Bmatrix} f_{xI+} \\ f_{yI+} \\ f_{xI-} \\ f_{yI-} \end{Bmatrix} \tag{9.3.8}$$

The external nodal forces at the master nodes can be obtained from the slave node external forces by the same transformation. The column matrix of nodal forces consists of the two force components f_{xI} and f_{yI} and the moment m_I. It can readily be seen that

they are conjugate in power to the velocities of the master nodes, i.e. the power of the forces at node I is given by $\mathbf{v}_I \ \mathbf{f}_I$; the superscripts "mast" have been dropped.

The major difference from the procedures in the standard continuum element is that in the evaluation of the constitutive law for the CB beam, the plane stress assumption (9.3.1) must be observed. Therefore, it is convenient to transform components of the stress and velocity strain tensors at each point of the beam to the corotational coordinate systems $\hat{x}, \hat{y},$. For this purpose, local base vectors $\hat{\mathbf{e}}_i$ are constructed so that $\hat{\mathbf{e}}_x$ is tangent to the lamina and $\hat{\mathbf{e}}_y$ is normal to the lamina, see Fig. 9.4.

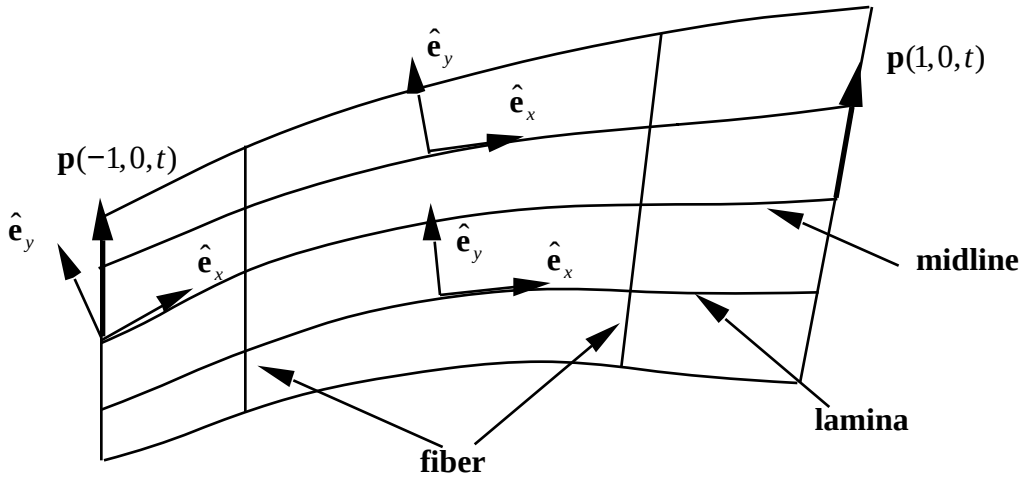

Figure 9.4 Schematic of DC beam showing lamina, the corotational unit vectors $\hat{\mathbf{e}}_x$, $\hat{\mathbf{e}}_y$ and the director $\mathbf{p}(\xi,t)$ at the ends; note $\mathbf{p}$ usually does not coincide with $\hat{\mathbf{e}}_y$.

The base vectors at any point are given by

$$\hat{\mathbf{e}}_x = \frac{x_{,\xi}\,\mathbf{e}_x + y_{,\xi}\,\mathbf{e}_y}{\left(x_{,\xi}^2 + y_{,\xi}^2\right)^{1/2}}, \qquad \hat{\mathbf{e}}_y = \frac{-y_{,\xi}\,\mathbf{e}_x + x_{,\xi}\,\mathbf{e}_y}{\left(x_{,\xi}^2 + y_{,\xi}^2\right)^{1/2}} \tag{9.3.9}$$

$$x_{,\xi} = \sum_I x_{I^*} N_{I^*,\xi}(\xi,\eta) \qquad y_{,\xi} = \sum_I y_{I^*} N_{I^*,\xi}(\xi,\eta)$$

The rate-of-deformation is transformed to the corotational system by Box 3.2?????:

$$\hat{\mathbf{D}} = \mathbf{R}^T \mathbf{D} \mathbf{R} \quad \text{where} \quad \mathbf{R} = \begin{bmatrix} \mathbf{e}_x \cdot \hat{\mathbf{e}}_x & \mathbf{e}_x \cdot \hat{\mathbf{e}}_y \\ \mathbf{e}_y \cdot \hat{\mathbf{e}}_x & \mathbf{e}_y \cdot \hat{\mathbf{e}}_y \end{bmatrix} \tag{9.3.10}$$

In the evaluation of the stress, the plane stress constraint $\hat{\sigma}_{yy} = 0$ must be observed. If the constitutive equation is in rate form, the constraint is expressed in the rate form $D\hat{\sigma}_{yy}/Dt = 0$. For example, for an isotropic hyperelastic material, the stress rate is given by LIU, CORRECTION NEEDS TO BE PUT IN

$$\frac{D}{Dt}\{\hat{\sigma}\} = \frac{D}{Dt}\begin{Bmatrix}\hat{\sigma}_{xx}\\ \hat{\sigma}_{yy}\\ \hat{\sigma}_{xy}\end{Bmatrix} = \frac{D}{Dt}\begin{Bmatrix}\hat{\sigma}_{xx}\\ 0\\ \hat{\sigma}_{xy}\end{Bmatrix} = \frac{E^{\sigma G}}{1-\upsilon^2}\begin{bmatrix}1 & \upsilon & 0\\ \upsilon & 1 & 0\\ 0 & 0 & \frac{1}{2}(1-\upsilon)\end{bmatrix}\begin{Bmatrix}\hat{D}_{xx}\\ \hat{D}_{yy}\\ 2\hat{D}_{xy}\end{Bmatrix} \tag{9.3.11}$$

In the above, the rate form of the plane stress condition $D\hat{\sigma}_{yy}/Dt = 0$ has been imposed to give $\hat{D}_{yy} = -\nu\hat{D}_{xx}$. Solving for the two other components gives

$$\frac{D\hat{\sigma}_{xx}}{Dt} = E^{\sigma G}\hat{D}_{xx}, \qquad \frac{D\hat{\sigma}_{xy}}{Dt} = \frac{E^{\sigma G}}{2(1+\upsilon)}\hat{D}_{xy} \tag{9.3.12}$$

As seen in the above, in an isotropic material, the rate of the axial stress is related to the axial rate-of-deformation by the tangent modulus $E^{\sigma G}$ for the Green-Naghdi rate.

For more general materials (including laws which lack symmetry in the moduli, such as nonassociated plasticity) the rate relation for the stress can be expressed as

$$\frac{D}{Dt}\begin{Bmatrix}\hat{\sigma}_{xx}\\ 0\\ \hat{\sigma}_{xy}\end{Bmatrix} = \begin{bmatrix}\hat{C}_{11} & \hat{C}_{12} & \hat{C}_{13}\\ \hat{C}_{21} & \hat{C}_{22} & \hat{C}_{23}\\ \hat{C}_{31} & \hat{C}_{32} & \hat{C}_{33}\end{bmatrix}^{\sigma G}\begin{Bmatrix}\hat{D}_{xx}\\ \hat{D}_{yy}\\ 2\hat{D}_{xy}\end{Bmatrix} \tag{9.3.13}$$

where $\hat{\mathbf{C}}$ is matrix of instantaneous moduli for the Green-Naghdi rate of Cauchy stress, as in plastic models given in Chapter 5, and the second equation enforces the plane stress condition.

The stress $\hat{\sigma}$ can be considered corotational, since the base vectors $(\hat{\mathbf{e}}_x, \hat{\mathbf{e}}_y)$ rotate almost exactly with the material. The rotation given through (9.3.9) differs somewhat from that given by a polar decomposition, but is usually a better rotation for composite or reinforced beams than that given by polar decomposition. The fibers of a composite and reinforcements tend to remain aligned with the lamina, and with this rotation, the tangent modulus $\hat{C}_{11}$ pertains to the lamina direction. If the system $(\hat{\mathbf{e}}_x, \hat{\mathbf{e}}_y)$ is not a good enough approximation of the rotation, it can be set by the polar decomposition theorem.

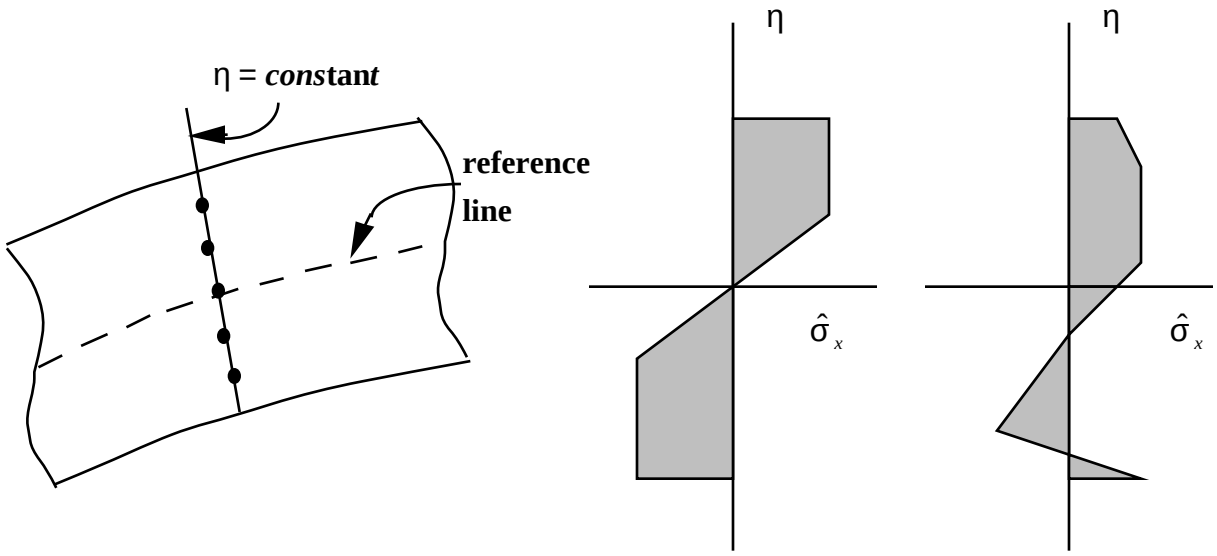

Figure 9.5. A stack of quadrature points and examples of axial stress distributions for an elastic-plastic material.

The slave internal nodal forces are obtained by the mechanics of the continuum element Example 4. and the integrals in (E4.2.11) are evaluated by numerical quadrature over the element domain. Neither full quadrature (4.5.27) nor the selective-reduced quadrature given (4.3.34b) can be used in a CB beam. Both quadrature schemes result in shear locking, to be described in Section 9.5. Shear locking can be avoided in this element by using a single stack of quadrature points along the axis $\xi = 0$ as shown in Fig. 9.5. The number of quadrature points required in the η direction depends on the material law and the accuracy desired. For a nonlinear hyperelastic material law, 3 Gauss quadrature points are often adequate. For an elastic-plastic law, a minimum of 5 quadrature points is needed. Gauss quadrature is not optimal for elastic-plastic laws since the lack of smoothness in the elastic-plastic constitutive response results in stress distributions with discontinuous derivatives, such as shown in Fig. 9.5. Therefore, the trapezoidal rule is often used.

To illustrate the selective-reduced integration procedure which circumvents shear locking, we consider a two-node beam element based on a 4-node quadrilateral continuum element. The nodal forces are obtained by integration with a single stack of quadrature points at $\xi = 0$ to avoid shear locking. The nodal forces at the slave nodes are obtained by (see Section 4.5.4):

$$\left[f_{xI^*}, f_{yI^*} \right]^{int} = \sum_{Q=1}^{n_Q} \begin{bmatrix} N_{I^*,x} & N_{I^*,y} \end{bmatrix} \begin{bmatrix} \sigma_{xx} & \sigma_{xy} \\ \sigma_{xy} & \sigma_{yy} \end{bmatrix} \overline{w}_Q a J_\xi \Big|_{(0,\eta_Q)} \tag{9.3.15}$$

where η_Q are the n_Q quadrature points through the thickness of the beam, $\overline{w}_Q$ are the quadrature weights, a is the dimension of the beam in the z-direction and J_ξ is the Jacobian determinant with respect to the parent element coordinates, (4.4.38). Note that the node numbers I^* can be related to the triplet number by Eq. (9.3.0) so the relationship to Eq. (9.3.8) is easily established. The stresses must be rotated back to the global system prior to evaluating the nodal internal forces by (9.3.15). The nodal internal forces can also be evaluated in terms of the corotational system by

$$\left[f_{\hat{x}I^*}, f_{\hat{y}I^*} \right]^{int} = \sum_{Q=1}^{n_Q} \left[N_{I,\hat{x}} \;\; N_{I,\hat{y}} \right] \begin{bmatrix} \hat{\sigma}_{xx} & \hat{\sigma}_{xy} \\ \hat{\sigma}_{xy} & 0 \end{bmatrix} \begin{bmatrix} R_{xx} & R_{yx} \\ R_{xy} & R_{yy} \end{bmatrix} \bar{w}_Q a J_\xi \Big|_{(0,\eta_Q)} \tag{9.3.16}$$

The stress component $\hat{\sigma}_{yy}$ vanishes in (9.316) because of the plane stress condition. The corotational approach is of advantage because the plane stress condition is more easily expressed in corotational components. While the use of the corotational form of the internal forces (9.3.16) eliminates the need to transform the stress components back to the global system after the constitutive update, some of the computational advantage is lost because the shape function derivatives must be evaluated in each corotational system. This computational effort can be reduced by using only one or two corotational systems per stack of quadrature points.

BOX?????

In summary, the procedure for computing the nodal forces in a CB beam element in a corotational, updated Lagrangian approach is:

1. the positions and velocities of the slave nodes are computed by (9.3.3) and (9.3.7) from the positions and velocities of the master nodes;
2. the rate-of-deformation is transformed to the corotational coordinate system at each quadrature point
3. the Cauchy stresses are computed at all quadrature points in the corotational coordinates with the plane stress condition $\hat{\sigma}_{yy} = 0$ enforced;
3. the stresses are transformed back to the global coordinates;
3. the nodal internal forces are computed at the slave nodes by standard method for continua, (E.4.2.11) as illustrated by (9.3.15-16);
4. the slave nodal forces are transformed to the master nodes by (9.3.8).

9.2.4.4. Mass Matrix. The mass matrix of the CB beam element can be obtained by using the transformation (4.5.39) using for $\hat{\mathbf{M}}$ the mass matrix for the underlying continuum element.

$$\mathbf{M} = \mathbf{T}^T \hat{\mathbf{M}} \mathbf{T} \tag{9.3.18a}$$

where

$$\mathbf{T} = \begin{bmatrix} \mathbf{T}_1 & \mathbf{0} & . & \mathbf{0} \\ \mathbf{0} & \mathbf{T}_2 & . & \mathbf{0} \\ . & . & . & . \\ \mathbf{0} & \mathbf{0} & . & \mathbf{T}_{n_N} \end{bmatrix} \tag{9.3.18b}$$

This mass matrix does not account for the time dependence of the $\mathbf{T}$ matrix. If we account for the time dependence of $\mathbf{T}$, the inertial force according to (4.5.42) is given by

$$\mathbf{f}^{inert} = \mathbf{T}^T \hat{\mathbf{M}} \dot{\mathbf{T}} \dot{\mathbf{v}} + \mathbf{T}^T \hat{\mathbf{M}} \dot{\mathbf{T}} \mathbf{v} \tag{9.3.17}$$

and $\hat{\mathbf{M}}$ is given in Example 4.2 and $\mathbf{T}_I$ is given by (9.3.7). The matrix $\dot{\mathbf{T}}_I$ is obtained by taking a time derivative of (9.3.7b) and using the fact that for node *I*, $\frac{d}{dt}(\omega_I \times \mathbf{r}_I) = \omega_I \times (\omega_I \times \mathbf{r}_I)$, which gives

$$\dot{\mathbf{T}}_I = \omega \begin{bmatrix} 1 & 0 & x_I - x_{I^+} \\ 0 & 1 & y_I - y_{I^+} \\ 1 & 0 & y_I - y_{I^-} \\ 0 & 1 & x_I - x_{I^-} \end{bmatrix} \tag{9.3.19}$$

From (9.3.17) and (9.3.19), it can be seen that the acceleration of the CB element will include a term proportional to the square of the angular velocity. Consequently the inertial term in the discrete ordinary differential equations are no longer linear in the velocities and the time integration of the equations becomes more complex. This second term in (9.3.17) is usually neglected.

Either the consistent or lumped mass of the continuum element, $\hat{\mathbf{M}}$, can be used to generate the mass matrix for the CB beam element. Equation (9.3.18a) does not yield a diagonal matrix even when the diagonal mass matrix of the continuum element is used.

Two techniques are used to obtain diagonal matrices:

1. The consistent mass matrix of the quadrilateral is transformed by (4.5.39) and the row sum technique is used.
2. The translational masses of the diagonal mass matrix are taken to be half the mass of the element and the rotational mass is taken to be the rotational inertia of half the beam about the node.

For a CB beam based on a rectangular 4-node continuum element, the second procedure yields (this is left as an exercize)

$$\mathbf{M} = \frac{\rho h_I^0 \ell_0 a_0}{420} \begin{bmatrix} 210 & 0 & 0 & 0 & 0 & 0 \\ 0 & 210 & 0 & 0 & 0 & 0 \\ 0 & 0 & \alpha \ell_0^2 & 0 & 0 & 0 \\ 0 & 0 & 0 & 210 & 0 & 0 \\ 0 & 0 & 0 & 0 & 210 & 0 \\ 0 & 0 & 0 & 0 & 0 & \alpha \ell_0^2 \end{bmatrix} \tag{9.3.20}$$

where α is often treated as a scale factor for the rotational inertia. This scale factor is chosen in explicit codes so that the stable time step depends only on the translational degrees of freedom, see Key and Beisinger (1971). LIU FILL IN

9.2.?. Equations of Motion. The equations of motion at a node are given by

$$\mathbf{M}_{IJ} \dot{\mathbf{v}}_J + \mathbf{f}_I^{int} = \mathbf{f}_I^{ext} \quad \textit{sum on } J \tag{9.3.21}$$

where the nodalo forces and nodal displacements

$$\mathbf{f}_I = \begin{Bmatrix} f_{xI} \\ f_{yI} \\ m_I \end{Bmatrix} \qquad \dot{\mathbf{d}}_I = \begin{Bmatrix} v_{xI} \\ v_{yI} \\ \omega_I \end{Bmatrix} \tag{9.3.22}$$

which are the master degrees of freedom, i.e. The equations are identical in form to (4.??). For a diagonal mass matrix the equations can be when written out as

$$\begin{bmatrix} M_{11} & 0 & 0 \\ 0 & M_{22} & 0 \\ 0 & 0 & M_{33} \end{bmatrix} \begin{Bmatrix} \dot{v}_{xI} \\ \dot{v}_{yI} \\ \dot{\omega}_I \end{Bmatrix} + \begin{Bmatrix} f_{xI} \\ f_{yI} \\ m_I \end{Bmatrix} = \begin{Bmatrix} f_{xI} \\ f_{yI} \end{Bmatrix}^{ext} \begin{Bmatrix} f_{xI} \\ f_{yI} \end{Bmatrix}^{int} \tag{9.3.23}$$

where M_{ii}, $i = 1$ to 3 are the assembled diagonal masses at node *I*. Although we have not derived these equations explicitly, they follow from (4.??) since we have only made transformation of variables. Showing this is left as an exercise. For equilibrium processes, the first term is dropped.

Tangent Stiffness. The tangential and load stiffnesses are obtained from the corresponding matrices for the underlying continuum element by the transformation (4.5.43). However, the continuum stiffnesses must reflect the plane stress assumption. This is illustrated in Example 9.1. These matrices do not need to be rederived for CB beams.

9.4. ANALYSIS OF CB BEAM

In order to obtain a better understanding of the CB beam, it is worthwhile to examine its motion from a viewpoint which more closely parallels classical beam theory. The analysis in this Section leads to discrete equations which are identical to those described in the previous section. It is more pleasing conceptually, but working in this framework is more burdensome, since the many of the entities needed for a standard implementation, such as the tangent stiffness and the mass matrix, have to be developed from scratch, whereas in the previous approach they are inherited from a continuum element with small modifications.

We start with the description of the motion. Recall that in the underlying continuum element, there are only two slave nodes along any fiber, i.e. in the thickness direction of the beam, so that the motion is linear in η. Consequently we can describe the motion of the CB beam by

$$\mathbf{x}(\xi, \eta, t) = \mathbf{x}^M(\xi, t) + \bar{\eta}(\xi, \eta)\mathbf{p}(\xi, t) \tag{9.4.1}$$

where

$$\bar{\eta}(\xi, \eta) = \tfrac{1}{2}\eta h^0(\xi) \tag{9.4.2}$$

The independent variables ξ and η are curvilinear coordinates with $\eta = 0$ corresponding to the reference line. The top and bottom surfaces of the beam are given by $\eta = 1$ and

$\eta = -1$, respectively. Note that although we use the same nomenclature for the curvilinear coordinates as for the parent element coordinates, (9.4.1) is independent of a parent element and ξ and η are an arbitrary set of curvilinear coordinates. The initial configuration is given by writing (9.4.1) at the initial time:

$$\mathbf{X}(\xi,\eta) = \mathbf{X}^M(\xi) + \bar{\eta}(\xi,\eta)\mathbf{p}_0(\xi) \tag{9.4.3}$$

where $\mathbf{p}_0(\xi)$ is the initial director and $\mathbf{X}^M(\xi)$ describes the initial reference line.

In this form of the motion, it is straightforward to show that all fibers are inextensible if the nodal fibers are inextensible. The length of a fiber is given by the distance between the top and bottom surfaces along the fiber, i.e. the distance between the points at $\eta = -1$ and $\eta = 1$ for a constant value of ξ. Using (9.4.3) it follows that the length of any fiber in the deformed configuration is given by

$$\|\mathbf{x}(\xi,1,t) - \mathbf{x}(\xi,-1,t)\| = \left\| \left(\mathbf{x}^M(\xi,t) + \frac{h^0(\xi)}{2}\mathbf{p}(\xi,t) \right) - \left(\mathbf{x}^M(\xi,t) - \frac{h^0(\xi)}{2}\mathbf{p}(\xi,t) \right) \right\|$$

$$= \|h^0(\xi)\mathbf{p}(\xi,t)\| = h^0(\xi)$$

where the last step follows from the fact that the director $\mathbf{p}$ is a unit vector. Hence the length of a fiber is always $h^0(\xi)$.

The displacement is obtained by subtracting (9.4.3) from (9.4.1), which gives

$$\mathbf{u}(\xi,\eta,t) = \mathbf{u}^M(\xi,t) + \bar{\eta}(\xi,\eta)\left(\mathbf{p}(\xi,t) - \mathbf{p}_0(\xi)\right) \tag{9.4.4}$$

Because the directors are unit vectors, the second term on the RHS of the above is a function of a single variable, the angle $\theta(\xi,t)$, which is measured counterclockwise from the *x*-axis as shown in Fig. 9.4. This can be clarified by expressing the second term of (9.4.4) in terms of the global base vectors:

$$\mathbf{u} = \mathbf{u}^M + \bar{\eta}\left(\mathbf{e}_x\left(\cos\theta - \cos\theta_0\right) + \mathbf{e}_y\left(\sin\theta - \sin\theta_0\right) \right) \tag{9.4.5}$$

$\theta_0(\xi)$ is the initial angle of the director at ξ. The velocity is the material time derivative of the displacement (9.4.5):

$$\mathbf{v}(\xi,\eta,t) = \mathbf{v}^M(\xi,t) + \bar{\eta}(\xi,\eta)\dot{\mathbf{p}}(\xi,t) \tag{9.4.6}$$

Using (9.2.1a), the above can be written

$$\mathbf{v} = \mathbf{v}^M + \bar{\eta}\,\omega \times \mathbf{p} \tag{9.4.7}$$

where $\omega\left(\xi, t\right)$ is the angular velocity of the director. Noting as before that the only nonzero component of this angular velocity is normal to the plane, the vectors are expressed in terms of the base vectors as follows

$$\omega = \omega \mathbf{e}_z \qquad \mathbf{p} = \hat{\mathbf{e}}_x \cos\hat{\theta} + \hat{\mathbf{e}}_y \sin\hat{\theta} \qquad \mathbf{v}^M = \hat{v}_x^M \hat{\mathbf{e}}_x + \hat{v}_y^M \hat{\mathbf{e}}_y \tag{9.4.7.b}$$

where $\hat{\theta}$ is the angle between the tangent and the director, as shown in Fig. 9.6.

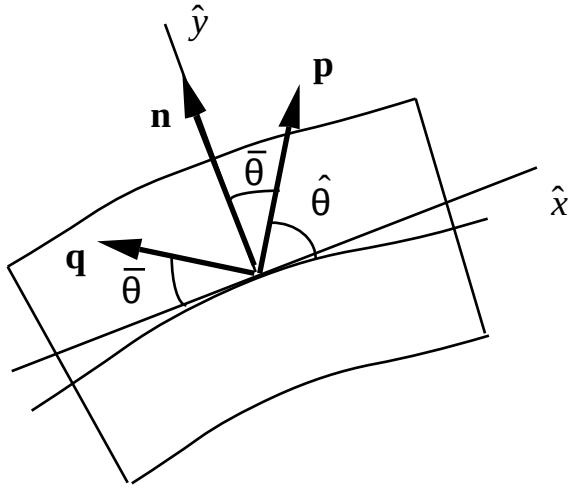

Figure 9.6 Nomenclature for CB beam in two dimensions showing director **p** and normal **n**.

The velocity can then be written as

$$\mathbf{v} = \hat{v}_x^M \hat{\mathbf{e}}_x + \hat{v}_y^M \hat{\mathbf{e}}_y + \bar{\eta}\,\omega\left(-\hat{\mathbf{e}}_x \sin\hat{\theta} + \hat{\mathbf{e}}_y \cos\hat{\theta}\right) \tag{9.4.8}$$

We define vector **q** by

$$\mathbf{q} = \mathbf{e}_z \times \mathbf{p} = -\hat{\mathbf{e}}_x \sin\hat{\theta} + \hat{\mathbf{e}}_y \cos\hat{\theta} \tag{9.4.10}$$

Then,

$$\mathbf{v} = \mathbf{v}^M + \hat{y}\omega\mathbf{q} \tag{9.4.11}$$

Noting (9.4.2) and Fig. 9.6, it can be seen that

$$\bar{\eta} = \frac{\hat{y}}{\sin\hat{\theta}} = \frac{\hat{y}}{\cos\bar{\theta}} \tag{9.4.11b}$$

The corotational components of the velocity are then obtained by writing (9.4.6) in the corotational basis with (9.4.11) used to eliminate the *y* coordinate:

$$\begin{bmatrix} \hat{v}_x \\ \hat{v}_y \end{bmatrix} = \begin{bmatrix} \hat{v}_x^M \\ \hat{v}_y^M \end{bmatrix} + \omega \hat{y} \begin{bmatrix} -1 \\ \tan\bar{\theta} \end{bmatrix} \tag{9.4.12}$$

It can be seen by comparing the above to (9.2.2-3) that when $\bar{\theta} = 0$, the above corresponds exactly to the velocity field of classical Mindlin-Reissner theory, and as long as $\bar{\theta}$ is small, it is a good approximation. However, analysts often let $\bar{\theta}$ take on large values, like $\frac{\pi}{4}$, by placing the slave nodes so that the director is not aligned with the normal. When the angle between the director and the normal is large, the velocity field differs substantially from that of classical Mindlin-Reissner theory.

The acceleration is given by the material time derivative of the velocity:

$$\dot{\mathbf{v}} = \dot{\mathbf{v}}^M + \bar{\eta}\left(\dot{\omega} \times \mathbf{p} + \omega \times (\omega \times \mathbf{p})\right) \tag{9.4.9}$$

so as indicated in (9.3.17), the accelration depends quadratically on the angular velocities.

The dependent variables for the beam are the two components of the midline velocity, $\mathbf{v}^M(\xi, t)$ and the angular velocity $\omega(\xi, t)$; alternatively one can let the midline displacement $\mathbf{u}^M(\xi, t)$ and the current angle of the director, $\theta(\xi, t)$, be the dependent variables. Thus the constraints introduced by the assumptions of the CB beam theory change the dependent variables from the two translational velocity components to two translational components and a rotation. However, the new dependent variables are functions of a single space variable, ξ, whereas the independent variables of the continuum are functions of two space variables. This reduction in the dimensionality of the problem is the major benefit of structural theories.

The development of expressions for the rate-of-deformation tensor is somewhat involved. The following is based on Belytschko, Wong and Stolarski(1989) specialized to two dimensions. We start with the implicit differentiation formula (4.4.36)

$$\mathbf{L} = \mathbf{v}_{,\mathbf{x}} = \mathbf{v}_{,\xi} \mathbf{x}_{,\xi}^{-1}$$

$$\hat{\mathbf{D}} = sym \begin{bmatrix} \frac{\partial \hat{v}_i}{\partial \hat{x}_j} \end{bmatrix} = \begin{bmatrix} \frac{\partial \hat{v}_x^M}{\partial \hat{x}} - \hat{y}\frac{\partial \omega}{\partial \hat{x}} & \frac{1}{2}\left(\frac{\partial \hat{v}_y^M}{\partial \hat{x}} - \omega + \frac{\partial \omega}{\partial \hat{x}} \tan\bar{\theta}\right) \\ sym & \omega \tan\bar{\theta} \end{bmatrix} \tag{9.4.13}$$

The effects of deviations of the director from the normal can be seen by comparing the above with (9.2.4). The axial velocity strain, which is predominant in bending response, agrees exactly with the Mindlin-Reissner theory: it varies linearly through the thickness of the beam, with the linear field entirely due to rotation of the cross-section. However, the above transverse shear $\hat{D}_{xy}$ and normal velocity strains $\hat{D}_{yy}$ differ substantially from those of the classical Mindlin-Reissner theory (9.2.4) when the angle $\hat{\theta}$ between the director and the normal to the lamina is large. These differences effect the plane stress

assumption. The motion associated with the modified Mindlin-Reissner theory can generate a significant nonzero axial velocity strain through Poisson effects.

The above tortuous approach is seldom used for the calculation of the velocity strrains in a CB beam. It makes sense only when the nodal internal fores are computed from resultant stresses. Otherwise the standard continuum expressions given in Chapter 4 are utilized. The objective of the above development was to show the characteristics of the velocity strain of a CB beam element, particularly its distribution through the thickness of the beam. The predominantly linear variation of the velocity strains through the thickness is the basis for developing resultant stresses.

Resultant Stresses. In classical beam and shell theories, the stresses are treated in terms of their integrals, known as resultant stresses. In the following, we examine the resultant stresses for CB beam theory, but to make the development more manageable, we assume the director to be normal to the reference surface, i.e. that $\bar{\theta} = 0$. We consider a curved beam in two dimensions with the reference line parametrized by r; $0 \le r \le L$, where r has physical dimensions of length, in contrast to the curvilinear coordinate ξ, which is nondimensional. To define the resultant stresses, we will express the virtual internal power (4.6.12) in terms of corotational components of the Cauchy stress. We omit the power due to $\hat{\sigma}_{yy}$, which vanishes due to the plane stress assumption (4.6.12), giving

$$\delta P^{int} = \int_0^L \iint_A \left(\delta \hat{D}_x \hat{\sigma}_x + 2\delta \hat{D}_{xy} \hat{\sigma}_{xy} \right) dA dr \qquad (9.4.13b)$$

In the above, the three-dimensional domain integral has been changed to an area integral and a line integral over the arc length of the reference line. The above integral is exactly equivalent to the integral over the volume if the directors at the endpoints are normal to the reference line. If the directors are not normal to the reference line at the endpoints, then the volume in (9.4.14) differs from the volume of the continuum element as shown in Fig. 9.7. This is usually not significant.

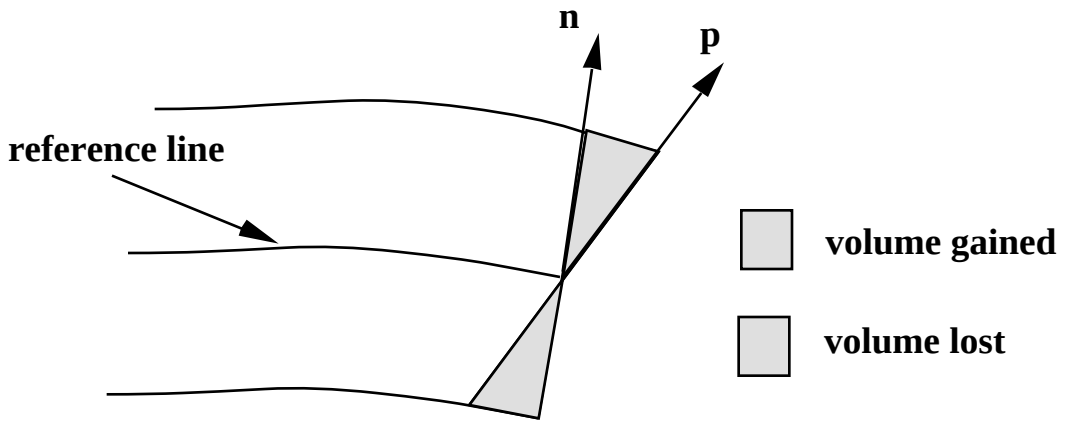

Figure 9.7 Comparison of volume integral in CB beam theory with line integral

Substituting (9.4.13b) into (9.4.13) gives

$$\delta P^{int} = \int_0^L \int_A \left(\frac{\partial \left(\delta \hat{v}_x^M \right)}{\partial \hat{x}} \hat{\sigma}_{xx} - \frac{\partial (\delta \omega)}{\partial \hat{x}} \hat{y} \hat{\sigma}_{xx} \right.$$
$$\left. + \left(-\delta \omega + \frac{\partial \left(\delta \hat{v}_y^M \right)}{\partial \hat{x}} \right) \hat{\sigma}_{xy} \right) dA dr \qquad (9.4.14)$$

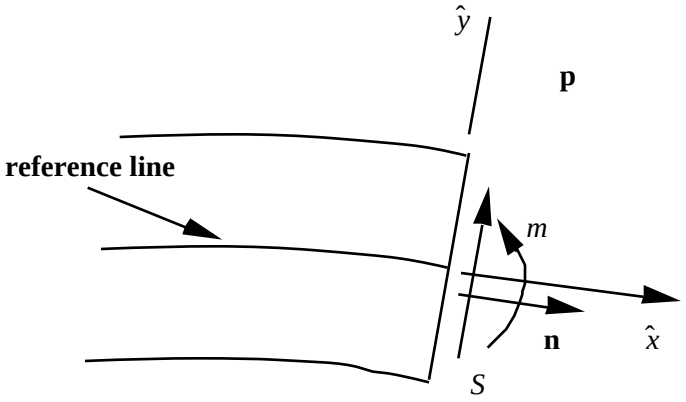

Figure 9.8. Resultant stresses in 2D beam.

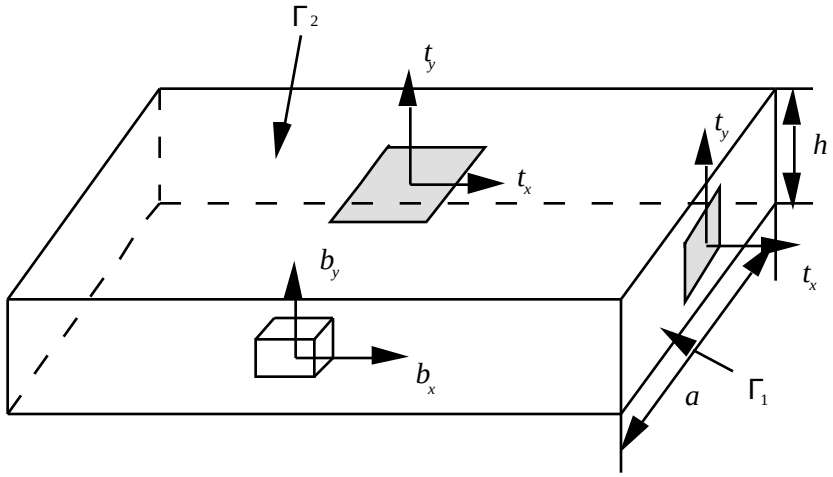

9.9. An example of external loads on a CB beam.

The following area integrals are defined

membrane force $\quad n = \int_A \hat{\sigma}_{xx} dA$

moment $\quad m = -\int_A y \hat{\sigma}_{xx} dA \qquad (9.4.15)$

shear $\quad s_y = \int_A \hat{\sigma}_{xy} dA$

The above are known as resultant stresses or generalized stresses; they are shown in Fig. 9.8 in their positive directions. The resultant n is the normal force, also called the

membrane force or axial force. This is the net force tangent to the midline due to the stresses in the beam. The moment *m* is the first moment of the stresses above the reference line. The shear force *s* is the net resultant of the transverse shear stresses. These definitions correspond with the customary definitions in texts on structures or mechanics of materials.

With these definitions, the internal virtual power (9.4.14) becomes

$$\delta P^{int} = \int_0^L \underbrace{\frac{\partial\left(\delta\hat{v}_x^M\right)}{\partial\hat{x}}}_{axial} n + \underbrace{\frac{\partial(\delta\omega)}{\partial\hat{x}}}_{bending} m + \underbrace{-\delta\omega + \frac{\partial\left(\delta\hat{v}_y^M\right)}{\partial\hat{x}}}_{shear} q\, dr \tag{9.4.16}$$

The physical names of the various powers are indicated. The axial or membrane power is the power expended on stretching the beam, the bending power the energy expended on bending the beam. The transverse shear power arises also from bending of the beam (see Eq. (???)); it vanishes for thin beams where the Euler-Bernoulli assumption is applicable.

The external power is defined in terms of resultants of the tractions subdivided into axial and bending power in a similar way. We assume $\bar{t}_z = 0$ and that **p** is coincident with $\hat{y}$ at the ends of the beam and consider only the tractions for the specific example shown in Fig. 9.9; the director is assumed collinear with the normal, so only the terms in classical Mindlin-Reissner theory are developed. The virtual external power is obtained from (B4.2.5), which in terms of corotational components gives

$$\delta P^{ext} = \int_{\Gamma_1 \Gamma_2} \left(\delta\hat{v}_x \hat{t}_x + \delta\hat{v}_y \hat{t}_y\right) d\Gamma + \int_{\Omega} \left(\delta\hat{v}_x \hat{b}_x + \delta\hat{v}_y \hat{b}_y\right) d\Omega \tag{9.4.17}$$

Substituting Eq. (9.4.12) into the above yields

$$\begin{aligned} \delta P^{ext} = & \int_{\Gamma_1 \Gamma_2} \left(\left(\delta\hat{v}_x^M - \delta\omega\hat{y}\right)\hat{t}_x + \left(\delta\hat{v}_y^M\right)\hat{t}_y\right) d\Gamma \\ & + \int_{\Omega} \left(\left(\delta\hat{v}_x^M - \delta\omega\hat{y}\right)\hat{b}_x + \left(\delta\hat{v}_y^M\right)\hat{b}_y\right) d\Omega \end{aligned} \tag{9.4.18}$$

The applied forces are now subdivided into those applied to the ends of the beam and those applied over the interior. For this example, only the right hand end is subjected to prescribed tractions, see Fig. 9.9. The generalized external forces are now defined similarly to the resulotant stresses by taking the zeroth and first moments of the tractions:

$$n^* = \int_{\Gamma_1} \hat{t}_x\, dA, \quad s^* = \int_{\Gamma_1} \hat{t}_y\, dA, \quad m^* = -\int_{\Gamma_1} \hat{y}\hat{t}_x\, dA = \tag{9.4.19}$$

where the last equality follows from the fact that the director is assumed normal to the midline at the boundaries. The tractions between the end points and the body forces are subsumed as generalized body forces

$$\hat{f}_x = \int_{\Gamma_2} \hat{t}_x \, d\Gamma + \int_{\Omega} \hat{b}_x d\Omega, \quad \hat{f}_y = \int_{\Gamma_2} \hat{t}_y \, d\Gamma + \int_{\Omega} \hat{b}_y d\Omega, \quad M = -\int_{\Gamma_2} \hat{y}\hat{t}_x \, d\Gamma + \int_{\Omega} \hat{y}\hat{b}_y d\Omega \tag{9.4.20}$$

Since the dependent variables have been changed from $v_i(x, y)$ to $v_i^M(r)$ and $\omega(r)$ by the modified Mindlin-Reissner constraint, the definitions of boundaries are changed accordingly: the boundaries become the end points of the beam. Any loads applied between the endpoints are treated like body forces. The boundaries with prescribed forces are denoted by Γ_n, Γ_m and Γ_s which are the end points at which the normal (axial) force, moment, and shear force are prescribed, respectively. The external virtual power (9.4.17), in light of the definitions (9.4.19-20), becomes

$$\delta P^{ext} = \int \left(\delta\hat{v}_x \hat{f}_x + \delta\hat{v}_y \hat{f}_y + \delta\omega M \right) dr + \delta\hat{v}_x n^* \Big|_{\Gamma_n} + \delta\hat{v}_y s^* \Big|_{\Gamma_s} + \delta\omega m^* \Big|_{\Gamma_m} \tag{9.4.21}$$

9.3.?. Boundary Conditions. The velocity (essential) boundary conditions for the CB beam are usually expressed in terms of corotational coordinates so that they have a clearer physical meaning. The velocity boundary conditions are

$$\begin{aligned} \hat{v}_x^M &= \hat{v}_x^M \qquad \text{on } \Gamma_{\hat{v}_x} \\ \hat{v}_y^M &= \hat{v}_y^M \qquad \text{on } \Gamma_{\hat{v}_y} \\ \omega &= \omega \qquad \text{on } \Gamma_{\omega} \end{aligned} \tag{9.4.18}$$

where the subscript on Γ indicates the boundary on which the particular displacement is prescribed. The angular velocity. of course, is independent of the orientation of the coordinate system so we have not superposed hat on it.

The generalized traction boundary conditions are:

$$\begin{aligned} n &= n^* \qquad \text{on } \Gamma_n \\ s &= s \qquad \text{on } \Gamma_s \\ m &= m \qquad \text{on } \Gamma_m \end{aligned} \tag{9.4.19}$$

Note that (9.4.18) and (9.4.19) are sequentially conditions on kinematic and kinetic variables which are conjugate in power. Each pair yields a power, i.e., $n\hat{v}_x^M$ is the power of the axial force on the boundary, $s\hat{v}_y^M$ is the power of the transverse force and $m\omega$ is the power of the moment. Since variables which are conjugatge in power can not be prescribed on the same boundary, but one of the pair must be prescribed on any boundary, it follows then that

$$\begin{aligned} \Gamma_n \quad \Gamma_{v_x} &= \Gamma \quad \Gamma_n \cap \Gamma_{v_x} = 0 \\ \Gamma_s \quad \Gamma_{v_y} &= \Gamma \quad \Gamma_s \cap \Gamma_{v_y} = 0 \\ \Gamma_m \quad \Gamma_{v_\omega} &= \Gamma \quad \Gamma_m \cap \Gamma_{\omega} = 0 \end{aligned} \tag{9.4.20}$$

So on a boundary point either the moment or rotation, the normal force or the velocity $\hat{v}_x^M$, the shear or the velocity $\hat{v}_y^M$ must be prescribed, but no pair can be described on the smae boundary. Even for CB beams, boundary conditions are prescribed in terms of resultants. The velocity boundary conditions can easily be imposed on the nodal degrees of freedom given in (9.3.22), since the midline velocities correspond to the nodal velociities. The traction boundary conditions are

Weak Form. The weak form for the momentum equation for a beam is given by

$$\delta P^{inert} + \delta P^{int} = \delta P^{ext} \qquad \left(\delta v_x, \delta v_y, \delta\omega\right) \quad U_0 \tag{9.4.21}$$

where the virtual powers are defined in (9.4.16)and (9.4.21) and U_0 is the space of piecewise differentiable functions, i.e.C^0 functions, which vanish on the corresponding prescribed displacement boundaries. The functions need only be C^0 since only the first derivatives of the dependent variables appear in the virtual power expressions.

Strong Form. We will not derive the strong form equivalent to (9.4.21) for an arbitrary geometry. This can be done, see Simo and Fox(1989) for example, but it is awkward without curvilinear tensors. Instead, we will develop the strong form for a straight beam of uniform cross-section which lies along the x-axis, with inertia and applied moments neglected. Equation (9.4.21) can then be simplified to

$$\begin{aligned}&\int_0^L \left(\delta v_{x,x} n + \delta\omega_{,x} m + \left(\delta v_{y,x} - \delta\omega\right)s - \delta v_x f_x - \delta v_y f_y\right)dx \\ &\quad - \left(\delta v_x n^*\right)\Big|_{\Gamma_n} - \left(\delta\omega m^*\right)\Big|_{\Gamma_m} - \left(\delta v_y s^*\right)\Big|_{\Gamma_s} = 0\end{aligned} \tag{9.4.22}$$

The hats have been dropped since the local coordinate system coincides with the global system at all points. The procedure for finding the equivalent strong form then parallels the procedure used in Section 4.3. The idea is to remove all derivatives of test functions which appear in the weak form, so that the above can be written as products of the test functions with a function of the resultant forces and their derivatives. This is accomplished by using integration by parts, which is sketched below for each of the terms in the weak form:

$$\int_0^L \delta v_{x,x} n dx = \int_0^L -\delta v_x n_{,x} dx + \left(\delta v_x n\right)\Big|_{\Gamma_n} + \left\langle \delta v_x n \right\rangle \tag{9.4.23}$$

$$\int_0^L \delta\omega_{,x} m dx = \int_0^L -\delta\omega m_{,x} dx + \left(\delta\omega m\right)\Big|_{\Gamma_m} + \left\langle \delta\omega m \right\rangle \tag{9.4.24}$$

$$\int_0^L \delta v_{y,x} s dx = \int_0^L -\delta v_y s_{,x} dx + \left(\delta v_y s\right)\Big|_{\Gamma_s} + \left\langle \delta v_y s \right\rangle \tag{9.4.25}$$

In each of the above we have used the fundamental theorem of calculus as given in Section 2.? for a piecewise continuously differentiable function and the fact that the test

functions vanish on the prescribed displacement boundaries, so the boundary term only applies to the complementary boundary points, which are given by (9.4.20). Substituting (9.4.23) to (9.4.25) into (9.4.22) gives

$$\int_0^L \Big(\delta v_x\big(n_{,x} + f_x\big) + \delta\omega\big(m_{,x} + s\big) + \delta v_y\big(s_{,x} + f_y\big)\Big)dx + \delta v_x\langle n\rangle + \delta v_y\langle s\rangle + \\ \delta\omega\langle m\rangle + -\delta v_x\big(n^* - n\big)\Big|_{\Gamma_n} + \delta\omega\big(m^* - m\big)\Big|_{\Gamma_m} + \delta v_y\big(s^* - s\big)\Big|_{\Gamma_s} = 0 \tag{9.4.26}$$

Using the density theorem as given in Section 4.3 then gives the following strong form:

$$n_{,x} + f_x = 0, \quad s_{,x} + f_y = 0, \quad m_{,x} + s = 0, \\ \langle n\rangle = 0,\ \langle s\rangle = 0,\ \langle m\rangle = 0 \\ n = n^* \text{ on } \Gamma_n, \quad s = s^* \text{ on } \Gamma_s, \quad m = m^* \text{ on } \Gamma_m \tag{9.4.27}$$

which are respectively, the equations of equilibrium, the internal continuity conditions, and the generalized traction (natural) boundary conditions.

The above equilibrium equations are well known in structural mechanics. These equilibrium equations are not equivalent to the continuum equilibrium equations, $\sigma_{ij,j} + b_i = 0$. Instead, they are a *weak form of the continuum equilibrium equations*. Their suitability for beams is primarily based on experimental evidence. The error due to the structural assumption can not be bounded rigorously for arbitrary materials. Thus the applicability of beam theory, and by extension the shell theories to be considered later, rests primarily on experimental evidence.

Finite Element Approximation. When the motion is treated in the form (9.4.1) as a function of a single variable, the finite element approximation is constructed by means of one-dimensional shape functions $N_I(\xi)$:

$$\mathbf{x}(\xi,\eta,t) = \sum_{I=1}^{n_N}\Big(\mathbf{x}_I^M(t) + \bar{\eta}_I\mathbf{p}_I(t)\Big)N_I(\xi) \tag{9.4.24}$$

As is clear from in the above, the *product of the thickness with the director is interpolated*. If they are interpolated independently, the second term in the above is quadratic in the shape functions and differs from (9.3.2a). It follows immediately from the above that the original configuration of the element is given by

$$\mathbf{X}(\xi,\eta) = \sum_{I=1}^{n_N}\Big(\mathbf{X}_I^M + \bar{\eta}_I\mathbf{p}_I^0\Big)N_I(\xi) \tag{9.4.25}$$

The displacement is obtained by taking the difference of (9.4.24) and (9.4.25), which gives

$$\mathbf{u}(\xi,\eta,t) = \sum_{I=1}^{n_N}\Big(\mathbf{u}_I^M(t) + \bar{\eta}_I\big(\mathbf{p}_I(t) - \mathbf{p}_I^0\big)\Big)N_I(\xi)$$

Taking the material time derivative of the above gives the velocity

$$\mathbf{v}(\xi,\eta,t) = \sum_{I=1}^{n_N} \left(\mathbf{v}_I^M(t) + \bar{\eta}_I \left(\omega \mathbf{e}_z \times \mathbf{p}_I(t) \right) \right) N_I(\xi)$$

This velocity field is identical to the velocity field generated by substituting (9.3.6) into (9.5.2b). Thus the mechanics of any element generated by this approach will be identical to that of an element implemented directly as a continuum element with the modified Mindlin-Reissner constraints applied only at the nodes, i.e. with the modified Mindlin-Reissner assumptions applied to the discrete equations. Therefore we will not pursue this approach further.

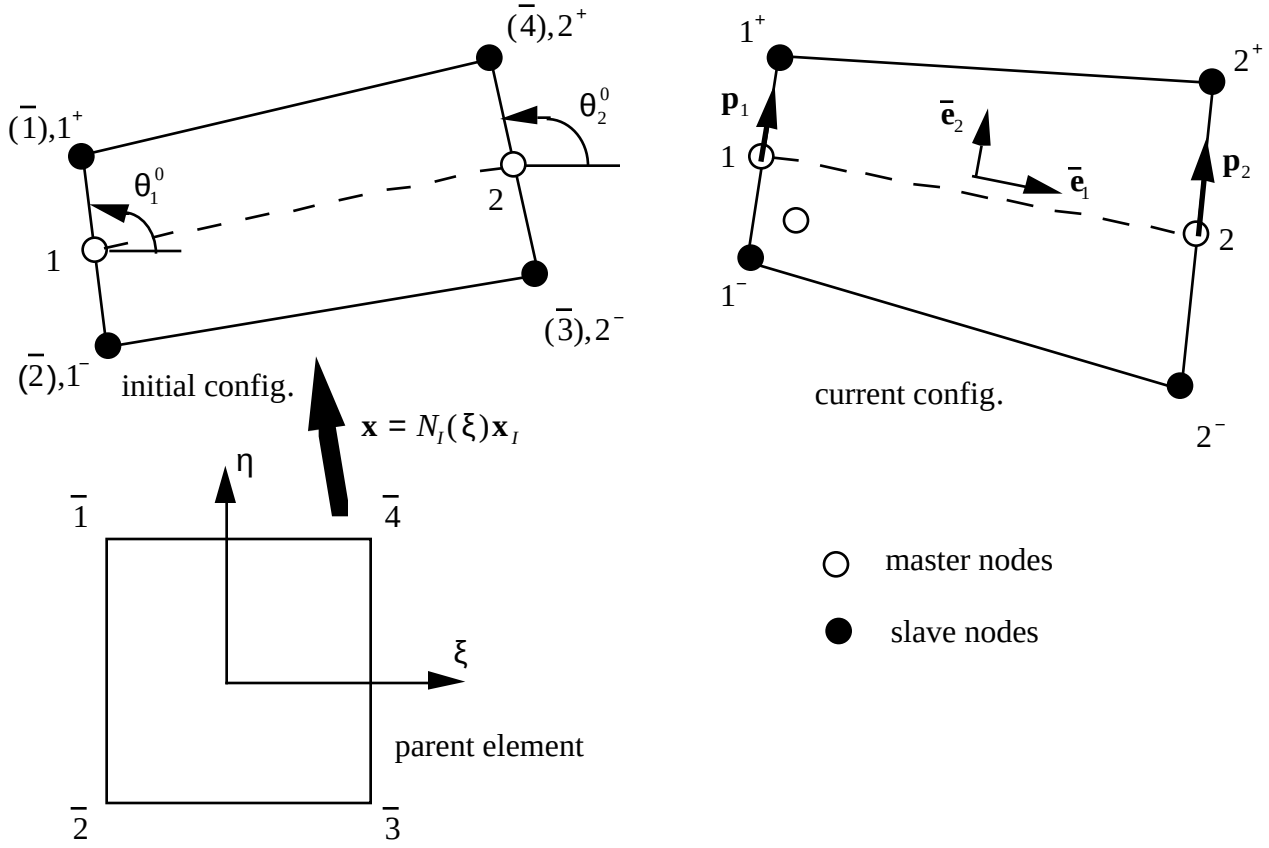

Fig. 9.10 Two-node CB beam element based on 4-node quadrilateral continuum element.

Example 9.1 Two-node beam element. The CB beam theory is used to formulate a 2-node CB beam element based on a 4-node, continuum quadrilateral. The element is shown in Fig. 9.10. We place the reference line (midline) midway between the top and bottom surfaces; the line coincides with $\xi = 0$ in the parent domain; although this placement is not necessary it is convenient. The master nodes are placed at the intersections of the reference line with the edges of the element. The slave nodes are the

corner nodes and are labeled by the two numbering schemes described previously in Fig. 9.10.

This motion of the 4-node continuum element

$$\mathbf{x} = \sum_{I=1}^{4} x_{\bar{I}}(t) N_{\bar{I}}(\xi,\eta) \tag{E9.1.2}$$

where $N_I(\xi,\eta)$ are the standard 4-node isoparametric shape functions

$$N_I(\xi,\eta) = \frac{1}{4}(1+\xi_I\xi)(1+\eta_I\eta) \tag{E9.1.3}$$

The motion of the element when given in terms of one-dimensional shape functions by (9.3.3) is:

$$\begin{aligned}\mathbf{x}(\xi,\eta,t) &= \mathbf{x}^M(\xi,t) + \bar{\eta}\,\mathbf{p}(\xi,t) \\ &= \mathbf{x}_1(t)(1-\xi) + \mathbf{x}_2(t)\xi + \bar{\eta}\,\mathbf{p}_1(t)(1-\xi) + \bar{\eta}\,\mathbf{p}_2(t)\xi\end{aligned} \tag{E9.1.1}$$

Eqs. (E9.1.1) and (E9.1.3) are equivalent if

$$x_1(t) = \frac{1}{2}\left(x_{\bar{1}} + x_{\bar{2}}\right) = \frac{1}{2}\left(x_{1^+} + x_{1^-}\right) \qquad x_2(t) = \frac{1}{2}\left(x_{\bar{3}} + x_{\bar{4}}\right) = \frac{1}{2}\left(x_{2^+} + x_{2^-}\right) \tag{E9.1.4}$$

$$\mathbf{p}_1(t) = \frac{\left(x_{\bar{2}} - x_{\bar{1}}\right)\mathbf{e}_x + \left(y_{\bar{2}} - y_{\bar{1}}\right)\mathbf{e}_y}{\left(\left(x_{\bar{2}} - x_{\bar{1}}\right)^2 + \left(y_{\bar{2}} - y_{\bar{1}}\right)^2\right)^{1/2}} \qquad \mathbf{p}_2(t) = \frac{\left(x_{\bar{4}} - x_{\bar{3}}\right)\mathbf{e}_x + \left(y_{\bar{4}} - y_{\bar{3}}\right)\mathbf{e}_y}{\left(\left(x_{\bar{4}} - x_{\bar{3}}\right)^2 + \left(y_{\bar{4}} - y_{\bar{3}}\right)^2\right)^{1/2}} \tag{E9.1.5a}$$

Thus the motions given in Eqs. (E9.1.2) and (E9.1.3) are alternate descriptions of the same motion. Eqs. (E9.1.4) define the location of the master nodes. Eqs. (E9.1.5) define the orientations of the directors.

The degrees of freedom of this CB beam element are

$$\mathbf{d}^T = \left[u_{x1},\, u_{y1}, \theta_1, u_{x2}, u_{y2}, \theta_2\right] \tag{E9.1.6}$$

where θ_I are the angles between the directors and the *x*-axis measured positively in a counterclockwise direction from the positive x-axis. The nodal velocities are

$$\dot{\mathbf{d}}^T = \left[\dot{u}_{x1}, \dot{u}_{y1}, \omega_1, \dot{u}_{x2}, \dot{u}_{y2}, \omega_2\right] \tag{E9.1.7}$$

The nodal forces are conjugate to the nodal velocities in the sense of power, so

$$\mathbf{f}^T = \left[\, f_{x1}, f_{y1}, m_1, f_{x2}, f_{y2}, m_2\right] \tag{E9.1.8}$$

where m_I are nodal moments.

The nodal velocities of the slave nodes are next expressed in terms of the master nodal velocities by (9.3.7). The relations are written for each triplet of nodes: a master node and the two associated slave nodes. For each triplet of nodes, the (9.3.7) specialized to the geometry of this example is

$$\mathbf{v}_I^S = \mathbf{T}_I \mathbf{v}_I^M \quad \text{(no sum on } I\text{)} \tag{E9.1.9}$$

where

$$\mathbf{v}_I^S = \begin{Bmatrix} v_{xI^-} \\ v_{yI^-} \\ v_{xI^+} \\ v_{yI^+} \end{Bmatrix}, \quad \mathbf{T}_I = \begin{bmatrix} 1 & 0 & \frac{h}{2} p_x & 1 & 0 & \frac{1}{2} y_{,\xi 12} \\ 0 & 1 & -\frac{h}{2} p_y & 0 & 1 & \frac{1}{2} x_{,\xi 21} \\ 1 & 0 & -\frac{h}{2} p_x & 1 & 0 & \frac{1}{2} y_{,\xi 34} \\ 0 & 1 & \frac{h}{2} p_y & 0 & 1 & \frac{1}{2} x_{,\xi 43} \end{bmatrix}, \quad \mathbf{v}_I^M = \begin{Bmatrix} v_{xI} \\ v_{yI} \\ \theta_I \end{Bmatrix} \tag{E9.1.10}$$

Once the slave node velocities are known, the rate-of-deformation can be computed at any point in the element by Eq. (E4.2.c).

The rate-of-deformation is be computed at all quadrature points in the corotational coordinate system of the quadrature point. The two node element avoids shear locking if a single stack of quadrature points $\xi = (0, \eta_Q)$, $Q = 1$ to n_Q. The strain measures are computed in the global coordinate system using the equation given in Example 4.2 and 4.10.

The constitutive equation is evaluated at the quadrature points of the element in a corotational coordinate system given by Eq. (9.3.9) with

$$\hat{\mathbf{e}}_x = \frac{x_{,\xi}\, \mathbf{e}_x + y_{,\xi} \mathbf{e}_y}{\left(\left(x_{,\xi} \right)^2 + \left(y_{,\xi} \right)^2 \right)^{\frac{1}{2}}} \qquad \hat{\mathbf{e}}_y = \hat{\mathbf{e}}_z \times \hat{\mathbf{e}}_x \tag{E9.1.11}$$

where

$$x_{,\xi} = \sum_{I=1}^{4} x_I N_{I,\xi} \qquad y_{,\xi} = \sum_{I=1}^{4} y_I N_{I,\xi} \tag{E9.1.13}$$

A hypoelastic law for isotropic and anisotropic laws is given by (9.3.11) or (9.3.13), respectively.

The internal forces are then transformed to the master nodes for each triplet by (4.5.36). This gives

$$\begin{Bmatrix} f_{xI} \\ f_{yI} \\ m_I \end{Bmatrix} = \mathbf{T}_I^T \begin{Bmatrix} f_{xI^+} \\ f_{yI^+} \\ f_{xI^-} \\ f_{yI^-} \end{Bmatrix} \tag{E9.1.14}$$

Evaluating the first and third term of the above left hand matrix gives

$$f_{xI} = f_{xI^+} + f_{xI^-} \qquad f_{yI} = f_{yI^+} + f_{yI^-} \tag{E.9.1.15a}$$

$$m_1 = \frac{1}{2}\left(y_{\bar{1}\bar{2}} f_{x1} + x_{\bar{2}\bar{1}} f_{y1}\right) \tag{E.9.1.15b}$$

So the transformation gives what is expected from equilibrium of the slave node with the master node. The master node force is the sum of the slave node forces and the master node moment is the moment of the slave node forces about the master node.

This element formulation can also be applied to constitutive equations in terms of the PK2 stress and the Green strain. The computation of the Green strain tensors requires the knowledge of θ_I and x_I. The director in the initial and current configurations is given by

$$p_{xI}^0 = \cos\theta_I^0, \quad p_{yI}^0 = \sin\theta_I^0 \qquad p_{xI} = \cos\theta_I, \quad p_{yI} = \sin\theta_I \tag{E9.1.11}$$

The positions of the slave nodes can then be computed by specializing (9.4.1) to the nodes, which gives

$$\begin{aligned}
X_{\bar{1}} &= X_1 + \tfrac{h}{2} p_{x1}, & Y_{\bar{1}} &= Y_1 + \tfrac{h}{2} p_{y1}^0 & x_{\bar{1}} &= x_1 + \tfrac{h}{2} p_{x1}, & y_{\bar{1}} &= y_1 + \tfrac{h}{2} p_{y1} \\
X_{\bar{2}} &= X_1 - \tfrac{h}{2} p_{x1}^0, & Y_{\bar{2}} &= Y_1 - \tfrac{h}{2} p_{y1}^0 & x_{\bar{2}} &= x_1 - \tfrac{h}{2} p_{x1}, & y_{\bar{2}} &= y_1 - \tfrac{h}{2} p_{y1} \\
X_{\bar{3}} &= X_2 - \tfrac{h}{2} p_{x2}^0, & Y_{\bar{3}} &= Y_2 - \tfrac{h}{2} p_{y2}^0 & x_{\bar{3}} &= x_2 - \tfrac{h}{2} p_{x2}, & y_{\bar{3}} &= y_2 - \tfrac{h}{2} p_{y2} \\
X_{\bar{4}} &= X_2 + \tfrac{h}{2} p_{x2}^0, & Y_{\bar{4}} &= Y_2 + \tfrac{h}{2} p_{y2}^0 & x_{\bar{4}} &= x_2 + \tfrac{h}{2} p_{x2}, & y_{\bar{4}} &= y_2 + \tfrac{h}{2} p_{y2}
\end{aligned} \tag{E9.1.12}$$

The displacement of the slave nodes is then obtained by taking the difference of the nodal coordinates. The displacement of any point can then be obtained by the continuum displacement field

$$\mathbf{u} = \sum_{\bar{I}=\bar{1}}^{4} \mathbf{u}_{\bar{I}} N_{\bar{I}}$$

The Green strain can then be computed by (3.3.6) and the PK2 stress by the constitutive law. After transforming the PK2 stress to the Cauchy stress by Box 3.2, the nodal forces can be computed as before.

Velocity Strains for Rectangular Element. When the underlying continuum element is rectangular (because the directors are in the *y* direction), and the beam is along the x direction, the velocity field (9.4.8) is

$$\mathbf{v} = \mathbf{v}^M - y\omega\mathbf{e}_x$$

where we have specialized Eq. (9.4.8) to $\theta = \pi/2$. Writing out the components of the above and immediately substituting the one-dimensional two-node shape functions gives

$$v_x = v_{x1}^M(1-\xi) + v_{x2}^M\xi - y\left(\omega(1-\xi) - \omega_2\xi\right)$$

$$v_y = v_{y1}^M(1-\xi) + v_{y2}^M\xi$$

The velocity strain is then given by Eq. (3.3.10):

$$D_{xx} = \frac{\partial v_x}{\partial x} = \frac{1}{\ell}\left(v_{x2}^M - v_{x1}^M\right) - \frac{y}{\ell}\left(\omega_2 - \omega_1\right)$$

$$2D_{xy} = \frac{\partial v_y}{\partial x} + \frac{\partial v_x}{\partial y} = \frac{1}{\ell}\left(v_{y2}^M - v_{y1}^M\right) - \left(\omega_1(1-\xi) + \omega_2\xi\right)$$

$$D_{yy} = 0$$

The material tangent and goemetric stiffness of this elementis given by LIU-give result with some explanation

9.5 CONTINUUM BASED SHELL IMPLEMENTATION

In this Section, the degenerated continuum (CB) approach to shell finite elements is developed. This approach was pioneered by Ahmad(1970); a nonlinear version of this theory was presented by Hughes and Liu(1981). In the CB approach to shell theory, as for CB beams, it is not necessary to develop the complete formulation, i.e. developing a weak form, discretizing the problem by using finite elemeny interpolatns, etc. Instead the shell element is developed in this Section by imposing the constraints pf the shell theory on a continuum element. Subsequently, we will examine CB shells from a more theoretical viewpoint by imposing the constraints on thhe test and trial functions prior to construction of the weak form.

Assumptions in Classical Shell Theories. To describe the kinematic assumptions for shells, we need to define a reference surface, often called a midsurface. The reference surface, as the second name implies, is generally placed midway between the top and bottom surfaces of the shell. As in nonlinear beams, the exact placement of the reference surface in nonlinear shells is irrelevant.

Before developing the CB shell theory, we briefly review the kinematic assumptions of classical shell theories. Similar to beams, there are two types of kinematic assumptions, those that admit transverse shear and those that don't. The theory which admit transverse shear are called Mindlin-Reissner theories, whereas the theory which does not admit transverse shear is called Kirchhoff-Love theory. The kinematic assumptions in these shell theories are:

1. the normal to the midsurface remains straight (Mindlin-Reissner theory).
2. the normal to the midsurface remains straight and normal (Kirchhoff-Love theory)

Experimental results show that the Kirchhoff-Love assumptions are the most accurate in predicting the behavior of thin shells. For thicker shells, the Mindlin-Reissner assumptions are more accurate because transverse shear effects become important. Transverse shear effects are particularly important in composites. Mindlin-Reissner theory can also be used for thin shells: in that case the normal will remain approximately normal and the transverse shears will almost vanish.

One point which needs to be made is that these theories were originally developed for small deformation problems, and most of their experimental verification has been made for small strain cases. Once the strains are large, it is not clear whether it is better to assume that the *current normal remains straight* or that the *initial normal remains straight.* Currently, in most theoretical work, the initial normal is assumed to remain straight. This choice is probably made because it leads to a cleaner theory. We know of no experiments that show an advantage of this assumption over the assumption that the current normal remain instantaneously straight.

Degenerated Shell Methodology. In the implementation and theory of CB shell elements, the shell is modeled by a single layer of three dimensional elements, as shown in Fig. 9.11?. The motion is then constrained to reflect the modified Mindlin-Reissner assumptions.

We consider a shell element, such as the one shown in Fig. 9.11, which is associated with a three dimensional continnjum element. The parent element coordinates are ξ_i, $i = 1$ to 3; we also use the notation $\xi_1 \equiv \xi$, $\xi_2 \equiv \eta$, and $\xi_3 \equiv \zeta$. In the shell, the coordinates ξ_i are curvilinear coordinates. The midsurface is the surface given by $\zeta = 0$. Each surface of constant ζ is called a *lamina.* The reference surface is parametrized by the two curvilinear coordinates (ξ, η) or ξ_α in indicial notation (Greek letters are used for indices with a range of 2). Lines along the ζ axis are called *fibers,* and the unit vector along a fiber is called a *director.* These definitions are analogous to the corresponding definitions for beams given previously.

In the CB shell theory, the major assumptions are the modified Mindlin-Reissner kinematic assumption and the plane stress assumption:

1. fibers remain straight;
2. the stress normal to the midsurface vanishes.

Often it is assumed that the fibers are inextensional but we omit this assumption. These assumptions differs from those of classical Mindlin-Reissner theory in that the rectilinear constraint applies to fibers, not to the normals. This modification is chosen because, as in beams, the Mindlin-Reissner kinematic assumption cannot be imposed exactly in a CB element with C^0 interpolants. In models based on the modified Mindlin-Reissner theory, the nodes should be placed so that the fiber direction is as close as possible to normal to the midsurface.

For thin shells, the behavior of CB shells will approximate the behavior of a Kirchhoff-Love shell: normals to the midsurface will remain normal, so directors which are originally normal to the midsurface will remain normal, and the transverse shears will vanish. The normality constraint is based on physical observations, and even when this constraint is not imposed on a numerical model, the results will tend towards this behavior for thin shells.

We will consider shells where the deformations are large enough so that the thickness may change substantially with deformation. The thickness change arises from the conservation of matter, but is usually imposed on the model through the constitutive equations, which reflect the conservation of matter. In order to model the thickness change exactly, it is necessary to integrate the thickness strains along the entire fiber. Here we present a simpler and computationally less demanding theory which only accounts for a linear variation of the thickness strain through the depth of the shell. This is more accurate than theories which incorporate only the overall thickness change and is usually very accurate, since the major effect which needs to be modeled, in addition to the thickness change due to elongational straining, are the consequences of the linear bending field.

The motion of the shell is given by

$$\mathbf{x}(\xi,\eta,\zeta,t) = \mathbf{x}^M(\xi,\eta,t) + \zeta\, h^-\mathbf{p}(\xi,\eta,t) \quad \text{for } \zeta < 0 \tag{9.5.1a}$$

$$\mathbf{x}(\xi,\eta,\zeta,t) = \mathbf{x}^M(\xi,\eta,t) + \zeta\, h^+\mathbf{p}(\xi,\eta,t) \quad \text{for } \zeta > 0 \tag{9.5.1b}$$

where h^- and h^+ are the distances from the midsurface to the top and bottom surfaces along the director, respectively. The above will be written in the compact form

$$\mathbf{x} = \mathbf{x}^M + \bar{\zeta}\mathbf{x}^B \tag{9.5.2}$$

where

$$\mathbf{x}^B = \mathbf{p} \tag{9.5.2b}$$

$$\bar{\zeta} = \zeta\, h^+ \quad \text{when } \zeta > 0, \qquad \bar{\zeta} = \zeta\, h^- \quad \text{when } \zeta < 0 \tag{9.5.3}$$

In the above, $\mathbf{x}^B$ characterizes the motion due to bending; although this decomposition of the motio, it becomes more useful for other kinematic quantities.

The coordinates of the shell in the original configuration are obtained by evaluating (9.5.2) at the initial time

$$\mathbf{X}(\xi,\eta,\zeta) = \mathbf{X}^M(\xi,\eta) + \bar{\zeta}\mathbf{p}_0(\xi,\eta) = \mathbf{X}^M + \bar{\zeta}\mathbf{X}^B \tag{9.5.4}$$

where $\mathbf{p}_0 = \mathbf{p}(\xi,\eta,0)$. The displacement field is obtained by taking the difference of (9.5.2) and (9.5.4):

$$\mathbf{u}(\xi,\eta,\zeta,t) = \mathbf{u}^M + \bar{\zeta}(\mathbf{p} - \mathbf{p}_0) = \mathbf{u}^M + \bar{\zeta}\mathbf{u}^B \tag{9.5.5a}$$

where

$$\mathbf{u}^M = \mathbf{x}^M - \mathbf{X}^M \qquad \mathbf{u}^B = \mathbf{p} - \mathbf{p}_0 \tag{9.5.5b}$$

As can be seen from the above, the bending displacement field $\mathbf{u}^B$ is the difference between two unit vectors. Therefore the bending field can be described by two dependent

variables. The motion is then described by 5 dependent variables: the three translations of the midsurface, $\mathbf{u}^M = \left[u_x^M, u_y^M, u_z^M\right]$ and the two dependent variables which describe the bending displacement, $\mathbf{u}^B$, which remain to be defined.

The velocity field is obtained by taking the material time derivative of the displacement or motion, using (9.2.1) to write the rate of the director:

$$\mathbf{v}(\xi,\eta,\zeta,t) = \mathbf{v}^M(\xi,\eta,t) + \bar{\zeta}\boldsymbol{\omega}(\xi,\eta,t)\times\mathbf{p} + \dot{\bar{\zeta}}\mathbf{p} \tag{9.5.6}$$

The last term in the above represents the change in thickness of the shell. It will not be retained in the equations of motion, since it represents an insignificant inertia. But it will be used in updating the geometry, so it will effect the internal nodal forces, which depend on the current geometry. The variable $\dot{\bar{\zeta}}$ will be obtained from the constitutive equation or conservation of matter. The velocity field can also be written as

$$\mathbf{v}(\xi,\eta,\zeta,t) = \mathbf{v}^M + \bar{\zeta}\mathbf{v}^B + \dot{\bar{\zeta}}\mathbf{p} \tag{9.5.7}$$

where

$$\mathbf{v}^B = \bar{\zeta}\boldsymbol{\omega}\times\mathbf{p} \tag{9.5.8}$$

As can be seen from the above, the velocity of any point in the shell consists of the sum of the velocity of the reference plane, the bending velocity, and the velocity due to the change in thickness. The bending velocity is defined by the rotation of the director. Only the two components of the angular velocity in the plane tangent to the director **p** are relevant. The component parallel to the **p** vector is irrelevant since it causes no change in the director **p**. This component is called the *drilling component or the drill* for short.

Local and Corotational Coordinates. Three coordinate systems are defined:

1. the global Cartesian system, (x, y, z) with base vectors $\mathbf{e}_i$.
2. the corotational Cartesian coordinates $(\hat{x}, \hat{y}, \hat{z})$ with base vectors $\hat{\mathbf{e}}_i$, which are constructed so that the plane defined by $\hat{\mathbf{e}}_1(\xi,t)$ and $\hat{\mathbf{e}}_2(\xi,t)$ is tangent to the lamina As indicated, the corotational base vectors are functions of the element coordinates and time. In practice, these coordinate systems are constructed only at the quadrature points of the element, but conceptually, the corotational coordinate system is defined at every point of the shell. Several methods have been proposed for the construction of the corotational systems, and they will be described later.
3. nodal coordinate systems associated with the master nodes; they are denoted by superposed bars $\bar{\mathbf{e}}_{iI}(t)$, where the subscript the node. The nodal coordinates system is defined by

$$\bar{\mathbf{e}}_{zI}(t) = \mathbf{p}_I(t) \tag{9.5.9}$$

The orientation of the two other base vectors is described later.

Finite Element Approximation of Motion. The underlying finite element for a CB shell theory is a three-dimensional isoparametric element with $2n_N$ slave nodes. In order to meet the modified Mindlin-Reissner assumption, the continuum element may have at most two slave nodes along any fiber. As a consequence of this restriction, the motion will be linear in ζ. The description is Lagrangian and either an updated or total Lagrangian formulation can be employed. We will emphasize the updated Lagrangian formulation, but remind the reader that in the updated Lagrangian formulation the strain can be described by the Green strain tensor and the PK2 stress when it is advantageous for a particular constitutive law. Moreover any updated Lagrangian formulation can easily be changed to a Lagrangian formulation by a transformation of stresses and change in the domain of integration.

The formulation may have either 5 or 6 degrees of freedom per master node. We will emphasize the 5 degree-of-freedom formulations and discuss the relative merits later. The degrees of freedom in the 5 degree-of-freedom formulation are

$$\mathbf{v}_I = \left[v_{xI},\ v_{yI},\ v_{zI},\ \bar{\omega}_{xI},\ \bar{\omega}_{yI} \right]^T \tag{9.5.9b}$$

the $\bar{\omega}_{zI}$ component, the drilling angular velocity component, has been omitted; see (9.5.9) for the definition of the nodal coordinate system. The nodal forces are conjugate to the nodal velocities in the sense of power, so they are given by

$$\mathbf{f}_I = \left[f_{xI},\ f_{yI},\ f_{zI},\ \bar{m}_{xI},\ \bar{m}_{yI} \right]^T \tag{9.5.9c}$$

At the intersections of the slave nodal fibers with the reference surface, we define master nodes as shown in Fig. 9.7. The finite element approximation to the motion in terms of the motion of the slave nodes is

$$\mathbf{x}\left(\xi^e, t\right) \equiv \varphi^h\left(\xi^e, t\right) = \sum_{\bar{I}=1}^{2n_N} \mathbf{x}_{\bar{I}}(t) N_{\bar{I}}\left(\xi^e\right) = \sum_{I^+=1}^{n_N} \mathbf{x}_{I^+}(t) N_{I^+}\left(\xi^e\right) + \sum_{I^-=1}^{n_N} \mathbf{x}_{I^-}(t) N_{I^-}\left(\xi^e\right) \tag{9.5.10}$$

where $N_{\bar{I}}\left(\xi^e\right)$ are standard isoparametric, three dimensional shape functions and ξ^e are the parent element coordinates. Recall that in a Lagrangian element, the element coordinates can be used as surrogate material coordinates. The above gives the motion for a single element; the assembly of element motions to obtain the motion of the complete body is standard.

Two notations are used for the slave nodes: nodal indices with superposed bars, which refer to the original node numbers of the underlying three dimensional element and node numbers with plus and minus superscripts, which refer to the master node numbers. Nodes I^+ and I^- are, respectively, the slave nodes on the top and bottom surfaces of the fiber which passes through master node *I.*

The velocity field of the underlying continuum element is given by

$$\mathbf{v}\left(\xi^e,\ t\right) = \frac{\partial \varphi^h\left(\xi^e,\ t\right)}{\partial t} = \sum_{\bar{I}=1}^{2n_N} \dot{\mathbf{x}}_{\bar{I}}(t) N_{\bar{I}}\left(\xi^e\right) \tag{9.5.12}$$

where $\dot{\mathbf{x}}_I$ is the velocity of slave node *I*. To achieve a velocity field compatible with (9.5.6), the velocity of the slave nodes is given in terms of the translational velocities of the master nodes $\mathbf{v}_I^M = \left[v_{xI}^M, v_{yI}^M, v_{zI}^M\right]^T$ and the angular velocities of the director $\omega_I = \left[\bar{\omega}_{xI}, \bar{\omega}_{yI}\right]^T$ by

$$\mathbf{v}_{I^+} = \mathbf{v}_I^M + h^+ \omega_I \times \mathbf{p}_I - \dot{h}_I^+ \mathbf{p}_I \qquad \mathbf{v}_{I^-} = \mathbf{v}_I^M + h_I^- \omega_I \times \mathbf{p}_I + \dot{h}_I^- \mathbf{p}_I \tag{9.5.13}$$

$$h = \int_0^1 h_0 F_{\zeta\zeta}\, d\zeta$$

where $\dot{h}_I^+$ and $\dot{h}_I^-$ are the velocities of slave nodes I^+ and I^- in the direction of the director, respectively. These are obtained from integrating the through-the thickness strains obtained from the constitutive equation because of the plane stress assumption, as described later. They are omitted in the formulation of the equations of motion, for neither momentum balance nor equilibrium is enforced in the direction of $\mathbf{p}$.

The relationship between the slave and master nodal velocities for each triplet of nodes along a fiber can then be written in matrix form as

$$\begin{Bmatrix} \bar{\mathbf{v}}_{I^+} \\ \bar{\mathbf{v}}_{I^-} \end{Bmatrix} = \mathbf{T}_I \bar{\mathbf{v}}_I \qquad \text{no sum on } I \tag{9.5.14}$$

where the vector have been expressed in the nodal coordinate system of the master node for convenience. For a 5 degree of freedom per node formulation

$$\bar{\mathbf{v}}_{I^+} = \left[\bar{v}_{xI},\ \bar{v}_{yI^+},\ \bar{v}_{zI^+}\right]^T \qquad \bar{\mathbf{v}}_{I^-} = \left[\bar{v}_{xI^-},\ \bar{v}_{yI^-},\ \bar{v}_{zI^-}\right]^T \tag{9.5.15}$$

$$\bar{\mathbf{v}}_I = \left[\bar{v}_{xI},\ \bar{v}_{yI},\ \bar{v}_{zI},\ \bar{\omega}_{xI},\ \bar{\omega}_{yI}\right] \tag{9.5.16}$$

$$\mathbf{T}_I = \begin{bmatrix} \mathbf{I}_{3\times 3} & \Lambda^+ \\ \mathbf{I}_{3\times 3} & \Lambda^- \end{bmatrix} \tag{9.5.17}$$

$$\Lambda^+ = h_I^+ \begin{bmatrix} 0 & 1 \\ -1 & 0 \\ 0 & 0 \end{bmatrix} \qquad \Lambda^- = h_I^- \begin{bmatrix} 0 & 1 \\ -1 & 0 \\ 0 & 0 \end{bmatrix} \tag{9.5.18}$$

For a 6 degree-of-freedom per master node formulation it is more convenient to write (9.5.14) in terms of global components:

$$\begin{Bmatrix} \mathbf{v}_{I^+} \\ \mathbf{v}_{I^-} \end{Bmatrix} = \mathbf{T}_I \mathbf{v}_I \qquad \text{no sum on } I \tag{9.5.19}$$

$$\mathbf{v}_{I^+} = \left[v_{xI}, v_{yI^+}, v_{zI^+} \right]^T \qquad \mathbf{v}_{I^-} = \left[v_{xI^-}, v_{yI^-}, v_{zI^-} \right]^T \tag{9.5.20}$$

$$\mathbf{v}_I = \left[v_{xI}, v_{yI}, v_{zI}, \omega_{xI}, \omega_{yI}, \omega_{zI} \right] \tag{9.5.22}$$

$$\Lambda^+ = h_I^+ \begin{bmatrix} 0 & p_z & -p_y \\ -p_z & 0 & p_x \\ p_y & -p_x & 0 \end{bmatrix} = \begin{bmatrix} 0 & z_{I+} - z_I & y_I - y_{I+} \\ z_I - z_{I+} & 0 & x_{I+} - x_I \\ y_{I+} - y_I & x_I - x_{I+} & 0 \end{bmatrix} \tag{9.5.21}$$

$$\Lambda^- = -h_I^- \begin{bmatrix} 0 & p_z & -p_y \\ -p_z & 0 & p_x \\ p_y & -p_x & 0 \end{bmatrix} = \begin{bmatrix} 0 & z_{I-} - z_I & y_I - y_{I-} \\ z_I - z_{I-} & 0 & x_{I-} - x_I \\ y_{I-} - y_I & x_I - x_{I-} & 0 \end{bmatrix} \tag{9.5.23}$$

Nodal Internal Forces. The nodal forces at the slave nodes, i.e. the nodes of the underlying continuum element, are obtained by the usual procedures for continuum elements, see Chapter 4. Of course, the plane stress assumption and computation of the thickness change must be considered in the procedures at the continuum level.

The nodal internal and external forces at the master nodes can be obtained from the slave nodal forces by Eq. (4.3.36), which using (9.5.14) gives

$$\mathbf{f}_I = \mathbf{T}_I \begin{Bmatrix} \mathbf{f}_{I^+} \\ \mathbf{f}_{I^-} \end{Bmatrix} \qquad \text{no sum on } I \tag{9.5.24}$$

where for a 6 degree-of-freedom formulation

$$\mathbf{f}_I = \left[f_{xI}, f_{yI}, f_{zI}, m_{xI}, m_{yI}, m_{zI} \right] \tag{9.5.25}$$

and $\mathbf{T}_I$ is given by (9.5.19-23). In the above, m_{iI} are the nodal moments at the master nodes.

Tangent Stiffness. The tangent stiffness matrix can be obtained from that of the underlying continuum element by the standard transformation for stiffness matrices, Section

$$\mathbf{K}_{IJ} = \mathbf{T}_I^T \overline{\mathbf{K}}_{IJ} \mathbf{T}_J \quad \text{no sum on I or J} \tag{9.5.26}$$

where $\overline{\mathbf{K}}_{IJ}$ is the tangent stiffness matrix for the continuum element.

The rate-of-deformation is computed in the corotational coordinates system with base vectors $\hat{\mathbf{e}}_i$. The equations for the rate-of-deformation in the corotational coordinates, ; are

$$\hat{D}_{ij} = \frac{1}{2}\left(\frac{\partial \hat{v}_i}{\partial \hat{x}_j} + \frac{\partial \hat{v}_j}{\partial \hat{x}_i}\right)$$

The rate-of-deformation $\hat{D}_{zz}$ is computed from the conservation of mass or the condition that the normal stress $\hat{\sigma}_{zz}$ vanishes. This is discussed in more detail in Section ??.

Applying these equations to the velocity field (9.5.6-7) gives

$$\hat{D}_{xx} = \frac{\partial \hat{v}_x}{\partial \hat{x}} = \frac{\partial \hat{v}_x^M}{\partial \hat{x}} + \zeta \frac{\partial \hat{v}_x^B}{\partial \hat{x}} \approx$$

$$\hat{D}_{yy} = \frac{\partial \hat{v}_y}{\partial \hat{y}} = \frac{\partial \hat{v}_y^M}{\partial \hat{y}} + \zeta \frac{\partial \hat{v}_y^B}{\partial \hat{y}} \approx$$

$$\hat{D}_{xy} = \frac{1}{2}\left(\frac{\partial \hat{v}_x}{\partial \hat{y}} + \frac{\partial \hat{v}_y}{\partial \hat{x}}\right) = \frac{1}{2}\left(\frac{\partial \hat{v}_x^M}{\partial \hat{y}} + \frac{\partial \hat{v}_y^M}{\partial \hat{x}}\right) + \frac{1}{2}\zeta\left(\frac{\partial \hat{v}_x^B}{\partial \hat{y}} + \frac{\partial \hat{v}_y^B}{\partial \hat{x}}\right) =$$

$$\hat{D}_{xz} = \frac{1}{2}\left(\frac{\partial \hat{v}_x}{\partial \hat{z}} + \frac{\partial \hat{v}_z}{\partial \hat{x}}\right) = \frac{1}{2}\left(\frac{\partial \hat{v}_y^M}{\partial \hat{x}} + \zeta \frac{\partial \hat{v}_y^B}{\partial \hat{x}}\right) =$$

In deriving the above, we have used the fact that the tangent plane to the lamina is coincident with the $\hat{x}, \hat{y}$ plane, so functions of ξ and η are independent of $\hat{z}$. The above equations are very similar to the equations we derived for a plate, Exercise ??. However, it is implicit in Eqs.(??) that the $\hat{x}, \hat{y}$ plane is constructed so that it is tangent to the lamina which passes through the point at which the rate-of-deformation is evaluated. As a consequence additional terms appear in the actual rate-of-deformation fields; these are explored in Example ???.

The $\hat{D}_{xx}$, $\hat{D}_{yy}$ and $\hat{D}_{xy}$ components of the rate-of-deformation consist of a membrane part that is constant through the depth of the shell and a bending part which varies linearly through the depth of the shell. The transverse shears $\hat{D}_{xz}$ and $\hat{D}_{yz}$ are constant through the thickness. This characteristic of the transverse shears does not agree with actual behavior of shells and is dealt with in many cases by a shear correction factor.

Discrete momentum equation. The discrete equations for the shell are obtained via the principle of virtual power. As mentioned before, the only difference in the way the principle of virtual power is applied to a shell element is that the kinematic constraints are taken into account. We will use the same systematic procedure as before of identifying the virtual power terms by the physical effects from which they arise and then developing corresponding nodal forces. The main difference we will see is that in the shell theory nodal moments arise quite naturally, so we will treat the nodal moments separately. If the angular velocity and the director are expressed in terms of shape functions, the product of shape functions will not be compatible with the reference

continuum element and the result will not satisfy the reproducing conditions for linear polynomials.

Inconsistencies and Idiosyncrasies of Structural Theories. The introduction of both the Mindlin-Reissner and Kirchhoff-Love assumptions introduces several inconsistencies into the resulting theory. In the Mindlin-Reissner theory, the shear stresses $\hat{\sigma}_{xz}$ and $\hat{\sigma}_{yz}$ are constant through the depth of the shell. However, unless a shear traction is applied to the top or bottom surfaces, the transverse shear must vanish at these surfaces because of the symmetry of the stress tensor. Furthermore, a simple analysis of the requirements of equilibrium in a beam shows that the transverse shear stress are quadratic through the depth of a beam, vanishing at the top and bottom surfaces. Therefore a constant shear stress distribution overestimates the shear energy . A correction factor, knownas a shear correction, is often used on the transverse shear to reduce the energy associated with it, and accurate estimates of this factor can be made for elastic beams and shells. For nonlinear materials, however, it is difficult to estimate a shear correction factor.

The inconsistency of Kirchhoff-Love theory is even more drastic, since the kinematic assumption results in a vanishing transverse shear. In a beam, it is well known in structural theories that the shear must be nonzero if the moment is not constant. Thus the Kirchhoff-Love kinematic assumption is quite inconsistent with equilibrium. Nevertheless, comparison with experiments shows that it is quite accurate, and for thin, homogeneous shells it is more effective and just as accurate as the Mindlin-Reissner theory. Transverse shear simply does not play an important role in the deformation of thin structures, so its inclusion has little effect, but Mindlin-Reissner theories are nevertheless used in finite elements because of the simplicity of the CB shell approach.

The use of the modified Mindlin-Reisner CB models pose additional possibilities for severe errors. If the directors are not normal to the midsurface, the motion deviates markedly from the motion which has been verified experimentally for thin and thick beams and shells. Bathe shows results for CB shells elements modeling a frame with a right angle corner which are at least reasonable. However, when a right angle is included in the model, the assumption that the fiber direction be near to the normal to the midsurface obviously no longer holds. In view of this, it would be foolhardy to use CB elements without modifying the construction of the director in the vicinity of sharp corners.

The zero normal stress, i.e. the plane stress, assumption is also inconsistent when a normal traction is applied to either surface of the shell. Obviously, the normal stress must equal the applied normal traction for equilibrium. However, it is neglected in structural theories because it is much smaller than the axial stresses, so the energy associated with it is much smaller and it has little effect on the deformation.

Another effect of which the analyst should remain aware is boundary effects in shells. Certain boundary conditions result in severe edge effects where the behavior changes dramatically in a narrow boundary layer. The standard boundary conditions also can result in singularities at corners, (MORE DETAIL)

An important reason for using the structural kinematic assumptions is that they improve the conditioning of the discrete equations. If a shells is modeled with three-dimensional continuum elements, the degrees of freedom are the translations at all of the nodes. The mode associated with through-the-thickness velocity strains $\hat{D}_{zz}$ then has very large eigenvalues, so the conditioning of the equations is very poor. The conditioning of shell

equations is also not as good as that of standard continuum models, but it is substantially better than that of continuum models of thin shells.

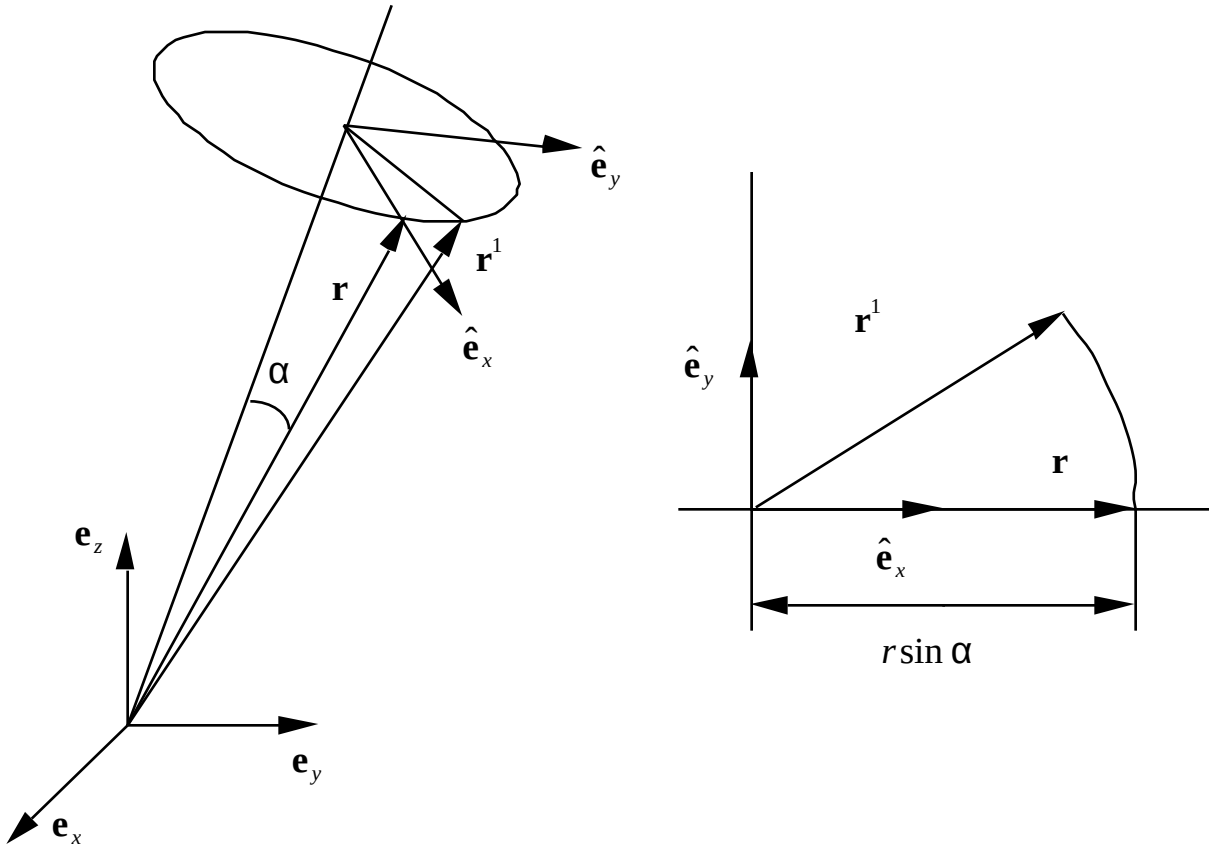

Fig. 9.?? Rotation of a vector $\mathbf{r}$ viewed as a rotation about a fixed axes $\theta = \theta \mathbf{e}$ according to Euler's theorem; on the right a top view along the θ axis is shown.

9.6. LARGE ROTATIONS

The treatment of large rotations in three dimensions for shells and beams is described in the following. This topic has been extensively explored in the literature on large displacement finite element methods and multi-body dynamics, Shabana (). Large rotations are usually treated by Euler angles in classical dynamics texts. However, Euler angles are nonunique for certain orientations and lead to awkward equations of motion. Therefore alternative techniques which lead to cleaner equations are usually employed. In addition, in 5 degree-of-freedom shells formulations, the rotation should be treated as two dependent variables. These factors are discussed in the following.

Euler's Theorem and Exponential Map. The fundamental concept in the treatment of large rotations is the theorem of Euler. This theorem states that in any rigid body rotation there exists a line which remains fixed, and the body rotates about this line This formula enables the development of general formulas for the rotation matrix: some special cases which will be described here are the Rodrigues formulas and the Hughes-Winget update. other techniques are quaternion, Cardona and Geradin().

The fundamental equation which evolves from Euler's theorem is the rotation formula which relates the components of a vector $\mathbf{r}$ in a rigid body which is rotated about the axis θ. The vector after the rotation is denoted by $\mathbf{r}'$ as shown in Fig. 9.?. The objective then is to obtain a rotation matrix $\mathbf{R}$ so that

$$\mathbf{r}' = \mathbf{R}\mathbf{r} \tag{9.6.1}$$

The nomenclature to be used is shown in Fig. ?, where the line segment about which the body rotates is denoted by the unit vector $\mathbf{e}$. We will first derive the formula

$$\mathbf{r}' = \mathbf{r} + \sin\theta\, \mathbf{e}\times\mathbf{r} + (1-\cos\theta)\mathbf{e}\times(\mathbf{e}\times\mathbf{r}) \tag{9.6.2}$$

The schematic on the right of Fig. ? shows the body as viewed along the $\mathbf{e}$ axis. It can be seen from this schematic that

$$\mathbf{r}' = \mathbf{r} + \mathbf{r}_{PQ} = \mathbf{r} + \alpha\, \sin\theta\mathbf{e}_2 + \alpha(1-\cos\theta)\mathbf{e}_3 \tag{9.6.3}$$

where $\alpha = r\sin\varphi$. From the definition of the cross product it follows that

$$\alpha\mathbf{e}_2 = r\sin\varphi\mathbf{e}_2 = \mathbf{e}\times\mathbf{r}, \quad \alpha\mathbf{e}_3 = r\sin\varphi\mathbf{e}_3 = \mathbf{e}\times(\mathbf{e}\times\mathbf{r}) \tag{9.6.4}$$

Substituting the above into () yields Eq. ().

We now develop a matrix so that (??) can be written in the form of a matrix multiplication. For this purpose, weuse the same scheme as in (3.2.35) to define a skew-symmetric tensor $\Omega(\theta)$ so that

$$\Omega(\theta)\mathbf{r} = \theta\times\mathbf{r} \tag{9.6.5}$$

In other words, we define a matrix $\Omega(\theta)$ that has the same effect on $\mathbf{r}$ as the cross product with θ. Recall from (3.2.35) that the skew-symmetric tensor equivalent to a cross product with a vector can be obtained by defining $\Omega(\theta)$ by $\Omega_{ij}(\theta) = e_{ijk}\theta_k$ where e_{ijk} is the alternator tensor. From this definition of the $\Omega(\theta)$ matrix it follows that

$$\Omega(\mathbf{e})\mathbf{r} = \mathbf{e}\times\mathbf{r}, \quad \Omega^2(\mathbf{e})\mathbf{r} = \Omega(\mathbf{e})\Omega(\mathbf{e})\mathbf{r} = \mathbf{e}\times(\mathbf{e}\times\mathbf{r}) \tag{9.6.6}$$

Comparing the above terms with (), it can be seen that (??) can be written as

$$\mathbf{r}' = \mathbf{r} + \sin\theta\,\Omega(\mathbf{e})\mathbf{r} + (1-\cos\theta)\Omega^2(\mathbf{e})\mathbf{r} \tag{9.6.7}$$

so that comparison with () shows that

$$\mathbf{R} = \mathbf{I} + \sin\theta\,\Omega(\mathbf{e}) + (1-\cos\theta)\Omega^2(\mathbf{e}) \tag{9.6.8}$$

In writing the rotation matrix, it is often useful to define a vector θ along the axis of rotation $\mathbf{e}$ with length θ, the angle of rotation. The vector θ is sometimes called a pseudovector because sequential rotations cannot be added as vectors to obtain the final

rotation, i.e. if the pseudovector θ_{12} corresponds to the rotation θ_1 followed by the rotation θ_2 then $\theta_{12} \neq \theta_{21}$. This property of rotations is often illustrated in introductory physics texts by rotating an object such as a book 90 degrees about the x-axis followed by a 90 degree rotation about the y-axis and comparing this with a 90 degree rotation about the y-axis followed by a 90 degree rotation about the x-axis.

An important way to describe rotation is the *exponential map*, which gives the rotation matrix **R** by

$$\mathbf{R} = exp\left(\Omega(\theta)\right) = \sum_n \frac{\Omega^n(\theta)}{n!} = \mathbf{I} + \Omega(\theta) + \frac{\Omega^2(\theta)}{2} + \frac{\Omega^3(\theta)}{6} + ... \tag{9.6.9}$$

This form of the rotation matrix can be used to obtain accurate approximation to the rotation matrix for small rotations. To develop the exponential map from (9.6.8) we note that the matrix $\Omega(\theta)$ satisfies the following recurrence relation

$$\Omega^{n+1}(\theta) = -\theta\Omega^n(\theta) \tag{9.6.10}$$

This relationship can be obtained easily by using the interpretation of $\Omega(\theta)$ as a matrix which replicates the cross-product as given in Eq. (9.6.5) and that it scales with θ. The trigonometric functions $sin\theta$ and $cos\theta$ can be expanded in Taylor's series

$$sin\theta = \theta - \frac{\theta^3}{3!} + \frac{\theta^5}{5!} - ..., \qquad cos\theta = 1 - \frac{\theta^2}{2!} + \frac{\theta^4}{4!} - ... \tag{9.6.11}$$

yielding (9.6.9).

9.7. SHEAR AND MEMBRANE LOCKING

Among the most troublesome characteristics of shell elements are shear and membrane locking. Shear locking results from the spurious appearance of transverse shear in deformation modes that should be free of transverse shear. More precisely, it emanates from the inability of many elements to represent deformation modes in which the transverse shear should vanish. Since the shear stiffness is often significantly greater than the bending stiffness, the spurious shear absorbs a large part of the energy imparted by the external forces and the predicted deflections and strains are much too small, hence the name shear locking.

The observed behavior of thin beams and shells indicates that the normals to the midline remain straight and normal, and that hence the transverse shears vanish. This behavior can be viewed as a constraint on the motion of the continuum. While the normality constraint is not exactly enforced in the shear-beam or CB shell theories, the normality constant always appears as a penalty term in the energy. The penalty factor increases as the thickness decreases, see Example (??), so as the thickness decreases shear locking becomes more prominent. Shear locking does not appear in C^1 elements, since the motion in C^1 elements is such that the normals remain normal. In C^0 (and CB structural) elements, the normal can rotate relative to the midline, so spurious transverse shear and locking can appear.

Membrane locking results from the inability of shell finite elements to represent inextensional modes of deformation. A shell can bend without stretching: take a piece of paper and see how easily you can bend it. However stretching a piece of paper is almost impossible. Shells behave similarly: their bending stiffness is small but their membrane stiffness is large. So when the element cannot bend without stretching, the energy is incorrectly shifted to membrane energy, resulting in underprediction of displacements and strains. Membrane locking is particularly important in simulation of buckling since many buckling modes are completely or nearly inextensible.

The situation for shear and membrane locking is similar to the volumetric locking described in Chapter 8: a finite element approximation to motion cannot represent a motion in a constrained medium that satisfies the constraint, where the constraint is much stiffer than the stiffness experienced by the correct motion. In the case of volumetric locking, the constraint is incompressibility, while the in the case of shear and membrane locking the strains are the normality constraint of Kirchhoff-Love behavior and the inextensibility constraint. This is summarized in Table 9.??. It should be noted that the Kirchhoff-Love behavior of thin shells, and the counterpart in Euler-Bernoulli beams, is not an exact constraint. For thicker shells and beams, some transverse shear is expected, but just as elements that lock exhibit poor performance for nearly incompressible materials, shell elements which lock in shear perform poorly for thick shells where transverse shear is expected.

Table 9
Analogy of Locking Phenomena

Constraint	Shortcoming of finite element motion	Locking type
incompressibility isochoric motion J = constant, $v_{i,i} = 0$	volumetric strain appears in element	volumetric locking
Kirchhoff-Love constraint $\hat{D}_{xz} = \hat{D}_{yz} = 0$	transverse shear strain appears in pure bending	shear locking
Inextensibility constraint	membrane strain appears in inextensional mode	membrane locking

Shear Locking. This description of shear and membrane locking closely follows Stolarski, Belytschko and Lee ( ). To illustrate shear locking, we consider the two-node beam element described in Example 9.1; for simplicity, consider the element being along the x-axis. Since shear and membrane locking occur in linear response of beams and shells, our examination will be made in the context of linear theory. The transverse shear strain is given by

$$2\varepsilon_{xy} = \frac{1}{\ell}\left(u^M_{x2} - u^M_{x1}\right) - \theta_1(1-\xi) - \theta_2\xi \tag{9.7.1}$$

We now consider the element in a state of pure bending, where the moment $m(x)$ is constant. From the equilibrium equation, Eq. (??), the shear $s(x)$ should vanish when the

moment is constant. We now consider a specific deformation mode of the element where the moment is constant:

$$u_{x1} = u_{x2} = 0,\ \theta_1 = -\theta_2 = \alpha\ . \tag{9.7.2}$$

It is easy to verify the bending moment is constant for this element, and anyway the deformation can be seen to be a pure bending mode. For these nodal displacements, Eq. (9.7.1) gives

$$2\varepsilon_{xy} = \alpha\left(2\xi - 1\right) \tag{9.7.3}$$

Thus the transverse shear strain, and hence the transverse shear stress, are nonzero is most of the element, which contradicts the expected behavior that the transverse shear vanish in when the moment is constant.

To explain why this parasitic transverse shear has such a large effect, the energies associated with the various strains are examined for a linear, elastic beam of unit depth with a rectangular cross-section. The bending energy is the energy associated with the linear portion of the axial strains, which is given by

$$W_{bend} = \frac{E}{2}\int_\Omega y^2\theta_{,x}^2 d\Omega = \frac{Eh^3}{24}\int_0^\ell \theta_{,x}^2 dx = \frac{Eh^3}{24\ell}\left(\theta_2 - \theta_1\right)^2 = \frac{Eh^3\alpha^2}{6\ell} \tag{9.7.4a}$$

where the rotations associated with the bending mode (9.7.2) have been used in the last expression.

The shear energy for the beam is given by

$$W_{shear} = \frac{E}{(1+\nu)}\int_\Omega \varepsilon_{xy}^2 d\Omega = \frac{Eh}{(1+\nu)}\int_0^\ell \left(\theta - u_{z,x}\right)^2 dx = \frac{Eh\ell\alpha^2}{3(1+\nu)} \tag{9.7.4b}$$

The ratio of these two energies is given approximately by

$$\frac{W_{shear}}{W_{bend}} \approx \left(\frac{\ell}{h}\right)^2$$

Thus for a thin element with the length ℓ greater than the thickness h the shear energy is greater than the bending energy. Since the shear energy should vanish in pure bending, the effect of this parasitic shear energy is a significant underprediction of the total displacement. As the length of the element decreases due to mesh refinement, the ratio of shear to bending energy in each element decreases, but the convergence tends to be very slow. However, in contrast the volumetric locking, where often no convergence is observed with refinement, elements that lock in shear converge to the correct solution, but very slowly.

Equation (9.7.3) immediately suggests why underintegration can alleviate shear locking in this element: note that the transverse shear vanishes at $\xi = \frac{1}{2}$, which

corresponds to the quadrature point in one-point quadrature. Thus, the spurious transverse shear is eliminated by underintegration of the shear-related terms.

Membrane Locking. In the following, we will use linear strain displacement equations, which are only valid for small strains and rotations to explain shear and membrane locking. To illustrate membrane locking we will use the Marguerre shallow beam equation. The Marguerre equations are

$$\varepsilon_x = u^M_{x,x} + w^0_{,x} u_{z,x} - y\theta_{,x} \tag{9.7.5a}$$

$$2\varepsilon_{xy} = u_{z,x} - \theta \tag{9.7.5b}$$

It should be stressed that while these kinematic relations are different from the CB beam equations, they in fact closely approximate the CB equations for shallow beams, i.e. when $w^0(x)$ is small. The mechanical behavior predicted by the various theories for a thin beam is almost identical if the assumptions of the theories are met. For shallow beams, Marguerre theory gives very accurate results.

Consider a three-node beam element. In an inextensional mode, the membrane strain ε_x must vanish, so by integrating the expression for $u^M_{x,\,x}$ in (9.7.5a) for y=0 it follows that

$$u^M_{x3} - u^M_{x1} = -\int_0^\ell w^0_{,x} w_{,x}\, dx \tag{9.7.6}$$

Consider a beam in a pure bending mode so $\theta_1 = -\theta_3 = \alpha$. In the absence of transverse shear it follows from Eq. (9.4.5b) that

$$u_{z2} = \int_0^{\ell/2} \theta(x)\, dx = \frac{\alpha \ell^2}{4} \tag{9.7.7}$$

Consider a beam in an initially symmetric configuration, so $\theta^0_1 = \theta^0_3 = \alpha_0$, $\theta^0_2 = 0$. Then Eq. (9.7.6) is satisfied if $u_{x1} = -u_{x3} = \frac{\alpha_0 \alpha \ell}{6}$, $u_{x2} = 0$. Evaluation of the membrane strain via Eqs. (??) and (9.7.5a) then gives

$$\varepsilon_x = \alpha\alpha_0 \left(\frac{1}{3} - \xi^2 \right) \tag{9.7.8}$$

Thus, in this particular inextensional mode of deformation, the extensional strain does not vanish throughout the beam. If an element is developed with a quadrature scheme which includes quadrature points where the extensional strain does not vanish, the element will exhibit membrane locking.

The possibility of membrane locking in the three-node curved beam can also be determined by examining the orders of the displacement fields. The variables

u_x, u_y, and w^0 are quadratic, and the quadratic fields are actuated in a pure bending mode. Since $u_{x,x}$ is linear, the membrane strain Eq. (9.7.5a) cannot vanish uniformly throughout the element in a pure bending mode if W^0 is nonzero. Thus membrane locking can be said to originate from the inability of the finite element interpolant to represent inextensional motions. Shear locking can be explained similarly as the inability of finite element interpolants to represent pure bending modes.

From the preceding, an obvious remedy to membrane and shear locking would be to match the order of the interpolants of different components of the motion. For example, is a cubic field u_x would improve the representation of an inextensional mode for quadratic u_y. However, it is difficult to accomplish this within the framework of CB elements based on isoparametric elements without disturbing the element's capacity to represent rigid body motion, which is crucial for convergence.

If the element is rectilinear, w^0 vanishes and membrane locking will not occur because bending will not generate membrane strains, see Eq. (9.7.5a). Membrane locking does not occur in flat shell elements or straight beam elements. Thus, the two-node beam never exhibits membrane locking and the four-node quadrilateral shell only manifests membrane locking in warped configurations.

Shear locking in the three-node beam is less obvious than for the two-node beam. The shear strain in this element is given by

$$\begin{aligned} 2\varepsilon_{xy} = u_{z,\theta} - \theta = \frac{1}{\ell}\left[(2\xi - 1)u_{z1} - 4\xi u_{z2} + (2\xi + 1)u_{z3}\right] \\ - \tfrac{1}{2}(\xi^2 - \xi)\theta_1 - (\xi^2 - 1)\theta_2 - \tfrac{1}{2}(\xi^2 - \xi)\theta_3 \end{aligned} \tag{9.7.9}$$

Consider a state of pure bending, $\theta_1 = -\theta_3 = \alpha$, $\theta_2 = 0$, $u_{z1} = u_{z3}$ and $u_{z2} = \dfrac{\alpha\ell}{4}$. Using these nodal displacements in Eq. (9.7.9) gives a vanishing transverse shear throughout the element. However, consider nodal displacements for another bending mode in which the transverse shear should vanish, $u_z^M = \alpha\xi^3$, $\theta = u_{z,x} = \dfrac{6\alpha\xi^2}{\ell}$. According to Eq. (9.7.9)

$$2\varepsilon_{xy} = \frac{\alpha}{\ell}\left(1 - 3\xi^2\right) \tag{9.7.10}$$

so the finite element approximation gives nonzero shear.

Remarkably, the shear in Eq. (9.7.10) and the membrane strains in Eq. (9.7.8) vanish at the points $\xi = \pm 1\sqrt{3}$, which correspond to the Gauss quadrature points for two-point quadrature. These are often called the Barlow points because Barlow [53] first pointed out that at these points of an eight-node isoparametric element, if the nodal displacements are set by a cubic field, the stresses obtained via the strain-displacement equations and stress-strain laws also correspond to those obtained from a cubic displacement field. He concluded that "if the element is used to represent a general cubic displacement field, the stresses at the 2×2 Gauss points will have the same degree of

accuracy as the nodal displacements." While it is not clear whether the Barlow hypothesis applies directly to elements such as the nine-node Lagrange shell element, the serendipitous features of the Gauss quadrature points in quadratic elements are undeniable.

Although this model for membrane locking is based on the shallow shell equations, it correctly predicts the performance of elements developed by other shell theories or degenerated continuum elements. The mechanical behavior of elements is almost independent of the underlying shell theory as long as the element is shallow. Moreover, as meshes are refined, elements increasingly conform to the shallow shell hypothesis. However, the extension of these concepts and analyses to general shell elements is quite difficult, particularly when the element is not rectangular. For non-rectangular elements, the development of reduced quadrature schemes or assumed strain fields for shells which avoid both shear and membrane locking has been a challenging task which is not fully resolved for elements of quadratic order or higher.

The fact that the shear strain vanishes at the Barlow points explains the success of reduced integration as introduced by Zienkiewicz et al. [54]. When the shear strain is only sampled at the Barlow points in integrating the shear stiffness, it will not sample the spurious shear which occurs along the remainder of the beam. Similarly, the shear strain in the two-node element, (3.1.7) vanishes at $\xi = 0$. Therefore, if the shear is only sampled at this point, shear locking is avoided (see [55]).

The alleviation or complete elimination of these two locking phenomena has been a central thrust of plate and shell element research. This has not proven an easy task, particularly when combined with the goal of not permitting any spurious singular zero energy modes in the element.

9.8 ASSUMED STRAIN ELEMENTS

To circumvent the difficulties of shear and membrane locking, it is necessary to develop assumed shear and membrane strain fields which avoid spurious (or parasitic) shear and membrane strains. Shear and membrane locking can also be avoided by selective-reduced integration, but selective-reduced integration is not as successful in shells as in continua. For example, in the quadrilateral four-node shell element described in Hughes (?? p ?), the element with selective-reduced integration still possesses a spurious singular mode, the w-hourglass mode, see Belytschko and Tsay (??). Thus while selective-reduced integration provides robust elements for continua, it is not as successful for shells.

The assumed strain methods are based on mixed variational principles, such as the Hu-Washizu and the Simo-Hughes B-bar simplification. When the CB shell methodology is employed, the mixed principles can be employed in the same form as given for continua; for those who have not yet appreciated CB shell theory, one element in their attractiveness is that it eliminates for reformulating the many ingredients of continuous finite elements for shells.

The Hu-Washizu weak form is then given by

$$\delta\pi^{HW}\left(\mathbf{u},\ \bar{\sigma},\ \bar{\mathbf{D}}\right) = \int_{\Omega}\left[\delta\mathbf{D}:\bar{\sigma} - \delta\bar{\sigma}\left(\bar{V}_s\mathbf{v} - \bar{\mathbf{D}}\right)\right]d\Omega - \delta W^{ext} \tag{9.8.1}$$

where we note that $\hat{\sigma}_{zz} = 0$ because of the plane-stress assumption.

The essence of the assumed strain approach is then to design transverse shear fields and membrane strain fields so that shear and membrane locking are mitigated. This is done by eliminating the strains which are parasitic: transverse shear strains in bending and membrane strains in inextensional bending. Furthermore, these strain fields must be designed so that the correct rank of the stiffness matrix is retained to avoid spurious singular modes. In the following, we concentrate on the B-bar form of the mixed field implementation, so once the strain fields have been designed, the internal nodal forces at the slave nodes are given by

$$\{f\}^{int} = \int \overline{\mathbf{B}}^T \{\sigma\} \tag{9.8.2}$$

9.8.2. Assumed Strain Four-Node Quadrilateral. The shape functions and motion of the four-node quadrilateral shell element based on the 8-node hexahedron were given in Example ??. The objective here is to construct the shear and membrane strain fields so that locking is avoided.

The construction of the transverse shear field for the four-node quadrilateral is motivated by Eq. (9.7.3), the transverse shear distribution for a beam in bending. We examine this first for a rectangular shell element. A rectangular shell element behaves similarly to a beam, so when a bending moment is applied as shown in Figure 9.?, the transverse shear σ_{xz} should vanish. When the material is isotropic, this can be met if $\overline{D}_{xz}$ vanishes, and this can be effected by making it constant in the x-direction. So the assumed shear is taken to be

$$\overline{D}_{xz} = \alpha_1$$

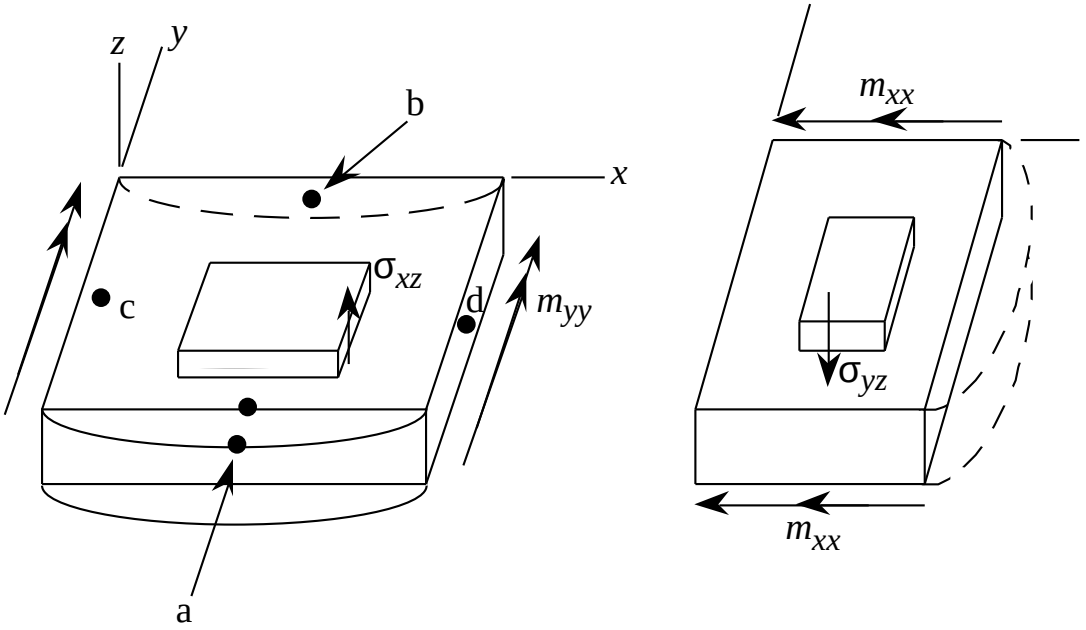

Figure 9.?. Rectangular element under pure bending showning the transverse shear which is activated, if not suppressed, by assumed strain methods.

However, a constant transverse shear leads to a rank deficiency in the element. To restore stability, a linear dependence on y is added: this extra field has no effect on the behavior on bending due to the moment m_{yy}, so the unlocking is not disturbed. So

$$\overline{D}_{xz} = \alpha_1 + \alpha_2 y$$

In the application of the Hu-Washizu weak form, the parameters would be found by the discrete compatibility equations. However, this complicates the computation of the element. Instead, the above shear fields are interpolated directly from values of the shear at selected points. In this case, the midpoints of the edges are chosen as interpolation points. The shear field is given by

$$D_{xz} = \frac{1}{2}\left(D_{xz}(\xi_a,\, t) + D_{xz}(\xi_b,\, t)\right) + \frac{1}{2} D_{xz}(\xi_a,\, t)(1-\eta) + \frac{1}{2} D_{xz}(\xi_b,\, t)(1+\eta)$$

where

$$\xi_a = \left(-\frac{1}{2},\, -1,\, 0\right) \qquad \xi_b = \left(\frac{1}{2},\, 1,\, 0\right)$$
$$\xi_c = \left(-1,\, \frac{1}{2},\, 0\right) \qquad \xi_d = \left(1,\, \frac{1}{2},\, 0\right)$$

The points are shown in Figure 9.?. We have used η instead of y since $y = 2b\eta$ in this element. By similar arguments, see Figure 9.?, the transverse shear $\overline{D}_{yz}$ is interpolated by

$$\overline{D}_{yz} = \frac{1}{2}\left(D_{yz}(\xi_c,\, t) + D_{yz}(\xi_d,\, t)\right) + \frac{1}{2} D_{yz}(\xi_c,\, t)(1-\xi) + \frac{1}{2} D_{yz}(\xi_d,\, t)(1+\xi)$$

To extend this technique to quadrilaterals, it was noted that $D_{\xi z}$ vanishes when the moment $m_{\eta\eta}$ is constant, and $D_{\eta z}$ vanishes when $m_{\xi\xi}$ is constant.

The assumed strain field given here was first constructed on the basis of physical arguments by MacNeal () an identical field was used by Hughes and Tezduyar (??); the referential interpolation was given by Wempner and Talislides (??). Dvorkin and Bathe (??) constructed the field given in the previous references on the basis of interpolation.

The basic idea is to assume the transverse shears so that under a constant movement about the η-axis, the resulting transverse shear, $D_{z\xi}$ is constant, with a similar argument for $D_{z\eta}$. The resulting shear fields are

$$\overline{D}_{z\xi}(\xi,\, \eta, \zeta,\, t) = \alpha_1 + \alpha_2 \eta \tag{9.8.5a}$$

$$\overline{D}_{z\eta}(\xi,\, \eta,\, t) = \beta_1 + \beta_2 \xi \tag{9.8.5b}$$

where α_i and β_i are arbitrary parameter. As can be seen from the above, the shear $D_{z\xi}$ has no variation in the ξ direction, so when a moment is applied about the ξ axis, the

relevant shear is constant. However, a η dependence has been added to stabilize the elment, i.e. to correct the rank. Analogous reasoning is used for the construction of the shear field $\overline{D}_{z\eta}$.

To avoid the Hu-Washizu weak form, the midpoints of the edges are chosen as interpolation. The shear fields are given by

$$\overline{D}_{z\xi}(\xi,\ \eta,\zeta,\ t)=\frac{1}{2}D_{z\xi}(0,\ -1,0,\ t)(1-\eta)+\frac{1}{2}D_{z\xi}(0,\ 1,0,\ t)(1+\eta)$$

$$\overline{D}_{z\eta}(\xi,\ \eta,\zeta,\ t)=\frac{1}{2}D_{z\eta}(-1,\ 0,0,\ t)(1-\xi)+\frac{1}{2}D_{z\xi}(1,\ 0,0,\ t)(1+\eta)$$

where $D_{z\xi}(\xi,\ \overline{\Delta},\ t)$ and $D_{z\eta}(\xi_a,\ \eta_a,0,\ t)$ are the velocity strains computed at the midpoints of the edges from the velocity field.

Assumed strain fields for the nine-node shell that avoid membrane and shear locking have been given by Huang and Hinton (1986) and Bucalem and Bathe (1993). We just briefly describe the latter.

In this scheme, the velocity strains $D_{\xi\xi}$ and $D_{\xi\xi}$ are interpolated by using the corresponding velocity strains computed at the six points shown in Figure ?? and a linear-quadratic isoparametric field, so

$$\overline{D}_{\xi\xi}\ = D_{\xi\xi}\ (\xi_I,\ \eta_J,\ 0,\ t)\ N_{IJ}(\xi,\ \eta)$$

$$\overline{D}_{\xi\zeta}\ = D_{\xi\zeta}\ (\xi_I,\ \eta_J,\ 0,\ t)\ N_{IJ}(\xi,\ \eta)$$

where $N_{IJ}(\xi,\ \eta)$ are shape functions formed by the product of Lagrange interpolants linear in ξ and quadratic in η so that

$$N_{IJ}(\xi_K,\ \eta_L)=\delta_{IK}\delta_{JL}$$

Note that the curvilinear components are interpolated, including the replacement of $D_{\xi Z}$ by $D_{\xi\xi}$; it is not clear whether the latter offers any advantage. The interpolation of $D_{\xi\xi}$ is convenient because it relates the component interpolated to the parent element coordinates, so that the stiffness of the element is independent of the orientation of the element. Although no motivation is given for the selection of the interpolation points in Bathe (1998), the beam example in the previous Section sheds some light on it: at the Gauss quadrature points $\pm 3^{-1/2}$, the transverse shear vanishes in bending and the membrane straine vanished in inextensional bending. Thus the element should not exhibit spurious transverse shears or membrane strains. The higher order interpolation in the η direction provides stability.

The velocity strains $\overline{D}_{\eta\eta}$ and $\overline{D}_{\eta\zeta}$ are interpolated with the rotated image of (??). The shear component $\overline{D}_{\xi\eta}$ is interpolated with another set of points shown in Figure 9.?.

9.9. ONE-POINT QUADRATURE ELEMENTS.

In explicit software and large scale implicit software, the most widely used shell elements are four-node quadrilaterals with one-point quadrature. Here the one-point quadrature refers to the number of quadrature points in the reference plane: actually, anywhere from three to thirty or more quadrature are used through the thickness, depending on the complexity of the nonlinear material response. Therefore, we often refer to one stack of quadrature points. The number of quadrature points is actually one only for resultant stress theories. For CB elements the motion of the element is based on eight-node hexahedron continuum element, although the description of the motion is often simplified to the four-node quadrilateral shape functions on the reference surface.

These elements are the most commonly used in large-scale analysis because they work well with diagonal mass matrices and are extremely robust. Higher order elements, such as those based on quadratic isoparametrics, converge more rapidly to smooth solutions. However, most large-scale analyses involve nonsmooth problems, with elasto-plasticity, contact-impact, etc., so the greater approximation power of higher order elements is not realizable in these problems.

Since only one stack of quadrature points are used, the element is, unless hourglass control is added, rank-deficient and unstable. Therefore, hourglass control is required to stabilize the element. In the following, the various forms of hourglass control are also described.

We will first summarize the elements which have been most frequently used in software. We then describe two of these elements in more detail, drawing on the material which precedes this to abbreviate the description.

The elements used most frequently are listed in Table X, along with some of the most prominent features and drawbacks. The earliest is the Belytschko-Tsay (BT) element, which is based on Belytschko and Tsay (1983) and Belytschko, Liu, and Tsay (1984). It is constructed by combining a flat, four-node element with a plane quadrilateral four-node membrane. As indicated in Table X, it dos not respond correctly when its configuration is warped (this shortcoming manifests itself primarily when one or two lines of elements are used to model twisted beams, as described later). However, the element is very robust and fast. Whereas most of the other elements often fail when subjected to severe distortions, the BT element seldom aborts a computation. This is highly valued in industrial settings.

The Hughes-Liu (HL) element, partially described in Hughes and Liu (1981), is CB shell element. In explicit codes, it is used with a single stack of quadrature points, so it also requires hourglass control and the techniques developed in Belytschko, Liu and Tsay (1984) are used. It is significantly slower than the BT element.

The BWC element corrects the twist, i.e., the warped configuration defect in the BT element. Otherwise, it is quite similar. In the BL element, the so-called physical hourglass control described in Chapter 8 is implemented. This hourglass control is based on a multifield variational principle, so it is theoretically possible to exactly reproduce the behavior of a fully integrated element. However, in practice this is possible only for

elastic response, since the homogeneity of the strain and stress state are crucial in obtaining closed form expressions for the physical hourglass control. Nevertheless, this form of hourglass control provides a substantial advantage; it can be increased to moderately large values without inducing locking; whereas in the BT element high values of the hourglass control parameters result in locking.

Both the BL element and the fully integrated element are afflicted with another shortcoming. In problems with large distortions, these elements fail suddenly and dramatically, aborting the simulation. So the advantage of single quadrature point elements does not reside only in their superior speed, in addition, they tend to be more robust.

The YASE element (yet another shell element) incorporates the Pian-Sumihara (1984) membrane field for improved membrane response in beam bending, i.e., for improved flexural performance, as described in Section 8.?. Otherwise, it is identical to the BT element.

The BT, BWC, and BL elements are based on a discrete Mindlin-Reissner theory which is not continuum-based. "Discrete" refers to the fact that the assumption is only applied to the motion at the quadrature point. The motion is constrained by requiring the current normal to remain straight. This can be viewed as another modification of the Mindlin-Reissner assumption in its extension to large deformations; rather than requiring the initial normal to remain straight, the current normal is required to remain straight. The effectiveness of this assumption as compared to the assumption in Section 9.8 can be judged only by comparison to experiment. The velocity in the element is given by… A corotational coordinate system is used. Although in the original papers the corotational coordinate system was aligned with $\hat{e}_x$ along $\mathbf{x}_{,\xi}$, this can lead to difficulties, so the technique descried in Section 8.?. is used.

The current configuration of the element is shown in Figure 9.?. As can be seen, $\hat{e}_z$ is always normal to the reference surface at the location of the quadrature point stack. The velocity field is given by Eq. (9.8.7) with the thickness rate dropped:

$$\mathbf{v}(\xi,\ t) = \mathbf{v}^M(\xi,\ \eta,\ t) + \bar{\zeta}\left(\omega(\xi,\ \eta,\ t) \times \tilde{\mathbf{p}}(\xi,\ \eta,\ t)\right) \tag{9.9.1}$$

where a curlicue is superimposed on the nodal director $\tilde{\mathbf{p}}_I$ to indicate that it may differs from the director as defined in Section 9.8. The finite element approximation to the motion is

$$\mathbf{v}(\xi,\ t) = \sum_{I=1}^{4} \left(v_I(t) + \bar{\zeta}\,\omega_I(t) \times \mathbf{p}_I\right) N_I(\xi,\ \eta) \tag{9.9.2}$$

Converting the cross-product to a scalar product, the above can be written

$$\mathbf{v}(\xi,\ t) = \sum_{I=1}^{4} \left(v_I(t) + \bar{\zeta}\,\Omega\,\mathbf{p}_I\right) N_I(\xi,\ \eta) \tag{9.9.2c}$$

where N_I are the four-node isoparametric shape functions.

The rate-of-deformation tensor in corotational form is

$$\{\mathbf{D}\}^T = \left\{ D_{\hat{x}\hat{x}},\ D_{\hat{y}\hat{y}},\ 2D_{\hat{x}\hat{y}},\ 2D_{\hat{x}\hat{z}},\ 2D_{\hat{y}\hat{z}} \right\} \tag{9.9.2b}$$

where $D_{\hat{z}\hat{z}}$ is omitted since it does not contribute to the power because of the plane stress condition. The components are evaluated by Eq. (3.2.39).

The rate-of-deformation is evaluated by using a linear expansion of the Jacobian J in corotational coordinate system $[\hat{x}, \hat{y}]$. It has been found that a linear expansion captures the major effects, such as twist, for thin shells. To make this expansion, the shape functions are considered in three-dimensional form. The linear expansion is of the shape function derivatives is then

$$\begin{Bmatrix} N_{I,\hat{x}} \\ N_{I,\hat{y}} \end{Bmatrix} = \begin{Bmatrix} N_{I,\hat{x}} \\ N_{I,\hat{y}} \end{Bmatrix} + \xi \begin{Bmatrix} b^c_{xI} \\ b^c_{yI} \end{Bmatrix} \tag{9.9.3}$$

where

$$\begin{Bmatrix} b^c_{xI} \\ b^c_{yI} \end{Bmatrix} = \frac{1}{J} \begin{bmatrix} p_{\hat{y},\eta} & -p_{\hat{y},\xi} \\ -p_{\hat{x},\eta} & p_{\hat{x},\xi} \end{bmatrix} \begin{Bmatrix} N_{I,\xi} \\ N_{I,\eta} \end{Bmatrix} \tag{9.9.4}$$

The director $\mathbf{p}$ is taken to be the normal in the current configuration (the director changes with time and is not the tangent to a material fiber). Setting $\mathbf{p}$ to the normal to the reference surface

$$\mathbf{p} = \frac{1}{p^*} \begin{Bmatrix} -\hat{z}^M_{,\hat{x}} \\ -\hat{z}^M_{,\hat{y}} \\ 1 \end{Bmatrix} = -\frac{1}{p^*} \sum_{I=1}^{4} \hat{z}_I \begin{Bmatrix} b_{xI} + (\xi\eta)_{,\hat{x}}\, \gamma_I \\ b_{yI} + (\xi\eta)_{,\hat{y}}\, \gamma_I \\ 1 \end{Bmatrix} \tag{9.9.5}$$

where

$$p^* = \left(1 + \hat{z}^2_{,\hat{x}} + \hat{z}^2_{,\hat{y}}\right)^{1/2} \tag{9.9.6}$$

and γ_I is the consistent hourglass operator given in Section 8.?. At the origin $(\xi\eta)_{,\hat{x}} = (\xi\eta)_{,\hat{y}} = 0$, because

$$(\xi\eta)_{,\hat{x}} = \xi\eta_{,\hat{x}} = \xi_{,\hat{x}}\eta = 0 \tag{9.9.7}$$

The director $\mathbf{p}$ is constructed normal to the $\hat{x} - \hat{y}$ plane at the origin, so from and Eq. (9.9.7), it follows that

$$\sum_{I=1}^{4} b_{xI}\hat{z}_I = \sum_{I=1}^{4} b_{yI}\hat{z}_I = 0 \tag{9.9.8}$$

Therefore, $p^* = 1$ at the origin of the reference plane, i.e. at the quadrature point.

Taking the derivatives of $p_{\hat{x}}$ and $p_{\hat{y}}$ with respect to ξ and η (and neglecting the terms related to $p_{,\xi}$ and $p_{,\eta}$, which can be shown to be small) gives

$$p_{\hat{x},\xi} = -\hat{z}_{,\hat{x}\xi} = -z_\gamma \eta_{,\hat{x}} \tag{9.9.9}$$

$$p_{\hat{x},\eta} = -\hat{z}_{,\hat{x}\eta} = -z_\gamma \xi_{,\hat{x}} \tag{9.9.10}$$

$$p_{\hat{y},\xi} = -\hat{z}_{,\hat{y}\xi} = -z_\gamma \eta_{,\hat{y}} \tag{9.9.11}$$

$$p_{\hat{y},\eta} = -\hat{z}_{,\hat{y}\eta} = -z_\gamma \xi_{,\hat{y}} \tag{9.9.12}$$

where

$$z_\gamma = \sum_{I=1}^{4} \gamma_I \hat{z}_I \tag{9.9.13}$$

From Eq. (4.?.?)

$$\begin{bmatrix} \xi_{,\hat{x}} & \xi_{,\hat{y}} \\ \eta_{,\hat{x}} & \eta_{,\hat{x}} \end{bmatrix} = \frac{1}{J} \begin{bmatrix} \hat{y}_{,\eta} & -\hat{x}_{,\eta} \\ -\hat{y}_{,\xi} & \hat{x}_{,\xi} \end{bmatrix} = \frac{1}{4J} \begin{bmatrix} \hat{y}_\eta & -\hat{x}_\eta \\ -\hat{y}_\xi & \hat{x}_\xi \end{bmatrix} \tag{9.9.14}$$

where

$$\hat{y}_\eta = \eta^t \hat{\boldsymbol{y}} = \sum_{I=1}^{4} \eta_I \hat{y}_I \tag{9.9.15}$$

It follows from Eqs. (9.9.3) and (9.9.10-14) that

$$\begin{Bmatrix} b^c_{xI}(\mathbf{0}) \\ b^c_{yI}(\mathbf{0}) \end{Bmatrix} = \frac{z_\gamma}{16J^2} \begin{Bmatrix} \xi_I \hat{x}_{,\eta} + \eta_I \hat{x}_{,\xi}(\mathbf{0}) \\ \xi_I \hat{y}_{,\eta} + \eta_I \hat{y}_{,\xi}(\mathbf{0}) \end{Bmatrix} \tag{9.9.16}$$

$$= \frac{2z_\gamma}{A^2} \begin{bmatrix} \hat{x}_{13} & \hat{x}_{42} & \hat{x}_{31} & \hat{x}_{24} \\ \hat{y}_{13} & \hat{y}_{42} & \hat{y}_{31} & \hat{y}_{24} \end{bmatrix} \tag{9.9.17}$$

Thus, the $\mathbf{b}^c$ column vector involves the same terms as the $\mathbf{b}$ matrix given in (???).

REMARK. Method $\hat{z}$ couples curvatures to translations only for warped elements, i.e., when the nodes are not coplanar, if which case $z_\gamma \neq 0$

The corotational rate-of-deformation at the quadrature point $\xi = \eta = 0$ is then given by

$$\hat{D}_{\alpha\beta} = \hat{D}^M_{\alpha\beta} + \bar{\xi}\,\kappa_{\alpha\beta} \tag{9.9.18}$$

where the membrane components of the rate of deformation are

$$\hat{D}^M_x = \frac{1}{2A}\left(\hat{y}_{24}\hat{\upsilon}_{x13} + \hat{y}_{13}\hat{\upsilon}_{x42}\right) \tag{9.9.19a}$$

$$\hat{D}^M_y = \frac{1}{2A}\left(\hat{x}_{42}\hat{\upsilon}_{y13} + \hat{x}_{13}\hat{\upsilon}_{y24}\right) \tag{9.9.19b}$$

$$2\hat{D}^M_{xy} = \frac{1}{2A}\left(\hat{x}_{42}\hat{\upsilon}_{x13} + \hat{x}_{13}\hat{\upsilon}_{x24} + \hat{y}_{24}\hat{\upsilon}_{y13} + \hat{y}_{31}\hat{\upsilon}_{y24}\right) \tag{9.9.19c}$$

The curvatures are given by

$$\kappa_x = \frac{1}{2A}\left(\hat{y}_{24}\hat{\omega}_{y13} + \hat{y}_{31}\hat{\omega}_{y42}\right) + \frac{2z_\gamma}{A^2}\left(\hat{x}_{13}\hat{\upsilon}_{x13} + \hat{x}_{42}\hat{\upsilon}_{x24}\right) \tag{9.9.20a}$$

$$\kappa_y = -\frac{1}{2A}\left(\hat{x}_{42}\hat{\omega}_{x13} + \hat{x}_{13}\hat{\omega}_{x24}\right) + \frac{2z_\gamma}{A^2}\left(\hat{y}_{13}\hat{\upsilon}_{y13} + \hat{y}_{42}\hat{\upsilon}_{y24}\right) \tag{9.9.20b}$$

$$\begin{aligned} 2\kappa_{xy} = {} & \frac{1}{2A}\left(\hat{x}_{42}\hat{\omega}_{y13} + \hat{x}_{13}\hat{\omega}_{y24} - \hat{y}_{24}\hat{\omega}_{x13} + \hat{y}_{31}\hat{\omega}_{x24}\right) \\ & + \frac{2z_\gamma}{A^2}\left(\hat{x}_{13}\hat{\upsilon}_{y13} + \hat{x}_{42}\hat{\upsilon}_{y24} + \hat{y}_{13}\hat{\upsilon}_{x13} + \hat{y}_{42}\hat{\upsilon}_{x24}\right) \end{aligned} \tag{9.9.20c}$$

The last terms in the curvature expressions would not vanish in an arbitrary coordinate system for a rigid body rotation. However, for the coordinate system used here, the nodal velocities $\hat{\upsilon}_x$ and $\hat{\upsilon}_y$ are proportional to $z_\gamma \mathbf{h}$ in rigid body rotation and it can be shown that the curvatures vanish for rigid body rotation.

The hourglass strain rates are computed as in [2]; some modifications are needed to exactly satisfy the patch test. The transverse shear velocity strains are computed as described in the previous section. The stresses $\hat{\sigma}$ and the hourglass stresses Q^M_1, Q^M_2, Q^B_1, Q^B_2, and Q^B_3 are then computed by the constitutive equation. The nodal force expressions then emanate from the transpose of the kinematic relations.

If the corotational coordinate system $\hat{x}_1$, $\hat{x}_2$ is updated according to the spin as described in [2], the rate of the stress corresponds to the Green-Naghdi rate. The formulation thus requires a constitutive law which relates the Green-Naghdi rate to the corotational stretching tensor (13). Under these conditions, the formulation is valid for large membrane strains.

Shear Projection. To calculate the shear strains, a projection is made on the angular velocities

$$\bar{\omega}_n^a = \frac{1}{2}\left(\omega_{nI}^a + \omega_{nJ}^a\right) + \frac{1}{\ell_{IJ}}\left(\hat{\upsilon}_{zJ} - \hat{\upsilon}_{zI}\right) \tag{9.9.21}$$

where the superscript *a* refers to side *a* and the subscript *n* refers to a component normal to side *I*; see Figure 9.?. This projection leads to a transverse shear field which is identical to the MacNeal-Wempner-Bathe-Dvorkin field. The angular velocities $\bar{\omega}_{iI}$ are obtained from $\bar{\theta}_n^J$ by

$$\bar{\omega}_{\hat{x}I} = \left(\mathbf{e}_n^I \ \mathbf{e}_{\hat{x}}\right)\bar{\omega}_n^a + \left(\mathbf{e}_n^K \ \mathbf{e}_{\hat{x}}\right)\bar{\omega}_n^b \tag{9.9.24a}$$

$$\bar{\omega}_{\hat{y}I} = \left(\mathbf{e}_n^I \ \mathbf{e}_{\hat{y}}\right)\bar{\omega}_n^a + \left(\mathbf{e}_n^K \ \mathbf{e}_{\hat{y}}\right)\bar{\omega}_n^b \tag{9.9.24b}$$

where $\mathbf{e}_i$ and $\mathbf{e}_n$ are unit vectors defined in Figure 9.?.

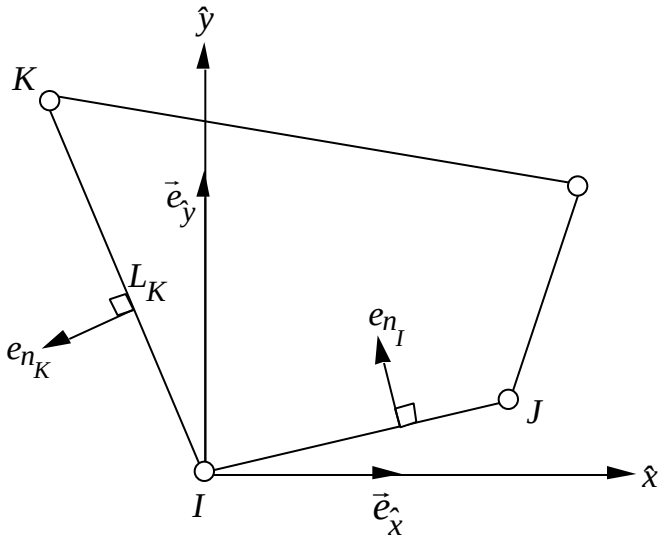

Node and side numbering

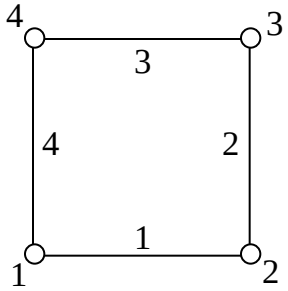

Numbering sequence

a	*J*	*K*
1	2	4
2	2	1
3	4	2
4	1	3

Figure 9.?. Numbering scheme for shear projection.

The transverse shears at the quadrature point then are given by

$$2\hat{D}_{xz} = -\sum_{I=1}^{4} N_I(\xi, \eta)\bar{\omega}_{\hat{y}I} \tag{9.9.22}$$

$$2\hat{D}_{yz} = -\sum_{I=1}^{4} N_I(\xi, \eta)\bar{\omega}_{\hat{x}I} \tag{9.9.23}$$

The transverse shears do not depend on $\hat{\upsilon}_z$, because these velocities vanish at the quadrature point.

Evaluating the resulting forms for the transverse shear at the quadrature point, $\xi = \eta = 0$, gives

$$\begin{Bmatrix} D_{xz} \\ D_{yz} \end{Bmatrix} = \sum_{I=1}^{4} [\mathbf{B}_s] \begin{Bmatrix} \hat{\upsilon}_{zI} \\ \hat{\omega}_{xI} \\ \hat{\omega}_{yI} \end{Bmatrix} \tag{9.9.25}$$

$$\mathbf{B}_I^s = \frac{1}{4} \begin{bmatrix} 2(\bar{x}_{JI} - \bar{x}_{IK}) & (\hat{x}_{JI}\bar{y}_{JI} + \hat{x}_{IK}\bar{y}_{IK}) & -(\hat{x}_{JI}\bar{x}_{JI} + \hat{x}_{IK}\bar{x}_{IK}) \\ 2(\bar{y}_{JI} - \bar{y}_{IK}) & (\hat{y}_{JI}\bar{x}_{JI} + \hat{y}_{IK}\bar{x}_{IK}) & -(\hat{x}_{JI}\bar{y}_{JI} + \hat{x}_{IK}\bar{y}_{IK}) \end{bmatrix} \tag{9.9.26}$$

$$\bar{x}_{JI} = \hat{x}_{JI} \Big/ \left(L^{JI}\right)^2, \quad \bar{y}_{JI} = \hat{y}_{JI} \Big/ \left(L^{JI}\right)^2, \quad L^{\mathrm{JI}} = \sqrt{\hat{x}_{JI}^2 + \hat{y}_{JI}^2} \tag{9.9.27}$$

Table 9.2
4-Node Quadrilateral Shell Elements

Element	Ref.	Passes Patch Test	Correct in Twist	Speed	Robustness
Belytschko-Tsay (BT)	[ ]	No	No		High
Hughes-Liu (HL)	[ ]	No	Yes		High*
Belytschko-Wong-Chang (BWC)	[ ]	No	Yes		Moderate
Belytschko-Leviathan (BL)	[ ]	Yes	Yes		Moderate to Low
YASE		No	No		Moderate
Full Quadrature MacNeal-Wempner (Bathe-Dvorkin)		Yes	Yes		Moderate to Low

References

S. Ahmad, B.B. Irons, and O.C. Zienkiewicz (1970) "Analysis of Thick and Thin Shell Structures by Curved Finite Elements," IJNME, VOL2, 419-451.

T. Belytschko, B.L. Wong and H.-Y. Chiang "Advances in one-point quadrature shell elements," Comp. Method. Applied Mechanics and Engr., Vol. 96, 93-107 (1992).

B.E. Engelmann, R.G. Whirley and G.L. Goudreau, "A Simple shell element formulation for large-scale elastoplastic analysis," Lawrence Livermore National Laboratory, Report UCRL-99677 (1989).

T. Belytschko, H. Stolarski, W.K. Liu, N. Carpenter and J.S.-J. Ong, "Stress projection for membrane and shear locking in shell finite elements," Comput. Methods Appl. Mech. Engrg., 51, 221-258 (1985).

T. Belytschko and C.S. Tsay, "A stabilization procedure for the quadrilateral plate element with one-point quadrature," Internat. J. Numer. Methods Engrg., Vol. 19, 405-419 (1981).

T. Belytschko, J.I. Lin, and C.S. Tsay, "Explicit Algorithms for the nonlinear dynamics of shells," Comput. Methods Appl. Mech. Engrg., Vol 42, 225-251 (1984).

T. Belytschko, B.I. Wong, and H.-Y. Chiang, "Advances in one-point quadrature shell elements," Comput. Methods Appl. Mech. Engrg., Vol 96, 93-107 (1992).

T. Belytschko, B.I. Wong, and H. Stolarski, "Assumed strain stabilization procedure for the 9-node Lagrange Shell element," Internat. J. Numer. Methods Engrg., Vol 28, 385-414 (1989).

M. Mucalern and K.J. Bathe, "Higher Order MITC General Shell Elements," Internat. J. Numer. Methods Engrg., Vol 36, 3729-3754 (1993).

N. Buechter and E. Ramm(1992), "Shell theory versus degenration-a comparison of large rotaion finite element analysis," IJNME, 34, 39-59, (1992).

E.N. Dvorkin and K.J. Bathe, "A Continuum mechanics based four-node shell element for general nonlinear analysis," Engrg. Comput. Vol. 1, 77-88 (1984).

B.E. Engelmann and R.G. Whirley, "A new elastoplastic shell element formulation for DYNA3D," Lawrence Livermore National Laboratory, Report UCRL-JC-104826 (1990).

J.O. Hallquist and R.G. Whirley, "DYNA3D Users manual: nonlinear dynamic analysis of structures in three dimensions, UCID-19592, Rev. 5, Lawrence Livermore National Laboratory, California (1989).

H.C. Huang and E. Hinton, "A New Nine-Node Degenerated Shell Element with Enhanced Membrane and Shear Interpolants," Internat. J. Numer. Methods Engrg., Vol 22, 73-92 (1986).

T.J.R. Hughes and W.K. Liu, "Nonlinear finite element analysis of shells: Part 1. Three-dimensional Shells," Comput. Methods Appl. Methods Engrg., Vol. 2, 419-451 (1970).

T.J.R. Hughes and W.K. Liu (1981) "Nonlinear Finite Element Analysis of Shells: Part 2, Two-dimensional Shells," CMAME, 26, pp332-362.

J.M. Jang and P.M. Pinsky, "An assumed covariant strain based nine-node shell element," Internat. J. Numer. Methods Engrg., Vol 24, 2389-2411 (1988).

K.C. Park and G.M. Stanley, "An assume covariant strain based nine-node shell element," Journal of Applied Mechanics, Vol 53, 278-290 (1987).

J.C. Simo and D.D. Fox (1989) "On a stress resultant geometrically exact shell model, Part I: Formulation and optimal parametrization," CMAME, 72, 267-304.

G.M. Stanley (1985), Continuum-Based Shell Elements," Ph.D. thesis, Stanford University.

G. Wempner, D. Talaslidis, and C.M. Hwang, "A simple and efficient approximation of shells via finite quadrilateral elements," J. Appl. Mech. ASME, Vol 49, 331-362 (1982)

H. Solarski et al review paper

LIST OF FIGURES

LIST OF TABLES

Exercise 9.?. Consider a flat plate in the x-y plane governed by the Mindlin-Reissner theory. The velocity fieldis given by

$$\mathbf{v} = z\,\omega \times \mathbf{n} = z\left(\omega_y \mathbf{e}_x - \omega_x \mathbf{e}_y\right)$$

Show that the rate-of-deformation is computed is given by

$$\hat{D}_{xx} = \frac{\partial \hat{v}_x^M}{\partial \hat{x}} + \hat{z}\frac{\partial \hat{\omega}_y}{\partial \hat{x}}, \qquad \hat{D}_{yy} = \frac{\partial \hat{v}_y^M}{\partial \hat{y}} - \hat{z}\frac{\partial \hat{\omega}_x}{\partial \hat{y}}$$

$$\hat{D}_{xy} = \frac{1}{2}\left(\frac{\partial \hat{v}_x^M}{\partial \hat{y}} + \frac{\partial \hat{v}_x^M}{\partial \hat{x}}\right) + \frac{\hat{z}}{2}\left(\frac{\partial \hat{\omega}_y}{\partial \hat{y}} - \frac{\partial \hat{\omega}_x}{\partial \hat{x}}\right)$$

$$\hat{D}_{xz} = \frac{1}{2}\left(\hat{\omega}_y + \frac{\partial \hat{v}_z^M}{\partial \hat{x}}\right), \qquad \hat{D}_{yz} = \frac{1}{2}\left(-\hat{\omega}_x + \frac{\partial \hat{v}_z^M}{\partial \hat{y}}\right)$$

$$D_{xy} = \frac{1}{2}\left(\frac{\partial v_x^M}{\partial y} + \frac{\partial v_y^M}{\partial x}\right) - \hat{z}\frac{\partial^2 v_z}{\partial x \partial y}, \qquad D_{xz} = D_{yz} = 0$$

Discrete momentum equation. The discrete equations for the shell are obtained via the principle of virtual power. As mentioned before, the only difference in the way the principle of virtual power is applied to a shell element is that the kinematic constraints are taken into account. We will use the same systematic procedure as before of identifying the virtual power terms by the physical effects from which they arise and then developing corresponding nodal forces. The main difference we will see is that in the shell theory nodal moments arise quite naturally, so we will treat the nodal moments separately. Boundary conditions in shells are often expressed in specialized forms, but we will first

If the angular velocity and the director are expressed in terms of shape functions, the product of shape functions will not be compatible with the reference continuum element and the result will not satisfy the reproducing conditions for linear polynomials. Therefore, the bending velocities $\mathbf{v}^B(\xi,\eta)$ are approximated directly.

EXAMPLE 9.?. Consider the three-node element shown, which is an application of the degenerated continuum concept to beams. The shape functions are quadratic in ξ. Develop the velocity field and the rate-of-deformation in the corotational coordinates. Give an expression for the nodal forces. If the nodes are placed at angles of 0˚, 5˚, and 10˚, what is the maximum angle between the pseudonormal *p* and the true normal to the midline?

Expand the rate-of-deformation in ξ and retain only the linear terms for an element with nodes placed along a circular arch. Compare the result with the equation.

Consider the beam element with the master nodes along the *x*-axis as shown in Figure 9.?. Develop the expression for the rate-of-deformation and compare to the Midlin-Reissner equations.

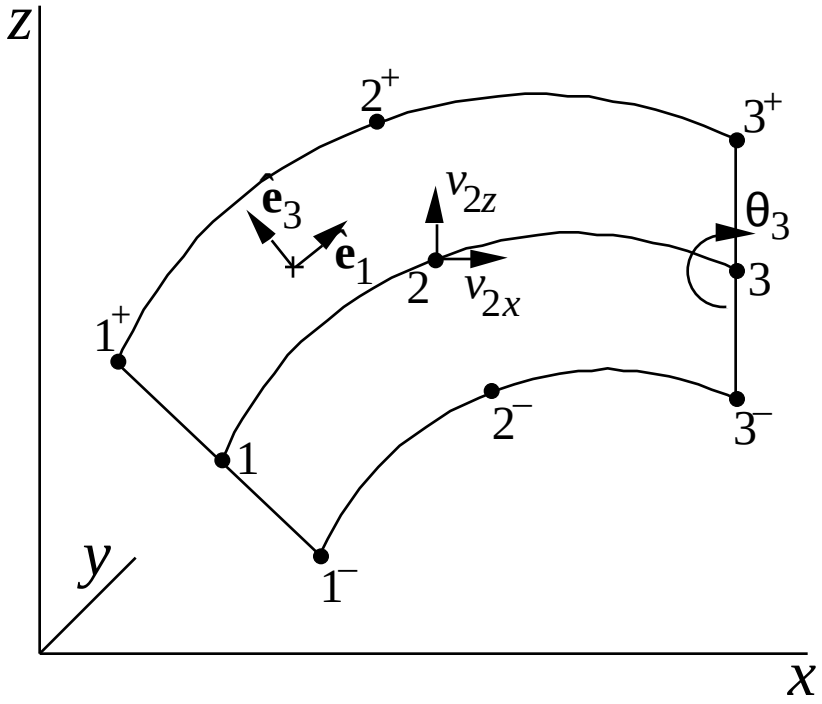

Figure 9.?.

EXERCISE. Consider the lumped mass for a rectangle.

$$\hat{\mathbf{M}} = \frac{1}{8} m \mathbf{I}_{2\times 2}$$

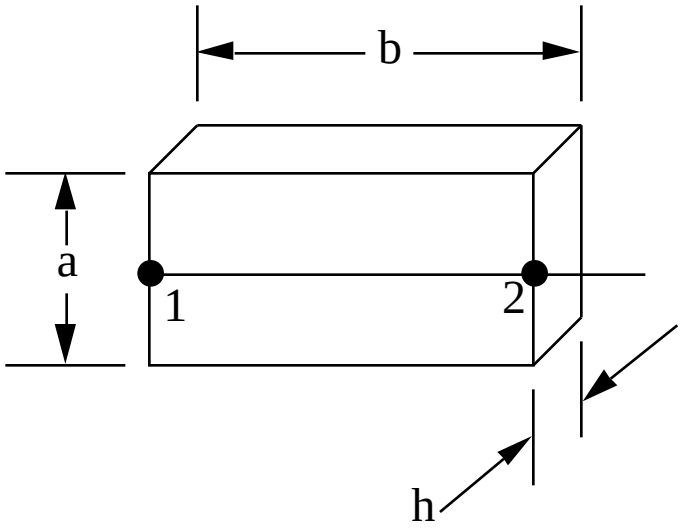

Figure 9.?.

$$m = \frac{1}{8}\rho_0 a_0 b_0 h_0$$

where ρ_0, a_0, b_0, and h_0 are the initial density and dimensions of the rectangular continuum element underlying the beam element. Using the transformation (???), develop a mass matrix and diagonalize the result with the row-sum technique.

EXERCISE. Starting with the consistent mass matrix for a rectangular continuuem element (from Przemienicki)

$$\hat{\mathbf{M}} = \begin{bmatrix} & & & & & \\ & & & & & \\ & & & & & \\ & & & & & \\ & & & & & \end{bmatrix}$$

a.) develop a consistent mass using Eq. (9.3.17), i.e. $\mathbf{M} = \mathbf{T}^T \hat{\mathbf{M}} \mathbf{T}$ for a beam element lying along the *x*-axis as shown.

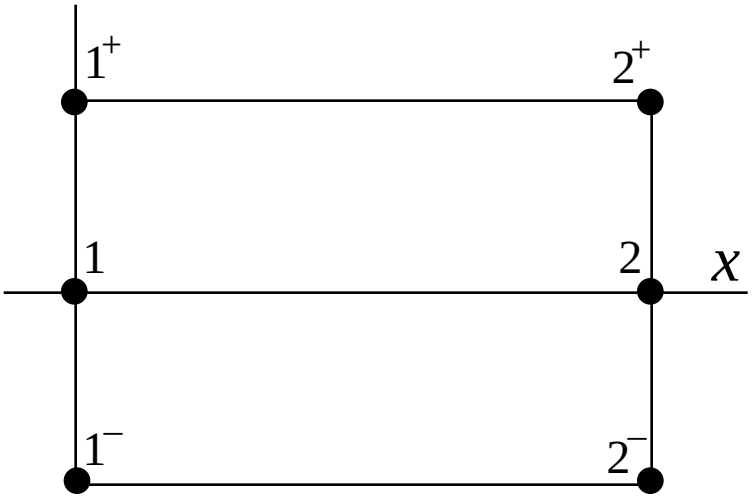

Figure 9.?

b.) develop the complete inertia term including the time-dependent term in Eq. (9.3.17).

The idea of using covariant components of velocity-strains (or strains) has already been explored in Chapter 8. It enables the assumed strain field to be tailored more precisely to arbitrarily shaped elements, independent of node numbering.

CHAPTER 10
CONTACT-IMPACT

by Ted Belytschko
Northwestern University

X.1 INTRODUCTION

This Chapter introduces the treatment of problems with contact and impact. Many problems in the simulation of prototype tests and manufacturing processes involve contact and impact. For example, in the simulation of a drop test on a product, the various parts must be separated by so-called sliding interfaces which can model contact, sliding and separation. In the simulation of manufacturing processes, sliding interfaces are also important: the modeling of the surfaces between the die and workpiece in sheet metal forming, the modeling of the tool-workpiece interface in machining, the modeling of extrusion are some examples of where sliding interfaces are needed. In crashworthiness simulation of automobiles, many components, including the engine, wheels, radiator, etc. can contact during the crash and their surfaces automatically must be treated as sliding interfaces. The treatment of impact always requires a subsequent treatment of contact, since bodies which impact will stay in contact until rarefaction waves result in release.

In this Chapter, the governing equations and finite element procedures for problems with contact-impact are introduced for Lagrangian meshes; the modeling of contact with Eulerian meshes introduces difficulties which have not been resolved yet. The governing equations for bodies in contact are identical to the equations introduced previously, except that it is necessary to add the kinetic and kinematic conditions on the contact interface. The key condition is the *condition of impenetrability:* namely, the condition that two bodies cannot interpenetrate. The general condition of impenetrability cannot be expressed as a useful equation, so several approaches to developing specialized forms of these conditions have evolved. We will consider two of these forms: a rate form which is useful for explicit dynamics methods and a form based on closest point projection; the latter is primarily useful for implicit methods. Friction is treated by both the classical Coulomb friction models and by interface constitutive models wherein the tangential tractions are developed through constitutive laws in terms of relative normal and tangential velocities of the interface.

Next, the weak forms of the governing equations are developed. Four approaches to treating the contact surface conditions are considered:

1. the Lagrange multiplier method;

2. the penalty method;

3. the augmented Lagrangian method;

4. the perturbed Lagrangian method.

The weak form for contact-impact for the Lagrange multiplier methods differs from the weak form for single bodies in that they are inequalities; they are often called weak

inequalities or variational inequalities. In penalty methods, these inequalities are incorporated by means of the Heaviside step function. It will be shown that the weak forms are equivalent to the strong forms.

The discretization of contact problems is similar to problems without contact except that in Lagrange multiplier methods, the Lagrange multiplier fields must be approximated. The Lagrange multiplier fields are constrained fields which must observe the inequality that they be nonnegative across the contact interface (the sign of the inequality depends on the structure of the weak form; the Lagrange multipliers may also be contrained to be nonpositive). These constraints on the Lagrange multiplier ultimately imply the constraint that the normal tractions be compressive. In penalty methods, the traction inequalities emerge from the Heaviside step function which is embedded in the penalty force.

Contact-impact problems are among the most difficult nonlinear problems because the response in contact-impact problems is not smooth. The velocities normal to the contact interface are discontinuous in time when impact occurs. When Coulomb friction models are used, the tangential velocities along the interface are discontinuous when stick-slip behavior is encountered. These characteristics of contact-impact problems introduce significant difficulties in the time integration of the governing equations and impair the performance of numerical algorithms. Therefore, the appropriate choice of methodologies and algorithms is crucial in the successful treatment of these problems. Techniques such as regularization are highly useful in obtaining robust solution procedures, but the analyst must understand their effect so that important aspects of the response are not eliminated.

The implementation of contact-impact for general models is quite difficult. In our discussion of implementation, we will begin with the simplest examples, one dimensional problems, which illustrate how the contact inequalities are imposed. We will then sketch some of the difficulties that arise in large-scale multidimensional problems, but we will not dwell on these since many of the approaches are based more on heuristics and computer science than computational mechanics.

X.2 CONTACT INTERFACE EQUATIONS

X.2.1. Notation and Preliminaries. Contact-impact algorithms in general purpose software can treat the interaction of many bodies, but for purposes of simplicity, we limit ourselves to two bodies as illustrated in Fig. 1. The treatment of multi-body contact is identical: the interaction of any pair of bodies is exactly like the two body problem. We have denoted the configurations of the two bodies by Ω^A and Ω^B and denote the union of the two bodies by Ω. The boundaries of the bodies are denoted by Γ^A and Γ^B. Although the two bodies are interchangeable with respect to their mechanics, it is sometimes useful to express the equations in term of one of the bodies, which is called the master; body A is designated as the master, body B as the slave. When we wish to distinguish field variables that are associated with a particular body, we append a superscript *A* or *B*; when neither of these superscripts appears, the field variable applies to the union of the two bodies. Thus the velocity field $\mathbf{v}(\mathbf{X},t)$ refers to the velocity field in both bodies, whereas $\mathbf{v}^A(\mathbf{X},t)$ refers to the velocity in body *A*.

The contact interface consists of the intersection of the surfaces of the two bodies and is denoted by Γ^c.

$$\Gamma^c = \Gamma^A \cap \Gamma^B \tag{X.2.1}$$

This contact interface consists of the two physical surfaces of the two bodies which are in contact, but since they are theoretically coincident we refer to a single interface Γ^c. In numerical solutions, the two surfaces will usually not be coincident. In those cases, Γ^c refers to the master surface. Moreover, although the two bodies may be in contact on several disjoint interfaces, we designate their union by a single symbol Γ^c. The contact interface is a function of time, and its determination is an important part of the solution of the contact-impact problem.

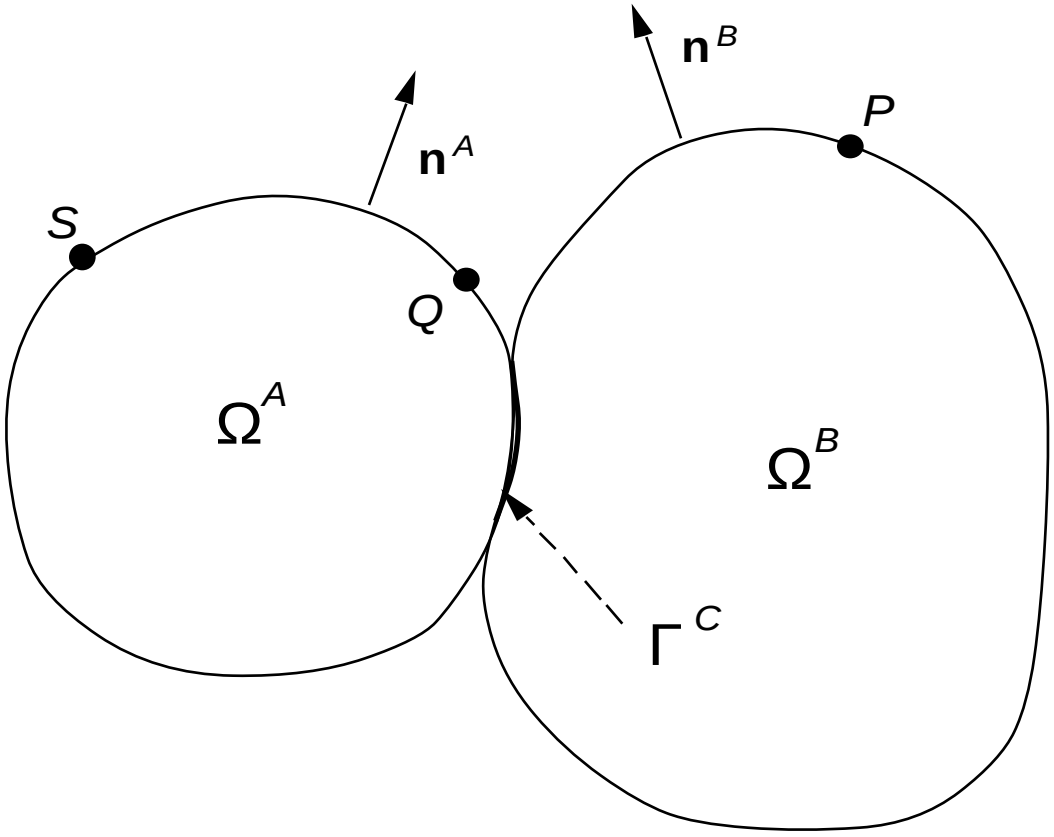

Figure 1. Model problem for contact-impact showing notation.

In constructing the equations, it is convenient to express vectors in terms of local components of the contact surface. A local coordinate system is set up at each point of the master contact surface as shown in Fig. 2. At each point, we can construct unit vectors tangent to the surface of the master body $\hat{\mathbf{e}}_1^A \equiv \hat{\mathbf{e}}_x^A$ and $\hat{\mathbf{e}}_2^A \equiv \hat{\mathbf{e}}_y^A$. The procedure for obtaining these unit vectors is identical to that used in shell elements, see Chapter 8. The normal for body *A* is given by

$$\mathbf{n}^A = \hat{\mathbf{e}}_1^A \times \hat{\mathbf{e}}_2^A \tag{X.2.2}$$

On the contact surface

$$\mathbf{n}^A = -\mathbf{n}^B \tag{X.2.3}$$

that is, the normals of the two bodies are in opposite directions.

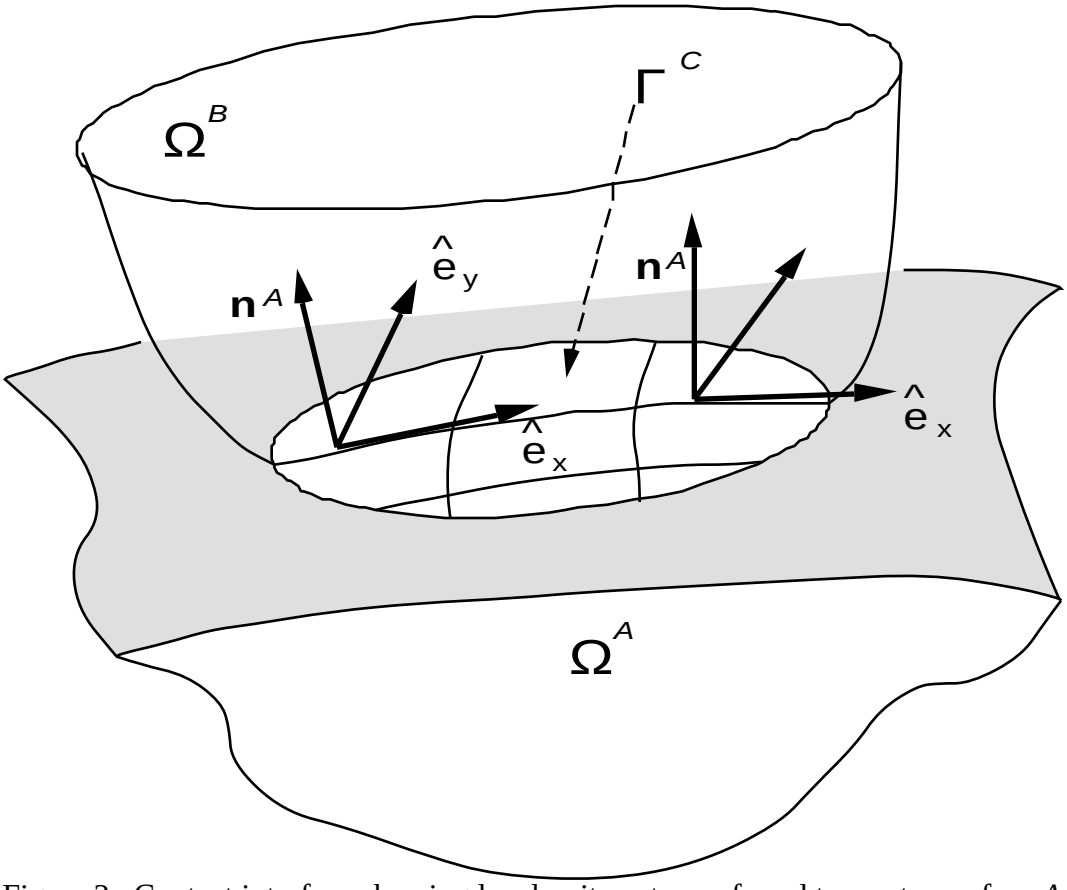

Figure 2. Contact interface showing local unit vectors referred to master surface *A*.

The velocity fields can be expressed in the local coordinates of the contact surface by

$$\mathbf{v}^A = v_N^A \mathbf{n}^A + \hat{v}_\alpha^A \hat{\mathbf{e}}_\alpha^A = v_N^A \mathbf{n}^A + \mathbf{v}_T^A \tag{X.2.4a}$$

$$\mathbf{v}^B = v_N^B \mathbf{n}^A + \hat{v}_\alpha^B \hat{\mathbf{e}}_\alpha^A = v_N^A \mathbf{n}^B + \mathbf{v}_T^A \tag{X.2.4b}$$

where the range of Greek subscripts is 2 in three dimensional problems. When the problem is two dimensional, the contact surface becomes a line, so we have a single unit vector $\hat{\mathbf{e}}_1 \equiv \hat{\mathbf{e}}_x$ tangent to this line; the range of the Greek subscripts in (4) is then one and the tangential component is a scalar. As can be seen in the above, the components are

expressed in terms of the local coordinate system of the master surface. The normal velocities are given by

$$v_N^A = \mathbf{v}^A \ \mathbf{n}^A \quad v_N^B = \mathbf{v}^B \ \mathbf{n}^A \tag{X.2.5}$$

which can easily be seen by taking the dot product of the expressions in (4) with $\mathbf{n}^A$ and using the fact that the normal is orthogonal to the unit vectors tangent to the plane $\hat{\mathbf{e}}_i^A$.

The bodies are governed by the standard field equations given in Boxes 4.1 and 5.1: conservation of mass, momentum and energy, a strain measure, and the constitutive equations. Contact adds the following conditions: the bodies can not interpenetrate and the tractions must satisfy momentum conservation on the interface. Furthermore, the normal traction across the contact interface cannot be tensile. We classify the requirements on the displacements and velocities as kinematic conditions and the requirements on the tractions as kinetic conditions.

X.2.2. Impenetrability Condition. In a multi-body problem, the bodies must observe the impenetrability condition. The impenetrability condition for a pair of bodies can be stated as

$$\Omega^A \cap \Omega^B = 0 \tag{X.2.6}$$

that is, the intersection of the two bodies is the null set. In other words, the two bodies are not allowed to overlap, which can also be viewed as a compatibility condition. The impenetrability condition is highly nonlinear for large displacement problems, and in general cannot be expressed as an algebraic or differential equation in terms of the displacements. The difficulty arises because in an arbitrary motion it is impossible to anticipate which points of the two bodies will contact. For example, in Fig. 1, if the bodies are spinning, it is possible for point *P* to contact point *Q*, whereas a different relative motion can result in contact of point *P* with point *S*. Consequently, an equation which expresses the fact that point *P* does not penetrate body *A* cannot be written except in general terms such as (6).

Because it is not feasible to express Eq. (6) in terms of the displacements, it is convenient to express the impenetrability equations in rate form or incremental form in each stage of the process. The rate form of the impenetrability condition is applied to those portions of bodies *A* and *B* which are already in contact , i.e. to those points which are on the contact surface Γ^c. It can be written as

$$\gamma_N = (\mathbf{v}^A - \mathbf{v}^B) \ \mathbf{n}^A \equiv v_N^A - v_N^B \le 0 \ on \Gamma^c \tag{X.2.7}$$

where v_N^A and v_N^B are defined in Eq. (5). Here $\gamma_N(\mathbf{X}, t)$ is the rate of interpenetration of the two bodies; see Fig. 3. The impenetrability condition (7) restricts the interpenetration rate for any points on the contact surface to be negative, i.e. Eq. (7) expresses the fact that when the two bodies are in contact, then they must either remain in contact ($\gamma_N = 0$) or they must separate ($\gamma_N < 0$). When (7) is met for all points which are in contact, the impenetrability condition is met exactly. However, the equivalence between (7) and (6) does not hold when (7) is only observed at discrete points in time as in most numerical

methods, since interpenetration is then possible for points which are close but not on the contact surface during the intervening time intervals.

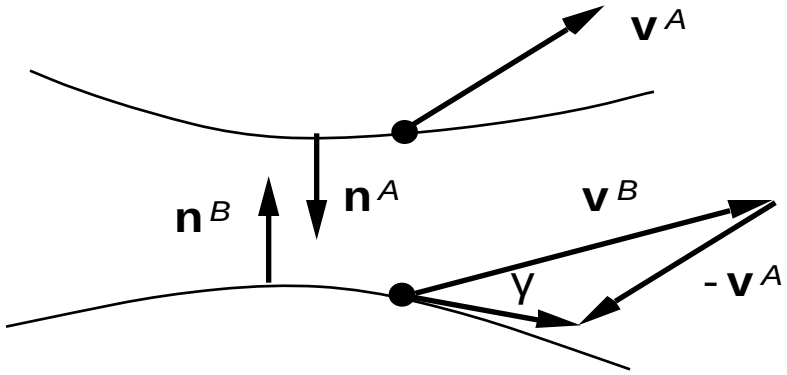

Figure 3. Nomenclature for velocities on contact surface; the same nomenclature and relations hold for incremental displacements $\Delta\mathbf{u}$ or variations $\delta\mathbf{u}$ or $\delta\mathbf{v}$; the contacting surfaces are shown separated for clarity.

Equation (7) can introduce discontinuities in the velocity time histories. Prior to contact, the normal velocities are not equal whereas subsequent to impact, the normal velocity components must observe (7). These discontinuities in time complicate the time integration of the discrete equations.

Equation (7) is useful only for point-pairs that are in contact or separated by small distances, since it defines the interpenetration rate exactly only when the two surfaces are coincident. However, it gives the correct sign on the interpenetration and is representative of the speed of relative surface motion when the gap between the two surfaces is small. When the interpentration is moderately large or used as the basis of the contact traction calculation, Eq. (7) is not recommended because the rate γ_N is not integrable and therefore depends on the path of interpenetration. Later in this Section, formulas are discussed which are applicable for moderate amounts of interpenetration .

Many authors use the quantity $-\gamma_N$ to characterize the interaction of the two bodies and call it the gap rate. The *gap rate is the negative of the interpenetration rate*; we prefer to use the term interpenetration rate. Some authors define an interpenetration but call it a gap. It may appear inconsistent to speak of an interpenetration rate when impenetrability is a fundamental condition on the solution. However, in many numerical methods, a small amount of interpenetration is allowed, and inequality (7) will not be observed exactly.

The relative tangential velocity is given by

$$\gamma_T = \hat{\gamma}_{Tx}\hat{\mathbf{e}}_x - \hat{\gamma}_{Ty}\hat{\mathbf{e}}_y = \mathbf{v}_T^A - \mathbf{v}_T^B \qquad \text{(X.2.8)}$$

The middle term is included to illustrate that the relative tangential velocity in three dimensions is a two-component vector which can be expressed in terms of the local

coordinates of each point on the contact surface. As can be seen from (8), the expression for the relative tangential velocity is similar to the expression for the normal relative velocities, Eq. (2).

X.2.3. Traction Conditions. The tractions must observe the balance of momemtum across the contact interface. Since the interface has no mass, this requires that the sum of the tractions on the two bodies vanish

$$\mathbf{t}^A + \mathbf{t}^B = 0 \qquad \text{(X.2.9a)}$$

The tractions on the surfaces of the two bodies are defined by Cauchy's law

$$\mathbf{t}^A = \sigma^A \ \mathbf{n}^A \quad or \ t_i^A = \sigma_{ij}^A n_j^A \qquad \text{(X.2.9b)}$$

$$\mathbf{t}^B = \sigma^B \ \mathbf{n}^B \quad or \ t_i^B = \sigma_{ij}^B n_j^B \qquad \text{(X.2.9c)}$$

The normal tractions are defined by

$$t_N^A = \mathbf{t}^A \ \mathbf{n}^A \quad or \ t_N^A = t_j^A n_j^A \qquad \text{(X.2.9d)}$$

$$t_N^B = \mathbf{t}^B \ \mathbf{n}^A \quad or \ t_N^B = t_j^B n_j^A \qquad \text{(X.2.9e)}$$

Note that the normal components, like all local components on the contact surface, refer to the master body. The momentum balance condition on the normal tractions can be obtained by taking a dot product of Eq. (8a) with the normal vector $\mathbf{n}^A$, which gives

$$t_N^A + t_N^B = 0 \qquad \text{(X.2.9f)}$$

We do not consider any adhesion between the contact surfaces in the normal direction, so the normal tractions cannot be tensile. We will subsequently often use the phrase that the normal tractions must be compressive, although the normal tractions can also vanish. The condition that the normal tractions cannot be tensile can be stated as

$$t_N \equiv t_N^A(\mathbf{x},t) = -t_N^B(\mathbf{x},t) \le 0 \qquad \text{(X.2.9g)}$$

The condition that the normal tractions be compressive requires t_N^B to be positive since t_N^B is the projection of the traction on body *B* onto the unit normal of *A*, which points into body *B*.

The tangential tractions are defined by

$$\mathbf{t}_T^A = \mathbf{t}^A - t_N^A \mathbf{n}^A \qquad \mathbf{t}_T^B = \mathbf{t}^B - t_N^B \mathbf{n}^A \qquad \text{(X.2.10a)}$$

so the tangential tractions are the total tractions projected on the master contact surface. Momentum balance requires that

$$\mathbf{t}_T^A + \mathbf{t}_T^B = 0 \qquad \text{(X.2.10b)}$$

The above equation can be obtained by substituting (10a) into (9a) and using (9f).

When a frictionless model of contact is used, the tangential tractions vanish:

$$\mathbf{t}_T^A = \mathbf{t}_T^B = 0 \qquad \text{(X.2.10c)}$$

We have used the phrase "frictionless model of contact" to emphasize that it is not implied that friction is absent, but rather that friction is neglected in the model because it is deemed unimportant. Subsequently we shall just say frictionless contact, but it should be understood that friction never vanishes in reality.

Although one of the bodies has been chosen as the master body in developing the preceding contact interface equations, these equations are symmetrical with respect to the bodies when the two contact surfaces are coincident and Eq. (3) is observed. Thus it does not matter which body is chosen as the master body. However, when the two surfaces are not coincident, as in most numerical solutions, then the choice of the master body changes the equations somewhat.

X.2.4. Unitary Contact Condition. Conditions (7) and (9g) can be combined into a single equation

$$t_N \gamma_N = 0 \qquad \text{(X.2.10d)}$$

which is called the *unitary contact condition.* This equation also expresses the fact that the contact forces do no work. That this condition must hold on the contact surface can be seen as follows: when the bodies are in contact and remain in contact, $\gamma_N = 0$, whereas when contact ceases, $\gamma_N \le 0$ but the normal traction must vanish, so the product always vanishes. It will also be seen that this is a Kuhn-Tucker condition when a Lagrange multiplier approach is used, for the normal traction is then equivalent to a Lagrange multiplier, and the unitary condition states that the product of the Lagrange multiplier and the constraint on the velocities vanishes.

X.2.5. Surface Description*. In penalty treatments of the contact conditions and for some interface constitutive equations, it is useful to allow a certain amount of interpenetration on the contact interface and to compute it precisely. To develop such expressions for the interpenetration, a referential description of the contact surface is used. If the reference coordinates in a three dimensional problem are $\xi \equiv (\xi_1, \xi_2, \xi_3)$, i.e. $\xi \in R^3$, then the contact surface can be described by a manifold $\zeta = (\zeta_1, \zeta_2)$ i.e. $\zeta \in R^2$. These referential coordinates will be usually element reference coordinates in FE discretizations; an example is given later. In two dimensions, $\xi \in R^2$ and $\zeta \in R^1$, so the contact surface is a curve.

The contact surface can be described by the reference coordinates of either body, but it is conventional to choose one body as the master and use the reference coordinates of the master body for the contact interface. Body A is chosen to be the master and the contact interface is described by $\mathbf{x}^A(\zeta,t)=\varphi^A(\zeta,t)$. The covariant base vectors are given by

$$\mathbf{a}_\alpha=\frac{\partial\varphi^A}{\partial\zeta^\alpha}\equiv\varphi^A_{,\alpha}\equiv\mathbf{x}^A_{,\alpha} \tag{X.2.11a}$$

In the above, the second through fourth term in (11) are different expressions for the same equation. The normal vector is given by

$$\mathbf{n}=\mathbf{a}_1\times\mathbf{a}_2/\|\mathbf{a}_1\times\mathbf{a}_2\| \tag{X.2.11b}$$

The covariant base vectors $\mathbf{a}_\alpha$ are useful primarily in derivations; they are tangent to the surface but not necessarily orthogonal nor of unit length. The variable Cartesian base vectors $\hat{\mathbf{e}}_\alpha$ are orthonormal and can be constructed from $\mathbf{a}_\alpha$ by $\mathbf{e}_1=\mathbf{a}_1/\|\mathbf{a}_1\|$, $\mathbf{e}_2=\mathbf{n}\times\mathbf{e}_1$, where $\mathbf{n}$ is given above; a better choice of $\mathbf{e}_\alpha$ is given in Chapter (Shells).

X.2.6. Interpenetration Measure. In many implementations of contact, the impenetrability condition is relaxed, i.e. a certain amount of interpenetration is permitted. When the points of two contacting areas have interpenetrated, it is useful to write the interpenetration $g_N(\zeta^\alpha,t)$ in the form of an explicit equation. We follow here the work of Wriggers(1995) and Wriggers and Miehe(1992). Consider a situation such as shown in Fig. 4, where point P has penetrated body A. The objective is to find the penetration, which is denoted by $g_N(\zeta^\alpha,t)$

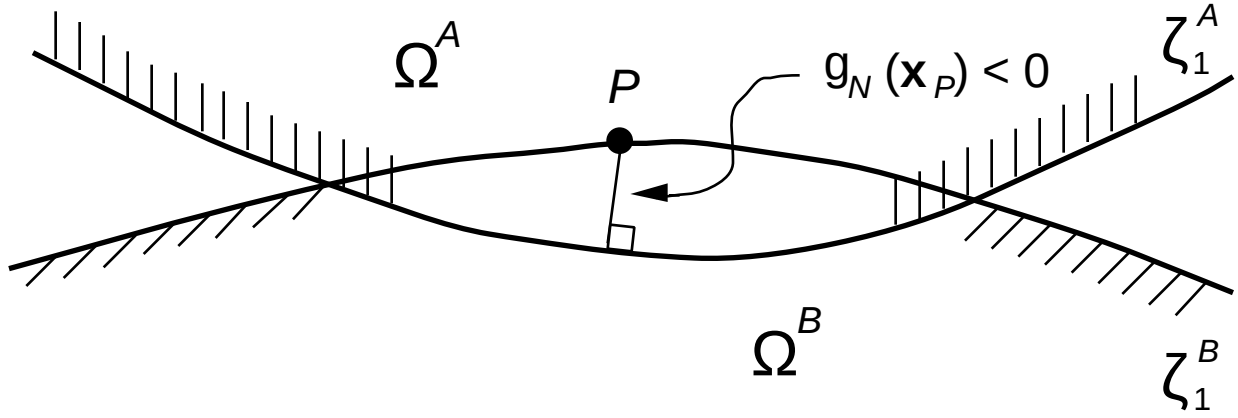

Figure 4. Interpenetration of point P on body slave$B$ defined as orthonormal projection from master body A..

The interpenetration is defined as the minimum distance from point P on body B to a point on body A. The distance between P and any point on A is given by

$$l_{AB} = \left\| \mathbf{x}^B(\zeta, t) - \mathbf{x}^A(\bar{\zeta}, t) \right\|$$
$$\equiv \left[(x^B - x^A)^2 + (y^B - y^A)^2 + (z^B - z^A)^2 \right]^{\frac{1}{2}}$$

The referential coordinates $\bar{\zeta}$ and ζ pertain to bodies *A* and *B*, respectively. The interpenetration $g_N(\zeta,t)$ is then defined as the *minimum distance* of point *P* to the surface of *A* when point *P* has penetrated body *A*:

$$g_N(\zeta,t) = \min_{\bar{\zeta}} \left\| \mathbf{x}^B(\zeta, t) - \mathbf{x}^A(\bar{\zeta}, t) \right\|$$
$$\text{if } \left[\mathbf{x}^B(\zeta, t) - \mathbf{x}^A(\bar{\zeta}, t) \right] \mathbf{n}^A \le 0 \qquad \text{(X.2.12)}$$

otherwise $g_N(\zeta,t) = 0$

According to this definition, $g_N(\zeta,t)$ is positive when interpenetration occurs and vanishes when the bodies have not interpenetrated.

To evaluate the $g_N(\zeta,t)$, the referential coordinate $\bar{\zeta}$ which minimizes the interpenetration must be found, i.e. we must find the location of the point $\mathbf{x}^A(\bar{\zeta}, t)$ on the master body which corresponds to the stationary point of the distance, so we take the derivative of l_{AB} with respect to $\bar{\zeta}$ and set the result to zero. This yields

$$\frac{\partial l_{AB}}{\partial \bar{\zeta}^\alpha} = \frac{\mathbf{x}^B(\zeta,t) - \mathbf{x}^A(\bar{\zeta},t)}{\left\| \mathbf{x}^B(\zeta,t) - \mathbf{x}^A(\bar{\zeta},t) \right\|} \frac{\partial \mathbf{x}^A(\bar{\zeta},t)}{\partial \bar{\zeta}^\alpha} \equiv \mathbf{e} \cdot \mathbf{a}_\alpha = 0 \qquad \text{(X.2.13)}$$

where $\mathbf{a}_\alpha$ is given by Eq.(11) and $\mathbf{e} = (\mathbf{x}^B - \mathbf{x}^A) / \left\| \mathbf{x}^B - \mathbf{x}^A \right\|$, so $\mathbf{e}$ is a unit vector from body *A* to body *B*. The last term in the above shows that the distance is minimum, i.e. the derivative vanishes, when $\mathbf{e}$ is orthogonal to the two tangent vectors $\mathbf{a}_\alpha$. This implies that $\mathbf{e}$ is normal to the surface of *A*. Thus $\mathbf{x}^A\left(\bar{\zeta}, t\right)$ is the orthogonal projection of the point *P* with coordinates $\mathbf{x}^B$ onto the master surface. This is a result that permeates mathematics: the shortest distance is always the orthogonal projection. The result is illustrated in Fig 4 in two dimensions. Note that when the bodies have interpenetrated, $\mathbf{e}$ is opposite to the direction of the outward pointing normal, so $\mathbf{e} = -\mathbf{n}^A$. Therefore the interpenetration $g_N(\zeta,t)$ is the distance from *P* to the surface *A* along the direction opposite to the normal of *A*. As a matter of fact, the result developed in this section is obvious from the definition: since the point corresponding to $\bar{\zeta}$ is the minimizer of the distance, it must be the orthogonal projection.

The minimizer $\bar{\zeta}$ is determined by solving the nonlinear algebraic equations (13). In three-dimensional problems, (13) involves two equation in two unknowns, in two dimensions a single equation. Once $\bar{\zeta}$ is determined, the interpenetration g_N can be found by Eq. (12).

This approach to defining the interpenetration poses difficulties when the two bodies are not smooth and locally convex. For example, in the situation shown in Fig. 5 the minimizer of l_{AB} is not unique: there are two points which are orthogonal projections of the point *P*. In these situations, it is difficult to develop schemes which lead to a uniquely defined measure of the interpenetration. Furthermore, if the discontinuous surface is the slave, the point of maximum interpenetration is not reflected in the interpenetration measure $g_N(\zeta,t)$ because the point of maximum interpenetration is not the orthogonal projection of any point on the master surface.

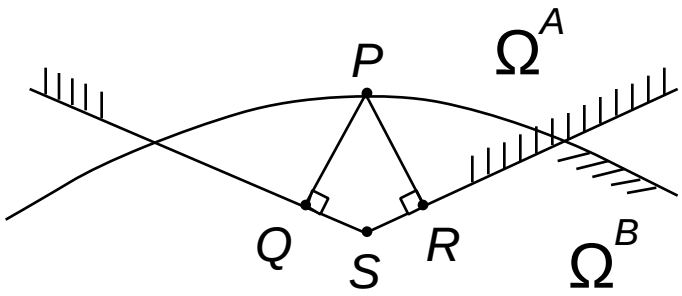

Figure 5. Penetration by a surface with a kink showing the resulting nonuniqueness of the point of orthogonal projection.

X.2.7. Path Independent Form of Interpentration Rate. In this Section, the rate of interpenetration will be developed from the interpenetration formula (12) and compared to the rate formula developed previously, Eq. (7). The rate of $g_N(\zeta,t)$ provides a path-independent measure of the interpentration rate so its derivative is integrable, in contrast to γ_N, which is not integrable. The rate $\dot{g}_N(\zeta,t)$ can be found by taking the derivative of $g_N(\zeta,t)$ in Eq. (12):

$$\dot{g}_N = \frac{d}{dt}(\min l_{AB}) = \frac{\mathbf{x}^B(\zeta,t) - \mathbf{x}^A(\bar{\zeta},t)}{\left\|\mathbf{x}^B(\zeta,t) - \mathbf{x}^A(\bar{\zeta},t)\right\|} \left(\frac{\partial \mathbf{x}^B(\zeta,t)}{\partial t} - \frac{\partial \mathbf{x}^A(\bar{\zeta},t)}{\partial t} \right) \quad \text{(X.2.14)}$$

Based on the discussion following Eq. (13), we know that the minimimum is attained when $\mathbf{x}^B - \mathbf{x}^A / \left\|\mathbf{x}^B - \mathbf{x}^A\right\|$ corresponds to the normal to body *B*. Using this fact and that $\mathbf{v}^B = \partial \mathbf{x}^B(\zeta,t) / \partial t$, the above can be rewritten as

$$\dot{g}_N = \mathbf{n}^B \left(\mathbf{v}^B - \frac{\partial \mathbf{x}^A(\bar{\zeta},t)}{\partial t} \right) \quad \text{(X.2.15)}$$

It is important to observe that $\bar{\zeta}$ is not a material coordinate, because in order to remain the closest point projection, this point moves independently of the material. Thus the second term in the parenthesis of the RHS of (15) is not a material velocity. The point can be considered an ALE point: it is neither fixed in space nor coincident with a material point. Using the concept of ALE derivatives from Section X, which is based on the chain rule, it follows that

$$\frac{\partial \mathbf{x}^A(\bar{\zeta}_\alpha, t)}{\partial t} = \mathbf{v}^A - \frac{\partial \mathbf{x}^A}{\partial \bar{\zeta}^\alpha}\frac{d\bar{\zeta}^\alpha}{dt} \equiv \mathbf{v}^A - \mathbf{x}^A_{,\alpha}\bar{\zeta}^\alpha_{,t} \tag{X.2.16}$$

Substituting (16) into (15), and using Eq. (2) it follows that

$$\dot{g}_N = \mathbf{n}^B\left(\mathbf{v}^B - \mathbf{v}^A - \mathbf{x}^A_{,\alpha}\bar{\zeta}^\alpha_{,t}\right) = \mathbf{n}^A\ \mathbf{v}^A - \mathbf{n}^A\ \mathbf{v}^B + \mathbf{n}^A\ \mathbf{x}^A_{,\alpha}\bar{\zeta}^\alpha_{,t} \tag{X.2.17a}$$

Comparing Eqs. (7) and (17a), it can be seen that the normal interpenetration rate differs from the normal projection of the relative velocities γ_N unless $\bar{\zeta}^\alpha_{,t} = 0$. Whenever the two surfaces of the contacting bodies are coincident $\bar{\zeta}_{,t} = 0$, so

$$\gamma_N = \dot{g}_N \quad \textit{when} \quad g_N << 1 \tag{X.2.17b}$$

X.2.8. Tangential Relative Velocity for Interpentrated Bodies. If the bodies have interpenetrated, Eq. (8) does not give the relative tangential velocities of two points on the contact surfaces; Eq. (8) is exact only when the two bodies are in contact but have not interpenetrated. To obtain a relation for the tangential velocities which holds for interpenetrated bodies, we follow Wriggers(1995) and Wriggers. In this approach, the relative tangential velocity is defined in terms of the velocities of a point *P* on body *B* and its closest point projection. The relative velocity is then projected onto the master surface. So the relative tangential velocity is defined by

$$\dot{\mathbf{g}}_T = \bar{\zeta}^\alpha_{,t}\mathbf{a}_\alpha \tag{X.2.17c}$$

which involves the rate $\bar{\zeta}^\alpha_{,t}$ which appears in Eq. (16). This rate $\bar{\zeta}^\alpha_{,t}$ can be obtained from Eq. (13) as follows. Since Eq. (13) always holds for the point which is the closest point projection, the derivative of the LHS must vanish, i.e. multiplying Eq.(13) by $\left\|\mathbf{x}^B - \mathbf{x}^A\right\|$ and using Eq. (11), $\mathbf{a}_\alpha = \partial \mathbf{x}^A / \partial \zeta^\alpha$, we have

$$\frac{d}{dt}\left[\left(\mathbf{x}^B(\zeta, t) - \mathbf{x}^A(\bar{\zeta}, t)\right)\ \mathbf{a}_\alpha\right] = 0 \tag{X.2.18}$$

To expand the time derivative of the covariant base vector $\mathbf{a}_\alpha$ use (see Section X)

$$\frac{d\mathbf{a}_\alpha}{dt} = \frac{d}{dt}\left(\frac{\partial \mathbf{x}^A}{\partial \zeta^\alpha}\right) = \frac{\partial}{\partial \zeta_\alpha}\left(\frac{d\mathbf{x}^A}{dt}\right) + \frac{\partial \mathbf{x}^A}{\partial \zeta^\beta}\frac{d\zeta^\beta}{dt}$$

$$= \frac{\partial}{\partial \zeta_\alpha}\left(\mathbf{v}^A + \mathbf{x}^A_{,\beta}\zeta^\beta_{,t}\right) = \mathbf{v}^A_{,\alpha} + \mathbf{x}^A_{,\alpha\beta}\zeta^\beta_{,t} \qquad \text{(X.2.19)}$$

The remaining step are as follows (the independent variables are suppressed when convenient):

(derivative of product in (18))

$$\left(\mathbf{x}^B_{,t}(\zeta,t) - \mathbf{x}^A_{,t}(\bar{\zeta},t)\right)\ \mathbf{a}_\alpha + (\mathbf{x}^B - \mathbf{x}^A)\ \mathbf{a}_{\alpha,t} = 0 \qquad \text{(X.2.20)}$$

(using $\mathbf{v}^{BA} \equiv \mathbf{v}^B - \mathbf{v}^A$, $\mathbf{x}^{BA} \equiv \mathbf{x}^B - \mathbf{x}^A$, Eq. (19) for $\mathbf{a}_{\alpha,t}$)

$$(\mathbf{v}^{BA} - \mathbf{x}^A_{,\beta}\bar{\zeta}^\beta_{,t})\ \mathbf{a}_\alpha + \mathbf{x}^{BA}\ (\mathbf{v}^A_{,\alpha} + \mathbf{x}^A_{,\alpha\beta}\bar{\zeta}^\beta_{,t}) = 0 \qquad \text{(X.2.21)}$$

(using $g_N\mathbf{n}^A = \mathbf{x}^B - \mathbf{x}^A \equiv \mathbf{x}^{BA}$, $\mathbf{x}^A_{,\beta} = \mathbf{a}_\beta$ Eq. (11))

$$(\mathbf{a}_\alpha\ \mathbf{a}_\beta - g_N\mathbf{n}^A\ \mathbf{x}^A_{,\alpha\beta})\bar{\zeta}^\beta_{,t} = g_N\mathbf{n}^A\ \mathbf{v}^A_{,\alpha} + \mathbf{v}^{BA}\ \mathbf{a}_\alpha \qquad \text{(X.2.22)}$$

The above is a system of two linear algebraic equations in the two unknowns $\bar{\zeta}^\beta_{,t}$; all terms on the right hand side are known. Once the time derivatives $\bar{\zeta}^\beta_{,t}$ are known, $\dot{\mathbf{g}}_T$ can be determined from (17c). The first terms on the LHS and RHS of the above equations are of fundamental importance in the theory of surfaces: they are the first and second fundamental forms of the surface.

When $g_N = 0$ (or when g_N is sufficiently small), Eq. (22) can be simplified to

$$\mathbf{a}_\alpha\ \mathbf{a}_\beta\bar{\zeta}^\beta_{,t} = (\mathbf{v}^B - \mathbf{v}^A)\ \mathbf{a}_\alpha \qquad \text{(X.2.23)}$$

Taking the tensor product of the above with $\mathbf{a}^\alpha$ we obtain

$$\dot{\mathbf{g}}_T = \mathbf{a}_\beta\bar{\zeta}^\beta_{,t} = (\mathbf{v}^B - \mathbf{v}^A)\mathbf{a}_\alpha\ \ \mathbf{a}^\alpha = \mathbf{v}^B_T - \mathbf{v}^A_T \qquad \text{(X.2.24)}$$

where the second line follows from the fact that the projection of any vector on the surface is the tangential component. Since the RHS by Eq. (8) is $-\gamma_T$, we can see that when that the surfaces are coincident, i.e. when $g_N = 0$, then

$$\dot{\mathbf{g}}_T = -\gamma_T \qquad \text{(X.2.25)}$$

Thus the displacement-based definition of relative tangential velocity, Eqs. (17c) and (22), is consistent with the tangential velocity defined in Eq. (8) in the absence of interpenetration (except for the sign, which is irrelevant)

The kinetic and kinematic contact interface equations are summarized in Box X.1.

Example 5.2.1. Consider the two surfaces shown in Fig. 6, which have partially interpenetrated as shown. The master body is a 9-node isoparametric element, so the 3 nodes of surface *A* are defined by a quadratic mapping:

$$\begin{bmatrix} x \\ y \end{bmatrix}^A = (1-r^2)\begin{bmatrix} 2 \\ 1 \end{bmatrix} + \tfrac{1}{2} r(1+r)\begin{bmatrix} 3 \\ 3 \end{bmatrix}$$

$$r \equiv \zeta^A, \quad -1 \le r \le 1$$

The surface of the slave body *B* is a horizontal line given by

$$\begin{bmatrix} x \\ y \end{bmatrix}^B = \begin{bmatrix} 4s \\ 1.5 \end{bmatrix}, \quad s \equiv \zeta^B, \quad 0 \le s \le 1$$

The interpenetration in the example has been exaggerated. Note that $\mathbf{n}^B \neq -\mathbf{n}^A$ along the interface.

Part A. For the point *P* on slave surface *B* with coordinates (1,1.5), find the interpenetration.

The first step is to find the orthogonal projection point *Q* which minimizes l_{PQ}:

BOX X.1. Contact Interface Conditions

kinetic conditions

$$\mathbf{t}^A + \mathbf{t}^B = 0$$

normal: $t_N^A + t_N^B = 0, \quad t_N^A \equiv \mathbf{t}^A \ \mathbf{n}^A, \quad t_N^B \equiv \mathbf{t}^B \ \mathbf{n}^A, \quad t_N \equiv t_N^A \le 0$

tangential: $\mathbf{t}_T^A + \mathbf{t}_T^B = 0, \quad \mathbf{t}_T^A \equiv \mathbf{t}^A - t_N^A \mathbf{n}^A, \quad \mathbf{t}_T^B \equiv \mathbf{t}^B - t_N^B \mathbf{n}^A$

kinematic conditions in velocity form

$$\gamma \equiv \gamma_N = \left(\mathbf{v}^A - \mathbf{v}^B\right) \ \mathbf{n}^B \equiv v_N^A - v_N^B \le 0$$

$$\gamma_T = \mathbf{v}_T^A - \mathbf{v}_T^B = \mathbf{v}^A - \mathbf{v}^B - \left(\mathbf{v}^A - \mathbf{v}^B\right) \ \mathbf{n}^A$$

unitary contact condition

$$t_N \gamma_N = 0$$

kinematic conditions and definitions in displacement form

$$g \equiv g_N = \min_{\bar{\zeta}} \left\| \mathbf{x}^B(\zeta, t) - \mathbf{x}^A(\bar{\zeta}, t) \right\| \quad \text{if } \left[\mathbf{x}^B(\zeta, t) - \mathbf{x}^A(\bar{\zeta}, t)\right] \ \mathbf{n}^A \le 0$$

$$\dot{g}_N = \mathbf{n}^B \left(\mathbf{v}^B - \mathbf{v}^A - \mathbf{x}_{,\alpha}^A \dot{\bar{\zeta}}^\alpha\right) = \mathbf{n}^A \ \mathbf{v}^A - \mathbf{n}^A \ \mathbf{v}^B + \mathbf{n}^A \ \mathbf{x}_{,\alpha}^A \dot{\bar{\zeta}}^\alpha$$

$$\dot{\mathbf{g}}_T = \dot{\bar{\zeta}}^\alpha \mathbf{a}_\alpha \quad \text{where } (\mathbf{a}_\alpha \ \mathbf{a}_\beta - g \mathbf{n}^A \mathbf{v}_{,\alpha\beta}) \dot{\bar{\zeta}}^\beta = g \mathbf{n}^A \ \mathbf{v}_{,\alpha}^A + \left(\mathbf{v}^B - \mathbf{v}^A\right) \mathbf{a}_\alpha$$

$$l_{PQ} = \left\| \mathbf{x}^B(\zeta^B) - \mathbf{x}^A(\zeta^A) \right\| = \left((x^B - x^A)^2 + (y^B - y^A)^2 \right)^{1/2}$$

$$= \left\{ \left[1 - \left(2(1-r^2) + \tfrac{3}{2} r(1+r)\right)\right]^2 + \left[\tfrac{3}{2} - \left((1-r^2) + \tfrac{3}{2} r(1+r)\right)\right]^2 \right\}^{1/2}$$

The minimizer satisfies

$$0 = \frac{dl_{PQ}}{dr} = \frac{1}{l_{PQ}} (r^3 + 3r + \tfrac{3}{4})$$

The root is found numerically to be r= -0.2451, so $(x_Q, y_Q) = (1.6023, 0.6624)$.

X.3 FRICTION MODELS

X.3.1. Classification. The models used for the computation of the tangential tractions are collectively called friction models. There are basically three types of friction models:

1. Coulomb friction models, which are based on the classical theories of friction commonly taught in undergraduate mechanics and physics courses;

2. Interface constitutive equations, which approximate the behavior of the tangential forces by equations similar to constitutive equations used for materials;

3. Asperity-lubricant models, which model the behavior of the physical characteristics of the interface, often on a microscale.

The demarcations between these classes are not sharp; some models adopt features of more than one of the above classes, but the above roughly describes the current state of affairs.

X.3.2. Coulomb Friction. Coulomb friction models originate from classical friction, which is used for the total frictional forces between rigid bodies. In the application of classical Coulomb friction models to continua, they are applied at each point of the contact interface. A direct translation of the Coulomb friction law to a pointwise law gives

if A and B are in contact at $\mathbf{x}$, *then*

$$a)\ \text{if} \|\mathbf{t}_T(\mathbf{x},t)\| < -\mu_F t_N(\mathbf{x},t),\ \gamma_T(\mathbf{x},t) = 0 \qquad \text{(X.3.1a)}$$

$$b)\ \text{if} \|\mathbf{t}_T(\mathbf{x},t)\| = -\mu_F t_N(\mathbf{x},t),\ \gamma_T(\mathbf{x},t) = -\alpha(\mathbf{x},t)\mathbf{t}_T(\mathbf{x},t),\ \ \alpha \geq 0 \qquad \text{(X.3.1b)}$$

where α is a variable which is determined from the solution of the complete problem. The condition that the two bodies are in contact at a point implies that the normal traction $t_N \leq 0$, so the RHS of the two expressions, $-\mu_F t_N$, is always positive. Condition (a) is known as the stick condition, for when the tangential traction at a point is less than the critical value, no relative tangential motion is permitted according to this condition, i.e. *the two bodies stick*. Condition (b) corresponds to frictional sliding, and the second part of that equation expresses the fact that the tangential traction arising from friction must be in the direction opposite to the direction of the relative tangential velocity.

The classical Coulomb friction law closely resembles a rigid-plastic constitutive equation. If the tangential velocity γ_T is interpreted as a strain and the tangential traction components are interpreted as stresses, the first relation in Eq. (1a) can be interpreted as a yield function. According to (1), when the yield criterion is not met, the tangential velocity vanishes. Once the yield function is satisfied, the tangential velocity is in the

direction of the tangential traction but its magnitude is unspecified. These attributes of the response parallel the rigid plastic model desribed in Section 6.?.

There are several alternative ways of stating Coulomb's law which are equivalent to the above. For example, Demkowicz and Oden(1981) state Coulomb's law as (the spatial dependence of the variables has been dropped for simplicity):

$$\begin{aligned} &\textit{if A and B are in contact at } x, \textit{ then} \\ &\|\mathbf{t}_T\| \le -\mu_F t_N \quad \textit{and} \quad \mathbf{t}_T \cdot \mathbf{v}_T + \mu_F |t_N| |\gamma_T| = 0 \end{aligned} \tag{X.3.2}$$

The stick condition of Coulomb friction is its most troublesome characteristic, since it introduces discontinuities in the time history of the relative tangential velocity. When the motion of point changes from relative slipping to sticking, the relative tangential velocity γ_T discontinuously jumps to zero. Thus the tangential velocities at that point are not smooth, but exhibit the same discontinous character as the normal velocities at the time of impact. Furthermore, the inequalities result in the Coulomb friction law result in weak forms which involve inequalities. Therefore, Coulomb friction is difficult to handle in numerical solutions and we consider it only for some special cases.

X.3.3. Interface Constitutive Equations. A different approach to defining interface laws has been pioneered by Michalowski and Mroz (1978) and Curnier(1984). This approach is motivated by the theory of plasticity and the analogy between Coulomb friction and rigid-perfect plasticity we alluded to above. Interface constitutive equations can model behavior similar to Coulomb friction by means of the Mohr-Coulomb criterion (see Section XX). Plastic models of interface behavior are motivated by the fact that microscopic examination of even the smoothest surfaces reveals surface roughness due to asperities, such as shown in Fig. X.3.1. Even when the surfaces appear smooth, friction is generated by the interaction of these asperities during sliding. Sliding initially causes elastic deformations of these asperities, so a true stick condition cannot exist in actual siding, i.e. the stick condition is an idealization of observed behavior. The elastic deformation of the asperities is followed by "grinding" down of the asperities as the sliding proceeds. The elastic deformations of the asperities are reversible, whereas the grinding down is irreversible, so ascribing an elastic character to the initial sliding and a plastic character to subsequent sliding is natural.

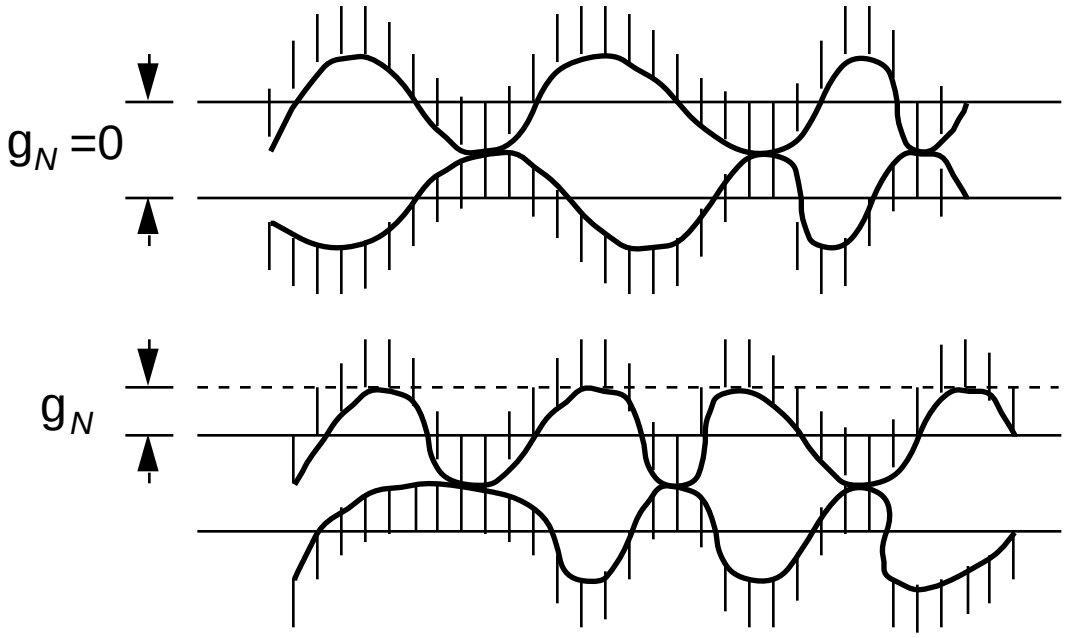

Figure X.3.1. Asperities on contacting surface.

As an example of an interface constitutive law we describe an adaptation of Curnier's plasticity theory for friction. This model contains all of the ingredients of a plasticity theory for continua: a decomposition of deformation into reversible and irreversible components, a yield function and a flow law. In this description of the model Curnier(1984), we have replaced displacements by rates, which appears appropriate for problems involving arbitrary time histories and large relative sliding.

In this theory, the rate of relative velocities γ is subdivided into that ascribed to adherence, which is the elastic deformation of the asperities, and that ascribed to slip, the grinding down of the asperities:

$$\gamma = \gamma^{adh} + \gamma^{slip} \equiv \gamma^{a} + \gamma^{s} \tag{X.3.3}$$

Here γ^{adh} is the reversible part, γ^{slip} is the irreversible part. A wear function is defined by

$$D^{c} = \int_0^t (\gamma_T^s \ \gamma_T^s)^{\frac{1}{2}} dt \tag{X.3.4}$$

which is reminiscent of the definition of effective plastic strain.

Two functions are defined to construct the plastic interface law:

1. a yield function, $f(\mathbf{t})$

2. a potential function for the flow law, $h(\mathbf{t})$

The yield function determines the onset of plastic response, the potential function the relationship between the slip (plastic strain rate) and the tangential tractions.

The theory is similar to the nonassociative plasticity theories given in Section ?. Therefore, we will only sketch the steps so that the equations are available and to enable us to point out the need for nonassociative plasticity in a model of frictional sliding.

The yield function for Coulomb type behavior is obtained from Eq. (1):

$$f(t_N, \mathbf{t}_T) = \|\mathbf{t}_T\| + \mu_F t_N = 0 \qquad \text{(X.3.5)}$$

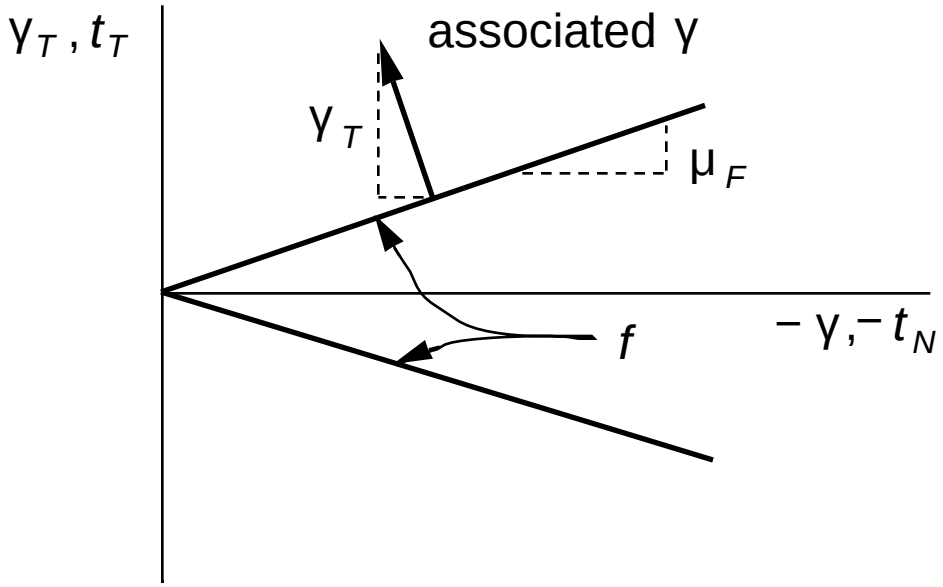

Figure X.3.2. Coulomb yield surface in two dimensions.

In two dimensions this yield function takes the form shown in Fig. X.3.2: $\mathbf{t}_T = t_T \hat{\mathbf{e}}_x$ in that case, so the yield function consists of two lines with slopes $\pm\mu_F$ as shown. For the three-dimensional case, $\mathbf{t}_T = \hat{t}_\alpha \hat{\mathbf{e}}_\alpha = \hat{t}_x \hat{\mathbf{e}}_x + \hat{t}_y \hat{\mathbf{e}}_y$, we can write Eq. (5) as

$$f(t_N, \mathbf{t}_T) = (\hat{t}_x^2 + \hat{t}_y^2)^{1/2} + \mu_F t_N = 0 \qquad \text{(X.3.6)}$$

so the yield function is a cone as shown in Fig. X.3.3.

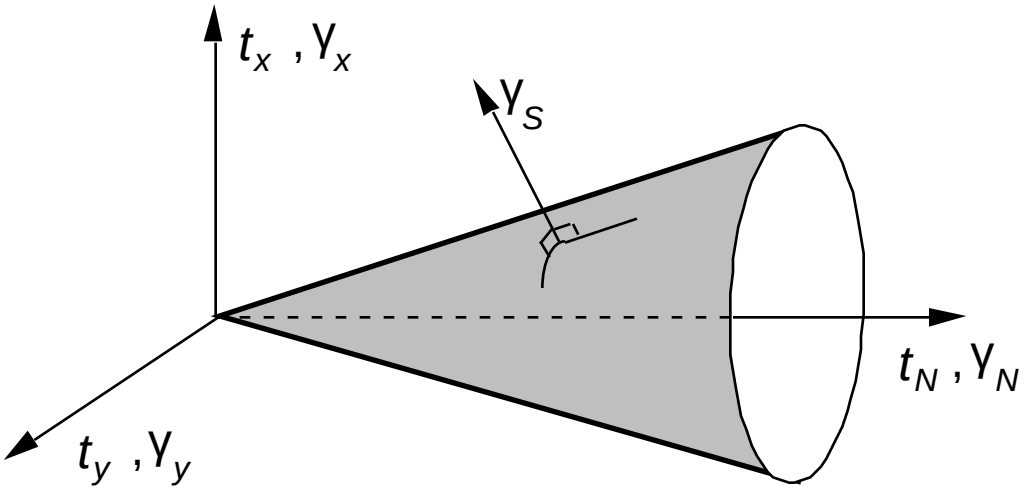

Figure X.3.3. Coulomb surface for contact in 3D.

In a nonassociative theory, the potential function for the slip differs from the yield function. One possible potential function for a nonassociative theory is

$$h(t_N, \mathbf{t}_T) = \|\mathbf{t}_T\| - \beta = 0 \qquad \text{(X.3.7)}$$

where β is a constant whose magnitude is irrelevant. This potential function is also shown in Fig. X.3.4.

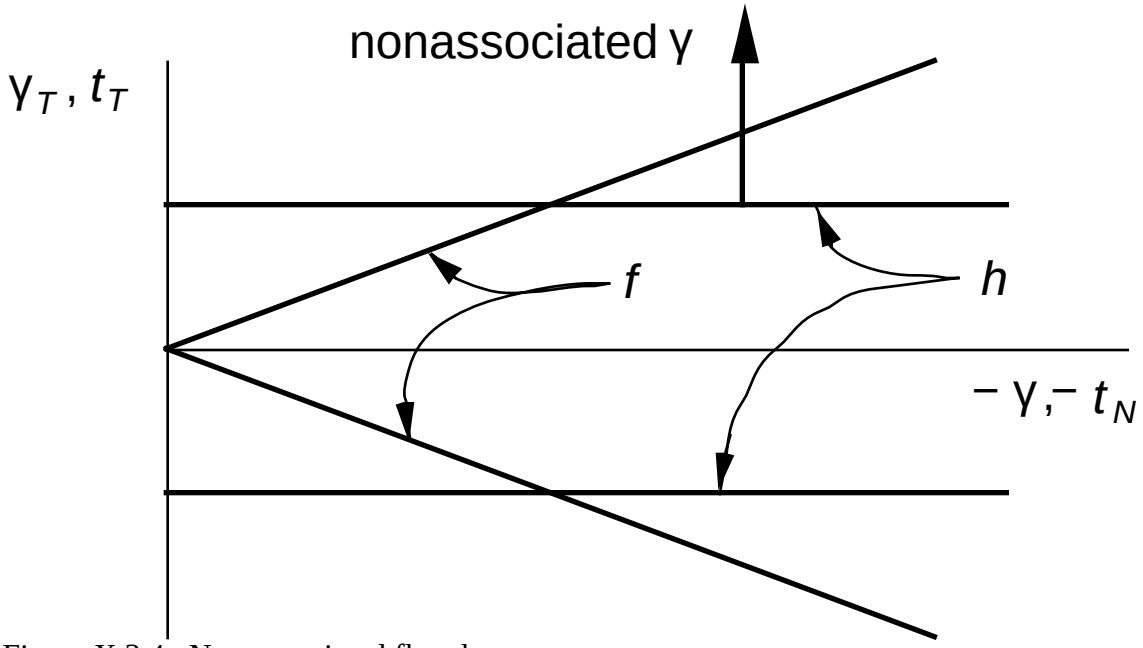

Figure X.3.4. Non-associated flow law.

To write the complete relations for a plasticity theory of friction in two and three dimensions, it is convenient to define

$$\mathbf{g} = \begin{Bmatrix} \gamma_N \\ \mathbf{g}_T \end{Bmatrix} \text{ in 2D}, \quad \mathbf{g} = \begin{Bmatrix} \gamma_N \\ \mathbf{g}_T \end{Bmatrix} = \begin{Bmatrix} \gamma_N \\ \hat{\gamma}_x \\ \hat{\gamma}_y \end{Bmatrix} \text{ in 3D} \tag{X.3.10}$$

$$\mathbf{Q} = \begin{Bmatrix} t_N \\ t_T \end{Bmatrix} \text{ in 2D}, \quad \mathbf{Q} = \begin{Bmatrix} t_N \\ \mathbf{t}_T \end{Bmatrix} = \begin{Bmatrix} t_N \\ \hat{t}_x \\ \hat{t}_y \end{Bmatrix} \text{ in 3D} \tag{X.3.11}$$

The adhesive strains are then related to the stresses by

$$\dot{\mathbf{Q}} = \mathbf{C}_F \mathbf{g}^{adh} \quad \text{or} \quad \dot{\mathbf{Q}}_i = C_{ij}^F \gamma_j^{adh} \tag{X.3.12}$$

which is the counterpart of the linear elastic law for continua. Usually $\mathbf{C}_F$ is diagonal since little experimental information is available on coupling between different components of the frictional traction and the relative motion.

The adhesive slip rates are given by the nonassociative flow law. Perfectly-plastic sliding, in which there is no increase in the tractions with the accumulation of slip, closely resembles Coulomb friction and is given by

$$\mathbf{g}^{slip} = \alpha \frac{\partial h}{\partial \mathbf{Q}} \quad \text{or} \quad \gamma_i^{slip} = \alpha \frac{\partial h}{\partial Q_i} \tag{X.3.13}$$

We define

$$\mathbf{f}_Q = \frac{\partial f}{\partial Q} \qquad \mathbf{h}_Q = \frac{\partial h}{\partial Q} \tag{X.3.14}$$

The steps for developing the constitutive equation for the frictional surface are then:

$$\mathbf{f}_Q^T \dot{\mathbf{Q}} = 0 \qquad \text{consistency} \tag{X.3.15}$$

$$\dot{\mathbf{Q}} = \mathbf{C}\left(\mathbf{g} - \mathbf{g}^{slip}\right) \qquad \text{(12) and (3)} \tag{X.3.16}$$

$$\mathbf{f}_Q^T \mathbf{C}\left(\mathbf{g} - \alpha \mathbf{h}_Q\right) = 0 \qquad \text{(13) and (15) into (16)} \tag{X.3.17}$$

$$\alpha = \frac{\mathbf{f}_Q^T \mathbf{C} \mathbf{g}}{\mathbf{f}_Q^T \mathbf{C} \mathbf{h}_Q} \qquad \text{solve (17) for } \alpha \tag{X.3.18}$$

$$\dot{\mathbf{Q}} = \mathbf{C}\left(\mathbf{g} - \frac{\mathbf{f}_Q^T \mathbf{C} \mathbf{g}}{\mathbf{f}_Q^T \mathbf{C} \mathbf{h}_Q} \mathbf{h}_Q\right) \qquad \text{(18) and (??) into (16)} \tag{X.3.19}$$

Since the above is a traction rate, it is not objective (i.e. frame invariant) so a frame-invariant rate must be used for integration.

$$\mathbf{Q}\ (\zeta,t) = \frac{\partial \mathbf{Q}(\zeta,t)}{\partial t} - \mathbf{Q}\ \mathbf{W} \qquad \text{(X.3.20)}$$

where $\mathbf{Q}$ is a frame invariant rate and $\mathbf{W}$ is the projection of the spin given by Eq. (3.X.X) onto the surface. In the above, $\partial \mathbf{Q}/\partial t$ is the rate of the tractions due to the slip rates. The update proccedures are analogous to that in elasto-plasticity and are discussed in Section X.

The reason for choosing a nonassociative flow law can be clarified by considering sliding in a two dimensional problem. If we were to use an associated flow law, the irreversible slips are given by $\gamma_N^{slip} = \alpha \dfrac{\partial f}{\partial t_N} = -\alpha\mu_F$ $\gamma_T^{slip} = \alpha \dfrac{\partial f}{\partial t_T} = -\alpha\, sign(t_T)$. Since $\alpha \geq 0$, this implies that, $\gamma_N^{slip} < 0$ so the bodies would separate after the onset of slip (recall γ_N is positive in interpenetration). If the slips are then given by the potential flow laws using the nonassociated potential (7), the slips in two dimensions can be written as

$$\gamma_N^{slip} = \alpha \frac{\partial h}{\partial t_N} = 0 \qquad \text{(X.3.21)}$$

$$\gamma_T^{slip} = \alpha \frac{\partial h}{\partial t_T} = \alpha \qquad \text{(X.3.22)}$$

Thus the normal slip vanishes, i.e. that no irreversible normal interpenetration occurs during to sliding.

Hardening can also be incorporated in a manner analogous to the procedure in elasto-plasticity. The constitutive equation for the interface is then developed as in plasticity with hardening, see Section ?. Under large pressures, the asperities are often significantly ground down, and some degree of permanent change occurs in the normal interpentration. This can be modeled by a cap model such as described in Section ?.

X.4 WEAK FORMS

X.4.1. Notation and Preliminaries. The weak form of the momentum equation and the contact interface conditions will be developed for a Lagrangian mesh. This development is also applicable to an ALE mesh when the contact surface is treated as Lagrangian. For simplicity, we start with frictionless contact and defer the treatment of tangential tractions to the last part of this Section. We restrict the following developments to the case where all traction or velocity components are prescribed on a traction or dispacement boundary, respectively.

The contact surface is neither a traction nor a displacement boundary. Thus the total boundary of body A is given by

$$\Gamma^A = \Gamma_t^A \quad \Gamma_u^A \quad \Gamma^c \qquad \text{(X.4.2a)}$$

$$\Gamma_t^A \cap \Gamma_u^A = 0 \quad \Gamma_t^A \cap \Gamma^c = 0 \quad \Gamma_u^A \cap \Gamma^c = 0 \tag{X.4.2b}$$

Similar relations hold for body *B*.

The trial solutions are in the space of *kinematically admissible velocities*, and as in Chapter 4 we choose the velocities to be the cardinal dependent variable. The trial solution is $\mathbf{v}(\mathbf{X},t) \quad U$ where the space of trial functions is defined by

$$U = \left\{ \mathbf{v}(\mathbf{X},t) \middle| \mathbf{v} \quad C^0\left(\Omega^A\right), \mathbf{v} \quad C^0\left(\Omega^B\right), \mathbf{v} = \bar{\mathbf{v}} \, on \, \Gamma_u \right\} \tag{X.4.3}$$

The space is similar to that for the single body problem, but the velocities are separately approximated in the two bodies; the velocity fields in U are not required to be continuous across the contact interface. (*while the admissible velocity fields are here given as C^0, i.e. in H^1, for purposes of convergence analysis in linear elastostatics the displacements for the contact problem are defined in the space $H^{1/2}$, see Kikuchi and Oden(1988). This is the same space that is used in fracture mechanics problems to handle the singular stresses at the crack tip. In contact problems, singularities occur at the edge of the contact zone so the same space must be used in convergence analysis. However, unlike in fracture mechanics, these singularities do not appear to be of any engineering significance, since the roughness of surfaces appears to eliminate the appearance of even near singular behavior in the stresses.)

The space of test functions is defined by

$$U_0 = U \cap \left\{ \delta\mathbf{v}(\mathbf{X}) \middle| \quad \delta\mathbf{v} = 0 \, on \, \Gamma_u \right\} \tag{X.4.4}$$

which parallels the definition in Section 4.3: The test functions are identical to the trial functions except that they vanish on prescribed displacement boundaries.

X.4.2. Lagrange Multiplier Weak Form. A common approach to imposing the contact constraints is by means of Lagrange multipliers. We will follow the description given by Belytschko and Neal(1991). Let the Lagrange multiplier trial functions $\lambda\left(\zeta^\alpha, t\right)$ and the corresponding test functions be in the following spaces

$$\lambda\left(\zeta^\alpha, t\right) \quad J^+, \; J^+ = \left\{ \lambda\left(\zeta^\alpha, t\right) \middle| \lambda \quad C^{-1}, \lambda \geq 0 \, on \, \Gamma^c \right\} \tag{X.4.5}$$

$$\delta\lambda(\zeta^\alpha) \quad J^-, \; J^- = \left\{ \delta\lambda(\zeta^\alpha) \middle| \delta\lambda \quad C^{-1}, \delta\lambda \leq 0 \, on \, \Gamma^c \right\} \tag{X.4.6}$$

The weak form is:

$$\text{if } \delta P_L(\mathbf{v}, \delta\mathbf{v}, \lambda, \delta\lambda) \equiv \delta P + \delta G_L \geq 0 \quad \delta\mathbf{v} \quad U_0, \quad \delta\lambda \quad J^- \tag{X.4.7}$$

$$\delta G_L = \int_{\Gamma^c} \delta(\lambda g_N) d\Gamma \qquad \text{(X.4.8)}$$

where δP is defined in Table B4.2 and $v \quad U$, $\lambda \quad J^+$. This weak form is equivalent to the momentum equation, the traction boundary conditions and the following contact interface conditions: impenetrability (2.7), momentum balance on normal tractions (2.9f) and the frictionless condition (2.10c). The restriction of the normal interface traction to be compressive will result from the constraints on the trial set of Lagrange multipliers. Note that the above *weak form is an inequality.*

The above is a standard way of appending a constraint to a weak form by means of a Lagrange multipliers: compare to the Hu-Washizu variational principle. The only difference from the Hu-Washizu form is that the constraint is an inequality.

The equivalence of the weak form to the momentum equation, the traction boundary conditions and the contact conditions is shown by a procedure that parallels that given in Section 4.2. Recall that δP is given in Box 4.1 as

$$\delta P = \int_\Omega \left[\delta v_{i,j} \sigma_{ji} - \delta v_i (\rho b_i - \rho \dot{v}_i) \right] d\Omega - \int_{\Gamma_t} \delta v_i \bar{t}_i d\Gamma \qquad \text{(X.4.9)}$$

where we have used commas to denote derivatives with respect to the spatial variables and a superposed dot to denote the material time derivative. All integrals in the above apply to the union of both bodies, i.e. $\Omega = \Omega^A \quad \Omega^B$, $\Gamma_t = \Gamma_t^A \quad \Gamma_t^B$. The first step is to integrate the internal virtual power by parts and apply Gauss's theorem:

$$\int_\Omega \left(\delta v_i \sigma_{ji} \right)_{,j} d\Omega = \int_{\Gamma_t} \delta v_i \sigma_{ji} n_j d\Gamma + \int_{\Gamma^c} (\delta v_i^A t_i^A + \delta v_i^B t_i^B) d\Gamma \qquad \text{(X.4.12)}$$

We have used the fact that the integral over the displacement boundary Γ_u vanishes because $\delta v_i = 0$ on Γ_u and Cauchy's law (9b-c) has been applied to obtain the expressions in the last integral. The first integral on the right hand side of the above applies to both bodies, as can be seen from the definition (2c). The contact surface integral appears for each body when Gauss's theorem is applied, so to express the result as a single integral, the field variables associated with the two bodies have been specifically indicated the superscripts *A* and *B.*

The integrand of the second integral on the RHS of the above is now broken up into components normal and tangential to the contact surface. In indicial notation this gives

$$\delta v_i^A t_i^A = \delta v_N^A t_N^A + \delta \hat{v}_\alpha^A \hat{t}_\alpha^A \qquad \text{(X.4.13)}$$

where, as usual in this book, the range of alpha is 1 for two dimesional problems and 2 for three dimensional problems. A similar relationship can be written for body *B*. The above is clearer to some people in vector notation, where using (2.10a) we can write

$$\begin{aligned}\delta\mathbf{v}^A\ \mathbf{t}^A &= (\delta v_N^A \mathbf{n}^A + \delta\mathbf{v}_T^A)\ (t_N^A \mathbf{n}^A + \mathbf{t}_T^A) \\ &= \delta v_N^A t_N^A + \delta\mathbf{v}_T^A\ \mathbf{t}_T^A\end{aligned} \tag{X.4.14}$$

The simplification to the second line is obtained by noting that $\mathbf{n}$ is normal to the tangent vectors $\mathbf{t}_N$ and $\mathbf{v}_N$. The second term in (14) is an alternative expression for $\hat{t}_\alpha \hat{v}_\alpha$.

Substituting Eqs. (12) and (13) into (9) gives

$$\begin{aligned}\delta P = &\int_{\Gamma_C} \delta v_i(\rho v_i - b_i - \sigma_{ij,j})\, d\Omega + \int_{\Gamma_t} \delta v_i(\sigma_{ji} n_j - \bar{t}_i)\, d\Gamma \\ &+ \int_{\Gamma_c} (\delta v_N^A t_N^A + \delta v_N^B t_N^B + \delta\hat{v}_\alpha^A \hat{t}_\alpha^A + \delta\hat{v}_\alpha^B \hat{t}_\alpha^B)\, d\Gamma\end{aligned} \tag{X.4.16}$$

Now consider Eq. (8):

$$\delta G_L = \int_{\Gamma_C} \delta(\lambda\gamma_N) d\Gamma = \int_{\Gamma_C} (\delta\lambda\gamma_N + \delta\gamma_N\lambda) d\Gamma \tag{X.4.17}$$

Substituting Eq.(2.2) into the above gives

$$\delta G_L = \int_{\Gamma_c} (\delta\lambda\gamma_N + \lambda(\delta v_N^A - \delta v_N^B))\, d\Gamma \tag{X.4.18}$$

Combining Eqs. (16) and (18) yields

$$\begin{aligned}0 \le \delta P_L = &\int_\Omega \delta v_i \left(\sigma_{ji,j} - \rho b_i - \rho\dot{v}_i\right) d\Omega + \int_{\Gamma_t} \delta v_i(\sigma_{ji} n_j - \bar{t}_i)\, d\Gamma \\ &+ \int_{\Gamma_c} [\delta v_N^A(t_N^A + \lambda) + \delta v_N^B(t_N^B - \lambda) + (\delta\hat{v}_\alpha^A \hat{t}_\alpha^A + \delta\hat{v}_\alpha^B \hat{t}_\alpha^B) + \delta\lambda\gamma_N]\, d\Gamma\end{aligned} \tag{X.4.19}$$

Extracting the strong form from the weak inequality is similar to the procedure described in Section 4.2. Whenever the test function is unconstrained, there is then no restriction on the sign of the term which multiplies the test function and the term must vanish by the density theorem. Thus it follows from the first two integrals of the above that

$$\sigma_{ji,j} - \rho b_i = \rho\dot{v}_i \quad in\ \Omega \tag{X.4.20}$$

$$\sigma_{ji} n_j = \bar{t}_i \quad on\ \Gamma_t \tag{X.4.21}$$

i.e. that the momentum equation and the natural boundary conditions are satisfied in bodies *A* and *B*. In all terms of the integrand on the contact surface except the last, the test function is also unconstrained, and we obtain the equalities

$$\hat{t}_\alpha^A = 0 \ \textit{and} \quad \hat{t}_\alpha^B = 0 \ \textit{on} \Gamma^c, \quad \textit{or} \ \mathbf{t}_T^A = \mathbf{t}_T^A = 0 \ \textit{on} \ \Gamma^c \tag{X.4.22}$$

$$\lambda = -t_N^A \ \textit{and} \ \lambda = t_N^B \ \textit{on} \ \Gamma^c \tag{X.4.23}$$

By eliminating λ from (23) we obtain the momentum balance condition on the normal tractions

$$t_N^A + t_N^B = 0 \ \textit{on} \ \Gamma^c \tag{X.4.25a}$$

Since the space of trial functions for λ is constrained to be positive, see Eq. (5), it follows from (23) that the normal traction on the contact interface is compressive. Thus we can write

$$t_N^A + t_N^B = 0 \ \textit{on} \ \Gamma^c \tag{X.4.25b}$$

In the last term of the integrand of Eq.(18), the variation $\delta\lambda$ is constrained to be negative. Therefore, it cannot be deduced that its coefficient γ_N vanishes. However it can be deduced that the coefficient must be nonpositive, i.e. that the weak *inequality* is equivalent to

$$\gamma_N \le 0 \ \textit{on} \ \Gamma^c \tag{X.4.26}$$

which is the interpenetration inequality (2.2).

Equations (20-22) and (25-26) constitute the strong form corresponding to the weak form given in Eq. (7). This set of equations includes the momentum equation and the traction (natural) boundary conditions on both bodies. On the contact surface, the strong form enforces the momentum balance of the normal tractions and the inequality on the interpenetration rate. The compressive character of the normal tractions follows from the restriction on the Lagrange multiplier field (5).

X.4.3. Contribution of Virtual Power to Contact Surface. At this point, for the purpose of simplifying subsequent proofs, we observe that the only contribution of δP to the conditions on the contact interface is the term in Eq. (12). We call this term δP_1 and from (12) it can be seen that it is given by

$$\begin{aligned} \delta P_1(\Gamma^c) &= \int_{\Gamma^c} (\delta v_i^A t_i^A + \delta v_i^B t_i^B)\, d\Gamma \\ &= \int_{\Gamma^c} (\delta v_N^A t_N^A + \delta v_N^B t_N^B + \delta \mathbf{v}_T^A \ \mathbf{t}_T^A + \delta \mathbf{v}_T^B \ \mathbf{t}_T^B)\, d\Gamma \end{aligned} \tag{X.4.27}$$

The remaining terms in δP are equivalent to the momentum equation and traction boundary conditions, so by replacing δP by δP_1 the momentum equation and traction boundary conditions are observed.

If the contact surface is frictionless, then the last two terms in the integrand of (27a) vanish, so the contribution of δP to the contact interace is

$$\delta P_2(\Gamma^c) \equiv \int_{\Gamma^c} (\delta v_N^A t_N^A + \delta v_N^B t_N^B)\, d\Gamma \qquad \text{(X.4.28)}$$

Replacing δP by δP_2 implies the momentum equation, the traction boundary conditions, and the frictionless condition (10c). These results will be used in the proofs which follow.

X.4.4. Penalty Method with Rate-dependent Penalty. In the penalty method, the impenetrabilty constraint is imposed as a penalty normal traction along the contact surface. In contrast to the Lagrange multiplier method, the penalty method allows some interpenetration. However, it is easier to implement and is quite widely used. We consider two forms of the penalty method:

1. a penalty which is proportional to the square of the normal interpentration rate γ_N;

2. a penalty which can be an arbitrary function of the interpenetration and its rate.

The second is more useful for applications in nonlinear problems, because a strictly velocity-dependent penalty allows too much interpenetration. However, the interpenetration-rate dependent penalty leads to a form which is of interest in the elastostatic problem when we replace velocities by displacements, so it is included.

In the penalty methods, we use the same test and trial functions for the velocities as in the Lagrange multiplier method, Eqs. (3) and (4), respectively. The equivalence of the weak form to the strong form for the penalty method can be stated as follows:

$$\text{if } \mathbf{v} \in U \text{ and } \delta P_p(\mathbf{v}, \delta\mathbf{v}) = \delta P + \delta G_p = 0 \qquad \forall \delta\mathbf{v} \in U_0 \qquad \text{(X.4.29a)}$$

$$\text{where } \delta G_p = \int_{\Gamma^C} \frac{\beta}{2} \delta(\gamma_N^2)\, H(\gamma_N)\, d\Gamma \qquad \text{(X.4.29b)}$$

then the momentum equation and natural boundary conditions are satisfied in the two bodies and the normal tractions on Γ^c satisfy momentum balance and are compressive, and vice versa

In the above $H(\gamma_N)$ is the Heaviside step function,

$$H(\gamma_N) = \begin{cases} 1 & \text{if } \gamma_N \geq 0 \\ 0 & \text{if } \gamma_N = 0 \end{cases} \qquad \text{(X.4.30)}$$

The functional δP is defined in Eq. (9) and β is an arbitrary parameter known as the *penalty parameter*. The penalty parameter can be a function of the spatial coordinates. The weak form associated with the penalty method is not an inequality; the discontinuous nature of the contact-impact problem is introduced by the Heaviside step function in Eq. (29b). This weak form does not include the impenetrability condition, which is satisfied only approximately in the penalty method.

To show that the weak form implies the strong form, we begin by taking the variation of δG_P, which gives

$$\delta G_P = \int_{\Gamma_C} \beta \gamma_N \, \delta\gamma_N H(\gamma_N) \, d\Gamma \tag{X.4.31}$$

Using Eq. (2.3) in the above gives

$$\delta G_P = \int_{\Gamma_C} \beta \gamma_N^+ (\delta v_N^A - \delta v_N^B) \, d\Gamma \tag{X.4.32}$$

where

$$\gamma_N^+ = \gamma_N H(\gamma_N) \tag{X.4.34}$$

We then combine the above term with the contact term, $\delta P_2(\Gamma_C)$ in Eq. (28), i.e. with what remains from δP after extracting the momentum equation and natural boundary conditions (which means that these strong forms are already implied). This yields

$$\delta P_P = \int_{\Gamma_C} \left[\delta v_N^A (t_N^A + \beta \gamma_N^+) + \delta v_N^B (t_N^B - \beta \gamma_N^+) \right] d\Gamma = 0 \tag{X.4.33}$$

The arbitrariness of δv_N^A and δv_N^B on Γ^c then yields

$$t_N^A + \beta \gamma_N^+ = 0 \quad on \Gamma^c \tag{X.4.35}$$

$$t_N^B - \beta \gamma_N^+ = 0 \quad on \Gamma^c \tag{X.4.36}$$

Combining the two above equations gives

$$t_N^A = - t_N^B = - \beta \gamma_N^+ \le 0 \tag{X.4.37}$$

where the inequality follows from Eq. (34). Thus the weak form implies that the normal tractions satisfy momentum balance and are compressive. The weak form, unlike the Lagrange multiplier technique, does not enforce the continuity of the velocities of the two bodies across the contact interface; in fact, the velocities will be discontinuous across the interface. The magnitude of the discontinuity can be obtained from (37), which gives

$$\gamma_N^+ = v_N^A - v_N^B = t_N^A / \beta$$

Thus the discontinuity in the relative normal velocity component is inversely proportional to the penalty parameter β; as β is increased, the diccontinuity will decrease.

X.4.5. Interpenetration-dependent Penalty. The above form of the penalty method often performs quite poorly since it may allow excessive interpenetration. The normal traction is applied only when the relative velocities lead to continued interpenetration. As soon as the relative velocities of contiguous points of the two

surfaces become equal or negative, the normal traction vanishes. Substantial interpenetration may consequently persist in the solution. Therefore, in penalty methods, it is recommended that the normal traction also be a function of the interpenetration as defined in (2.12). For this purpose, we define the following relation for the normal traction :

$$p = p(g_N, \dot{g}_N)\, H(g_N) \tag{X.4.38}$$

where g_N is defined in Eq. (2.12). The weak form is then given by Eq. (28) with

$$\delta G_p = \int_{\Gamma_C} \delta \dot{g}_N p \, d\Gamma \tag{X.4.39}$$

The same procedure as before then gives

$$t_N^A + p = 0 \quad on\ \Gamma^c \tag{X.4.40}$$

$$t_N^B - p = 0 \quad on\ \Gamma^c \tag{X.4.41}$$

Combining the two above equations gives

$$t_N^A = -t_N^B = -p(g_N, \dot{g}_N)\, H(g_N) \tag{X.4.42}$$

Thus the tractions are always compressive and satisfy momentum balance. The tractions are functions of the interpenetration and rate of interpenetration. An example of a suitable penalty function is

$$p = (\beta_1 g_N + \beta_2 \dot{g}_N) H(\beta_1 g_N + \beta_2 \dot{g}_N) \tag{X.4.43a}$$

where β_1, β_2 are penalty parameters whose selection is discussed in Section ?. The step function in this expression avoids tensile normal tractions across the interface.

X.4.6. Perturbed Lagrangian Weak Form. The perturbed Lagrangian method is primarily of interest in small displacement elastostatics. In the perturbed Lagrangian method, the weak form is

$$\text{if } v \quad U, \lambda \quad C^{-1} \text{ and } \delta P_{PL} = \delta P + \delta G_{PL} \geq 0 \qquad \delta v \quad U_0, \delta\lambda \quad C^{-1} \tag{X.4.44}$$

In the above

$$\delta G_{PL} = \int_{\Gamma_C} \delta\lambda \left(\dot{g}_N^+ - \frac{1}{2\beta} \lambda^2 \right) d\Gamma \tag{X.4.45}$$

where $\dot{g}_N^+$ is defined by Eqs. (34) and (2.3) and β is a large constant, analogous to a penalty parameter. It can be seen that the second term in the above integrand is a perturbation of the Lagrangian multiplier, Eq. (8); the quadratic perturbation term is small since β is large.

In this weak form, the test and trial functions for the Lagrange multiplier are unconstrained. This weak form is equivalent to the momentum equation, the traction boundary condition and the momentum balance and traction inequalities (2.9g) on the contact interface. It will be shown that as in the penalty method, the impenetrability condition (2.7) is only met approximately.

The equivalence to the strong form is shown as follows. From (45),

$$\delta G_{PL} = \int_{\Gamma_C} (\delta\lambda \gamma_N^+ + \lambda \delta\gamma_N - \frac{1}{\beta} \lambda \delta\lambda) \, d\Gamma \qquad \text{(X.4.46)}$$

Combining δG_{PL} with the terms that emerge from δP once the momentum equation, traction boundary conditions and frictionless interface conditions are met, $\delta P_2(\Gamma^c)$ in Eq. (27), yields

$$\begin{aligned} 0 = \delta G_{PL} + \delta P_2 = & \int_{\Gamma^c} \delta\lambda \left(\gamma_N^+ - \frac{\lambda}{\beta} \right) d\Gamma \\ & + \int_{\Gamma^c} \delta v_N^A \left(t_N^A + \lambda \right) + \delta v_N^B \left(t_N^B - \lambda \right) d\Gamma \end{aligned} \qquad \text{(X.4.47)}$$

Since the test functions δv_N^A and δv_N^B are arbitrary, it follows that

$$t_N^A = -\lambda \ \ on \ \Gamma^c \qquad \text{(X.4.48a)}$$

$$t_N^B = \lambda \ \ on \ \Gamma^c \qquad \text{(X.4.48b)}$$

The test function $\delta\lambda$ is constrained to be negative, so the variational inequality yields

$$\lambda = \beta \gamma_N^+ \ on \ \Gamma^c \qquad \text{(X.4.48c)}$$

Combining the above yields

$$t_N^A = -t_N^B = -\beta \gamma_N^+ = -\beta (v_N^A - v_N^B) H (\gamma_N) \ \ on \ \Gamma^c \qquad \text{(X.4.49)}$$

So the tractions satisfy momentum balance and are compressive on the contact interface.

The above strong form of the contact surface conditions are almost identical to those which emanate from the penalty method. This similarity is also found in the discrete equations, so the perturbed Lagrangian is a penalty method in disguise.

X.4.7. Augmented Lagrangian. The augmented Lagrangian formulation has been developed to exploit improved methods for solving the Lagrange multiplier problem, c.f. Bertsekas (1984). The weak form is given by

$$\delta P_{AL}(\mathbf{v}, \delta\mathbf{v}, \lambda, \delta\lambda) = \delta P + \delta G_{AL} \geq 0 \qquad \delta\mathbf{v} \quad U_0, \ \delta\lambda \quad J^- \qquad \text{X.4.51)}$$

$$\delta G^{AL} = \int_{\Gamma_C} \delta \left[\lambda g_N(\mathbf{v}) + \frac{\alpha}{2} g_N^2(\mathbf{v}) \right] d\Gamma \qquad \text{(X.4.52)}$$

where $v \in U$, $\lambda \in J^+(\Gamma_C)$; $g_N(\mathbf{v})$ is defined by Eq. (2.3) and α is a positive parameter determined as part of the solution process.

The equivalence of this weak form to the strong form is shown in the following. Expanding the integrand in (52) gives

$$\delta G_{AL} = \int_{\Gamma_C} \left[\delta\lambda g_N + \lambda (\delta v_N^A + \delta v_N^B) + \alpha g_N (\delta v_N^A - \delta v_N^B) \right] d\Gamma \qquad \text{(X.4.53)}$$

where Eq. (2.3) has been used for δg. Combining the above with the terms associated with δG_{PL} from Eq. (28) gives

$$\int_{\Gamma_C} \left[\delta\lambda g + \delta v_N^A (\lambda + \alpha g + t_N^A) + \delta v_N^B (\lambda + \alpha g - t_N^B) \right] d\Gamma \geq 0 \qquad \text{(X.4.54)}$$

Since all of the variations are arbitrary, we obtain that on Γ_c

$$\delta\lambda: \qquad g_N = v_N^A - v_N^B \leq 0 \qquad \text{(X.4.55)}$$

$$\delta v_N^A: \qquad \lambda = -\alpha g - t_N^A \qquad \text{(X.4.56)}$$

$$\delta v_N^B: \qquad \lambda = -\alpha g + t_N^B \qquad \text{(X.4.57)}$$

Eqs. (56) and (57) can be combined to yield

$$t_A^N = -t_B^N = -\lambda - \alpha g \leq 0 \qquad \text{(X.4.58)}$$

where the inequality follows because $\lambda \geq 0$ and $g \geq 0$ when interpenetration occurs. Thus the normal interface traction is compressive and satisfies momentum balance.

X.4.8. Tangential Tractions by Lagrange Multipliers. All of the above formulations can be modified to handle interface friction laws by adding a term to the weak form which enforces continuity of the tangential tractions. We simply let

$$\delta P_C = \delta P + \delta G_N + \delta G_T \qquad \text{(X.4.59)}$$

where

$$\delta P_C \geq 0 \quad \text{if} \quad \delta G_N = \delta G_L \text{ or } \delta G_{AL} \qquad \text{X.4.60a)}$$

and

$$\delta P_C = 0 \quad \text{if} \quad \delta G_N = \delta G_P \text{ or } \delta G_{PL} \qquad \text{(X.4.60b)}$$

The tangential weak form is given by

$$\delta G_T = \int_{\Gamma_C} \delta\gamma_T \;\; \mathbf{t}_T \, d\Gamma \equiv \int_{\Gamma_C} \delta\hat{\gamma}_\alpha \hat{t}_\alpha \, d\Gamma \tag{X.4.61}$$

where $\mathbf{t}_T$ is a traction which is computed by a friction model. We have put hats on the expressions which are expressed in indicial notation to indicate that these components are in the local coordinates of the tangent plane of the contact interface.

To obtain the equations, we take what remains from δP after extracting the momentum equation and traction boundary conditions, Eq. (27a) . The normal kinetic and possibly kinematic conditions are then extracted as indicated in the preceding sections. What remains is combined with δG_T, giving

$$0 = \delta P_1(\Gamma_C) + \delta G + \delta G_T = \int_{\Gamma_c} (\delta v_\alpha^A t_\alpha^A + \delta v_\alpha^B t_\alpha^B + \delta\hat{\gamma}_\alpha \hat{t}_\alpha) \, d\Gamma \tag{X.4.62}$$

$$\equiv \int_{\Gamma_c} (\delta \mathbf{v}_T^A \;\; \mathbf{t}_T^A + \delta \mathbf{v}_T^B \;\; t_T^B + \delta\gamma_T \;\; \mathbf{t}_T) \, d\Gamma$$

Note that $\mathbf{t}_T$ differs from $\mathbf{t}_T^A$ and $\mathbf{t}_T^B$; $\mathbf{t}_T$ is the prescribed traction, which can be computed by an interface constitutive equation, whereas $\mathbf{t}_T^A$ and $\mathbf{t}_T^B$; are the tractions on the interface which result from the interior stresses by Eqs. (2.9b-c). Using the definition of γ_T, Eq. (2.8) we can write $\delta\gamma_T = \delta\mathbf{v}_T^A - \delta\mathbf{v}_T^B$. Substituting into the above we have, after rearranging the terms

$$0 = \delta P_1(\Gamma_C) + \delta G_T = \int_{\Gamma_c} \left[\delta \mathbf{v}_T^A \;\; (\mathbf{t}_T^A + \mathbf{t}_T) + \delta \mathbf{v}_T^B \;\; (\mathbf{t}_T^B - \mathbf{t}_T) \right] d\Gamma \tag{X.4.63}$$

From this we can extract

$$\mathbf{t}_T^A = -\mathbf{t}_T \qquad \mathbf{t}_T^B = \mathbf{t}_T \tag{X.4.64}$$

Eliminating $\mathbf{t}_T$ from the above we have

$$\mathbf{t}_T^A + \mathbf{t}_T^B = 0 \quad \text{or} \quad \hat{t}_\alpha^A + \hat{t}_\alpha^B = 0 \tag{X.4.65}$$

Thus the additional term δG_T in the weak form corresponds to the momentum balance of the tangential tractions on the contact interface. Without this term in the weak form, the tangential tractions vanish, i.e. the interface is frictionless.

This approach can be viewed as considering the $\hat{x}$ and $\hat{y}$ components of the contact surfaces to be prescribed traction surfaces. The traction term in the external power would then be equivalent (61).

When the stick condition applies to a part of the contact interface, it is possible to use a Lagrange multiplier to impose the constraint of no tangential slip. The form of the term is similar to that which imposes the interpenetration condition, (8). It is given by

$$\delta G_T = \int_{\Gamma_C} \delta(\gamma_T \ \mathbf{t}_T)\, d\Gamma \equiv \int_{\Gamma_C} \delta(\hat{\gamma}_\alpha \hat{t}_\alpha)\, d\Gamma \qquad \text{(X.4.66)}$$

This tangential weak form is associated with an equality, so if the original weak form to which it is appended is an equality, then the weak form remains an equality, whereas if the original weak is an inequality it remains an inequality. The strong forms corresponding to (66) are (65) and $\gamma_T = 0$.

BOX X.2 Weak Forms

$\delta P_C = \delta P + \delta G + \delta G_T$ note $\gamma \equiv \gamma_N$

Tangential tractions: $\delta G = \int_{\Gamma^c} \delta\gamma_T \ \lambda_T \, d\Gamma \equiv \int_{\Gamma^c} \delta\hat{\gamma}_\alpha \hat{\lambda}_\alpha \, d\Gamma$

Lagrangian: $\delta G = \delta G_L = \int_{\Gamma^c} \delta(\lambda\gamma)\, d\Gamma, \quad \delta P_C \geq 0$

Penalty: $\delta G = \delta G_P = \int_{\Gamma^c} \frac{1}{2}\beta\delta(\gamma^2)\, d\Gamma, \quad \delta P_C = 0$

Augmented Lagrangian: $\delta G = \delta G_{AL} = \int_{\Gamma^c} \delta(\lambda\gamma + \frac{\alpha}{2}\gamma^2)\, d\Gamma, \quad \delta P_C \geq 0$

Perturbed Lagrangian: $\delta G_N = \delta G_{PL} = \int_{\Gamma^c} \delta(\lambda\gamma - \frac{1}{2\beta}\lambda^2)\, d\Gamma, \quad \delta P_C = 0$

X.5 FINITE ELEMENT DISCRETIZATION

X.5.1 Overview. In the following, the finite element equations for the various treatments of contact-impact are developed. The weak statements for all of the approaches to the contact-impact problem, (penalty, Lagrange multiplier, etc.) involve a sum of the standard virtual power and a contribution from the contact interface. The standard virtual power is discretized exactly as in the absence of contact, so we will use the results developed in Chapter 4. This Section concentrates on the discretization of the various contact interface weak forms.

The developments that follow here are applicable to both updated and total Lagrangian formulations. However in total Lagrangian formulations, the contact interface conditions must be imposed in terms of the tractions on the deformed surface areas. The following discretizations are also applicable to ALE formulations as long as the nodes on the contact surface are Lagrangian. *They are not directly applicable to Eulerian formulations* since we assume that we have at our disposal a referential coordinate that describes the contact surface. Such a coordinate system cannot easily be defined in an Eulerian mesh. In a Lagrangian mesh, the contact surface corresponds to a subset of the boundary of the mesh.

We will first develop the FEM discretization for the Lagrangian multiplier method in indicial notation. Indicial notation enables us to go through some subtle steps which will subsequently be glossed over in the matrix derivations; anyone who wishes to replicate these steps for other formulations can rederive these in indicial notation.

X.5.2 Lagrange Multiplier Method. For the purpose of developing a finite element discretization, the velocities and the Lagrange multipliers must be approximated as functions of space and time. The velocity $\mathbf{v}(\mathbf{X},t)$ is approximated by C^0 interpolants in each body as in the single body problem; as can be seen from (4.3), continuity of velocities between two bodies across the contact interface is not built into the approximation, so the interpenetration condition will emanate from the discretization of the weak form. The velocity field can also be expressed in terms of the reference coordinates ζ on the contact surface when needed. As in Chapter 4, we note that the approximation of the velocity field directly defines the approximation of the displacement field.

The finite element approximation for the velocity field is expressed in terms of the material coordinates since we are dealing with a Lagrangian mesh. It can alternatively be written in terms of the element reference coordinates, since as pointed out in Chapter 4 the two sets of coordinates are equivalent. To clarify certain issues, we will initially discard the summation convention on repeated nodal indices and indicate sums explicitly. The velocity field is

$$v_i^A(\mathbf{X},t) = \sum_{I \in \Omega^A} N_I(\mathbf{X}) v_{Ii}^A(t) \qquad \text{(X.5.1a)}$$

$$v_i^B(\mathbf{X},t) = \sum_{I \in \Omega^B} N_I(\mathbf{X}) v_{Ii}^B(t) \qquad \text{(X.5.1b)}$$

If the node numbers of bodies *A* and *B* are treated as distinct, then the two velocity fields can be written as a single expression

$$v_i(\mathbf{X},t) = \sum_{I \in \Omega^A \cup \Omega^B} N_I(\mathbf{X}) v_{Ii}(t) \equiv N_I(\mathbf{X}) v_{Ii}(t) \qquad \text{(X.5.1c)}$$

where the last expression uses the implicit summation convention on node numbers

The Lagrange multiplier field $\lambda(\zeta,t)$, as can be seen from (4.5) and (4.6), is approximated by a C^{-1} field on the contact surface. The Lagrange multiplier field need only be piecewise continuous because its derivatives do not appear in any of the weak forms. We will use the element coordinates of the master body, ζ, as the independent variables in approximating the Lagrange multiplier field.

$$\lambda(\zeta,t) = \sum_{I \ \Gamma_\lambda^c} \Lambda_I(\zeta)\lambda_I(t) \equiv \Lambda_I(\zeta)\lambda_I(t) \qquad \lambda(\zeta,t) \ge 0 \tag{X.5.2}$$

The shape functions for the Lagrange multiplier field often differ from those used for the velocities, so different symbols have been used for the two approximations. Moreover, when the nodes of bodies *A* and *B* are not coincident, the mesh structure differs from that for the velocity field and a subscript λ has been added to Γ^c to indicate this fact. The need for a different nodal structure for the Lagrange multipliers is discussed in more detail later.

The test functions are given by

$$\delta v_i(\mathbf{X}) = N_I(\mathbf{X})\delta v_{Ii} \tag{X.5.3}$$

$$\delta\lambda(\zeta) = \Lambda_I(\zeta)\delta\lambda_I \qquad \delta\lambda(\zeta) \le 0 \tag{X.5.4}$$

where the implicit sums are defined in Eqs. (1) and (2).

To develop the semidiscrete equations, the above approximations for the velocity and Lagrange multiplier fields and the test functions are substituted into the weak form, Eq. (BX.2.3), which is repeated below:

$$\delta P + \int_{\Gamma^c} \delta(\lambda g_N)\, d\Gamma \ge 0 \tag{X.5.5}$$

The terms emerging from δP are identical to the nodal forces developed in Chapter 4, so they will not be rederived; the results are given in Table B4.1. From Eq. (B4.1.?) it follows that

$$\delta P = \delta v_{Ii}(\, f_{Ii}^{int} - f_{Ii}^{ext} + M_{IJij}\dot{v}_{Jj}) \equiv \delta\mathbf{d}^T(\,\mathbf{f}^{int} - \mathbf{f}^{ext} + \mathbf{M}\ddot{\mathbf{d}}) \equiv \delta\mathbf{d}^T\mathbf{f}^{res} \tag{X.5.6}$$

The interpenetration rate can be expressed in terms of the nodal velocities by using (2.7) and (8):

$$g_N = \sum_{I \ \Gamma^c \cap \Gamma^A} N_I v_{Ii}^A n_i^A + \sum_{I \ \Gamma^c \cap \Gamma^B} N_I v_{Ii}^B n_i^B \tag{X.5.7}$$

where the first sum, as indicated, is over the nodes of body *A* which are on the contact interface, and the second sum is over the nodes of body *B* which are on the contact interface. If we assign these nodes distinct node numbers, we can eliminate the distinction between nodes of body *A* and *B* and express the above as

$$\gamma_N = N_I v_{In} \tag{X.5.8}$$

(lower case *n* is used to indicate some of the normal components in this equation and the following). The range of the sum on the repeated index I is implied and defined in (7). The normal components are defined as in (2.5) by

$$v_{In} = v_{Ii}^A n_i^A \ \ if\ I in\ A, \quad v_{In} = v_{Ii}^B n_i^A \ \ if\ I in\ B \tag{X.5.9}$$

Then using the approximations (1-4) it follows that

$$\int_{\Gamma^c} \delta(\lambda\gamma_N)\, d\Gamma = \delta v_{In} \hat{G}_{IJ}^T \lambda_J + \delta\lambda_I \hat{G}_{IJ} v_{Jn} \tag{X.5.10}$$

where

$$\hat{G}_{IJ} = \int_{\Gamma^c} \Lambda_I N_J d\Gamma \tag{X.5.11}$$

A superposed hat has been placed on $\hat{G}_{IJ}$ to indicate that it pertains to the velocities in the local coordinate system of the contact interface. Combining Eqs. (5), (6), and (10) we can write the weak form as

$$\sum_I \delta v_{Ii} f_{Ii}^{res} + \sum_I \delta v_{In} \hat{G}_{IJ}^T \lambda_J + \sum_I \delta\lambda_I \hat{G}_{IJ} v_{Jn} \geq 0 \tag{X.5.12}$$

where the implicit sum on the index J holds, but the sums on the index I are explicitly stated to indicate the relevant nodes.

The governing equations must be extracted carefully because of the inequalities and the different roles different velocity components play in this equation. The equations for nodes which are not on the contact interface can be directly extracted from the first sum since the nodal velocities are arbitrary, which yields the standard nodal equations of motion at the nodes which are not on the contact interface

$$f_{Ii}^{res} = 0 \ \text{ or } \ M_{IJ} \dot{\mathbf{v}}_{Jj} = f_{Ii}^{ext} - f_{Ii}^{int} \quad for I \quad \Omega - \Gamma^c \tag{X.5.13}$$

To obtain the equations on the contact interface, what remains of the first sum after extracting Eq. (13) is rewritten in the local coordinate systems of the contact interface and combined with the second sum, giving

$$\sum_I \int_{\Gamma^c} (\delta v_{In} f_{In}^{res} + \delta\hat{v}_{I\alpha} \hat{f}_{I\alpha}^{res} + \delta v_{In} \hat{G}_{IJ}^T \lambda_J) + \sum_I \delta\lambda_I \hat{G}_{IJ} v_{Jn} \geq 0 \tag{X.5.14}$$

Since the tangential nodal velocities are unconstrained, the weak inequality yields an equality for the coefficients of the nodal velocities. First we set the coefficient of $\delta\hat{v}_{I\alpha}$ to zero, which gives

$$\hat{f}^{res}_{I\alpha} = 0 \;\; or \;\; M_{IJ}\dot{\hat{v}}_{J\alpha} = \hat{f}^{ext}_{I\alpha} - \hat{f}^{int}_{I\alpha} \;\; for \; I \quad \Gamma^c \tag{X.5.15}$$

The equation for the normal component at the contact interface nodes involves the first and third terms of the first sum in (13) and gives

$$f^{res}_{In} + \hat{G}^T_{IJ}\lambda_J = 0 \;\; or \;\; M_{IJ}\dot{v}_{Jn} + f^{ext}_{In} - f^{int}_{In} + \hat{G}^T_{IJ}\lambda_J = 0 \quad for I \quad \Gamma^c \tag{X.5.16}$$

To extract the equations associated with the Lagrange multipliers, we note that the variations of the nodal Lagrange multipliers must be negative. Therefore the inequality (5) implies

$$\hat{G}_{IJ}v_{Jn} \le 0 \tag{X.5.17}$$

In addition, we have from Eq. (4.6) the requirement that the test function for the Lagrange multiplier field must be positive

$$\lambda(\zeta, t) \ge 0 \tag{X.5.18}$$

The above inequality is difficult to enforce. For elements with piecewise linear displacements along the edges, this condition is often enforced only at the nodes by $\lambda_I \ge 0$. This simplification is only appropriate with piecewise linear approximations since the local minima of the Lagrange multipliers then occur at the nodes.

The above equations, in conjunction with the strain-displacement equations and the constitutive equation, comprise the complete system of equations for the semidiscrete model. The semidiscrete equations consist of the equations of motion and the contact interface conditions. The equations of motion for nodes not on the contact interface are unchanged from the unconstrained case. On the contact interface, additional forces $\hat{G}_{IJ}\lambda_J$ which represent the normal contact tractions appear. In addition, the impenetrability constraint in weak form (17) must be imposed. Like the equations without contact, the semidiscrete equations are ordinary differential equations, but the variables are subject to algebraic inequality constraints on the velocities and the Lagrange multipliers. These inequality constraints substantially complicate the time integration, since the smoothness which is implicitly assumed by most time integration procedures is lost.

For purposes of implementation, it is convenient to write the above equations in matrix form in global components. Let the interpenetration rate be defined in terms of the nodal velocities by

$$\gamma = \Phi_{Ii}(X)v_{Ii}(t) \tag{X.5.19}$$

where

$$\Phi_{Ii}(X) = \begin{cases} N_I n_i^A \; if \; I on A \\ N_I n_i^B \; if \; I on B \end{cases} \tag{X.5.20}$$

The contact weak term is then given by

$$\delta G_L = \int_{\Gamma_c} \delta(\lambda_I \Lambda_I \Phi_{Jj} v_{Jj})\, d\Gamma = \lambda^T \mathbf{G} \mathbf{v} \qquad \text{(X.5.21a)}$$

where

$$G_{JjI} = \int_{\Gamma_c} \Lambda_I \Phi_{Jj}\, d\Gamma \qquad \mathbf{G} = \int_{\Gamma_c} \Lambda^T \Phi\, d\Gamma \qquad \text{(X.5.21b)}$$

The equations of motion can be written in matrix form by combining this form with matrix forms of the internal, external and inertial power, which gives

$$\delta \mathbf{v}^T \left(\mathbf{f}^{int} - \mathbf{f}^{ext} + \mathbf{M}\ddot{\mathbf{d}} \right) + \delta \left(\mathbf{v}^T \mathbf{G}^T \lambda \right) = 0 \qquad \delta \mathbf{v} \quad U^h \qquad \delta \lambda \quad J^{h-} \qquad \text{(X.5.22)}$$

We will skip the steps represented by Eqs. (7-17) and invoke the arbitrariness of $\delta \mathbf{v}$ and $\delta \lambda$. The matrix forms of the equations of motion and the interpenetration condition are

$$\mathbf{M}\ddot{\mathbf{d}} + \mathbf{f}^{int} - \mathbf{f}^{ext} + \mathbf{G}^T \lambda = \mathbf{0} \qquad \text{(X.5.23a)}$$

$$\mathbf{G}\mathbf{v} \le 0 \qquad \text{(X.5.23b)}$$

The construction of the interpolation, and hence the nodal arrangement, for the Lagrange multipliers poses some difficulties. In general, the nodes of the two contacting bodies are not coincident, as shown in Fig. 5.1. Therefore it is necessary to develop a scheme to deal with noncontiguous nodes. One possibility is indicated in Fig. 5.1, where the nodes for the Lagrange multiplier field are chosen to be the nodes of the master body which are in contact. This is a simple

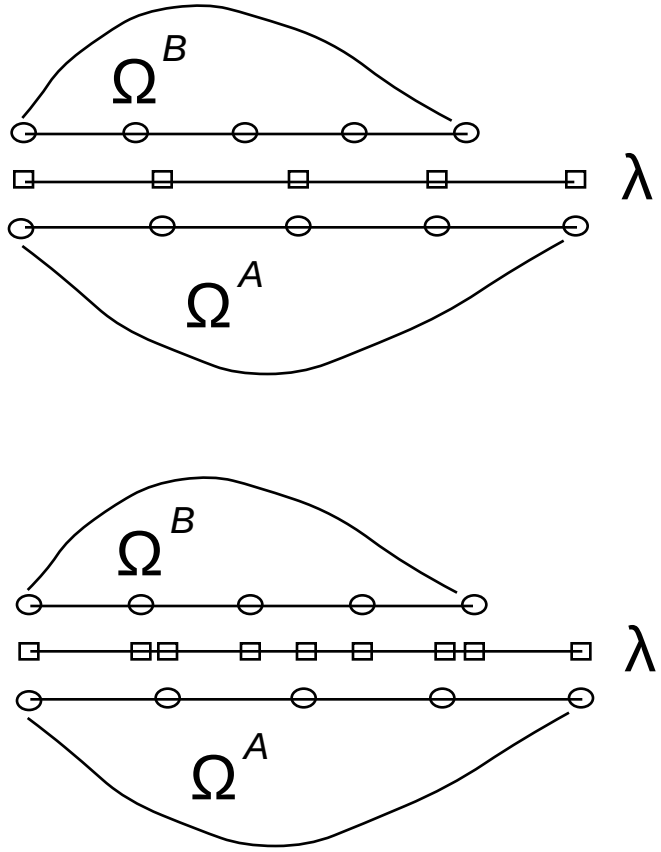

Figure. X.5.1. Nodal arrangements for two contacting bodies with noncontiguous nodes showing (a) a Lagrange multiplier mesh based on the master body and (b) an independent Lagrange multiplier mesh.

scheme, but when the nodes of body B are much more finely spaced a coarse nodal structure for the Lagrange multipliers will lead to interpenetration. An alternative is to place Lagrange multiplier nodes wherever a node appears in either body *A* or *B*, as shown in Fig. 5.1b. The disadvantage of that scheme is that when nodes of A and B are closely spaced, the Lagrange multiplier element is then very small. This can lead to ill-conditioning of the equations.

X.5.3. Assembly of Interface Matrix. The **G** matrix can be assembled from "element" matrices like any other global finite element matrix. To illustrate the assembly procedure, let the nodal velocities and Lagrange multipliers of element *e* be expressed in terms of the global matrices by

$$\mathbf{v}_e = \mathbf{L}_e \mathbf{v} \quad \lambda_e = \mathbf{L}_e^{\lambda} \lambda \tag{X.5.24a}$$

with identical relations for the test functions

$$\delta\mathbf{v}_e = \mathbf{L}_e \mathbf{v} \quad \delta\lambda_e = \mathbf{L}_e^{\lambda} \delta\lambda$$

Substituting into (18) gives

$$\lambda^{\mathbf{T}}\mathbf{G}\mathbf{v} = \int_{\Gamma^c} \lambda\gamma d\Gamma = \sum_e \int_{\Gamma_e^c} \lambda\gamma d\Gamma = \lambda^T \left(\mathbf{L}_e^{\lambda}\right)^T \int_{\Gamma_e^c} \Phi^T \Lambda d\Gamma\, \mathbf{L}_e \mathbf{v}$$

Since (18) must hold for arbitrary $\dot{\mathbf{d}}$ and λ it can be seen by comparing the first and last term of the above that

$$\mathbf{G} = \sum_e \left(\mathbf{L}_e^{\lambda}\right)^T \mathbf{G}_e \mathbf{L}_e, \qquad \mathbf{G}_e = \int_{\Gamma_e^c} \Lambda^T \varphi d\Gamma \tag{X.5.25}$$

Thus the assembly of $\mathbf{G}$ from $\mathbf{G}_e$ is identical to assembly of global matrices such as the stiffness matrix.

X.5.4. Lagrange Multipliers for Small-Displacement Elastostatics. We will call the analysis of small-displacement problems with linear, elastic materials small-displacement elastostatics. We have used the nomenclature of small-displacement, elastostatics rather than linear elasticity because these problems are not linear due to the inequality constraint on the displacements which arises from the contact condition. For small-displacement elastostatics, the governing relations for the impenetrability constraint can be obtained from the preceding by replacing the velocities by the displacements. Thus Eq. (2.7) and (19) are replaced by

$$g_N = \left(\mathbf{u}^A - \mathbf{u}^B\right) \mathbf{n}^A \le 0 \;\; on \Gamma^c \qquad g_N = \Phi \mathbf{d} \tag{X.5.26}$$

The discretization procedure is then identical to the above except for substituting velocities by displacements and omitting the inertia, giving

$$\delta\mathbf{d}^T\left(\mathbf{f}^{int} - \mathbf{f}^{ext}\right) + \delta\left(\mathbf{d}^T\mathbf{G}\lambda\right) = 0 \quad \delta\mathbf{d} \quad U \quad \delta\lambda \quad J^- \tag{X.5.27}$$

Since the internal nodal forces are not effected by contact, for the small displacement elastostatic problem they can be expressed in terms of the stiffness matrix by

$$\mathbf{f}^{int} = \mathbf{K}\mathbf{d} \tag{X.5.26a}$$

Taking the variation of the second term and using the arbitrariness of $\delta\mathbf{d}$ and the arbitrary but negative character of $\delta\lambda$ gives

$$\begin{bmatrix} \mathbf{K} & \mathbf{G}^T \\ \mathbf{G} & \mathbf{0} \end{bmatrix} \begin{Bmatrix} \mathbf{d} \\ \lambda \end{Bmatrix} \le \begin{Bmatrix} \mathbf{f}^{ext} \\ \mathbf{0} \end{Bmatrix} \tag{X.5.27}$$

This is the standard form for Lagrange multiplier problems except that an equality has been replaced by an inequality in the second matrix equation.

If we recall other Lagrange multiplier problems, two properties of this system come to mind:

1. the system of linear algebraic equations is no longer positive definite;

2. the equations as given above are not banded and it is difficult to find an arrangement of unknowns so that they are banded;

3. the number of unknowns is increased as compared to the system without the contact constraints.

In addition, for the contact problem, the solution of the equations is complicated by the presence of the inequalities. These are very difficult to deal with and often the small-displacement, elastostatic problem is posed as a quadratic programming problem, see Section ?. These difficulties also arise in the nonlinear implicit solution of contact problems.

A major disadvantage of the Lagrange multiplier method is the need to set up a nodal and element topology for the Lagrange multipliers. As we have seen in the simple two dimensional example, this can introduce complications even in two dimensions. In three dimensions, this task is far more complicated. In penalty methods we see there is no need to set up an additional mesh.

In comparison to the penalty method, the advantage of the Lagrange multiplier method is that there are no user-set parameters and the contact constraint can be met almost exactly when the nodes are contiguous. When the nodes are not contiguous, impenetrability can be violated slightly, but not as much as in penalty methods. However, for high velocity impact, Lagrange multipliers often result in very noisy solutions. Therefore, Lagrange multiplier methods are most suited for static and low velocity problems.

X.5.5. Penalty Method for Nonlinear Frictionless Contact. The nonlinear discretization is developed only for the second form of the penalty method, (X.4.47). In the penalty method only the velocity field needs to be approximated. Again, the velocity field is C^0 within each body, but no stipulation of continuity between bodies need be made. Continuity between bodies on the contact interface is enforced by the penalty method. We only develop the weak penalty term

$$\delta G_p = \int_{\Gamma_c} \delta\gamma p(g,\gamma)\, d\Gamma \tag{X.5.28}$$

since the other weak terms are unchanged from the unconstrained problem. Substituting

$$\delta G_P = \delta \mathbf{v}^T \int_{\Gamma_c} \varphi^T p\, d\Gamma \equiv \delta \mathbf{v}^T \mathbf{f}^c \tag{X.5.29}$$

where φthe second equality defines $\mathbf{f}^c$ by

$$\mathbf{f}^c = \int_{\Gamma_c} \varphi^T p\, d\Gamma \tag{X.5.30}$$

Note the similarity of this formula to that for the internal forces; they express the same thing, the relation between discrete forces and continuous tractions. Using (29) and (6) in the weak form (4.28) with (4.39) the above definition of $\mathbf{f}^c$ gives

$$\delta P = \delta \mathbf{v}^T \mathbf{f}^{res} + \delta \mathbf{v}^T \mathbf{f}^c \qquad \text{(X.5.31)}$$

So using the arbitrariness of $\delta \mathbf{v}$ and (5.6) gives

$$\mathbf{f}^{int} - \mathbf{f}^{ext} + \mathbf{M}\mathbf{a} + \mathbf{f}^c = 0 \qquad \text{(X.5.32)}$$

Thus in the penalty method the number of equations is unchanged from the unconstrained problem. The inequalities (B1.3) do not appear explicitly among the discrete equations but are enforced by appearance of the step function in the calculation of the contact penalty forces by (30) and (4.38).

X.5.6. Penalty for Small-Displacement Elastostatics. For small-displacement elastostatics, we replace velocities by displacements as previously. Equation (4.43a) with $\beta_2 = 0$ and (26b) give

$$p = \beta_1 g_N = \beta_1 \varphi \mathbf{d} \qquad \text{(X.5.33)}$$

Substituting the above into (30) gives

$$\mathbf{f}^c = \int_{\Gamma^c} \varphi^T p(g_N) H(\gamma)\, d\Gamma = \int_{\Gamma} \beta_1 \varphi^T \varphi H(\gamma)\, d\Gamma\, \mathbf{d}$$

or

$$\mathbf{f}^c = \mathbf{P}_c \mathbf{d}, \qquad \mathbf{P}_c = \int_{\Gamma} \beta_1 \varphi^T \varphi H(\gamma)\, d\Gamma \qquad \text{(X.5.34)}$$

Substituting (34) and (26a) into (32) after dropping the inertial term, gives,

$$(\mathbf{K} + \mathbf{P}_c)\mathbf{d} = \mathbf{f}^{ext} \qquad \text{(X.5.35)}$$

This is a system of algebraic equations of the same order as the problem without contact impact. The contact interface constraints appear strictly through the penalty forces $\mathbf{P}_c \mathbf{d}$. The algebraic equations are not linear because as can be seen from (34), the matrix $\mathbf{P}_c$ involves the Heaviside step function of the gap, which depends on the displacements.

In contrast to the Lagrange multiplier methods it can be seen that:

1. the number of unknowns does not increase due to the enforcement of the contact constraints.

2. the system equations remain positive definite since $\mathbf{K}$ is positive definite and $\mathbf{G}$ is positive definite.

The disadvantage of the penalty approach is that the enforcement of the impenetrability condition is only approximate and its effectiveness depends on the appropriateness of the penalty parameters. If the penalty parameters is too small, excessive interpenetration occurs causing errors in the solution. In impact problems, small penalty parameters reduce the maximum computed stresses. We have seen some shenanigans in calculations where analysts met stress criteria by reducing the penalty parameters. Picking the correct

penalty parameter is a challenging problem. Some guidelines are given in Section ?, where we discuss implementation of various solution procedures with penalty methods.

X.5.7. Augmented Lagrangian. In the augmented Lagrangian method, the weak contact term is

$$\delta G_{AL} = \int_{\Gamma_c} \delta(\lambda\gamma + \frac{\alpha}{2}\gamma^2)\, d\Gamma \tag{X.5.36}$$

Using the approximation for the velocity $v(\mathbf{X},t)$ and the Lagrange multiplier $\lambda(\xi,t)$ gives

$$\delta G_{AL} = \int_{\Gamma_C} \delta(\lambda^T \Lambda^T \varphi \mathbf{v} + \frac{\alpha}{2}\mathbf{v}^T \varphi^T \varphi \mathbf{v})\, d\Gamma$$

Taking the variations gives (X.5.37)

$$\delta G_{AL} = \delta\lambda^T \mathbf{G}\mathbf{v} + \delta\mathbf{v}^T \mathbf{G}^T \lambda + \delta\mathbf{v}^T \mathbf{P}_c(\alpha)\mathbf{v} \tag{X.5.38}$$

where $\mathbf{P}_c(\alpha)$ is defined by (34). Writing out the weak form $\delta P_{AL} = \delta P + \delta G_{AL} \geq 0$ using Eqs. (36-38) then gives

$$\mathbf{f}^{int} - \mathbf{f}^{ext} + \mathbf{M}\mathbf{a} + \mathbf{G}^T\lambda + \mathbf{P}_c\mathbf{v} = 0 \tag{X.5.40a}$$

$$\mathbf{G}\mathbf{v} \leq 0 \tag{X.5.40b}$$

Comparing Eqs. (40) with (23) and (35), we can see that the augmented Lagrangian method gives contact forces which are a sum of those in the Lagrangian method and the penalty method. The impenetrability constraint (40b), is the same as in the Lagrange multiplier method.

For small-displacement elastostatics, we use the same procedure as before. We change the dependent variables to displacements so we replace the nodal velocities by nodal displacements, and using(??) and (27a), the counterpart of Eqs. (39) and (40)

$$\begin{bmatrix} \mathbf{K} + \mathbf{P}_c & \mathbf{G}^T \\ \mathbf{G} & \mathbf{O} \end{bmatrix} \begin{Bmatrix} \mathbf{d} \\ \lambda \end{Bmatrix} \leq \begin{Bmatrix} \mathbf{f}^{ext} \\ \mathbf{O} \end{Bmatrix} \tag{X.5.41}$$

which further illustrates that the augmented Lagrangian method is a synthesis of penalty and Lagrange multiplier methods , Eqs. (27) and (35).

X.5.8. Perturbed Lagrangian. The semidiscretization of the perturbed Lagrangian formulation is obtained by using (4.45) with velocity and Lagrange multiplier approximations are given by Eqs. (1) and (2), respectively. We won't go through the steps, since they are identical to the previous discretizations. The discrete equations are

$$\mathbf{f}^{int} - \mathbf{f}^{ext} + \mathbf{M}\mathbf{a} + \mathbf{G}^T\lambda = \mathbf{O} \tag{X.5.42}$$

$$\mathbf{G}\mathbf{v} - \mathbf{H}\lambda = \mathbf{O} \tag{X.5.43}$$

Equation (42) corresponds to the momentum equation, Eq. (43) to the impenetrability condition. The matrix $\mathbf{G}$ is defined by Eq. (21b) and

$$\mathbf{H} = \int_{\Gamma_c} \frac{1}{\beta} \Lambda^T \Lambda \, d\Gamma \tag{X.5.44}$$

The constraint equations (43) can be eliminated to yield a single system of equations. Solving Eq.(43) for λ and substituting into (42) gives

$$\mathbf{f}^{int} - \mathbf{f}^{ext} + \mathbf{M}\mathbf{a} + \mathbf{G}^T \mathbf{H}^{-1} \mathbf{G} = 0 \tag{X.5.45}$$

The above is similar to the discrete penalty equation (35) with the penalty parameter β appearing through $\mathbf{H}$ in (44). The last term in the above equations represents the contact forces.

The semidiscrete equations for small-displacement elastostatics for the perturbed Lagrangian methods are

$$\begin{bmatrix} \mathbf{K} & \mathbf{G}^T \\ \mathbf{G} & -\mathbf{H} \end{bmatrix} \begin{Bmatrix} \mathbf{d} \\ \lambda \end{Bmatrix} = \begin{Bmatrix} \mathbf{f}^{ext} \\ \mathbf{O} \end{Bmatrix} \tag{X.5.46}$$

Comparing the above to the Lagrangian method, Eq. (27), we can see that it differs only in the lower left submatrix, which is $\mathbf{0}$ in the Lagrangian method but consists of the matrix $\mathbf{H}$ in the perturbed Lagrangian method.

BOX X.3 Semidiscrete Equations for Nonlinear Contact

$$\mathbf{f} = \mathbf{f}^{ext} - \mathbf{f}^{int}$$

Lagrange Multiplier

$$\mathbf{Ma} - \mathbf{f} + \mathbf{G}^T\lambda = 0, \quad \mathbf{Gv} \le 0, \quad \lambda(x) \ge 0$$

Penalty

$$\mathbf{Ma} - \mathbf{f} + \mathbf{f}^c = 0, \quad \mathbf{f}^c = \int_{\Gamma^c} \Phi^T p(g_N) H(g_N) d\Gamma$$

Augmented Lagrangian

$$\mathbf{Ma} - \mathbf{f} + \mathbf{G}^T\lambda + \mathbf{P}_c\mathbf{v} = 0, \quad \mathbf{Gv} \le 0$$

Perturbed Lagrangian

$$\mathbf{Ma} - \mathbf{f} + \mathbf{G}^T\lambda = 0, \quad \mathbf{Gv} - \mathbf{H}\lambda = 0$$

$$\mathbf{G} = \int_{\Gamma^c} \Lambda^T \varphi \, d\Gamma \qquad \mathbf{H} = \int_{\Gamma^c} \Lambda^T \Lambda \, d\Gamma \qquad \mathbf{P}_c = \int_{\Gamma^c} \alpha \varphi^T \varphi \, d\Gamma$$

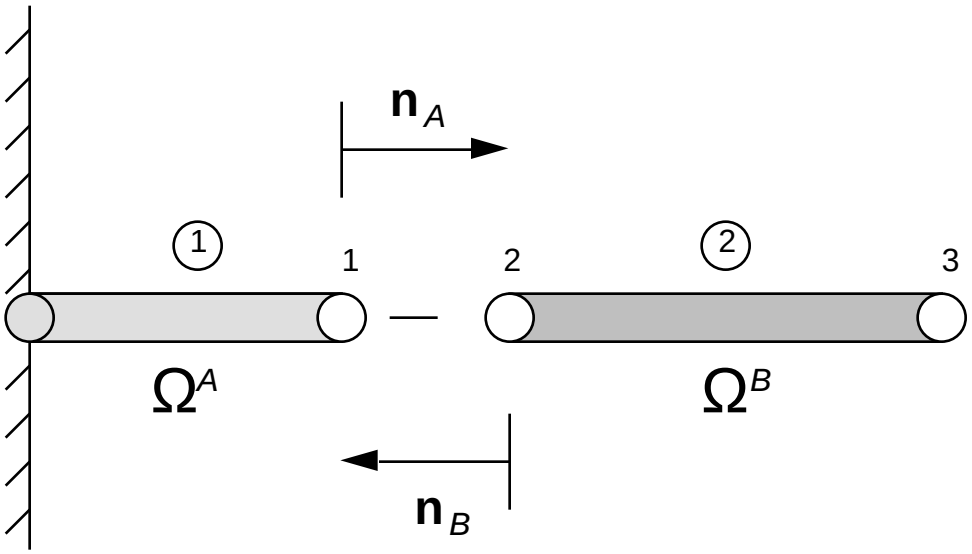

Figure X.5.1. One dimensional example of contact; example 1.

Example X.5.1. Finite Element Equations for One Dimensional Contact-Impact. Consider the two rods shown in Fig. X.5.1. We consider a rod of unit cross-sectional area. The contact interface consists of the nodes at the ends of the rods, which are numbered 1 and 2. The unit normals, as shown in Fig. X.5.1, are $n_x^A = 1, n_x^B = -1$. The contact interface in one-dimensional problems is rather odd since it consists of a single point. The velocity fields in the two elements which border the contact interface are given by

$$v(\xi,t) = \mathbf{N}(\xi,t)\dot{\mathbf{d}} = \left[\xi^A,\ 1-\xi^B,\ \xi^B\right]\dot{\mathbf{d}} \tag{X.5.47}$$

where the column matrix of nodal velocities is

$$\dot{\mathbf{d}}^T = \left[v_1 \quad v_2 \quad v_3\right] \tag{X.5.48}$$

The **G** matrix is given by Eqs. (20) and (21); in a one-dimensional problem, the integral is replaced by a single function value, with the function evaluated at the contact point:

$$\begin{aligned}\mathbf{G}^T &= \left[\xi^A\ n^A,\ (1-\xi^B)n^B,\ \xi^B\right]\Big|_{\xi^A=1,\,\xi^B=0} \\ &= \left[(1)(+1),\ 1(-1),\ 0\right] \\ &= \left[1,\ -1,\ 0\right]\end{aligned} \tag{X.5.49}$$

The impenetrability condition in rate form, (23b), is given by

$$\mathbf{G}^T\dot{\mathbf{d}} \le 0 \ \textit{or}\ \left[1 \quad -1 \quad 0\right]\dot{\mathbf{d}} = v_1 - v_2 \le 0 \tag{X.5.50}$$

The last equation can easily be obtained by inspection: when the two nodes are in contact, the velocity of node 1 must be less or equal than the velocity of node 2 to preclude overlap. If they are equal, they remain in contact, whereas when the inequality holds, they release. These conditions are not sufficient to check for initial contact, which should be checked in terms of the nodal displacements: $x_1 - x_2 \ge 0$ indicates contact has occurred during the previous time step.

Since there is only one point of contact, only a single Lagrange multiplier appears in the equations of motion. The equations of motion, Eqs. (BX.3.2) are then

$$\begin{bmatrix} M_{11} & M_{12} & M_{13} \\ M_{21} & M_{22} & M_{23} \\ M_{31} & M_{32} & M_{33} \end{bmatrix} \begin{Bmatrix} \ddot{d}_1 \\ \ddot{d}_2 \\ \ddot{d}_3 \end{Bmatrix} - \begin{Bmatrix} f_1 \\ f_2 \\ f_3 \end{Bmatrix} + \begin{Bmatrix} 1 \\ -1 \\ 0 \end{Bmatrix} \lambda_1 = 0 \tag{X.5.51}$$

and

$$\lambda_1 \ge 0 \tag{X.5.52}$$

The last terms in (51) are the nodal forces resulting from contact between nodes 1 and 2. The forces on the nodes are equal and opposite and vanish when the Lagrange multiplier vanishes. The equations of motion are identical to the equations for an unconstrained finite element mesh except at the nodes which are in contact. The equations for a diagonal mass matrix with unit area can be written as

$$\begin{aligned} M_1 a_1 - f_1 + \lambda_1 &= 0 \\ M_2 a_2 - f_2 - \lambda_1 &= 0 \\ M_3 a_3 - f_3 &= 0 \end{aligned} \qquad \text{(X.5.53)}$$

where $a_I = \ddot{d}_I$.

The equations for small-displacement elastostatics, Eq. (27) can be written by combining the **G** matrix, Eq. (49), with the assembled stiffness as in (27c) giving

$$\begin{bmatrix} k_1 & 0 & 0 & 1 \\ 0 & k_2 & -k_2 & -1 \\ 0 & -k_2 & k_2 & 0 \\ 1 & -1 & 0 & 0 \end{bmatrix} \begin{Bmatrix} d_1 \\ d_2 \\ d_3 \\ \lambda_1 \end{Bmatrix} = \begin{Bmatrix} f_1^{ext} \\ f_2 \\ f_3 \\ 0 \end{Bmatrix} \qquad \text{(X.5.54)}$$

where k_I is the stiffness of element *I*. The assembled stiffness matrix in the absence of contact, i.e. the upper left hand 3x3 matrix, is singular, but with the addition of the contact interface conditions, the complete 4x4 matrix becomes regular.

Penalty Method. To write the equation for the penalty method, we will use the penalty law $p = \beta g = \beta(x_1 - x_2)\,H(g) = \beta(X_1 - X_2 + u_1 - u_2)\,H(g)$. Then evaluating Eq. (30) gives

$$\mathbf{f}^c = \int_{\Gamma^c} \varphi^T p \, d\Gamma = \begin{Bmatrix} 1 \\ -1 \\ 0 \end{Bmatrix} \beta g \qquad \text{(X.5.55)}$$

The above integral consists of the integrand evaluated at the interface point since Γ^c is a point. Equations (32) for a diagonal mass are then

$$\begin{aligned} M_1 a_1 - f_1 + \beta g &= 0 \\ M_2 a_2 - f_2 - \beta g &= 0 \\ M_3 a_3 - f_3 &= 0 \end{aligned} \qquad \text{(X.5.56)}$$

The equations are identical to that for the Lagrange multiplier method, (53) except that the Lagrange multiplier is replaced by the penalty force.

To construct the small displacement, elastostatic equations for the penalty method, we first evaluate $\mathbf{P}_c$ by Eq. (34):

$$\mathbf{P}_c = \int_{\Gamma_c} \beta_1 \varphi^T \varphi H(g)\, d\Gamma = \beta_1 H(\gamma) \begin{bmatrix} +1 \\ -1 \\ 0 \end{bmatrix} \begin{bmatrix} +1 & -1 & 0 \end{bmatrix}$$

$$= \beta_1 H(g) \begin{bmatrix} +1 & -1 & 0 \\ -1 & +1 & 0 \\ 0 & 0 & 0 \end{bmatrix} \tag{X.5.57}$$

If we define $\bar{\beta} = \beta_1 H(g)$, and add $\mathbf{P}_c$ to the linear stifness, then the resulting equations are

$$\begin{bmatrix} k_1 + \bar{\beta} & -\bar{\beta} & \\ -\bar{\beta} & k_2 + \bar{\beta} & -k_2 \\ & -k_2 & k_2 \end{bmatrix} \begin{Bmatrix} d_1 \\ d_2 \\ d_3 \end{Bmatrix} = \begin{Bmatrix} f_1 \\ f_2 \\ f_3 \end{Bmatrix}^{ext} \tag{X.5.58}$$

It can be seen from the above equation that the penalty method simply adds a spring with a spring constant $\bar{\beta}$ between nodes 1 and 2. The above equation is nonlinear since $\bar{\beta}$ is a nonlinear function of $g = u_1 - u_2$.

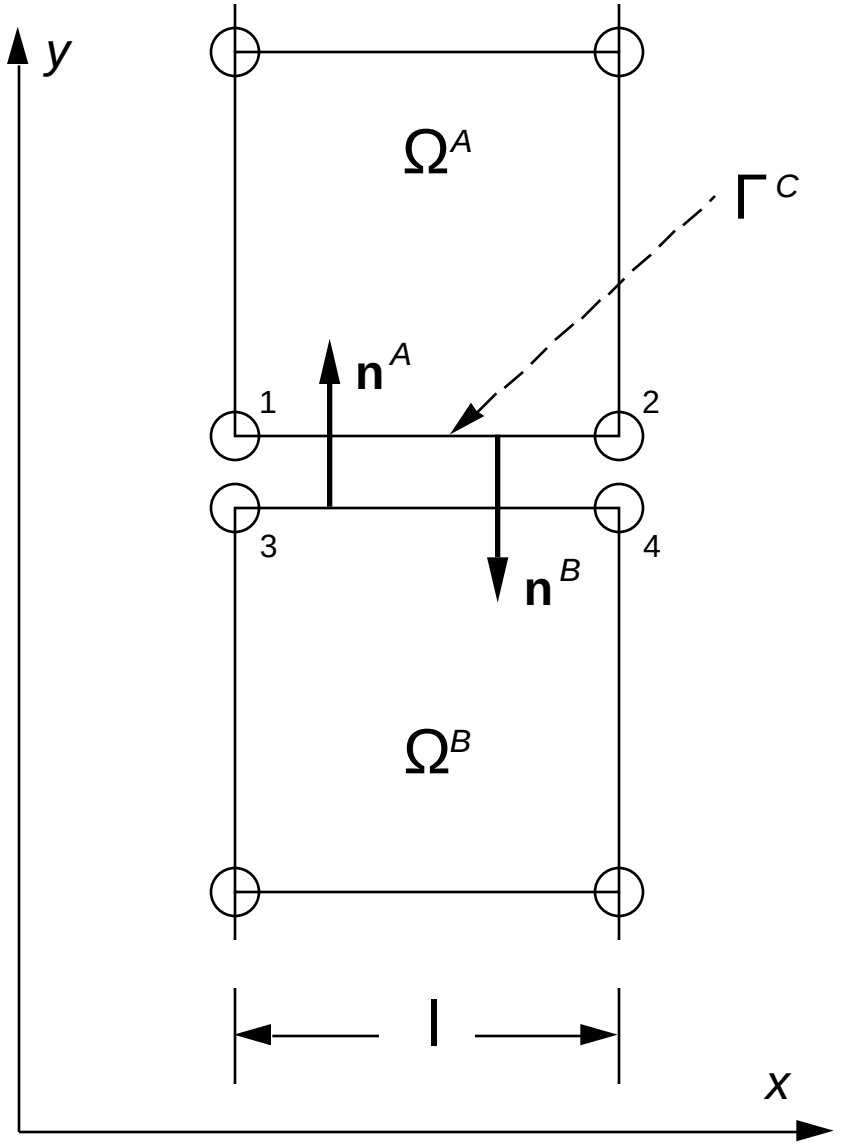

Figure X.5.2

Example X2. Two Dimensional Example. Figure 2 shows two dimensional bodies modeled by 4-node quadrilaterals which are in contact along a line parallel to the *x*-axis. The approximations along the contact surface are written in terms of the element coordinates of one of the master body *A*., which in this case is the identical to that of body *B*. The velocity field along the contact interface is given by

$$\begin{Bmatrix} v_x(\xi,t) \\ v_y(\xi,t) \end{Bmatrix} = \begin{bmatrix} N_1 & 0 & N_2 & 0 & N_3 & 0 & N_4 & 0 \\ 0 & N_1 & 0 & N_2 & 0 & N_3 & 0 & N_4 \end{bmatrix} \mathbf{v} \tag{X.5.59}$$

where

$$\mathbf{v}^T = \begin{bmatrix} v_{1x} & v_{1y} & v_{2x} & v_{2y} & v_{3x} & v_{3y} & v_{4x} & v_{4y} \end{bmatrix}^T \tag{X.5.60}$$

$$N_1 = N_3 = 1 - \xi, N_2 = N_4 = \xi, \xi = x / l \tag{X.5.61}$$

The unit normals are given by $\mathbf{n}^A = \begin{bmatrix} 0 & -1 \end{bmatrix}^T, \mathbf{n}^B = \begin{bmatrix} 0 & 1 \end{bmatrix}^T$ so the Φ matrix is given by Eq. (20):

$$\Phi = \begin{bmatrix} N_1 n_1^A & N_1 n_2^A & N_2 n_1^A & N_2 n_2^A & N_3 n_1^B & N_3 n_2^B & N_4 n_1^B & N_4 n_2^B \end{bmatrix}$$

$$= \begin{bmatrix} -N_1 & 0 & -N_2 & 0 & N_3 & 0 & N_4 & 0 \end{bmatrix} \tag{X.5.62}$$

The Lagrange multiplier field is approximated by the same linear field (we will discuss appropriate fields later)

$$\lambda(\xi, t) = \Lambda\lambda = \begin{bmatrix} N_1 & N_2 \end{bmatrix} \begin{Bmatrix} \lambda_1 \\ \lambda_2 \end{Bmatrix} \tag{X.5.63}$$

where the same shape functions as in (61) are used. The $\mathbf{G}$ matrix is given by

$$\mathbf{G} = \int_{\Gamma_c} \Lambda^T \Phi \, d\Gamma = \frac{l}{6} \begin{bmatrix} 0 & -2 & 0 & -1 & 0 & 2 & 0 & 1 \\ 0 & -1 & 0 & -2 & 0 & 1 & 0 & 2 \end{bmatrix} \tag{X.5.64}$$

The terms of the rows resemble the terms of the consistent mass for a rod, and the behavior for this Lagrange multiplier field is similar: a contact at node 1 results in forces at node 2, and vice versa. Nodal forces due to contact are strictly in the *y* direction; all *x*-components of forces from contact in this example will vanish since the odd rows of the $\mathbf{G}$ matrix vanish. This is consistent with what is expected physically, since the contact surface is along the x-direction and the contact interface is frictionless.

MISCELLANEOUS TOPICS

Regularization. The penalty approach may be thought of as a regularization of the interface conditions; the exact solution of the impact of two rods leads to solutions discontinuous in time, cf. Fig. . A regularization procedure in mathematics is a procedure which by an artifact replaces a problem whose solutions are difficult to deal with because of warts such as discontinuities or singularities by one with smoother, more regular solutions. The classic example of regularization is von Neumann's addition of artificial viscosity to the Euler fluid equations to smooth shocks. Without this artificial viscosity, solutions of the Euler equations in the vicinity of shocks by the central difference method are so oscillatory that they look like lash. Von Neumann showed that his regularization conserves momentum, so only part of the system is modified by regularization.

The penalty method plays the same role as artificial viscosity in impact. With the Lagrange multiplier method, the velocities are discontinuous in time at the point of impact, and these discontinuities propagate through the body as waves and result in considerable noise. The penalty regularization preserves momentum conservation, and the other *conservation* equations are also observed exactly. It only relaxes one condition,

the impenetrability condition, by allowing some overlap of the two bodies. It is a small price to pay for smoother solutions if the interpenetration is small.

The Curnier-Mroz plasticity models of friction can also be considered regularization, in this case, of the discontinuous character of the friction laws. The discontinuous nature of Coulomb friction can be gleamed from a simple illustration. Consider an element on a rigid surface with interface tractions modeled by Coulomb friction. A vertical force is applied to the top nodes, a horizontal force on the two left-hand nodes as shown, and we neglect the deformability of the element. If the vertical force is kept constant while the horizontal force has the time history shown, the velocity will have the time history shown in Fig. Xd. The discontinuity in time arises because the inequalities in the Coulomb friction law embody Heaviside step functions exactly as they embodied in the interpenetration inequalities.

The Curnier-Mroz friction model eliminates the discontinuity as shown in Fig. X. Regularization of Coulomb friction differs from regularization of interpenetration in that, superficially at least, it smoothes the response by introducing additional mechanics to the model, namely the asperities, whereas the relaxation of the interpenetrability condition appears to be quite *ad hoc* and not motivated by physical arguments. In fact, one can also attribute some interpenetration of the idealized bodies which comprise the models in contact-impact problems to compression of asperities. Usually, however, the penalty parameters are not chosen by such physical characteristics, but instead by the desirability of eliminating frequencies above a certain threshold.

REFERENCES

T. Belytschko and M.O. Neal (1991), "Contact-Impact by the Pinball Algorithm with Penalty and Lagrangian Methods," *Int. J. for Numerical Methods in Engineering*, 31. 547-572.

D.P. Bertsekas (1984), *Constrained Optimization and Lagrange Multiplier Methods*, Academic Press, New York.

A. Curnier (1984), "A Theory of Friction," *Int. J. Solids and Structures*, **20**, 637-647.

Demkowicz and J. T. Oden (1981), *On some existence and uniqueness results in contact problems with nonlocal friction*, Texas Institute of Computational Mechanics (TICOM) Report 81-13, University of Texas at Austin.

N. Kikuchi and J.T. Oden, *Contact Problems in Elasticity: A Study of Variational Inequalities and Finite Element Methods*, SIAM ????

R. Michalowski and Z. Mroz (1978), "Associated and non-associated sliding rules in contact friction problems," *Archives of Mechanics*, **30**, 259-276.

P. Wriggers (1995), "Finite Element Algorithms for Contact Problems," *Archives of Computational Methods in Engineering*, **2**,4, pp. 1-49.

P. Wriggers and C. Miehe (1994), "Contact Constraints within Coupled Thermomechanical Analysis - a Finite Element Model," *Comp. Meth. in Appl. Mech. and Eng.*, **113**, 301-319.

ERRATA

1. p.38 should read

$$G_{JjI} = \int_{\Gamma_c} \Lambda_I \Phi_{Jj} \, d\Gamma \qquad \mathbf{G} = \int_{\Gamma_c} \Lambda^T \Phi \, d\Gamma \tag{X.5.21b}$$

2. in Box X.3 last equation should read

$$\mathbf{G} = \int_{\Gamma_c} \Lambda^T \varphi \, d\Gamma$$

3. equation before (X.5.55) should read

$$p = \beta g = \beta (x_1 - x_2) H(g) = \beta (X_1 - X_2 + u_1 - u_2) H(g)$$

X.6. EXPLICIT METHODS OF TIME INTEGRATION

In this Section we describe the procedures for treating contact impact with explicit time integration. Explicit time integration is well suited to contact-impact problems because the small time steps imposed by numerical stability can treat the discontinuities in contact-impact. The large time steps made possible by unconditionally stable implicit methods are not effective for discontinous response. Furthermore, contact-impact also introduces discontinuities in the Jacobian, which impedes the convergence of Newton methods.

Another advantage of explicit algorithms is that the bodies can first be integrated completely independently, as if they were not in contact. This uncoupled solution correctly indicates which parts of the body are in contact. The contact conditions are imposed after the two bodies have been updated in an uncoupled manner; no iterations are needed to establish the contact interface. An explicit algorithm with contact-impact is almost identical to the algorithm described in Chapter X except that the bodies are checked for interpenetration. In each time step, the displacements and velocities of those nodes which have penetrated into another body are modified to reflect momentum balance and impenetrability on the interface.

We will here describe several implementations of contact-impact algorithms in explicit methods. Only the Lagrange multiplier and the penalty methods will be considered. the issues to be discussed include: 1. the approximations for the Lagrange multiplier fields; 2. structure of the algorithm; 3. effects of contact-impact methods on numerical stability. We will also describe certain characteristics of explicit solutions which arise from the physics and numerical characteristics of the contact-impact problem. In order to illustrate the characteristics of contact-impact in a simple setting, we first consider a one dimensional problem.

Example of Contact in One Dimension. The one-dimensional example is shown in Fig. ??. We first consider the premise that uncoupled updates of bodies A and B followed by modifications of the interpenetrating nodes for contact-impact lead to consistent solutions. For the two points R and S, which correspond to nodes 1 and 2,

respectively, of bodies A and B, there are four possibilities during a contact-impact problem

1. R and S are not in contact and do not contact during the time step;

2. R and S are not in contact but impact during the time step;

3. R and S are in contact and remain in contact;

4. R and S are in contact and separate during a time step, often known as release.

For case 3, the statement "remain in contact" does not imply that if two points must remain contiguous, because relative tangential motion, or sliding, which separates contiguous points is always possible. When two bodies remain in contact, they are assumed not to separate.

All of these possibilities can be correctly accounted for by integrating the two bodies independently as if they were not in contact and subsequently adjusting the velocities and the displacements. The possibilities which need to be explained are cases 2, 3 and 4.

The governing equations for the nodes 1 and 2 have been given in Example Eq. (53); although the problem shown in Fig. ?? is somewhat different, the equations for the contact nodes are unchanged. We will show that when the velocities from the uncoupled update predict initial or continuing contact, then the Lagrange multiplier $\lambda \geq 0$. The accelerations of nodes 1 and 2 when the two bodies are updated as uncoupled are

$$M_1 \bar{a}_1 - f_1 = 0 \ , \ \ M_2 \bar{a}_2 - f_2 = 0$$

where bars have been superposed on the accelerations to indicate that these are trial accelerations computed with the uncoupled bodies, as can be seen from the absence of the Lagrange multipliers. The central difference form of the update of Eqs. (53)

$$M_1 v_1^+ - M_1 v_1^- - \Delta t f_1 + \Delta t \lambda = 0$$

$$M_1 v_2^+ - M_1 v_2^- - \Delta t f_2 - \Delta t \lambda = 0$$

When the bodies contact during the time step, these equations must be solved with the subsidiary condition $v_1^+ = v_2^+$. Eliminating λ from the above equations by adding them and using the equality $v_1^+ = v_2^+$ gives

$$v_1^+ = v_2^+ = \frac{M_2 v_1^- + M_2 v_1^- + \Delta t \left(f_1 + f_2 \right)}{M_1 + M_2}$$

where all unmarked variables are a time step *n*. By means of the above equations, the updated velocities can be updated whenever impact occurs or the nodes were in contact in the previous time step. The above equations can be recognized to be the well known equations of conservation of mass for plastic impact of rigid bodies; more will be said on this later.

We will now show that whenever the updated velocities of any nodes which interpenetrate are computed by ( ), then the Lagrange multiplier will be positive, i.e. the interface force will be compressive. In other words, if the two nodes are updated as if the bodies were uncoupled and if the velocities are subsequently modified by (), then the Lagrange multipliers will have the correct sign, This amounts to showing that

if $\bar{v}_1^+ \geq \bar{v}_2^+$, then $\lambda \geq 0$.

Multiplying Eq top by M2 and Eq. bot by M1 and subtract bot form top; this gives

$$M_1 M_2 \left(v_1^- - v_2^- \right) + \Delta t \left(M_2 f_1 - M_1 f_2 \right) = \lambda \Delta t \left(M_1 + M_2 \right)$$

Substituting the expressions for f1 and f2 from () into the above and rearranging gives

$$\frac{\Delta t \left(M_1 + M_2 \right)}{M_1 M_2} \lambda = \left(v_1^- - v_2^- \right) + \Delta t \left(\bar{a}_1 - \bar{a}_2 \right) = \bar{v}_1^+ - \bar{v}_2^+$$

where the last equality is obtained by using the central difference formulas for the uncoupled integration of the two bodies: $\bar{v}_I^+ = v_I^- + \Delta t a_I$. The coefficient of λ is positive, so the sign of the RHS gives the sign of λ. Thus Eq () has been demonstrated.

To examine this finding in more detail, we now consider the three of the cases listed above (case 1 is trivial since it requires no modification of the nodal velocities since there is no contact):

case 2 (not in contact /contacts during Δt): then $\bar{v}_1^+ \succ \bar{v}_2^+$ and $\lambda \geq 0$ by Eq ()

case 3 (in contact/remains in contact): then $\bar{v}_1^+ \succ \bar{v}_2^+$ and $\lambda \geq 0$ by Eq ()

case 4 (in contact/release during Δt): then $\bar{v}_1^+ \prec \bar{v}_2^+$ and $\lambda \prec 0$ by Eq ()

Thus the velocities obtained by uncoupled integration correctly predict the sign of the Lagrange multiplier λ.

Two other interesting properties of explicit integration that can be learned from this example are:

1. initial contact, i.e. impact cannot occur in the same time step as release;

2. energy is dissipated during impact;

The first statement rests on the fact that the Lagrange multiplier at time step *n* is computed so that the velocities at time step *n*+1/2 match. Hence there is no mechanism in an explicit method for forcing release during the time step in which impact occurs. This property is consistent with the mechanics of wave propagation. In the mechanics of impacting bodies, release is caused by rarefaction waves which are generated when the compressive waves due to impact reflect from a free surface and reach the point of contact. When the magnitude of these rarefaction is sufficient to cause tension across the contact interface, release occurs. Therefore the minimum time required for release

subsequent to impact is two traversals of the distance to the nearest free surface. The stable time step, you may recall, allows the any wave generated by impact to move at most to the node nearest to the contact nodes. Therefore, in explicit time integration, there is insufficient time in a stable time step for the waves to traverse twice the distance to the nearest free surface.

The second statement can be explained by Eq. () which shows that the post-impact velocities are obtained by the plastic impact conditions,for rigid bodies, which always dissipate energy. The energy dissipated when two rods as shown in Fig.() are at constant but equal velocities is given by

As can be seen from the above, the amount of dissipation decreases with the refinement of the mesh. In the continuos impact problem, no energy is dissipated because the condition of equal velocities after impact is limited to the impact surfaces. A surface is a set of measure zero in three dimensions, so a change of energy over the surface has no effect on the total energy. (For one-dimensional problems the impact surface is a point, which is also a set of measure zero.) In a discrete model, the impacting nodes represent the material layer of thickness $h/2$ adjacent to the contact surface. Therefore, the dissipation in a discrete model is always finite. The correspondence between the continuous model and the discrete model also substantiates the correctness of the plastic impact condition. Since release cannot occur until the rarefaction waves reach the contact interface, the velocities of the two contacting bodies must be equal until that time. Thus it is inappropriate to use impact conditions other than perfectly plastic impact for discrete models of continuous systems. It should be stressed that such arguments do not apply to strictly multi-body models, where each node represents a body whose stiffness is not modeled, or to structural models, where the thickness direction has no deformability. The release and impact conditions are then more complex.

Penalty Method. The discrete equation at the impacting nodes for the two body problem can be taken directly from those given in Eq. ():

$$M_1 a_1 - f_1 + f_1^c = 0$$

$$M_2 a_2 - f_2 - f_2^c = 0$$

where the contact forces f_I^c replace the Lagrange multiplier replace the Lagrange multiplier in (). When the nodes are initially almost coincident, then $X_1 = X_2$ and the interface normal traction can be written as

$$f^c = p = \beta_1 g + \beta_1 \dot{g} = \beta_1 (u_1 - u_2) H(g) + \beta_2 (v_1 - v_2) H(\dot{g})$$

The unitary condition is now approximately enforced by the step functions in the normal contact force; it is violated since the normal traction is positive while the interpenetration rate is positive, so its product no longer vanishes. The post-impact velocities are now given by

The velocities of the two nodes are not equal since the penalty method only enforces the impenetrability constraint approximately. As the penalty parameter is increased, the condition of impenetrability is observed more closely. However, as indicated in the next paragraph, in dynamics the penalty parameter cannot be made arbitrarily large.

The condition that release not occur in the same time step as impact, which has been described to be a natural consequence of the physics of contact and numerical stability conditions of explicit intergrators, is not automatically satisifed by the penalty method. If the penalty force is very large, it is possible for the relative nodal velocity to reverse, so that decreasing gap rate is is followed in the same time step by an increasing gap rate. In view of the behavior of the continuous model described previously, which does not permit release until rarefaction waves reflected from the free surfaces reach the contact interface, this possibility in penalty methods does not appear physically correct. This anomaly can be eliminated by placing an upper bound on the penalty force, so that the impact is at most perfectly plastic. In other words, the penalty force should be bounded so that the velocities at the end of the impact time step are given by (). This yields the following upper bound on the contact force:

This bopund can be very useful since it provides a

In contrast to the Lagrange multiplier method, the penalty method usually decreases the stable time step. An estimate of the stable time step can be made by using the linear stiffness for the penalty method given in Eq. () in conjunction with the eigenvalue element inequality. In using the element eigenvalue inequlitu, a group of elements consisting of the penalty spring and the two surrounding elements should be used, since the penalty element has no mass by itself and therefore has an infinite frequency. This analysis shows that the stable time step for an interpenetration dependent penalty is given by

where α is given by

The decrease in the time step depends on the stiffness of the penalty spring. As the interpenetration stifness b is increased, the stable time step decreases. As in the case of the Lagrange multiplier method, this estimate of the stable time step is not a conservative estimate, even though it is based on the element eigenvalue inequaality. The analysis presumes linear behavior, whereas contact-impact is a very non-linear process.

EXPLICIT ALGORITHM

A flowchart for explicit time integration with contact-impact is shown in Box ??. As can be seen from the flowchart, the contact impact conditions are enforced immediately after the boundary conditions. Prior to the contact-impact step, all nodes in the model have been updated as if they were not in contact, including the nodes which were in contact in the previous time step. The nodes which are in contact are not treated differently in the rest of the algorithm. Some difficulties may occur dus to making the contact-impact

modifications after the boundary condition enforcement. For example, for a pair of contacting nodes on a plane of symmetry, it is possible for the contact-impact modifications to result in violation of the condition that the velocities normal to the plane of symmetry vanish. This can occur when the normal of the element adjacent to the plane of symmetry does not lie in that plane. Therefore, boundary conditions sometimes have to be imposed at contact nodes after the modifications.

The CONTACT module is limited to low-order elements in which the maximum interpenetration always occurs of the nodes of the master or slave body. It is then only necessary to check all nodes for interpenetration into elements of another body. The second statement in the *CONTACT* nevertheless conceals many challenging tasks. In a large model, on the order of 10^5 nodes may have to be checked against penetration into a similar number of elements. Obviously a brute force approach to this task is not going to work. Some of the strategies for dealing with this task are described in Section ?.

The

Box X.?
Flowchart for Explicit Integration with Contact-Impact

Main Program

1. initial conditions and setup: $t = 0$, $n = 0$, set $\mathbf{v}^0, \sigma^0$
2. get nodal forces $\mathbf{f}^t = \left(\mathbf{f}^{ext} - \mathbf{f}^{int}\right)^t$
3. velocity update: if $n \succ 0$, $\mathbf{v}^{\Delta t/2} = \mathbf{v}^0 + \mathbf{M}^{-1}\mathbf{f}^0$;
   otherwise $\mathbf{v}^{t+\Delta t/2} = \mathbf{v}^{t-\Delta t/2} + \mathbf{M}^{-1}\mathbf{f}^t$
4. displacement update: $\mathbf{d}^{t+\Delta t} = \mathbf{d}^t + \Delta t \mathbf{v}^{t+\Delta t/2}$
5. modify velocities and displacements for velocity boundary conditions
6. go to *CONTACT*
7. get $\mathbf{f}^{t+\Delta t} = \left(\mathbf{f}^{ext} - \mathbf{f}^{int}\right)^{t+\Delta t}$
8. accelerations: $\mathbf{a}^t = \mathbf{M}^{-1}\mathbf{f}^t$
9. if *if* $t \prec END$, go to 3

CONTACT

1. find node-element pairs which are in contact;
2.

Lagrange multiplier method. The discrete equations for the system are obtained by combining the semidiscrete equations with an explicit integration formula. For simplicity, we consider here only the central difference method. Substituting an expression for the accelerations at time step *n*, Eq.(), we obtain from () that

$$\mathbf{M}\left(\mathbf{v}^{n+1/2} - \mathbf{v}^{n-1/2}\right) - \mathbf{f}^n + \mathbf{G}^T\lambda^n = 0$$

Referring to the flowchart in Box X, it can be seen that when the contact conditions are enforced, the nodal forces at time step *n* are already known. However the Lagrange

multiplier are unknown. If we combine the above with the velocity constraint, Eq. () in Box ?, we obtain

$$\begin{bmatrix} \mathbf{M} & \Delta t\mathbf{G}^T \\ \mathbf{G} & \mathbf{0} \end{bmatrix} \begin{Bmatrix} \mathbf{v}^{n+1/2} \\ \lambda^n \end{Bmatrix} = \begin{Bmatrix} \Delta t\mathbf{f}^n + \mathbf{M}\mathbf{v}^{n-1/2} \\ \mathbf{0} \end{Bmatrix}$$

If a consistent mass matrix is used, solving for these variables appears to involve a system of equations which is larger than the unconstrained system, since the Lagrange multipliers have been added. In fact, for most systems, the size of the matrix can be reduced substantially, since trial values of $\mathbf{v}^{n+1/2}$ are already known and only the velocities of nodes on the contact interface are modified by contact .

In the above, everything on the right hand side is known at time step n when the modifications for the contact are made. The unknowns are λ^n and $\mathbf{v}^{n+1/2}$, although trial values for the nodal velocities have already been obtained by the uncoupled update. The solution for the Lagrange multipliers is obtained by first solving the top of the above equation for $\mathbf{v}^{n+1/2}$ and then solving for λ^n, which gives

$$\mathbf{G}\mathbf{M}^{-1}\mathbf{G}^T\lambda^n \le -\left(\mathbf{M}^{-1}\mathbf{f}^n + \tfrac{1}{\Delta t}\mathbf{v}^{n+1/2}\right) \equiv \mathbf{r}w$$

When the mass matrix is diagonal, the solution for the Lagrange multipliers can be streamlined by taking advantage of the fact that the inverse of the mass matrix consists of the reciprocals of the diagonal terms. To preserve the symmetric structure of the equations we take the square root of the mass matrix and multiply $\mathbf{G}$, and define the resulting matrix as $\overline{\mathbf{G}}$:

$$\overline{\mathbf{G}} = \mathbf{M}^{-1/2}\mathbf{G} \quad \overline{G}_{ab} = M_{ad}^{-1/2} G_{db}$$

Equations () can then be written as

$$\overline{\mathbf{G}}\,\overline{\mathbf{G}}^T\lambda^n = \mathbf{r}$$

An interesting characteristic of these equations is that they are already in the form of a triangulation. It is only necessary to eliminate all terms of the $\overline{\mathbf{G}}$ matrix to obtain a matrix from which the solution can easily be found. Moreover, the above equations involve only the nodes on the contact interfaces. Thus the system of equations to be solved is usually much smaller than the complete model. Nevertheless, for large-scale explicit solutions, the burden of solving these equations is too great, so simplifications are usually made to avoid solving these equations; these are discussed later.

Lagrange multiplier interpolation. In order to develop explicit forms of Eq.(), the interpolation for the Lagrange multipliers must be defined. We have already mentioned in Section X.5.2 that the construction of these interpolants can be complicated when the nodes of the bodies are noncontiguous. As indicated there, two possibilities are: 1. the master body mesh is chosen to be the $\mathbf{l}$ mesh; 2. construct a new mesh. Examples of the G matrix for noncontiguous nodes have already been described in Example XX. We now

explore the consequences of various **l** approx imations and their effects on computational efficency.

The implementation of implicit time integration and statics will be combined because the procedure are almost identical. The reader is urged to consult Sections X, where these topics are discussed for problems without contact. As in the aforementioned, both classes of problems are treated by the Newton method.

In the Newton method, the solution to the discrete equations is found by using a local linear model for the nonlinear equations. The linear model is based on a linearization of the governing discrete equations. We will consider the Lagrange multiplier methods and the penalty methods. In both cases, as before, we write the nonlinear equations in the form

$$\bar{\mathbf{f}}(\mathbf{d}, \dot{\mathbf{d}}, \lambda) = 0$$

where $\mathbf{d}$, $\dot{\mathbf{d}}$, and λ are, respectively, the nodal displacements, nodal velocities, and discrete Lagrange multipliers at time $t + \Delta t$; λ appears only in the Lagrange multiplier method. The internal force is only a function of $\mathbf{d}$, i.e. the material is rate-independent. The extension to rate dependent materials involves a combination of the techniques described here and in Section X, but they obscure the effects of contact-impact, so are omitted in this exposition.

In the Lagrange multiplier method the governing equations are

$$0 = \bar{f}(\mathbf{d}, \dot{\mathbf{d}}, \lambda, t) = \mathbf{M}\ddot{\mathbf{d}}(t) + \mathbf{f}^{int}(\mathbf{d}) - f^{ext}(\mathbf{d}, t) - \mathbf{G}(\mathbf{d})\lambda(t)$$

where the independent variables are indicated in the above. All of the above terms are functions of time since $\mathbf{d} = \mathbf{d}/t$. The development is restricted to rate-independent materials, so the internal nodal forces are only functions of the nodal displacements, see Section X.

We now expand the nodal forces by the chain rule, giving

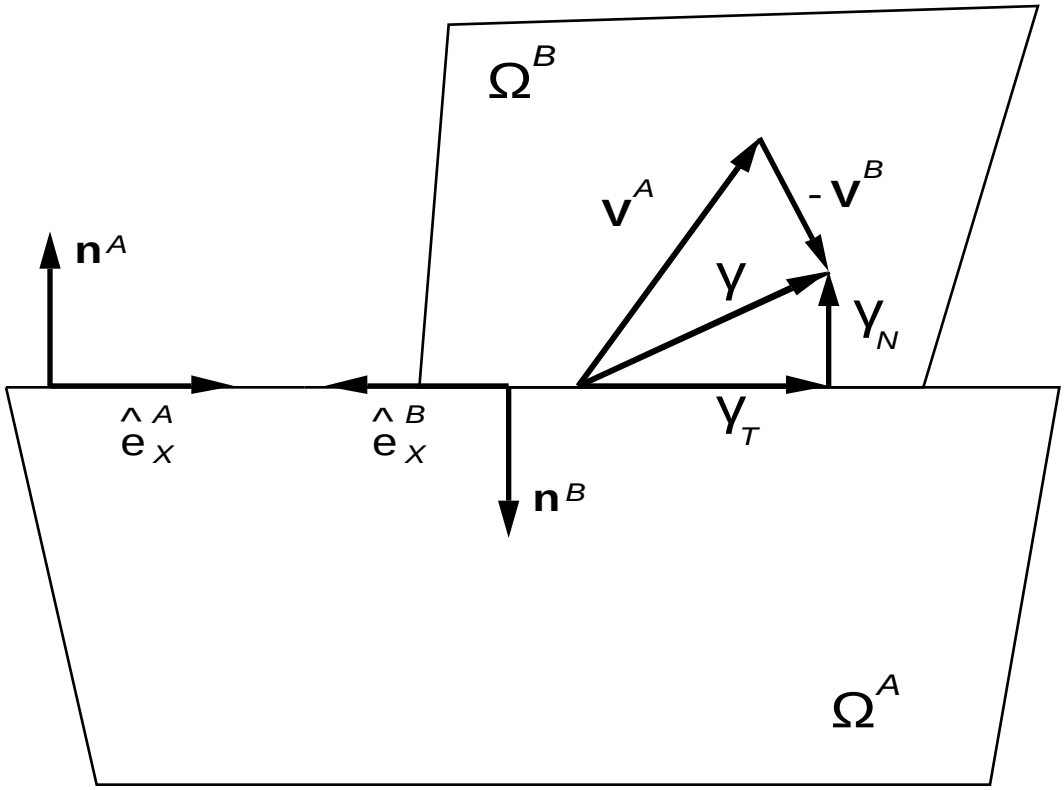

Figure 4. Illustration of nomenclature in a two dimensional contact problem.

An interesting simplification of the above example is shown in Fig. . The equations for this system can be obtained by just eliminating rows 1 and 3 and columns 1 and 3, giving

$$\begin{bmatrix} k_2 & -1 \\ -1 & 0 \end{bmatrix} \begin{Bmatrix} d_1 \\ \lambda_1 \end{Bmatrix} = \begin{Bmatrix} f_1 \\ 0 \end{Bmatrix}$$

The potential energy $\Pi(d,\lambda) = \frac{1}{2} k_2 d^2 - f_1 d$ is plotted for $f_1 =$ in Fig. as a function of d and λ ; to obtain the plot, Eqs. ( ) have been solved.

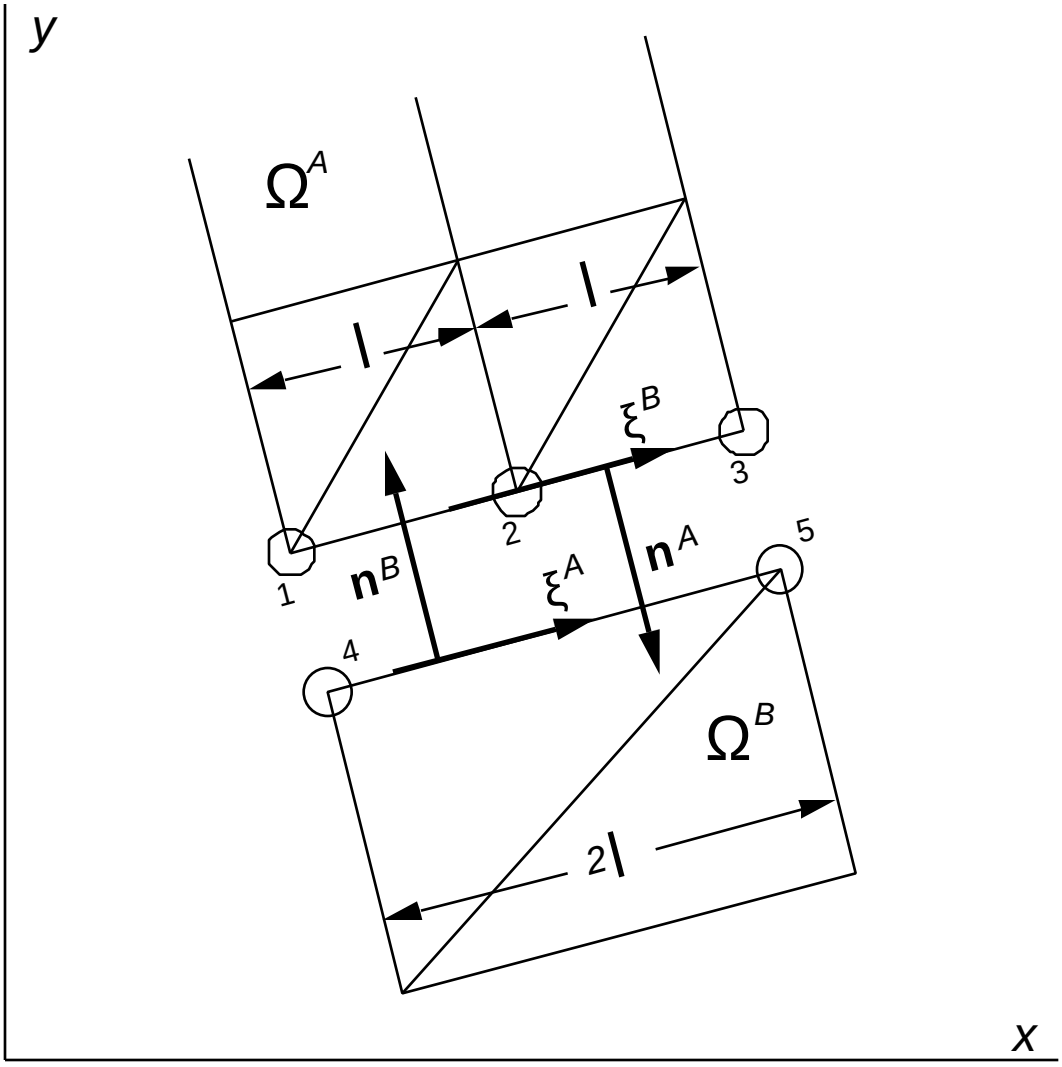

Figure 9.

Example X3. Figure 9 shows the two two-dimensional bodies of unit thickness which are in contact along a line; a total of 5 nodes are in contact, 3 nodes from body A, 2 nodes from body B.. The nodes on the endpoints are coincident, but the center node of body A is not coincident with a node on body B. This example introduces some of the difficulties arising from noncoincident nodes. We will restrict our attention to the nodes which are in contact, since the equation at the other nodes are unchanged. The nodal velocities of the contact nodes are denoted by $\mathbf{d}_c$ where $\dot{\mathbf{d}}_c^T = \begin{bmatrix} v_1 & v_2 & v_3 & v_4 & v_5 \end{bmatrix}$. The elements in the two bodies are bilinear 4-node quadrilaterals, so the displacement and velocity fields along the contact lines are linear, and will be represented by

$$v(\xi,t) = \sum_{I=1}^{5} N_I(\xi) v_I(t)$$

where $\xi = (s - s_I) / l_I$ along each of the segments.

There are many choices for the approximation of the Lagrange multiplier field, but a good choice is usually a field of the same order as that of the field being constrained. In this case the tractions are constrained and the tractions are piecewise constant, so we let

$$\lambda(x,t) = \lambda_1(t) \;\; for \; 0 \le s \le \frac{l}{2}$$

$$\lambda(s,t) = \lambda_2(t) \;\; for \; l/2 \le s \le l$$

where s parametrizes the contact line.

The G matrix here will be assembled from the segment, or element, matrices. The **T** matrix is constant along the line joining nodes 1 and 3 and given by

$$T = \begin{bmatrix} s & -c \\ 0 & 0 \\ c & s \end{bmatrix}, \quad c = \cos\theta, \; s = \sin\theta$$

The element G matrices are then given by

$$\mathbf{G}_{e=1} = \mathbf{G}_{e=2} = \int_0^1 \begin{bmatrix} s(1-\xi) \\ -c(1-\xi) \\ s\xi \\ -c\xi \end{bmatrix} [1] l d\xi = \frac{l}{2} \begin{bmatrix} s \\ -c \\ s \\ -c \end{bmatrix}$$

$$\mathbf{G}_{e=3} = \int_0^{1/2} \begin{bmatrix} -s(1-\xi) \\ c(1-\xi) \\ -s\xi \\ c\xi \end{bmatrix} [1 \quad 0] 2l d\xi + \int_{1/2}^1 \begin{bmatrix} -s(1-\xi) \\ c(1-\xi) \\ -s\xi \\ c\xi \end{bmatrix} [0 \quad 1] 2l d\xi = \frac{l}{4} \begin{bmatrix} -3s & -s \\ 3c & c \\ -s & -3s \\ c & 3c \end{bmatrix}$$

Assembling the three matrices gives

$$\mathbf{G}^T = \frac{l}{4} \begin{bmatrix} 2s & -2c & 2s & -2c & 0 & 0 & -3s & 3c & -s & c \\ 0 & 0 & 2s & -2c & 2s & -2c & -s & c & -3s & -3c \end{bmatrix}$$